

NIST NCSTAR 1-6D

**Federal Building and Fire Safety Investigation of the
World Trade Center Disaster**

Global Structural Analysis of the Response of the World Trade Center Towers to Impact Damage and Fire

Mehdi S. Zarghamee
Yasuo Kitane
Ömer O. Erbay
Therese P. McAllister
John L. Gross

NIST NCSTAR 1-6D

**Federal Building and Fire Safety Investigation of the
World Trade Center Disaster**

**Global Structural Analysis of the
Response of the World Trade Center
Towers to Impact Damage and Fire**

Mehdi S. Zarghamee
Yasuo Kitane
Ömer O. Erbay
Simpson Gumpertz & Heger Inc.

Therese P. McAllister
John L. Gross
*Building and Fire Research Laboratory
National Institute of Standard and Technology*

September 2005



U.S. Department of Commerce
Carlos M. Gutierrez, Secretary

Technology Administration
Michelle O'Neill, Acting Secretary for Technology

National Institute of Standards and Technology
William Jeffrey, Director

Disclaimer No. 1

Certain commercial entities, equipment, products, or materials are identified in this document in order to describe a procedure or concept adequately or to trace the history of the procedures and practices used. Such identification is not intended to imply recommendation, endorsement, or implication that the entities, products, materials, or equipment are necessarily the best available for the purpose. Nor does such identification imply a finding of fault or negligence by the National Institute of Standards and Technology.

Disclaimer No. 2

The policy of NIST is to use the International System of Units (metric units) in all publications. In this document, however, units are presented in metric units or the inch-pound system, whichever is prevalent in the discipline.

Disclaimer No. 3

Pursuant to section 7 of the National Construction Safety Team Act, the NIST Director has determined that certain evidence received by NIST in the course of this Investigation is "voluntarily provided safety-related information" that is "not directly related to the building failure being investigated" and that "disclosure of that information would inhibit the voluntary provision of that type of information" (15 USC 7306c).

In addition, a substantial portion of the evidence collected by NIST in the course of the Investigation has been provided to NIST under nondisclosure agreements.

Disclaimer No. 4

NIST takes no position as to whether the design or construction of a WTC building was compliant with any code since, due to the destruction of the WTC buildings, NIST could not verify the actual (or as-built) construction, the properties and condition of the materials used, or changes to the original construction made over the life of the buildings. In addition, NIST could not verify the interpretations of codes used by applicable authorities in determining compliance when implementing building codes. Where an Investigation report states whether a system was designed or installed as required by a code *provision*, NIST has documentary or anecdotal evidence indicating whether the requirement was met, or NIST has independently conducted tests or analyses indicating whether the requirement was met.

Use in Legal Proceedings

No part of any report resulting from a NIST investigation into a structural failure or from an investigation under the National Construction Safety Team Act may be used in any suit or action for damages arising out of any matter mentioned in such report (15 USC 281a; as amended by P.L. 107-231).

**National Institute of Standards and Technology National Construction Safety Team Act Report 1-6D
Natl. Inst. Stand. Technol. Natl. Constr. Sfty. Tm. Act Rpt. 1-6D, 476 pages (September 2005)
CODEN: NSPUE2**

U.S. GOVERNMENT PRINTING OFFICE
WASHINGTON: 2005

For sale by the Superintendent of Documents, U.S. Government Printing Office
Internet: bookstore.gpo.gov — Phone: (202) 512-1800 — Fax: (202) 512-2250
Mail: Stop SSOP, Washington, DC 20402-0001

ABSTRACT

Simpson Gumpertz & Heger Inc (SGH) developed global models of the World Trade Center (WTC) towers using finite elements to gain an understanding of the roles of the aircraft impact damage and the subsequent fires in the WTC towers with respect to structural stability and sequential failures of components and subsystems and to determine the probable sequence of structural responses that led to initiation of global collapse. The study was conducted as part of the investigation on the WTC disaster by the National Institute of Standards and Technology (NIST).

The developed finite-element global models of the WTC towers simulated the structural performance of the part of the buildings in and above the aircraft impact zone. These models captured the nonlinear responses of the towers subjected to the aircraft impact damage and the subsequent fire effects. The nonlinearities included in the global models were temperature-dependent material properties such as thermal expansion, plasticity and creep of metals, large deflection and the resulting instability, and failure modes of members and connections.

NIST provided temperature-dependent nonlinear material properties, estimates of aircraft impact damage to structural members, and temperature time histories of structural elements, which were used as input in this study.

The finite element analyses (FEA) of the global models and of the component and subsystem models showed that the key structural responses that led to the collapse of the towers were as follows: 1) floor sagging caused by the failure of thermally-weakened truss members, resulting in pull-in forces between the floor and the exterior wall, and in some cases, disconnection of the floor from the exterior wall; 2) downward displacement of the core due to aircraft impact damage and shortening of the remaining core columns from increased load, plasticity, creep of steel at high temperatures, and buckling resulting from fire-induced high temperatures, and unloading of the core; 3) bowing and buckling of exterior walls caused by the pull-in forces and loss of lateral support from the sagged floors, and floor/wall disconnections at high temperatures; and 4) redistribution of gravity loads among the columns locally, among the exterior walls, and between the exterior walls and the core, resulting from impact damage, relative thermal expansion, shortening of core columns, tilting of the tower above the impact zone, and bowing and buckling of exterior walls.

In WTC 1, the aircraft impact caused damage to the north and south walls, floors, some core columns, and insulation. The subsequent fires caused sagging of the floors on the south side of the office area, where insulation was damaged, and inward bowing of the south wall. The damage to the core columns resulted in local load redistribution to the remaining core columns. The subsequent fire-induced high temperatures caused the core to displace downward from plasticity and high creep strains in high stress and high temperatures. The downward displacement of the core resulted in load redistribution from the core to the exterior walls. With continuously increased bowing, the entire width of the south wall buckled inward. The section of the building above the impact zone tilted to the south as instability progressed horizontally to the adjacent east and west walls. Global collapse occurred as potential energy of the falling upper structure exceeded the strain energy capacity in the deforming structural members.

In WTC 2, the aircraft impact caused damage to the south and north exterior walls, floors, and columns in the southeast corner of the core. The floor damage and the subsequent fires caused sagging of the floors and local floor/wall disconnections, and resulted in bowing and buckling of the east wall. The damage to the core columns and fire-induced high temperatures resulted in local load redistribution to the remaining core columns in the southeast corner, which redistributed the core column loads to the east and south wall columns, as the core leaned toward the south and east. With continuously increased bowing, the entire width of the east wall buckled inward. The section of the building above the impact zone tilted to the east and south as instability progressed horizontally to the adjacent north and south walls. Global collapse occurred when the potential energy of the falling upper structure exceeded the strain energy capacity in the deforming structural members.

The results of global analysis of both WTC 1 and WTC 2 showed that global collapse of both towers was initiated by the instability of the exterior walls pursuant to their excessive inward bowing which progressed horizontally to adjacent walls.

Keywords: Collapse, creep, large deflection, nonlinear finite element analysis, plasticity, stability, structural response to damage, structural response to fire, World Trade Center.

TABLE OF CONTENTS

Abstract	iii
List of Figures	vii
List of Tables	xxv
List of Acronyms and Abbreviations	xxix
Preface	xxxix
Acknowledgments.....	xli
Executive Summary	xliii
Chapter 1	
Introduction	1
1.1 Objective	1
1.2 Background.....	1
1.3 Method of Approach	3
1.4 Report Organization.....	4
Chapter 2	
Global Models	7
2.1 Description of Global Models.....	7
2.2 Impact Damage	12
2.2.1 Introduction	12
2.2.2 Initial Damage Sets.....	12
2.2.3 Final Damage Sets	23
2.3 Temperature Effects.....	34
2.4 Thermal Behavior of Floors.....	35
2.5 Fire-Induced Damage.....	36
2.5.1 Floor/Wall Disconnections	36
2.5.2 Pull-in Forces.....	37
2.5.3 Floor/Wall Disconnections and Pull-in Forces Included in the Global Model.....	39
Chapter 3	
Isolated Wall and Core Model Analyses	61
3.1 Introduction.....	61
3.2 Exterior Wall Buckling.....	61

3.2.1	Finite Element Analysis of WTC 1 Exterior Wall	65
3.2.2	FEA of WTC 2 Exterior Wall	102
3.3	Core Column Shortening and Downward Displacement of Core	134
3.3.1	FEA of WTC 1 Core.....	135
3.3.2	FEA of WTC 2 Core.....	154
Chapter 4		
Global Analysis		167
4.1	Conversion from SAP2000 to ANSYS	167
4.1.1	ANSYS Models	168
4.1.2	Validation of Translated ANSYS Global Models	170
4.2	Global Analysis with Creep	173
4.2.1	Introduction	173
4.2.2	Modifications to the Global Model with Creep and Inelastic Buckling of Columns	173
4.2.3	Boundary Conditions and Loading Steps	179
4.2.4	Simulation of WTC 1 Collapse	179
4.2.5	Simulation of WTC 2 Collapse	245
Chapter 5		
Collapse Sequence		309
5.1	Introduction.....	309
5.2	WTC 1 Collapse Sequence	312
5.3	WTC 2 Collapse Sequence	319
5.4	Discussion.....	329
Appendix A		
FEA of Floors		331
Appendix B		
Floor Truss Dynamic Response Due to Impact of Dropping Floor		373
Appendix C		
Global Analysis Without Creep		377

LIST OF FIGURES

Figure P-1.	The eight projects in the federal building and fire safety investigation of the WTC disaster.	xxxiii
Figure 2-1.	Column designations.....	11
Figure 2-2.	Structural damage condition on the exterior walls of WTC 1 for all cases of impact damage.	13
Figure 2-3.	Structural damage condition on the exterior walls of WTC 2 for all cases of impact damage.	14
Figure 2-4.	Core columns and core beams in the WTC 1 global model without aircraft impact damage.	14
Figure 2-5.	Core columns and core beams in the WTC 2 global model without aircraft impact damage.	15
Figure 2-6.	Case A _i structural damage condition on the core columns of WTC 1.	15
Figure 2-7.	Case C _i structural damage condition on the core columns of WTC 2.....	16
Figure 2-8.	Revised Case C _i structural damage condition on the core columns of WTC 2.....	16
Figure 2-9.	Case A _i insulation damage conditions for WTC 1 floor trusses and beams.	17
Figure 2-10.	Case A _i structural damage conditions for WTC 1.....	18
Figure 2-11.	Case C _i insulation damage conditions for WTC 2 floor trusses and beams.....	19
Figure 2-12.	Case C _i Structural damage conditions for WTC 2 floors.....	20
Figure 2-13.	Case D _i insulation damage conditions for WTC 2 floor trusses and beams.	21
Figure 2-14.	Case D _i Structural damage conditions for WTC 2 floors.....	22
Figure 2-15.	Case A structural damage condition on the core columns of WTC 1.....	23
Figure 2-16.	Case C structural damage condition on the core columns of WTC 2.	24
Figure 2-17.	Case B structural damage condition on the core columns of WTC 1 (including heavily damaged columns).....	24
Figure 2-18.	Case D structural damage condition on the core columns of WTC 2 (including heavily damaged columns).....	25
Figure 2-19.	Case A insulation damage condition for WTC 1 floor trusses and beams.....	26
Figure 2-20.	Case A structural damage condition for WTC 1 floors.....	27
Figure 2-21.	Case C insulation damage condition for WTC 2 floor trusses and beams.	28
Figure 2-22.	Case C structural damage condition for WTC 2 floors.....	29
Figure 2-23.	Case B insulation damage conditions for WTC 1 floor trusses and beams.	30
Figure 2-24.	Case B structural damage conditions for WTC 1 floors.	31
Figure 2-25.	Case D insulation damage conditions for WTC 2 floor trusses and beams.	32

Figure 2–26. Case D structural damage conditions for WTC 2 floors. 33

Figure 2–27. Comparison of vertical displacement of a simplified truss model at Column 333 extracted from the full floor model of Floor 96 of WTC 1 for Case B_i temperature condition at 40 min with and without creep..... 39

Figure 2–28. Locations of floor/wall disconnections and pull-in forces for the global analysis of WTC 1 between 0 min and 10 min for Case B conditions..... 41

Figure 2–29. Locations of floor/wall disconnections and pull-in forces for the global analysis of WTC 1 between 10 min and 20 min for Case B conditions..... 42

Figure 2–30. Locations of floor/wall disconnections and pull-in forces for the global analysis of WTC 1 between 20 min and 30 min for Case B conditions..... 43

Figure 2–31. Locations of floor/wall disconnections and pull-in forces for the global analysis of WTC 1 between 30 min and 40 min for Case B conditions..... 44

Figure 2–32. Locations of floor/wall disconnections and pull-in forces for the global analysis of WTC 1 between 40 min and 50 min for Case B conditions..... 45

Figure 2–33. Locations of floor/wall disconnections and pull-in forces for the global analysis of WTC 1 between 50 min and 60 min for Case B conditions..... 46

Figure 2–34. Locations of floor/wall disconnections and pull-in forces for the global analysis of WTC 1 between 60 min and 70 min for Case B conditions..... 47

Figure 2–35. Locations of floor/wall disconnections and pull-in forces for the global analysis of WTC 1 between 70 min and 80 min for Case B conditions..... 48

Figure 2–36. Locations of floor/wall disconnections and pull-in forces for the global analysis of WTC 1 between 80 min and 90 min for Case B conditions..... 49

Figure 2–37. Locations of floor/wall disconnections and pull-in forces for the global analysis of WTC 1 between 90 min and 100 min for Case B conditions..... 50

Figure 2–38. Locations of floor/wall disconnections and pull-in forces for the global analysis of WTC 2 between 0 min and 10 min for Case D conditions. 54

Figure 2–39. Locations of floor/wall disconnections and pull-in forces for the global analysis of WTC 2 between 10 min and 20 min for Case D conditions. 55

Figure 2–40. Locations of floor/wall disconnections and pull-in forces for the global analysis of WTC 2 between 20 min and 30 min for Case D conditions. 56

Figure 2–41. Locations of floor/wall disconnections and pull-in forces for the global analysis of WTC 2 between 30 min and 40 min for Case D conditions. 57

Figure 2–42. Locations of floor/wall disconnections and pull-in forces for the global analysis of WTC 2 between 40 min and 50 min for Case D conditions. 58

Figure 2–43. Locations of floor/wall disconnections and pull-in forces for the global analysis of WTC 2 between 50 min and 60 min for Case D conditions. 59

Figure 3–1. Isolated exterior wall segments from WTC 1 and WTC 2 (horizontal lines show spandrels and vertical lines show column). 62

Figure 3–2. Boundary conditions applied on the isolated exterior wall segment on the south wall of WTC 1. 62

Figure 3–3.	Case A temperature condition of south wall columns of WTC 1 at 10 min.	66
Figure 3–4.	Case A temperature condition of south wall columns of WTC 1 at 20 min.	66
Figure 3–5.	Case A temperature condition of south wall columns of WTC 1 at 30 min.	67
Figure 3–6.	Case A temperature condition of south wall columns of WTC 1 at 40 min.	67
Figure 3–7.	Case A temperature condition of south wall columns of WTC 1 at 50 min.	67
Figure 3–8.	Case A temperature condition of south wall columns of WTC 1 at 60 min.	68
Figure 3–9.	Case A temperature condition of south wall columns of WTC 1 at 70 min.	68
Figure 3–10.	Case A temperature condition of south wall columns of WTC 1 at 80 min.	68
Figure 3–11.	Case A temperature condition of south wall columns of WTC 1 at 90 min.	69
Figure 3–12.	Case A temperature condition of south wall columns of WTC 1 at 100 min.	69
Figure 3–13.	Case A temperature condition of south wall spandrels of WTC 1 at 10 min.	69
Figure 3–14.	Case A temperature condition of south wall spandrels of WTC 1 at 20 min.	70
Figure 3–15.	Case A temperature condition of south wall spandrels of WTC 1 at 30 min.	70
Figure 3–16.	Case A temperature condition of south wall spandrels of WTC 1 at 40 min.	70
Figure 3–17.	Case A temperature condition of south wall spandrels of WTC 1 at 50 min.	71
Figure 3–18.	Case A temperature condition of south wall spandrels of WTC 1 at 60 min.	71
Figure 3–19.	Case A temperature condition of south wall spandrels of WTC 1 at 70 min.	71
Figure 3–20.	Case A temperature condition of south wall spandrels of WTC 1 at 80 min.	72
Figure 3–21.	Case A temperature condition of south wall spandrels of WTC 1 at 90 min.	72
Figure 3–22.	Case A temperature condition of south wall spandrels of WTC 1 at 100 min.	72
Figure 3–23.	Response of Isolated south wall model of WTC 1 after aircraft impact.	73
Figure 3–24.	Vertical displacements of isolated south wall model of WTC 1 for Case A temperature condition (downward displacement is negative).	74
Figure 3–25.	Out-of-plane displacements of isolated south wall model of WTC 1 for Case A temperature condition (inward displacement is positive).	75
Figure 3–26.	Axial load in columns of isolated south wall model of WTC 1 for Case A temperature condition (compression is negative).	76
Figure 3–27.	Plastic strain in columns of isolated south wall model of WTC 1 for Case A temperature condition at 100 min (compressive strain is negative).	77
Figure 3–28.	Axial load in columns of south wall of WTC 1 at 100 min: isolated wall model for Case A temperature condition compared to global model without creep for Case Ai conditions (compression is positive).	77
Figure 3–29.	Responses of isolated south wall model of WTC 1 after corrective loads from the global model were applied (Case A temperature condition at 100 min).	78
Figure 3–30.	Total additional vertical load versus additional vertical displacement during push- down analysis of isolated south wall model of WTC 1 for Case A temperature condition (compression is positive).	79

Figure 3–31. Additional vertical load per column at different additional vertical displacements during push-down analysis of isolated south wall model of WTC 1 for Case A temperature condition (compression is positive). 79

Figure 3–32. Response of isolated south wall model of WTC 1 to Case A temperature condition and push down at the end of the push-down analysis. 80

Figure 3–33. Location of the out-of-plane supports and floor/wall disconnections between exterior wall and the floor (WTC 1 south wall for Case B conditions at 100 min)..... 82

Figure 3–34. Case B temperature condition of south wall columns of WTC 1 at 10 min. 82

Figure 3–35. Case B temperature condition of south wall columns of WTC 1 at 20 min. 83

Figure 3–36. Case B temperature condition of south wall columns of WTC 1 at 30 min. 83

Figure 3–37. Case B temperature condition of south wall columns of WTC 1 at 40 min. 83

Figure 3–38. Case B temperature condition of south wall columns of WTC 1 at 50 min. 84

Figure 3–39. Case B temperature condition of south wall columns of WTC 1 at 60 min. 84

Figure 3–40. Case B temperature condition of south wall columns of WTC 1 at 70 min. 84

Figure 3–41. Case B temperature condition of south wall columns of WTC 1 at 80 min. 85

Figure 3–42. Case B temperature condition of south wall columns of WTC 1 at 90 min. 85

Figure 3–43. Case B temperature condition of south wall columns of WTC 1 at 100 min..... 85

Figure 3–44. Case B temperature condition of south wall spandrels of WTC 1 at 10 min. 86

Figure 3–45. Case B temperature condition of south wall spandrels of WTC 1 at 20 min. 86

Figure 3–46. Case B temperature condition of south wall spandrels of WTC 1 at 30 min. 86

Figure 3–47. Case B temperature condition of south wall spandrels of WTC 1 at 40 min. 87

Figure 3–48. Case B temperature condition of south wall spandrels of WTC 1 at 50 min. 87

Figure 3–49. Case B temperature condition of south wall spandrels of WTC 1 at 60 min. 87

Figure 3–50. Case B temperature condition of south wall spandrels of WTC 1 at 70 min. 88

Figure 3–51. Case B temperature condition of south wall spandrels of WTC 1 at 80 min. 88

Figure 3–52. Case B temperature condition of south wall spandrels of WTC 1 at 90 min. 88

Figure 3–53. Case B temperature condition of south wall spandrels of WTC 1 at 100 min. 89

Figure 3–54. Vertical displacement of isolated south wall model of WTC 1 for Case B temperature condition (downward displacement is negative)..... 90

Figure 3–55. Out-of-plane displacement of isolated south wall model of WTC 1 for Case B temperature condition (inward displacement is positive). 91

Figure 3–56. Axial load in columns of isolated south wall model of WTC 1 for Case B temperature condition (compression is negative). 92

Figure 3–57. Plastic strain in columns of isolated south wall model of WTC 1 for Case B temperature condition at 100 min (compressive strain is negative)..... 93

Figure 3–58. Axial load in columns of south wall of WTC 1 at 100 min: isolated wall model for Case B temperature condition compared to global model without creep for Case A_i conditions (compression is positive)..... 93

Figure 3–59. Response of isolated south wall model of WTC 1 after corrective loads from the global model were applied (Case B temperature condition at 100 min).	94
Figure 3–60. Total additional vertical load versus additional vertical displacement during push-down analysis of isolated south wall model of WTC 1 for Case B temperature condition (compression is positive).	95
Figure 3–61. Additional load per column at different additional vertical displacements during push-down analysis of isolated south wall model of WTC 1 for Case B temperature condition (compression is positive).	95
Figure 3–62. Response of isolated south wall model of WTC 1 to Case B temperature condition and push-down.	96
Figure 3–63. Locations of floor/wall disconnections and pull-in forces used between 80 min and 100 min of Case B temperature for south wall of WTC 1.	98
Figure 3–64. Response of isolated south wall model of WTC 1 at 80 min of Case B temperature condition with floor/wall disconnections and 6 kip pull-in forces over five floors.	99
Figure 3–65. Response of isolated south wall model of WTC 1 at 90 min of Case B temperature condition with floor/wall disconnections and 6 kip pull-in forces over five floors.	100
Figure 3–66. Response of isolated south wall model of WTC 1 at 100 min of Case B temperature condition with floor/wall disconnections and 6 kip pull-in forces over five floors.	101
Figure 3–67. Axial load in columns between Floors 98 and 99 of isolated south wall model of WTC 1 at 80 min, 90 min, and 100 min of Case B temperature condition with floor/wall disconnections and 6 kip pull-in forces over five floors (compression is positive).....	102
Figure 3–68. Column temperatures on the east wall of WTC 2 for Case C temperature condition at 10 min, 20 min, and 30 min.	104
Figure 3–69. Column temperatures on the east wall of WTC 2 for Case C temperature condition at 40 min, 50 min, and 60 min.	105
Figure 3–70. Location of the out-of-plane supports and floor/wall disconnections between exterior wall and the floor (WTC 2 east wall for Case C conditions at 60 min).	106
Figure 3–71. Vertical displacement of isolated east wall model of WTC 2 for Case C temperature distribution (downward displacement is negative; displacements scaled ten times).	107
Figure 3–72. Vertical displacement of isolated east wall model of WTC 2 for Case C temperature distribution at 60 min (downward displacement is negative; displacements scaled ten times).....	108
Figure 3–73. Out-of-plane displacement of isolated east wall model of WTC 2 for Case C temperature condition (inward displacement is positive; displacements scaled ten times).....	109
Figure 3–74. Out-of-plane displacement of isolated east wall model of WTC 2 for Case C temperature distribution at 60 min (inward displacement is positive; displacements scaled ten times).....	110
Figure 3–75. Axial load on columns of isolated east wall model of WTC 2 under Case C temperature condition (compression is negative).	111
Figure 3–76. Axial load on columns of isolated east wall model of WTC 2 for Case C temperatures distribution at 60 min (compression is negative).	112

Figure 3–77. Comparison of axial load in columns at Floor 83 of isolated east wall model of WTC 2 at 60 min for Case C temperature conditions and the global model without creep for Case C_i conditions (compression is positive). 113

Figure 3–78. Vertical and out-of-plane displacements of isolated east wall model of WTC 2 after column forces were corrected to those of global modal without creep for Case C_i conditions (displacements scaled ten times). 113

Figure 3–79. Vertical and out-of-plane displacements of isolated east wall model of WTC 2 after Case C temperature condition and push down analysis (displacements scaled five times)..... 114

Figure 3–80. Axial load on east wall columns of isolated east wall model of WTC 2 after Case C temperature condition and push-down (compression is negative). 114

Figure 3–81. Additional vertical load versus additional vertical displacement during push–down analysis of isolated east wall model of WTC 2 for Case C temperature condition..... 115

Figure 3–82. Variation of additional vertical load applied to columns of isolated east wall model of WTC 2 at different levels of additional vertical displacements imposed after Case C temperature condition (compression is positive). 115

Figure 3–83. Column temperatures on the east wall of WTC 2 for Case D temperature condition at 10 min, 20 min, and 30 min. 117

Figure 3–84. Column temperatures on the east wall of WTC 2 for Case D temperature condition at 40 min, 50 min, and 60 min. 118

Figure 3–85. Location of the out-of-plane supports and floor/wall disconnections between exterior wall and the floor (WTC 2 east wall for Case D conditions at 60 min)..... 119

Figure 3–86. Vertical displacement of isolated east wall model of WTC 2 for Case D temperature condition (downward displacement is negative; displacements scaled ten times)..... 120

Figure 3–87. Vertical displacement of isolated east wall model of WTC 2 for Case D temperature condition at 60 min (downward displacement is negative; displacements scaled ten times)..... 121

Figure 3–88. Out-of-plane displacement of isolated east wall model of WTC 2 for Case D temperature condition (inward displacement is positive; displacements scaled ten times)..... 122

Figure 3–89. Out-of-plane displacement of isolated east wall model of WTC 2 for Case D temperature condition at 60 min (inward displacement is positive; displacements scaled ten times)..... 123

Figure 3–90. Axial load on east wall columns of isolated east wall model of WTC 2 for Case D temperature condition (compression is negative). 124

Figure 3–91. Axial load on east wall columns of isolated east wall model of WTC 2 for Case D temperature condition at 60 min (compression is negative). 125

Figure 3–92. Comparison of axial load in columns at Floor 83 of isolated east wall model of WTC 2 at 60 min for Case D temperature conditions and the global model without creep for Case C_i structural damage condition and Case D_i temperature condition (compression is positive). 126

Figure 3–93. Vertical and out-of-plane displacements of columns of isolated east wall model of WTC 2 after column forces were corrected to those of global model without creep for Case C _i structural damage condition and Case D _i temperature condition (displacements scaled ten times).....	126
Figure 3–94. Vertical and out-of-plane displacements of isolated east wall model of WTC 2 after Case D temperature condition and push down (displacements scaled five times).....	127
Figure 3–95. Axial load on east wall columns of isolated east wall model of WTC 2 after Case D temperature condition and push down (compression is negative).	127
Figure 3–96. Additional vertical load applied to columns versus additional vertical during displacement for push-down analysis of isolated east wall model of WTC 2 for after Case D temperature condition (compression is positive; see Fig. 3–95 for column locations).....	128
Figure 3–97. Variation of additional vertical load applied to columns of isolated east wall model of WTC 2 at different levels of additional vertical displacements imposed after Case D temperature condition (compression is positive).	128
Figure 3–98. Out-of-plane displacements of the east wall of WTC 2 estimated by NIST from photographs (inward displacement is positive; displacements are in in.).....	129
Figure 3–99. Out-of-plane displacement of isolated east wall model of WTC 2 with 0.5 kip and 5.0 kip pull-in force with uniform magnitude distribution at 20 min and 18 min (inward displacement is positive).....	130
Figure 3–100. Out-of-plane displacement of isolated east wall model of WTC 2 with 0.5 kip pull-in force with uniform magnitude distribution at 32 min (inward displacement is positive).....	130
Figure 3–101. Out-of-plane displacement of isolated east wall model of WTC 2 with nonuniform pull-in force with magnitude of 1.0 kip on the south half and 4.0 kip on the north half (inward displacement is positive).	132
Figure 3–102. Out-of-plane displacement of isolated east wall model of WTC 2 with nonuniform pull-in force with magnitude of 1.5 kip on the south half and 5.0 kip on the north half (inward displacement is positive).	133
Figure 3–103. Isolated core models.....	134
Figure 3–104. Vertical displacement of isolated core model of WTC 1 after aircraft impact (downward displacement is negative).....	136
Figure 3–105. Vertical displacement of isolated core model of WTC 1 for Case A temperature condition at 10 min (downward displacement is negative).....	136
Figure 3–106. Vertical displacement of isolated core model of WTC 1 for Case A temperature condition at 20 min (downward displacement is negative).....	137
Figure 3–107. Vertical displacement of isolated core model of WTC 1 for Case A temperature condition at 30 min (downward displacement is negative).....	137
Figure 3–108. Vertical displacement of isolated core model of WTC 1 for Case A temperature condition at 40 min (downward displacement is negative).....	138
Figure 3–109. Vertical displacement of isolated core model of WTC 1 for Case A temperature condition at 50 min (downward displacement is negative).....	138

Figure 3–110. Vertical displacement of isolated core model of WTC 1 for Case A temperature condition at 70 min (downward displacement is negative)..... 139

Figure 3–111. Vertical displacement of isolated core model of WTC 1 for Case A temperature condition at 100 min (downward displacement is negative)..... 139

Figure 3–112. Horizontal displacement of isolated core model of WTC 1 for Case A temperature condition at 100 min. 140

Figure 3–113. Axial load in columns of isolated core model of WTC 1 after aircraft impact (compression is negative)..... 141

Figure 3–114. Axial load in columns of isolated core model of WTC 1 for Case A temperature condition at 100 min (compression is negative). 142

Figure 3–115. Plastic strain in columns of isolated core model of WTC 1 for Case A temperature condition at 100 min (compressive strain is negative)..... 143

Figure 3–116. Vertical displacement after push down of isolated core model of WTC 1 for Case A temperature condition (downward displacement is negative)..... 144

Figure 3–117. Total additional vertical load versus additional vertical displacement during push-down analysis of isolated core model of WTC 1 for Case A temperature condition (compression is positive). 144

Figure 3–118. Additional axial load (kip) in columns at Floor 98 when the total axial load reached the maximum during push down analysis of isolated core model of WTC 1 for Case A temperature condition (compression is positive)..... 145

Figure 3–119. Vertical displacement of isolated core model of WTC 1 for Case B temperature condition at 10 min (downward displacement is negative)..... 146

Figure 3–120. Vertical displacement of isolated core model of WTC 1 for Case B temperature condition at 20 min (downward displacement is negative)..... 146

Figure 3–121. Vertical displacement of isolated core model of WTC 1 for Case B temperature condition at 30 min (downward displacement is negative)..... 147

Figure 3–122. Vertical displacement of isolated core model of WTC 1 for Case B temperature condition at 40 min (downward displacement is negative)..... 147

Figure 3–123. Vertical displacement of isolated core model of WTC 1 for Case B temperature condition at 50 min (downward displacement is negative)..... 148

Figure 3–124. Vertical displacement of isolated core model of WTC 1 for Case B temperature condition at 70 min (downward displacement is negative)..... 148

Figure 3–125. Vertical displacement of isolated core model of WTC 1 for Case B temperature condition at 100 min (downward displacement is negative)..... 149

Figure 3–126. Horizontal displacement of isolated core model of WTC 1 for Case B temperature condition at 100 min. 150

Figure 3–127. Axial load in columns of isolated core model of WTC 1 for Case B temperature condition at 100 min (compression is negative). 151

Figure 3–128. Plastic strain in columns of isolated core model of WTC 1 for Case B temperature condition at 100 min (compressive strain is negative)..... 152

Figure 3–129. Vertical displacement after push down of isolated core model of WTC 1 for Case B temperature condition (downward displacement is negative)..... 153

Figure 3–130. Total additional vertical load versus additional vertical displacement relationship obtained from push down analysis of isolated core model of WTC 1 for Case B temperature condition (compression is positive).	153
Figure 3–131. Additional axial load (kip) in columns at Floor 98 when the total axial load reached the maximum during push down analysis of the WTC 1 core for Case B temperature condition (compression is positive).	154
Figure 3–132. Vertical displacement of isolated core model of WTC 2 for Case C temperature condition (downward displacement is negative).	156
Figure 3–133. Vertical displacement of isolated core model of WTC 2 for Case C temperature condition at 60 min (downward displacement is negative).	157
Figure 3–134. Axial load in core columns of isolated core model of WTC 2 for Case C temperature condition at 60 min (compression is negative).	158
Figure 3–135. Axial plastic strains in core columns of isolated core model of WTC 2 for Case C temperature condition at 60 min (compressive strain is negative).	159
Figure 3–136. Vertical displacement after push down of isolated core model of WTC 2 for Case C temperature condition (downward displacement is negative).	160
Figure 3–137. Additional average vertical load versus additional vertical displacement during push-down analysis of isolated core model of WTC 2 for Case C temperature condition (compression is positive; core column locations are shown in Fig. 3–136).	160
Figure 3–138. Vertical displacement of isolated core model of WTC 2 for Case D temperature condition (downward displacement is negative).	162
Figure 3–139. Vertical displacement of isolated core model of WTC 2 for Case D temperature condition at 60 min (downward displacement is negative).	163
Figure 3–140. Axial load in core columns of isolated core model of WTC 2 for Case D temperature condition at 60 min (compression is negative).	164
Figure 3–141. Axial plastic strains in core columns of isolated core model of WTC 2 for Case D temperature condition at 60 min (compressive strain is negative).	165
Figure 3–142. Vertical displacement after push down of isolated core model of WTC 2 for Case D temperature condition (downward displacement is negative).	166
Figure 3–143. Additional average vertical load versus additional vertical displacement during push-down analysis of isolated core model of WTC 2 for Case D temperature condition.	166
Figure 4–1. Coordinate system used in the analysis models.	167
Figure 4–2. Office and core area floors and core beams.	169
Figure 4–3. Location and IDs of outriggers and supporting columns.	170
Figure 4–4. Displaced shape of WTC 1 at the end of gravity analysis.	171
Figure 4–5. Displaced shape of WTC 2 at the end of gravity analysis.	171
Figure 4–6. Comparison of vertical displacement between WTC 1 models with and without construction sequence.	177
Figure 4–7. Comparison of vertical displacement between WTC 2 models with and without construction sequence.	178

Figure 4–8. Vertical displacement of exterior wall of WTC 1 before aircraft impact (downward displacement is negative). 186

Figure 4–9. Vertical displacement of exterior wall of WTC 1 after aircraft impact for Case B conditions (downward displacement is negative). 187

Figure 4–10. Vertical displacement of exterior wall of WTC 1 at 80 min for Case B conditions (downward displacement is negative). 188

Figure 4–11. Vertical displacement of exterior wall of WTC 1 at 100 min for Case B conditions (downward displacement is negative). 189

Figure 4–12. Vertical displacement of north wall of WTC 1 before aircraft impact. 190

Figure 4–13. Vertical displacement of north wall of WTC 1 after aircraft impact for Case B conditions (downward displacement is negative). 190

Figure 4–14. Vertical displacement of north wall of WTC 1 at 80 min for Case B conditions (downward displacement is negative). 191

Figure 4–15. Vertical displacement of north wall of WTC 1 at 100 min for Case B conditions with 5 kip pull-in forces (downward displacement is negative). 191

Figure 4–16. Vertical displacement of east wall of WTC 1 before aircraft impact (downward displacement is negative). 192

Figure 4–17. Vertical displacement of east wall of WTC 1 after aircraft impact for Case B conditions (downward displacement is negative). 192

Figure 4–18. Vertical displacement of east wall of WTC 1 at 80 min for Case B conditions (downward displacement is negative). 193

Figure 4–19. Vertical displacement of east wall of WTC 1 at 100 min for Case B conditions with 5 kip pull-in forces (downward displacement is negative). 193

Figure 4–20. Vertical displacement of south wall of WTC 1 before aircraft impact (downward displacement is negative). 194

Figure 4–21. Vertical displacement of south wall of WTC 1 after aircraft impact for Case B conditions (downward displacement is negative). 194

Figure 4–22. Vertical displacement of south wall of WTC 1 at 80 min for Case B conditions (downward displacement is negative). 195

Figure 4–23. Vertical displacement of south wall of WTC 1 at 100 min for Case B conditions with 5 kip pull-in forces (downward displacement is negative). 195

Figure 4–24. Vertical displacement of core of WTC 1 before aircraft impact (downward displacement is negative). 196

Figure 4–25. Vertical displacement of core of WTC 1 after aircraft impact for Case B conditions (downward displacement is negative). 197

Figure 4–26. Vertical displacement of core of WTC 1 at 50 min for Case B conditions (downward displacement is negative). 198

Figure 4–27. Vertical displacement of core of WTC 1 at 80 min for Case B conditions (downward displacement is negative). 199

Figure 4–28. Vertical displacement of core of WTC 1 at 100 min for Case B conditions with 5 kip pull-in forces (downward displacement is negative). 200

Figure 4–29. Vertical displacement of core columns of WTC 1 before aircraft impact (downward displacement is negative).	201
Figure 4–30. Vertical displacement of core columns of WTC 1 after aircraft impact for Case B conditions (downward displacement is negative).	202
Figure 4–31. Vertical displacement of core columns of WTC 1 at 80 min for Case B conditions (downward displacement is negative).	203
Figure 4–32. Vertical displacement of core columns of WTC 1 at 100 min for Case B conditions with 5 kip pull-in forces (downward displacement is negative).	204
Figure 4–33. Vertical displacement at Floor 99 of WTC 1 before aircraft impact.	205
Figure 4–34. Change in vertical displacement at Floor 99 of WTC 1 from the time before impact to the time after impact for Case B conditions.	205
Figure 4–35. Change in vertical displacement at Floor 99 of WTC 1 from the time before impact to 50 min for Case B conditions.	206
Figure 4–36. Change in vertical displacement at Floor 99 of WTC 1 from the time before impact to 80 min for Case B conditions.	206
Figure 4–37. Change in vertical displacement at Floor 99 of WTC 1 from the time before impact to 100 min for Case B conditions with 5 kip pull-in forces.	207
Figure 4–38. Out-of-plane displacement of south wall of WTC 1 before aircraft impact (inward displacement is positive).	208
Figure 4–39. Out-of-plane displacement of south wall of WTC 1 after aircraft impact for Case B conditions (inward displacement is positive).	208
Figure 4–40. Out-of-plane displacement of south wall of WTC 1 at 80 min (at the end of Analysis Step 17) for Case B conditions (inward displacement is positive).	209
Figure 4–41. Out-of-plane displacement of south wall of WTC 1 at 100 min for Case B conditions with 5 kip pull-in forces (inward displacement is positive).	209
Figure 4–42. Time history of maximum out-of-plane displacement of south wall of WTC 1 for Case B conditions with 5 kip pull-in forces (from Analysis Step 18 to Step 21).	210
Figure 4–43. Out-of-plane displacement of south wall of WTC 1 at 100 min for Case B conditions with 4 kip pull-in forces (inward displacement is positive).	210
Figure 4–44. Axial load in exterior columns of north wall of WTC 1 before aircraft impact (compression is negative).	211
Figure 4–45. Axial load in exterior columns of north wall of WTC 1 after aircraft impact for Case B conditions (compression is negative).	211
Figure 4–46. Axial load in exterior columns of north wall of WTC 1 at 80 min for the Case B conditions (compression is negative).	212
Figure 4–47. Axial load in exterior columns of north wall of WTC 1 at 100 min for Case B conditions with 5 kip pull-in forces (compression is negative).	212
Figure 4–48. Axial load in exterior columns of east wall of WTC 1 before aircraft impact (compression is negative).	213
Figure 4–49. Axial load in exterior columns of east wall of WTC 1 after aircraft impact for Case B conditions (compression is negative).	213

Figure 4–50. Axial load in exterior columns of east wall of WTC 1 at 80 min for the Case B conditions (compression is negative). 214

Figure 4–51. Axial load in exterior columns of east wall of WTC 1 at 100 min for the Case B conditions with 5 kip pull-in forces (compression is negative). 214

Figure 4–52. Axial load in exterior columns of south wall of WTC 1 before aircraft impact (compression is negative). 215

Figure 4–53. Axial load in exterior columns of south wall of WTC 1 after aircraft impact for Case B conditions (compression is negative). 215

Figure 4–54. Axial load in exterior columns of south wall of WTC 1 at 80 min for Case B conditions (compression is negative). 216

Figure 4–55. Axial load in exterior columns of south wall of WTC 1 at 100 min for Case B conditions with 5 kip pull-in forces (compression is negative). 216

Figure 4–56. Variation of axial load in exterior columns at Floor 98 of north wall of WTC 1 for Case B conditions with 5 kip pull-in forces (compression is positive). 217

Figure 4–57. Variation of axial load in exterior columns at Floor 98 of east wall of WTC 1 for Case B conditions with 5 kip pull-in forces (compression is positive). 217

Figure 4–58. Variation of axial load in exterior columns at Floor 98 of south wall of WTC 1 for Case B conditions with 5 kip pull-in forces (compression is positive). 218

Figure 4–59. Variation of axial load in exterior columns at Floor 98 of west wall of WTC 1 for Case B conditions with 5 kip pull-in forces (compression is positive). 218

Figure 4–60. Axial load in core columns of WTC 1 before aircraft impact (compression is negative). 219

Figure 4–61. Axial load in core columns of WTC 1 after aircraft impact for Case B conditions (compression is negative). 220

Figure 4–62. Axial load in core columns of WTC 1 at 80 min for Case B conditions (compression is negative). 221

Figure 4–63. Axial load in core columns of WTC 1 at 100 min for Case B conditions with 5 kip pull-in forces (compression is negative). 222

Figure 4–64. Axial load in columns at Floor 98 of WTC 1 before aircraft impact (compression is positive). 223

Figure 4–65. Axial load in columns at Floor 98 of WTC 1 after aircraft impact for Case B conditions (compression is positive). 223

Figure 4–66. Axial load in columns at Floor 98 of WTC 1 at 80 min for Case B conditions (compression is positive). 224

Figure 4–67. Axial load in columns at Floor 98 of WTC 1 at 100 min for Case B conditions with 5 kip pull-in forces (compression is positive). 224

Figure 4–68. Maximum demand-to-capacity ratio for axial load in core columns between Floor 93 and Floor 99 of WTC 1 before aircraft impact. 232

Figure 4–69. Maximum demand-to-capacity ratio for axial load in core columns between Floor 93 and Floor 99 of WTC 1 after aircraft impact for Case B conditions. 232

Figure 4–70. Maximum demand-to-capacity ratio for axial load in core columns between Floor 93 and Floor 99 of WTC 1 at 80 min for Case B conditions.	233
Figure 4–71. Maximum demand-to-capacity ratio for axial load in core columns between Floor 93 and Floor 99 of WTC 1 at 100 min for Case B conditions with 5 kip pull-in forces.....	233
Figure 4–72. Maximum elastic-plus-plastic strain for columns between Floor 93 and Floor 99 of WTC 1 before aircraft impact (compressive strain is positive; strain values are in percent).	234
Figure 4–73. Maximum elastic-plus-plastic strain for columns between Floor 93 and Floor 99 of WTC 1 after aircraft impact for Case B conditions (compressive strain is positive; strain values are in percent).	234
Figure 4–74. Maximum elastic-plus-plastic strain for columns between Floor 93 and Floor 99 of WTC 1 at 10 min for Case B conditions (compressive strain is positive; strain values are in percent).	235
Figure 4–75. Maximum elastic-plus-plastic strain for columns between Floor 93 and Floor 99 of WTC 1 at 40 min for Case B conditions (compressive strain is positive; strain values are in percent).	235
Figure 4–76. Maximum elastic-plus-plastic strain for columns between Floor 93 and Floor 99 of WTC 1 at 80 min for Case B conditions (compressive strain is positive; strain values are in percent).	236
Figure 4–77. Maximum elastic-plus-plastic strain for columns between Floor 93 and Floor 99 of WTC 1 at 100 min for Case B conditions with 5 kip pull-in forces (compressive strain is positive; strain values are in percent).	236
Figure 4–78. Maximum elastic-plus-plastic-plus-creep strain for columns between Floor 93 and Floor 99 of WTC 1 at 10 min for Case B conditions (compressive strain is positive; strain values are in percent).	237
Figure 4–79. Maximum elastic-plus-plastic-plus-creep strain for columns between Floor 93 and Floor 99 of WTC 1 at 40 min for Case B conditions (compressive strain is positive; strain values are in percent).	237
Figure 4–80. Maximum elastic-plus-plastic-plus-creep strain for columns between Floor 93 and Floor 99 of WTC 1 at 80 min for Case B conditions (compressive strain is positive; strain values are in percent).	238
Figure 4–81. Maximum elastic-plus-plastic-plus-creep strain for columns between Floor 93 and Floor 99 of WTC 1 at 100 min for Case B conditions with 5 kip pull-in forces (compressive strain is positive; strain value are in percent).....	238
Figure 4–82. Axial load (kip) in core columns at Floor 105 of WTC 1 at 100 min for Case B conditions with 5 kip pull-in forces (compression is positive).	241
Figure 4–83. Tension demand-to-capacity ratio for core column splices at Floor 106 of WTC 1 at 100 min for Case B conditions with 5 kip pull-in forces.	241
Figure 4–84. Primary load path within the hat truss of WTC 1.	243
Figure 4–85. Location of the hat truss connections in the primary load path.	243
Figure 4–86. Vertical displacement of exterior wall of WTC 2 for Case D conditions (downward displacement is negative).	253

Figure 4–87. Vertical displacement of exterior wall of WTC 2 for Case D conditions (downward displacement is negative). 254

Figure 4–88. Vertical displacement at Floor 83 of WTC 2 for Case D conditions (downward displacement is positive). 255

Figure 4–89. Vertical displacement at Floor 83 of WTC 2 for Case D conditions (downward displacement is positive; note the tilt toward east and south). 256

Figure 4–90. Total displacements of WTC 2 above Floor 86 at 43 min of Case D conditions (deformed shape magnified 20 times). Note the tilt toward east and south. 257

Figure 4–91. Vertical displacement of core of WTC 2 for Case D conditions (downward displacement is negative). 258

Figure 4–92. Vertical displacement of core of WTC 2 for Case D conditions (downward displacement is negative). 259

Figure 4–93. Vertical displacement of 800 series core columns of WTC 2 for Case D conditions (downward displacement is negative). 260

Figure 4–94. Vertical displacement of 800 series core columns of WTC 2 for Case D conditions (downward displacement is negative). 261

Figure 4–95. Vertical displacement of 900 series core columns of WTC 2 for Case D conditions (downward displacement is negative). 262

Figure 4–96. Vertical displacement of 900 series core columns of WTC 2 for Case D conditions (downward displacement is negative). 263

Figure 4–97. Vertical displacement of 1000 series core columns of WTC 2 for Case D conditions (downward displacement is negative). 264

Figure 4–98. Vertical displacement of 1000 series core columns of WTC 2 for Case D conditions (downward displacement is negative). 265

Figure 4–99. Out-of-plane displacement of the east wall of WTC 2 for Case D conditions (inward displacement is positive). 266

Figure 4–100. Out-of-plane displacement of the east wall of WTC 2 for Case D conditions (inward displacement is positive). 267

Figure 4–101. Variation of maximum inward bowing of the east wall of WTC 2 over time for Case D conditions. 268

Figure 4–102. Lateral displacements above Floor 86 of WTC 2 in the x-direction (north-south) for Case D conditions. 269

Figure 4–103. Lateral displacements above Floor 86 of WTC 2 in the y-direction (east-west) for Case D conditions. 270

Figure 4–104. Axial load in the east wall of WTC 2 for Case D conditions (compression is negative). 271

Figure 4–105. Axial load in the east wall of WTC 2 for Case D conditions (compression is negative). 272

Figure 4–106. Axial load in the south wall of WTC 2 for Case D conditions (compression is negative). 273

Figure 4–107. Axial load in the south wall of WTC 2 for Case D conditions (compression is negative).....	274
Figure 4–108. Axial load in the north wall of WTC 2 for Case D conditions (compression is negative).....	275
Figure 4–109. Axial load in the north wall of WTC 2 for Case D conditions (compression is negative).....	276
Figure 4–110. Axial load in the east and the west wall columns at Floor 83 of WTC 2 for Case D conditions (compression is positive).....	277
Figure 4–111. Axial load in the south and the north wall columns at Floor 83 of WTC 2 for Case D conditions (compression is positive).....	278
Figure 4–112. Axial load in 800 series core columns of WTC 2 for Case D conditions (compression is negative).	279
Figure 4–113. Axial load in 800 series core columns of WTC 2 for Case D conditions (compression is negative).	280
Figure 4–114. Axial load in 900 series core columns of WTC 2 for Case D conditions (compression is negative).	281
Figure 4–115. Axial load in 900 series core columns of WTC 2 for Case D conditions (compression is negative).	282
Figure 4–116. Axial load in 1000 series core columns of WTC 2 for Case D conditions (compression is negative).....	283
Figure 4–117. Axial load in 1000 series core columns of WTC 2 for Case D conditions (compression is negative).....	284
Figure 4–118. Core column loads (kip) at Floor 83 of WTC 2 for Case D conditions (compression is positive).....	285
Figure 4–119. Core column loads (kip) at Floor 83 of WTC 2 for Case D conditions (compression is positive).....	286
Figure 4–120. Axial load in Floor 83 columns of WTC 2 for Case D conditions (compression is positive).....	287
Figure 4–121. Maximum elastic-plus-plastic strains for columns between Floor 78 and Floor 83 of WTC 2 for Case D conditions (compressive strain is positive; strain values are in percent).	288
Figure 4–122. Maximum elastic-plus-plastic strains for columns between Floor 78 and Floor 3 of WTC 2 for Case D conditions (compressive strain is positive; strain values are in percent).	289
Figure 4–123. Maximum elastic-plus-plastic-plus-creep strains for columns between Floor 78 and Floor 83 of WTC 2 for Case D conditions (compressive strain is positive; strain values are in percent).	290
Figure 4–124. Axial load in core columns (kip) at Floor 105 (at hat truss level) of WTC 2 for Case D conditions (compression is positive).	291
Figure 4–125. Axial load in core columns (kip) at Floor 105 (at hat truss level) of WTC 2 for Case D conditions (compression is positive).	292

Figure 4–126. Progressive failure of core column splices at Floor 105 of WTC 2 (compression is positive; values are in kip). 293

Figure 4–127. State of core column splices at Floor 105 of WTC 2. 294

Figure 4–128. Axial force in hat truss members of WTC 2 for Case D conditions (tension is positive)..... 295

Figure 4–129. Axial force in hat truss members of WTC 2 for Case D conditions (tension is positive)..... 296

Figure 4–130. Axial stress in hat truss members of WTC 2 for Case D conditions (tension is positive)..... 297

Figure 4–131. Axial stress in hat truss members of WTC 2 for Case D conditions (tension is positive)..... 298

Figure 4–132. Primary load path within the hat truss of WTC 2. 301

Figure 4–133. Location of hat truss connections that were in the primary load path..... 301

Figure 5–1. Vertical displacement of the truss model under thermal loading..... 311

Figure 5–2. Catenary action in the floor system..... 311

Figure 5–3. Total column loads at Floor 98 of the south wall of WTC 2 global model for Case B conditions (compression is positive). 315

Figure 5–4. Vertical displacements of full floor models of WTC 1 for Case Bi temperature condition at 100 min (downward displacement is negative)..... 316

Figure 5–5. Loss of vertical supports obtained in Floor 97 and Floor 98 full floor models of WTC 1 for Case Bi temperature condition at 100 min (1x displacement magnification). 316

Figure 5–6. Inward bowing of exterior columns of the South wall of WTC 1 at 10:23 a.m. (97 min after impact). Displacements were estimated by NIST from the analysis of this photograph..... 317

Figure 5–7. Inward bowing of south wall of WTC 1 global model with creep at 100 min for Case B conditions with 5 kip pull-in forces (5x displacement magnification). 318

Figure 5–8. Collapse initiation and tilting of WTC 1 (view from the northeast). 318

Figure 5–9. Vertical displacements of full floor models of WTC 2 for Case Di temperature condition at 40 min (downward displacement is negative)..... 323

Figure 5–10. Floor sagging observed on the east wall of WTC 2 at different times..... 324

Figure 5–11. Total column loads at Floor 83 of the east wall of WTC 2 global model for Case D conditions (compression is positive). 325

Figure 5–12. Maximum elastic + plastic + creep strain magnitudes for columns between Floor 78 and Floor 83 of WTC 2 global model for Case D conditions at 20 min, 30 min, and 40 min (compressive strain is positive; strain values are in percent)..... 326

Figure 5–13. Inward bowing of the east wall of WTC 2 global model for Case D conditions at 43 min at the instant of collapse initiation (deformed shape scaled four times). 327

Figure 5–14. Inward bowing of exterior columns of the west wall of WTC 2 just before collapse..... 327

Figure 5–15. Total displacements of WTC 2 global model above Floor 86 for Case D conditions at 43 min at collapse initiation (note the tilt toward east and south; deformed shape magnified 20 times). 328

Figure 5–16. Initiation of Collapse of WTC 2. Note the tilt toward east and south..... 328

Figure 5–17. Full floor model of Floor 96 of WTC 1 for Case B_i temperature condition at 100 min. ... 330

This page intentionally left blank.

LIST OF TABLES

Table P-1	Federal building and fire safety investigation of the WTC disaster.....	xxxii
Table P-2	Public meetings and briefings of the WTC Investigation	xxxv
Table 2-1.	Element types used in the global models.	8
Table 2-2.	Temperatures of exterior seats at east wall of Floor 82 of WTC 2.	51
Table 2-3.	Demand-to-capacity ratios of exterior seats at east wall of Floor 82 of WTC 2 predicted by the full floor model.....	52
Table 3-1.	Analysis steps conducted on WTC 1 isolated exterior wall model.....	64
Table 3-2.	Analysis steps conducted on WTC 2 isolated exterior wall model.....	64
Table 4-1.	Conversion from SAP2000 element types to ANSYS element types.....	168
Table 4-2.	Comparison of maximum displacements and base reactions of WTC 1 from translated ANSYS and SAP2000 models.	172
Table 4-3.	Comparison of maximum displacements and base reactions of WTC 2 obtained from translated ANSYS and SAP2000 models.	172
Table 4-4.	Comparison of axial forces in randomly selected elements from WTC 1 model at the end of gravity analysis.	172
Table 4-5.	Comparison of axial forces in randomly selected elements from WTC 2 model at the end of gravity analysis.	173
Table 4-6.	Global model properties before and after modifications for computational efficiency.	174
Table 4-7.	Comparison of total column loads between WTC 1 models with and without construction sequence	176
Table 4-8.	Comparison of total column loads between WTC 2 models with and without construction sequence	176
Table 4-9.	Analysis steps of WTC 1 ANSYS global model.	180
Table 4-10.	Total column loads at Floor 98 of WTC 1 for Case B conditions.	225
Table 4-11.	Total column loads at Floor 105 of WTC 1 for Case B conditions.	225
Table 4-12.	Total column loads on the north wall of WTC 1 for Case B conditions.....	226
Table 4-13.	Change in total column loads on the north wall of WTC 1 for Case B conditions from the state before aircraft impact.....	226
Table 4-14.	Total column loads on the east wall of WTC 1 for Case B conditions.....	227
Table 4-15.	Change in total column loads on the east wall of WTC 1 for Case B conditions from the state before aircraft impact.....	227

Table 4-16.	Total column loads on the south wall of WTC 1 for Case B conditions.....	228
Table 4-17.	Change in total column loads on the south wall of WTC 1 for Case B conditions from the state before aircraft impact.....	228
Table 4-18.	Summation of total column loads on the west wall of WTC 1 for Case B conditions.....	229
Table 4-19.	Change in total column loads on the west wall of WTC 1 for Case B conditions from the state before aircraft impact.....	229
Table 4-20.	Total column loads on the core of WTC 1 for Case B conditions.	230
Table 4-21.	Change in total column loads on the core of WTC 1 for Case B conditions from the state before aircraft impact.....	230
Table 4-22.	Change in total column loads before and after aircraft impact. (Loads after impact) – (Loads before impact)	231
Table 4-23.	Change in total column loads after aircraft impact and at 80 min for Case B conditions. (Loads at 80 min) – (Loads After Impact).....	231
Table 4-24.	Change in total column loads at 80 min and at 100 min for Case B conditions. (Loads at 100 min) – (Loads at 80 min).....	231
Table 4-25.	Tension capacity of core column splices at Floor 106.....	239
Table 4-26.	Axial load in core columns at Floor 105 of WTC 1 for Case B conditions	240
Table 4-27.	Demand-to-capacity ratio for axial load in outriggers of WTC 1 for Case B conditions (outrigger IDs are indicated in Fig. 4-3).....	242
Table 4-28.	Demand to capacity ratio for axial load in exterior columns supporting outriggers at Floor 107 of WTC 1 for Case B conditions.	242
Table 4-29.	Demand and capacity of the hat truss connections (kip) in the primary load path at 80 min (connection IDs are shown in Fig. 4-85).....	244
Table 4-30.	Analysis Steps of WTC 2 ANSYS global model with Case D conditions.	245
Table 4-31.	Total column loads (kip) at Floor 105 at different stages of splice failures at 40 min (compression is positive).	294
Table 4-32.	Demand-to-capacity ratios for outriggers of WTC 2 for Case D conditions (outrigger IDs are shown in Fig. 4-3).....	299
Table 4-33.	Demand to capacity ratios for columns supporting outriggers at Floor 107 of WTC 2 for Case D conditions.....	300
Table 4-34.	Demand and capacity of the hat truss connections (kip) in the primary load path at 40 min (connection IDs are shown in Fig. 4-133).....	302
Table 4-35.	Total column loads at Floor 83 of WTC 2 for Case D conditions.	302
Table 4-36.	Total column loads at Floor 105 of WTC 2 for Case D conditions.	303
Table 4-37.	Change in total column loads before and after aircraft impact. (Loads After Impact) – (Loads Before Impact)	303
Table 4-38.	Change in total column loads between 40 min and 43 min. (Loads at 43 min) – (Loads at 40 min)	303
Table 4-39.	Total column loads over the height for the east wall of WTC 2 for Case D conditions. ...	304

Table 4-40.	Total column loads over the height for the south wall of WTC 2 for Case D conditions.....	305
Table 4-41.	Total column loads over the height for the north wall of WTC 2 for Case D conditions.....	306
Table 4-42.	Total column loads over the height for the west wall of WTC 2 for Case D conditions.....	307
Table 4-43.	Total column loads over the height for the core of WTC 2 for Case D conditions.	308
Table 5-1.	Summary of main events that led to the collapse of WTC 1.	312
Table 5-2.	Observations on WTC 1 provided by NIST.....	312
Table 5-3.	Total column loads at Floor 98 and Floor 105 of WTC 1 global model for Case B conditions.....	315
Table 5-4.	Summary of main events that led to the collapse of WTC 2	319
Table 5-5.	Observations on WTC 2 provided by NIST.....	319
Table 5-6.	Total column loads at Floor 83 and Floor 105 of WTC 2 for Case D conditions.....	322

This page intentionally left blank.

LIST OF ACRONYMS AND ABBREVIATIONS

Acronyms

ARA	Applied Research Associates, Inc.
ASTM	American Society for Testing and Materials
BPS	Building Performance Study
CAEAI	Computer Aided Engineering Associates, Inc.
FEMA	Federal Emergency Management Agency
FEA	finite element analysis
LERA	Leslie E. Robertson Associates
NIST	National Institute of Standards and Technology
PANYNJ	The Port Authority of New York and New Jersey
SEAoNY	Structural Engineers Association of New York
SGH	Simpson Gumpertz & Heger Inc.
USC	United States Code
WTC	World Trade Center

Abbreviations

°C	degrees Celsius
°F	degrees Fahrenheit
ft	feet
in.	inch
L	liter
m	meter
µm	micrometer
min	minute
s	second
lb	pound
kip	a force equal to 1,000 pounds
pcf	pound per cubic foot

psf	pound per square foot
psi	pound per square inch
ksi	1,000 pounds per square inch

PREFACE

Genesis of This Investigation

Immediately following the terrorist attack on the World Trade Center (WTC) on September 11, 2001, the Federal Emergency Management Agency (FEMA) and the American Society of Civil Engineers began planning a building performance study of the disaster. The week of October 7, as soon as the rescue and search efforts ceased, the Building Performance Study Team went to the site and began its assessment. This was to be a brief effort, as the study team consisted of experts who largely volunteered their time away from their other professional commitments. The Building Performance Study Team issued its report in May 2002, fulfilling its goal “to determine probable failure mechanisms and to identify areas of future investigation that could lead to practical measures for improving the damage resistance of buildings against such unforeseen events.”

On August 21, 2002, with funding from the U.S. Congress through FEMA, the National Institute of Standards and Technology (NIST) announced its building and fire safety investigation of the WTC disaster. On October 1, 2002, the National Construction Safety Team Act (Public Law 107-231), was signed into law. The NIST WTC Investigation was conducted under the authority of the National Construction Safety Team Act.

The goals of the investigation of the WTC disaster were:

- To investigate the building construction, the materials used, and the technical conditions that contributed to the outcome of the WTC disaster.
- To serve as the basis for:
 - Improvements in the way buildings are designed, constructed, maintained, and used;
 - Improved tools and guidance for industry and safety officials;
 - Recommended revisions to current codes, standards, and practices; and
 - Improved public safety.

The specific objectives were:

1. Determine why and how WTC 1 and WTC 2 collapsed following the initial impacts of the aircraft and why and how WTC 7 collapsed;
2. Determine why the injuries and fatalities were so high or low depending on location, including all technical aspects of fire protection, occupant behavior, evacuation, and emergency response;
3. Determine what procedures and practices were used in the design, construction, operation, and maintenance of WTC 1, 2, and 7; and
4. Identify, as specifically as possible, areas in current building and fire codes, standards, and practices that warrant revision.

NIST is a nonregulatory agency of the U.S. Department of Commerce’s Technology Administration. The purpose of NIST investigations is to improve the safety and structural integrity of buildings in the United States, and the focus is on fact finding. NIST investigative teams are authorized to assess building performance and emergency response and evacuation procedures in the wake of any building failure that has resulted in substantial loss of life or that posed significant potential of substantial loss of life. NIST does not have the statutory authority to make findings of fault nor negligence by individuals or organizations. Further, no part of any report resulting from a NIST investigation into a building failure or from an investigation under the National Construction Safety Team Act may be used in any suit or action for damages arising out of any matter mentioned in such report (15 USC 281a, as amended by Public Law 107-231).

Organization of the Investigation

The National Construction Safety Team for this Investigation, appointed by the then NIST Director, Dr. Arden L. Bement, Jr., was led by Dr. S. Shyam Sunder. Dr. William L. Grosshandler served as Associate Lead Investigator, Mr. Stephen A. Cauffman served as Program Manager for Administration, and Mr. Harold E. Nelson served on the team as a private sector expert. The Investigation included eight interdependent projects whose leaders comprised the remainder of the team. A detailed description of each of these eight projects is available at <http://wtc.nist.gov>. The purpose of each project is summarized in Table P–1, and the key interdependencies among the projects are illustrated in Fig. P–1.

Table P–1. Federal building and fire safety investigation of the WTC disaster.

Technical Area and Project Leader	Project Purpose
Analysis of Building and Fire Codes and Practices; Project Leaders: Dr. H. S. Lew and Mr. Richard W. Bukowski	Document and analyze the code provisions, procedures, and practices used in the design, construction, operation, and maintenance of the structural, passive fire protection, and emergency access and evacuation systems of WTC 1, 2, and 7.
Baseline Structural Performance and Aircraft Impact Damage Analysis; Project Leader: Dr. Fahim H. Sadek	Analyze the baseline performance of WTC 1 and WTC 2 under design, service, and abnormal loads, and aircraft impact damage on the structural, fire protection, and egress systems.
Mechanical and Metallurgical Analysis of Structural Steel; Project Leader: Dr. Frank W. Gayle	Determine and analyze the mechanical and metallurgical properties and quality of steel, weldments, and connections from steel recovered from WTC 1, 2, and 7.
Investigation of Active Fire Protection Systems; Project Leader: Dr. David D. Evans; Dr. William Grosshandler	Investigate the performance of the active fire protection systems in WTC 1, 2, and 7 and their role in fire control, emergency response, and fate of occupants and responders.
Reconstruction of Thermal and Tenability Environment; Project Leader: Dr. Richard G. Gann	Reconstruct the time-evolving temperature, thermal environment, and smoke movement in WTC 1, 2, and 7 for use in evaluating the structural performance of the buildings and behavior and fate of occupants and responders.
Structural Fire Response and Collapse Analysis; Project Leaders: Dr. John L. Gross and Dr. Therese P. McAllister	Analyze the response of the WTC towers to fires with and without aircraft damage, the response of WTC 7 in fires, the performance of composite steel-trussed floor systems, and determine the most probable structural collapse sequence for WTC 1, 2, and 7.
Occupant Behavior, Egress, and Emergency Communications; Project Leader: Mr. Jason D. Averill	Analyze the behavior and fate of occupants and responders, both those who survived and those who did not, and the performance of the evacuation system.
Emergency Response Technologies and Guidelines; Project Leader: Mr. J. Randall Lawson	Document the activities of the emergency responders from the time of the terrorist attacks on WTC 1 and WTC 2 until the collapse of WTC 7, including practices followed and technologies used.

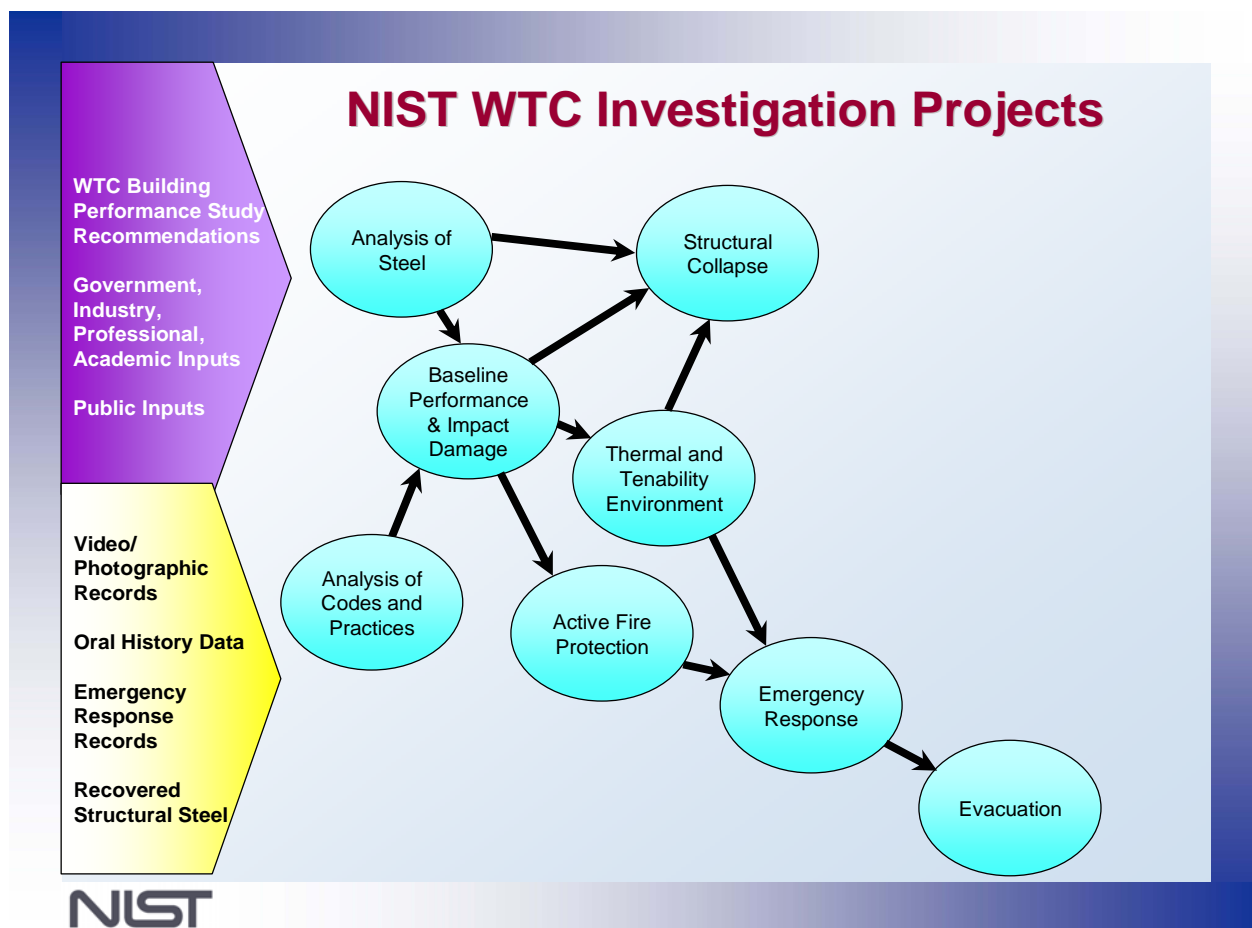


Figure P–1. The eight projects in the federal building and fire safety investigation of the WTC disaster.

National Construction Safety Team Advisory Committee

The NIST Director also established an advisory committee as mandated under the National Construction Safety Team Act. The initial members of the committee were appointed following a public solicitation. These were:

- Paul Fitzgerald, Executive Vice President (retired) FM Global, National Construction Safety Team Advisory Committee Chair
- John Barsom, President, Barsom Consulting, Ltd.
- John Bryan, Professor Emeritus, University of Maryland
- David Collins, President, The Preview Group, Inc.
- Glenn Corbett, Professor, John Jay College of Criminal Justice
- Philip DiNunno, President, Hughes Associates, Inc.

- Robert Hanson, Professor Emeritus, University of Michigan
- Charles Thornton, Co-Chairman and Managing Principal, The Thornton-Tomasetti Group, Inc.
- Kathleen Tierney, Director, Natural Hazards Research and Applications Information Center, University of Colorado at Boulder
- Forman Williams, Director, Center for Energy Research, University of California at San Diego

This National Construction Safety Team Advisory Committee provided technical advice during the Investigation and commentary on drafts of the Investigation reports prior to their public release. NIST has benefited from the work of many people in the preparation of these reports, including the National Construction Safety Team Advisory Committee. The content of the reports and recommendations, however, are solely the responsibility of NIST.

Public Outreach

During the course of this Investigation, NIST held public briefings and meetings (listed in Table P-2) to solicit input from the public, present preliminary findings, and obtain comments on the direction and progress of the Investigation from the public and the Advisory Committee.

NIST maintained a publicly accessible Web site during this Investigation at <http://wtc.nist.gov>. The site contained extensive information on the background and progress of the Investigation.

NIST's WTC Public-Private Response Plan

The collapse of the WTC buildings has led to broad reexamination of how tall buildings are designed, constructed, maintained, and used, especially with regard to major events such as fires, natural disasters, and terrorist attacks. Reflecting the enhanced interest in effecting necessary change, NIST, with support from Congress and the Administration, has put in place a program, the goal of which is to develop and implement the standards, technology, and practices needed for cost-effective improvements to the safety and security of buildings and building occupants, including evacuation, emergency response procedures, and threat mitigation.

The strategy to meet this goal is a three-part NIST-led public-private response program that includes:

- A federal building and fire safety investigation to study the most probable factors that contributed to post-aircraft impact collapse of the WTC towers and the 47-story WTC 7 building, and the associated evacuation and emergency response experience.
- A research and development (R&D) program to (a) facilitate the implementation of recommendations resulting from the WTC Investigation, and (b) provide the technical basis for cost-effective improvements to national building and fire codes, standards, and practices that enhance the safety of buildings, their occupants, and emergency responders.

Table P-2. Public meetings and briefings of the WTC Investigation.

Date	Location	Principal Agenda
June 24, 2002	New York City, NY	Public meeting: Public comments on the <i>Draft Plan</i> for the pending WTC Investigation.
August 21, 2002	Gaithersburg, MD	Media briefing announcing the formal start of the Investigation.
December 9, 2002	Washington, DC	Media briefing on release of the <i>Public Update</i> and NIST request for photographs and videos.
April 8, 2003	New York City, NY	Joint public forum with Columbia University on first-person interviews.
April 29–30, 2003	Gaithersburg, MD	NCST Advisory Committee meeting on plan for and progress on WTC Investigation with a public comment session.
May 7, 2003	New York City, NY	Media briefing on release of <i>May 2003 Progress Report</i> .
August 26–27, 2003	Gaithersburg, MD	NCST Advisory Committee meeting on status of the WTC investigation with a public comment session.
September 17, 2003	New York City, NY	Media and public briefing on initiation of first-person data collection projects.
December 2–3, 2003	Gaithersburg, MD	NCST Advisory Committee meeting on status and initial results and release of the <i>Public Update</i> with a public comment session.
February 12, 2004	New York City, NY	Public meeting on progress and preliminary findings with public comments on issues to be considered in formulating final recommendations.
June 18, 2004	New York City, NY	Media/public briefing on release of <i>June 2004 Progress Report</i> .
June 22–23, 2004	Gaithersburg, MD	NCST Advisory Committee meeting on the status of and preliminary findings from the WTC Investigation with a public comment session.
August 24, 2004	Northbrook, IL	Public viewing of standard fire resistance test of WTC floor system at Underwriters Laboratories, Inc.
October 19–20, 2004	Gaithersburg, MD	NCST Advisory Committee meeting on status and near complete set of preliminary findings with a public comment session.
November 22, 2004	Gaithersburg, MD	NCST Advisory Committee discussion on draft annual report to Congress, a public comment session, and a closed session to discuss pre-draft recommendations for WTC Investigation.
April 5, 2005	New York City, NY	Media and public briefing on release of the probable collapse sequence for the WTC towers and draft reports for the projects on codes and practices, evacuation, and emergency response.
June 23, 2005	New York City, NY	Media and public briefing on release of all draft reports for the WTC towers and draft recommendations for public comment.
September 12–13, 2005	Gaithersburg, MD	NCST Advisory Committee meeting on disposition of public comments and update to draft reports for the WTC towers.
September 13–15, 2005	Gaithersburg, MD	WTC Technical Conference for stakeholders and technical community for dissemination of findings and recommendations and opportunity for public to make technical comments.

- A dissemination and technical assistance program (DTAP) to (a) engage leaders of the construction and building community in ensuring timely adoption and widespread use of proposed changes to practices, standards, and codes resulting from the WTC Investigation and the R&D program, and (b) provide practical guidance and tools to better prepare facility owners, contractors, architects, engineers, emergency responders, and regulatory authorities to respond to future disasters.

The desired outcomes are to make buildings, occupants, and first responders safer in future disaster events.

National Construction Safety Team Reports on the WTC Investigation

A final report on the collapse of the WTC towers is being issued as NIST NCSTAR 1. A companion report on the collapse of WTC 7 is being issued as NIST NCSTAR 1A. The present report is one of a set that provides more detailed documentation of the Investigation findings and the means by which these technical results were achieved. As such, it is part of the archival record of this Investigation. The titles of the full set of Investigation publications are:

NIST (National Institute of Standards and Technology). 2005. *Federal Building and Fire Safety Investigation of the World Trade Center Disaster: Final Report on the Collapse of the World Trade Center Towers*. NIST NCSTAR 1. Gaithersburg, MD, September.

NIST (National Institute of Standards and Technology). 2006. *Federal Building and Fire Safety Investigation of the World Trade Center Disaster: Final Report on the Collapse of World Trade Center 7*. NIST NCSTAR 1A. Gaithersburg, MD.

Lew, H. S., R. W. Bukowski, and N. J. Carino. 2005. *Federal Building and Fire Safety Investigation of the World Trade Center Disaster: Design, Construction, and Maintenance of Structural and Life Safety Systems*. NIST NCSTAR 1-1. National Institute of Standards and Technology. Gaithersburg, MD, September.

Fanella, D. A., A. T. Derecho, and S. K. Ghosh. 2005. *Federal Building and Fire Safety Investigation of the World Trade Center Disaster: Design and Construction of Structural Systems*. NIST NCSTAR 1-1A. National Institute of Standards and Technology. Gaithersburg, MD, September.

Ghosh, S. K., and X. Liang. 2005. *Federal Building and Fire Safety Investigation of the World Trade Center Disaster: Comparison of Building Code Structural Requirements*. NIST NCSTAR 1-1B. National Institute of Standards and Technology. Gaithersburg, MD, September.

Fanella, D. A., A. T. Derecho, and S. K. Ghosh. 2005. *Federal Building and Fire Safety Investigation of the World Trade Center Disaster: Maintenance and Modifications to Structural Systems*. NIST NCSTAR 1-1C. National Institute of Standards and Technology. Gaithersburg, MD, September.

Grill, R. A., and D. A. Johnson. 2005. *Federal Building and Fire Safety Investigation of the World Trade Center Disaster: Fire Protection and Life Safety Provisions Applied to the Design and Construction of World Trade Center 1, 2, and 7 and Post-Construction Provisions Applied after Occupancy*. NIST NCSTAR 1-1D. National Institute of Standards and Technology. Gaithersburg, MD, September.

Razza, J. C., and R. A. Grill. 2005. *Federal Building and Fire Safety Investigation of the World Trade Center Disaster: Comparison of Codes, Standards, and Practices in Use at the Time of the Design and Construction of World Trade Center 1, 2, and 7*. NIST NCSTAR 1-1E. National Institute of Standards and Technology. Gaithersburg, MD, September.

Grill, R. A., D. A. Johnson, and D. A. Fanella. 2005. *Federal Building and Fire Safety Investigation of the World Trade Center Disaster: Comparison of the 1968 and Current (2003) New*

York City Building Code Provisions. NIST NCSTAR 1-1F. National Institute of Standards and Technology. Gaithersburg, MD, September.

Grill, R. A., and D. A. Johnson. 2005. *Federal Building and Fire Safety Investigation of the World Trade Center Disaster: Amendments to the Fire Protection and Life Safety Provisions of the New York City Building Code by Local Laws Adopted While World Trade Center 1, 2, and 7 Were in Use*. NIST NCSTAR 1-1G. National Institute of Standards and Technology. Gaithersburg, MD, September.

Grill, R. A., and D. A. Johnson. 2005. *Federal Building and Fire Safety Investigation of the World Trade Center Disaster: Post-Construction Modifications to Fire Protection and Life Safety Systems of World Trade Center 1 and 2*. NIST NCSTAR 1-1H. National Institute of Standards and Technology. Gaithersburg, MD, September.

Grill, R. A., D. A. Johnson, and D. A. Fanella. 2005. *Federal Building and Fire Safety Investigation of the World Trade Center Disaster: Post-Construction Modifications to Fire Protection, Life Safety, and Structural Systems of World Trade Center 7*. NIST NCSTAR 1-1I. National Institute of Standards and Technology. Gaithersburg, MD, September.

Grill, R. A., and D. A. Johnson. 2005. *Federal Building and Fire Safety Investigation of the World Trade Center Disaster: Design, Installation, and Operation of Fuel System for Emergency Power in World Trade Center 7*. NIST NCSTAR 1-1J. National Institute of Standards and Technology. Gaithersburg, MD, September.

Sadek, F. 2005. *Federal Building and Fire Safety Investigation of the World Trade Center Disaster: Baseline Structural Performance and Aircraft Impact Damage Analysis of the World Trade Center Towers*. NIST NCSTAR 1-2. National Institute of Standards and Technology. Gaithersburg, MD, September.

Faschan, W. J., and R. B. Garlock. 2005. *Federal Building and Fire Safety Investigation of the World Trade Center Disaster: Reference Structural Models and Baseline Performance Analysis of the World Trade Center Towers*. NIST NCSTAR 1-2A. National Institute of Standards and Technology. Gaithersburg, MD, September.

Kirkpatrick, S. W., R. T. Bocchieri, F. Sadek, R. A. MacNeill, S. Holmes, B. D. Peterson, R. W. Cilke, C. Navarro. 2005. *Federal Building and Fire Safety Investigation of the World Trade Center Disaster: Analysis of Aircraft Impacts into the World Trade Center Towers*, NIST NCSTAR 1-2B. National Institute of Standards and Technology. Gaithersburg, MD, September.

Gayle, F. W., R. J. Fields, W. E. Luecke, S. W. Banovic, T. Foecke, C. N. McCowan, T. A. Siewert, and J. D. McColskey. 2005. *Federal Building and Fire Safety Investigation of the World Trade Center Disaster: Mechanical and Metallurgical Analysis of Structural Steel*. NIST NCSTAR 1-3. National Institute of Standards and Technology. Gaithersburg, MD, September.

Luecke, W. E., T. A. Siewert, and F. W. Gayle. 2005. *Federal Building and Fire Safety Investigation of the World Trade Center Disaster: Contemporaneous Structural Steel Specifications*. NIST Special Publication 1-3A. National Institute of Standards and Technology. Gaithersburg, MD, September.

- Banovic, S. W. 2005. *Federal Building and Fire Safety Investigation of the World Trade Center Disaster: Steel Inventory and Identification*. NIST NCSTAR 1-3B. National Institute of Standards and Technology. Gaithersburg, MD, September.
- Banovic, S. W., and T. Foecke. 2005. *Federal Building and Fire Safety Investigation of the World Trade Center Disaster: Damage and Failure Modes of Structural Steel Components*. NIST NCSTAR 1-3C. National Institute of Standards and Technology. Gaithersburg, MD, September.
- Luecke, W. E., J. D. McColskey, C. N. McCowan, S. W. Banovic, R. J. Fields, T. Foecke, T. A. Siewert, and F. W. Gayle. 2005. *Federal Building and Fire Safety Investigation of the World Trade Center Disaster: Mechanical Properties of Structural Steels*. NIST NCSTAR 1-3D. National Institute of Standards and Technology. Gaithersburg, MD, September.
- Banovic, S. W., C. N. McCowan, and W. E. Luecke. 2005. *Federal Building and Fire Safety Investigation of the World Trade Center Disaster: Physical Properties of Structural Steels*. NIST NCSTAR 1-3E. National Institute of Standards and Technology. Gaithersburg, MD, September.
- Evans, D. D., R. D. Peacock, E. D. Kuligowski, W. S. Dols, and W. L. Grosshandler. 2005. *Federal Building and Fire Safety Investigation of the World Trade Center Disaster: Active Fire Protection Systems*. NIST NCSTAR 1-4. National Institute of Standards and Technology. Gaithersburg, MD, September.
- Kuligowski, E. D., D. D. Evans, and R. D. Peacock. 2005. *Federal Building and Fire Safety Investigation of the World Trade Center Disaster: Post-Construction Fires Prior to September 11, 2001*. NIST NCSTAR 1-4A. National Institute of Standards and Technology. Gaithersburg, MD, September.
- Hopkins, M., J. Schoenrock, and E. Budnick. 2005. *Federal Building and Fire Safety Investigation of the World Trade Center Disaster: Fire Suppression Systems*. NIST NCSTAR 1-4B. National Institute of Standards and Technology. Gaithersburg, MD, September.
- Keough, R. J., and R. A. Grill. 2005. *Federal Building and Fire Safety Investigation of the World Trade Center Disaster: Fire Alarm Systems*. NIST NCSTAR 1-4C. National Institute of Standards and Technology. Gaithersburg, MD, September.
- Ferreira, M. J., and S. M. Strege. 2005. *Federal Building and Fire Safety Investigation of the World Trade Center Disaster: Smoke Management Systems*. NIST NCSTAR 1-4D. National Institute of Standards and Technology. Gaithersburg, MD, September.
- Gann, R. G., A. Hamins, K. B. McGrattan, G. W. Mulholland, H. E. Nelson, T. J. Ohlemiller, W. M. Pitts, and K. R. Prasad. 2005. *Federal Building and Fire Safety Investigation of the World Trade Center Disaster: Reconstruction of the Fires in the World Trade Center Towers*. NIST NCSTAR 1-5. National Institute of Standards and Technology. Gaithersburg, MD, September.
- Pitts, W. M., K. M. Butler, and V. Junker. 2005. *Federal Building and Fire Safety Investigation of the World Trade Center Disaster: Visual Evidence, Damage Estimates, and Timeline Analysis*. NIST NCSTAR 1-5A. National Institute of Standards and Technology. Gaithersburg, MD, September.

Hamins, A., A. Maranghides, K. B. McGrattan, E. Johnsson, T. J. Ohlemiller, M. Donnelly, J. Yang, G. Mulholland, K. R. Prasad, S. Kukuck, R. Anleitner and T. McAllister. 2005. *Federal Building and Fire Safety Investigation of the World Trade Center Disaster: Experiments and Modeling of Structural Steel Elements Exposed to Fire*. NIST NCSTAR 1-5B. National Institute of Standards and Technology. Gaithersburg, MD, September.

Ohlemiller, T. J., G. W. Mulholland, A. Maranghides, J. J. Filliben, and R. G. Gann. 2005. *Federal Building and Fire Safety Investigation of the World Trade Center Disaster: Fire Tests of Single Office Workstations*. NIST NCSTAR 1-5C. National Institute of Standards and Technology. Gaithersburg, MD, September.

Gann, R. G., M. A. Riley, J. M. Repp, A. S. Whittaker, A. M. Reinhorn, and P. A. Hough. 2005. *Federal Building and Fire Safety Investigation of the World Trade Center Disaster: Reaction of Ceiling Tile Systems to Shocks*. NIST NCSTAR 1-5D. National Institute of Standards and Technology. Gaithersburg, MD, September.

Hamins, A., A. Maranghides, K. B. McGrattan, T. J. Ohlemiller, and R. Anleitner. 2005. *Federal Building and Fire Safety Investigation of the World Trade Center Disaster: Experiments and Modeling of Multiple Workstations Burning in a Compartment*. NIST NCSTAR 1-5E. National Institute of Standards and Technology. Gaithersburg, MD, September.

McGrattan, K. B., C. Bouldin, and G. Forney. 2005. *Federal Building and Fire Safety Investigation of the World Trade Center Disaster: Computer Simulation of the Fires in the World Trade Center Towers*. NIST NCSTAR 1-5F. National Institute of Standards and Technology. Gaithersburg, MD, September.

Prasad, K. R., and H. R. Baum. 2005. *Federal Building and Fire Safety Investigation of the World Trade Center Disaster: Fire Structure Interface and Thermal Response of the World Trade Center Towers*. NIST NCSTAR 1-5G. National Institute of Standards and Technology. Gaithersburg, MD, September.

Gross, J. L., and T. McAllister. 2005. *Federal Building and Fire Safety Investigation of the World Trade Center Disaster: Structural Fire Response and Probable Collapse Sequence of the World Trade Center Towers*. NIST NCSTAR 1-6. National Institute of Standards and Technology. Gaithersburg, MD, September.

Carino, N. J., M. A. Starnes, J. L. Gross, J. C. Yang, S. Kukuck, K. R. Prasad, and R. W. Bukowski. 2005. *Federal Building and Fire Safety Investigation of the World Trade Center Disaster: Passive Fire Protection*. NIST NCSTAR 1-6A. National Institute of Standards and Technology. Gaithersburg, MD, September.

Gross, J., F. Hervey, M. Izydorek, J. Mammoser, and J. Treadway. 2005. *Federal Building and Fire Safety Investigation of the World Trade Center Disaster: Fire Resistance Tests of Floor Truss Systems*. NIST NCSTAR 1-6B. National Institute of Standards and Technology. Gaithersburg, MD, September.

Zarghamee, M. S., S. Bolourchi, D. W. Eggers, Ö. O. Erbay, F. W. Kan, Y. Kitane, A. A. Liepins, M. Mudlock, W. I. Naguib, R. P. Ojdrovic, A. T. Sarawit, P. R. Barrett, J. L. Gross, and

T. P. McAllister. 2005. *Federal Building and Fire Safety Investigation of the World Trade Center Disaster: Component, Connection, and Subsystem Structural Analysis*. NIST NCSTAR 1-6C. National Institute of Standards and Technology. Gaithersburg, MD, September.

Zarghamee, M. S., Y. Kitane, Ö. O. Erbay, T. P. McAllister, and J. L. Gross. 2005. *Federal Building and Fire Safety Investigation of the World Trade Center Disaster: Global Structural Analysis of the Response of the World Trade Center Towers to Impact Damage and Fire*. NIST NCSTAR 1-6D. National Institute of Standards and Technology. Gaithersburg, MD, September.

McAllister, T., R. W. Bukowski, R. G. Gann, J. L. Gross, K. B. McGrattan, H. E. Nelson, L. Phan, W. M. Pitts, K. R. Prasad, F. Sadek. 2006. *Federal Building and Fire Safety Investigation of the World Trade Center Disaster: Structural Fire Response and Probable Collapse Sequence of World Trade Center 7*. (Provisional). NIST NCSTAR 1-6E. National Institute of Standards and Technology. Gaithersburg, MD.

Gilsanz, R., V. Arbitrio, C. Anders, D. Chlebus, K. Ezzeldin, W. Guo, P. Moloney, A. Montalva, J. Oh, K. Rubenacker. 2006. *Federal Building and Fire Safety Investigation of the World Trade Center Disaster: Structural Analysis of the Response of World Trade Center 7 to Debris Damage and Fire*. (Provisional). NIST NCSTAR 1-6F. National Institute of Standards and Technology. Gaithersburg, MD.

Kim, W. 2006. *Federal Building and Fire Safety Investigation of the World Trade Center Disaster: Analysis of September 11, 2001, Seismogram Data*. (Provisional). NIST NCSTAR 1-6G. National Institute of Standards and Technology. Gaithersburg, MD.

Nelson, K. 2006. *Federal Building and Fire Safety Investigation of the World Trade Center Disaster: The Con Ed Substation in World Trade Center 7*. (Provisional). NIST NCSTAR 1-6H. National Institute of Standards and Technology. Gaithersburg, MD.

Averill, J. D., D. S. Mileti, R. D. Peacock, E. D. Kuligowski, N. Groner, G. Proulx, P. A. Reneke, and H. E. Nelson. 2005. *Federal Building and Fire Safety Investigation of the World Trade Center Disaster: Occupant Behavior, Egress, and Emergency Communication*. NIST NCSTAR 1-7. National Institute of Standards and Technology. Gaithersburg, MD, September.

Fahy, R., and G. Proulx. 2005. *Federal Building and Fire Safety Investigation of the World Trade Center Disaster: Analysis of Published Accounts of the World Trade Center Evacuation*. NIST NCSTAR 1-7A. National Institute of Standards and Technology. Gaithersburg, MD, September.

Zmud, J. 2005. *Federal Building and Fire Safety Investigation of the World Trade Center Disaster: Technical Documentation for Survey Administration*. NIST NCSTAR 1-7B. National Institute of Standards and Technology. Gaithersburg, MD, September.

Lawson, J. R., and R. L. Vettori. 2005. *Federal Building and Fire Safety Investigation of the World Trade Center Disaster: The Emergency Response Operations*. NIST NCSTAR 1-8. National Institute of Standards and Technology. Gaithersburg, MD, September.

ACKNOWLEDGMENTS

The Authors would like to thank Glenn R. Bell and Ronald O. Hamburger of Simpson Gumpertz & Heger Inc. (SGH) for reviewing the report and assisting in its revision. The assistance of the SGH internal Structural Performance Review Committee (Glenn R. Bell, Ronald O. Hamburger, and Pedro J. Sifre) and the Computation/Modeling Review Committee (Said Bolourchi, Atis A. Liepins, and Peter R. Barrett of Computer Aided Engineering Associates, Inc., an SGH subconsultant in this project) is acknowledged. The authors would also like to thank the technical staff of Computer Aided Engineering Associates, Inc., for their effort at converting SAP2000 finite element models to ANSYS and for their assistance in finite element modeling in ANSYS.

This page intentionally left blank.

EXECUTIVE SUMMARY

E.1 INTRODUCTION

Simpson Gumpertz & Heger Inc. (SGH) developed global models of the World Trade Center (WTC) towers using finite elements and performed analyses of the global models to gain an understanding of the roles of the aircraft impact damage and the subsequent fires in the WTC towers in the structural stability and sequential failures of components and subsystems and to determine the probable sequence of structural responses that led to the global collapse initiation. The study was conducted as part of the investigation of the WTC disaster by the National Institute of Standards and Technology (NIST).

The work presented in this report was performed as a part of Project 6 of the NIST WTC investigation. This report complements the work performed by SGH on the structural response to the fire environment of connections such as truss seats and knuckles, components such as trusses and columns, and subsystems including full floors and exterior walls of the WTC towers.

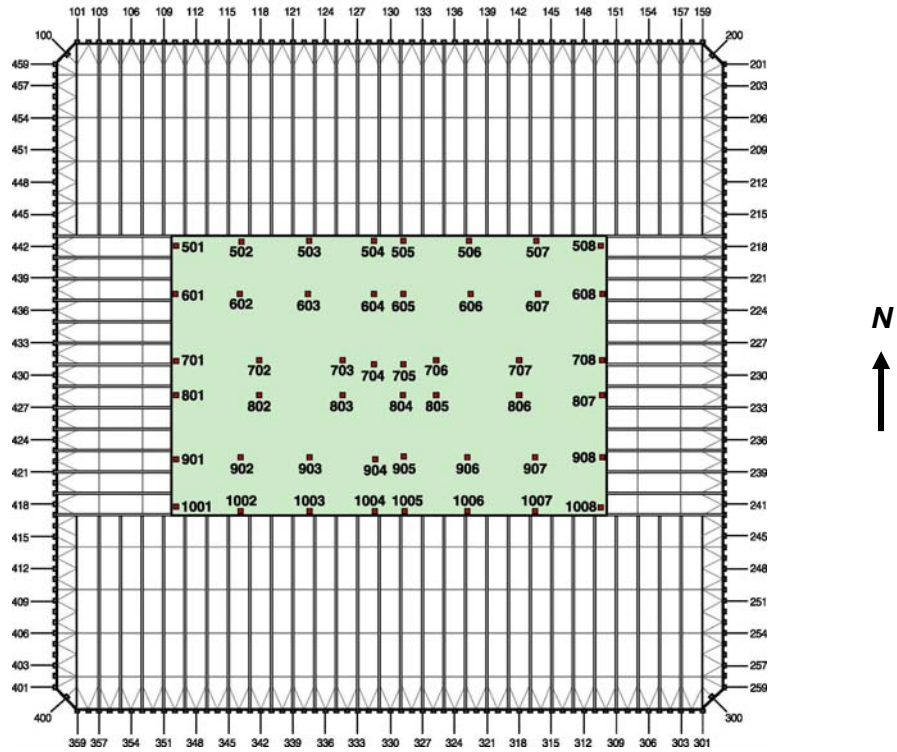
Global analyses of the WTC towers were also guided by observations. NIST examined photos and videos for visual evidence, damage estimates, and timeline of the collapse process in NIST NCSTAR 1-5A. A trial and error procedure was used in this study, which was (1) to identify the major observations at different times during the collapse process, (2) to determine the deviation between the observations and calculations, and to identify the likely assumptions that led to such deviations, and (3) to use the observations to correct the state of the structure at that time and continue the calculation to collapse initiation point. Actual observations based on NIST's examination of photos and videos are summarized in Tables E-1 and E-2 for WTC 1 and WTC 2, respectively. Columns that are referenced by column numbers can be located in Fig. E-1.

Table E–1. Observations on WTC 1 provided by NIST.

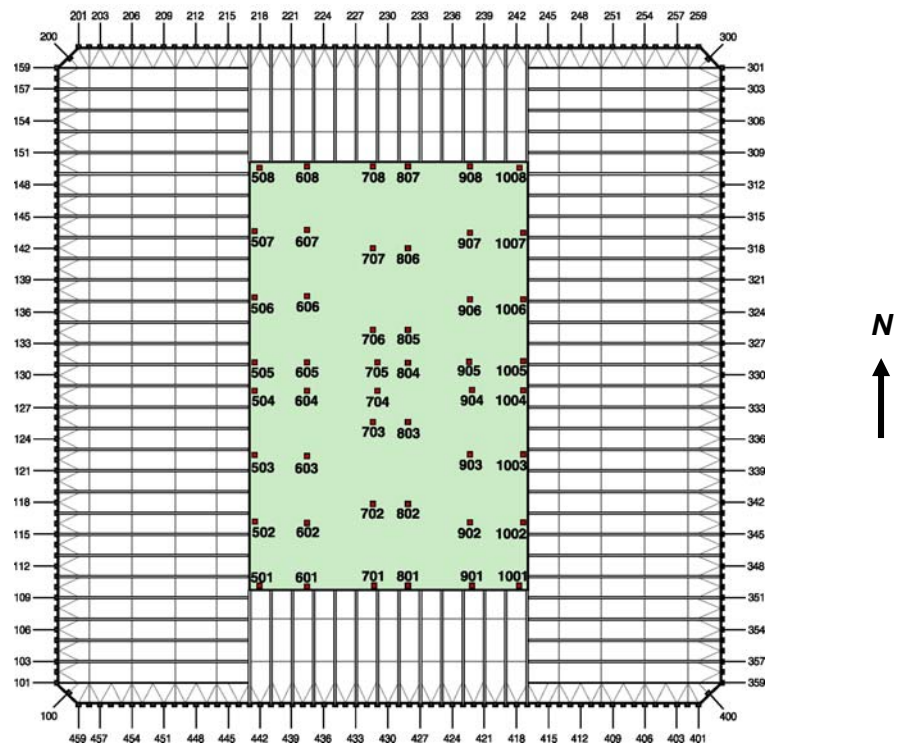
Time	Time from Impact (min)	Observation
8:46:26	0	Aircraft impact on the north wall of WTC 1 between Floor 93 and Floor 99 and Columns 112 and 151.
9:25:28	39	Fire on west side of south wall.
9:40	54	No bowing of columns was observed between Columns 301 and 323 on the east side of south wall.
10:18:43	92	Smoke suddenly expelled on Floor 92 north wall; Floor 94 east side of north wall; Floor 95 to Floor 98 on west side of north wall; Floor 95 and Floor 98 on north side of west wall; lower floor on south side.
10:22:59	97	Inward bowing from Floor 95 to about Floor 99 between Columns 308 and 326 (maybe to 340) on the south wall, maximum amplitude approximately 55 in. at Floor 97.
10:28:18	102	Smoke puff out of north edge and center of west wall; smoke and debris clouds out of the north, east, and west walls on Floor 98. Fire out of windows on the north, east, west, and south walls between Floor 92 and Floor 98, and on Floor 104.
10:28:20	102	WTC 1 began to collapse. First exterior sign of collapse was at Floor 98. Rotation of at least 8 degrees to the south occurred before the building section began to fall vertically under gravity.

Table E–2. Observations on WTC 2 provided by NIST.

Time	Time from Impact (min)	Observation
9:03	0	Aircraft impact on the south wall of WTC 2 between Floors 77 and 85, Columns 404 to 443.
9:21	18	Columns of the east wall bowed inward over the entire width of Floors 78 to 83; maximum of 7–9 in. at Floor 80.
9:38	35	Floor 83 disconnections on the east wall appeared to extend.
9:54	51	Columns of the east wall bowed inward between Floor 78 and Floor 84, 12–20 in. at Floor 80. East side of Floor 83 draped between Columns 310 to 342.
9:59	56	WTC 2 began to collapse. Column splices failed at every third panel and columns sprung back from inward bowing as collapse initiated on the east wall near the northeast corner Smoke and debris clouds were expelled from Floor 81 on the east, north, and west walls of the building. WTC 2 appeared to tilt around the base of Floor 82 and initial downward motion was visible at the same location. Tilt of approximately 3 to 4 degrees to the south and 7 to 8 degrees to the east occurred before building section fell. Kink (change in slope) on the southeast corner near Floor 94 (halfway along building section above failure). Kink (change in slope) and offset about at the Floor 106.



(a) WTC 1



(b) WTC 2

Figure E-1. Column designations.

E.2 GLOBAL MODEL ANALYSIS

E.2.1 Global Models

SGH developed global finite-element structural models of WTC towers in ANSYS to perform collapse analysis of WTC 1 and WTC 2 subjected to the combined effects of gravity and thermal loads. The geometry, the connectivity, and the member shapes of the global models for WTC 1 and WTC 2 were obtained from an ANSYS model converted from the reference SAP2000 model developed by NIST (NIST NCSTAR 1-2) and the study conducted by SGH on components and subsystems of the WTC towers. The global models were then modified by truncating the models below the aircraft impact zone and including changes to the modeling of columns, trusses, and slabs to capture the failure modes calculated in the structural analysis of components, connections, and subsystems of the WTC towers. Material properties of steel were modified to include: temperature-dependent material properties, such as thermal expansion, elastic properties, isotropic hardening plasticity, and creep. In addition, global models allowed geometrically nonlinear analysis and large deflection effects needed for elastic and inelastic structural instability at high temperatures.

E.2.2 Impact Damage

Aircraft impact damage to the structural members and the fireproofing of steel members of the WTC towers were determined in NIST NCSTAR 1-2 and NIST NCSTAR 1-6. In the global analysis the severed exterior wall columns, spandrels, core columns, core beams, and parts of the floors were removed at the appropriate stage of analysis.

The NIST investigation identified four aircraft impact damage sets (two damage sets for each tower) consisting of an impact damage condition and a fireproofing damage condition. These damage sets were named Case A and Case B for WTC 1 and Case C and Case D for WTC 2. Case B and Case D damage sets were used in the final global analyses. Case B and Case D impact damage sets for columns are shown in Figs. E-2 to E-5, where severed columns are shown as missing vertical lines. For comparison, core columns and beams before aircraft impact are shown in Figs. E-6 and E-7 for WTC 1 and WTC 2, respectively. (Note that the global models included only core beams that had moment connections; hence, Figs E-3 and E-5 do not show all the core beams that existed in the WTC towers.)

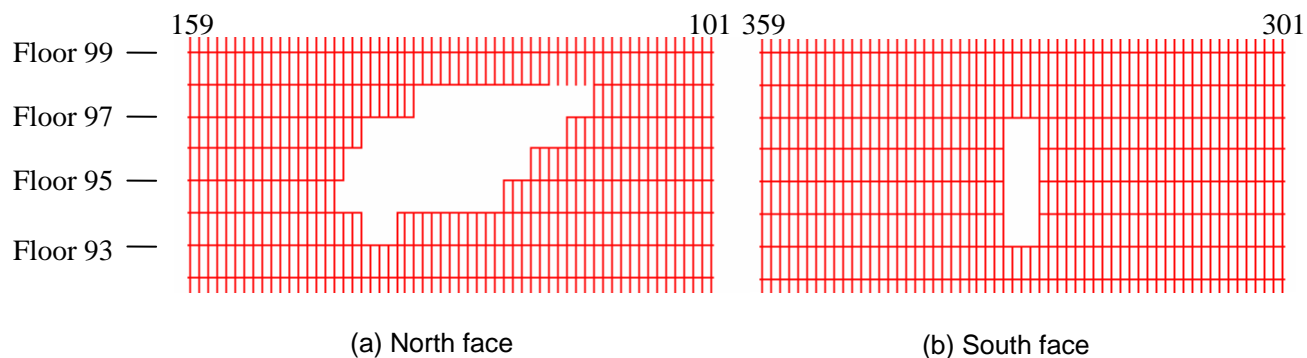


Figure E-2. Structural damage condition on the exterior walls of WTC 1 for all cases of impact damage.

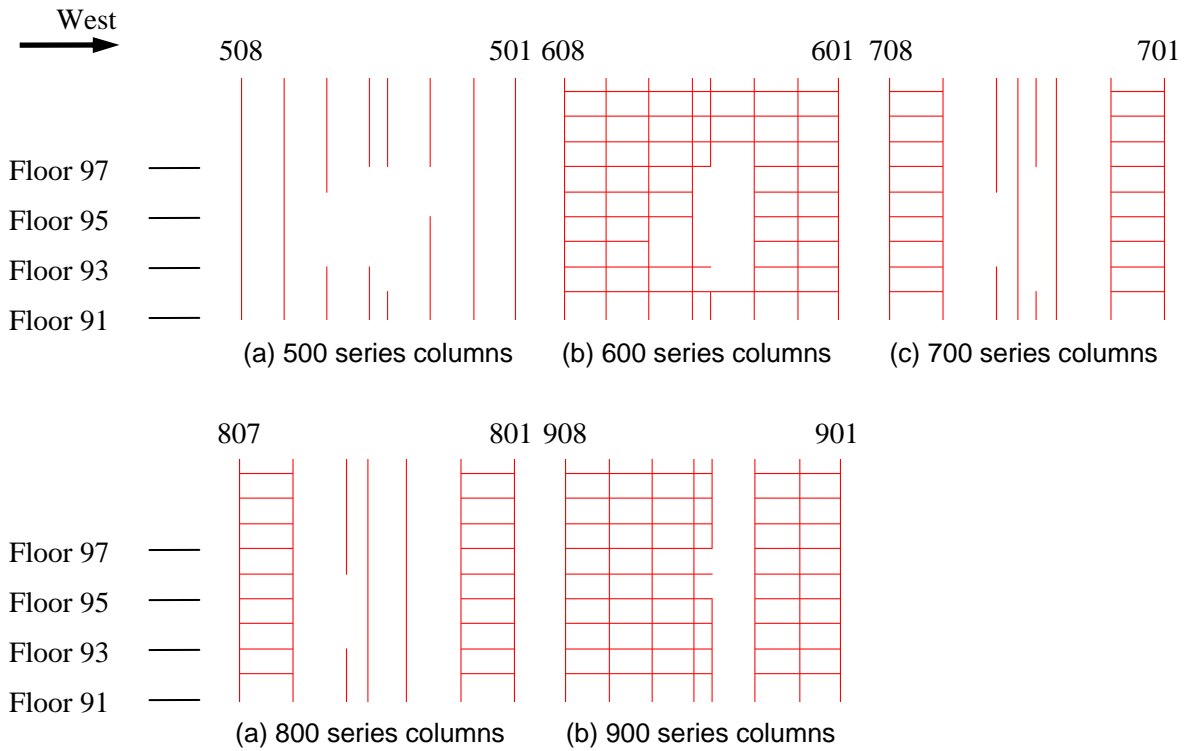


Figure E-3. Case B structural damage condition on the core columns of WTC 1 (including heavily damaged columns).

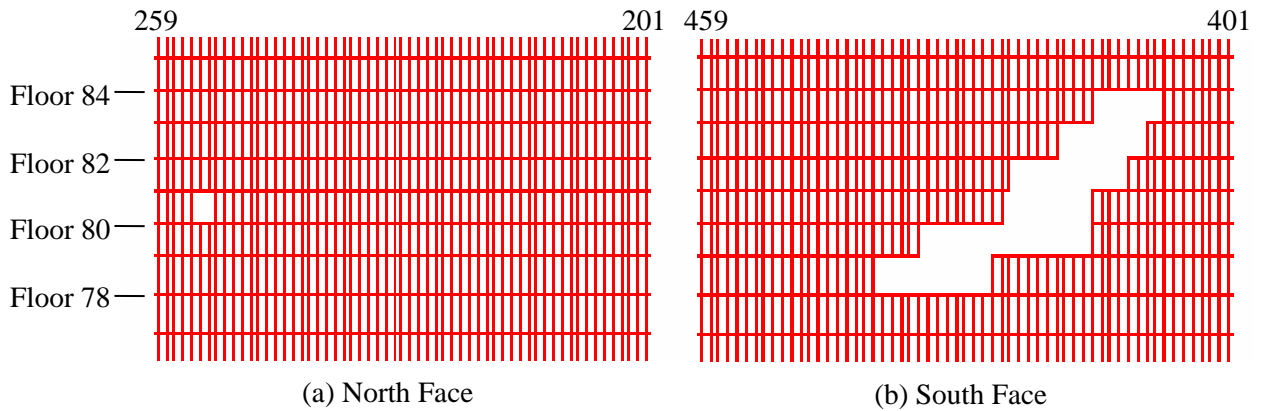


Figure E-4. Structural damage condition on the exterior walls of WTC 2 for all cases of impact damage.

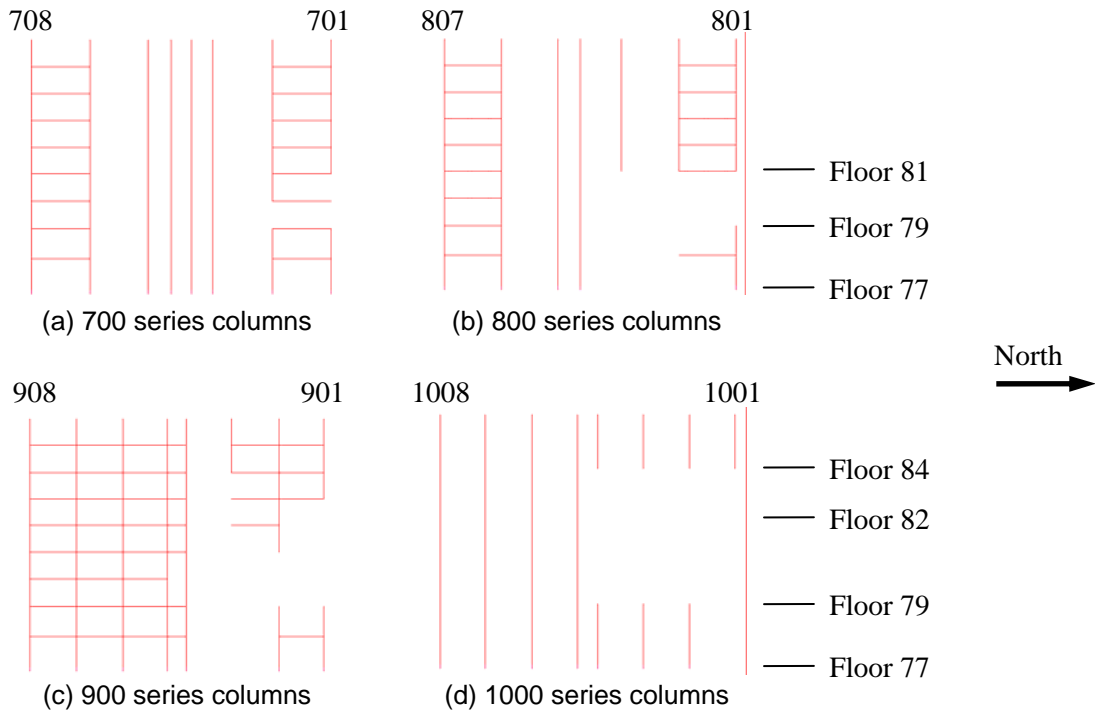


Figure E-5. Case D structural damage condition on the core columns of WTC 2 (including heavily damaged columns).

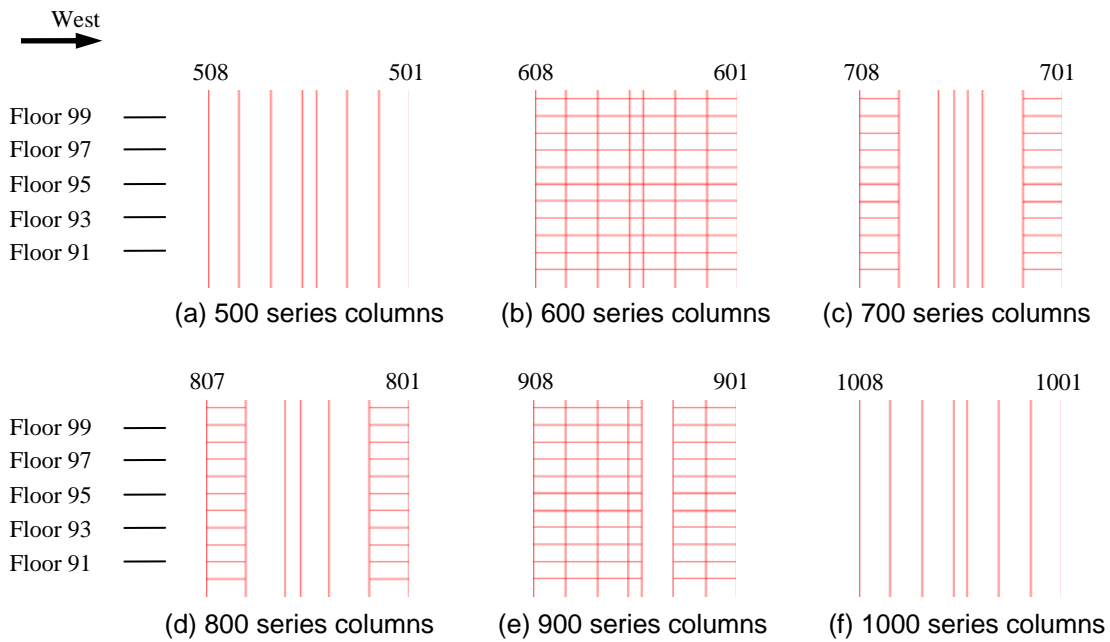


Figure E-6. Core columns and core beams in the WTC 1 global model without aircraft impact damage.

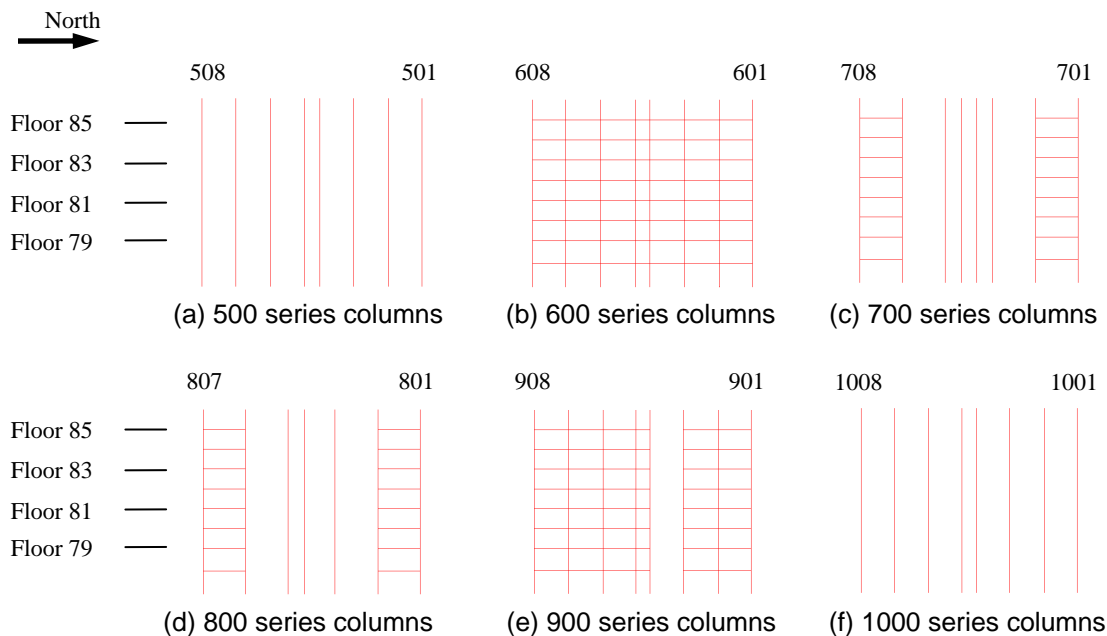


Figure E-7. Core columns and core beams in the WTC 2 global model without aircraft impact damage.

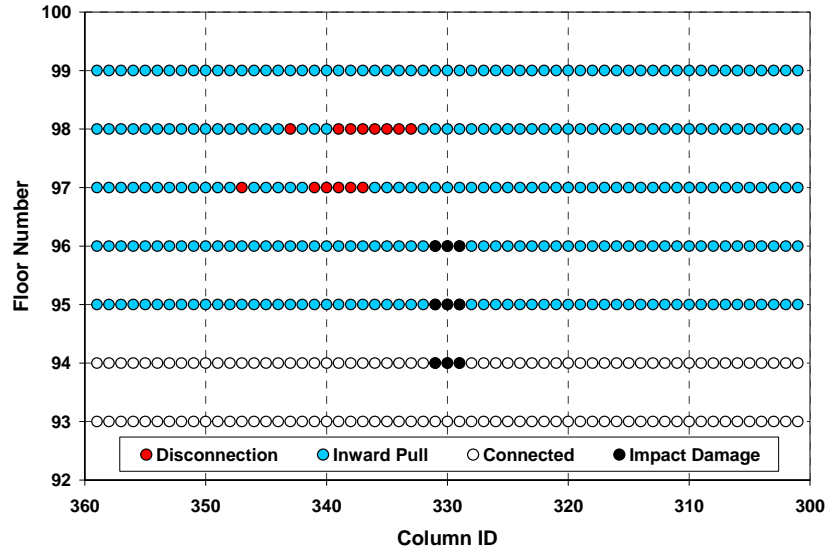
E.2.4 Loads and Boundary Conditions in the Global Models

The global models were fully restrained at the base of the vertical springs. The loads on the structure consisted of gravity loads and temperature loads. The gravity loads included dead load and live load (equal to 25 percent of the design live load). Temperature loads consisted of temperature time histories provided by NIST based on their fire dynamics and heat transfer analyses performed for different conditions of structural and fireproofing damage. Temperature data were provided for every structural node at 10 min intervals. Temperatures between the 10 min intervals were determined by linear interpolation.

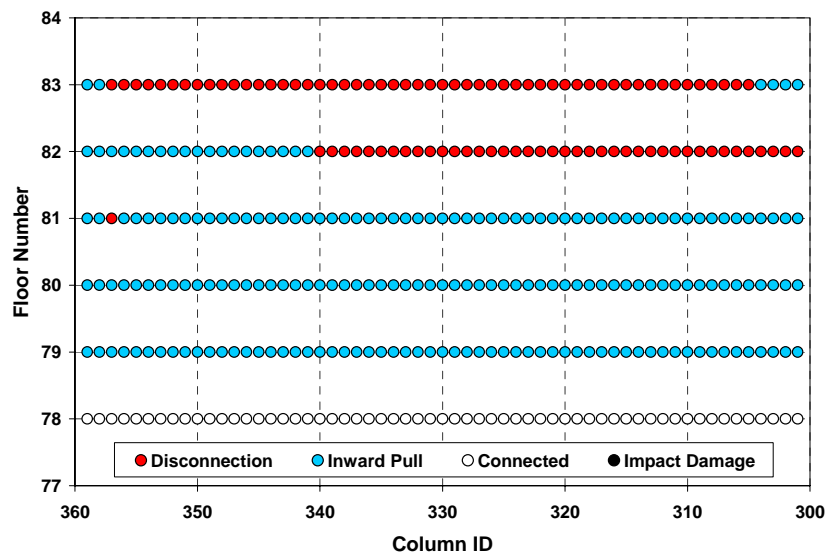
E.2.5 Fire-Induced Damage

It was not practical to develop global models that could capture all the failure modes found in the study of components, connections, and subsystems, and to perform global analyses within a reasonable time period. Since detailed modeling of the floors was not included in the global models, important floor behavioral modes could not be captured directly from the global analyses. Key floor behavioral modes include sagging that imposed pull-in forces on the exterior wall and failure of support of the trusses at the exterior wall resulting in local disconnection of the floor from the exterior wall. Moreover, the sagging and the resulting bowing of the exterior walls calculated from the full floor model did not match the observed inward bowing. To account for these effects, the pull-in forces on the exterior wall and floor/wall disconnections were input into the global models as fire-induced damage at certain points in time, as illustrated in Figure E-8. Fire-induced damage calculated by the full floor models were then calibrated to the damage observed by NIST through their examination of photographs and videos during the heating period up to the final collapse. In addition, the magnitudes of pull-in forces were determined

by trial and error to match the observed inward bowing of exterior walls using the isolated exterior wall models from the global models.



(a) South wall of WTC 1 between 80 min and 90 min



(b) East wall of WTC 2 between 40 min and 50 min

Figure E–8. Examples of locations of floor/wall disconnections and pull-in forces used in the collapse analyses of the global model with creep.

E.3 COLLAPSE SEQUENCE

The final global models were developed based on the following assumptions:

- Floor subsystem was modeled by plate elements with elastic properties without ability to simulate sagging and its effect on the development of pull-in forces and floor/wall disconnections. Pull-in forces resulting from floor sagging and floor/wall disconnections were determined based on the results of full floor models and isolated wall models and modified by visual observations. They were input in the global model analyses at different times as fire-induced damage.
- Spandrels were modeled by beam elements. Axial degree of freedom of the beam elements representing spandrels was released to enhance numerical efficiency and avoid thermally-induced buckling. The exterior wall subsystem analysis showed that large deformations and buckling of spandrels would not affect the stability of exterior columns significantly.
- Columns were modeled to capture inelastic buckling, but not the kink-type buckling initiated by the local buckling of plates and resulting in significant distortion of the cross section. The analysis of columns showed that when buckling occurs on a column that spans several floors and is at high temperatures, inelastic buckling, rather than kink-type buckling, governs its load deformation characteristic.
- The sections below the impact zones were removed, and the vertical stiffness of the removed sections was replaced with equivalent vertical springs. Preliminary analyses of the global models showed that sections below the impact zone did not contribute much to the overall behavior of the towers.
- Construction sequence was not considered to enhance computational efficiency. A comparative study showed that the total column load on each face of the exterior wall increased by 7 to 15 percent, and the total column load on the core decreased by about 10 percent, by neglecting the construction sequence.
- Structural members that were severed or heavily damaged by aircraft impact were removed from the final global models before gravity loads were applied to enhance computational efficiency.
- Break elements were not used in the final global models to represent component failures such as failure of column splices. However, the results of the global model analyses were examined to determine whether any component failure occurred and to what extent its failure impacted the collapse sequence.

The key structural events common to both towers are discussed below.

- Sagging of floors caused by the elevated steel temperatures resulting from loss of fireproofing. Elevated temperature caused buckling of the truss web diagonals, with the floor deforming into a catenary. The catenary action in this study refers to the combined action that results when the bending capacity of the truss is exceeded and additional load is carried

by the floor system acting as a tensile structure. Sagging of the floor resulted in pull-in forces at floor/exterior wall connections, and led to inward bowing of the exterior wall

- Bowing and buckling of the entire exterior wall of a tower under the combined effects of temperature, the redistributed gravity load, pull-in force from sagging floors, and loss of lateral support due to sagging or floor/wall disconnections. Floors deformed into catenaries did not restrain the exterior wall columns from buckling.
- Downward displacement of the core due to severed core columns from the aircraft impact and redistributed column loads to non-severed core columns, and shortening of the core columns caused by buckling, plasticity, and creep of core columns at elevated temperatures.
- Redistribution of gravity loads among exterior and interior columns resulting from damage due to aircraft impact, restrained thermal expansion, shortening of core columns, tilting of the tower above the impact region, and bowing and buckling of exterior walls. Redistribution of the loads from aircraft impact or fire-induced damaged columns, both in the core and exterior walls, was primarily to the neighboring columns. Redistribution of gravity loads from the core to the exterior walls and from the exterior walls to the core was primarily through the hat truss. Redistribution between adjacent exterior walls was primarily through the spandrels, and to a lesser extent through the hat truss. Major load redistribution mechanisms were as follows:
 - Aircraft impact reduced the load on the impacted wall and on the opposite wall through the pivoting action of the hat truss, and increased the load on side walls.
 - Thermal expansion caused increased loads in thermally restrained members.
 - Shortening of core columns caused a redistribution of the load from the core to the exterior walls.
 - Tilting of the tower redistributed the load among the exterior walls, resulting in increased load on the compressed part of the exterior walls.
 - Buckling of the exterior wall caused rapid unloading of the buckled wall and of the opposite wall through the pivoting action of the stiff hat truss and increased the load on the other two exterior walls.

The collapse sequences of the two towers are discussed separately below.

E.3.1 WTC 1 Collapse Sequence

The aircraft impacted the north wall of WTC 1 at 8:46 a.m. The aircraft severed exterior columns and floors on the north side of the tower and core columns and floor members between Floor 93 and Floor 98. The subsequent fires weakened structural subsystems, including the core columns, floors, and exterior walls. The core displaced downward, the floors sagged, and the south exterior wall bowed inward. At 10:28 a.m., about 102 min after the aircraft impact, WTC 1 began to collapse. The collapse sequence of WTC 1 consists of five main structural events: 1) aircraft impact, 2) unloading of core, 3) sagging of floors and floor/wall disconnections, 4) inward bowing of south wall, and 5) buckling of south wall and collapse initiation.

Aircraft Impact. The aircraft impacted WTC 1 at the north wall. The aircraft severed or heavily damaged Columns 112 to 151 between Floors 94 and 98 on the north wall. After breaching the building's perimeter, the aircraft continued to penetrate into the building. The north office area floor system sustained severe structural damage between Columns 112 and 145 at Floors 94 to 98. Core Columns 503, 504, 505, 506, 604, 704, 706, 805, and 904 were severed or heavily damaged between Floor 92 and Floor 97. The aircraft also severed a single exterior panel at the center of the south wall from Columns 329 to 331 between Floor 93 and Floor 96. In summary, 38 of 59 columns of the north wall, three of 59 columns of the south wall, and nine of 47 core columns were severed or heavily damaged. In addition, thermal insulation on floor framings and columns were damaged from the impact area to the south perimeter wall, primarily through the center of WTC 1 and over one-third to one-half of the core width.

Gravity loads in the columns that were severed were redistributed mostly to the neighboring columns. Due to the severe impact damage to the north wall, the wall section above the impact zone moved downward. The hat truss resisted the downward movement of the north wall and rotated about its east-west axis, which reduced the load on the south wall. As a result, the north and south walls each carried about 7 percent less gravity loads at Floor 98 after impact, the east and west walls each carried about 7 percent more loads, and the core carried about 1 percent more gravity loads at Floor 98 after impact. Column 705 buckled, and Columns 605 and 804 showed minor buckling.

Unloading of Core. Temperatures in the core area rose quickly, and thermal expansion of the core was greater than the thermal expansion of the exterior walls in early stages of the fire. This increased the gravity loads in the core columns until 10 min after impact. The additional gravity loads from adjacent severed columns and high temperatures caused high plastic and creep strains to develop in the core columns in the early stages of the fire. More columns buckled inelastically due to high temperatures. Creep strain continued to increase to the point of collapse. By 30 min, the plastic-plus-creep strains exceeded thermal expansion strains. Due to high plastic and creep strains and inelastic buckling of core columns, the core columns shortened, and the core displaced downward. At 100 min, the downward displacement of the core at Floor 99 became 2.0 in. on the average.

The shortening of core columns was resisted by the hat truss, which unloaded the core with time and redistributed the gravity loads from the core to the exterior walls. As a result, the north, east, south, and west walls at Floor 98 carried about 12 percent, 27 percent, 10 percent, and 22 percent more gravity loads, respectively, at 80 min than the state immediately after the impact, and the core carried about 20 percent less loads. The net increase in the total column load on the south wall, where exterior wall failure initiated, was only about 10 percent due to core downward displacement. At 80 min, the total core column loads reached their maximum. As the floor pulled in starting at 80 min on in the south side, the south exterior wall began to shed load to adjacent walls and the core.

Sagging of Floors and Floor/Wall Disconnections. The long-span trusses of Floor 95 through Floor 99 sagged due to high temperatures. While the fires were on the north side and the floors on the north side sagged first, the fires later reached the south side and the floors on the south side sagged. Full floor models underestimated the extent of sagging because cracking and spalling of concrete and creep in steel under high temperatures were not modeled, and because the extent of insulation damage was conservatively estimated. The sagging floors pulled in the south wall columns over Floors 95 to 99. In addition, the exterior seats on the south wall in the hot zone of Floors 97 and 98 began to fail due to their reduced vertical shear capacity at around 80 min, and by 100 min about 20 percent of the exterior seats on

the south wall of Floors 97 and 98 failed. Partial collapse of floor may have occurred at Floors 97 and 98, resulting from the exterior seat failures, as indicated by the observed smoke puff at 92 min (10:19 a.m.), but this phenomenon was not modeled.

Bowing of South Wall. The exterior columns on the south wall bowed inward as they were subjected to high temperatures, pull-in forces from the floors beginning at 80 min, and additional gravity loads redistributed from the core. Figure E-9 shows the observed and the estimated inward bowing of the south wall at 97 min after impact (10:23 a.m.). Since no bowing was observed on the south wall at 69 min (9:55 a.m.), it is estimated that the south wall began to bow inward at around 80 min when the floors on the south side began to substantially sag. The inward bowing of the south wall increased with time due to continuing floor sagging and increased temperatures on the south wall (Fig. E-10). At 97 min (10:23 a.m.), the maximum bowing observed was about 55 in.

Buckling of South Wall and Collapse Initiation. With continuously increased bowing, as more columns buckled, the entire width of the south wall buckled inward. Instability started at the center of the south wall and rapidly progressed horizontally toward the sides. As a result of the buckling of the south wall, the south wall significantly unloaded, redistributing its load to the softened core through the hat-truss and to the south side of the east and west walls through the spandrels. At 100 min, the north, east, and west walls at Floor 98 carried about 7 percent, 35 percent, and 30 percent more gravity loads than the state immediately after impact, and the south wall and the core carried about 7 percent and 20 percent less loads, respectively. The section of the building above the impact zone tilted to the south (observed at about 8°) as column instability progressed rapidly from the south wall along the adjacent east and west walls (see Fig. E-11), resulting in increased gravity load on the core columns. The release of potential energy due to downward movement of building mass above the buckled columns exceeded the strain energy that could be absorbed by the structure. Global collapse ensued.

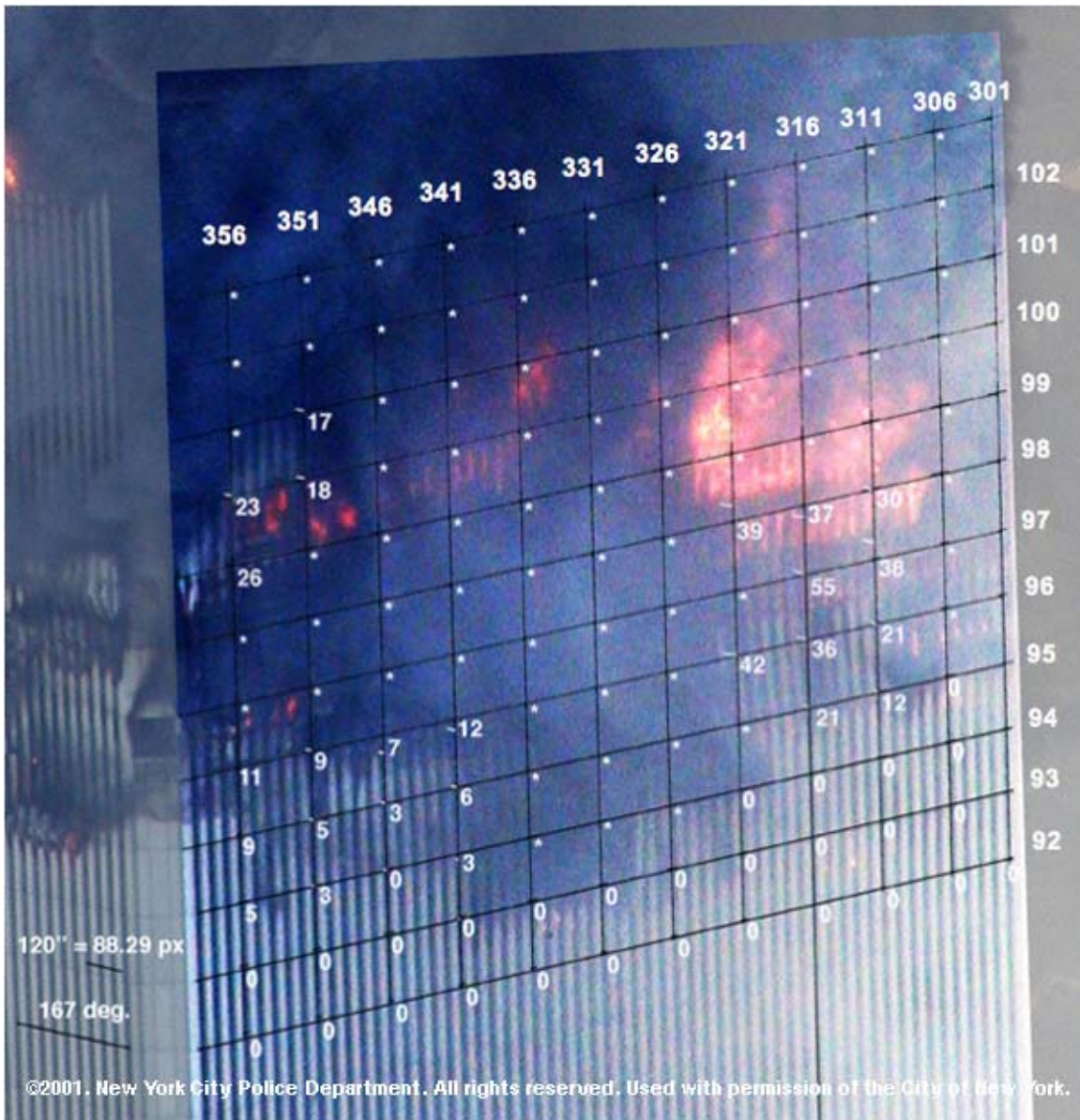


Figure E-9. Inward bowing of the south wall of WTC 1 at 10:23 a.m. Displacement estimated by NIST.

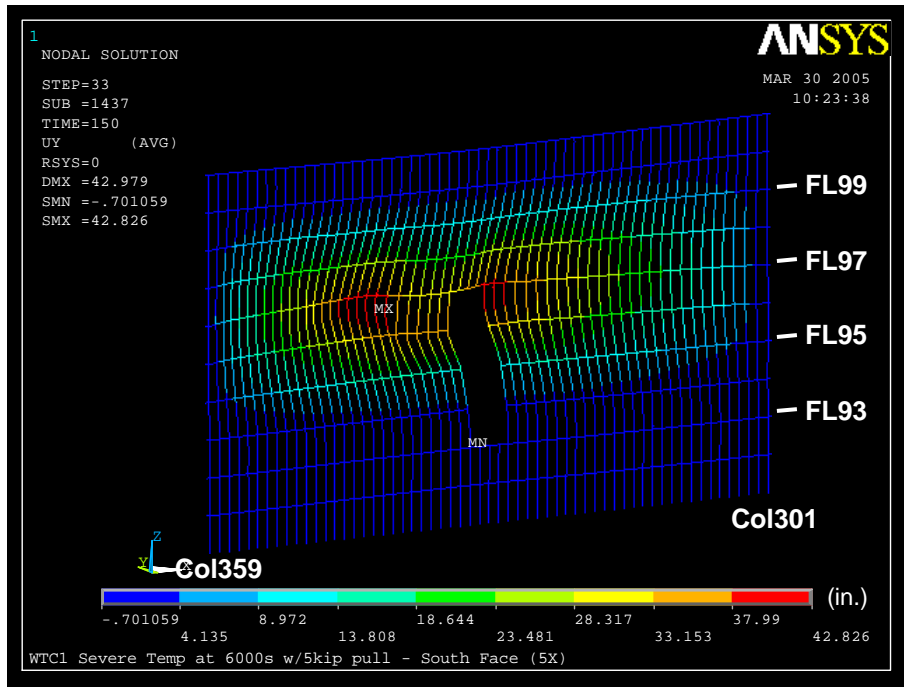


Figure E-10. Inward bowing of south wall of WTC 1 global model with creep at 100 min for Case B conditions with 5 kip pull-in forces (5x displacement magnification).



Figure E-11. Collapse initiation and tilting of WTC 1 (view from the northeast).

E.3.2 WTC 2 Collapse Sequence

The aircraft traveling in a north-northeast direction impacted the south wall of WTC 2 at 9:03 a.m. The aircraft mostly severed columns and floors that were on the east side of the building between Floor 78 and Floor 84. The subsequent fires were also on the east side of the building. At 9:59 a.m., about 56 min after the aircraft impact, the building started to collapse with the east wall buckling inward, followed by tilting of the building above Floor 82 to the east and south. The collapse sequence of WTC 2 consists of five main structural events: 1) aircraft impact, 2) sagging of floors and floor/wall disconnections, 3) bowing of the east wall, 4) unloading and tilting of core, and 5) buckling of east wall and collapse initiation.

Aircraft Impact. The aircraft impacted the south wall of WTC 2, severing a number of exterior columns on the south wall from Floor 78 to Floor 84. The south office area floor system sustained severe structural damage between Columns 410 and 436 from Floor 79 to Floor 83. Core columns 701, 702, 801, 802, 803, 901, 903, 1001, 1002, 1003, and 1004 were severed or heavily damaged between Floor 77 and Floor 84. The aircraft also severed Column 253 of the north wall. The aircraft damaged the floor framing and core columns at the southeast corner of the core. In summary, 32 of 59 columns of the south wall, two of 59 columns of the north wall, and 11 of 47 core columns were severed or heavily damaged. Thermal insulation was damaged from the impact area through the east half of the core to the north and east exterior walls. The floor truss seat connections over about one-quarter to one-half of the east side of the core were severed on Floor 80 and Floor 81 and over about one-third of the east wall on Floor 83.

Gravity loads in the columns that were severed on the south wall and in the southeast corner of the core were redistributed to adjacent intact columns and also to the columns on the east wall. In this redistribution, the total axial load on the core columns reduced by 6 percent, and the total axial load on the north wall columns reduced by 10 percent. The total axial load on the east wall columns increased by 24 percent, and the total axial load on the west and south wall columns increased by 2 percent to 3 percent. The large increases in loads in the east wall resulted from their proximity to the severed core columns at the southeast corner of the core. The total load on the south wall at Floor 83 did not change, as some of the loads from the core area were redistributed to that wall through the hat truss.

At Floor 105, splices in the columns at the southeast corner of the core failed (Columns 1001 and 1002 and most likely Columns 701, 801, 901, 902, and 1003). This increased the core tendency to lean toward southeast and also increased the vertical downward displacement of the core at the impact zone. After the core column splices failed, 73 percent of the loads released from the failing core columns were redistributed through the hat truss to the exterior walls.

About 20 percent ($= 227 \text{ kip} / 1,263 \text{ kip}$) of the redistributed load at the hat truss level of the south wall was transferred through columns and the rest of the load (about 1,000 kip) was transferred to the columns of the east and west walls through the spandrels.

After load redistribution following impact, the core was prevented from tilting excessively toward the east by the north and the south exterior walls through the action of floors and the hat truss.

Sagging of Floors and Floor/Wall Disconnections. Aircraft impact and high temperatures due to subsequent fires caused Floors 79 through 83 to sag. The sag was greater at Floor 80 and Floor 81 where the truss seats on the east side of the core failed at aircraft impact. High temperatures weakened the truss

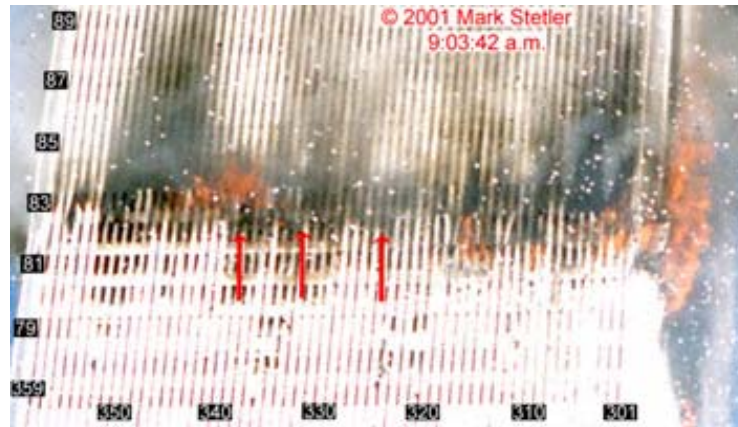
seats on the east exterior wall and caused truss seats to fail at Floor 83 and Floor 82 (see Fig. E-12) which in turn increased the sag in those floors. Floor sagging induced pull-in forces on the east wall columns, beginning approximately 10 min after impact and increasing with time.

Bowing of East Wall. The east wall columns bowed inward as a result of increasing temperatures (reduced strength and stiffness) and pull-in forces induced by sagging floors. The inward bowing in the east wall increased with time due to the combined effects of pull-in from sagging floors, increased axial loads, and a continuous increase in plastic and creep strains. As columns bowed, they shed load to adjacent unbowed columns, but the total column load on the east wall did not change significantly after impact until buckling of the east wall started near the collapse time.

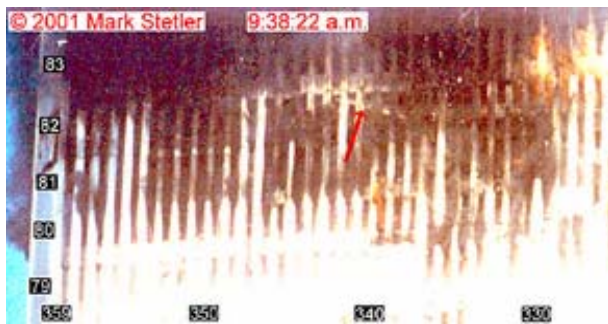
Unloading and Leaning of Core. With increasing time and temperatures, the core columns developed high plastic and creep strains, especially on the east side of the core. Plastic and creep strains exceeded the thermal expansion strains beginning about 30 min after the aircraft impact. High plastic and creep strains caused unloading on the east side core columns. This increased leaning of the core toward the east and transferred more loads to the east wall. Calculations showed that resistance to core leaning was provided by the north and south exterior walls, partly through the floors and partly through the hat truss. Leaning of the core resulted in tilting of the upper part of the tower as the east wall buckled.

Buckling of East Wall and Collapse Initiation. With continuously increased bowing and axial loads, the entire width of the east wall buckled inward (Fig. E-13). The instability started at the center of the wall and rapidly progressed horizontally toward the sides. As a result of the buckling of the east wall, the east wall significantly unloaded, redistributing its load to the softened core through the hat truss and to the east side of the south and north walls through the spandrels (see Fig. E-14). The section of tower above the buckled wall suddenly moved downward, and the building tilted toward the east (see Fig. E-15).

The section of the building above the impact zone tilted to the east and south (observed at about 7° to 8° to east and about 3° to 4° to south, Fig. E-16) as column instability progressed from the east wall to the adjacent south and north walls. The release of potential energy due to downward movement of the building mass above the buckled columns exceeded the strain energy that could be absorbed by the structure. Global collapse ensued.



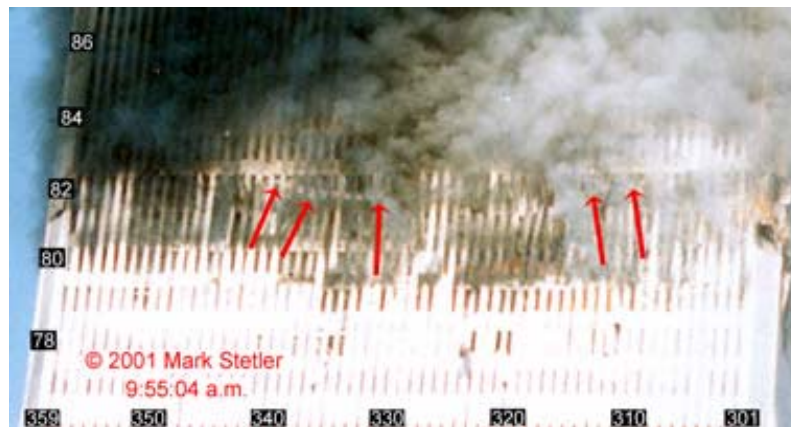
(a) After impact damage



(b) South side at 9:38 a.m.
(35 min after impact)

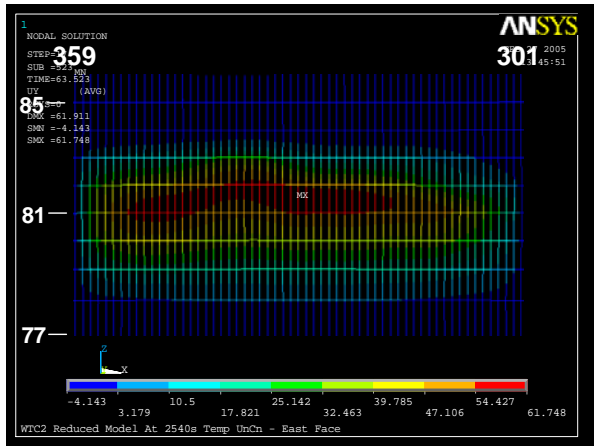


(c) North side at 9:38 a.m.
(35 min after impact)

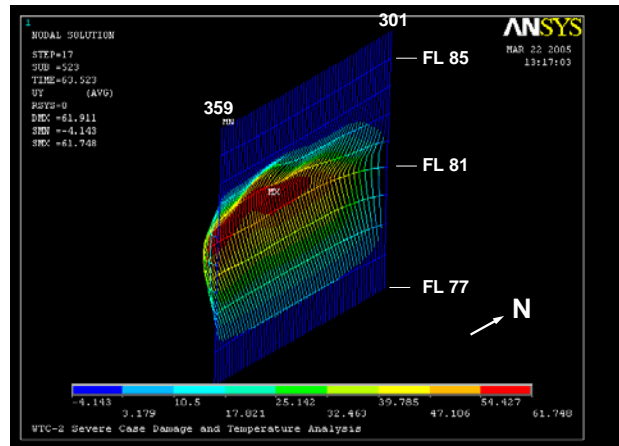


(d) At 9:54 a.m.
(51 min after impact)

Figure E-12. Floor sagging observed on the east wall of WTC 2 at different times.



(a) View from east



(b) View from southeast

Figure E-13. Inward bowing of the east wall of WTC 2 global model for Case D conditions at 43 min at the instant of collapse initiation (deformed shape scaled four times).



Figure E-14. Inward bowing of exterior columns of the west wall of WTC 2 just before collapse.

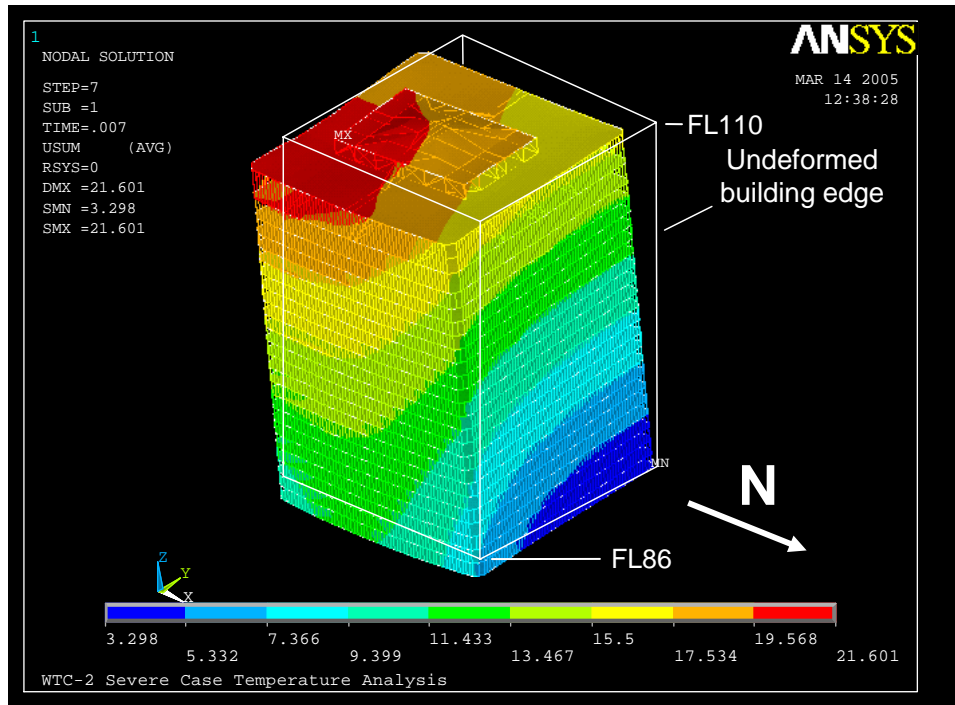


Figure E–15. Total displacements of WTC 2 global model above Floor 86 for Case D conditions at 43 min at collapse initiation (note the tilt toward east and south; deformed shape magnified 20 times).



Figure E–16. Initiation of collapse of WTC 2. Note the tilt toward east and south.

This page intentionally left blank.

Chapter 1

INTRODUCTION

1.1 OBJECTIVE

The objective of this report is to present the results of finite element analyses (FEA) performed by Simpson Gumpertz and Heger Inc. (SGH) on global models of the World Trade Center (WTC) towers. The purpose of the analyses is to determine the roles of aircraft impact damage and of subsequent fires in the probable sequence of structural responses that led to global collapse of the WTC towers.

This report complements the work that SGH performed on the structural response of components in the WTC towers, such as trusses and columns, connections such as truss seats and knuckles, and subsystems including full floors and exterior walls to the fire environment. Results were reported in NIST NCSTAR 1-6C¹.

1.2 BACKGROUND

On the morning of September 11, 2001, two Boeing 767 aircraft were hijacked after they left Boston's Logan International Airport for Los Angeles. At 8:46 a.m., American Airline Flight 11, traveling from the north at an estimated speed of 440 miles per hour, impacted near the center of the north face of WTC 1 between Floor 94 and Floor 98, 1,100 ft above the plaza level. At 9:03 a.m., United Airlines Flight 175, traveling at an estimated speed of 540 miles per hour from the south, impacted the south face of WTC 2 between Floor 78 and Floor 84, 901 ft above the plaza level (NIST NCSTAR 1).

Although both WTC towers suffered substantial damage over several floors, they withstood the aircraft impact damage without global collapse. Subsequent fires, ignited with aircraft fuel and fed by the building and aircraft contents, led to the collapse of the two towers. The collapse of WTC 2 occurred at 9:59 a.m., 56 min after impact, and the collapse of WTC 1 occurred at 10:28 a.m., 102 min after impact (NIST NCSTAR 1).

Since the collapse of these tall steel frame buildings were unprecedented, questions were raised about the safety of tall steel buildings in fires. Before drawing conclusions regarding the safety of tall steel buildings in fire, it is necessary to understand how and why the WTC towers collapsed. Various aspects of the WTC towers and their collapses have been investigated by many researchers and engineers (Bažant and Zhou 2002, FEMA 2002, Kausel et al. 2002, Levy and Abboud 2002, Usmani et al. 2003). NIST initiated a comprehensive investigation of the WTC disaster on August 21, 2002, and SGH was retained under contract in October, 2003. The work presented in this report was performed by SGH as part of Project 6 of the NIST WTC Investigation.

¹ This reference is to one of the companion documents from this Investigation. A list of these documents appears in the Preface to this report.

Aircraft impact damage to the structural components of the WTC buildings were investigated and reported in NIST NCSTAR 1-2 and NIST NCSTAR 1-2B. These studies assessed structural damage and thermal insulation damage caused by aircraft impact. Although the computed aircraft impact damage to the exterior wall system of each building can be validated from the many photographs and videos taken, aircraft impact damage to the interior columns and floor systems and to the insulation cannot be validated using this same technique.

NIST performed a fire dynamics study to estimate the thermal input to the building following the aircraft impact. The fire dynamics analysis depends on the distribution of the building and aircraft contents following the impact, the spread of aircraft fuel throughout the structure upon impact, the amount of fuel that ignited and burned off immediately upon impact, and the availability of air in fire-involved areas, flowing through broken windows and through damaged interior partitions and structures to support continued combustion. Of these factors, only the distribution of broken windows on the exterior of the building can be verified, through examination of photographic and video evidence. Other factors were estimated and validated against recorded smoke plumes and other data. These calculations were performed by NIST and were reported in NIST NCSTAR 1-5 and NIST NCSTAR 1-5F.

Based on the results of the fire dynamics model, NIST calculated the steel and concrete temperatures at various times from the time of aircraft impact for the estimated extent of remaining insulation. Before aircraft impact, WTC 1 had thicker insulation on floor trusses in the areas principally involved in the fires than did WTC 2. The columns, spandrels, and core beams had similar insulation in both of the towers. No insulation had been applied to the steel deck supporting the concrete slabs in either building, though there was overspray from application of insulation to the trusses. Based on the path of the debris determined from the aircraft impact analysis, NIST estimated the extent of the insulation that was dislodged from the structural components of the WTC towers. These estimates considered insulation to be removed only in areas where direct impact from debris was predicted. Possible additional dislodgement of insulation due to the shock and resulting vibration from the aircraft impact was neglected. The extent of dislodged insulation predicted by the aircraft impact analysis is discussed in NIST NCSTAR 1-6A, and the calculation of steel and concrete temperatures is presented in NIST NCSTAR 1-5G.

NIST determined mechanical and metallurgical properties of structural steel recovered from the WTC towers. NIST also estimated the mechanical properties of WTC steel for elevated temperatures. Results were reported in NIST NCSTAR 1-3 and NIST NCSTAR 1-3D. Temperature-dependent mechanical properties of WTC steel include modulus of elasticity, Poisson's ratio, coefficient of thermal expansion, yield strength, tensile strength, and nonlinear stress-strain relationship. NIST also predicted temperature-dependent creep properties for the WTC steels.

Prior to the development of the global finite element models of the WTC towers, SGH used hand and finite element analyses to study the structural behavior of subcomponents such as knuckles and connections, components, and subsystems. Results from structural analyses of truss seats and knuckles were used in a detailed model of a slice of a floor that included a single truss and a section of slab, which was referred to as the truss model. It was found that when subjected to elevated temperatures, the trusses sagged after diagonal web members buckled. Based on the truss model analyses, a simplified truss model was constructed and used in a model of a typical full floor. Full floor model analyses showed that in a fire environment floors sagged significantly at areas where insulation was dislodged, and exterior seats failed under extreme temperatures causing floors to disconnect from the exterior wall. The structural

performance of columns and exterior walls was studied with the analysis of single column and exterior wall subsystem models, which gave guidance in choosing element size and type for exterior columns in the global model that captured inelastic buckling behavior under elevated temperatures.

SGH developed global models that would simulate the key failure modes discovered in the analysis of components and subsystems. In addition, certain damage that could not be accurately modeled without significant loss of computational efficiency, such as certain fire-induced damage, were introduced to the global models at appropriate times. Types of fire-induced damage that were important in the collapse analysis of the global model included sagging of the floors that applied pull-in forces on the exterior columns and disconnections of floors from the exterior walls. The fire-induced damage incorporated in the global model is discussed in detail in Section 2.5.

1.3 METHOD OF APPROACH

SGH developed global finite element structural models of the WTC towers in ANSYS, based on reference structural models developed in SAP2000 (NIST NCSTAR 1-2A), and based on the studies that SGH conducted on components and subsystems of the WTC towers (NIST NCSTAR 1-6C). Owing to the existing limits of computational software and hardware, all potential structural behaviors and failure modes that could contribute to the collapse of the WTC towers were not explicitly included in the global models. A single global model that included all structural behaviors and failure modes would not be practical due to the extremely large time period required for analyses.

An alternative approach, a trial and error procedure, was used in this study to (1) perform global structural time history analyses for an assumed set of fire-induced damage, (2) identify major observations of subsequent fire-induced structural damage at different times up to the initiation of collapse, (3) determine the deviation between the calculated and observed fire-induced damage, (4) develop a structural explanation of the deviation, and (5) use the observed fire-induced damage to correct the state of the structure at that time and continue the calculation. This approach reduced the error margin (hence increased the accuracy) of the results due to epistemic uncertainties in modeling and load estimation by updating the response of the WTC towers according to observed facts at specific time points.

In developing the global models, the knowledge obtained from extensive investigation of components' and subsystems' responses to various temperature-dependent nonlinear actions was utilized. The pertinent structural actions and failure modes between and within components and subsystems that were obtained from the isolated model investigations allowed us to include or represent in a more efficient way all essential nonlinear responses in the global models without sacrificing accuracy and computation time. The important features of the detailed component and subsystem models and their influence on the global building response during the collapse process are discussed in NIST NCSTAR 1-6C. Similar discussions for two additional substructure models isolated from the global models (isolated core and exterior wall models) are provided in Chapter 3 of this report.

As discussed earlier, collapse analyses of the WTC towers were also guided by observations from the photos and videos taken during the collapse process. Visual evidence, damage estimates, and the timeline of the collapse process are reported in NIST NCSTAR 1-5A. The key observations of collapse sequences of the WTC towers are presented in Chapter 5.

The global and subsystem models were capable of capturing material nonlinearities due to plasticity and creep in steel, geometric nonlinearities due to large deflection, and elastic and inelastic buckling of the columns and other structural members at high temperatures.

The global models developed in this study were first validated against the SAP2000 models under gravity loads. Then, aircraft impact damage was included in these models by removing corresponding elements based on results from Project 2. Impact damage is discussed in detail in Section 2.2. The global models with impact damage were then subjected to temperature time histories derived from reconstructed fires in the WTC towers in Project 5.

Based on the results from FEA of the isolated and global models and the results of component and subsystem models, collapse sequences of WTC 1 and WTC 2 were identified as a conclusion of this study.

1.4 REPORT ORGANIZATION

This report presents results from the isolated models and the global models of the WTC towers. All the results are based on FEA and hand calculations. The “observed values” when used refer to the estimates obtained from photographs and videos.

This report consists of six chapters:

- Chapter 1 serves as an introduction of this report and includes objectives, background, and methods of approach of this study.
- Chapter 2 introduces the global models of WTC 1 and WTC 2. It gives general descriptions of the global models and of temperatures and aircraft impact and fire-induced damage used in the global model analyses.
- Chapter 3 gives the results from FEA of isolated wall and core models subjected to gravity and thermal loadings. The results shown in this chapter do not form a major link in the chain of collapse sequence arguments and may be skipped by those interested only in this chain of arguments.
- Chapter 4 describes the details of the global models and presents the results of FEA of the global models with creep subjected to gravity and thermal loadings.
- Chapter 5 presents the collapse sequences of WTC 1 and WTC 2 concluded from this study and provides supporting evidence.
- Chapter 6 provides a list of references.

This report also includes three appendices:

- Appendix A summarizes the results from FEA of full floor models.
- Appendix B summarizes a study on dynamic response of a floor to impact from collapse of a floor above.

- Appendix C summarizes the results of FEA of the global models without creep subjected to gravity and thermal loadings. The analyses presented in this appendix are preliminary global analyses and were primarily used to get a better understanding of the interaction between various structural components in the overall global response of the towers.

This page intentionally left blank.

Chapter 2

GLOBAL MODELS

2.1 DESCRIPTION OF GLOBAL MODELS

Simpson Gumpertz & Heger Inc. (SGH) developed two different finite element models to simulate the global structural behavior of the World Trade Center towers, WTC 1 and WTC 2, incorporating the aircraft impact damage and the fire environment that followed the impact. The finite element models of the towers were developed using ANSYS commercial structural analysis software package. The finite element models were developed to determine the roles of aircraft impact damage and of subsequent fires in the probable sequence of structural responses that led to global collapse of the WTC towers.

SGH obtained the basic building geometry, member types and cross sections, and their connectivity from models developed by Leslie E. Robertson Associates (LERA) as described in Chapter 4 of the National Institute of Standards and Technology (NIST) NCSTAR 1-6C. LERA developed the original models using SAP2000 structural analysis software.

The observation of photographic and video evidence of the behavior of both structures, following the time of aircraft impact and until collapse initiation, strongly suggested that nonlinear behavior and structural collapse initiation occurred within the upper portions of the structures, generally above the zone of aircraft impact. Therefore, to reduce the model size and improve solution time, the model of WTC 1 was truncated at Floor 89, five floors below the zone of impact, and a series of equivalent vertical linear springs were introduced at the base of this truncated model to represent the stiffness of the interior columns and exterior walls beneath the level of truncation. Similarly, the model of WTC 2 was truncated at Floor 73. This truncation is believed to have negligible effect on the predicted behavior of the structure.

As a first step in the analyses, the truncated SAP2000 models were converted to ANSYS. While the geometry from the SAP2000 model was directly transferable to ANSYS, it was necessary to substitute the elements with those from ANSYS element library. Table 2-1 summarizes the element types used in the ANSYS global models. The element names used in the table correspond to specific ANSYS (ANSYS, Inc. 2004) element formulations. All element types listed in Table 2-1 have temperature-dependent material properties.

In the original SAP2000 models, LERA represented the structural floors as rigid constraints with no out-of-plane stiffness. In order to capture the potential behavior of the floor slabs in transferring loads between the core and the exterior walls, these rigid constraints were replaced with grids of plate elements with the same membrane stiffness as the composite floor system (slab and trusses). Floors in the global models were not intended to capture floor response and failure modes during fires. Important failure modes were identified in the truss and full floor analyses and incorporated into the global models as floor/wall disconnections and pull-in forces at appropriate time intervals. See Chapter 7 in NIST NCSTAR 1-6C and Chapter 2 in this report for a detailed discussion of how floor behavior was modeled in the global analyses.

SGH next performed a series of modifications to the models, to simulate the structural damage resulting from the aircraft impacts and the effects of fire. The damage to the exterior walls was modeled by removing structural elements in a pattern that replicated the damage observed in available photographic and video evidence. The damage to interior structural elements was modeled based on aircraft impact simulations reported in NIST NCSTAR 1-2. The effects of fire damage to the structure were also included in the global models, based on thermal predictions developed by NIST, and the results of structural analyses performed by SGH of individual structural subsystems, including individual floor trusses, entire floor assemblies, and portions of exterior walls. Since projection of these subsystem analyses to global behavior entailed substantial uncertainty, visual photographic and video evidence of the behavior of the exterior structure were also used to benchmark the projections from the subsystem analyses.

The models were also modified to include a number of nonlinear behavioral modes including:

- Geometric nonlinearity associated with large deflections,
- Nonlinearity in stress-strain behavior as a function of applied loading and thermal effects, as described in Chapter 3 of NIST NCSTAR 1-6C,
- Creep behavior as the time-dependent effect of sustained stress and elevated temperatures on strain as described in Chapter 3 of NIST NCSTAR 1-6C,
- Failure of a connection between elements, resulting in a complete loss of load transfer ability and deformation compatibility.

The converted ANSYS models were validated against the SAP2000 models by comparing gravity load response, natural frequencies, and mode shapes.

Table 2–1. Element types used in the global models.

Name	Element Type	Description	Usage in the Model
BEAM188	3-D linear finite strain beam	BEAM188 is a linear (2-node) or a quadratic beam element in 3-D based on Timoshenko beam theory. Each node has six degrees of freedom or seven degrees of freedom (6+warping). Shear deformation effects are included. This element is supported for plasticity, creep, large deflection. A cross-section can be a built-up section referencing more than one material. Creep strain is calculated by implicit time integration method.	Exterior columns Core columns Core beams Spandrels Hat truss members
BEAM24	3-D thin-walled beam	BEAM24 is a 3-D beam element of arbitrary open or closed cross-section with axial, bending, and St. Venant torsional capabilities. Each node has six degrees of freedom. The element has plastic, creep, large deflection, and shear deflection capabilities. Creep strain is calculated by explicit time integration method.	Exterior columns Core columns
SHELL63	4-node elastic shell	SHELL63 has both bending and membrane capabilities. The element has six degrees of freedom at each node: three translations and three rotations. Large deflection capability is also included.	Floors

Name	Element Type	Description	Usage in the Model
SHELL181	4-node finite strain shell	SHELL181 is a 4-node shell element with six degrees of freedom at each node: three translations and three rotations. Plasticity, creep, and large deflection capabilities are supported. In nonlinear analyses, change in shell thickness is accounted for. SHELL181 may be used for layered applications.	Floors
LINK8	3-D truss	LINK8 is a uniaxial tension-compression element with three degrees of freedom at each node. It has plasticity, creep, and large deflection capabilities.	Vertical springs at the base

Damage modified the geometry and connectivity of and load distribution in the towers. Types of damage included in the global models were aircraft impact damage to the exterior wall that were visible and documented by photos and videos and interior damage resulting from the movement of aircraft impact debris through the interior space of the towers which were obtained from the aircraft impact analyses.

Structural damage caused by the fires, such as disconnection of the floor from the exterior wall, was determined from the structural analysis of the full floor subsystems. Some structural behaviors caused by the fires were not adequately captured by the full floor analysis, such as pull-in forces at the floor/wall connections. The pull-in forces were estimated through additional analyses with exterior wall models that were conducted to estimate the pull-in force required to match the observed inward bowing of the exterior walls.

The models were then analyzed for the effects of gravity and temperature loads. Gravity loads considered included: the dead load of the structure itself; superimposed dead load consisting of the estimated weights of ceilings, mechanical and electrical equipment, thermal insulation, and floor finishes; and live load, taken as 25 percent of design live load specified in the original construction documents. The use of 25 percent of the design live load as service live loads is discussed in NIST NCSTAR 1-2. Wind loads were negligible and were not considered (see NIST NCSTAR 1-6 for the recorded wind data).

Due to the height of the structures, substantial column shortening occurred under the application of dead loads. If these loads were applied to the model while the stiffness of the hat trusses was present, the hat trusses would restrain the downward deflection of the columns and in the process experience higher levels of stress. These stresses did not occur in the real buildings, because the columns experienced most of their dead load-induced shortening before the hat trusses were erected. In order to account for this effect, except for those simulations in which the effect of creep was also considered, the sequence of construction was considered during gravity load application. The loading of the structure was staged so that the stiffness of the hat trusses was not present when dead loads below Floor 106 level were applied. Construction sequence effects were not considered in the global analyses that included creep effects to enhance computational efficiency. The effect of construction sequence is discussed in more detail in Section 4.2.2.

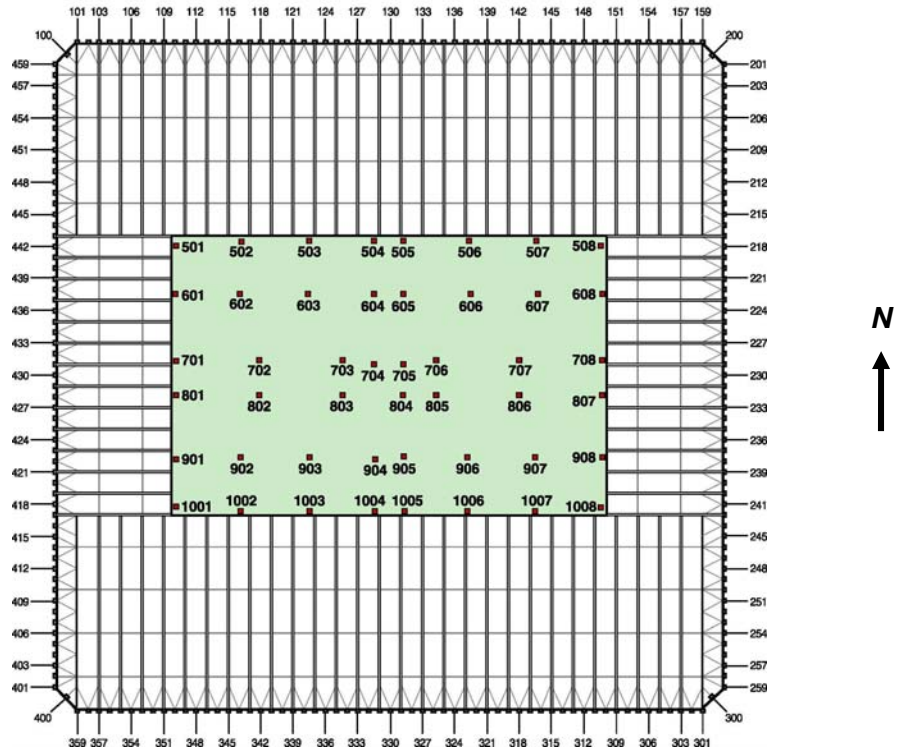
Thermal loading of a structure resulted in several effects:

- restrained axial thermal expansion of members causing local redistribution of loads, e.g., heated columns of WTC towers that attracted more load,
- differential thermal expansion across member depth, resulting in bowing if unrestrained or bending moment if restrained,
- reduction in the stiffness and strength of members, and
- high creep strain when accompanied by high stress.

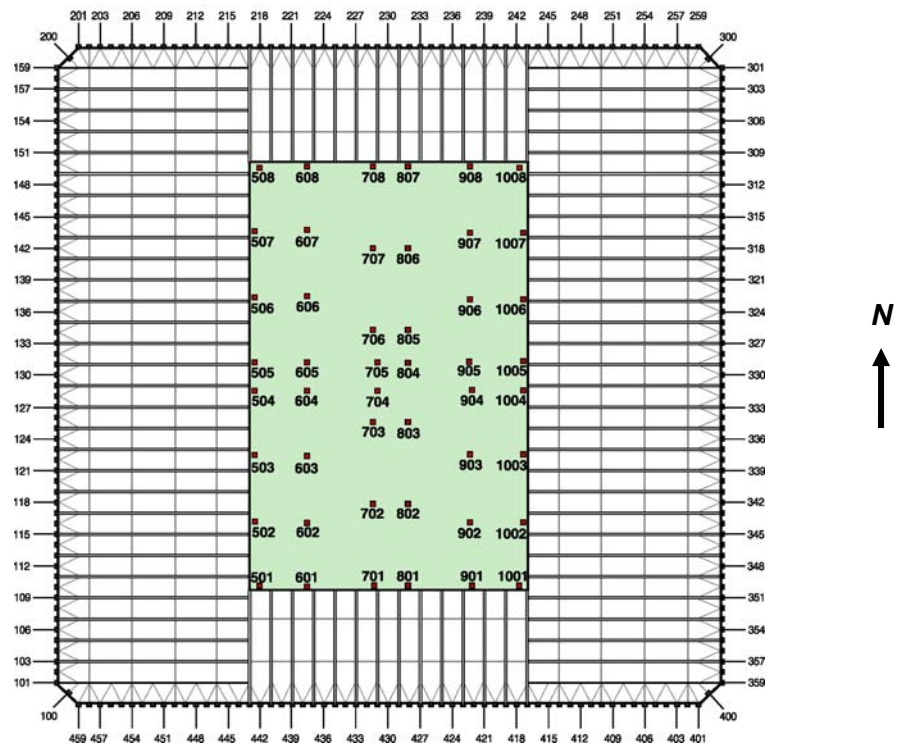
SGH applied thermal loading in the form of temperature time histories. NIST developed these temperature time histories using gas dynamic and heat transfer models. Each temperature time history corresponded to a unique set of assumptions regarding the extent of impact damage to the structure, glazing, fire separation elements, and insulation. Each temperature time history was defined discretely at 10 min time intervals which were linearly interpolated for times in between.

The behavior of columns in the two structures was significant to the collapse behavior of the towers. Throughout this report reference is made to the behavior of various columns and lines of columns, using the specific column numbering system found in the original PANYNJ structural drawings¹. In WTC 1, columns in the exterior north wall were assigned a number ranging from 101 at the west end to 159 at the east end. Columns in the exterior east wall were assigned a number ranging from 201 at the north end to 259 at the south end. Columns in the exterior south wall were assigned a number ranging from 301 at east end to 359 at the west end. Columns in the west wall were numbered sequentially from 401 at the south end to 459 at the north end. Columns 100, 200, 300 and 400 were located, respectively, at the northwest, northeast, southeast and southwest building corners. Within the rectangular core of the structure, there were six rows of either seven or eight columns each. Columns of the northern-most row were numbered 501 through 508 with column 501 located at the west end and 508 at the east end. Successive rows of columns, reading from north to south were designated 601-608, 701-708, 801-807, 901-908, and 1001-1008. This numbering scheme is illustrated in Fig. 2-1 (a). The column numbering system used for WTC 2 is similar. However, for WTC 2 Columns 101-159 were located along the west wall, Columns 201-259 along the north wall, 301-359 along the east wall, and Columns 401-459 along the south wall. Column 100 was located at the southwest corner, 200 at the northwest corner, 300 at the northeast corner and 400 at the southeast corner. In the core of WTC 2, Columns 501-508 were located along the extreme west side of the core and Columns 1000-1008 along the extreme east side of the core with the 600, 700, 800, and 900 series columns arranged progressively from west to east. Figure 2-1 (b) illustrates the column numbering system used in WTC 2.

¹ The technical data required to conduct the analyses of the WTC towers reported herein were obtained from drawings that were provided by the Port Authority of New York and New Jersey (PANYNJ) and their contractors.



(a) WTC 1



(b) WTC 2

Figure 2-1. Column designations.

2.2 IMPACT DAMAGE

2.2.1 Introduction

The extent of aircraft impact damage to the structural components of the WTC towers has been separately investigated as part of NIST Project 2 and was reported in NIST NCSTAR 1-2 and NIST NCSTAR 1-2B. SGH incorporated the results of these studies into the global models of the WTC towers to characterize the aircraft impact damage to exterior columns and spandrels, core columns, beams, and floors. Specifically, those elements identified in the aircraft impact studies as severed or heavily damaged were removed from the global models.

NIST's investigation initially identified two sets of aircraft impact damage for each of the two towers, consisting of a structural damage condition, which was damage to the structure, and a insulation damage condition, which affected the temperatures in members. These damage sets represent a *base case* and a *more severe case* of damage estimates. They were named as Case A_i and Case B_i for WTC 1 and Case C_i and Case D_i for WTC 2. These initial damage sets were used in early analyses to study the structural response of full floor subsystem models and global models without creep. The results of the full floor subsystem analyses were presented in Section 5.4 of NIST NCSTAR 1-6C and summarized in Appendix A of this report. The results of the global model analyses without creep are discussed in Section 4.1 of this report.

NIST refined the initial damage sets at later stages of the investigation and renamed them as Case A and Case B for WTC 1 and Case C and Case D for WTC 2. These damage sets were used in isolated wall and isolated core models and global models with creep. The results of the isolated wall and core models are discussed in Chapter 3, and the results of the global model analyses with creep are discussed in Section 4.2 of this report.

For each tower, the impact damage on the exterior columns and spandrels was primarily obtained from photographs and video footage that were taken before and during the collapse of the buildings. For this reason, the impact damage on the exterior columns and spandrels were the same for all damage sets for each tower. The differences between damage sets existed in the way that the impact damage was defined for the core columns, core beams, and floors. The initial and final damage sets are summarized in Sections 2.2.2 and 2.2.3.

The difference between Case A_i and Case B_i, Case C_i and Case D_i, Case A and Case B, and Case C and Case D damage sets are the structural damage condition in core columns and beams, floors, and the extent of insulation damage that ensued from the abrasion of flying debris on the structural components. The differences in insulation damage condition resulted in different temperatures of the structural components. For this reason, each impact damage set has an associated temperature set. Temperature sets have the same names as the impact damage sets.

2.2.2 Initial Damage Sets

Case A_i, Case B_i, Case C_i, and Case D_i damage sets were the initial aircraft impact damage sets defined by NIST. In terms of structural damage condition in exterior columns, Case A_i and Case B_i and similarly Case C_i and Case D_i damage sets were identical. For this reason, only one set of structural damage condition in exterior columns is presented for each tower. The structural damage condition for the floors

and core columns was not provided for Case B_i of WTC 1, and the structural damage condition for the core columns was not provided for Case D_i of WTC 2. The damage sets presented in this section were used in the full floor subsystem models and global models without creep.

The severed columns and spandrels on the exterior walls of WTC 1 and WTC 2 are shown in Figs. 2–2 and 2–3. For comparison, core columns and beams before aircraft impact are shown in Figs. 2–4 and 2–5 for WTC 1 and WTC 2, respectively. The severed columns in the core area for Case A_i of WTC 1 and for Case C_i and revised Case C_i are shown in Figs. 2–6, 2–7, and 2–8. The core column series that are not shown in these figures did not include severed columns. Since global models included only core beams that had moment connections at the ends as described in Chapter 4, these figures do not show all the core beams that existed in the WTC towers. The difference between Case C_i and revised Case C_i is only in the impact damage to the core columns (see Figs. 2–7 and 2–8). Revised Case C_i damage was received later and, consequently, was not included in some of the earlier analyses. The associated temperature sets are identical.

Case A_i, Case C_i, and Case D_i floor impact damage conditions are shown in Figs. 2–9 through 2–14. The figures show damage to structural elements, including slabs and supporting steel framing, as well as to the insulation on the framing. The shell elements of the floors and beam elements of core beams were removed from the global models at appropriate locations to replicate the areas of structural damage indicated in these figures. For regions where the floor slab was coarsely meshed in the global models, the elements were removed in such a way as to capture force discontinuities resulting from the structural damage in that region. This sometimes resulted in the removal of a somewhat larger floor area in the global models than indicated in Figs. 2–10, 2–12, and 2–14.

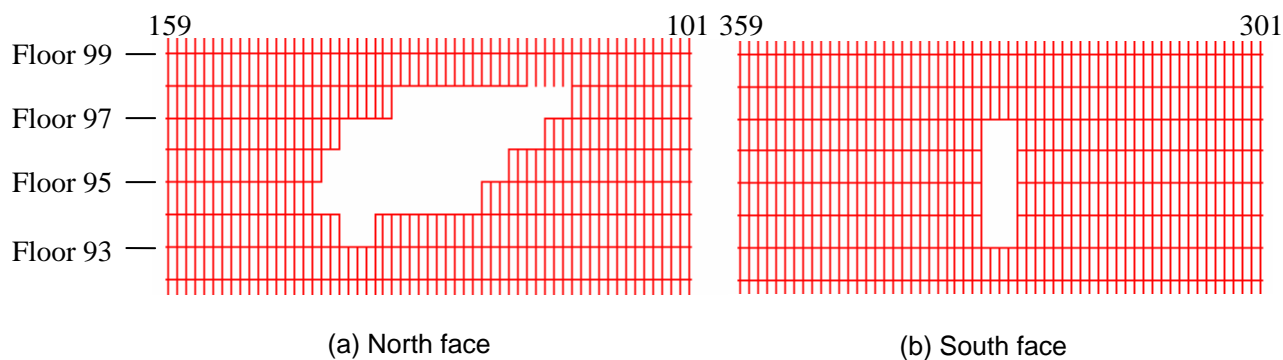


Figure 2–2. Structural damage condition on the exterior walls of WTC 1 for all cases of impact damage.

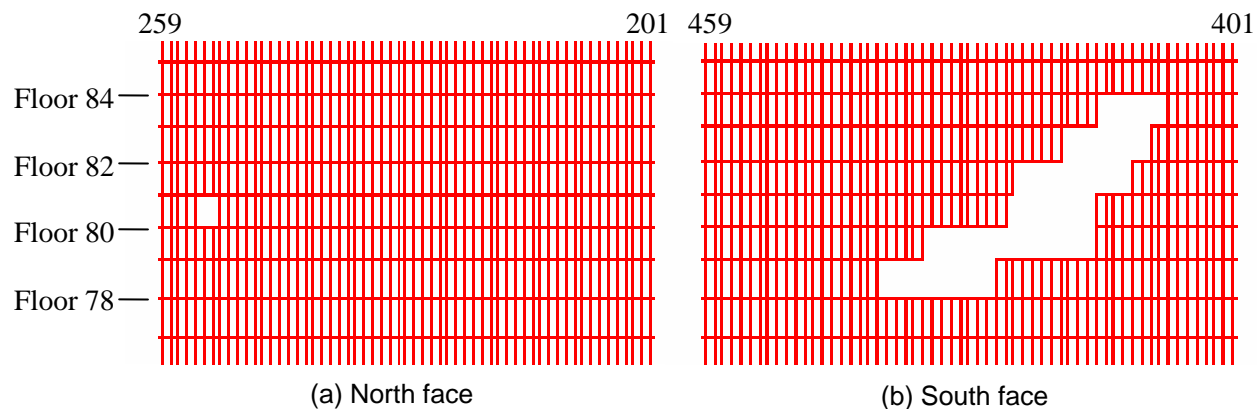


Figure 2-3. Structural damage condition on the exterior walls of WTC 2 for all cases of impact damage.

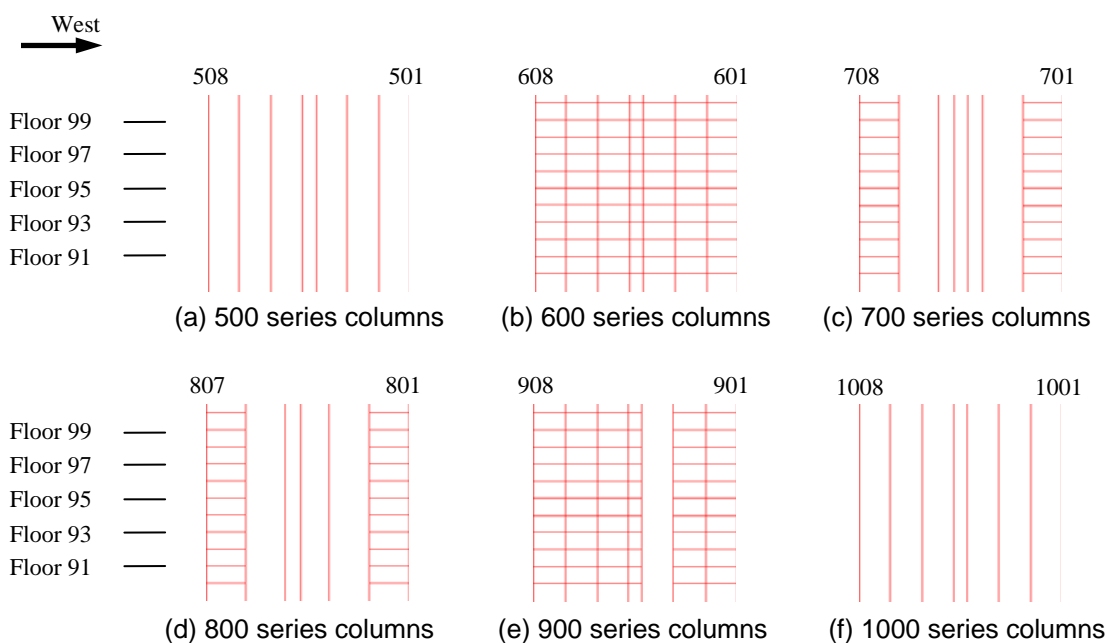


Figure 2-4. Core columns and core beams in the WTC 1 global model without aircraft impact damage.

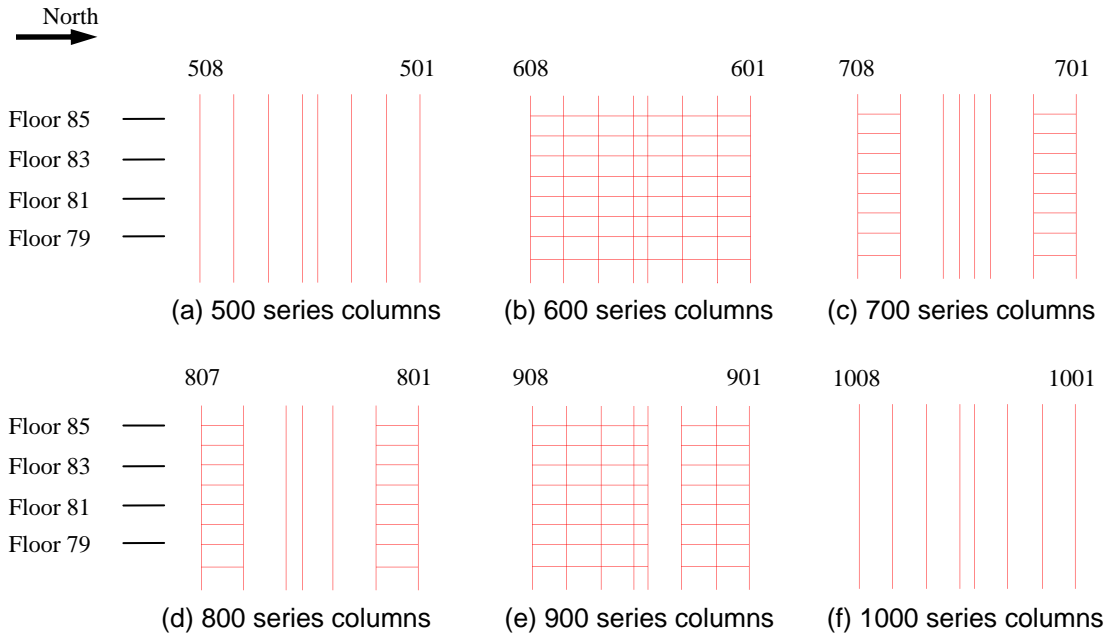


Figure 2–5. Core columns and core beams in the WTC 2 global model without aircraft impact damage.

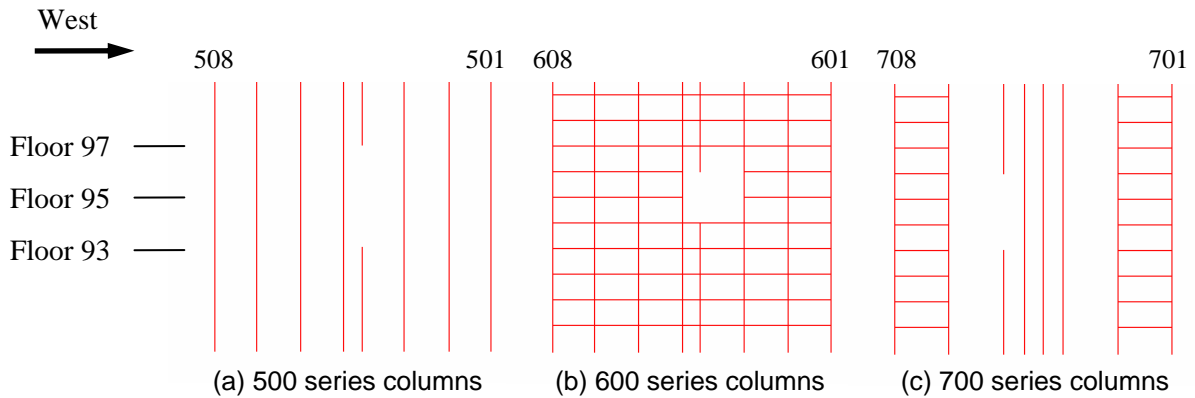


Figure 2–6. Case A_i structural damage condition on the core columns of WTC 1.

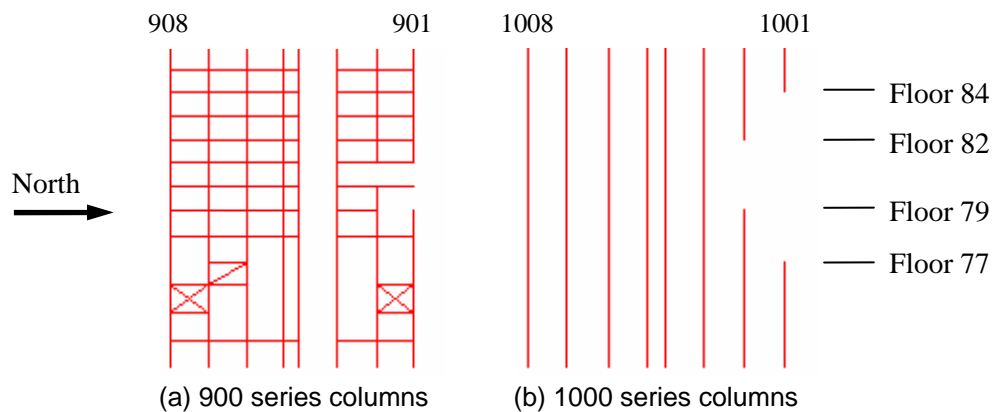


Figure 2-7. Case C_i structural damage condition on the core columns of WTC 2.

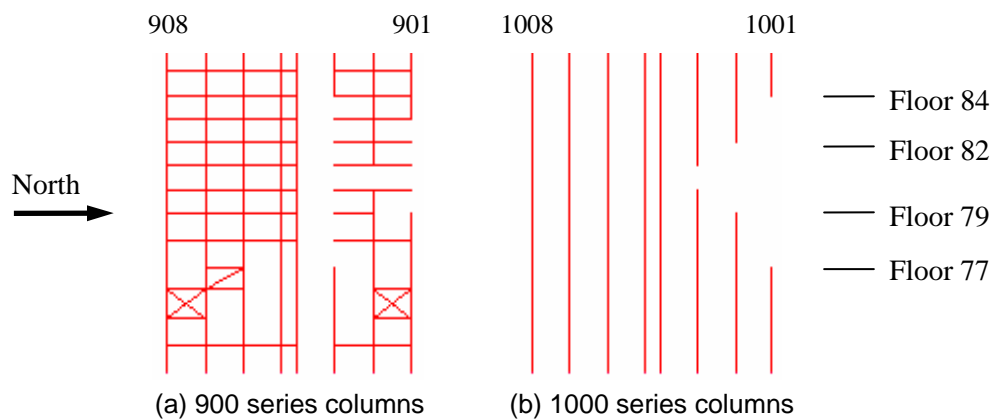


Figure 2-8. Revised Case C_i structural damage condition on the core columns of WTC 2.

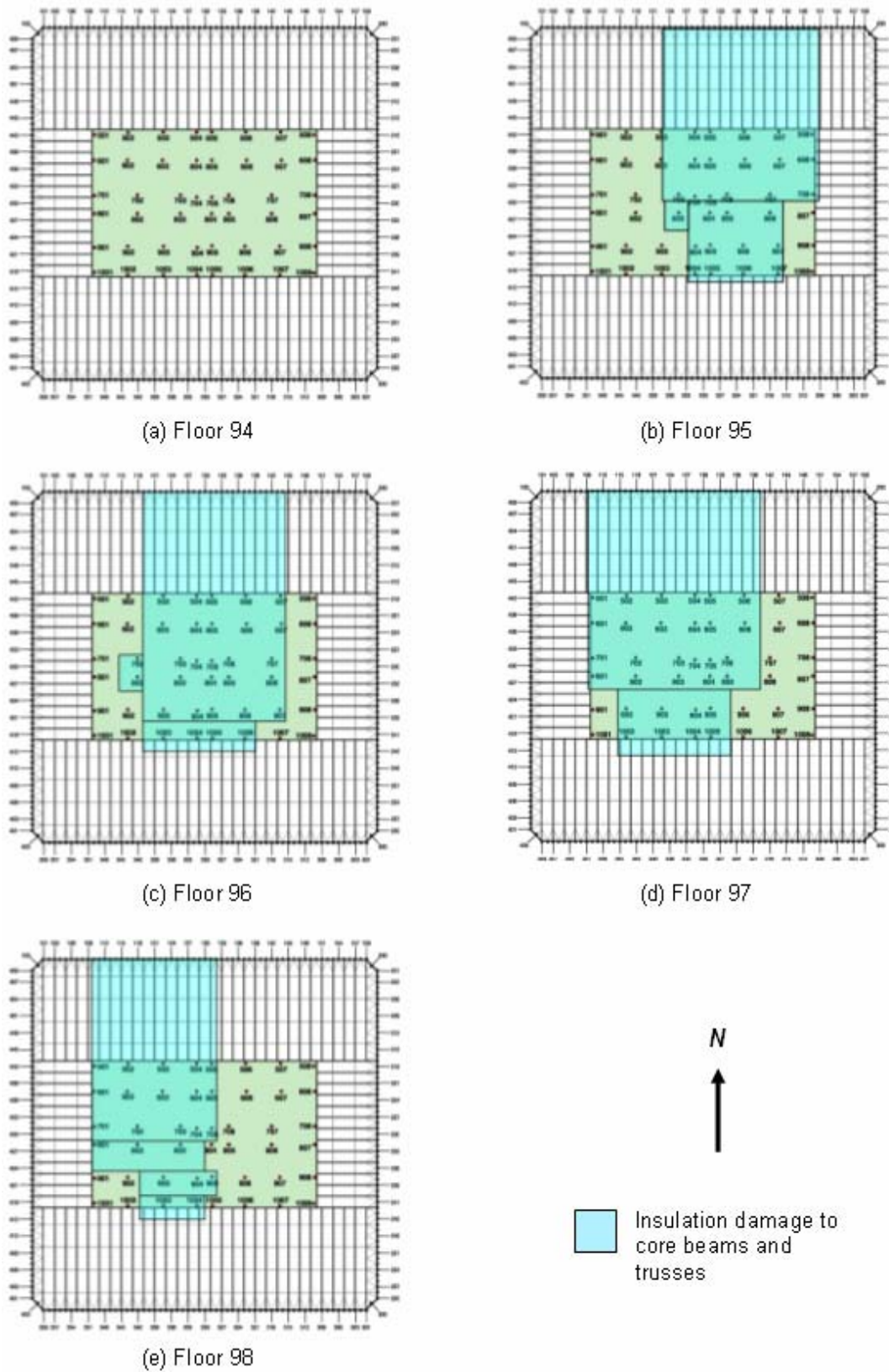


Figure 2-9. Case A_i insulation damage conditions for WTC 1 floor trusses and beams.

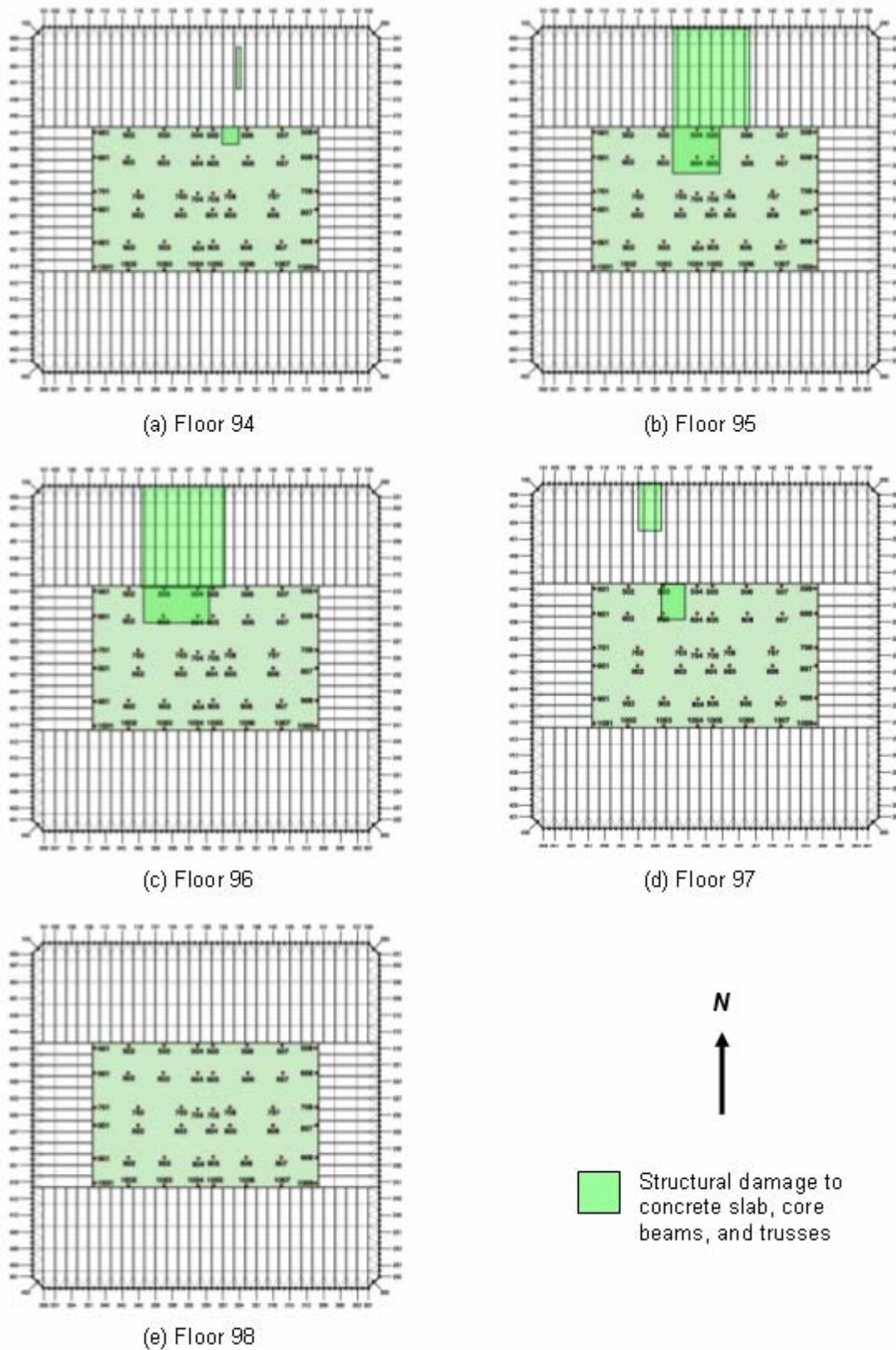


Figure 2–10. Case A; structural damage conditions for WTC 1.

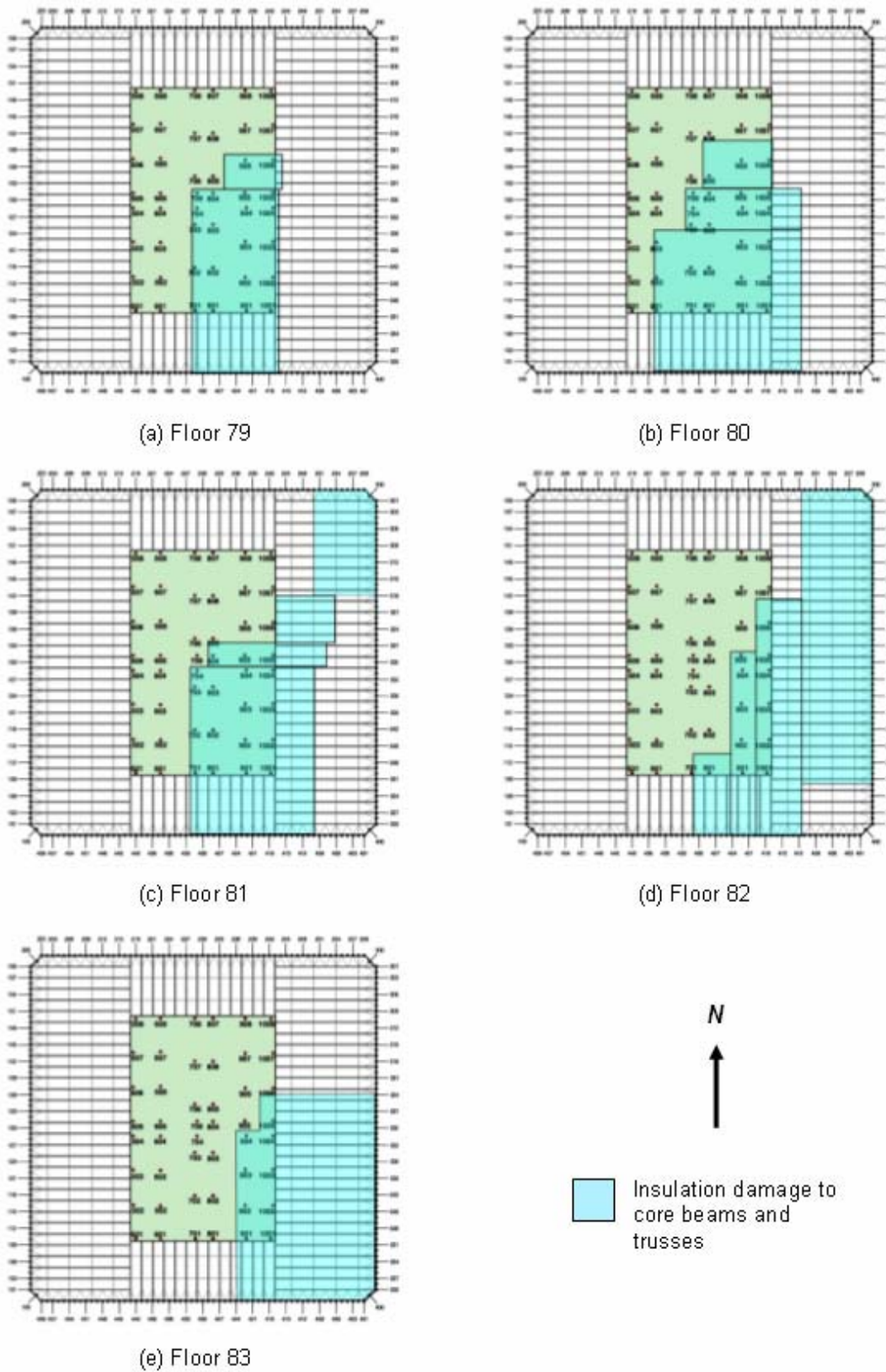


Figure 2–11. Case C_i insulation damage conditions for WTC 2 floor trusses and beams.

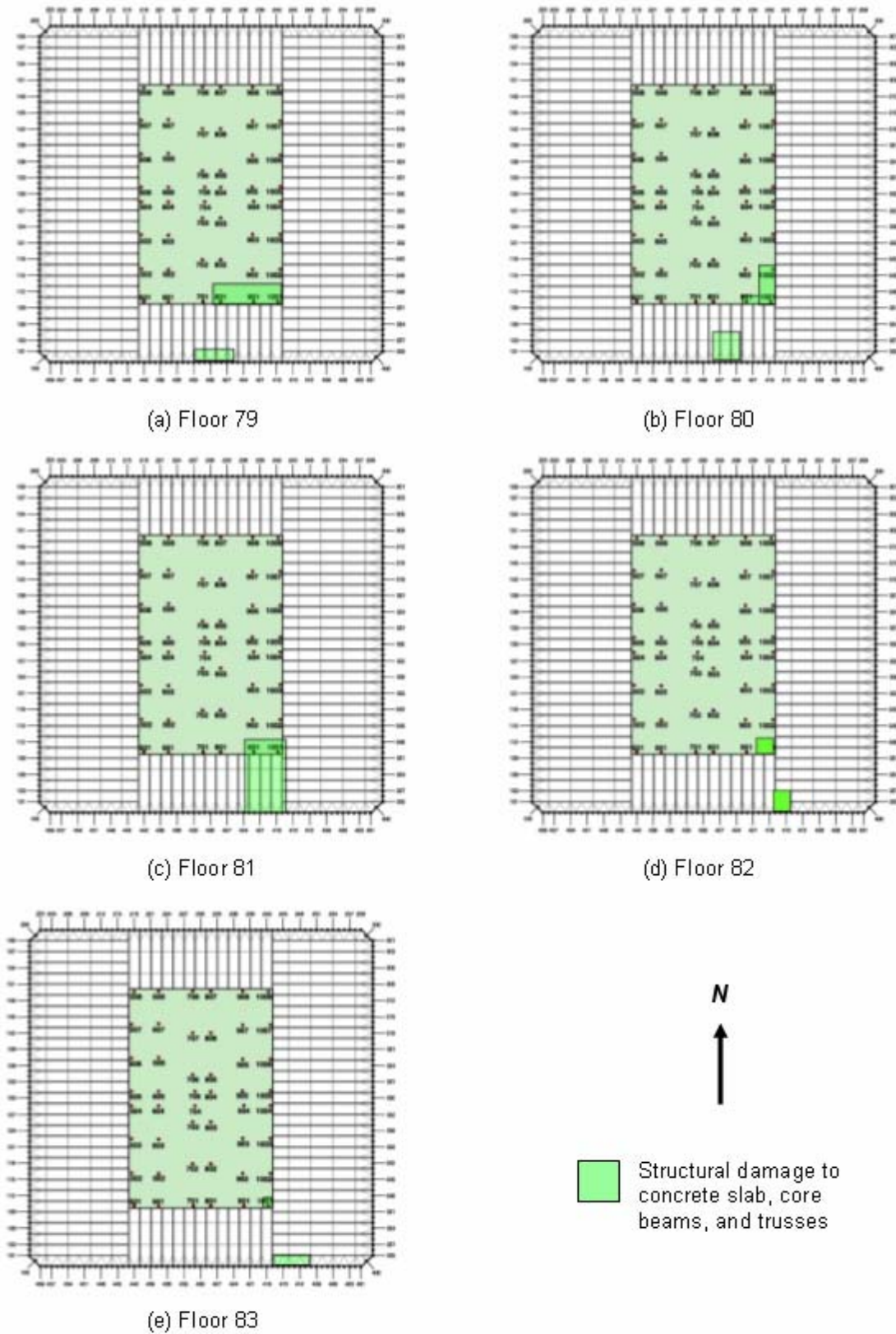


Figure 2–12. Case C, Structural damage conditions for WTC 2 floors.

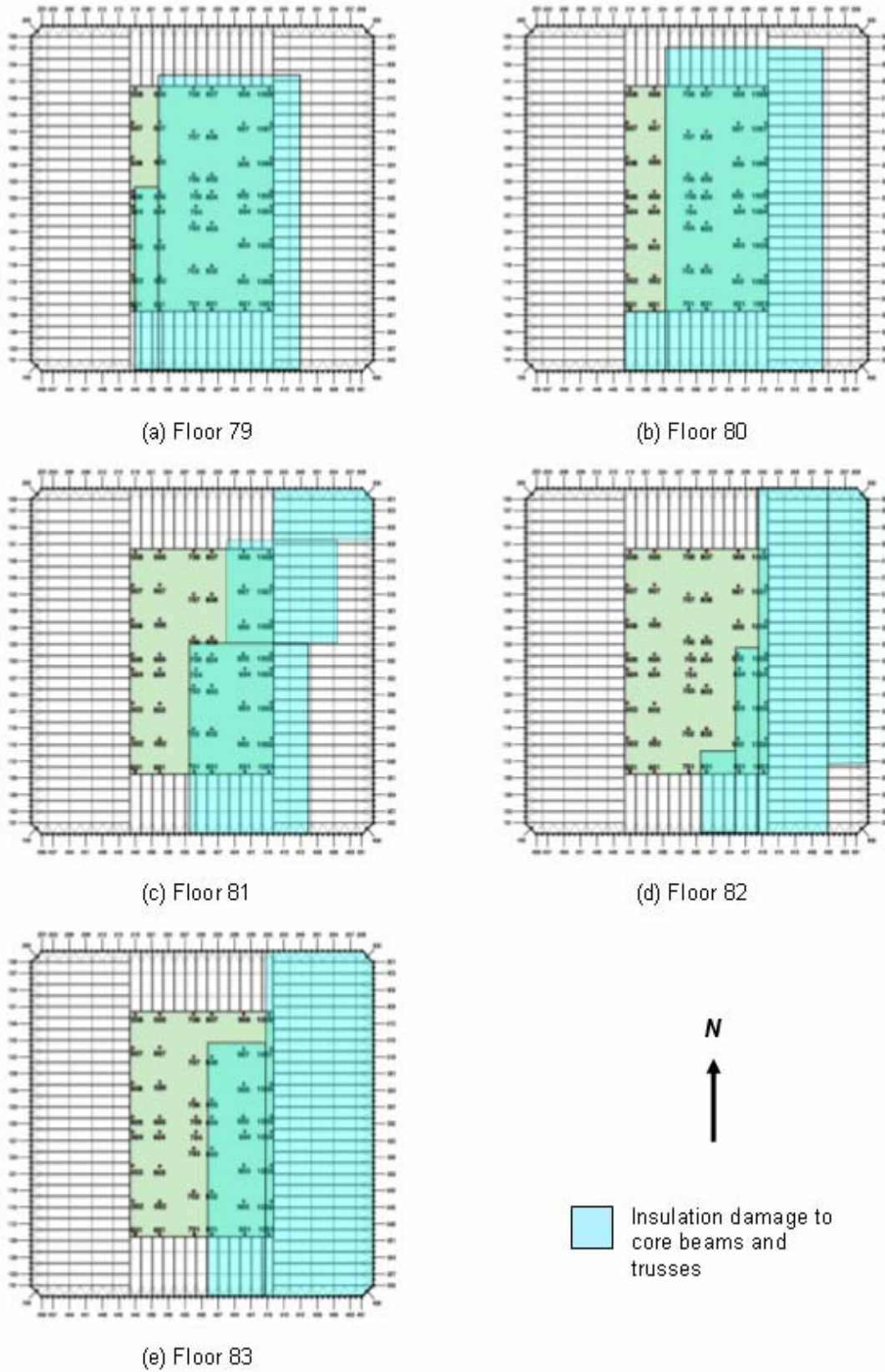


Figure 2–13. Case D_i insulation damage conditions for WTC 2 floor trusses and beams.

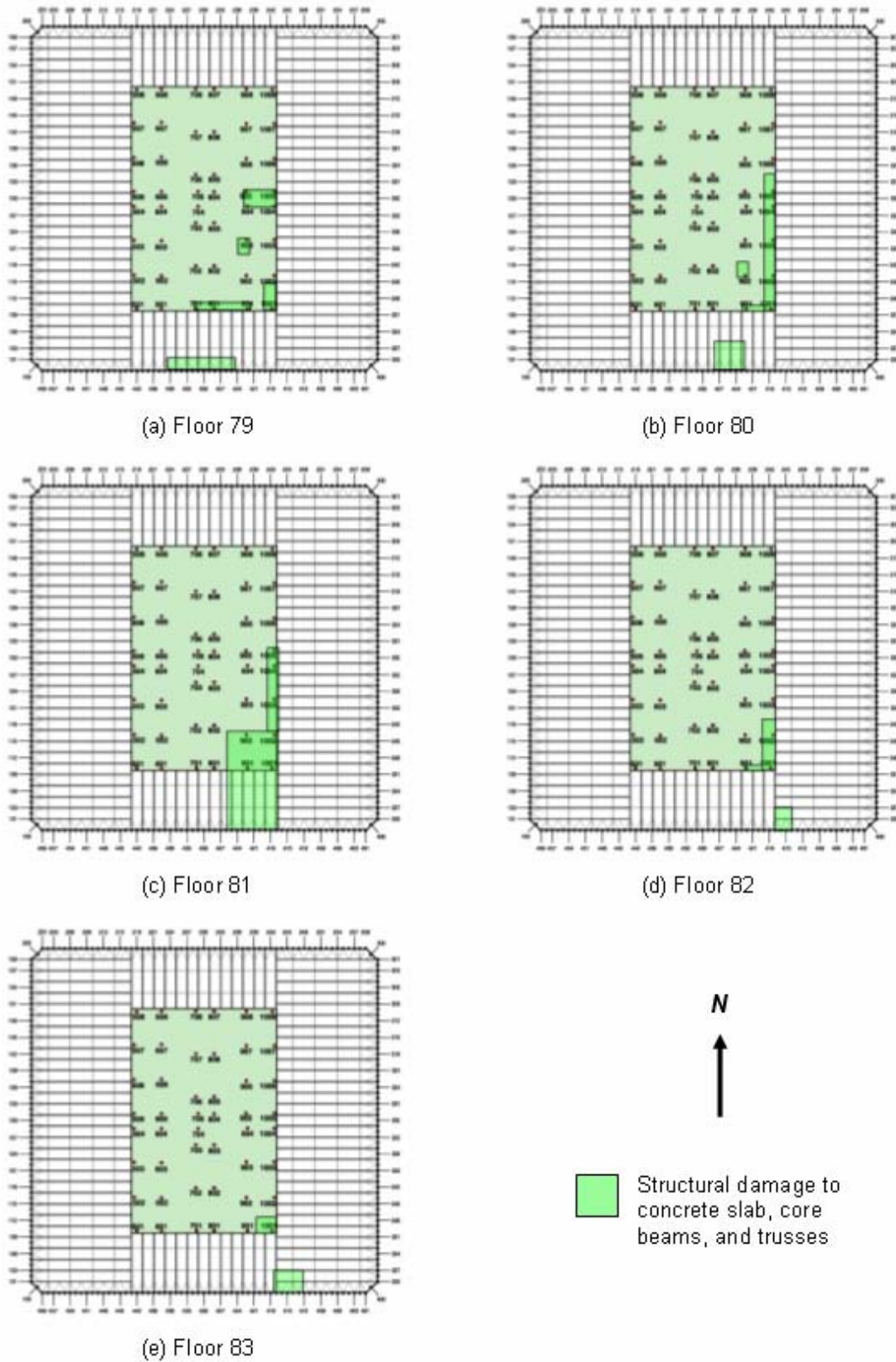


Figure 2–14. Case D, Structural damage conditions for WTC 2 floors.

2.2.3 Final Damage Sets

NIST provided a series of final damage sets for use in the global analyses. Two sets were provided for each of the two buildings, together with temperature time history data sets computed by NIST based on the damage set. The final damage sets for WTC 1 were designated Case A and Case B, respectively, representing different scenarios of aircraft impact damage to the structure and thermal insulation. The final damage sets for WTC 2 were designated Case C and Case D. The exterior wall damage contained in the final damage sets are identical to those in the contained in the initial damage sets, described in the previous section and illustrated in Figs. 2–2 and 2–3. However, the projected damage to floor and core elements differed from the initial damage sets. The final damage sets were used in SGH analyses of the isolated wall models, the isolated core models, and the global analyses with creep.

The severed columns in the core area of WTC 1 for Case A and Case B and WTC 2 for Case C and Case D are shown in Figs. 2–15 through 2–18. For Case B and Case D structural damage condition, heavily damaged core columns were also considered as severed and removed from the analysis. Columns removed from the global models are shown as missing vertical lines in these figures. For WTC 2, core column 902 was assigned a moderate damage state after aircraft impact at Floor 79 and Floor 80 by NIST. The preliminary analyses showed that this column buckled after aircraft impact and caused numerical problems in the temperature time history analyses. Therefore, in the Case D damage set, this column was also treated as heavily damaged and removed from the model. The core column series that are not shown in Figs. 2–15 through 2–18 did not include severed columns for all the cases or heavily damaged columns for Case B of WTC 1 and Case D of WTC 2.

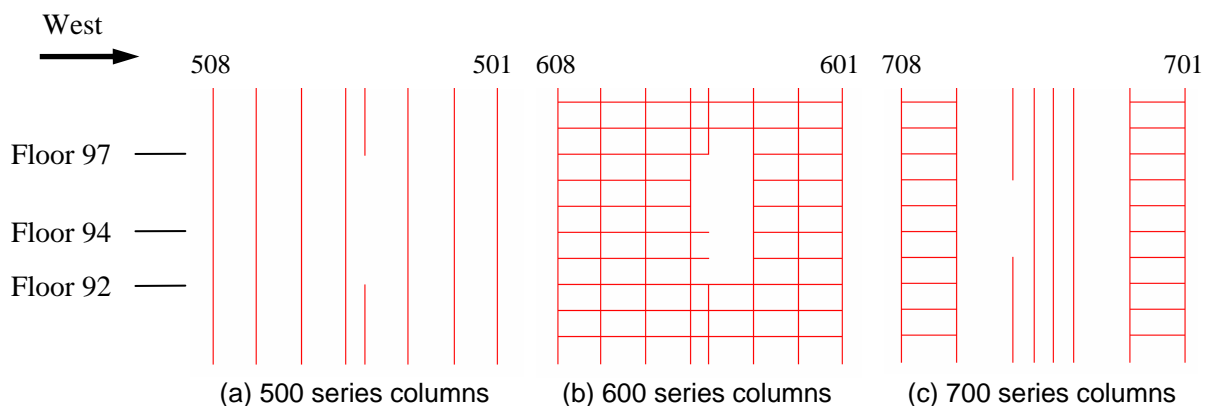


Figure 2–15. Case A structural damage condition on the core columns of WTC 1.

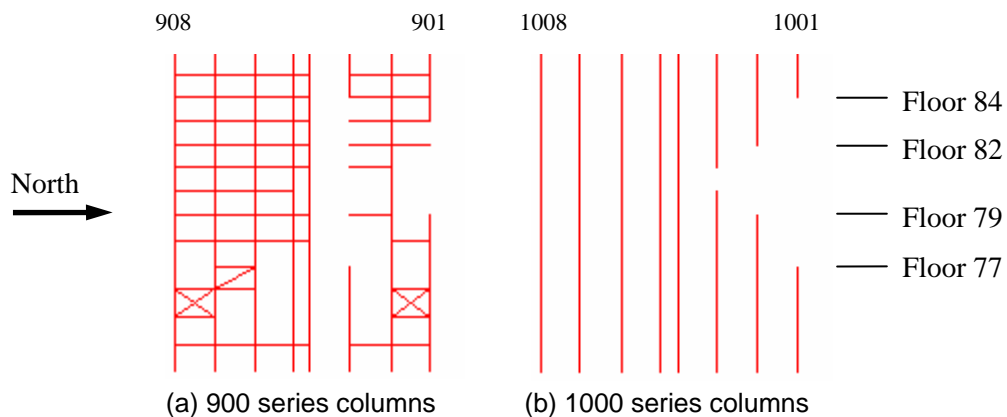


Figure 2–16. Case C structural damage condition on the core columns of WTC 2.

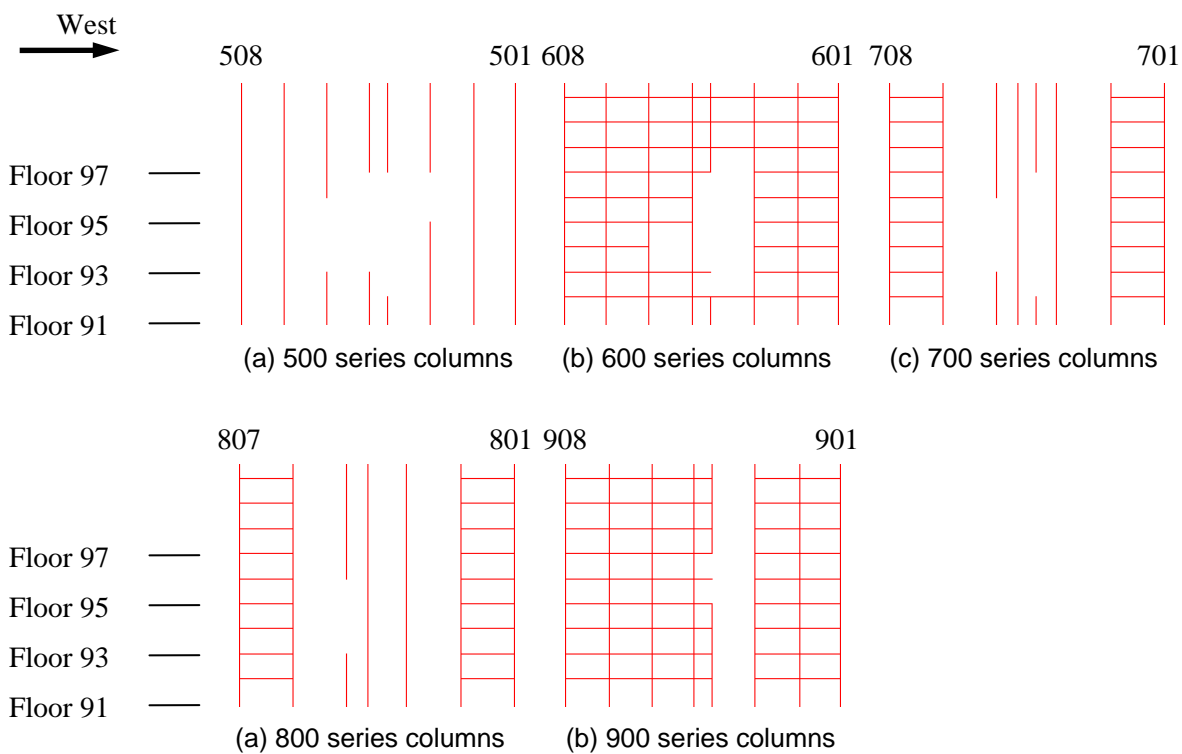


Figure 2–17 Case B structural damage condition on the core columns of WTC 1 (including heavily damaged columns).

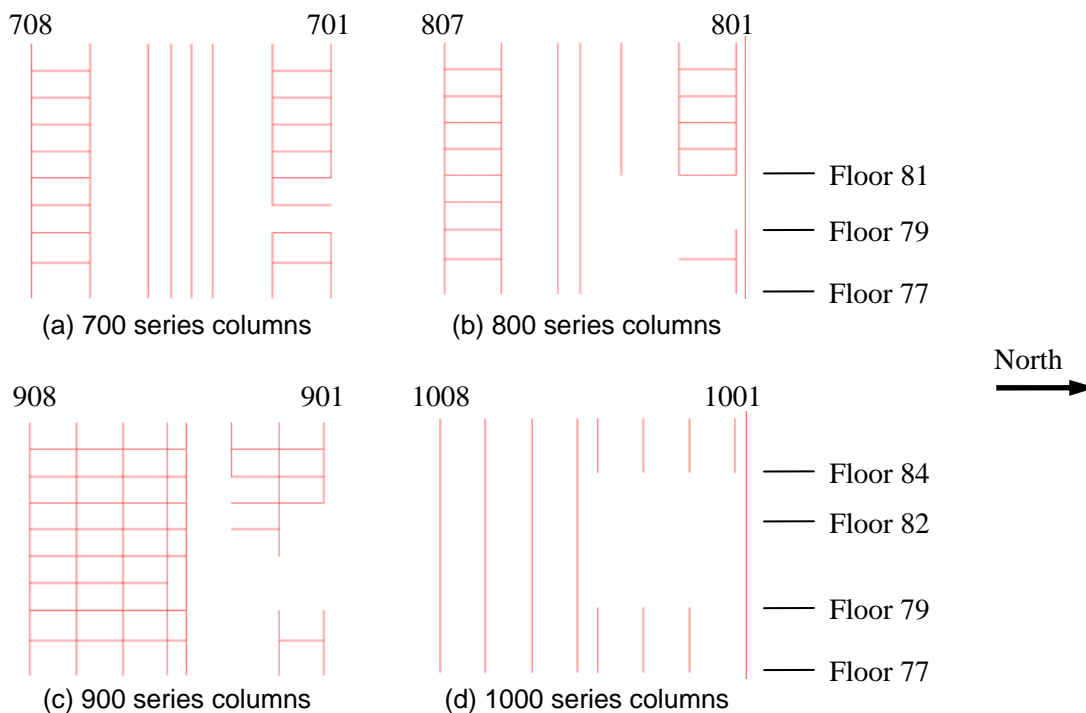


Figure 2-18. Case D structural damage condition on the core columns of WTC 2 (including heavily damaged columns).

The floor insulation and structural damage conditions are shown in Figs. 2-19 and 2-20 for Case A, in Figs. 2-23 and 2-24 for Case B, in Figs. 2-21 and 2-22 for Case C, and in Figs. 2-25 and 2-26 for Case D.

The shell elements of the floors and beam elements of core beams were removed from the global models at appropriate locations to replicate the areas of structural floor damage indicated in these figures. For the regions where the floor slab was coarsely meshed, the elements were removed in such a way as to capture force discontinuities resulting from the structural damage in that region. This sometimes resulted somewhat larger floor openings than indicated in Figs. 2-20, 2-22, 2-24, and 2-26. However, as discussed in Chapter 4, the dead and live loads of the floor system were applied as concentrated loads to the connecting columns; this minimized the effect of slightly larger floor openings.

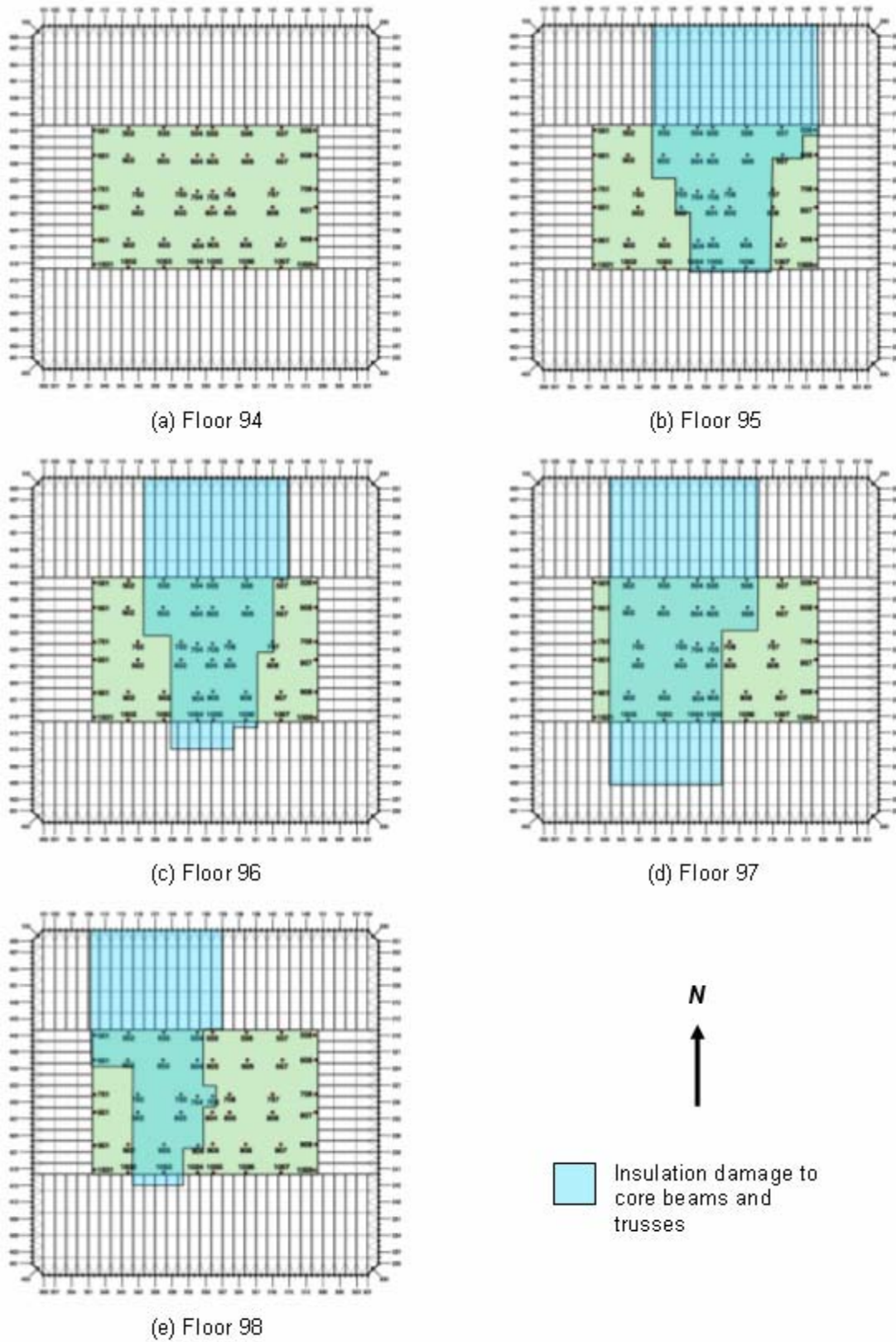


Figure 2–19. Case A insulation damage condition for WTC 1 floor trusses and beams.

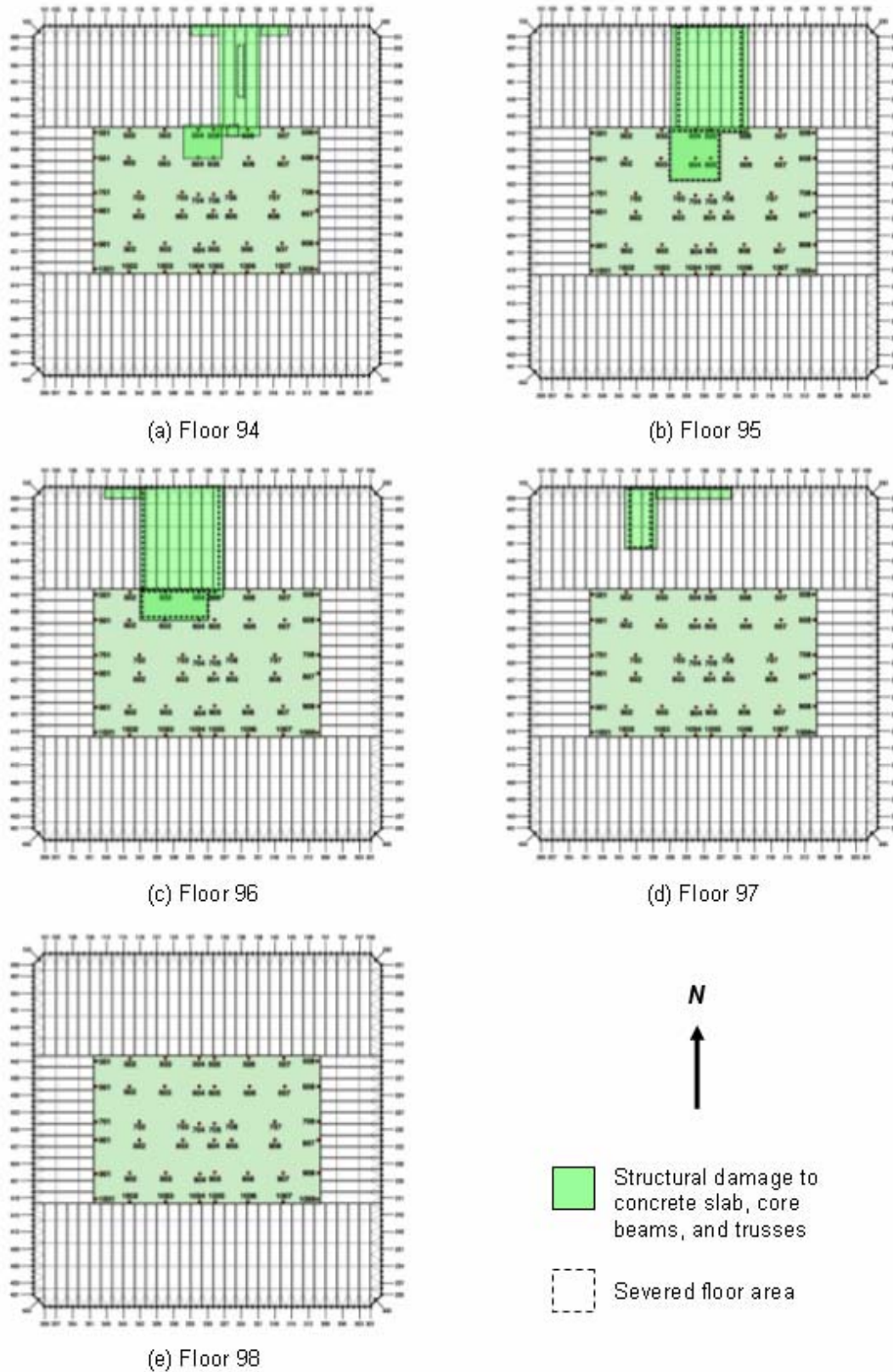


Figure 2-20. Case A structural damage condition for WTC 1 floors.

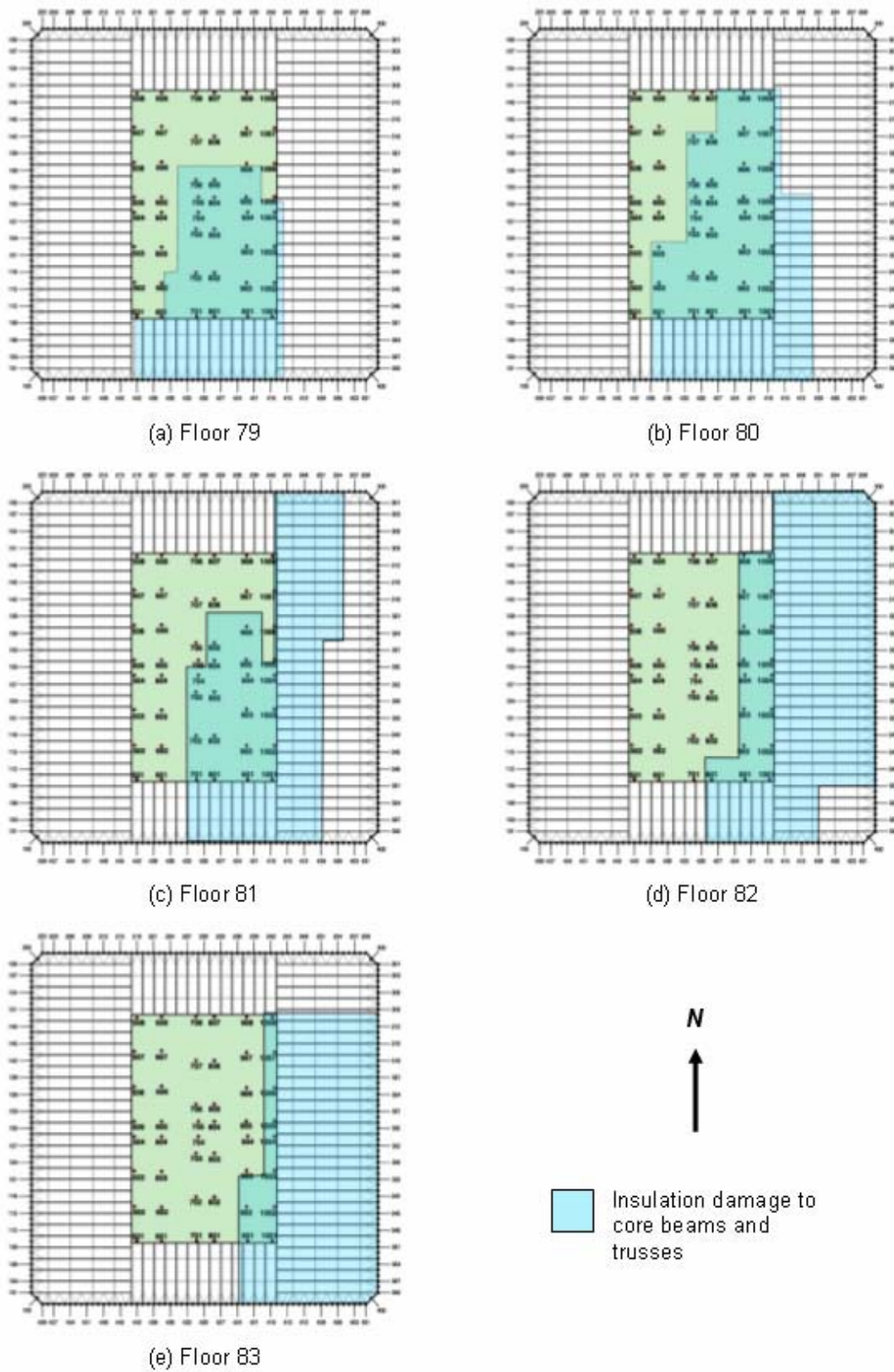


Figure 2–21. Case C insulation damage condition for WTC 2 floor trusses and beams.

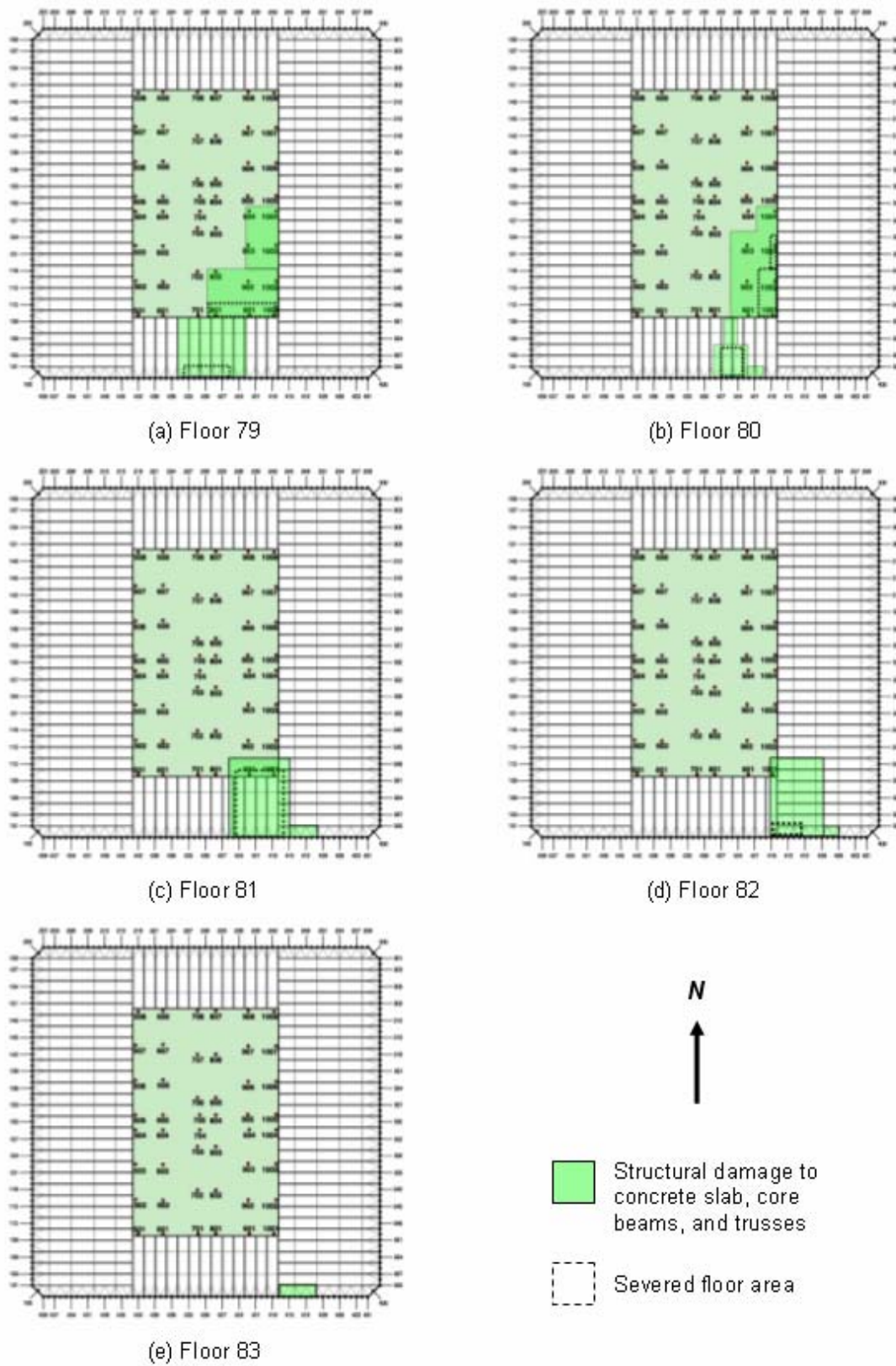


Figure 2-22. Case C structural damage condition for WTC 2 floors.

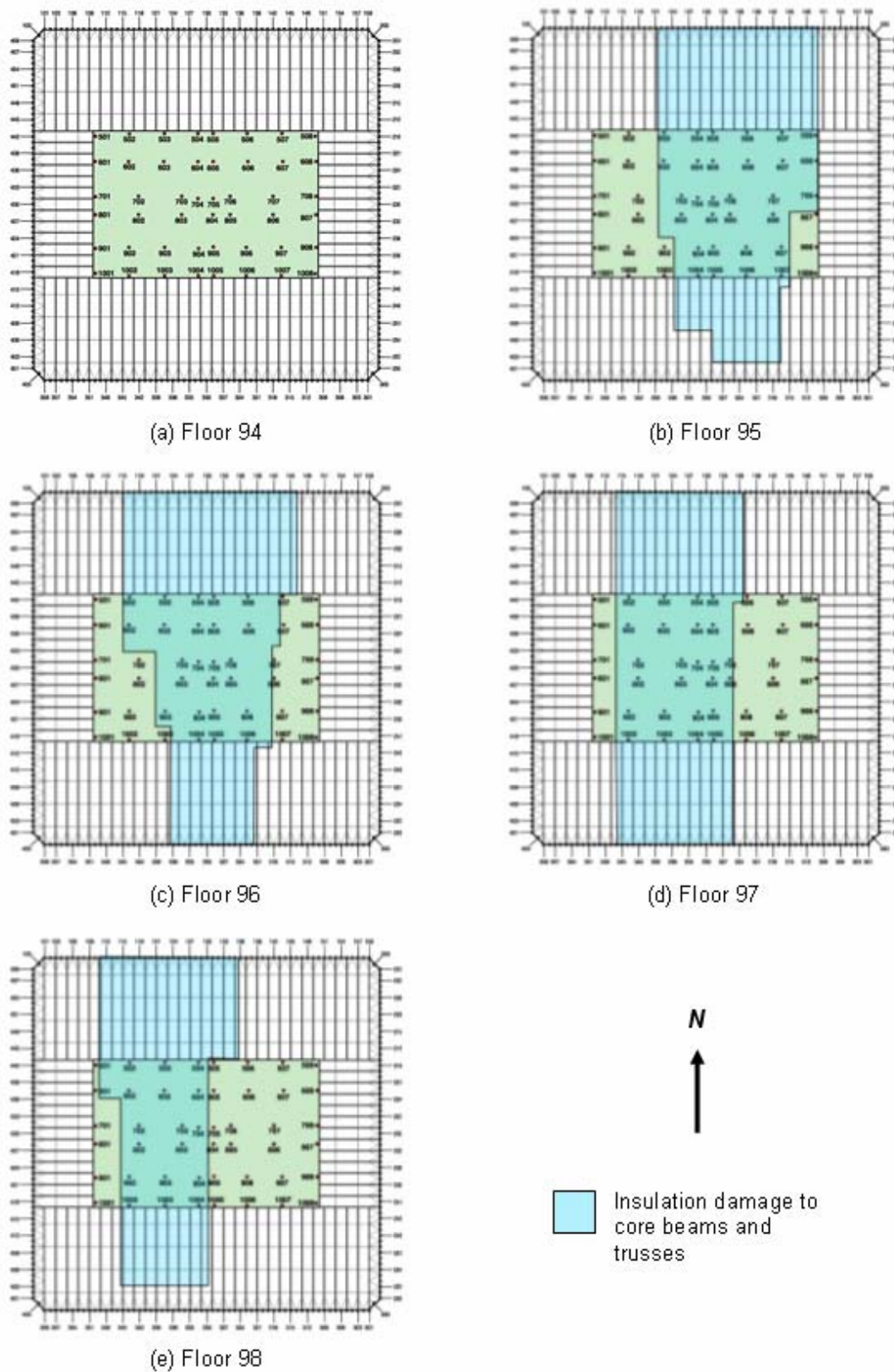


Figure 2–23. Case B insulation damage conditions for WTC 1 floor trusses and beams.

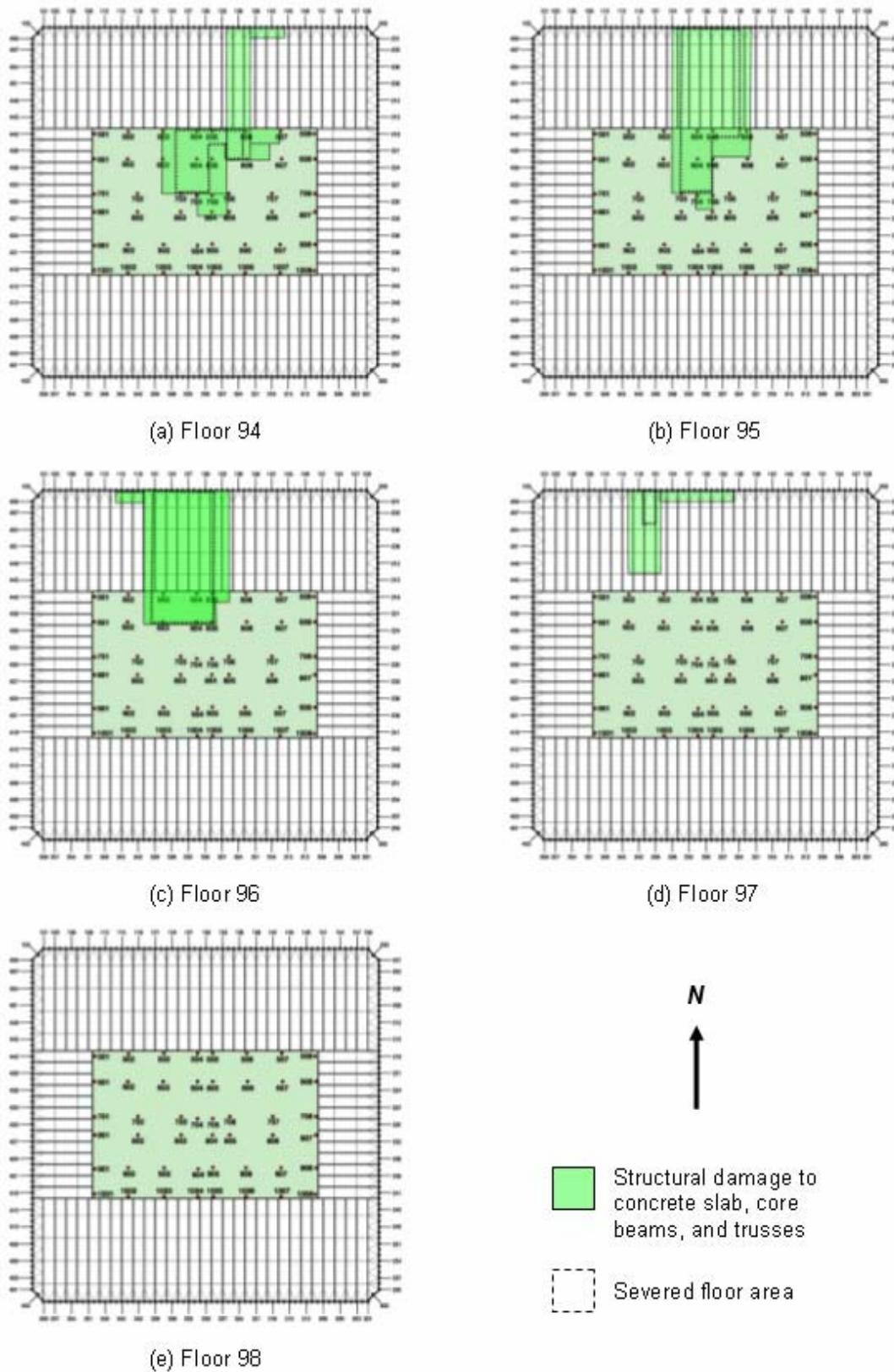


Figure 2-24. Case B structural damage conditions for WTC 1 floors.

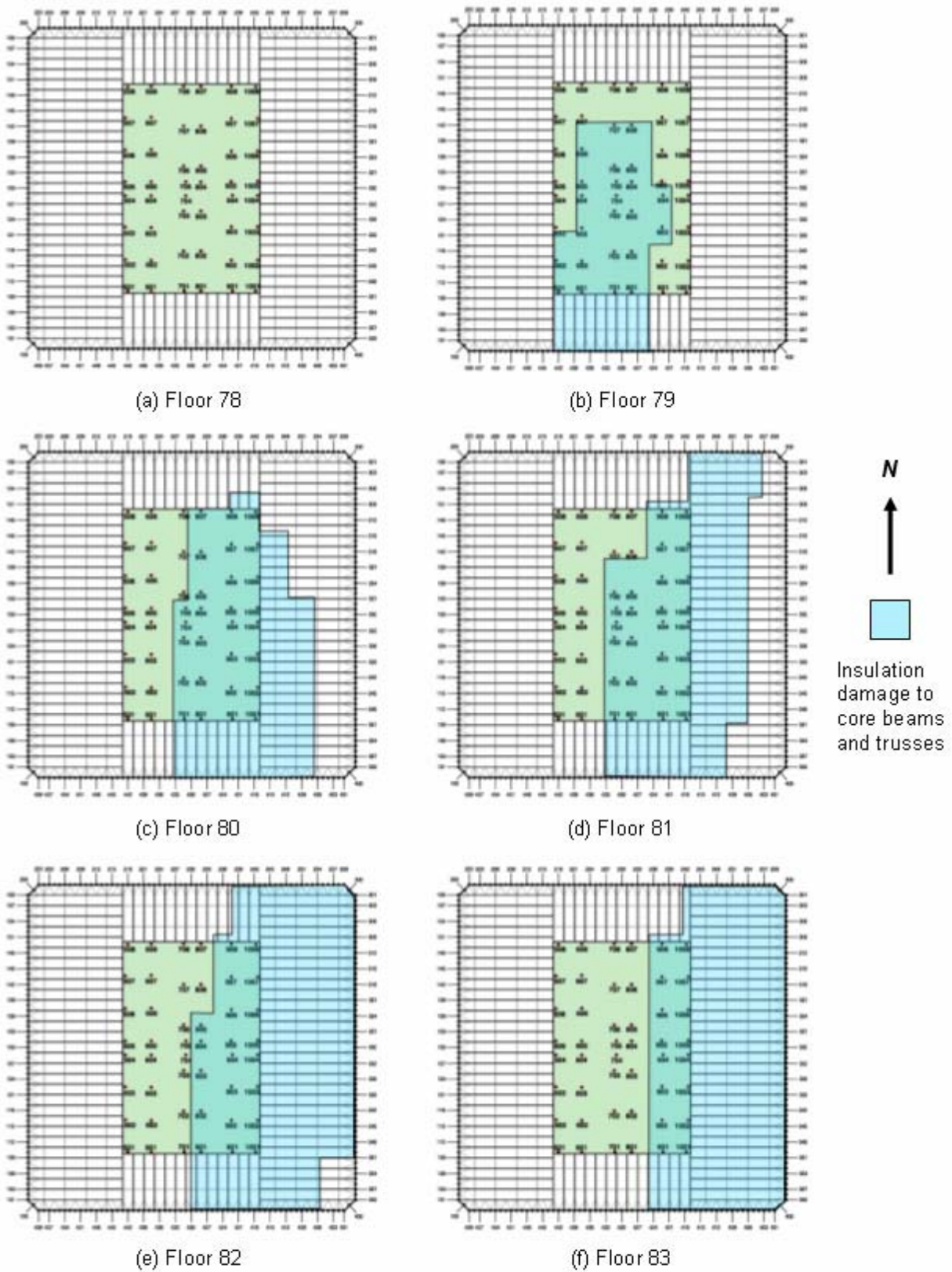


Figure 2–25. Case D insulation damage conditions for WTC 2 floor trusses and beams.

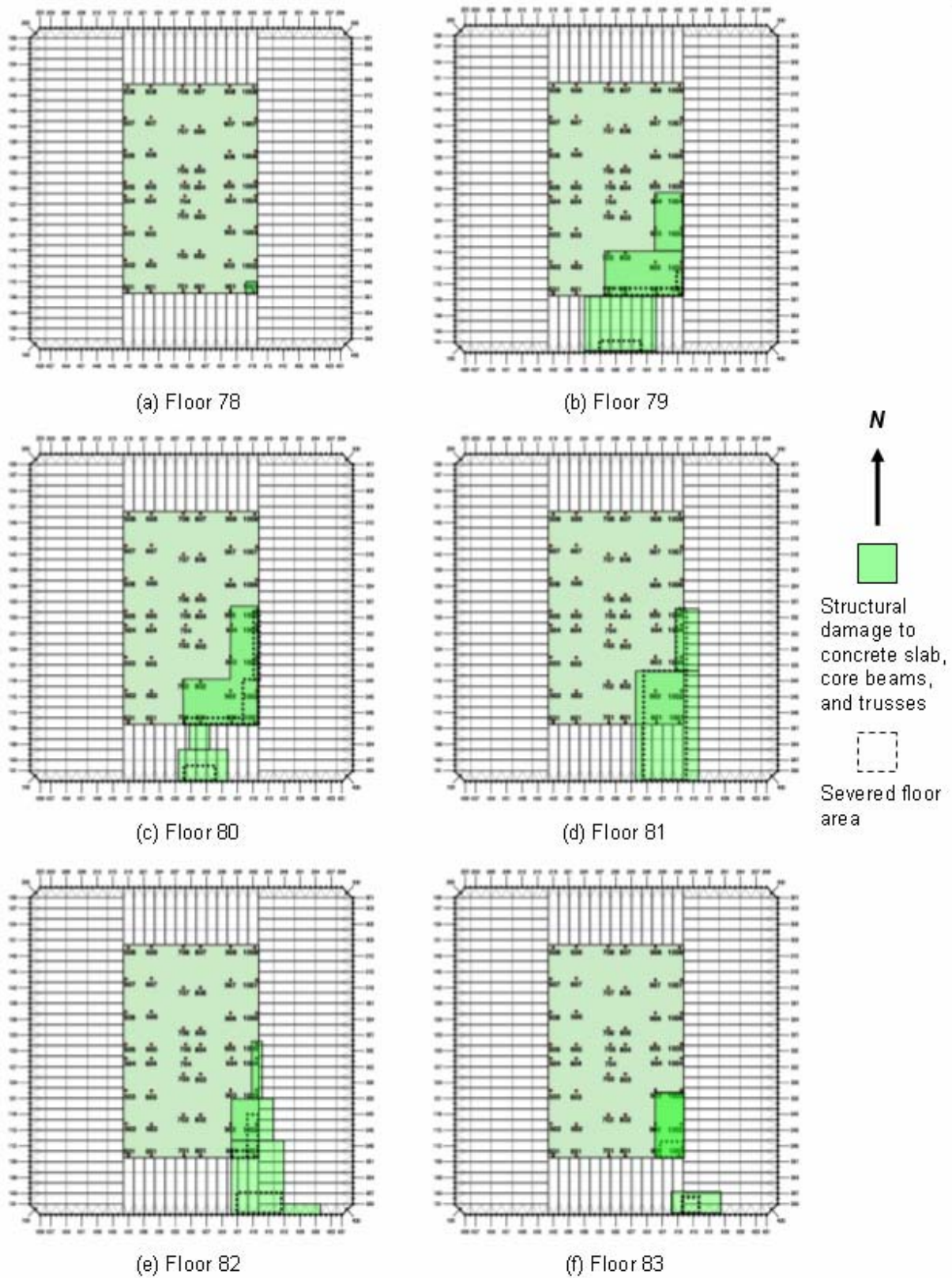


Figure 2-26. Case D structural damage conditions for WTC 2 floors.

2.3 TEMPERATURE EFFECTS

The fires resulting from the combustion of the jet fuel, followed by the combustion of building contents and the debris from the aircraft produced high-temperature gases that in turn increased the temperature of the exposed structural members. Fire is dynamic in nature. As fire consumes combustible materials in the area of ignition, the high temperature gases produced by the fire spread to other areas of the building, heating the structure and igniting combustible contents in these other areas. Even as the fire spreads, it consumes the fuel in areas already involved, extinguishing itself and allowing the structure in those areas to cool. As a result of this behavior, the temperature of the exposed structural members in the two towers varied with time, from the instant of aircraft impact until the final collapse. NIST performed a series of computational fluid dynamics analyses to predict the distribution with time of gas temperatures in various locations in the structures and also to produce temperature time histories for the structural members in the affected areas of the buildings. These analyses are reported in NIST NCSTAR 1-5.

In the analyses performed by NIST, a key factor in the calculation of the temperature distribution for the structural members was the extent of insulation that was in place after the impact. NIST assumed that any damage to the insulation was by direct abrasion from flying debris created as the aircraft impacted, disintegrated, and transited across the building. A series of aircraft impact analyses were performed to predict the pattern of debris flow as well as the probable damage to structural members inside the building. In these analyses, the trajectories of the debris flow and, therefore, of the extent and distribution of insulation damage predicted was dependent on the estimated values for aircraft speed and direction of travel, point of impact on the structure, and impact trajectory. The several damage sets (Case A_i, Case B_i, Case C_i, etc.) resulted from variation in the values of these parameters and, therefore, the estimated damage and temperature time histories. One temperature time history data set was derived for each set of structural and insulation damage². As discussed in Section 2.2, Case C_i and revised Case C_i have the same temperature time histories for structural components.

The high temperature gases produced by the fires primarily heated the floor trusses and the bottom face of the slabs through convection and the top face of the slabs through radiation. The temperatures predicted in the structural members depended on the extent of insulation assumed to be in place and on the material properties and geometry of the structural members. In the actual buildings, the temperature in the structural members varied through the length and cross section and changed with time. The temperature at every node in the global models was calculated by interpolation of temperatures from the thermal analysis, which had a much finer mesh than the global structural models. A linear temperature gradient was assumed across column cross sections and along the length of members. To reduce data handling, the continuous temperature time histories were replaced with piecewise linear time-histories without significant loss of accuracy. Consequently, snapshots of the spatial distribution of temperature were taken at 10 min intervals, initiating at the time of impact and extending through the time of collapse (or approximately the time of collapse) for each of the buildings (see NIST NCSTAR 1-5G for more discussion of the 10 min intervals).

² Temperature cases were formerly called by different names. Case A_i and Case C_i conditions were called “baseline case”, and Case B_i and Case D_i conditions were called “maximum damage case”. Case A and Case C conditions were called “best estimate case” or “realistic case”, and Case B and Case D conditions were called “upper bound case” or “severe case”. These former temperature case names may appear on graphics produced in ANSYS.

Structural response of a building to fire-induced temperature is a complex phenomenon involving the following phenomena:

- Axial thermal expansion of members as they heat and thermal contraction of members as they cool; if these members are restrained, this expansion and contraction can induce a change in the stress distribution in the structure.
- Differential thermal expansion of members across their cross section if they are heated unevenly, resulting in bowing of the members along their length; if members are under significant compression, this bowing can lead to onset of buckling.
- Significant reduction in modulus of elasticity and strength of steel and concrete as temperature increases beyond 500 °C (NIST NCSTAR 1-6C).
- Creep in steel at high stresses and high temperatures.

Creep is a time-dependent phenomenon and, in the analyses that SGH performed, was found to have resulted in shortening of core columns with high temperatures and high stresses.

In the global models, NIST-provided temperatures were applied to structural members between Floor 93 and Floor 99 in WTC 1 and between Floor 79 and Floor 83 in WTC 2. In each case, the temperatures were applied to exterior columns, spandrels, core columns and beams, and floor slabs.

In general, temperatures were assigned to the node locations in the global models. The distribution of temperature was assumed to be uniform throughout the member cross section except in the case of the exterior columns where temperature gradients within the cross section were considered in the direction normal to the exterior walls.

All temperatures reported in this study are in units of °C.

2.4 THERMAL BEHAVIOR OF FLOORS

It was not practically possible to develop global models that could capture all structural behaviors or failure modes found in the study of components and subsystems and to perform the global analysis within a reasonable time period. To enhance computational efficiency, selected modeling details were omitted in the global models, and structural behaviors or failure modes that could not be captured by the global models were introduced in the global analysis as fire-induced damage at appropriate points in time.

Key failure modes of the floor subsystem were identified in NIST NCSTAR 1-6C for components and subsystems subjected to temperature time histories. These analyses indicated that as floor system temperature increased, web diagonals in the floor trusses buckled, allowing the floors to sag. In extreme cases, the analyses showed loss of vertical support for individual trusses, as either the truss seats supporting the trusses lost strength and failed under the influence of vertical gravity loads or sagging of the trusses caused them to walk off the supporting seats.

This floor truss behavior was incorporated into the finite element models of entire individual floors that are referred to as full floor models. The models included representation of the floor slabs, trusses, beams, and columns that extended full height to the floors immediately above and below the level under

consideration. When an entire full floor model was subjected to the temperature time histories, the analyses showed that the floors sagged in areas where insulation was damaged and that individual floor trusses lost their vertical support at the exterior wall in some areas. However, it was found that these full floor models could not accurately capture the pull-in forces that the sagging floors were expected to apply to the exterior walls. Discussions on these pull-in forces can be found in Section 2.5.2.

Since detailed modeling of the floors was not included in the global analysis models, important floor behavioral modes could not be captured in these global analyses. Key floor behavioral modes include floor sagging that imposes pull-in forces on the exterior wall and loss of support of the trusses at the exterior wall resulting in local disconnection of the floor from the exterior wall. To account for these effects, pull-in forces on the exterior wall and disconnections of the floors from the wall were introduced in the global analyses at appropriate times as fire-induced damage. In the process of developing the fire-induced damage, the behaviors predicted by the full floor model analyses as well as the damage observed by NIST in their review of photographic and video evidence were both considered.

2.5 FIRE-INDUCED DAMAGE

Disconnections of the floors from the exterior walls caused by fire-induced connection failure between the floor and the exterior wall and pull-in forces on the exterior wall exerted by sagging floors were included in the global analyses as fire-induced damage. The locations of the floor/wall disconnections and the locations and magnitudes of the pull-in forces were determined based on a combination of the results from the full floor model analyses, the results from the isolated wall model analyses, and the actual observations in photographic and video evidence of WTC 1 and WTC 2.

2.5.1 Floor/Wall Disconnections

In areas where the connection of the floor to the exterior wall failed and the floor was locally disconnected from the exterior wall, the floor could no longer provide out-of-plane support for the wall at the locations of floor/wall disconnections, which resulted in a reduction of the buckling capacity of the exterior columns. In order to simulate this behavior in the global analyses, the connection between floor and wall elements was removed. When either one of the following conditions was encountered in the full floor analyses, the floor was disconnected from the exterior wall in the global model as it lost vertical support:

- Gusset plate failure + seat failure due to vertical shear
- Gusset plate failure + bolt shear-off + truss walk off the truss seat

Most disconnections obtained in the full floor models were due to the first of these conditions.

NIST performed extensive review of the available photographic and video evidence of the condition of the two towers prior to their collapse. Some of the photographs NIST reviewed were taken immediately after the aircraft impacts, while others were taken at various times leading up to the collapse. From this visual evidence, NIST constructed a time-variant map of the locations of observed floor/wall disconnections. During the global analyses, floor/wall disconnections were introduced at those locations and those times indicated in NIST's damage maps, if these disconnections had not previously been

indicated by the full-floor analyses. Although FEA results and the observations were generally in good agreement, the visual evidence suggested a somewhat greater extent of floor/wall disconnections.

2.5.2 Pull-in Forces

When the floor sagged while it was still connected to the exterior wall, the floor developed tensile forces that tended to pull the exterior wall inward. There were four types of structural elements that connected the floor system to the exterior wall system: 1) diagonal strap anchors that extended from the top chords of trusses to the spandrel (they are referred to as strap anchors in this report), 2) headed studs on the spandrels that extended into the floor slab edges, 3) gusset plates that were horizontal field-welded plates that joined the top chords of the trusses to the spandrels, and 4) seat bolts that fastened bearing angles to the seats that were attached to the spandrels.

Pull-in force was applied to the exterior column in the global analyses, where either one of the following conditions was encountered in the full floor analyses:

- Gusset plate failure + bolt shear-off + significant deflection (>25 in.) of the floor slab in that area (floor remains vertically connected)
- Tensile force between the exterior wall and the floor system

However, locations and magnitudes of pull-in forces were not accurately simulated by the full floor models for the following reasons:

- The full floor models did not and could not have an accurate set of boundary conditions on the columns. Columns extended from one floor below to one floor above, and the top and bottom of exterior columns were restrained in the direction normal to the exterior wall. These boundary conditions could not accurately portray the thermally-induced movements of floors above and below the floor being analyzed and could not accurately capture the stiffness of columns in the exterior walls. Photographs of the towers taken before collapse indicated that the exterior walls bowed inward over a height of several floors. Bowing of exterior columns as observed could not be captured in the floor model because the boundary condition of a full floor model could not be formulated to represent the observed bowing of the exterior wall over several floors.
- In the actual buildings, the strap anchors and studs must have been capable of transmitting a significant amount of force between the floor system and exterior wall. However, the full floor analysis with the strap anchors and studs resulted in sequential failure of these components and an extremely slow convergence in the analyses. Because these components were found to fail at early stages of fire, these elements were then removed from all the full floor models to obtain solution within a reasonable period of time. Therefore, in these analyses, the only structural elements in the full floor model that could transfer horizontal interface forces between the floor system and the exterior walls were the gusset plates and seat bolts. This caused premature failure of the gusset plates and seat bolts in the analyses, which resulted in horizontal floor/wall disconnections. In addition, friction between bearing angles and seats was not modeled in the full floor analyses. Therefore, the full-floor model did not show significant tension at the floor/exterior wall interface. In the real structures,

tension forces could develop between the floor system and walls following failure of the gusset plates and seat bolts through the mechanism of friction between the truss seats and bearing angles and through the strap anchors that had not failed.

- There is considerable uncertainty as to what the actual capacity of the strap anchor system was to transfer pull-in forces from the floors to the walls. Assuming that the strap anchors were installed as shown on the PANYNJ drawings, with only the minimum length and size of welds specified actually installed, the tensile capacity of the strap anchor system was controlled by the strength of weld at the strap anchors to the truss the top chords. Typically, 5/16 in., 4 in long fillet welds were specified for this joint. For a pair of floor trusses, joined to the wall by a pair of diagonal strap anchors, this translates into a computed tensile capacity of 68 kip at room temperature and 6.6 kip at 800 °C. In full floor model analyses that incorporated the strap anchors, these capacities were used. However, if longer welds were provided, say in excess of 6 in., or somewhat larger fillets were actually placed, the ultimate tensile strength of the strap anchor (1-1/2 in. x 5/8 in. flat plate) could have controlled the capacity of this system. In such a case, the strap anchors for a pair of floor trusses could develop a 101 kip tension force at room temperature and a 9.8 kip tension force at 800 °C.
- Assuming a coefficient of friction of 0.33 and vertical reaction at an exterior seat of 13 kip, the friction force can be as much as 4.3 kip for a pair of trusses. The capacity of the two 5/8 in.-diameter seat bolts present in each pair of trusses in shear is 44 kip at room temperature and 4.0 kip at 800 °C. Therefore, at elevated temperature, the combined action of friction and bolts could develop on the order of an 8 kip tension force at the exterior seat.
- Creep at high temperature was found to significantly increase the sag of a floor system. A thermal response analysis of a simplified truss model removed from the full floor model showed a significant increase in vertical deflection when creep was considered, as shown in Fig. 2–27. However, full floor models were made with BEAM188/189 element types and were not run with creep due to inherent convergence problems of BEAM188/189 when used under thermal loadings with materials having temperature-dependent creep property.
- In the full floor models, crushing or cracking of the concrete slab was neglected. Extreme temperatures can crack and spall concrete, further reducing the floor stiffness, and increasing both the floor sag and the floor/wall pull-in forces.
- NIST may have underestimated the amount of thermal insulation that was damaged by the aircraft impacts. The estimates developed by NIST were limited to the insulation on sections of framing that were exposed to direct abrasion by the debris field, predicted in the impact analyses. Potential loss of insulation due to impact shock and vibration effects was not included. More severe insulation damage would have resulted in higher temperatures of the trusses than those used in the full floor analyses. This in turn would result in larger areas in which the floors would have sagged.

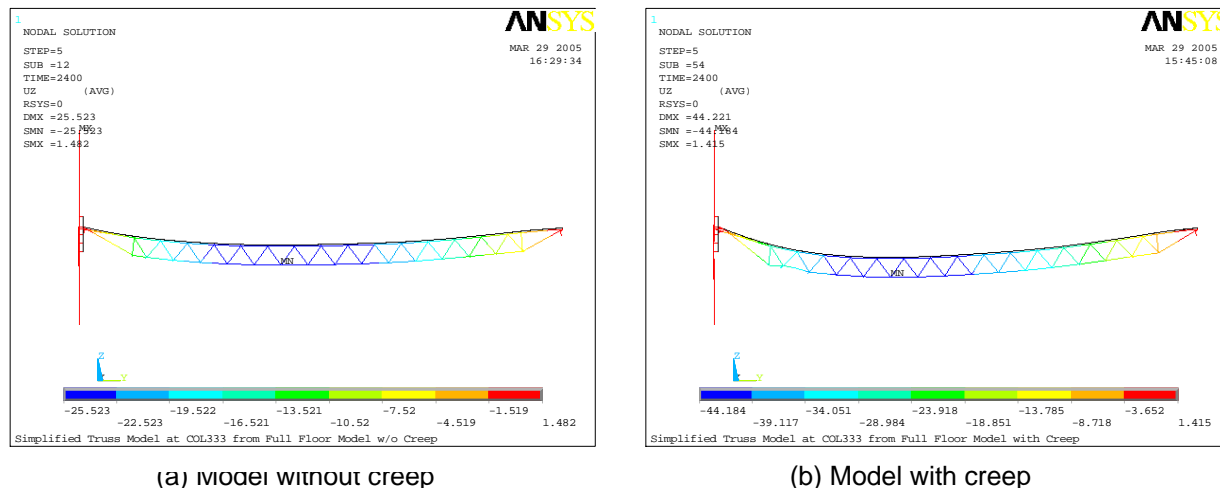


Figure 2–27. Comparison of vertical displacement of a simplified truss model at Column 333 extracted from the full floor model of Floor 96 of WTC 1 for Case B_i temperature condition at 40 min with and without creep.

Given these uncertainties and inaccuracies in the evaluation of the likely magnitude and location of pull-in forces on the exterior wall, in the global analyses, pull-in forces were applied in some locations where the full floor analyses did not predict the development of such behavior. The magnitude and location of pull-in forces were selected by trial and error to produce a computed bowing of the exterior walls that matched that observed in the photographic and video evidence, as discussed in Chapter 3.

In the actual buildings, floor attachment to the exterior wall occurred continuously along the length of the wall. Headed studs were spaced uniformly along the length of the wall. Pairs of trusses, with truss seats and gusset plates were present at alternate column locations, and diagonal strap anchors connected to the columns between those supporting trusses. Therefore, pull-in forces were applied to columns attached to trusses as well as those attached to strap anchors.

2.5.3 Floor/Wall Disconnections and Pull-in Forces Included in the Global Model

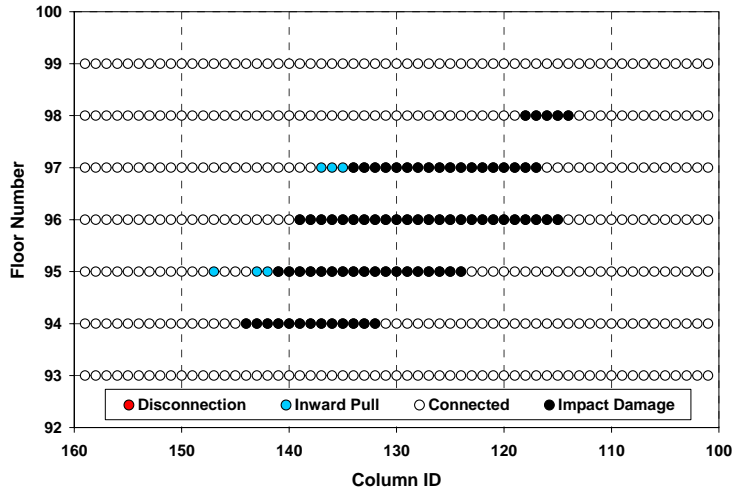
In the global models, nodal couplings tied the exterior columns to the floors. The nodal couplings were removed at locations of floor/wall disconnections. If disconnections were projected to occur or were observed in visual evidence at a time intermediate to the 10 min intervals used in the analyses, for example, between 10 min and 20 min, they were imposed starting at the earlier time point, in this example, at 10 min. Once a portion of a floor was disconnected from the exterior wall, it remained disconnected for the remainder of the analysis. Similarly, pull-in forces were also applied to the global models at the beginning of the 10 min time intervals in which they were predicted to occur or were observed, and they were maintained at a constant level for the 10 min time interval.

Outward expansion of the floors was not included in the global models. Floor analyses showed that the floors initially pushed exterior column outward by a few inches. However, significant outward bowing was not observed and several inches of outward deflection of exterior columns would not affect the global stability of the towers.

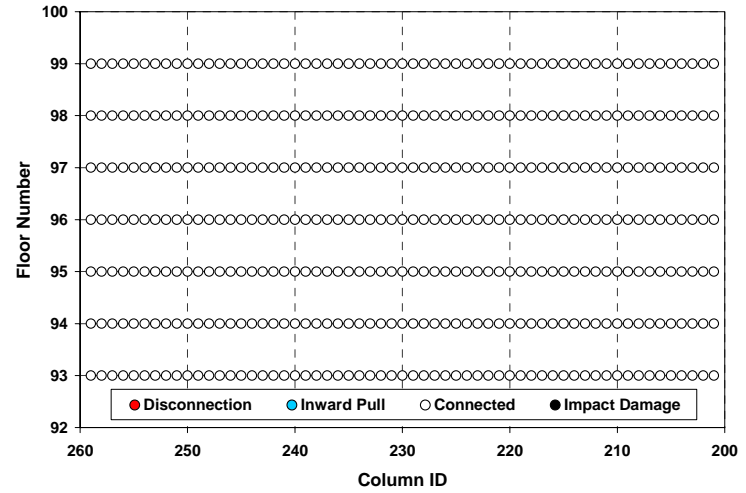
WTC 1

Figures 2–28 to 2–37 show the locations of floor/wall disconnections and pull-in forces imposed on the WTC 1 global model for Case B conditions. Each figure covers a 10 min time interval, the first initiating at 0 min, when the initial impact occurred, and the last initiating at 90 min. Until 80 min, the locations of floor/wall disconnections and pull-in forces were determined solely on the basis of full floor model analyses. After 80 min, the observations from the photographic and video evidence were also considered in determining these events to capture floor/wall disconnections and pull-in locations that were not evident in the full floor analyses. Section 3.2.1 discusses the process used to incorporate the actual observations.

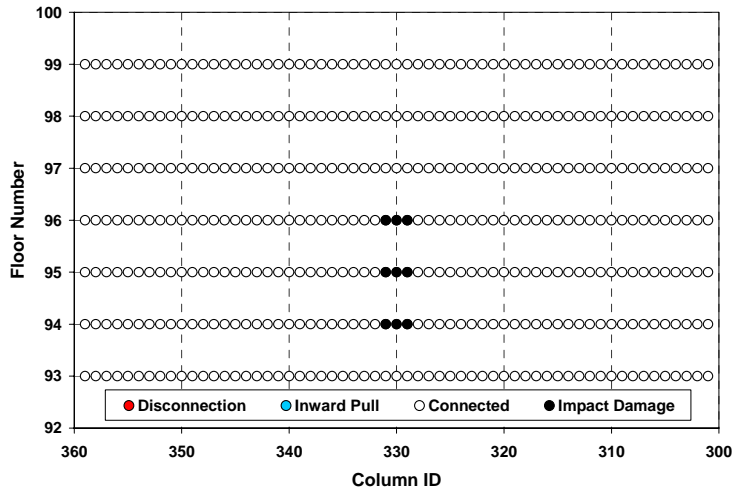
As is discussed in Chapter 5, inward bowing of the exterior south wall of WTC 1 was actually observed at 10:23 a.m., about 97 min after the aircraft impact (NIST NCSTAR 1-6), while inward bowing of the south wall was not observed in photos or videos at 9:55 a.m. (about 69 min after the aircraft impact). The observed inward bowing extended from Floors 95 to 99 between Columns 308 to 326 (possibly to 340), and the maximum bowing estimated by NIST from photographs was about 55 in. at Floor 97. Subsystem analyses of the full floors and the exterior walls suggested that this observed bowing of the south wall was caused by sagging of the floors. As the floors sagged, they imposed tension force on the exterior wall, and the exterior wall was pulled in. However, sagging of floors in such a wide range over five floors was not predicted by the full floor model analyses. Possible reasons for floor sagging in areas not predicted by the full floor analyses include loss of insulation outside of the areas considered by NIST when formulating the temperature time histories, the additional structural softening caused by concrete cracking and spalling, and debris weight from different sources including the aircraft, accumulation of debris from the impact, and partial floor collapse, none of which were modeled in the full floor analyses. To match the observations, the south wall was assumed to be pulled in by the floors between Floor 95 and Floor 99 across the entire width of the wall except at locations of floor/wall disconnections, starting at 80 min. The magnitude of the pull-in force was determined, by trial and error, by matching the observed bowing magnitude as discussed in Section 3.2.1. The pull-in forces were selected as 4 or 5 kip per column. Results from the analysis with 5 kip pull-in forces are presented in Chapter 4.



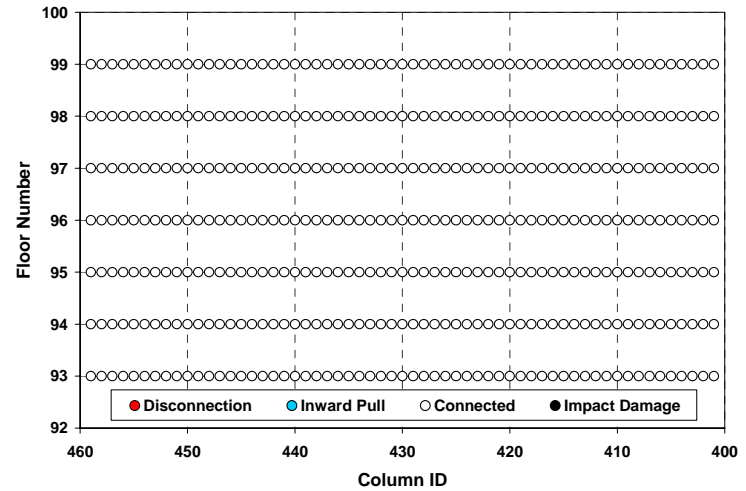
(a) North face



(b) East face

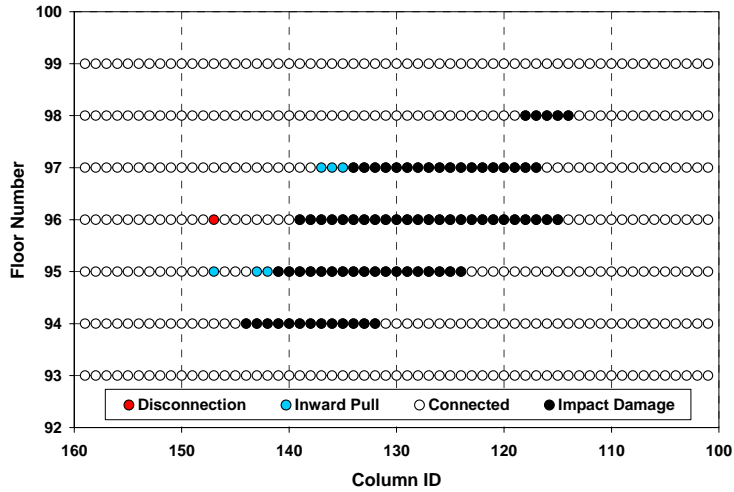


(c) South face

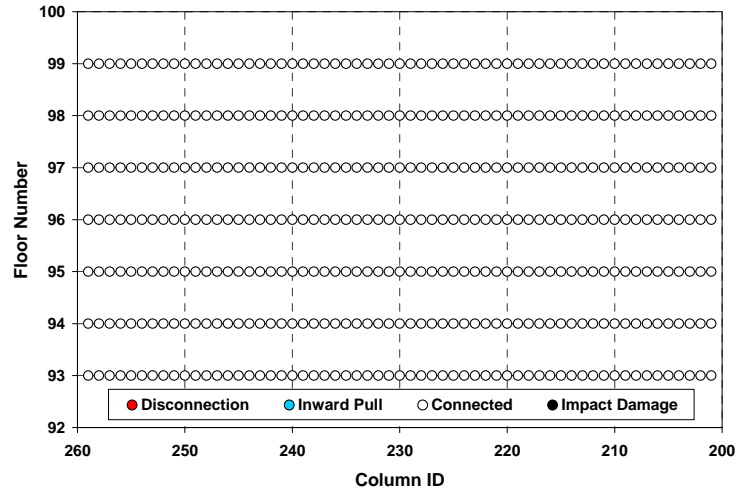


(d) West face

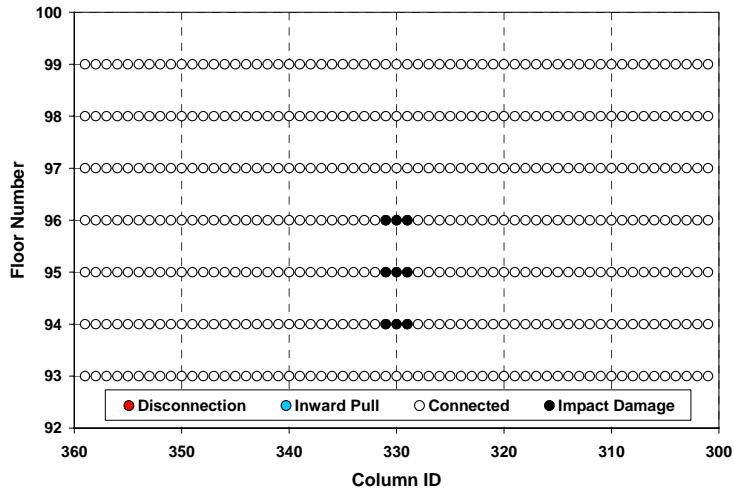
Figure 2–28. Locations of floor/wall disconnections and pull-in forces for the global analysis of WTC 1 between 0 min and 10 min for Case B conditions.



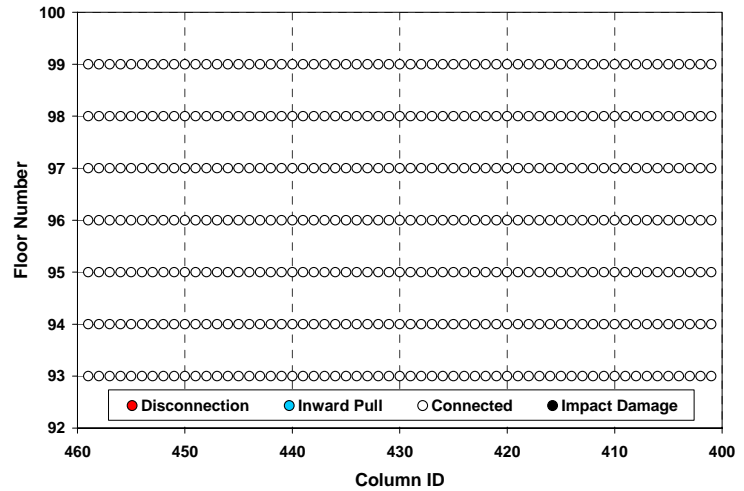
(a) North face



(b) East face

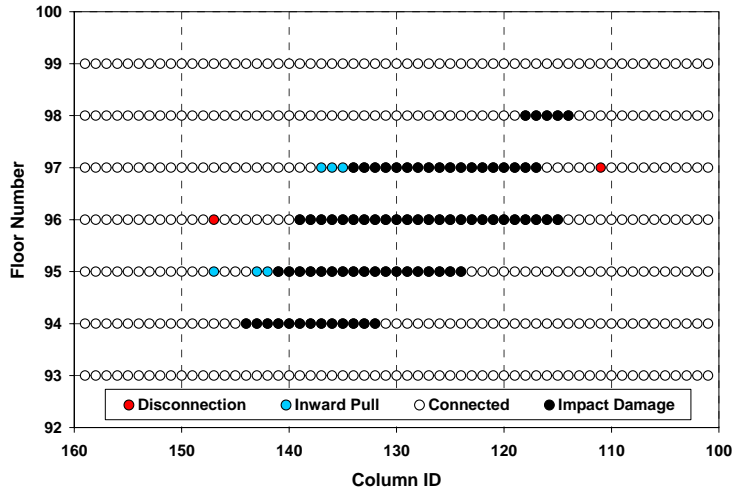


(c) South face

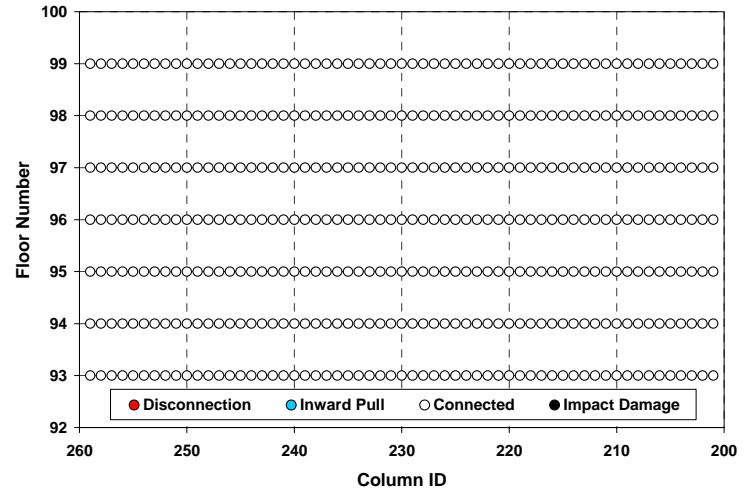


(d) West face

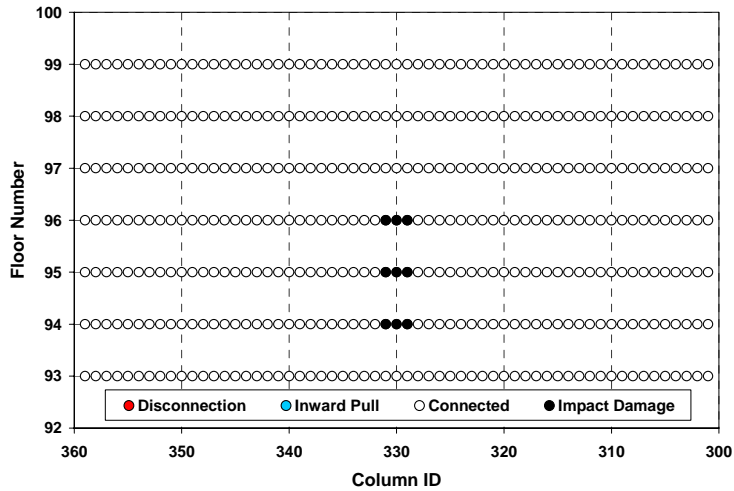
Figure 2–29. Locations of floor/wall disconnections and pull-in forces for the global analysis of WTC 1 between 10 min and 20 min for Case B conditions.



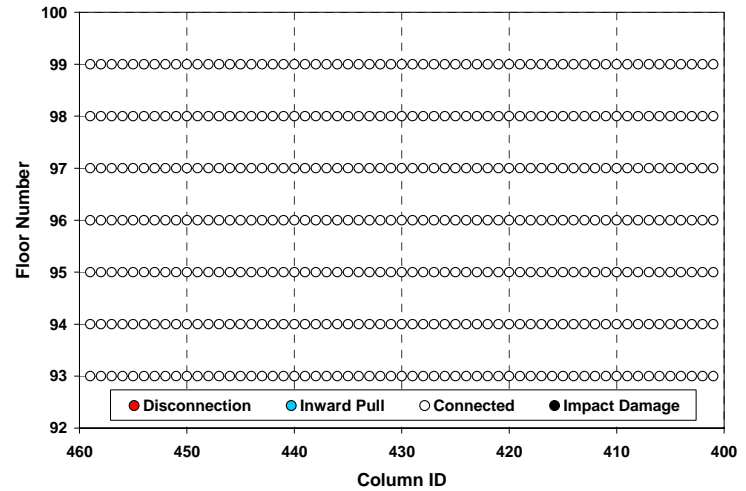
(a) North face



(b) East face

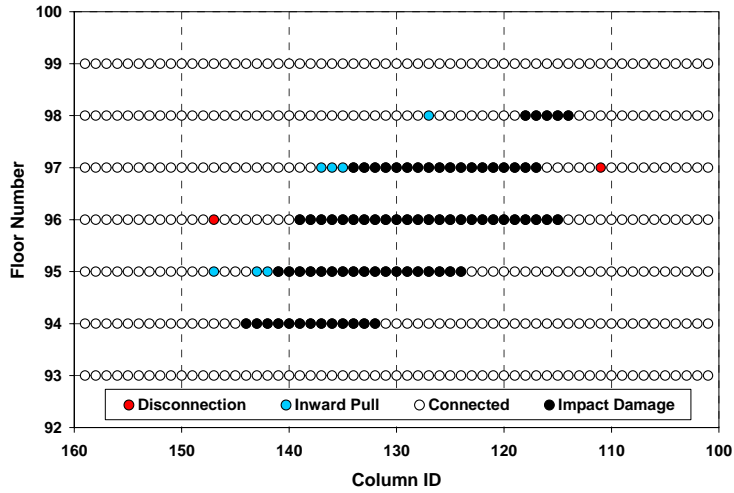


(c) South face

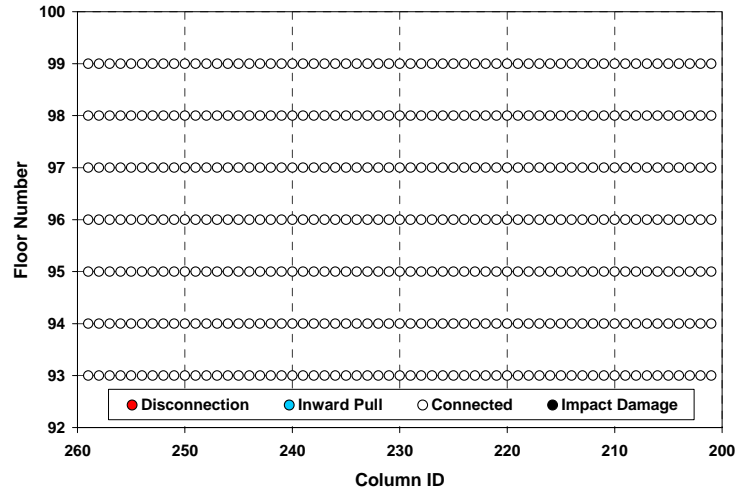


(d) West face

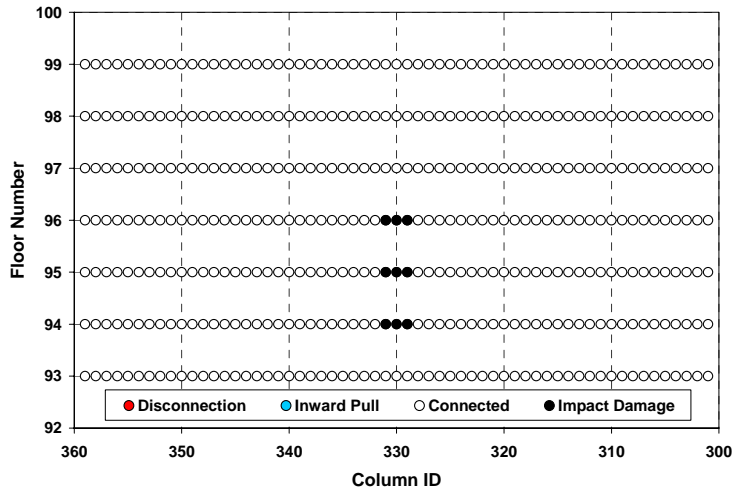
Figure 2–30. Locations of floor/wall disconnections and pull-in forces for the global analysis of WTC 1 between 20 min and 30 min for Case B conditions.



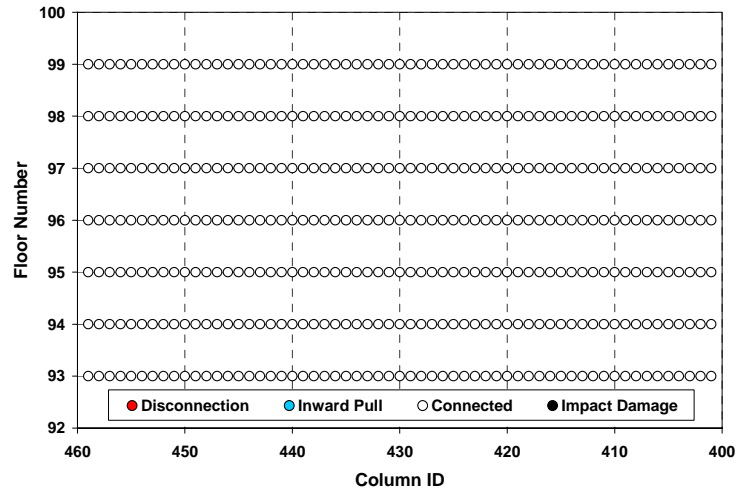
(a) North face



(b) East face

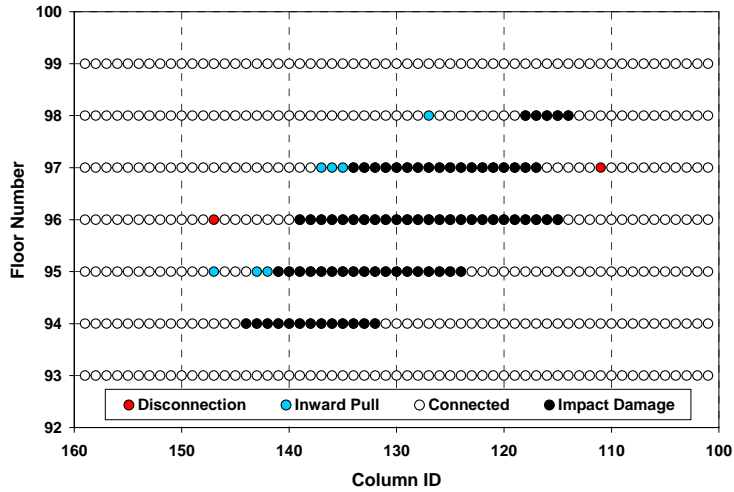


(c) South face

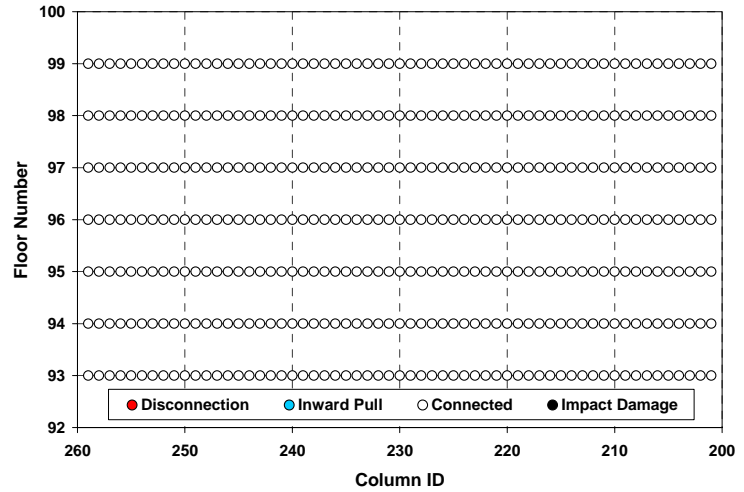


(d) West face

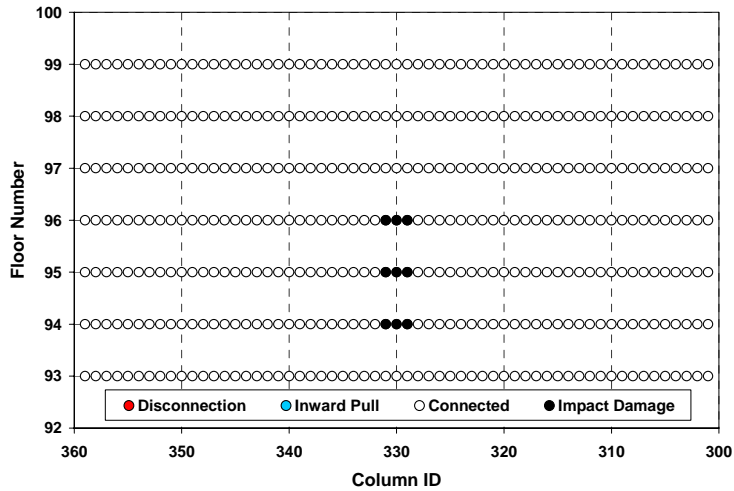
Figure 2–31. Locations of floor/wall disconnections and pull-in forces for the global analysis of WTC 1 between 30 min and 40 min for Case B conditions.



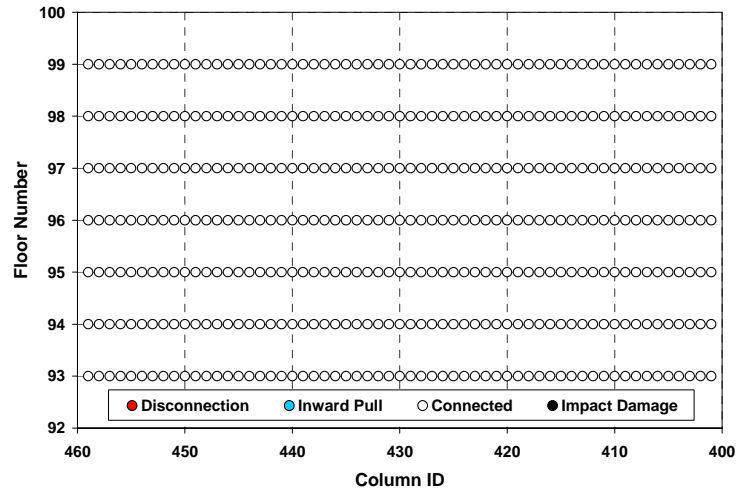
(a) North face



(b) East face

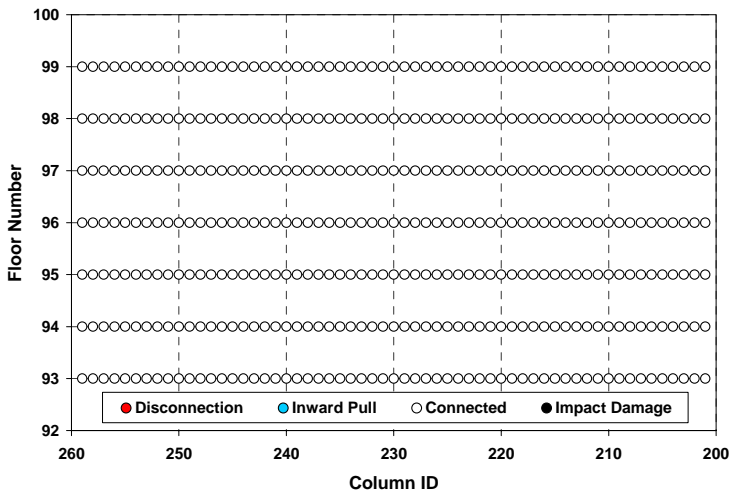


(c) South face

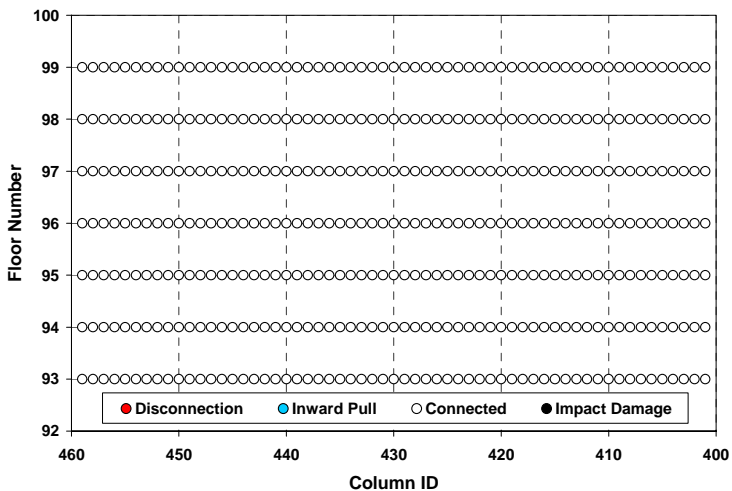


(d) West face

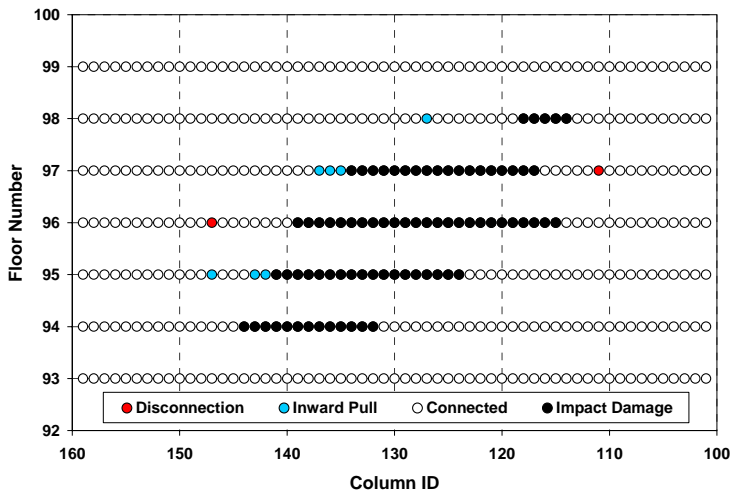
Figure 2-32. Locations of floor/wall disconnections and pull-in forces for the global analysis of WTC 1 between 40 min and 50 min for Case B conditions.



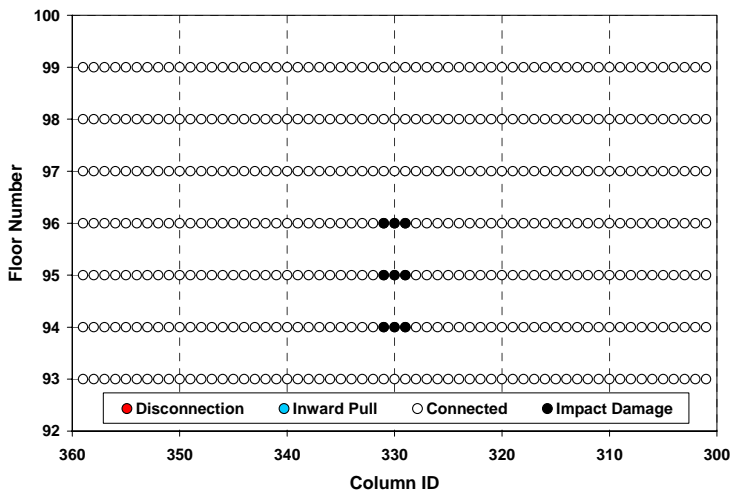
(b) East face



(d) West face

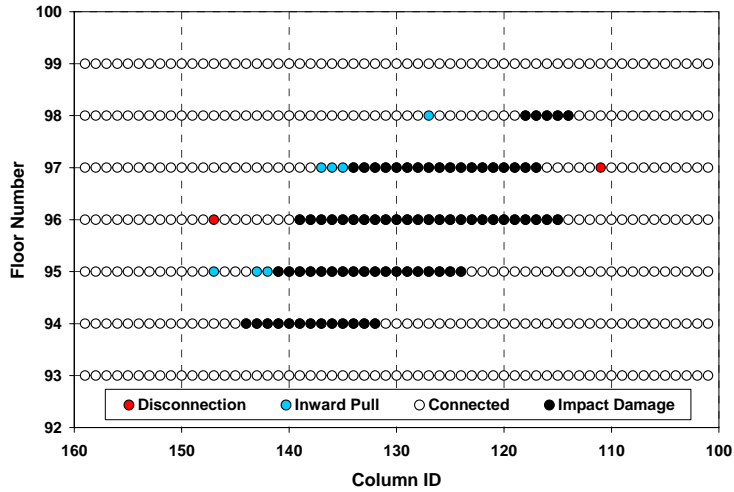


(a) North face

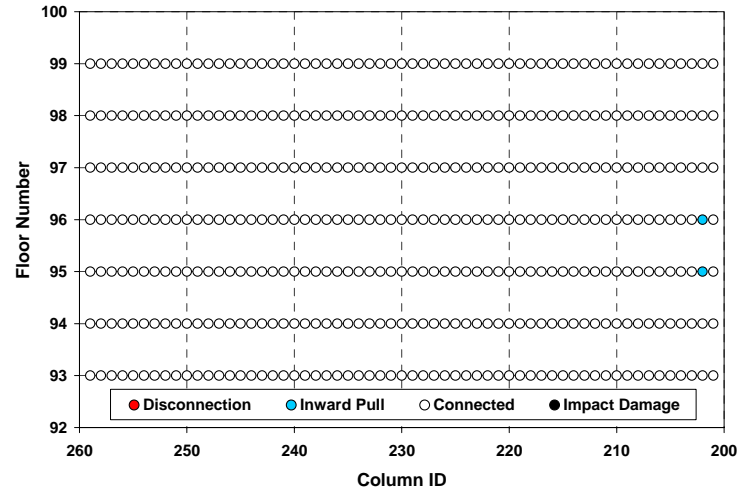


(c) South face

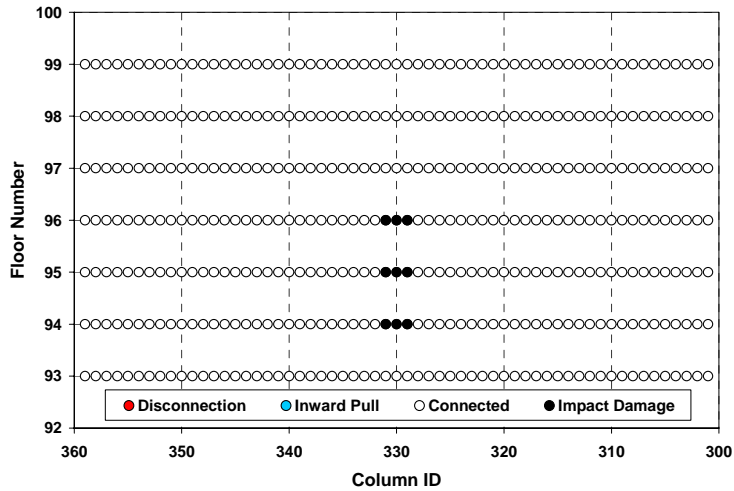
Figure 2–33. Locations of floor/wall disconnections and pull-in forces for the global analysis of WTC 1 between 50 min and 60 min for Case B conditions.



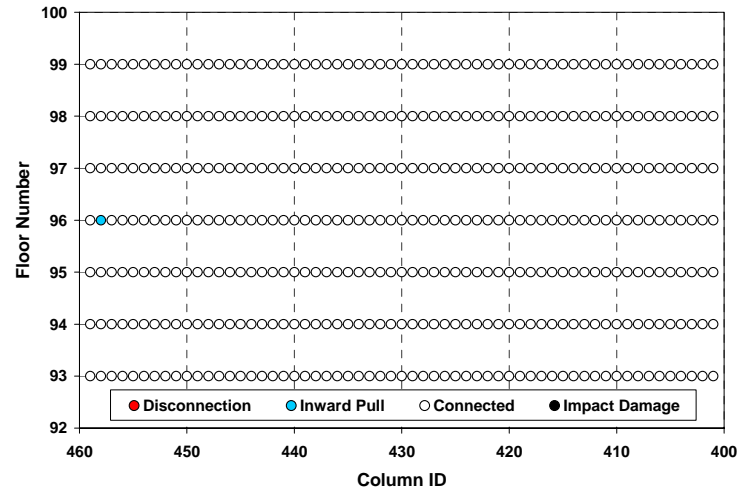
(a) North face



(b) East face

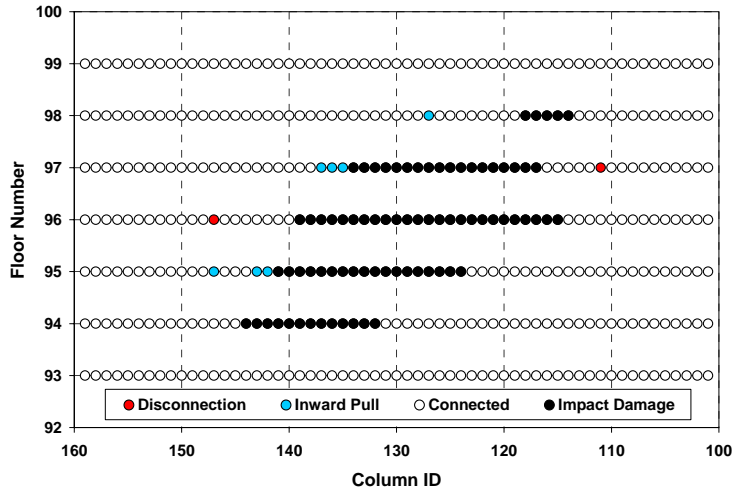


(c) South face

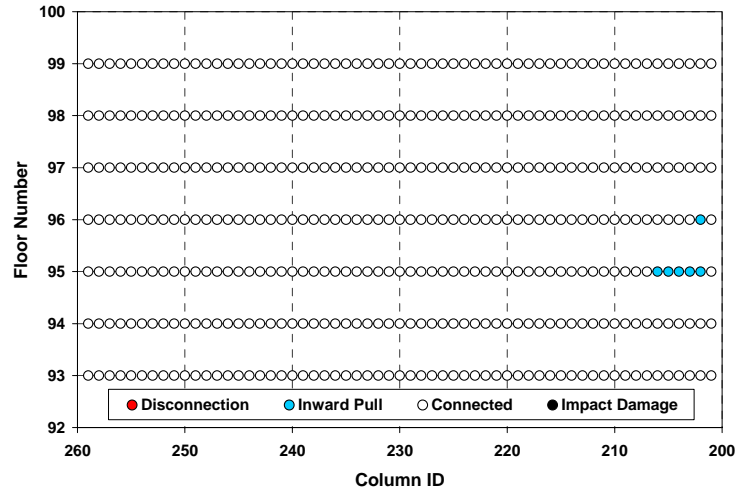


(d) West face

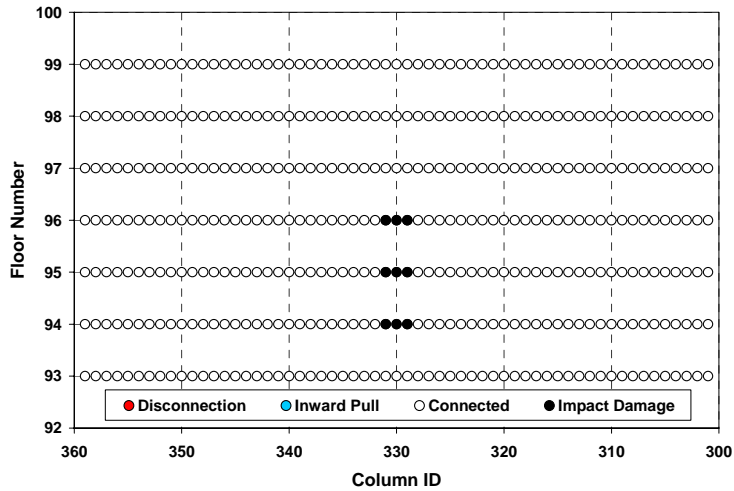
Figure 2–34. Locations of floor/wall disconnections and pull-in forces for the global analysis of WTC 1 between 60 min and 70 min for Case B conditions.



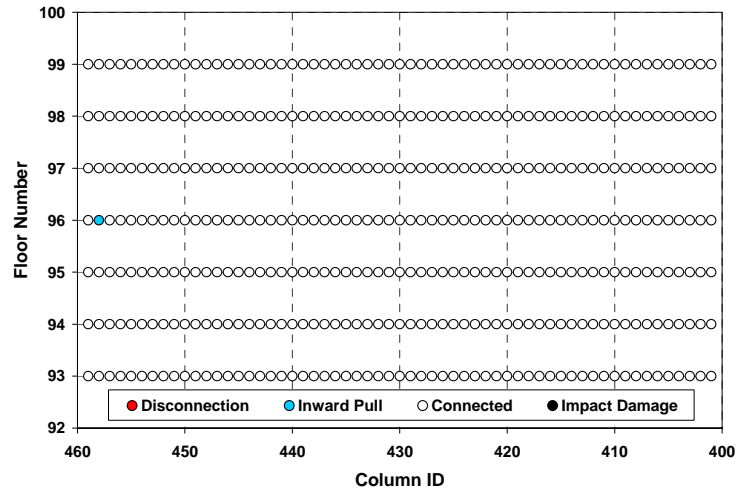
(a) North face



(b) East face

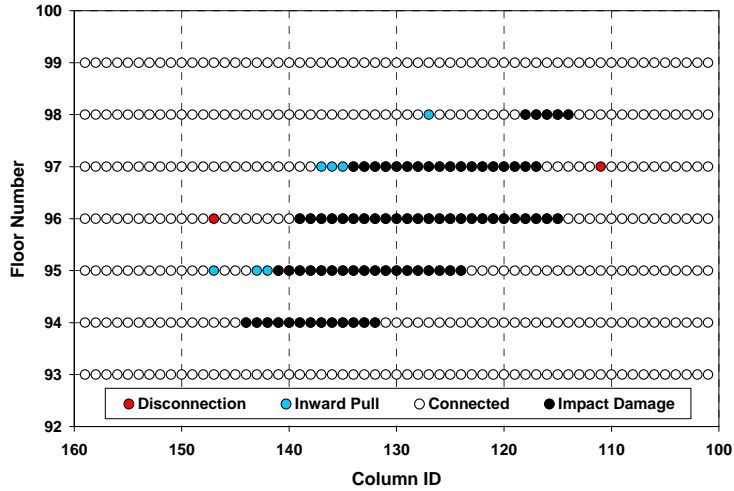


(c) South face

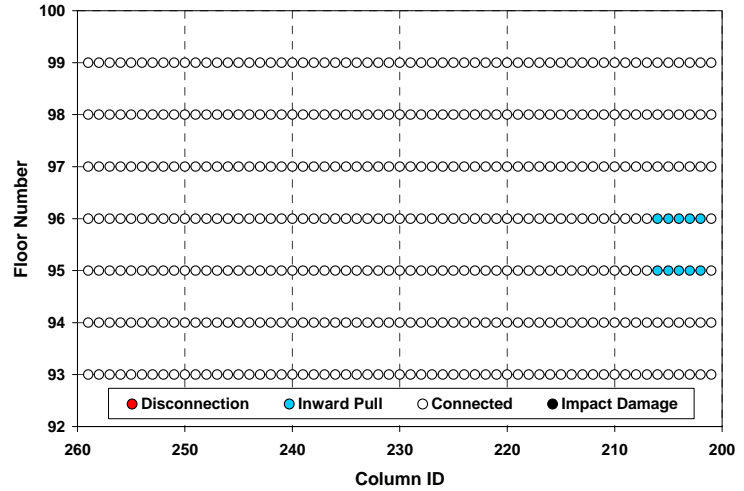


(d) West face

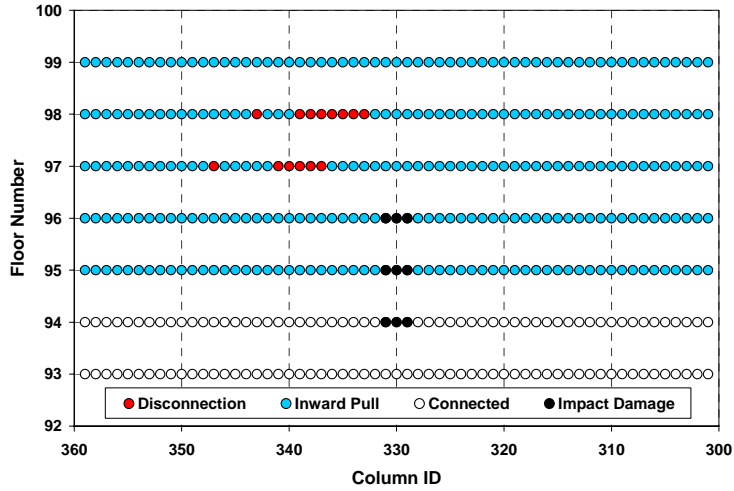
Figure 2–35. Locations of floor/wall disconnections and pull-in forces for the global analysis of WTC 1 between 70 min and 80 min for Case B conditions.



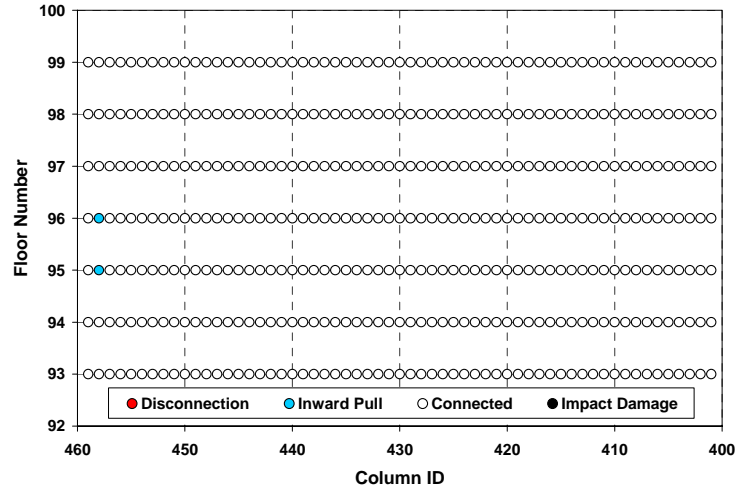
(a) North face



(b) East face

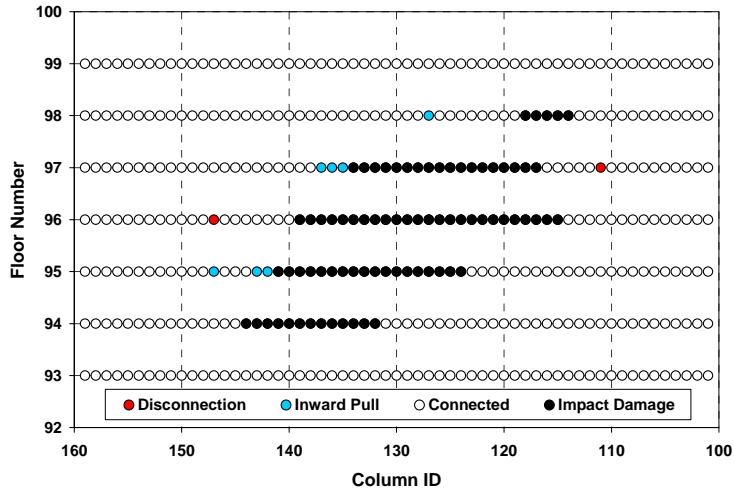


(c) South face

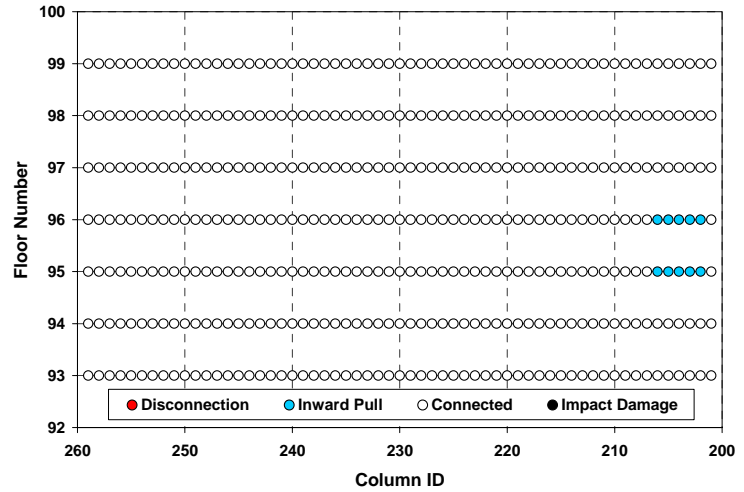


(d) West face

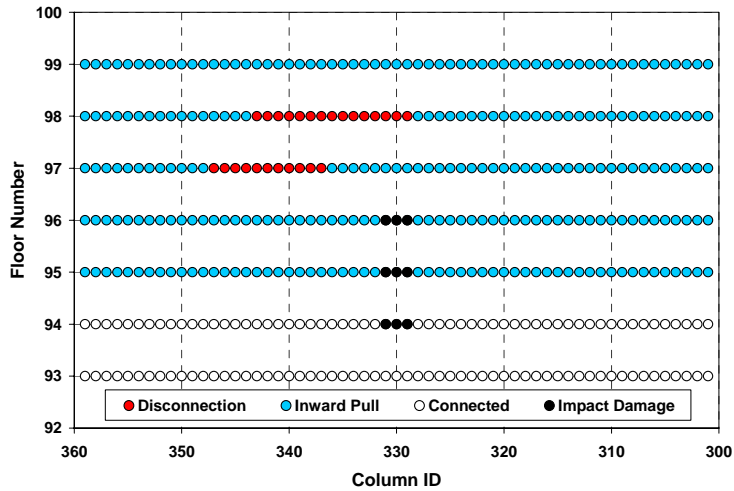
Figure 2-36. Locations of floor/wall disconnections and pull-in forces for the global analysis of WTC 1 between 80 min and 90 min for Case B conditions.



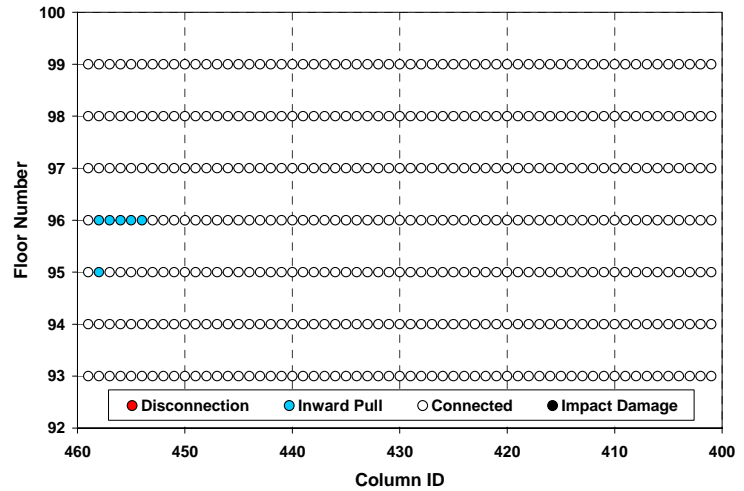
(a) North face



(b) East face



(c) South face



(d) West face

Figure 2-37. Locations of floor/wall disconnections and pull-in forces for the global analysis of WTC 1 between 90 min and 100 min for Case B conditions.

WTC 2

Figures 2–38 to 2–43 show the locations of floor/wall disconnections and pull-in forces imposed on the WTC 2 global model for Case D conditions. Each figure covers a 10 min time interval, the first initiating at 0 min, when the initial impact occurred, and the last initiating at 50 min.

In determining the locations of floor/wall disconnections from the full floor models, the results of Case C_i and Case D_i temperature conditions were considered jointly for the uncertainties in truss seat temperatures. This uncertainty is illustrated in Tables 2–2 and 2–3. Table 2–2 compares the temperature predicted for the exterior truss seats at selected columns of the east wall at Floor 82 at times of 30 min, 40 min, 50 min, and 60 min. Table 2–3 shows demand-to-capacity ratios for vertical support of these same exterior seats. Temperatures of the exterior seats at the east wall of Floor 82 rapidly dropped after 40 min in Case D_i; whereas, in Case C_i they continued to increase with time. Due to this difference, the truss seats that were very close to failure (such as the seat at Column 303) at 40 min of Case D_i did not fail at 50 min in the full floor analysis. If high temperatures had continued for a few more minutes for Case D_i, these seats would have failed. The actual temperature time history may not have descended rapidly between 40 min and 50 min, as is deduced from the consideration of piecewise linear temperature time history in this study.

The state of the floor/wall connections in the full floor analysis were reevaluated considering the effects of uncertainties in the seat capacities by comparing the demands to the seat capacities that were 10 percent lower than the calculated seat capacities. As a result of this comparison, the seats adjacent to the already disconnected seats at Floors 82 and 83 were found to be progressively failing, and the extent of floor/wall disconnection was extended to nearly the entire width of the east wall. These worst-case floor/wall disconnections were included in the floor/wall disconnections for Case D conditions in the global analysis.

Table 2–2. Temperatures of exterior seats at east wall of Floor 82 of WTC 2.

Column ID	Case C _i Temperatures (°C)				Case D _i Temperatures (°C)			
	30 min	40 min	50 min	60 min	30 min	40 min	50 min	60 min
301	763	788	811	813	818	819	507	345
303	752	774	809	808	822	820	509	348
305	750	769	807	804	823	821	513	348
307	750	769	804	799	823	821	511	342
309	727	748	787	790	822	816	485	334
311	677	698	738	758	816	804	458	328
313	636	657	700	724	809	803	487	342
315	591	605	632	662	816	794	481	347
317	574	580	615	637	815	799	494	351

Table 2–3. Demand-to-capacity ratios of exterior seats at east wall of Floor 82 of WTC 2 predicted by the full floor model.

Column ID	Case C _i Temperatures (°C)				Case D _i Temperatures (°C)			
	30 min	40 min	50 min	60 min	30 min	40 min	50 min	60 min
301	0.35	0.31	failed	failed	0.63	0.54	0.02	0.08
303	0.66	0.81	failed	failed	0.92	0.97	0.18	0.14
305	0.39	0.53	failed	failed	0.63	0.70	0.20	0.19
307	0.41	0.51	failed	failed	0.59	0.60	0.15	0.13
309	0.35	0.43	failed	failed	0.60	0.60	0.13	0.13
311	0.38	0.46	failed	failed	0.87	0.71	0.09	0.05
313	0.23	0.27	failed	failed	0.64	0.48	0.10	0.09
315	0.20	0.24	failed	failed	0.49	0.41	0.08	0.09
317	0.10	0.09	0.96	failed	0.45	0.50	0.14	0.13

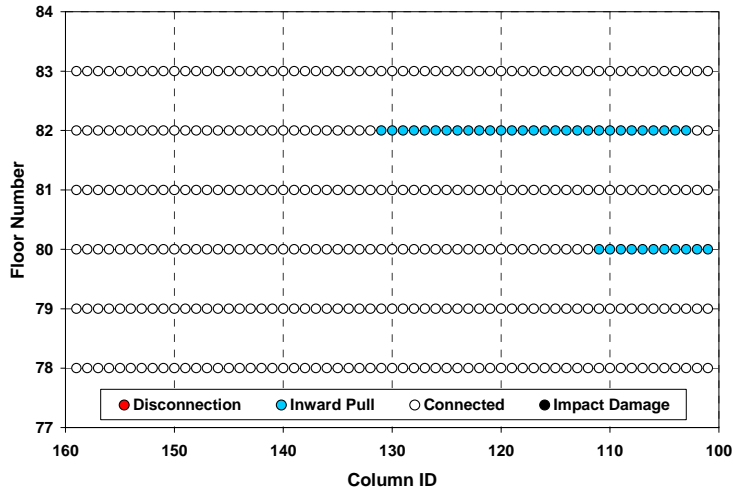
In addition to the reevaluation of the seat capacities, the location of floor/wall disconnections estimated from full floor analyses were compared and were updated based on the floor/wall disconnections observed in the photographs and videos. Observed floor/wall disconnections were provided for the east wall at 9:03 a.m., 9:38 a.m., and 9:55 a.m. and for the north wall at 9:10 a.m., 9:14 a.m., and 9:58 a.m. All observed floor/wall disconnections were included in the global analysis for Case D conditions at appropriate points in time, whether predicted by the full floor analyses or not.

As previously described above for the case of WTC 1, the photographic and video evidence was also reviewed by NIST to determine the extent of inward bowing of the east wall of WTC 2. These displacement measurements were used to update the location and the magnitude of the pull-in forces applied to the global model. The earliest observations of inward bowing for WTC 2 were made at 9:21 a.m., 18 min after impact (NIST NCSTAR 1-6), when the east wall was observed to be bowing inward between Column 301 and Column 345 between Floor 78 and Floor 83. At this time, NIST estimated the maximum inward deformation to be about 10 in. at Floors 80 and 81 between Column 322 and Column 329. To replicate this inward bowing, pull-in forces were applied at Floors 79, 80, 81, and 82. The full floor analyses correctly predicted the floors that were pulled in, but underestimated the location of the pull-in forces across the width of the east wall, relative to that required to replicate the observed bowing. The locations of pull-in forces predicted by the full-floor analyses were concentrated toward the south side of the east wall and typically ranged between Columns 329 and 359 at Floor 82 and between Columns 357 and 359 at Floor 79. The locations of pull-in forces estimated from the observation were used to augment those obtained from the full floor analyses. Based on this augmented data, at 20 min after impact, pull-in forces were applied over the entire width of the east wall at Floors 79, 80, 81, and 82 in the global analysis.

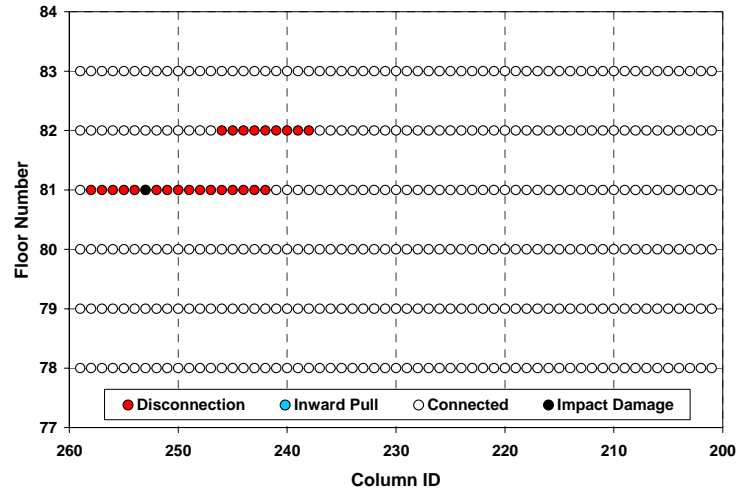
The photographic and video evidence, obtained at 9:53 a.m., about 50 min after impact (NIST NCSTAR 1-6), show the east wall bowing inward from Column 301 to Column 353 between Floor 77 and Floor 84. At this instant, NIST estimated the maximum inward deformation to be about 15 in. to 20 in. at Floor 81 between Column 320 and Column 330. To replicate this observed bowing geometry, a combination of pull-in forces and floor/wall disconnections were applied between Floor 77 and Floor 84. Except for Floor 78, which was not analyzed using a full floor model, the full floor analyses correctly predicted the floor levels at which the exterior wall was observed to be pulled in, but underestimated the locations of pull-in forces. The locations of the pull-in forces estimated from the full floor analyses were

concentrated toward the south side of the east wall and typically ranged between Column 333 and Column 359 at Floor 81 and between Column 355 and Column 359 at Floor 79. Based on the full floor analyses and the reevaluated seat capacities, Floor 83 was disconnected from the east wall between Column 302 and Column 357, and Floor 82 was disconnected between Column 301 and Column 349. For this reason, no pull-in forces were applied at these column locations. The locations of the pull-in forces estimated from the observations at 50 min were used to augment those estimated from the full floor analyses. As a result of this addition, at 50 min after impact, pull-in forces were applied over the entire width of the east wall at Floors 78, 79, 80, and 81, and between Column 350 and Column 359 at Floor 82.

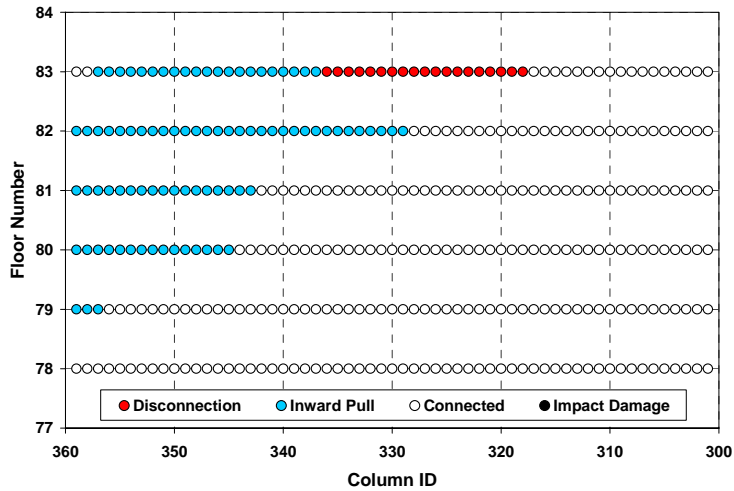
As is discussed in Section 3.2.2, the magnitude of the pull-in force was estimated through a trial and error process by applying different levels of pull-in forces to the isolated wall models and by comparing the resulting inward bowing to that estimated from observations at 9:21 a.m. and 9:53 a.m. From these comparative analyses, the magnitude of pull-in forces were determined to range from 1.0 to 2.0 kip on the south side of the east wall and 4.0 to 5.0 kip on the north side of the east wall. It was necessary to apply larger pull-in forces on the north side than on the south side of the east wall because column temperatures on the north side were higher than the column temperatures on the south side of the east wall. Higher temperatures resulted in more outward bowing of columns, and thus larger pull-in forces were required to overcome this outward bowing.



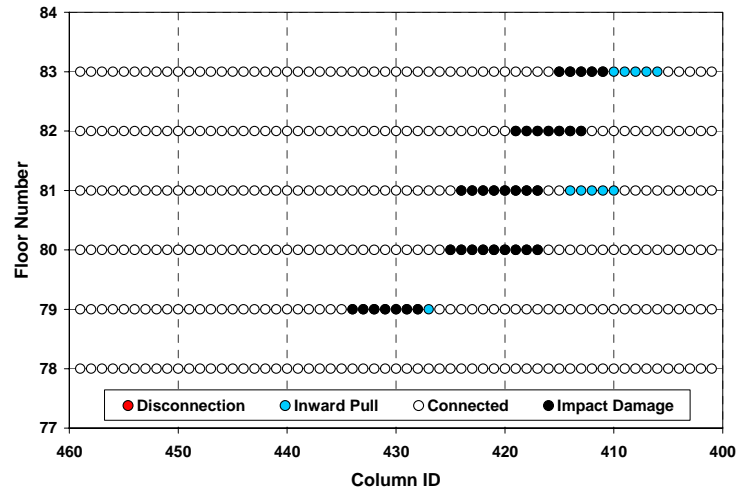
(a) West face



(b) North face

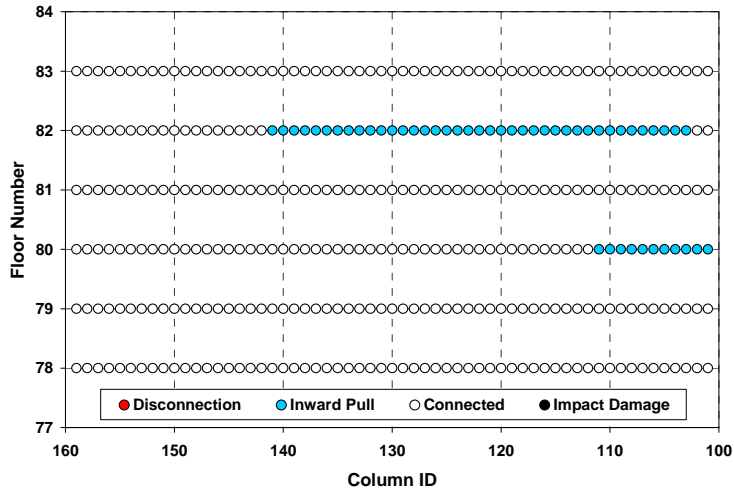


(c) East face

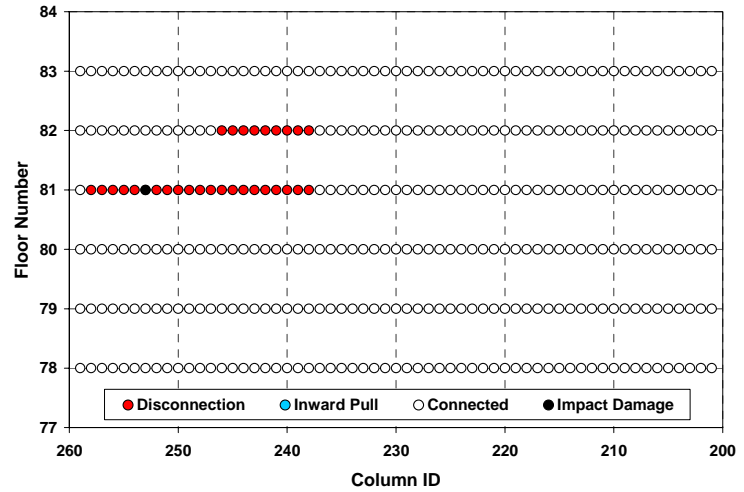


(d) South face

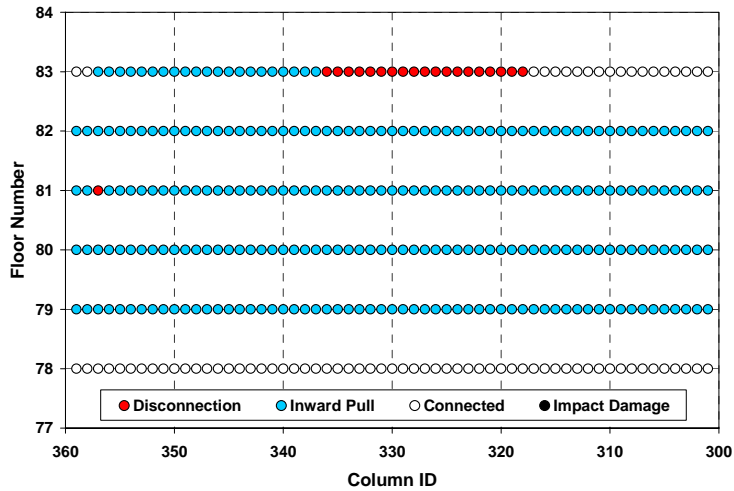
Figure 2-38. Locations of floor/wall disconnections and pull-in forces for the global analysis of WTC 2 between 0 min and 10 min for Case D conditions.



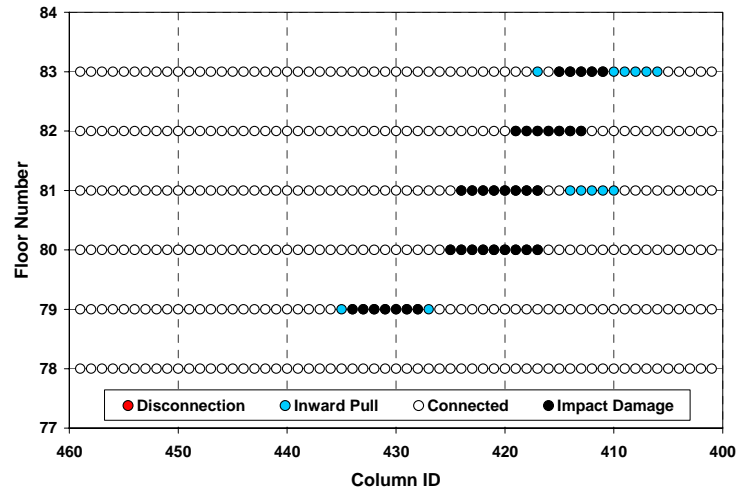
(a) West face



(b) North face

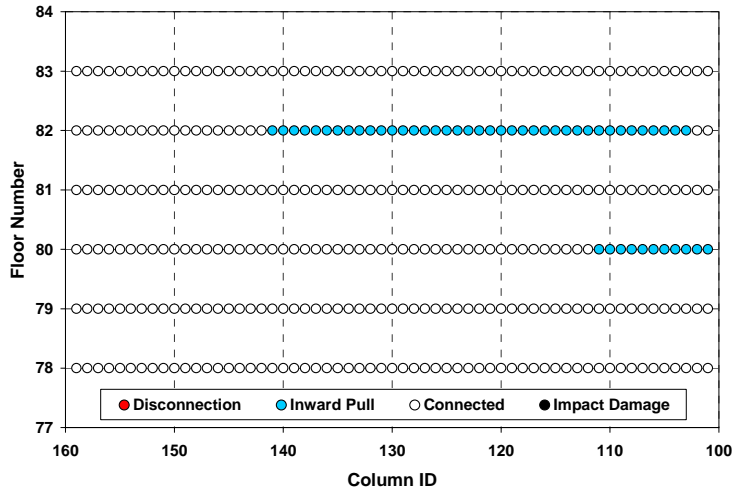


(c) East face

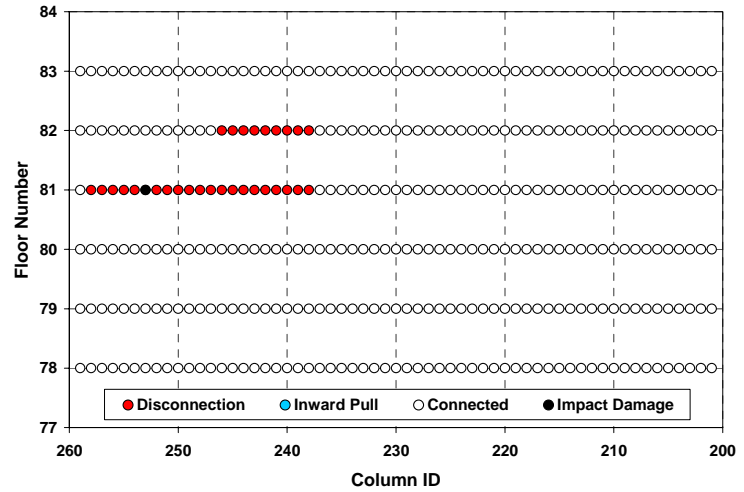


(d) South face

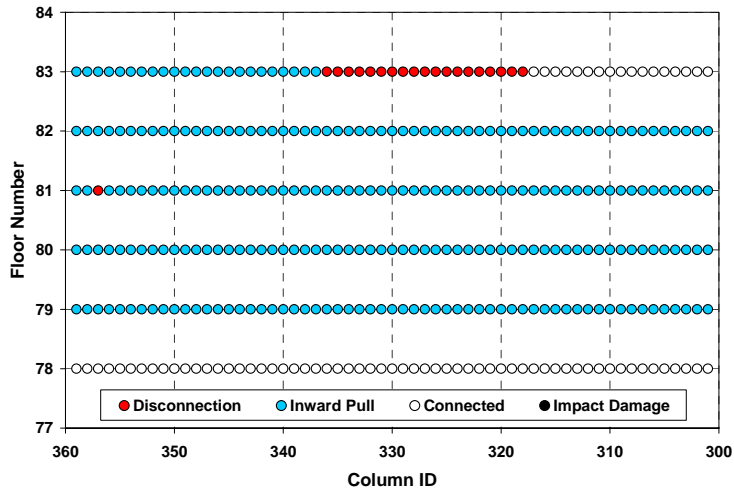
Figure 2-39. Locations of floor/wall disconnections and pull-in forces for the global analysis of WTC 2 between 10 min and 20 min for Case D conditions.



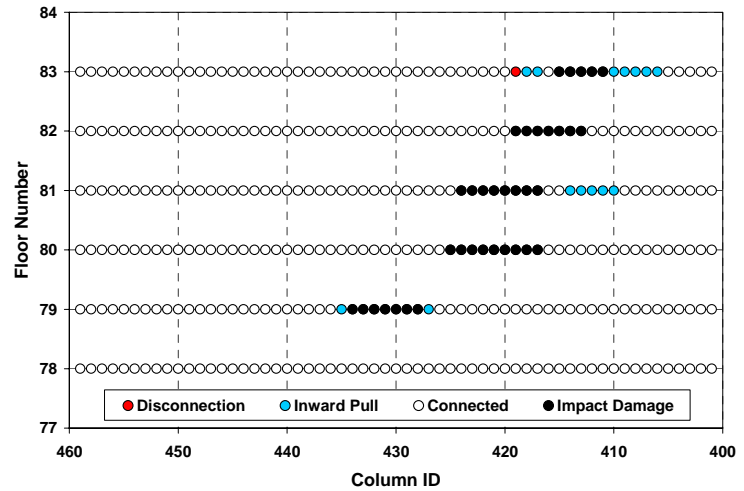
(a) West face



(b) North face

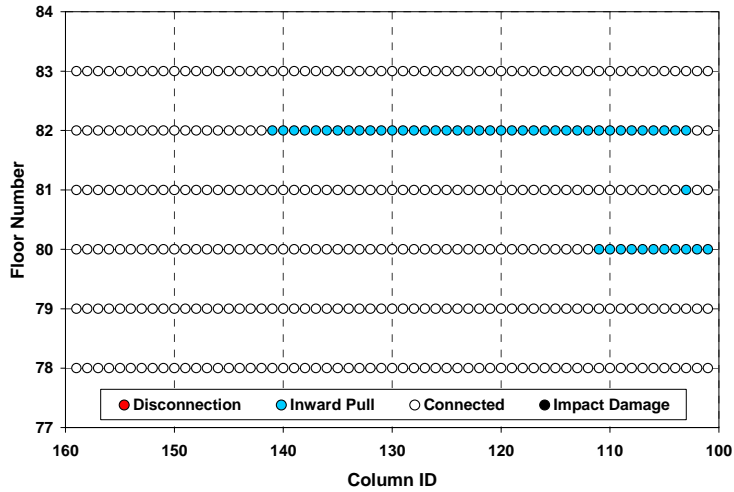


(c) East face

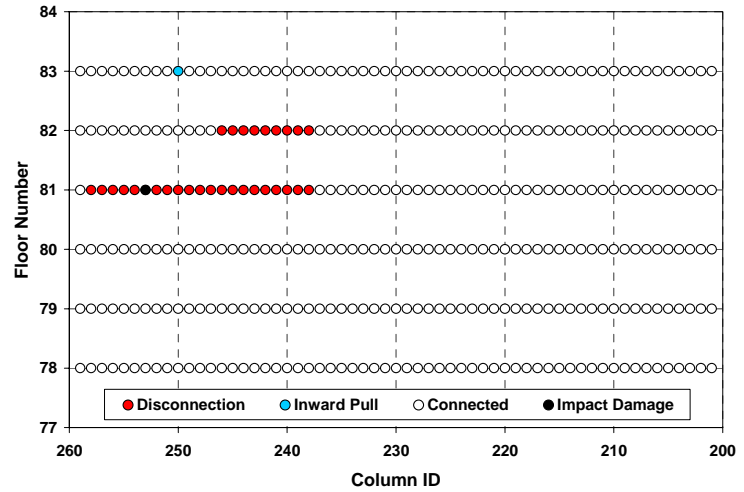


(d) South face

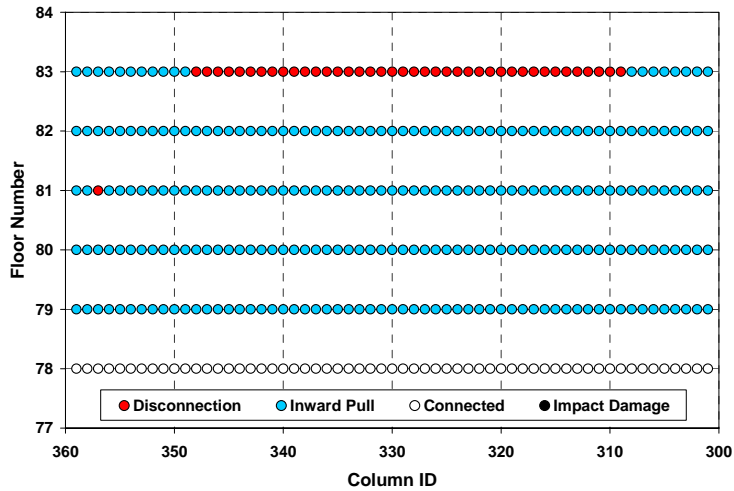
Figure 2-40. Locations of floor/wall disconnections and pull-in forces for the global analysis of WTC 2 between 20 min and 30 min for Case D conditions.



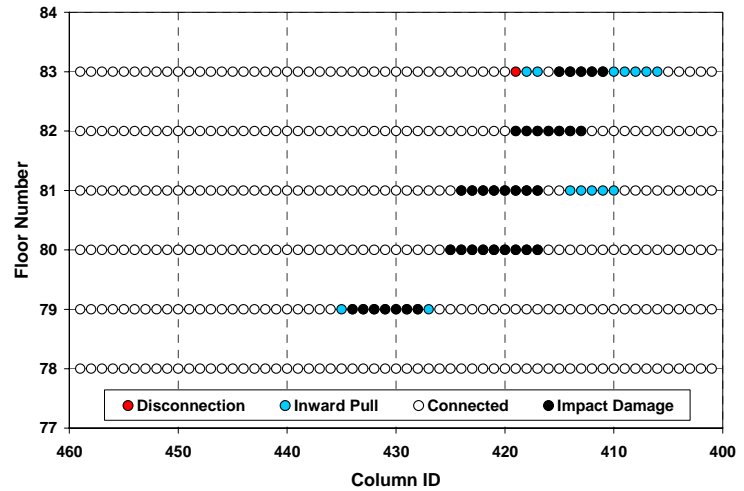
(a) West face



(b) North face

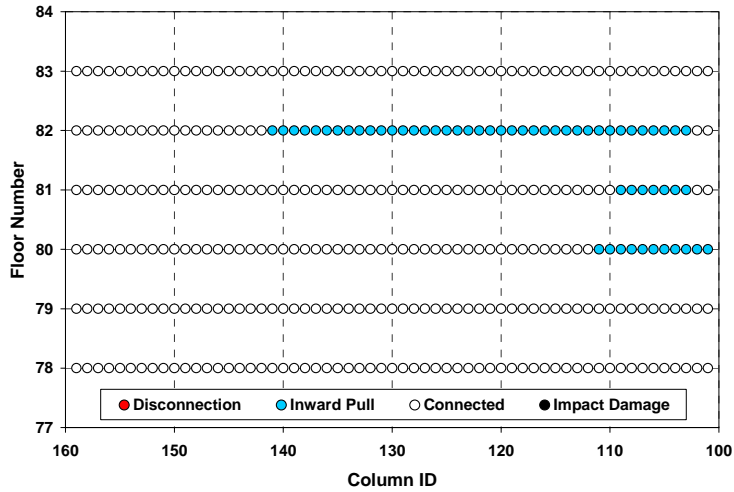


(c) East face

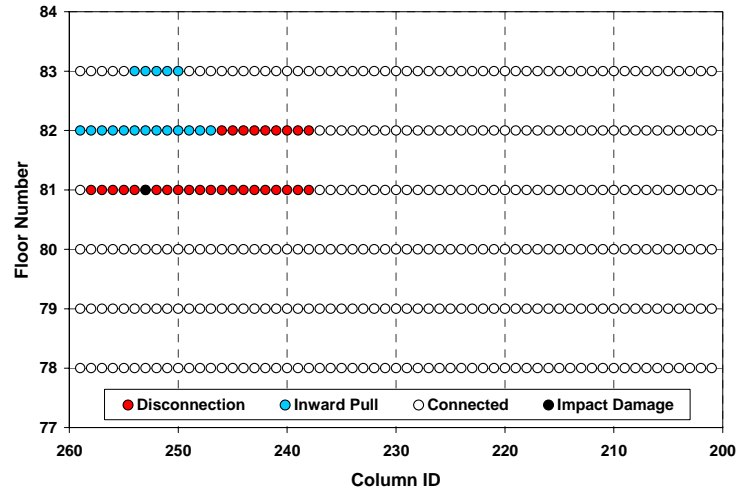


(d) South face

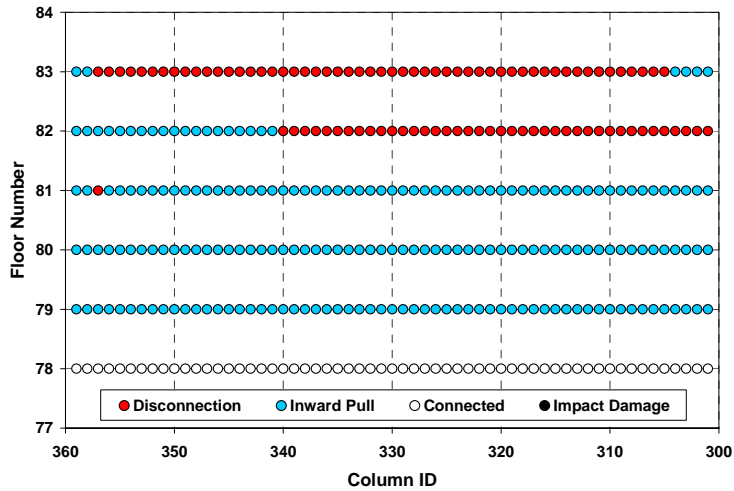
Figure 2-41. Locations of floor/wall disconnections and pull-in forces for the global analysis of WTC 2 between 30 min and 40 min for Case D conditions.



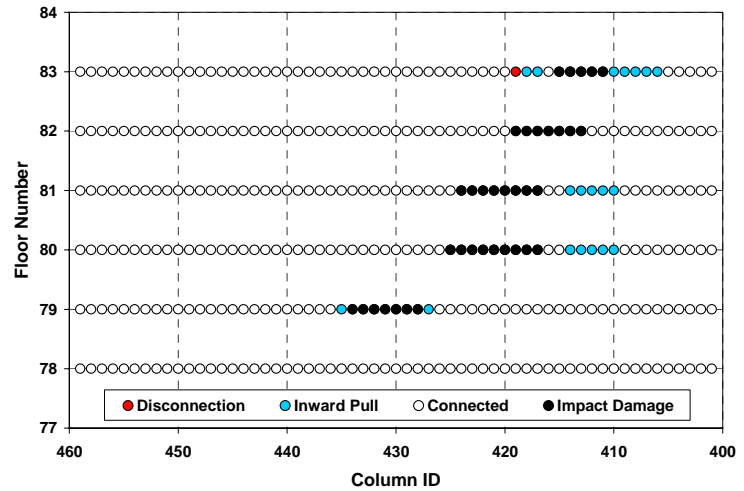
(a) West face



(b) North face

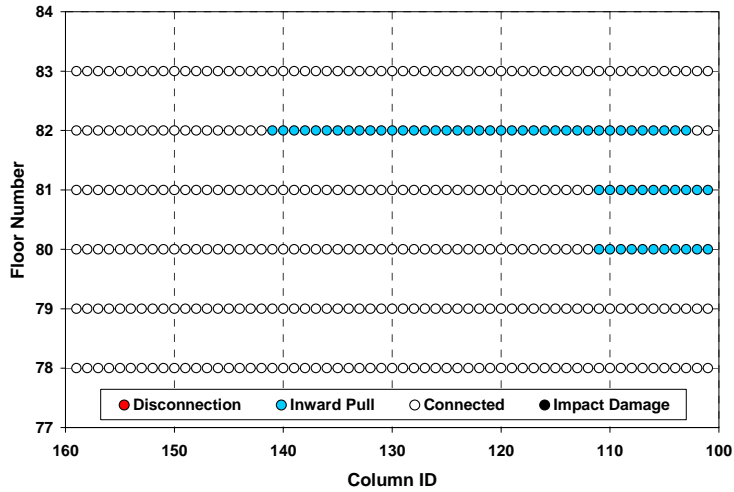


(c) East face

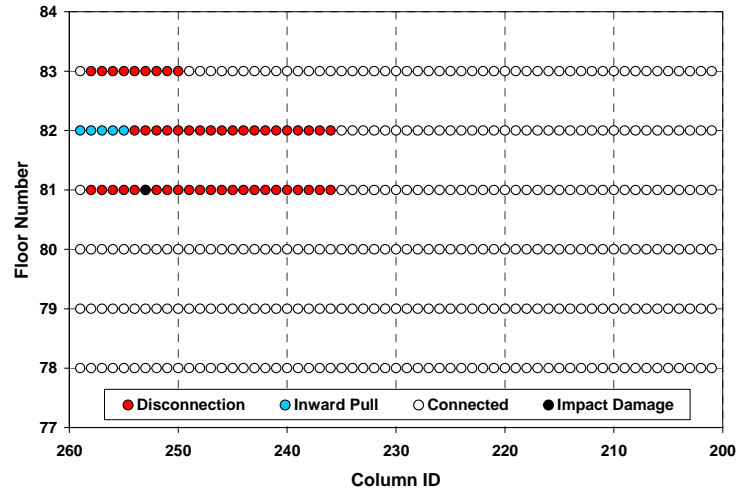


(d) South face

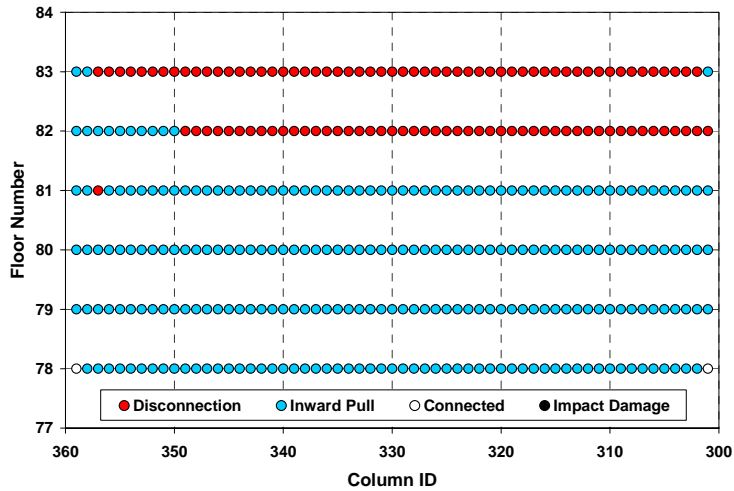
Figure 2-42. Locations of floor/wall disconnections and pull-in forces for the global analysis of WTC 2 between 40 min and 50 min for Case D conditions.



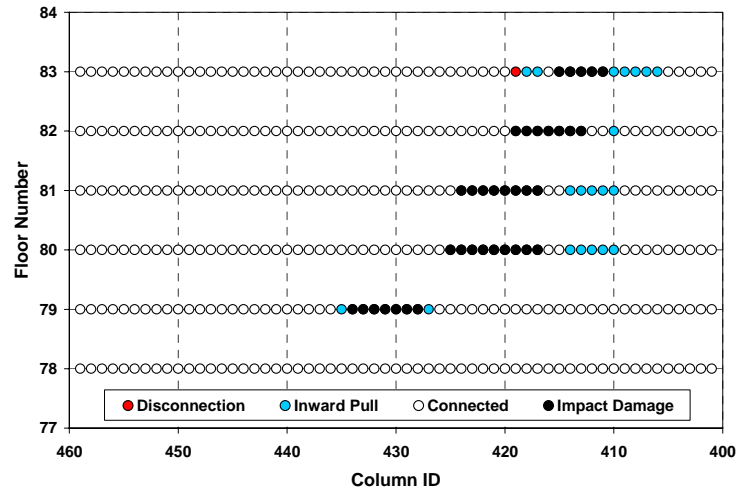
(a) West face



(b) North face



(c) East face



(d) South face

Figure 2-43. Locations of floor/wall disconnections and pull-in forces for the global analysis of WTC 2 between 50 min and 60 min for Case D conditions.

This page intentionally left blank.

Chapter 3

ISOLATED WALL AND CORE MODEL ANALYSES

3.1 INTRODUCTION

The isolated models were parts of the global models that were isolated and subjected to the same gravity and thermal loads as the global models. Obviously, the boundary conditions of the isolated models were not realistic, and the results cannot capture the interaction between the isolated model and the rest of the global model. Nevertheless, the isolated models provided insight into the structural behavior of the major parts of the global models under gravity and temperature time histories. Specifically, the trial values of the magnitude of pull-in forces resulted in calculated bowing of the exterior wall that did not agree well with the observed damage. Multiple analyses were required to match the results of calculations with the actual observations. Such multiple analyses could not have been performed on the global models within the time frame of this study and, therefore, were performed on the isolated models.

The isolated model analyses were performed pursuant to the global model analyses without creep and prior to the global model analyses with creep. The results shown in this chapter do not form a major link in the chain of collapse sequence arguments and may be skipped by those interested only in this chain of arguments.

The south exterior wall of WTC 1 and the east exterior wall of WTC 2 bowed and buckled as observed in photographs and videos. Both walls were isolated from the global models of WTC 1 and WTC 2. The isolated models were subjected to both Case A and Case B temperature conditions for WTC 1 and both Case C and Case D temperature conditions for WTC 2. In the following sections, the details of the isolated models, the results, and their comparison with the actual observations for different assumed input parameters are discussed.

3.2 EXTERIOR WALL BUCKLING

The south exterior wall of WTC 1 and the east exterior wall of WTC 2 were isolated from the global models and subjected to the combined effects of gravity loads and temperature time histories to determine whether the exterior walls of WTC 1 and WTC 2 would buckle as observed in the photographs and videos, and to determine conditions required to buckle them such as locations and magnitude of pull-in force from the sagging floors, locations of the floor/wall disconnections, and the need for additional vertical loads.

The isolated exterior walls from WTC 1 and WTC 2 are shown in Fig. 3–1. The exterior wall segment of WTC 1 included all the exterior columns from Column 301 to Column 359 and floors from Floor 89 to Floor 106. The exterior wall segment of WTC 2 included all the exterior columns from Column 301 to Column 359 and floors from Floor 73 to Floor 90. The springs at the base of the global models represent the vertical flexibility of the exterior walls below Floor 89 for WTC 1 and Floor 73 for WTC 2 for a uniform loading condition. For the south wall model of WTC 1, members that were severed by the aircraft impact were removed. The east wall of WTC 2 sustained no aircraft impact damage.

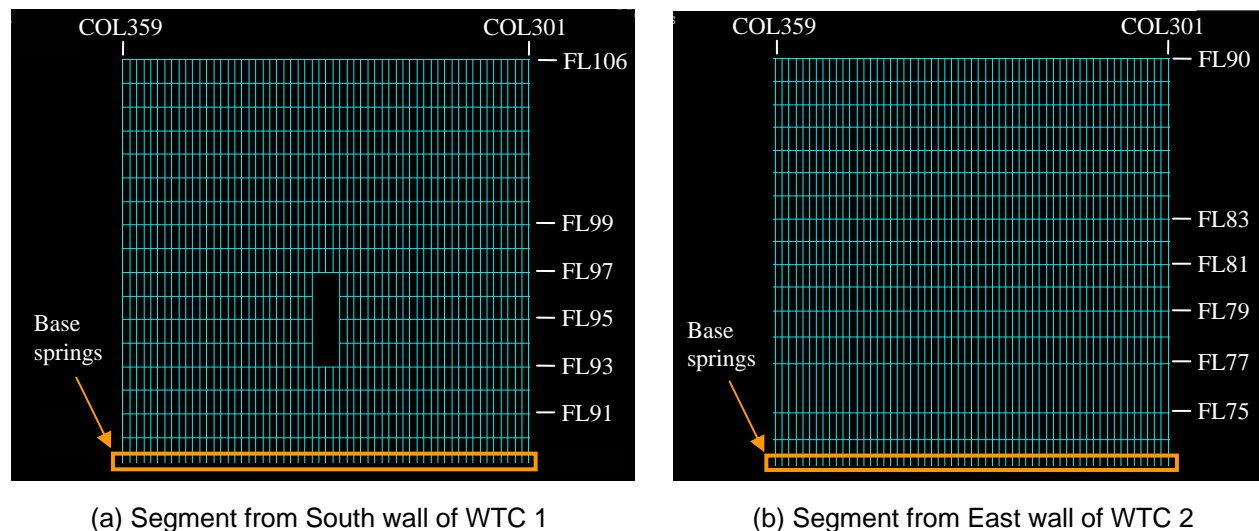


Figure 3–1. Isolated exterior wall segments from WTC 1 and WTC 2 (horizontal lines show spandrels and vertical lines show column).

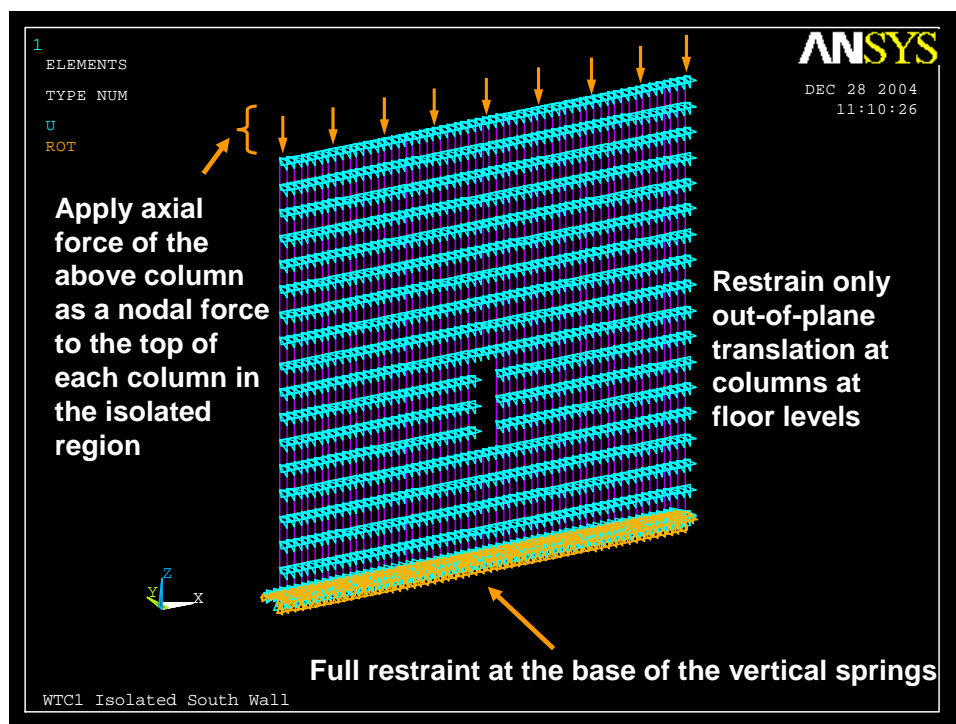


Figure 3–2. Boundary conditions applied on the isolated exterior wall segment on the south wall of WTC 1.

The applied boundary conditions for both isolated exterior wall models were identical and are shown for WTC 1 in Fig. 3–2. The isolated exterior wall models were fully restrained at the base of the vertical

springs. In the out-of-plane direction (direction *y*) they were supported at floor levels. At predetermined points in times, these supports were removed at locations where either calculations or observations showed floor/wall disconnections. For the east wall of WTC 2, there were floor/wall disconnections or pull-in forces calculated by the full floor models along the edges of the model (Column 301 and Column 359). In the analyses of the isolated wall model for Case C and Case D temperature conditions, the out-of-plane supports were removed at disconnections located on the edges of the model. However, in the analysis of the pull-in forces needed to match the observed bowing (see Section 3.2.2), the disconnections on the edges of the model were not modeled, and all nodes along the vertical edges of the model were restrained.

To represent the column loads after aircraft impact, a set of axial loads and moments were applied at the top of the isolated wall segments. These axial loads and moments, taken from the preliminary global model analyses with Case A (for WTC 1) and Case C and Case D (for WTC 2) structural damage conditions, represented the axial load and moment in the columns at the floor right above the top of the isolated wall segments after aircraft impact. For instance, for the WTC 2 exterior wall segment, the isolated wall terminates at Floor 90. In order to represent the axial load coming from Floor 90 and above, the axial loads from the columns between Floor 90 and Floor 91 of the global model were extracted at the end of the aircraft impact analysis and were applied on the top of the isolated wall model of WTC 2. In addition to the set of vertical loads applied at the top of the isolated walls, loads representing the dead and 25 percent of the design live loads of the floors were applied at each column node at floor levels.

The isolated exterior wall models were subjected to a set of loading conditions as summarized in Table 3–1 for WTC 1 and Table 3–2 for WTC 2. After the gravity analysis, the isolated exterior wall models were subjected to temperature loads at 10 min increments. The analyses were conducted with Case A and Case B temperature conditions for WTC 1 and Case C and Case D temperature conditions for WTC 2. For each temperature analysis, the column and spandrel temperatures at time *t* were ramped to the column and spandrel temperatures at time = *t* + 10 min. Before applying the temperatures, the out-of-plane supports were removed at disconnected column to exterior wall connections at or prior to *t* + 10 min. Once the temperature analyses were completed (WTC 1 was analyzed to 100 min and WTC 2 to 60 min), both isolated exterior wall models were pushed down by imposing additional displacements to determine additional axial-load-carrying capacity remaining in the exterior wall system. For push-down analysis, the vertical displacements at the top of the isolated exterior wall models at the end of temperature analyses were extracted. These displacements were applied on top of the isolated exterior wall models, and additional uniform displacement increments were imposed in a displacement-controlled analysis. During push-down analysis, the temperature of the columns and spandrels were kept constant at the values specified at the end of the temperature analyses (WTC 1 column and spandrel temperatures were kept at 100 min temperatures and WTC 2 column and spandrel temperatures were kept at 60 min temperatures). The results of isolated exterior wall model analyses are discussed in the following sections.

Table 3–1. Analysis steps conducted on WTC 1 isolated exterior wall model.

Analysis Step		Description
1	Gravity	Apply gravity loads with aircraft impact
2	Temperature at 10 min	Remove the out-of-plane supports at floor to exterior wall connections disconnected at or prior to 10 min. Apply column and spandrel temperatures at 10 min.
3	Temperature at 20 min	Remove the out-of-plane supports at floor to exterior wall connections disconnected at or prior to 20 min. Apply column and spandrel temperatures at 20 min.
4	Temperature at 30 min	Remove the out-of-plane supports at floor to exterior wall connections disconnected at or prior to 30 min. Apply column and spandrel temperatures at 30 min.
5	Temperature at 40 min	Remove the out-of-plane supports at floor to exterior wall connections disconnected at or prior to 40 min. Apply column and spandrel temperatures at 40 min.
6	Temperature at 50 min	Remove the out-of-plane supports at floor to exterior wall connections disconnected at or prior to 50 min. Apply column and spandrel temperatures at 50 min.
7	Temperature at 60 min	Remove the out-of-plane supports at floor to exterior wall connections disconnected at or prior to 60 min. Apply column and spandrel temperatures at 60 min.
8	Temperature at 70 min	Remove the out-of-plane supports at floor to exterior wall connections disconnected at or prior to 70 min. Apply column and spandrel temperatures at 70 min.
9	Temperature at 80 min	Remove the out-of-plane supports at floor to exterior wall connections disconnected at or prior to 80 min. Apply column and spandrel temperatures at 80 min.
10	Temperature at 90 min	Remove the out-of-plane supports at floor to exterior wall connections disconnected at or prior to 90 min. Apply column and spandrel temperatures at 90 min.
11	Temperature at 100 min	Remove the out-of-plane supports at floor to exterior wall connections disconnected at or prior to 100 min. Apply column and spandrel temperatures at 100 min.
12	Push Down	Extract the vertical displacements at the top of the isolated wall model and impose these displacements and additional uniform displacement increments with column and spandrel temperatures kept at 100 min.

Table 3–2. Analysis steps conducted on WTC 2 isolated exterior wall model.

Analysis Step		Description
1	Gravity	Apply gravity loads right after aircraft impact
2	Temperature at 10 min	Remove the out-of-plane supports at floor to exterior wall connections that were disconnected at or prior to 10 min. Apply column and spandrel temperatures at 10 min.
3	Temperature at 20 min	Remove the out-of-plane supports at floor to exterior wall connections that were disconnected at 20 min. Apply column and spandrel temperatures at 20 min.
4	Temperature at 30 min	Remove the out-of-plane supports at floor to exterior wall connections that were disconnected at 30 min. Apply column and spandrel temperatures at 30 min.
5	Temperature at 40 min	Remove the out-of-plane supports at floor to exterior wall connections that were disconnected at 40 min. Apply column and spandrel temperatures at 40 min.
6	Temperature at 50 min	Remove the out-of-plane supports at floor to exterior wall connections that were disconnected at 50 min. Apply column and spandrel temperatures at 50 min.
7	Temperature at 60 min	Remove the out-of-plane supports at floor to exterior wall connections that were disconnected at 60 min. Apply column and spandrel temperatures at 60 min.
8	Push Down	Extract the vertical displacements at the top of the isolated wall model and impose these displacements and additional uniform displacement increments with column and spandrel temperatures kept at 60 min.

3.2.1 Finite Element Analysis of WTC 1 Exterior Wall

Case A Temperature Condition

As calculated in the full-floor model analyses for Case A_i condition, described in Appendix A, the floors were assumed to remain connected to the south wall of WTC 1 throughout the temperature history for Case A condition.

Figures 3–3 to 3–12 show the temperature distributions of Case A condition in columns of the WTC 1 south wall from 10 min to 100 min. A linear temperature gradient in the direction normal to the exterior wall was assumed to exist in the cross section of beam elements for exterior columns. As Figs. 3–3 to 3–12 show, temperatures on the south wall were not very high; the peak temperature was only 455°C for Case A temperature condition. The temperature distributions of Case A condition in spandrels are shown in Figs. 3–13 to 3–22. Temperatures were assumed to be uniform over the entire cross section of beam elements for spandrels.

Figure 3–23 shows vertical displacements, out-of-plane displacements, and axial loads in columns of the WTC 1 south wall after the impact. In contour plots created by ANSYS, “MN” and “MX” indicate the locations of the minimum and maximum values, respectively. Columns from Column 329 to Column 331 between Floor 93 and Floor 97 were severed by the aircraft impact, and the maximum displacement occurred at Column 330 at Floor 106. Column 328 and Column 332 between Floor 93 and Floor 97 on both sides of the aircraft impact damage area were heavily loaded, and the maximum axial load was 377 kip at Column 332.

Figures 3–24 to 3–26 show vertical displacements, out-of-plane displacements, and axial loads in the columns of the WTC 1 south wall for Case A temperature condition, respectively. At 100 min, the maximum vertical displacement was nearly the same as the vertical displacement of 2.6 in. after the impact. The out-of-plane displacement was insignificant during thermal loading. The maximum out-of-plane displacement was 0.35 in. outward, occurring at Column 332 between Floor 96 and Floor 97. During thermal loading, the axial load in Column 332 between Floor 96 and Floor 97 increased from 377 kip to 756 kip.

Figure 3–27 shows plastic strains in columns at 100 min. The maximum plastic strain of 4 percent occurred in Column 332 between Floor 96 and Floor 97.

As described in Appendix C for the preliminary global model without creep and in Chapter 4 for the final global model with creep, gravity loads on the south wall varied under thermal loads as the loads were redistributed within the tower through the hat truss and the spandrels. Figure 3–28 compares the axial loads in columns derived from the preliminary global model without creep and with Case A_i structural damage condition to those of the isolated model wall model with Case A structural damage and temperature conditions. The preliminary global model without creep was the only available source for this comparison at that time. The differences in the axial loads were applied to the columns at Floor 99 as corrective loads. Figure 3–29 shows the response of the south wall after applying these corrective loads. The WTC 1 south wall remained stable after the application of these corrective loads.

To determine the additional load-carrying capacity of the south wall at the end of the temperature analysis at 100 min, the top of the isolated exterior wall model was pushed down by converting the model from a

force-control analysis to a displacement-control analysis and by imposing additional vertical displacement increments on top of the isolated model. The analysis was terminated at an additional vertical displacement of 13.2 in. This model reached a peak total vertical load at an additional vertical displacement of 11.3 in. Figure 3–30 shows the relationship between the total additional vertical load and the additional vertical displacement. Figure 3–31 shows additional vertical load per column at different additional vertical displacements of 2 in., 4 in., 6 in., 8 in., and 10 in. Figure 3–32 shows the response of the WTC 1 south wall at the additional displacement of 13.2 in. When an additional 2 in. of vertical displacement was imposed, the variation among the additional vertical loads on columns was within 50 kip for the average additional vertical load of about 160 kip. However, at an additional displacement of 10 in., the variation became large, indicating some columns were softer than others; the softer columns had reached their load-carrying capacities and were in the post-buckling regime. The WTC 1 south wall model carried an additional vertical load of 33,000 kip (560 kip per column on the average). Therefore, the south wall possessed significant reserve capacity after the application of Case A temperature condition.

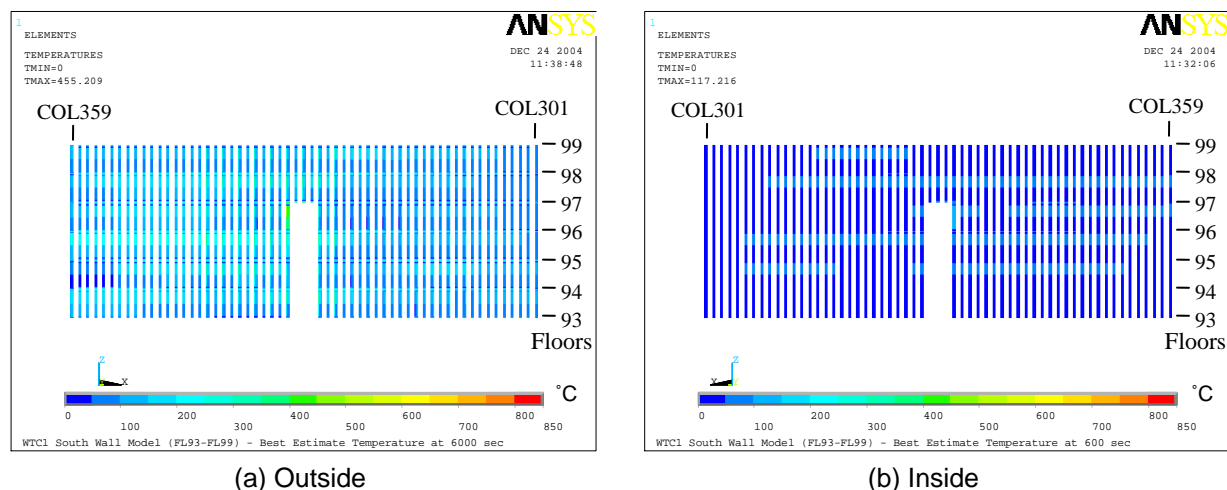


Figure 3–3. Case A temperature condition of south wall columns of WTC 1 at 10 min.

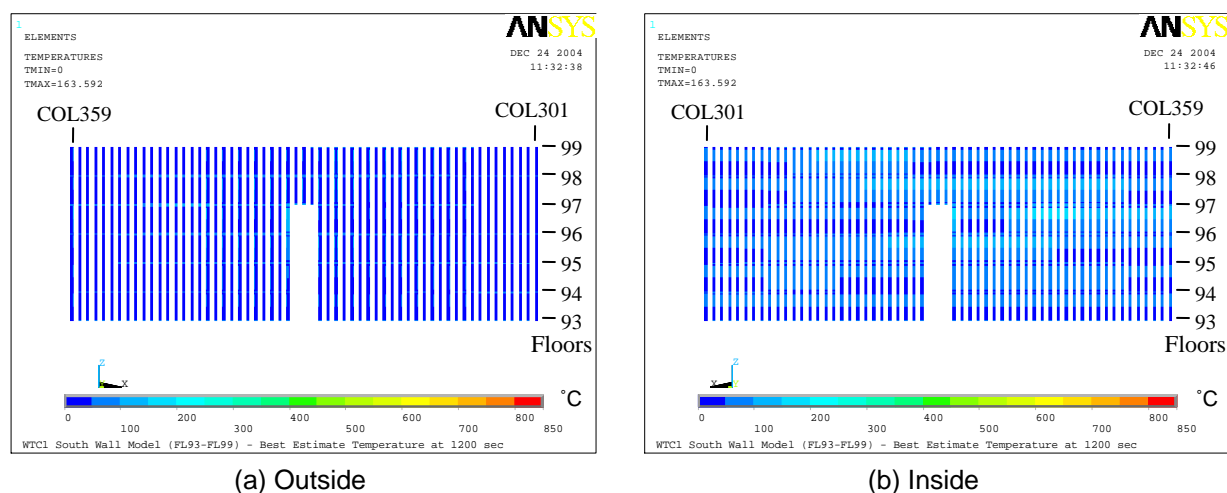
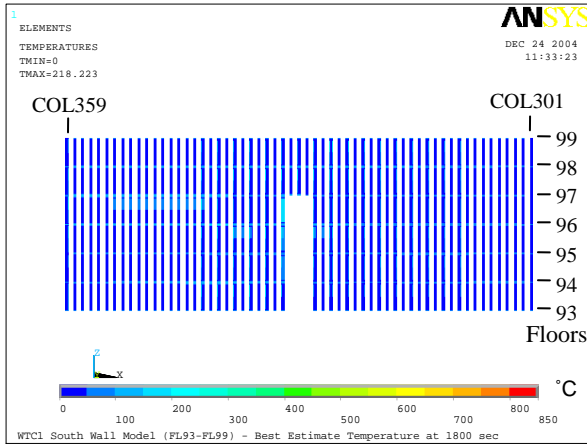
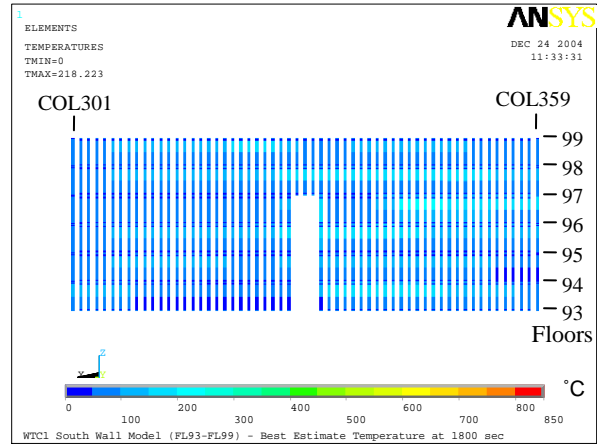


Figure 3–4. Case A temperature condition of south wall columns of WTC 1 at 20 min.

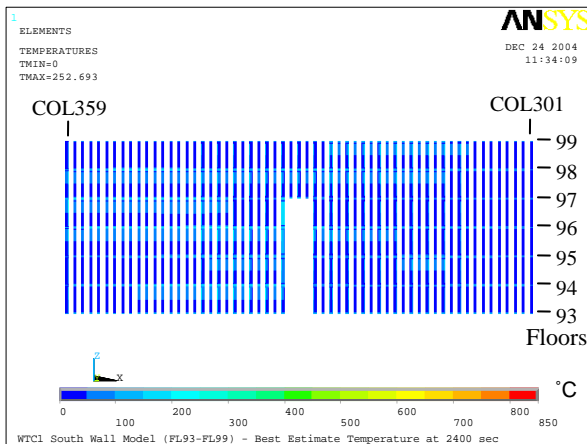


(a) Outside

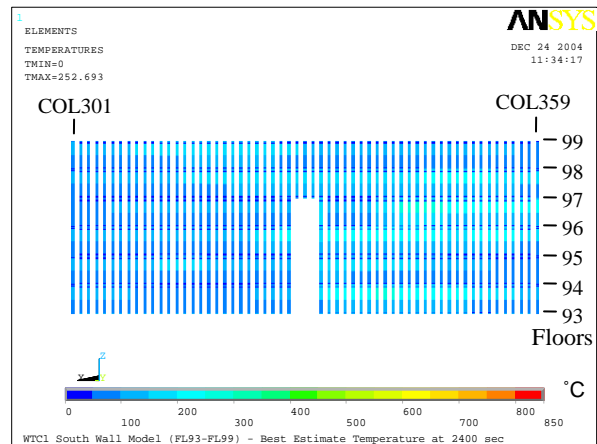


(b) Inside

Figure 3–5. Case A temperature condition of south wall columns of WTC 1 at 30 min.

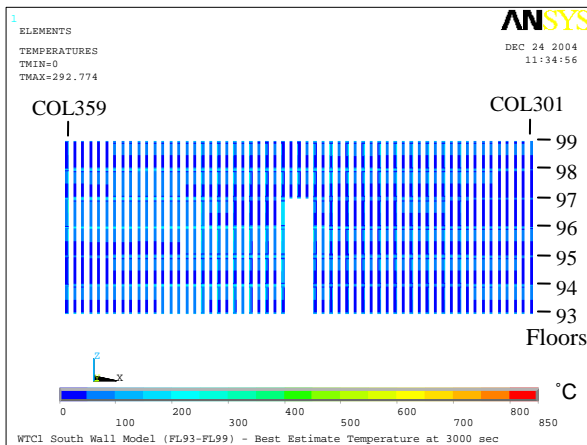


(a) Outside

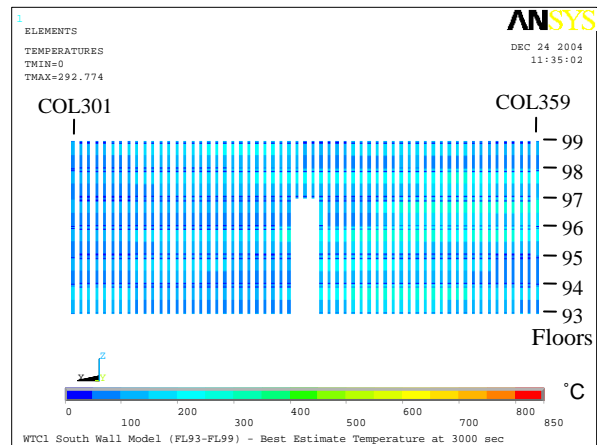


(b) Inside

Figure 3–6. Case A temperature condition of south wall columns of WTC 1 at 40 min.

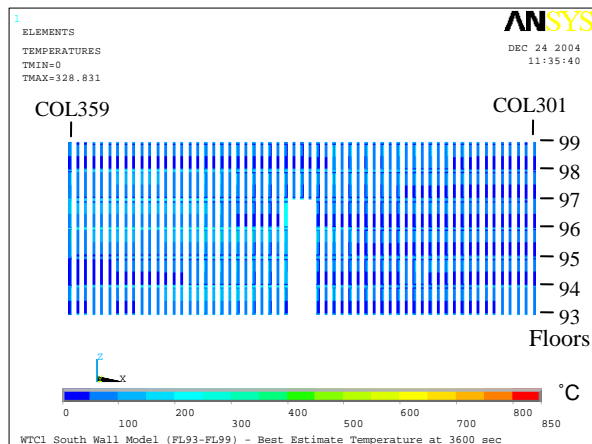


(a) Outside

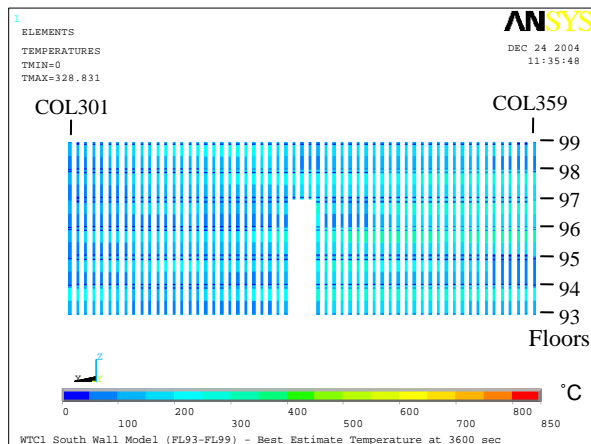


(b) Inside

Figure 3–7. Case A temperature condition of south wall columns of WTC 1 at 50 min.

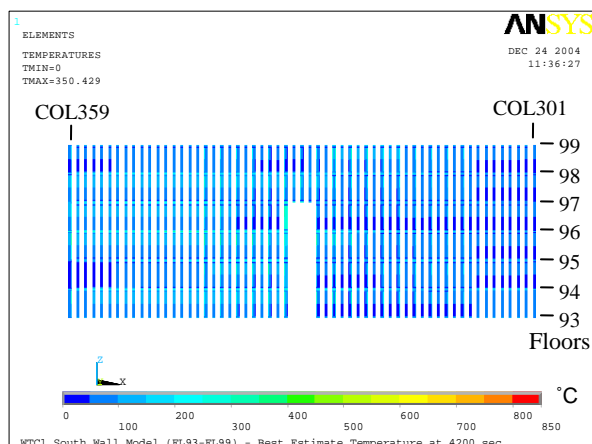


(a) Outside

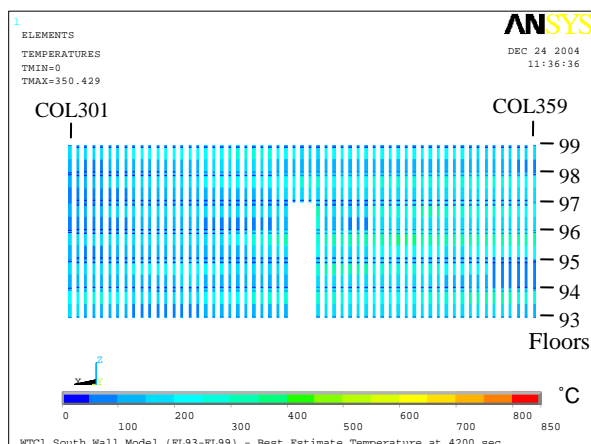


(b) Inside

Figure 3–8. Case A temperature condition of south wall columns of WTC 1 at 60 min.

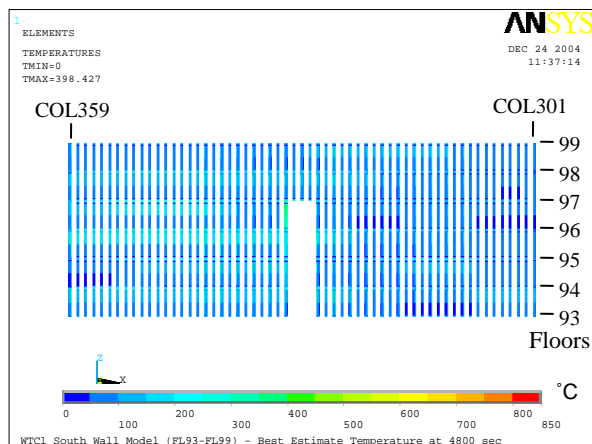


(a) Outside

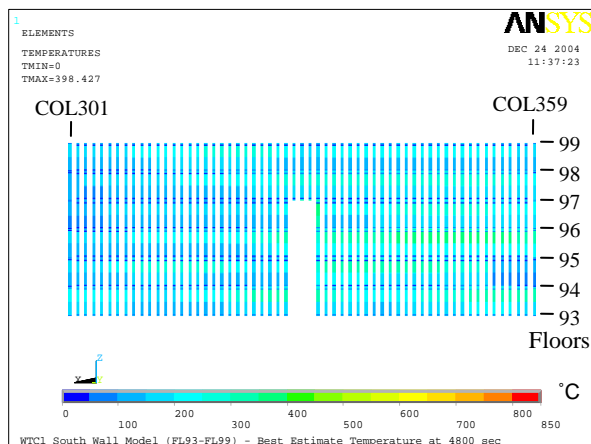


(b) Inside

Figure 3–9. Case A temperature condition of south wall columns of WTC 1 at 70 min.

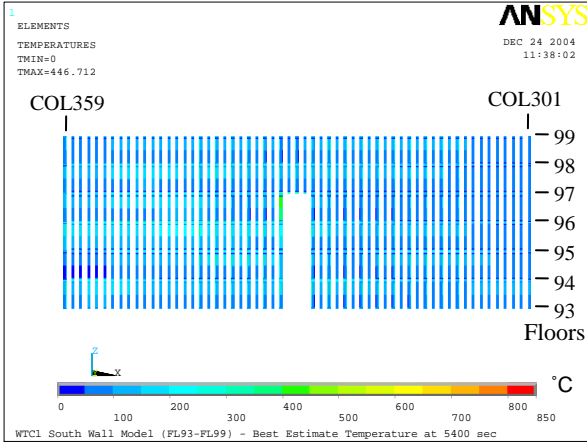


(a) Outside

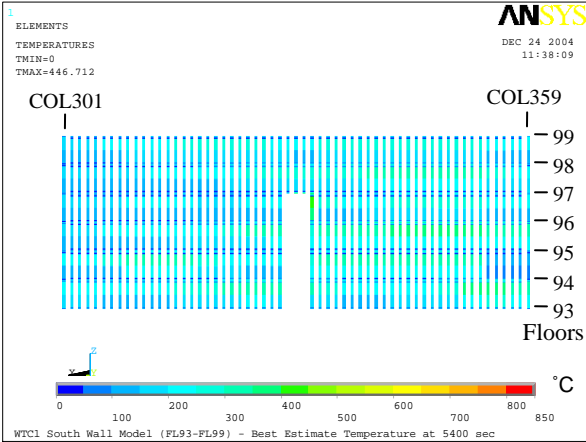


(b) Inside

Figure 3–10. Case A temperature condition of south wall columns of WTC 1 at 80 min.

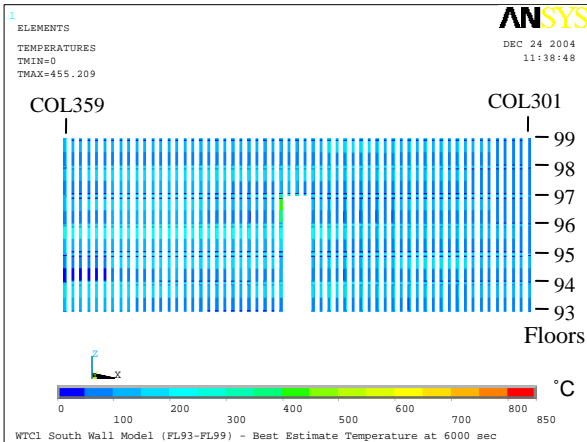


(a) Outside

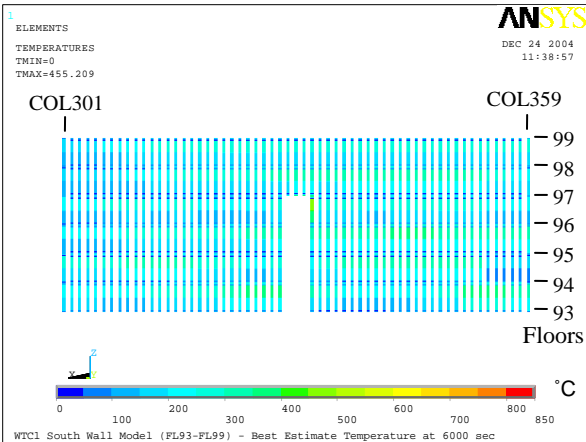


(b) Inside

Figure 3–11. Case A temperature condition of south wall columns of WTC 1 at 90 min.



(a) Outside



(b) Inside

Figure 3–12. Case A temperature condition of south wall columns of WTC 1 at 100 min.

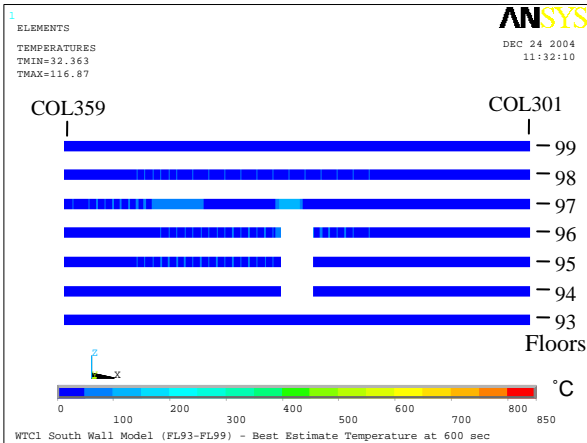


Figure 3–13. Case A temperature condition of south wall spandrels of WTC 1 at 10 min.

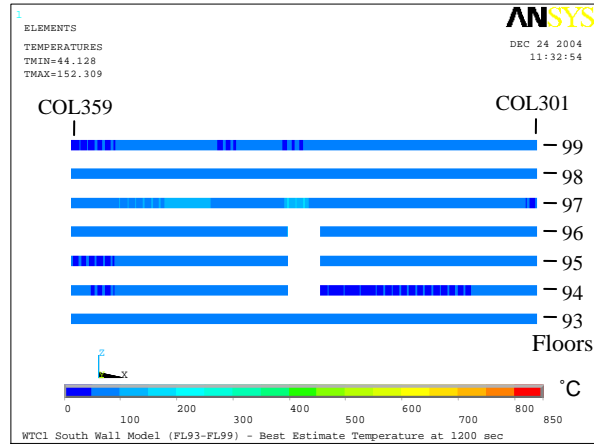


Figure 3–14. Case A temperature condition of south wall spandrels of WTC 1 at 20 min.

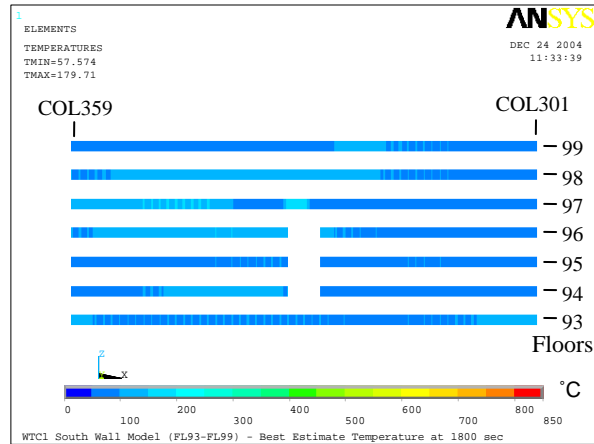


Figure 3–15. Case A temperature condition of south wall spandrels of WTC 1 at 30 min.

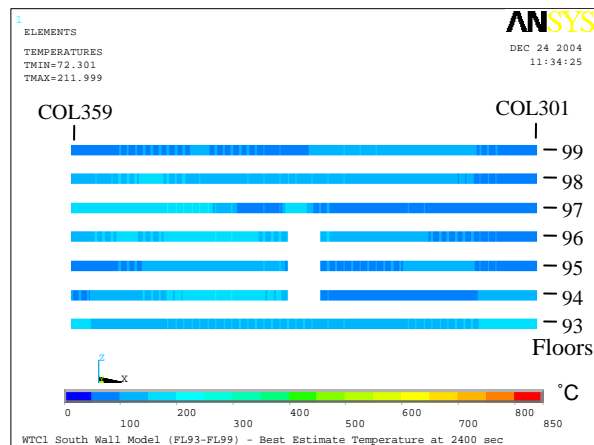


Figure 3–16. Case A temperature condition of south wall spandrels of WTC 1 at 40 min.

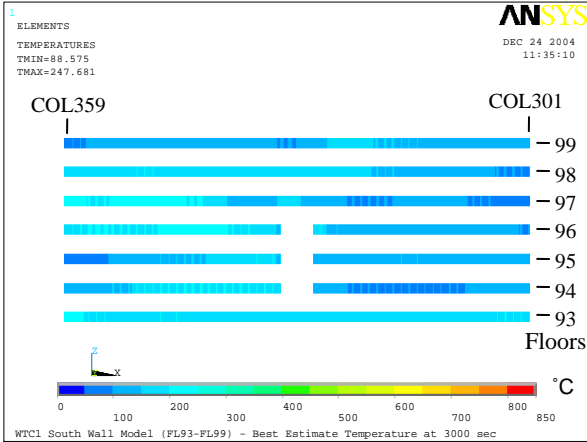


Figure 3–17. Case A temperature condition of south wall spandrels of WTC 1 at 50 min.

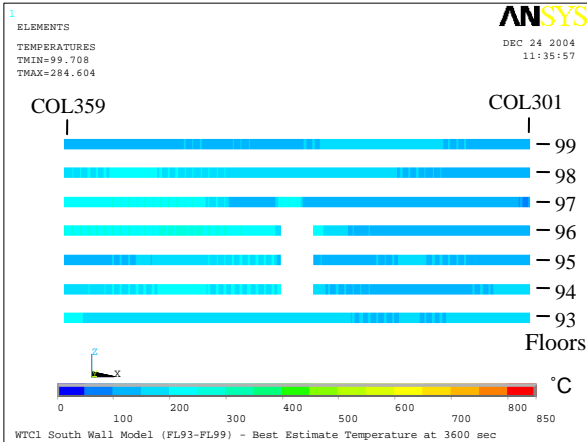


Figure 3–18. Case A temperature condition of south wall spandrels of WTC 1 at 60 min.

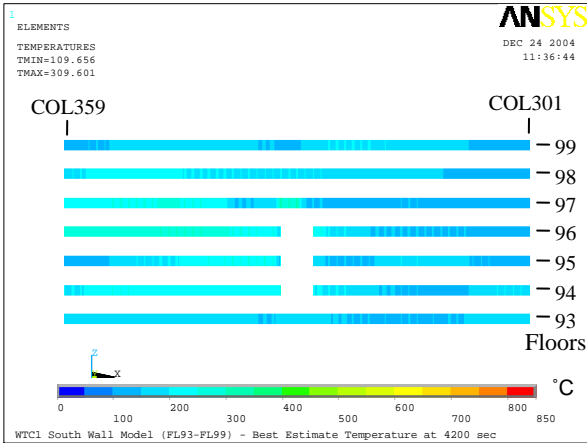


Figure 3–19. Case A temperature condition of south wall spandrels of WTC 1 at 70 min.

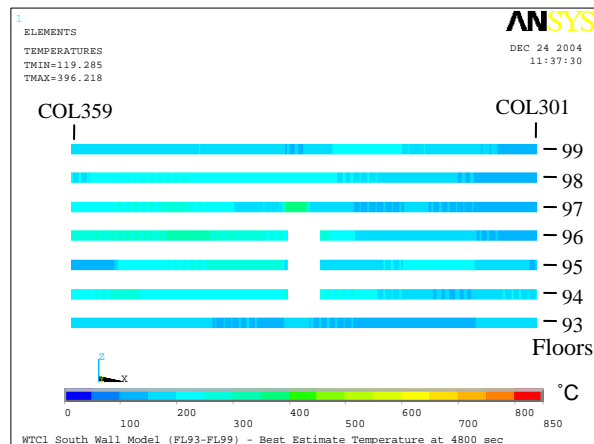


Figure 3–20. Case A temperature condition of south wall spandrels of WTC 1 at 80 min.

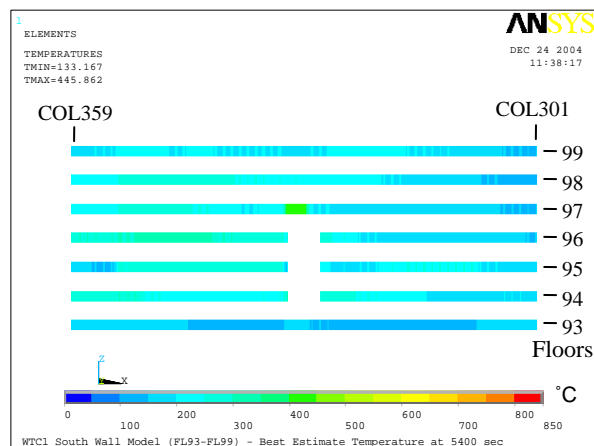


Figure 3–21. Case A temperature condition of south wall spandrels of WTC 1 at 90 min.

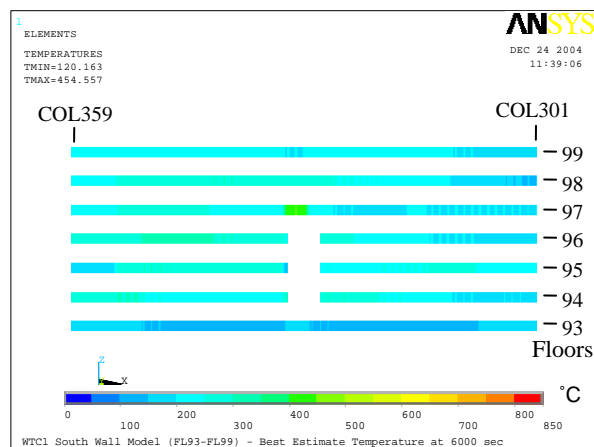
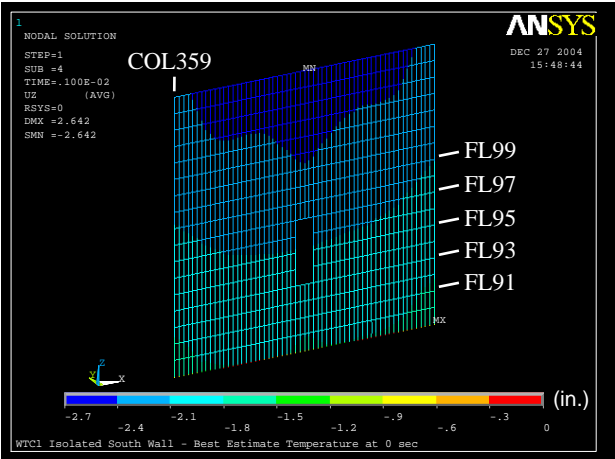
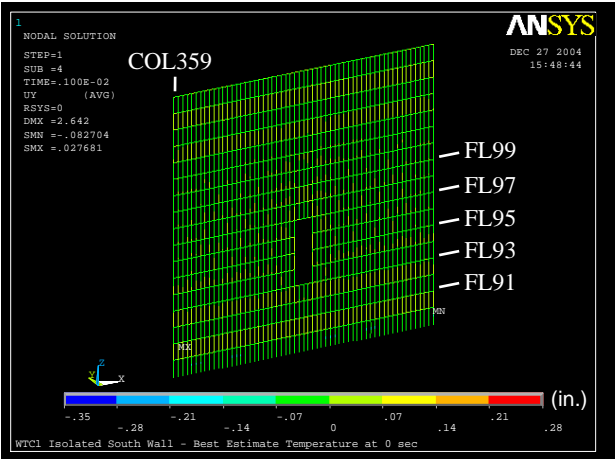


Figure 3–22. Case A temperature condition of south wall spandrels of WTC 1 at 100 min.



(a) Vertical displacement
(downward displacement is negative)

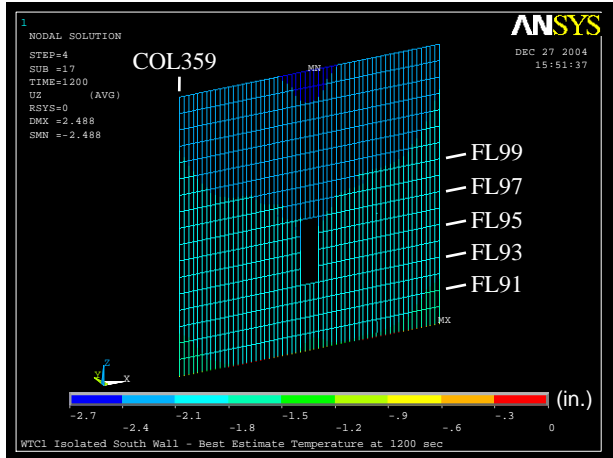


(b) Out-of-plane displacement
(inward displacement is positive)

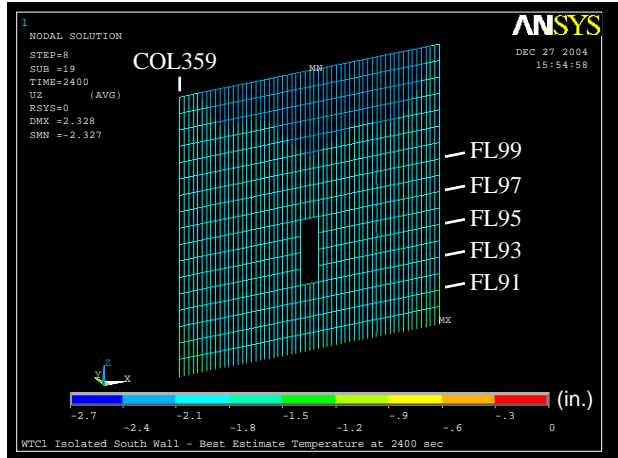


(c) Axial force in columns
(compression is negative)

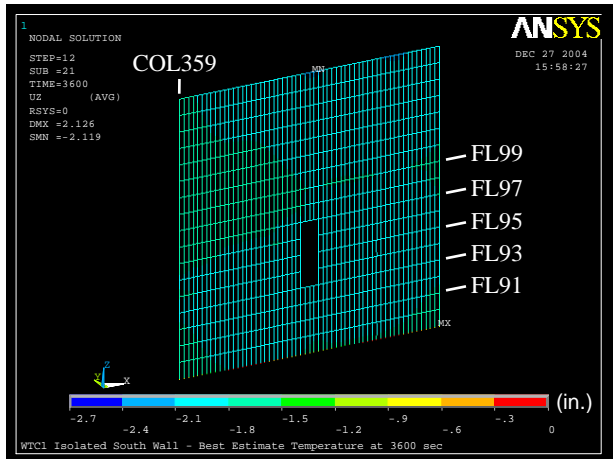
Figure 3–23. Response of Isolated south wall model of WTC 1 after aircraft impact.



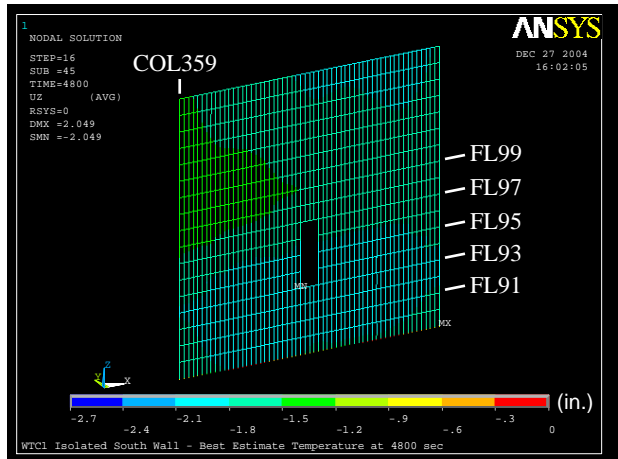
(a) At 20 min



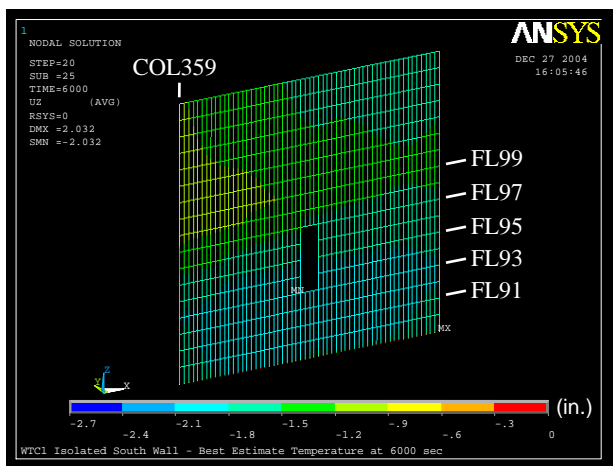
(b) At 40 min



(c) At 60 min

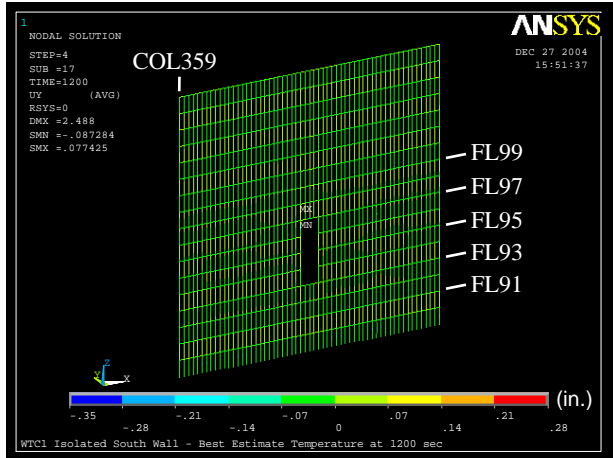


(d) At 80 min

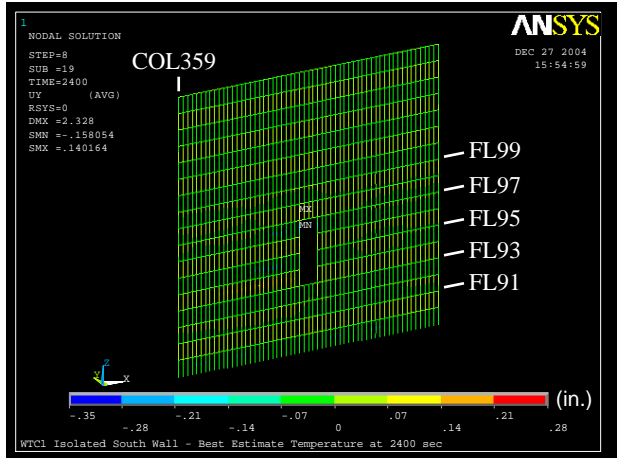


(e) At 100 min

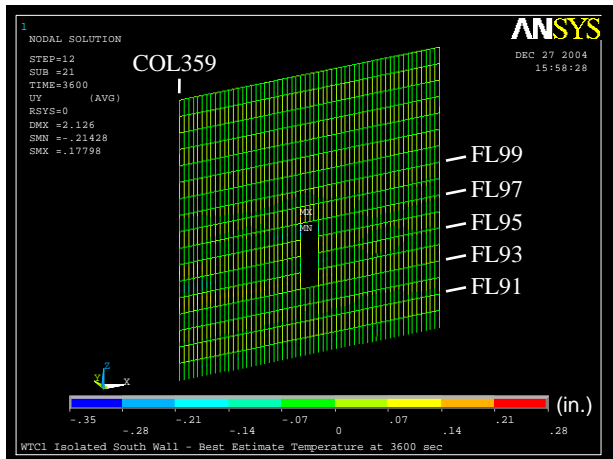
Figure 3–24. Vertical displacements of isolated south wall model of WTC 1 for Case A temperature condition (downward displacement is negative).



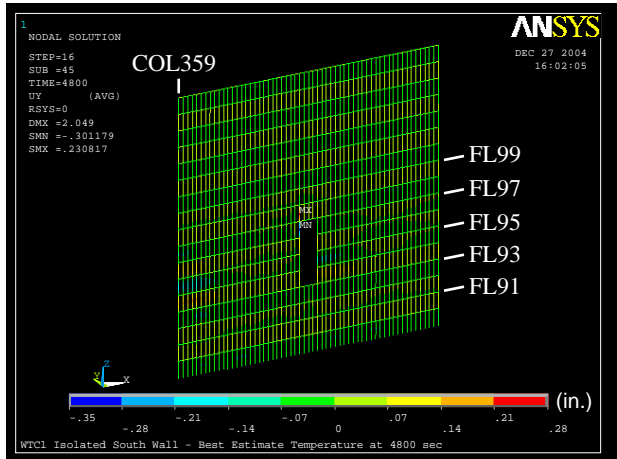
(a) at 20 min



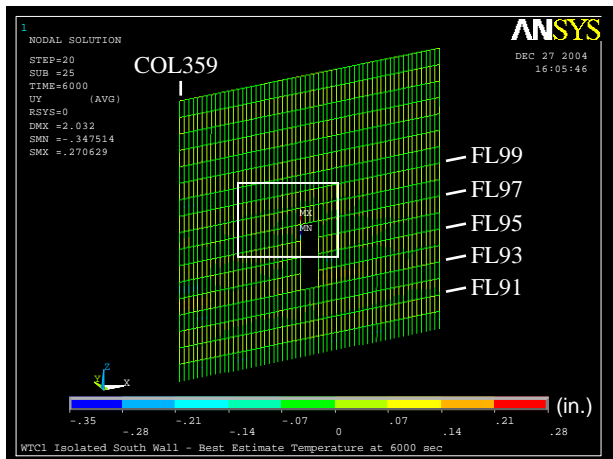
(b) at 40 min



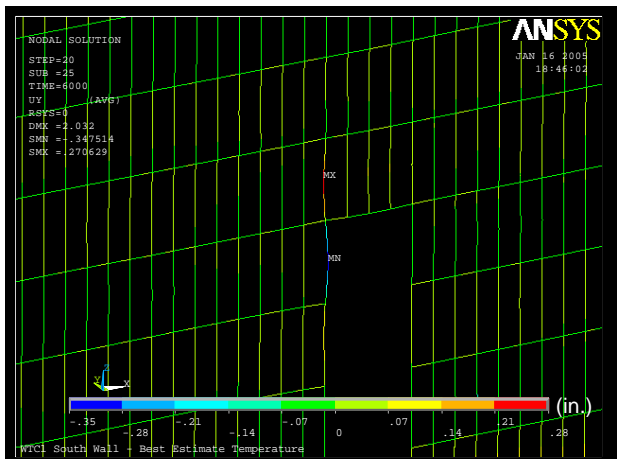
(c) at 60 min



(d) at 80 min

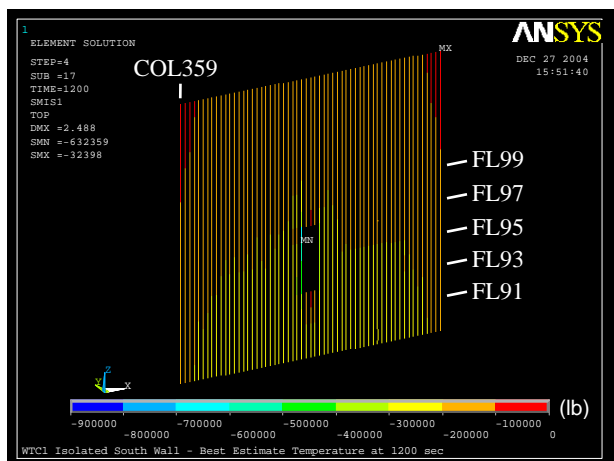


(e) at 100 min

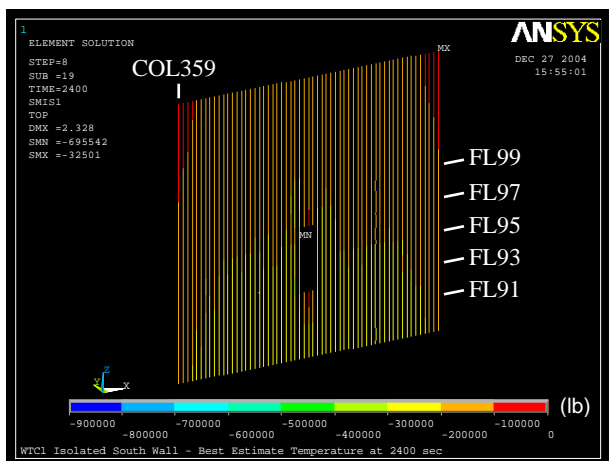


(f) Close-up view at 100 min
(30X displacement magnification)

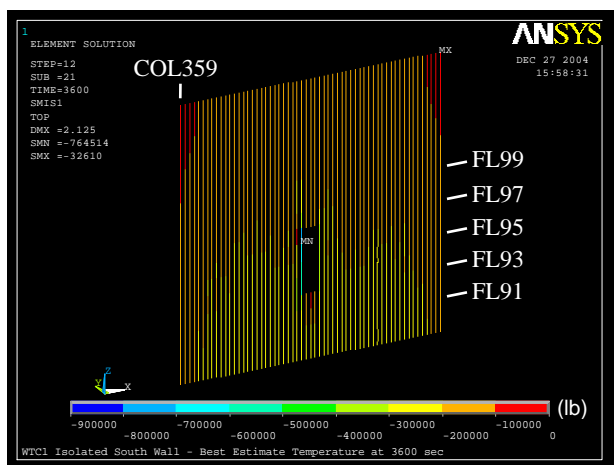
Figure 3–25. Out-of-plane displacements of isolated south wall model of WTC 1 for Case A temperature condition (inward displacement is positive).



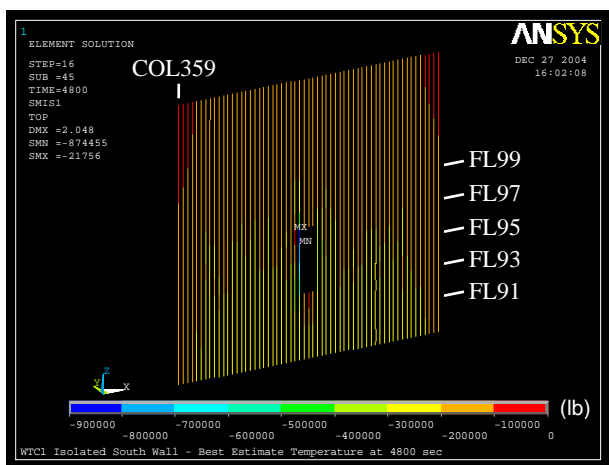
(a) at 20 min



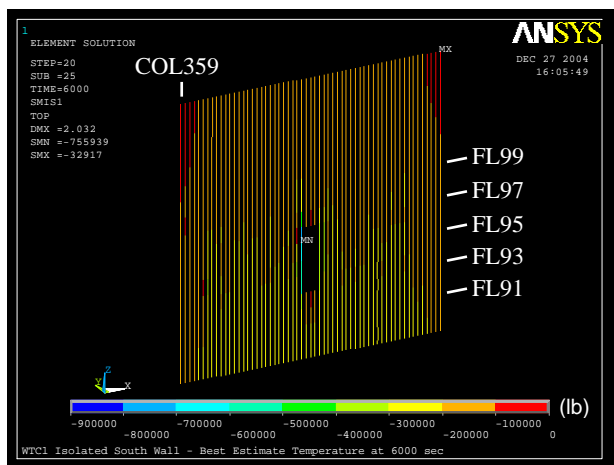
(b) at 40 min



(c) at 60 min



(d) at 80 min



(e) at 100 min

Figure 3–26. Axial load in columns of isolated south wall model of WTC 1 for Case A temperature condition (compression is negative).

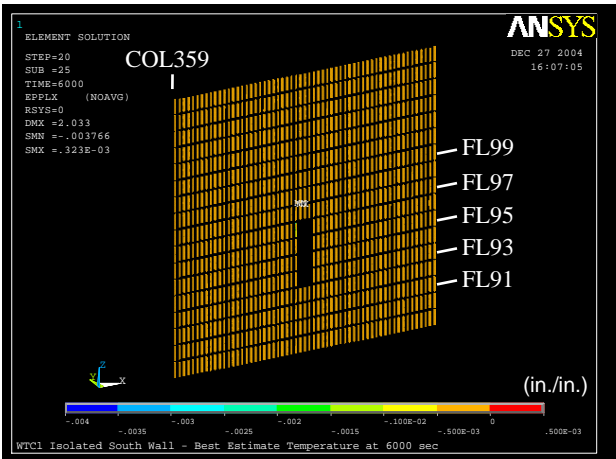


Figure 3–27. Plastic strain in columns of isolated south wall model of WTC 1 for Case A temperature condition at 100 min (compressive strain is negative).

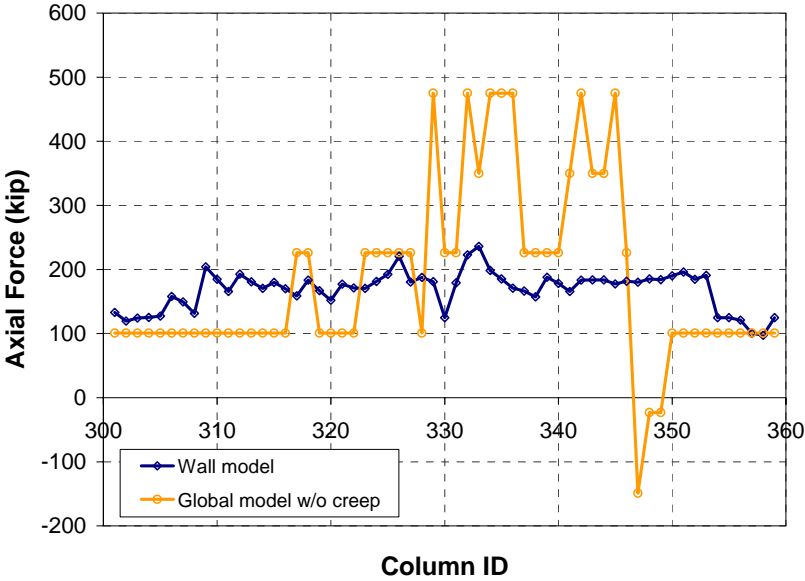
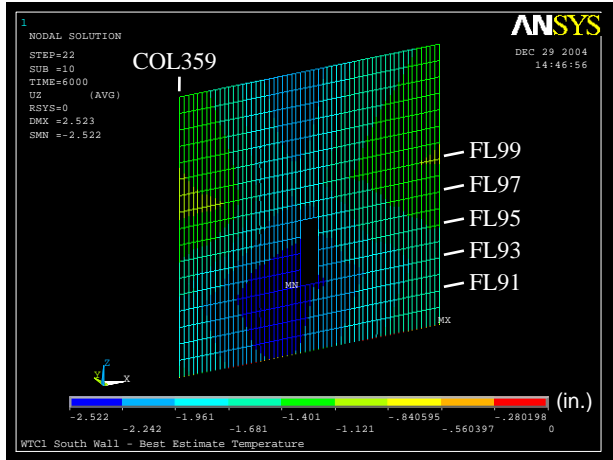
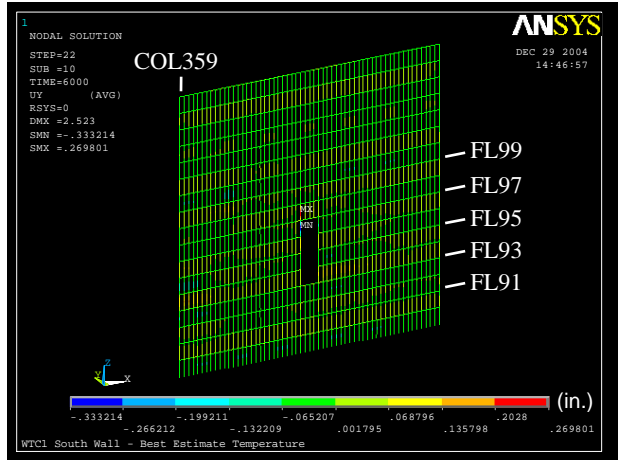


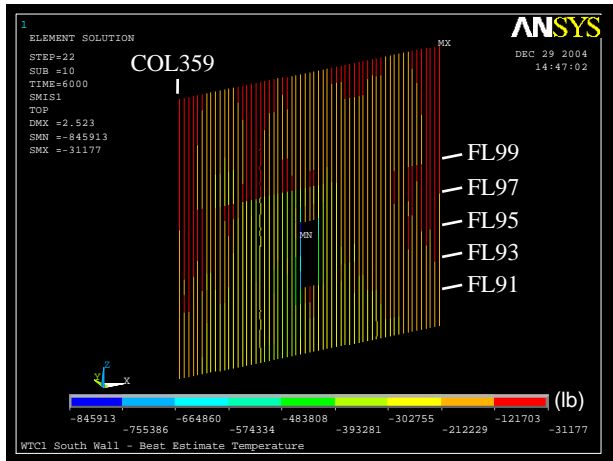
Figure 3–28. Axial load in columns of south wall of WTC 1 at 100 min: isolated wall model for Case A temperature condition compared to global model without creep for Case A_i conditions (compression is positive).



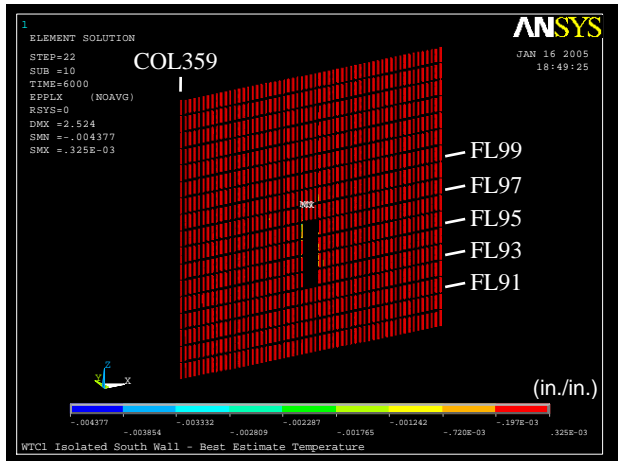
(a) Vertical displacement
(downward displacement is negative)



(b) Out-of-plane displacement
(inward displacement is positive)



(c) Axial force in columns
(compression is negative)



(d) Plastic strain in columns
(compressive strain is negative)

Figure 3–29. Responses of isolated south wall model of WTC 1 after corrective loads from the global model were applied (Case A temperature condition at 100 min).

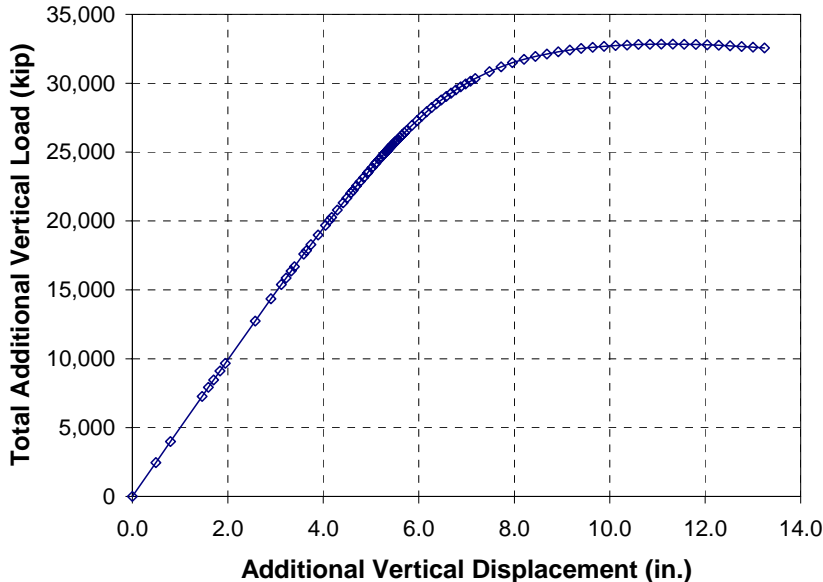


Figure 3–30. Total additional vertical load versus additional vertical displacement during push-down analysis of isolated south wall model of WTC 1 for Case A temperature condition (compression is positive).

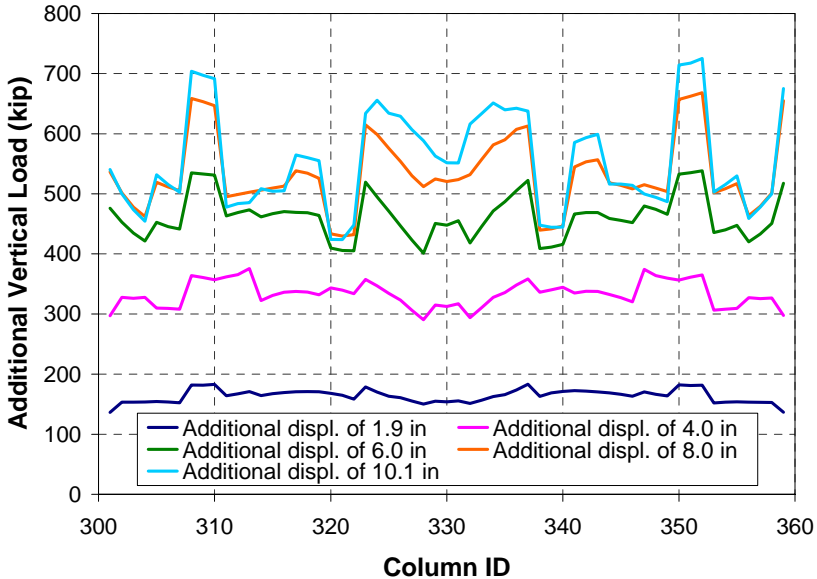
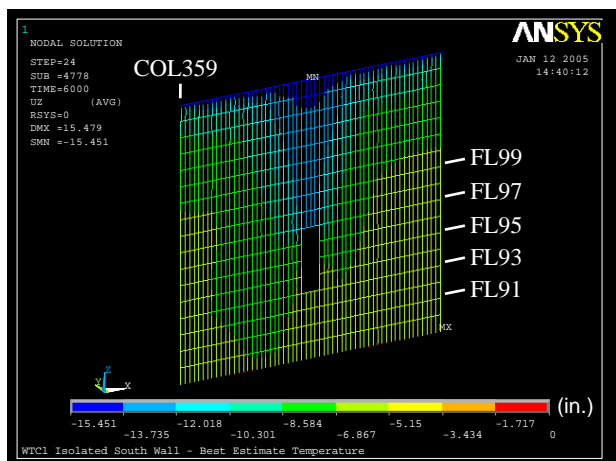
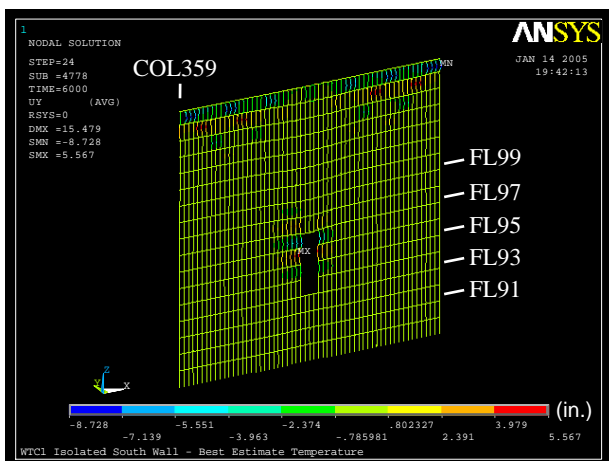


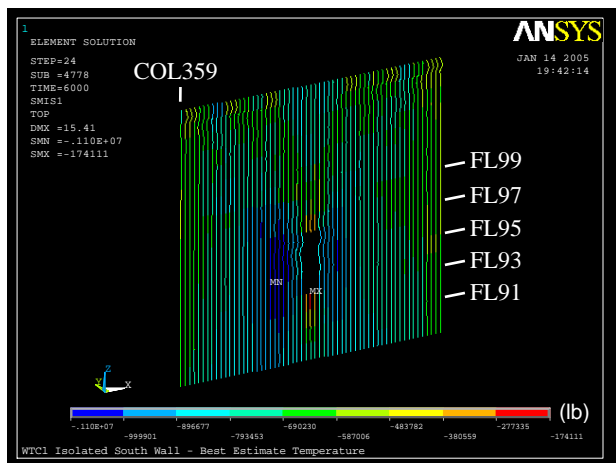
Figure 3–31. Additional vertical load per column at different additional vertical displacements during push-down analysis of isolated south wall model of WTC 1 for Case A temperature condition (compression is positive).



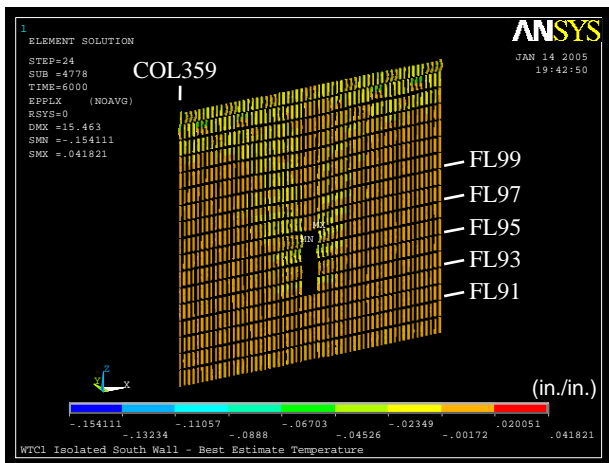
(a) Vertical displacement
(downward displacement is negative)



(b) Out-of-plane displacement
(inward displacement is positive,
5X displacement magnification)



(c) Axial force in columns
(compression is negative,
5X displacement magnification)



(d) Plastic strain in columns
(compressive strain is negative,
5X displacement magnification)

Figure 3–32. Response of isolated south wall model of WTC 1 to Case A temperature condition and push down at the end of the push-down analysis.

Case B Temperature Condition

In the full floor model analyses, described in Appendix A, Floors 97 and 98 disconnected from the exterior walls at several columns between 80 min and 90 min. Figure 3–33 shows locations of the out-of-plane supports of the exterior wall model of WTC 1 at 100 min.

Figures 3–34 to 3–43 show the temperature distributions of Case B condition in the south wall columns of WTC 1 from 10 min to 100 min. Figures 3–34 to 3–43 show that temperatures on the south wall became very high near the impact damage area, reaching 801°C. Figures 3–44 to 3–53 show the temperature distributions of Case B condition in spandrels. The temperatures of the spandrels are also quite high, reaching 778°C.

Figures 3–54 to 3–56 show the vertical displacements, the out-of-plane displacements, and the axial loads, respectively, in the south wall columns of WTC 1 for Case B temperature condition. Throughout the temperature time history the maximum vertical displacement changed negligibly, starting at 2.64 in. immediately after impact and ending at 2.60 in. at 100 min. The maximum inward out-of-plane displacement was 0.66 in. at Column 336 at Floor 98 at 100 min, while the maximum outward out-of-plane displacement was 2.3 in. at Column 342 at Floor 97. At these locations, the floor was disconnected from the exterior wall so that the unsupported length of the columns was two to three stories.

Figure 3–57 shows the plastic strains in the south wall columns at 100 min. The maximum plastic strain was only 0.5 percent at Column 325 at Floor 96.

Load redistribution to the south wall was accounted for by comparing the results of the isolated wall model to the global model, using a similar procedure to that described above for Case A (Fig. 3–58). The differences in axial loads in these two models were applied to the isolated wall model as corrective loads. Figure 3–59 shows the response of the south wall after applying these corrective loads. The WTC 1 south wall remained stable after the application of these corrective loads.

To determine the additional load-carrying capacity of the south wall at the end of the temperature analysis at 100 min, the top of the isolated exterior wall model was pushed down by converting the model from a force-control to a displacement-control analysis and by imposing additional vertical displacement increments on top of the isolated model. The analysis was terminated at an additional vertical displacement of 10.3 in. This model reached a peak total vertical load at an additional vertical displacement of 9.0 in. Figure 3–60 shows the relationship between the total additional vertical load applied and the additional vertical displacement applied. Figure 3–61 shows additional vertical load per column at different additional vertical displacements of 2 in., 4 in., 6 in., 8 in., and 10 in. Figure 3–62 shows the response of the WTC 1 south wall with the additional displacement of 10.3 in. When an additional 2 in. vertical displacement was imposed, the additional vertical load ranged from 110 kip to 200 kip, and the center columns, Column 330 to Column 340, started to buckle. Note that the additional load for the center columns dropped significantly after the onset of buckling. At an additional displacement of 10 in., the variation in columns loads became extremely large, and the additional column loads became negative at Column 332 to Column 337, indicating local instability of the exterior wall around Column 335. At the end of analysis, the outward displacement at Floor 97 increased as Column 332 to Column 337 between Floor 95 and Floor 96 buckled inward. If local instability of the exterior wall does not initiate a progressive instability (not captured by this model), the WTC 1 isolated south wall model could carry an additional vertical load of 23,000 kip (average column load of 390 kip).

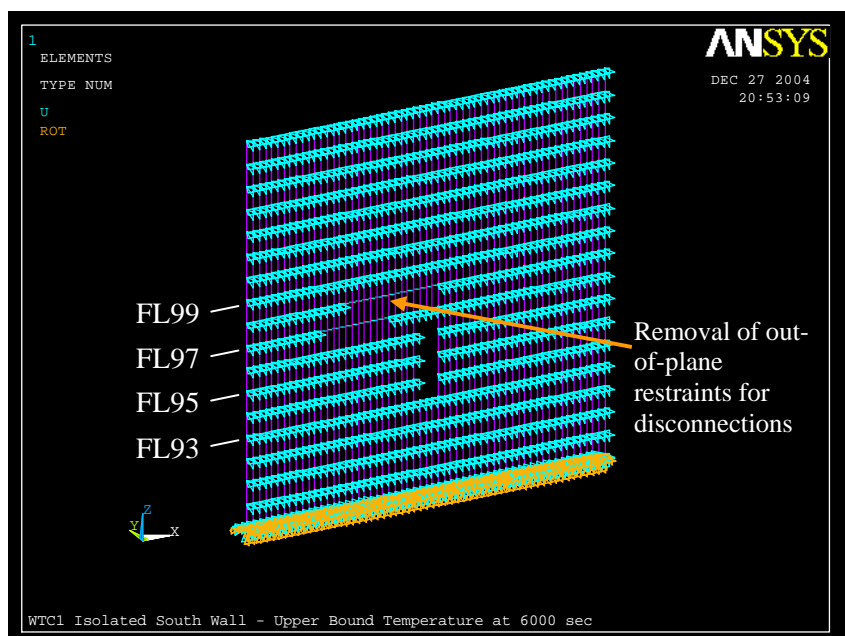
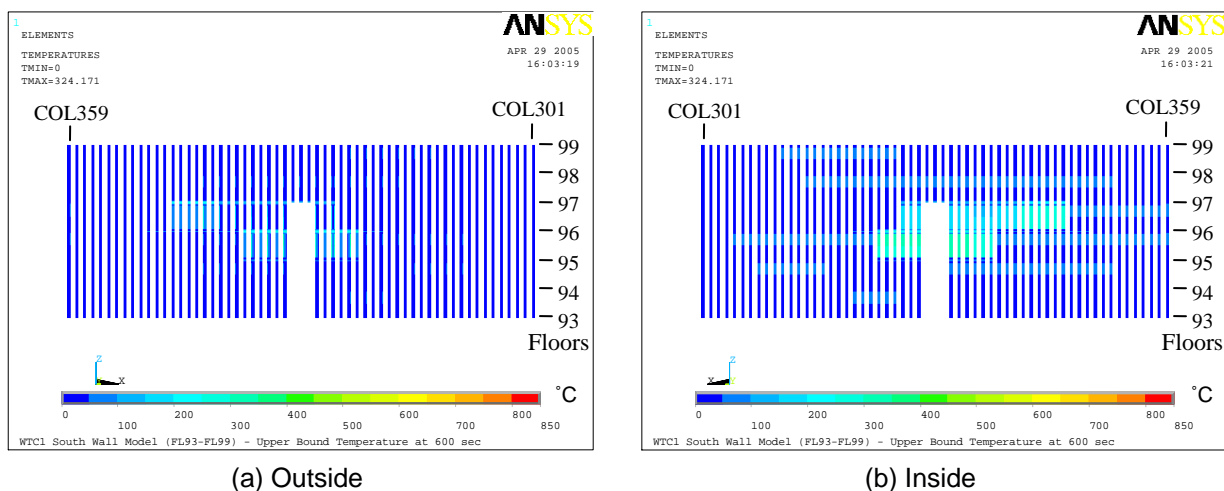


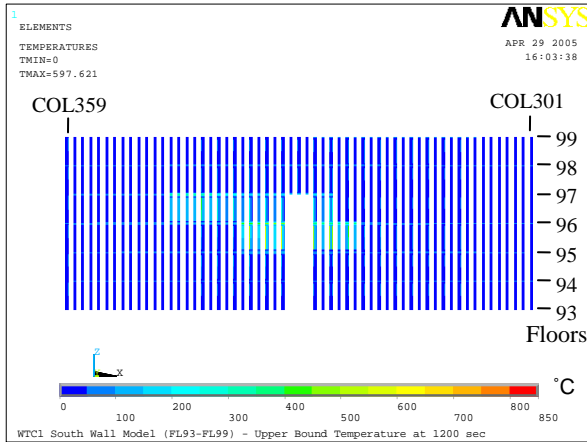
Figure 3–33. Location of the out-of-plane supports and floor/wall disconnections between exterior wall and the floor (WTC 1 south wall for Case B conditions at 100 min).



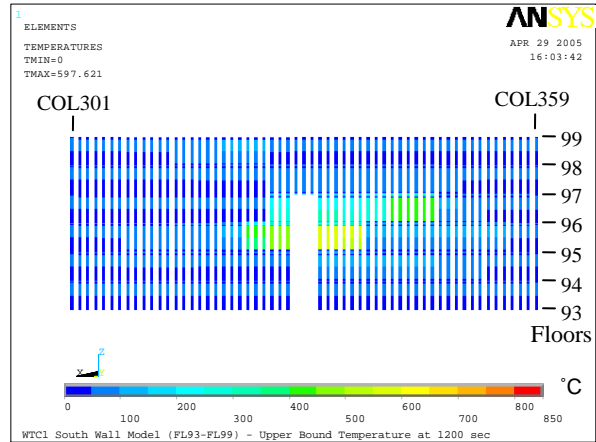
(a) Outside

(b) Inside

Figure 3–34. Case B temperature condition of south wall columns of WTC 1 at 10 min.

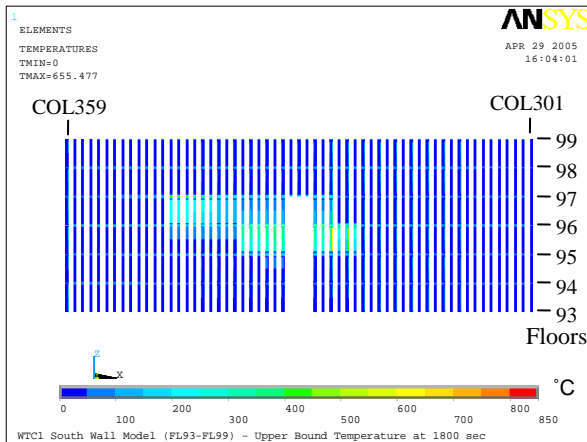


(a) Outside

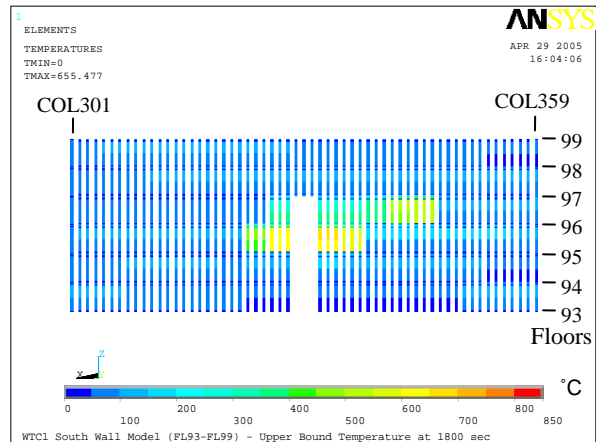


(b) Inside

Figure 3–35. Case B temperature condition of south wall columns of WTC 1 at 20 min.

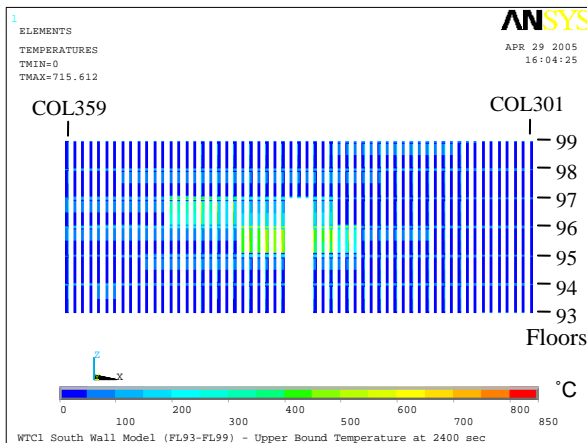


(a) Outside

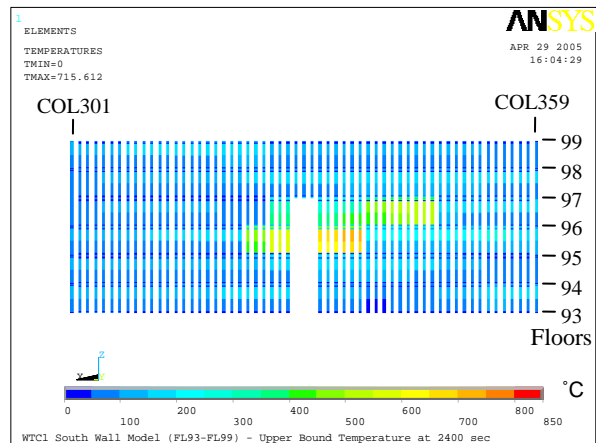


(b) Inside

Figure 3–36. Case B temperature condition of south wall columns of WTC 1 at 30 min.

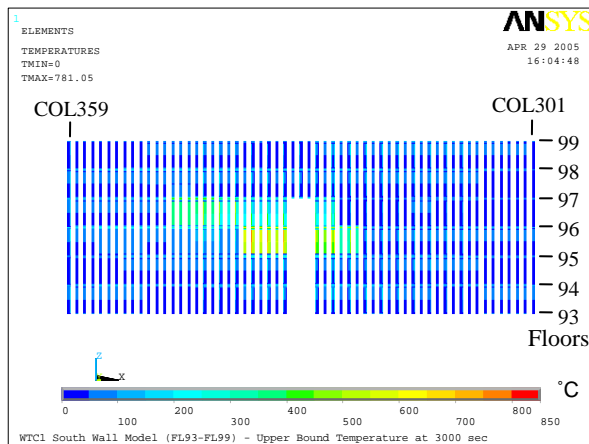


(a) Outside

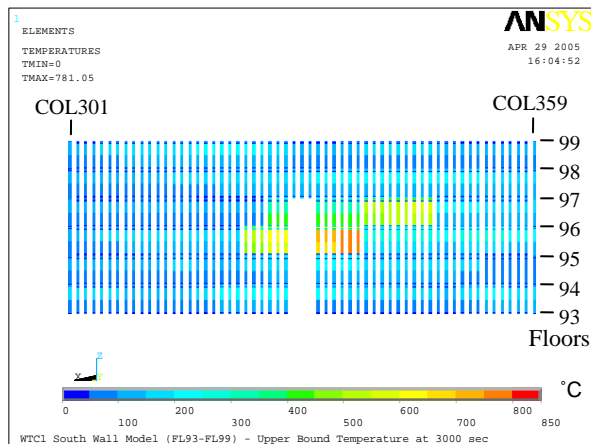


(b) Inside

Figure 3–37. Case B temperature condition of south wall columns of WTC 1 at 40 min.

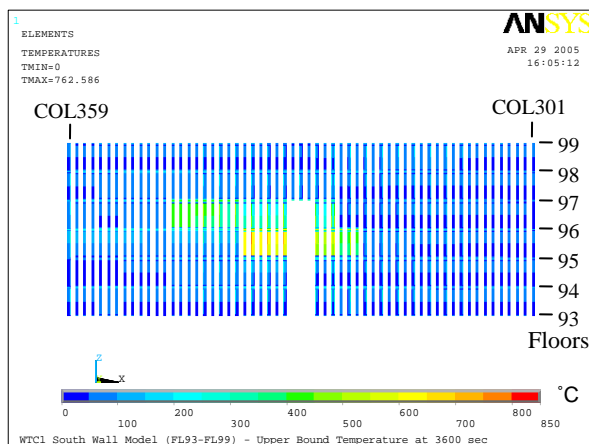


(a) Outside

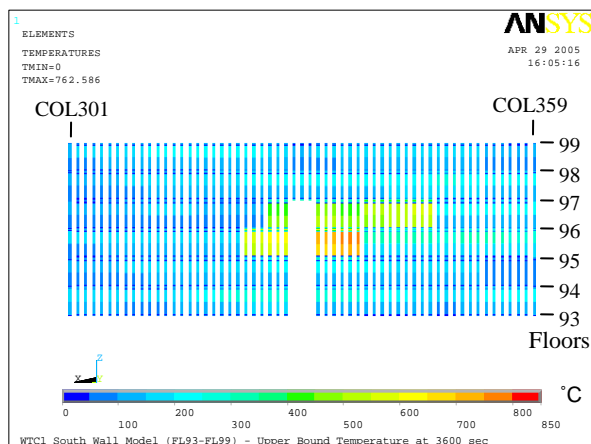


(b) Inside

Figure 3–38. Case B temperature condition of south wall columns of WTC 1 at 50 min.

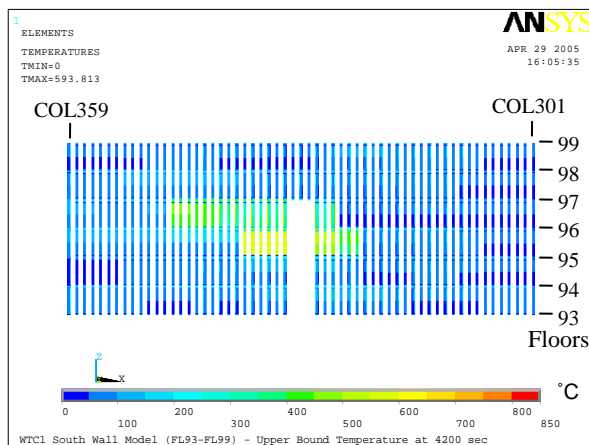


(a) Outside

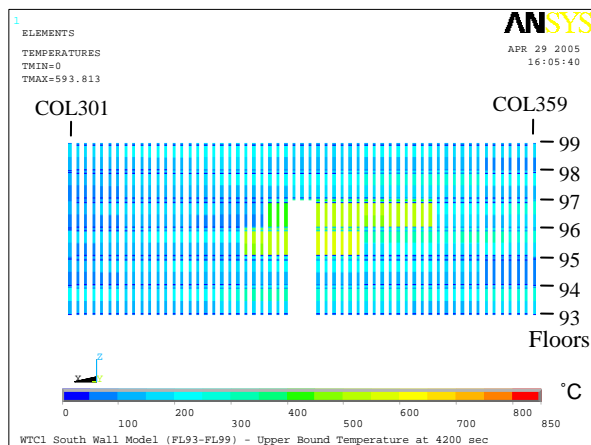


(b) Inside

Figure 3–39. Case B temperature condition of south wall columns of WTC 1 at 60 min.

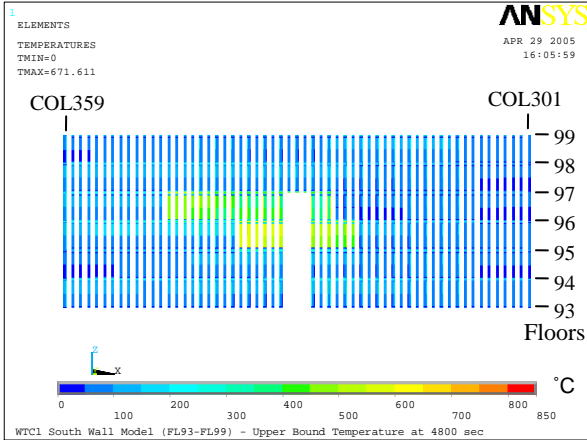


(a) Outside

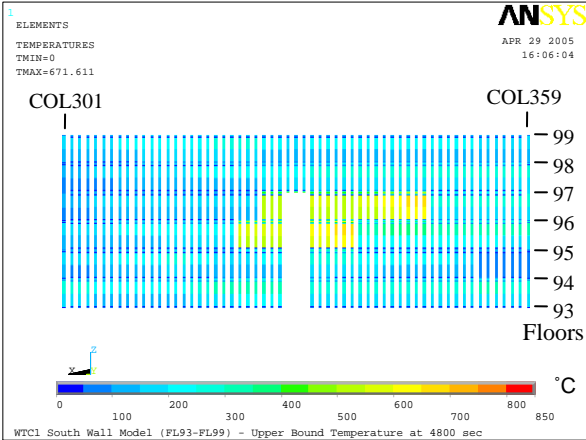


(b) Inside

Figure 3–40. Case B temperature condition of south wall columns of WTC 1 at 70 min.

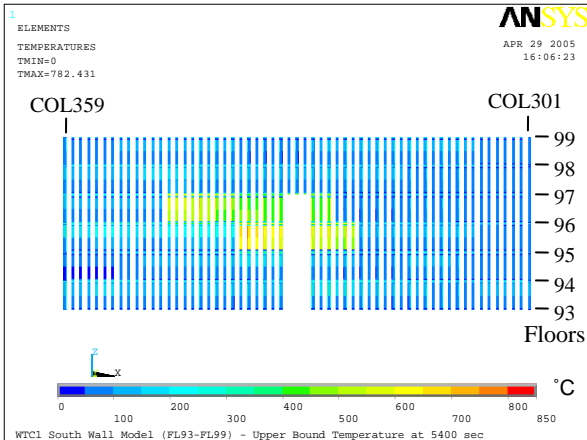


(a) Outside

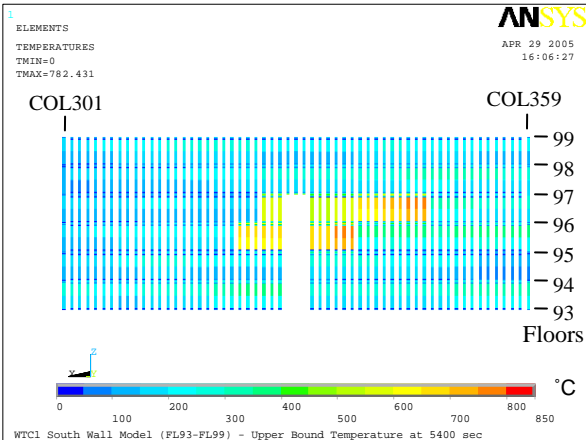


(b) Inside

Figure 3-41. Case B temperature condition of south wall columns of WTC 1 at 80 min.

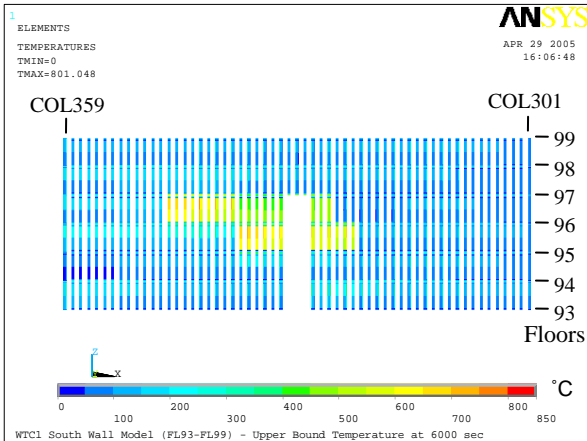


(a) Outside

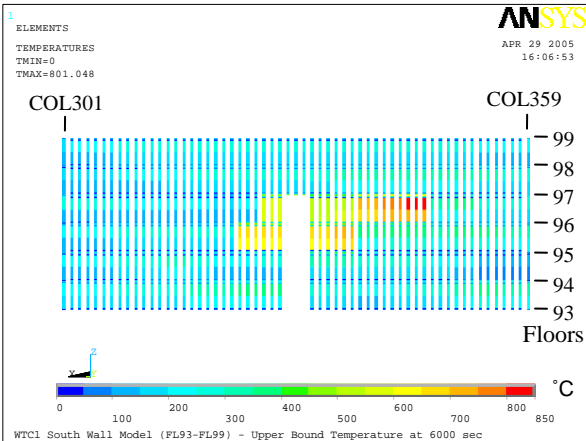


(b) Inside

Figure 3-42. Case B temperature condition of south wall columns of WTC 1 at 90 min.



(a) Outside



(b) Inside

Figure 3-43. Case B temperature condition of south wall columns of WTC 1 at 100 min.

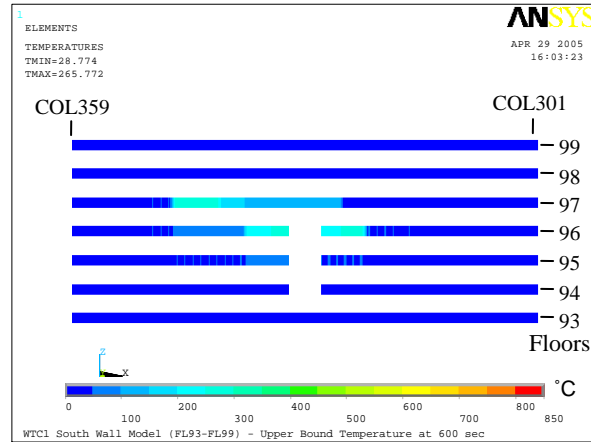


Figure 3–44. Case B temperature condition of south wall spandrels of WTC 1 at 10 min.

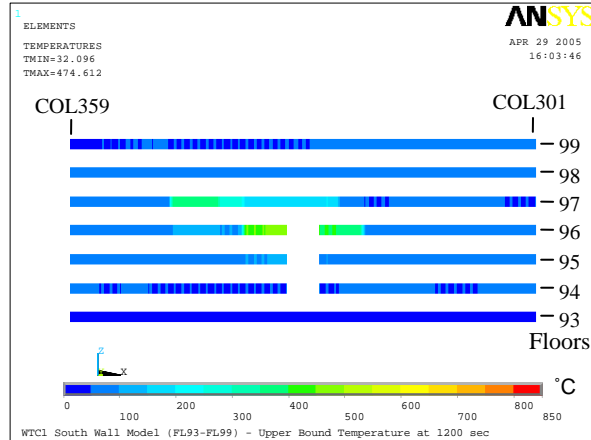


Figure 3–45. Case B temperature condition of south wall spandrels of WTC 1 at 20 min.

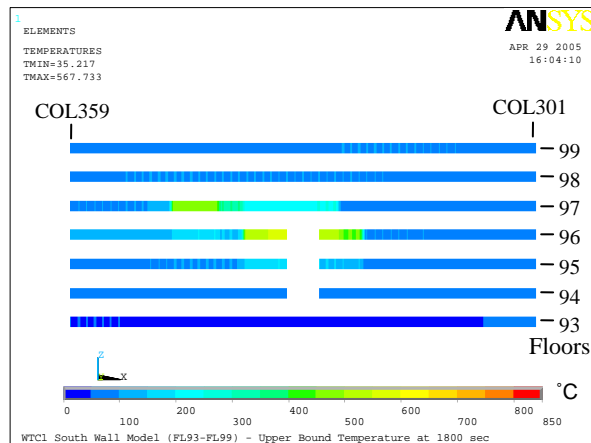


Figure 3–46. Case B temperature condition of south wall spandrels of WTC 1 at 30 min.

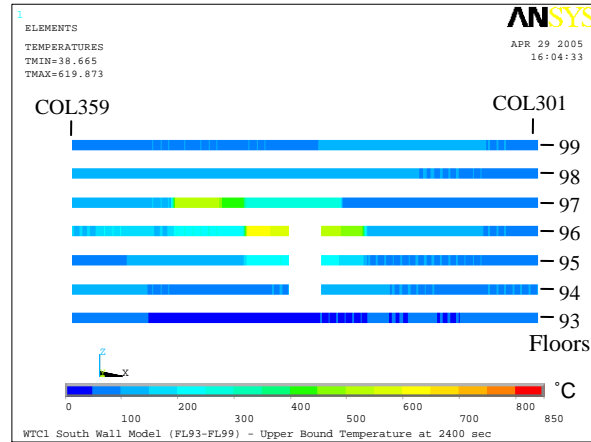


Figure 3–47. Case B temperature condition of south wall spandrels of WTC 1 at 40 min.

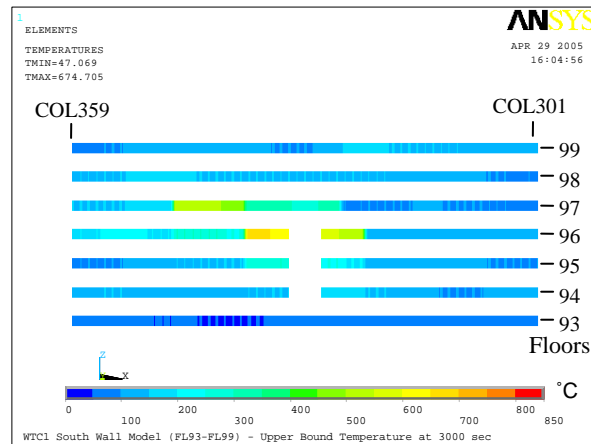


Figure 3–48. Case B temperature condition of south wall spandrels of WTC 1 at 50 min.

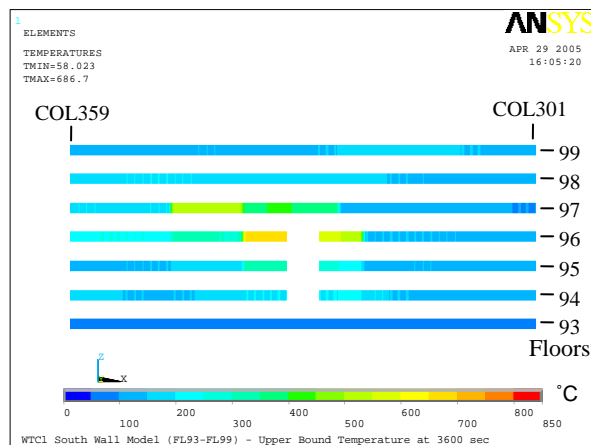


Figure 3–49. Case B temperature condition of south wall spandrels of WTC 1 at 60 min.

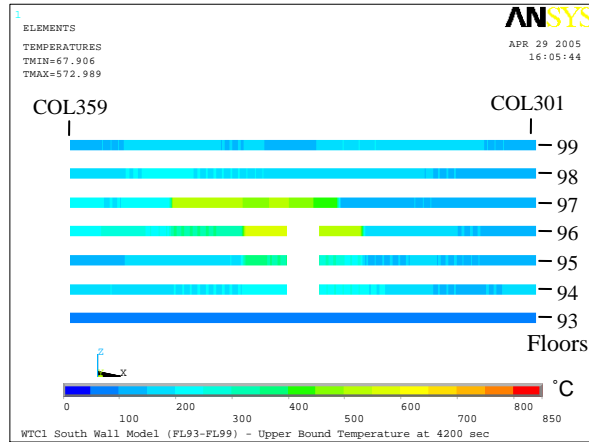


Figure 3–50. Case B temperature condition of south wall spandrels of WTC 1 at 70 min.

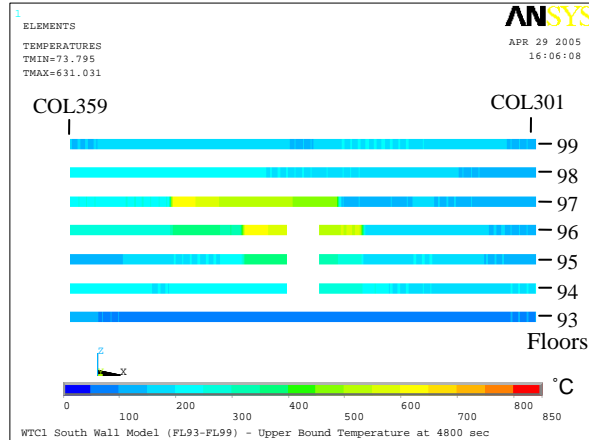


Figure 3–51. Case B temperature condition of south wall spandrels of WTC 1 at 80 min.

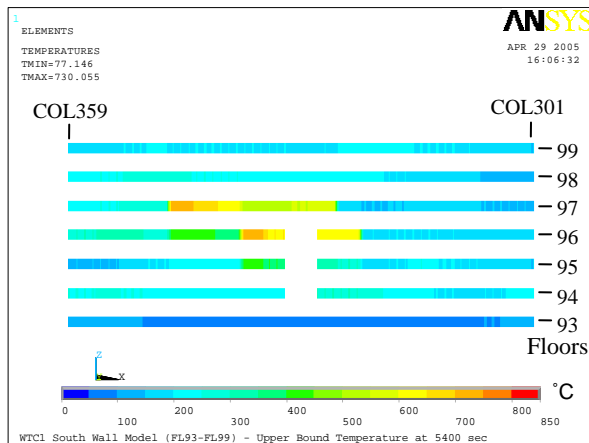


Figure 3–52. Case B temperature condition of south wall spandrels of WTC 1 at 90 min.

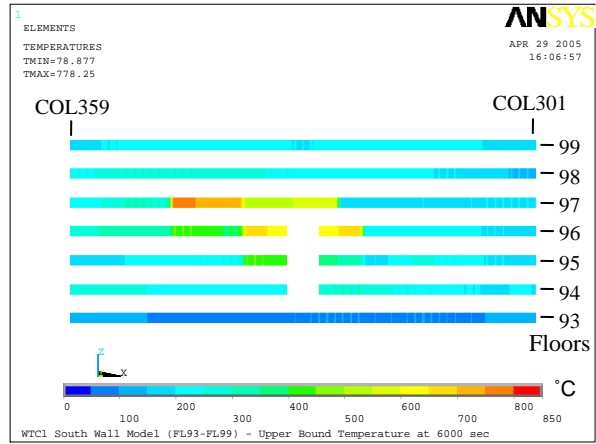
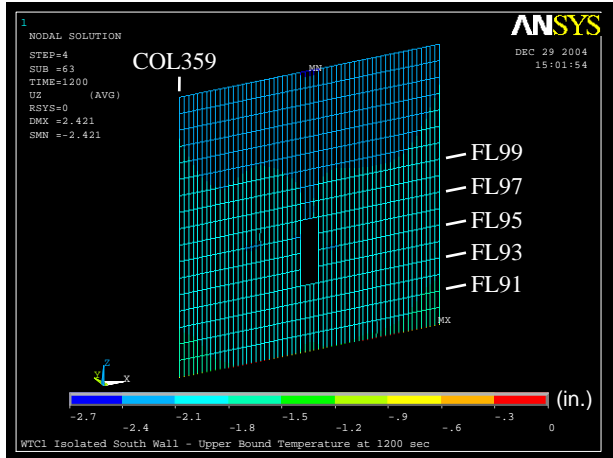
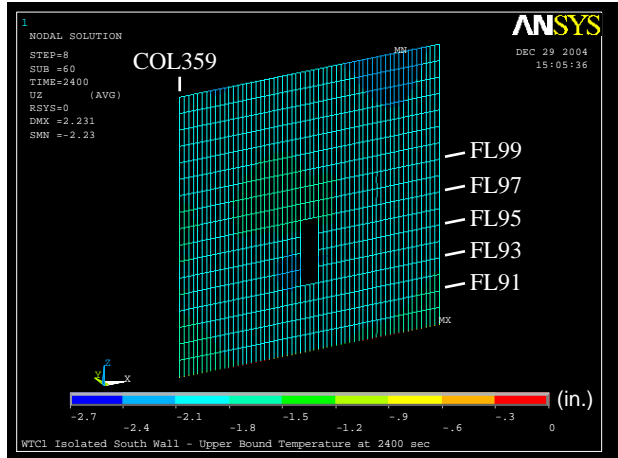


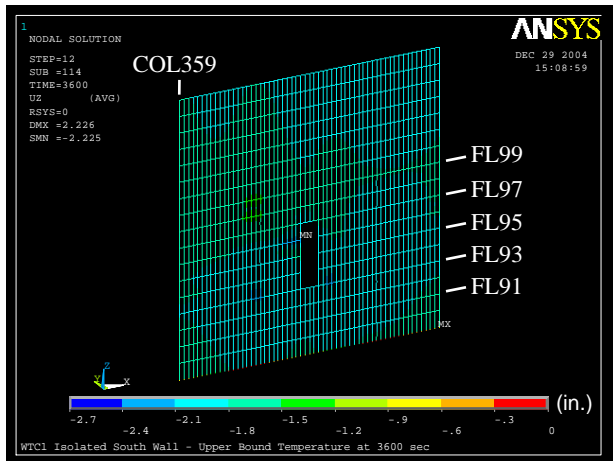
Figure 3–53. Case B temperature condition of south wall spandrels of WTC 1 at 100 min.



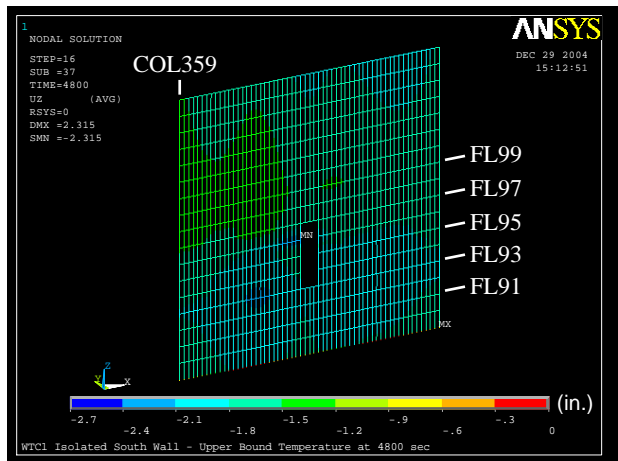
(a) At 20 min



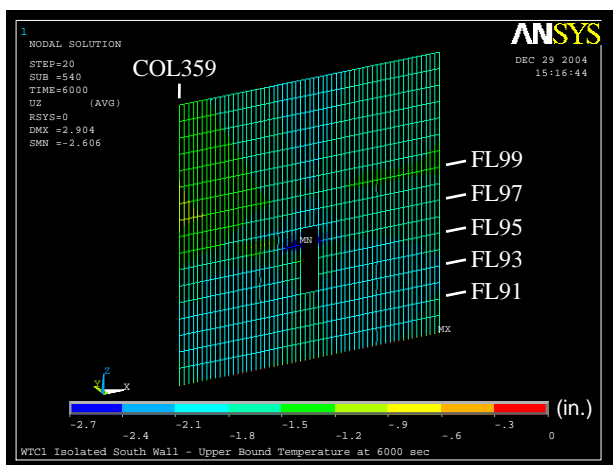
(b) At 40 min



(c) At 60 min

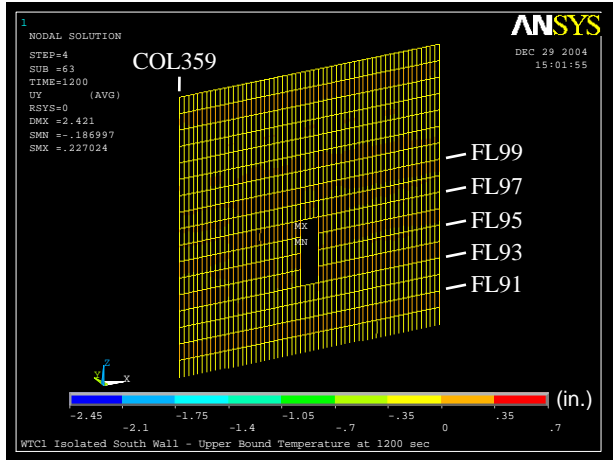


(d) At 80 min

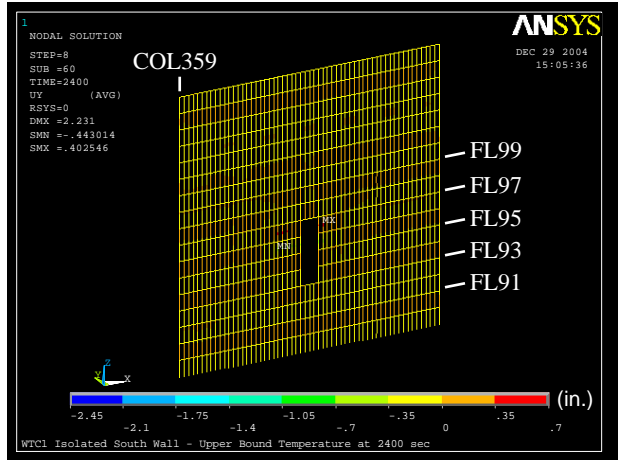


(e) At 100 min

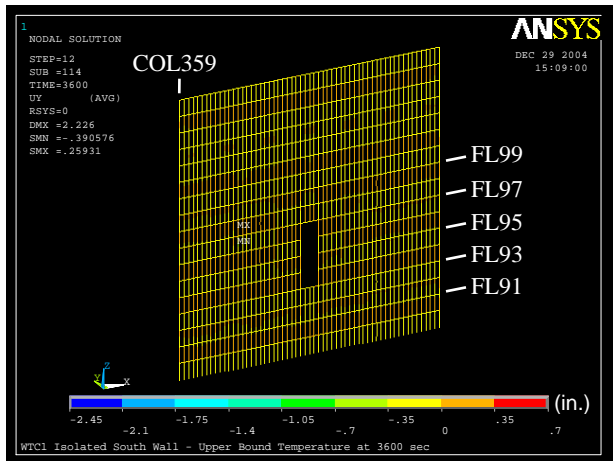
Figure 3–54. Vertical displacement of isolated south wall model of WTC 1 for Case B temperature condition (downward displacement is negative).



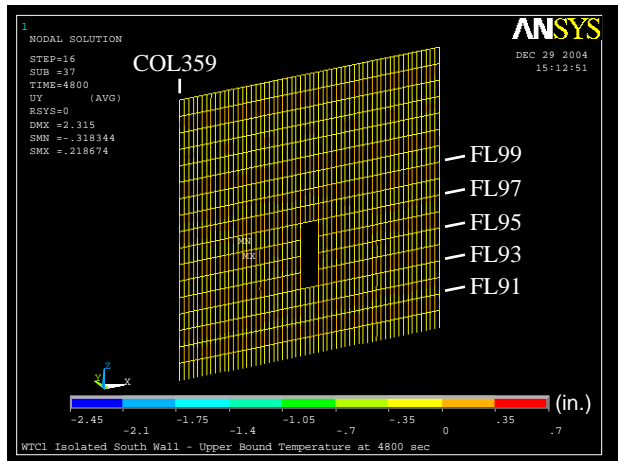
(a) At 20 min



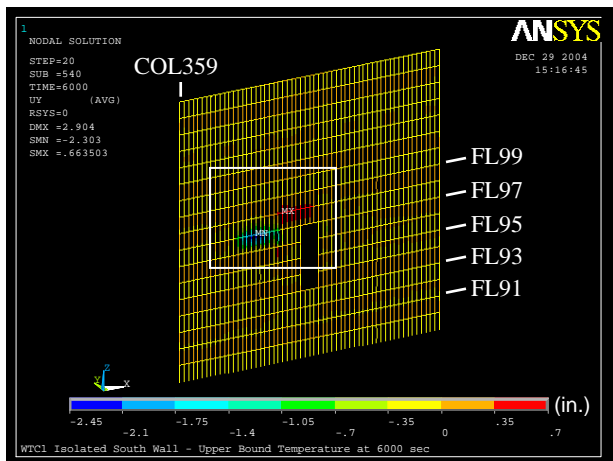
(b) At 40 min



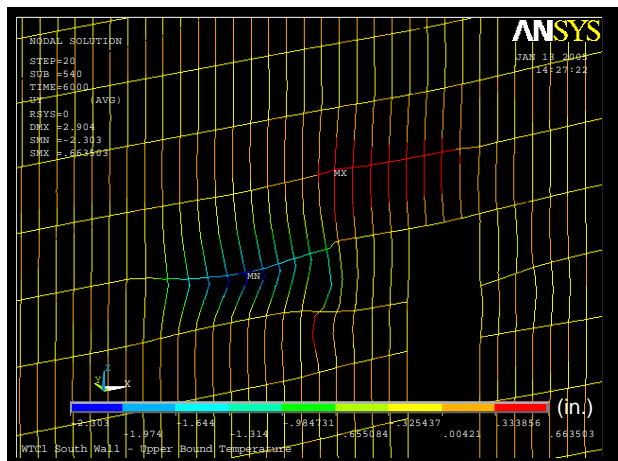
(c) At 60 min



(d) At 80 min

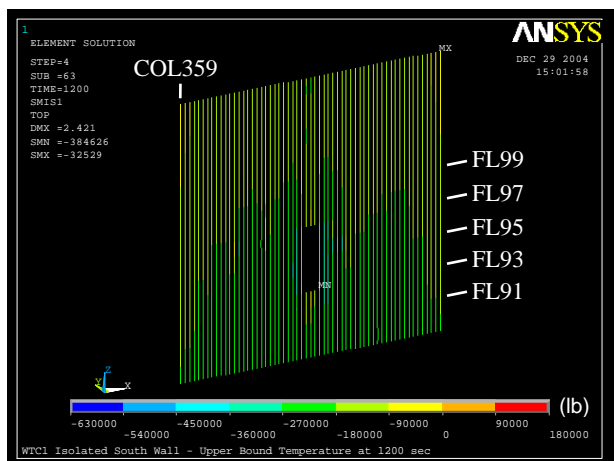


(e) At 100 min

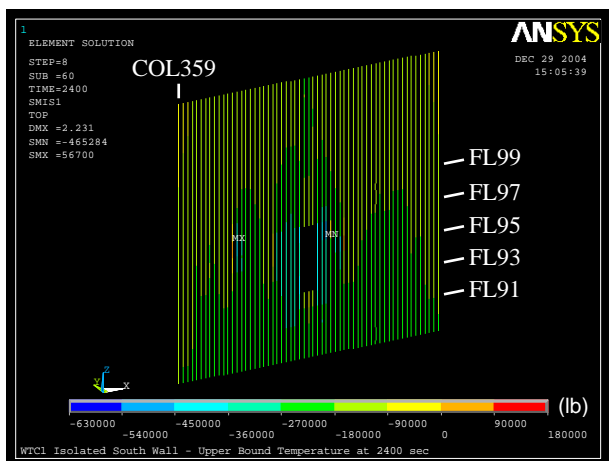


(f) At 100 min
(30X displacement magnification)

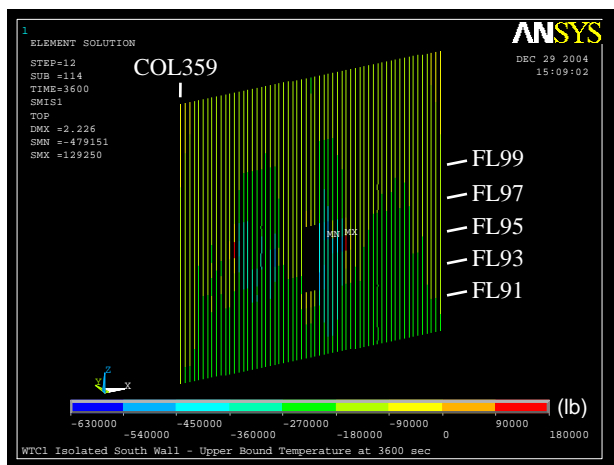
Figure 3–55. Out-of-plane displacement of isolated south wall model of WTC 1 for Case B temperature condition (inward displacement is positive).



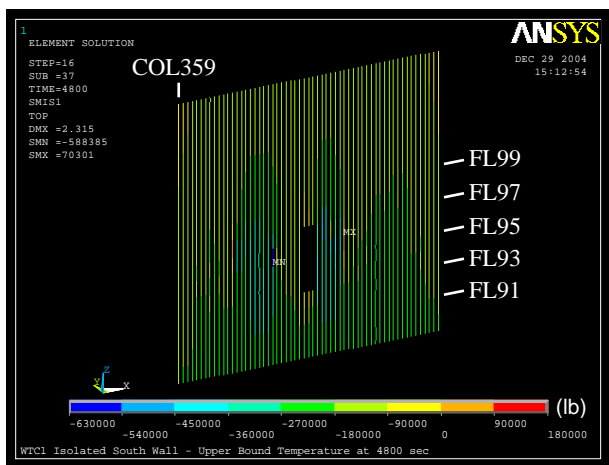
(a) At 20 min



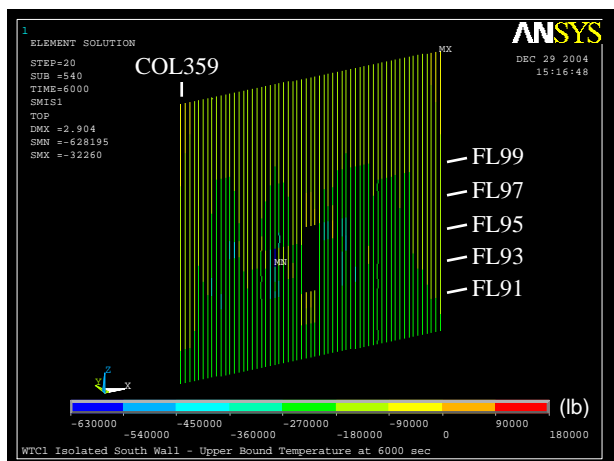
(b) At 40 min



(c) At 60 min

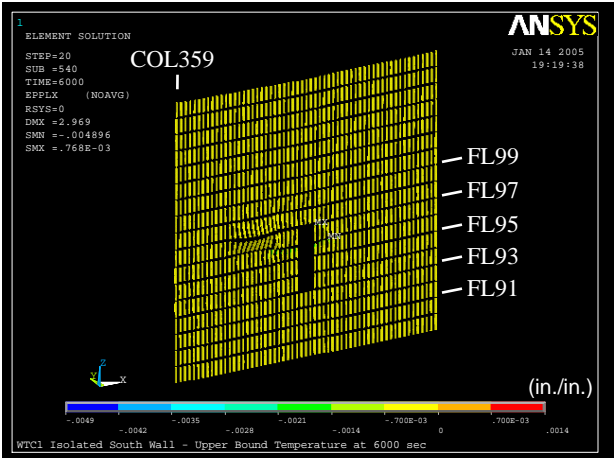


(d) At 80 min



(e) At 100 min

Figure 3-56. Axial load in columns of isolated south wall model of WTC 1 for Case B temperature condition (compression is negative).



(30X displacement magnification)

Figure 3–57. Plastic strain in columns of isolated south wall model of WTC 1 for Case B temperature condition at 100 min (compressive strain is negative).

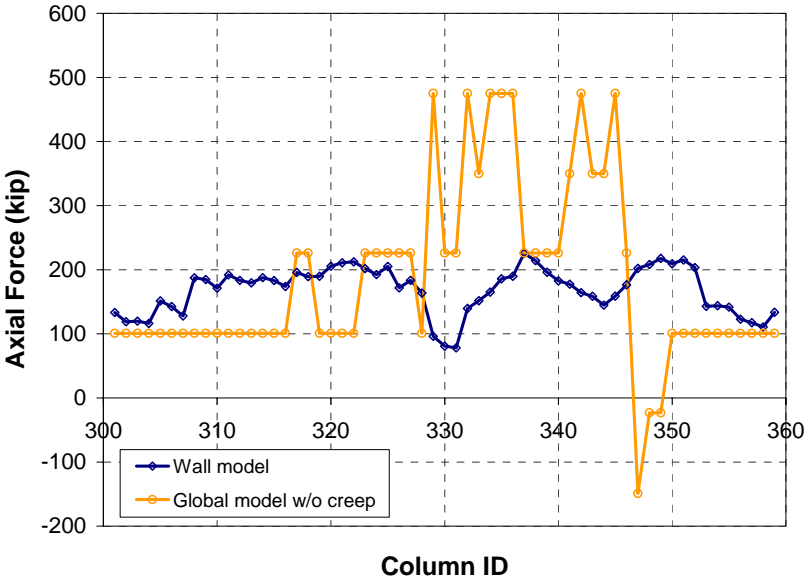
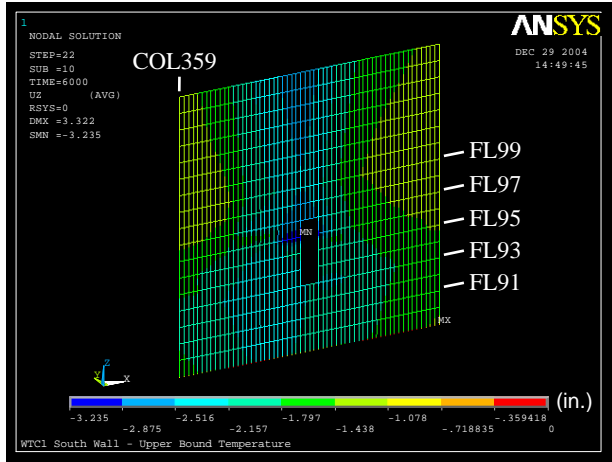
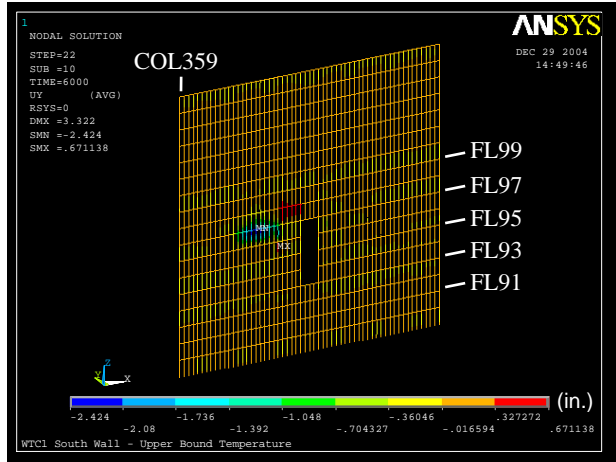


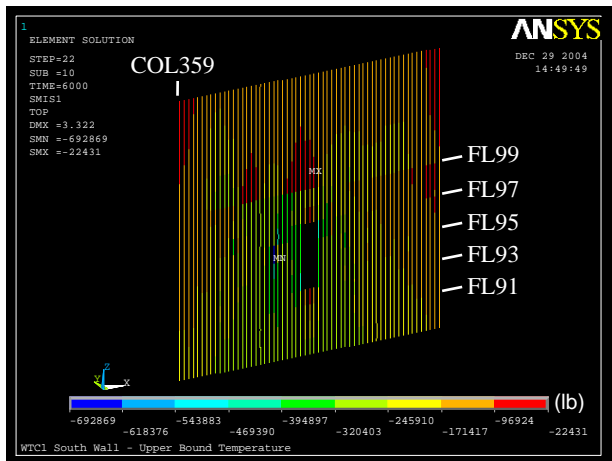
Figure 3–58. Axial load in columns of south wall of WTC 1 at 100 min: isolated wall model for Case B temperature condition compared to global model without creep for Case A_i conditions (compression is positive).



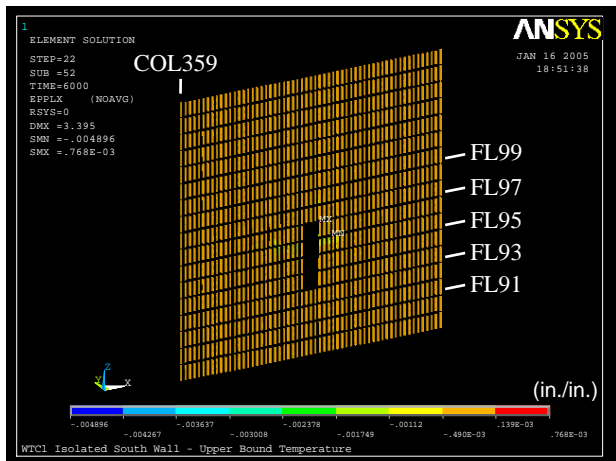
(a) Vertical displacement
(downward displacement is negative)



(b) Out-of-plane displacement
(inward displacement is positive)



(c) Axial force in columns
(compression is negative)



(d) Plastic strain in columns
(compressive strain is negative)

Figure 3–59. Response of isolated south wall model of WTC 1 after corrective loads from the global model were applied (Case B temperature condition at 100 min).

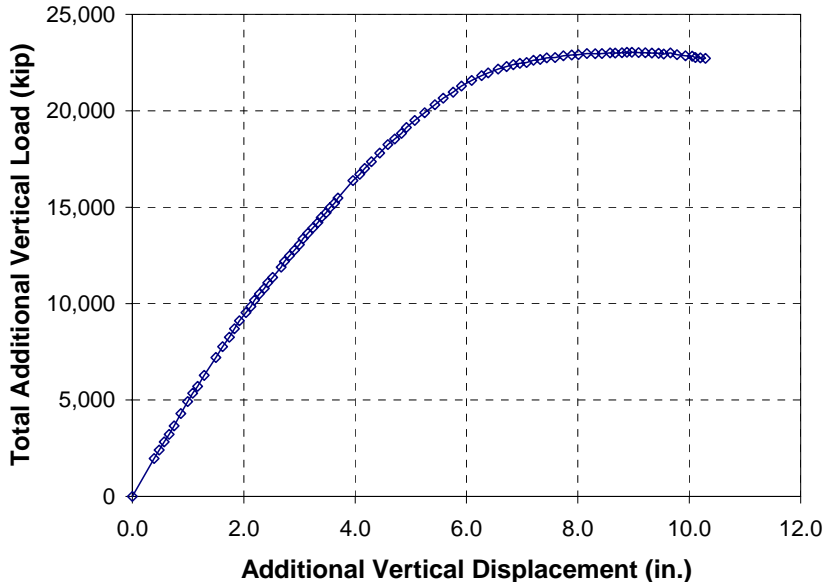


Figure 3–60. Total additional vertical load versus additional vertical displacement during push-down analysis of isolated south wall model of WTC 1 for Case B temperature condition (compression is positive).

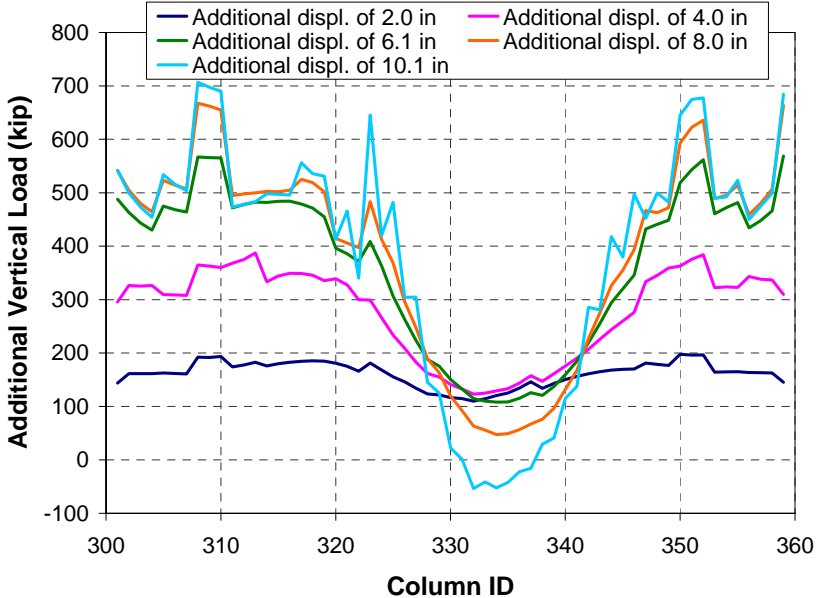
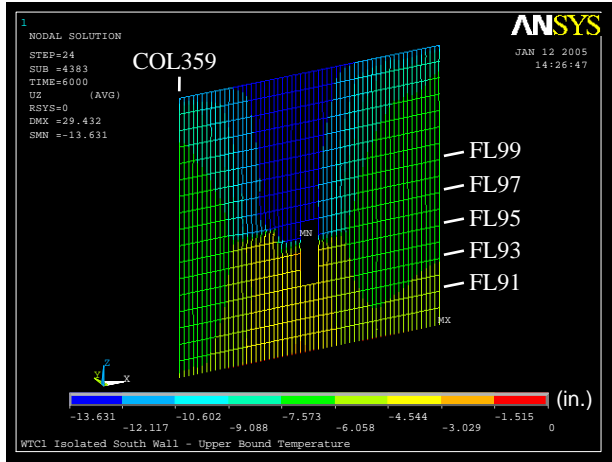
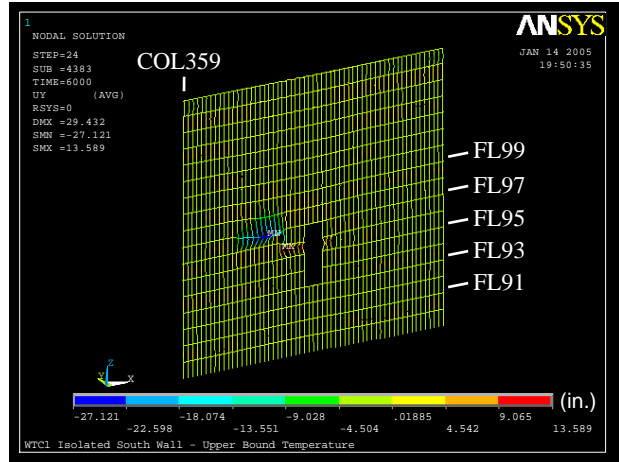


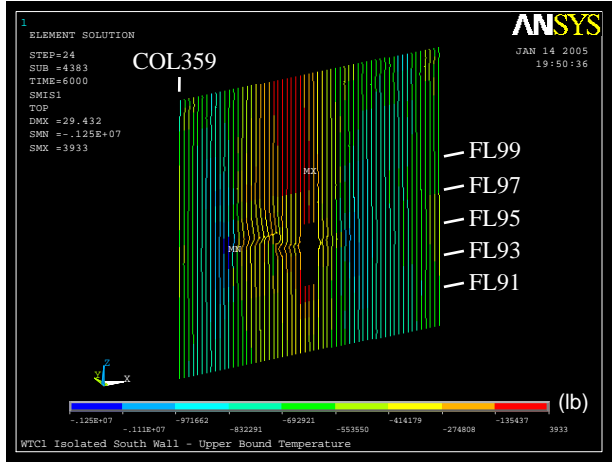
Figure 3–61. Additional load per column at different additional vertical displacements during push-down analysis of isolated south wall model of WTC 1 for Case B temperature condition (compression is positive).



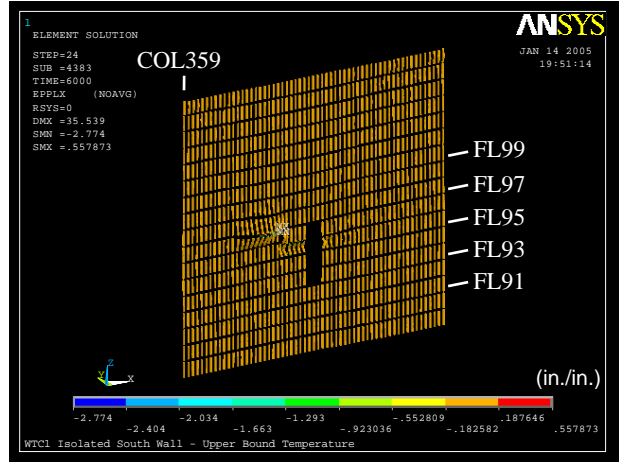
(a) Vertical displacement (downward displacement is negative)



(b) Out-of-plane displacement (inward displacement is positive, 3X displacement magnification)



(c) Axial force in columns (compression is negative, 3X displacement magnification)



(d) Plastic strain in columns (compressive strain is negative, 3X displacement magnification)

Figure 3–62. Response of isolated south wall model of WTC 1 to Case B temperature condition and push-down.

Pull-in Forces to Cause Observed Bowing

As discussed in Chapter 5, inward bowing of the exterior wall on the south face of WTC 1 can be seen in photographs of the event at 10:23 am (about 97 min after the aircraft impact), while no bowing of the south wall is evident at 9:55 am (about 68 min after the aircraft impact). The inward bowing at 97 min extended from Floors 95 to 99 between Columns 308 to 326 (possibly to 340); NIST estimated the maximum bowing to be 55 in. at Floor 97.

The isolated south wall model of WTC 1 did not bow inward under Case A temperature condition, and it bowed slightly over a very limited area under Case B temperature condition. The isolated wall model results did not capture the actual bowing.

The most plausible explanation for the discrepancy between the observed and modeled bowing of the exterior walls is that the pull-in forces were not captured in the full floor models, and floors sagged to a greater extent than these models predicted. Following are reasons the floor models likely underestimated sagging and did not accurately calculate pull-in forces.

- The exterior wall boundary conditions used in the floor models were realistic only if a single floor was heated. The floor trusses were supported on exterior columns that extended one story above and one story below the floor modeled. The far ends of the columns were restrained against translation in the direction normal to the exterior wall and rotation about the axis parallel to the exterior wall. This boundary condition was much stiffer in translation normal to the exterior wall than actually occurred for sequential floors heating simultaneously.
- The floor models did not include creep behavior in the steel or cracking of the concrete floors.
- The floor models did not include strap anchors or studs.
- More thermal insulation may have been dislodged from the trusses than estimated from the impact analysis. The impact analysis did not account for the effect of impact or vibrations on dislodging insulation.
- The floor models assumed a uniform live load. Debris accumulated in large piles was observed in some floor areas.

To model the effect of pull-in forces on inward bowing of the columns, trial values of pull-in forces were applied to the exterior columns of the south wall over five floors from Floor 95 to Floor 99 where bowing was observed.

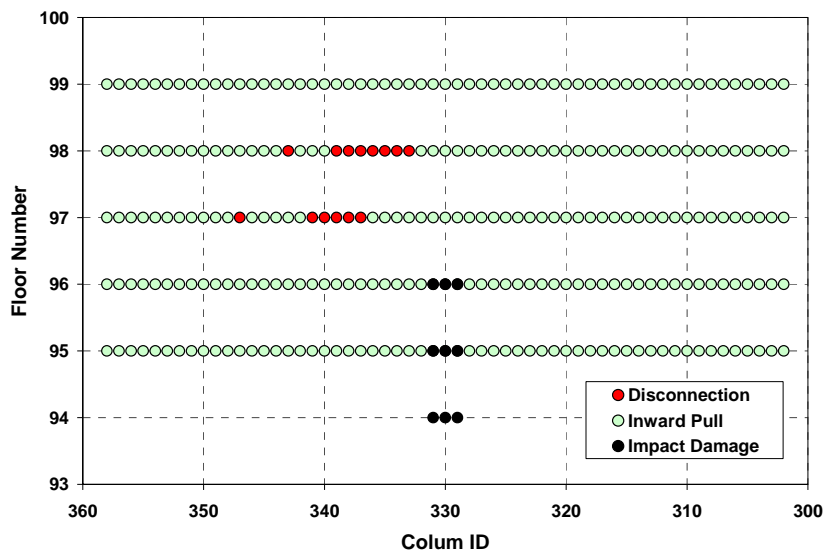
The magnitudes of the pull-in forces were determined by trial and error, matching the observed inward bowing of exterior walls for Case B temperature condition. The Case B temperature condition was used because temperatures of the south office area floors and south wall columns were much higher than those of the Case A temperature condition, and because the full floor models with the Case B_i temperature condition showed much larger floor sagging in the south office area than did the floor models with the Case A_i temperature condition.

The floor models for Case B temperature condition showed that floors began to disconnect from the south wall about 80 min after impact. In the temperature time histories of the Case B condition, temperatures of the south wall and south office area had begun to rise again after 80 min, having been relatively constant for some time. Consequently, pull-in forces were applied to the exterior wall model starting at 80 min and, the temperature time history was analyzed with these pull-in forces to 100 min. Figure 3–63 shows locations of floor/wall disconnections and pull-in forces for this analysis.

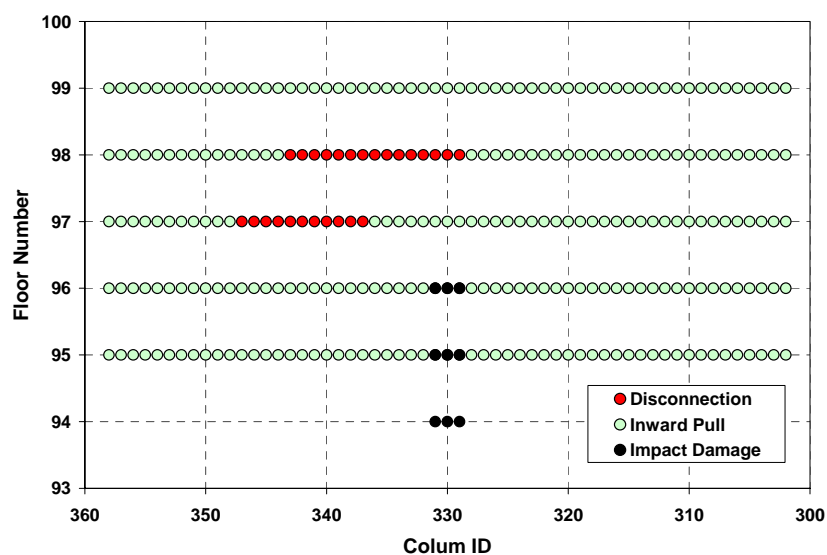
Figures 3–64, 3–65, and 3–66 show the results of the analysis performed with a 6 kip pull-in force per column. After applying 6 kip pull-in forces at 80 min, the maximum inward bowing increased to 12.2 in. as shown in Fig. 3–64. At 90 min, the maximum inward bowing became 19.0 in., and at 100 min, it reached 31.3 in., as shown in Figs. 3–65 and 3–66. The thermal loading from 80 min to 100 min increased the inward bowing significantly where there was inward bowing initially. Figure 3–67 shows the axial loads in columns between Floors 98 and 99 at 80 min, 90 min, and 100 min. At 100 min,

Columns 320 to 346 were in the post-buckling regime and were unloading. The maximum bowing of 31.3 in. was smaller than the observed maximum bowing of 55 in.. The wall remained stable at 100 min.

In the global model, the exterior wall boundary conditions were different from the isolated wall model: generally the stiffness against inward bowing in the global models was softer. In addition, the exterior walls were expected to carry additional gravity loads redistributed from the core due to downward displacement of the core resulting from creep and inelastic buckling. Consequently, it is likely that the inward bowing of the global model would be significantly larger than 31 in. with the same 6 kip pull-in forces. Therefore, 4 or 5 kip pull-in forces were selected for the WTC 1 global analysis.

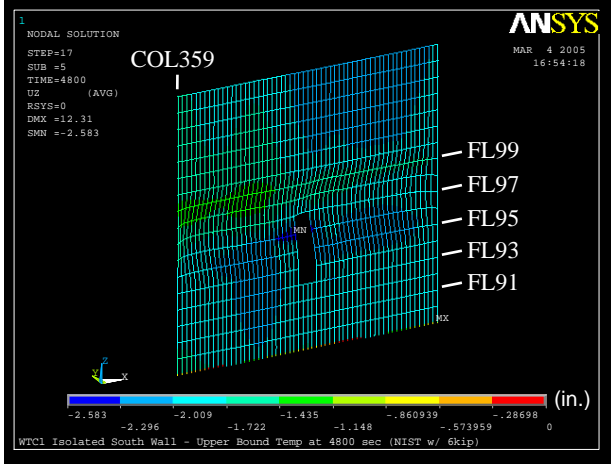


(a) Between 80 min and 90 min

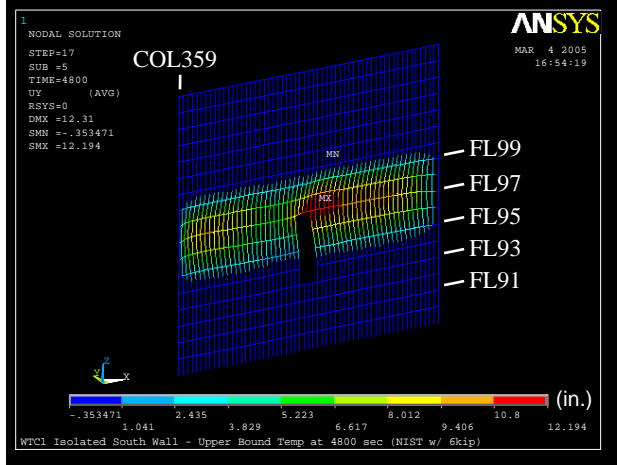


(b) Between 90 min and 100 min

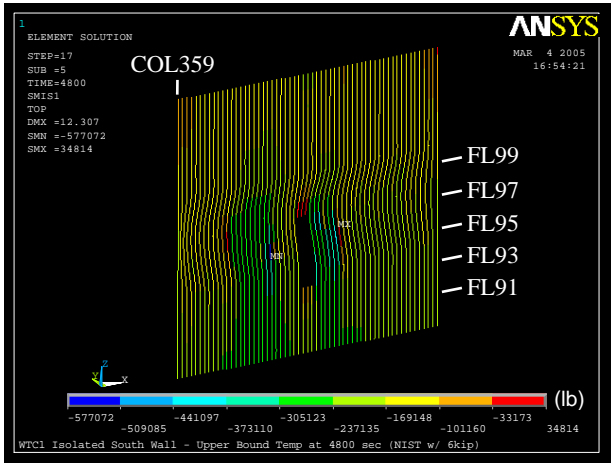
Figure 3–63. Locations of floor/wall disconnections and pull-in forces used between 80 min and 100 min of Case B temperature for south wall of WTC 1.



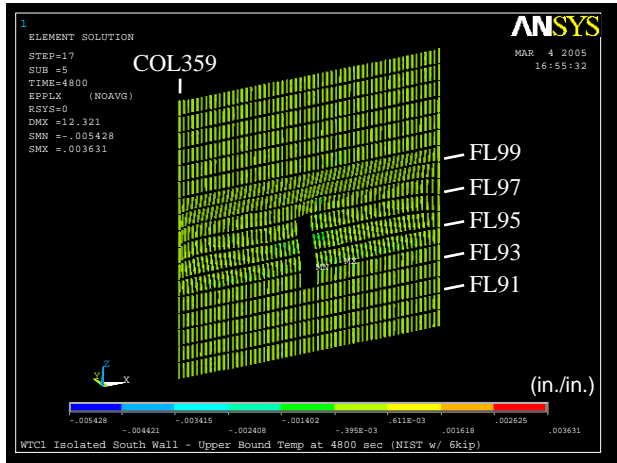
(a) Vertical displacement (downward displacement is negative, 10X displacement magnification)



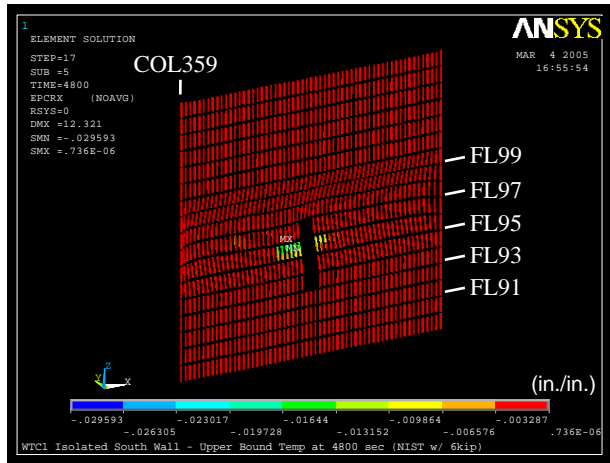
(b) Out-of-plane displacement (inward displacement is positive, 10X displacement magnification)



(c) Axial force in columns (compressive is negative, 10X displacement magnification)

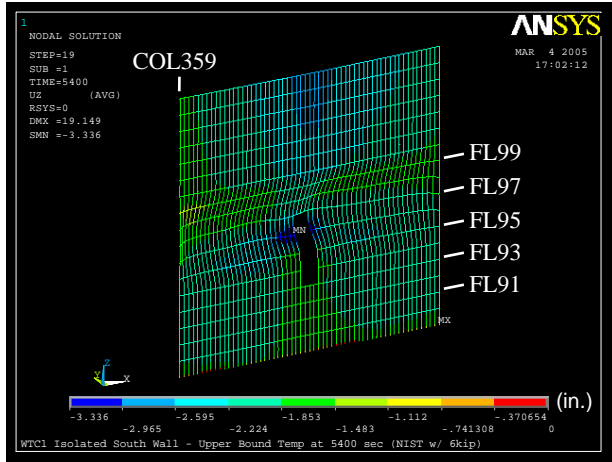


(d) Plastic strain in columns (compressive strain is negative, 10X displacement magnification)

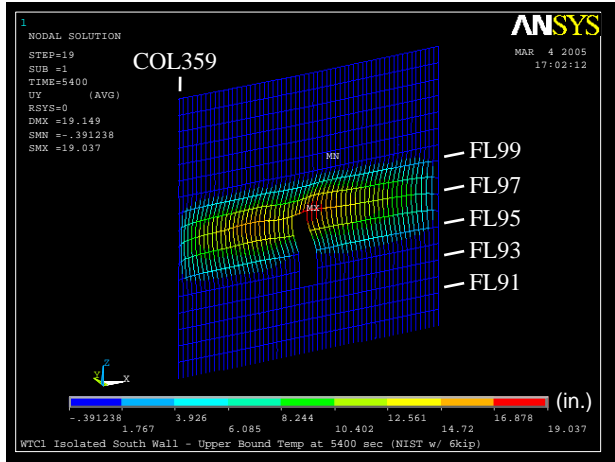


(e) Creep strain in columns (compressive strain is negative, 10X displacement magnification)

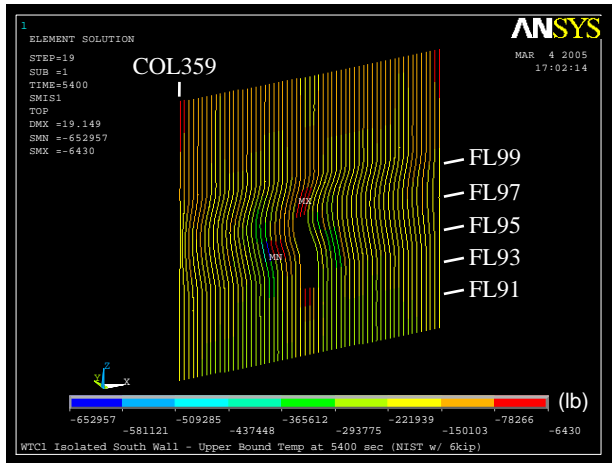
Figure 3–64. Response of isolated south wall model of WTC 1 at 80 min of Case B temperature condition with floor/wall disconnections and 6 kip pull-in forces over five floors.



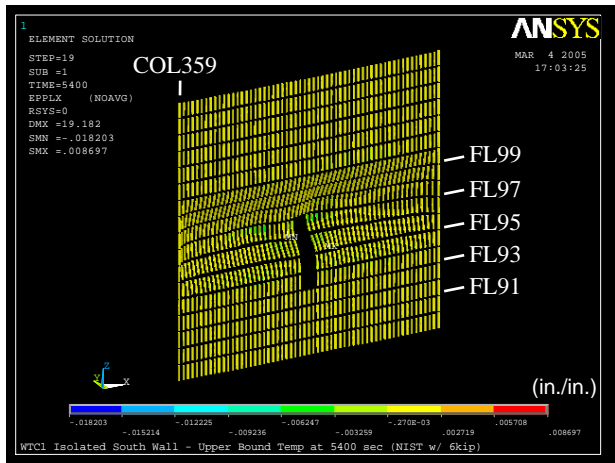
(a) Vertical displacement (downward displacement is negative, 10X displacement magnification)



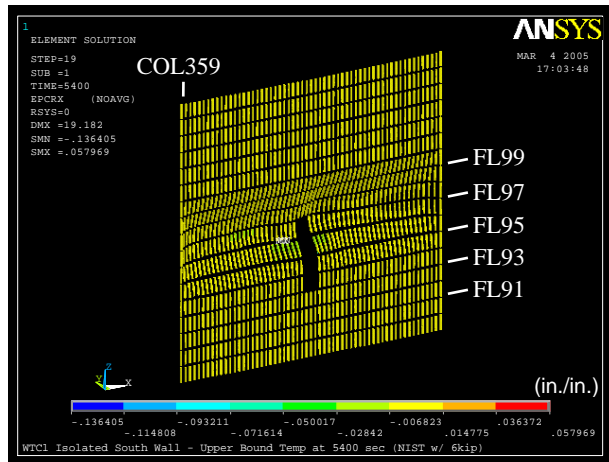
(b) Out-of-plane displacement (inward displacement is positive, 10X displacement magnification)



(c) Axial force in columns (compressive is negative, 10X displacement magnification)

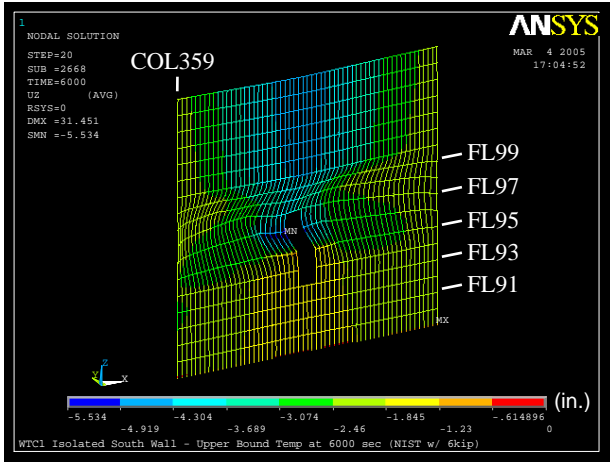


(d) Plastic strain in columns (compressive strain is negative, 10X displacement magnification)

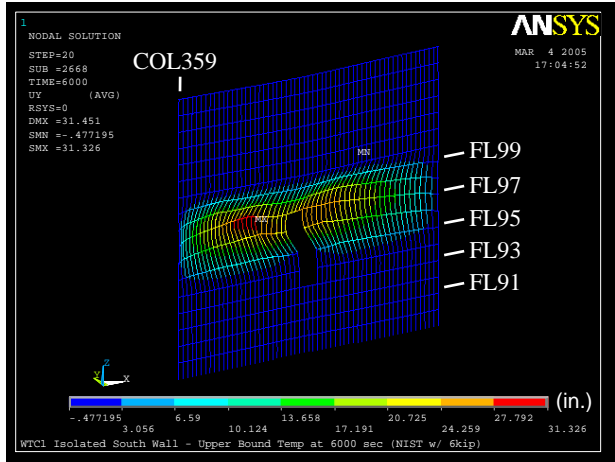


(e) Creep strain in columns (compressive strain is negative, 10X displacement magnification)

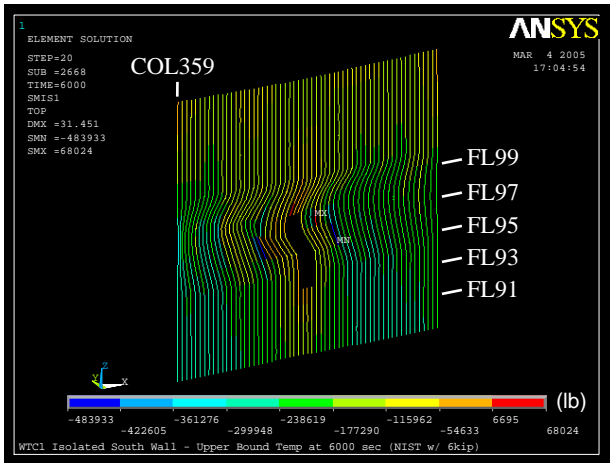
Figure 3–65. Response of isolated south wall model of WTC 1 at 90 min of Case B temperature condition with floor/wall disconnections and 6 kip pull-in forces over five floors.



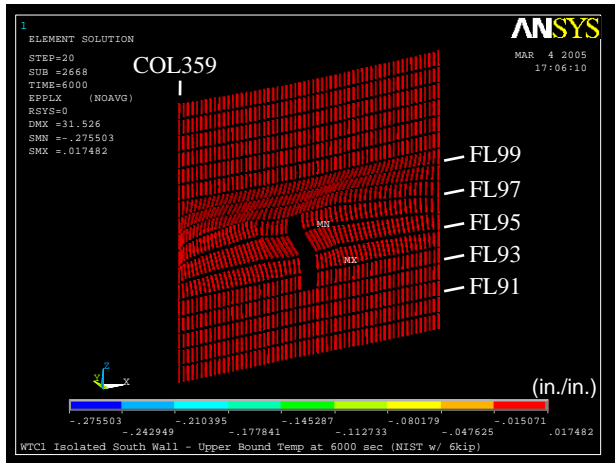
(a) Vertical displacement (downward displacement is negative, 10X displacement magnification)



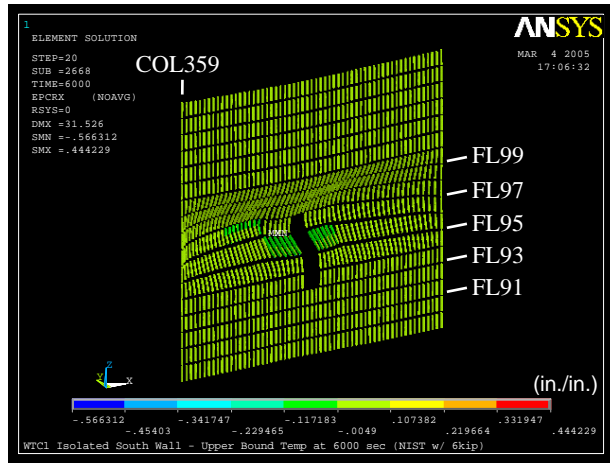
(b) Out-of-plane displacement (inward displacement is positive, 10X displacement magnification)



(c) Axial force in columns (compressive is negative, 10X displacement magnification)



(d) Plastic strain in columns (compressive strain is negative, 10X displacement magnification)



(e) Creep strain in columns (compressive strain is negative, 10X displacement magnification)

Figure 3–66. Response of isolated south wall model of WTC 1 at 100 min of Case B temperature condition with floor/wall disconnections and 6 kip pull-in forces over five floors.

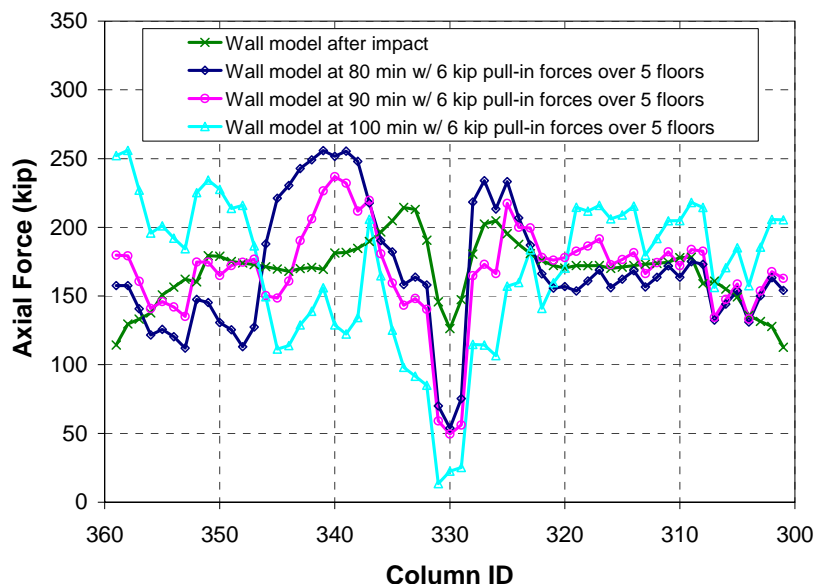


Figure 3–67. Axial load in columns between Floors 98 and 99 of isolated south wall model of WTC 1 at 80 min, 90 min, and 100 min of Case B temperature condition with floor/wall disconnections and 6 kip pull-in forces over five floors (compression is positive).

3.2.2 FEA of WTC 2 Exterior Wall

Case C Temperature Condition

Figures 3–68 and 3–69 show Case C temperature distributions in the columns of the isolated east exterior wall of WTC 2. The highest temperature, 850°C, occurred at 60 min in Column 303 between Floor 81 and Floor 82 for Case C temperature condition. Column temperatures were higher on the inside face of the exterior wall. Figure 3–70 shows the locations of the out-of-plane supports for Case C conditions at 60 min.

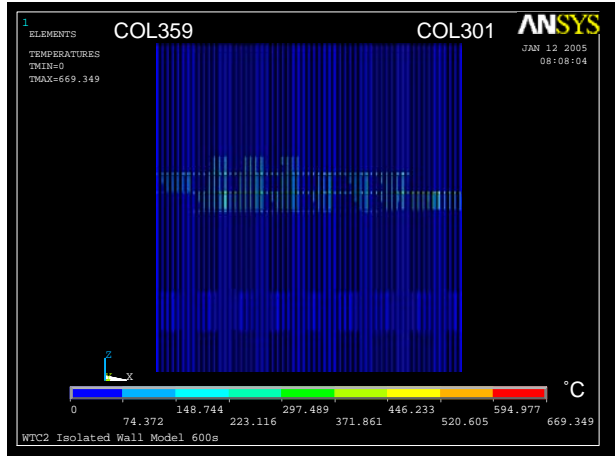
The vertical and the out-of-plane displacements at the end of the gravity load step after aircraft impact and at the end of each temperature step are shown in Figs. 3–71, 3–72, 3–73, and 3–74. The maximum vertical displacement of 3.6 in. occurred at Column 301 at Floor 90 at 60 min. The maximum out-of-plane deflection of 4.0 in. occurred at Column 302 at Floor 82 at 60 min (out-of-plane displacement is positive outward). The south side of the isolated east exterior wall displaced vertically after aircraft impact more than other parts of the east wall, as the impact damage was concentrated mostly on the southeast corner of the WTC 2. The maximum vertical displacement shifted to the north during the heating period. As time approached 60 min after the aircraft impact, the columns on the north side buckled, and the out-of-plane displacement increased.

The axial load distributions of the columns at the end of the gravity load step and each 10 min time interval are shown in Figs. 3–75 and 3–76. The maximum axial load occurred at Column 332 between Floor 83 and Floor 84 at 50 min. The axial load in this column increased from 330 kip after the aircraft

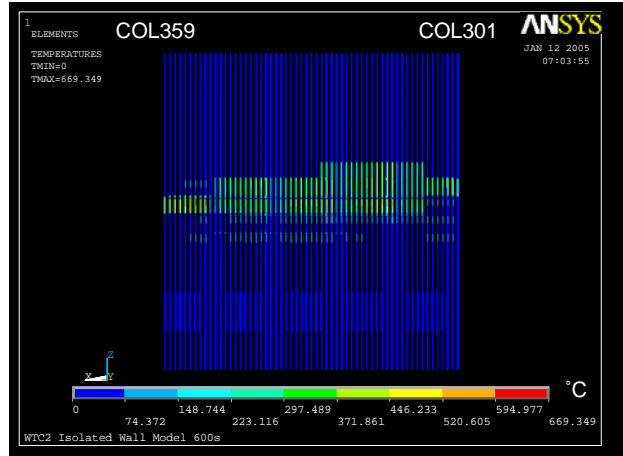
impact to 750 kip at 50 min. The axial load on the buckled columns on the north side of the isolated wall remained approximately constant throughout the temperature time history.

To consider the effect of load redistribution within the tower, the same corrective technique described earlier in this chapter for WTC 1 was used. The axial loads in columns between Floor 83 and Floor 84 in the isolated east wall model were compared with those obtained from the preliminary global model analysis without creep and with Case C₁ temperature and impact damage conditions (Appendix C). Column loads obtained from the preliminary global model and isolated exterior wall model at 60 min are shown in Fig. 3–77. The difference between the two column loads was applied to the columns of the isolated wall model at Floor 84 as corrective loads. The resulting vertical and out-of-plane displacements are shown in Fig. 3–78. The additional column loads increased the maximum vertical displacement by only 0.1 in., and the maximum out-of-plane displacement by less than 0.1 in.

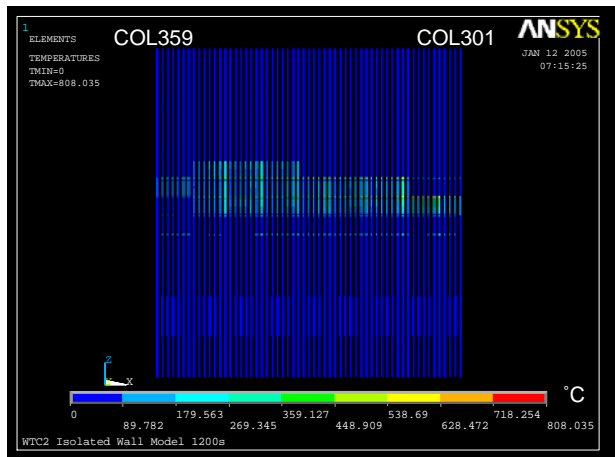
Also as described earlier for the WTC 1 isolated wall model, a push-down analysis of the WTC 2 isolated exterior wall model was performed. At an additional 5.6 in. of vertical displacement the model failed to converge, and the analysis was terminated. The vertical and out-of-plane displacements at the end of 5.6 in. of push down are shown in Fig. 3–79. At the end of push down, the maximum total vertical displacement increased to 9.4 in., and the maximum out-of-plane displacement increased to 17.2 in. Axial column loads are shown in Fig. 3–80. This figure also shows the location of the columns for which the load-deflection relationships are shown in Fig. 3–81. As can be seen from Fig. 3–81, the buckled columns on the north side of the isolated east exterior wall carried, on average, an additional 300 kip at 60 min temperatures, compared to 470 kip for the average of the entire east wall columns. The additional axial loads on individual columns at different additional vertical displacements are shown in Fig. 3–82.



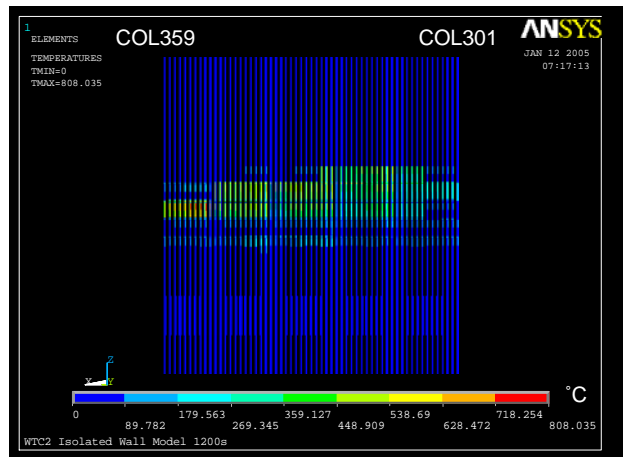
(a) Outside at 10 min



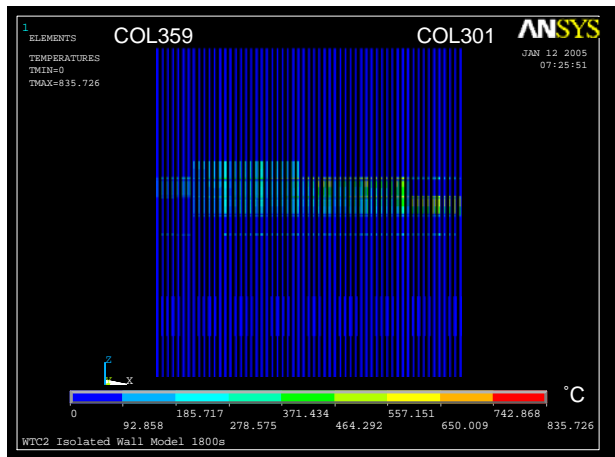
(b) Inside at 10 min



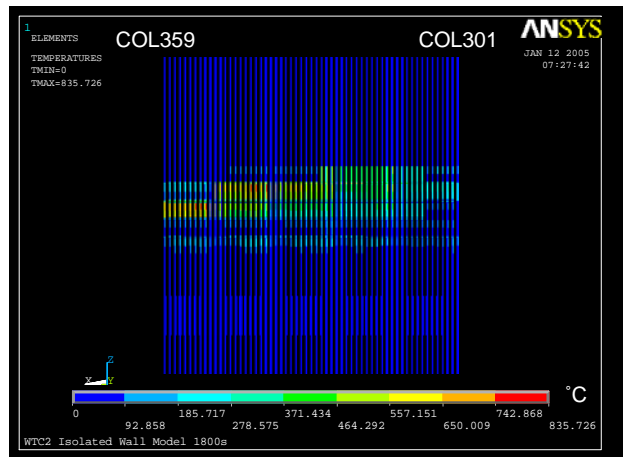
(c) Outside at 20 min



(d) Inside at 20 min

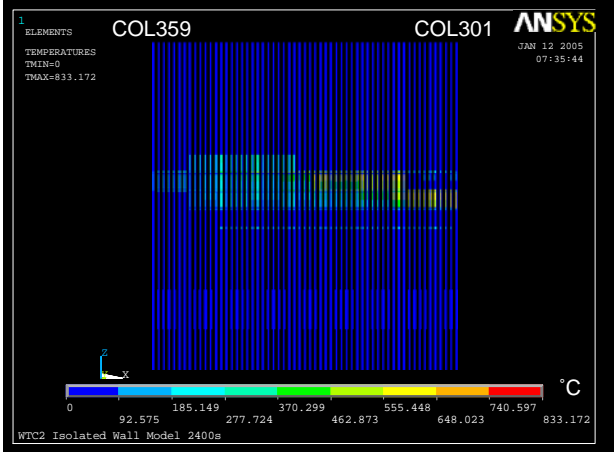


(e) Outside at 30 min

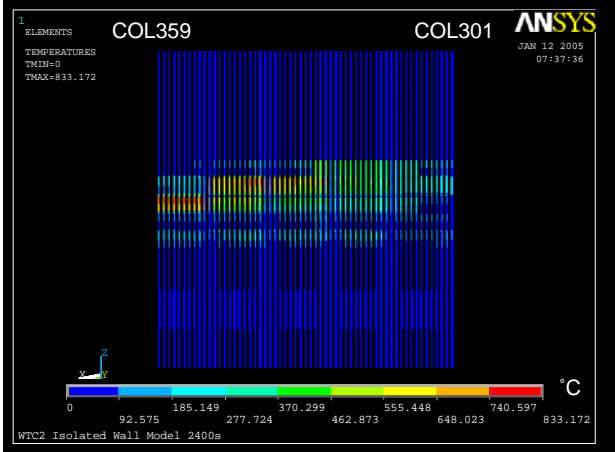


(f) Inside at 30 min

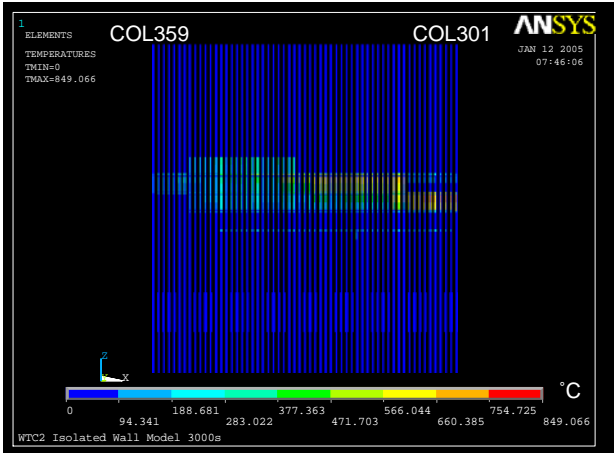
Figure 3–68. Column temperatures on the east wall of WTC 2 for Case C temperature condition at 10 min, 20 min, and 30 min.



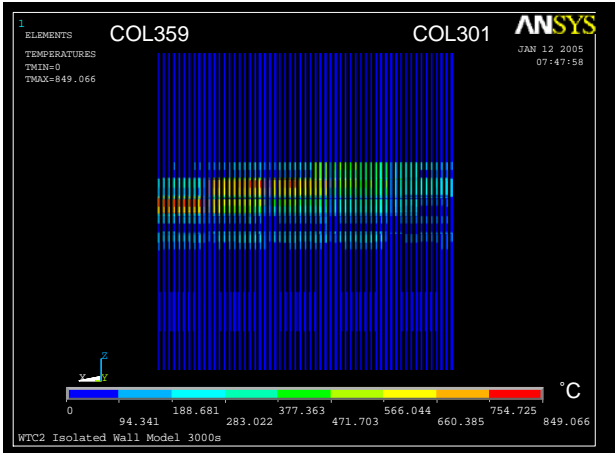
(a) Outside at 40 min



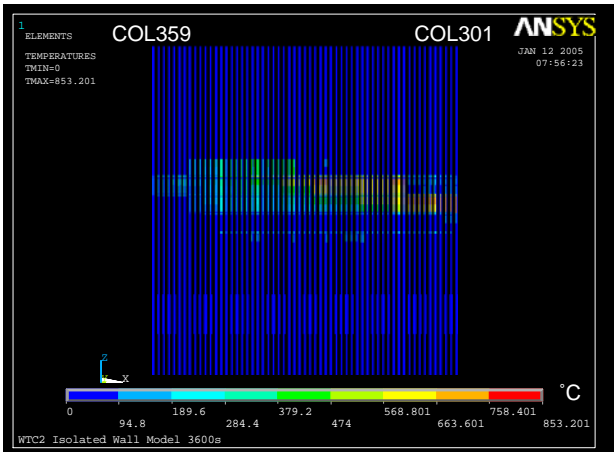
(b) Inside at 40 min



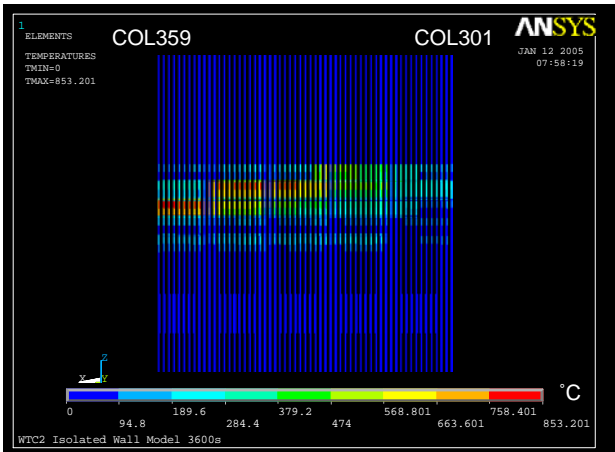
(c) Outside at 50 min



(d) Inside at 50 min



(e) Outside at 60 min



(f) Inside at 60 min

Figure 3–69. Column temperatures on the east wall of WTC 2 for Case C temperature condition at 40 min, 50 min, and 60 min.

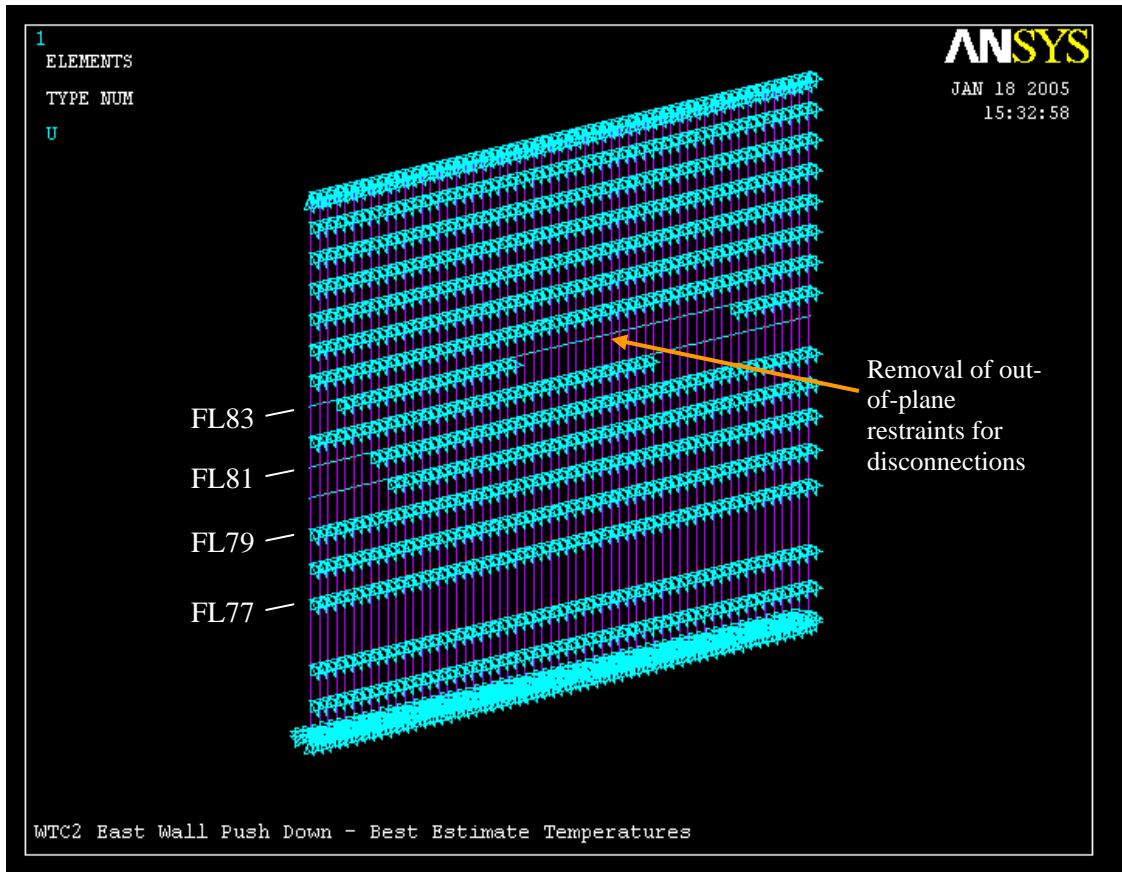
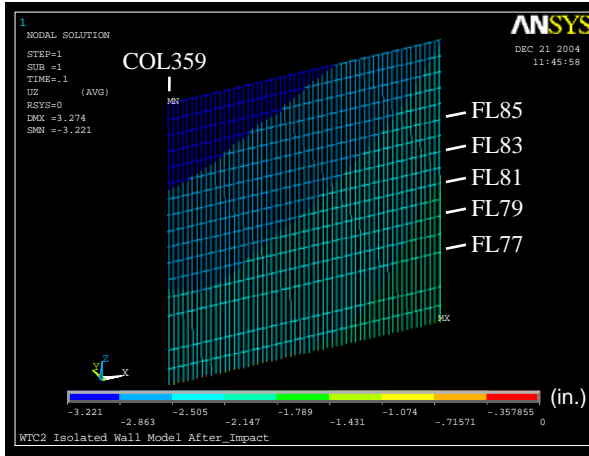
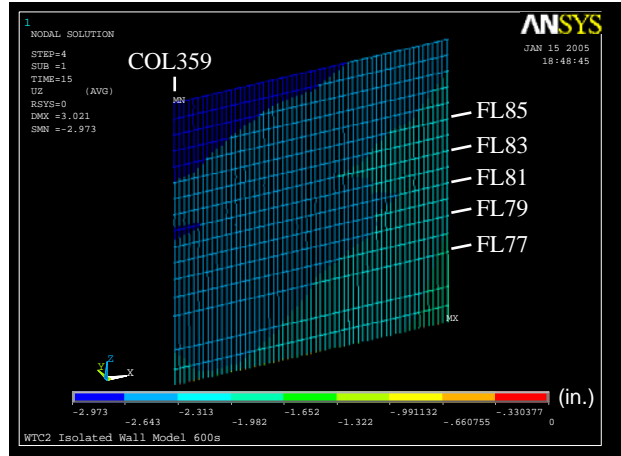


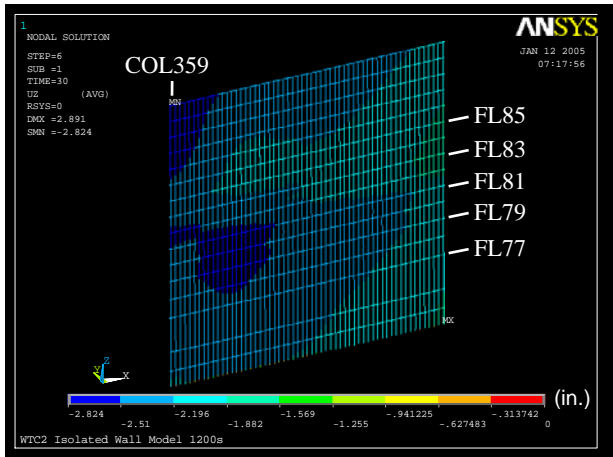
Figure 3–70. Location of the out-of-plane supports and floor/wall disconnections between exterior wall and the floor (WTC 2 east wall for Case C conditions at 60 min).



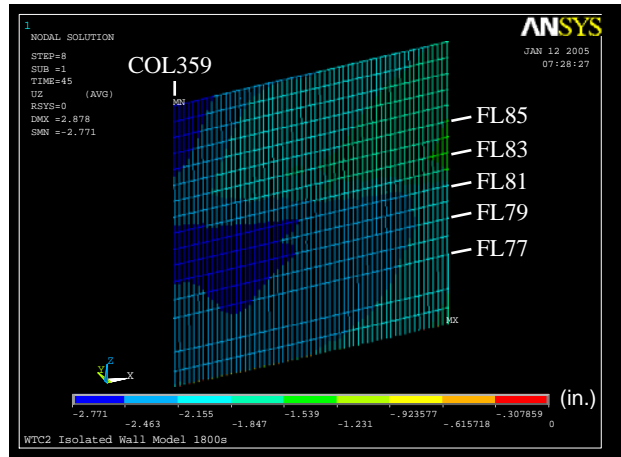
(a) After aircraft impact



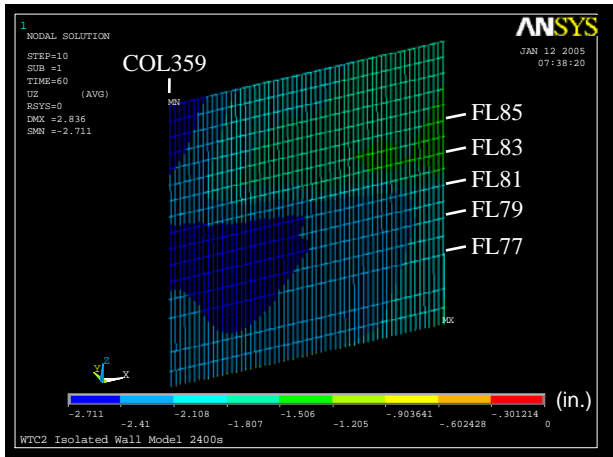
(b) At 10 min



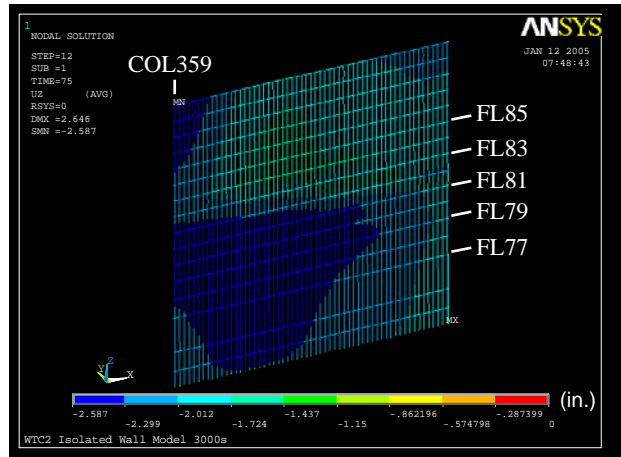
(c) At 20 min



(d) At 30 min



(e) At 40 min



(f) At 50 min

Figure 3–71. Vertical displacement of isolated east wall model of WTC 2 for Case C temperature distribution (downward displacement is negative; displacements scaled ten times).

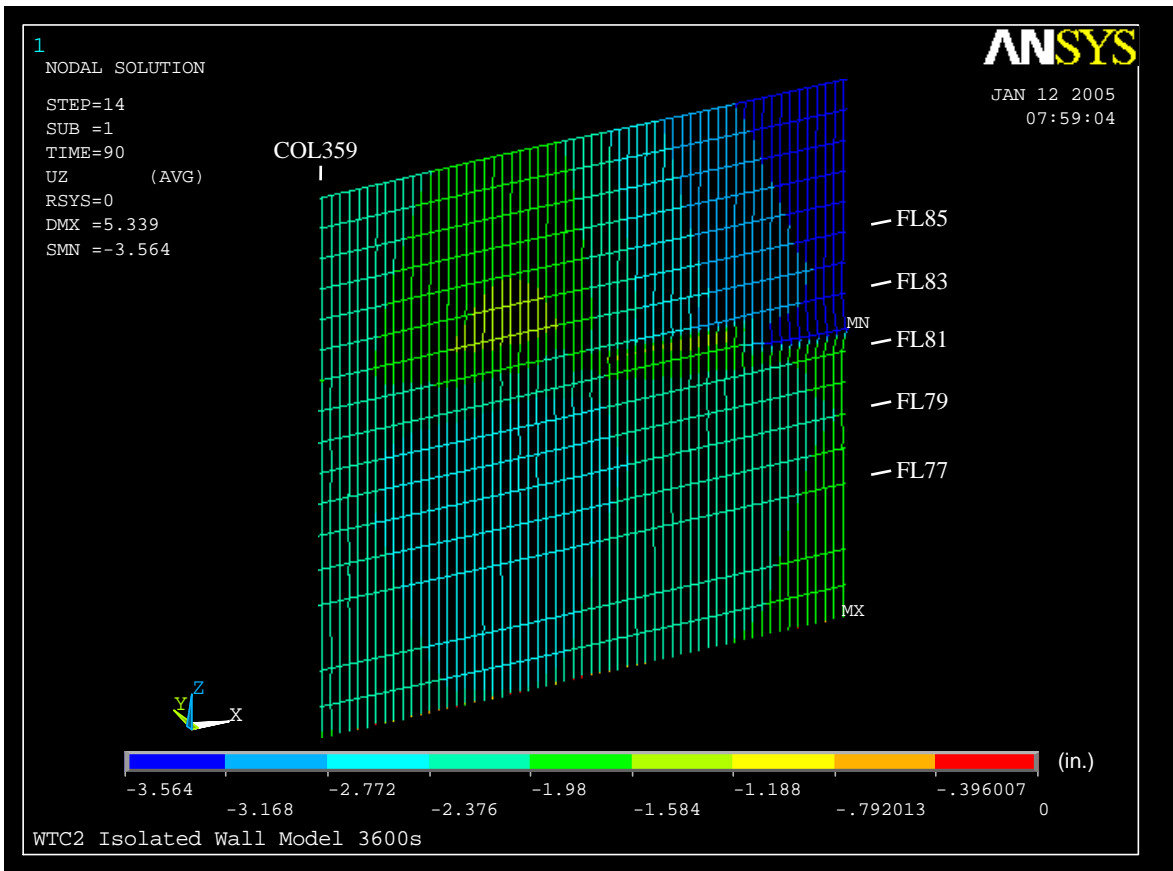
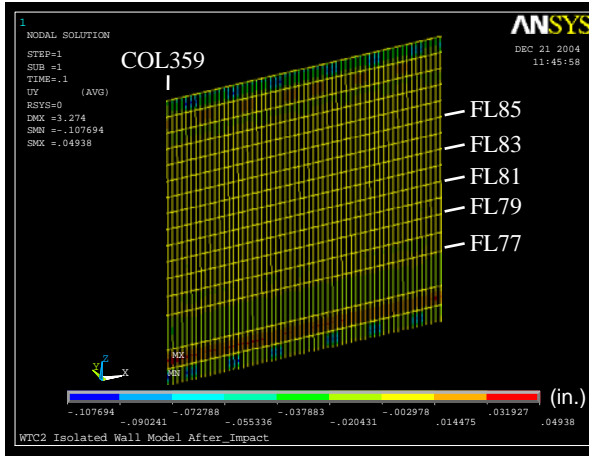
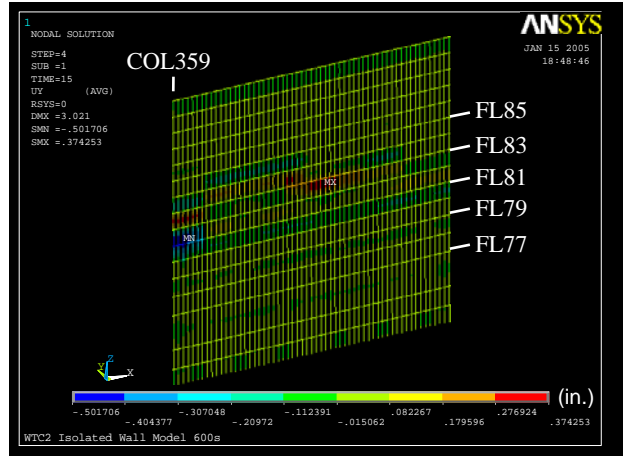


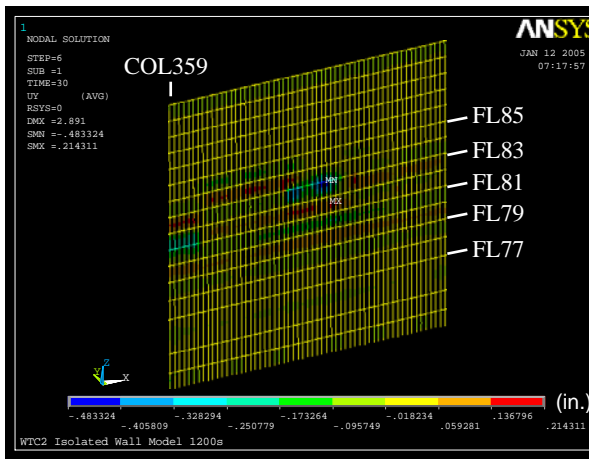
Figure 3–72. Vertical displacement of isolated east wall model of WTC 2 for Case C temperature distribution at 60 min (downward displacement is negative; displacements scaled ten times).



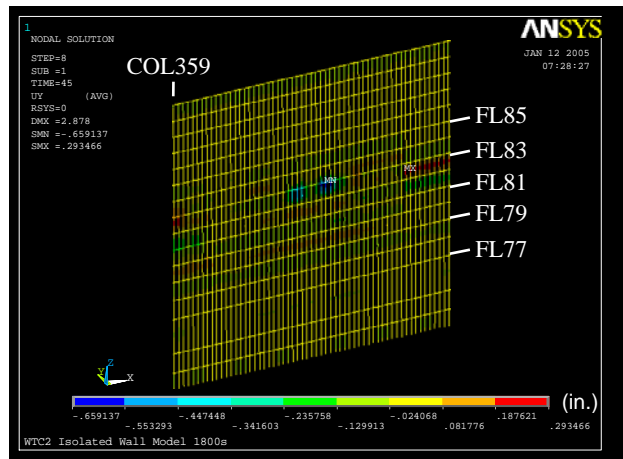
(a) After aircraft impact



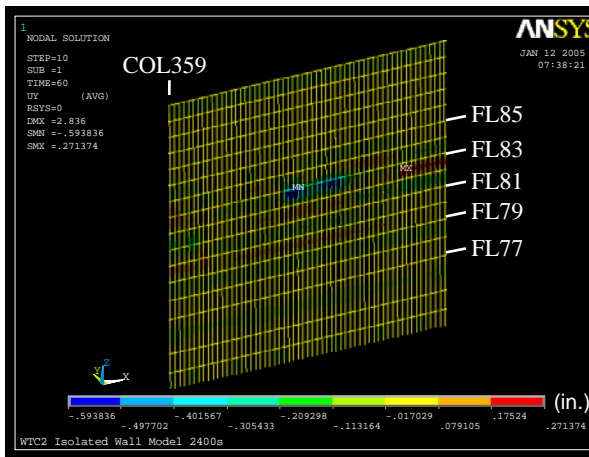
(b) At 10 min



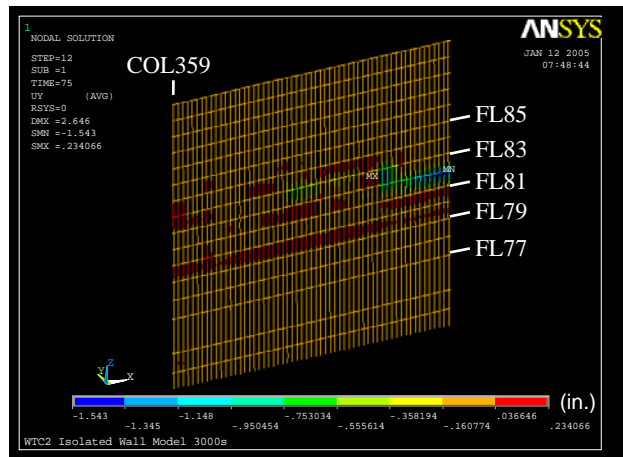
(c) At 20 min



(d) At 30 min



(e) At 40 min



(f) At 50 min

Figure 3–73. Out-of-plane displacement of isolated east wall model of WTC 2 for Case C temperature condition (inward displacement is positive; displacements scaled ten times).

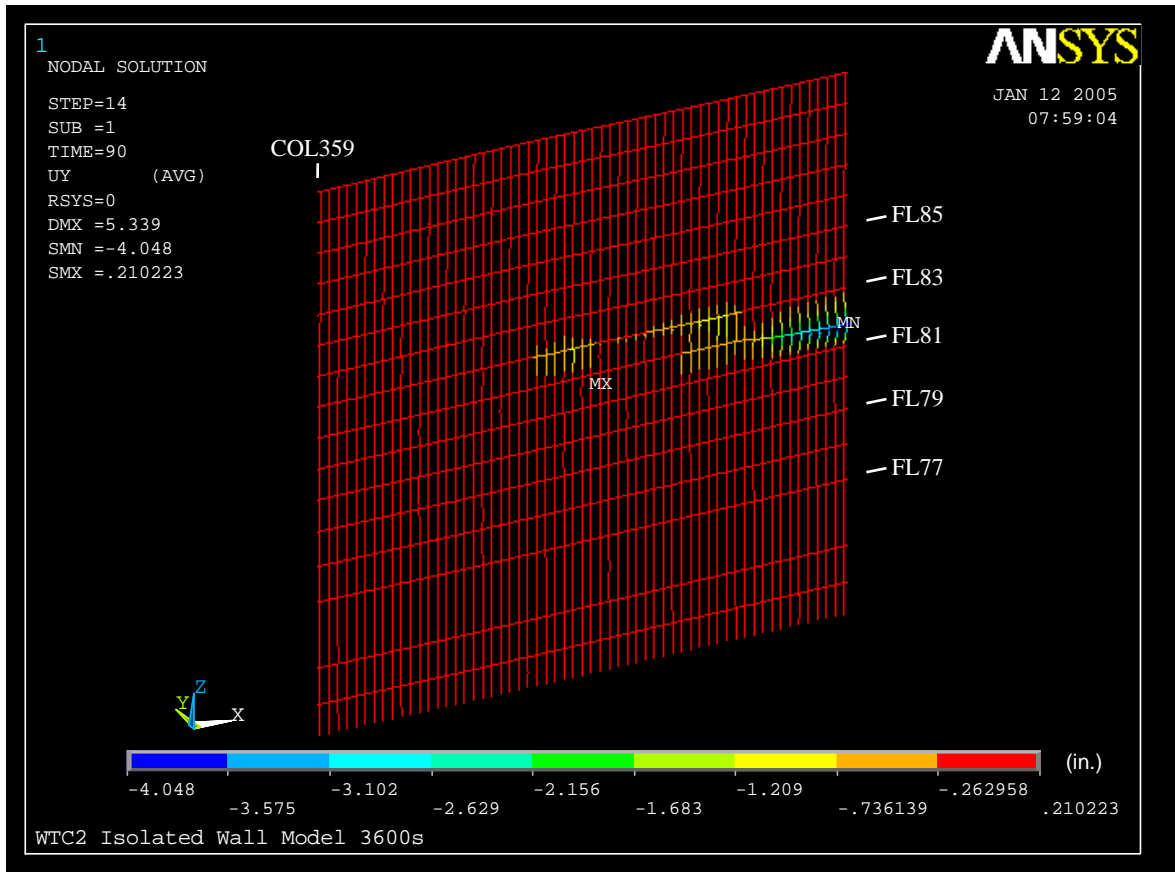


Figure 3–74. Out-of-plane displacement of isolated east wall model of WTC 2 for Case C temperature distribution at 60 min (inward displacement is positive; displacements scaled ten times).

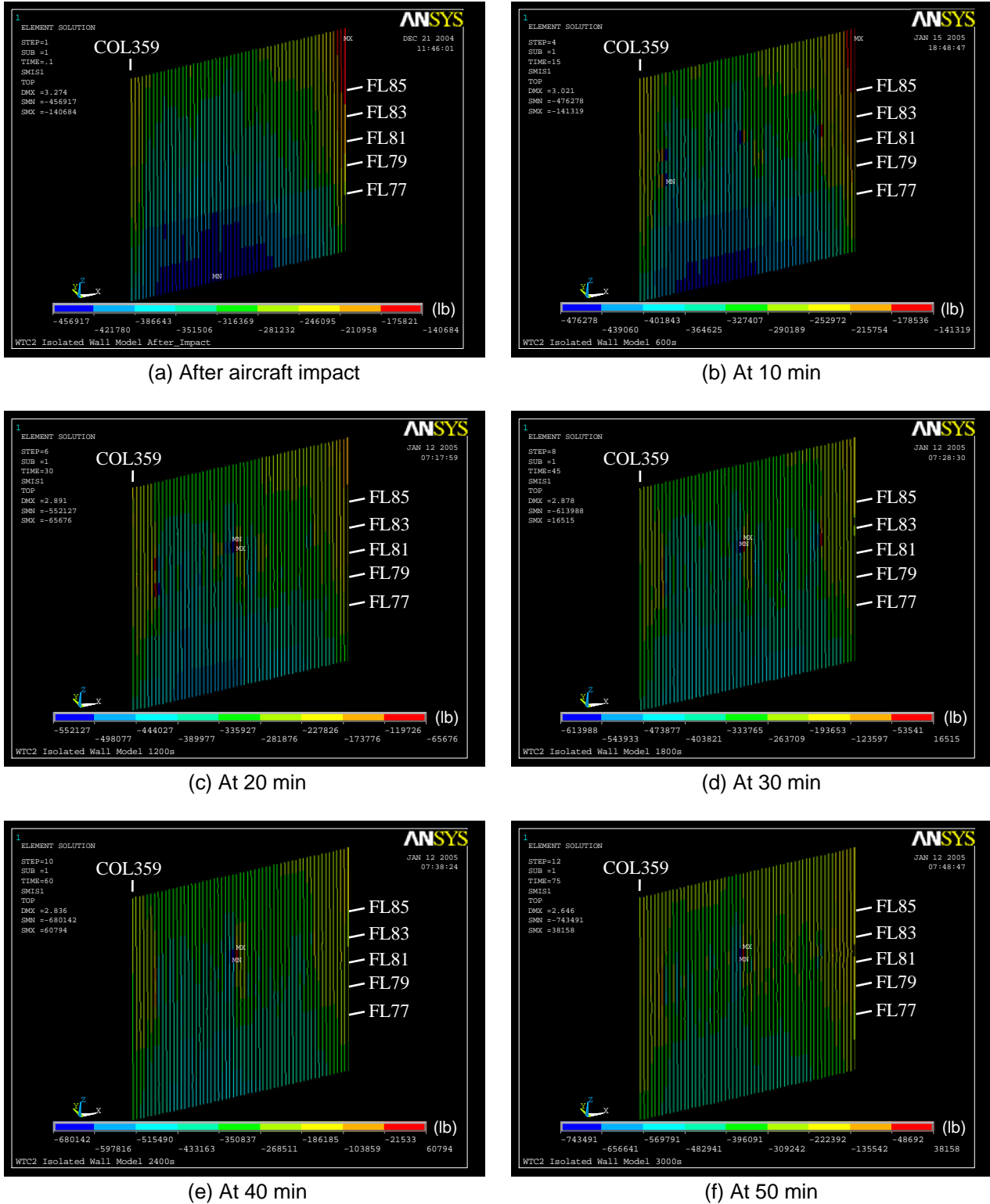


Figure 3–75. Axial load on columns of isolated east wall model of WTC 2 under Case C temperature condition (compression is negative).

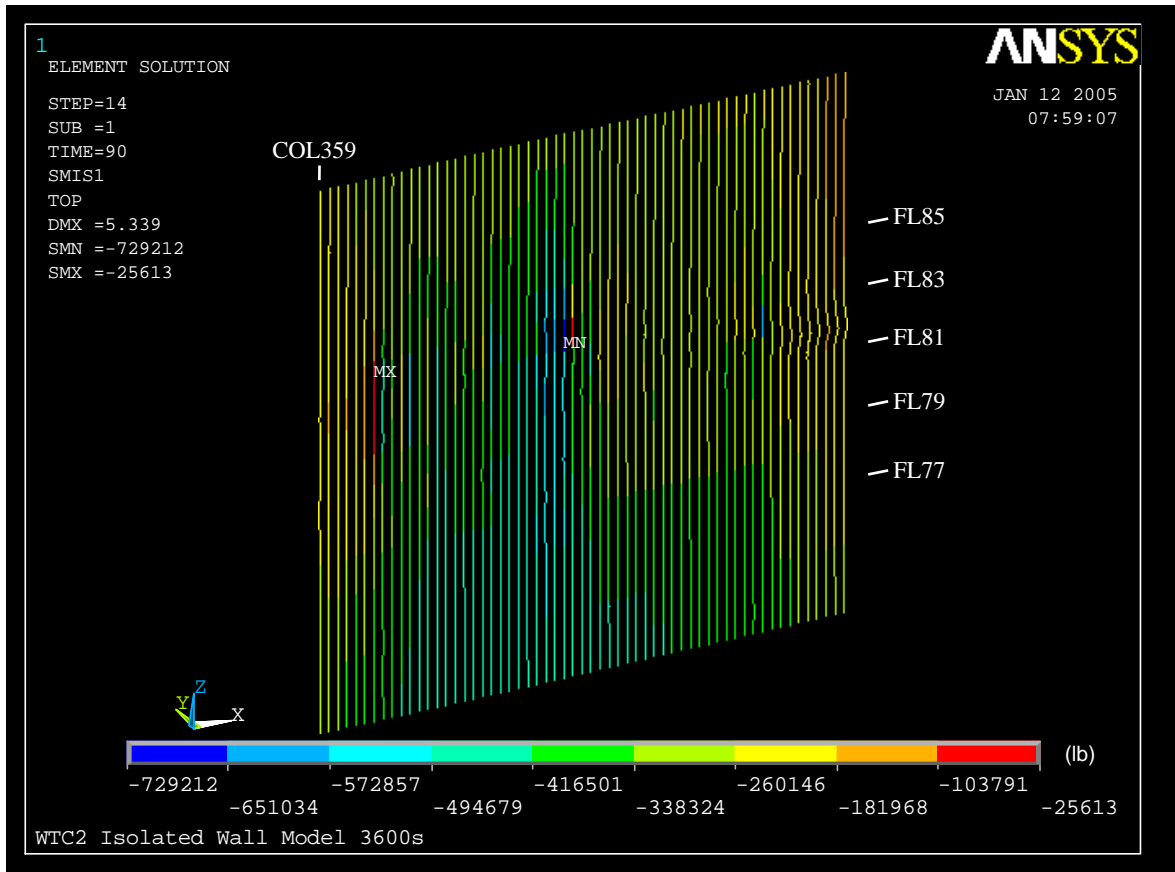


Figure 3–76. Axial load on columns of isolated east wall model of WTC 2 for Case C temperatures distribution at 60 min (compression is negative).

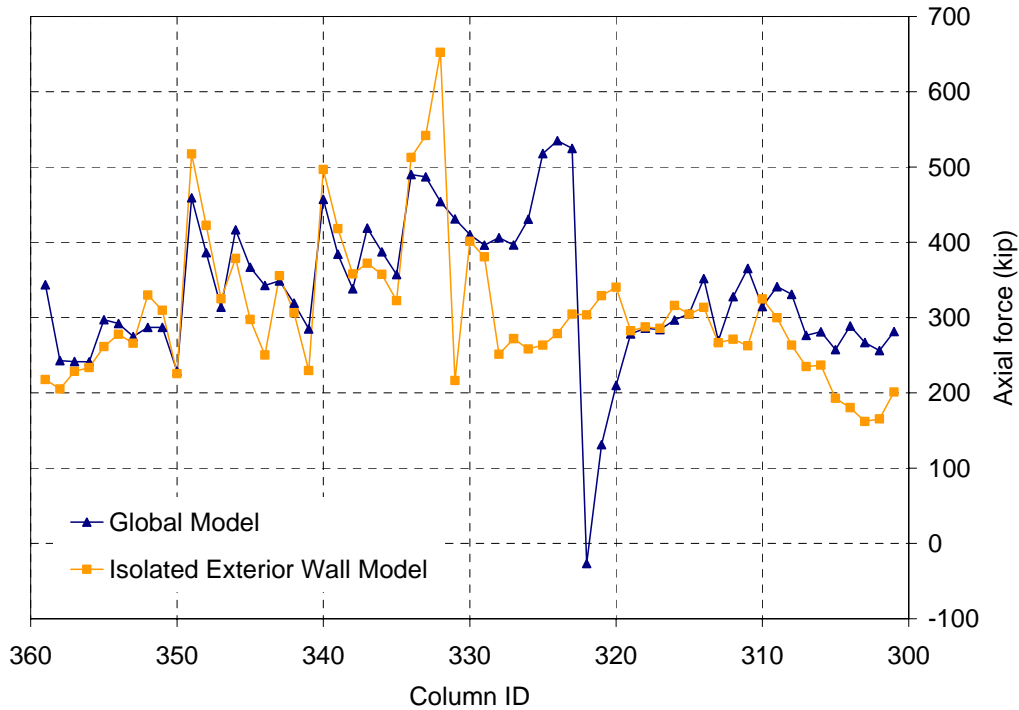
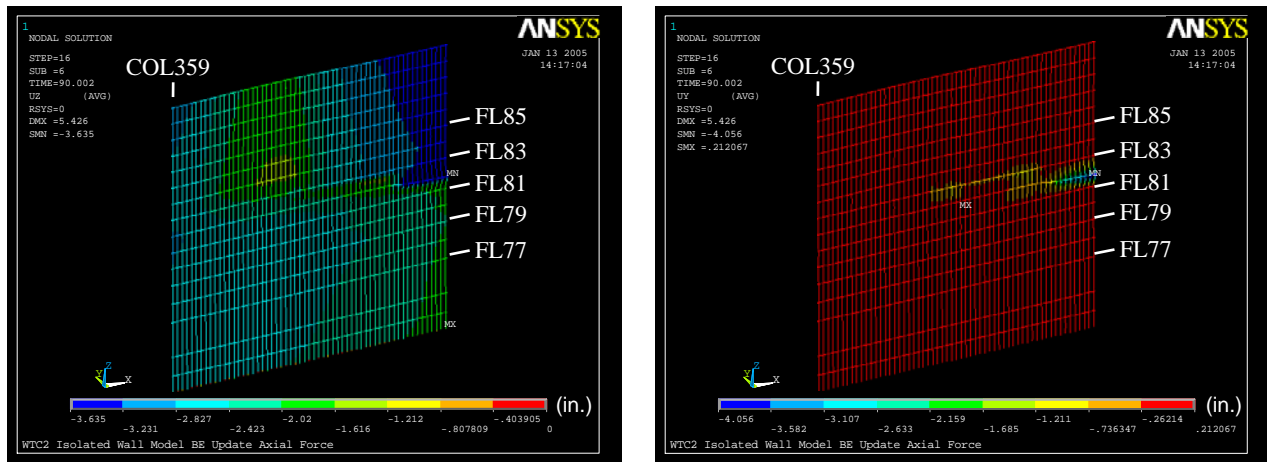


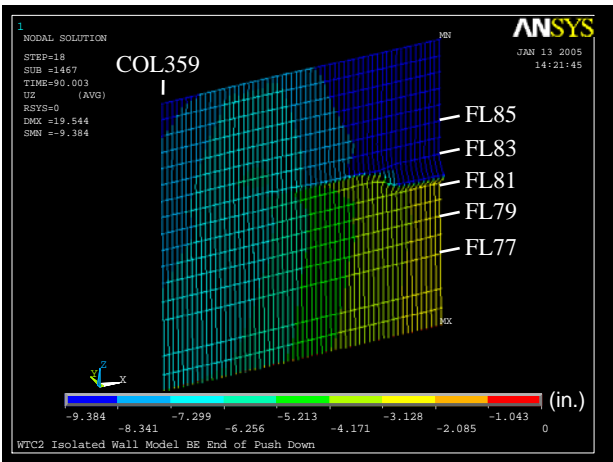
Figure 3–77. Comparison of axial load in columns at Floor 83 of isolated east wall model of WTC 2 at 60 min for Case C temperature conditions and the global model without creep for Case C_i conditions (compression is positive).



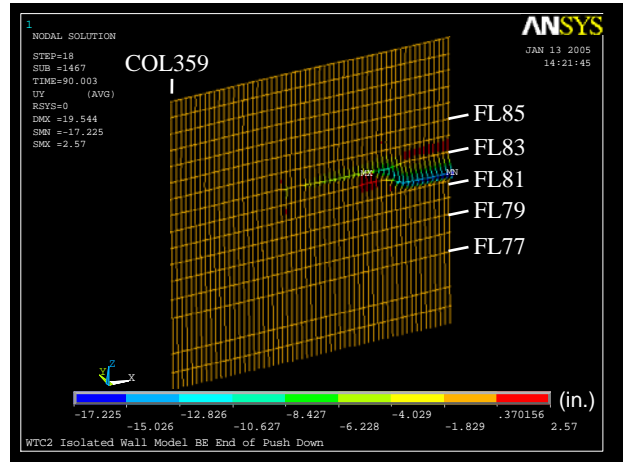
(a) Vertical displacement
(Downward displacement is negative)

(b) Out-of-plane displacement
(Inward displacement is positive)

Figure 3–78. Vertical and out-of-plane displacements of isolated east wall model of WTC 2 after column forces were corrected to those of global modal without creep for Case C_i conditions (displacements scaled ten times).



(a) Vertical displacement
(downward displacement is negative)



(b) Out-of-plane displacement
(Inward displacement is positive)

Figure 3–79. Vertical and out-of-plane displacements of isolated east wall model of WTC 2 after Case C temperature condition and push down analysis (displacements scaled five times).

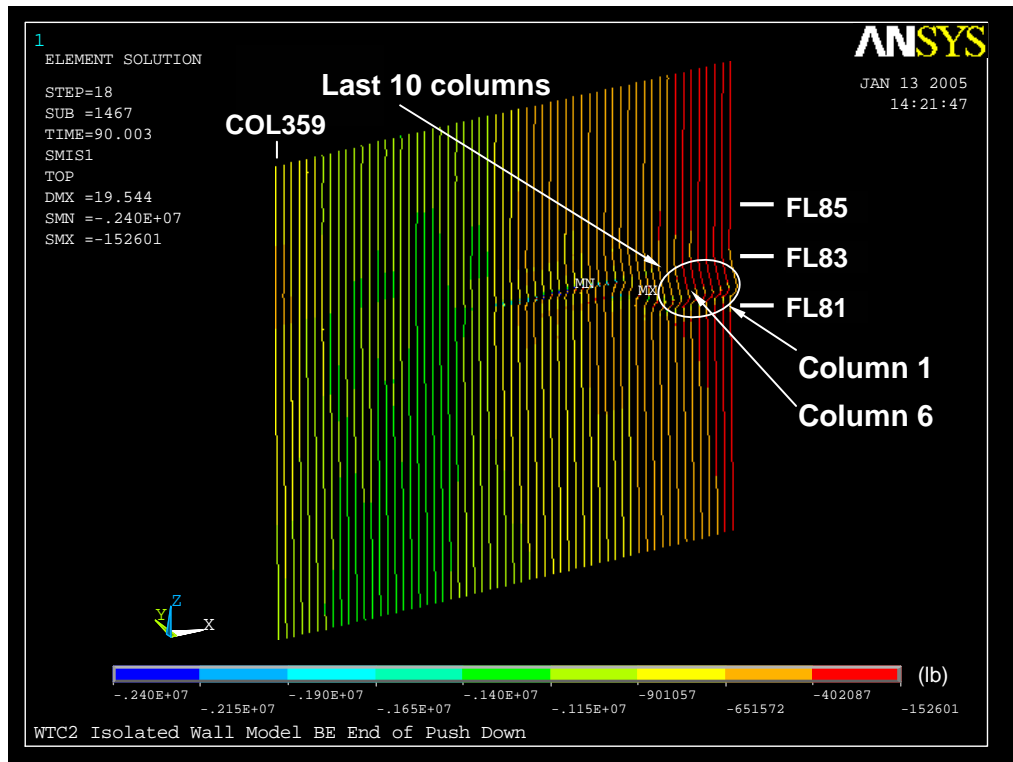


Figure 3–80. Axial load on east wall columns of isolated east wall model of WTC 2 after Case C temperature condition and push-down (compression is negative).

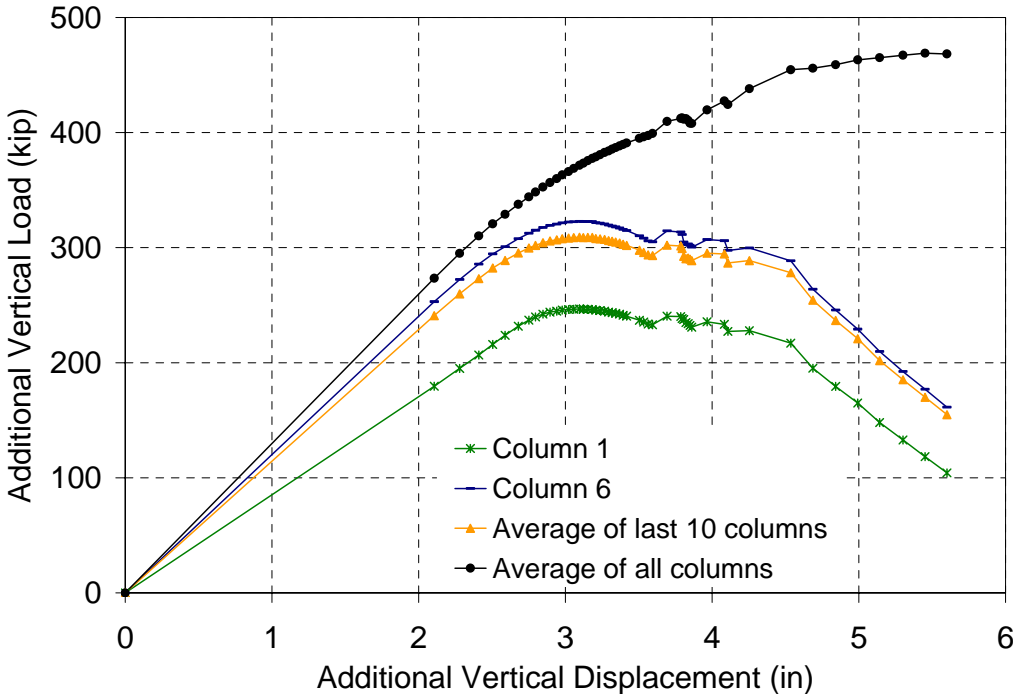


Figure 3–81. Additional vertical load versus additional vertical displacement during push-down analysis of isolated east wall model of WTC 2 for Case C temperature condition (compression is positive; see Fig. 3–80 for column locations).

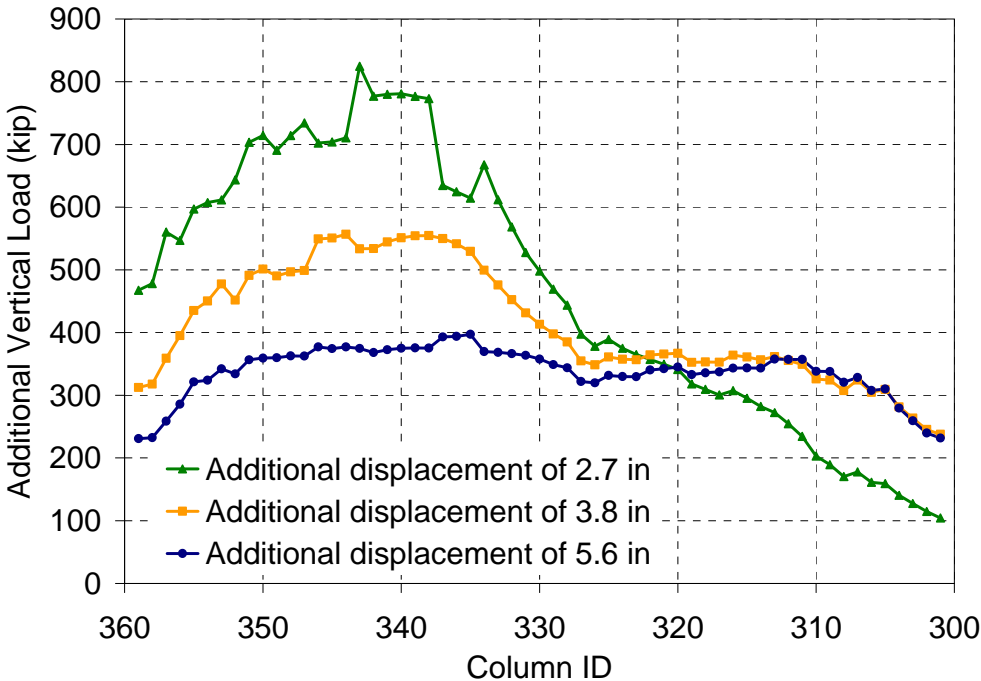


Figure 3–82. Variation of additional vertical load applied to columns of isolated east wall model of WTC 2 at different levels of additional vertical displacements imposed after Case C temperature condition (compression is positive).

Case D Temperature Condition

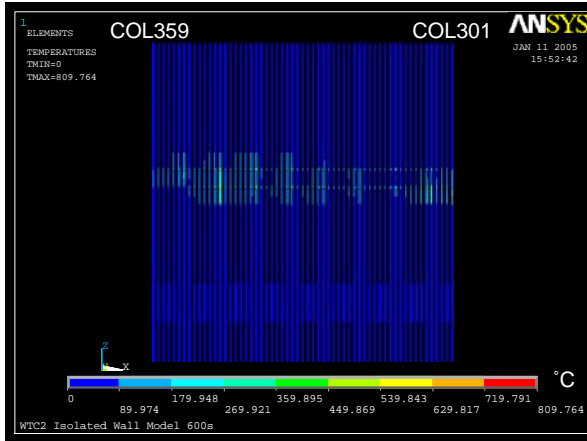
Figures 3–83 and 3–84 show Case D temperature distributions in the columns of the isolated east exterior wall model of WTC 2. The highest temperature, 845°C, occurred at 20 min in Column 307 between Floor 81 and Floor 82. Column temperatures were higher on the inside face of the exterior wall. Figure 3–85 shows the locations of the out-of-plane supports for Case D conditions at 60 min.

The vertical and the out-of-plane displacements at the end of the gravity load step after aircraft impact and at the end of each temperature step are shown in Figs. 3–86, 3–87, 3–88, and 3–89. The maximum vertical displacement of 3.2 in. occurred at Column 359 at Floor 90 immediately after aircraft impact. The maximum out-of-plane displacement of 7.8 in. occurred at Column 359 at Floor 81 at 60 min. (The out-of-plane displacement is positive inward.) The south side of the isolated exterior wall displaced vertically after aircraft impact more than other parts of the east wall, as impact damage was concentrated mostly on the southeast corner of the WTC 2. As time approached 60 min, the columns on the south side buckled, and the out-of-plane displacements increased.

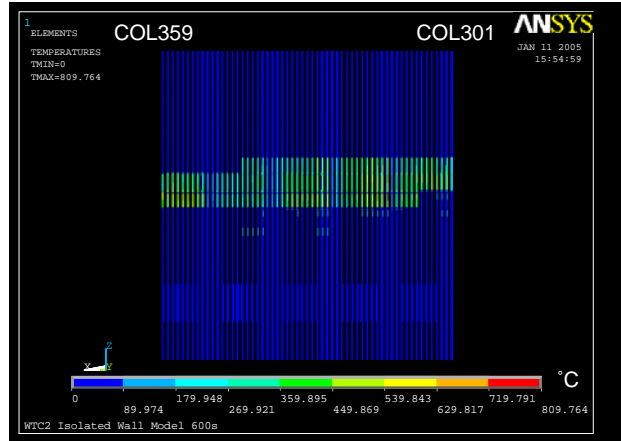
The axial load distributions on the columns at the end of the gravity load step and each time interval are shown in Figs. 3–90 and 3–91. The maximum axial load occurred at Column 301 between Floor 82 and Floor 83 at 10 min. The axial load in this column increased from 200 kip after aircraft impact to 920 kip at 10 min. The axial load of 920 kip was very close to the theoretical local buckling load of 985 kip for Column 301 at 314 °C and less than the yielding or Euler buckling load of the column. Since local buckling of plates in exterior columns could not be captured by the beam elements that were used in the model of the exterior wall, the model overestimated the buckling capacity of exterior columns. The axial loads on the buckled columns on the south side of the isolated wall remained approximately constant throughout the temperature time history.

To consider the effect of load redistribution within WTC 2, the same corrective technique as described earlier in this chapter for WTC 1 was used. The axial loads at 60 min in columns between Floor 83 and Floor 84 in the isolated exterior wall model were compared to the corresponding values from the global model without creep and with Case C_i structural damage condition and Case D_i temperature condition, as shown in Fig. 3–92. The difference between the two curves in Fig. 3–92 was then applied to the columns at Floor 84 as corrective loads. The resulting vertical and out-of-plane displacements are shown in Fig. 3–93. As can be seen, the additional loads increased the maximum vertical displacement by 0.4 in. and the maximum out-of-plane displacement by about 0.8 in.

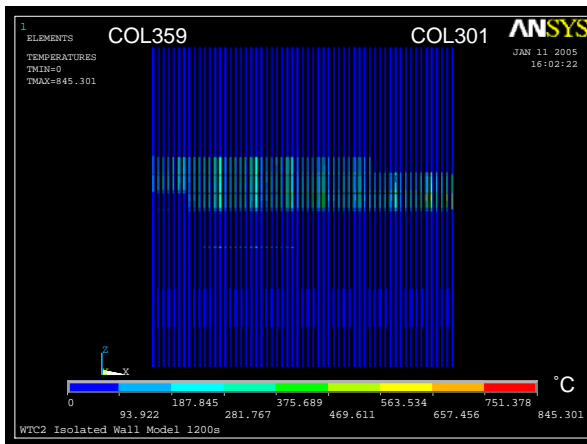
Also as described earlier for the WTC 1 isolated wall models, a push-down analysis of the WTC 2 isolated exterior wall model was performed. At an additional 5.3 in. of vertical displacement the model failed to converge, and the analysis was terminated. The vertical and out-of-plane displacements at the end of 5.3 in. of push down are shown in Fig. 3–94. At the end of push down, the maximum vertical displacement reached 8.0 in. and the maximum out-of-plane displacement reached 26.1 in. Figure 3–95 shows the column loads. This figure also shows the location of the columns, for which the load-deflection relationships are shown in Fig. 3–96. As can be seen from Fig. 3–96, the buckled columns on the south side of the isolated east exterior wall carried, on the average, an additional load of 410 kip at 60 min, compared to 630 kip for the average of the entire east wall columns. The additional axial loads on individual columns at different levels of additional vertical displacements are shown in Fig. 3–97.



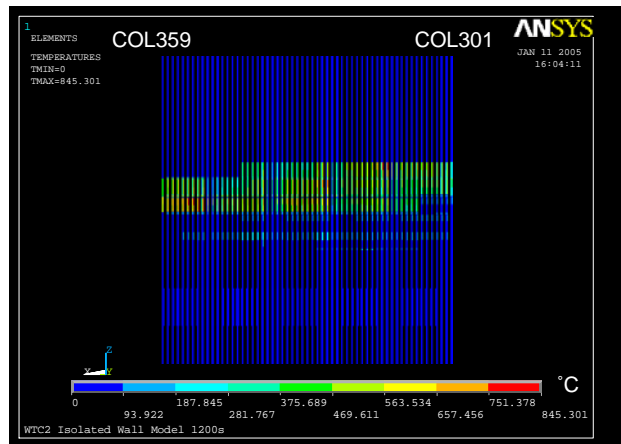
(a) Outside at 10 min



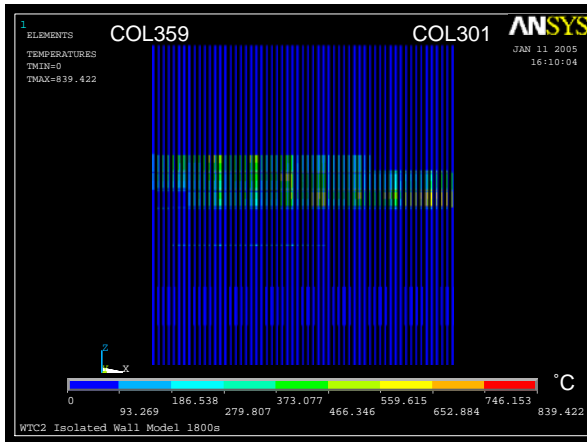
(b) Inside at 10 min



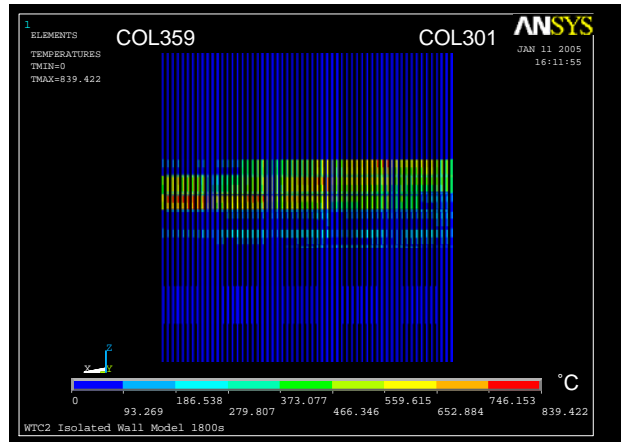
(c) Outside at 20 min



(d) Inside at 20 min

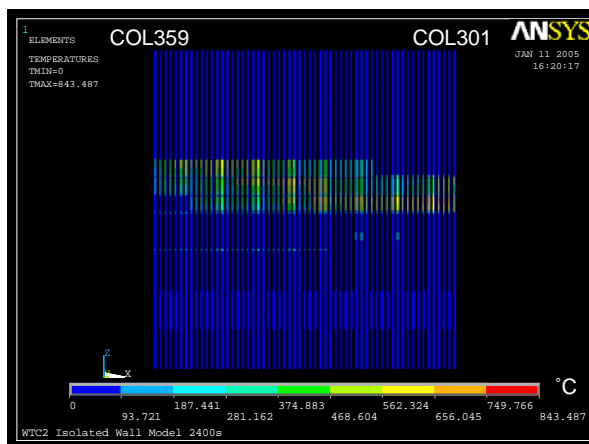


(e) Outside at 30 min

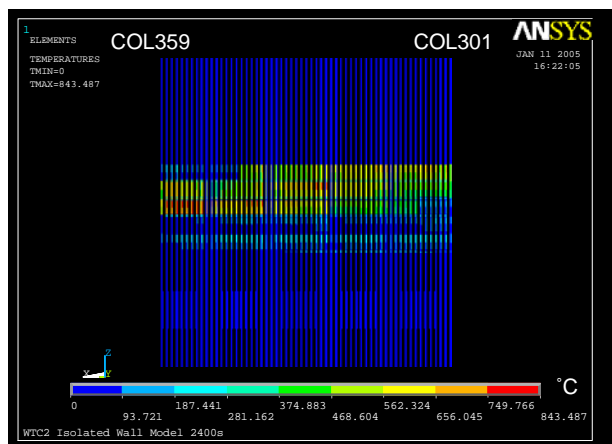


(f) Inside at 30 min

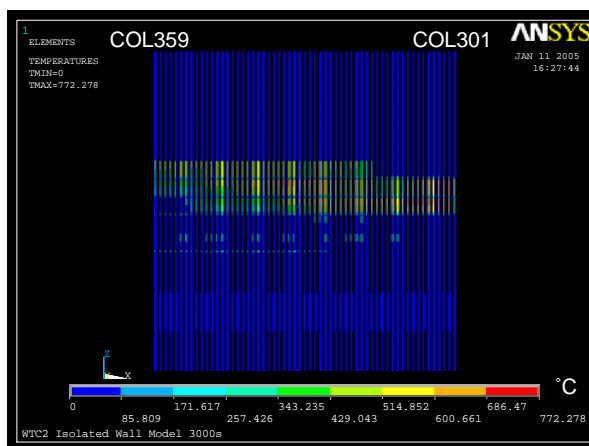
Figure 3–83. Column temperatures on the east wall of WTC 2 for Case D temperature condition at 10 min, 20 min, and 30 min.



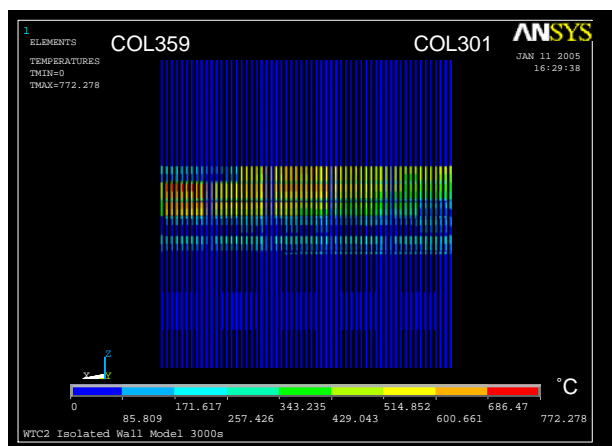
(a) Outside at 40 min



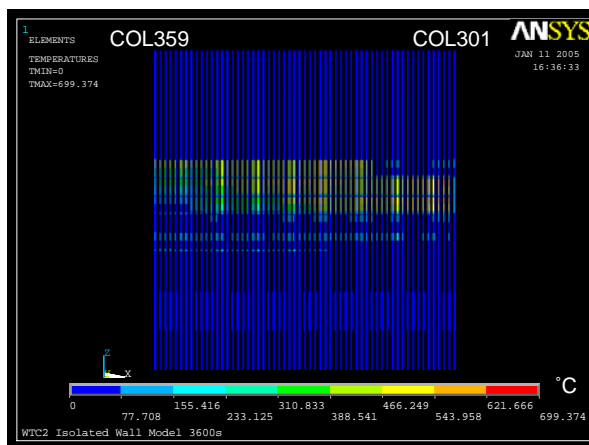
(b) Inside at 40 min



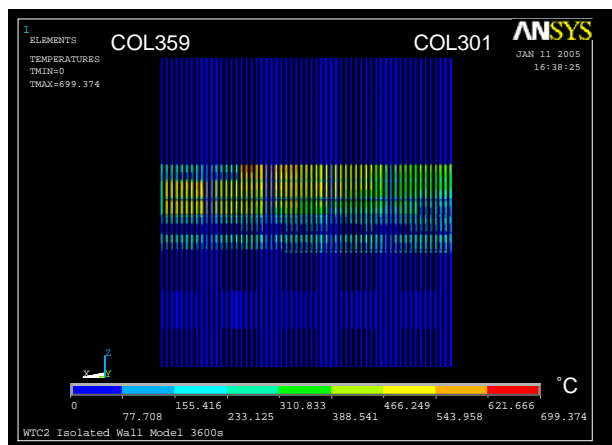
(c) Outside at 50 min



(d) Inside at 50 min



(e) Outside at 60 min



(f) Inside at 60 min

Figure 3–84. Column temperatures on the east wall of WTC 2 for Case D temperature condition at 40 min, 50 min, and 60 min.

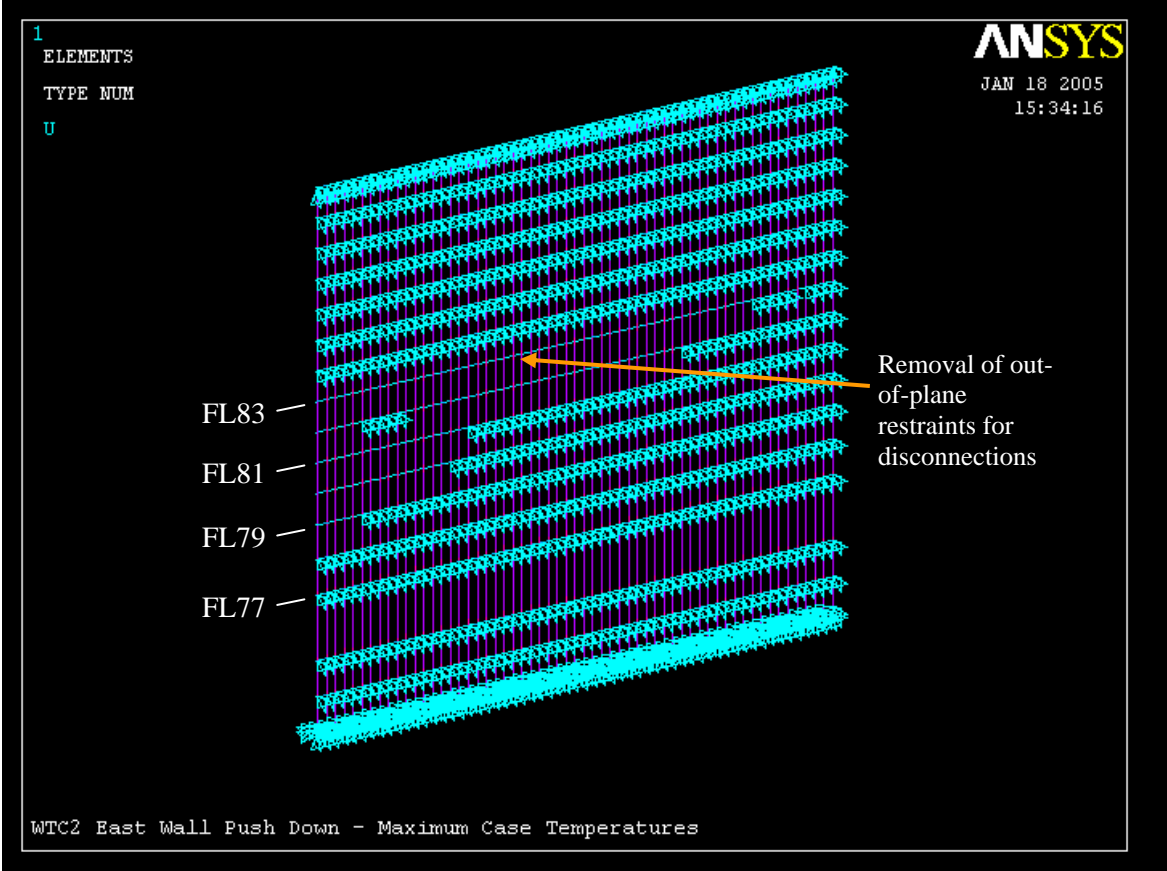
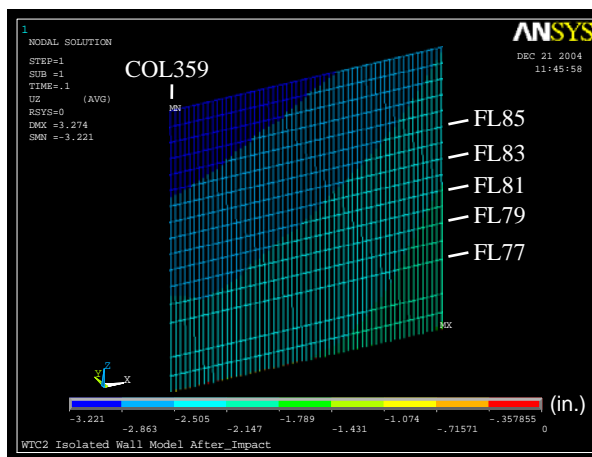
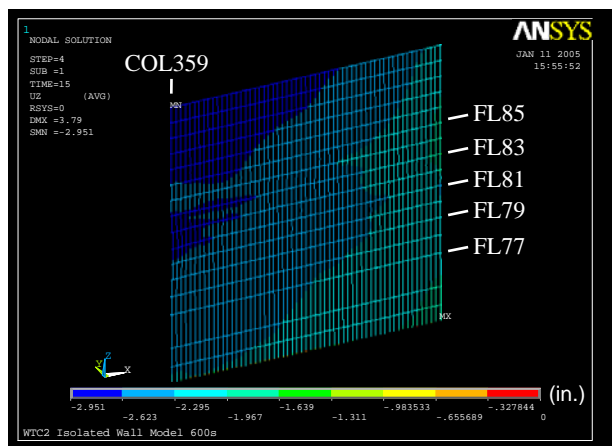


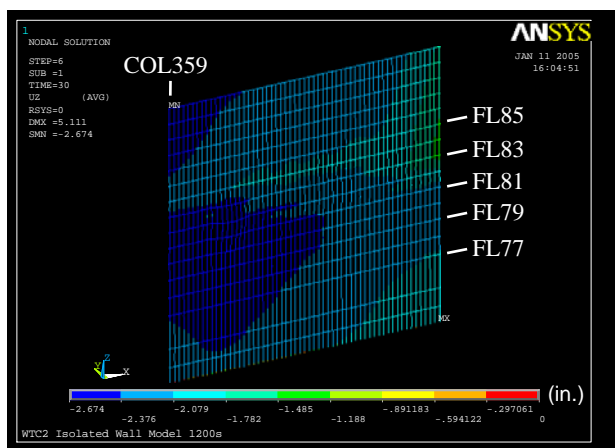
Figure 3–85. Location of the out-of-plane supports and floor/wall disconnections between exterior wall and the floor (WTC 2 east wall for Case D conditions at 60 min).



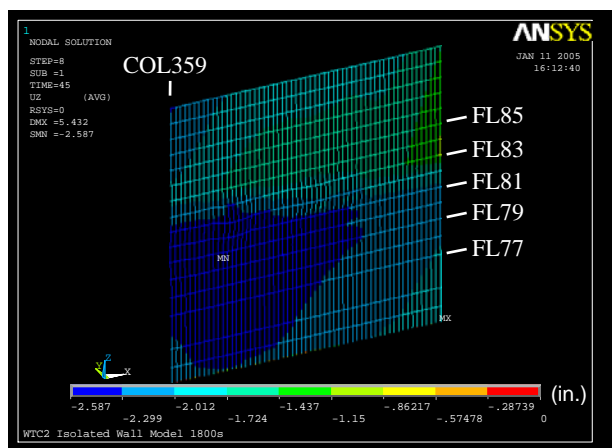
(a) After aircraft impact



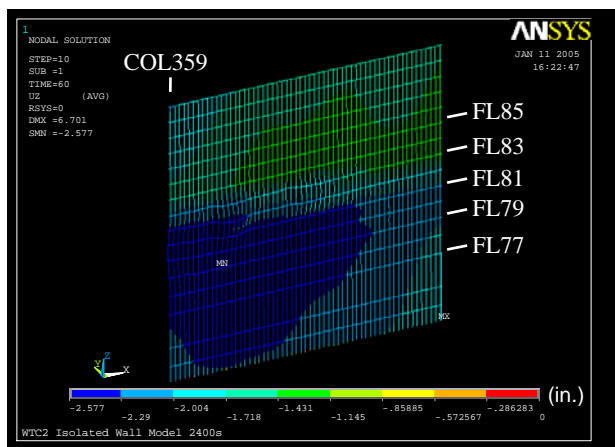
(b) At 10 min



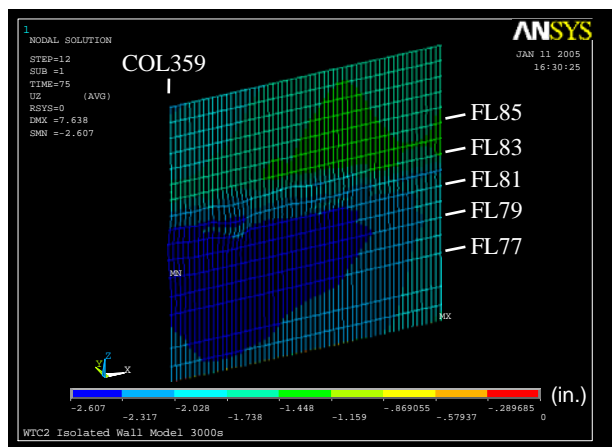
(c) At 20 min



(d) At 30 min



(e) At 40 min



(f) At 50 min

Figure 3–86. Vertical displacement of isolated east wall model of WTC 2 for Case D temperature condition (downward displacement is negative; displacements scaled ten times).

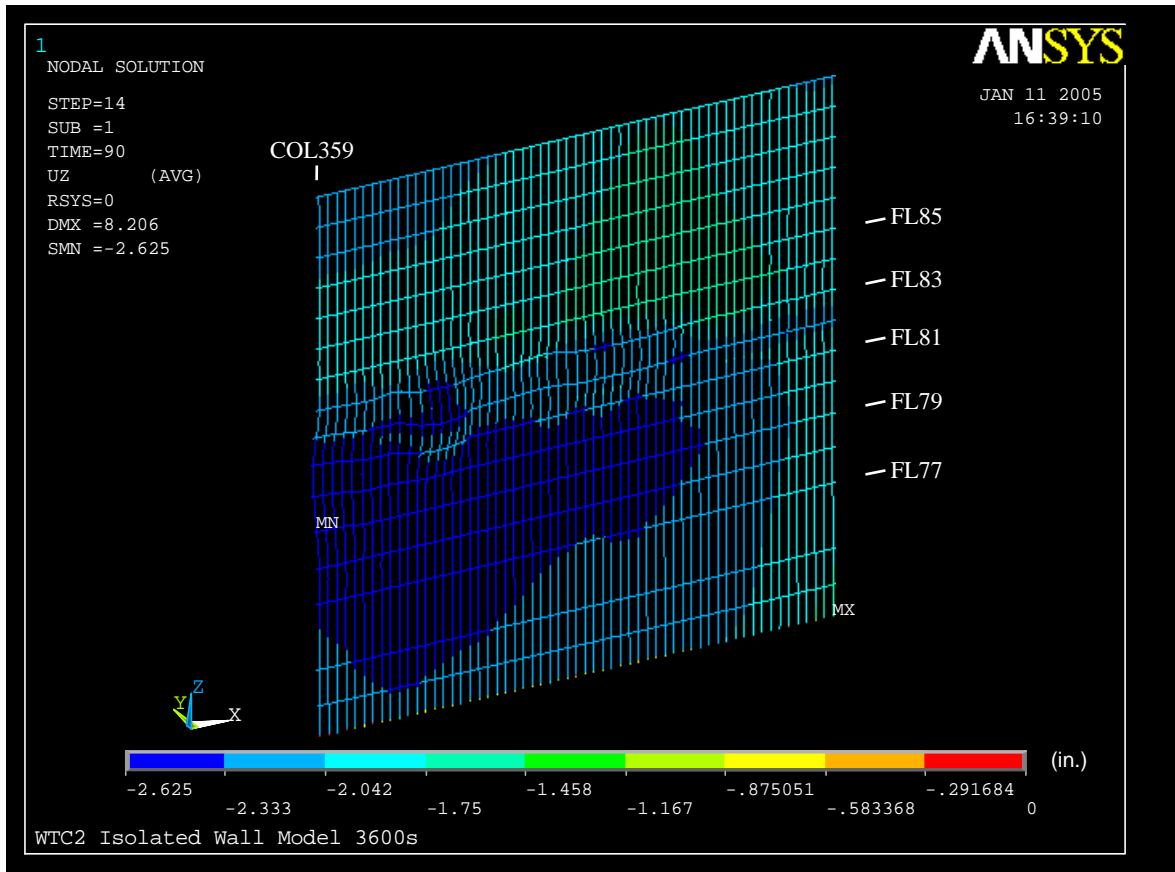
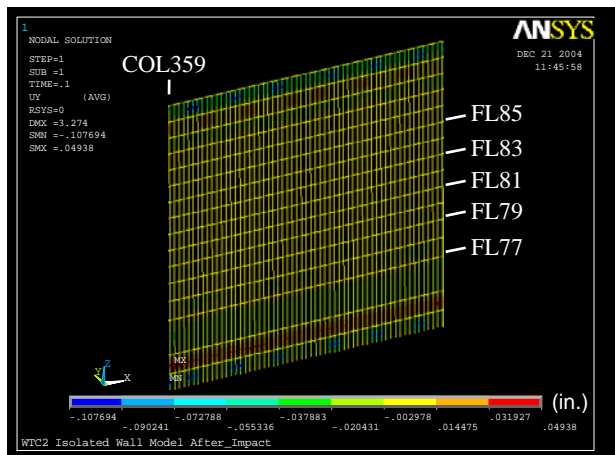
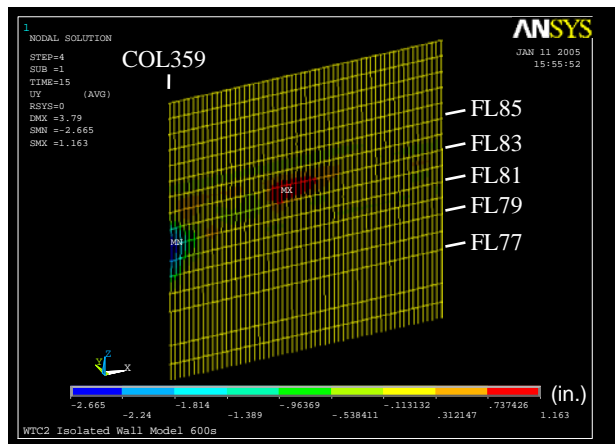


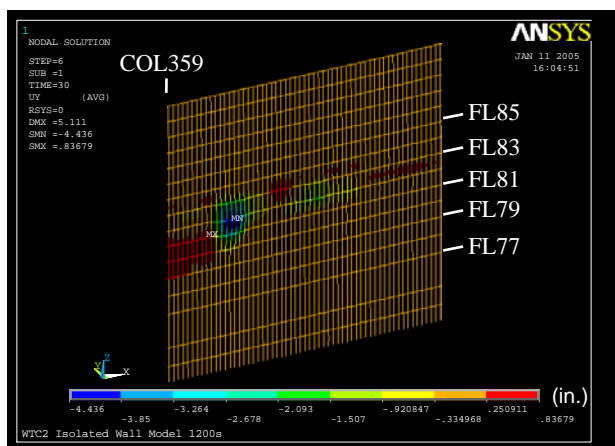
Figure 3–87. Vertical displacement of isolated east wall model of WTC 2 for Case D temperature condition at 60 min (downward displacement is negative; displacements scaled ten times).



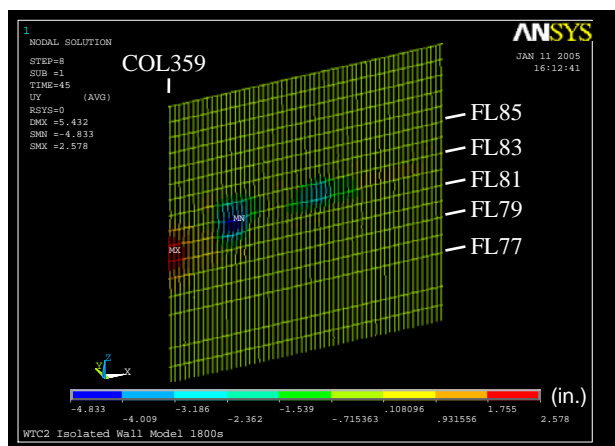
(a) After aircraft impact



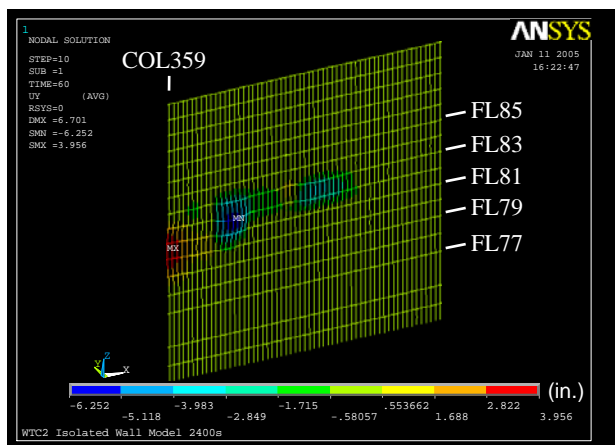
(b) At 10 min



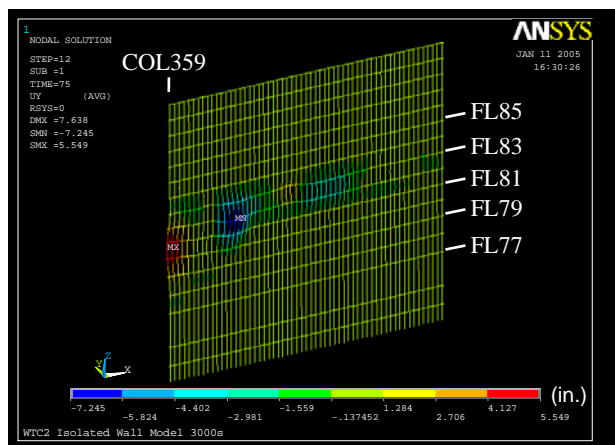
(c) At 20 min



(d) At 30 min



(e) At 40 min



(f) At 50 min

Figure 3–88. Out-of-plane displacement of isolated east wall model of WTC 2 for Case D temperature condition (inward displacement is positive; displacements scaled ten times).

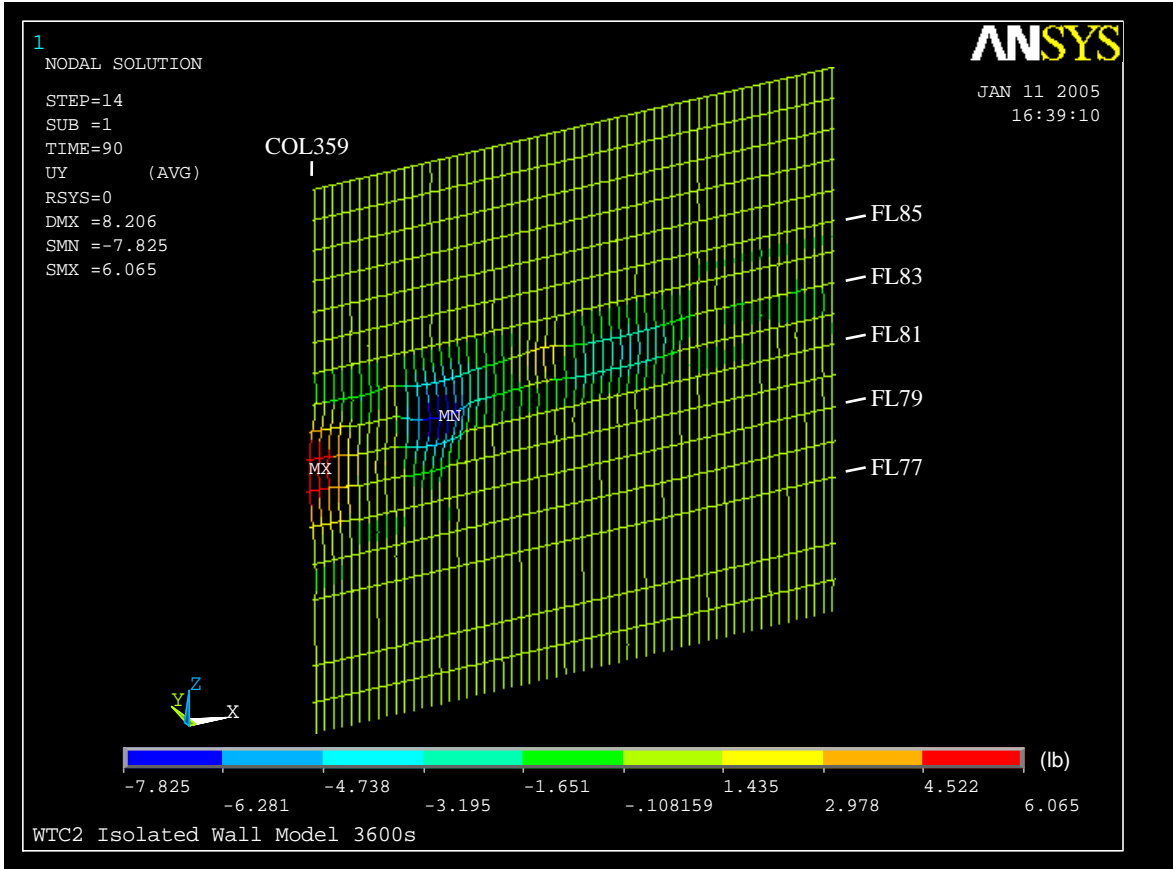
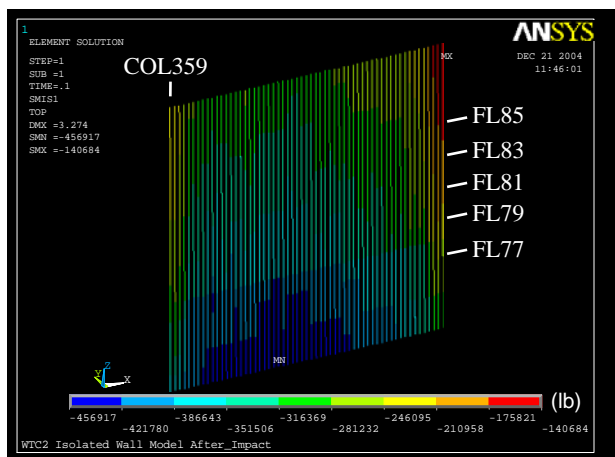
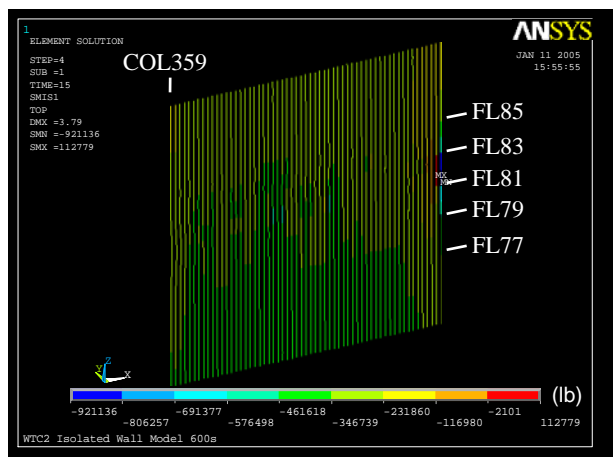


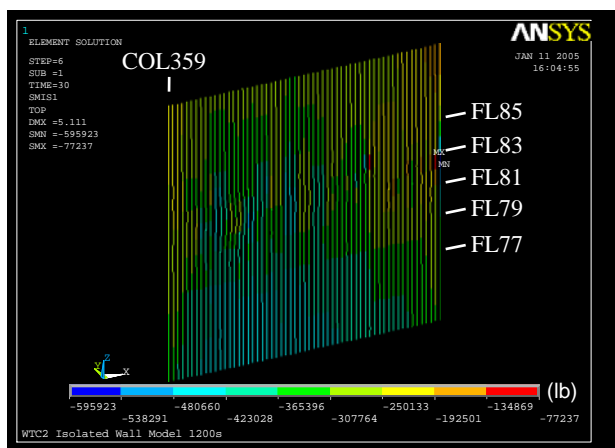
Figure 3–89 Out-of-plane displacement of isolated east wall model of WTC 2 for Case D temperature condition at 60 min (inward displacement is positive; displacements scaled ten times).



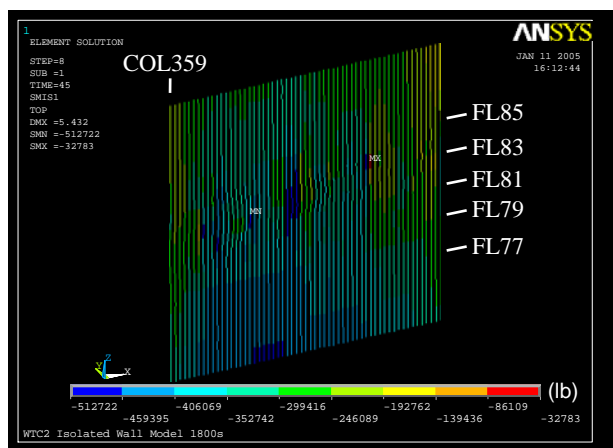
(a) After aircraft impact



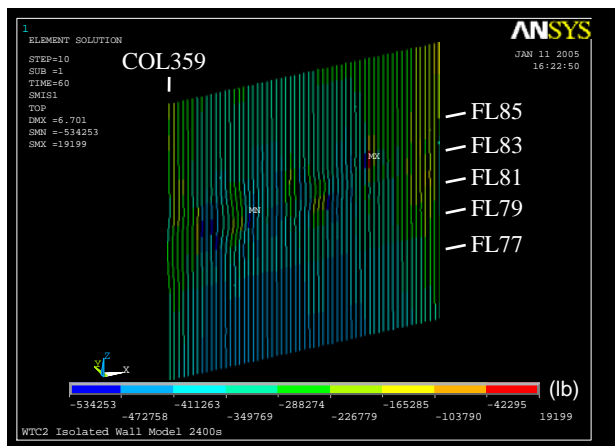
(b) At 10 min



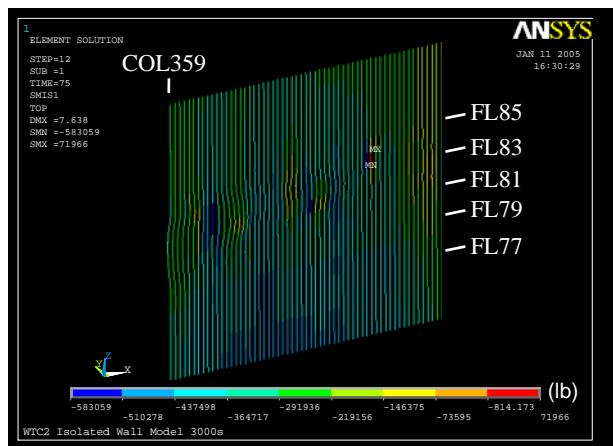
(c) At 20 min



(d) At 30 min



(e) At 40 min



(f) At 50 min

Figure 3–90. Axial load on east wall columns of isolated east wall model of WTC 2 for Case D temperature condition (compression is negative).

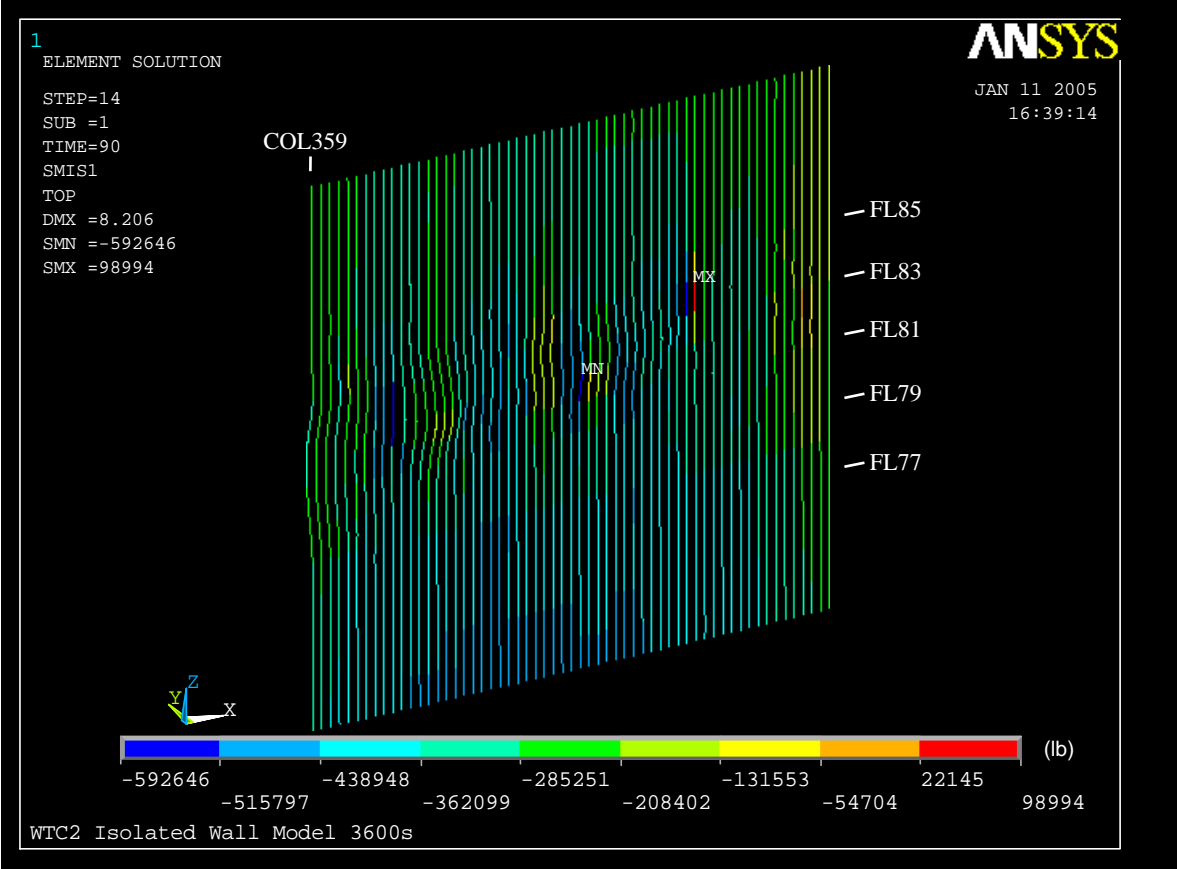


Figure 3–91. Axial load on east wall columns of isolated east wall model of WTC 2 for Case D temperature condition at 60 min (compression is negative).

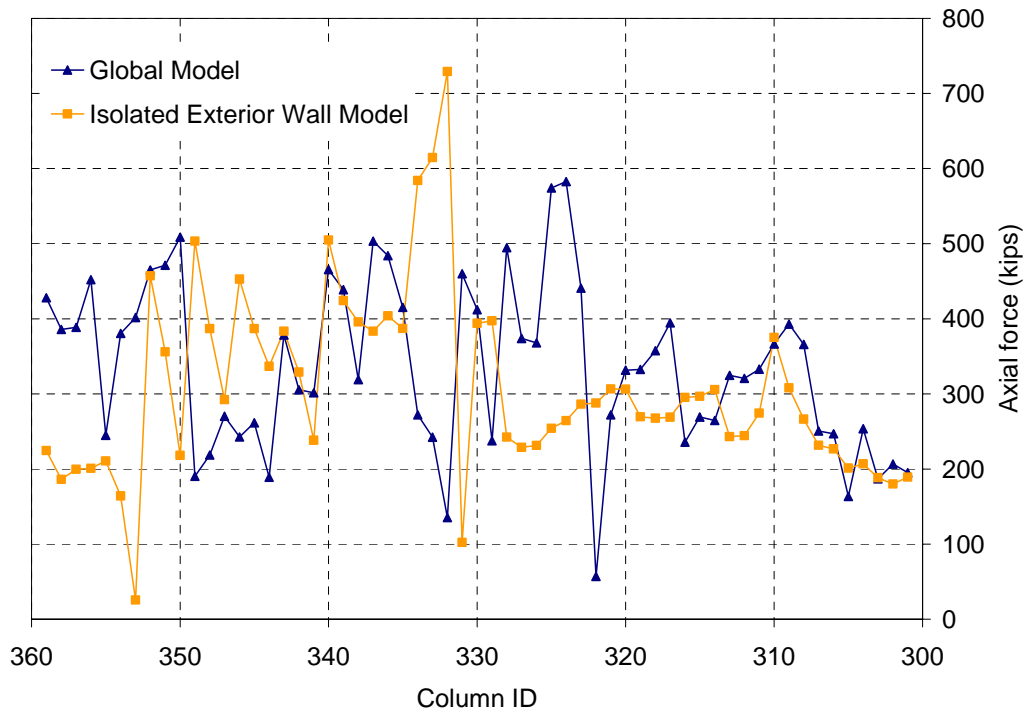
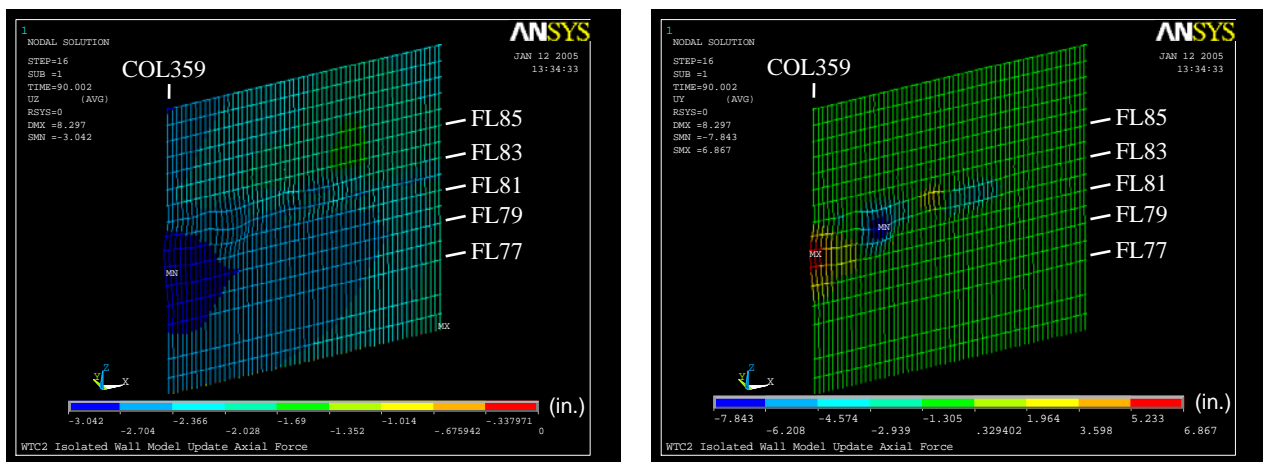


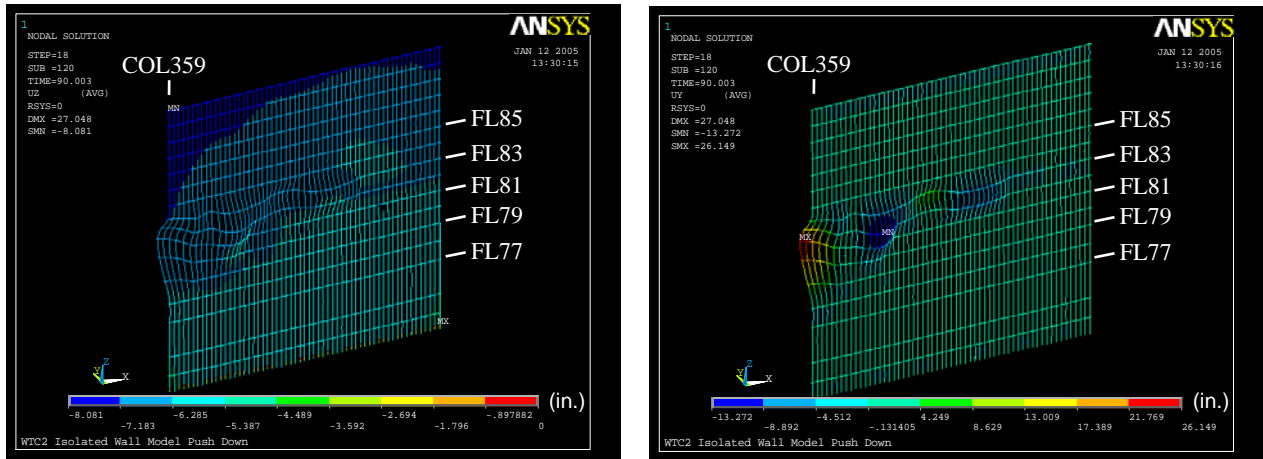
Figure 3–92. Comparison of axial load in columns at Floor 83 of isolated east wall model of WTC 2 at 60 min for Case D temperature conditions and the global model without creep for Case C_i structural damage condition and Case D_i temperature condition (compression is positive).



(a) Vertical displacement (downward displacement is negative)

(b) Out-of-plane displacement (inward displacement is positive)

Figure 3–93. Vertical and out-of-plane displacements of columns of isolated east wall model of WTC 2 after column forces were corrected to those of global model without creep for Case C_i structural damage condition and Case D_i temperature condition (displacements scaled ten times).



(a) Vertical displacement
(downward displacement is negative)

(b) Out-of-plane displacement
(inward displacement is positive)

Figure 3–94. Vertical and out-of-plane displacements of isolated east wall model of WTC 2 after Case D temperature condition and push down (displacements scaled five times).

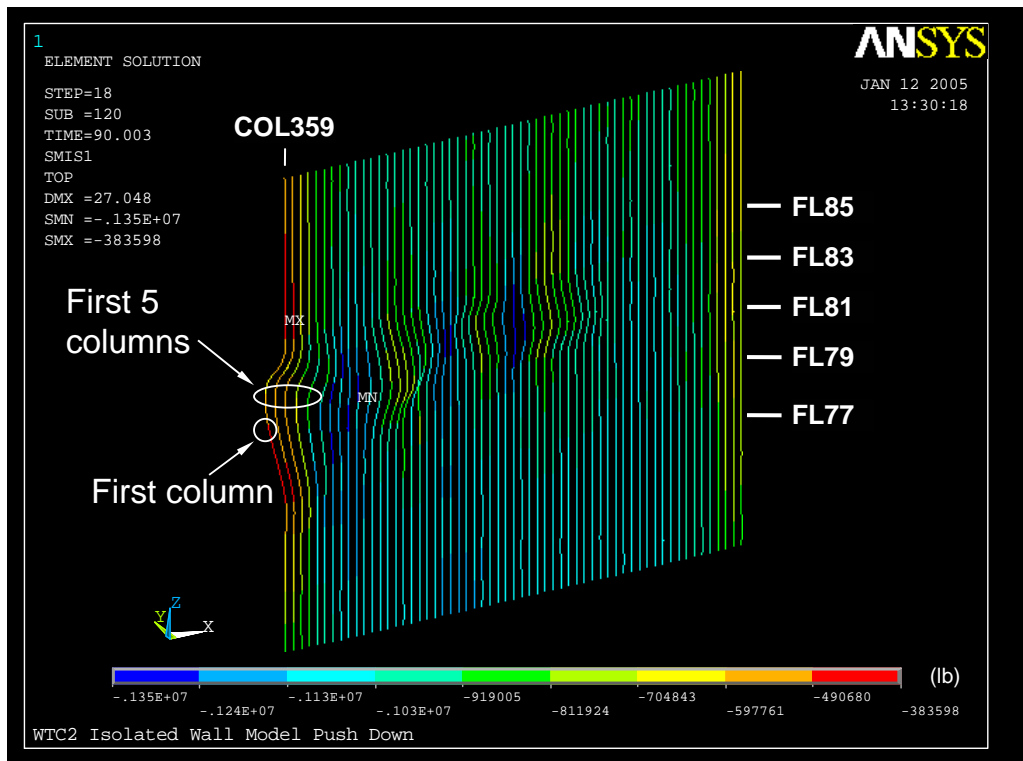


Figure 3–95. Axial load on east wall columns of isolated east wall model of WTC 2 after Case D temperature condition and push down (compression is negative).

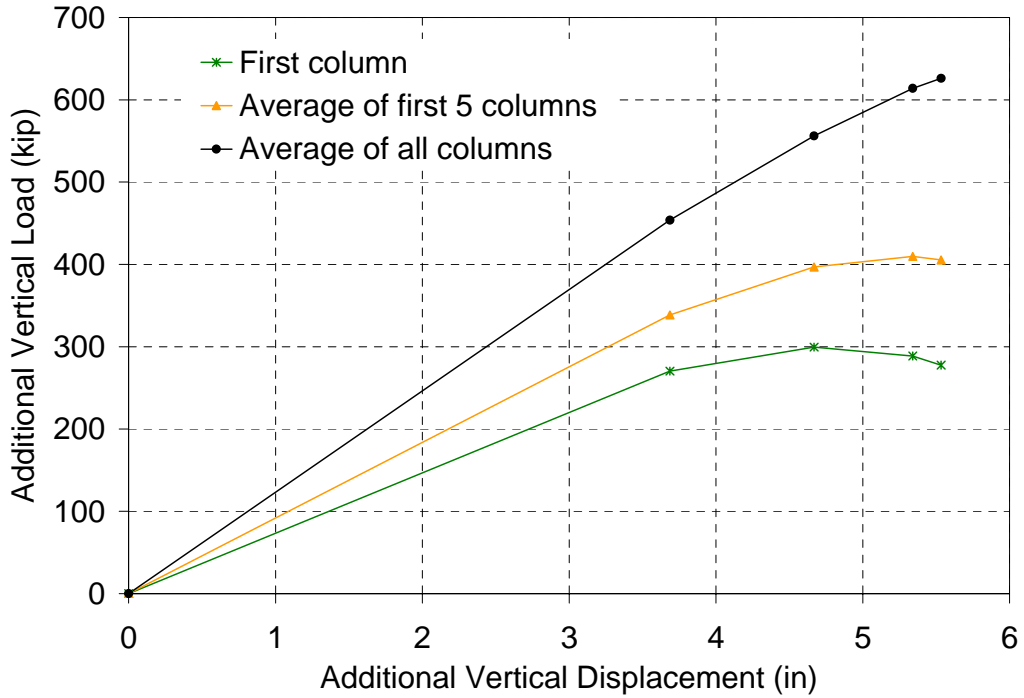


Figure 3–96. Additional vertical load applied to columns versus additional vertical during displacement for push-down analysis of isolated east wall model of WTC 2 for after Case D temperature condition (compression is positive; see Fig. 3–95 for column locations).

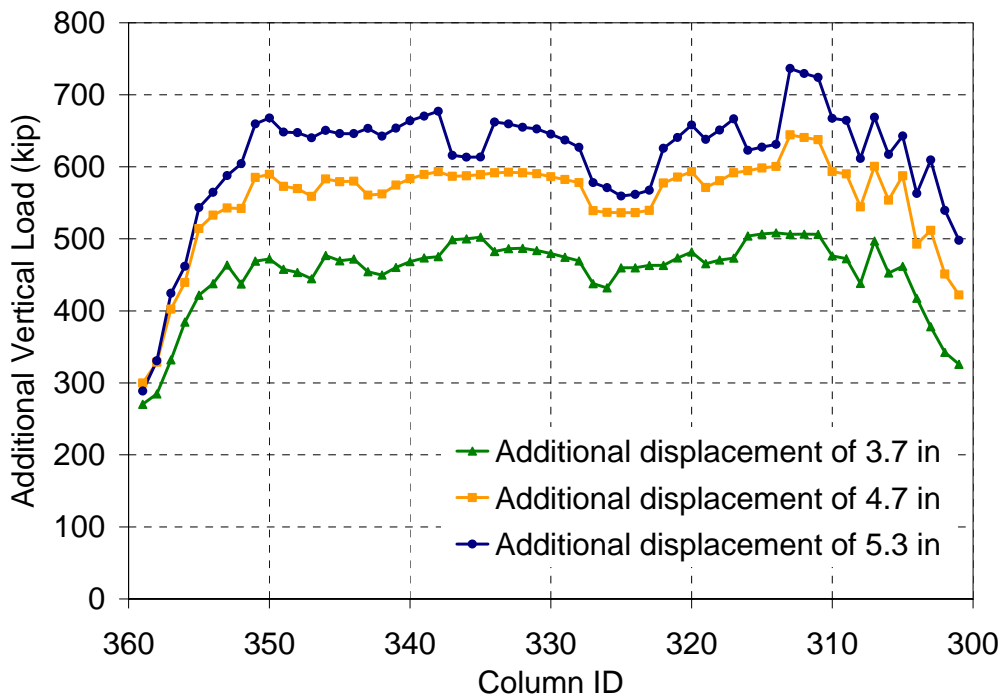


Figure 3–97. Variation of additional vertical load applied to columns of isolated east wall model of WTC 2 at different levels of additional vertical displacements imposed after Case D temperature condition (compression is positive).

Pull-in Forces to Cause Observed Bowing

As discussed in Section 2.5, the pull-in forces and their locations and the calculated floor/wall disconnections and pull-in locations were updated based on the observations from the photographs and videos. This section describes the analyses performed on the isolated wall model to estimate the magnitude of pull-in forces on the east wall of WTC 2, which would result in an inward bowing shape similar to that estimated from the photographs and videos. The estimated pull-in forces were used in the global analysis with Case D temperature condition.

The load steps that were used in the current analyses are similar to the load steps used in the earlier wall runs. At the beginning of each temperature load step, disconnections and lateral pull-in forces were applied to each floor connection to the east wall, as shown in Section 2.5. The magnitude and the distribution of the pull-in forces were obtained by trial and error. The magnitude of the pull-in force was kept constant till the end of the analysis, unless the column-floor connection fully disconnected before the analysis ended; at which point the pull-in force was set to zero. For each trial, the wall model was analyzed from the beginning (time = 0 min), accounting for large deflections and temperature-dependent plasticity and creep. The out-of-plane displacements calculated at the end of 20 min and 50 min were compared to the displacements estimated at the same points in time from the photographs, as shown in Fig. 3–98.

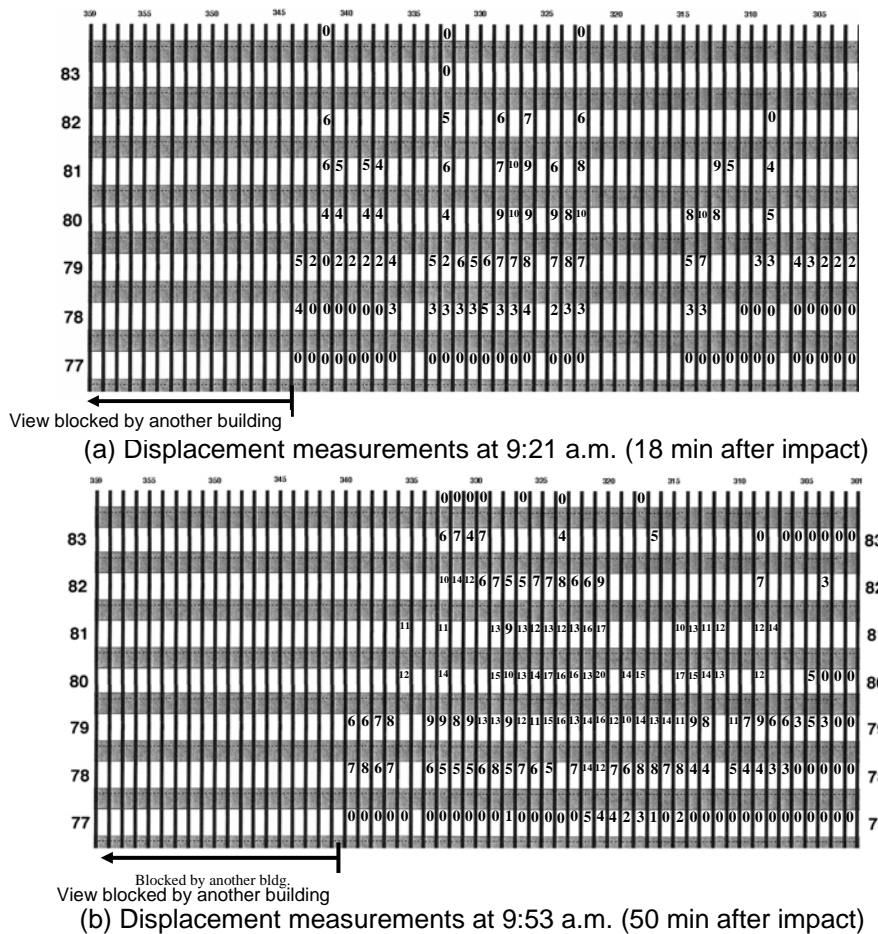


Figure 3–98. Out-of-plane displacements of the east wall of WTC 2 estimated by NIST from photographs (inward displacement is positive; displacements are in in.).

For the first set of trials, the pull-in forces were assumed to be uniformly distributed over the entire width of the model. Two different magnitudes for pull-in forces were tried: 0.5 kip and 5.0 kip. The analysis for 0.5 kip ran to 32 min, at which point it failed to converge. As shown in Fig. 3–99(a), the wall primarily bowed outward at 20 min (positive displacement direction is inward). These results disagreed with what was observed in the photographs and videos, indicating that the assumed magnitude of pull-in force of 0.5 kip was not sufficient to cause inward bowing. In a second trial, the 5.0 kip pull-in force was used. This analysis ran to 18 min, at which point it failed to converge. Contrary to the first trial with 0.5 kip pull-in force, the wall bowed inward, as shown in Fig. 3–99(b). The maximum inward displacement in this trial was 31 in. This value is about three times larger than the displacement estimated from photographs, indicating that the 5.0 kip pull-in force is greater than the actual magnitude of pull-in force. Based on these two runs, it was concluded that the magnitude of the pull-in forces for a uniform distribution is between 0.5 kip and 5.0 kip.

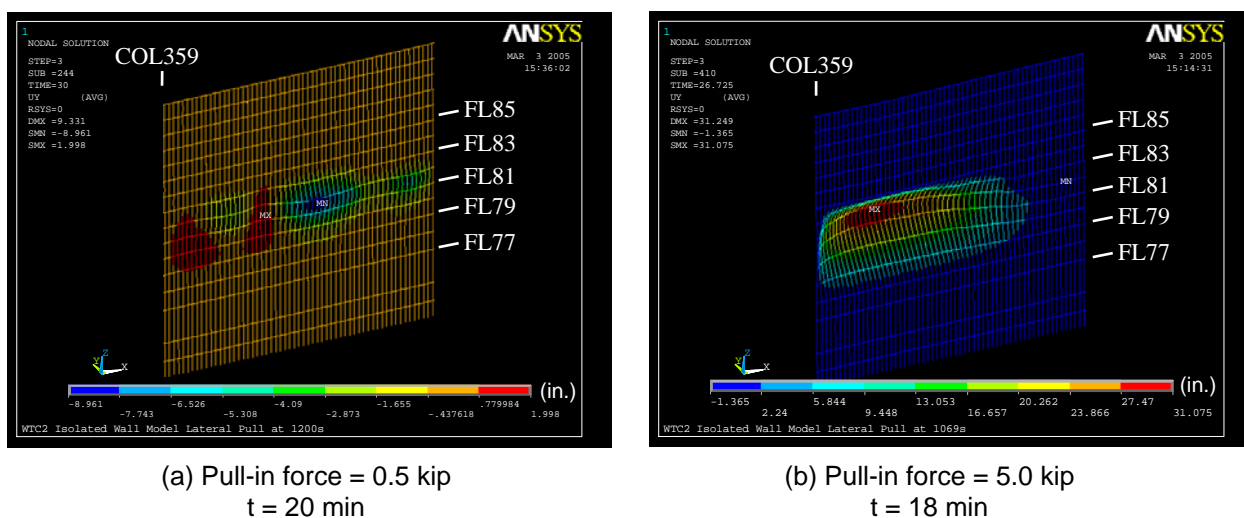


Figure 3–99. Out-of-plane displacement of isolated east wall model of WTC 2 with 0.5 kip and 5.0 kip pull-in force with uniform magnitude distribution at 20 min and 18 min (inward displacement is positive).

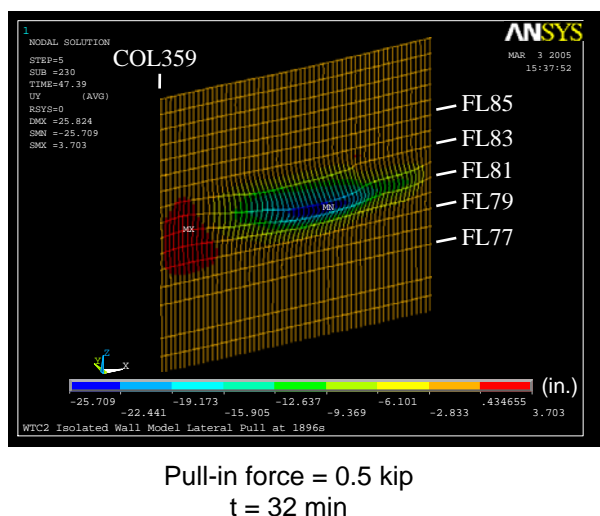
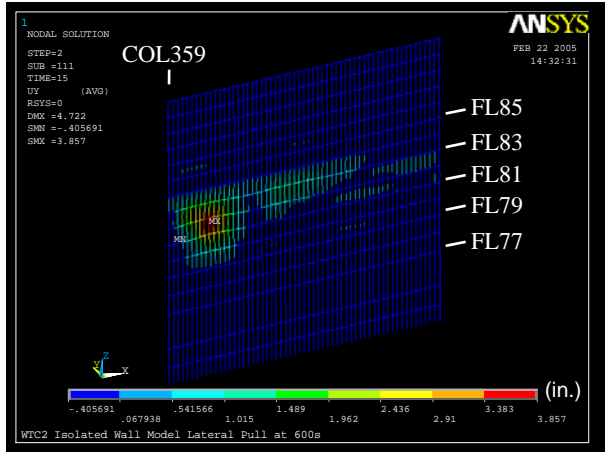


Figure 3–100. Out-of-plane displacement of isolated east wall model of WTC 2 with 0.5 kip pull-in force with uniform magnitude distribution at 32 min (inward displacement is positive).

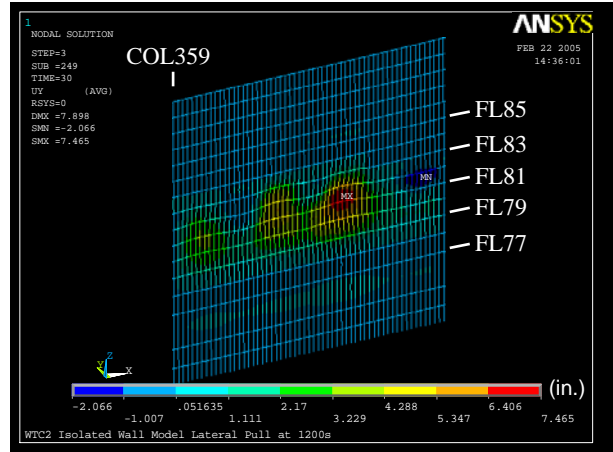
From these two runs, it was also possible to learn about the distribution of the pull-in forces over the width of the east wall. When a uniform distribution of a 0.5 kip pull-in force was used at 20 min over the entire width of the east wall, the resulting out-of-plane displacements were inward on the south side and outward on the north side of the wall, as shown in Fig. 3–99. The primary reasons for the outward bowing on the north side of the east wall are as follows: (1) the higher temperatures in the north side of the wall resulted in restrained thermal expansion and larger column loads; (2) the higher temperatures of the inside face of the columns, relative to the outside, caused higher plastic and creep strains and resulted in differential shortening of the inside relative to the outside; and (3) the plastic softening and creep of the inside caused an outward shift in the neutral axis, and a resulting outward bow of the columns. This phenomenon can be seen in the displacement results presented in Figs. 3–99 and 3–100, where inward displacements on the south side of the east wall became smaller and smaller and eventually changed to outward displacements toward the north side of the east wall. Consequently, a simple non-uniform pull-in force distribution was selected with higher loads on the north side to ensure inward bowing as observed in photographs and videos.

Two cases were analyzed for the second set of trials. In the first case, the magnitude of the pull-in forces on the south half of the east wall was set to 1.0 kip and the magnitude of the pull-in forces on the north half was set to 4.0 kip. The wall analysis with these pull-in force magnitudes ran to 60 min. Figure 3–101 shows the out-of-plane displacements at different stages of the analysis. As can be seen, the maximum inward bowing was 7.5 in. at 20 min, located approximately at the middle of Floor 81 of the east wall. This agreed well with the observed displacements, which showed maximum inward displacement of about 10 in. around the middle of Floor 81. In the earlier trial with a uniform 0.5 kip magnitude of pull-in force, the inward bowing started to decrease with increasing time after 20 min, and at around 40 min it bowed outward. The bowing at 50 min was mostly outward, disagreeing with the observed displacements. In the second trial, the magnitude of the pull-in force on the south half was increased from 1.0 to 1.5 kip, and on the north half was increased from 4.0 to 5.0 kip. This analysis ran to 50 min, at which point the analysis failed to converge. Figure 3–102 shows the magnitude of inward bowing at different stages of the analysis. The maximum inward bowing in this trial was 9.5 in. at 20 min, located approximately at the middle of Floor 81 of the east wall. This result agreed well with the observed displacements. The inward bowing continued to increase with time and reached a maximum of 37 in. at 50 min. As seen in Fig. 3–102, the location of the maximum displacements agreed well with the observations. However, the magnitude of the calculated displacements was about twice the magnitude of the observed displacements.

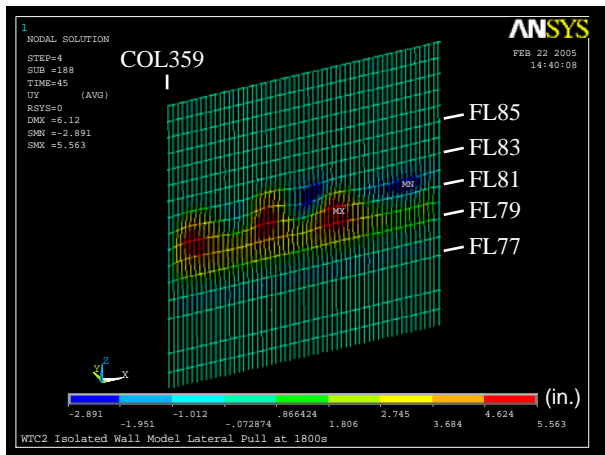
From these trial runs, it was concluded that the magnitude of pull-in forces ranged from 1.0 kip to 1.5 kip on the south half and from 4.0 kip to 5.0 kip on the north half of the east wall. Based on these ranges, and also considering the possible increase in column loads of the east face after impact for Case D conditions, a pull-in force of 1.0 kip on the south half and 4.0 kip on the north half of the east wall was initially selected for the global model analysis with creep. As will be discussed in Chapter 4, at 30 min, the magnitude of the pull-in force was increased to 1.5 kip on the south half and decreased to 3.0 kip on the north half of the east wall and kept constant after that time.



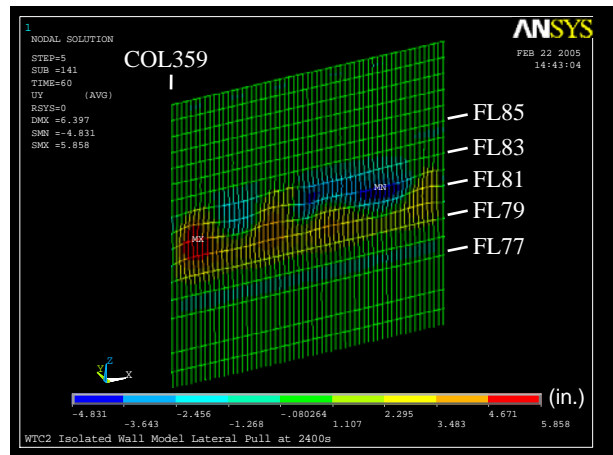
(a) At 10 min



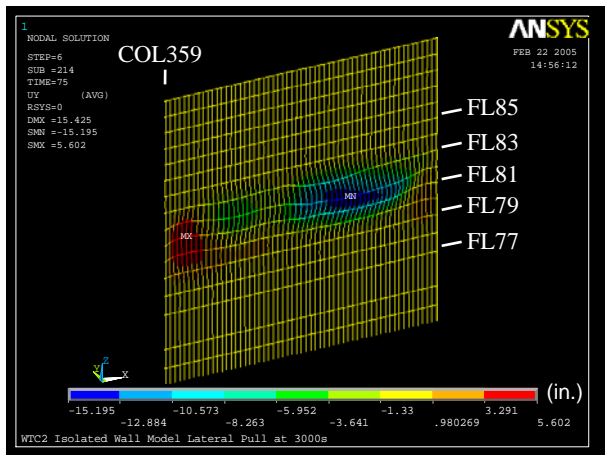
(b) At 20 min



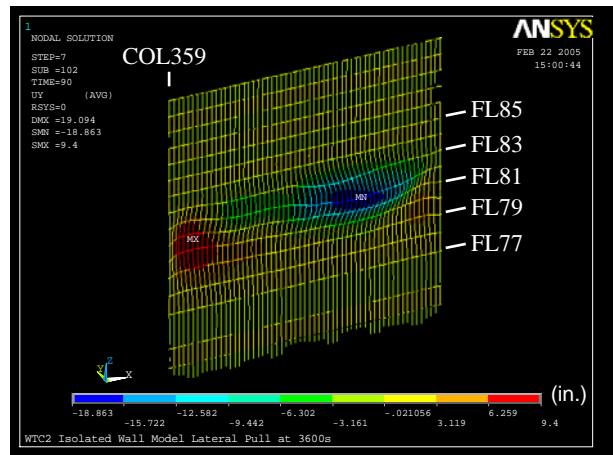
(c) At 30 min



(d) At 40 min

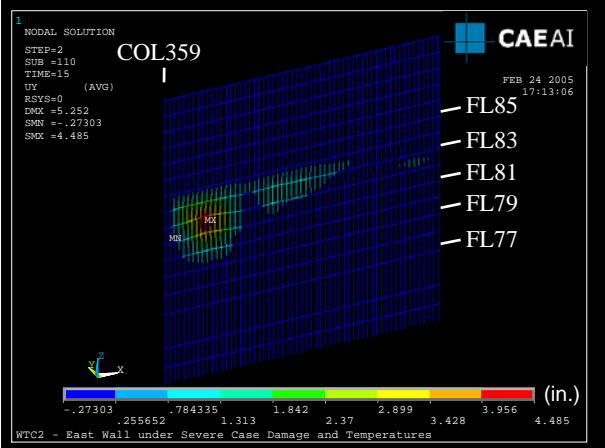


(e) At 50 min

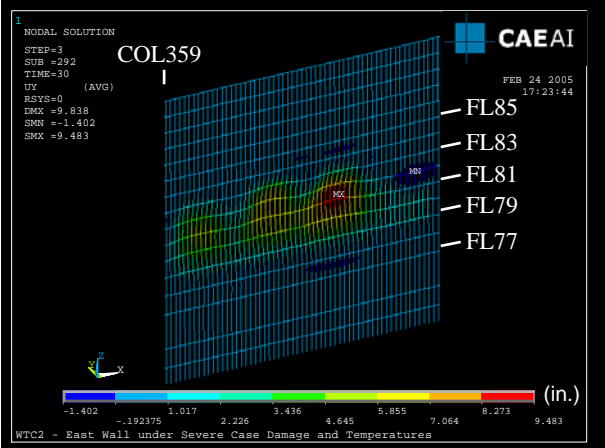


(f) At 60 min

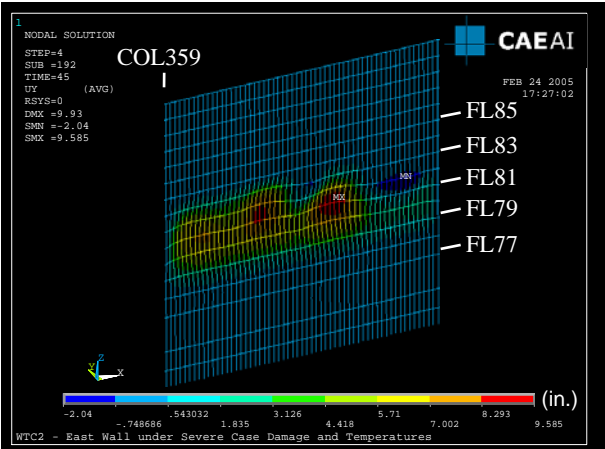
Figure 3–101. Out-of-plane displacement of isolated east wall model of WTC 2 with nonuniform pull-in force with magnitude of 1.0 kip on the south half and 4.0 kip on the north half (inward displacement is positive).



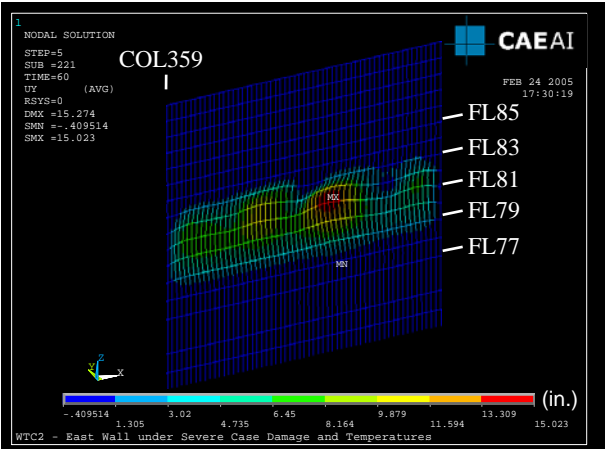
(a) At 10 min



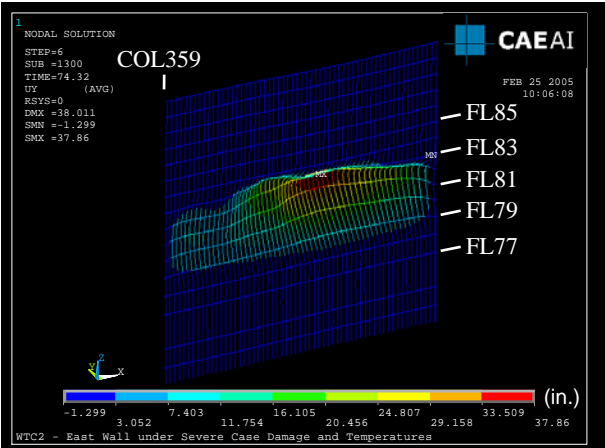
(b) At 20 min



(c) At 30 min



(d) At 40 min



(e) At 50 min

Figure 3–102. Out-of-plane displacement of isolated east wall model of WTC 2 with nonuniform pull-in force with magnitude of 1.5 kip on the south half and 5.0 kip on the north half (inward displacement is positive).

3.3 CORE COLUMN SHORTENING AND DOWNWARD DISPLACEMENT OF CORE

To examine whether or not the core columns shortened and the core displaced downward when subjected to fire-induced temperature loads, the core models were isolated from the global models of WTC 1 and WTC 2. The isolated core models extended from Floor 89 to Floor 106 for WTC 1 and from Floor 73 to Floor 106 for WTC 2, and did not include any parts of their hat trusses. At the base of the models, vertical springs connected Floor 89 and Floor 73 to fixed ground; the spring stiffness represented the vertical stiffness of the columns below. The isolated core models included core columns, core beams, and core slabs, as in the global models (see Chapter 4 for details).

The WTC 2 core model was restrained in two horizontal directions at every floor level to represent the lateral restraint of the exterior walls. Without the lateral restraints, the WTC 2 core model would tilt significantly, due to the extensive impact damage to the southeast part of the core. The WTC 1 core model was not restrained in the horizontal directions at floor levels.

Gravity dead and live loads were directly obtained from the global models and applied to the core model nodes. Internal forces and moments of the columns of Floor 106 of the global models after aircraft impact were imposed at the ends of the Floor 106 columns of the isolated core models. Only the Case A structural damage condition was used for the WTC 1 core model, and only the Case C structural damage condition was used for the WTC 2 core model. The isolated core models with Case B and Case D structural damage conditions were also run, but the models did not converge, even with lateral restraints.

The models were then subjected to two temperature conditions for each tower: Case A and Case B (for WTC 1) and Case C and Case D (for WTC 2). Temperature data were provided at 10 min intervals up to 100 min for WTC 1 and up to 60 min for WTC 2.

Since the models included only the core, the load transfer between the core and the exterior wall through either the hat truss or floors was not captured.

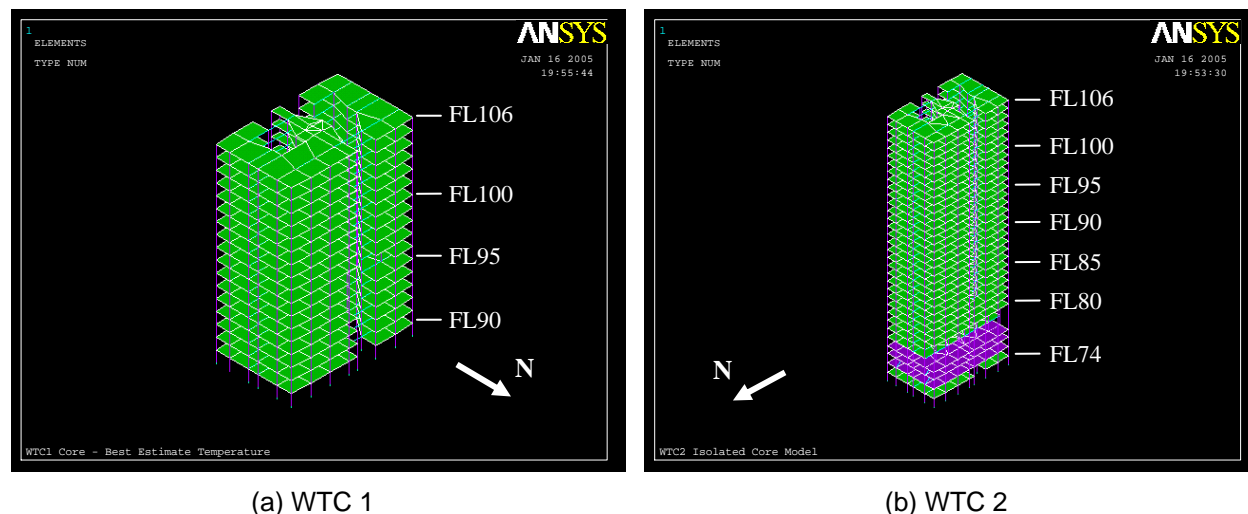


Figure 3–103. Isolated core models.

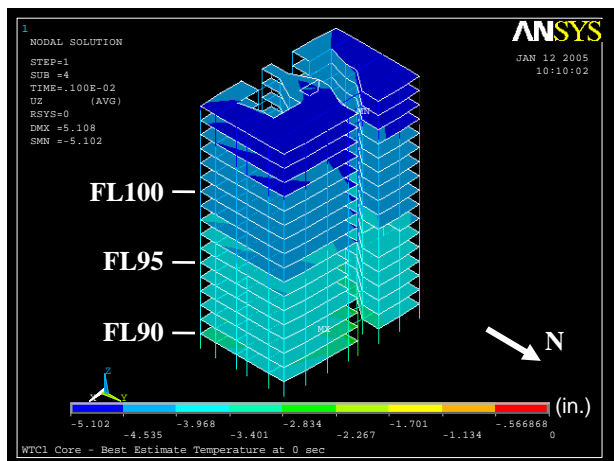
3.3.1 FEA of WTC 1 Core

Case A Temperature Condition

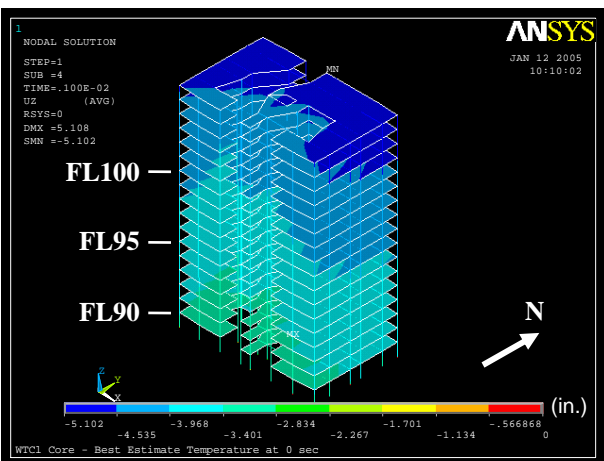
Figures 3–104 to 3–111 show the vertical displacements of the WTC 1 isolated core model subjected to Case A temperatures from aircraft impact to 100 min. At 30 min, the vertical displacement of the northwest corner at Column 501 became large above Floor 98, and grew larger with time. The core started to tilt toward the northwest corner at 30 min, and the analysis was terminated due to nonconvergence. The analysis was restarted at 30 min by restraining corner Column 501 in the horizontal directions at floor levels above Floor 98 to represent lateral restraint from the exterior walls and office floors. At 100 min, the maximum vertical displacement of 21.7 in. occurred at Column 501. Figures 3–114 and 3–115 show axial loads and plastic strains in the core columns at 100 min. Columns at the northwest corner experienced large plastic strains. The maximum plastic strain was about 14 percent.

The vertical displacement at Floor 106 at 100 min ranged from 3.3 in. to 21.7 in. The maximum vertical displacement of the south side was limited to 11.2 in. at Column 1004. The average vertical displacement of Floor 106 was 7.4 in. The average vertical displacement of the south side at Floor 106 was 6.0 in. Considering the average vertical displacement of 5 in. after the aircraft impact, the average additional downward displacement of the core due to thermal loads was about 2 in.

To determine the additional axial load-carrying capacity of the core, the isolated core model at 100 min was pushed down by imposing additional incremental vertical displacement. The analysis was converted from a force-control analysis to a displacement-control analysis by imposing the vertical displacements calculated at 100 min under force control and then imposing additional vertical displacement increments on the top of the columns at Floor 106. The analysis was terminated when the additional vertical displacement reached 9.5 in. Figure 3–116 shows the total vertical displacements of the model at the end of the push-down analysis. Figure 3–117 shows the relationship between the total additional vertical force and the additional vertical displacement. The additional vertical force reached its maximum at 7.2 in. of additional vertical displacement. Figure 3–118 shows the additional axial loads in columns of Floor 98 when the total additional vertical force is at its maximum. The maximum total additional vertical force of 37,142 kip was about 95 percent of the total column force at Floor 98 prior to push-down. Therefore, the core still had significant reserve capacity at the end of Case A temperature condition.

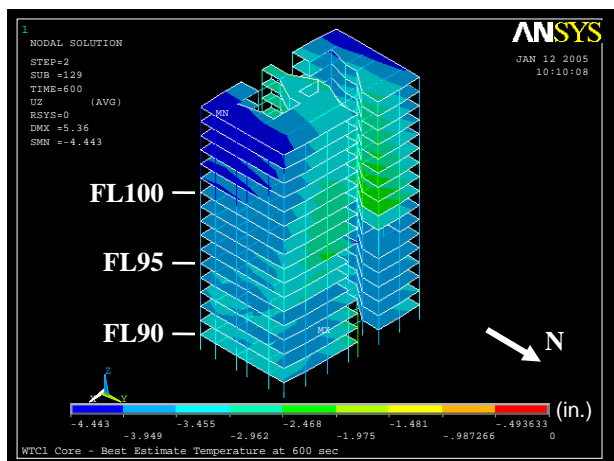


(a) North and east sides

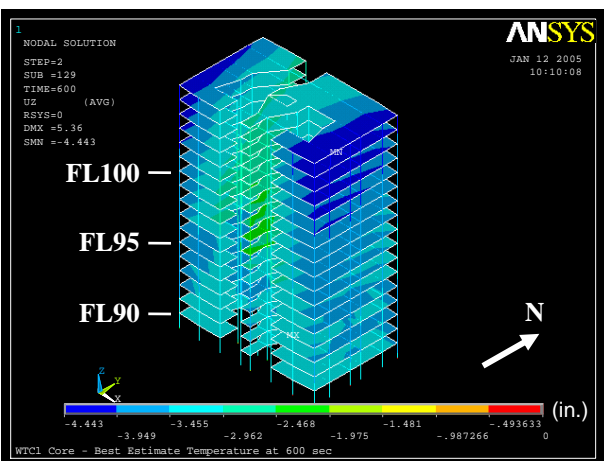


(b) South and east sides

Figure 3–104. Vertical displacement of isolated core model of WTC 1 after aircraft impact (downward displacement is negative).

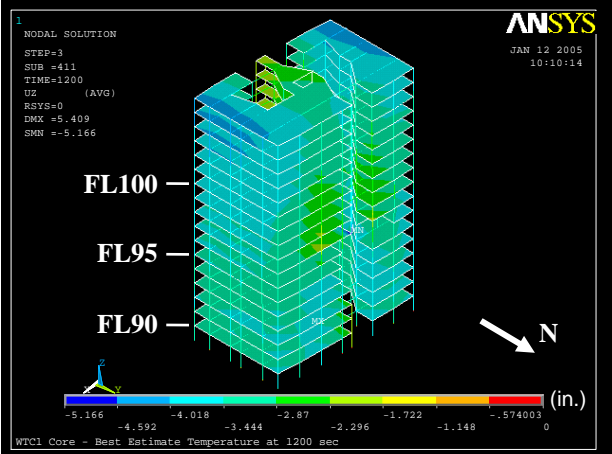


(a) North and east sides

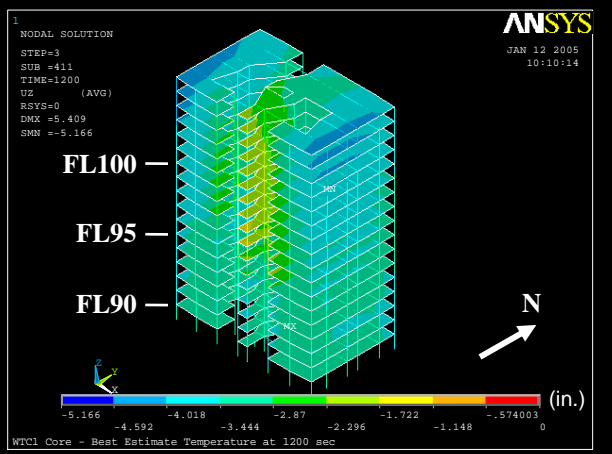


(b) South and east sides

Figure 3–105. Vertical displacement of isolated core model of WTC 1 for Case A temperature condition at 10 min (downward displacement is negative).

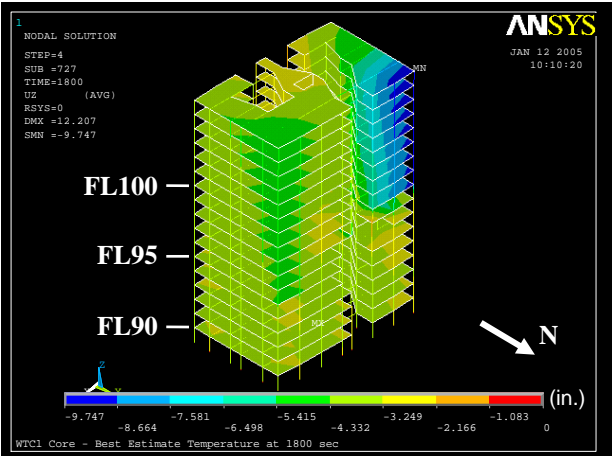


(a) North and east sides

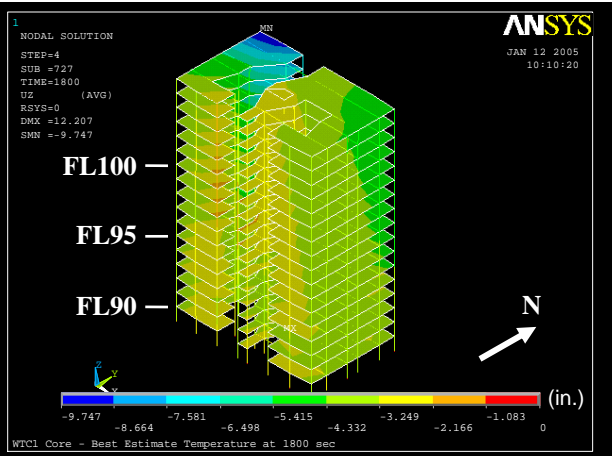


(b) South and east sides

Figure 3-106. Vertical displacement of isolated core model of WTC 1 for Case A temperature condition at 20 min (downward displacement is negative).

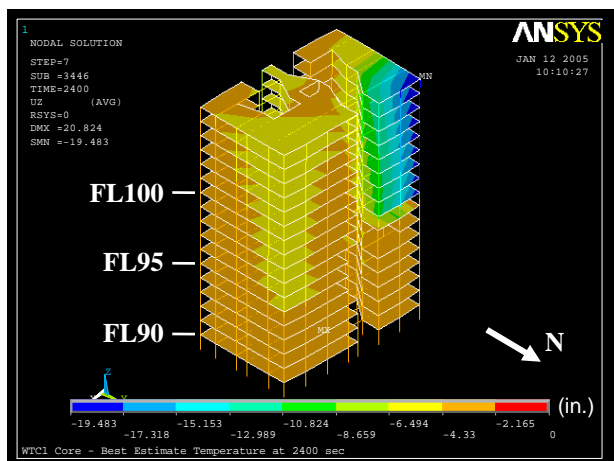


(a) North and east sides

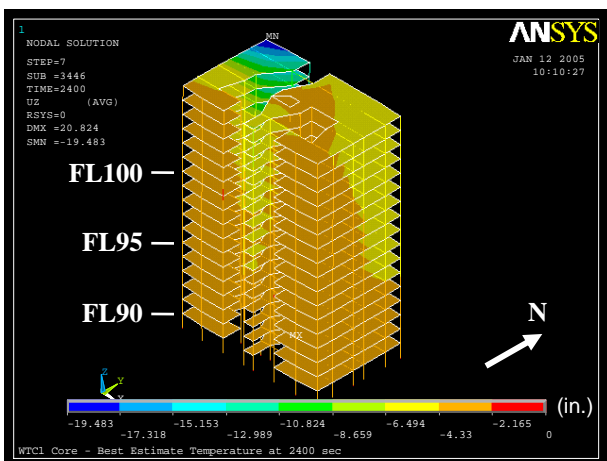


(b) South and east sides

Figure 3-107. Vertical displacement of isolated core model of WTC 1 for Case A temperature condition at 30 min (downward displacement is negative).

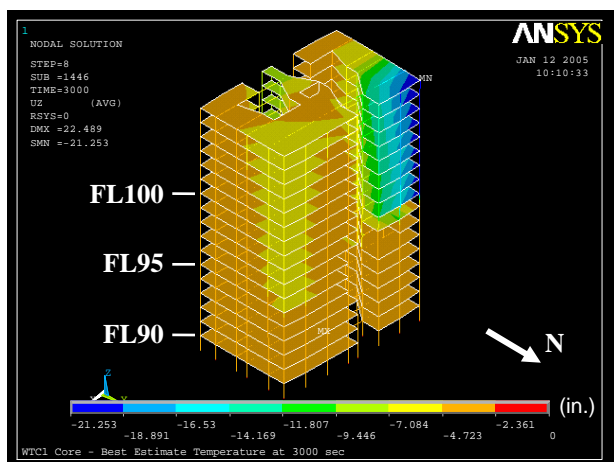


(a) North and east sides

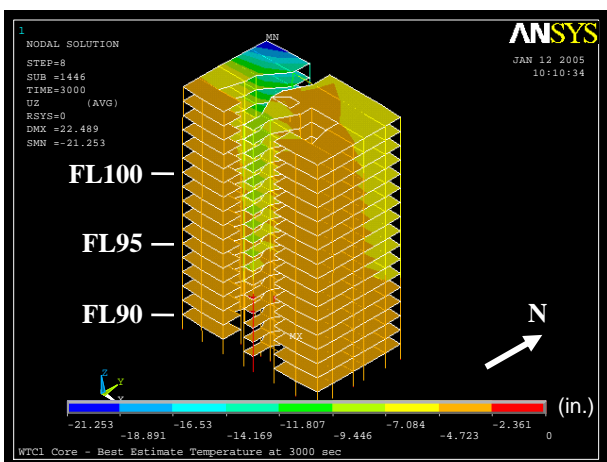


(b) South and east sides

Figure 3–108. Vertical displacement of isolated core model of WTC 1 for Case A temperature condition at 40 min (downward displacement is negative).

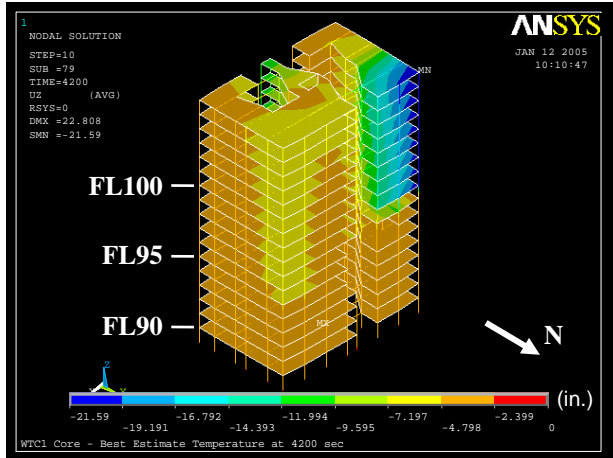


(a) North and east sides

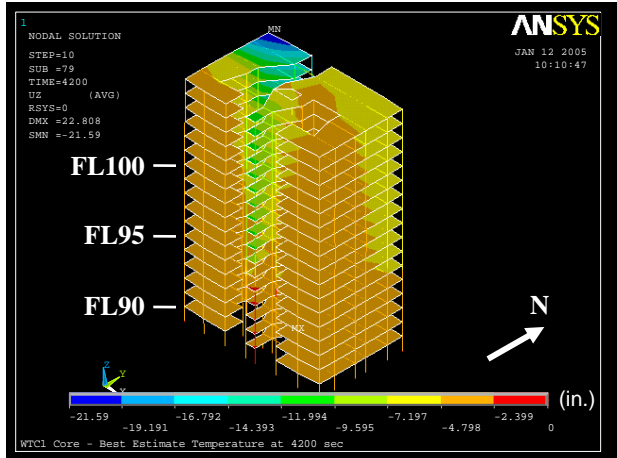


(b) South and east sides

Figure 3–109. Vertical displacement of isolated core model of WTC 1 for Case A temperature condition at 50 min (downward displacement is negative).

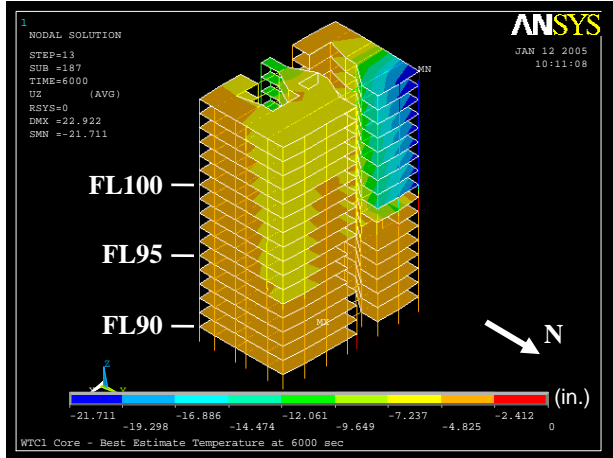


(a) North and east sides

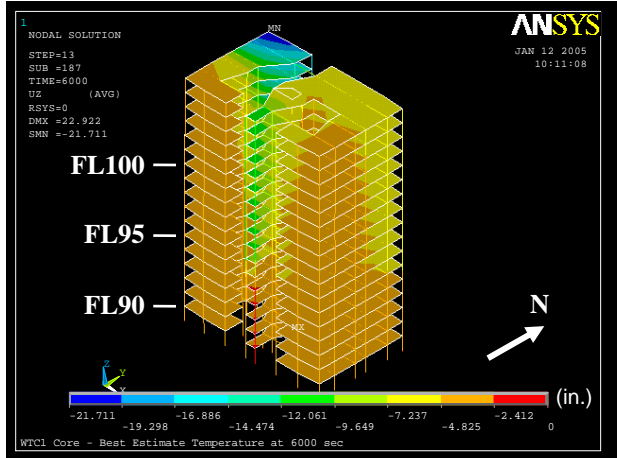


(b) South and east sides

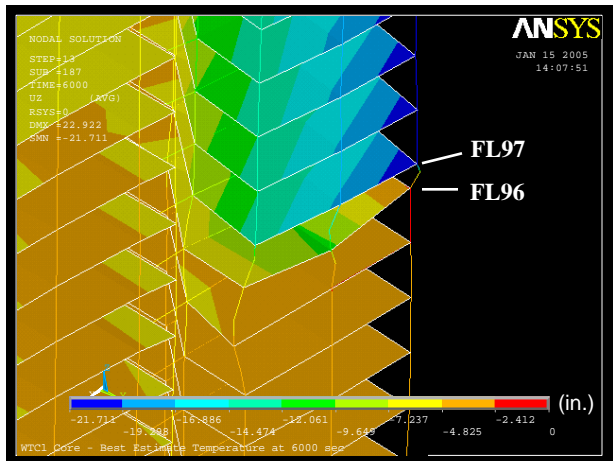
Figure 3-110. Vertical displacement of isolated core model of WTC 1 for Case A temperature condition at 70 min (downward displacement is negative).



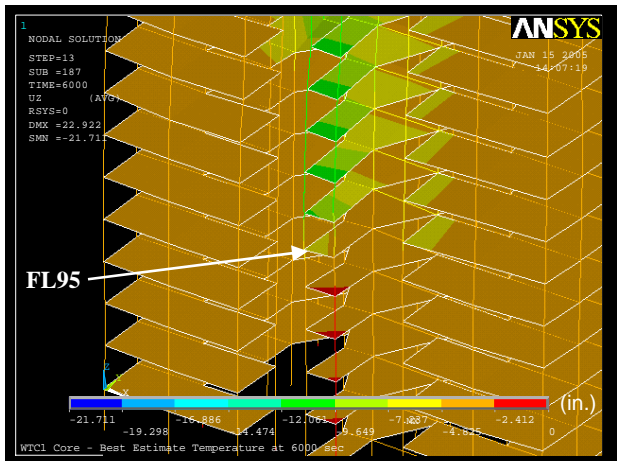
(a) North and east sides



(b) South and east sides

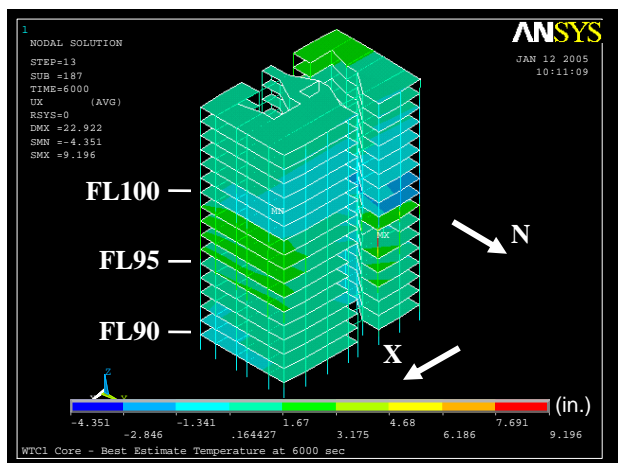


(c) Northwest corner
 (5X displacement magnification)

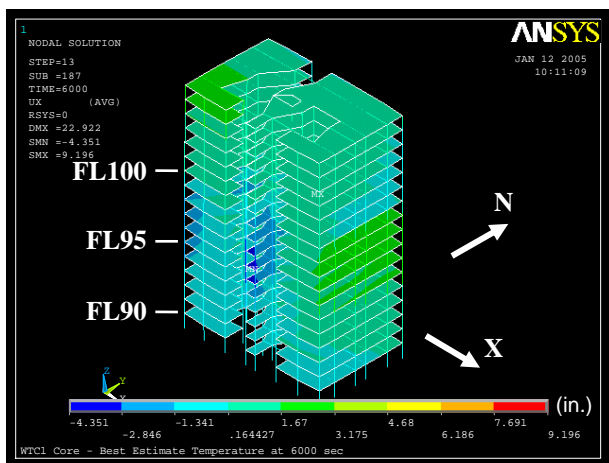


(b) South side
 (5X displacement magnification)

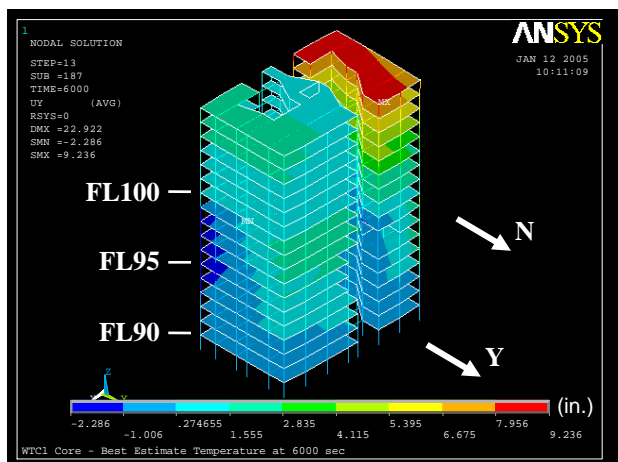
Figure 3-111. Vertical displacement of isolated core model of WTC 1 for Case A temperature condition at 100 min (downward displacement is negative).



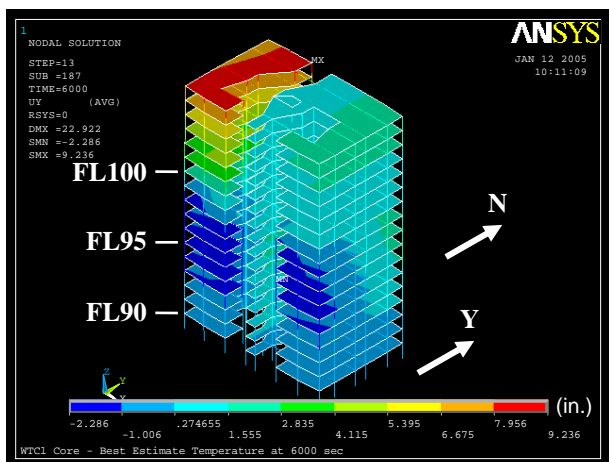
(a) X-displacement of north and east sides



(b) X-displacement of south and east sides

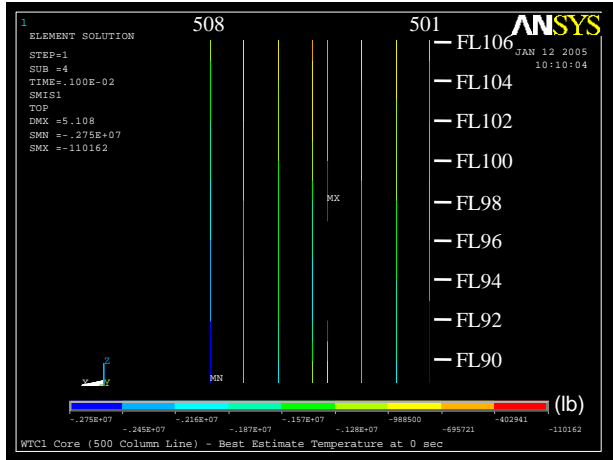


(c) Y-displacement of north and east sides

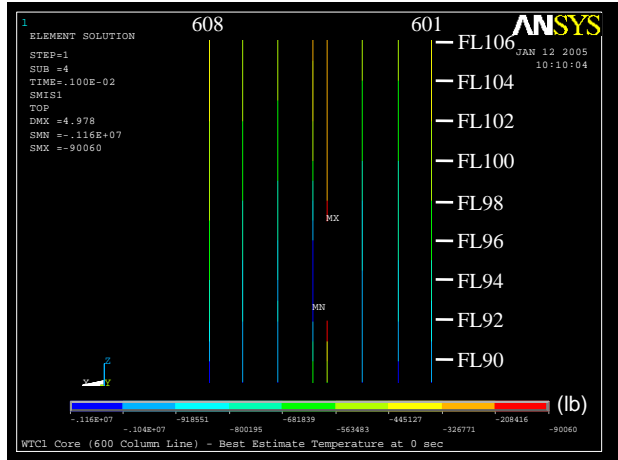


(d) Y-displacement of south and east sides

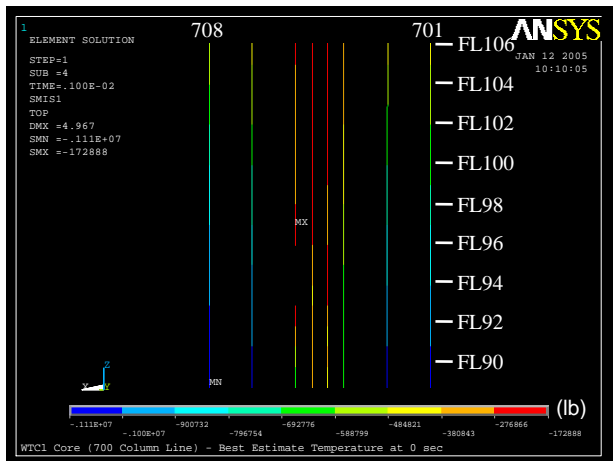
Figure 3–112. Horizontal displacement of isolated core model of WTC 1 for Case A temperature condition at 100 min.



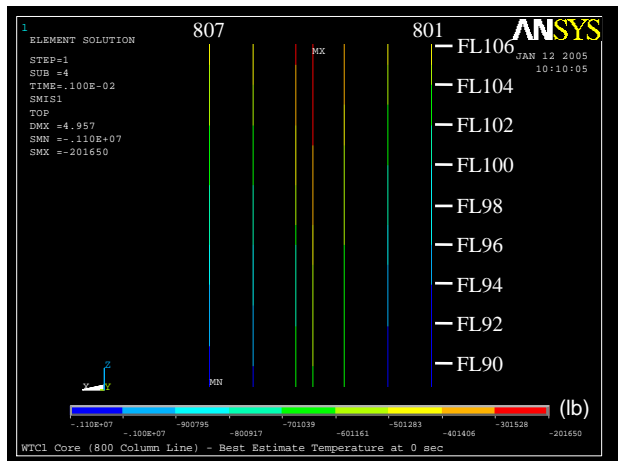
(a) 500 series columns



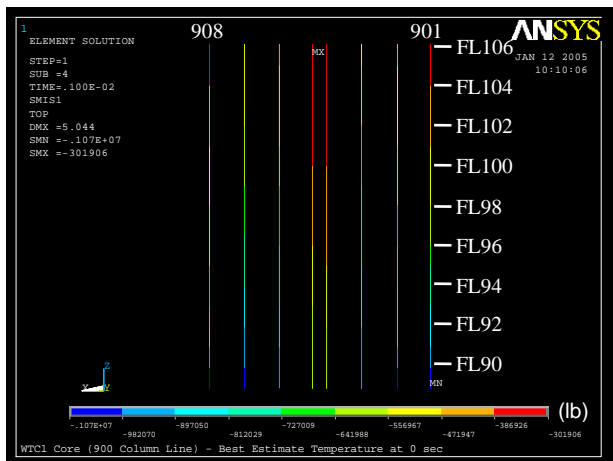
(b) 600 series columns



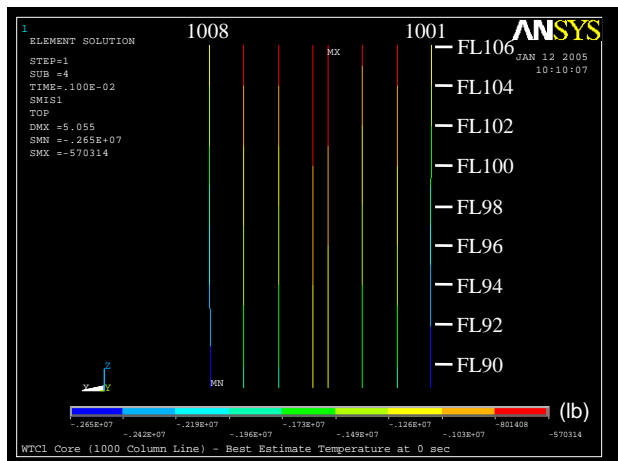
(c) 700 series columns



(d) 800 series columns

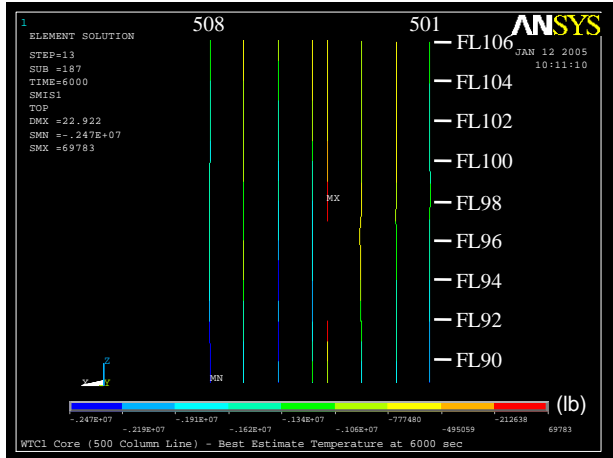


(e) 900 series columns

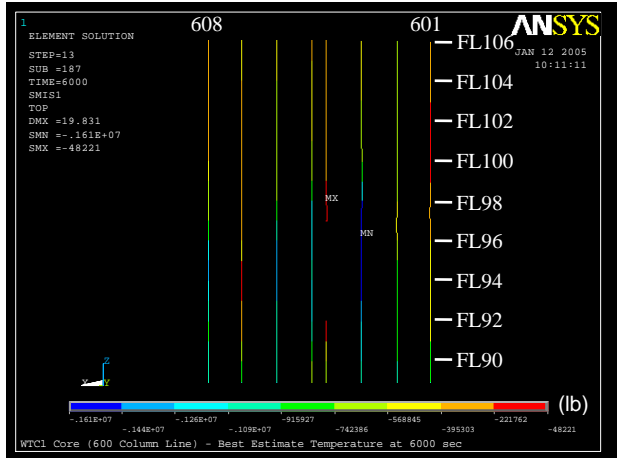


(f) 1000 series columns

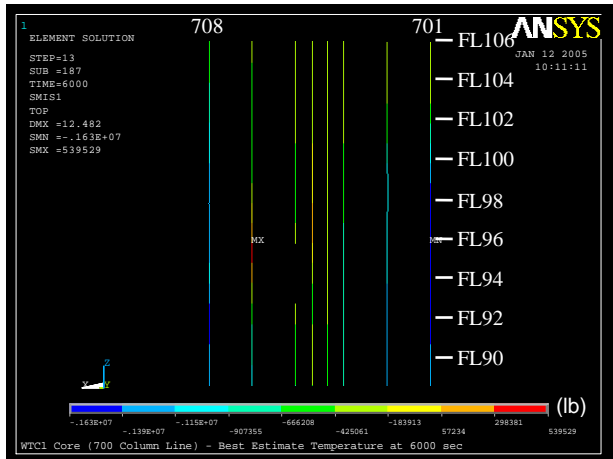
Figure 3–113. Axial load in columns of isolated core model of WTC 1 after aircraft impact (compression is negative).



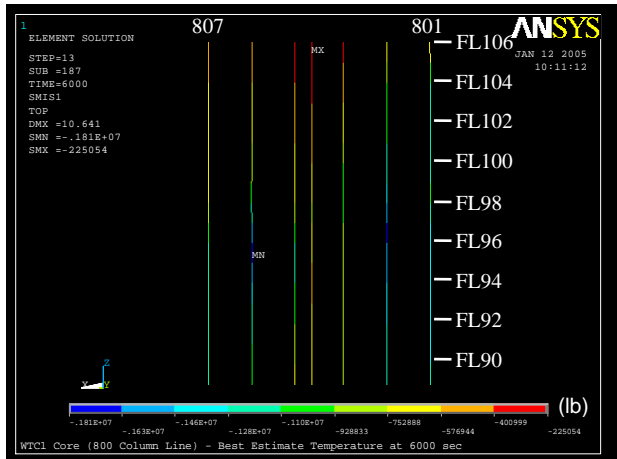
(a) 500 series columns



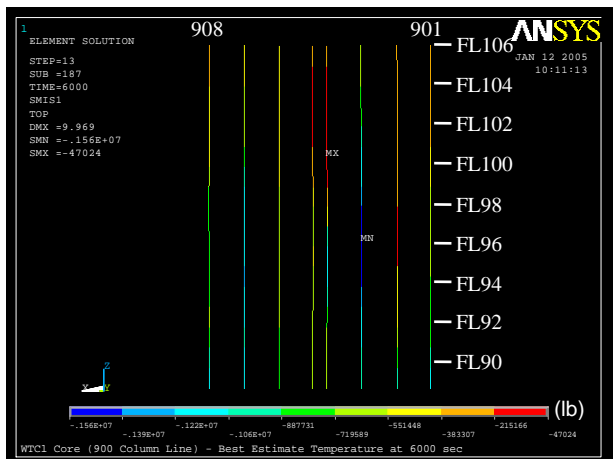
(b) 600 series columns



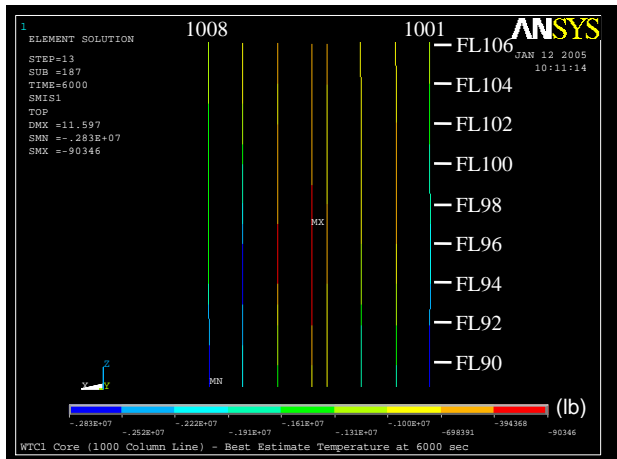
(c) 700 series columns



(d) 800 series columns

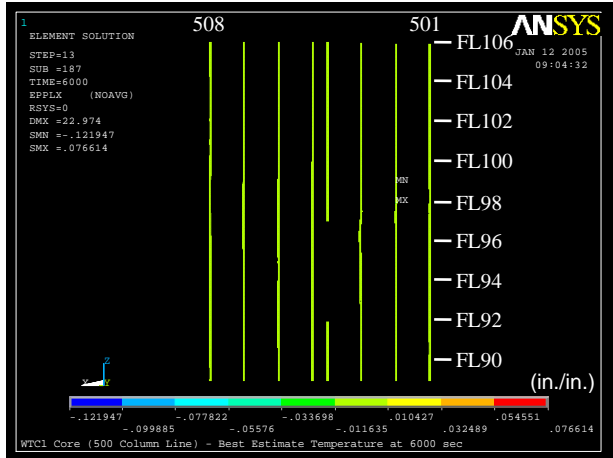


(e) 900 series columns

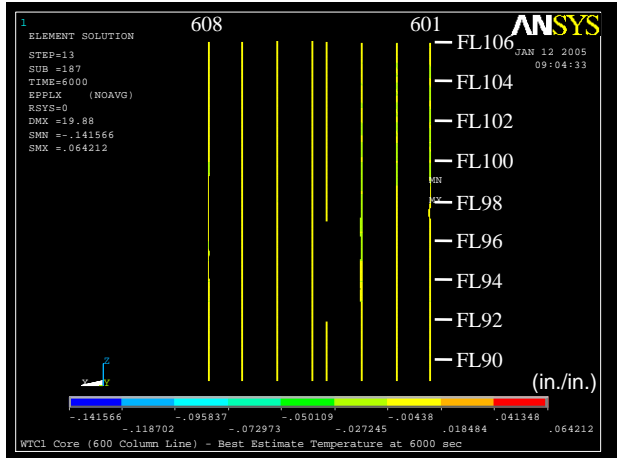


(f) 1000 series columns

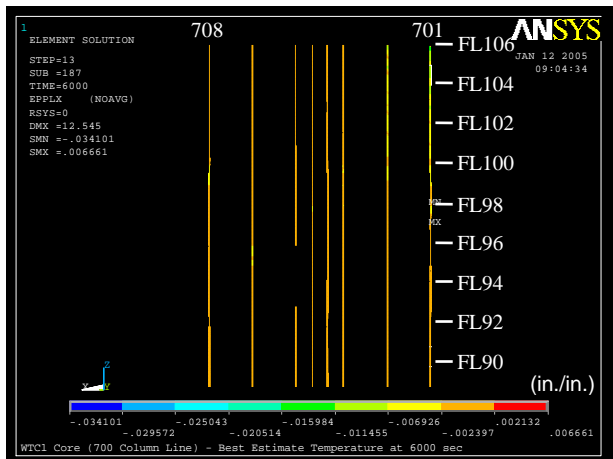
Figure 3–114. Axial load in columns of isolated core model of WTC 1 for Case A temperature condition at 100 min (compression is negative).



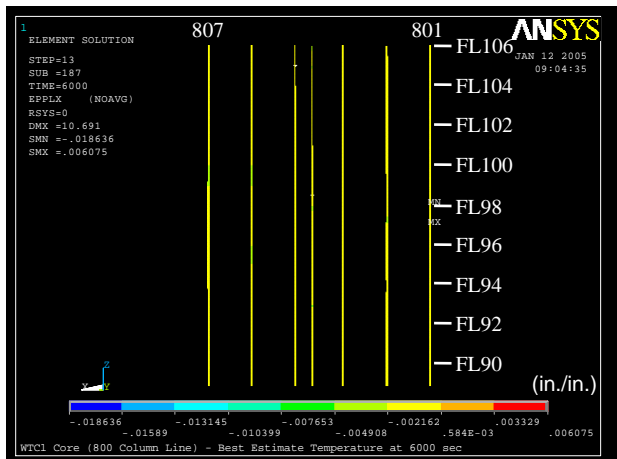
(a) 500 series columns



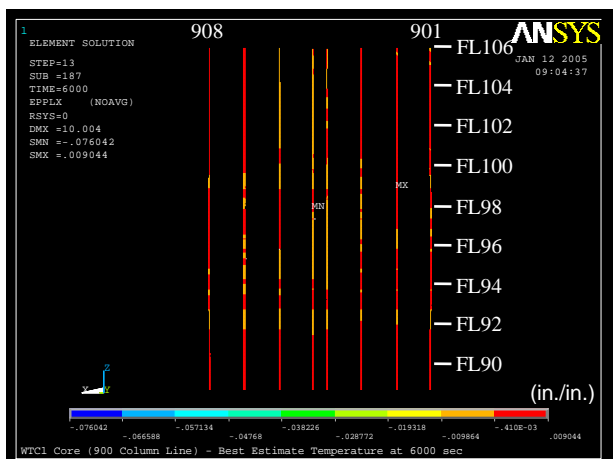
(b) 600 series columns



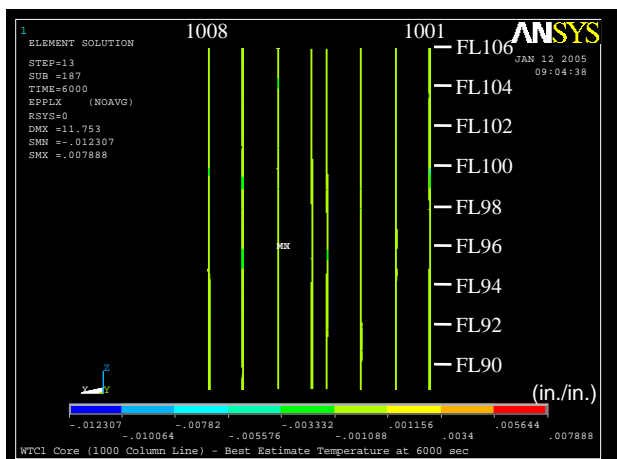
(c) 700 series columns



(d) 800 series columns

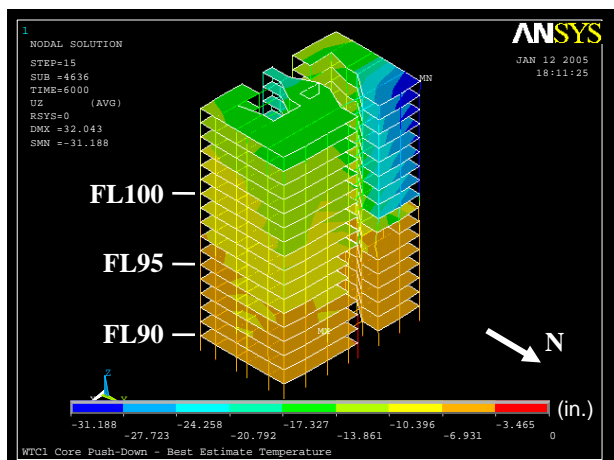


(e) 900 series columns

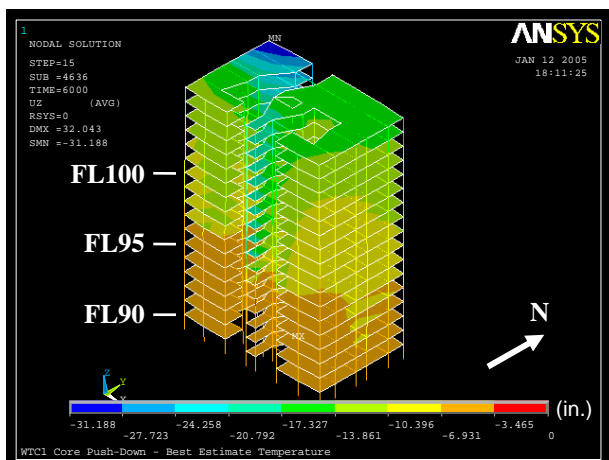


(f) 1000 series columns

Figure 3–115. Plastic strain in columns of isolated core model of WTC 1 for Case A temperature condition at 100 min (compressive strain is negative).



(a) North and east sides



(b) South and east sides

Figure 3–116. Vertical displacement after push down of isolated core model of WTC 1 for Case A temperature condition (downward displacement is negative).

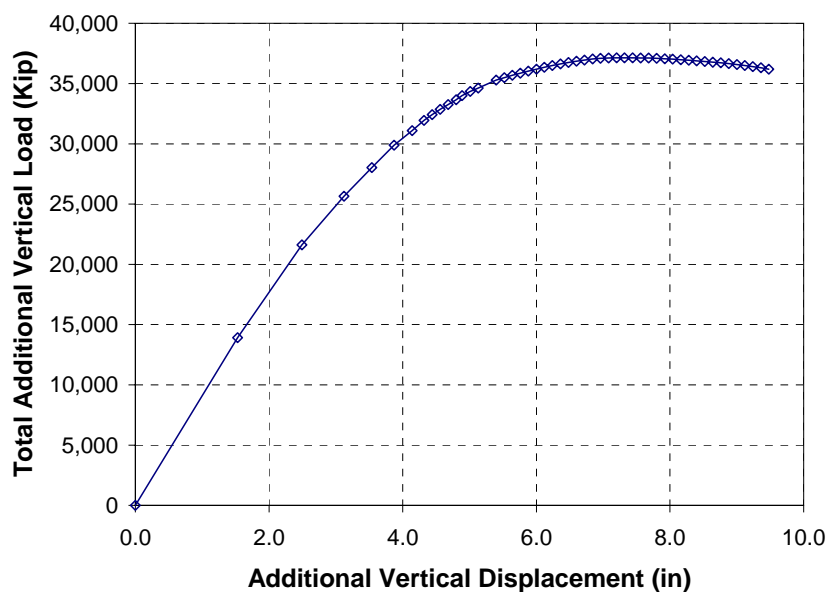


Figure 3–117. Total additional vertical load versus additional vertical displacement during push-down analysis of isolated core model of WTC 1 for Case A temperature condition (compression is positive).

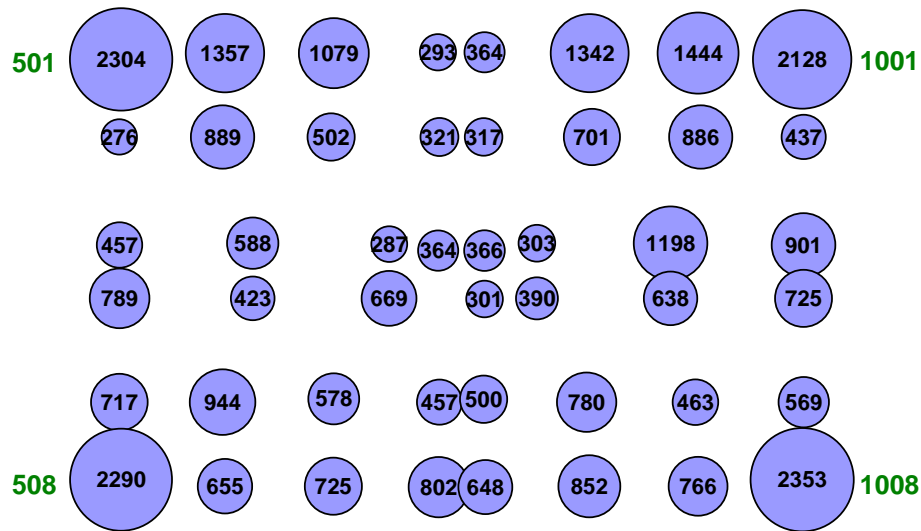


Figure 3–118. Additional axial load (kip) in columns at Floor 98 when the total axial load reached the maximum during push down analysis of isolated core model of WTC 1 for Case A temperature condition (compression is positive).

Case B Temperature Condition

Figures 3–119 to 3–125 show the vertical displacements of the WTC 1 isolated core model subjected to Case B temperature condition. At 30 min, the vertical displacement of the south side above Floor 96 between Column 1004 and Column 1005 became large. At 100 min, the maximum vertical displacement was 44.2 in. on the south side at Column 1005.

Figures 3–127 and 3–128 show axial loads and plastic strains in columns at 100 min. The following columns buckled: Column 904 spanning Floor 97 and Floor 98, Column 1004 spanning Floor 97 and Floor 98, Column 1005 spanning Floor 95 and Floor 96, and Column 1006 spanning Floor 95 and Floor 96. These columns also experienced large localized plastic strains.

The northeast corner, where the largest displacement occurred for Case A temperature condition, did not displace significantly for Case B temperature condition. The vertical displacement at Floor 106 ranged from 4.8 to 44.2 in. The average vertical displacement of Floor 106 was 11.9 in. The average displacement of the south face was 20 in. Considering the 5 in. displacement after the aircraft impact, the average additional downward displacement of the core due to thermal loads was about 7 in.

To determine the additional axial load-carrying capacity of the core, a push-down analysis was performed for Case B temperature condition in the same manner as described for the isolated core model for Case A temperature condition. The analysis was terminated when an additional vertical displacement of 9.4 in. was applied to the top. Figure 3–129 shows vertical displacements of the model at the end of analysis. Figure 3–130 shows the relationship between the total additional vertical force and the additional vertical displacement. The total additional vertical force reached its maximum at an additional displacement of 4.9 in. Figure 3–131 shows the additional axial loads in columns of Floor 98 when the total additional vertical force was at its maximum. The maximum total additional vertical force of 24,002 kip was about

61 percent of the total column force at Floor 98 prior to push-down. Thus, the reserve capacity of the core at the end of Case B temperature condition was substantial, but less than that of Case A temperature condition.

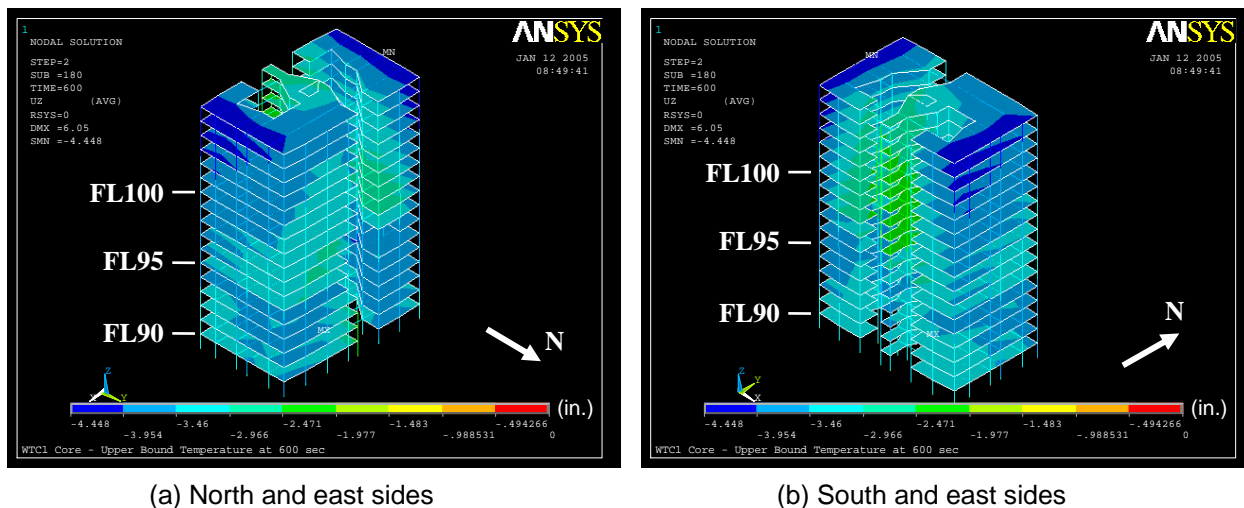


Figure 3–119. Vertical displacement of isolated core model of WTC 1 for Case B temperature condition at 10 min (downward displacement is negative).

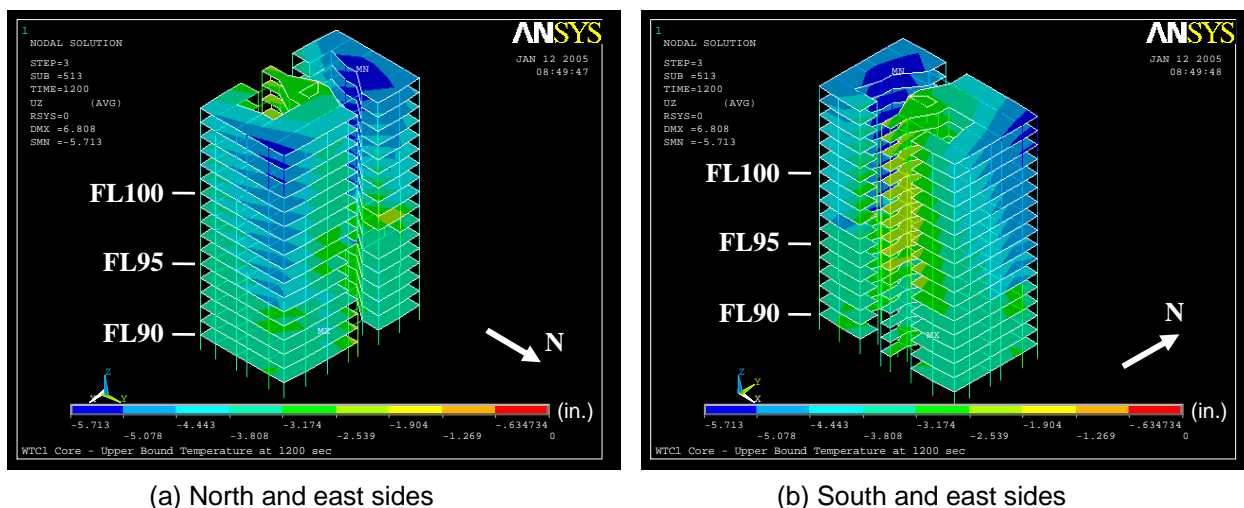
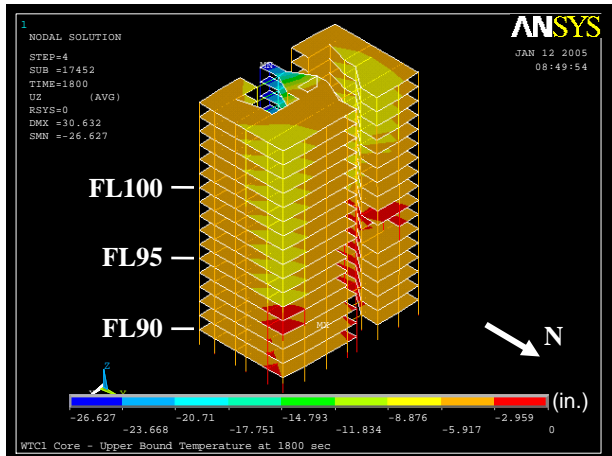
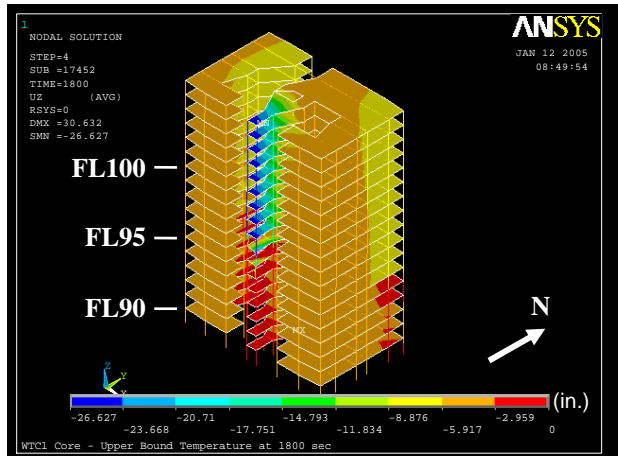


Figure 3–120. Vertical displacement of isolated core model of WTC 1 for Case B temperature condition at 20 min (downward displacement is negative).

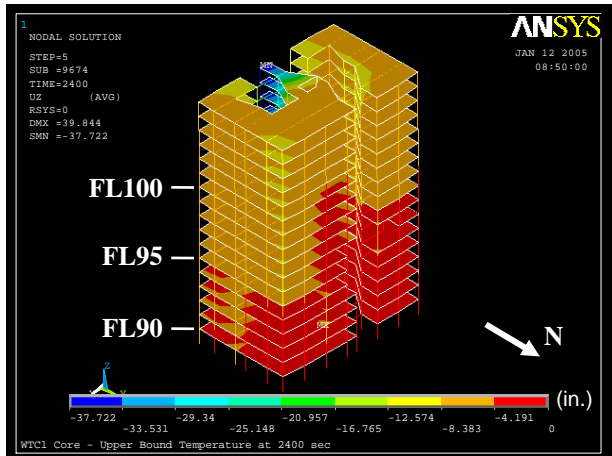


(a) North and east sides

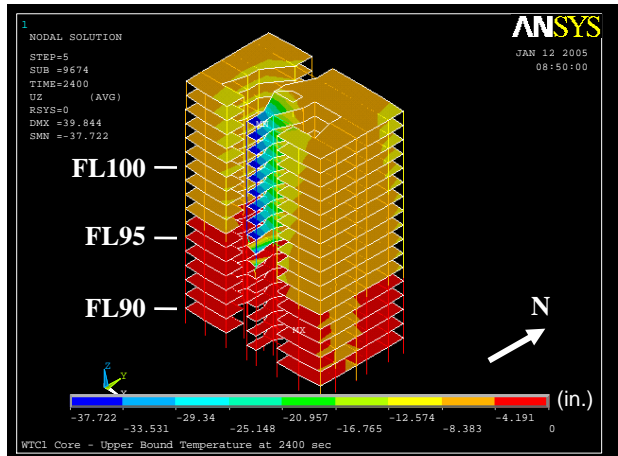


(b) South and east sides

Figure 3–121. Vertical displacement of isolated core model of WTC 1 for Case B temperature condition at 30 min (downward displacement is negative).

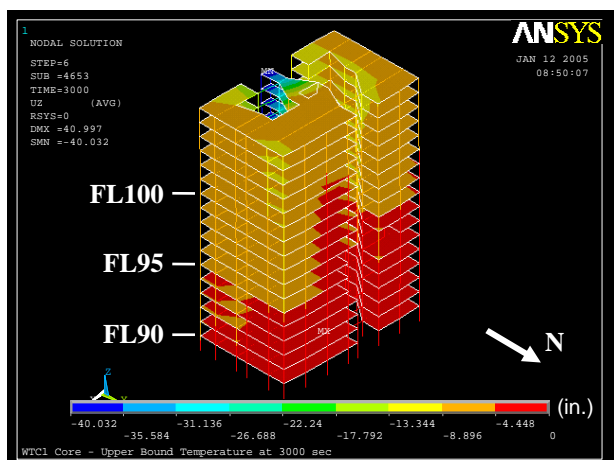


(a) North and east sides

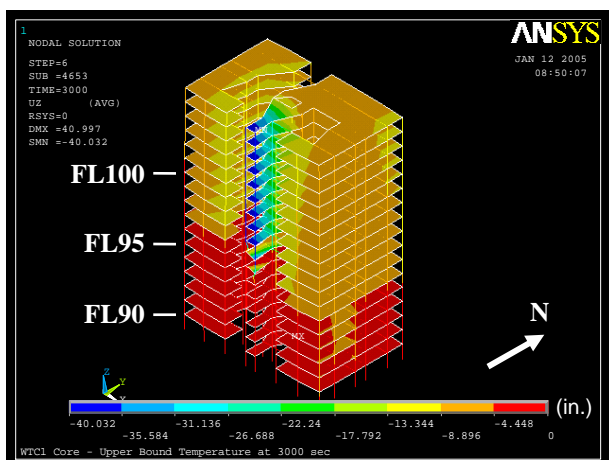


(b) South and east sides

Figure 3–122. Vertical displacement of isolated core model of WTC 1 for Case B temperature condition at 40 min (downward displacement is negative).

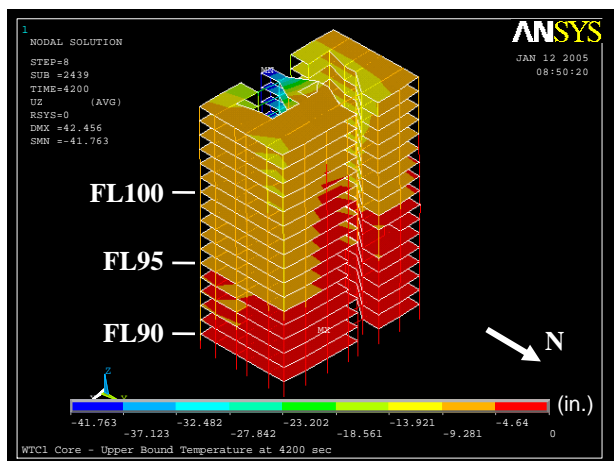


(a) North and east sides

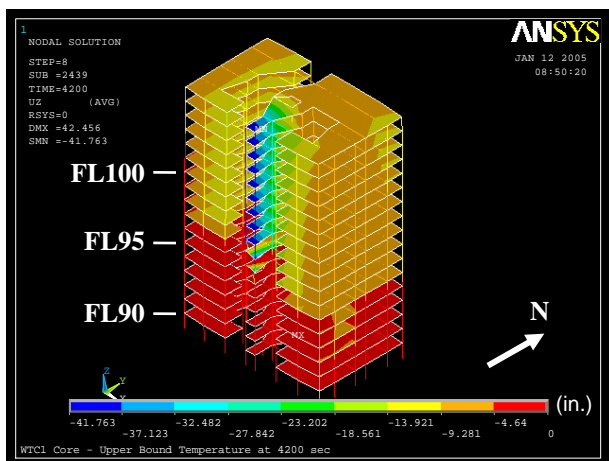


(b) South and east sides

Figure 3–123. Vertical displacement of isolated core model of WTC 1 for Case B temperature condition at 50 min (downward displacement is negative).

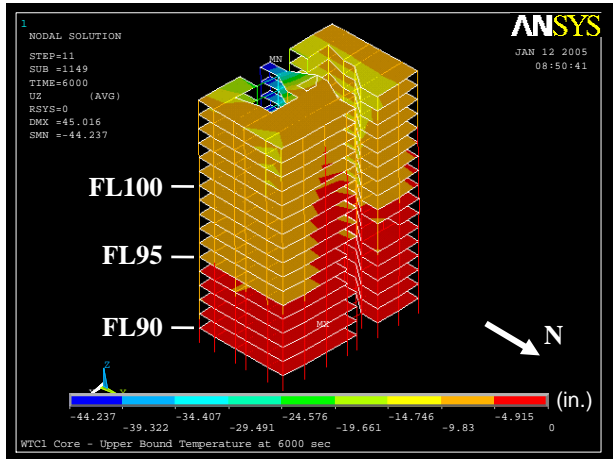


(a) North and east sides

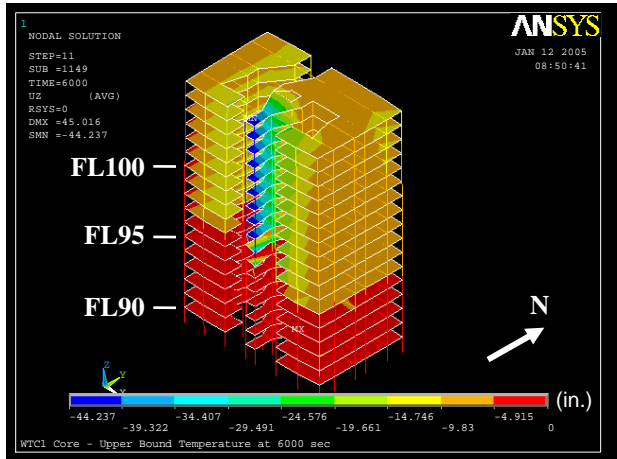


(b) South and east sides

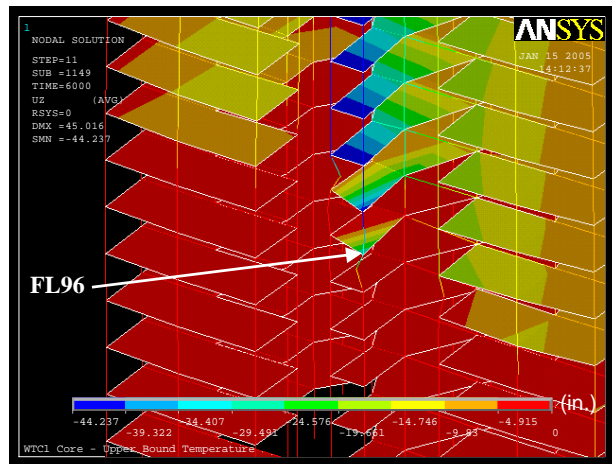
Figure 3–124. Vertical displacement of isolated core model of WTC 1 for Case B temperature condition at 70 min (downward displacement is negative).



(a) North and east sides

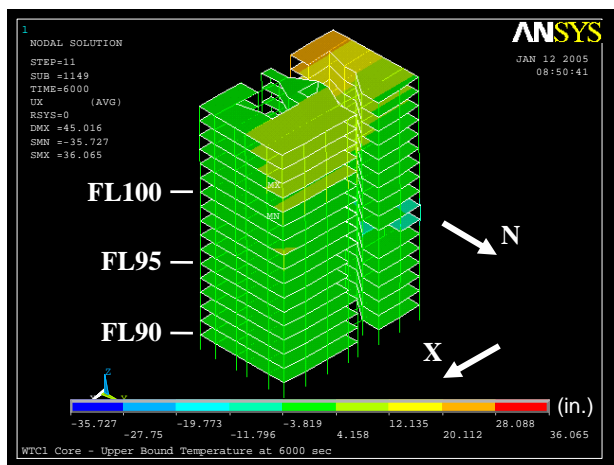


(b) South and east sides

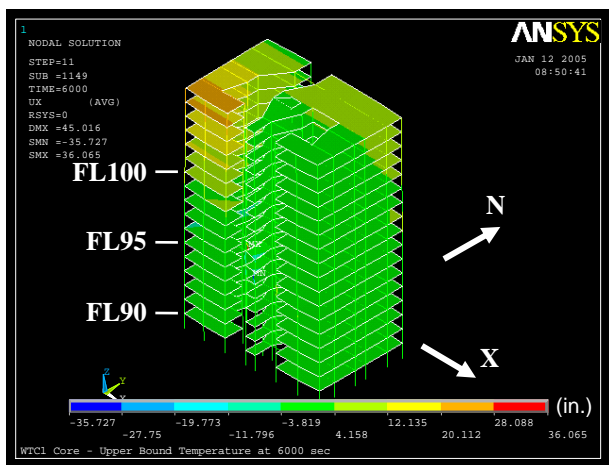


(c) South side
(1X displacement magnification)

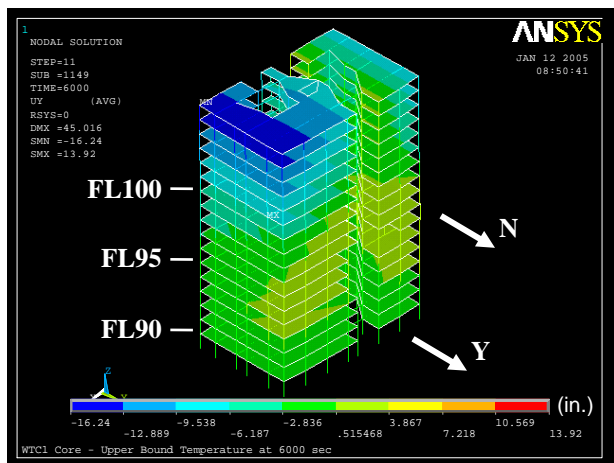
Figure 3–125. Vertical displacement of isolated core model of WTC 1 for Case B temperature condition at 100 min (downward displacement is negative).



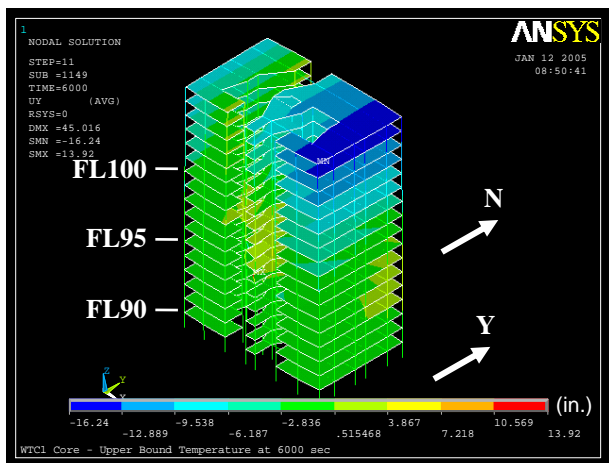
(a) X-displacement of north and east sides



(b) X-displacement of south and east sides

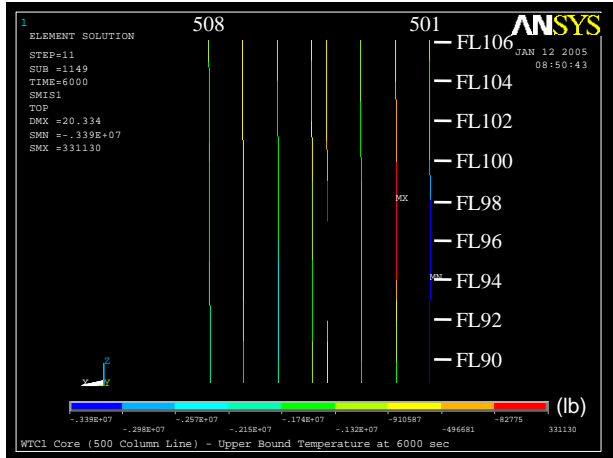


(c) Y-displacement of north and east sides

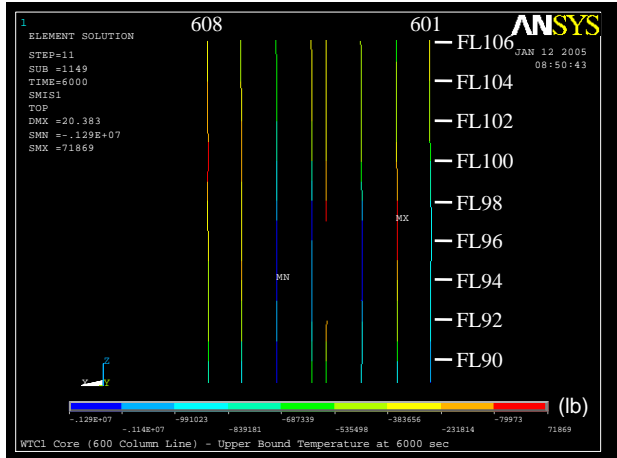


(d) Y-displacement of south and east sides

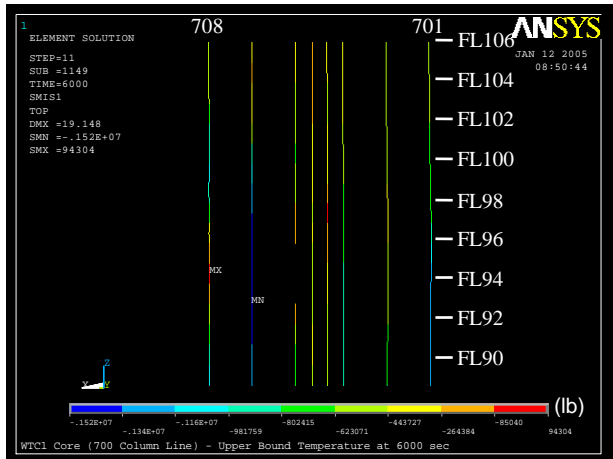
Figure 3–126. Horizontal displacement of isolated core model of WTC 1 for Case B temperature condition at 100 min.



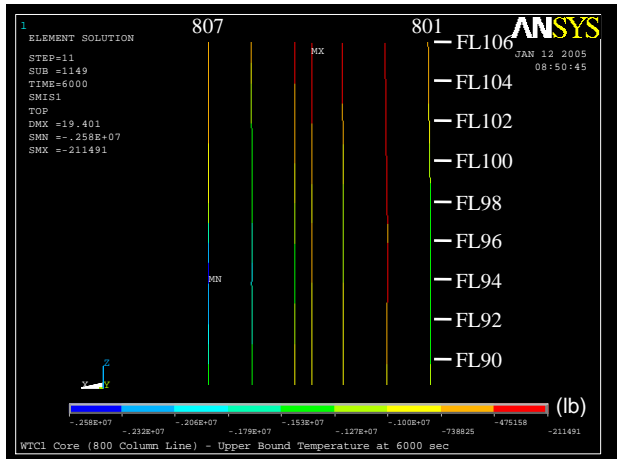
(a) 500 series columns



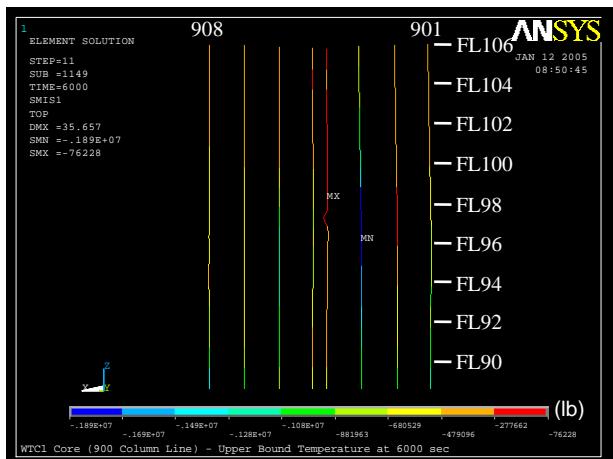
(b) 600 series columns



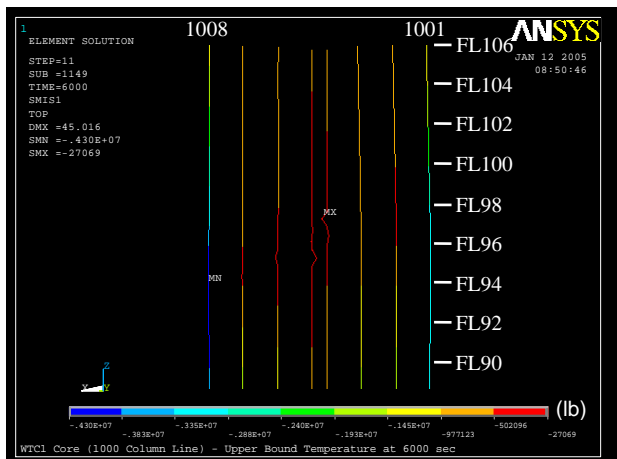
(c) 700 series columns



(d) 800 series columns

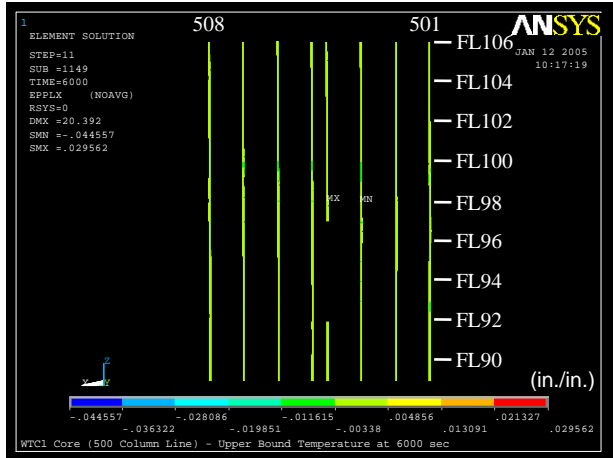


(e) 900 series columns

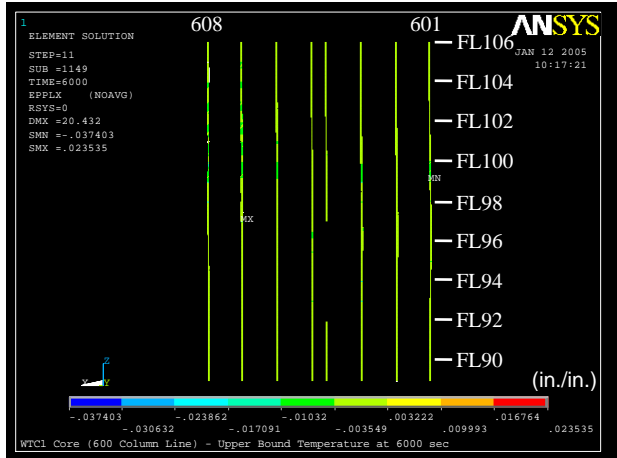


(f) 1000 series columns

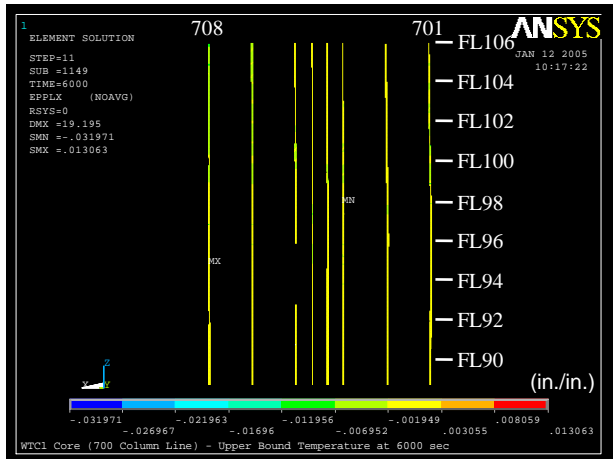
Figure 3–127. Axial load in columns of isolated core model of WTC 1 for Case B temperature condition at 100 min (compression is negative).



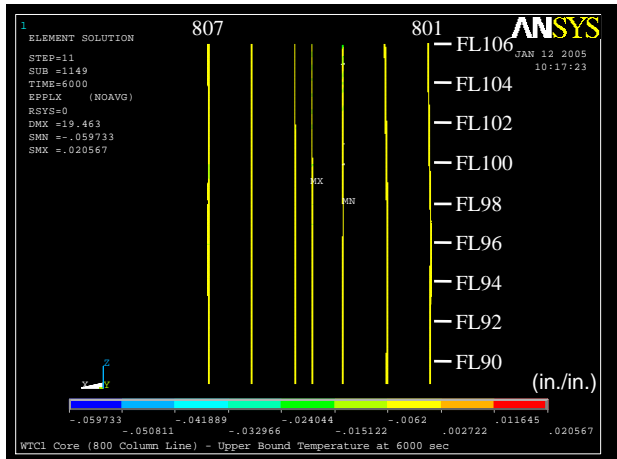
(a) 500 series columns



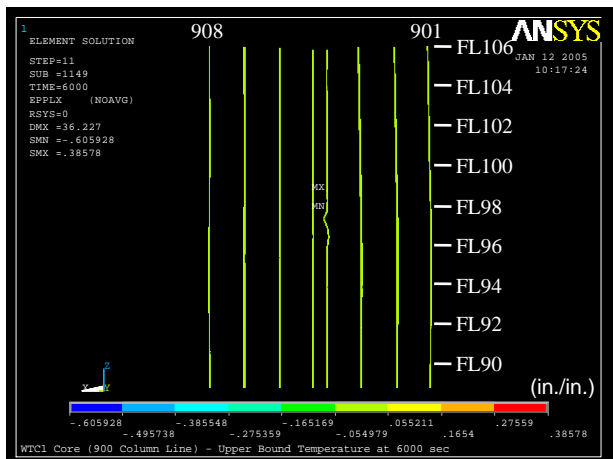
(b) 600 series columns



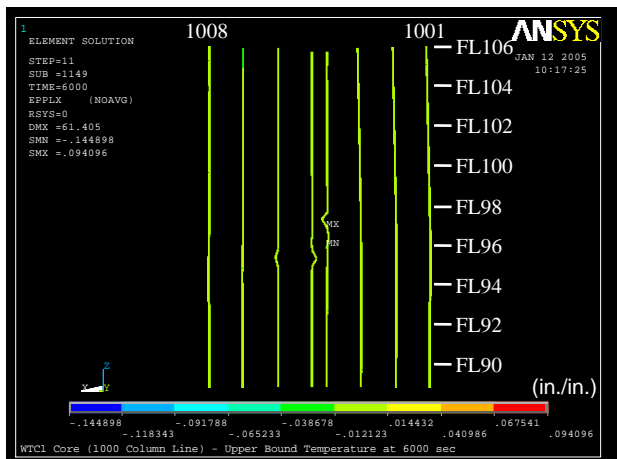
(c) 700 series columns



(d) 800 series columns



(e) 900 series columns



(f) 1000 series columns

Figure 3–128. Plastic strain in columns of isolated core model of WTC 1 for Case B temperature condition at 100 min (compressive strain is negative).

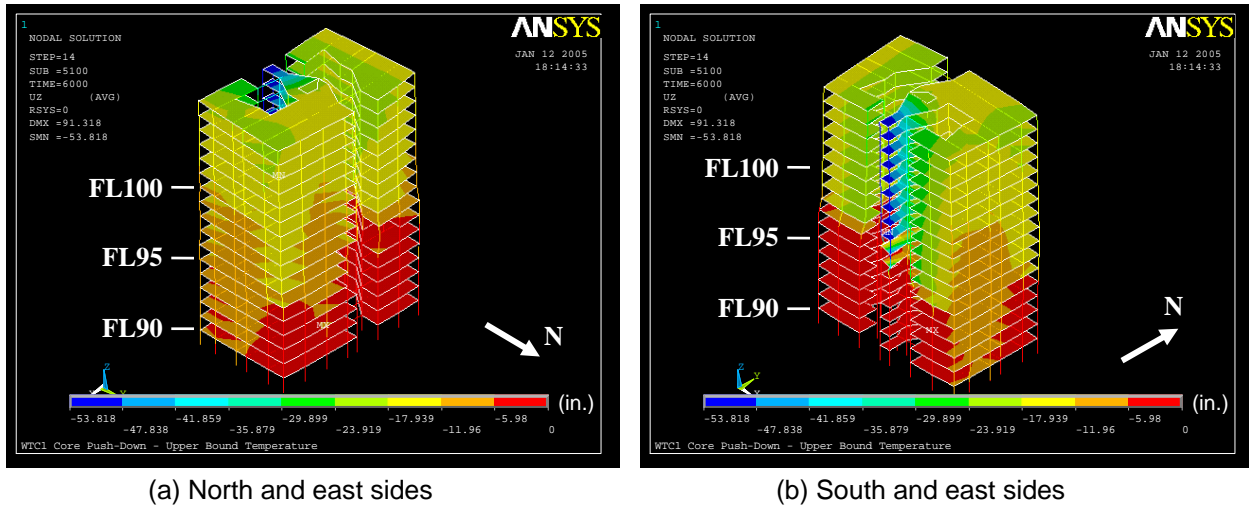


Figure 3–129. Vertical displacement after push down of isolated core model of WTC 1 for Case B temperature condition (downward displacement is negative).

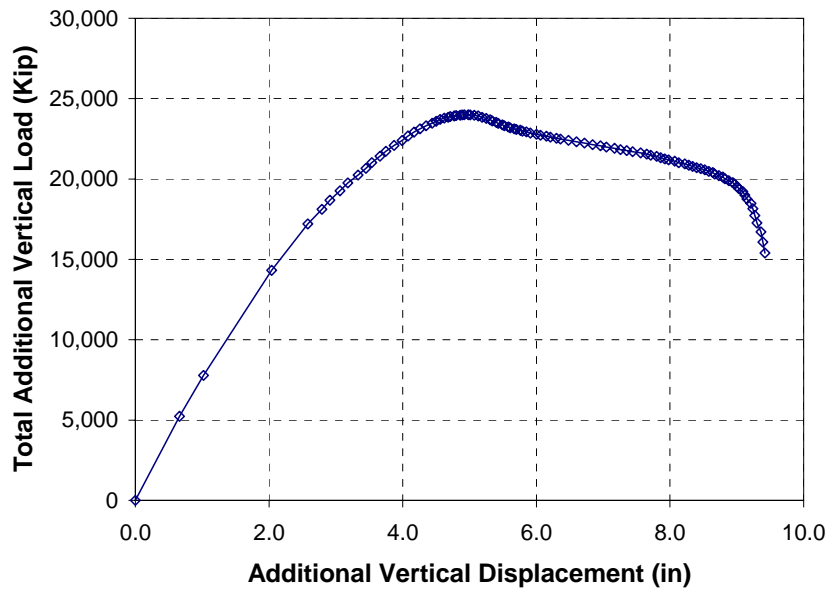


Figure 3–130. Total additional vertical load versus additional vertical displacement relationship obtained from push down analysis of isolated core model of WTC 1 for Case B temperature condition (compression is positive).

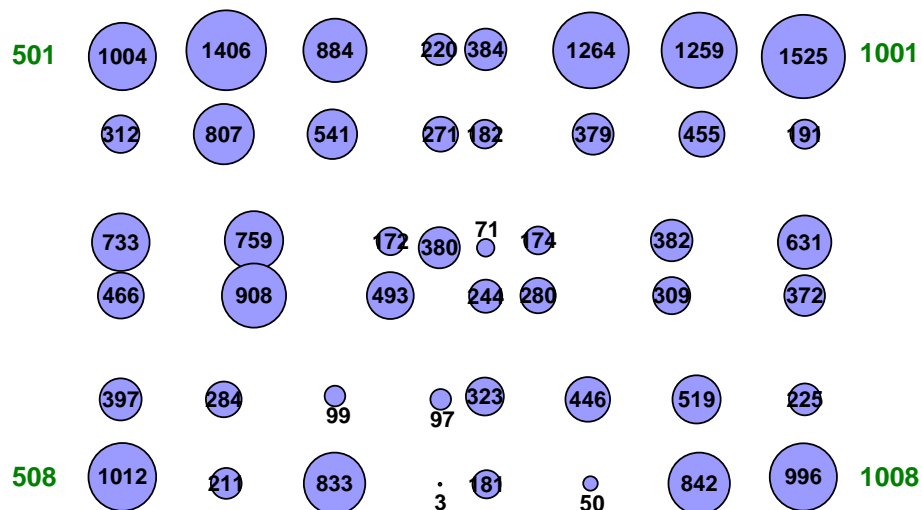


Figure 3–131. Additional axial load (kip) in columns at Floor 98 when the total axial load reached the maximum during push down analysis of the WTC 1 core for Case B temperature condition (compression is positive).

3.3.2 FEA of WTC 2 Core

Case C Temperature Condition

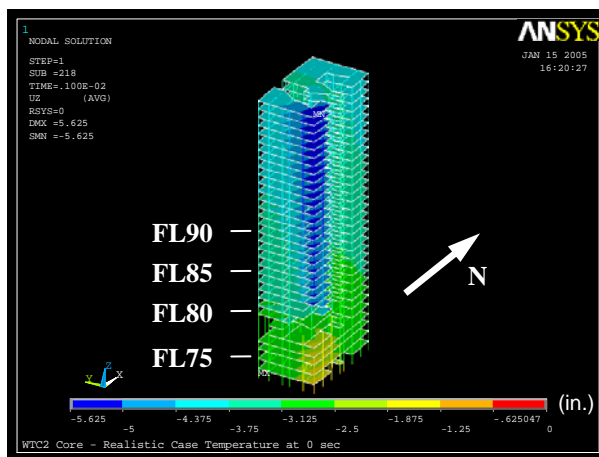
The isolated core model of WTC 2 was unstable after the aircraft impact damage, tilting excessively towards the southeast corner. To simulate the restraining effect of office floors and the exterior walls, the isolated core model was restrained in the horizontal directions at all floors.

Figures 3–132 to 3–133 show the vertical displacements of the WTC 2 isolated core model when subjected to Case C temperature condition from just after the aircraft impact to 60 min. The vertical displacement was always the highest at the southeast corner of the core as the aircraft impact severed the southeast corner core columns in Floors 79 to 82. After aircraft impact damage, the vertical displacement of the southeast corner was 5.6 in. This displacement increased to 6.1 in. at 60 min. Figures 3–134 and 3–135 show axial load and plastic strain in columns at 60 min. Columns at the southeast corner experienced plastic strains immediately following aircraft impact. The maximum plastic strain in the 900-series core columns was 1.2 percent, and 0.5 percent in the 1000 series core.

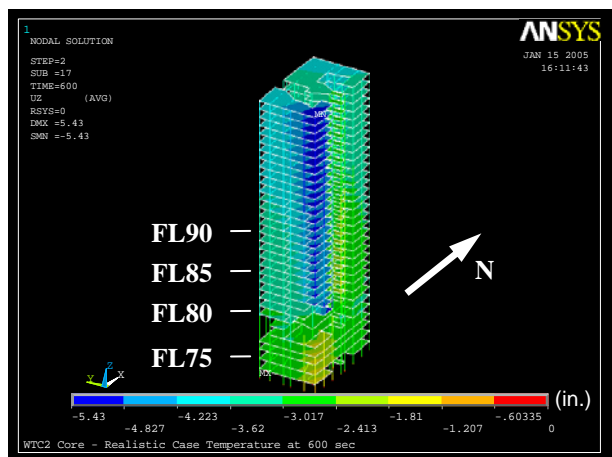
The vertical displacement of the core at Floor 106 at 60 min ranged from 2.3 in. to 5.3 in. The maximum vertical displacement of the southeast corner was less than 5.3 in. at Column 1001. The average vertical displacement of Floor 106 at 60 min was 3.7 in., close to the 3.9 in. average vertical displacement after the aircraft impact. None of core columns buckled during thermal loading.

Similar to the WTC 1 isolated core models, the WTC 2 isolated core model was pushed down following the analysis for Case C temperature condition to determine the additional axial load-carrying capacity of the core. The analysis was terminated at an additional vertical displacement of 17.0 in. even though the core was still continuing to carry more axial load. The vertical displacements at the end of 17.0 in. push-down are shown in Fig. 3–136. Figure 3–137 shows the relationship between the additional

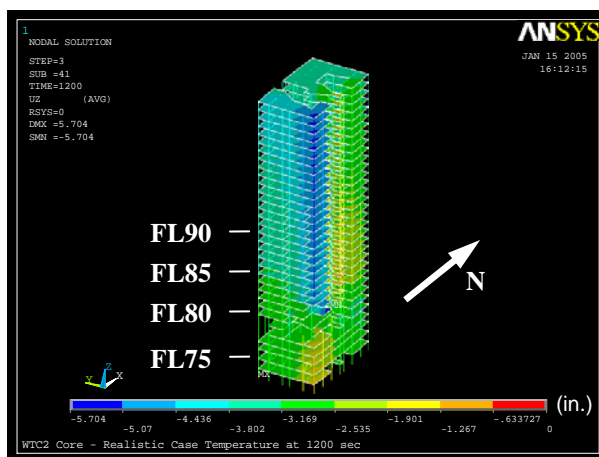
displacements and the average additional vertical load of corner columns, corner and middle columns on the east face, and all core columns (these column locations are shown in Fig. 3-136). The columns on the southeast corner of the isolated core at 60 min temperature condition carried an additional load of about 900 kip without failure, compared to about 1,500 kip for the average of the entire core columns prior to push-down. The additional load was about 1.6 times that of the average load in Floor 82 columns at 60 min temperature condition.



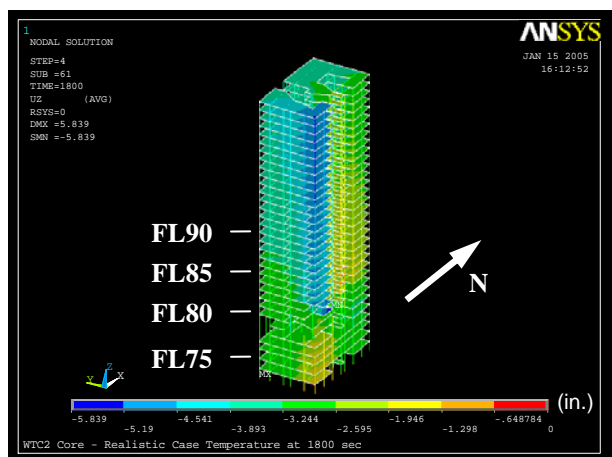
(a) After aircraft impact



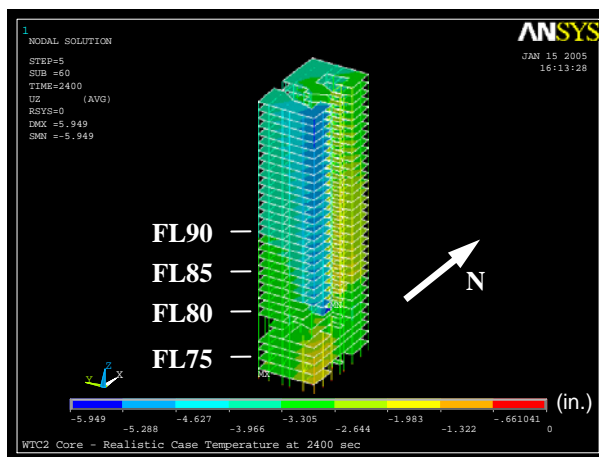
(b) At 10 min



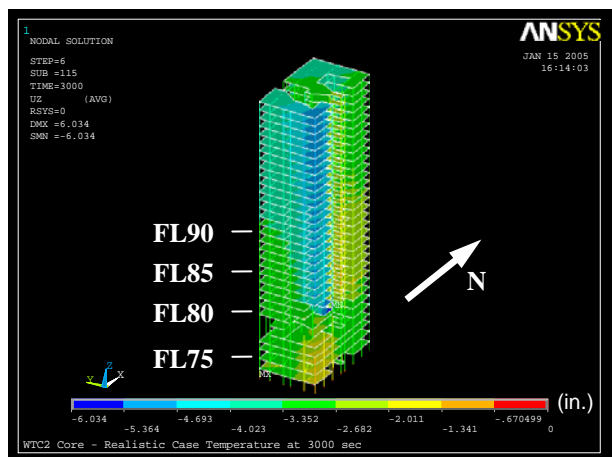
(c) At 20 min



(d) At 30 min



(e) At 40 min



(f) At 50 min

Figure 3–132. Vertical displacement of isolated core model of WTC 2 for Case C temperature condition (downward displacement is negative).

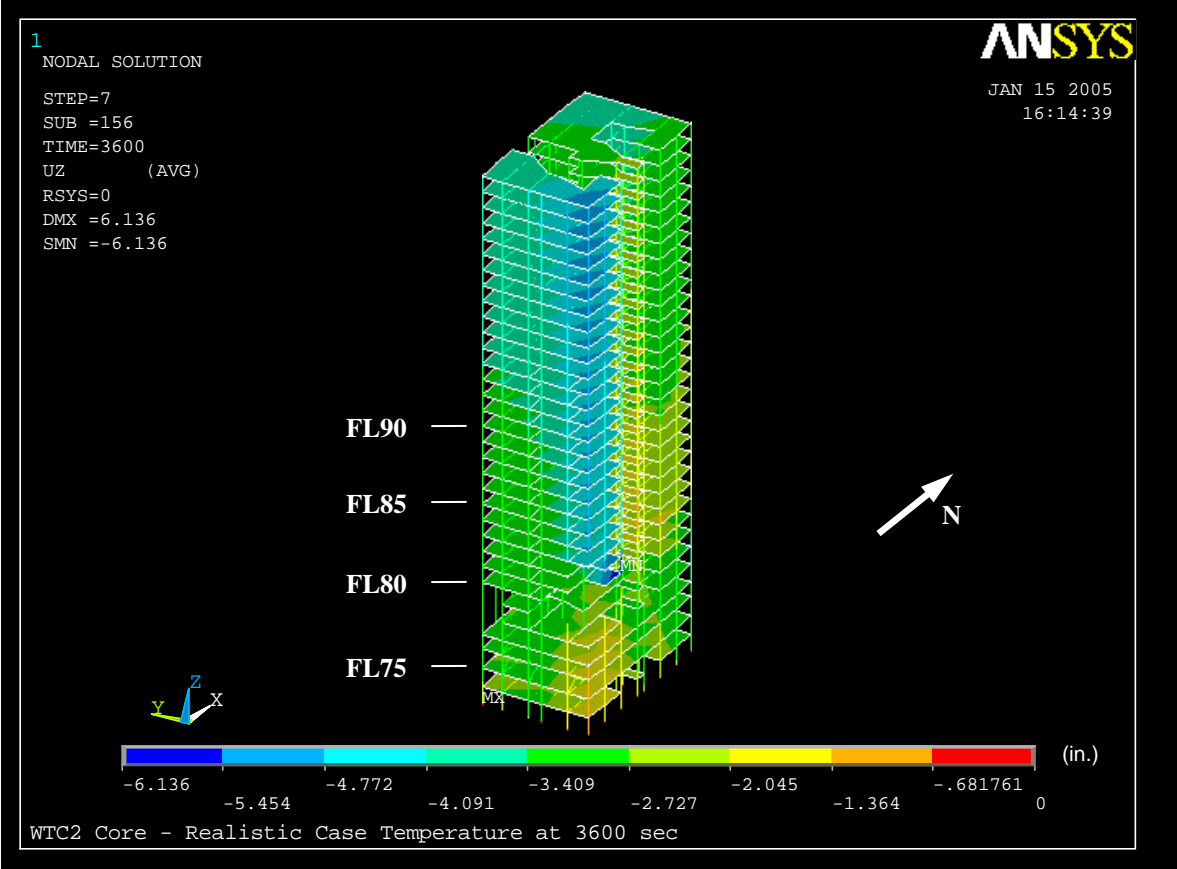
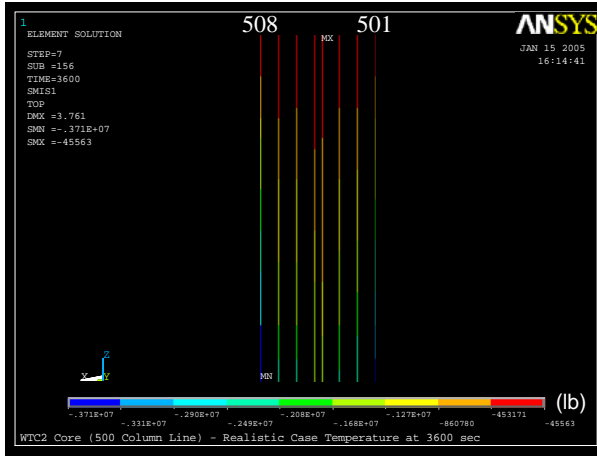
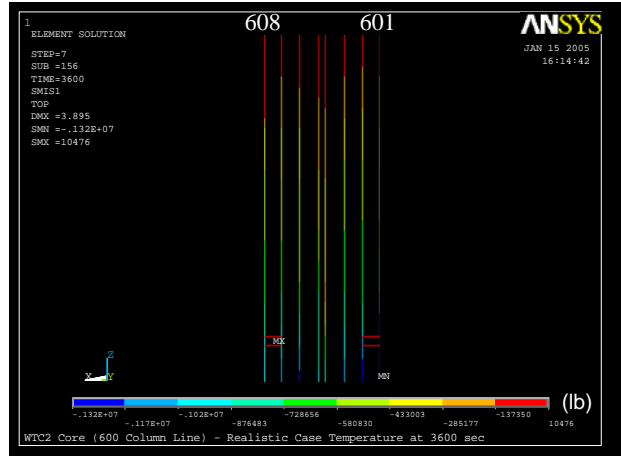


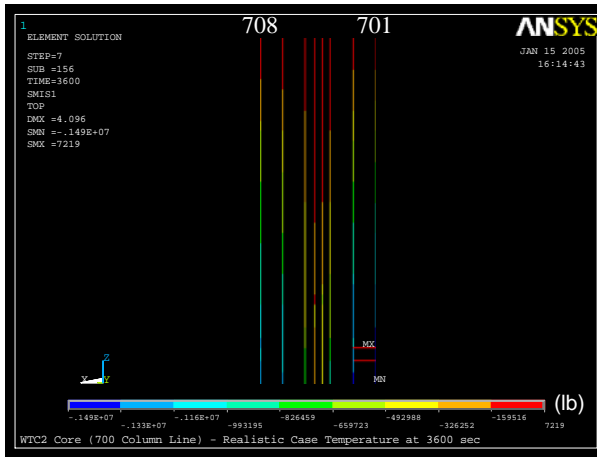
Figure 3-133. Vertical displacement of isolated core model of WTC 2 for Case C temperature condition at 60 min (downward displacement is negative).



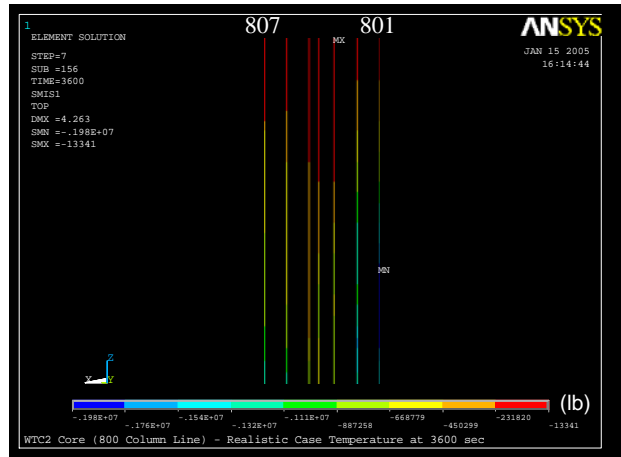
(a) 500 series columns



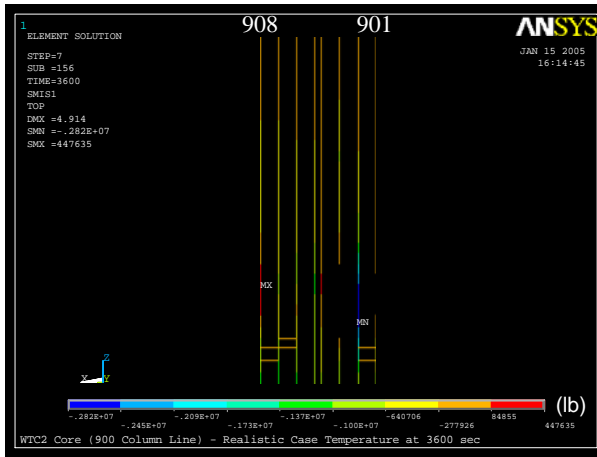
(b) 600 series columns



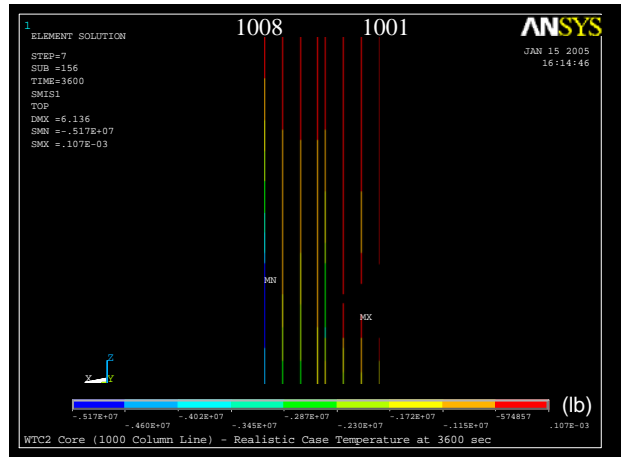
(c) 700 series columns



(d) 800 series columns

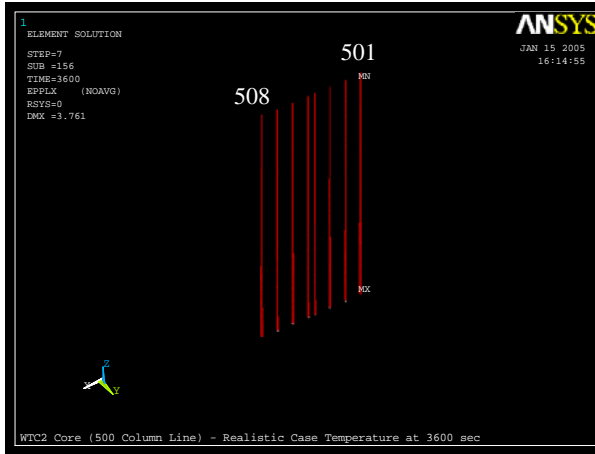


(e) 900 series columns

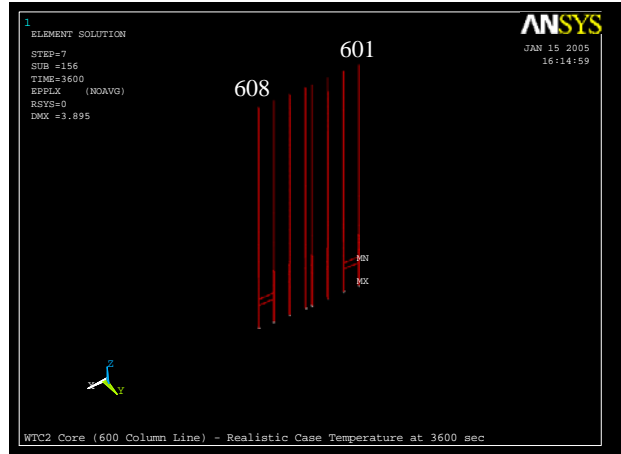


(f) 1000 series columns

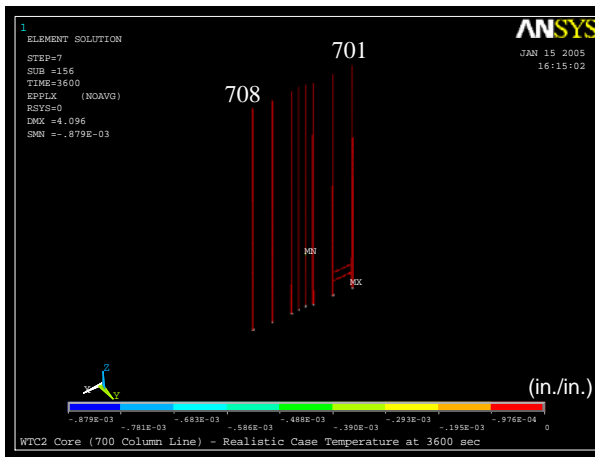
Figure 3–134. Axial load in core columns of isolated core model of WTC 2 for Case C temperature condition at 60 min (compression is negative).



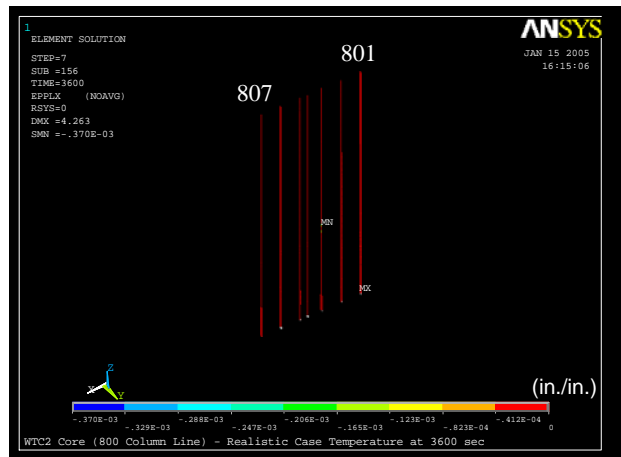
(a) 500 series columns



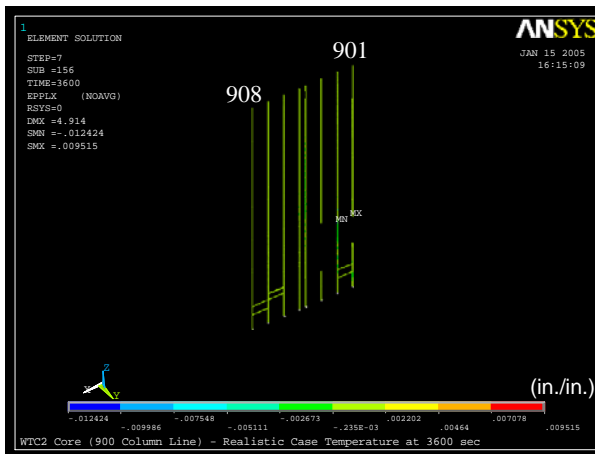
(b) 600 series columns



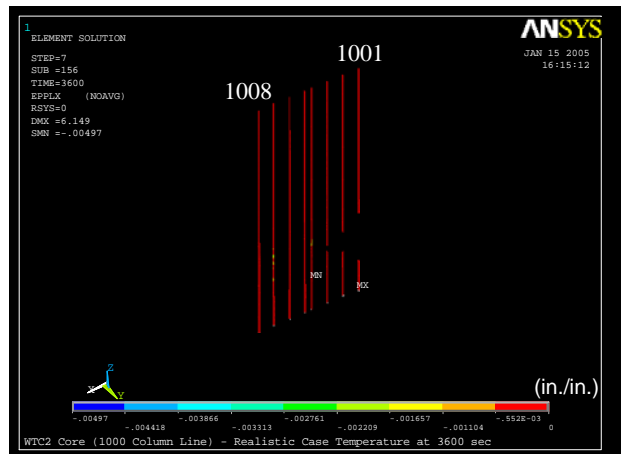
(c) 700 series columns



(d) 800 series columns



(e) 900 series columns



(f) 1000 series columns

Figure 3–135. Axial plastic strains in core columns of isolated core model of WTC 2 for Case C temperature condition at 60 min (compressive strain is negative).

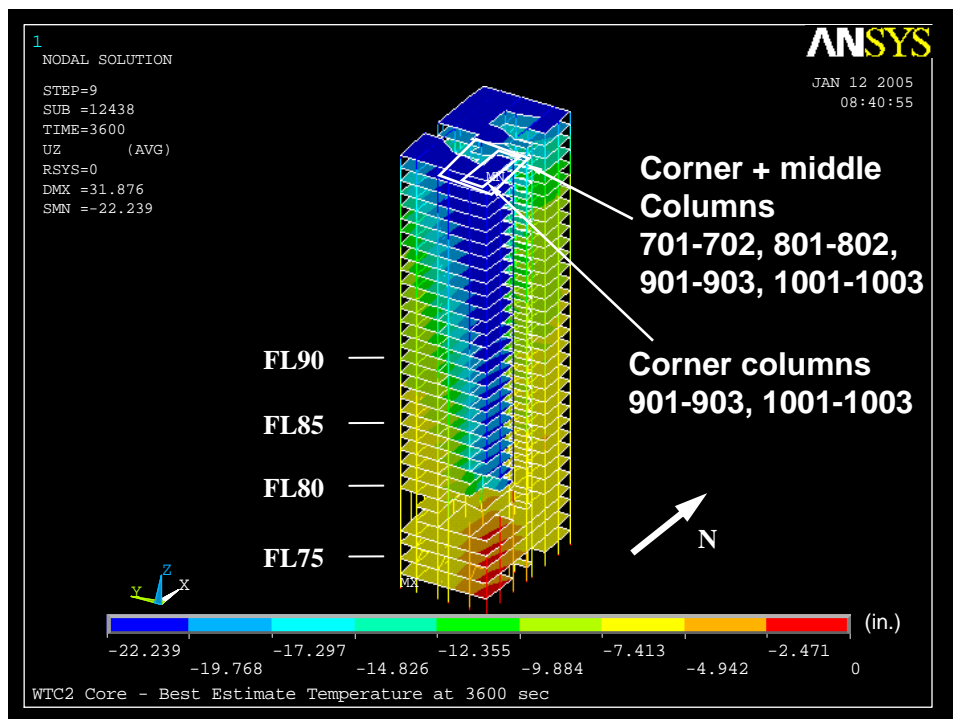


Figure 3–136. Vertical displacement after push down of isolated core model of WTC 2 for Case C temperature condition (downward displacement is negative).

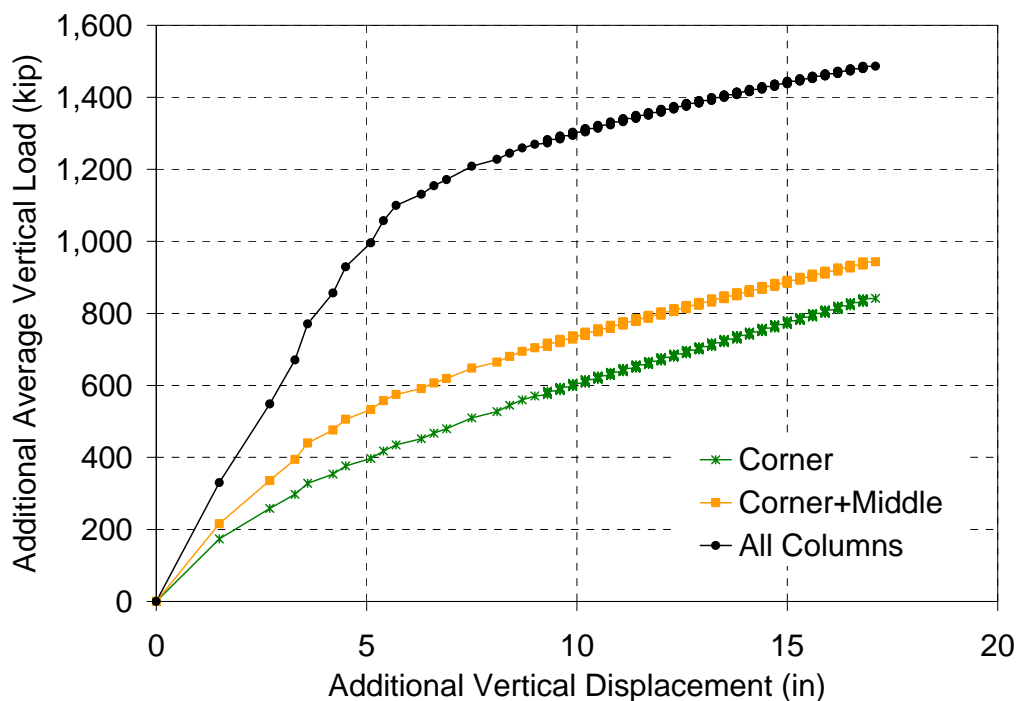


Figure 3–137. Additional average vertical load versus additional vertical displacement during push-down analysis of isolated core model of WTC 2 for Case C temperature condition (compression is positive; core column locations are shown in Fig. 3–136).

Case D Temperature Condition

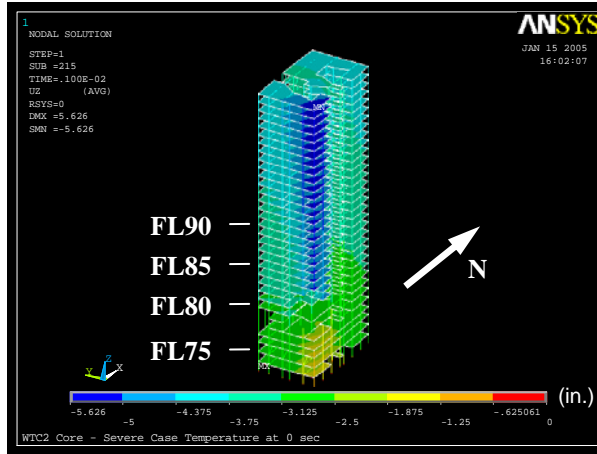
As mentioned in the previous section for Case C temperature condition, the isolated core model of WTC 2 was unstable after the aircraft impact damage, so the model was restrained in the horizontal directions.

Figures 3–138 to 3–139 show the vertical displacements of the WTC 2 isolated core model subjected to Case D temperature condition from just after the aircraft impact to 60 min. The vertical displacement was always the highest at the southeast corner of the core as the aircraft impact severed the southeast corner core columns in Floors 79 to 82. After aircraft impact damage, the vertical displacement of the southeast corner was 5.6 in. This displacement increased to 8.2 in. at 60 min. Figures 3–140 and 3–141 show axial load and plastic strain in columns at 60 min. Columns at the southeast corner experienced plastic strains immediately following aircraft impact. The maximum plastic strain in the 900-series core columns was 2.5 percent, and 0.7 percent in the 1000 series core columns.

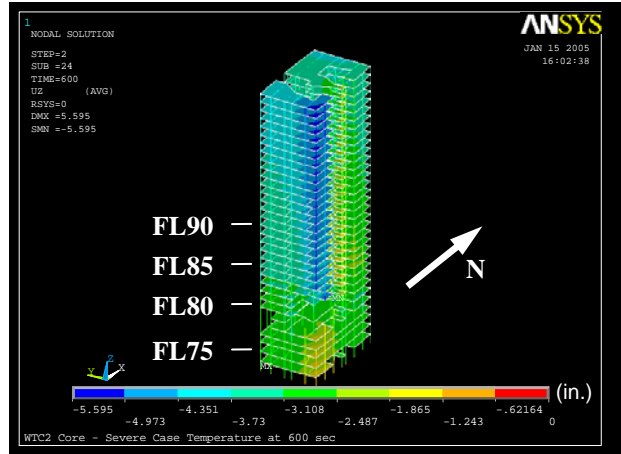
The vertical displacement of the core at Floor 106 at 60 min ranged from 3.3 in. to 6.0 in. The maximum vertical displacement of the southeast corner was less than 6.0 in. at Column 1001. The average vertical displacement of Floor 106 after thermal loading at 60 min was 4.1 in., similar to the 3.9 in. average vertical displacement after the aircraft impact. None of core columns buckled during thermal loading.

To determine the additional axial load-carrying capacity of the core, the isolated core model was pushed down following the analysis for Case D temperature condition as described before. The top of the isolated core was pushed down an additional 30.0 in. The analysis was stopped even though the core was continued to carry additional load. The vertical displacement at the end of 30.0 in. push-down is shown in Fig. 3–142. Figure 3–143 shows the relationship between the additional vertical displacement and the average additional vertical load on core columns, the corner columns, and the corner and middle columns shown in Fig. 3–143. As it can be seen from Fig. 3–143 at 60 min temperature condition, the columns on the southeast corner of the isolated core continued to carry, on the average, an additional load of about 1,200 kip without failure, compared to about 1,700 kip for the average of the entire core columns prior to push down. The additional load on the core columns was about 1.8 times that of the average load in Floor 82 columns at 60 min temperature condition.

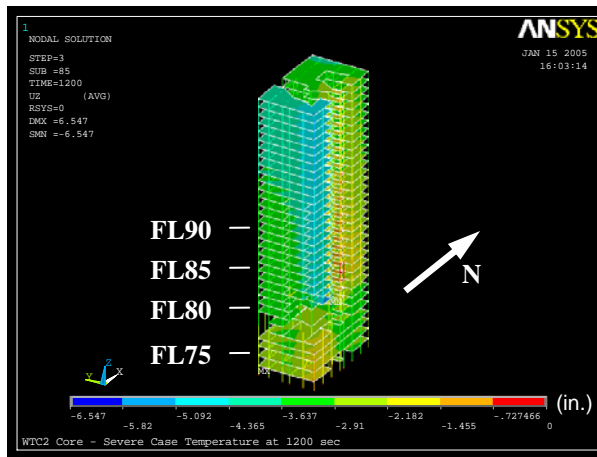
The results of the isolated core models of WTC 2 show that significant downward displacement of the core and core column buckling are not likely to occur for WTC 2 during the global analysis.



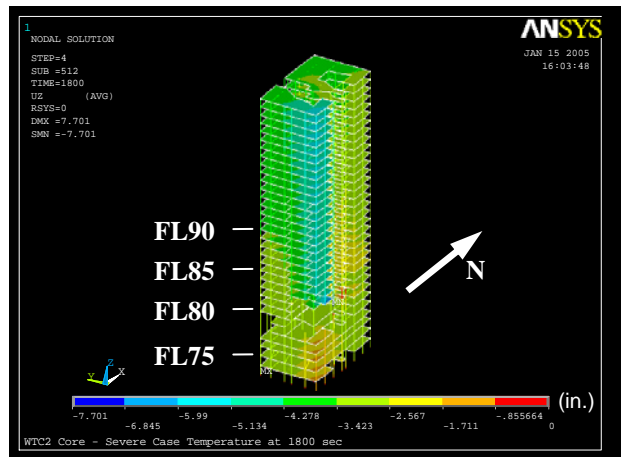
(a) After aircraft impact



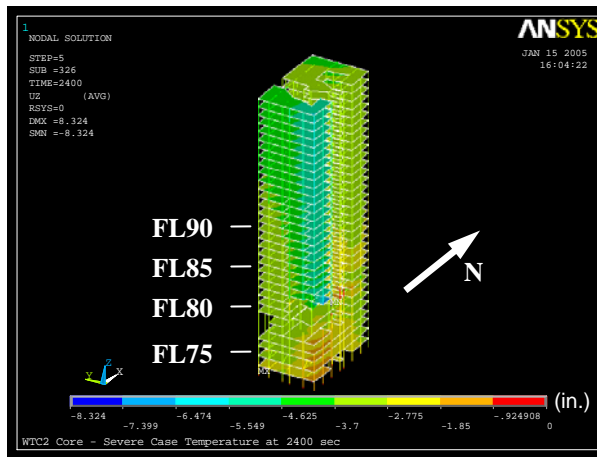
(b) At 10 min



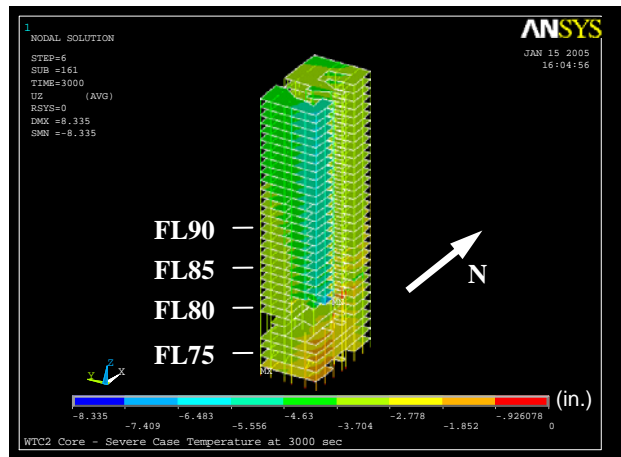
(c) At 20 min



(d) At 30 min



(e) At 40 min



(f) At 50 min

Figure 3–138. Vertical displacement of isolated core model of WTC 2 for Case D temperature condition (downward displacement is negative).

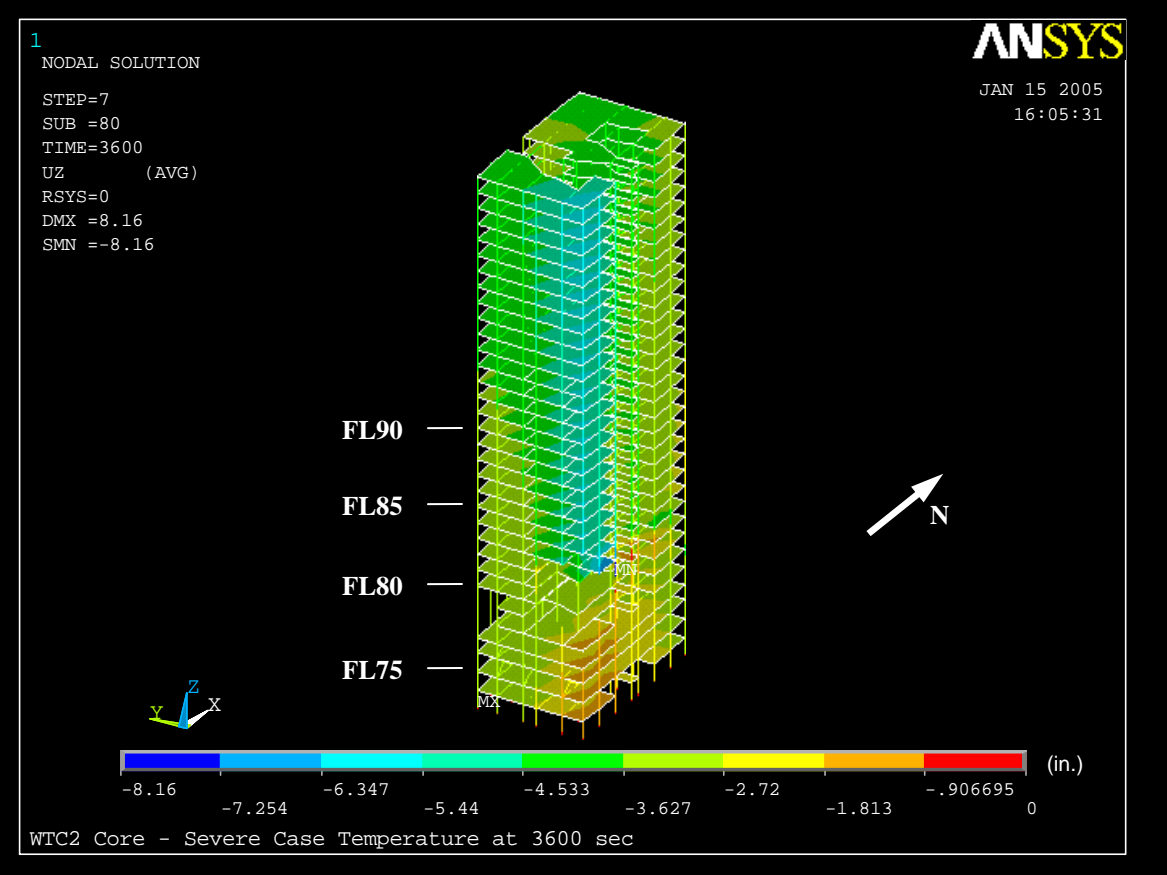
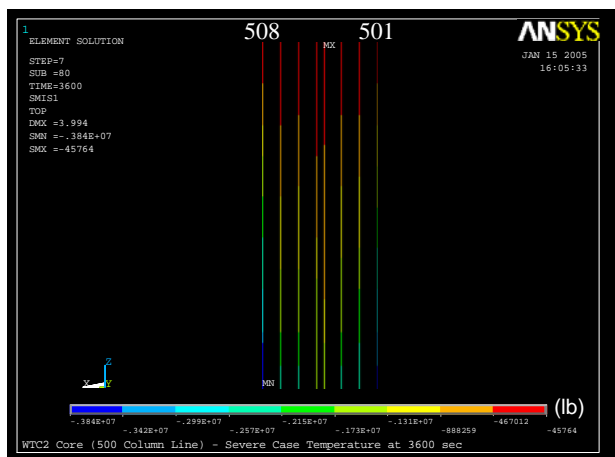
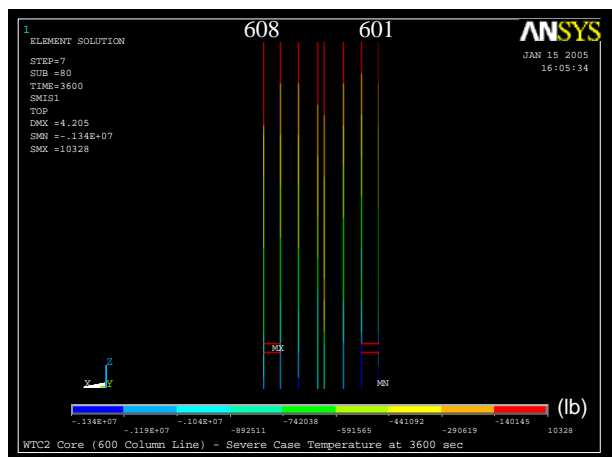


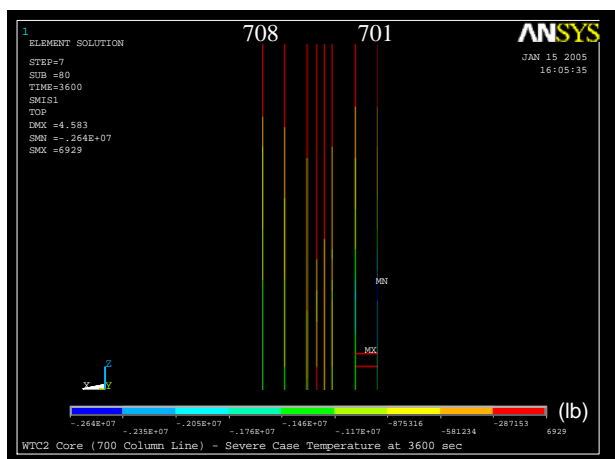
Figure 3-139. Vertical displacement of isolated core model of WTC 2 for Case D temperature condition at 60 min (downward displacement is negative).



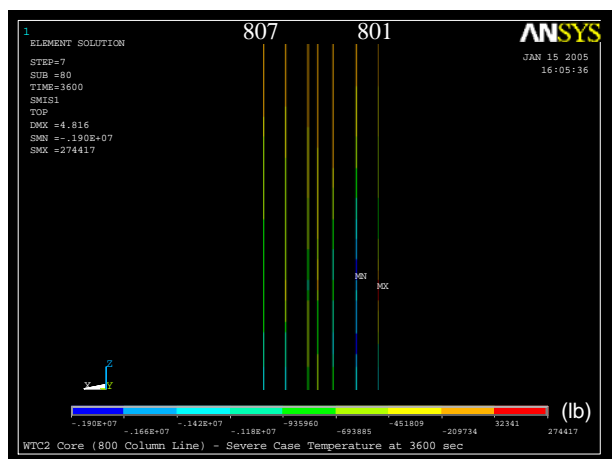
(a) 500 series columns



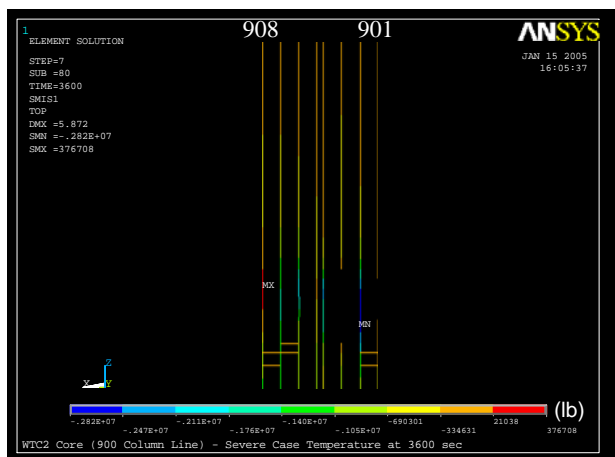
(b) 600 series columns



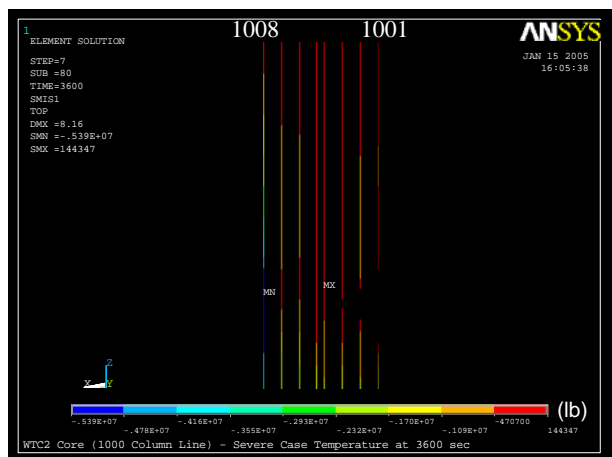
(c) 700 series columns



(d) 800 series columns

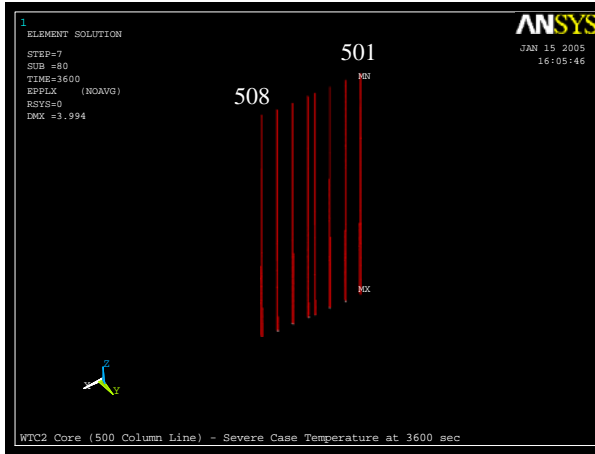


(e) 900 series columns

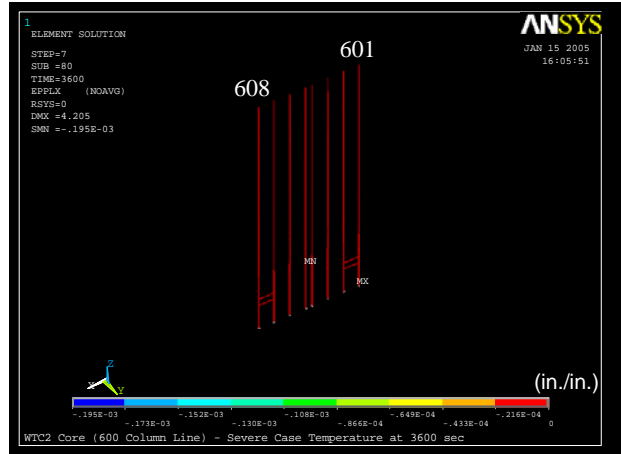


(f) 1000 series columns

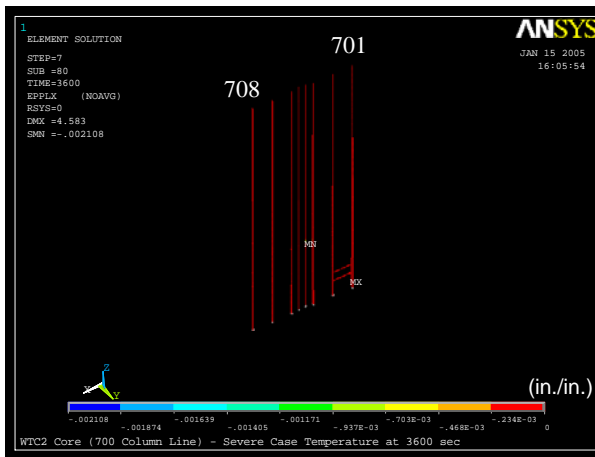
Figure 3–140. Axial load in core columns of isolated core model of WTC 2 for Case D temperature condition at 60 min (compression is negative).



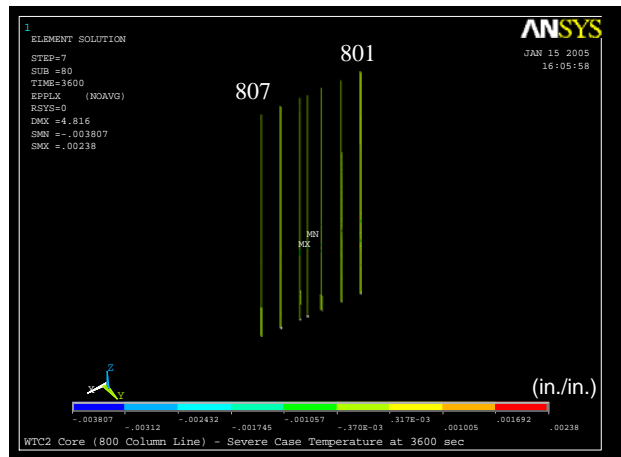
(a) 500 series columns



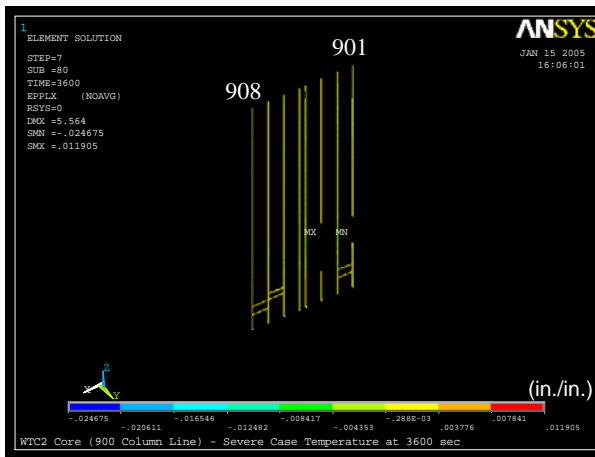
(b) 600 series columns



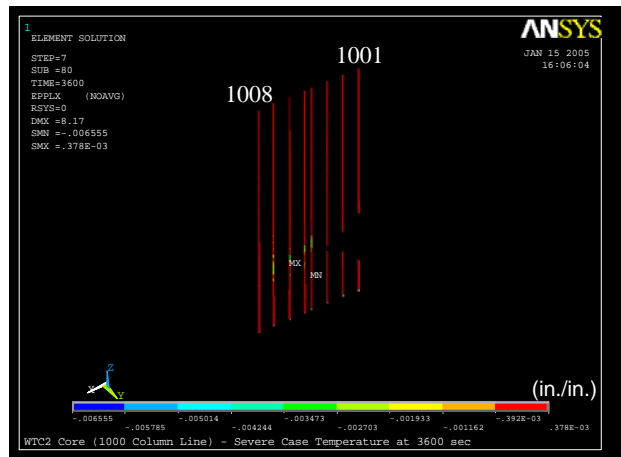
(c) 700 series columns



(d) 800 series columns



(e) 900 series columns



(f) 1000 series columns

Figure 3–141. Axial plastic strains in core columns of isolated core model of WTC 2 for Case D temperature condition at 60 min (compressive strain is negative).

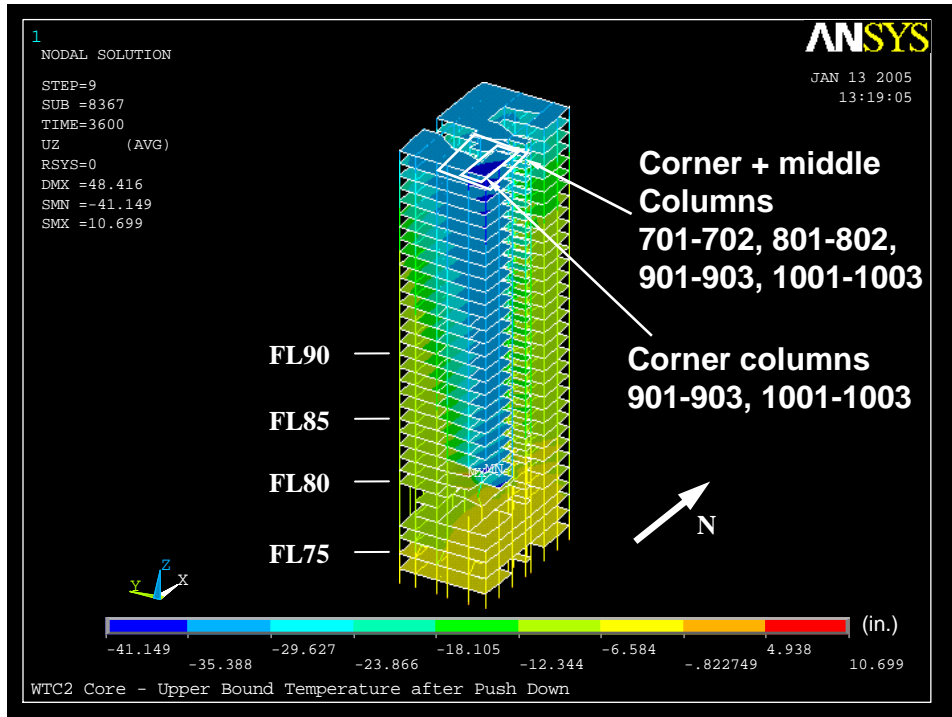


Figure 3–142. Vertical displacement after push down of isolated core model of WTC 2 for Case D temperature condition (downward displacement is negative).

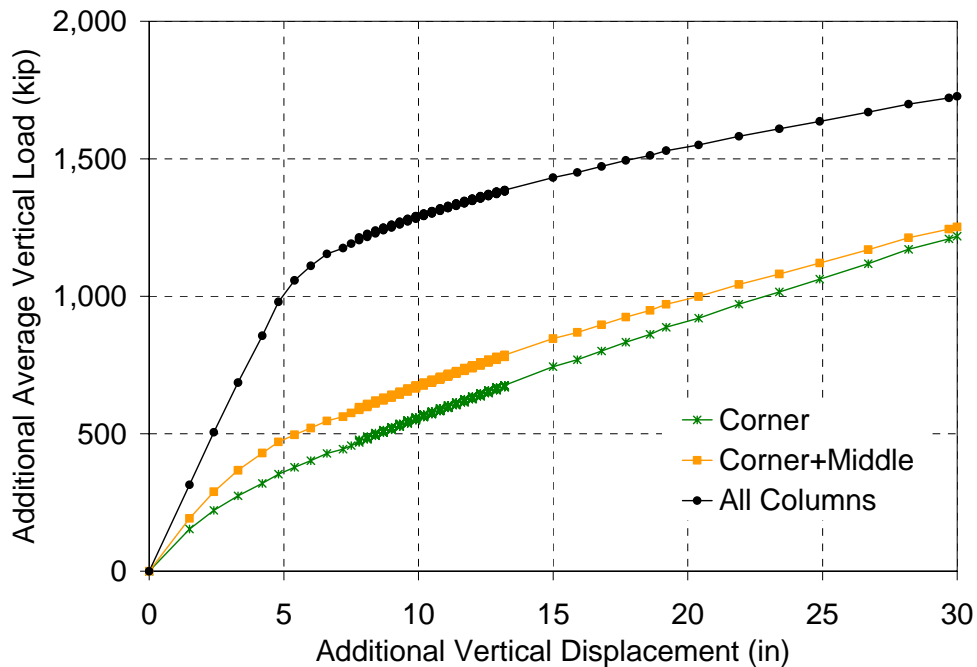


Figure 3–143. Additional average vertical load versus additional vertical displacement during push-down analysis of isolated core model of WTC 2 for Case D temperature condition. (compression is positive; core column locations are indicated in Fig. 3–142.)

Chapter 4

GLOBAL ANALYSIS

4.1 CONVERSION FROM SAP2000 TO ANSYS

Simpson, Gumpertz & Heger, Inc. (SGH) performed global analysis of the WTC 1 and WTC 2 towers using global models of the two towers developed in ANSYS as described in Chapter 2. The models were subjected to the aircraft impact damage and the temperature time histories resulting from the ensuing fire environments. The global models described in this report, and the reference models in NIST NCSTAR 1-2A, used the same coordinate system. As illustrated in Fig. 4–1, the z-axis in this coordinate system is parallel to the vertical axis of the building, the x axis is parallel to the long direction of the building's central core, and the y-axis is parallel to the short direction of the central core. In the WTC 1 models, the origin of the coordinate system is located at the southeast corner of the building with the y-axis extending to the north. In the WTC 2 models, the origin is located at the northeast corner of the building with the y-axis extending west.

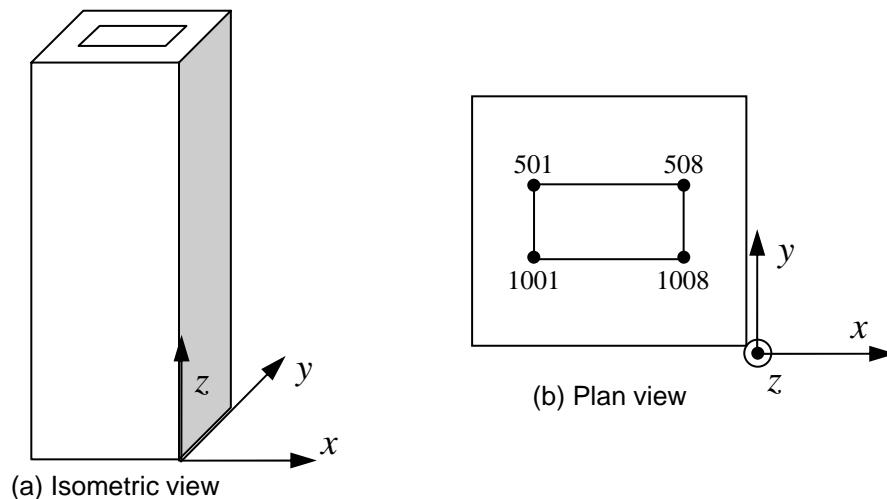


Figure 4–1. Coordinate system used in the analysis models.

The SAP2000 global models in NIST NCSTAR 1-2A were linearly elastic and included interior and exterior columns, spandrels, hat truss members, and floor slabs at mechanical floors. Only the mechanical floors were individually modeled. The other floor slabs were modeled using a set of coupling equations in the software to slave the displacement of certain nodes to the displacement of other nodes. In this case, these coupling equations provided full rigidity within the plane of the floor slabs (the x-y plane) and full flexibility out of this plane.

As most of the structural action that led to the collapse of the buildings took place within and above the aircraft-impacted floors, the reference models were truncated for each building below the lowest damaged floors. The model of WTC 1 was truncated at Floor 89, five floors below the zone of impact, and a series of equivalent vertical linear springs were introduced at the base of this truncated model to represent the

stiffness of the interior columns and exterior walls beneath the level of truncation. Similarly, the model of WTC 2 was truncated at Floor 73.

The truncated SAP2000 models were converted to ANSYS and modified to capture the failure modes of floors and columns and to enhance numerical efficiency. The global models included geometric and temperature-dependent material nonlinearities, including creep.

4.1.1 ANSYS Models

The ANSYS models were the direct translation of the truncated SAP2000 models. During the translation of the models, the coordinates of the nodes, cross sectional properties of members, including orientation and offset of the cross sections, nodal loads, material properties, and member end releases were automatically converted from each SAP2000 database into an ANSYS database. Table 4–1 summarizes the conversion used in translating the element types between SAP2000 and ANSYS. Comparison of the results obtained for the gravity analysis of WTC 1 and WTC 2 from the SAP2000 models and translated ANSYS models are discussed in the next section.

Table 4–1 summarizes the correspondence between element types contained in the SAP2000 model and those in the converted ANSYS model. Table 2–1 previously presented a description of the various ANSYS elements used in the global models. Gravity load analyses of the two buildings were then performed using both the truncated SAP2000 and converted ANSYS models to verify the fidelity of the conversion.

Table 4–1. Conversion from SAP2000 element types to ANSYS element types.

SAP2000 Element Types	ANSYS Element Types
Frame/Cable elements	BEAM188/189 later changed to BEAM24
Shell elements	SHELL63 later changed to SHELL181
Springs	LINK8

Following these analyses, the linear, elastic material properties of the converted ANSYS models were replaced with temperature-dependent inelastic material properties as defined for all material types in Chapter 3 of NIST NCSTAR 1-6C. These material types were assigned to the elements according to their material and cross sectional properties and their locations in the buildings. In the SAP2000 global model, each cross section was assigned a yield value representing the material capacity for that cross section. During the translation to ANSYS, a different name was given to each cross section and material combination, which resulted in a unique material index. Using this material index, the material properties of all elements were replaced with temperature-dependent inelastic material properties. In the actual buildings, the rectangular tube columns in the exterior wall were typically fabricated from four plates, Plate 1 (see Chapter 6 of NIST NCSTAR 1-6C for more information) and could have a different specified yield strength than the rest (Plates 2 and 3). Examination of drawings in the region of interest showed that all these plates had the same yield strength. Therefore, in the translation process, all plates in the same column cross section were considered to be of the same material.

The ANSYS models were also modified to include representation of the floor slabs, which except at mechanical floors, were not included in the SAP2000 models. Floor elements added into the ANSYS model included the core slabs, those core beams that were framed with moment connections at their ends,

and the office area slabs. Figure 4–2 shows the analytical representation of the core and office area floors and the core beams included in the models. Beams in the core that were framed without moment connections were not included in the model because they cannot transfer shear between columns without significant relative displacement. However, their axial stiffness was combined with in-plane stiffness of the floor slab, and then shell elements with this composite in-plane stiffness were used to model the floor.

An equivalent concrete thickness and modulus was calculated for the office area floors to match the in-plane stiffness of the composite floor system which included the concrete slab, the floor trusses, and the floor seats. The thickness of the core slab was taken from the PANYNJ drawings, but the elastic modulus was adjusted to match the in-plane stiffness of the composite floor that included the steel beams and the concrete slab. Both core and office area floor slabs were modeled with linear-elastic material properties for lightweight concrete. Later analyses with these models indicated that these slabs, composite with their framing members, could redistribute load locally amongst neighboring columns and transfer lateral loads to the exterior walls as collapse initiated and WTC 2 began to tilt.

Floors in the global models also provided diaphragm stiffness at each level. However, the floors were not modeled with sufficient detail to capture such floor behaviors under elevated temperatures as sagging and failure of floor-wall connections. Instead, these effects were incorporated into the global analyses as fire-induced damage, as described in Section 2.5.

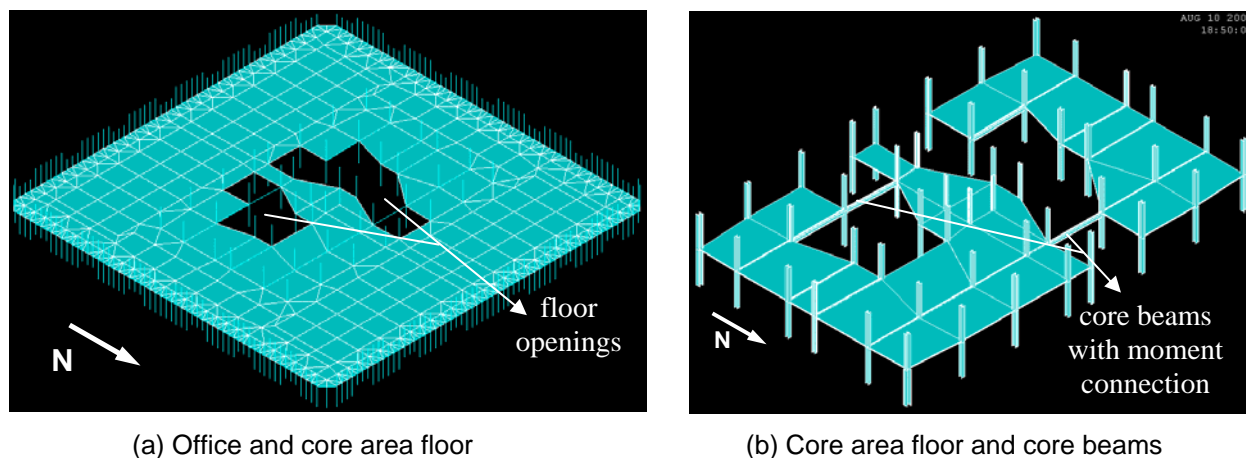


Figure 4–2. Office and core area floors and core beams.

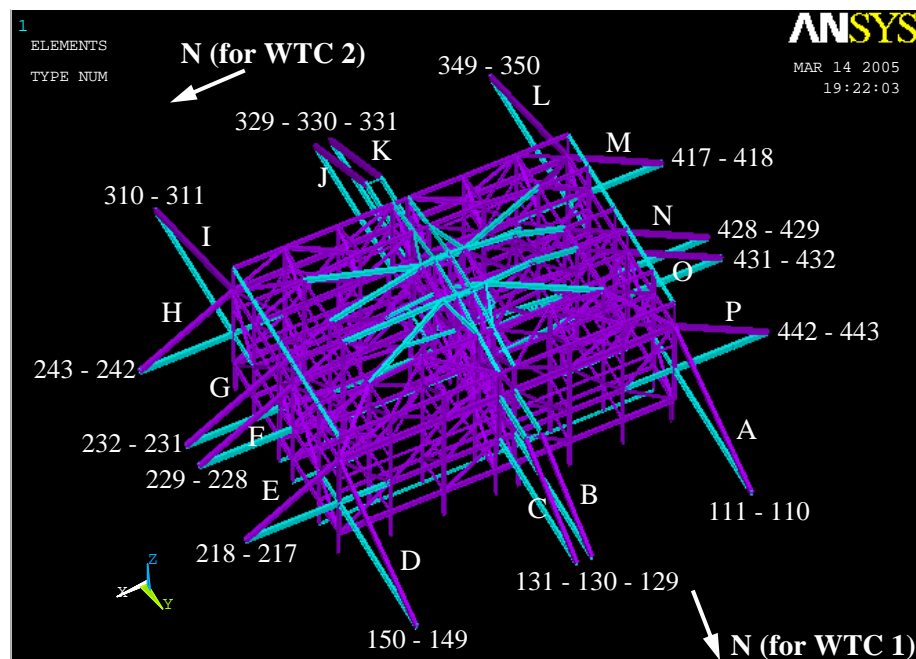


Figure 4–3. Location and IDs of outriggers and supporting columns.

Due to the limitations of the BEAM188 element used to model spandrels, columns, and truss members, a set of preliminary global analyses were conducted without including creep and inelastic buckling in the core and exterior wall columns, as discussed in Appendix C of this report. Plasticity and large deflection were the only nonlinearities included in those analyses. Later, the BEAM188 element was replaced with the BEAM24 element to eliminate the limitations on creep and inelastic buckling. As shown in the global analyses that included consideration of creep and buckling, described in Section 4.2, creep strains and inelastic column buckling played a very significant role in the collapse of the towers.

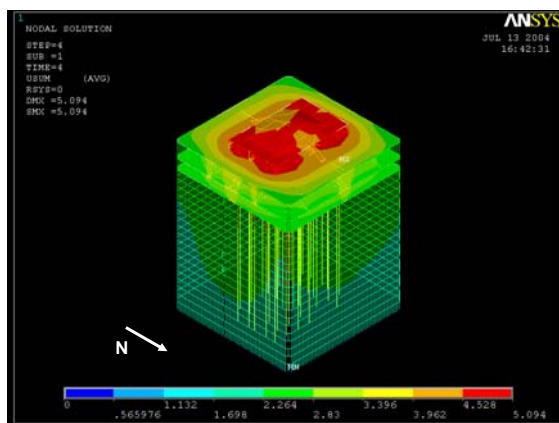
Figure 4–3 shows the hat trusses in the global models. The hat trusses connected the exterior walls and the core columns. As seen in the figure, four outrigger members on each face of the core extended outward from the core to the exterior walls. Hat truss members were provided with plasticity in the preliminary global models without creep and in the final WTC 1 global model with creep. The hat truss of the WTC 2 global model with creep was part of the “superstructure” where elastic properties were used. Further discussion of this is presented in Section 4.2.2. The hat trusses were not modeled with sufficient detail to capture the onset of buckling. However, the yield strength of the outrigger elements in the final WTC 1 model was set so that compressive yielding would occur when axial load reached the compressive capacity of the members.

4.1.2 Validation of Translated ANSYS Global Models

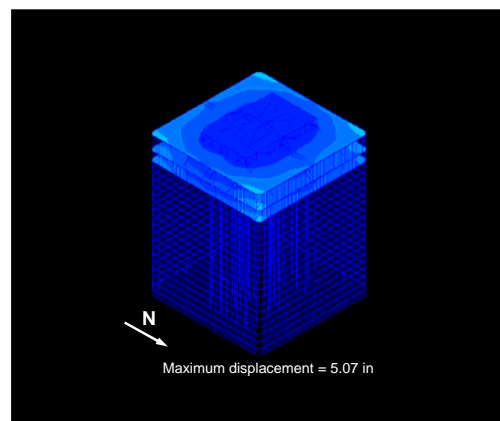
In order to verify the accuracy of the conversion of the building models from SAP2000 to ANSYS, prior to adding material nonlinearities and elements representing the floor slabs to the ANSYS models, the translated ANSYS models were subjected to gravity dead and live loads, and the ANSYS results were compared to the results of SAP2000 global models. The comparison included the calculated overall displaced shapes, the maximum displacements, vertical base reactions at each construction stage, and element forces for a set of randomly selected members from different parts of the buildings.

The gravity analysis was performed in three stages to simulate construction sequencing in the actual erection of the buildings. In Stage 1 the portion of the towers up to and including Floor 106 was analyzed under self-weight. In Stage 2 the members above Floor 106 were added, and the analysis was performed for the effects of dead loads of the newly added members. In Stage 3, the superimposed dead load and 25 percent of the design live load was added at each floor level to obtain an estimate of the deformations and stresses in each building under normal occupancy conditions.

Figure 4–4 shows the deformed shape calculated for WTC 1 by the ANSYS model and the truncated SAP 2000 model, following Stage 3 analysis. Figure 4–5 provides a similar comparison for WTC 2.

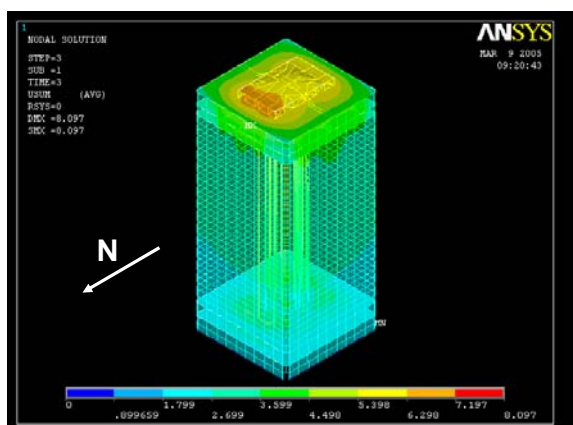


(a) WTC 1 ANSYS Model at Stage 3

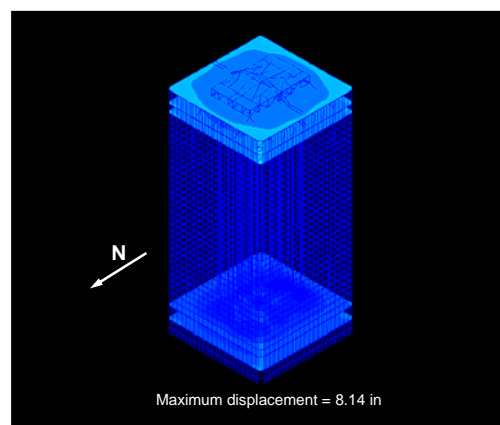


(b) WTC 1 SAP2000 Model at Stage 3
(Displacement is only shown on shell elements.)

Figure 4–4. Displaced shape of WTC 1 at the end of gravity analysis.



(a) WTC 2 ANSYS Model at Stage 3



(b) WTC 2 SAP2000 Model at Stage 3
(Displacement is only shown on shell elements.)

Figure 4–5. Displaced shape of WTC 2 at the end of gravity analysis.

Table 4–2 summarizes the maximum displacement and vertical reactions at the base for all stages of the gravity analysis of WTC 1, and Table 4–3 presents similar data for WTC 2. As can be seen, the deformed shapes as well as the maximum displacements and vertical reactions obtained from the analyses performed with the ANSYS models agree well with the results of the similar analyses performed with

SAP2000. The maximum difference in displacements between the two models was less than 1.4 percent for WTC 1 and 0.7 percent for WTC 2. The maximum difference between base reactions predicted by the two analyses was 1.2 percent for WTC 1 and 0.3 percent for WTC 2.

Table 4–4 presents a comparison of the axial forces computed from the ANSYS and SAP2000 analyses for a randomly selected set of elements from different parts of WTC 1. Table 4–5 presents similar data for WTC 2. The agreement between the results obtained from the ANSYS and SAP2000 analyses is quite good.

Table 4–2. Comparison of maximum displacements and base reactions of WTC 1 from translated ANSYS and SAP2000 models.

Stage	Maximum Vertical Displacement (in.)			Base Reaction Sum (kip)		
	ANSYS	SAP2000	Percent Difference	ANSYS	SAP2000	Percent Difference
1	-2.87	-2.83	1.4	55,600	54,940	1.2
2	-4.76	-4.74	0.4	98,470	97,850	0.6
3	-5.09	-5.07	0.4	107,040	106,450	0.6

Table 4–3. Comparison of maximum displacements and base reactions of WTC 2 obtained from translated ANSYS and SAP2000 models.

Stage	Maximum Vertical Displacement (in.)			Base Reaction Sum (kip)		
	ANSYS	SAP2000	Percent Difference	ANSYS	SAP2000	Percent Difference
1	-5.87	-5.91	-0.7	125,050	124,680	0.3
2	-7.67	-7.71	-0.5	166,950	166,980	-0.02
3	-8.10	-8.14	-0.5	180,250	180,360	-0.06

Table 4–4. Comparison of axial forces in randomly selected elements from WTC 1 model at the end of gravity analysis.

Location and Type of Selected Element	Axial Force (kip)	
	ANSYS	SAP2000
Exterior Column 302 at Floor 104	-77	-69
Spandrel between Columns 124 and 125 at Floor 102	0	0
Outrigger member between at Floor 110	-39	-48
Vertical hat truss member at 1005 core column line at Floor 109	-74	-91
Horizontal hat truss member at Floor 107	21	19
Horizontal hat truss member at Floor 108	170	150
Core Column 602 at Floor 97	-738	-745
Core Column 501 at Floor 93	-2,180	-2,190
Core Column 1001 at Floor 89	-2,570	-2,590
Spandrel between Columns 339 and 340 at Floor 100	0	0

Table 4–5. Comparison of axial forces in randomly selected elements from WTC 2 model at the end of gravity analysis.

Location and Type of Selected Element	Axial Force (kip)	
	ANSYS	SAP2000
Core beam at Floor 107	11	6
Inclined truss member at hat truss at Floor 107	-34	-4
Inclined truss member at hat truss at Floor 108	36	8
Inclined truss member at hat truss at Floor 108	-580	-670
Core Column 502 at Floor 87	-1,930	1,940
Core Column 1001 at Floor 82	-3,270	-3,290
Core Column 1002 at Floor 87	-1,910	-1,920
Core Column 1008 at Floor 82	-3,400	3,520
Core Column 1003 at Floor 107	-590	-608
Exterior Column 122 at Floor 82	-313	-313
Exterior Column 329 at Floor 82	-228	-230
Exterior Column 130 at Floor 107	-222	-202
Spandrel between Columns 138 and 139 at Floor 83	0	0
Spandrel between Columns 447 and 448 at Floor 87	0	0

4.2 GLOBAL ANALYSIS WITH CREEP

4.2.1 Introduction

This section presents the results of analyses conducted with global models that included consideration of plasticity, geometric nonlinearity relating to large displacements, inelastic buckling, and creep, and are referred to hereafter as global models or global analysis with creep. As noted earlier, a preliminary set of global analyses were conducted on models that did not include creep and could not simulate inelastic buckling of columns with fidelity. The results of these preliminary analyses are presented in Appendix C of this report, and are referred to as global analysis without creep. Due to the limited non-linear features in the preliminary global models without creep, global instability could not be captured during temperature time history analyses.

The results of the global analyses with creep are presented in Section 4.2.4 for WTC 1 and in Section 4.2.5 for WTC 2.

4.2.2 Modifications to the Global Model with Creep and Inelastic Buckling of Columns

Preliminary global analyses with creep resulted in an unacceptably slow rate of convergence. This was due to the size of the models and the nonlinear effects of temperature-dependent material properties, especially creep. To reduce the size of the global models and to enhance the computational efficiency without adversely affecting the fidelity of the results, a set of modifications were made. These modifications and their effects on the analysis results are discussed in this section. Table 4–6 summarizes the number of degrees of freedom, number of elements, and number of constraint equations in WTC 1 and WTC 2 global models before and after the modifications.

Table 4–6. Global model properties before and after modifications for computational efficiency.

Item	WTC 1		WTC 2	
	Before Modifications	After Modifications	Before Modifications	After Modifications
Number of Degrees of Freedom	291,670	265,760	487,260	196,900
Number of Constraint Eqs.	31,680	28,330	53,890	12,560
Number of Elements	63,880	57,680	106,460	38,130
Number of Beam Elements	48,200	43,600	81,280	32,540
Number of Shell Elements	15,680	14,080	25,180	5,490

Removal of Floors below Impact Zone

The parts of structures below the impact zones (Floor 89 to Floor 91 in WTC 1 and Floor 73 to Floor 77 in WTC 2) contributed little to the overall behavior of the buildings. Previous analyses of subsystem models and preliminary global models showed that the elements below the impact zone did not experience plastic deformations or buckling. Therefore, they were eliminated to further reduce the size of the models. With this modification, the global model for WTC 2 was truncated at Floor 77 just above the mechanical floors and the global model for WTC 1 was truncated at Floor 91.

Release of Axial Degree of Freedom of Spandrels

The spandrel elements in the exterior wall were modeled using BEAM188 elements. These elements caused convergence problems when thermal expansion caused buckling of spandrels. Based on visual evidence, buckling of spandrels did not compromise their ability to transfer shear and bending moment and did not play a very important role in the collapse sequence. Therefore, the axial degree of freedom was released on these spandrel elements, avoiding buckling due to development of large axial force in the spandrels. However, these BEAM188 elements could still transfer shear and bending moments. The coefficient of thermal expansion of spandrels was also removed so that the spandrels would not expand with temperatures.

Removal of Coefficient of Thermal Expansion from the Slab in the Office Area

Since trusses were not modeled individually, the office area slab buckled easily when thermal expansion was restrained by the exterior wall. Artificial buckling of the slab caused convergence problems in the global analysis. Since buckling of the slab in the actual buildings was resisted by the joists, and was not observed in any of the detailed full floor models, this slab buckling mode was considered unlikely to represent real building behavior. Consequently, the coefficient of thermal expansion for the slab in the office area was set to zero.

Neglecting the thermal expansion of the office area slabs did introduce small errors in the out-of-plane bending of columns extending between a hot floor and a cool floor, but such errors were small for columns extending between two hot floors. The error introduced by this modification was not expected to change failure modes or collapse sequence in the global analysis, because thermal expansion of floors was limited to less than a few inches (see Appendix A). The full floor models thermally expanded and pushed

outward on the columns until the thermal expansion was overcome by the floor sagging and the floors pulled inward on the exterior columns..

Use of Superelement in WTC 2

The term “superelement” is used to indicate substructuring, in which a portion of a large model expected to remain elastic is condensed out from the model as a whole. In this technique, the stiffness, damping and mass matrices for the substructure elements are calculated once and used throughout the analysis without any further change. One can calculate stresses and strains in individual elements in the superelement allowing verification of the assumption that the substructure elements remain elastic, or nearly so. The WTC 2 model was suitable for such modification as earlier analyses indicated that the section of the building above Floor 86 would remain nearly elastic. Therefore, this portion of the structure was converted into a superelement.

The use of this superelement in the WTC 2 analyses reduced the solution time required to complete a single iteration by a factor of three. However, it was recognized that if the hat truss members became inelastic and highly nonlinear, such nonlinearities could not be captured. Moreover, when the superelement is used, the effects of construction sequence on the load distribution between core and wall elements cannot be represented, since the birth and death option cannot be used in a superelement. As shown below, the effect of not including construction sequence was evaluated and found to introduce an error of less than 12 percent for vertical displacement.

To evaluate whether any member in the hat truss exceeded its elastic limits, the stresses in all elements within the superelement were calculated at the end of each time interval. For this purpose, a separate model that included the elements at and above Floor 86 was created. In this model, the material properties of all elements were replaced with elastic material properties. At each time interval, the displacements that were obtained from the global model at Floor 86 were imposed on the new model at the same level. Dead and live loads were also applied on the model. Member forces were calculated and compared with their capacities. The results are discussed in Section 4.2.5.

Change from BEAM188 to BEAM24 Elements

In the global models without creep, columns were modeled by BEAM188 (3D linear finite strain beam) elements. The analysis could not be conducted with elements of this type capturing time dependent creep behavior of steel. Frequent convergence problems occurred when thermally induced creep and buckling of columns was in process. Different element types were tested to determine whether thermally induced buckling and creep could be captured. Finally, BEAM24 element was selected, and the element type for the columns was changed from BEAM188 to BEAM24 (3D thin-walled beam).

Construction Sequence

Construction sequence was not included in the global models with creep. The effect of neglecting construction sequence was examined for both buildings. When construction sequence was not included in the analysis, the total axial loads in columns along the exterior walls increased by 7 percent to 15 percent. Similarly, the total column loads supported by the core columns decreased by about 10 percent.

Tables 4–7 and 4–8 indicate the differences in column loads when construction sequence either was or was not considered.

Table 4–7. Comparison of total column loads between WTC 1 models with and without construction sequence

	North		South		East		West		Core	
	w/ Const	w/o Const								
Floor 93 - 94	12,307	13,145	12,383	13,191	8,910	10,036	8,933	10,049	47,525	43,638
Floor 94 - 95	11,922	12,760	11,999	12,806	8,580	9,708	8,605	9,723	45,573	41,682
Floor 95 - 96	11,450	12,281	11,530	12,329	8,339	9,475	8,365	9,492	43,598	39,703
Floor 96 - 97	11,065	11,895	11,145	11,944	8,012	9,151	8,040	9,170	41,633	37,735
Floor 97 - 98	10,602	11,426	10,686	11,478	7,763	8,911	7,793	8,932	39,669	35,767
Floor 98 - 99	10,217	11,040	10,302	11,092	7,439	8,591	7,471	8,613	37,714	33,808

Note: Compression is positive. Units are in kip.

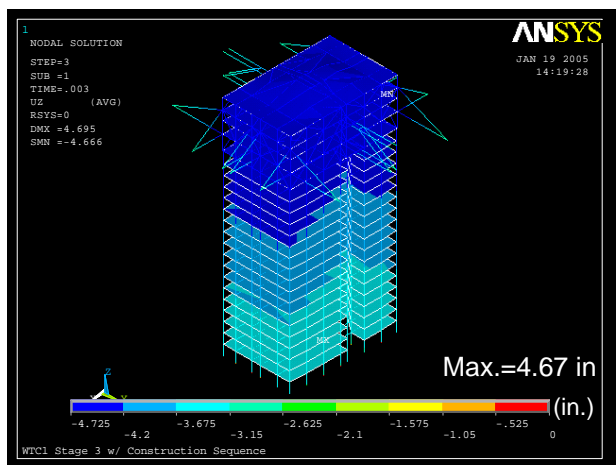
Table 4–8. Comparison of total column loads between WTC 2 models with and without construction sequence

	North		South		East		West		Core	
	w/ Const	w/o Const								
Floor 78 - 79	13,536	15,304	13,442	15,000	18,861	20,169	18,805	20,119	78,104	72,156
Floor 79 - 80	12,965	14,723	12,877	14,424	18,650	19,970	18,596	19,923	76,197	70,246
Floor 80 - 81	12,892	14,675	12,810	14,379	17,959	19,257	17,903	19,207	74,160	68,206
Floor 81 - 82	12,367	14,141	12,292	13,851	17,728	19,036	17,673	18,989	71,824	65,866
Floor 82 - 83	12,279	14,078	12,208	13,789	17,064	18,353	17,008	18,301	69,777	63,815
Floor 83 - 84	11,775	13,567	11,712	13,284	16,816	18,114	16,761	18,114	67,793	61,828

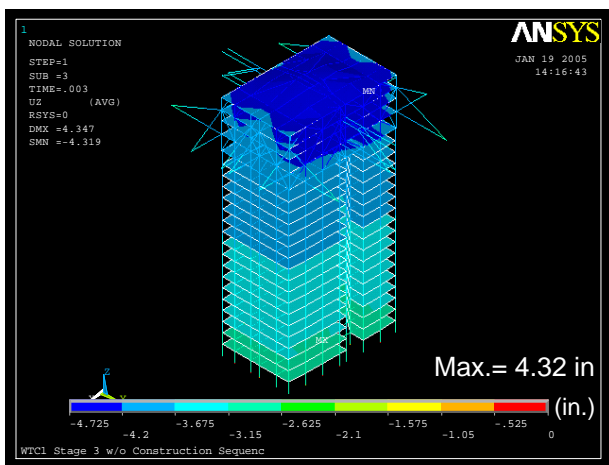
Note: Compression is positive. Units are in kip.

The calculations showed that the outriggers in the WTC 1 simulations were more highly stressed when the construction sequence was not considered. Since it was believed that the hat truss played an important role in transferring loads in WTC 1, the yield strengths of the materials for these outriggers in WTC 1 were artificially increased to account for the incorrect increase in compressive stresses when construction sequence was not considered.

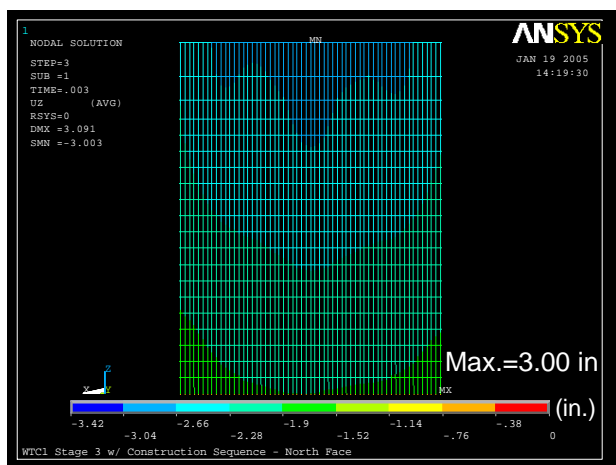
The difference in maximum displacement calculated with and without consideration of construction sequence was within 12 percent for both WTC 1 and WTC 2. Figures 4–6 and 4–7 present the differences in calculated displacements for analyses in which construction sequence either was or was not considered, respectively, for WTC 1 and WTC 2. In these figures, the results presented for global analyses with creep for the state of the structure before aircraft impact are for the analyses in which construction sequence was neglected; they differ from the corresponding results presented in Appendix C for global analyses without creep as those analyses included the effects of the construction sequence.



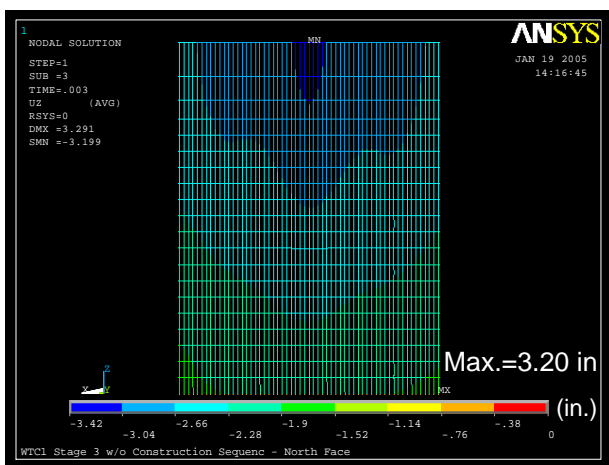
(a) Core w/ construction sequence



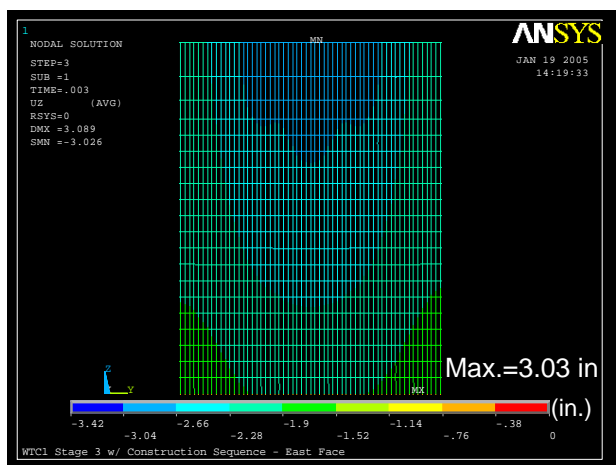
(b) Core w/o construction sequence



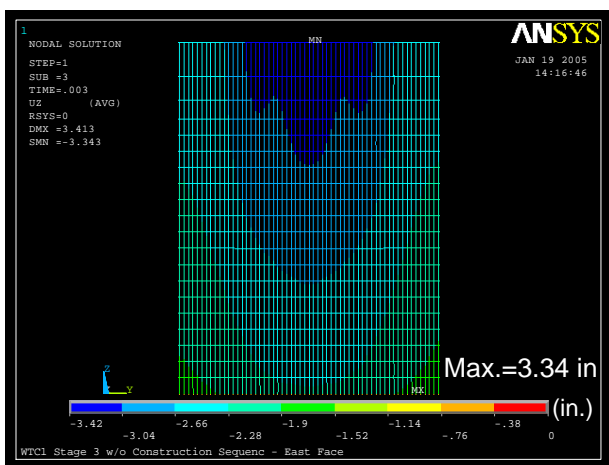
(c) North face w/ construction sequence



(d) North face w/o construction sequence

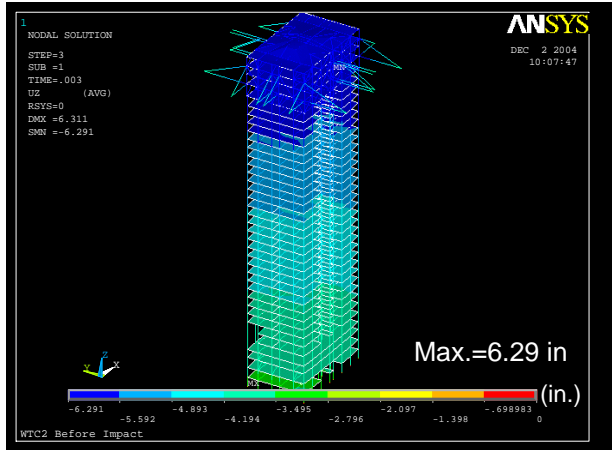


(e) East face w/ construction sequence

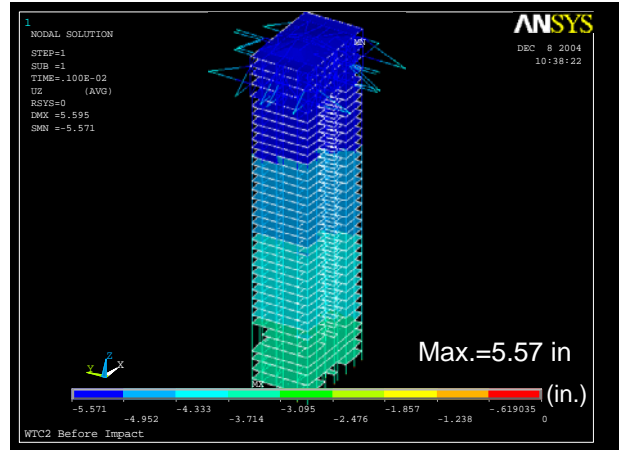


(f) East face w/o construction sequence

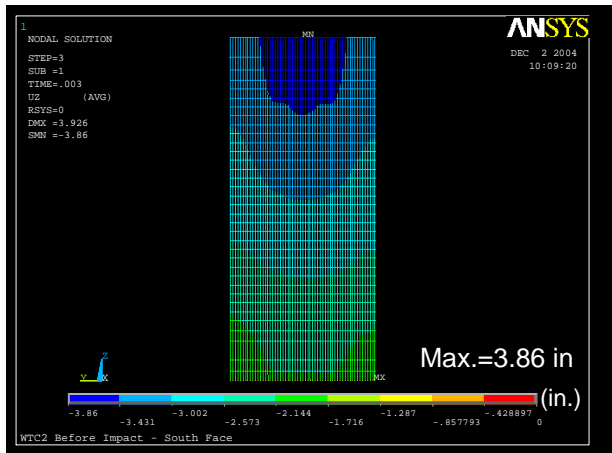
Figure 4–6. Comparison of vertical displacement between WTC 1 models with and without construction sequence.



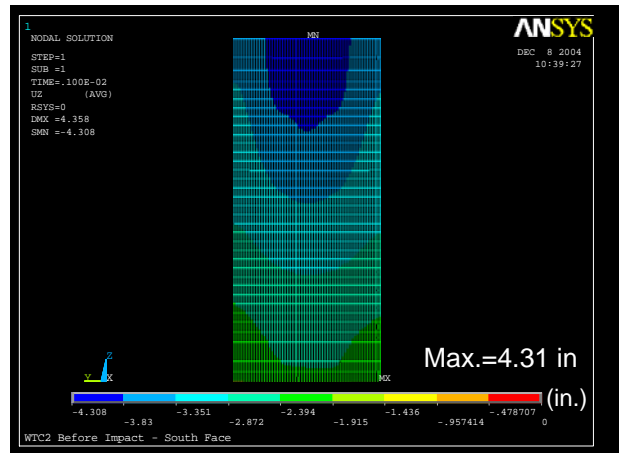
(a) Core w/ construction sequence



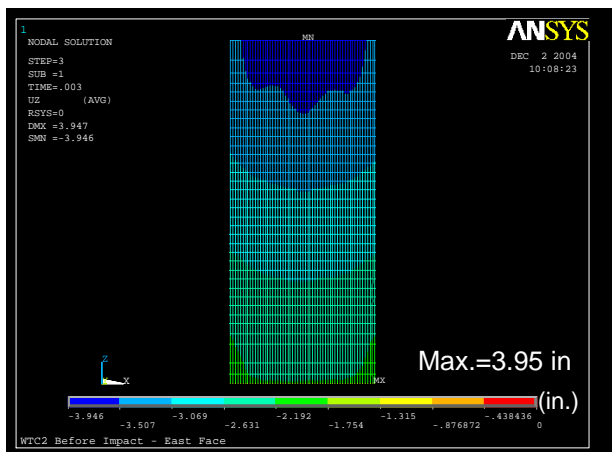
(b) Core w/o construction sequence



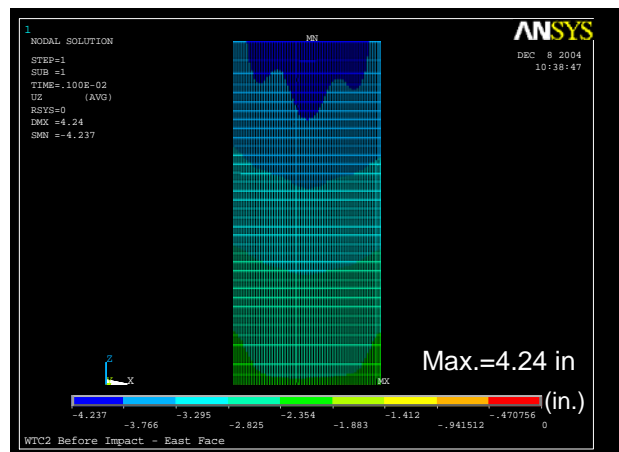
(c) South face w/ construction sequence



(d) South face w/o construction sequence



(e) East face w/ construction sequence



(f) East face w/o construction sequence

Figure 4–7. Comparison of vertical displacement between WTC 2 models with and without construction sequence.

4.2.3 Boundary Conditions and Loading Steps

The global models with creep were vertically supported on elastic springs at Floor 91 for WTC 1 and Floor 77 for WTC 2. These elastic springs represented the axial flexibility of the portion of the building below these floors. The models were fixed against horizontal translation at these floors.

The collapse analysis of WTC 1 considered creep and was performed only for Case B damage conditions and temperature time histories; and that for WTC 2 was only performed for Case D. Section 2.2.3 of this report provides a description of these damage conditions. Severed and heavily damaged core columns were removed in the global model with creep, while only severed columns were removed in the global models without creep.

To reduce the size of the global models as much as possible, members that were predicted to have been severed or heavily damaged by the aircraft impact were removed from the models before applying the gravity load. The floor dead and live loads were applied at each column node at the floor levels. These forces were taken directly from the ANSYS global models converted from the reference SAP2000 global models. WTC 1 and WTC 2 global models were then subjected to Case B and Case D temperature conditions, respectively. NIST provided temperature data at 10 min intervals ranging from 0 min to 100 min for WTC 1 and to 60 min for WTC 2. For the first loading step of temperature analysis, temperatures of the structural elements were linearly ramped up from room temperature to the temperatures at 10 min. After the first step, the temperatures were linearly ramped from the temperatures at the end of the previous time step to those at the end of current time step.

4.2.4 Simulation of WTC 1 Collapse

The global model of WTC 1, described in the previous section, was used to simulate the response of the building to aircraft impact damage and the ensuing fire environment. Studies performed on the isolated exterior wall and core models and on the full floor subsystem models indicated that the calculated response of these models to the Case B impact damage and temperature time history set, as described in Section 2.2.3, more closely matched the structural behavior observed in the visual evidence than did analyses using the Case A data set. Therefore, only the Case B impact damage and temperature time history set was used in the final global analyses.

The gravity loading, consisting of the structure's self weight, superimposed dead load, and 25 percent of the design live loads, was applied as a concentrated joint load at each column-floor node, without consideration of construction sequence effects. Then the temperature time history was applied in a series of load steps. Table 4–9 summarizes the sequence of analyses that were performed. The results of each analysis step were used as the initial conditions for the next analysis step. The steps consisted of alternate applications of fire damage, in the form of floor/wall disconnections or pull-in forces, followed by application of temperature change. Section 2.5 describes the methods by which floor/wall disconnections and pull-in forces were determined and applied.

After application of the Case B aircraft impact damage set, which included severe damage on the north face and to the north side of the core, the results of analysis showed slight tilting of the portion of the structure above the damaged area, to the north. In early stages of the application of the temperature time history, temperatures increased significantly in the core columns where thermal insulation was projected to be damaged. The resulting thermal expansion of these core columns was larger than the thermal

expansion of the exterior walls which occurred at the same time. Therefore, as the core columns in the model expanded, they were restrained by the stiff hat truss, resulting in increased compressive forces in the core columns. This effect first became significant at 20 min. By 50 min some of the core columns under the influence of the high temperatures and high compressive loads began to exhibit buckling and large creep strains. As buckling and creep strains accumulated, the core began to displace downward. Again, the movement of the tops of the core columns was restrained by the hat truss which now began to redistribute loads from the core columns to the exterior walls. At 80 min, pull-in forces were applied to the south wall, based on the observed evidence. At 87 min, the south wall started to bow inward significantly, initiating the buckling of the south wall that triggered the collapse sequence.

Table 4–9. Analysis steps of WTC 1 ANSYS global model.

Analysis Step	Description
1	Dead and 25 percent of the design live loads were applied on the model of WTC 1 with impact damage.
2	Floor/wall disconnections and pull-in forces that were projected to occur between 0 min and 10 min were applied.
3	Column and spandrel temperatures were linearly ramped up from room temperature of 20°C to temperatures at 10 min.
4	Floor/wall disconnections and pull-in forces that were projected to occur between 10 min and 20 min were applied.
5	Column and spandrel temperatures were linearly changed from temperatures at 10 min to 20 min.
6	Floor/wall disconnections and pull-in forces that were projected to occur between 20 min and 30 min were applied.
7	Column and spandrel temperatures were linearly changed from temperatures at 20 min to 30 min.
8	Floor/wall disconnections and pull-in forces that were projected to occur between 30 min and 40 min were applied.
9	Column and spandrel temperatures were linearly changed from temperatures at 30 min to 40 min.
10	Floor/wall disconnections and pull-in forces that were projected to occur between 40 min and 50 min were applied.
11	Column and spandrel temperatures were linearly changed from temperatures at 40 min to 50 min.
12	Floor/wall disconnections and pull-in forces that were projected to occur between 50 min and 60 min were applied.
13	Column and spandrel temperatures were linearly changed from temperatures at 50 min to 60 min.
14	Floor/wall disconnections and pull-in forces that were projected to occur between 60 min and 70 min were applied.
15	Column and spandrel temperatures were linearly changed from temperatures at 60 min to 70 min.
16	Floor/wall disconnections and pull-in forces that were projected to occur between 70 min and 80 min were applied.
17	Column and spandrel temperatures were linearly changed from temperatures at 70 min to 80 min.
18	Floor/wall disconnections and pull-in forces that were projected to occur between 80 min and 90 min were applied.
19	Column and spandrel temperatures were linearly changed from temperatures at 80 min to 90 min.
20	Floor/wall disconnections and pull-in forces that were projected to occur between 90 min and 100 min were applied.
21	Column and spandrel temperatures were linearly changed from temperatures at 90 min to 100 min.

Figures 4–8 to 4–23 show the calculated vertical displacements for the exterior walls of WTC 1, before the aircraft impact, immediately after impact, at 80 min after impact (at the end of Step 17), and 100 min after impact. Figures 4–24 to 4–32 show similar data for the core columns. Figure 4–33 shows the calculated vertical displacement of Floor 99 before the aircraft impact. Figures 4–34 to 4–37 show changes in vertical displacement at Floor 99 from the state before the aircraft impact. Before aircraft impact, the maximum vertical displacements of the exterior walls and the core were respectively calculated as 3.3 in. and 4.2 in. (see Figs. 4–8 and 4–24). As indicated in Fig. 4–33, the core had larger vertical displacements by about 1 in. than the exterior walls at Floor 99. Since the construction sequence was not considered in the analysis, this difference in the vertical displacements changed initial loading conditions of columns. As shown in Table 4–7, the total column loads on the north and south walls increased by 7 percent at the impacted floors, the total column loads on the east and west walls increased by about 14 percent, and the total column loads on the core decreased by about 9 percent, by ignoring the construction sequence. Owing to impact damage on the north face and the north side of the core, WTC 1 tilted slightly to the north after the aircraft impact as can be seen in Fig. 4–34. The maximum calculated displacement of the north wall increased from 3.1 in. to 5.9 in. as shown in Figs. 4–12 and 4–13, and the maximum displacement of the south wall decreased from 3.2 in. to 3.0 in. as shown in Figs. 4–20 and 4–21. The calculated vertical displacement for the east and west walls only increased slightly.

In the early stages of thermal loading, the temperatures in the core area were rising. At 50 min, the calculated downward displacement of the core from plasticity, creep, and buckling of core columns was 1.6 in. on average at Floor 99, as shown in Fig. 4–35. At 100 min, the downward displacement of the core was at 2.0 in. on average at Floor 99. Average increases of the downward vertical displacement at Floor 99 of the north, east, south, and west faces were 1.7 in., -0.24 in., -0.51 in., and -0.24 in. at 100 min, respectively. As the bowing of the south wall increased, a section of the south wall above the bowed-in area moved downward as shown in Fig. 4–37.

Figures 4–38 to 4–41 show the calculated out-of-plane displacements for the south wall before and after the aircraft impact, at 80 min (at the end of Step 17), and 100 min after impact. In these figures, inward displacement is shown as positive. Figure 4–42 shows a plot of the variation of maximum calculated out-of-plane displacement in the south wall between 80 min and 100 min. Until pull-in forces were applied to the columns on the south wall over Floor 95 to Floor 99 at 80 min (Step 18), no inward bowing had occurred. This matches the available video evidence. After the pull-in forces were applied, the bow initiated and grew to 15.5 in. At about 87 min into the analysis, the inward bow began to increase significantly. By 90 min, the rate of increase in inward bowing of the south wall slowed, and gravity loads were redistributed to the east and west walls and the core. The predicted inward bowing gradually increased to approximately 43 in. at 100 min. However, the south wall did not show instability (buckling) at 100 min.

Analyses of isolated exterior wall substructure models and of the global model showed that the amount of inward bowing predicted for the wall was highly sensitive to the magnitude of the applied pull-in forces. For a comparison, when pull-in forces were revised from the 5 kip magnitude used in the analyses discussed above to 4 kip, the predicted inward bowing of the south wall decreased dramatically from nearly 43 in. at 100 min to approximately 15 in. Minor upward adjustment of the pull-in forces, from the 5 kip used in the analyses, would have produced wall instability by 100 min. It is likely that the pull-in forces in the actual building increased with time, and that likely, this inward bowing of the south wall did trigger instability, which initiated the global structural collapse.

Figures 4–44 to 4–55 show calculated axial loads in exterior columns before and after the aircraft impact, at 80 min (at the end of Step 17), and 100 min after impact. Figures 4–56 to 4–59 show the variation of calculated axial loads in exterior columns along the different building faces at Floor 98 at different points in time. Figures 4–60 to 4–63 show axial loads for the core columns before and after the aircraft impact, at 80 min (at the end of Step 17), and 100 min. Figures 4–64 to 4–67 show the magnitude of axial load in each column at Floor 98; the size of axial load is proportional to the size of the circles. Tables 4–10 and 4–11 show the total column loads on each of the exterior walls and the core at Floor 98 and Floor 105, respectively. Tables 4–12, 4–14, 4–16, 4–18, and 4–20 show total column loads on each of the exterior walls and the core at different floors from Floor 93 to Floor 105. Tables 4–13, 4–15, 4–17, 4–19, and 4–21 show the predicted changes in the total column loads of each of the exterior walls and the core at various times in the analysis. Tables 4–22 to 4–24 show the difference in total column loads at Floor 98 and Floor 105 between the states before and after aircraft impact, just after aircraft impact to 80 min (at the end of Step 17), and between 80 min (at the end of Step 17) and 100 min.

After aircraft impact, gravity loads that were previously carried by severed columns were redistributed to other columns within the building. For example, Table 4–10 shows that the exterior columns of the north wall at Floor 98 carried 10,974 kip load before the aircraft impact, and 10,137 kip just after aircraft impact, a net reduction of 837 kip. Table 4–11 shows that columns along the north wall at Floor 105 lost 732 kip of column loads as a result of the impact damage. Therefore, 732 kip out of 837 kip was transferred by the hat truss to other portions of the structure, and the rest was redistributed to the adjacent walls by the Vierendeel behavior of the walls themselves. Table 4–22 shows this load redistribution. Due to the impact damage and the northward tilting of the building after impact, the south wall also lost gravity loads. Approximately 600 kip was transferred from the south wall by the hat truss. The east and west walls and the core gained respectively gained 466 kip, 472 kip, and 400 kip, respectively.

As described above, during early stages of the thermal analysis, thermal expansion of the core area was greater than that of the exterior walls. As this expansion occurred, the total column loads in the core increased until 20 min into the analysis, as shown in Tables 4–20 and 4–21. After 20 min, the core began to shed gravity loads as it displaced downward, under the influence of column creep and buckling. This behavior continued until the south wall initiated inward bowing. At 80 min, about 6,800 kip of the gravity load in the core was transferred by the hat truss to the exterior walls, as shown in Table 4–11. The north, east, south, and west walls respectively gained 1,234 kip, 2,470 kip, 1,063 kip, and 2,021 kip from this behavior. As shown in Table 4–23, the primary load redistribution path during the thermal loading up to 80 min was through the hat truss.

Figure 4–58 shows that after 80 min, Columns 318 to 346 on the south wall unloaded as they bowed inward. The vertical displacement of the south wall simultaneously increased as shown in Figs. 4–23 and 4–37, and the south wall shed 1,485 kip of the gravity load between 80 min and 100 min. As a result, the east and west walls and the core all gained gravity loads. Figure 4–58 also shows load redistribution within the south wall. As the columns near the center of the south wall unloaded after 80 min, the axial loads on the columns on the east and west sides of the south wall increased.

Figures 4–68 to 4–71 show the calculated axial load demand-to-capacity ratio of each core column before and after the aircraft impact, at 80 min (at the end of Step 17), and 100 min. Compressive capacities of the core columns were calculated using Eq. E2-1 in the American Institute of Steel Construction's Manual of Steel Construction Load and Resistance Factor Design (AISC LRFD) for inelastic buckling with an effective length factor, K , of unity and a resistance factor of unity. At 100 min, a large number of core

columns (501, 601, 603, 606, 701, 703, 705, 707, 801, 804, 806, 807, 901, 903, 904, 905, 906, 908, and 1001) exhibited demand-to-capacity ratios larger than 0.7. Eight columns (501, 606, 705, 707, 804, 806, 807, and 908) exhibited ratios larger than 1.0. Although there is some significant uncertainty associated with calculation of both the load on these columns and the buckling capacity, this indicates that at this time step, the core had either initiated or was close to initiating buckling-induced failure.

Figures 4–72 to 4–77 show the maximum strains in each column between Floor 93 and Floor 99 before and after aircraft impact, at 10 min (at the end of Step 3), 40 min (at the end of Step 9), 80 min (at the end of Step 18), and 100 min. These figures include elastic and inelastic strain, but no creep effects.

Figures 4–78 to 4–81 show the same data, but include the additional effects of creep. Before the aircraft impact, all of the columns were loaded within their elastic range. After the aircraft impact, columns close to removed columns (which included both severed and highly damaged columns) developed plastic strain. Plastic strain of the core columns increased significantly for the first 40 min, and then remained almost constant until 100 min. At 100 min, the maximum elastic-plus-plastic strain was 0.98 percent at Column 603. From 80 min to 100 min, plastic strain increased in almost all the bowed columns on the south face. However, creep strain was found to be far greater than plastic strain as can be seen in Figs. 4–78 to 4–81, especially in the core. At 40 min, 22 of 38 core columns that were not severed or highly damaged by aircraft impact had creep strains larger than 1.0 percent. After 40 min, the creep strains of core columns on the south side of the core slowly increased. The maximum elastic-plus-plastic-plus-creep strain at 100 min was 7.3 percent in Column 1006. As temperature increased on the south wall in the later times, creep strain in columns on the south wall also increased. By 100 min, creep strain increased in about 20 columns on the south face; the maximum elastic-plus-plastic-plus-creep strain in the columns on the south face reached 2.9 percent.

At 100 min, the core was weakened on the south side and had shortened by 1.6 in., and the south wall had bowed inward to approximately 43 in. from pull-in forces at Floors 95 to 99 and was unloading to the core and the adjacent east and west walls.

Based on the observations and the calculated results of the analysis, reported above, the following sequence of events likely occurred as the south wall reached instability and buckled:

- As columns buckled, they shed load through Vierendeel action to adjacent columns in the south wall, in turn buckling these columns.
- The inward bowing of the south wall increased as additional columns buckled.
- As a result of this behavior, instability progressed horizontally across the wall.
- When instability engulfed the entire south wall, the wall continued to shed load to the east and west walls and to the core.

The onset of this load redistribution can be found in Table 4–24. The section of the building above the impact zone began tilting to the south as column instability progressed rapidly from the south wall along the adjacent east and west walls, resulting in increase of the gravity load on the core columns and in turn contributing to the buckling failure of these columns and initiating global collapse of the structure.

Since the global model did not include elements capable of capturing failure of column or hat truss element splices, nor buckling of hat truss outriggers, the conditions of the connections and the members in the primary load path to and through the hat truss were evaluated at different time intervals. This evaluation included the core column splices for tension, outriggers and supporting columns for compression, and the hat truss connections that were in the primary load path for tension.

Before the aircraft impact, core column splices were under compression. After the impact and with increasing plastic and creep strains, the core displaced downward, and some core columns became suspended from the hat truss. In fact, as shown in Table 4–26 and Fig. 4–82, Columns 503, 504, 505, 602, 603, 604, 605, 702, and 802 were calculated to be in tension at Floor 105 at 100 min. To evaluate the condition of the core column splices at Floor 106, the tension capacities of these splices were calculated using the AISC LRFD procedures and compared to the calculated tensile forces at each time interval. Table 4–25 shows the calculated tension capacities of core column splices at Floor 106, and Fig. 4–83 shows tensile demand-to-capacity ratios for the core column splices at Floor 106 at 100 min. It was found that tension forces in core columns were less than the capacities of the splices.

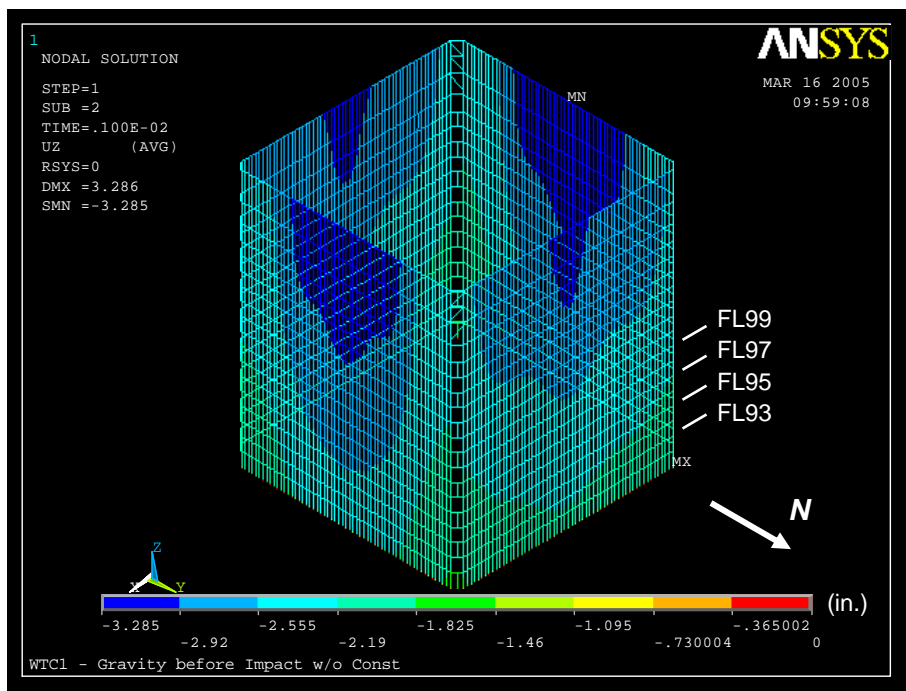
Sixteen outrigger members (four on each face) were present and participated in transfer of gravity loads between the core columns and the exterior walls, as shown in Fig. 4–3. In the global model, each of these outriggers was represented by one BEAM24 element; therefore, buckling of the member could not be captured, although material nonlinearity was included. Table 4–27 presents axial load demand-to-capacity ratios of the outrigger members. Capacities of outriggers were calculated using AISC LRFD Eq. E2-1 with an effective length factor $K=0.75$ and a resistance factor of unity. To check against calculated capacities, axial loads obtained from the global model were adjusted for the additional axial load caused by ignoring construction sequence. Analyses predicted that Outrigger E reached its axial load capacity (see Fig. 4–3 for designations of outrigger members). Because the material properties of the outriggers in the global model were set so that they would yield when the axial load in the outrigger reached its compressive capacity, the axial load in Outrigger E did not change after reaching its capacity as unloading in the post-buckling regime was not modeled. This may have resulted in an underestimate of the force redistribution to the other outriggers.

Table 4–28 shows the computed demand-to-capacity ratios for axial loads of exterior columns supporting the outriggers. Each of these exterior columns was also modeled by only one element (BEAM188) in the global model; therefore, buckling of the columns were not captured in the analysis. Compressive capacities of these columns were also calculated using AISC LRFD Eq. E2-1 with an effective length factor $K=0.75$ and a resistance factor of unity. This analysis showed that the axial loads in these columns were well below their inelastic buckling capacities.

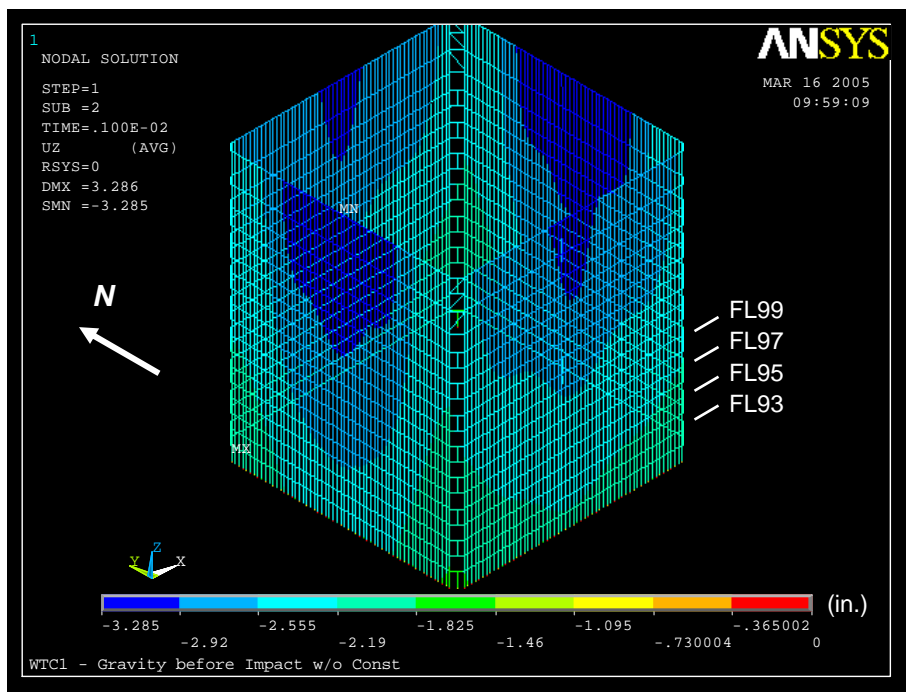
For effective load transfer from the core columns to the outriggers to occur, the capacities of the hat truss connections in the intermediate load path could not be exceeded. To investigate this issue, the hat truss connections that were in this load path were identified, and their capacities were compared to the calculated forces transferred through them. The load path was identified by selecting the hat truss members that were predicted to have an absolute axial stress of 25 ksi or more. The hat truss stresses were evaluated at 80 min (at the end of Step 17) as at this time they had reached their predicted maxima. Only the connections that were transferring tensile forces were evaluated. Figure 4–84 shows the members determined to be in the primary load path. Figure 4–85 shows the location of the critical hat truss connections that were evaluated. The capacities of the connections were calculated using the AISC LRFD procedures. Table 4–29 summarizes capacities, demands, and the conditions of the connections

identified in Fig. 4–85. As can be seen in Table 4–29, none of the connections exceeded their capacities. The state of the outriggers and core column splices at Floor 105 were discussed in the earlier paragraphs.

Based on these evaluations, it can be stated that even though one outrigger reached its capacity, the hat truss was capable of redistributing loads between the core and the exterior walls, and therefore, the evaluations described above are valid.

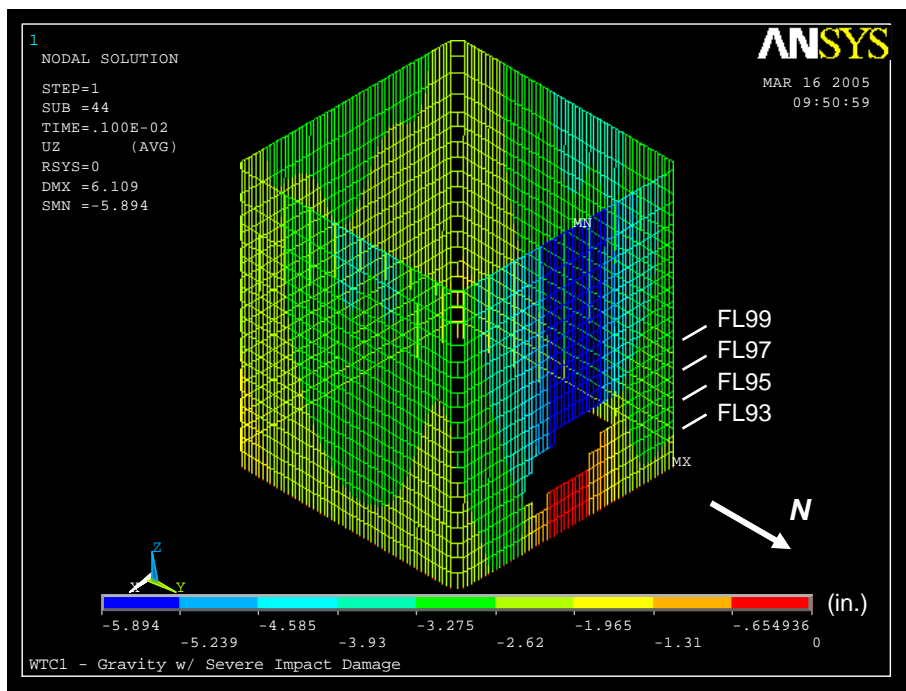


(a) North and east sides

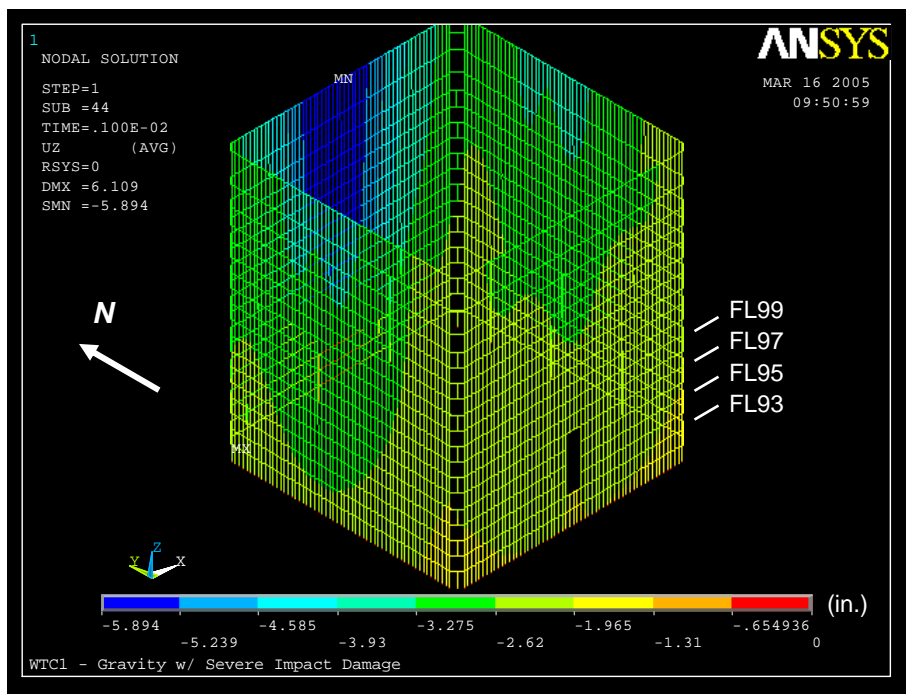


(b) South and west sides

Figure 4–8. Vertical displacement of exterior wall of WTC 1 before aircraft impact (downward displacement is negative).

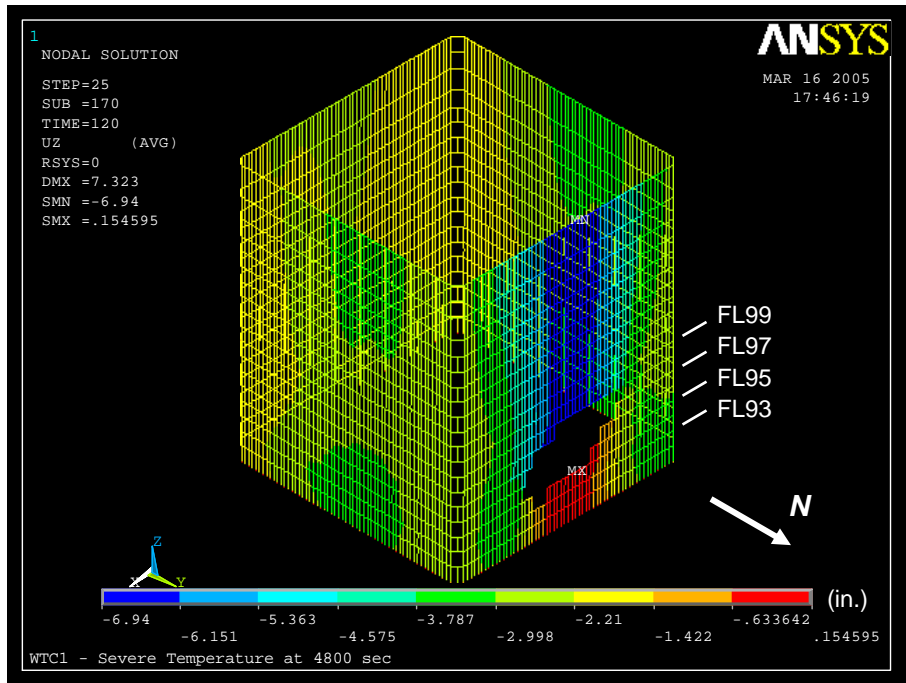


(a) North and east sides

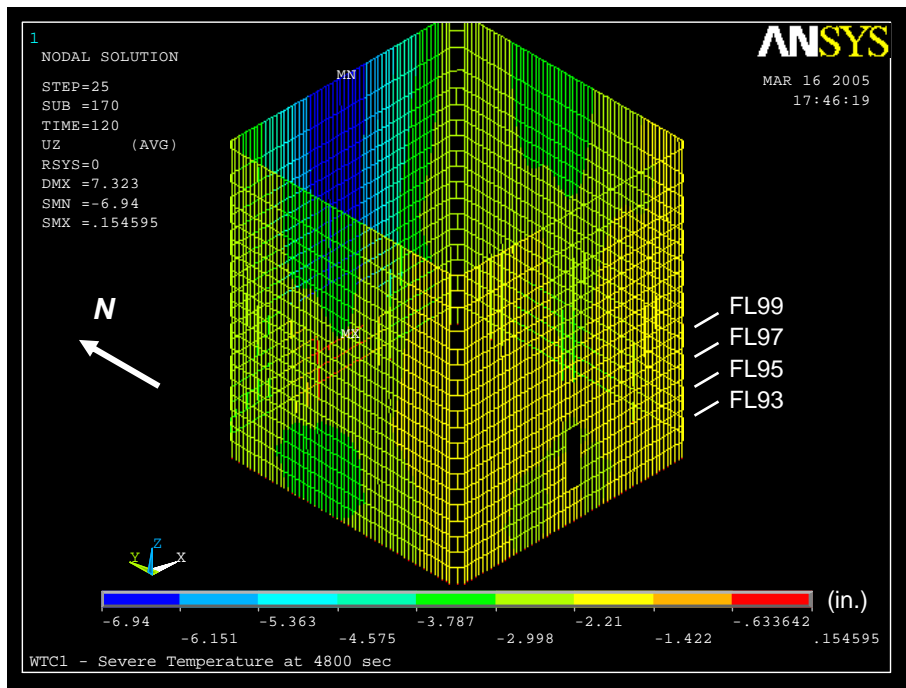


(b) South and west sides

Figure 4–9. Vertical displacement of exterior wall of WTC 1 after aircraft impact for Case B conditions (downward displacement is negative).

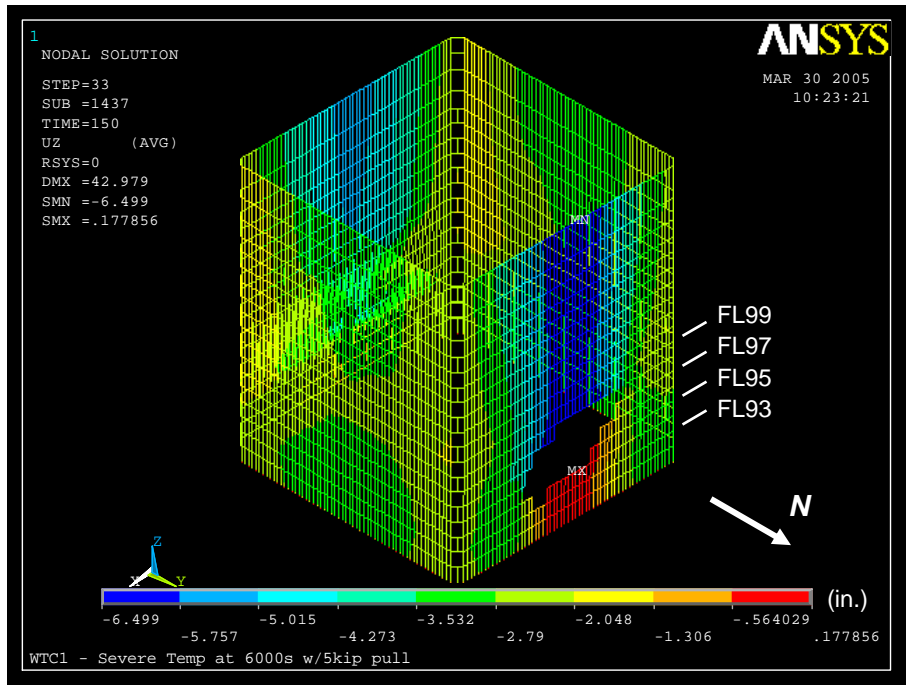


(a) North and east sides

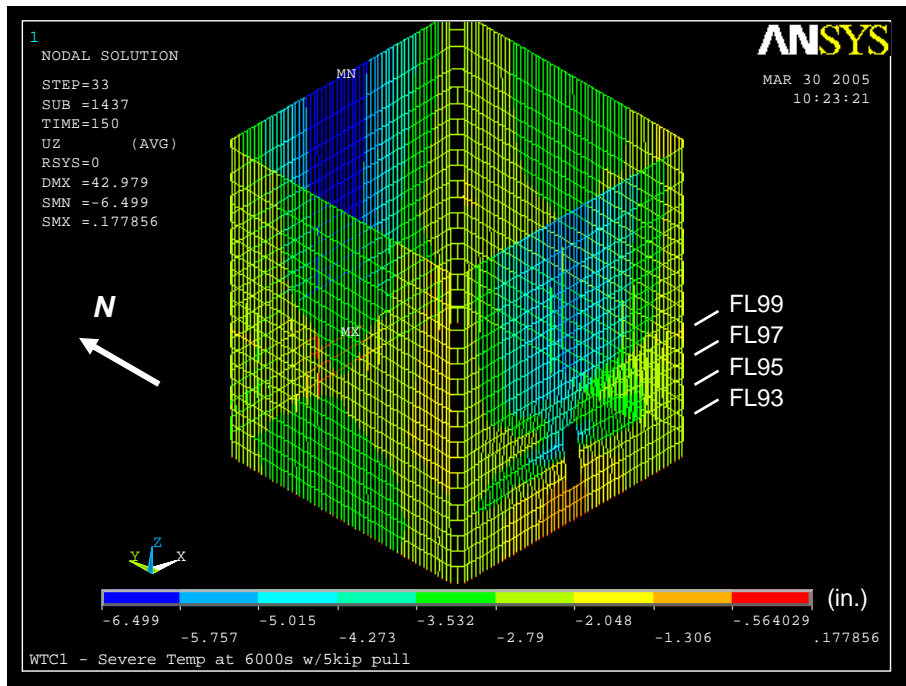


(b) South and west sides

Figure 4–10. Vertical displacement of exterior wall of WTC 1 at 80 min for Case B conditions (downward displacement is negative).



(a) North and east sides



(b) South and west sides

Figure 4–11. Vertical displacement of exterior wall of WTC 1 at 100 min for Case B conditions (downward displacement is negative).

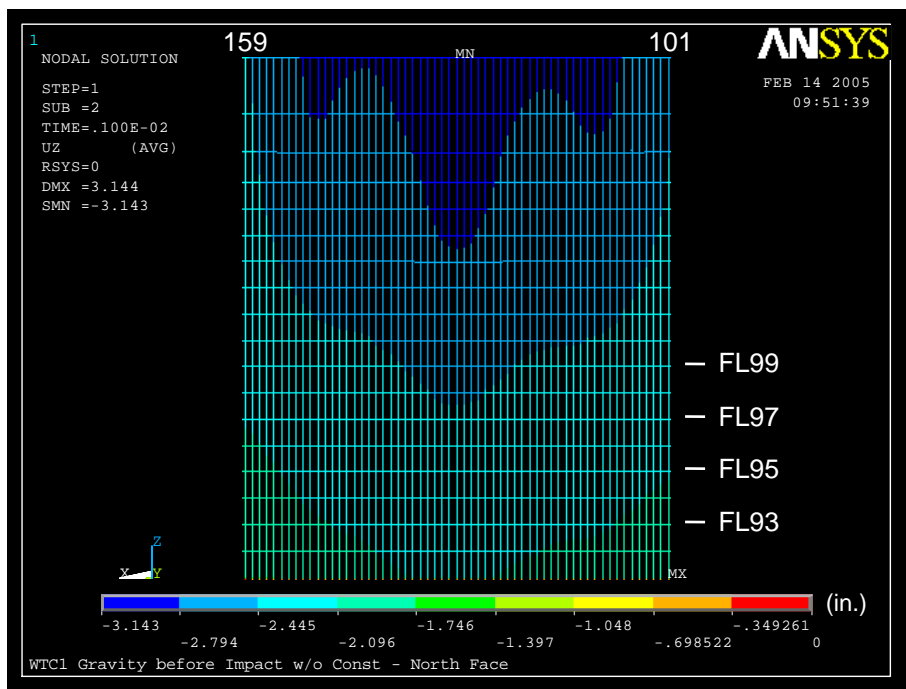


Figure 4–12. Vertical displacement of north wall of WTC 1 before aircraft impact.

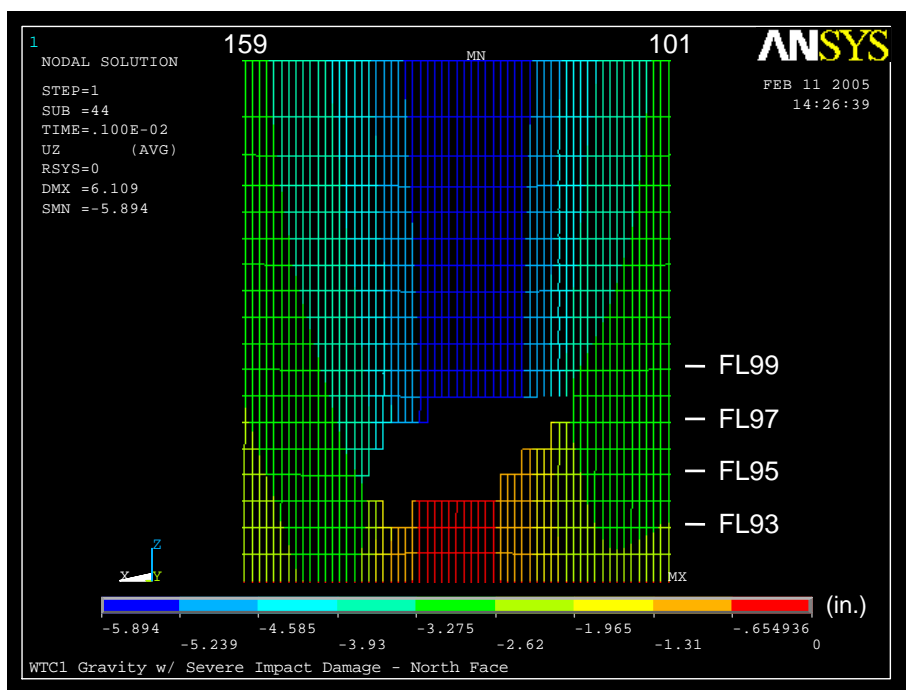


Figure 4–13. Vertical displacement of north wall of WTC 1 after aircraft impact for Case B conditions (downward displacement is negative).

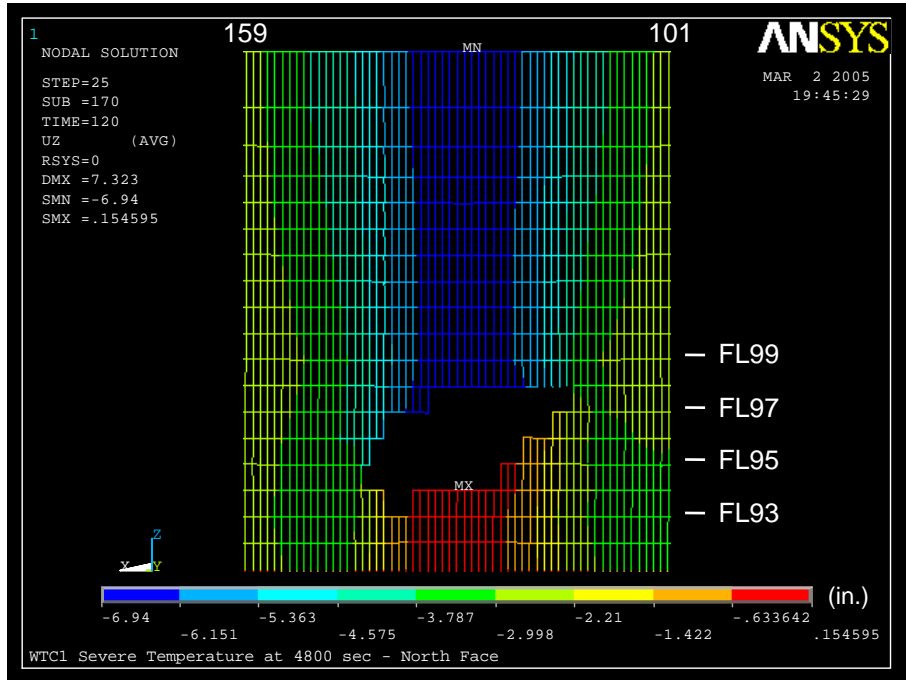


Figure 4–14. Vertical displacement of north wall of WTC 1 at 80 min for Case B conditions (downward displacement is negative).

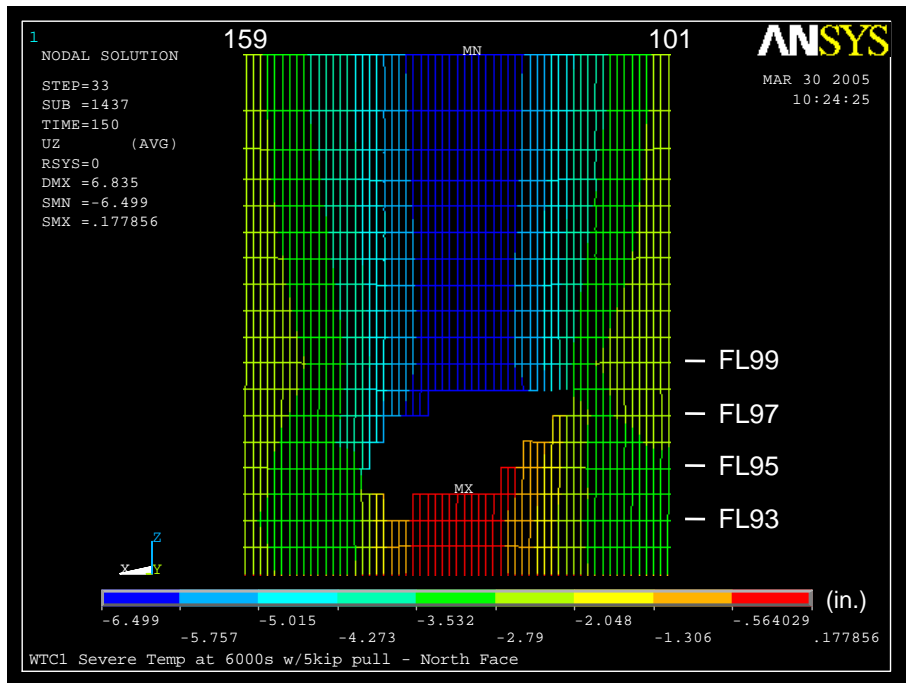


Figure 4–15. Vertical displacement of north wall of WTC 1 at 100 min for Case B conditions with 5 kip pull-in forces (downward displacement is negative).

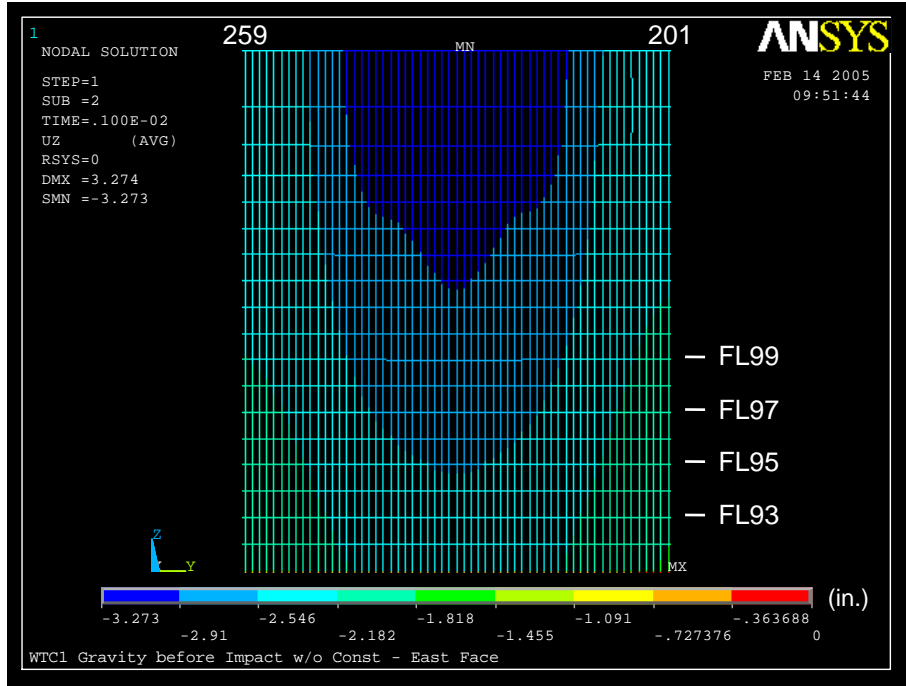


Figure 4–16. Vertical displacement of east wall of WTC 1 before aircraft impact (downward displacement is negative).

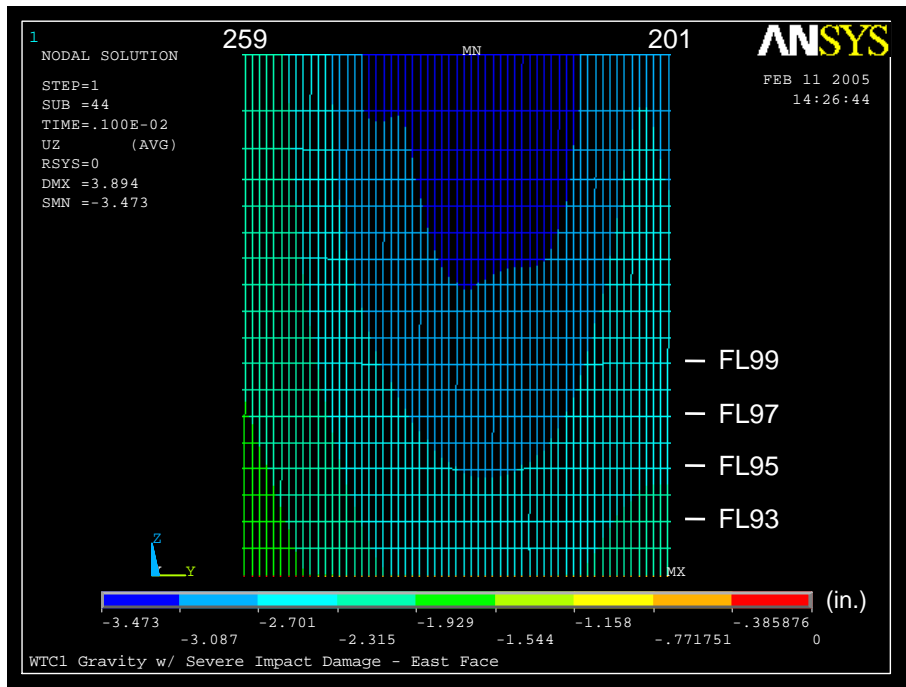


Figure 4–17. Vertical displacement of east wall of WTC 1 after aircraft impact for Case B conditions (downward displacement is negative).

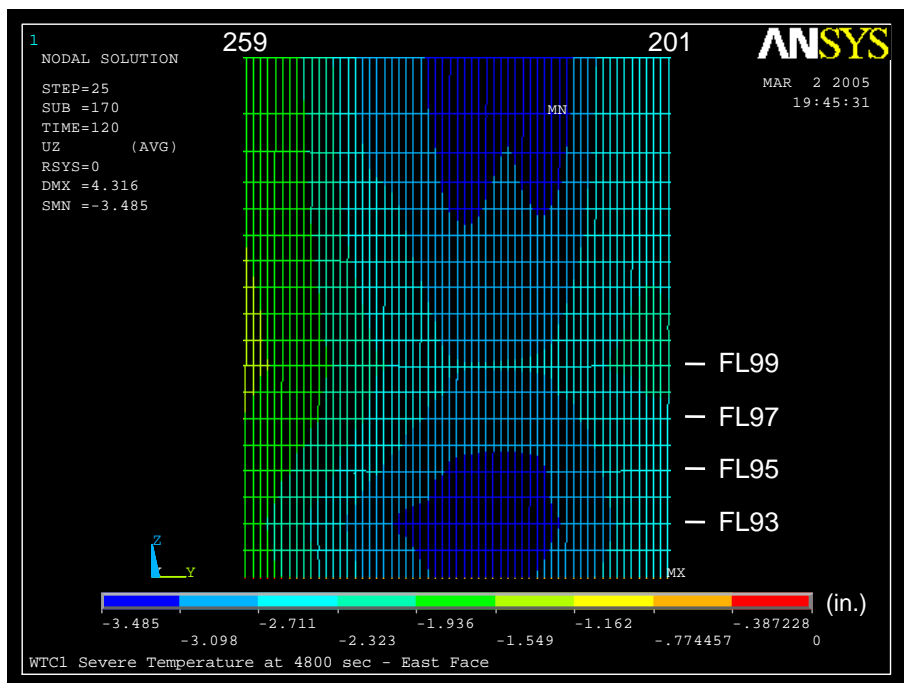


Figure 4–18. Vertical displacement of east wall of WTC 1 at 80 min for Case B conditions (downward displacement is negative).

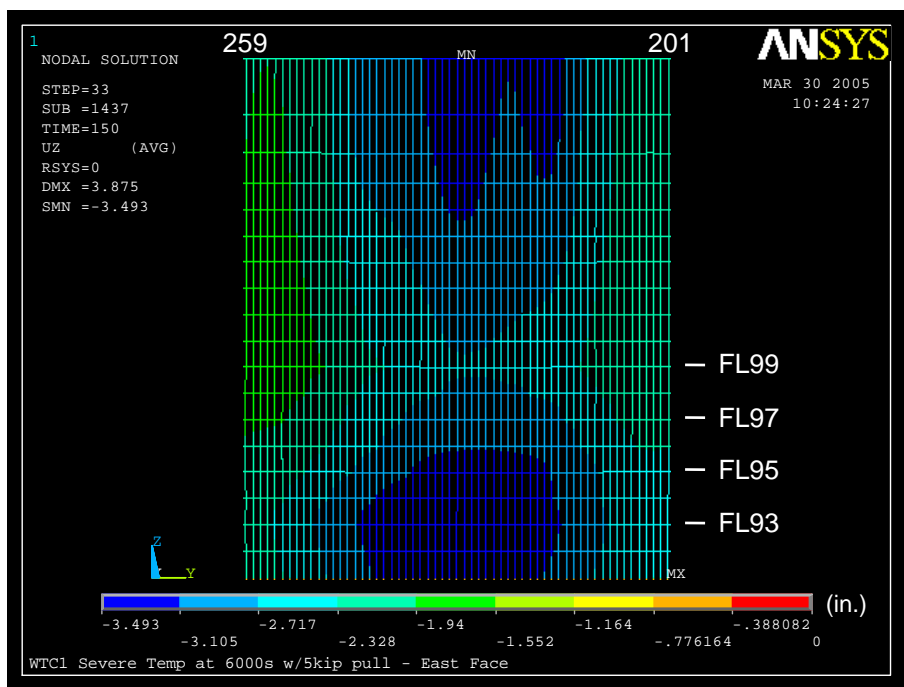


Figure 4–19. Vertical displacement of east wall of WTC 1 at 100 min for Case B conditions with 5 kip pull-in forces (downward displacement is negative).

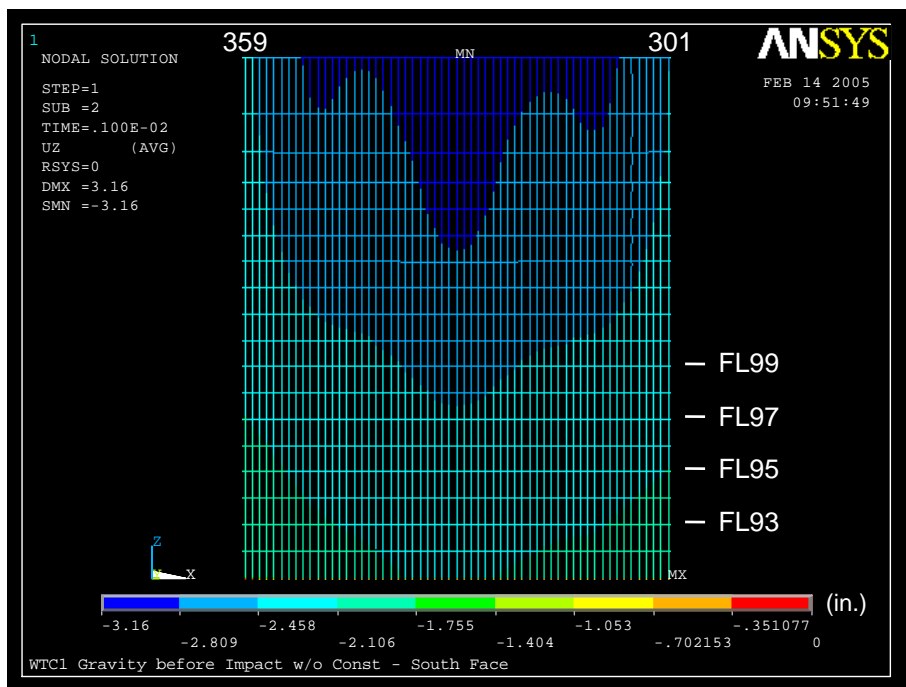


Figure 4–20. Vertical displacement of south wall of WTC 1 before aircraft impact (downward displacement is negative).

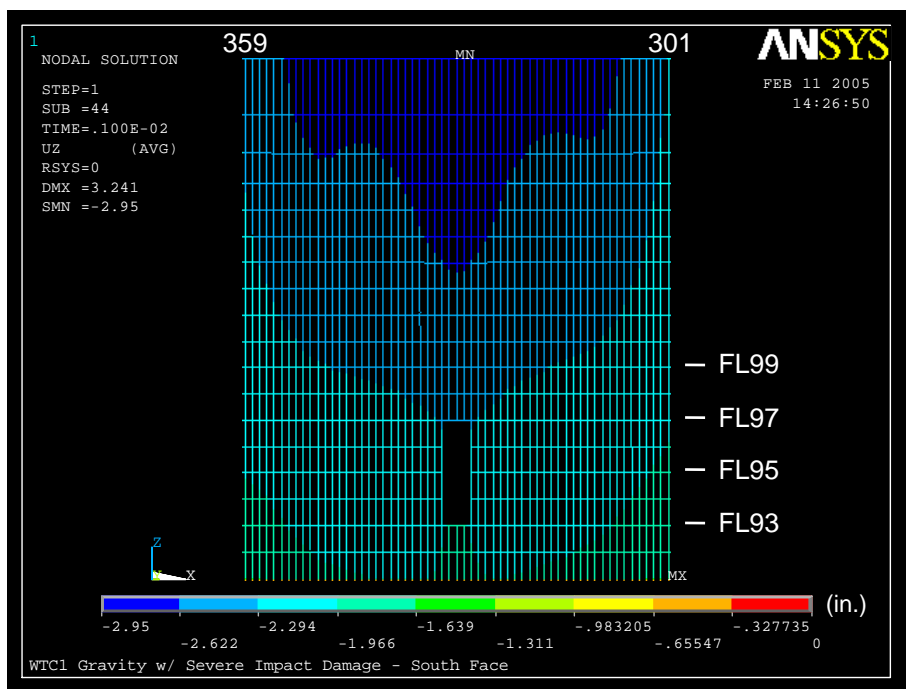


Figure 4–21. Vertical displacement of south wall of WTC 1 after aircraft impact for Case B conditions (downward displacement is negative).

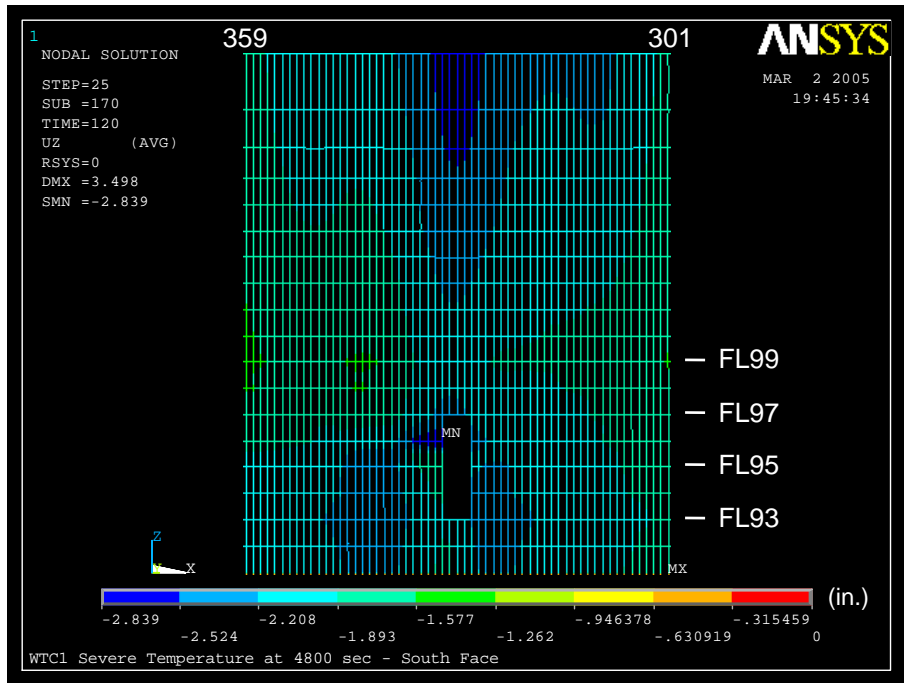


Figure 4–22. Vertical displacement of south wall of WTC 1 at 80 min for Case B conditions (downward displacement is negative).

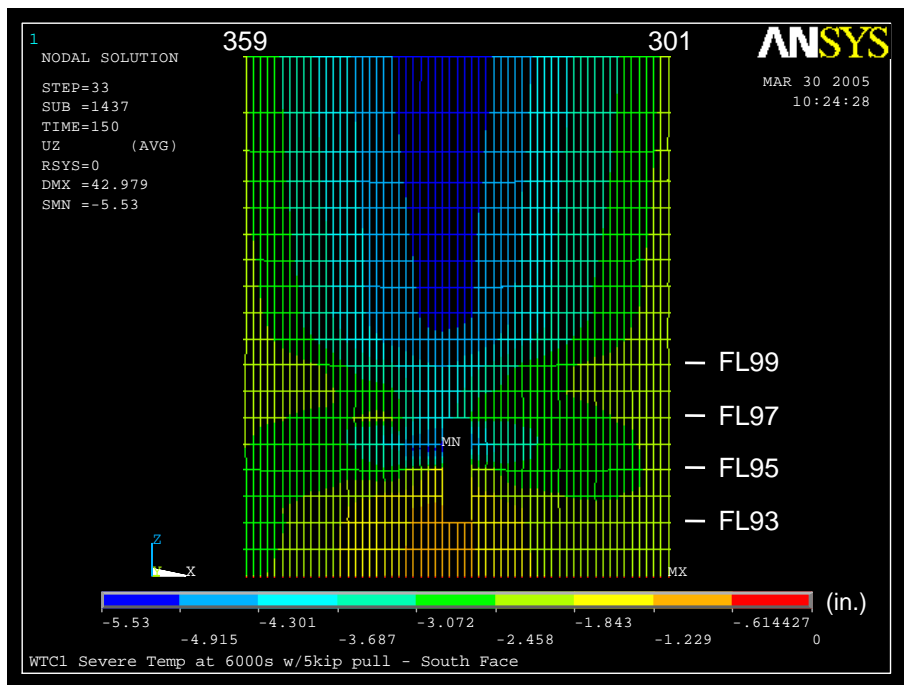
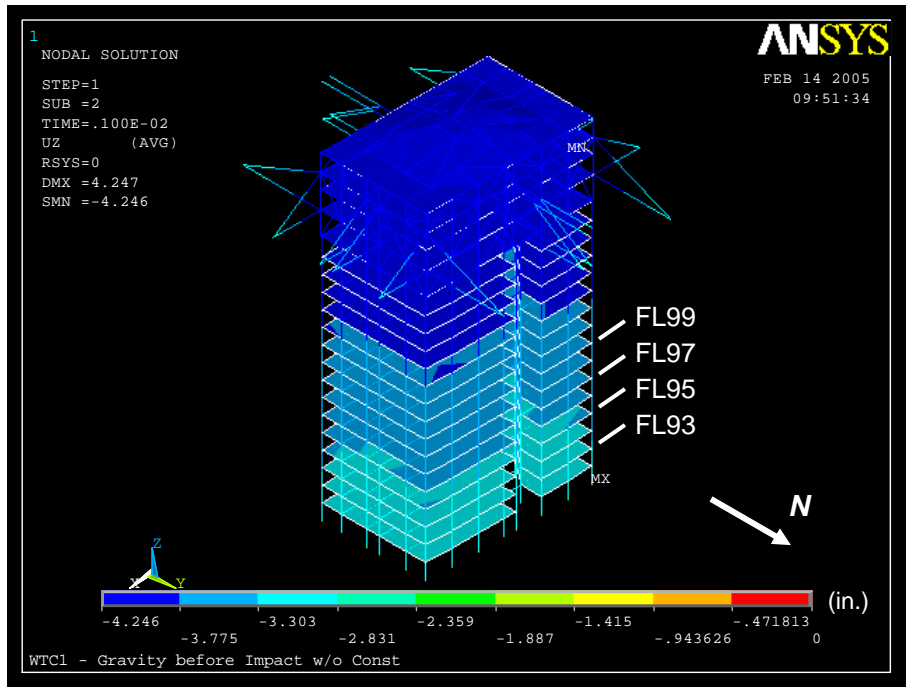
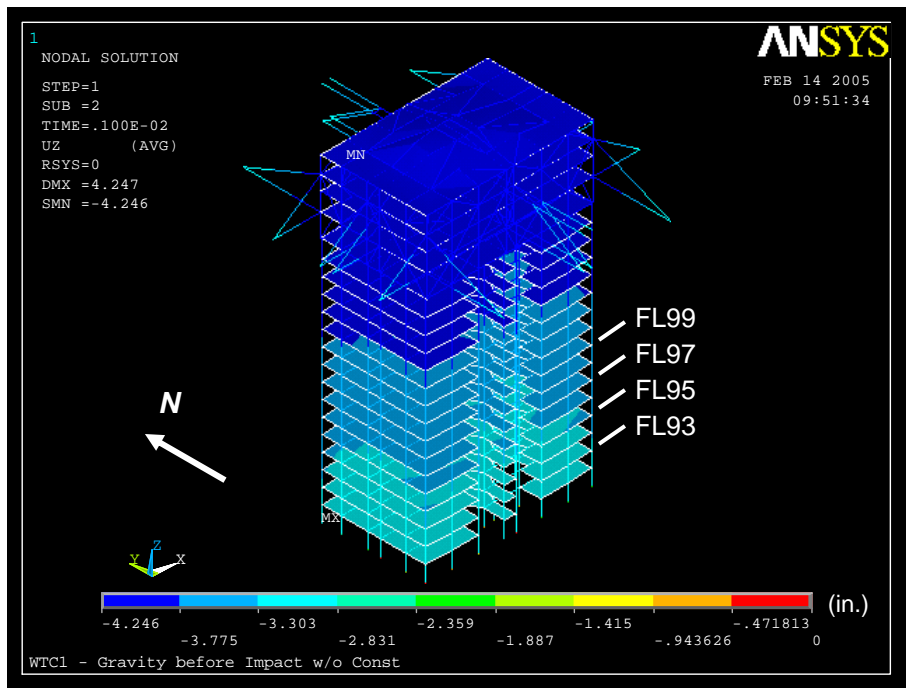


Figure 4–23. Vertical displacement of south wall of WTC 1 at 100 min for Case B conditions with 5 kip pull-in forces (downward displacement is negative).

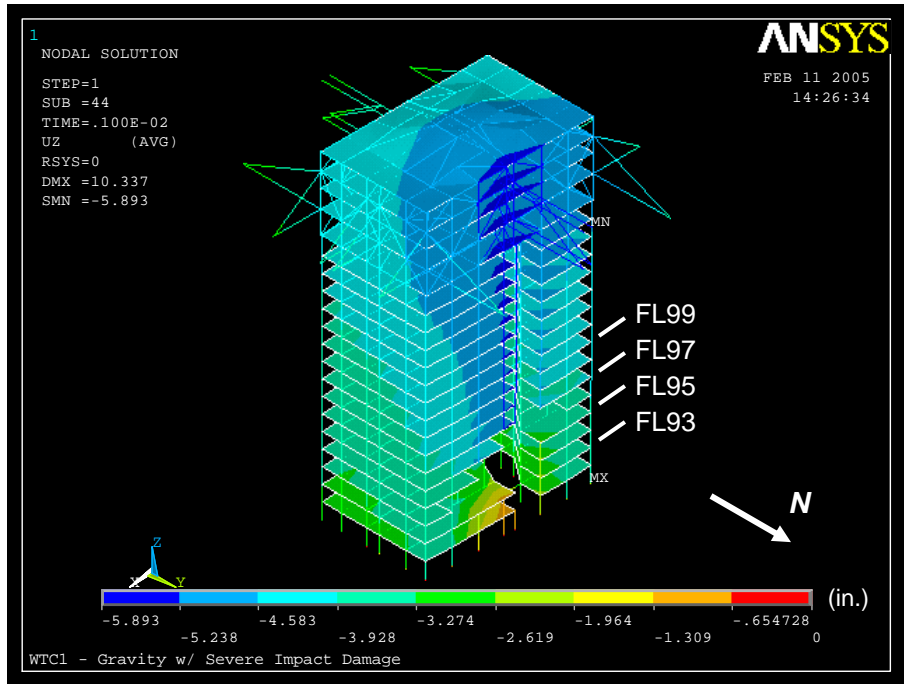


(a) North and east sides

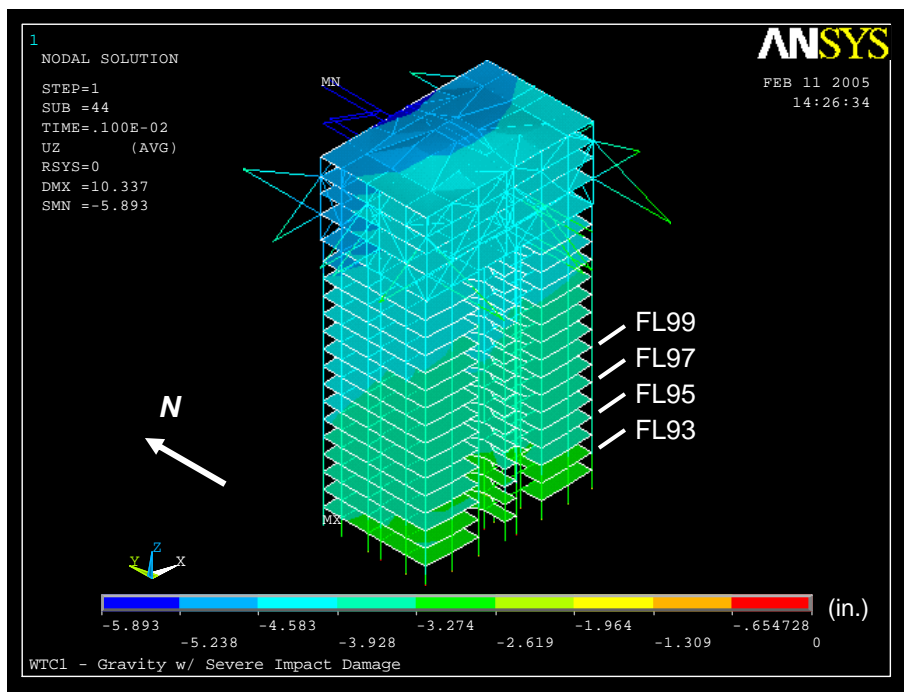


(b) South and west sides

Figure 4–24. Vertical displacement of core of WTC 1 before aircraft impact (downward displacement is negative).

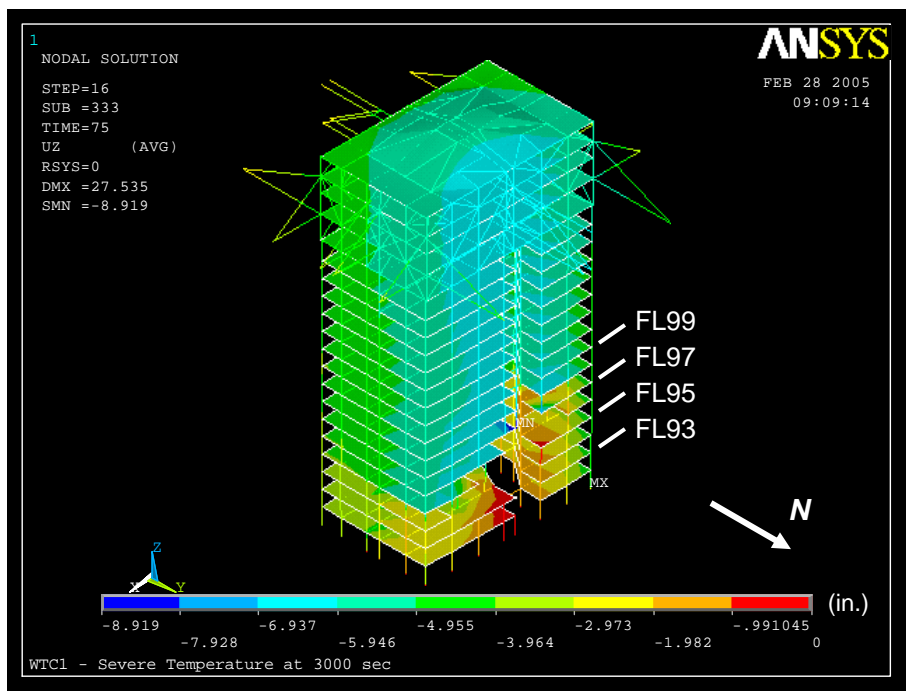


(a) North and east sides

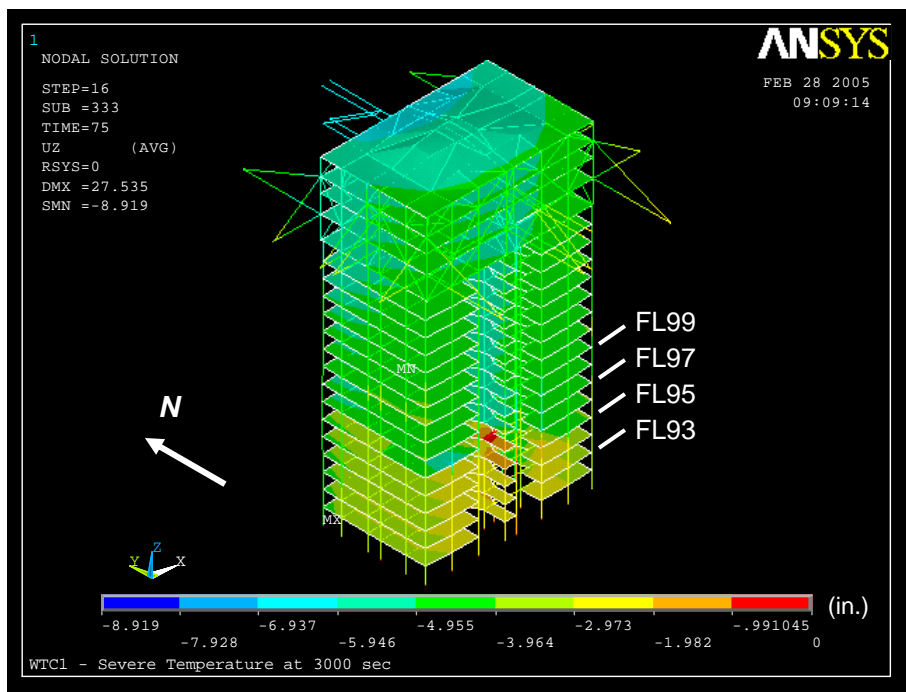


(b) South and west sides

Figure 4–25. Vertical displacement of core of WTC 1 after aircraft impact for Case B conditions (downward displacement is negative).

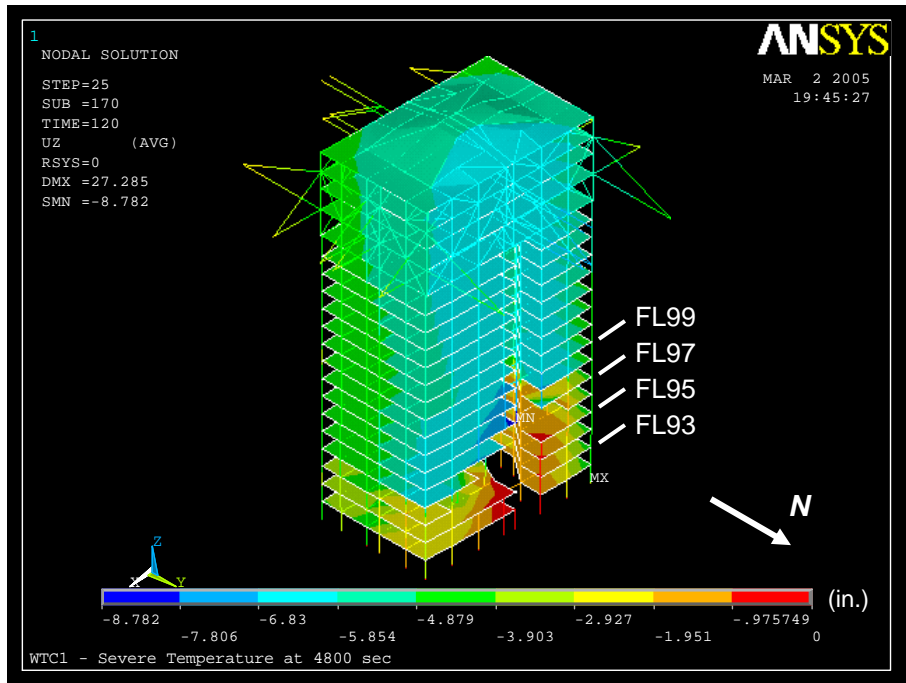


(a) North and east sides

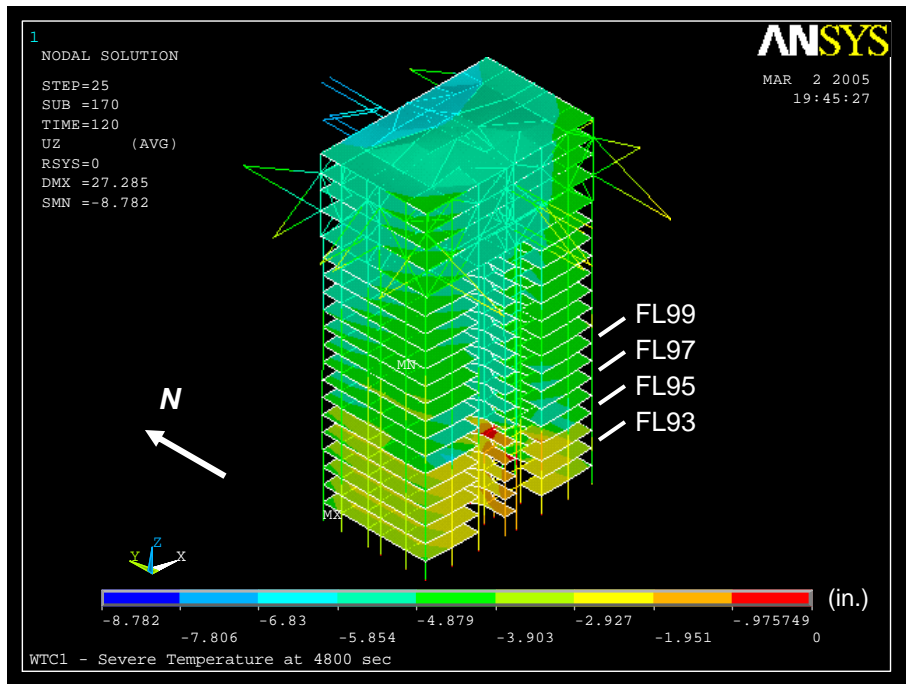


(b) South and west sides

Figure 4–26. Vertical displacement of core of WTC 1 at 50 min for Case B conditions (downward displacement is negative).

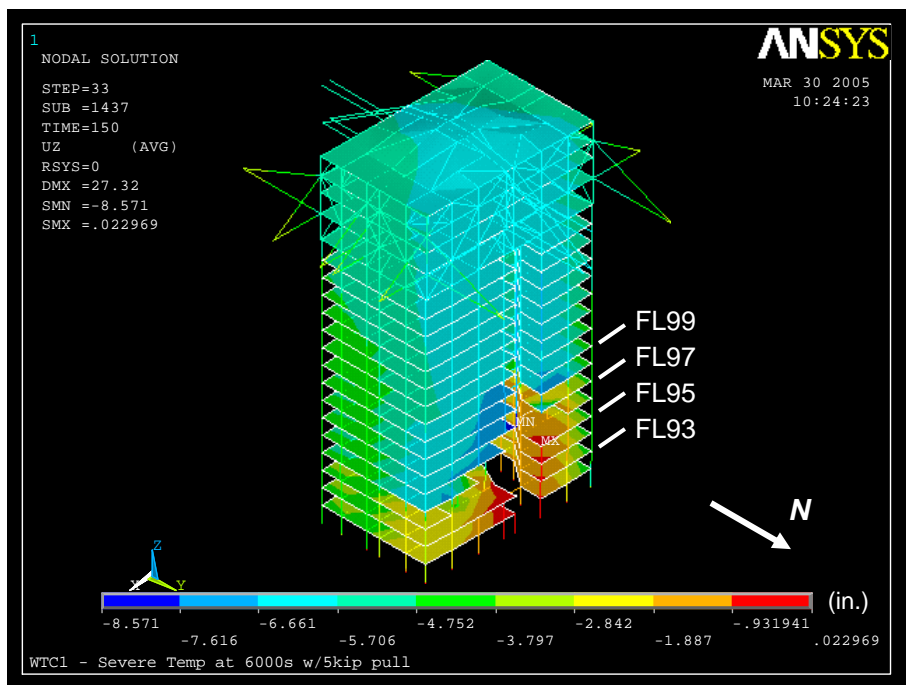


(a) North and east sides

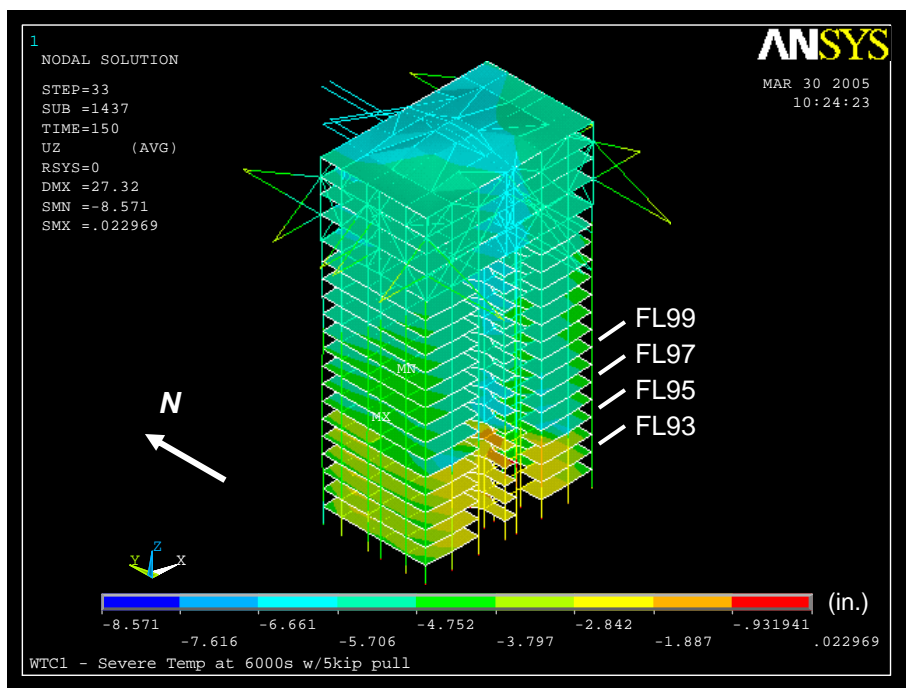


(b) South and west sides

Figure 4-27. Vertical displacement of core of WTC 1 at 80 min for Case B conditions (downward displacement is negative).

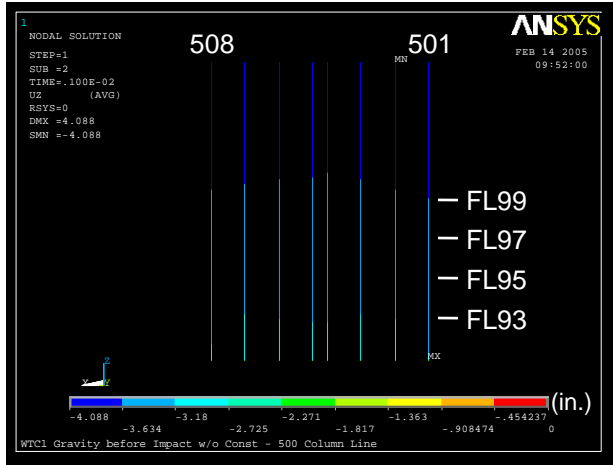


(a) North and east sides

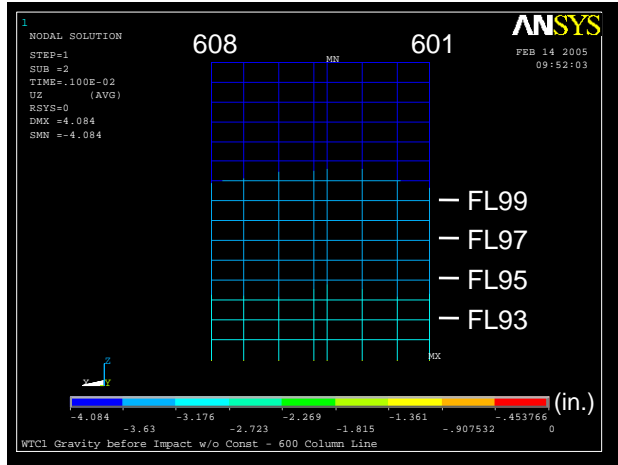


(b) South and west sides

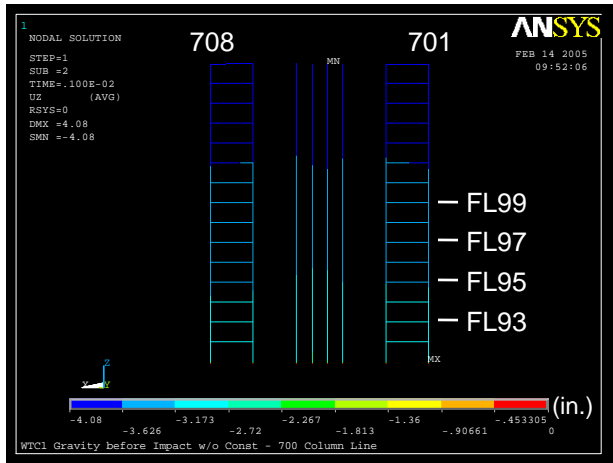
Figure 4–28. Vertical displacement of core of WTC 1 at 100 min for Case B conditions with 5 kip pull-in forces (downward displacement is negative).



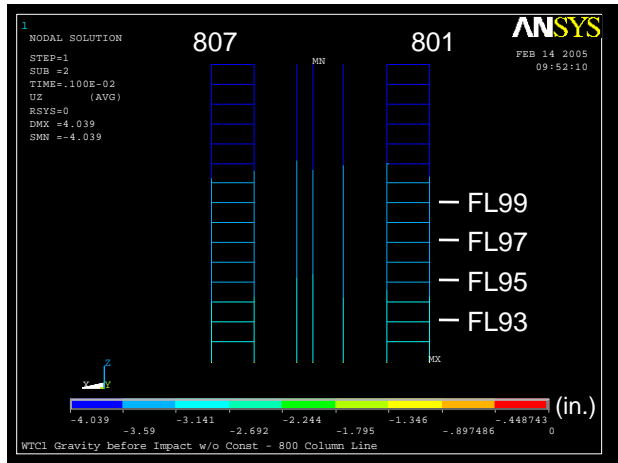
(a) 500 series columns



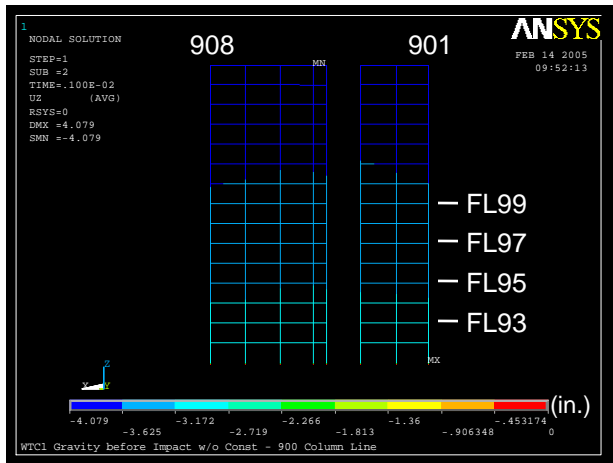
(b) 600 series columns



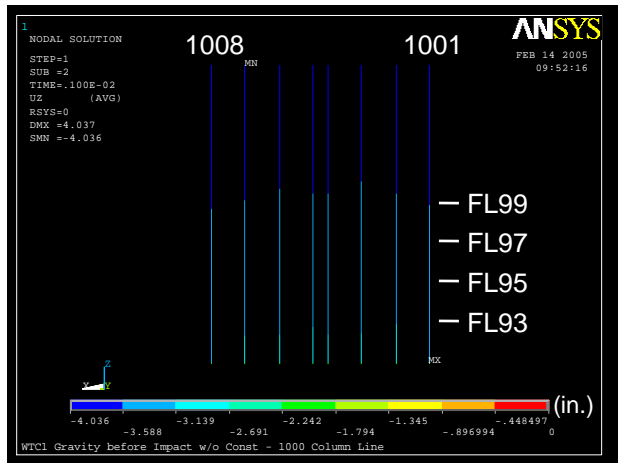
(c) 700 series columns



(d) 800 series columns

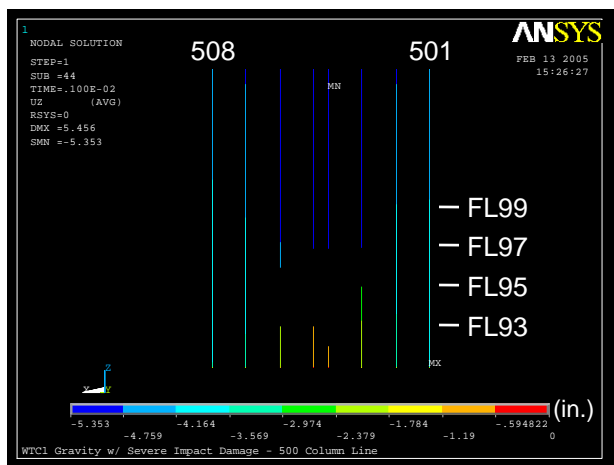


(e) 900 series columns

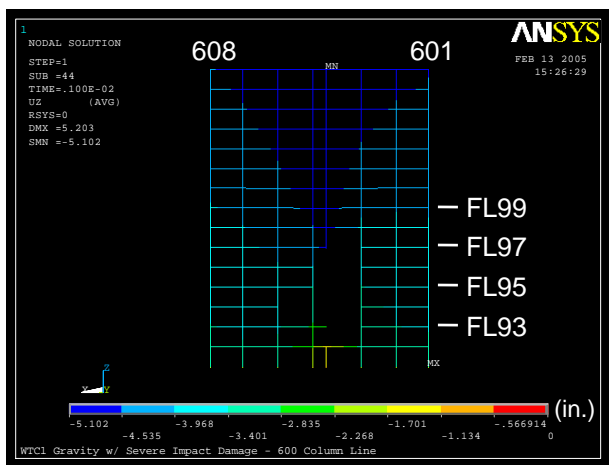


(f) 1000 series columns

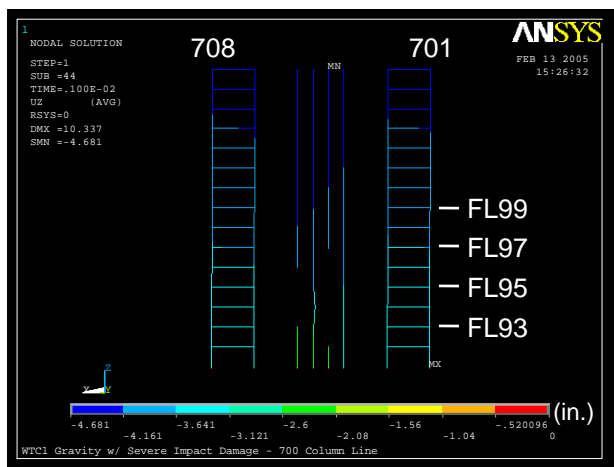
Figure 4–29. Vertical displacement of core columns of WTC 1 before aircraft impact (downward displacement is negative).



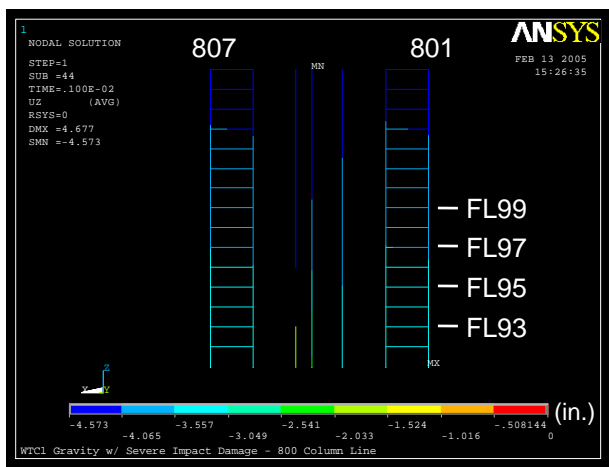
(a) 500 series columns



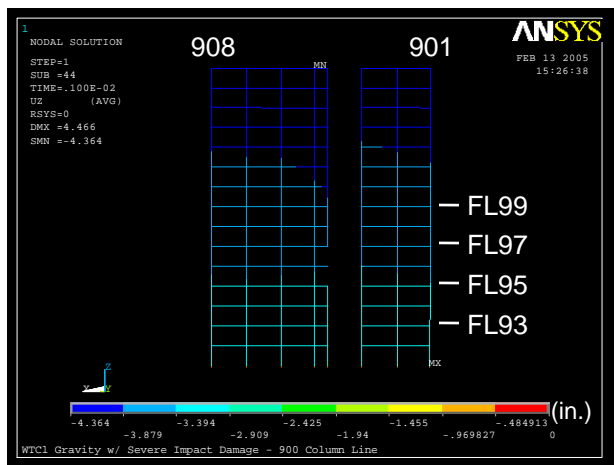
(b) 600 series columns



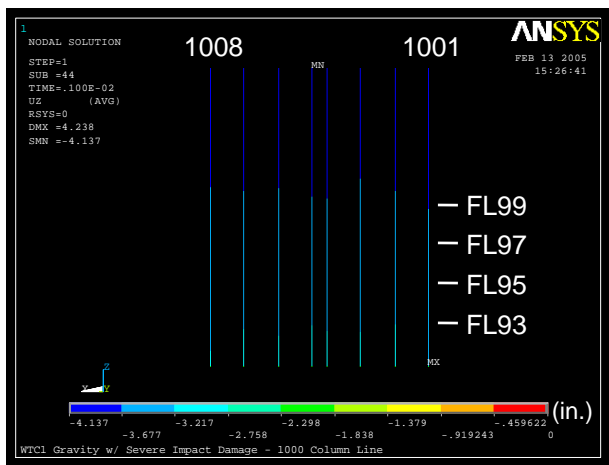
(c) 700 series columns



(d) 800 series columns

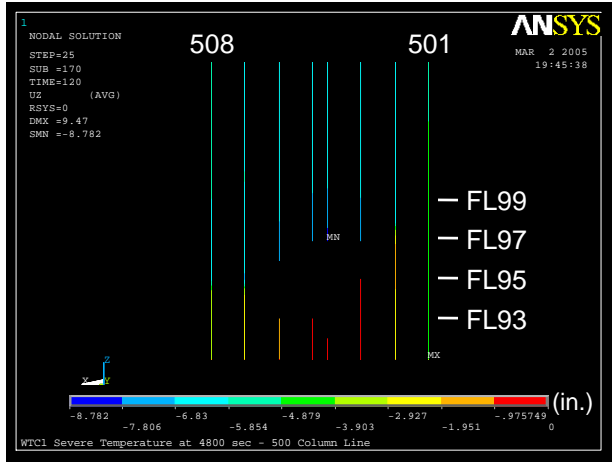


(e) 900 series columns

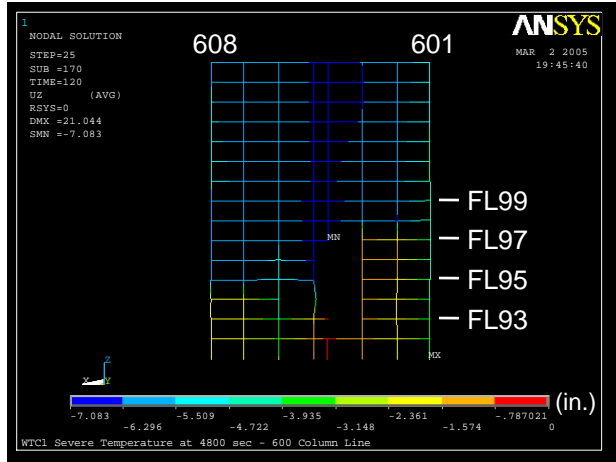


(f) 1000 series columns

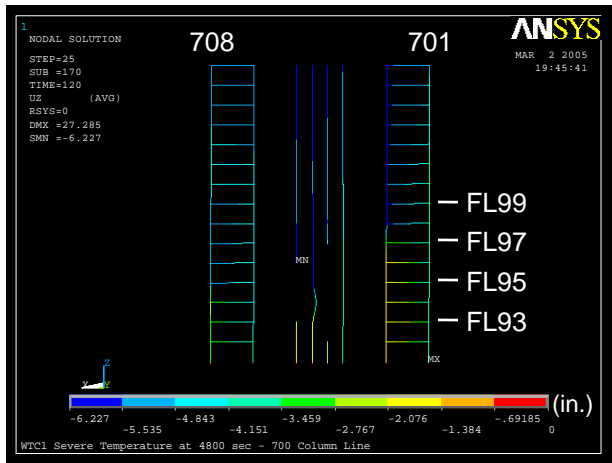
Figure 4–30. Vertical displacement of core columns of WTC 1 after aircraft impact for Case B conditions (downward displacement is negative).



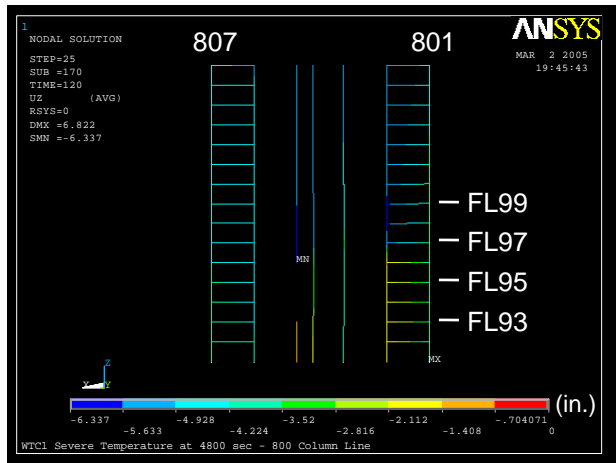
(a) 500 series columns



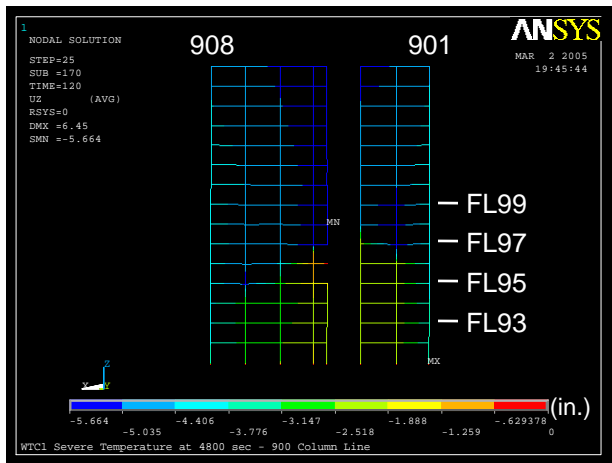
(b) 600 series columns



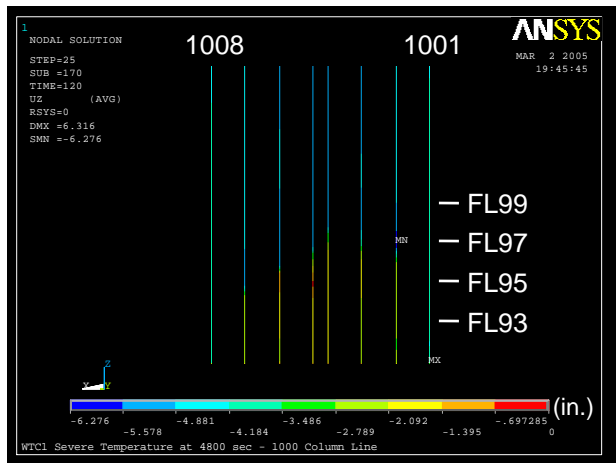
(c) 700 series columns



(d) 800 series columns

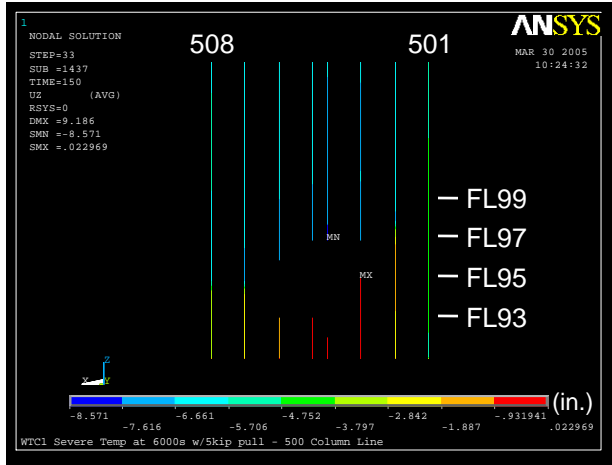


(e) 900 series columns

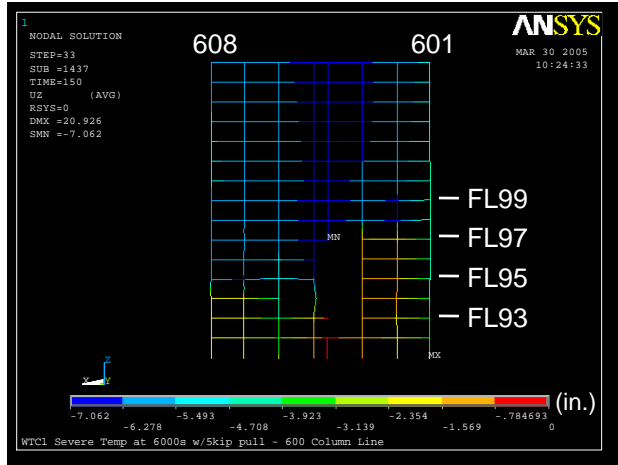


(f) 1000 series columns

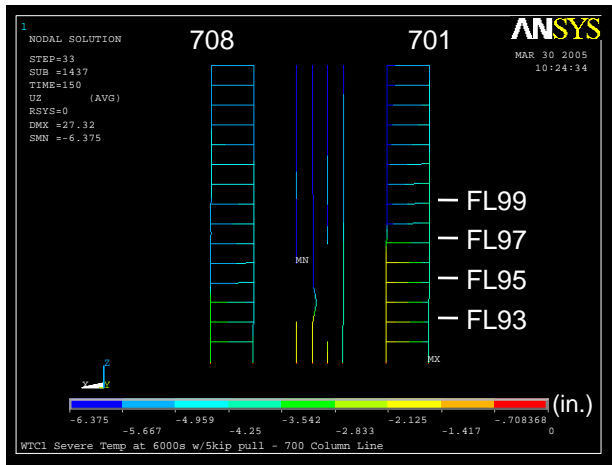
Figure 4–31. Vertical displacement of core columns of WTC 1 at 80 min for Case B conditions (downward displacement is negative).



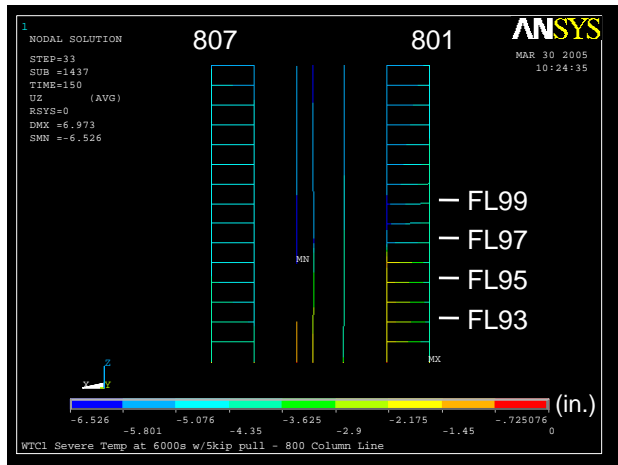
(a) 500 series columns



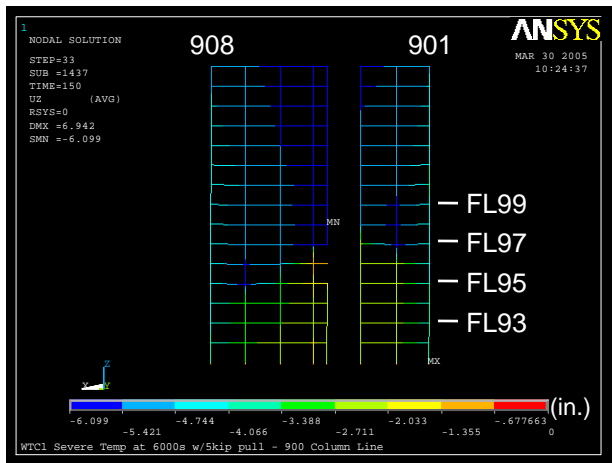
(b) 600 series columns



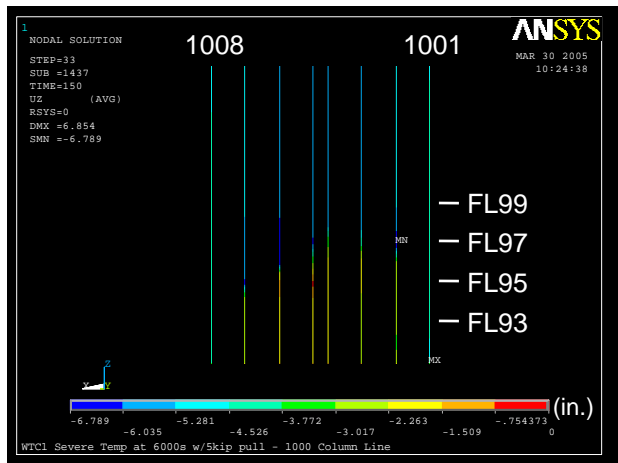
(c) 700 series columns



(d) 800 series columns



(e) 900 series columns



(f) 1000 series columns

Figure 4–32. Vertical displacement of core columns of WTC 1 at 100 min for Case B conditions with 5 kip pull-in forces (downward displacement is negative).

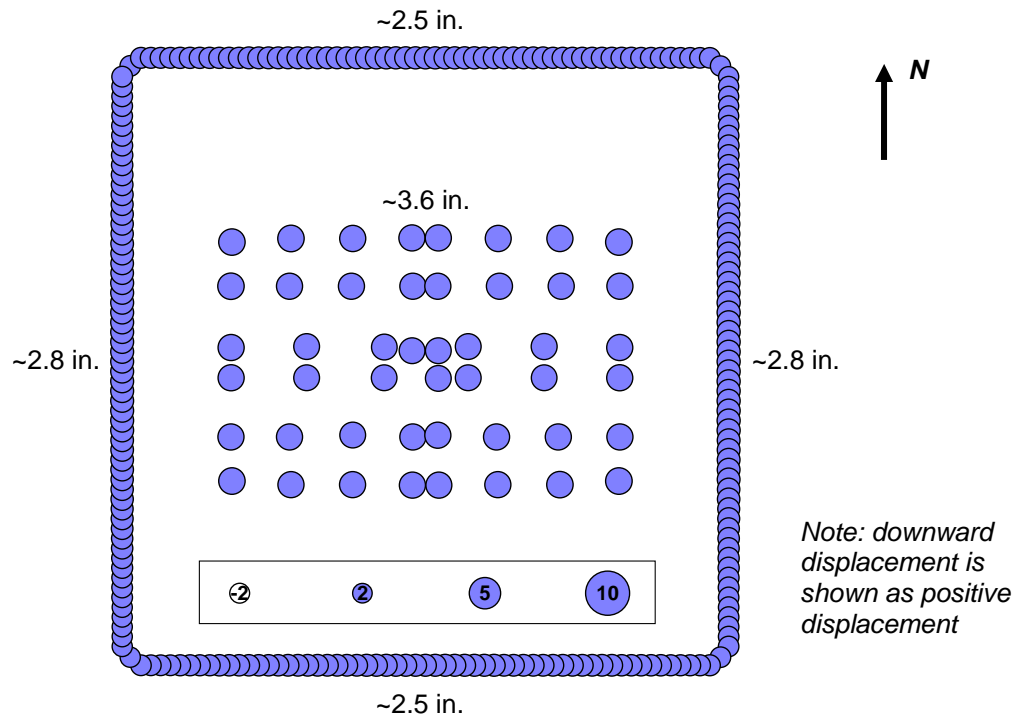


Figure 4-33. Vertical displacement at Floor 99 of WTC 1 before aircraft impact.

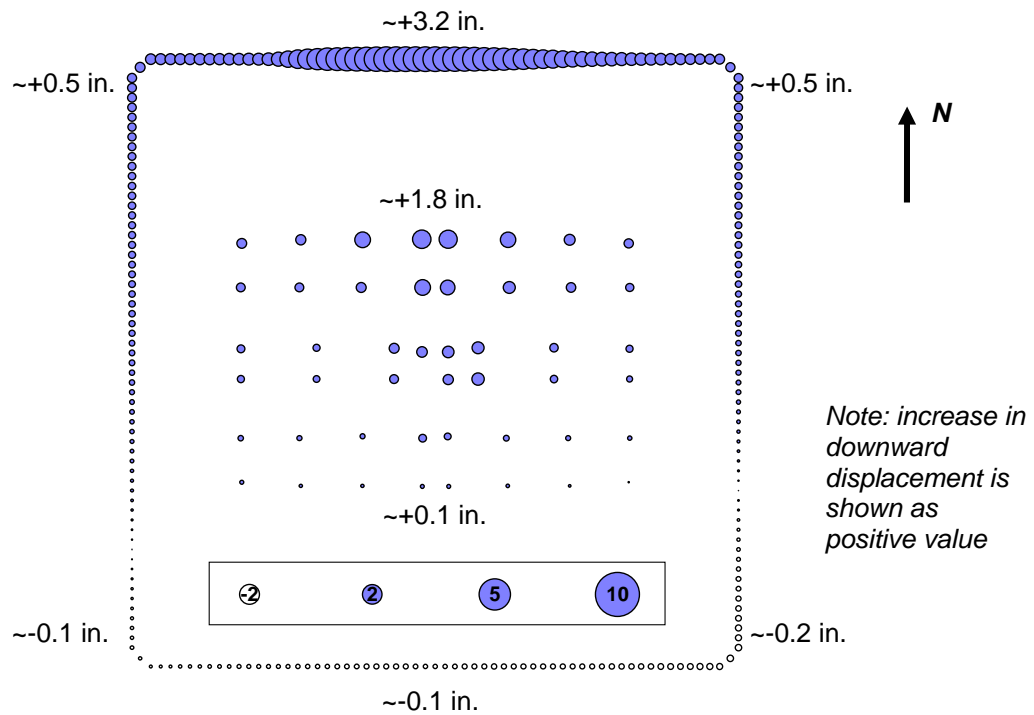


Figure 4-34. Change in vertical displacement at Floor 99 of WTC 1 from the time before impact to the time after impact for Case B conditions.

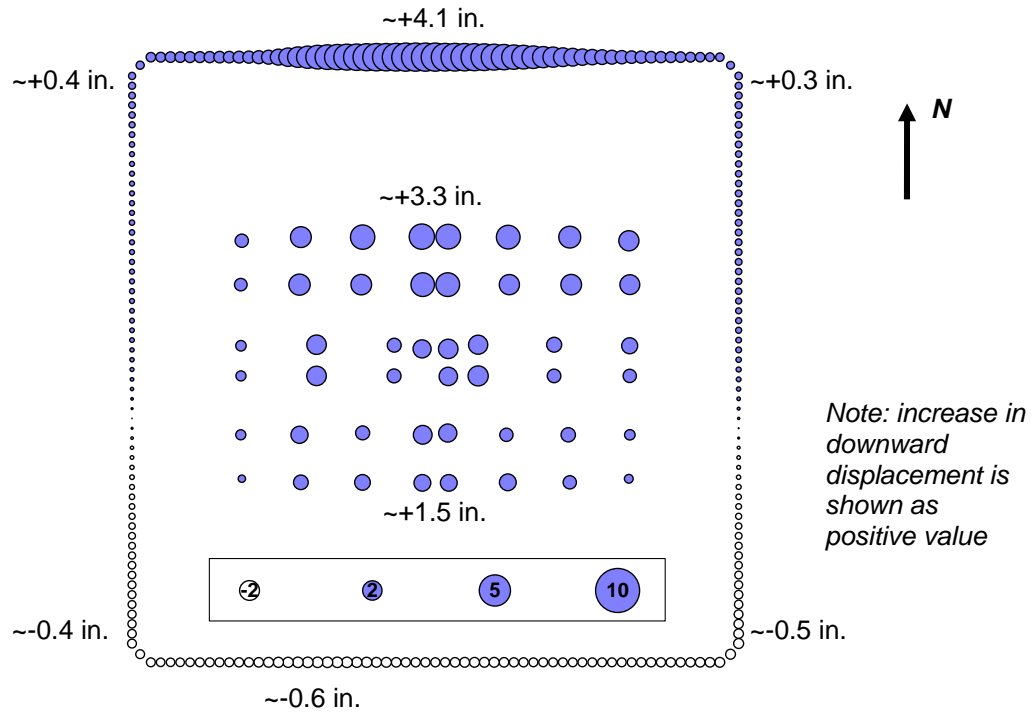


Figure 4–35. Change in vertical displacement at Floor 99 of WTC 1 from the time before impact to 50 min for Case B conditions.

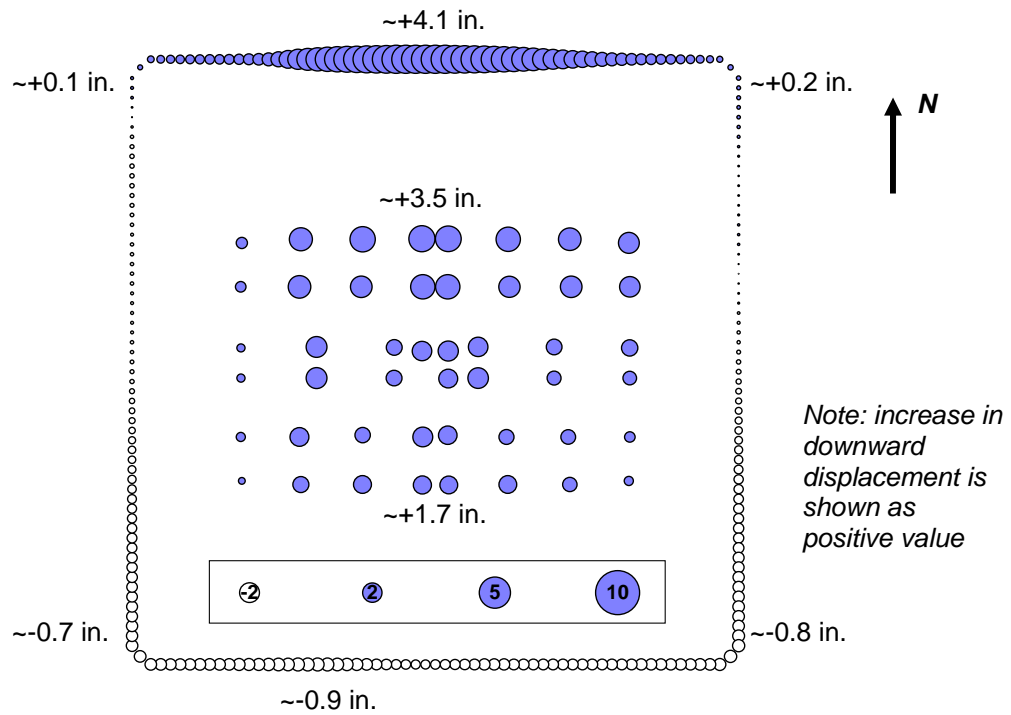


Figure 4–36. Change in vertical displacement at Floor 99 of WTC 1 from the time before impact to 80 min for Case B conditions.

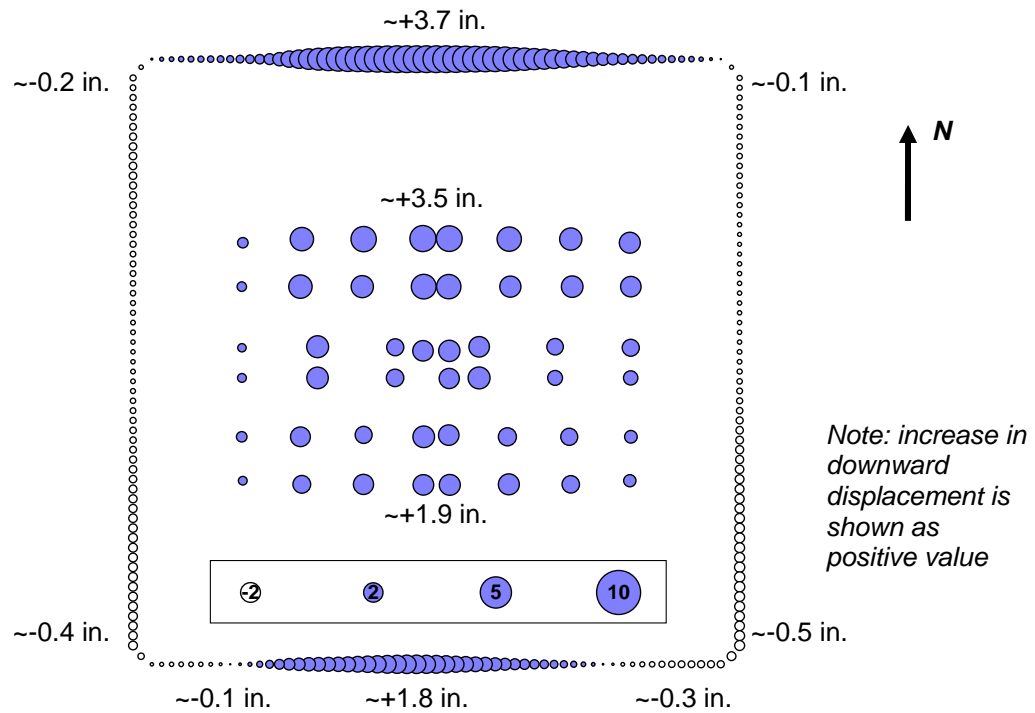


Figure 4–37. Change in vertical displacement at Floor 99 of WTC 1 from the time before impact to 100 min for Case B conditions with 5 kip pull-in forces.

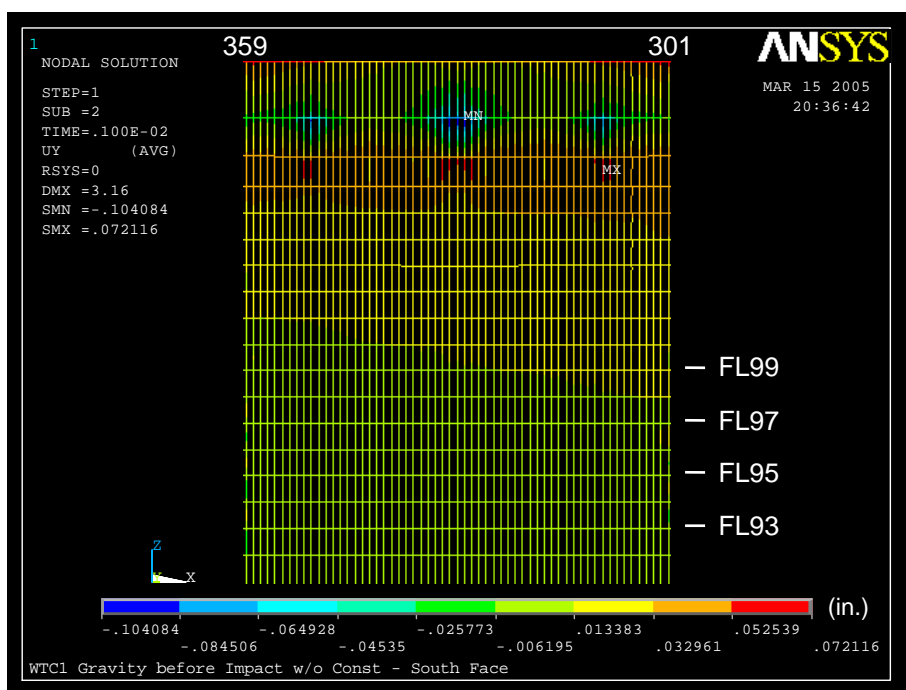


Figure 4–38. Out-of-plane displacement of south wall of WTC 1 before aircraft impact (inward displacement is positive).

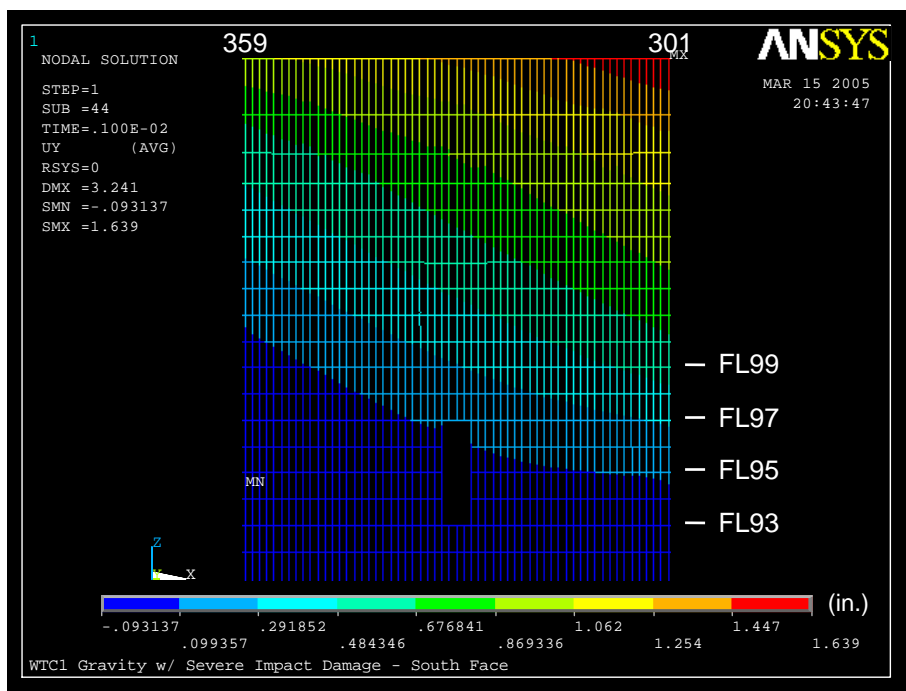


Figure 4–39. Out-of-plane displacement of south wall of WTC 1 after aircraft impact for Case B conditions (inward displacement is positive).

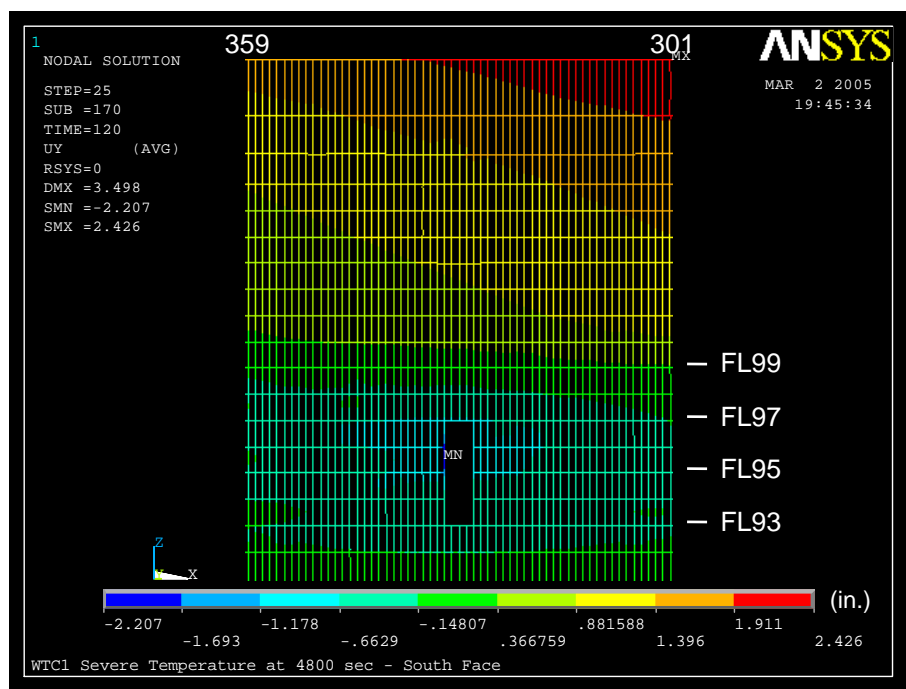


Figure 4–40. Out-of-plane displacement of south wall of WTC 1 at 80 min (at the end of Analysis Step 17) for Case B conditions (inward displacement is positive).

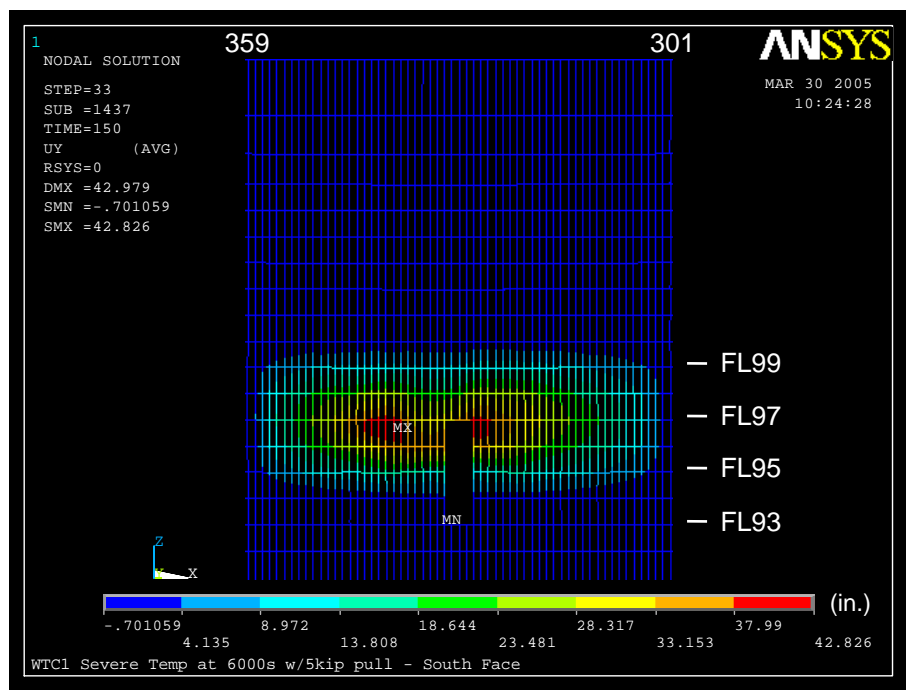


Figure 4–41. Out-of-plane displacement of south wall of WTC 1 at 100 min for Case B conditions with 5 kip pull-in forces (inward displacement is positive).

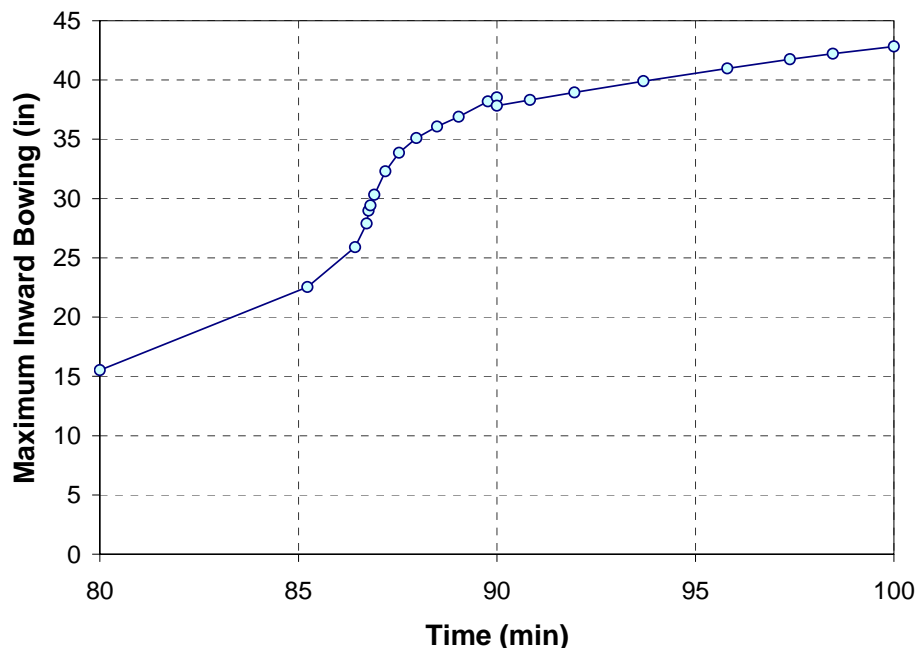


Figure 4-42. Time history of maximum out-of-plane displacement of south wall of WTC 1 for Case B conditions with 5 kip pull-in forces (from Analysis Step 18 to Step 21).

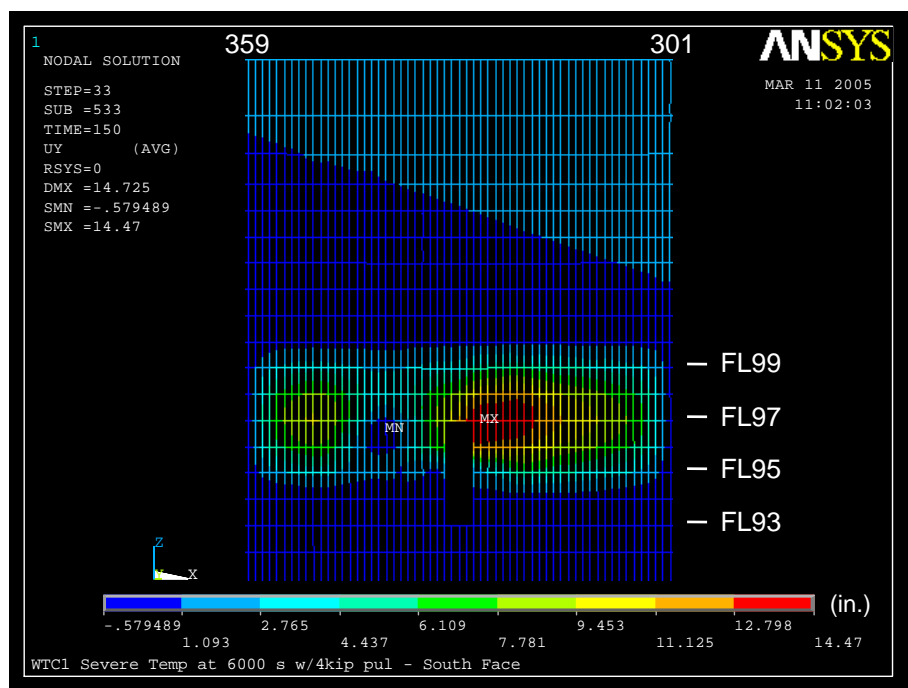


Figure 4-43. Out-of-plane displacement of south wall of WTC 1 at 100 min for Case B conditions with 4 kip pull-in forces (inward displacement is positive).

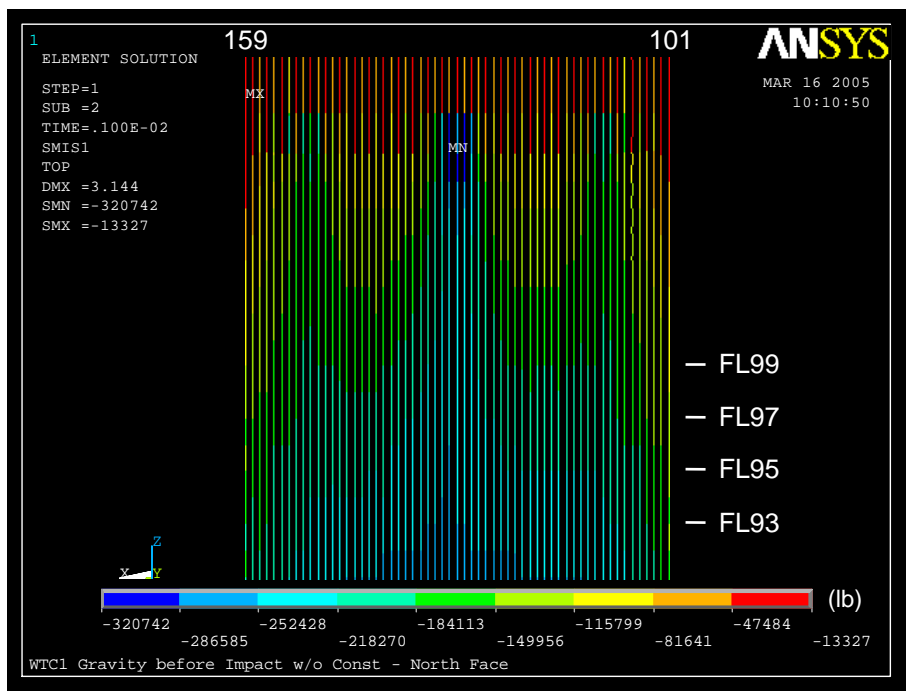


Figure 4–44. Axial load in exterior columns of north wall of WTC 1 before aircraft impact (compression is negative).

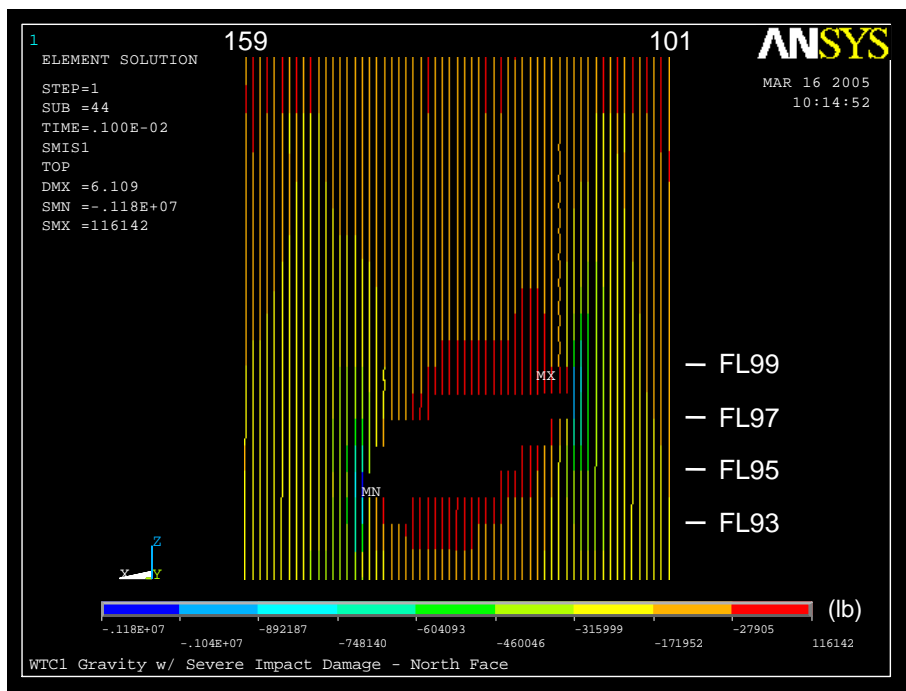


Figure 4–45. Axial load in exterior columns of north wall of WTC 1 after aircraft impact for Case B conditions (compression is negative).

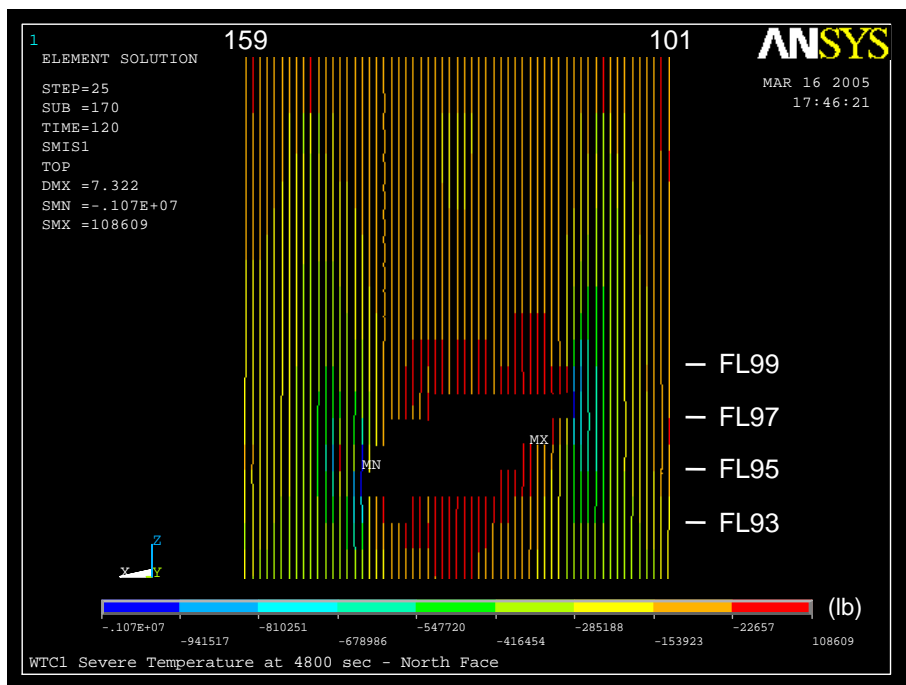


Figure 4–46. Axial load in exterior columns of north wall of WTC 1 at 80 min for the Case B conditions (compression is negative).

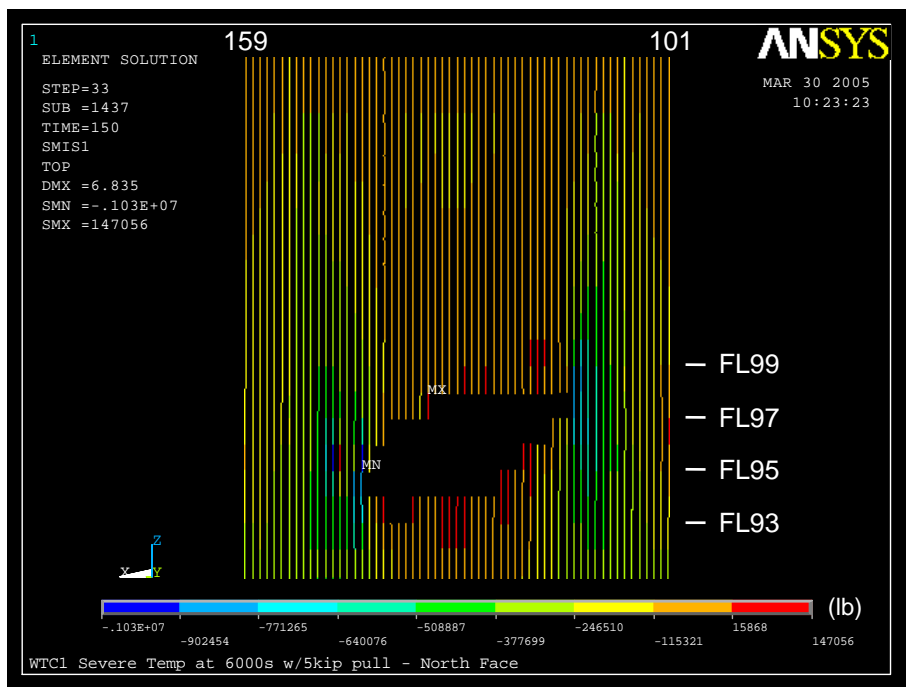


Figure 4–47. Axial load in exterior columns of north wall of WTC 1 at 100 min for Case B conditions with 5 kip pull-in forces (compression is negative).

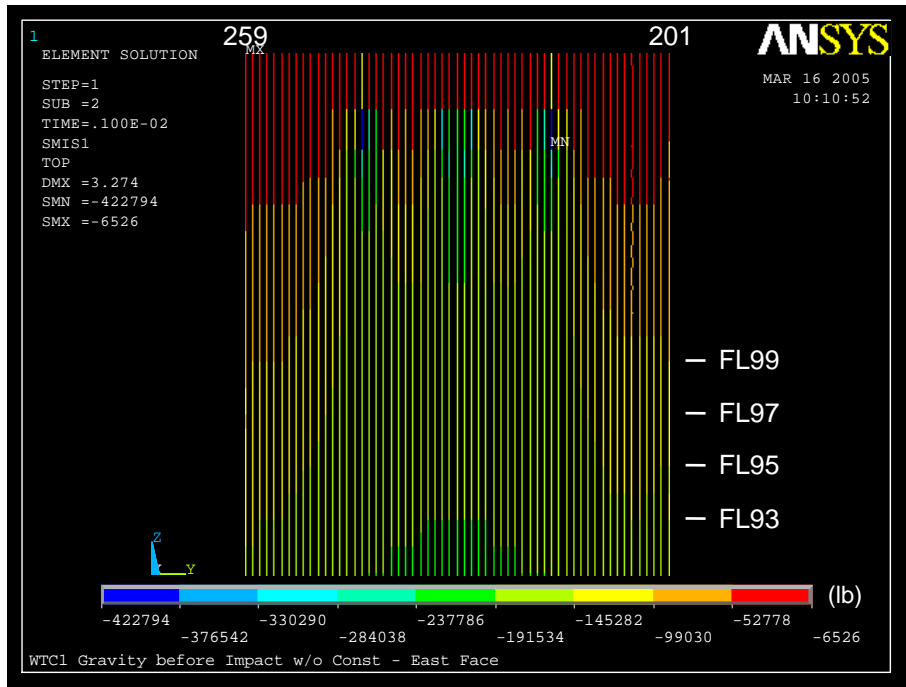


Figure 4–48. Axial load in exterior columns of east wall of WTC 1 before aircraft impact (compression is negative).

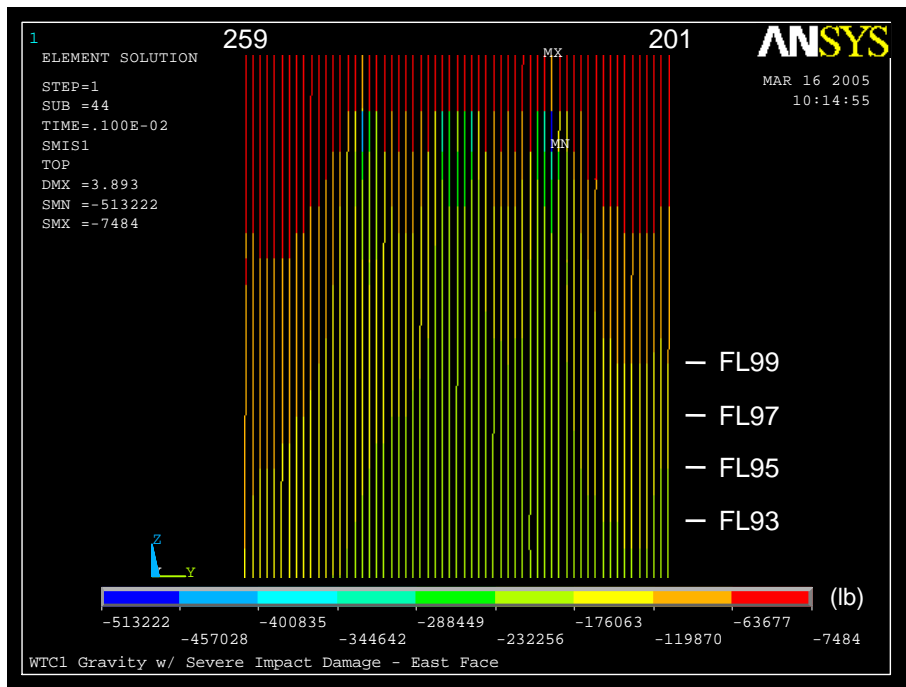


Figure 4–49. Axial load in exterior columns of east wall of WTC 1 after aircraft impact for Case B conditions (compression is negative).

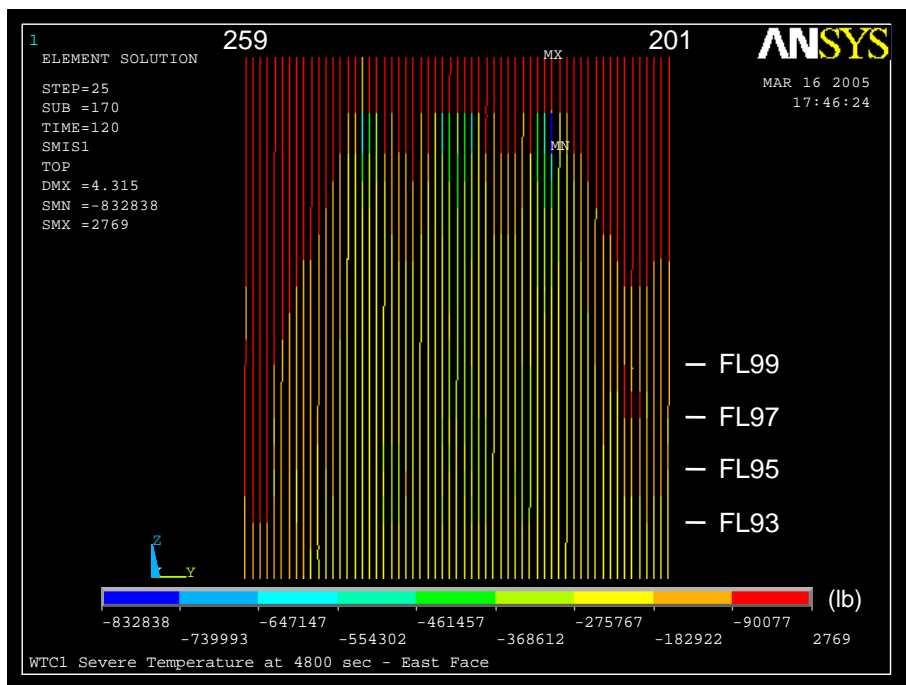


Figure 4–50. Axial load in exterior columns of east wall of WTC 1 at 80 min for the Case B conditions (compression is negative).

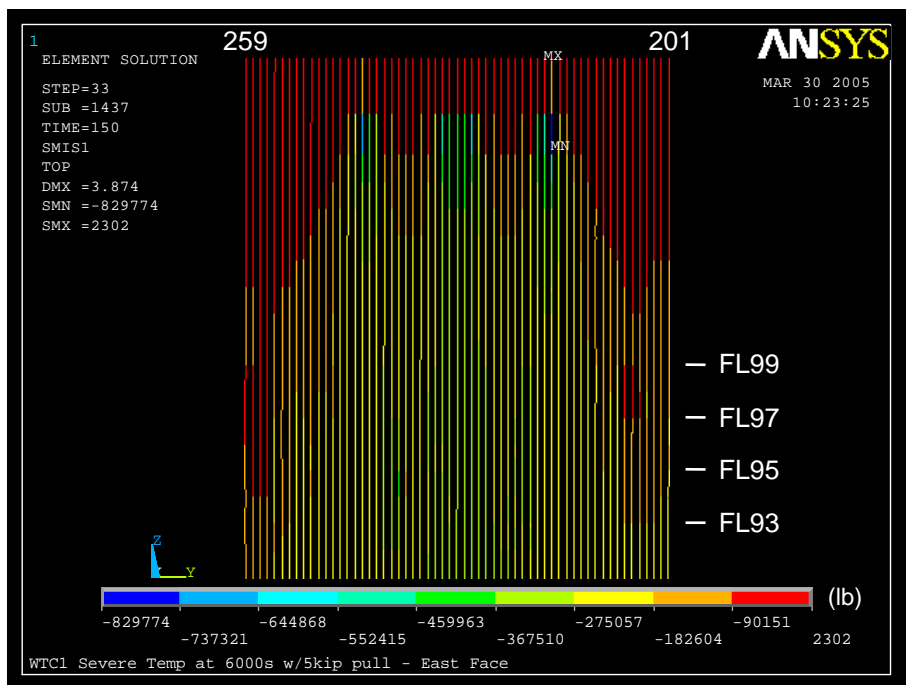


Figure 4–51. Axial load in exterior columns of east wall of WTC 1 at 100 min for the Case B conditions with 5 kip pull-in forces (compression is negative).

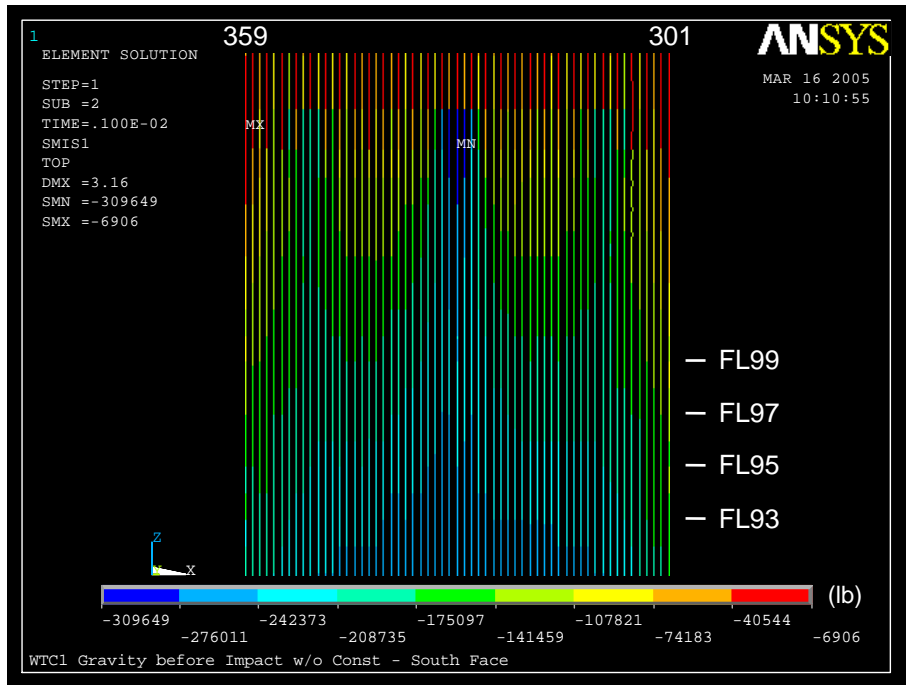


Figure 4–52. Axial load in exterior columns of south wall of WTC 1 before aircraft impact (compression is negative).

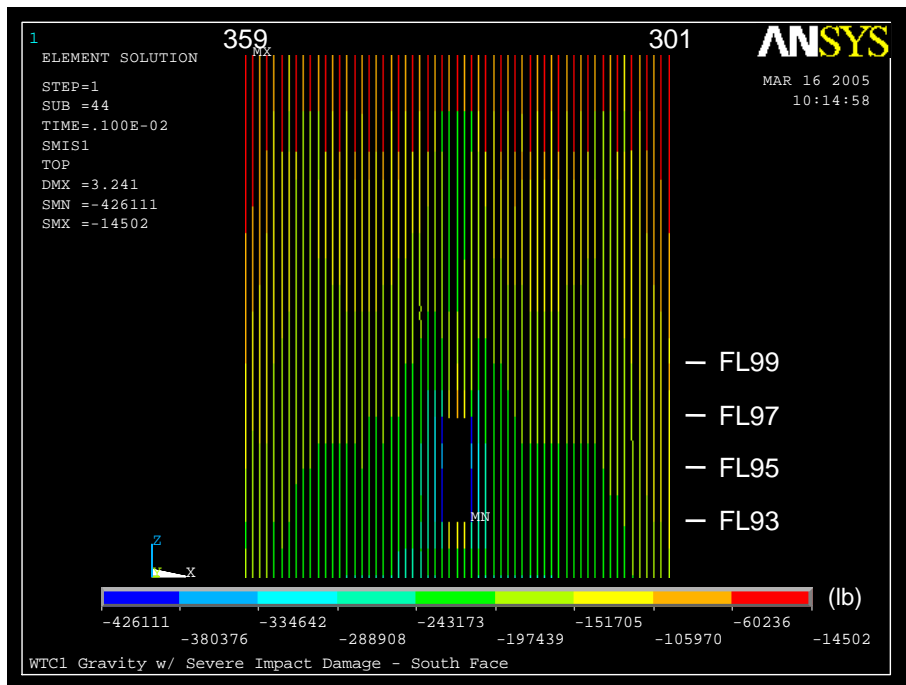


Figure 4–53. Axial load in exterior columns of south wall of WTC 1 after aircraft impact for Case B conditions (compression is negative).

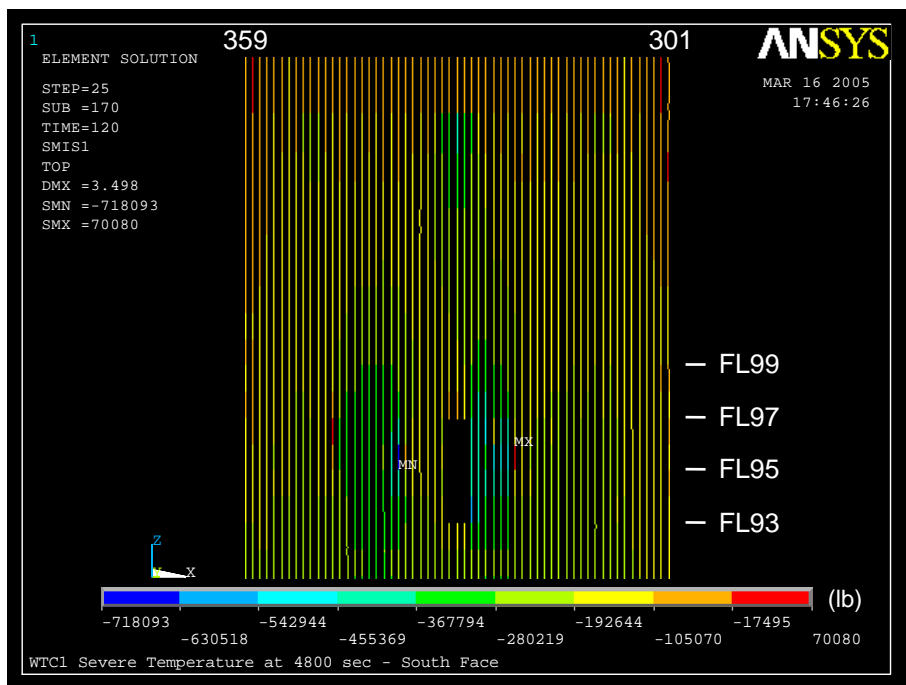


Figure 4–54. Axial load in exterior columns of south wall of WTC 1 at 80 min for Case B conditions (compression is negative).

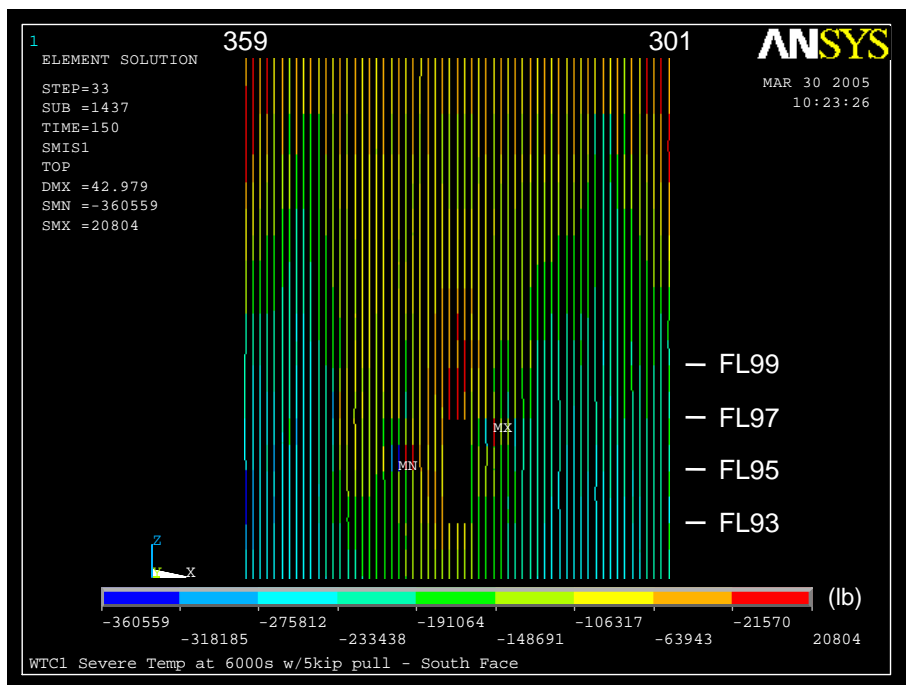


Figure 4–55. Axial load in exterior columns of south wall of WTC 1 at 100 min for Case B conditions with 5 kip pull-in forces (compression is negative).

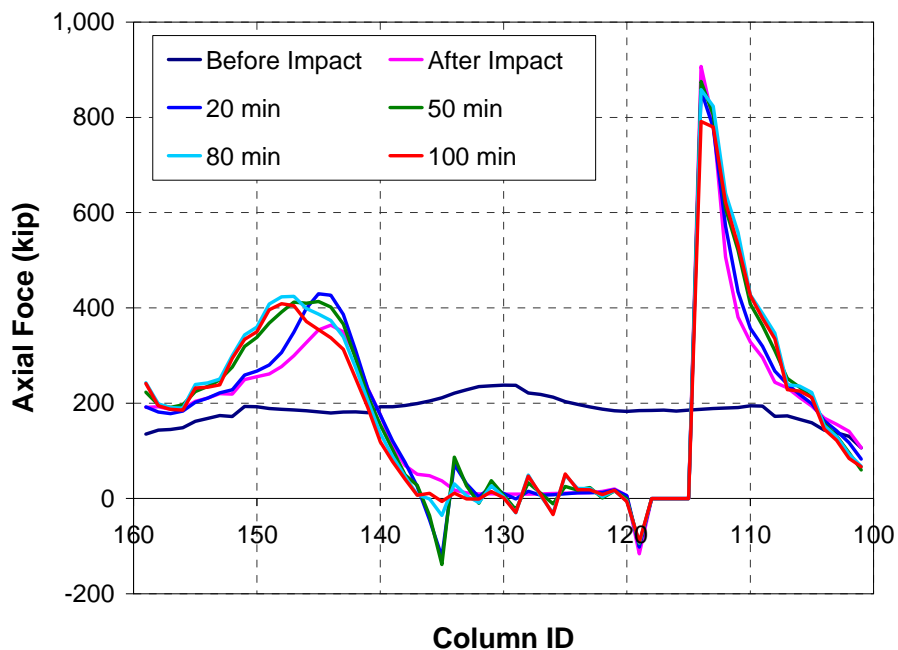


Figure 4–56. Variation of axial load in exterior columns at Floor 98 of north wall of WTC 1 for Case B conditions with 5 kip pull-in forces (compression is positive).

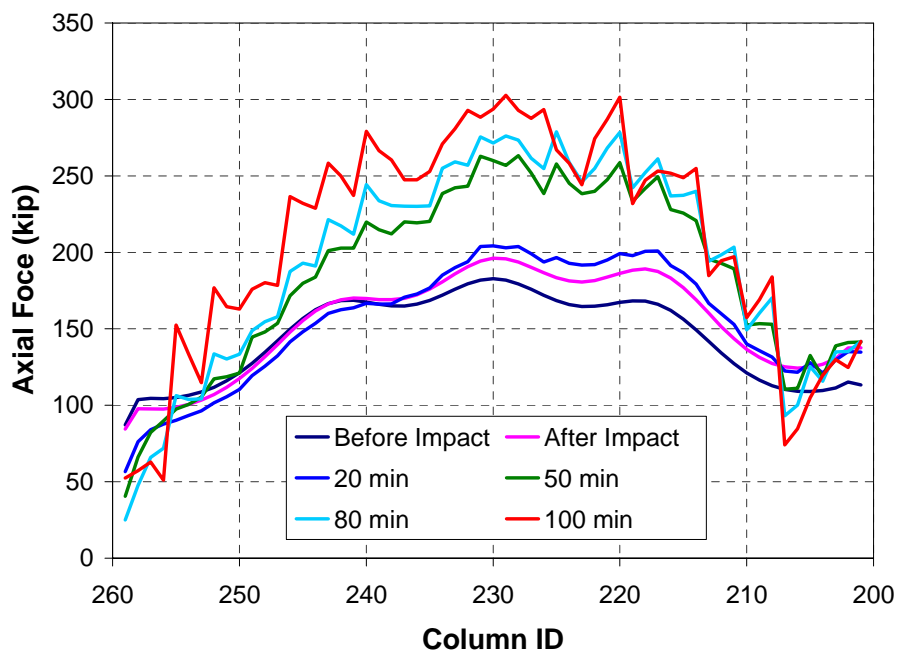


Figure 4–57. Variation of axial load in exterior columns at Floor 98 of east wall of WTC 1 for Case B conditions with 5 kip pull-in forces (compression is positive).

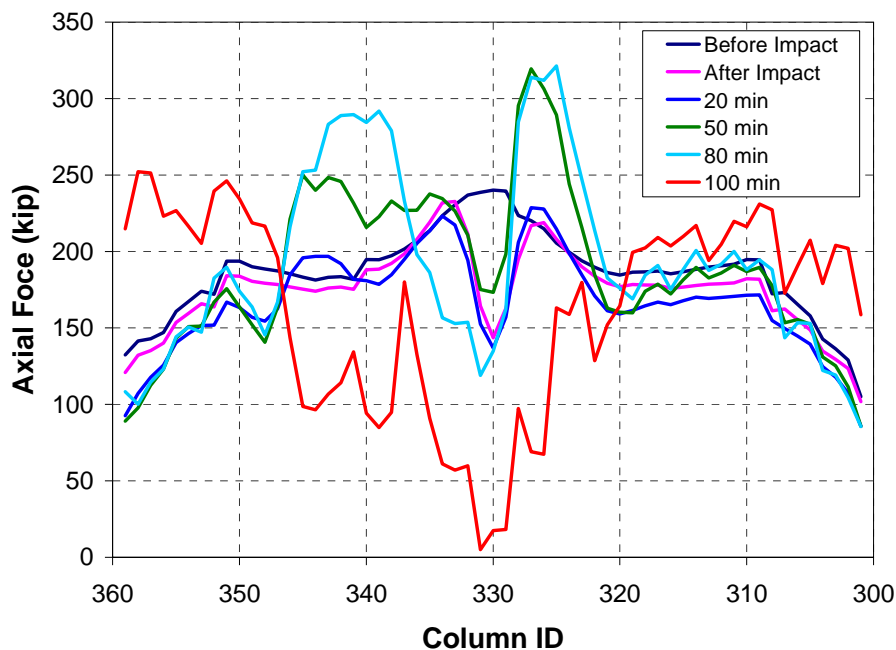


Figure 4–58. Variation of axial load in exterior columns at Floor 98 of south wall of WTC 1 for Case B conditions with 5 kip pull-in forces (compression is positive).

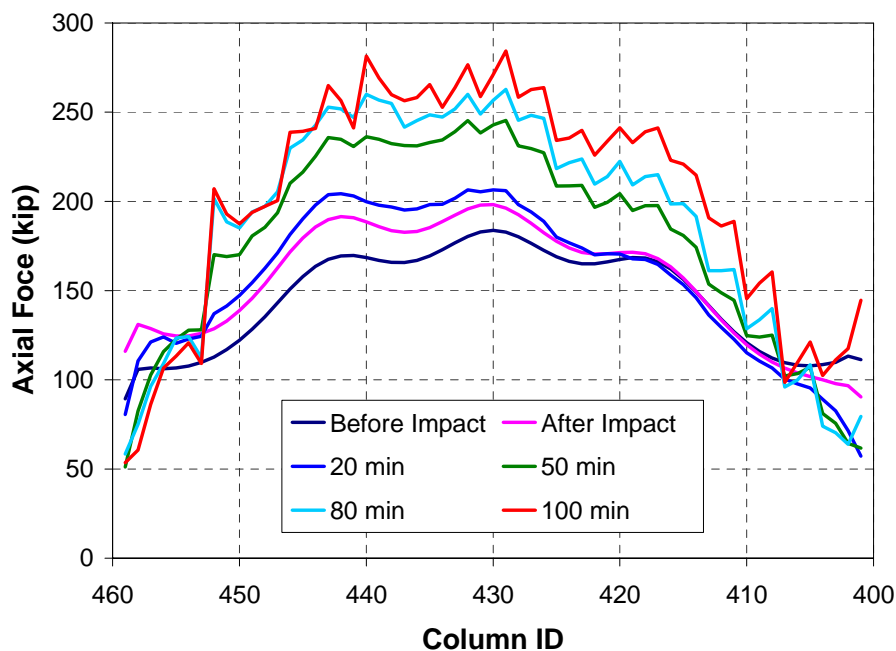
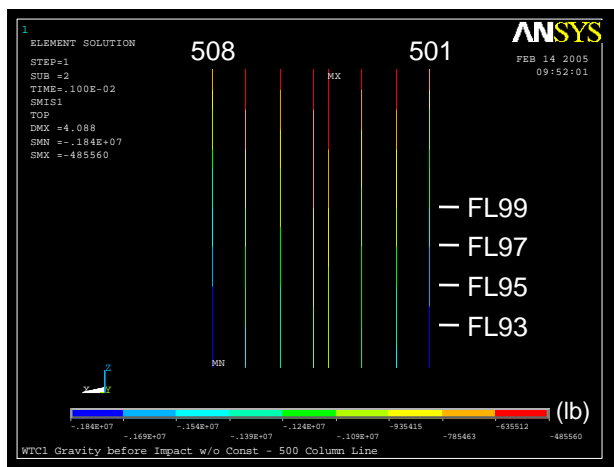
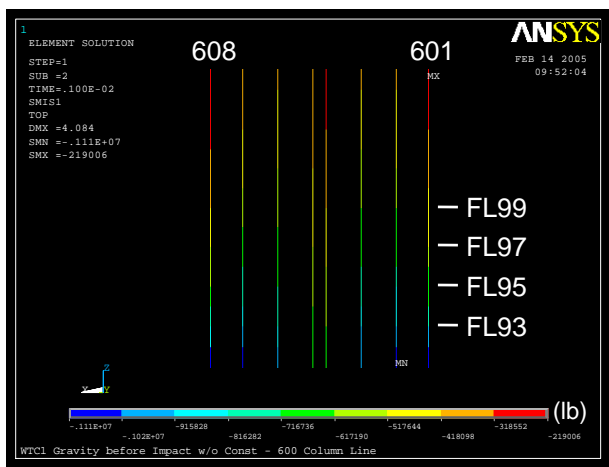


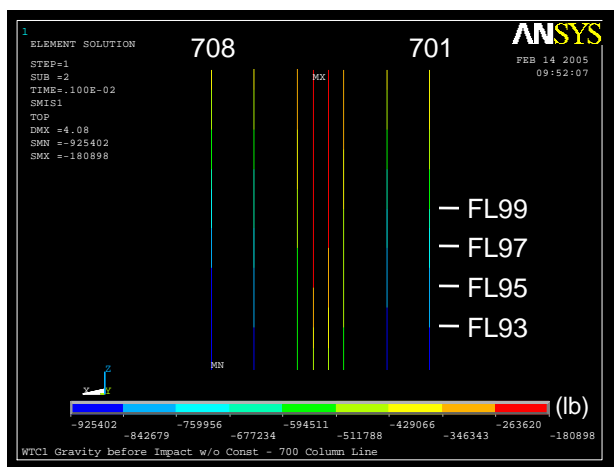
Figure 4–59. Variation of axial load in exterior columns at Floor 98 of west wall of WTC 1 for Case B conditions with 5 kip pull-in forces (compression is positive).



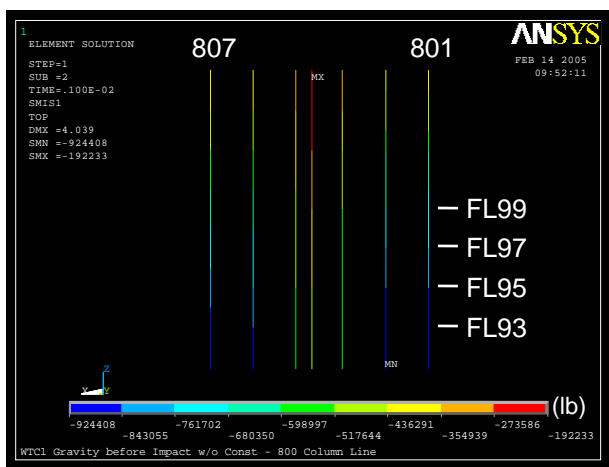
(a) 500 series columns



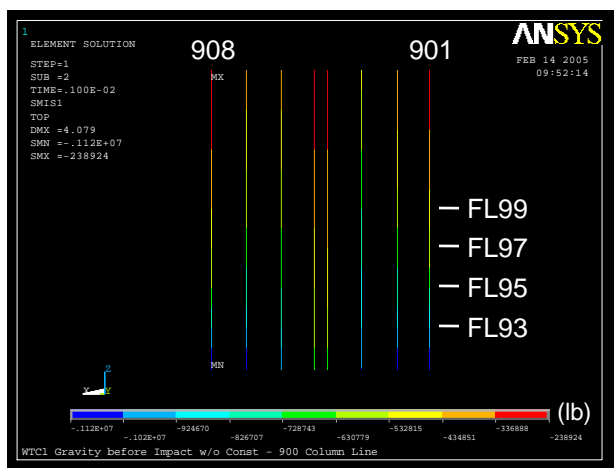
(b) 600 series columns



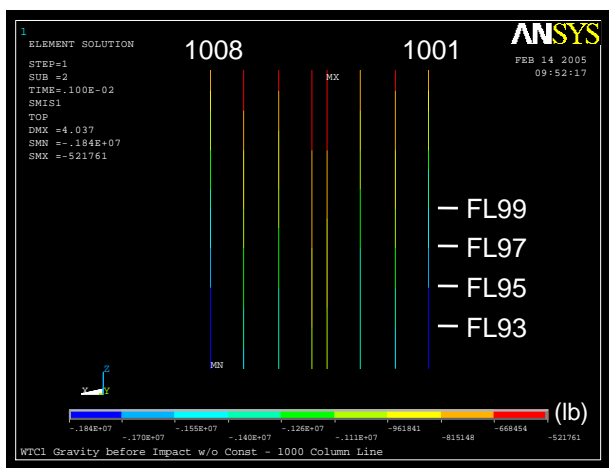
(c) 700 series columns



(d) 800 series columns

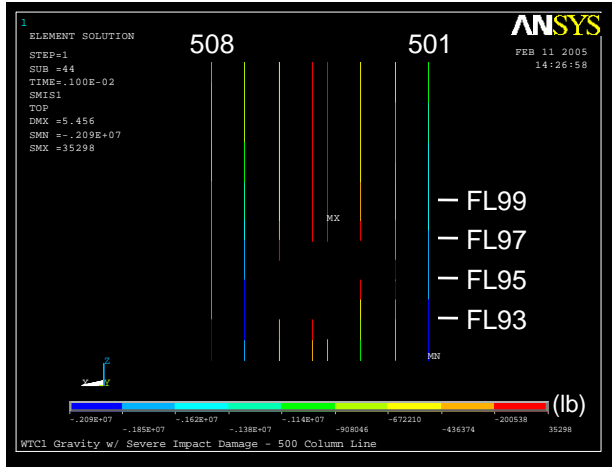


(e) 900 series columns

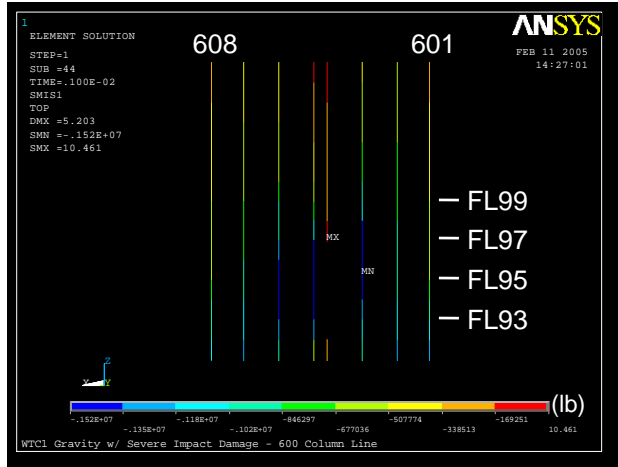


(f) 1000 series columns

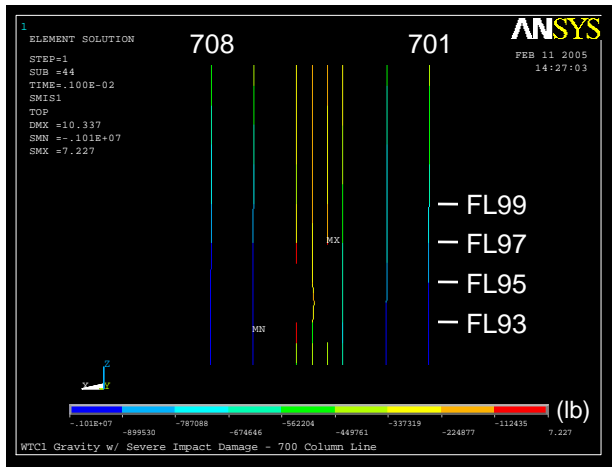
Figure 4–60. Axial load in core columns of WTC 1 before aircraft impact (compression is negative).



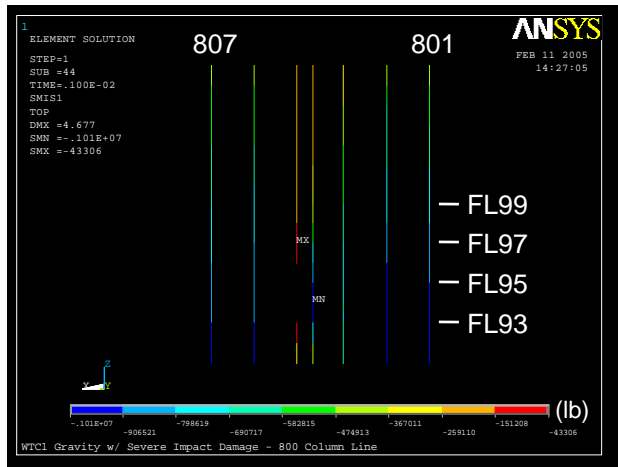
(a) 500 series columns



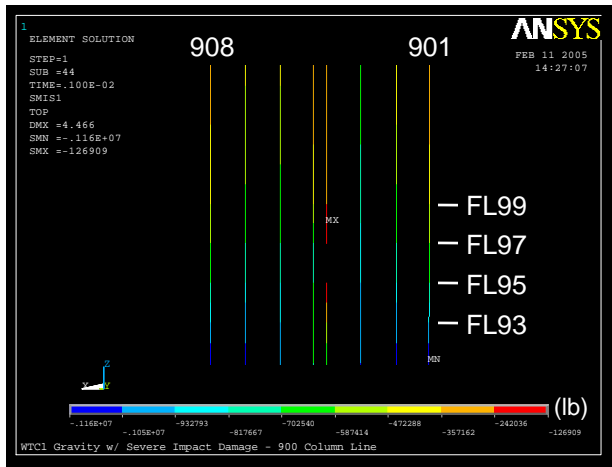
(b) 600 series columns



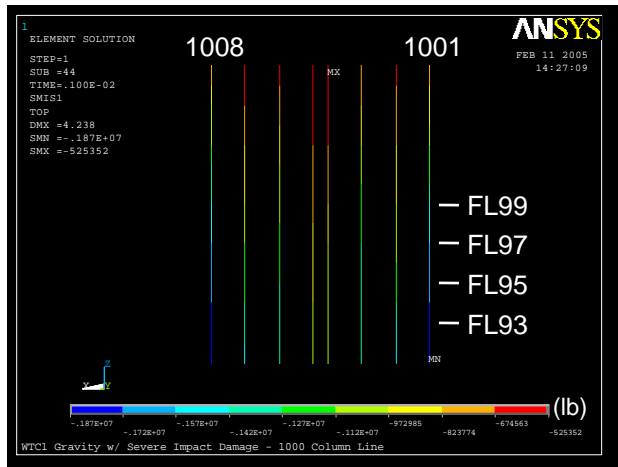
(c) 700 series columns



(d) 800 series columns

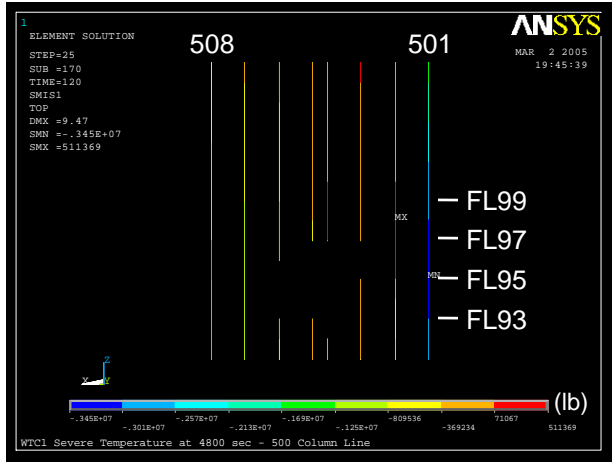


(e) 900 series columns

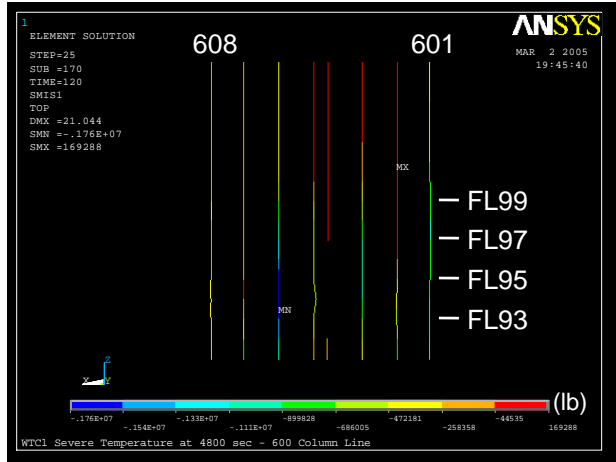


(f) 1000 series columns

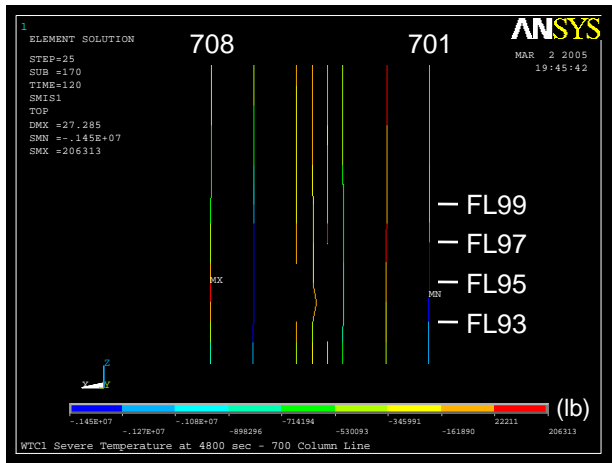
Figure 4–61. Axial load in core columns of WTC 1 after aircraft impact for Case B conditions (compression is negative).



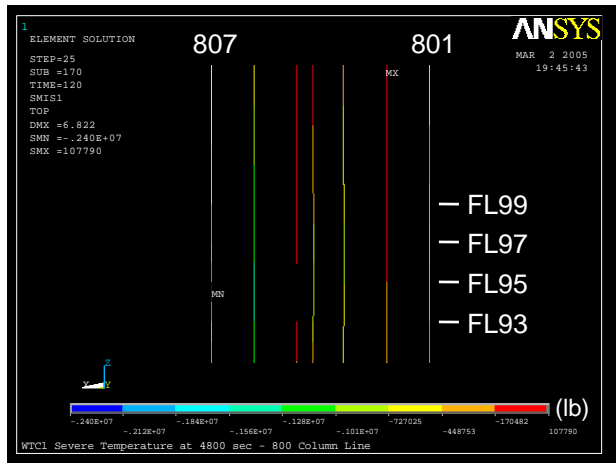
(a) 500 series columns



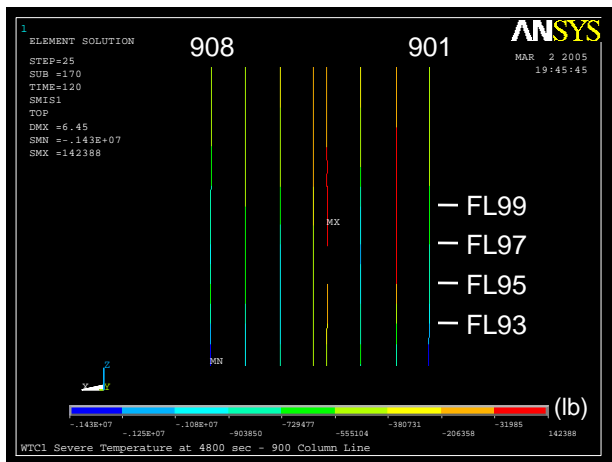
(b) 600 series columns



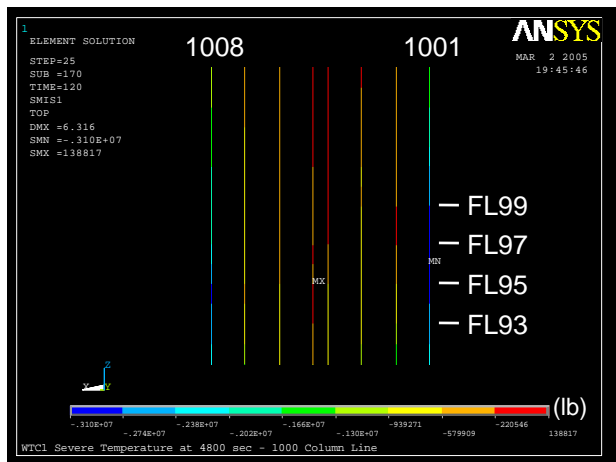
(c) 700 series columns



(d) 800 series columns



(e) 900 series columns

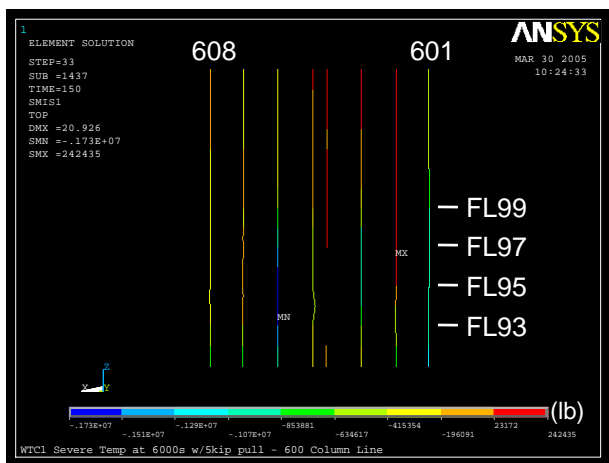


(f) 1000 series columns

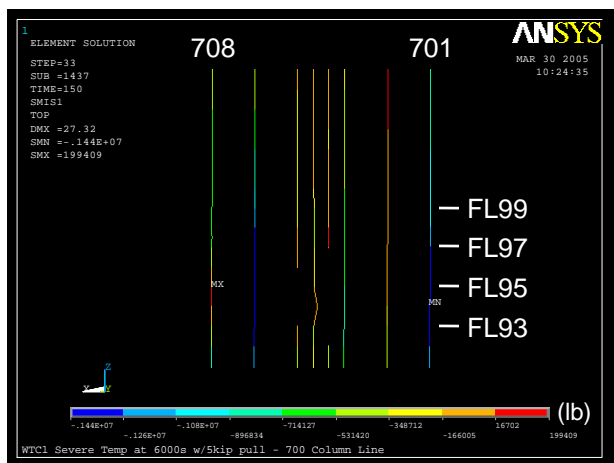
Figure 4–62. Axial load in core columns of WTC 1 at 80 min for Case B conditions (compression is negative).



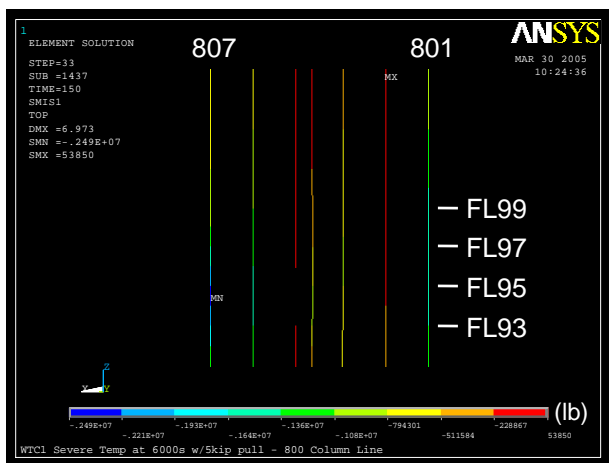
(a) 500 series columns



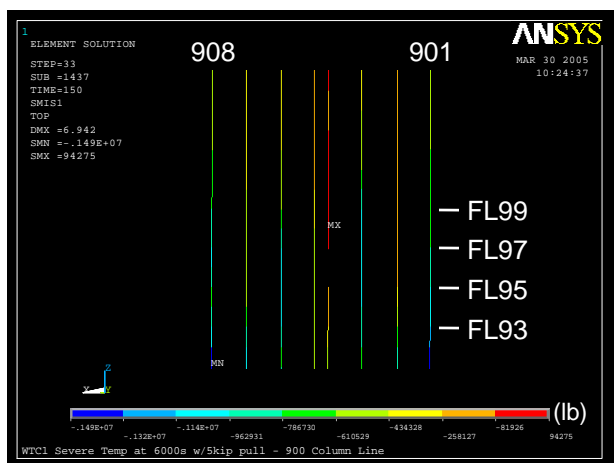
(b) 600 series columns



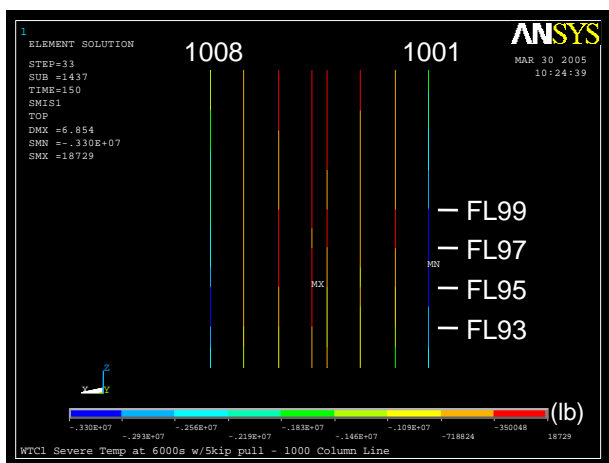
(c) 700 series columns



(d) 800 series columns



(e) 900 series columns



(f) 1000 series columns

Figure 4–63. Axial load in core columns of WTC 1 at 100 min for Case B conditions with 5 kip pull-in forces (compression is negative).

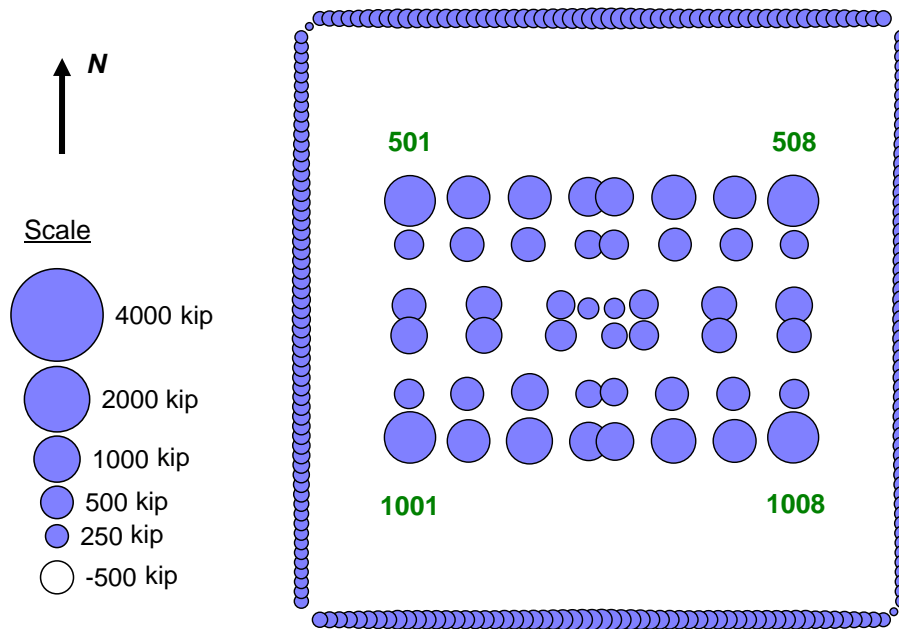


Figure 4-64. Axial load in columns at Floor 98 of WTC 1 before aircraft impact (compression is positive).

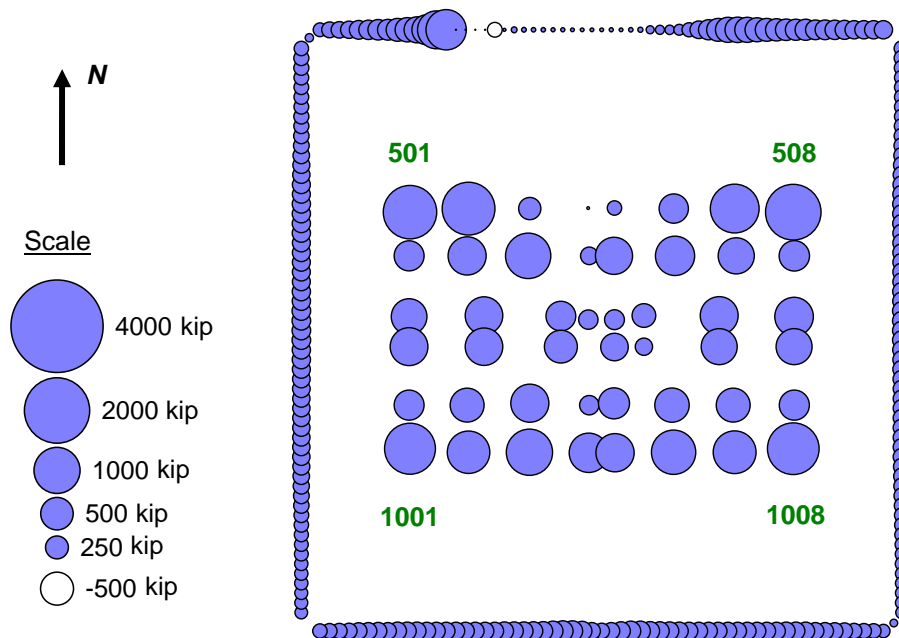


Figure 4-65. Axial load in columns at Floor 98 of WTC 1 after aircraft impact for Case B conditions (compression is positive).

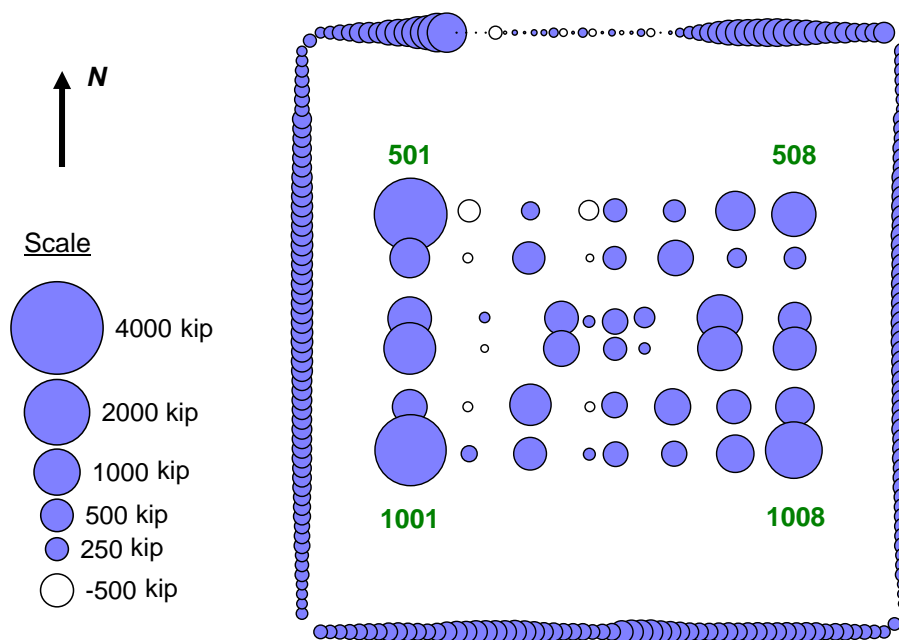


Figure 4–66. Axial load in columns at Floor 98 of WTC 1 at 80 min for Case B conditions (compression is positive).

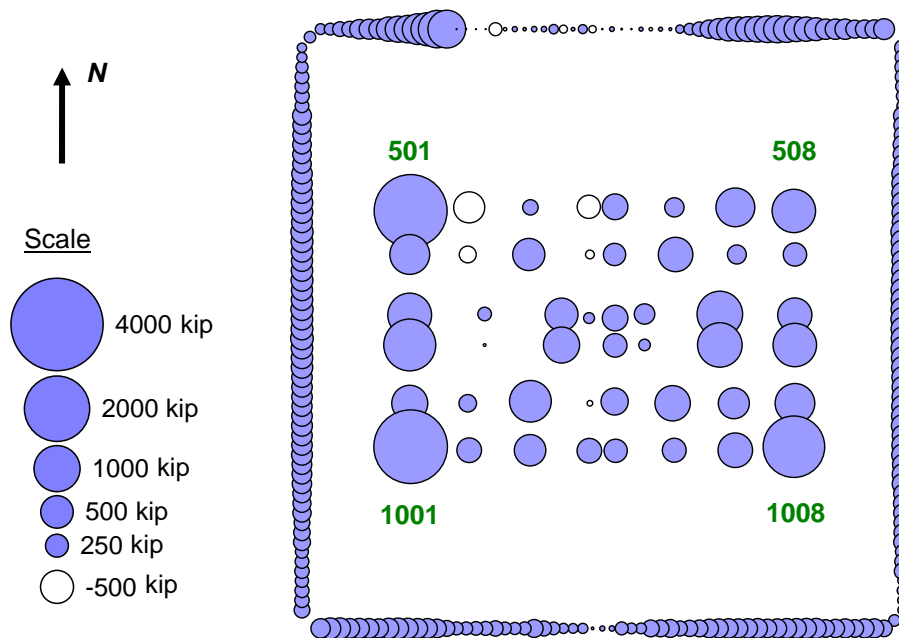


Figure 4–67. Axial load in columns at Floor 98 of WTC 1 at 100 min for Case B conditions with 5 kip pull-in forces (compression is positive).

Table 4–10. Total column loads at Floor 98 of WTC 1 for Case B conditions.

Row	Analysis Step	North	East	South	West	Core	Total
(1)	Before Impact	10,974	8,545	11,025	8,572	34,029	73,144
(2)	After Impact	10,137	9,071	10,356	9,146	34,429	73,139
(3)	10 min	9,796	8,490	9,848	8,536	36,473	73,143
(4)	20 min	10,437	9,108	9,900	9,202	34,495	73,143
(5)	30 min	10,913	10,034	10,420	9,715	32,060	73,142
(6)	40 min	11,068	10,599	11,004	10,178	30,294	73,142
(7)	50 min	11,149	10,908	11,192	10,458	29,435	73,141
(8)	60 min	11,205	11,168	11,285	10,716	28,766	73,141
(9)	70 min	11,286	11,366	11,343	10,939	28,205	73,138
(10)	80 min	11,376	11,555	11,409	11,119	27,681	73,140
(11)	90 min	10,916	11,991	9,949	11,657	28,587	73,099
(12)	100 min	10,828	12,249	9,638	11,905	28,478	73,098
(13)	(2) - (1)	-837	526	-668	574	400	-5
(14)	(10) - (2)	1,239	2,484	1,052	1,973	-6,748	1
(15)	(12) - (2)	692	3,178	-719	2,759	-5,951	-41
(16)	(12) - (10)	-548	694	-1,771	786	797	-42

Note: Compression is positive. Units are in kip.

Table 4–11. Total column loads at Floor 105 of WTC 1 for Case B conditions.

Row	Analysis Step	North	East	South	West	Core	Total
(1)	Before Impact	8,026	6,562	8,092	6,604	20,361	49,645
(2)	After Impact	7,294	7,028	7,488	7,076	20,761	49,646
(3)	10 min	6,944	6,461	6,981	6,469	22,790	49,646
(4)	20 min	7,551	7,075	7,057	7,158	20,806	49,647
(5)	30 min	8,020	7,998	7,569	7,685	18,377	49,648
(6)	40 min	8,193	8,571	8,129	8,147	16,608	49,649
(7)	50 min	8,285	8,878	8,315	8,428	15,743	49,650
(8)	60 min	8,351	9,130	8,414	8,687	15,069	49,650
(9)	70 min	8,435	9,319	8,481	8,914	14,502	49,651
(10)	80 min	8,528	9,497	8,551	9,097	13,978	49,651
(11)	90 min	8,096	9,847	7,327	9,506	14,876	49,652
(12)	100 min	8,023	10,076	7,066	9,720	14,767	49,653
(13)	(2) - (1)	-732	466	-604	472	400	1
(14)	(10) - (2)	1,234	2,470	1,063	2,021	-6,783	5
(15)	(12) - (2)	730	3,048	-422	2,644	-5,993	7
(16)	(12) - (10)	-504	579	-1,485	623	790	2

Note: Compression is positive. Units are in kip.

Table 4–12. Total column loads on the north wall of WTC 1 for Case B conditions.

Floor	Before Impact	After Impact	10 min	20 min	30 min	40 min	50 min	60 min	70 min	80 min	90 min	100 min
105	8,026	7,294	6,944	7,551	8,020	8,193	8,285	8,351	8,435	8,528	8,096	8,023
104	8,470	7,723	7,373	7,984	8,453	8,623	8,715	8,779	8,863	8,956	8,521	8,447
103	8,868	8,102	7,752	8,363	8,830	8,997	9,087	9,150	9,233	9,325	8,888	8,813
102	9,307	8,529	8,179	8,795	9,264	9,429	9,518	9,580	9,663	9,755	9,314	9,238
101	9,696	8,897	8,545	9,161	9,627	9,787	9,873	9,933	10,015	10,106	9,663	9,586
100	10,143	9,334	8,982	9,605	10,073	10,230	10,315	10,374	10,455	10,546	10,094	10,017
99	10,527	9,700	9,347	9,970	10,436	10,590	10,672	10,726	10,802	10,890	10,437	10,359
98	10,974	10,137	9,796	10,437	10,913	11,068	11,149	11,205	11,286	11,376	10,916	10,828
97	11,359	10,370	10,027	10,649	11,112	11,258	11,329	11,387	11,467	11,558	11,103	11,024
96	11,826	10,648	10,235	10,982	11,472	11,634	11,712	11,762	11,838	11,920	11,449	11,359
95	12,211	10,827	10,404	11,124	11,593	11,749	11,825	11,880	11,963	12,052	11,589	11,501
94	12,688	11,132	10,739	11,442	11,928	12,091	12,179	12,244	12,326	12,415	11,941	11,846
93	13,072	11,349	10,934	11,599	12,062	12,217	12,301	12,358	12,439	12,527	12,069	11,984

Note: Compression is positive. Units are in kip.

Table 4–13. Change in total column loads on the north wall of WTC 1 for Case B conditions from the state before aircraft impact.

Floor	After Impact	10 min	20 min	30 min	40 min	50 min	60 min	70 min	80 min	90 min	100 min
105	-732	-1,082	-475	-6	167	259	325	409	502	70	-3
104	-747	-1,096	-486	-17	154	245	310	393	486	51	-22
103	-765	-1,116	-505	-38	130	219	282	365	457	20	-54
102	-778	-1,128	-512	-43	122	211	273	356	448	7	-69
101	-798	-1,151	-534	-69	92	178	237	319	410	-33	-109
100	-809	-1,160	-538	-70	88	172	231	313	404	-49	-126
99	-827	-1,180	-557	-92	63	144	199	275	362	-91	-168
98	-837	-1,178	-537	-61	94	175	231	312	402	-58	-145
97	-988	-1,332	-710	-247	-101	-29	28	108	199	-256	-335
96	-1,178	-1,590	-844	-354	-192	-114	-64	12	94	-377	-467
95	-1,383	-1,807	-1,087	-618	-462	-386	-331	-247	-159	-622	-710
94	-1,556	-1,949	-1,247	-760	-598	-510	-445	-362	-273	-748	-843
93	-1,724	-2,138	-1,474	-1,011	-855	-772	-714	-634	-546	-1,004	-1,089

Note: Compression is positive. Units are in kip.

Table 4–14. Total column loads on the east wall of WTC 1 for Case B conditions.

Floor	Before Impact	After Impact	10 min	20 min	30 min	40 min	50 min	60 min	70 min	80 min	90 min	100 min
105	6,562	7,028	6,461	7,075	7,998	8,571	8,878	9,130	9,319	9,497	9,847	10,076
104	6,840	7,316	6,748	7,363	8,287	8,861	9,168	9,421	9,612	9,792	10,152	10,386
103	7,153	7,641	7,072	7,690	8,617	9,192	9,501	9,757	9,949	10,131	10,505	10,744
102	7,416	7,911	7,342	7,961	8,888	9,462	9,771	10,028	10,223	10,406	10,792	11,035
101	7,731	8,240	7,669	8,294	9,226	9,802	10,113	10,373	10,570	10,756	11,154	11,404
100	7,987	8,501	7,930	8,556	9,488	10,063	10,376	10,637	10,836	11,024	11,439	11,691
99	8,305	8,831	8,256	8,886	9,822	10,399	10,715	10,982	11,188	11,381	11,797	12,051
98	8,545	9,071	8,490	9,108	10,034	10,599	10,908	11,168	11,366	11,555	11,991	12,249
97	8,866	9,397	8,811	9,443	10,384	10,963	11,284	11,543	11,741	11,931	12,353	12,608
96	9,108	9,633	9,038	9,642	10,562	11,121	11,429	11,689	11,890	12,082	12,512	12,767
95	9,432	9,960	9,374	9,990	10,927	11,491	11,803	12,061	12,255	12,445	12,874	13,137
94	9,667	10,192	9,611	10,204	11,119	11,670	11,969	12,221	12,412	12,593	13,004	13,266
93	9,995	10,527	9,965	10,579	11,511	12,067	12,366	12,618	12,810	12,995	13,445	13,709

Note: Compression is positive. Units are in kip.

Table 4–15. Change in total column loads on the east wall of WTC 1 for Case B conditions from the state before aircraft impact.

Floor	After Impact	10 min	20 min	30 min	40 min	50 min	60 min	70 min	80 min	90 min	100 min
105	466	-101	513	1,436	2,009	2,316	2,568	2,757	2,935	3,285	3,514
104	475	-92	523	1,447	2,020	2,328	2,581	2,772	2,952	3,312	3,545
103	488	-81	538	1,465	2,039	2,348	2,604	2,797	2,978	3,352	3,592
102	496	-74	545	1,473	2,046	2,356	2,612	2,807	2,991	3,376	3,620
101	509	-62	563	1,495	2,071	2,383	2,643	2,840	3,025	3,424	3,673
100	514	-57	569	1,501	2,076	2,389	2,650	2,849	3,036	3,452	3,704
99	526	-49	581	1,517	2,094	2,410	2,676	2,883	3,075	3,491	3,745
98	526	-55	564	1,489	2,054	2,363	2,623	2,821	3,010	3,446	3,704
97	531	-55	577	1,518	2,097	2,418	2,677	2,875	3,065	3,487	3,742
96	525	-70	535	1,454	2,013	2,321	2,582	2,782	2,975	3,404	3,659
95	528	-59	558	1,494	2,059	2,371	2,629	2,823	3,012	3,442	3,705
94	525	-56	538	1,453	2,004	2,302	2,554	2,745	2,927	3,337	3,600
93	532	-30	584	1,516	2,072	2,370	2,623	2,815	3,000	3,450	3,714

Note: Compression is positive. Units are in kip.

Table 4–16. Total column loads on the south wall of WTC 1 for Case B conditions.

Floor	Before Impact	After Impact	10 min	20 min	30 min	40 min	50 min	60 min	70 min	80 min	90 min	100 min
105	8,092	7,488	6,981	7,057	7,569	8,129	8,315	8,414	8,481	8,551	7,327	7,066
104	8,532	7,918	7,411	7,484	7,996	8,560	8,746	8,844	8,909	8,979	7,729	7,462
103	8,929	8,307	7,800	7,869	8,382	8,947	9,133	9,230	9,295	9,364	8,077	7,799
102	9,365	8,734	8,226	8,292	8,806	9,375	9,562	9,658	9,722	9,789	8,478	8,194
101	9,753	9,114	8,605	8,667	9,180	9,751	9,937	10,032	10,094	10,161	8,808	8,514
100	10,197	9,548	9,038	9,094	9,608	10,182	10,368	10,463	10,523	10,590	9,229	8,932
99	10,581	9,924	9,414	9,466	9,979	10,554	10,738	10,829	10,886	10,951	9,504	9,194
98	11,025	10,356	9,848	9,900	10,420	11,004	11,192	11,285	11,343	11,409	9,949	9,638
97	11,409	10,736	10,224	10,262	10,761	11,327	11,503	11,586	11,638	11,703	10,278	9,959
96	11,874	11,167	10,664	10,713	11,230	11,811	11,996	12,087	12,145	12,198	10,765	10,454
95	12,258	11,518	11,007	11,044	11,548	12,116	12,293	12,380	12,436	12,488	11,004	10,676
94	12,733	11,954	11,451	11,498	12,016	12,601	12,790	12,885	12,946	13,007	11,505	11,175
93	13,116	12,309	11,795	11,832	12,339	12,913	13,094	13,181	13,239	13,291	11,850	11,518

Note: Compression is positive. Units are in kip.

Table 4–17. Change in total column loads on the south wall of WTC 1 for Case B conditions from the state before aircraft impact.

Floor	After Impact	10 min	20 min	30 min	40 min	50 min	60 min	70 min	80 min	90 min	100 min
105	-604	-1,111	-1,035	-523	37	223	322	389	459	-765	-1,026
104	-614	-1,121	-1,048	-536	28	214	312	377	447	-803	-1,070
103	-622	-1,129	-1,060	-548	18	204	301	366	435	-852	-1,130
102	-632	-1,140	-1,074	-560	10	196	293	356	424	-887	-1,171
101	-639	-1,148	-1,087	-573	-2	184	279	341	408	-945	-1,239
100	-650	-1,160	-1,103	-590	-15	171	266	326	392	-968	-1,266
99	-656	-1,166	-1,115	-601	-27	157	249	305	370	-1,077	-1,387
98	-668	-1,176	-1,125	-605	-21	167	260	319	384	-1,075	-1,387
97	-673	-1,185	-1,147	-648	-82	94	177	229	294	-1,131	-1,450
96	-707	-1,210	-1,161	-644	-62	122	213	271	324	-1,109	-1,420
95	-740	-1,251	-1,214	-710	-142	35	122	178	230	-1,254	-1,582
94	-779	-1,283	-1,236	-717	-132	57	152	213	274	-1,229	-1,558
93	-808	-1,321	-1,284	-778	-204	-23	65	122	175	-1,266	-1,598

Note: Compression is positive. Units are in kip.

Table 4–18. Summation of total column loads on the west wall of WTC 1 for Case B conditions.

Floor	Before Impact	After Impact	10 min	20 min	30 min	40 min	50 min	60 min	70 min	80 min	90 min	100 min
105	6,604	7,076	6,469	7,158	7,685	8,147	8,428	8,687	8,914	9,097	9,506	9,720
104	6,880	7,365	6,759	7,447	7,973	8,436	8,717	8,977	9,204	9,387	9,814	10,031
103	7,190	7,689	7,085	7,773	8,299	8,763	9,045	9,306	9,533	9,716	10,168	10,391
102	7,451	7,964	7,360	8,046	8,570	9,035	9,317	9,577	9,804	9,987	10,455	10,681
101	7,764	8,292	7,690	8,376	8,902	9,367	9,650	9,912	10,139	10,322	10,821	11,052
100	8,018	8,561	7,961	8,644	9,168	9,634	9,918	10,180	10,407	10,589	11,103	11,335
99	8,334	8,893	8,293	8,973	9,495	9,963	10,248	10,512	10,740	10,924	11,460	11,702
98	8,572	9,146	8,536	9,202	9,715	10,178	10,458	10,716	10,939	11,119	11,657	11,905
97	8,892	9,483	8,875	9,551	10,073	10,539	10,823	11,087	11,315	11,500	12,025	12,270
96	9,132	9,742	9,114	9,767	10,267	10,719	11,000	11,260	11,485	11,675	12,234	12,487
95	9,455	10,087	9,464	10,142	10,656	11,119	11,402	11,662	11,887	12,075	12,636	12,889
94	9,688	10,341	9,713	10,386	10,891	11,344	11,616	11,862	12,082	12,266	12,848	13,112
93	10,015	10,698	10,076	10,775	11,297	11,764	12,047	12,306	12,531	12,719	13,308	13,571

Note: Compression is positive. Units are in kip.

Table 4–19. Change in total column loads on the west wall of WTC 1 for Case B conditions from the state before aircraft impact.

Floor	After Impact	10 min	20 min	30 min	40 min	50 min	60 min	70 min	80 min	90 min	100 min
105	472	-135	554	1,081	1,543	1,824	2,083	2,310	2,493	2,902	3,116
104	485	-121	567	1,094	1,557	1,838	2,097	2,324	2,507	2,934	3,152
103	499	-105	583	1,109	1,573	1,855	2,116	2,343	2,526	2,978	3,201
102	514	-91	595	1,120	1,584	1,866	2,127	2,354	2,536	3,004	3,230
101	528	-73	612	1,138	1,603	1,886	2,148	2,376	2,558	3,057	3,289
100	543	-57	626	1,150	1,616	1,900	2,162	2,389	2,572	3,085	3,318
99	558	-41	638	1,161	1,628	1,913	2,177	2,406	2,589	3,126	3,368
98	574	-36	630	1,143	1,606	1,886	2,145	2,367	2,547	3,085	3,333
97	592	-17	660	1,182	1,647	1,931	2,195	2,424	2,608	3,133	3,378
96	611	-18	636	1,135	1,587	1,868	2,128	2,354	2,544	3,103	3,355
95	632	9	687	1,201	1,664	1,947	2,207	2,431	2,620	3,181	3,434
94	654	25	698	1,203	1,657	1,929	2,174	2,394	2,578	3,160	3,425
93	683	61	760	1,282	1,749	2,032	2,291	2,515	2,704	3,293	3,556

Note: Compression is positive. Units are in kip.

Table 4–20. Total column loads on the core of WTC 1 for Case B conditions.

Floor	Before Impact	After Impact	10 min	20 min	30 min	40 min	50 min	60 min	70 min	80 min	90 min	100 min
105	20,361	20,761	22,790	20,806	18,377	16,608	15,743	15,069	14,502	13,978	14,876	14,767
104	22,340	22,740	24,771	22,786	20,355	18,586	17,720	17,045	16,478	15,953	16,853	16,744
103	24,311	24,712	26,744	24,758	22,326	20,555	19,690	19,014	18,447	17,922	18,821	18,712
102	26,267	26,668	28,701	26,715	24,282	22,510	21,644	20,968	20,401	19,875	20,775	20,666
101	28,228	28,628	30,663	28,677	26,242	24,469	23,603	22,926	22,359	21,833	22,734	22,625
100	30,177	30,576	32,614	30,628	28,192	26,420	25,554	24,876	24,310	23,783	24,686	24,577
99	32,127	32,525	34,565	32,579	30,139	28,363	27,497	26,819	26,250	25,724	26,634	26,524
98	34,029	34,429	36,473	34,495	32,060	30,294	29,435	28,766	28,205	27,681	28,587	28,478
97	35,988	36,387	38,425	36,458	34,031	32,275	31,422	30,760	30,203	29,674	30,592	30,487
96	37,956	38,217	40,264	38,305	35,878	34,129	33,279	32,617	32,060	31,540	32,455	32,349
95	39,925	39,872	41,961	39,998	37,573	35,816	34,974	34,314	33,758	33,240	34,151	34,044
94	41,903	41,551	43,648	41,681	39,251	37,503	36,655	35,995	35,441	34,924	35,847	35,742
93	43,859	43,304	45,394	43,429	40,998	39,247	38,400	37,742	37,188	36,673	37,561	37,455

Note: Compression is positive. Units are in kip.

Table 4–21. Change in total column loads on the core of WTC 1 for Case B conditions from the state before aircraft impact.

Floor	After Impact	10 min	20 min	30 min	40 min	50 min	60 min	70 min	80 min	90 min	100 min
105	400	2,430	445	-1,984	-3,752	-4,617	-5,292	-5,858	-6,383	-5,484	-5,593
104	400	2,431	446	-1,985	-3,754	-4,620	-5,295	-5,862	-6,387	-5,487	-5,596
103	400	2,432	447	-1,985	-3,756	-4,622	-5,297	-5,864	-6,390	-5,490	-5,599
102	400	2,433	448	-1,986	-3,757	-4,623	-5,300	-5,867	-6,392	-5,492	-5,601
101	400	2,435	449	-1,986	-3,758	-4,624	-5,301	-5,868	-6,395	-5,493	-5,603
100	399	2,436	451	-1,985	-3,757	-4,623	-5,301	-5,867	-6,394	-5,491	-5,600
99	399	2,438	452	-1,988	-3,763	-4,630	-5,308	-5,876	-6,402	-5,493	-5,602
98	400	2,444	466	-1,969	-3,735	-4,594	-5,263	-5,824	-6,348	-5,443	-5,552
97	399	2,437	470	-1,956	-3,713	-4,566	-5,228	-5,785	-6,314	-5,396	-5,501
96	261	2,307	349	-2,079	-3,827	-4,677	-5,339	-5,897	-6,417	-5,501	-5,607
95	-53	2,037	73	-2,352	-4,108	-4,950	-5,610	-6,167	-6,685	-5,773	-5,880
94	-352	1,745	-223	-2,653	-4,401	-5,248	-5,908	-6,462	-6,979	-6,056	-6,162
93	-556	1,534	-431	-2,861	-4,613	-5,460	-6,117	-6,671	-7,186	-6,298	-6,405

Note: Compression is positive. Units are in kip.

**Table 4–22. Change in total column loads before and after aircraft impact.
(Loads after impact) – (Loads before impact)**

Row	Floor	North	East	South	West	Core
(1)	Floor 98	-837	526	-668	574	400
(2)	Floor 105	-732	466	-604	472	400
(3)	(2) - (1)	105	-60	64	-103	0

Note: Increase in compression is shown as positive. Units are in kip.

Table 4–23. Change in total column loads after aircraft impact and at 80 min for Case B conditions.

(Loads at 80 min) – (Loads After Impact)

Row	Floor	North	East	South	West	Core
(1)	Floor 98	1,239	2,484	1,052	1,973	-6,748
(2)	Floor 105	1,234	2,470	1,063	2,021	-6,783
(3)	(2) - (1)	-5	-15	11	48	-35

Note: Increase in compression is shown as positive. Units are in kip.

Table 4–24. Change in total column loads at 80 min and at 100 min for Case B conditions.

(Loads at 100 min) – (Loads at 80 min)

Row	Floor	North	East	South	West	Core
(1)	Floor 98	-548	694	-1,771	786	797
(2)	Floor 105	-504	579	-1,485	623	790
(3)	(2) - (1)	44	-115	285	-163	-7

Note: Increase in compression is shown as positive. Units are in kip.

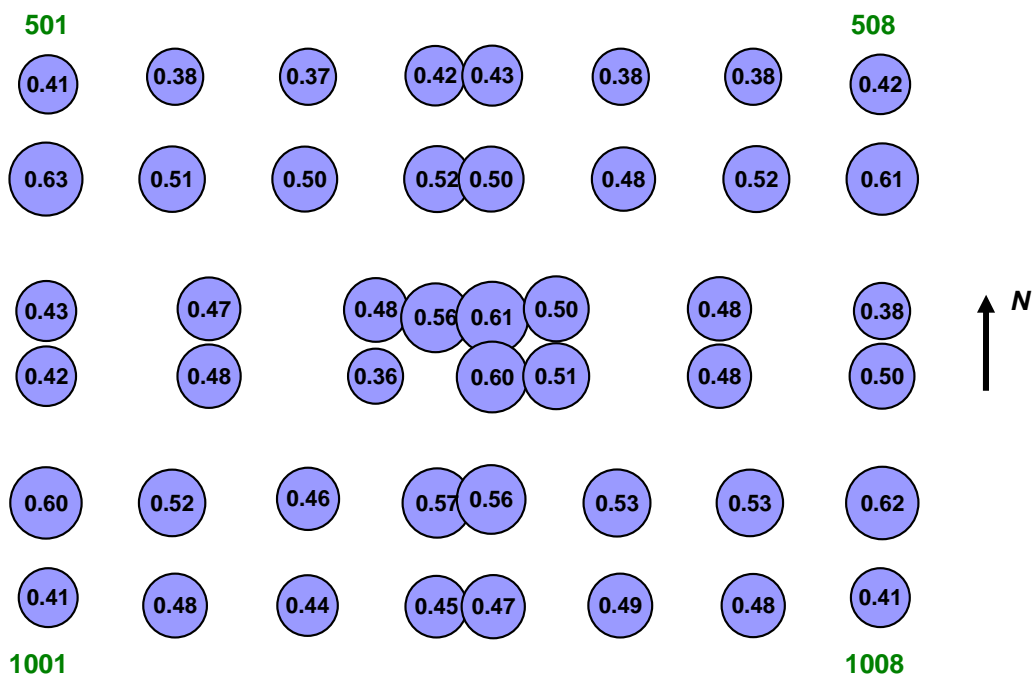


Figure 4-68. Maximum demand-to-capacity ratio for axial load in core columns between Floor 93 and Floor 99 of WTC 1 before aircraft impact.

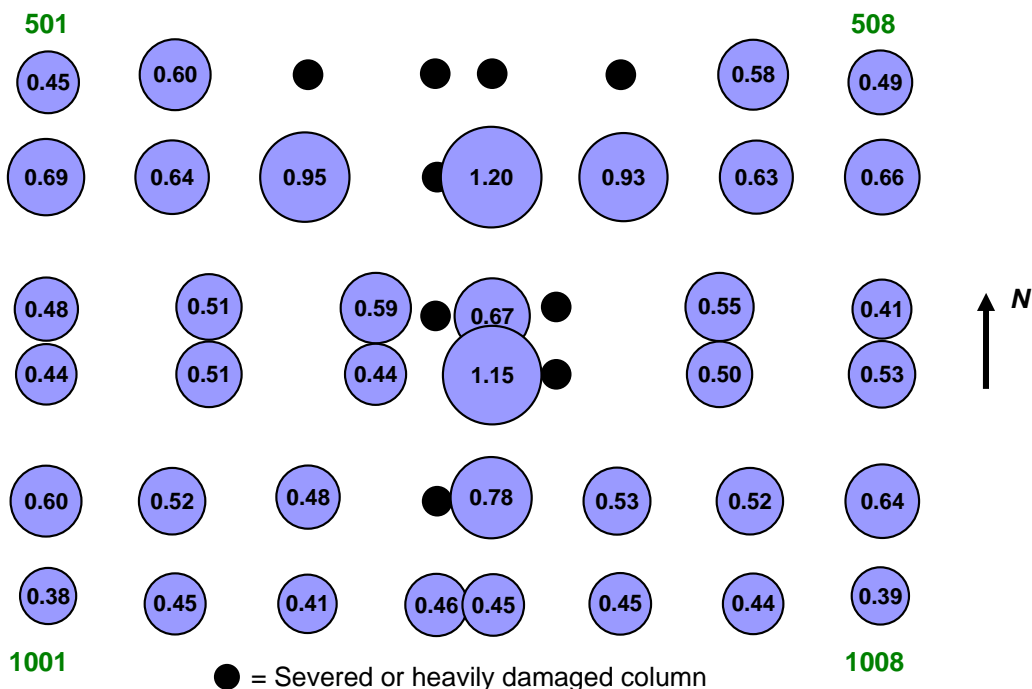


Figure 4-69. Maximum demand-to-capacity ratio for axial load in core columns between Floor 93 and Floor 99 of WTC 1 after aircraft impact for Case B conditions.

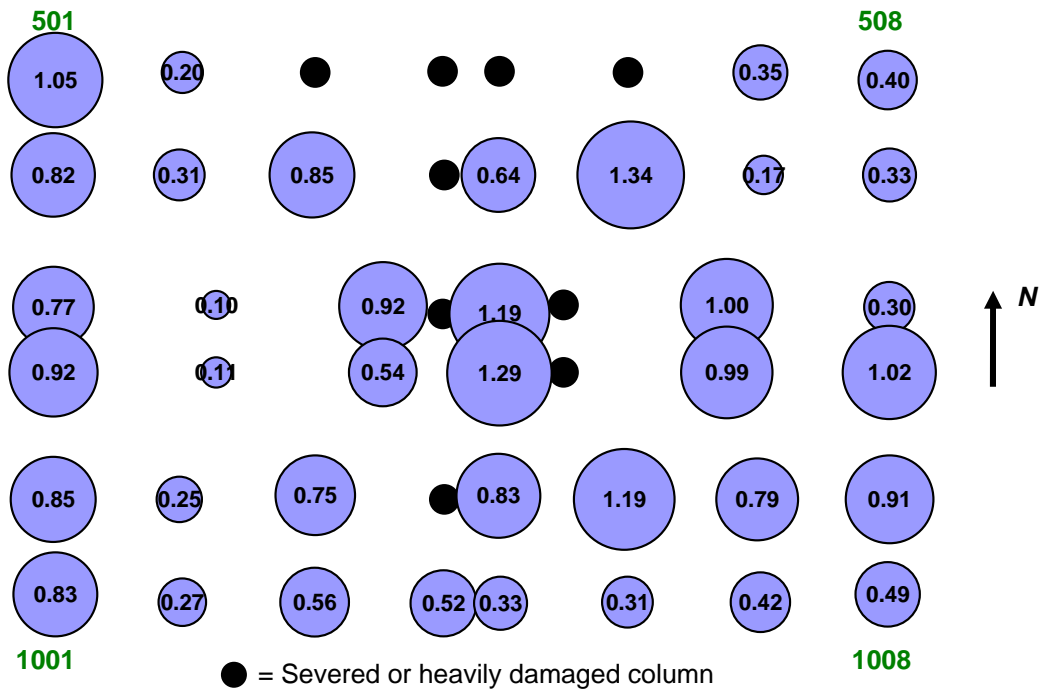


Figure 4–70. Maximum demand-to-capacity ratio for axial load in core columns between Floor 93 and Floor 99 of WTC 1 at 80 min for Case B conditions.

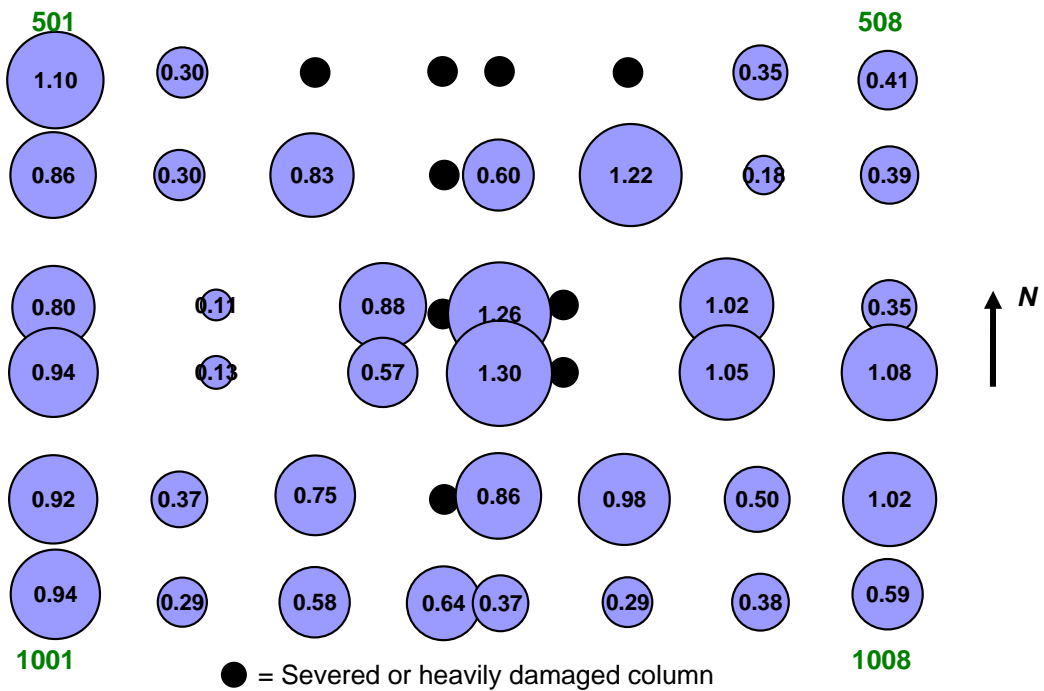


Figure 4–71. Maximum demand-to-capacity ratio for axial load in core columns between Floor 93 and Floor 99 of WTC 1 at 100 min for Case B conditions with 5 kip pull-in forces.

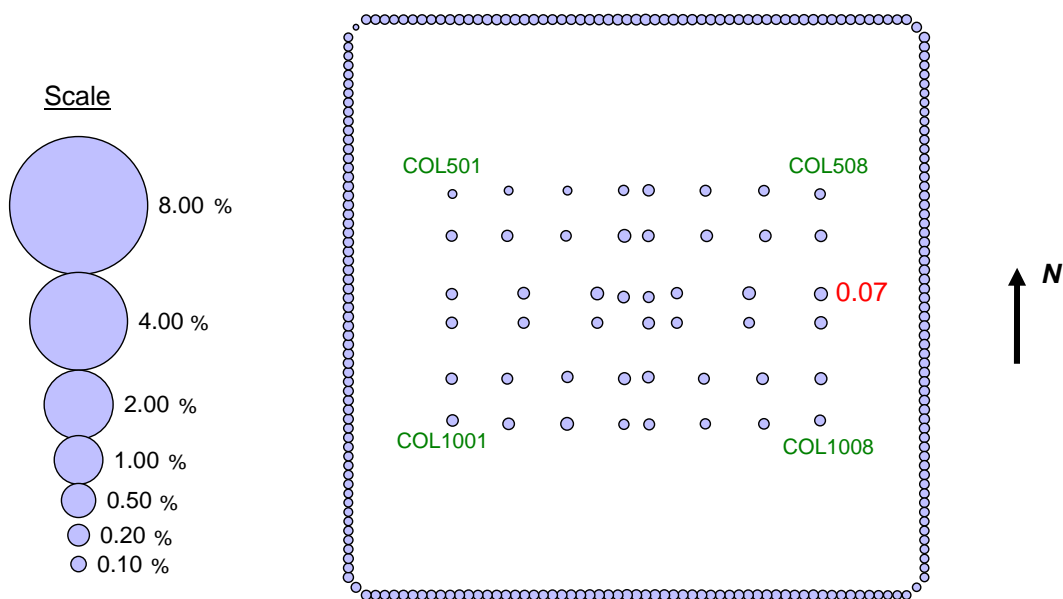


Figure 4-72. Maximum elastic-plus-plastic strain for columns between Floor 93 and Floor 99 of WTC 1 before aircraft impact (compressive strain is positive; strain values are in percent).

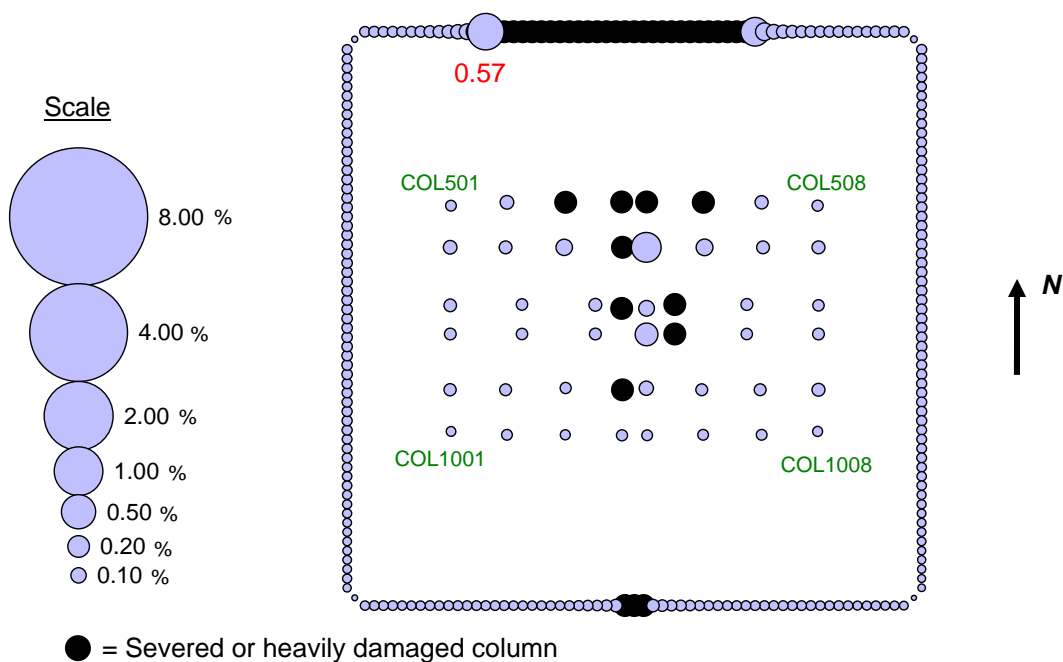


Figure 4-73. Maximum elastic-plus-plastic strain for columns between Floor 93 and Floor 99 of WTC 1 after aircraft impact for Case B conditions (compressive strain is positive; strain values are in percent).

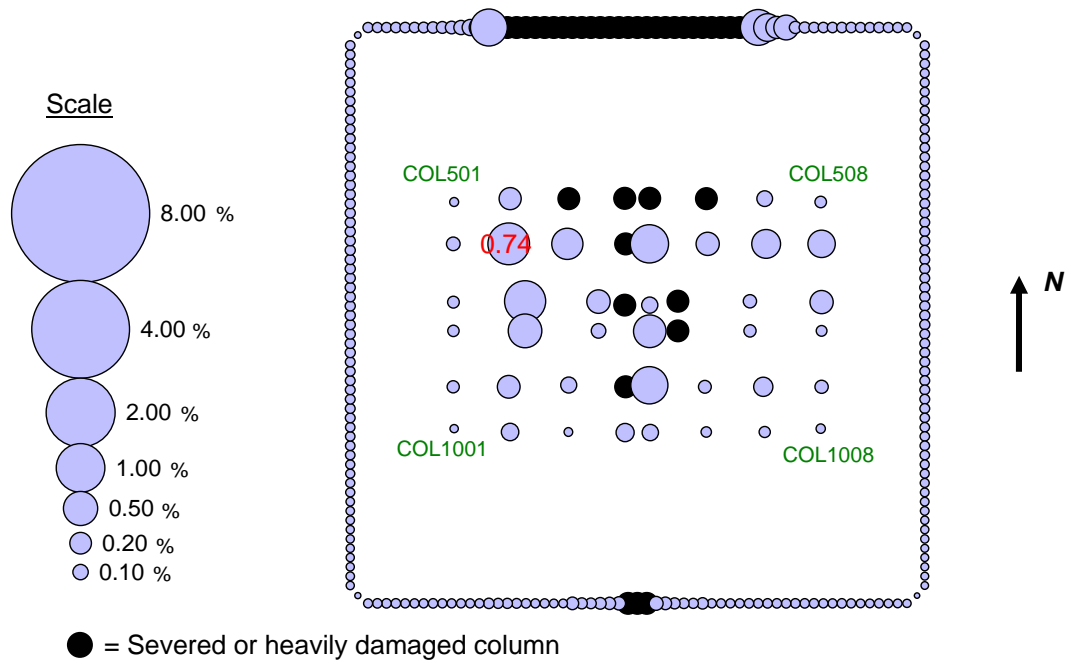


Figure 4-74. Maximum elastic-plus-plastic strain for columns between Floor 93 and Floor 99 of WTC 1 at 10 min for Case B conditions (compressive strain is positive; strain values are in percent).

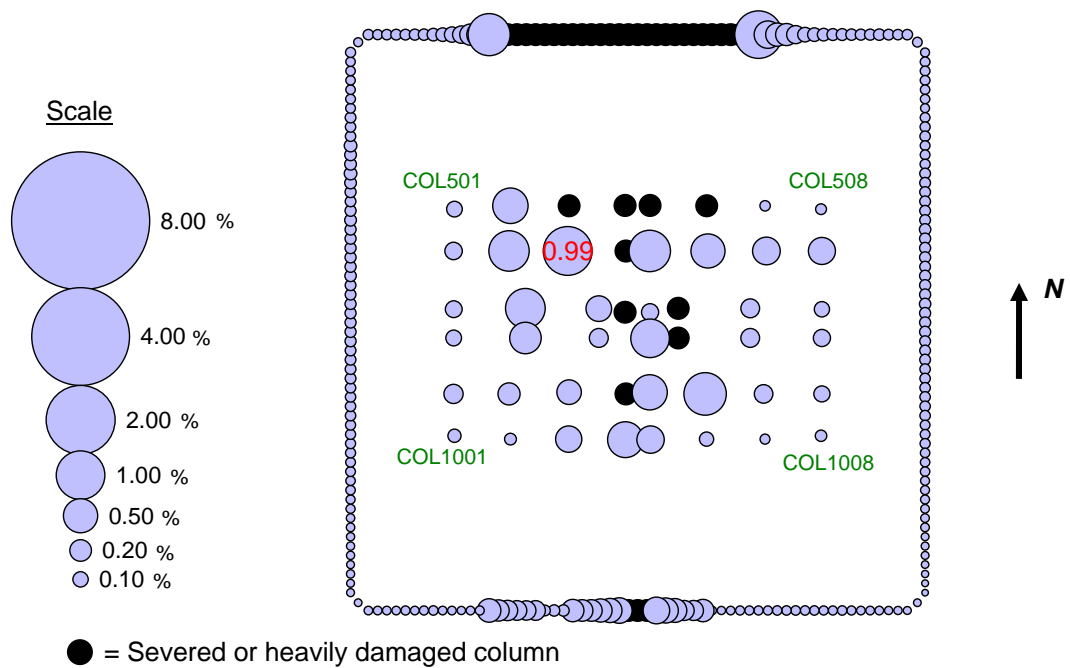


Figure 4-75. Maximum elastic-plus-plastic strain for columns between Floor 93 and Floor 99 of WTC 1 at 40 min for Case B conditions (compressive strain is positive; strain values are in percent).

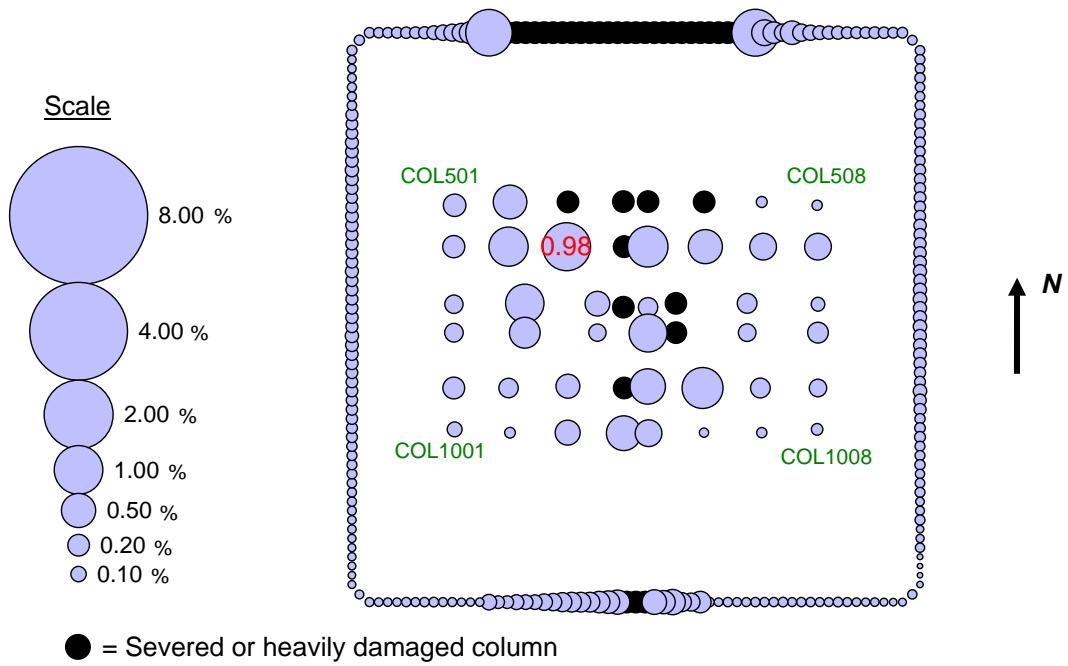


Figure 4-76. Maximum elastic-plus-plastic strain for columns between Floor 93 and Floor 99 of WTC 1 at 80 min for Case B conditions (compressive strain is positive; strain values are in percent).

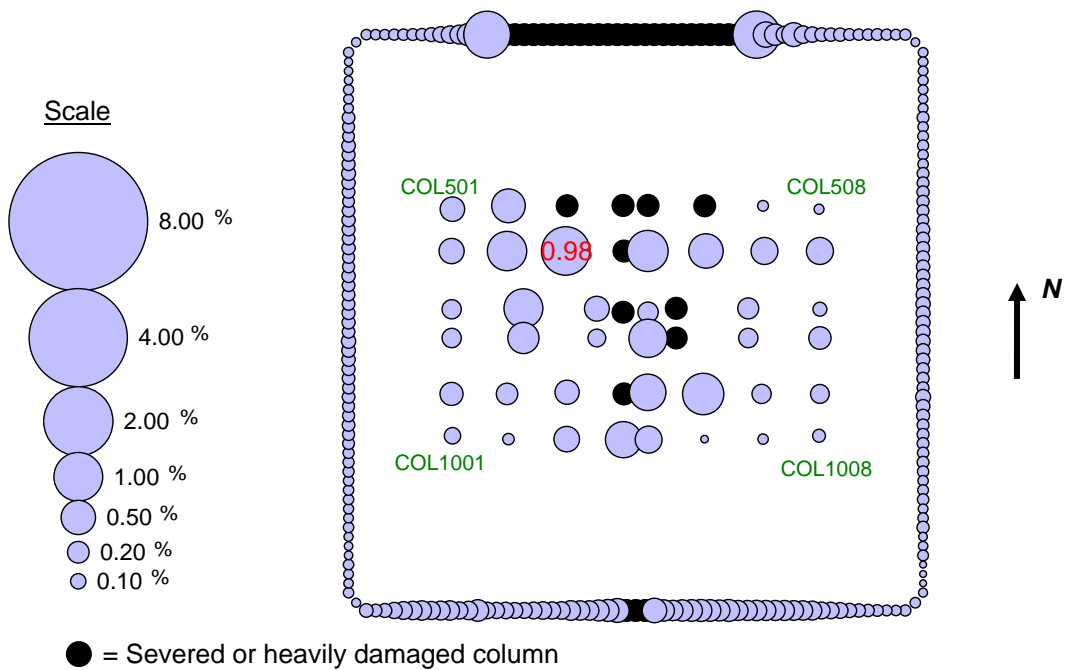


Figure 4-77. Maximum elastic-plus-plastic strain for columns between Floor 93 and Floor 99 of WTC 1 at 100 min for Case B conditions with 5 kip pull-in forces (compressive strain is positive; strain values are in percent).

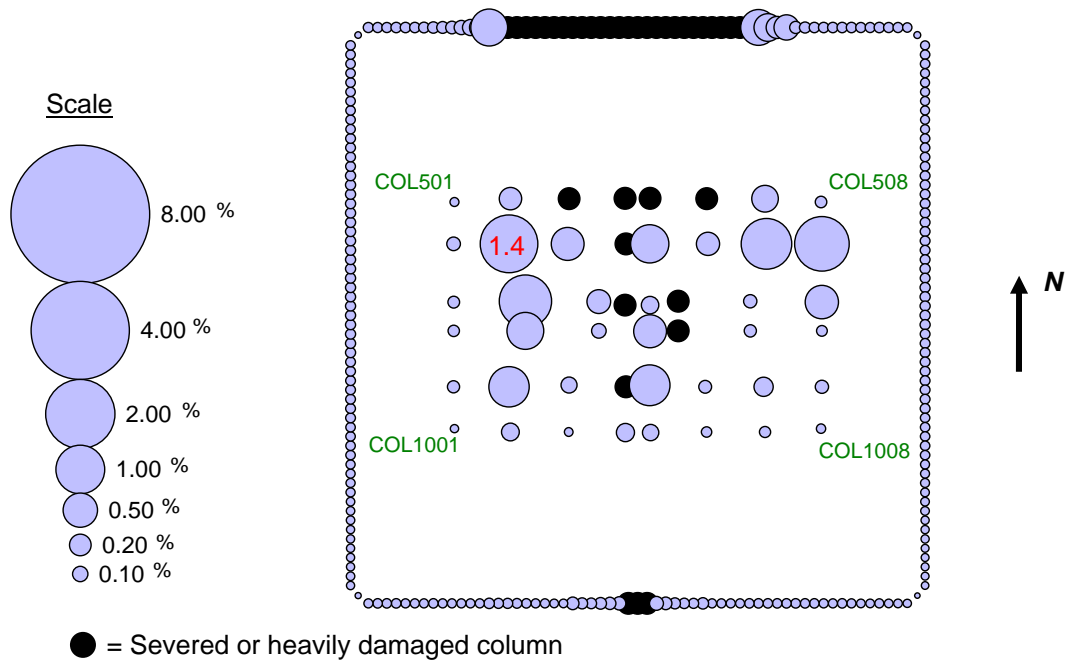


Figure 4-78. Maximum elastic-plus-plastic-plus-creep strain for columns between Floor 93 and Floor 99 of WTC 1 at 10 min for Case B conditions (compressive strain is positive; strain values are in percent).

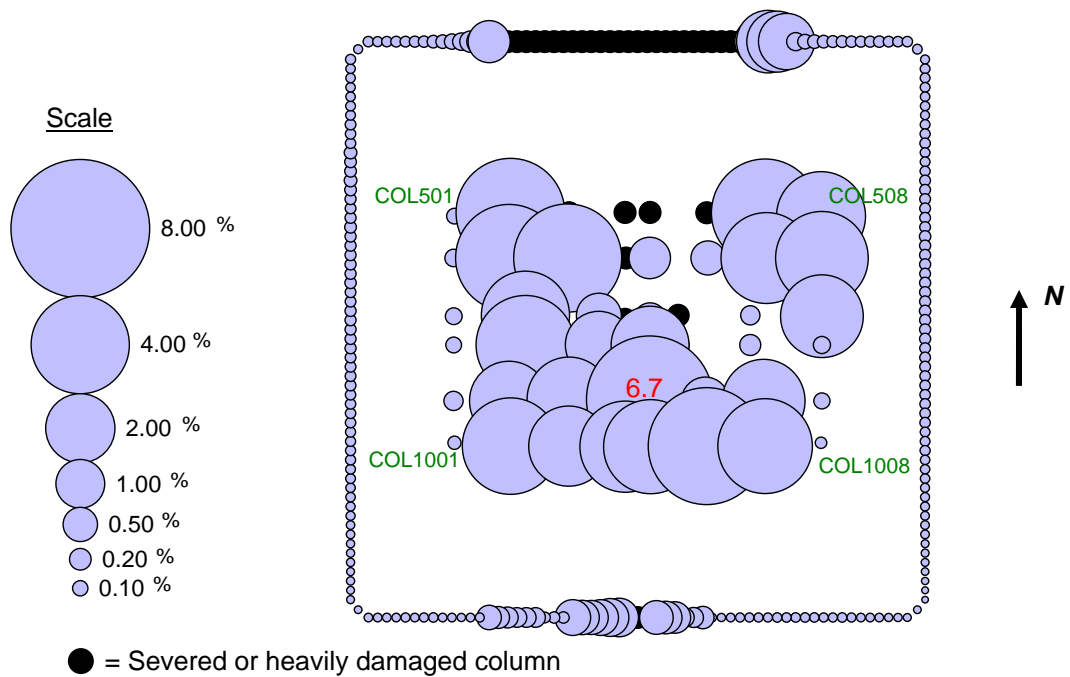


Figure 4-79. Maximum elastic-plus-plastic-plus-creep strain for columns between Floor 93 and Floor 99 of WTC 1 at 40 min for Case B conditions (compressive strain is positive; strain values are in percent).

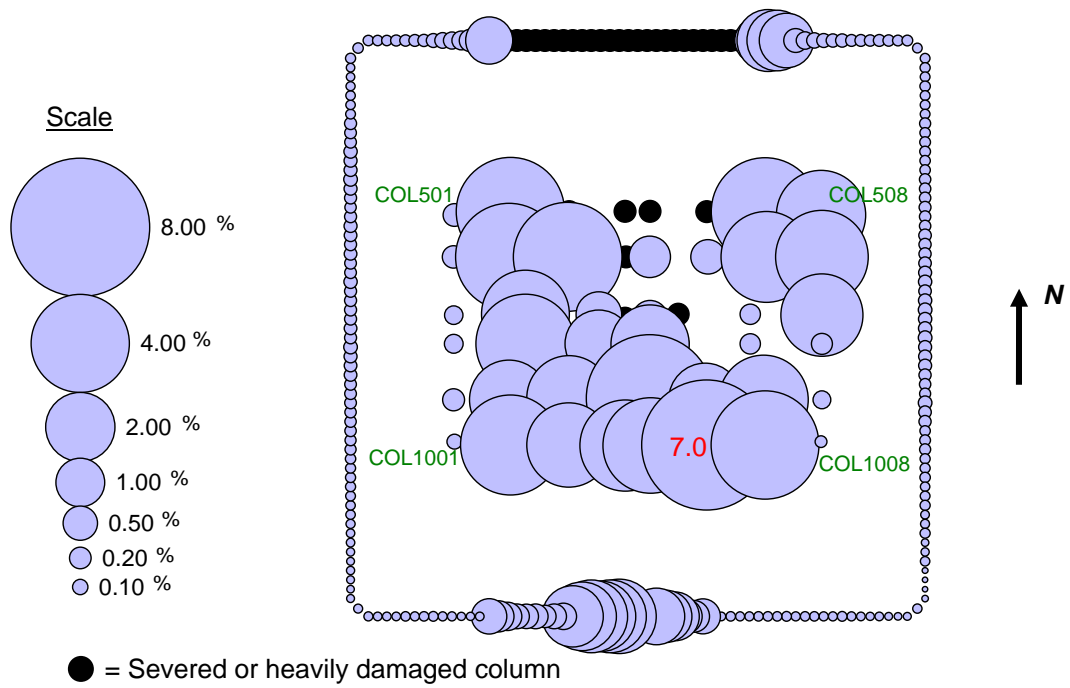


Figure 4–80. Maximum elastic-plus-plastic-plus-creep strain for columns between Floor 93 and Floor 99 of WTC 1 at 80 min for Case B conditions (compressive strain is positive; strain values are in percent).

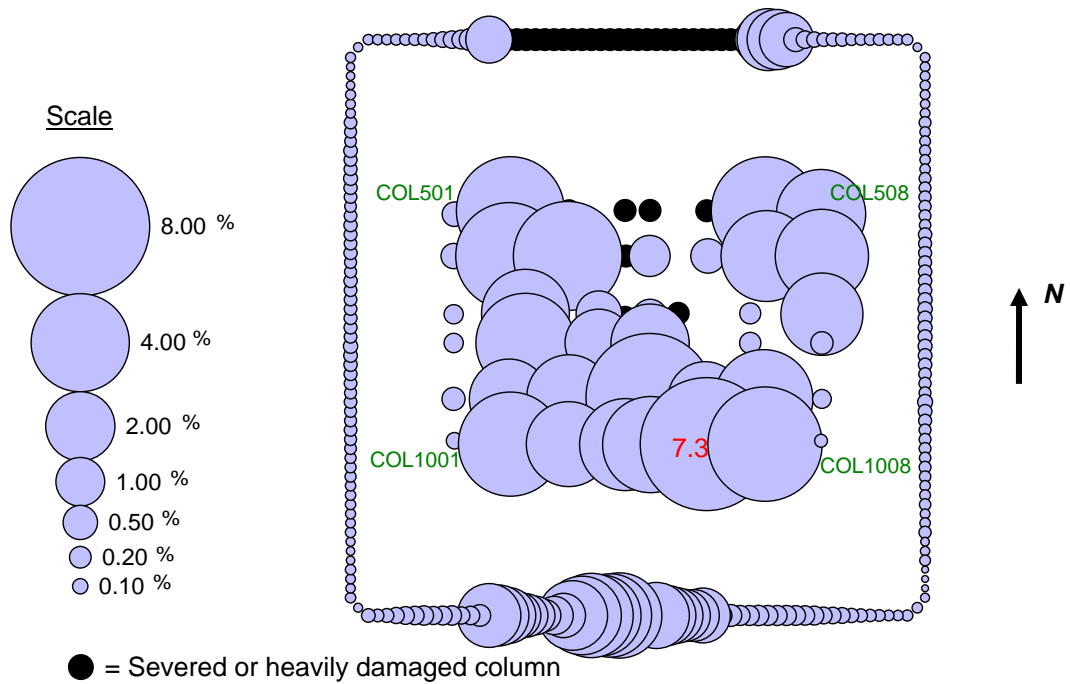


Figure 4–81. Maximum elastic-plus-plastic-plus-creep strain for columns between Floor 93 and Floor 99 of WTC 1 at 100 min for Case B conditions with 5 kip pull-in forces (compressive strain is positive; strain value are in percent).

Table 4–25. Tension capacity of core column splices at Floor 106

Col #	Column Line					
	500	600	700	800	900	1000
1	460	335	335	335	335	460
2	335	335	335	335	335	335
3	335	335	335	335	460	460
4	335	335	335	335	335	335
5	335	335	335	335	335	335
6	335	335	335	335	335	335
7	335	335	335	335	335	335
8	460	335	335		335	460

Note: Units are in kip.

Table 4–26. Axial load in core columns at Floor 105 of WTC 1 for Case B conditions

Column ID	Before Impact	After Impact	10 min	20 min	30 min	40 min	50 min	60 min	70 min	80 min	90 min	100 min
501	753	1,033	976	1,326	1,504	1,634	1,690	1,703	1,661	1,635	1,595	1,563
502	567	751	996	569	416	353	303	266	210	156	90	44
503	632	469	631	312	129	57	23	-13	-63	-118	-190	-240
504	486	1	-49	-17	-34	-39	-32	-34	-36	-44	-70	-82
505	576	82	27	18	3	-8	-8	-8	-8	-16	-42	-52
506	629	512	544	311	311	324	320	313	314	315	281	266
507	558	676	774	466	328	313	304	296	303	312	284	275
508	743	1,057	1,185	1,108	587	493	469	455	448	430	399	389
601	219	272	239	341	383	413	423	432	432	427	427	420
602	395	524	612	310	206	153	103	69	30	-5	-21	-45
603	408	475	525	315	118	15	-28	-64	-94	-126	-130	-137
604	275	131	85	45	7	-16	-28	-38	-45	-51	-50	-52
605	320	149	70	20	-3	-17	-23	-28	-34	-38	-36	-37
606	408	428	415	334	327	325	313	303	295	291	298	299
607	371	447	470	350	286	268	247	232	224	222	230	235
608	224	296	335	255	165	149	134	123	116	113	123	128
701	355	418	363	518	594	658	684	705	718	722	733	733
702	395	529	652	232	145	85	17	-34	-73	-98	-88	-89
703	266	288	380	456	456	425	407	387	368	351	344	334
704	224	221	237	214	189	165	147	132	121	113	119	117
705	181	159	146	135	125	117	110	103	99	96	98	95
706	276	227	195	178	167	161	153	146	141	137	138	133
707	386	447	472	514	524	514	491	471	456	445	448	449
708	391	491	540	420	448	470	462	451	446	445	470	482
801	398	450	374	536	630	706	742	762	777	788	818	834
802	398	473	622	167	110	69	1	-55	-91	-108	-73	-54
803	298	298	417	542	521	470	445	423	402	383	389	383
804	192	173	179	166	146	136	125	119	119	116	127	127
805	329	188	145	105	85	85	76	72	73	71	86	86
806	395	454	502	567	631	652	642	635	630	620	626	624
807	362	432	439	399	449	480	489	493	497	498	528	540
901	253	273	217	280	343	398	422	436	450	460	496	517
902	385	425	470	268	241	193	152	112	95	88	135	167
903	523	606	833	847	653	491	435	393	358	336	358	349
904	298	287	397	322	192	116	71	47	43	42	76	77
905	278	271	332	259	150	96	66	55	60	59	89	89
906	406	464	507	646	616	516	477	455	409	354	351	319
907	413	457	485	534	513	468	456	458	455	441	438	425
908	239	274	242	274	321	350	366	378	387	392	425	438
1001	762	735	605	721	915	1,112	1,212	1,301	1,370	1,405	1,595	1,685
1002	614	611	759	560	527	432	405	382	367	353	453	465
1003	745	744	855	1,079	990	555	426	286	214	182	299	271
1004	522	525	809	719	416	194	106	46	15	15	148	150
1005	534	546	830	685	359	176	94	50	27	20	135	132
1006	637	634	682	904	661	408	348	321	288	242	273	230
1007	587	578	582	727	624	500	478	476	463	435	438	408
1008	758	785	687	770	902	991	1,030	1,055	1,067	1,070	1,216	1,274

Note: Compression is positive. Units are in kip.

Note: Shading indicates when core columns were in tension.

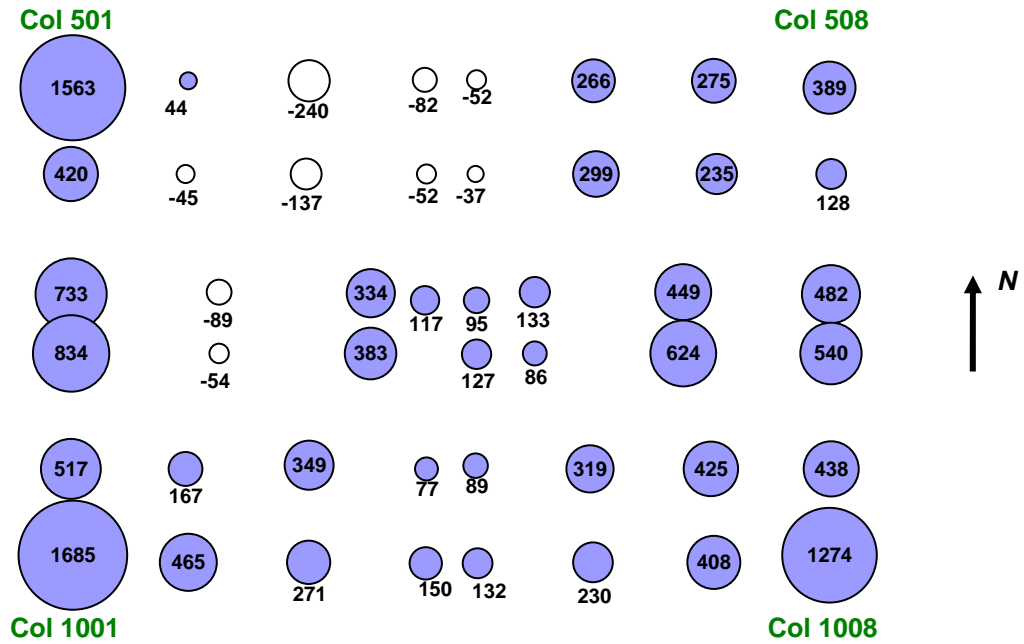


Figure 4–82. Axial load (kip) in core columns at Floor 105 of WTC 1 at 100 min for Case B conditions with 5 kip pull-in forces (compression is positive).

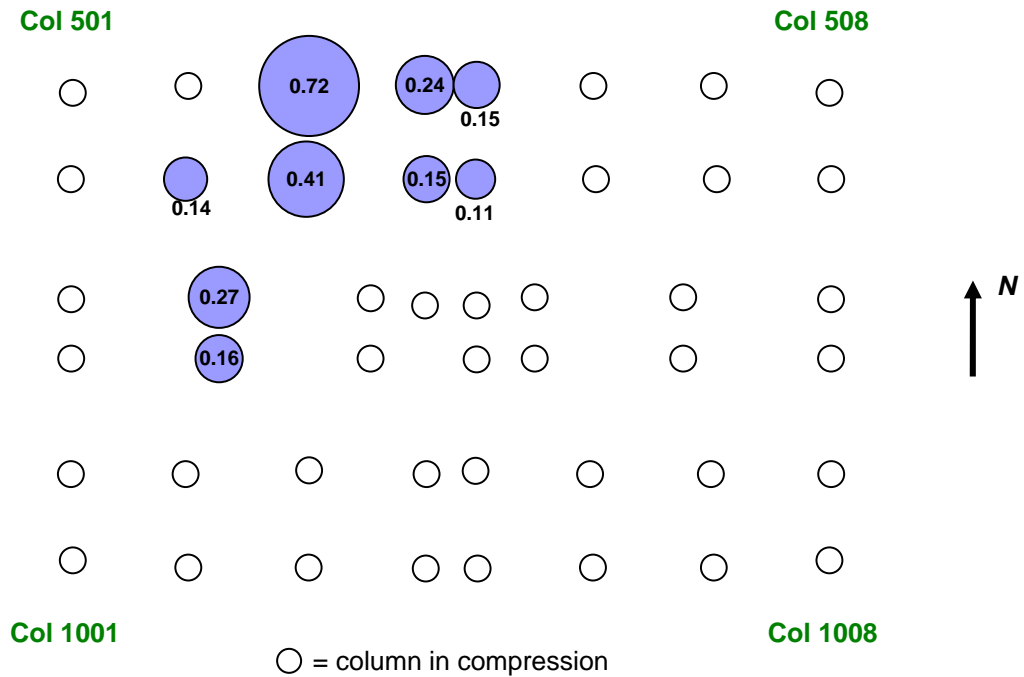


Figure 4–83. Tension demand-to-capacity ratio for core column splices at Floor 106 of WTC 1 at 100 min for Case B conditions with 5 kip pull-in forces.

Table 4–27. Demand-to-capacity ratio for axial load in outriggers of WTC 1 for Case B conditions (outrigger IDs are indicated in Fig. 4–3).

Outrigger ID	Bfr Imp	Afr Imp	10 min	20 min	30 min	40 min	50 min	60 min	70 min	80 min	90 min	100 min
North												
A	0.26	0.35	0.26	0.40	0.49	0.53	0.56	0.59	0.62	0.65	0.54	0.52
B	0.22	-0.07	-0.13	-0.04	0.02	0.04	0.06	0.07	0.08	0.09	0.03	0.03
C	0.21	-0.05	-0.11	-0.02	0.04	0.06	0.08	0.08	0.09	0.11	0.05	0.04
D	0.25	0.35	0.29	0.45	0.61	0.67	0.70	0.72	0.73	0.75	0.65	0.63
East												
E	0.32	0.48	0.38	0.56	0.75	0.83	0.88	0.92	0.94	0.97	0.95	0.96
F	0.23	0.28	0.21	0.30	0.41	0.48	0.52	0.55	0.57	0.59	0.62	0.64
G	0.23	0.26	0.20	0.26	0.35	0.42	0.46	0.49	0.51	0.54	0.58	0.61
H	0.33	0.31	0.23	0.25	0.36	0.46	0.51	0.55	0.58	0.60	0.72	0.77
South												
I	0.25	0.12	0.04	0.03	0.12	0.20	0.23	0.26	0.27	0.28	0.28	0.28
J	0.21	0.10	0.01	0.03	0.13	0.24	0.28	0.29	0.30	0.31	0.04	-0.02
K	0.21	0.10	0.01	0.03	0.13	0.24	0.27	0.28	0.30	0.31	0.02	-0.04
L	0.26	0.12	0.02	0.05	0.11	0.20	0.24	0.27	0.29	0.31	0.19	0.18
West												
M	0.33	0.33	0.22	0.29	0.36	0.44	0.49	0.53	0.56	0.58	0.69	0.73
N	0.24	0.27	0.20	0.28	0.34	0.40	0.44	0.47	0.50	0.52	0.56	0.58
O	0.24	0.29	0.22	0.31	0.38	0.43	0.47	0.50	0.53	0.55	0.59	0.61
P	0.33	0.48	0.39	0.54	0.64	0.71	0.75	0.79	0.83	0.87	0.88	0.90

Table 4–28. Demand to capacity ratio for axial load in exterior columns supporting outriggers at Floor 107 of WTC 1 for Case B conditions.

Column ID	Bfr Imp	Afr Imp	10 min	20 min	30 min	40 min	50 min	60 min	70 min	80 min	90 min	100 min
North												
110	0.30	0.40	0.35	0.43	0.48	0.51	0.53	0.54	0.56	0.58	0.52	0.51
111	0.24	0.31	0.28	0.33	0.36	0.37	0.38	0.39	0.40	0.41	0.37	0.37
129	0.28	0.00	-0.05	0.02	0.08	0.10	0.11	0.11	0.12	0.14	0.09	0.08
130	0.30	0.04	0.00	0.06	0.11	0.13	0.14	0.15	0.16	0.17	0.12	0.11
131	0.30	0.02	-0.03	0.04	0.10	0.12	0.13	0.13	0.14	0.16	0.10	0.10
149	0.25	0.30	0.28	0.33	0.39	0.41	0.42	0.43	0.43	0.44	0.41	0.40
150	0.25	0.31	0.29	0.36	0.43	0.46	0.48	0.49	0.49	0.50	0.45	0.44
East												
217	0.20	0.26	0.23	0.29	0.38	0.41	0.43	0.45	0.46	0.47	0.46	0.47
218	0.25	0.34	0.28	0.38	0.51	0.57	0.60	0.63	0.65	0.67	0.66	0.67
228	0.30	0.35	0.28	0.36	0.47	0.53	0.57	0.59	0.62	0.64	0.67	0.69
229	0.22	0.25	0.20	0.26	0.34	0.38	0.41	0.43	0.45	0.46	0.49	0.50
231	0.22	0.25	0.20	0.25	0.32	0.37	0.40	0.42	0.43	0.45	0.48	0.49
232	0.30	0.33	0.27	0.33	0.42	0.48	0.52	0.55	0.57	0.59	0.63	0.65
242	0.25	0.25	0.20	0.21	0.28	0.33	0.36	0.39	0.40	0.42	0.50	0.53
243	0.20	0.20	0.17	0.18	0.22	0.25	0.27	0.29	0.30	0.31	0.36	0.38
South												
310	0.30	0.23	0.19	0.19	0.23	0.28	0.29	0.31	0.31	0.32	0.33	0.33
311	0.24	0.20	0.18	0.17	0.20	0.22	0.23	0.24	0.24	0.25	0.25	0.25
329	0.27	0.17	0.10	0.12	0.20	0.29	0.32	0.33	0.33	0.34	0.10	0.05
330	0.34	0.23	0.14	0.16	0.26	0.37	0.40	0.41	0.41	0.43	0.13	0.07
331	0.27	0.18	0.10	0.12	0.21	0.30	0.32	0.32	0.33	0.34	0.10	0.05
349	0.24	0.20	0.17	0.18	0.20	0.22	0.23	0.25	0.25	0.26	0.22	0.22
350	0.31	0.23	0.18	0.20	0.23	0.27	0.30	0.31	0.33	0.33	0.28	0.28
West												
417	0.21	0.21	0.17	0.19	0.22	0.25	0.27	0.29	0.30	0.31	0.35	0.37
418	0.25	0.25	0.19	0.23	0.27	0.32	0.34	0.37	0.38	0.40	0.46	0.49
428	0.30	0.34	0.27	0.35	0.41	0.46	0.49	0.52	0.55	0.56	0.60	0.62
429	0.23	0.26	0.20	0.26	0.31	0.35	0.37	0.40	0.41	0.43	0.46	0.47
431	0.23	0.26	0.21	0.27	0.32	0.36	0.39	0.41	0.43	0.44	0.47	0.48
432	0.30	0.35	0.28	0.37	0.43	0.48	0.51	0.54	0.57	0.59	0.62	0.64
442	0.25	0.34	0.28	0.37	0.44	0.48	0.51	0.54	0.57	0.59	0.60	0.62
443	0.21	0.26	0.23	0.29	0.33	0.36	0.37	0.39	0.41	0.43	0.43	0.44

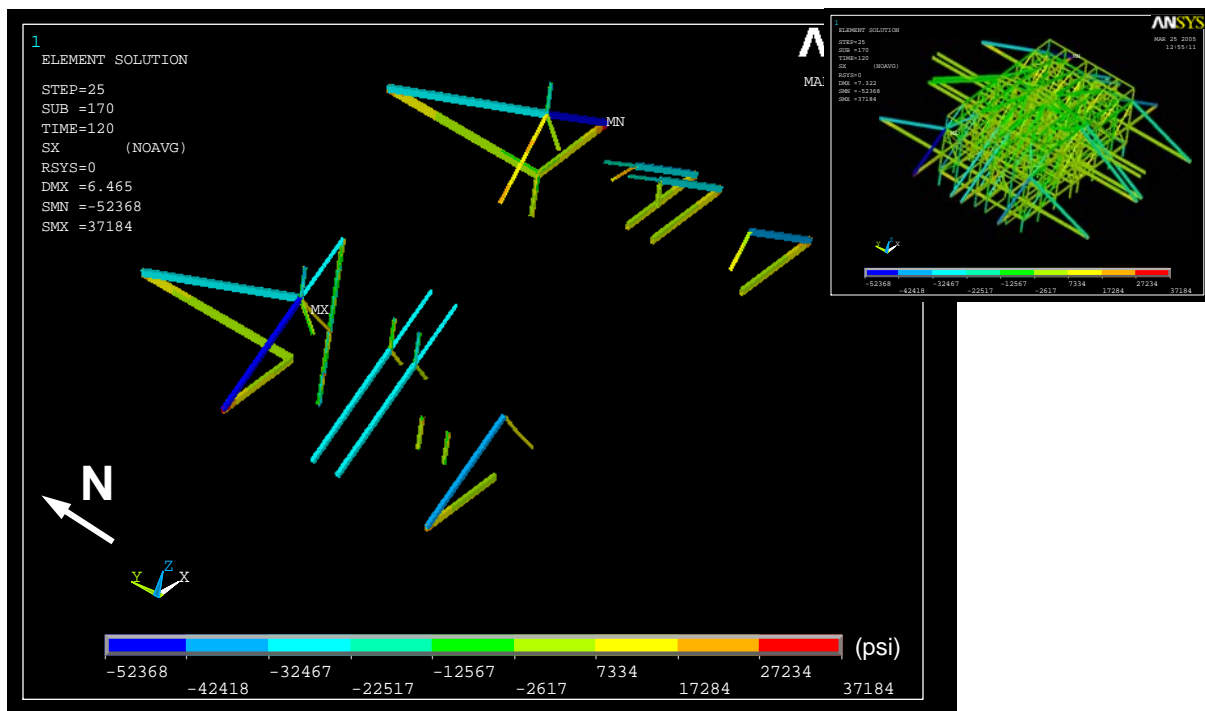


Figure 4–84. Primary load path within the hat truss of WTC 1.

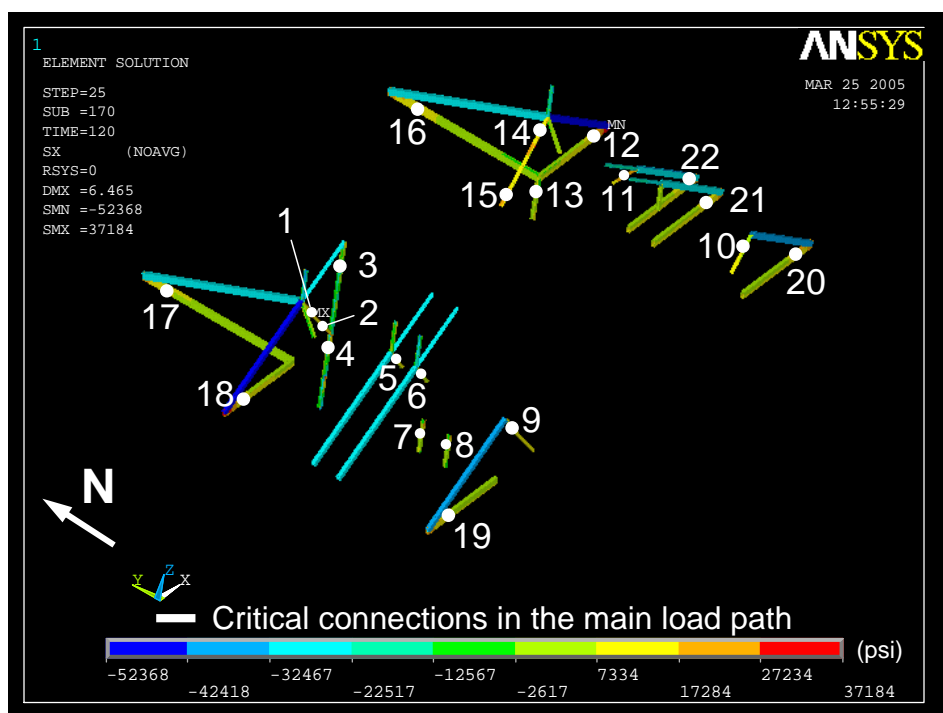


Figure 4–85. Location of the hat truss connections in the primary load path.

Table 4–29. Demand and capacity of the hat truss connections (kip) in the primary load path at 80 min (connection IDs are shown in Fig. 4–85).

Connection ID	Location		Tension Capacity		Demand Force (tension)	State
	Floor	Column	Yield	Ultimate		
1	110	501	1,250	1,250	680	Safe
2	108	502	1,250	1,250	680	Safe
3	111	502	1,930	1,930	80	Safe
4	108	502	520	520	100	Safe
5	110	701	1,340	1,340	390	Safe
6	107	702	950	950	370	Safe
7	110	801	1,340	1,340	140	Safe
8	107	802	335	260	140	Safe
9	110	1001	1,250	1,250	400	Safe
10	110	1008	1,250	1,250	290	Safe
11	110	708	1,340	1,340	360	Safe
12	108	217-218	4,520	5,880	1,810	Safe
13	108	508	870	760	410	Safe
14	110	508	1,250	1,250	530	Safe
15	108	507	1,250	1,250	530	Safe
16	108	149-150	2,640	2,640	1,310	Safe
17	108	110-111	2,640	2,640	1,170	Safe
18	108	442-443	4,520	5,880	1,650	Safe
19	108	417-418	4,520	5,880	1,200	Safe
20	108	242-243	4,520	5,880	1,230	Safe
21	108	231-232	3,010	3,920	1,070	Safe
22	108	228-229	3,010	3,920	1,150	Safe

4.2.5 Simulation of WTC 2 Collapse

The global model of WTC 2, as described in Sections 4.1.1 to 4.2.3, was used to simulate the response of the building to aircraft impact damage and the ensuing fire environment. Studies performed on the isolated exterior wall and core models and on the full floor subsystem models indicated that the calculated response of these models to the Case D damage and temperature time history set more closely matched the structural behavior observable in photographic and video evidence than did analyses using Case C. Therefore, in this global analysis only the Case D damage and temperature time history set were used. Section 2.2 of this report provides a description of the Case D structural impact damage set. The analysis started with dead and 25 percent of the design live loads taken directly from the reference SAP2000 models and applied as concentrated loads at each column-floor node. Table 4–30 summarizes the sequence of analyses that were performed. Section 2.5 gives the locations of floor/wall disconnections and pull-in forces at different analysis steps. The results of each analysis step were used as the initial conditions for the next analysis step.

Table 4–30. Analysis Steps of WTC 2 ANSYS global model with Case D conditions.

Analysis Step	Description
1	Dead and 25 percent of the design live loads were applied on the model of WTC 2 with impact damage.
2	Floor/wall disconnections and pull-in forces that were projected to occur between 0 min and 10 min were applied.
3	Column and spandrel temperatures were linearly ramped up from room temperature of 20 °C to temperatures at 10 min.
4	Floor/wall disconnections and pull-in forces that were projected to occur between 10 min and 20 min were applied.
5	Column and spandrel temperatures were linearly changed from temperatures at 10 min to 20 min.
6	Floor/wall disconnections and pull-in forces that were projected to occur between 20 min and 30 min were applied.
7	Column and spandrel temperatures were linearly changed from temperatures at 20 min to 30 min.
8	Floor/wall disconnections and pull-in forces that were projected to occur between 30 min and 40 min were applied.
9	Column and spandrel temperatures were linearly changed from temperatures at 30 min to 40 min.
10	Floor/wall disconnections and pull-in forces that were projected to occur between 40 min and 50 min were applied.
11	Column and spandrel temperatures were linearly changed from temperatures at 40 min to 50 min.

Figures 4–86 through 4–133 summarize the results of the global analyses with creep for the analysis steps described in Table 4–30. The vertical displacements of the exterior wall and the core area are presented in Figs. 4–86 through 4–98. For the exterior wall, the vertical displacements were about 2.0 in. to 3.0 in. before the aircraft impact. As indicated in Fig. 4–88, the core had larger vertical displacements by about 1 in. than the exterior walls at Floor 83 before aircraft impact. Since construction sequence was not considered in the analysis, this difference in the vertical displacements changed initial loading conditions of the columns. As shown in Table 4–8, the total column loads on the east and west walls increased by 7 percent at the impacted floors, the total column loads on the north and south walls increased by about 13 percent, and the total column loads on the core decreased by about 8 percent, by ignoring the construction sequence. After aircraft impact, the vertical displacements increased to 7.4 in. on the south wall

(Fig. 4–86). Due to thermal expansion of columns, the vertical downward displacements recovered slightly initially and eventually increased as shortening due to plastic and creep deformations became larger than the thermal expansion. However, the vertical displacements remained around 7.5 in. until 43 min at which point they increased rapidly to 11.3 in. on the east and south faces with the bowing of the east wall. When the east wall reached instability and buckled, the northwest corner of the exterior wall lifted up about 2.0 in., which indicated that the tower was tilting toward the southeast around an axis passing through the southwest and the northeast corners (Fig. 4–87). The tilting of the tower is also illustrated in Figs. 4–88 and 4–89, where the vertical displacements at Floor 83 are presented. As can be seen, with increasing time the displacements on the southeast corner increased, whereas the displacements on the northwest corner decreased. The likely axis about which the tower was tilted is indicated in Fig. 4–89. The axis location in Fig. 4–89 was based upon the distribution of plastic and creep strains, which is presented later in this Section. Figure 4–90 shows the total displacements above Floor 86 when the east wall buckled and collapse initiated. For reference, the undeformed tower is also shown. The tilt toward the southeast is clearly visible.

Analysis of the structure without aircraft impact damage indicates vertical displacements at the top of the building of approximately 4 in. (Figs. 4–91, 4–93, 4–95, and 4–97). Analysis with the estimated aircraft impact damage in place indicates that vertical displacements at the southeast corner of the core increased to approximately 10 in. (Figs. 4–91 and 4–97). As with displacements on the exterior wall, vertical downward displacement of the core was predicted to be somewhat recovered in the initial periods of the fire, due to thermal expansion, and then increased with time as inelastic and creep deformations of the heated and heavily loaded columns increased substantially. When the east wall reached instability and buckled, at 43 min, the core displacements suddenly increased to 13 in. at the southeast corner (Figs. 4–92, 4–94, 4–96, and 4–98).

Figures 4–99 through 4–101 show the out-of-plane displacements of the east wall at various analysis steps. As shown in Fig. 4–99, there was no out-of-plane displacement on the east wall before the aircraft impact. After aircraft impact, the south side of the east wall at Floor 86 displaced outward about 2.0 in., whereas the north side at the same floor remained approximately at the same displacement as before aircraft impact. This shows a slight twist about the z-axis. With increasing time and temperatures, the east wall bowed and the inward displacements increased (Fig. 4–100). At 20 min the maximum inward displacement reached 9.5 in. toward the center of the east wall. This maximum inward displacement agrees well with the maximum inward displacement (~10 in.) that was measured from the photographs and videos at the same time (at 9:21 am which is approximately 18 minutes after the aircraft impact). After 20 min, the inward displacements steadily increased until at 43 min they rapidly increased to 62 in. (Figs. 4–100 and 4–101). At this point, the east wall reached instability and buckled over the entire width of the wall.

Figures 4–102 and 4–103 show the lateral displacements of the exterior wall above Floor 86 after aircraft impact and at the instant of the east wall buckling. After aircraft impact, Floor 110 moved toward the east about 5.0 in. and toward the south about 5.1 in. There was also a slight twist about the z-axis of the tower which was about 0.0007 radian at Floor 110. The twist about the z-axis was calculated by taking the difference between the average in-plane displacement of the two opposing exterior walls (such as the east and the west walls) at Floor 110 and dividing the result by the distance between these walls (~200 ft). With the buckling of the east wall, the lateral displacements increased rapidly. The lateral displacements

of the north exterior wall increased to 15.2 in. toward the east, and of the south exterior wall increased to 6.7 in. toward south. The twist around the z-axis of the tower increased to 0.0010 radian at Floor 110.

Figures 4–104 through 4–111 show the variation of axial loads on the exterior wall columns at different analysis steps. Typically, before aircraft impact, the load distribution along the width of the walls was symmetric with respect to the centerline of each wall. After aircraft impact, the loads in the severed columns redistributed. As a result of this redistribution, the column loads on the south side of the east and west walls and on the east side of south wall increased. This was due to leaning of the tower toward the southeast as the aircraft impact severed columns on the east side of the south wall and on the southeast corner of the core (Figs. 4–104, 4–106, 4–108, 4–110, and 4–111). After redistribution, at Floor 83 the column loads on the south wall increased from about 250 kip before aircraft impact to 400 kip to 800 kip in general and to 1,500 kip at the edges of the severed area after aircraft impact. The column loads on the south side of the east wall at Floor 83 increased from about 350 kip before aircraft impact to about 450 kip after aircraft impact. The column loads on the east side of the north wall at Floor 83 did not change significantly; however, the column loads on the west side of the north wall at Floor 83 decreased from about 250 kip before aircraft impact to about 200 kip after aircraft impact. The column loads on the south side of the west wall at Floor 83 increased from about 300 kip before aircraft impact to about 380 kip after aircraft impact. The column loads on the north side of the west wall at Floor 83, however, decreased from about 300 kip before aircraft impact to 250 kip after aircraft impact. Over the duration of the fires the column load distributions remained constant except for some localized changes due to relative temperatures. When the east wall buckled, the load distribution significantly changed. The columns over nearly the whole width of the east wall unloaded about 400 kip on the average at Floor 83. Similarly, the columns on the west face unloaded about 65 kip on the average. This was due to the increased tilting of the tower toward the east, as the east wall buckled. A part of the loads from the east and the west walls were redistributed to the east side of the south and the north walls. The column loads on the east side of the south wall increased from about 500 kip to 800 kip after aircraft impact, and to 800 kip to 1,100 kip after east wall buckling. The column loads on the east side of the north wall increased from about 200 kip to 250 kip after aircraft impact, and to 300 kip to 500 kip after east wall buckling.

Figures 4–112 through 4–119 show the core column loads at different analysis steps. Before the aircraft impact the loads on the core columns were distributed symmetrically with respect to the center of the core. The slight difference between corner columns on the south side (Columns 501 and 1001) and north side (Columns 508 and 1008) of the core was due to slightly higher dead and live loads in the north side columns. After aircraft impact, some portion of the loads in the severed columns was redistributed to the adjacent intact columns within the core. The tilt toward the southeast also influenced the load redistribution within the core. Columns 506, 507, 508, and 1008 at the northwest and northeast corners unloaded; other intact core columns increased in load (Fig. 4–118). The maximum load in the 800 series core columns increased from about 1,400 kip before aircraft impact to about 1,700 kip after aircraft impact (Fig. 4–112). The maximum load in the 900 series core columns increased from about 1,250 kip before aircraft impact to about 1,900 kip after aircraft impact (Fig. 4–114). Although the maximum load in the 1000 series core columns reduced from about 4,300 kip before aircraft impact to about 3,000 kip after aircraft impact (Fig. 4–116), the average load on the remaining intact 1000 series columns increased about 360 kip at Floor 83 (Fig. 4–118).

Over the duration of the fires, some of the core columns, especially the ones on the east side of the core, unloaded due to yielding and creeping at high temperatures. Loads in softening columns were

redistributed to the adjacent columns with lower temperatures. During buckling of the east wall, the loads in the core columns, especially the ones at the northeast corner of the core, increased significantly. For instance, at Floor 83 the load in core column 1008 increased from 2,820 kip after aircraft impact to 5,320 kip at 43 min, the load in core column 907 increased from 1,290 kip to 2,330 kip, and the load in core column 805 increased from 950 kip to 1,480 kip (Figs. 4–118 and 4–119).

Figure 4–120 shows the axial loads in the columns at Floor 83 before aircraft impact and after the buckling of the east wall. This figure illustrates the load redistribution among the exterior wall and core columns. The tilting of the building about an axis likely located through the shaded area occurred after the buckling of the east wall and weakening of the core. Comparison of column loads before aircraft impact and after the east wall buckled clearly shows the unloading over the entire width of the east wall and increased loads at the east side of the south and north walls.

Figures 4–121, 4–122, and 4–123 show the maximum of the elastic-plus-plastic strains and elastic-plus-plastic-plus-creep strains in the columns between Floor 78 and Floor 83 for different analysis steps. The elastic-plus-plastic strains, which were less than 0.05 percent before the aircraft impact, reached about 0.60 percent in the exterior columns and about 0.35 percent in the core columns after the aircraft impact. With increasing temperatures the plastic strains increased, especially on the east wall and the east side of the core. When the east wall buckled, the elastic-plus-plastic strains reached their maximum of 2.2 percent in the east wall and 0.9 percent in the east side core columns. The creep strains also increased with increasing temperatures to the same level as the elastic-plus-plastic strains in the east wall (1.0 percent to 2.0 percent), to about 2 to 6 times that in the core columns (2.0 percent to 6.0 percent), and to about 10 times that in the east side of the north wall (4.0 percent to 5.0 percent).

The state of the hat truss members and the connections were checked as the global model did not include break elements to capture column and hat truss splice failures or sufficient beam elements to capture buckling of hat truss outriggers. The condition of the connections and the members in the primary load path of the hat truss was evaluated at different time intervals. Evaluations were performed for the core column splices for tensile capacity, outriggers and supporting columns for compressive capacity, and hat truss connections in the primary load path for tensile capacity. The demand forces that were used in the evaluation were obtained from the “superelement” since the hat truss was part of it for the WTC 2 global model with creep. The results for elements within the superelement were obtained by back-substitution. For this purpose the elastic model that was used to generate the stiffness matrix for the superelement was used. This elastic model essentially represents the portion of the building from Floor 86 and above and is referred to as the “top model” hereinafter. The displacements obtained at the interface nodes between the “superelement” and the nonlinear portion of the building (Floor 86 and below) were applied to the base of the “top model” at the end of each analysis step together with the nodal loads representing the dead and the 25 percent of the design live loads.

Figures 4–124 and 4–125 show the loads on the core column splices at the hat truss level at different analysis steps. As can be noticed, each splice was under compressive load before the aircraft impact. After the aircraft impact, the splices at severed core column lines started to carry tensile loads. To evaluate the condition of the core column splices at Floor 106, the tensile capacities of these splices were determined using the AISC LRFD procedures and were compared to the tensile forces obtained at 40 min, since at this time point the tensile forces at core column splices were at their maxima. The evaluation of core column splices required an iterative procedure as splice failures were not modeled in the “top model”. The iteration procedure was required due to the slight nonlinearity of the problem where the

failure of a few splices did not alter boundary conditions of the “top model” significantly. In the first iteration, the state of the “top model” was calculated using the interface nodal displacements at 40 min. Once equilibrium was reached, the columns exceeding their splice capacity were identified (in the first iteration Columns 1001 and 1002 were identified (see Fig. 4–126) and removed). This removal represented the splice failure at that column location. Before removing the columns, the displacement boundary conditions applied at the bottom of these column lines (at Floor 86) were replaced with the reaction forces that were obtained at the end of the first iteration. This conversion from displacement to force boundary condition allowed the remaining portion of the column lines to displace in the vertical direction when the columns were removed at Floor 105 to simulate splice failure. After the removal of the columns, the “top model” was reanalyzed to redistribute the released tensile force due to splice failure. Once equilibrium was reached, the remaining core column splices were reevaluated and any additional splice failures were identified. This iterative procedure was repeated until none of the remaining splices exceeded their tension capacity. A stable state was reached at the end of the fourth iteration. Figure 4–126 summarizes the iteration sequence and the splices that failed at each iteration. Figure 4–127 shows the state of the core column splices at the end of the fourth iteration.

In the global analyses, none of the splice failures were represented as those elements were part of the “superelement” which remained elastic throughout the analysis. However, the inclusion of splice failures is not expected to significantly affect the load redistribution in the global analysis. The loads on columns with failed splices would have redistributed through the core slab and core beams with moment connections to adjacent core columns, which in turn would transfer these extra loads to the hat truss. To quantify the amount of load that was redistributed to the hat truss through the adjacent core columns, the total column loads on each face and at the core area were extracted at Floor 105 at the end of each iteration. Table 4–31 summarizes these total column loads together with the magnitude of total tensile load released and total tensile load retransferred to the hat truss at each iteration. In Table 4–31, the Column “TTLRSF” represents the total tensile load that was released due to splice failure and is equal to the summation of the load carried by the circled columns in Fig. 4–126 up to and including the current iteration. In Table 4–31, the Column “Core” between Rows 6 and 9 represents the load that was transferred to the base of the “top model” through the core columns. The sum of Column “TTLRSF” and Column “Core” represents the total tensile load that was transferred to the hat truss after the splice failures (labeled as “TTLRHT” in Table 4–31). As can be seen, about 73 percent ($= 2,728 \text{ kip} / 3,717 \text{ kip}$) of the released tension load was transferred to the hat truss after the fourth iteration. The core slab and the core beams with moment connections were the primary components that transferred the released load to the adjacent core columns and to the hat truss. Capacity calculations have shown that the core slab and the core beams in the top 20 stories had enough cumulative capacity to redistribute the released load to the adjacent core columns. As a result of load redistribution, the loads on the southeast corner outriggers were reduced, but the loads on adjacent outriggers increased.

Figures 4–128 through 4–130 show the axial loads and stresses in the hat truss members at different analysis steps. With the aircraft impact, the maximum axial load on the outriggers, which was about 1,900 kip before the aircraft impact, increased to about 3,400 kip at the southeast corner. This increase remained almost constant over the duration of the fires. After the buckling of the east wall the maximum load slightly increased to 3,500 kip. The axial stresses in the outriggers also increased as a result of the aircraft impact. The maximum axial stress of 28.4 ksi before aircraft impact increased to 55.0 ksi after the buckling of the east wall. The specified grade of steel for the outriggers was 50 ksi. The tests conducted on this grade of steel showed an average yield strength of about 54 ksi. Considering this yield

strength and the 10 percent increase in the hat truss forces due to neglecting construction sequence, it was concluded that the outriggers of the hat truss did not exceed their elastic limits. To check against buckling, the buckling capacities of these outriggers as well as the supporting columns were calculated. The buckling calculations were performed using the AISC LRFD Eqs. E2-1 and E2-3 with an effective length factor “K” of 0.75 and a resistance factor of 1.0. The calculated capacities were then compared with the axial compressive forces obtained from the analysis and corrected to account for the load increase due to construction sequence. The location of the outriggers and the supporting columns are shown in Fig. 4-3. Tables 4-32 and 4-33 summarize the resulting demand-to-capacity ratios for the outriggers and the supporting columns, respectively. Except for one outrigger, designated Outrigger L, none of the outriggers or supporting columns was predicted to buckle.

Outrigger L was located at the southeast corner of the core, and above the severed core columns. With the splice failures in Columns 1001, 1002, and adjacent core columns, the load on this outrigger reduced and the load redistributed to other outriggers. With the load redistribution after splice failures, the demand-to-capacity ratio on Outrigger L reduced from 1.3 to 1.1 (Col “40* min” in Table 4-32). To investigate whether the buckling of the Outrigger L would cause additional outriggers to buckle, the element representing Outrigger L was removed from the “top model.” Removal of Outrigger L from the “top model” represents an upper bound solution as the load in the outrigger would not drop to zero after buckling. After removal of Outrigger L, the adjacent outriggers increased in load however, as presented in Col “40** min” of Table 4-32, none of the remaining outriggers exceeded their buckling or yield capacities.

In the global analysis, it was assumed that the connections in the hat truss area were adequate to transfer the loads from the core columns to the outriggers. The structural adequacy of the “primary” connections, those hat truss connections between members that were predicted to have axial tensile or compressive stress of 25 ksi or more, was evaluated. To perform this evaluation, the results at 40 min were used, since at 40 min the stresses in the hat truss members were at their maxima. Only connections that transferred tensile forces were evaluated. Figure 4-132 shows the members in the primary load path. Figure 4-133 shows the location of the critical hat truss connections that were evaluated in this study. The connections between the horizontal tie-backs and the outriggers were not evaluated as they were found to have significant capacity in the WTC 1 connection evaluations. Connection capacities were calculated using AISC LRFD procedures. Table 4-34 summarizes capacities, demands, and the predicted condition of the evaluated connections. As can be seen in Table 4-34, before redistribution of load due to column splice failure, none of the connections exceeded their capacities except the connections associated with the 1001 core column line. After load redistribution, the demand was less than the yield capacities for all connections. Based on this, and the other evaluations of column splices and hat truss members discussed above, it was concluded that the hat truss was capable of transferring loads from core columns to the outriggers without any connection failures.

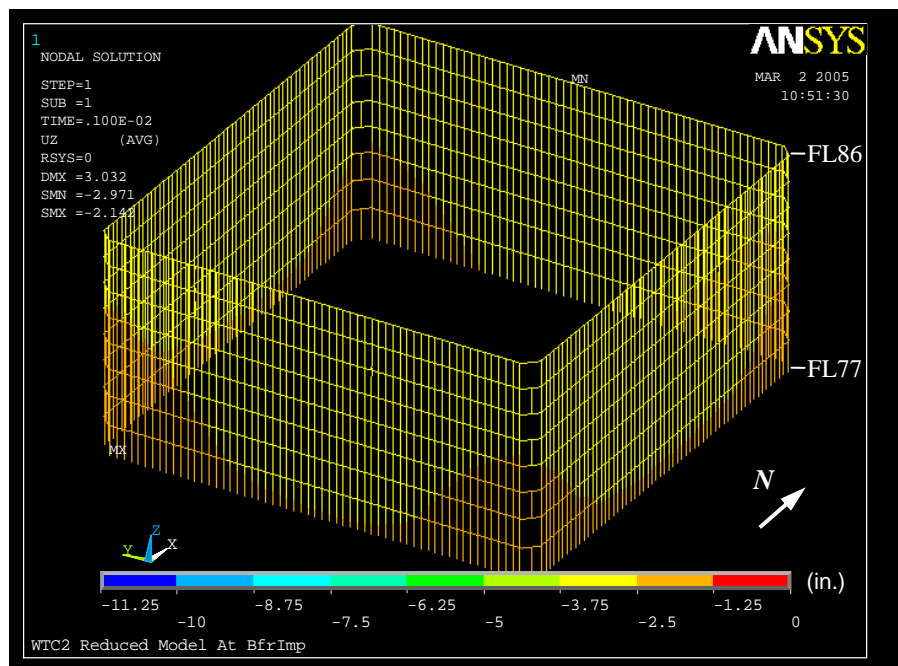
Tables 4-35 and 4-36 summarize the total column loads at each exterior face and the core for Floor 83 and Floor 105. The first seven rows of Tables 4-35 and 4-36 provide the total loads at each analysis step. The rows from 8 through 13 give the change in total column loads at each analysis step with respect to the total column loads before aircraft impact. For instance, Row 8 gives the difference between the total column loads before and after aircraft impact. A positive value between Row 8 and Row 13 indicates that the total compressive load has increased in that analysis stage as compared to the total compressive load before the aircraft impact. Based on these tables, after the aircraft impact, the core and the north wall

unloaded and their loads were redistributed to the south, west, and especially to the east wall at Floor 83. A similar load redistribution pattern was found for Floor 105. The comparison of the total column loads before and after aircraft impact at Floor 83 and Floor 105 is presented in Table 4–37. The second row in this table represents the amount of load redistributed through the hat truss, and the third row represents the amount of load redistributed through the spandrels and the floors. Based on this table, it can be stated that about 94 percent (3,740 kip/4,000 kip) of the load that was unloaded from the core was redistributed through the hat truss to the east, south, and west walls, and the remaining 6 percent was redistributed through the floors to the exterior walls. A similar calculation for the east wall indicates that about 62 percent (2,699 kip/4,368 kip) of the load increase on the east wall came through the hat truss and the remaining 38 percent came through the Vierendeel action of the wall. Rows 8, 9, 10, and 11 of Table 4–35, show that the loads in the various walls and the core itself did not significantly change until the core unloaded at about 30 min. At 30 min the total column loads on the east wall increased by about 1,200 kip (from 5,567 kip to 4,368 kip) and the core unloaded about 850 kip (from 4,861 kip to 4,007 kip) and the north wall unloaded about 420 kip (from 1,797 kip to 1,374 kip) at Floor 83. Similarly, at Floor 105 and at 30 min the total column loads in the various walls and core remained almost constant until initiation of buckling of the east wall. After 40 min, the east wall suddenly unloaded about 8,540 kip, the west wall unloaded about 2,860 kip, the core experienced a load increase of about 5,600 kip, the north wall increased by about 2,310 kip, and the south wall increased by about 2,820 kip at Floor 83 (Table 4–38). Comparison of the load redistribution that took place at Floor 105 with the one at Floor 83 indicates that about 100 percent of the additional core load came from the east and the west walls through the hat truss. For the east wall, about 46 percent (3,901 kip/8,539 kip) of the relieved load was redistributed through the hat truss to the core, and the remainder was redistributed through Vierendeel action to the south and north walls. After the redistribution, at 43 min, the load in the core had recovered to the same level as the total load before the aircraft impact.

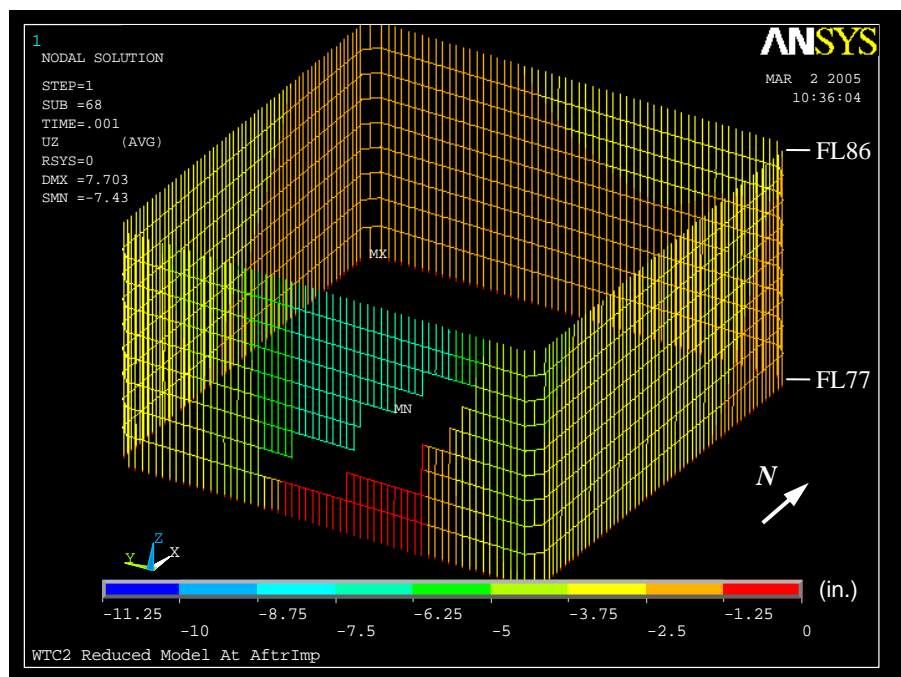
Tables 4–39 through 4–43 summarize the loads in the east, south, north, west walls, and the core at several floor levels. The tables also indicate the change in column load at each stage of the analysis, compared to the load present before aircraft impact. These load changes are provided in Columns 8 through 13. As described before, the changes in loads at Floor 105 represent the load redistribution through the hat truss. The changes in loads along the height of the tower indicate the load redistribution through the exterior wall and the floor system. In referring to the changes in loads after the aircraft impact (Col 8 in the tables), it can be concluded that the total column loads along the height of the core and the west wall remained almost constant. This indicates that almost all load redistribution from and to these portions of the tower went through the hat truss. The total column loads in the east wall increased at the hat truss level and continued to increase with distance from the hat truss. The north wall showed the opposite trend; at the hat truss level the wall unloaded and continued to unload further with distance from the hat truss. The unloading took place primarily through Vierendeel action, to the east wall. After the buckling of the east wall, the change in loads (Col 13 in the tables) indicates that the hat truss was the primary load path for the portion of the load picked up by the core. The east and west walls unloaded at the hat truss level and at lower floors. Both walls steadily picked up more load at lower floors through the action of spandrels.

During the load redistribution, the floor slabs played a significant role in restraining the core in the lateral direction. The aircraft impact damage to the core and the ensuing fire environment caused the core to lean toward the south and east. In fact, calculations show that the isolated core would not have been stable. The resistance to core leaning was provided by the exterior wall. The load was transferred to the

exterior walls by shear either through slabs or hat truss. To identify the contribution of the floor slabs to the lateral restraint of the core, the moment of the core column loads around the center of the building in the x- and y-directions at Floor 83 and Floor 105 were computed for WTC 2. Before impact, there was no eccentricity in the load, and the moments thus calculated were small. After impact and at the end of temperature histories, the moment in the x-direction was 5,905,640 kip-in at Floor 83 and 2,282,320 kip-in at Floor 105. Similarly, the moment in the y-direction was 5,051,130 kip-in at Floor 83 and 2,196,440 kip-in at Floor 105. The change in moment from Floors 83 to 105 was due to the lateral resistance of provided by the slabs and the exterior walls to the core. The results of calculations show that the overturning moment reduced by about 55 percent to 60 percent along the height of the tower. This reduction was due to the lateral resistance provided by the floor slabs. The remaining 40 percent to 45 percent was resisted by the hat truss.

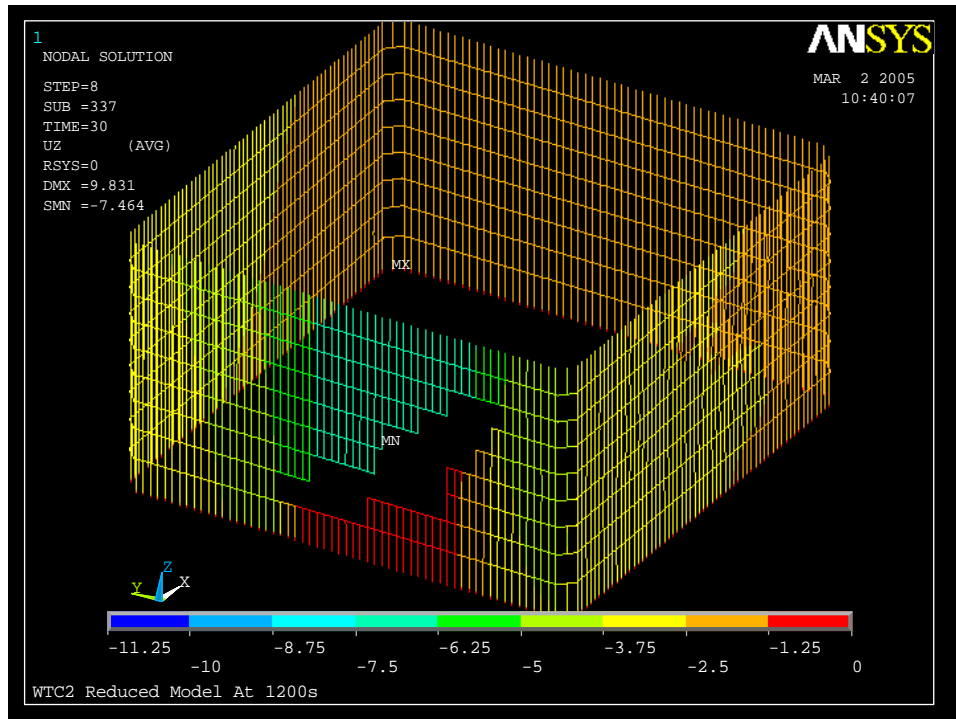


(a) Before impact

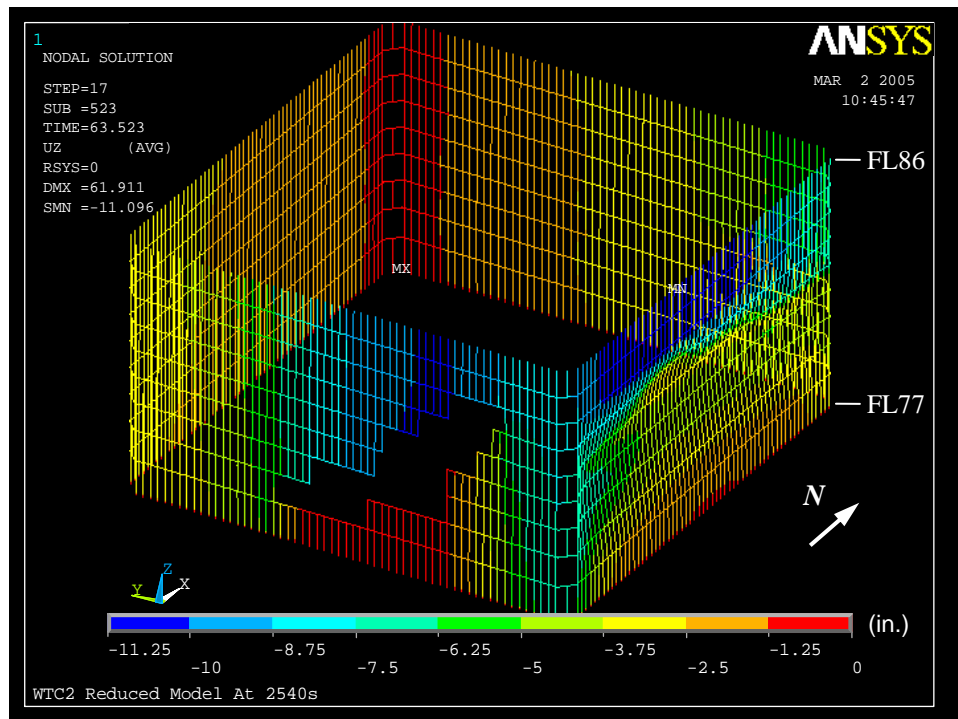


(b) After impact

Figure 4–86. Vertical displacement of exterior wall of WTC 2 for Case D conditions (downward displacement is negative).



(a) 20 min



(b) 43 min

Figure 4–87. Vertical displacement of exterior wall of WTC 2 for Case D conditions (downward displacement is negative).

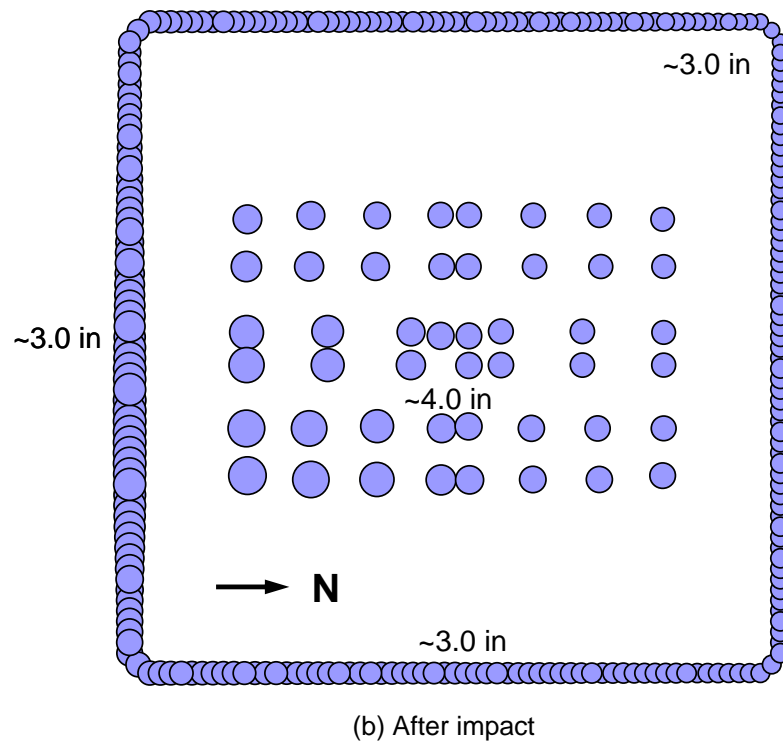
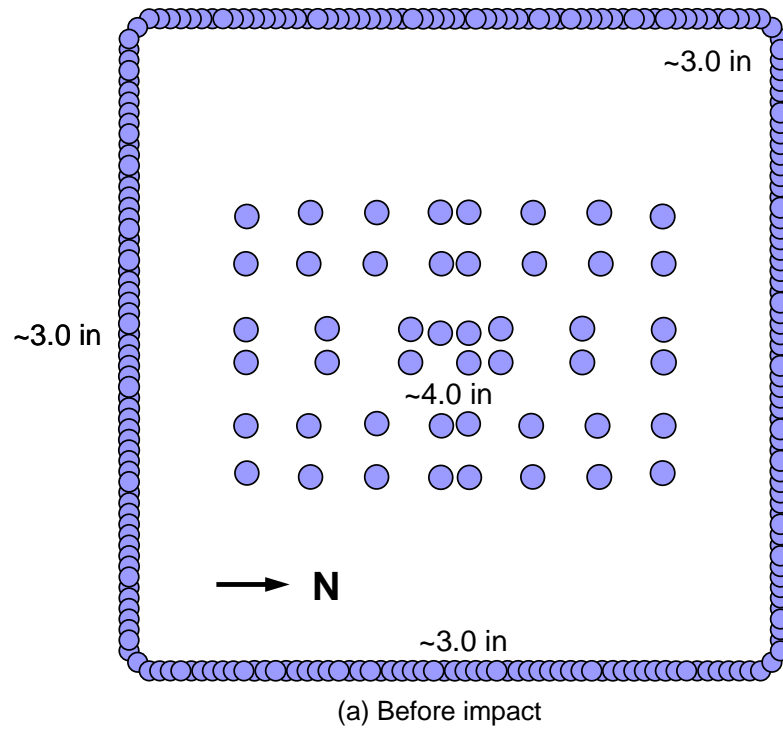


Figure 4–88. Vertical displacement at Floor 83 of WTC 2 for Case D conditions (downward displacement is positive).

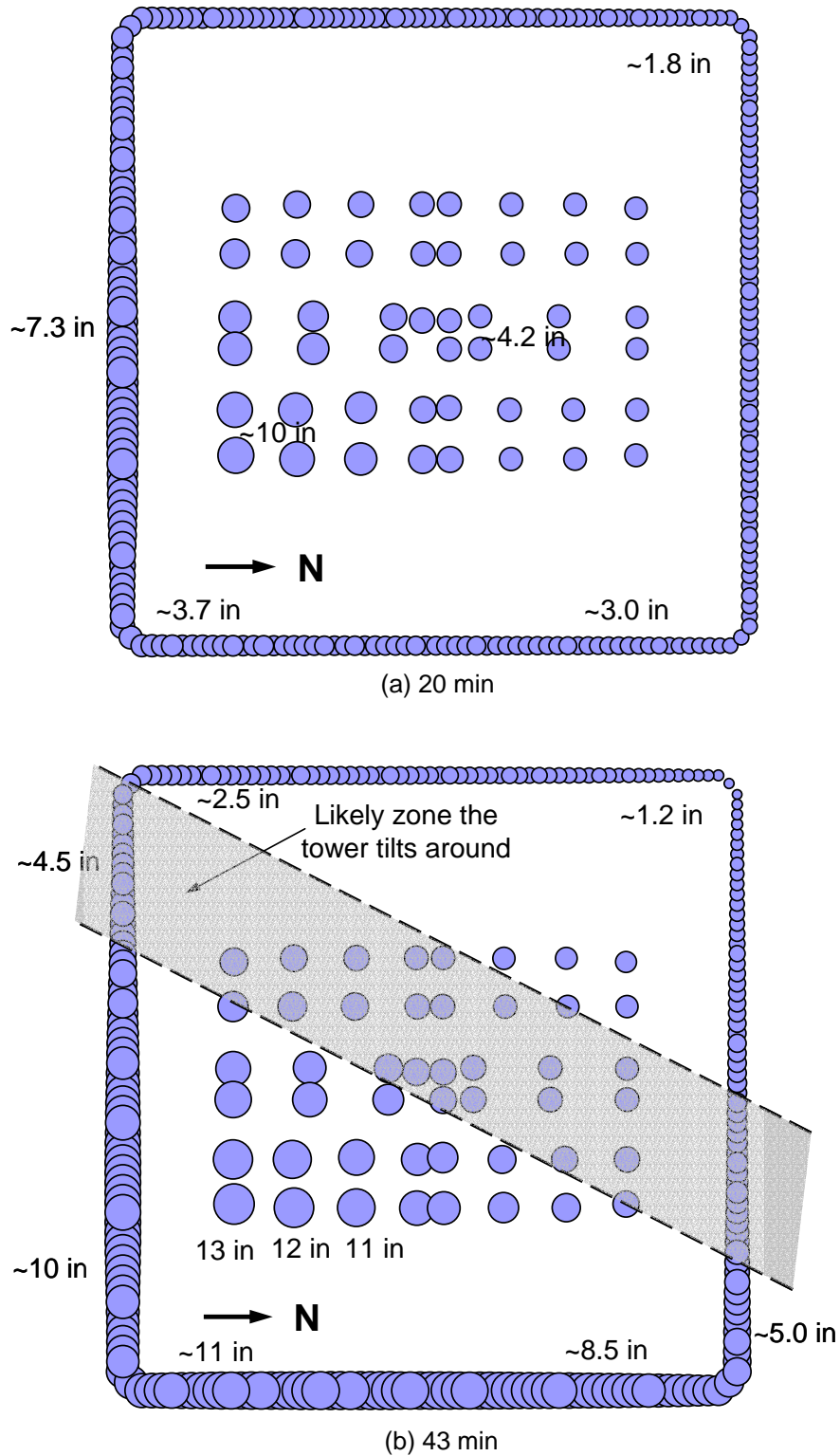


Figure 4–89. Vertical displacement at Floor 83 of WTC 2 for Case D conditions (downward displacement is positive; note the tilt toward east and south).

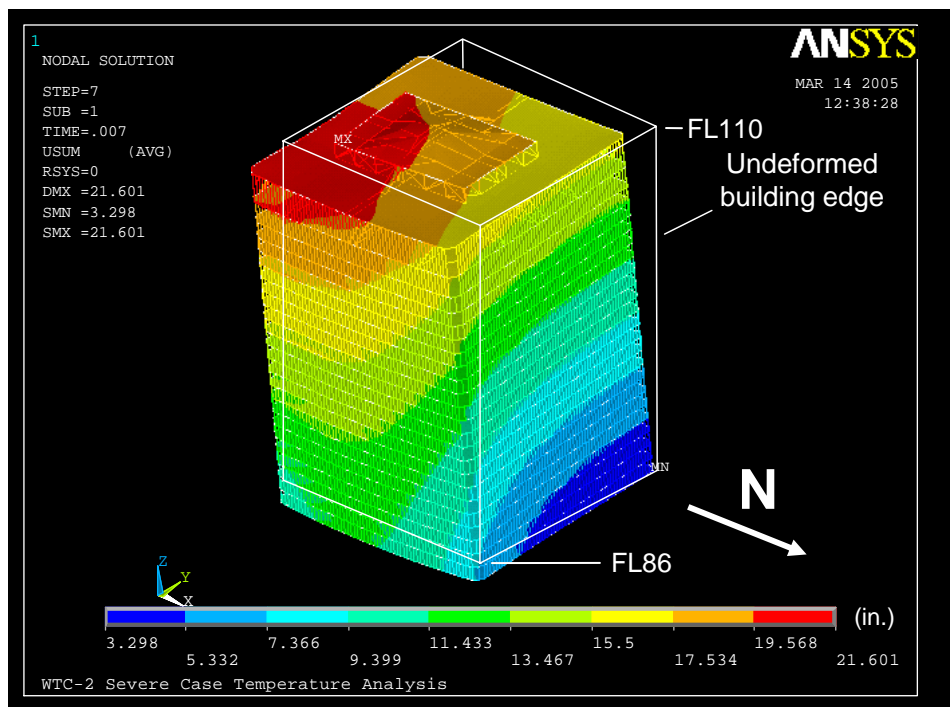
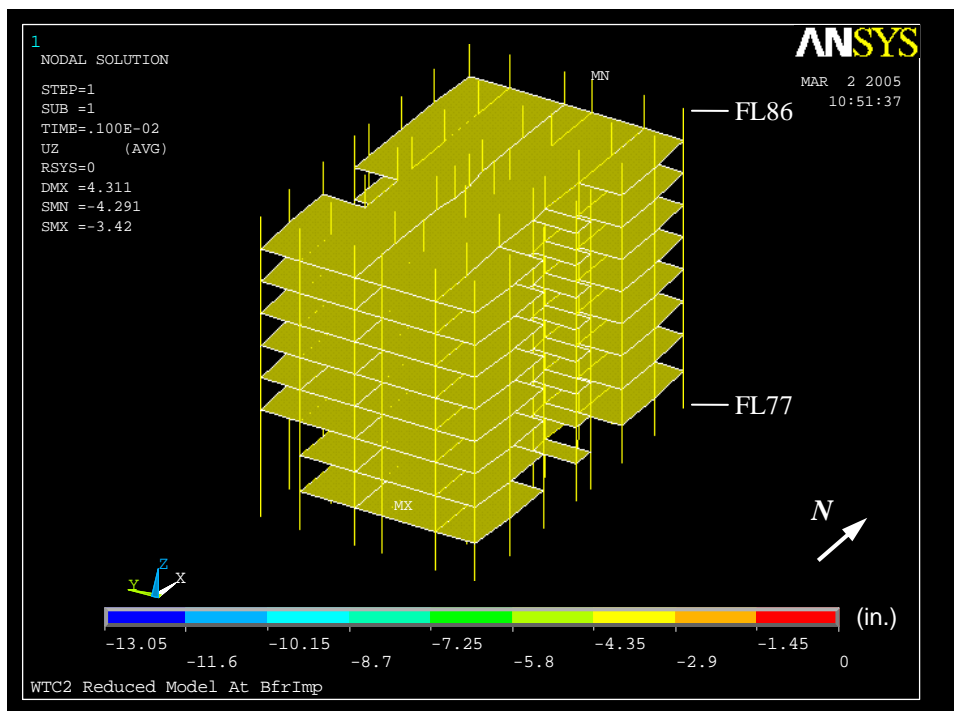
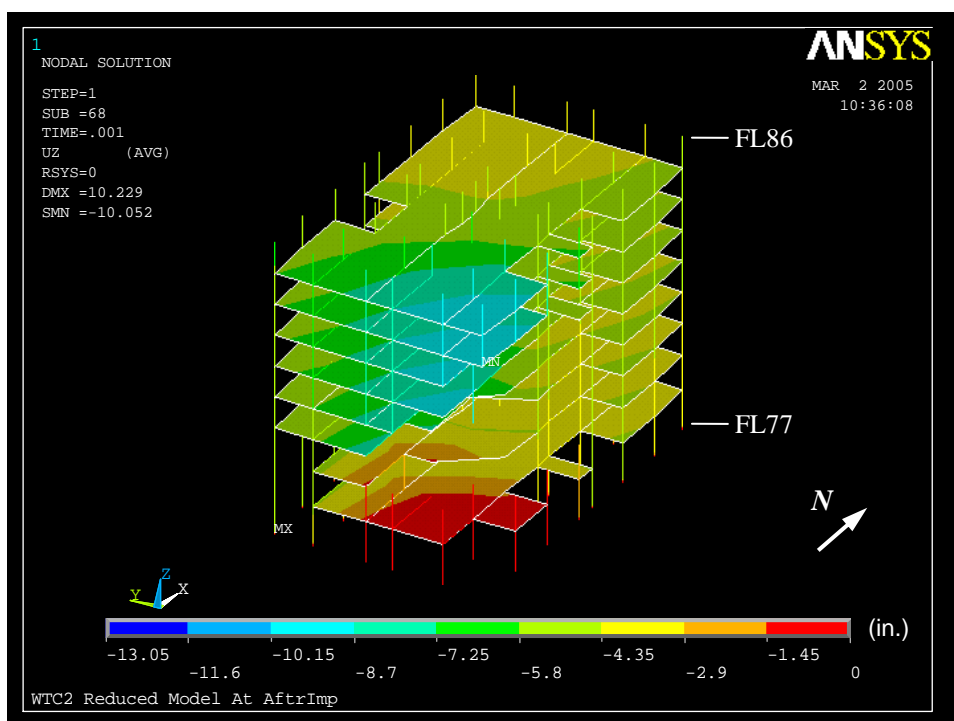


Figure 4–90. Total displacements of WTC 2 above Floor 86 at 43 min of Case D conditions (deformed shape magnified 20 times). Note the tilt toward east and south.

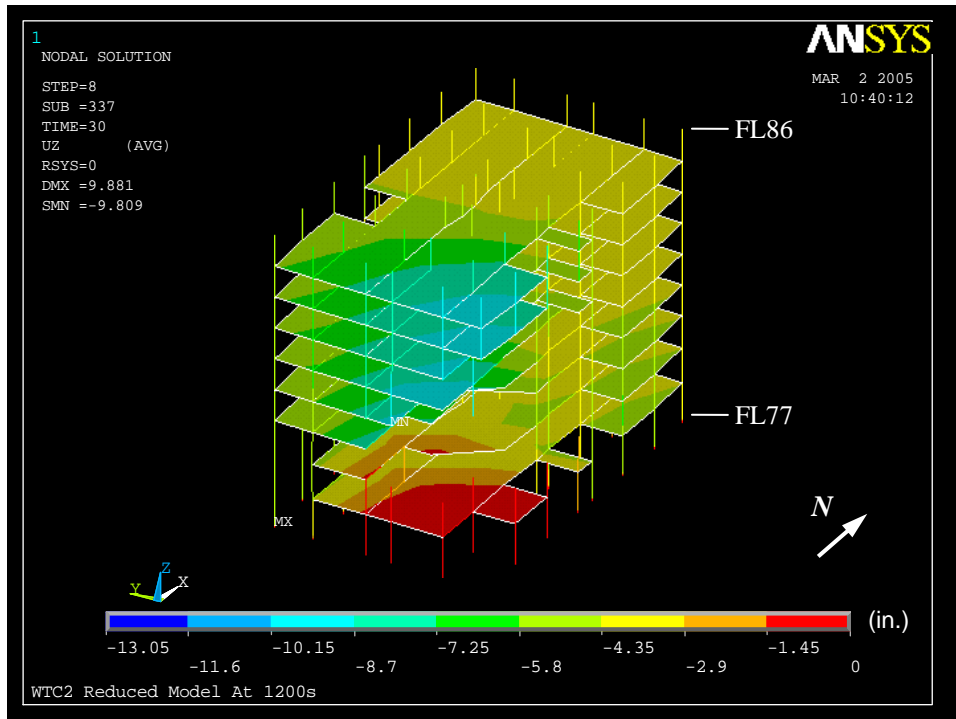


(a) Before impact

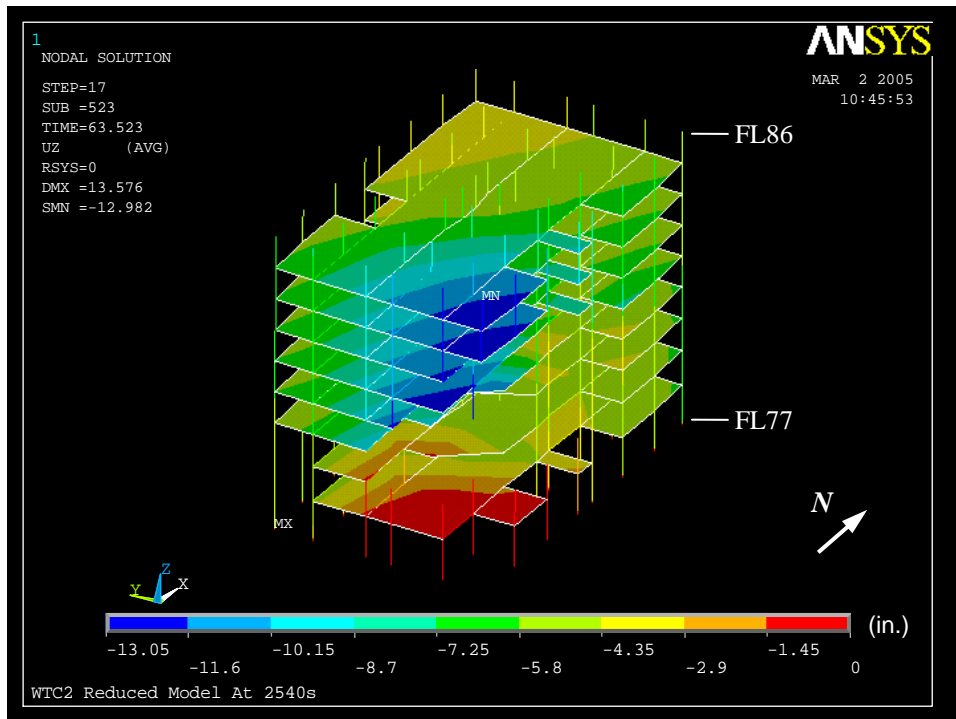


(b) After impact

Figure 4–91. Vertical displacement of core of WTC 2 for Case D conditions (downward displacement is negative).

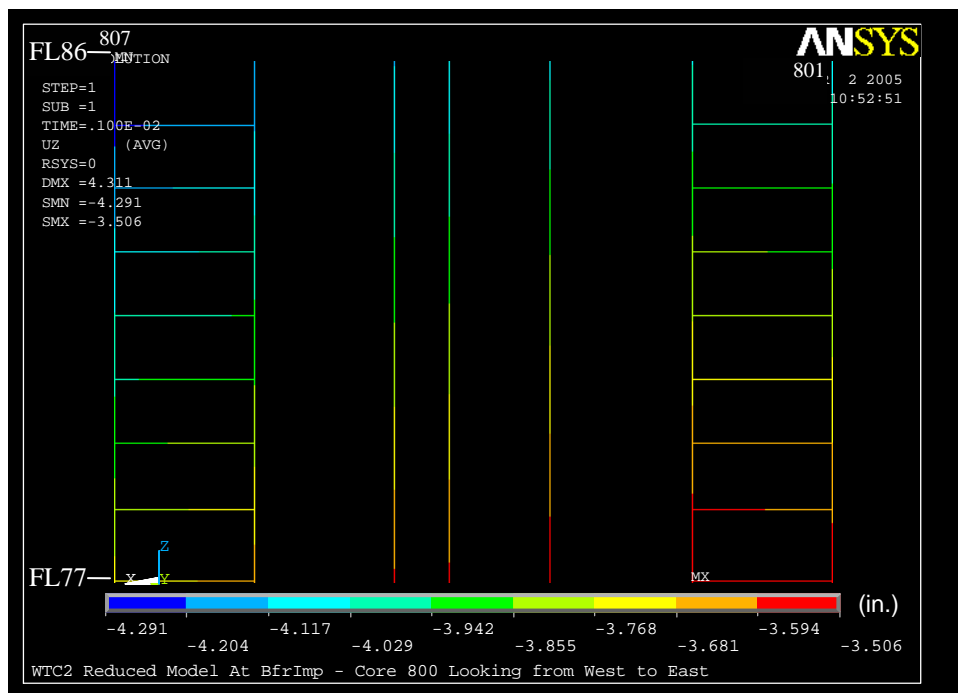


(a) 20 min

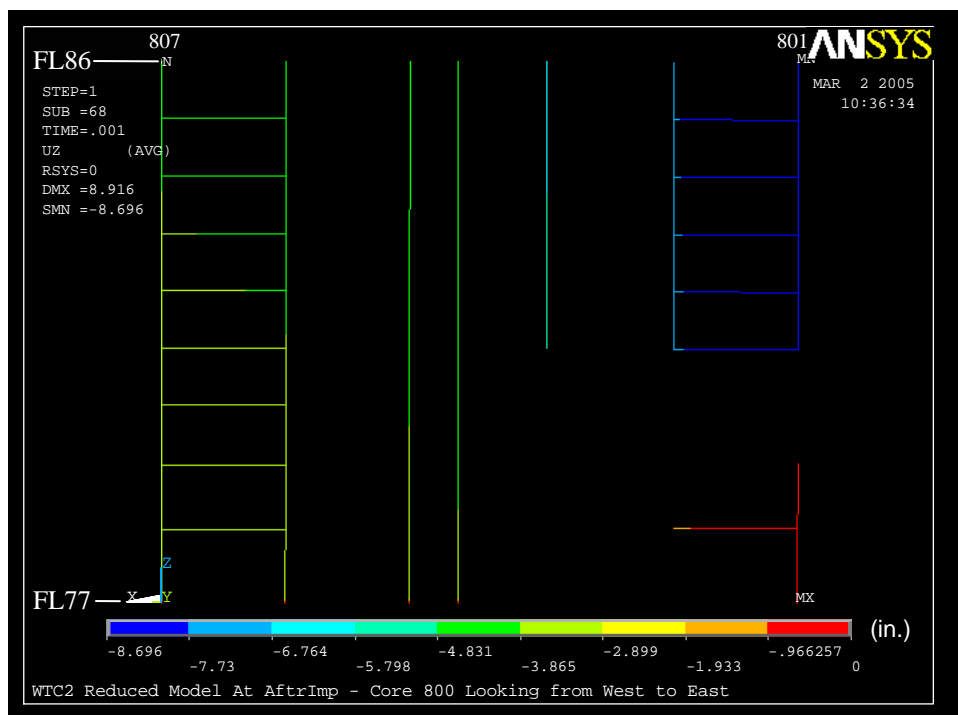


(b) 43 min

Figure 4–92. Vertical displacement of core of WTC 2 for Case D conditions (downward displacement is negative).

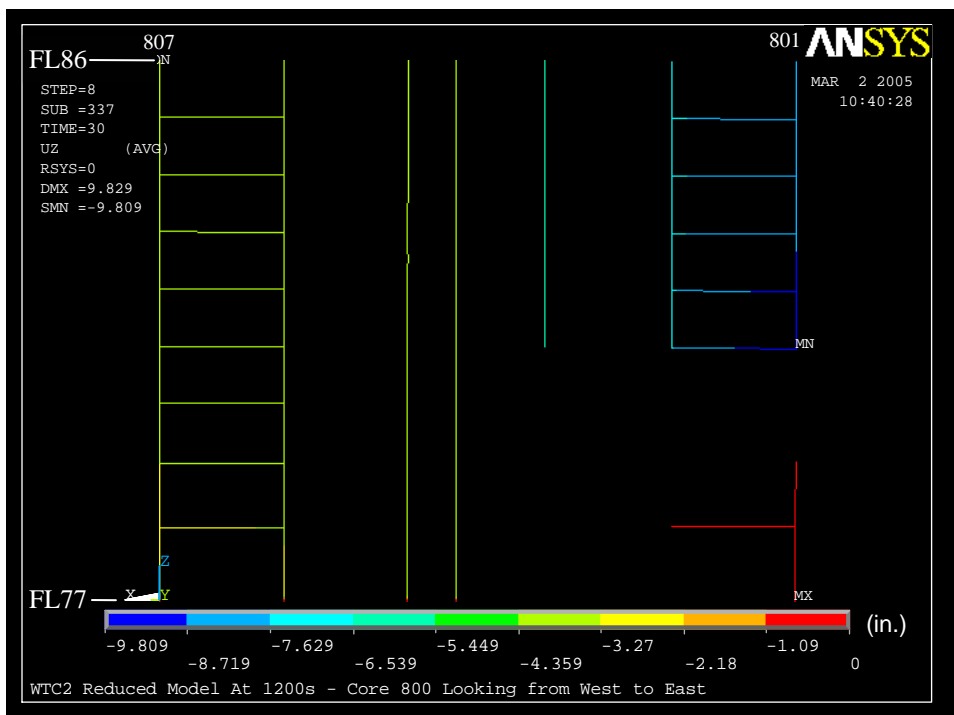


(a) Before impact

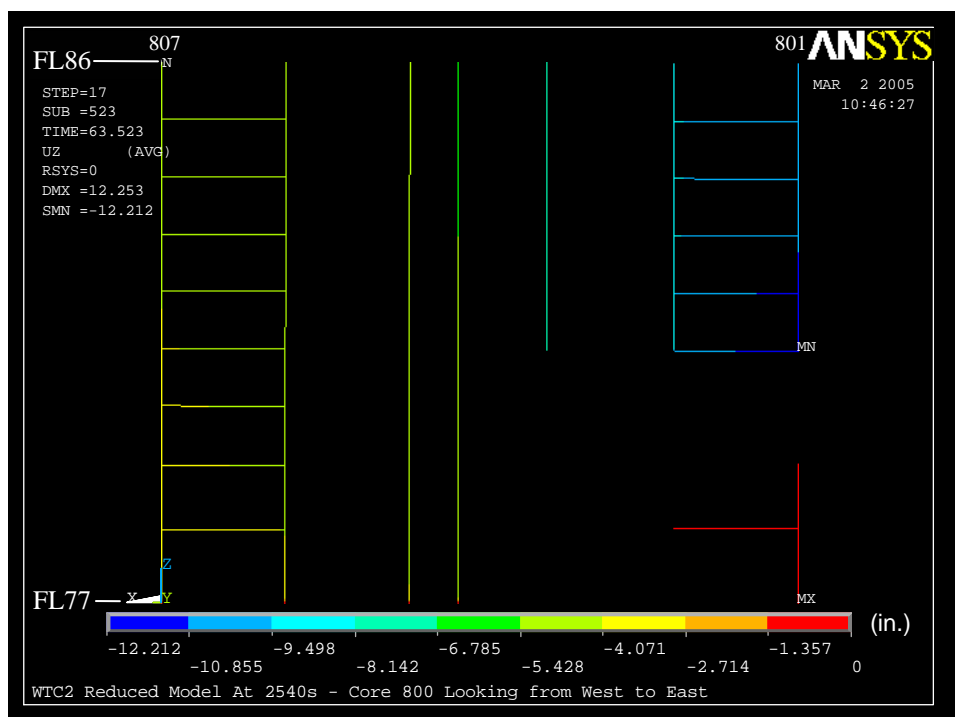


(b) After impact

Figure 4-93. Vertical displacement of 800 series core columns of WTC 2 for Case D conditions (downward displacement is negative).

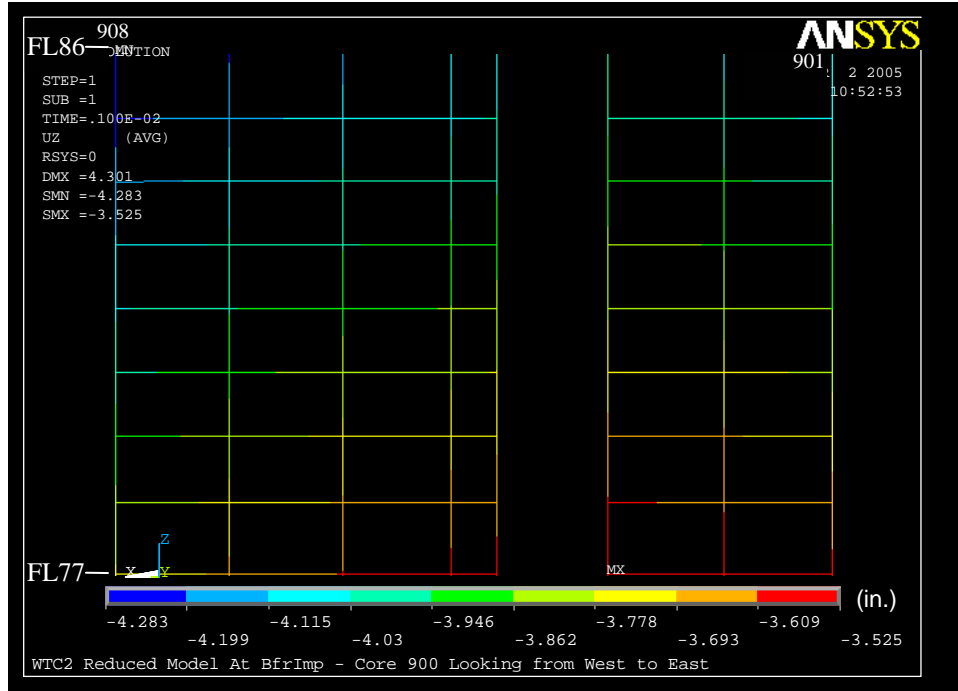


(a) 20 min

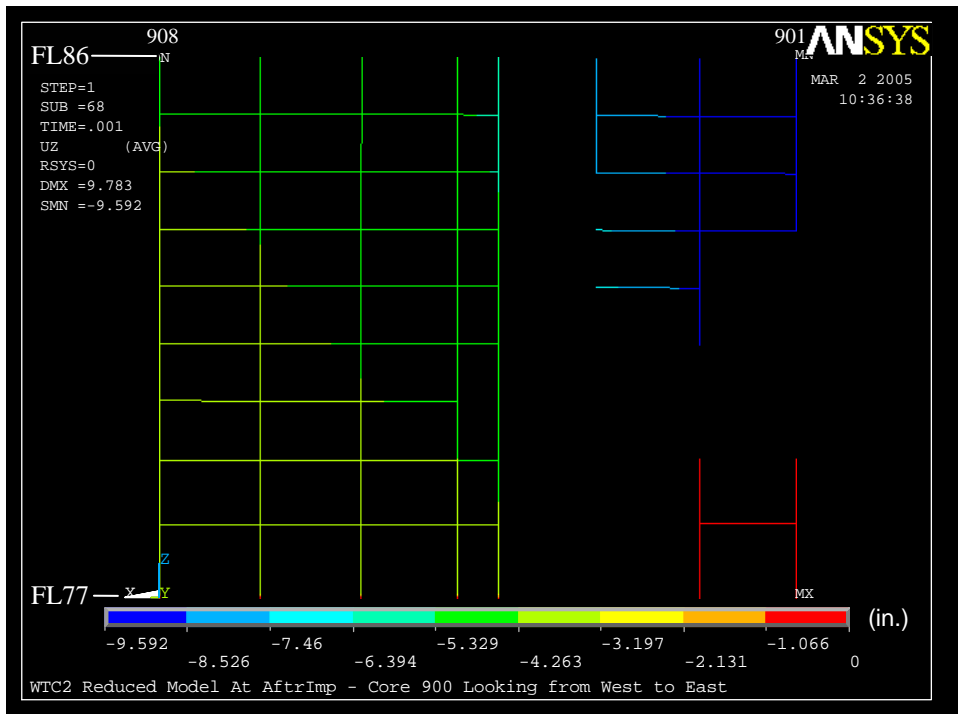


(b) 43 min

Figure 4-94. Vertical displacement of 800 series core columns of WTC 2 for Case D conditions (downward displacement is negative).

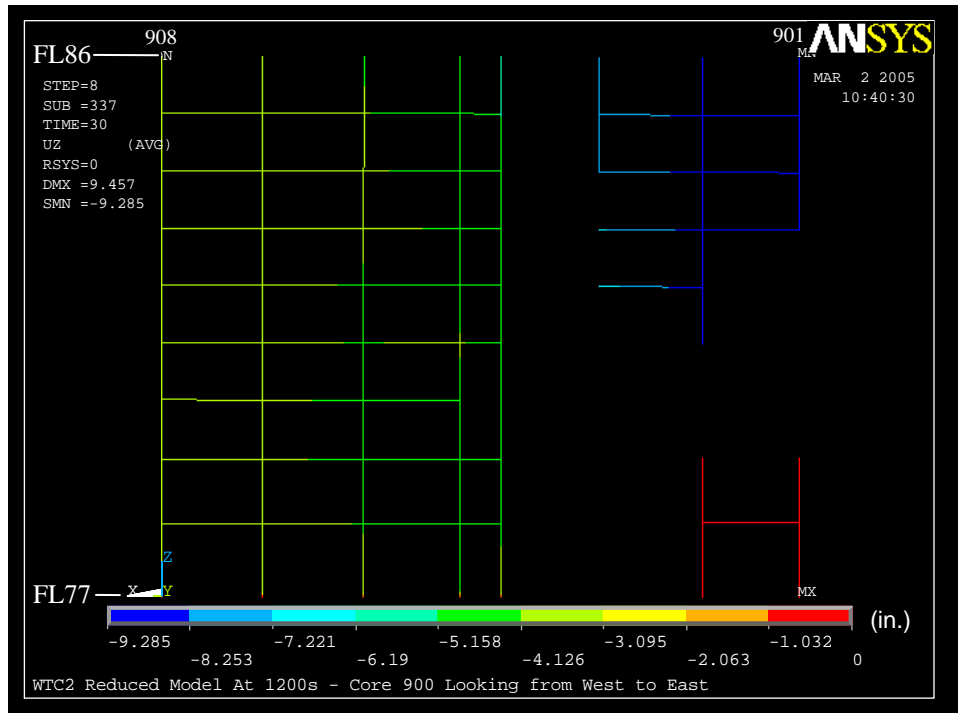


(a) Before impact

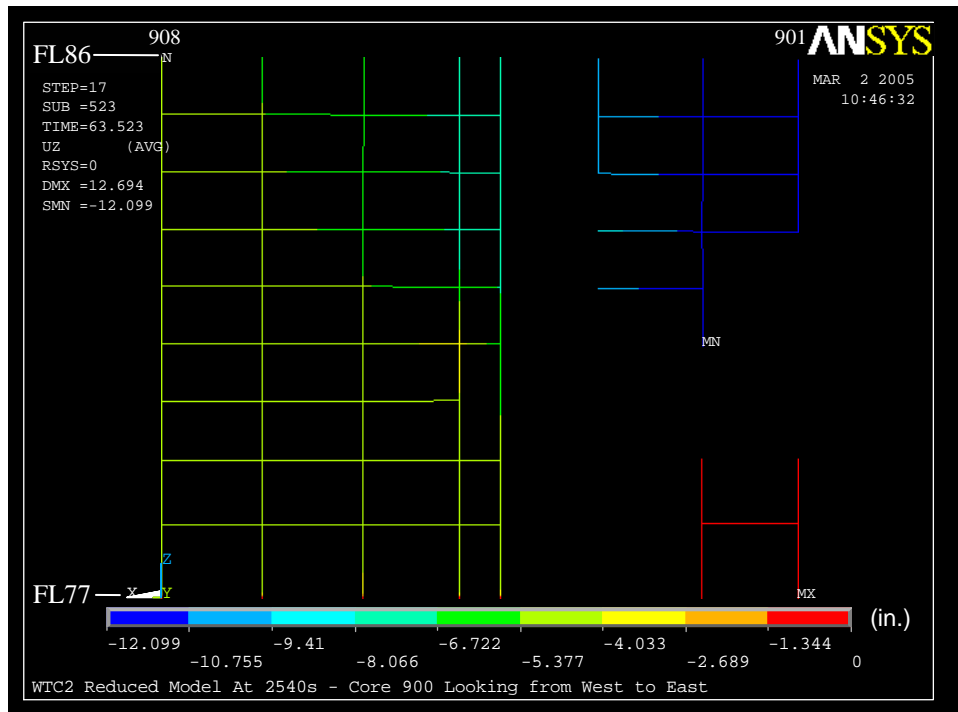


(b) After Impact

Figure 4-95. Vertical displacement of 900 series core columns of WTC 2 for Case D conditions (downward displacement is negative).

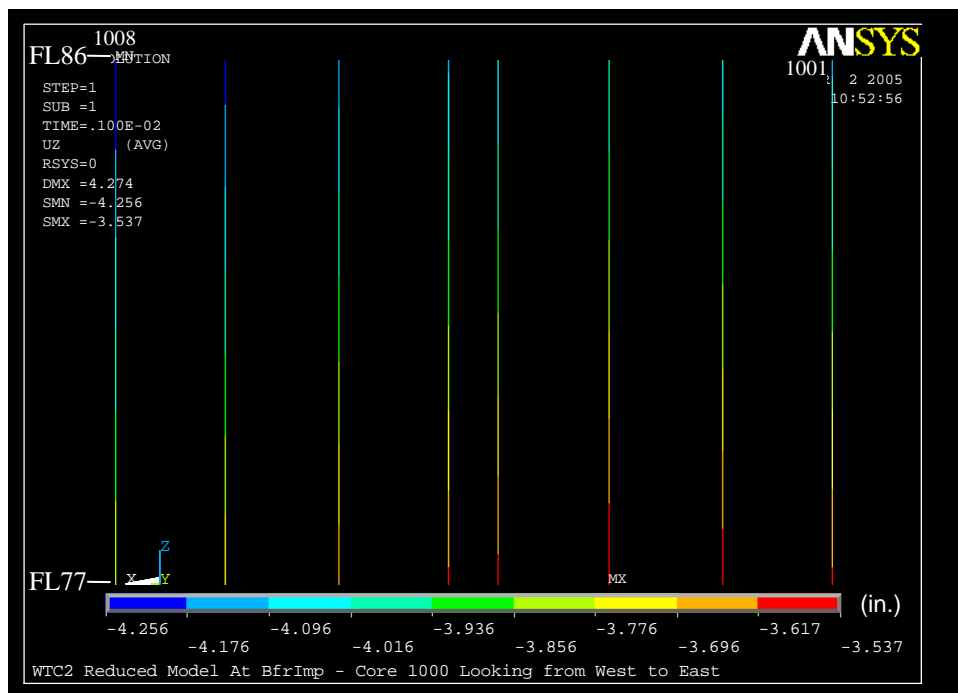


(a) 20 min

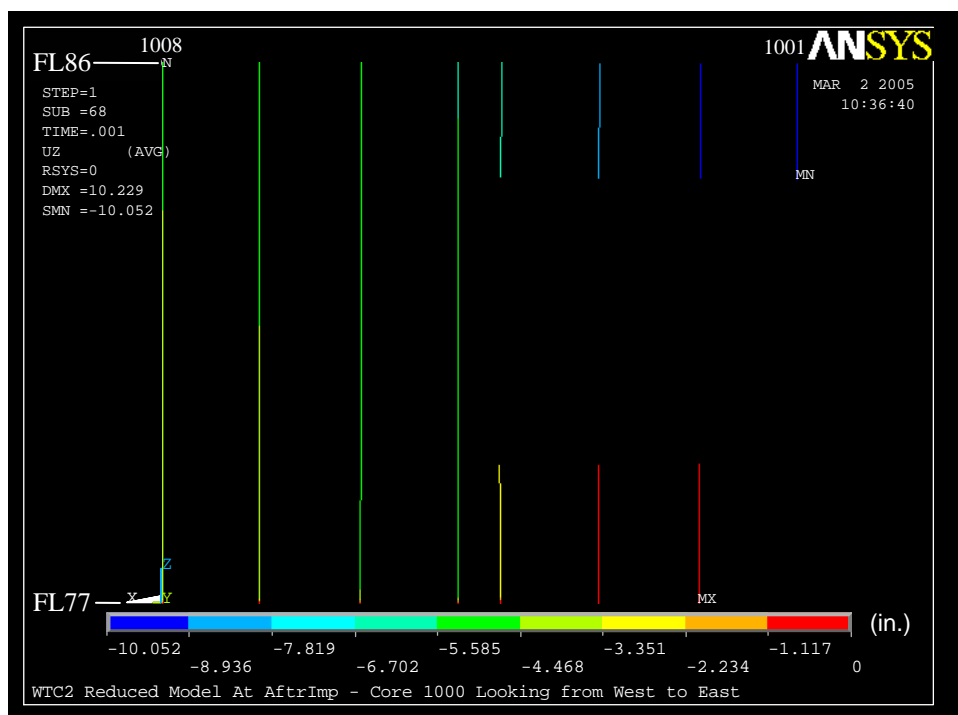


(b) 43 min

Figure 4-96. Vertical displacement of 900 series core columns of WTC 2 for Case D conditions (downward displacement is negative).

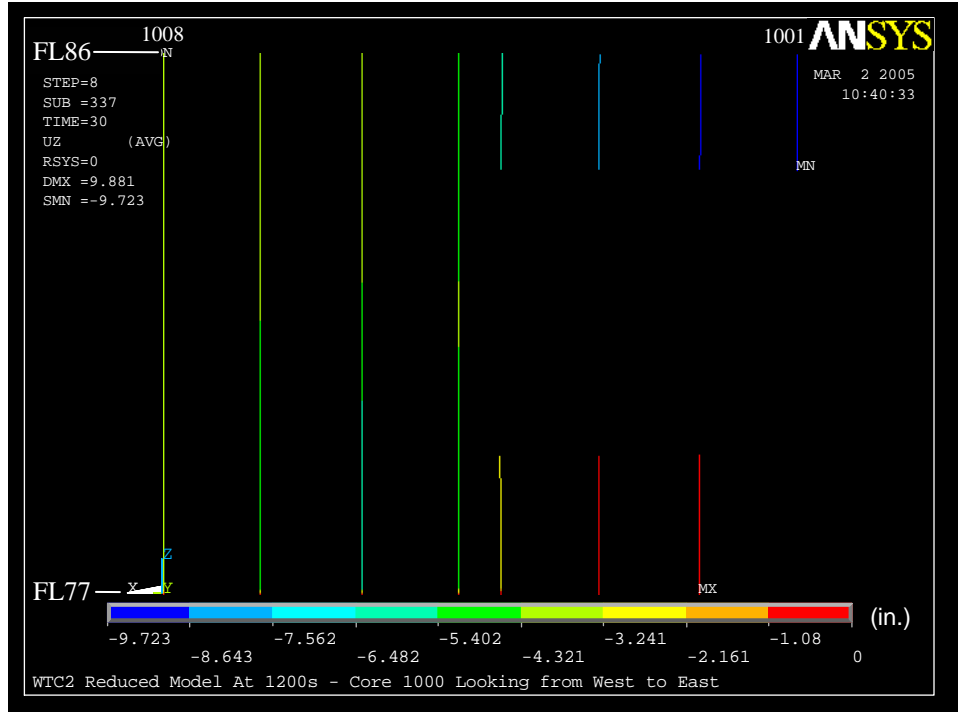


(a) Before impact

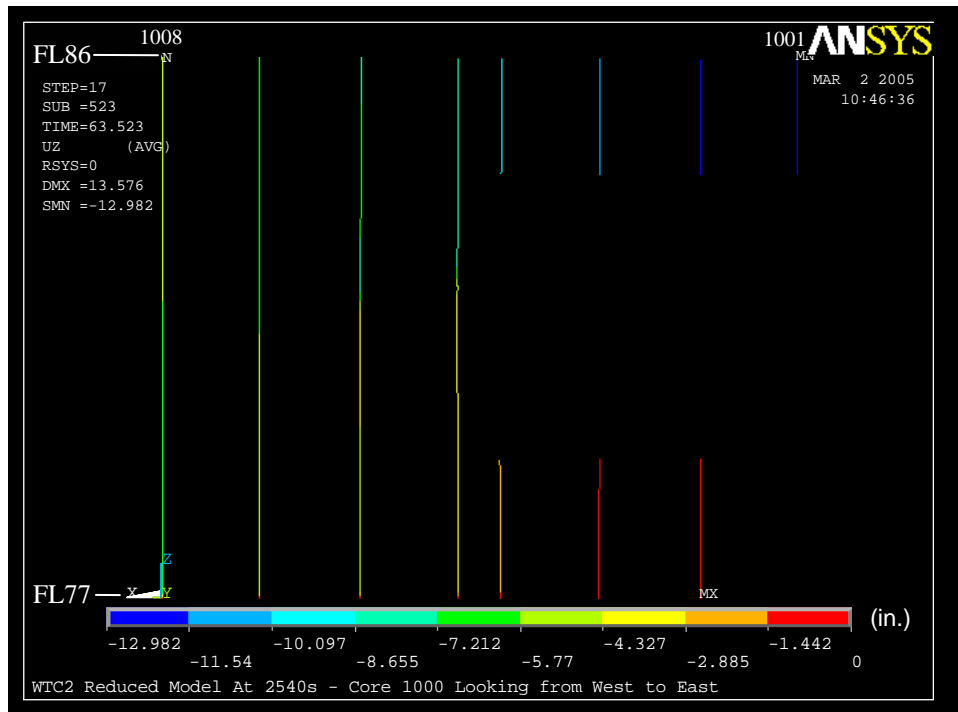


(b) After impact

Figure 4-97. Vertical displacement of 1000 series core columns of WTC 2 for Case D conditions (downward displacement is negative).

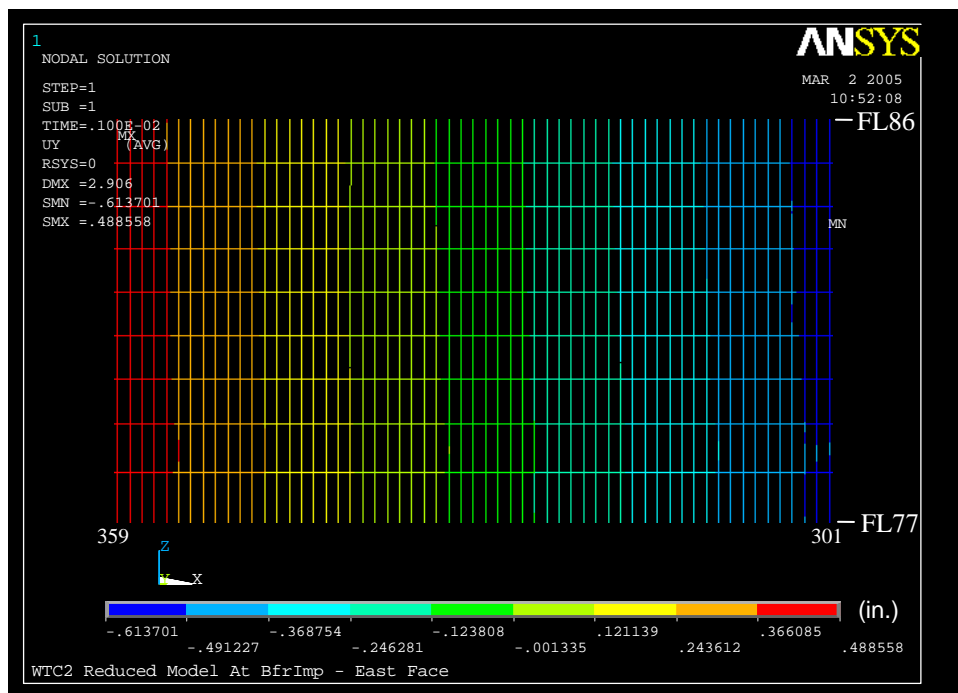


(a) 20 min

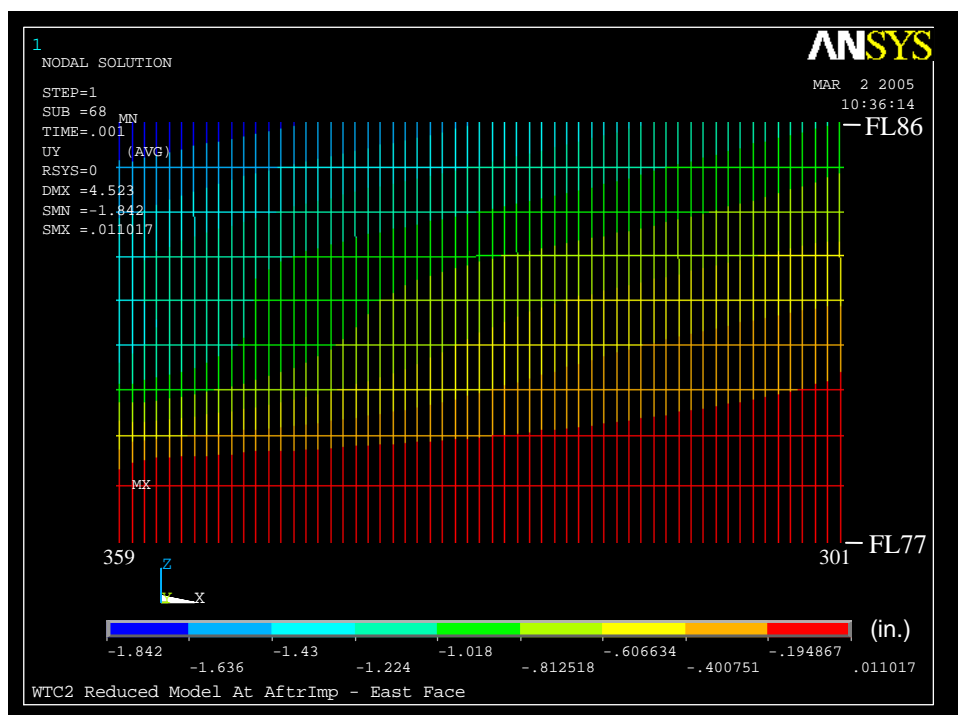


(b) 43 min

Figure 4–98. Vertical displacement of 1000 series core columns of WTC 2 for Case D conditions (downward displacement is negative).

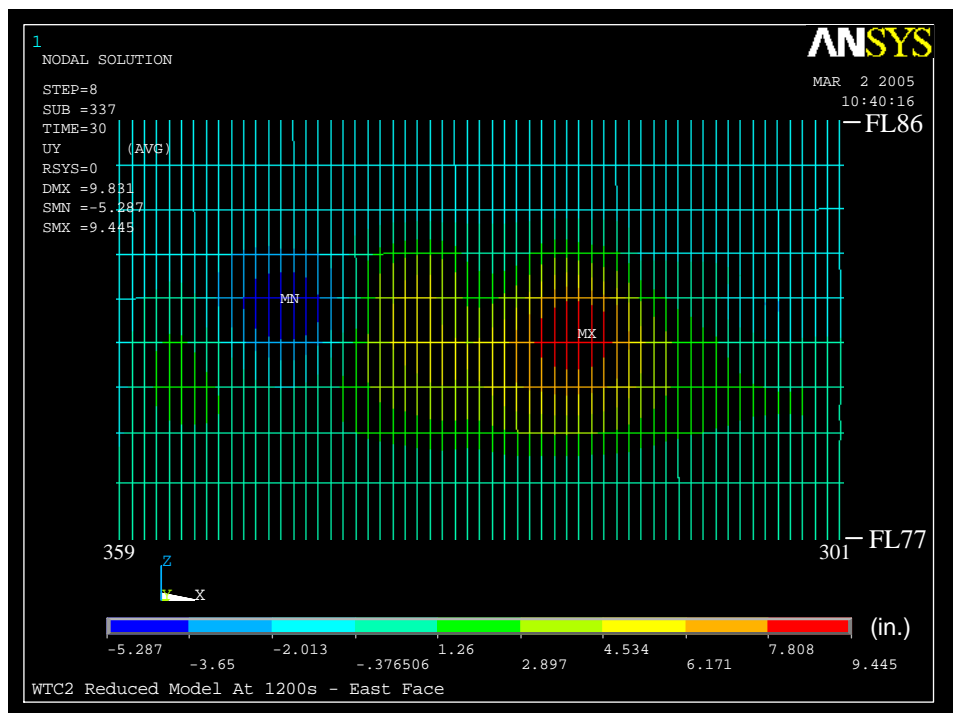


(a) Before impact

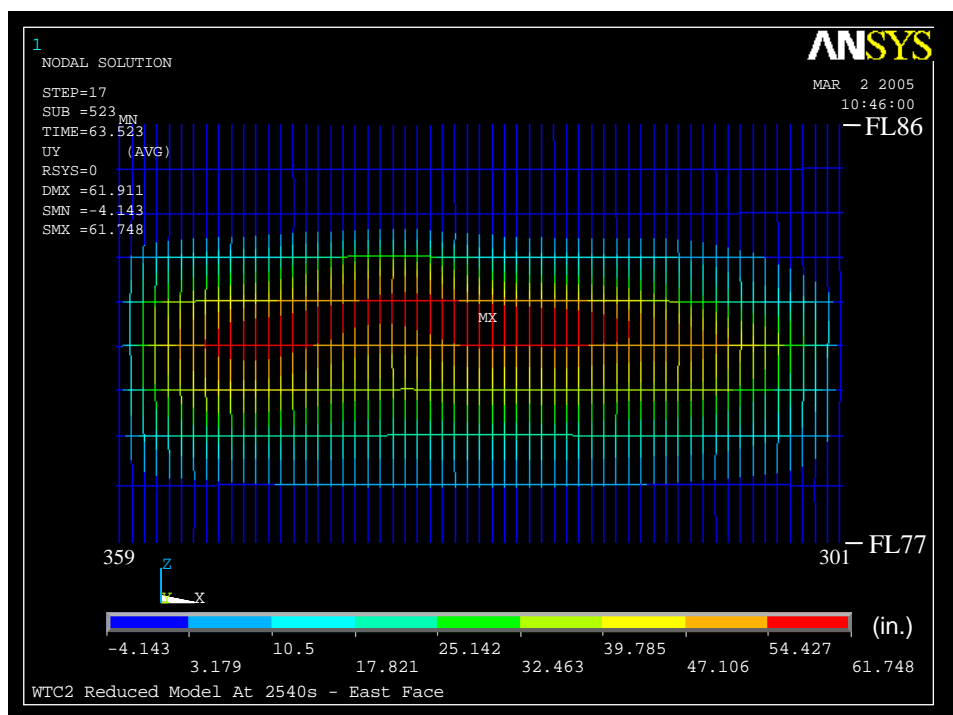


(b) After impact

Figure 4-99. Out-of-plane displacement of the east wall of WTC 2 for Case D conditions (inward displacement is positive).



(a) 20 min



(b) 43 min

Figure 4-100. Out-of-plane displacement of the east wall of WTC 2 for Case D conditions (inward displacement is positive).

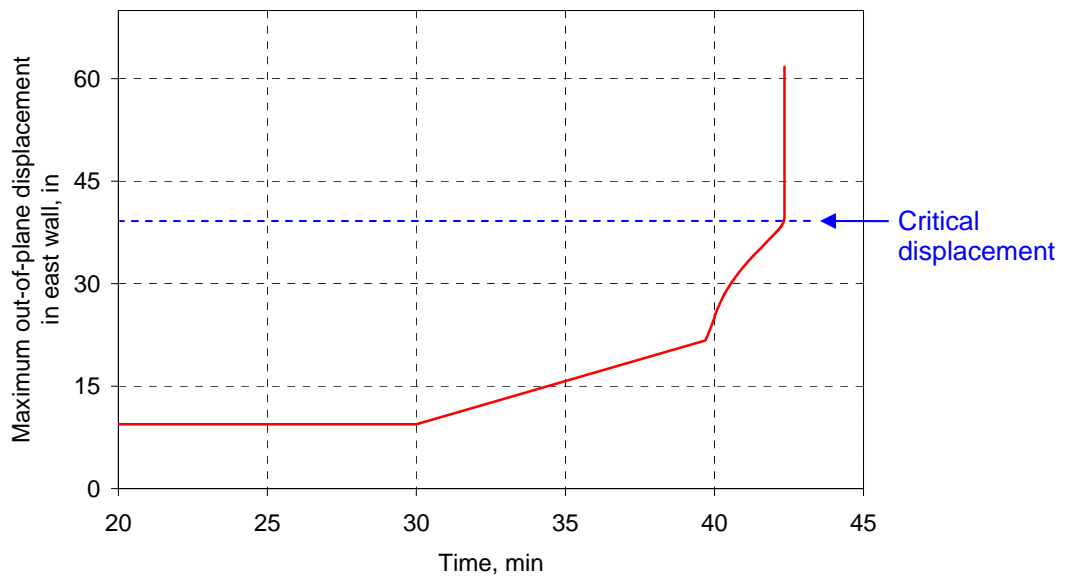
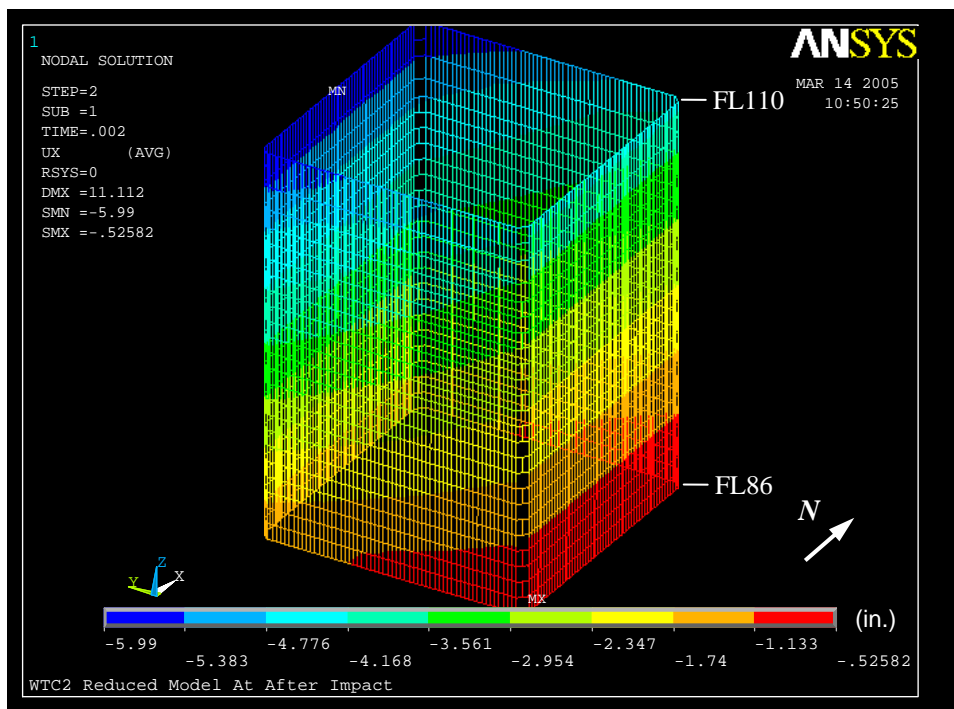
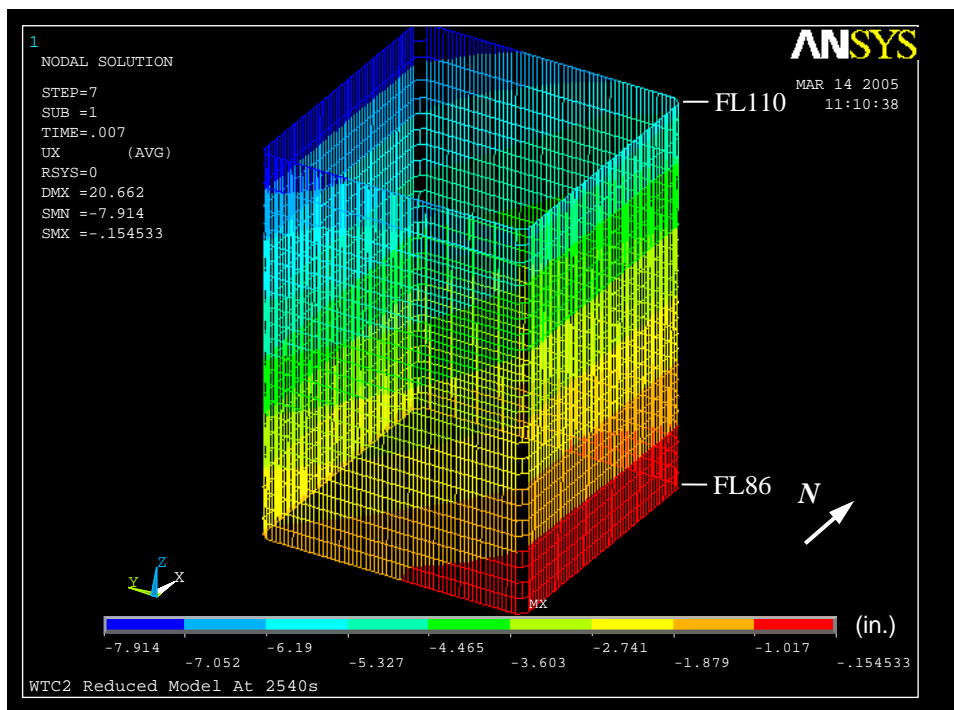


Figure 4–101. Variation of maximum inward bowing of the east wall of WTC 2 over time for Case D conditions.

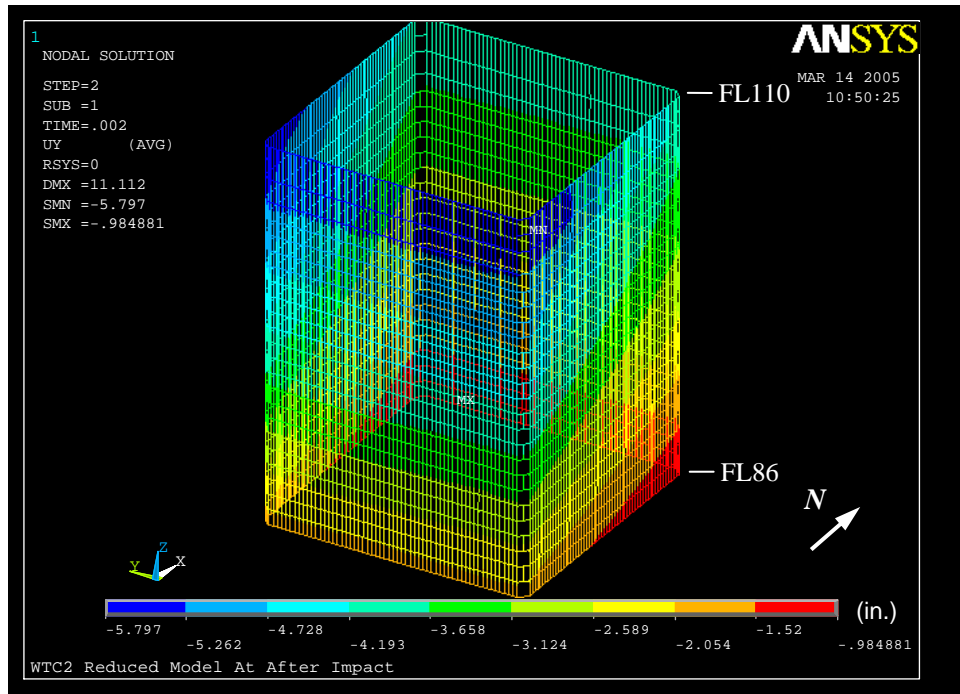


(a) After impact

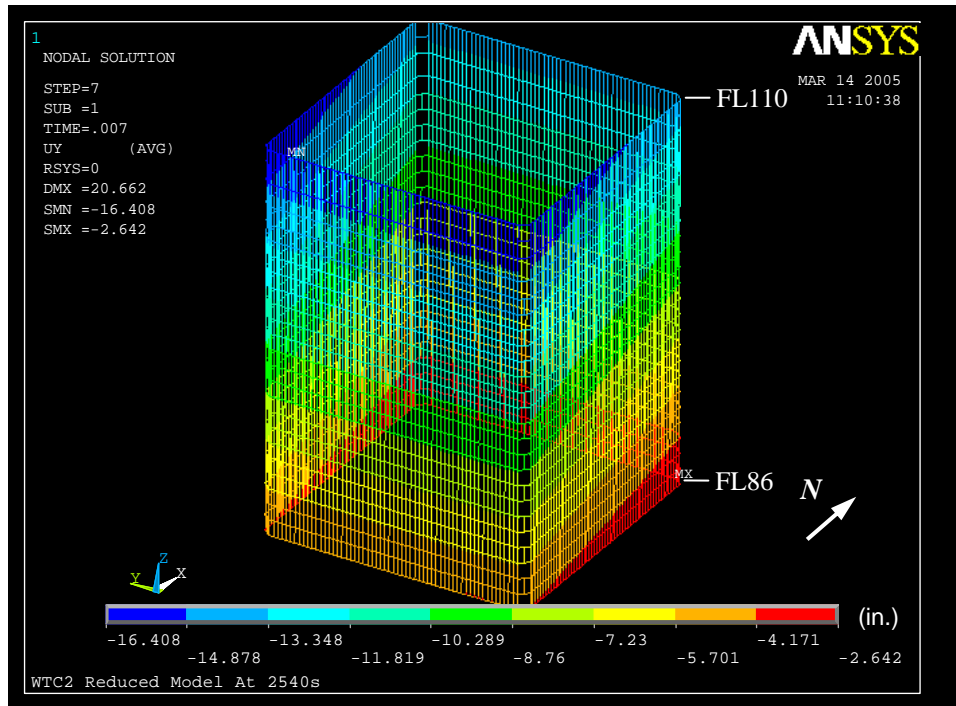


(b) 43 min

Figure 4-102. Lateral displacements above Floor 86 of WTC 2 in the x-direction (north-south) for Case D conditions.

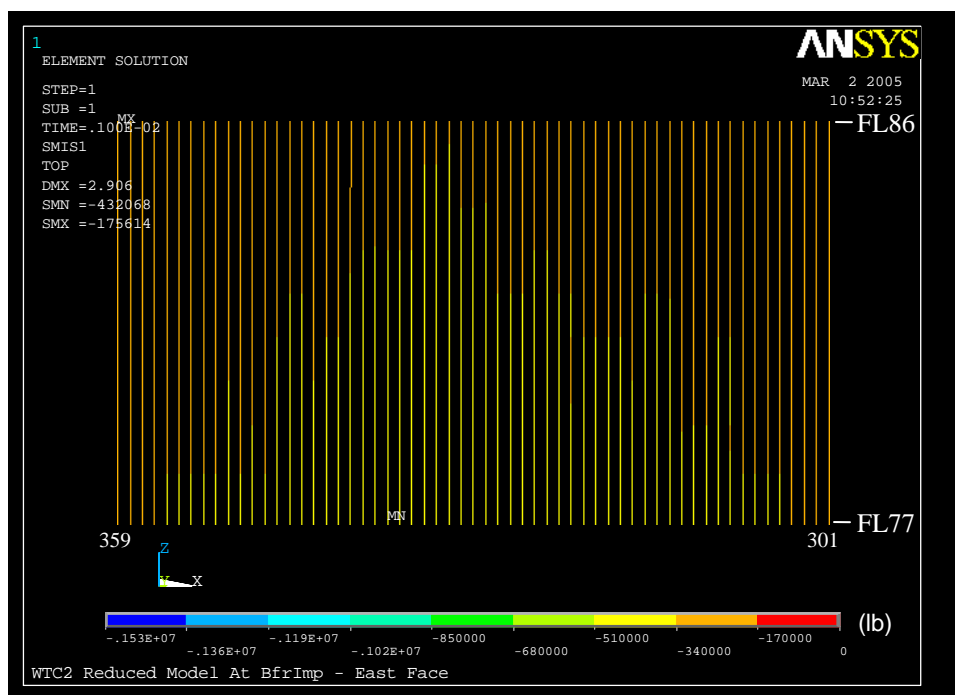


(a) After impact

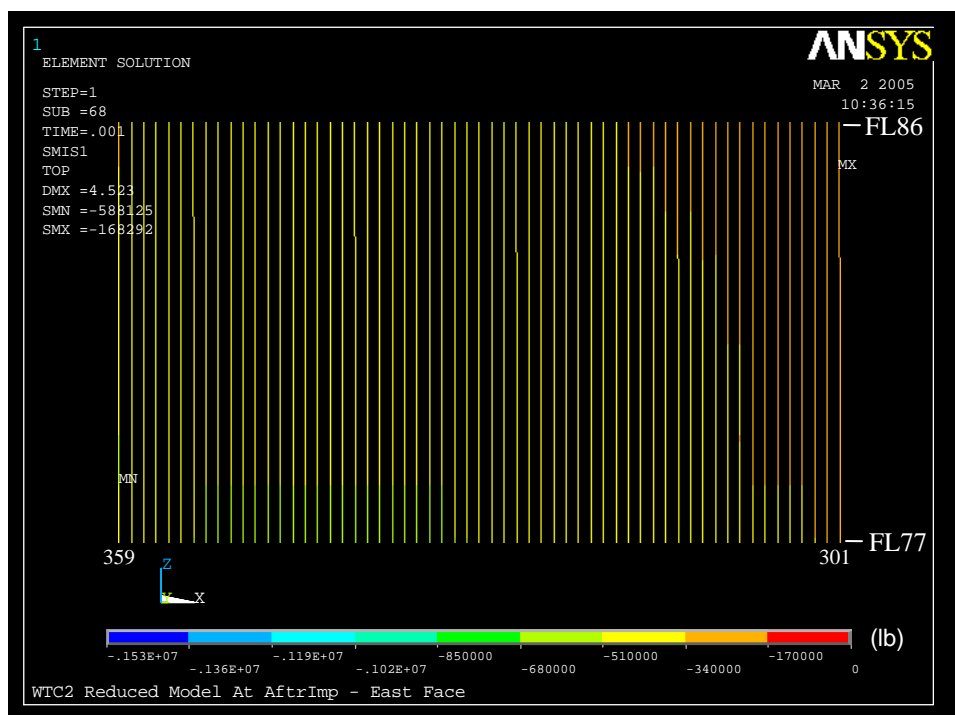


(b) 43 min

Figure 4–103. Lateral displacements above Floor 86 of WTC 2 in the y-direction (east-west) for Case D conditions.

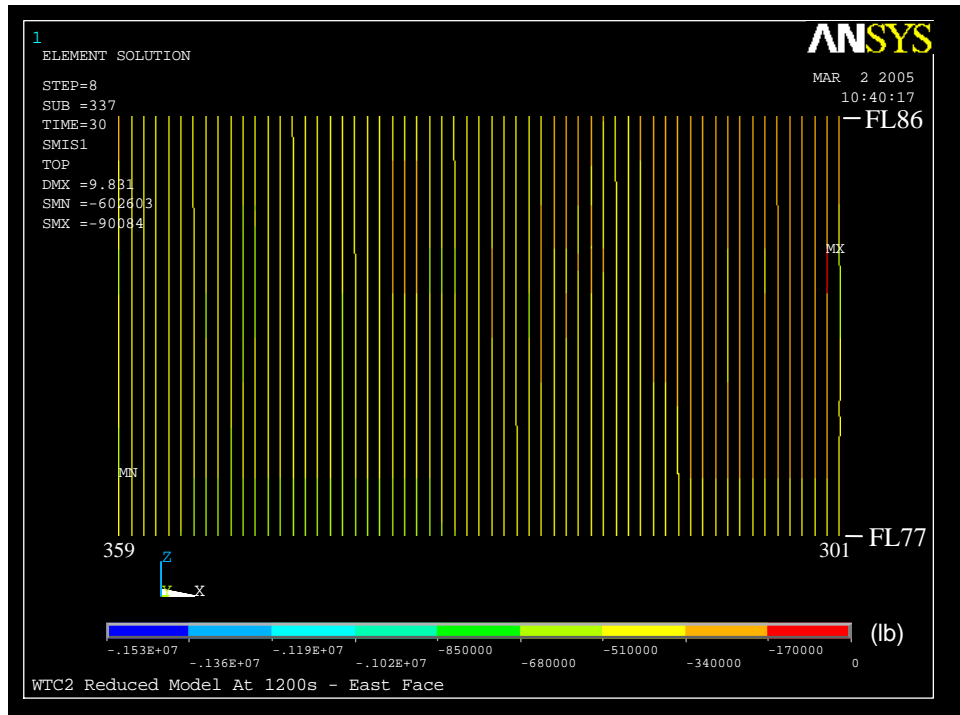


(a) Before impact

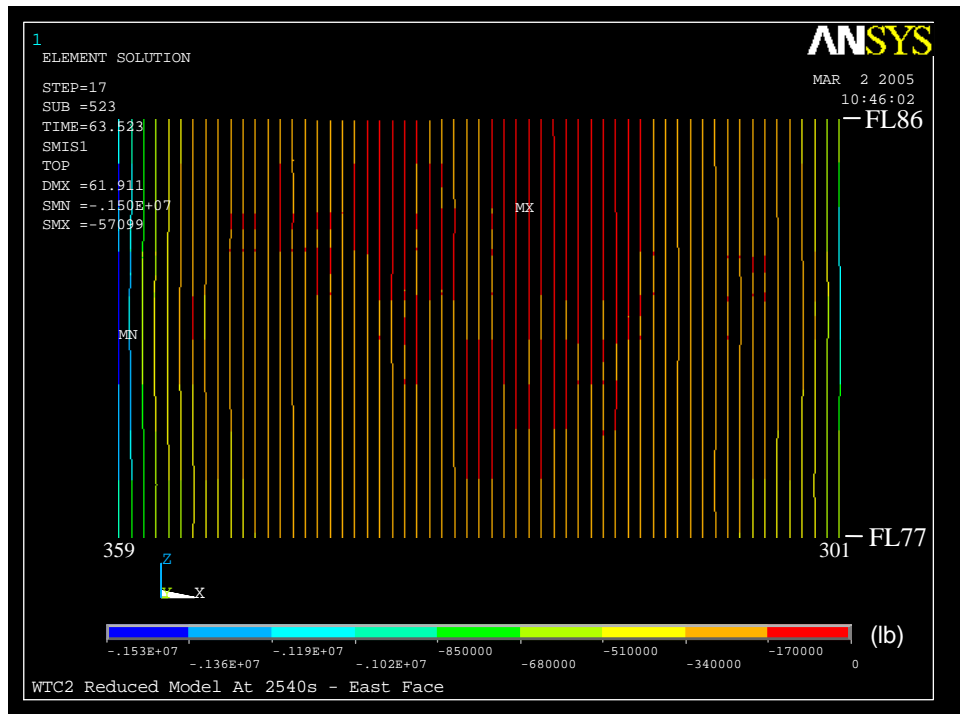


(b) After impact

Figure 4-104. Axial load in the east wall of WTC 2 for Case D conditions (compression is negative).

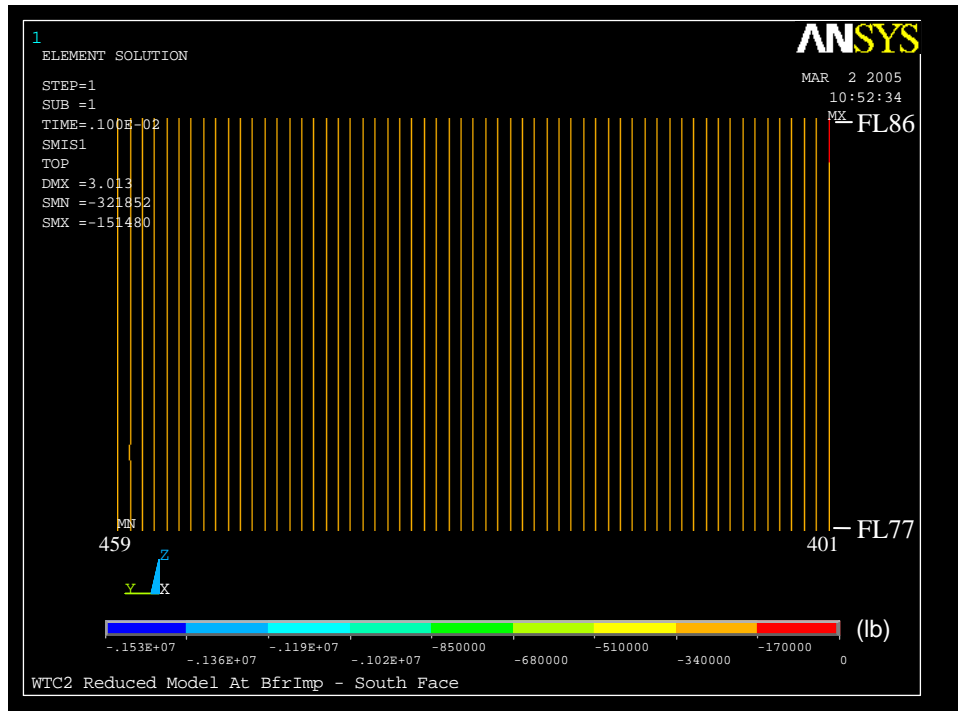


(a) 20 min

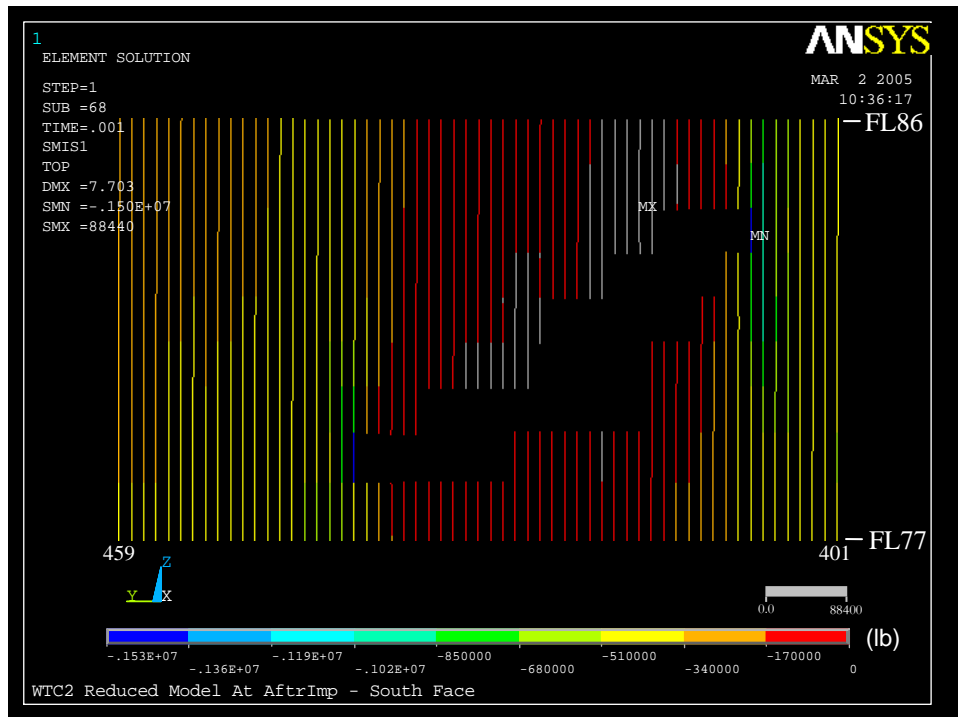


(b) 43 min

Figure 4-105. Axial load in the east wall of WTC 2 for Case D conditions (compression is negative).

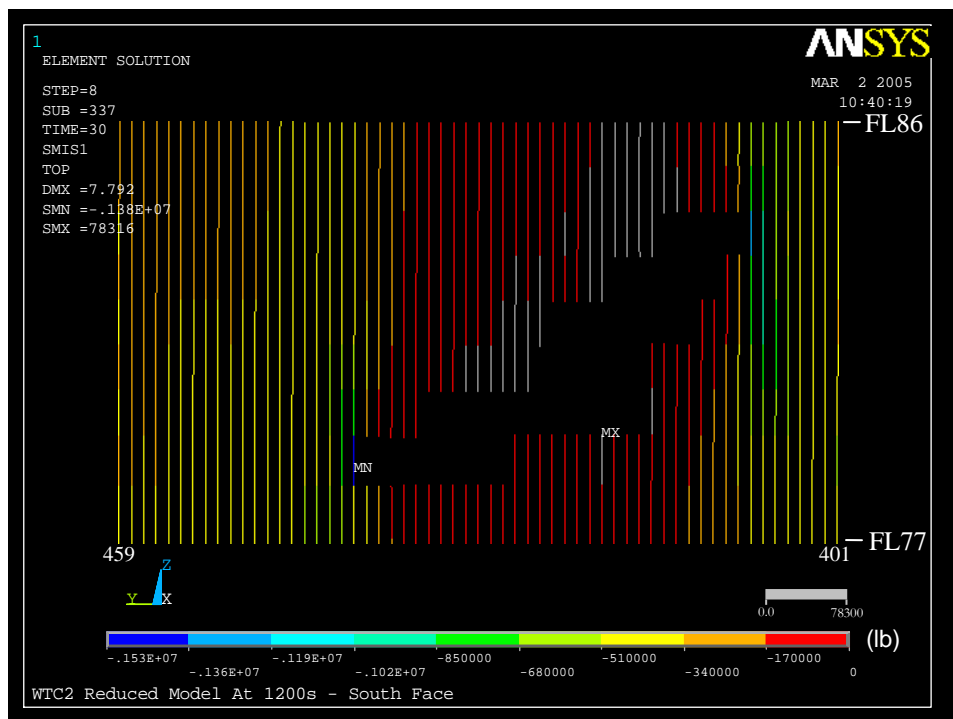


(a) Before impact

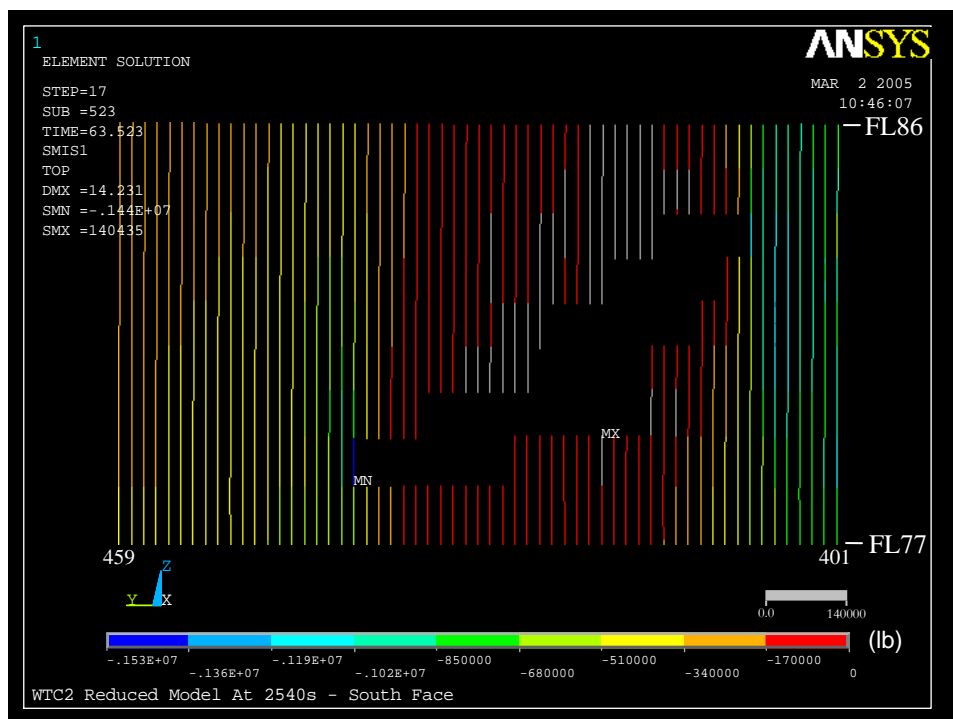


(b) After impact

Figure 4-106. Axial load in the south wall of WTC 2 for Case D conditions (compression is negative).

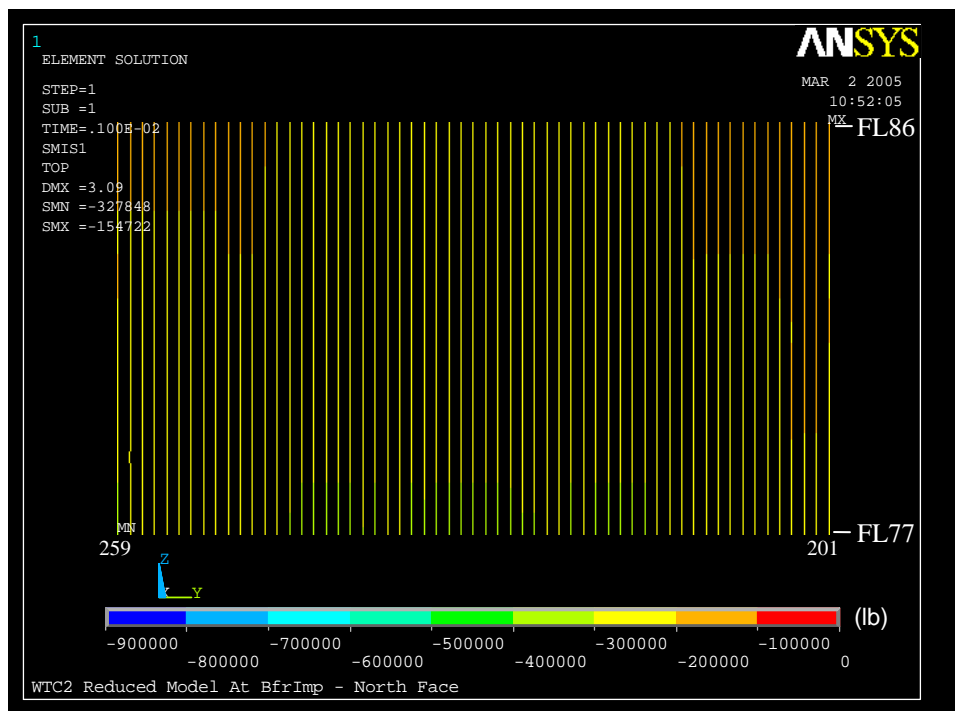


(a) 20 min

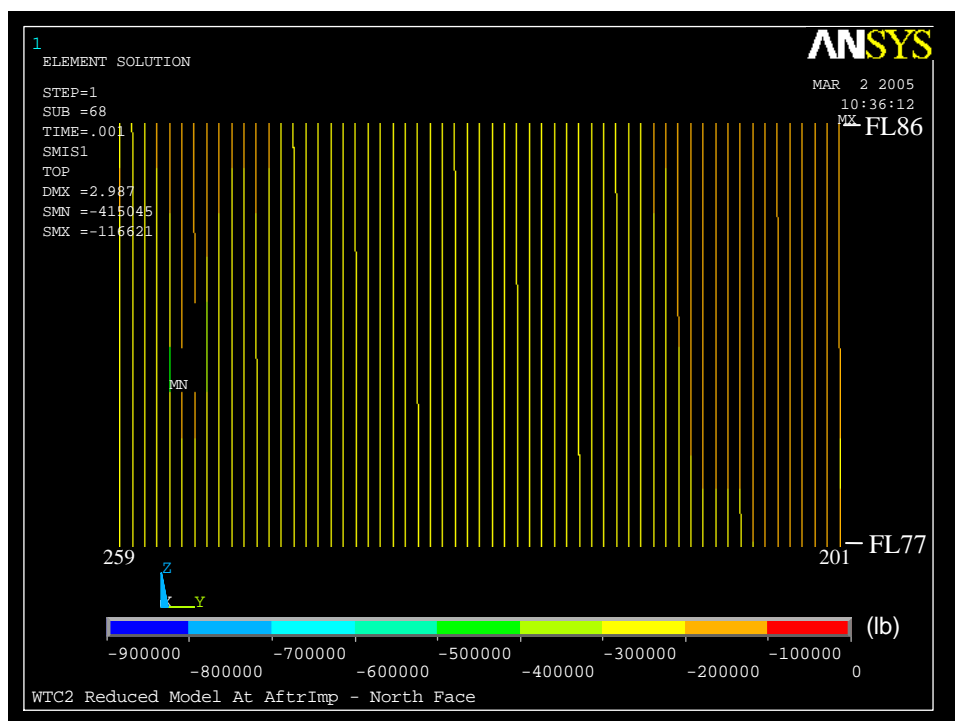


(b) 43 min

Figure 4-107. Axial load in the south wall of WTC 2 for Case D conditions (compression is negative).

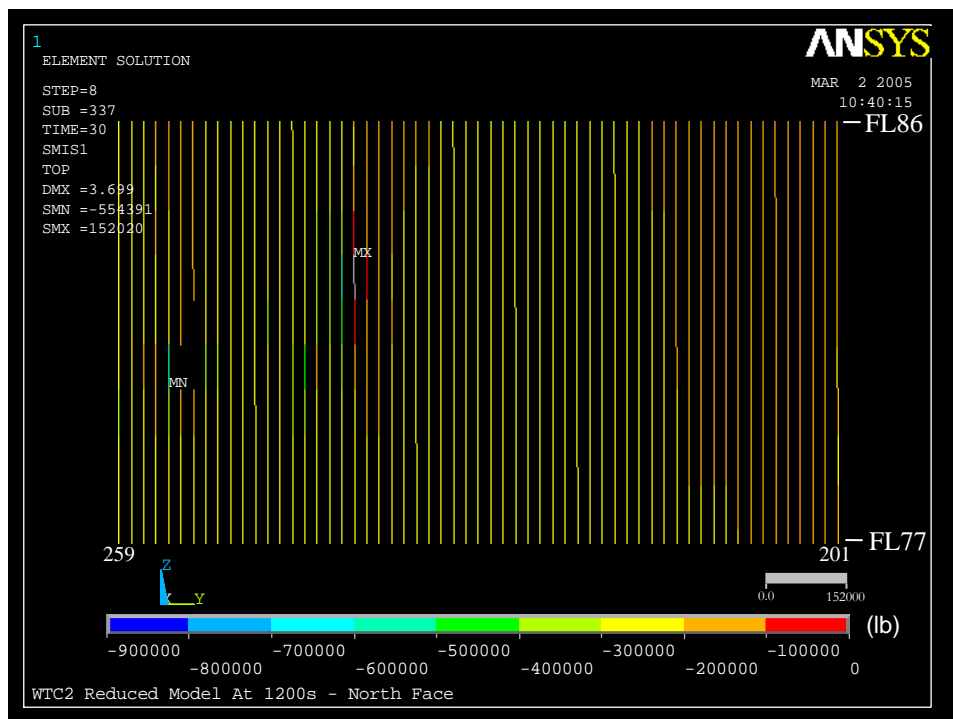


(a) Before impact

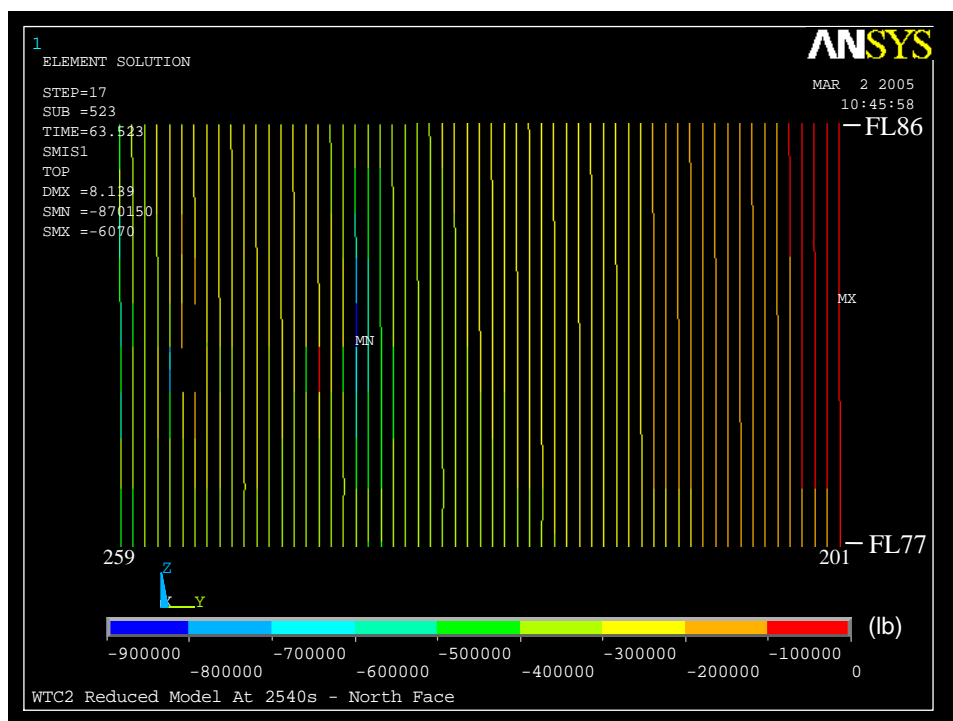


(b) After impact

Figure 4-108. Axial load in the north wall of WTC 2 for Case D conditions (compression is negative).

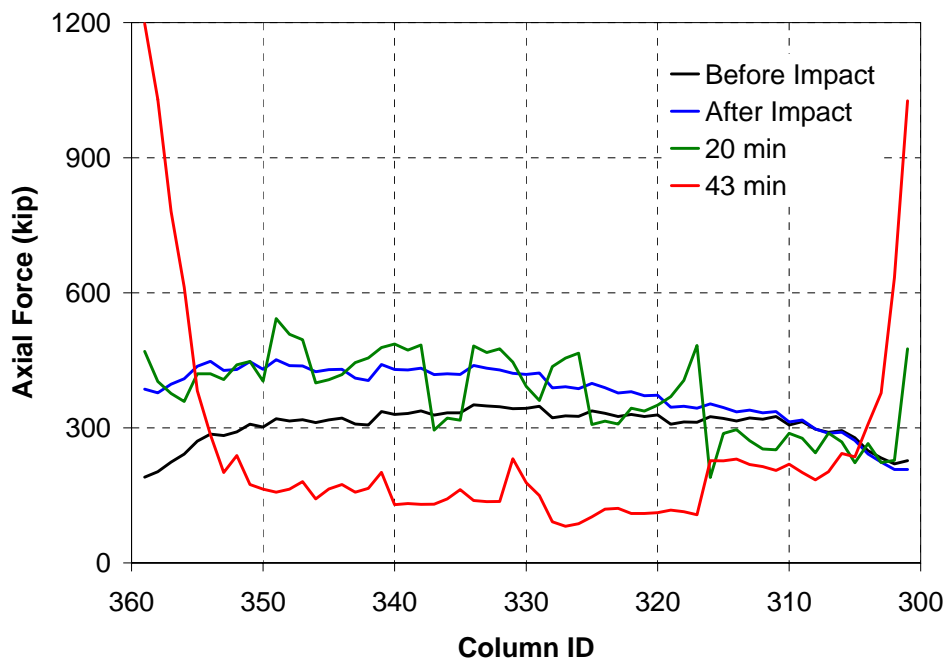


(a) 20 min

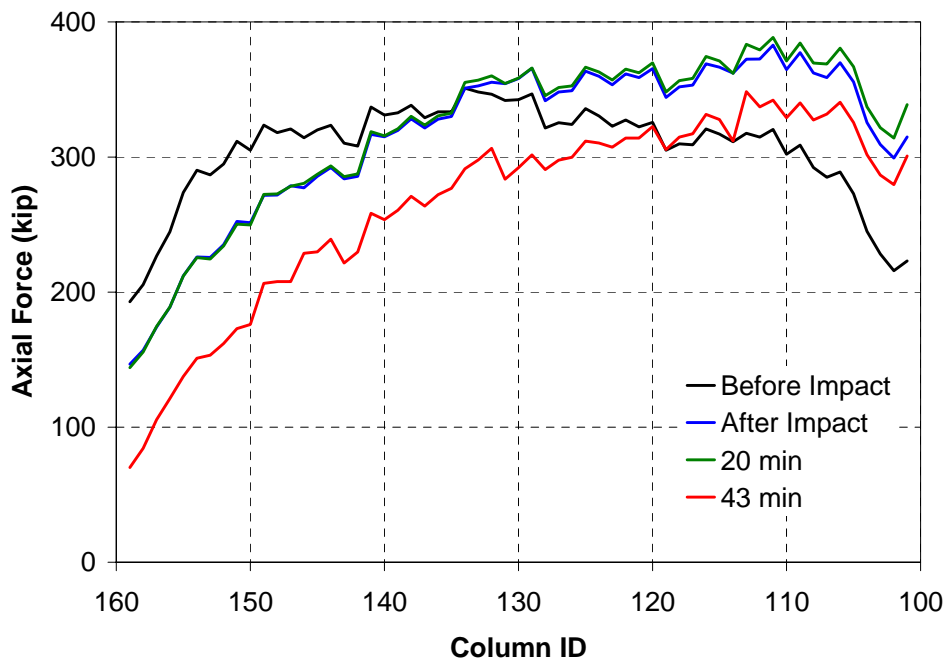


(b) 43 min

Figure 4–109. Axial load in the north wall of WTC 2 for Case D conditions (compression is negative).



(a) East wall



(b) West wall

Figure 4–110. Axial load in the east and the west wall columns at Floor 83 of WTC 2 for Case D conditions (compression is positive).

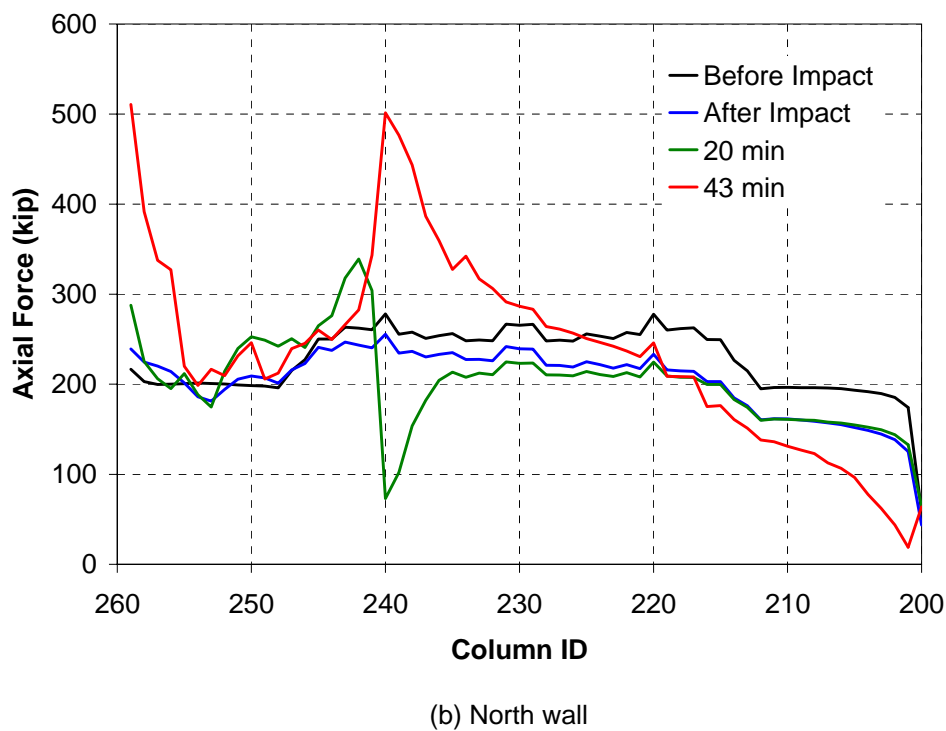
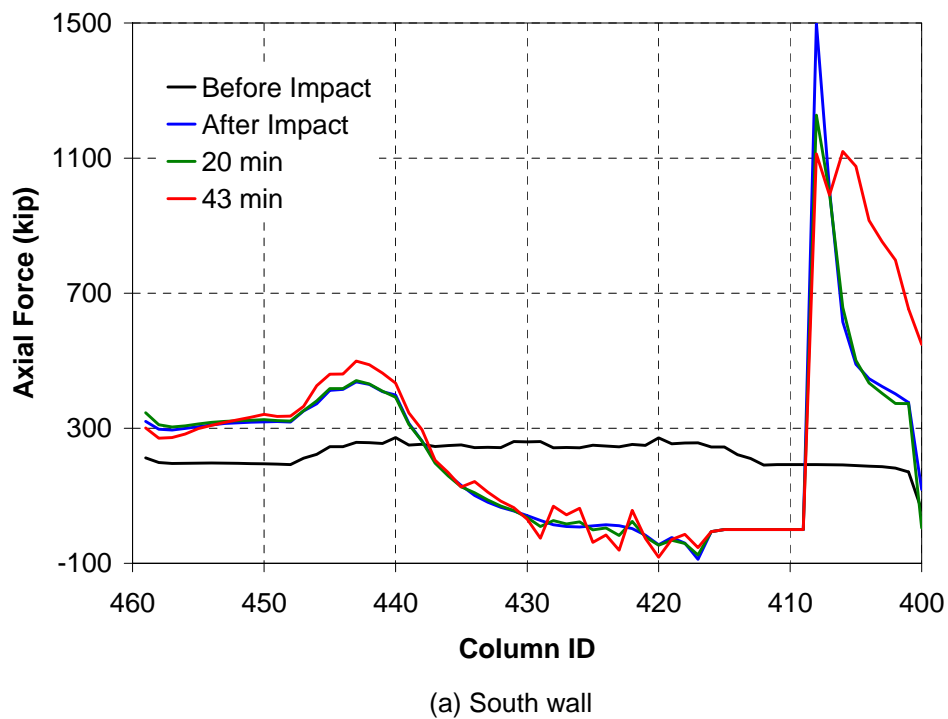
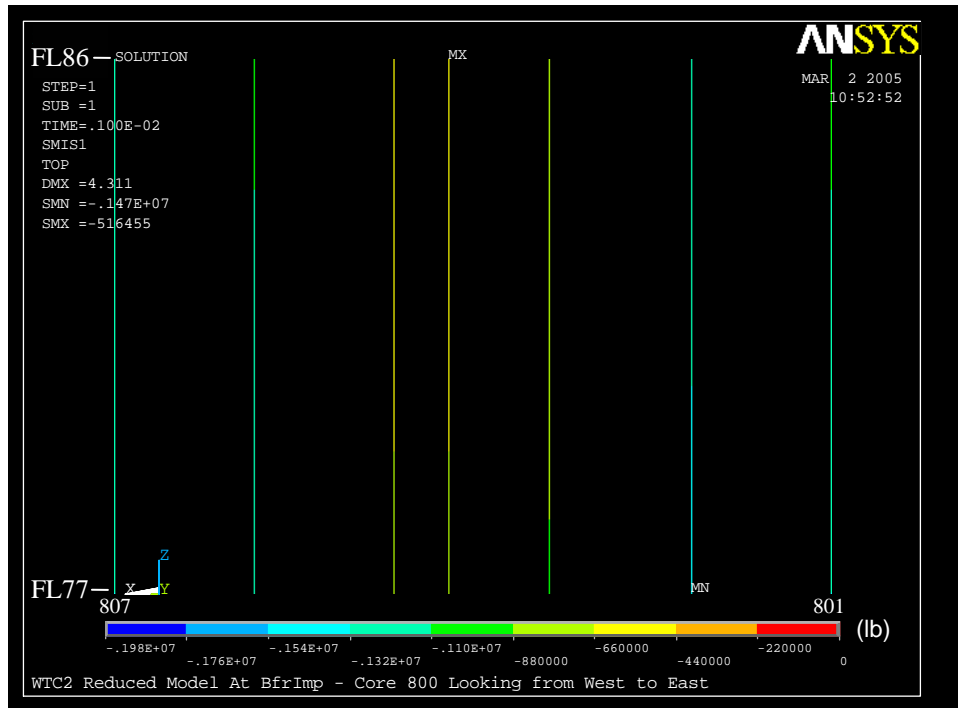
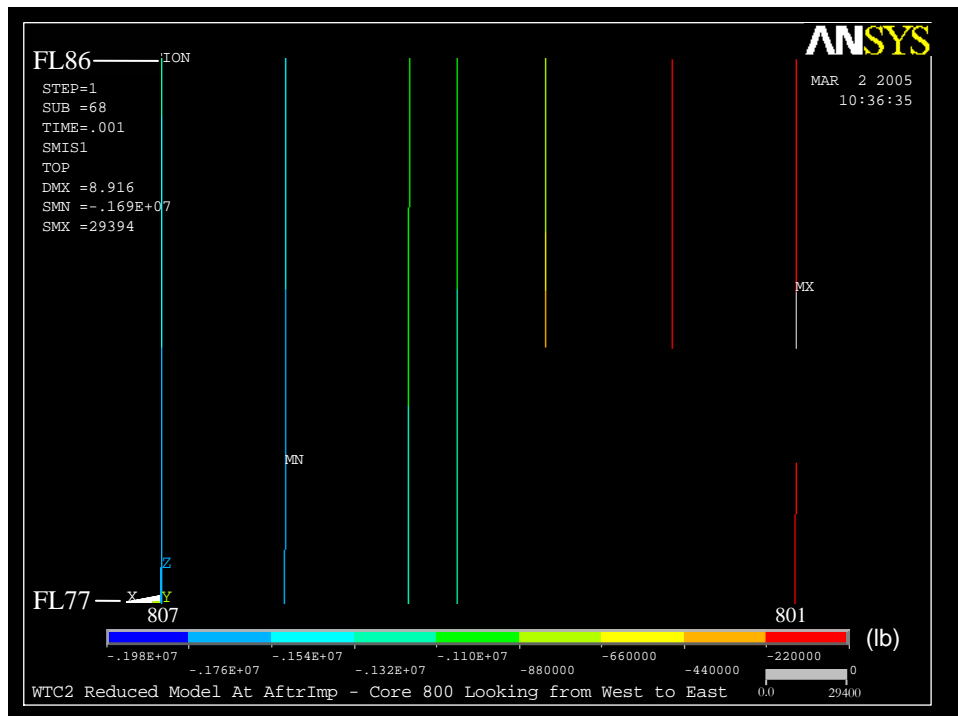


Figure 4–111. Axial load in the south and the north wall columns at Floor 83 of WTC 2 for Case D conditions (compression is positive).

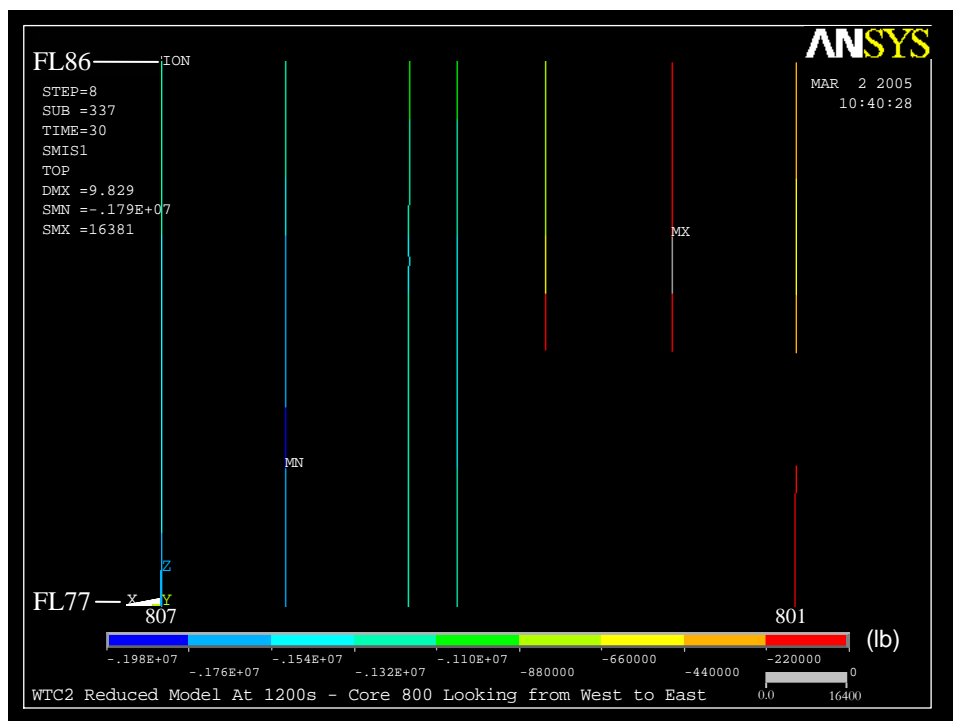


(a) Before impact

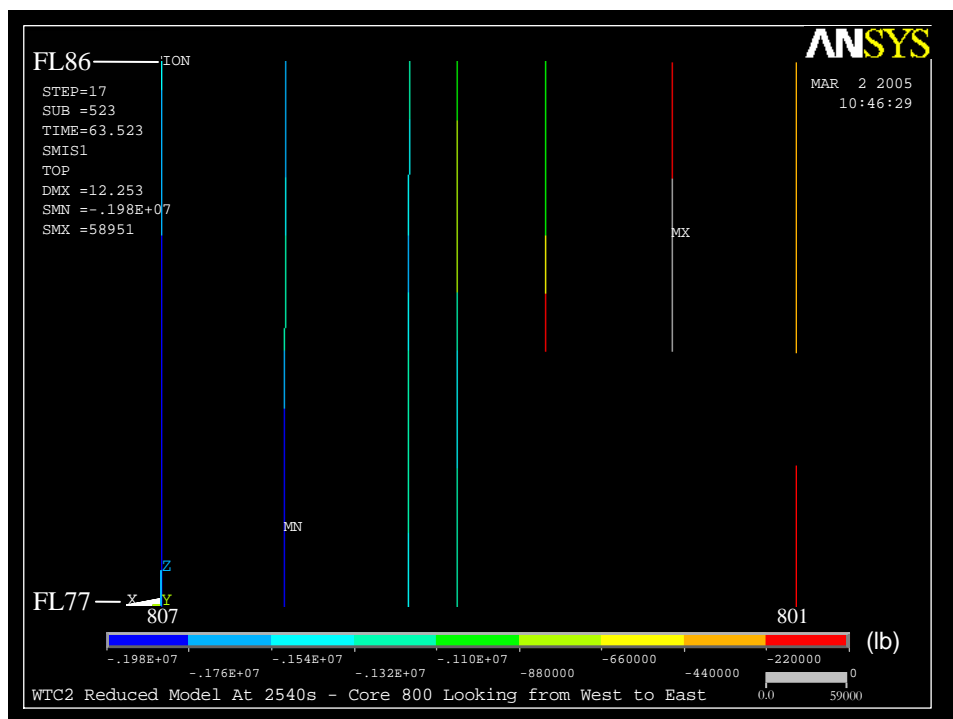


(b) After impact

Figure 4-112. Axial load in 800 series core columns of WTC 2 for Case D conditions (compression is negative).

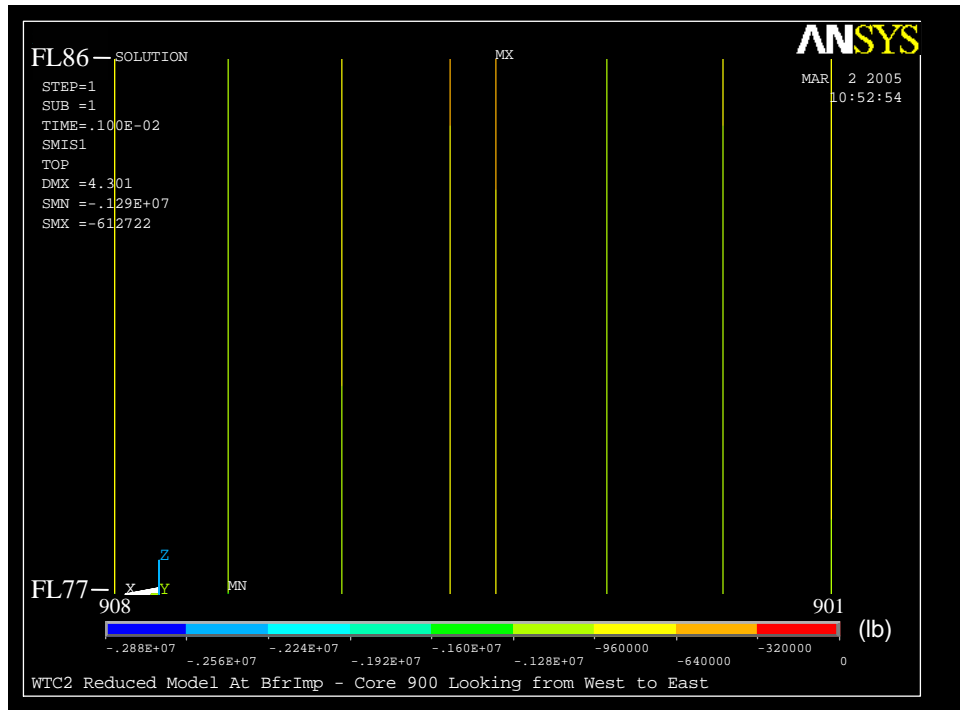


(a) 20 min

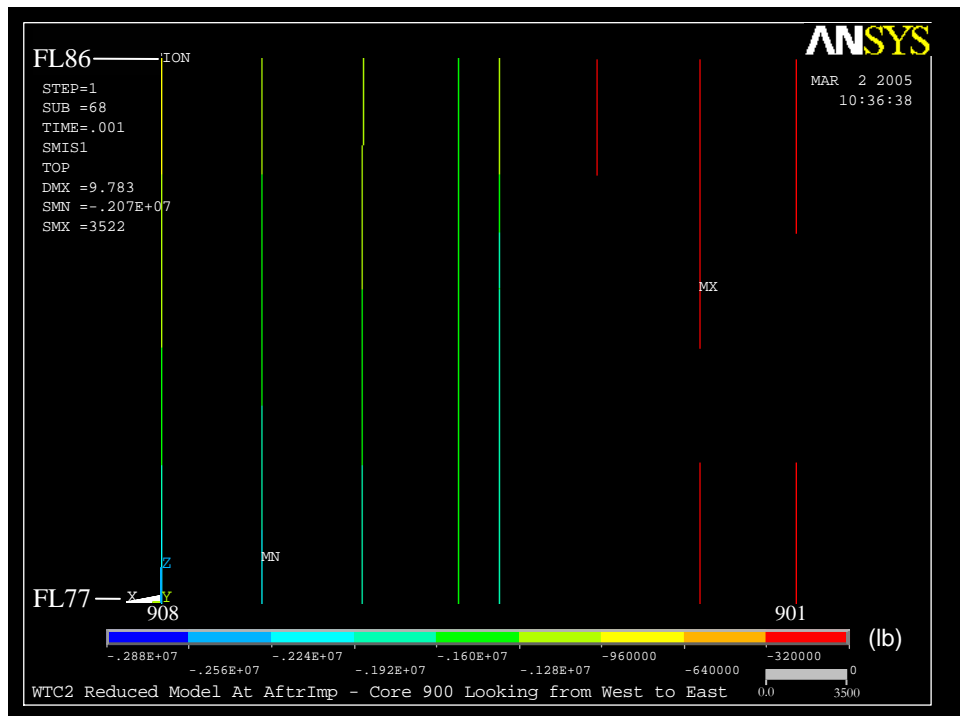


(b) 43 min

Figure 4-113. Axial load in 800 series core columns of WTC 2 for Case D conditions (compression is negative).

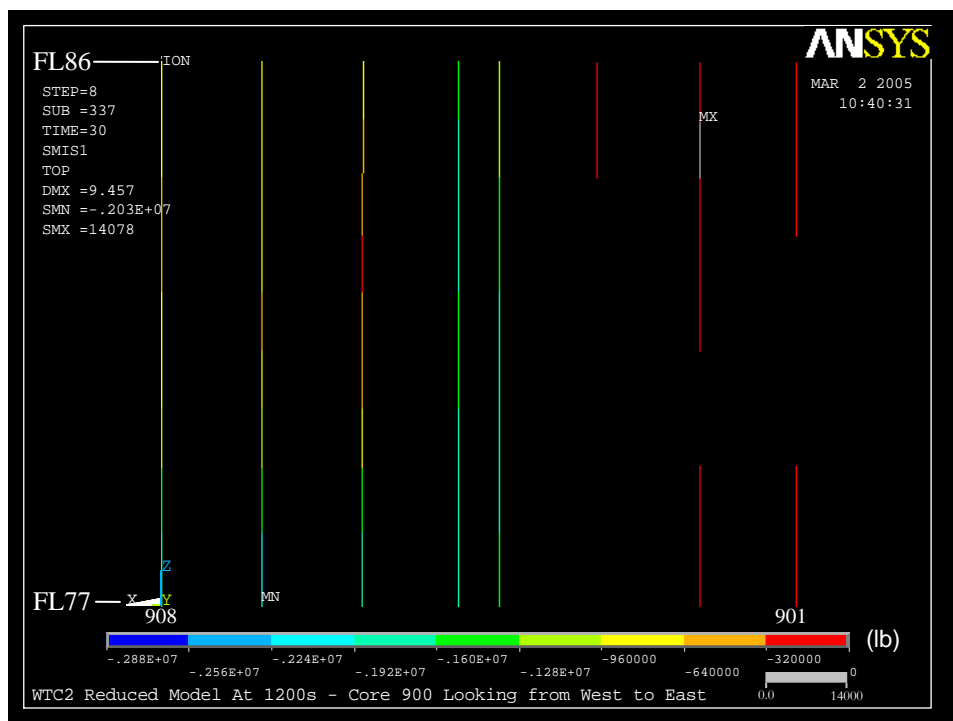


(a) Before impact

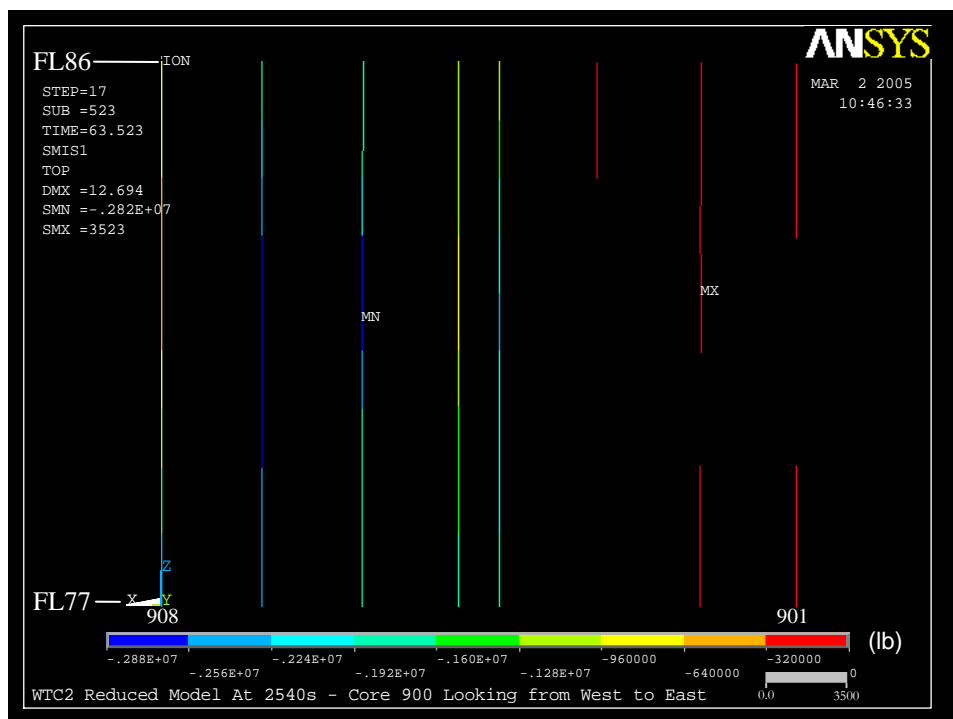


(b) After impact

Figure 4-114. Axial load in 900 series core columns of WTC 2 for Case D conditions (compression is negative).

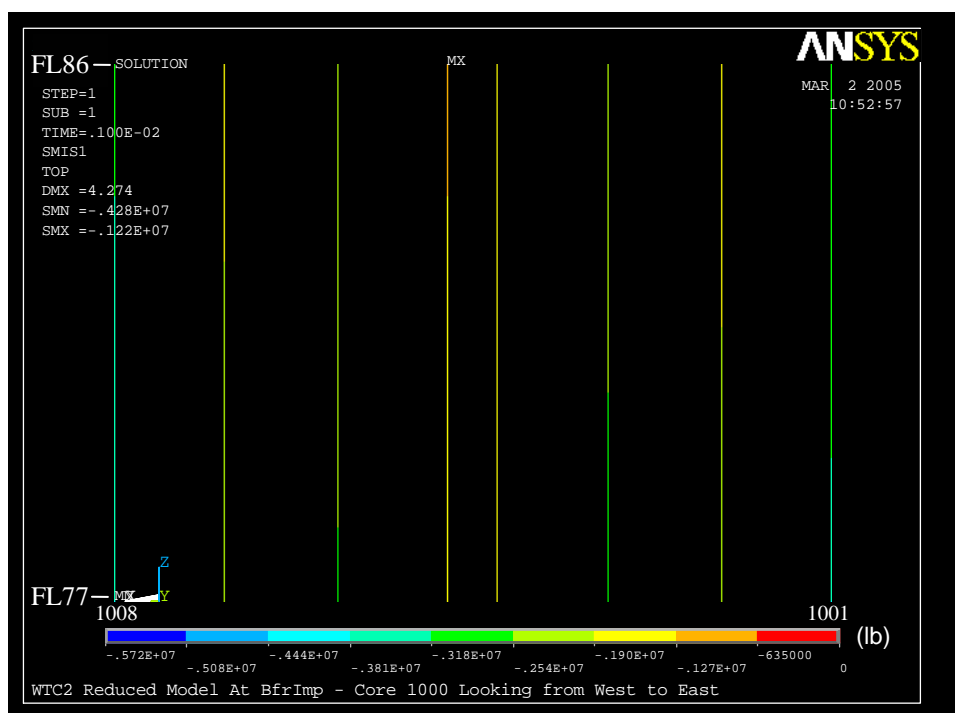


(a) 20 min

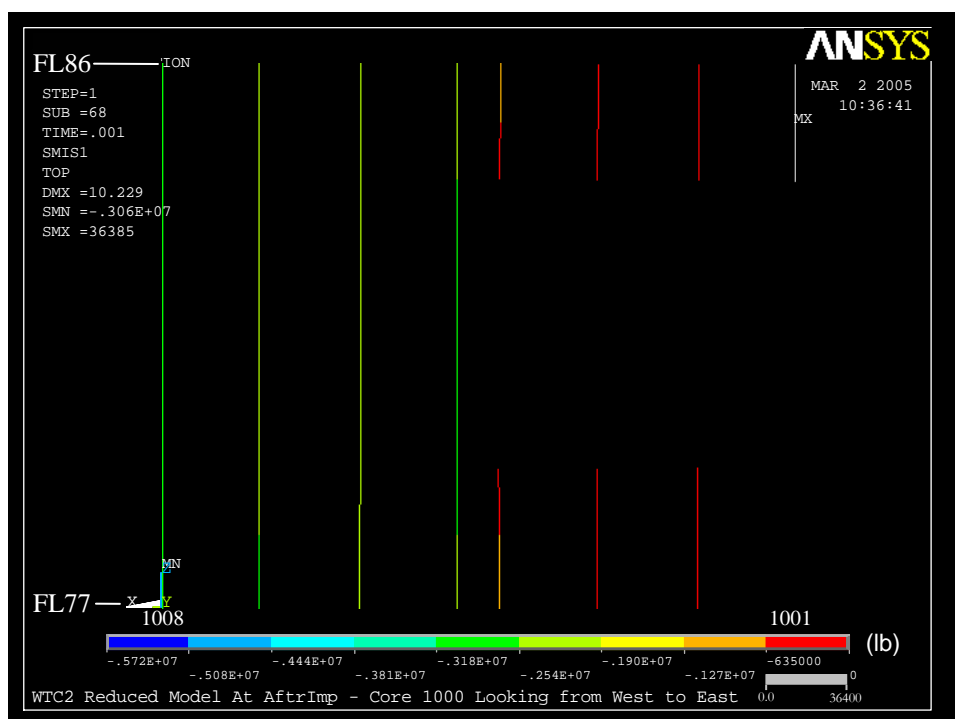


(b) 43 min

Figure 4-115. Axial load in 900 series core columns of WTC 2 for Case D conditions (compression is negative).

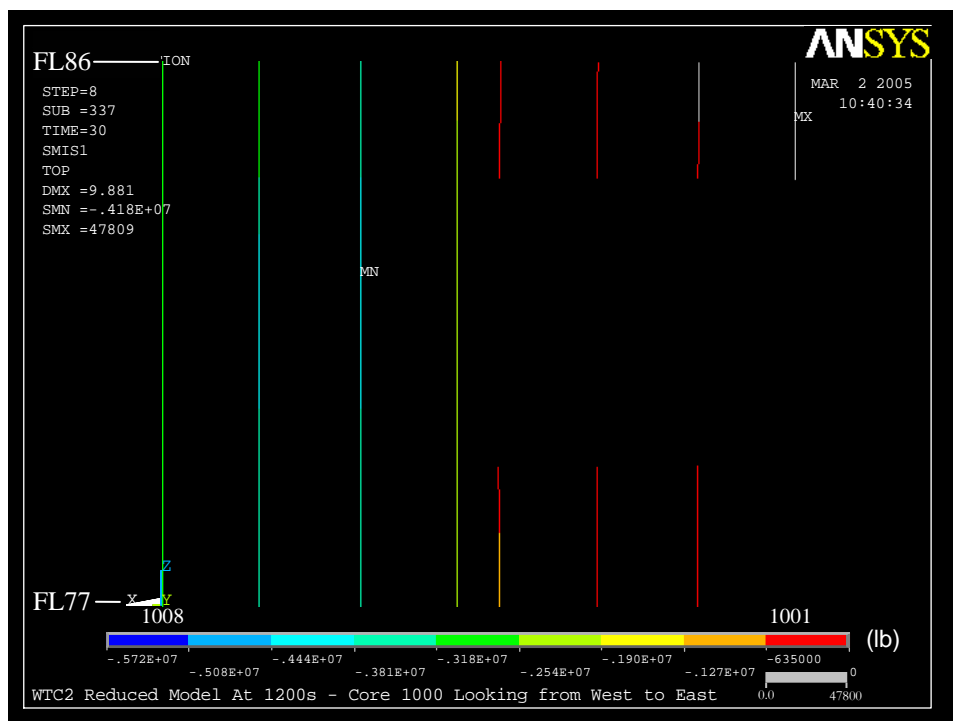


(a) Before impact

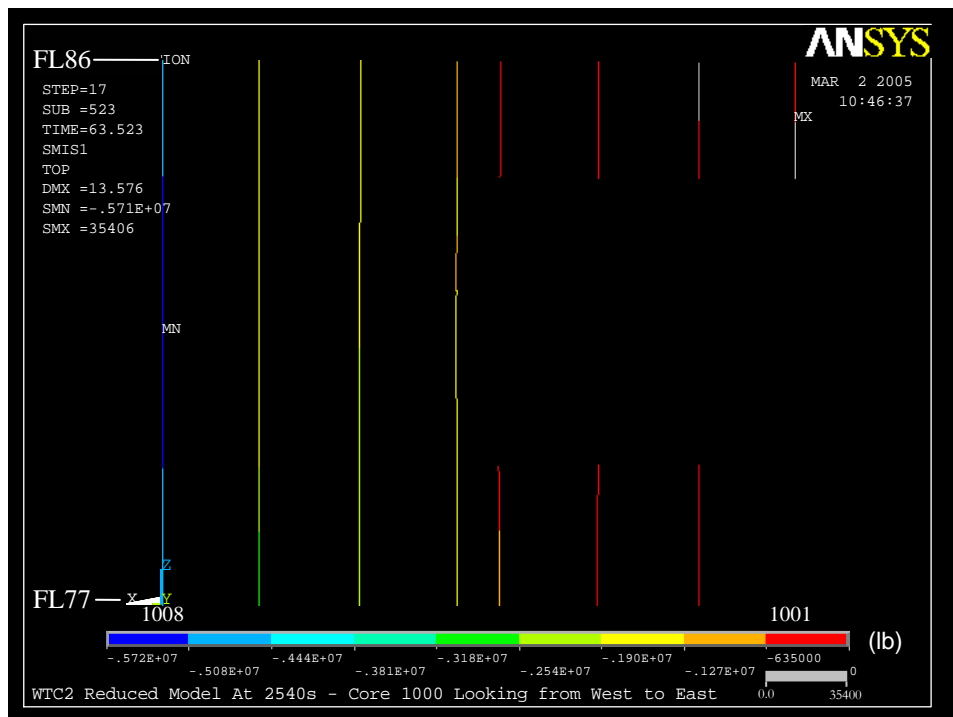


(b) After impact

Figure 4-116. Axial load in 1000 series core columns of WTC 2 for Case D conditions (compression is negative).



(a) 20 min



(b) 43 min

Figure 4-117. Axial load in 1000 series core columns of WTC 2 for Case D conditions (compression is negative).

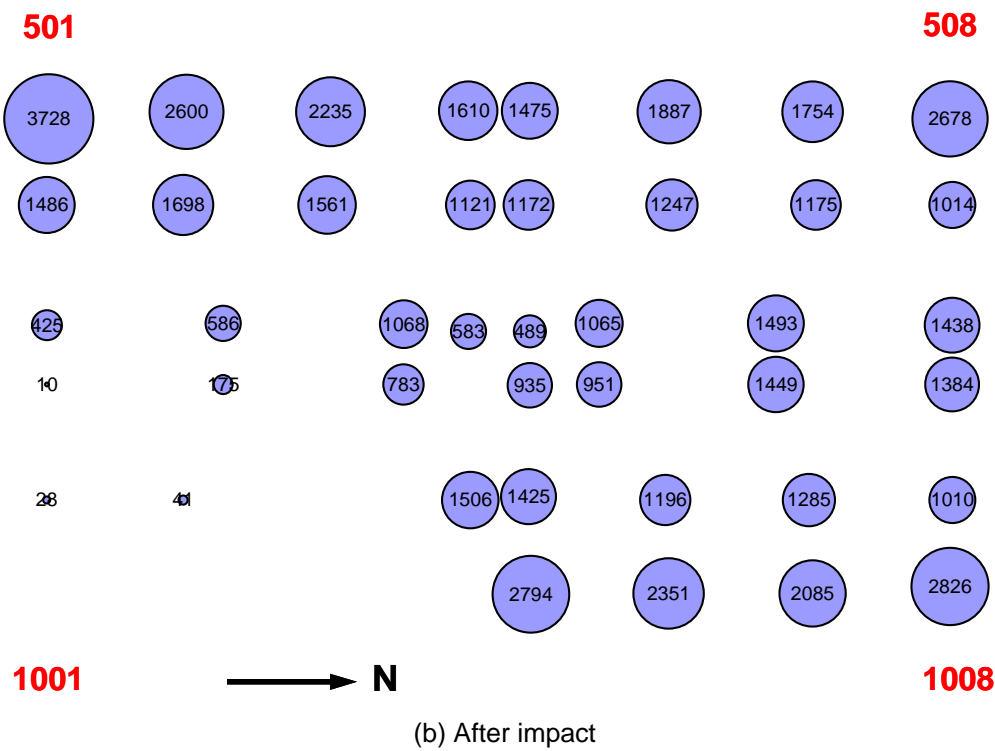
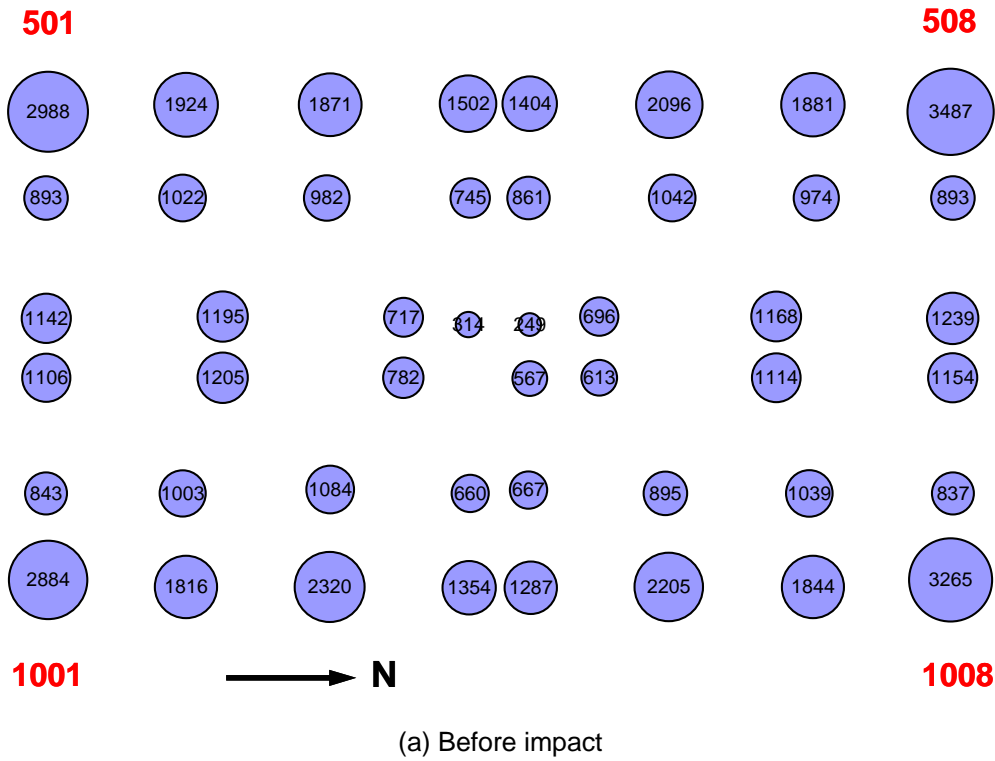


Figure 4-118. Core column loads (kip) at Floor 83 of WTC 2 for Case D conditions (compression is positive).

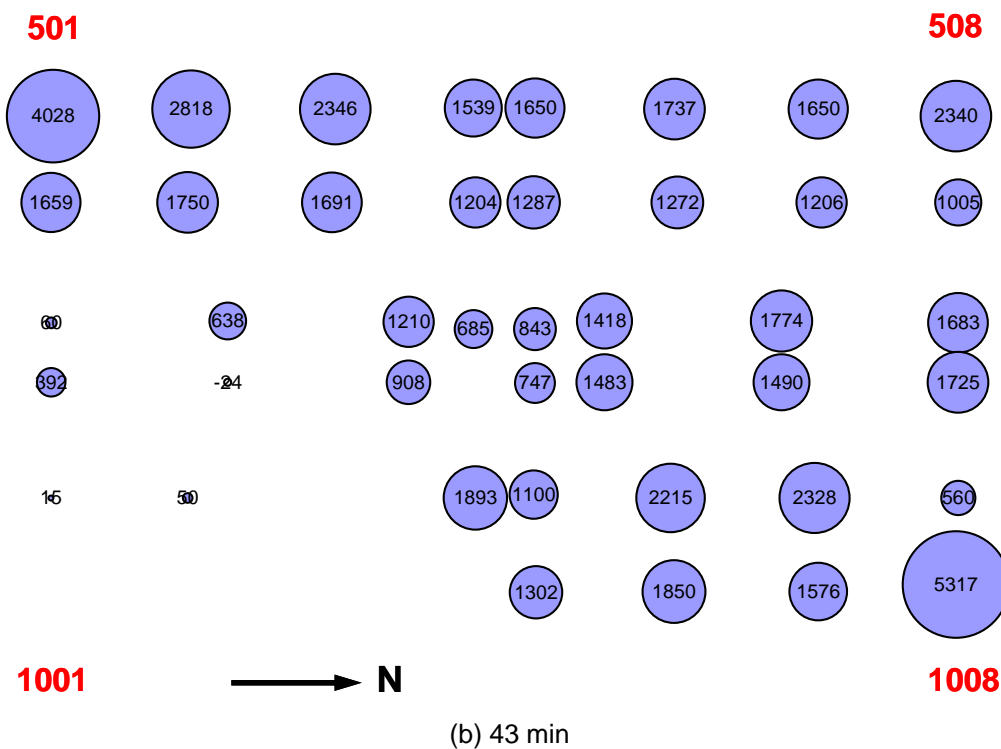
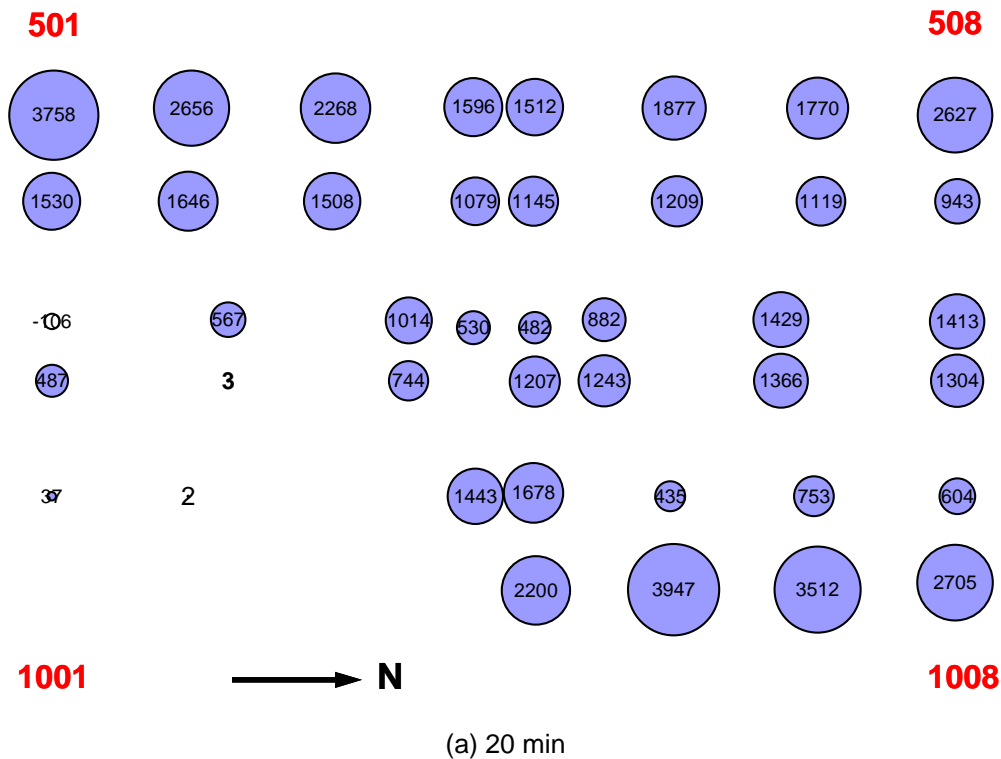


Figure 4-119. Core column loads (kip) at Floor 83 of WTC 2 for Case D conditions (compression is positive).

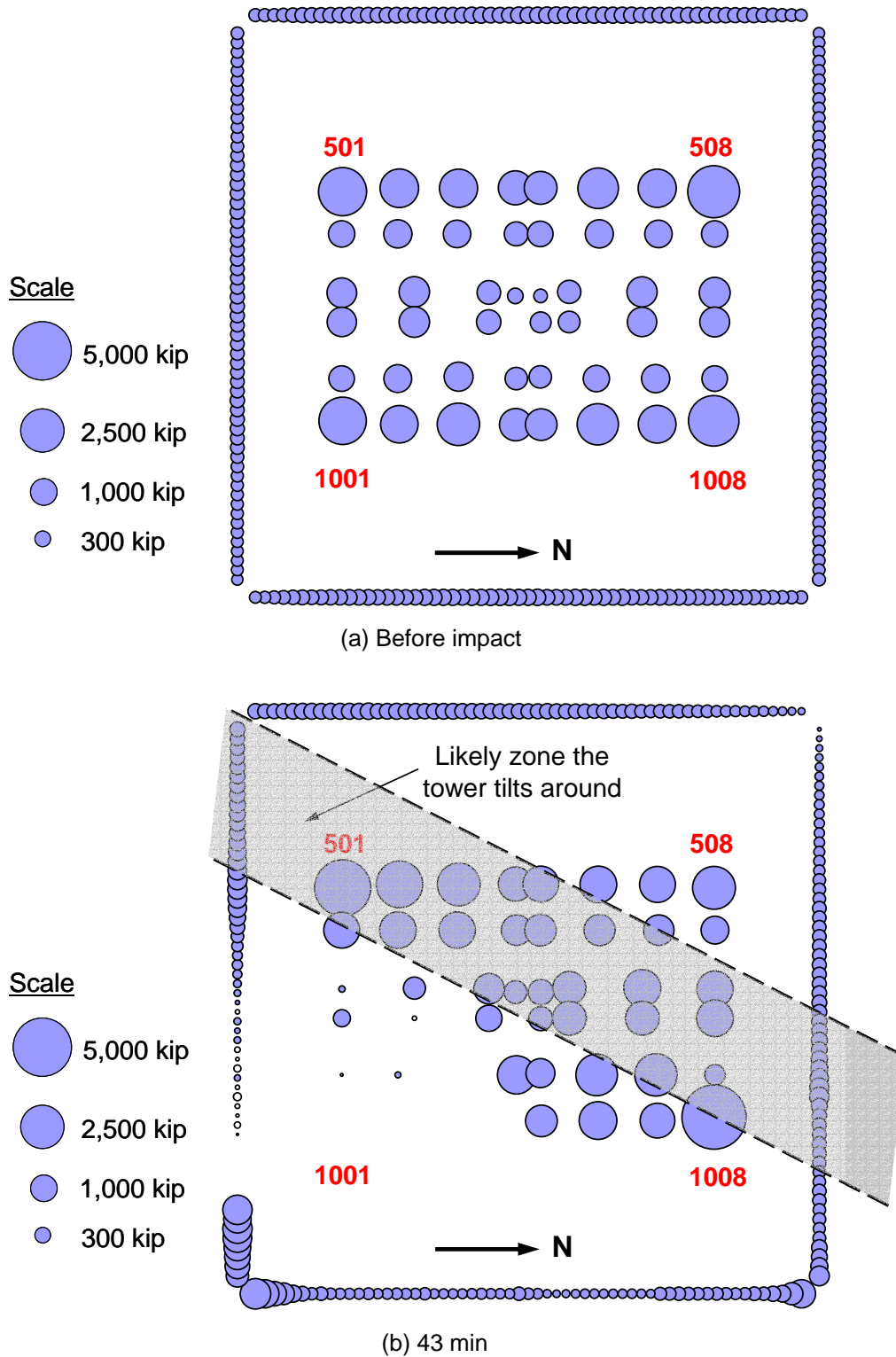


Figure 4–120. Axial load in Floor 83 columns of WTC 2 for Case D conditions (compression is positive).

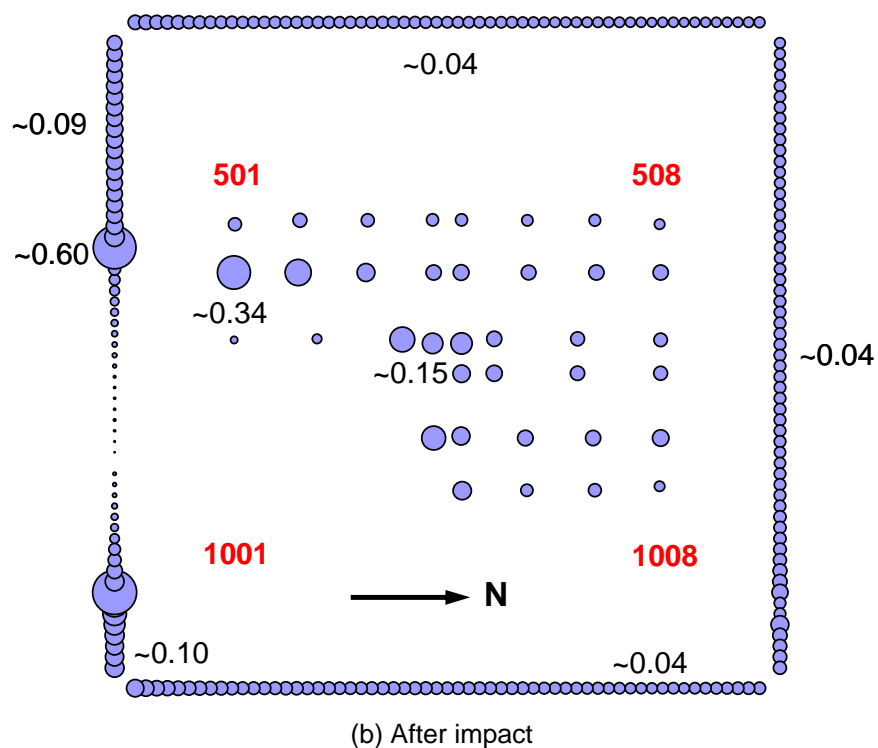
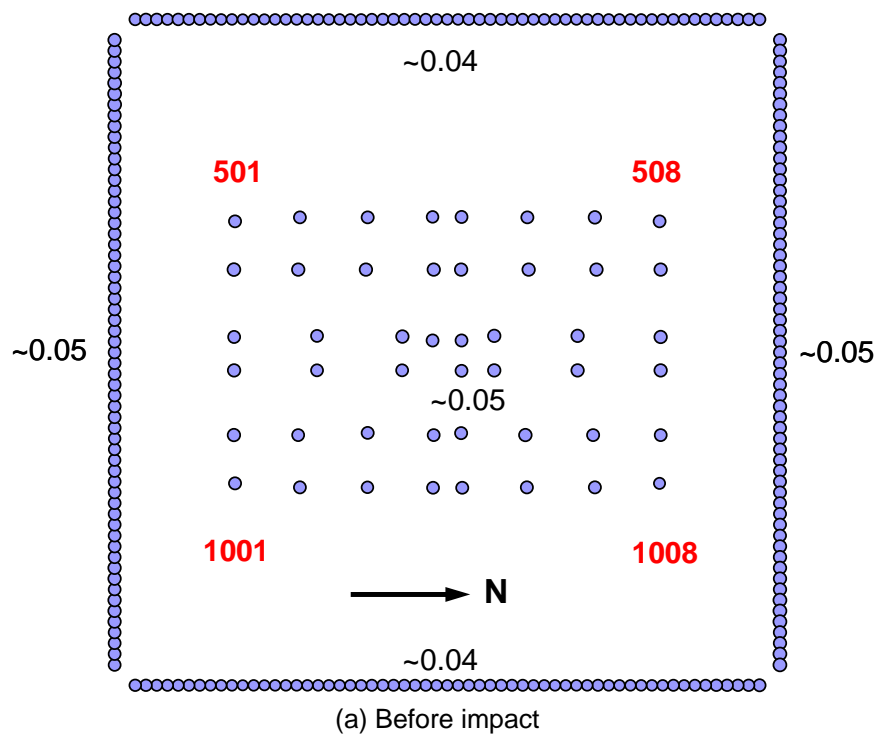


Figure 4–121. Maximum elastic-plus-plastic strains for columns between Floor 78 and Floor 83 of WTC 2 for Case D conditions (compressive strain is positive; strain values are in percent).

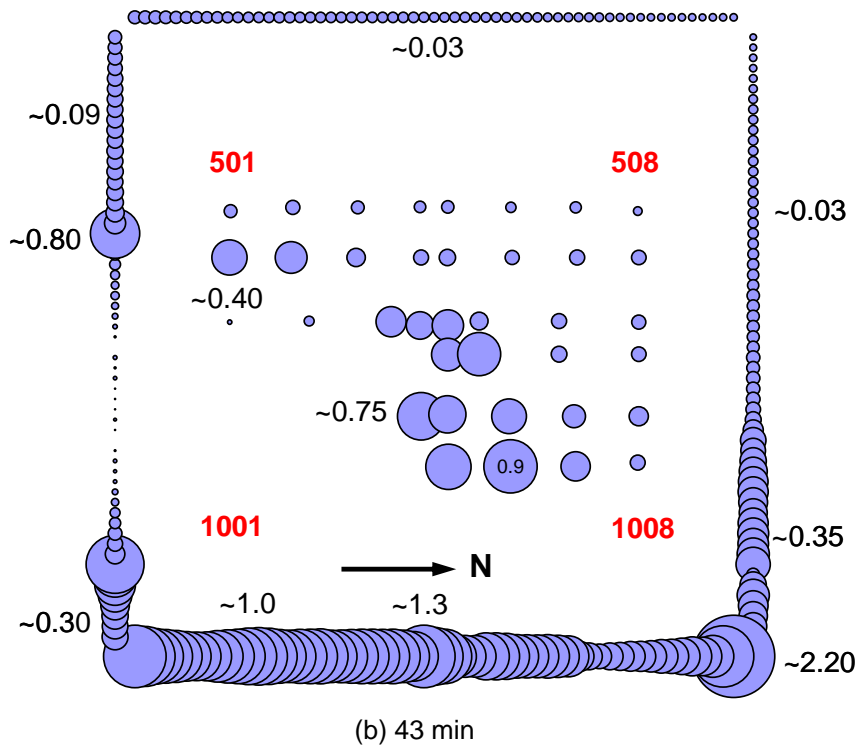
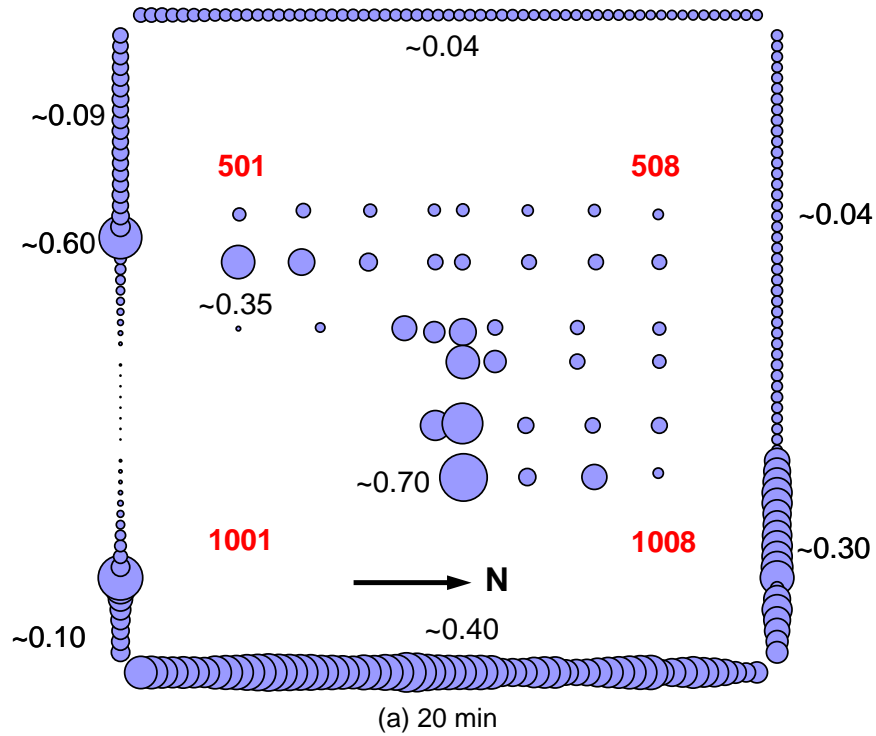


Figure 4–122. Maximum elastic-plus-plastic strains for columns between Floor 78 and Floor 3 of WTC 2 for Case D conditions (compressive strain is positive; strain values are in percent).

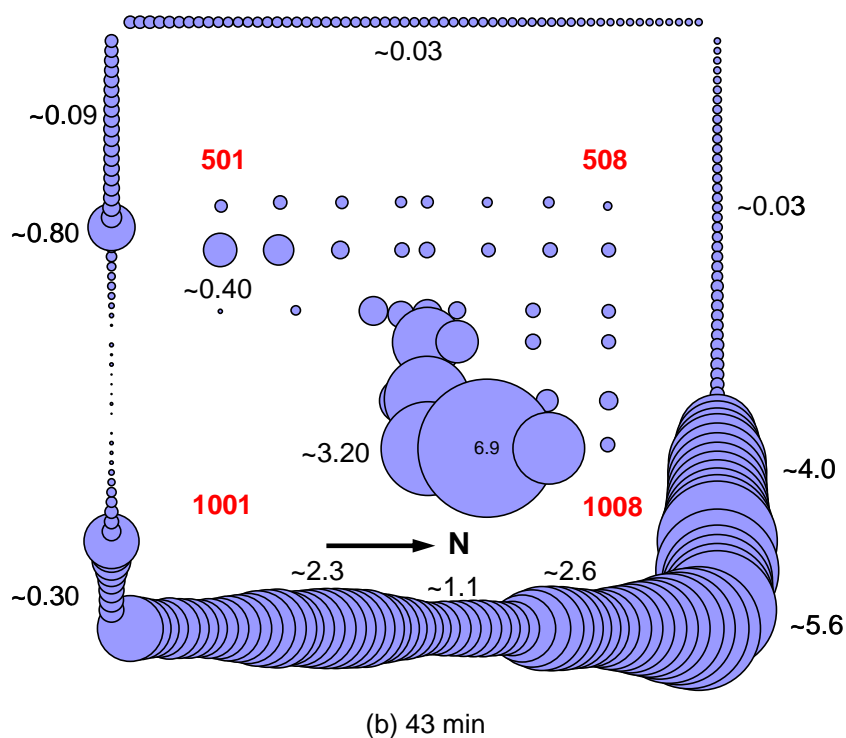
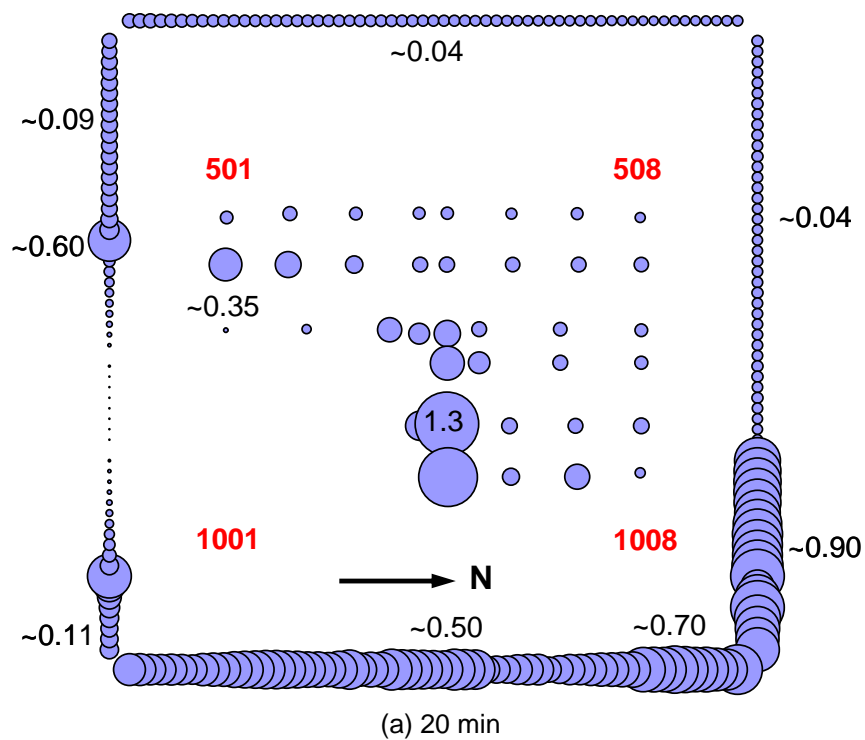


Figure 4–123. Maximum elastic-plus-plastic-plus-creep strains for columns between Floor 78 and Floor 83 of WTC 2 for Case D conditions (compressive strain is positive; strain values are in percent).

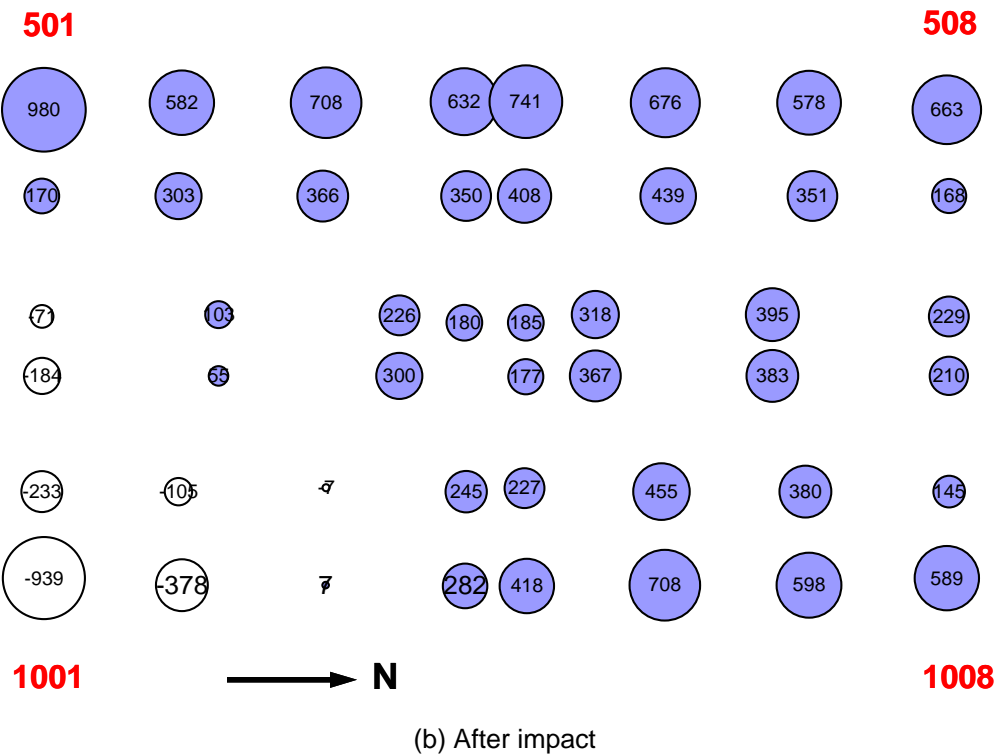
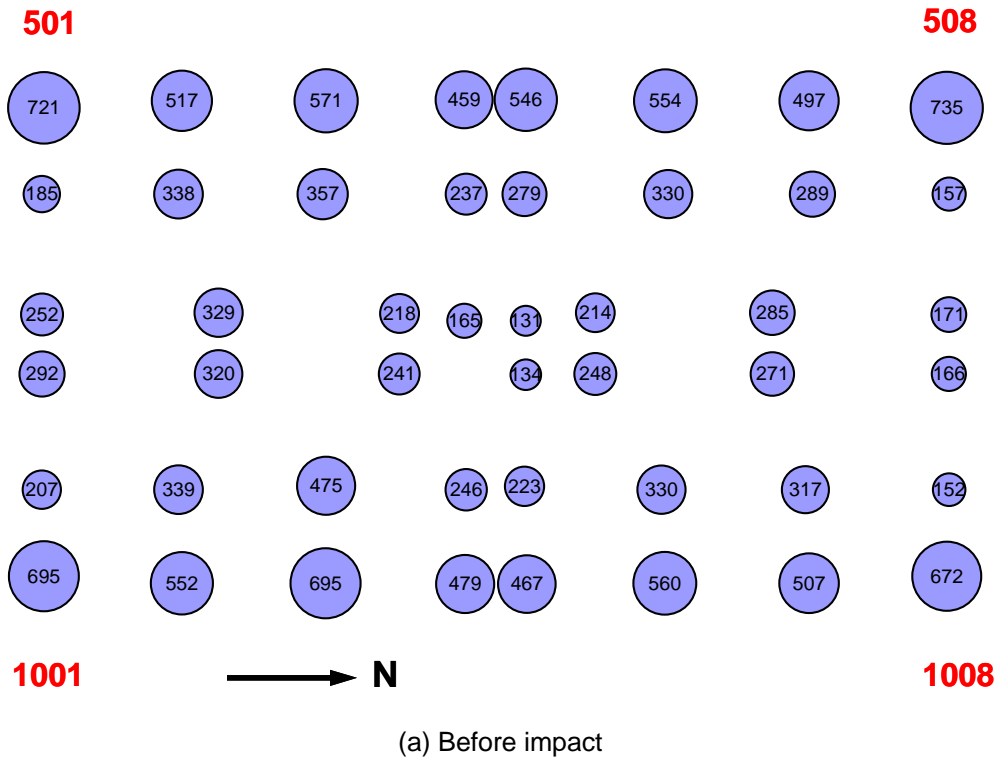
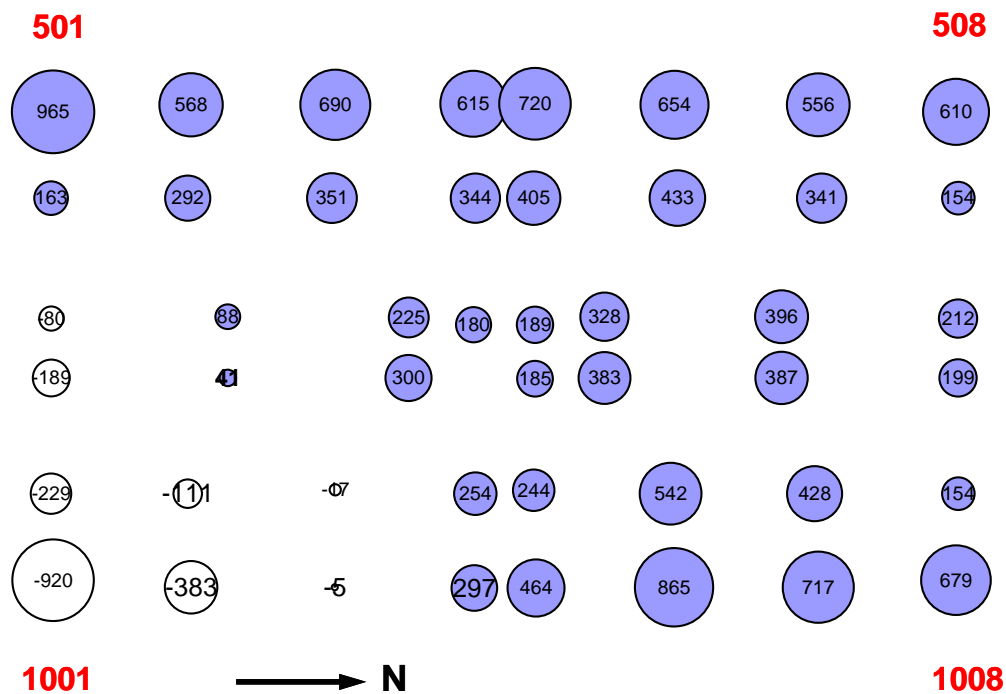
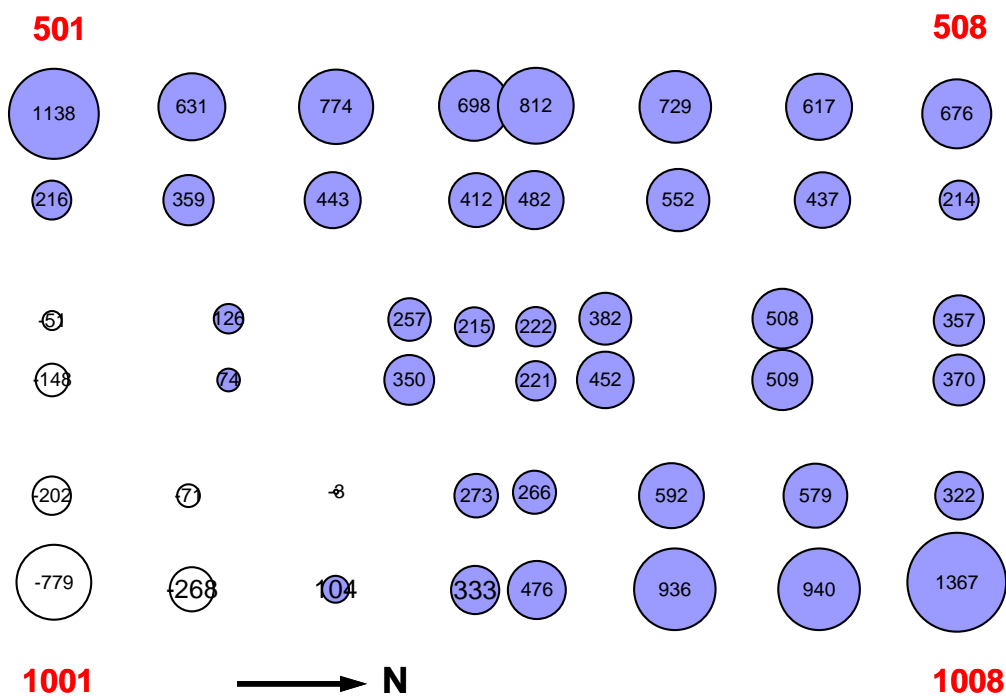


Figure 4–124. Axial load in core columns (kip) at Floor 105 (at hat truss level) of WTC 2 for Case D conditions (compression is positive).



(a) 20 min



(b) 43 min

Figure 4–125. Axial load in core columns (kip) at Floor 105 (at hat truss level) of WTC 2 for Case D conditions (compression is positive).

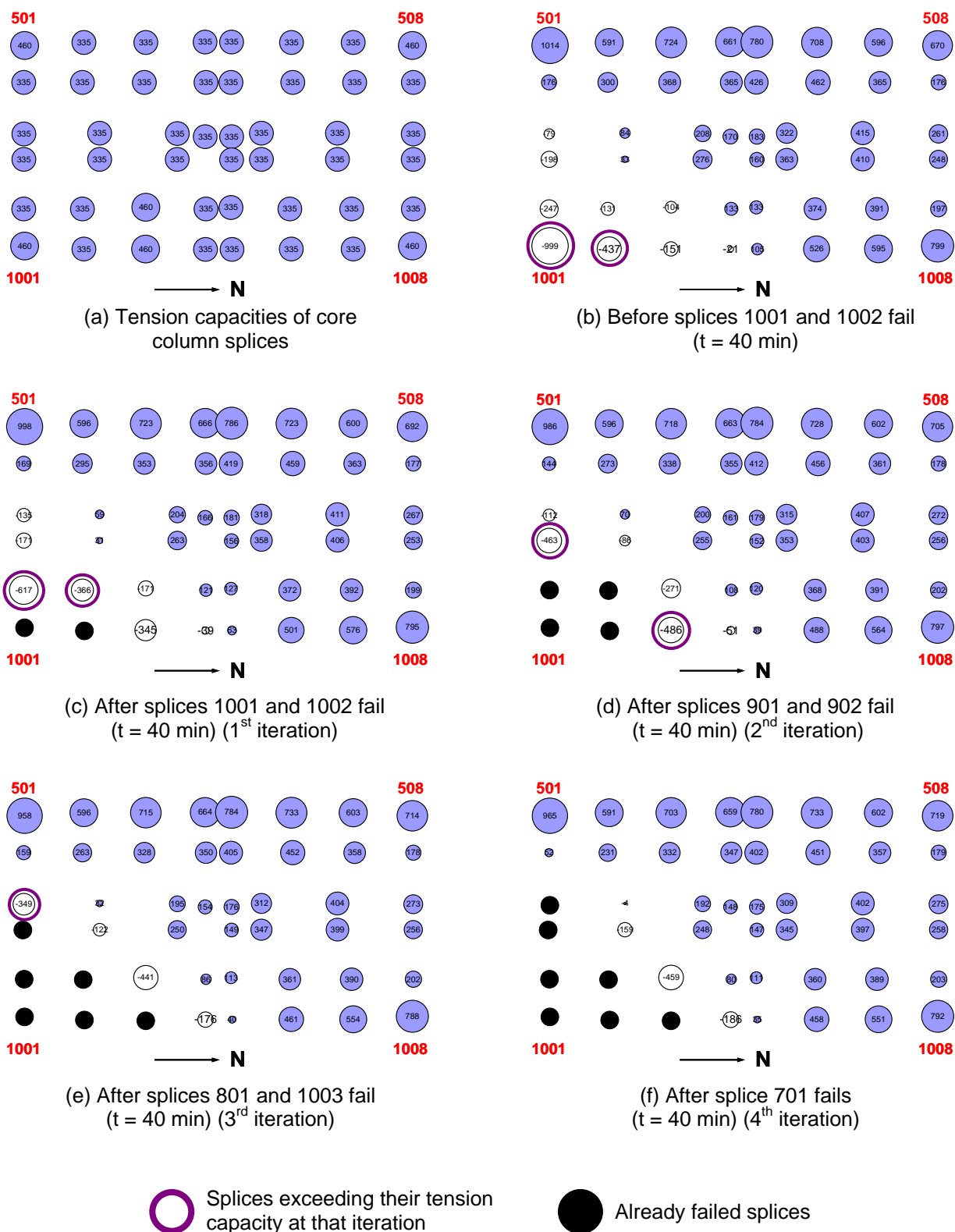


Figure 4–126. Progressive failure of core column splices at Floor 105 of WTC 2 (compression is positive; values are in kip).

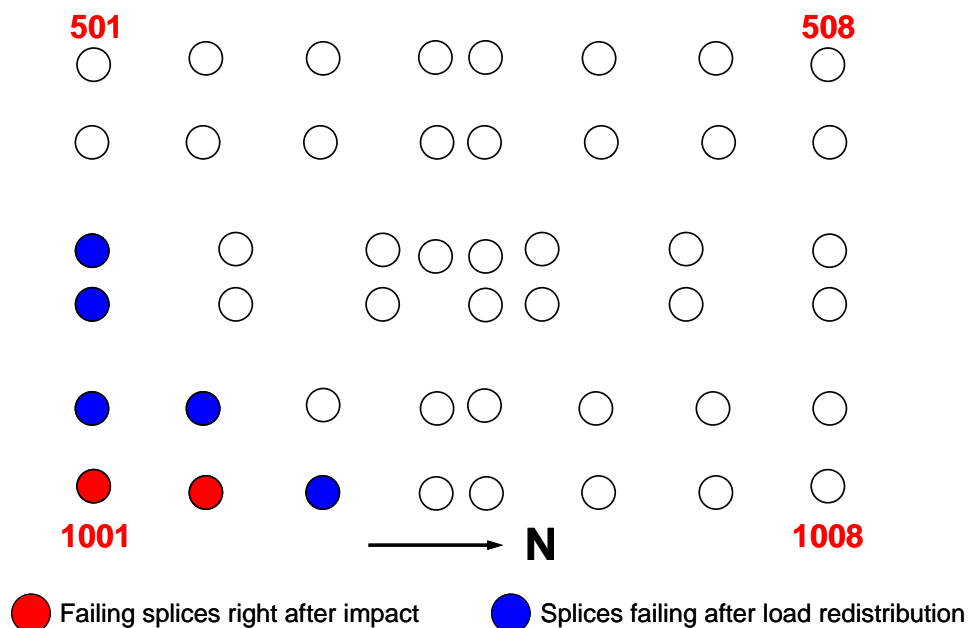


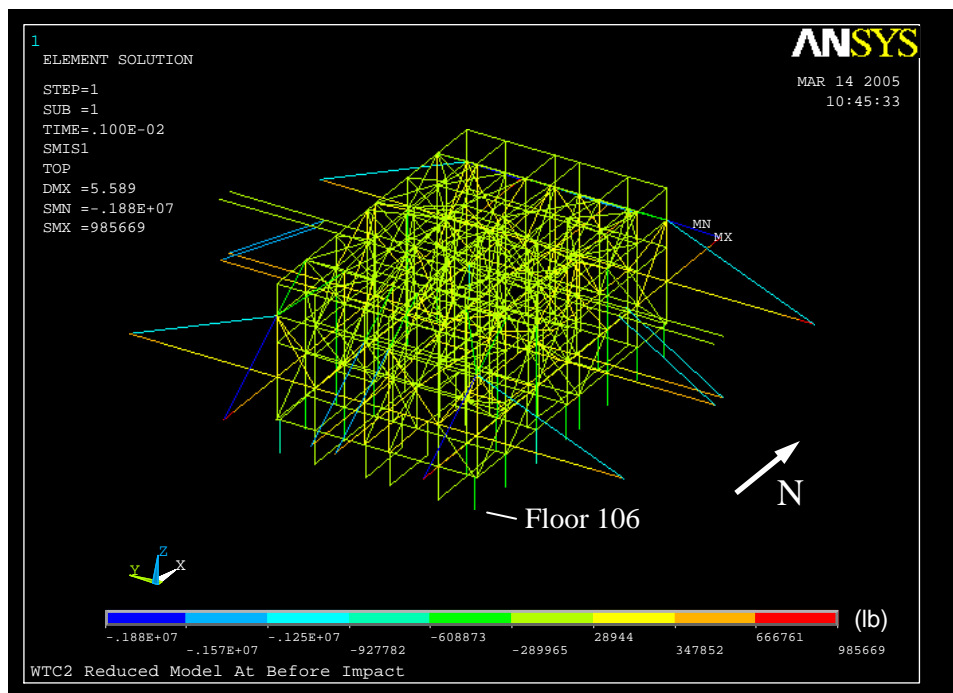
Figure 4–127. State of core column splices at Floor 105 of WTC 2.

Table 4–31. Total column loads (kip) at Floor 105 at different stages of splice failures at 40 min (compression is positive).

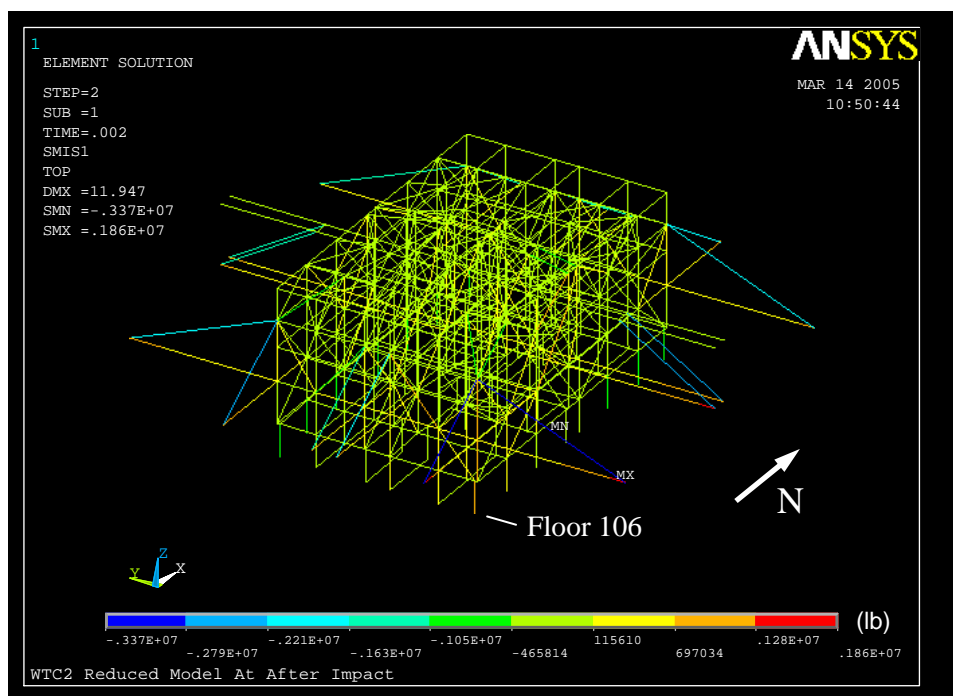
Row	Analysis Status	West	East	North	South	Core	TLRSF*	TLRHT**
(1)	Before Splice Failure (t = 40 min)	9185	11913	6537	8706	12402	0	0
(2)	Splices 1001 and 1002 fail	9221	11747	6577	8432	12761	-1436	-1077
(3)	Splices 901 and 902 fail	9227	11644	6612	8206	13045	-2419	-1776
(4)	Splices 801 and 1003 fail	9241	11550	6629	8043	13267	-3368	-2503
(5)	Splice 701 fails	9229	11533	6649	7925	13391	-3717	-2728
(6)	(2)-(1)	36	-166	40	-274	359	-1436	-1077
(7)	(3)-(2)	6	-103	35	-226	284	-983	-699
(8)	(4)-(3)	13	-93	17	-163	222	-949	-727
(9)	(5)-(4)	-11	-17	20	-117	124	-349	-225
(10)	(6)+(7)+(8)+(9)	44	-380	112	-780	989	-3717	-2728

* Total load released by the splice failure

** Total load retransferred to the hat-truss

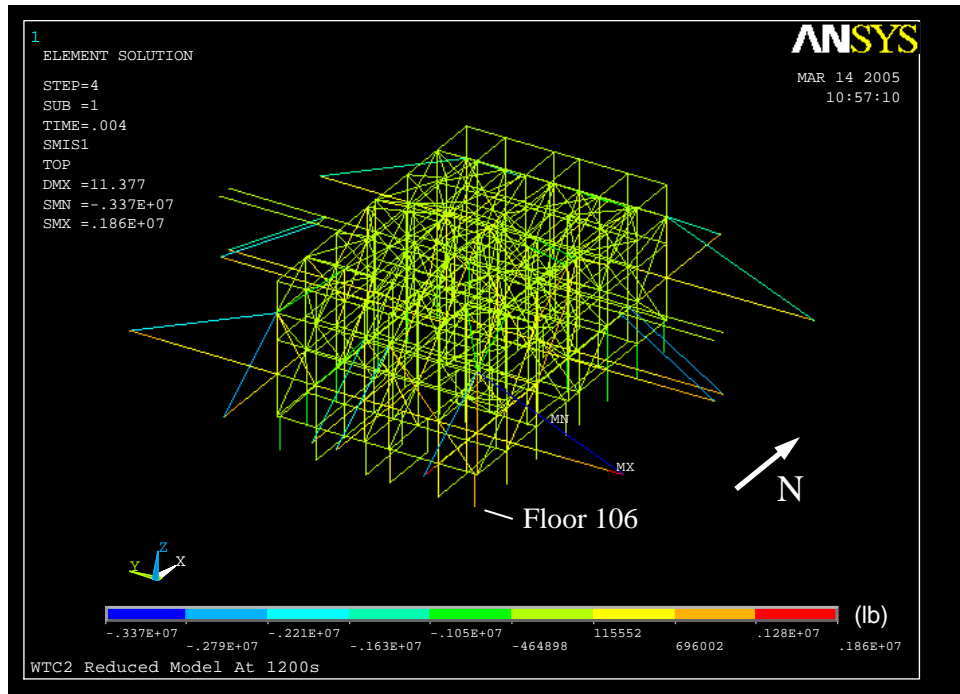


(a) Before impact

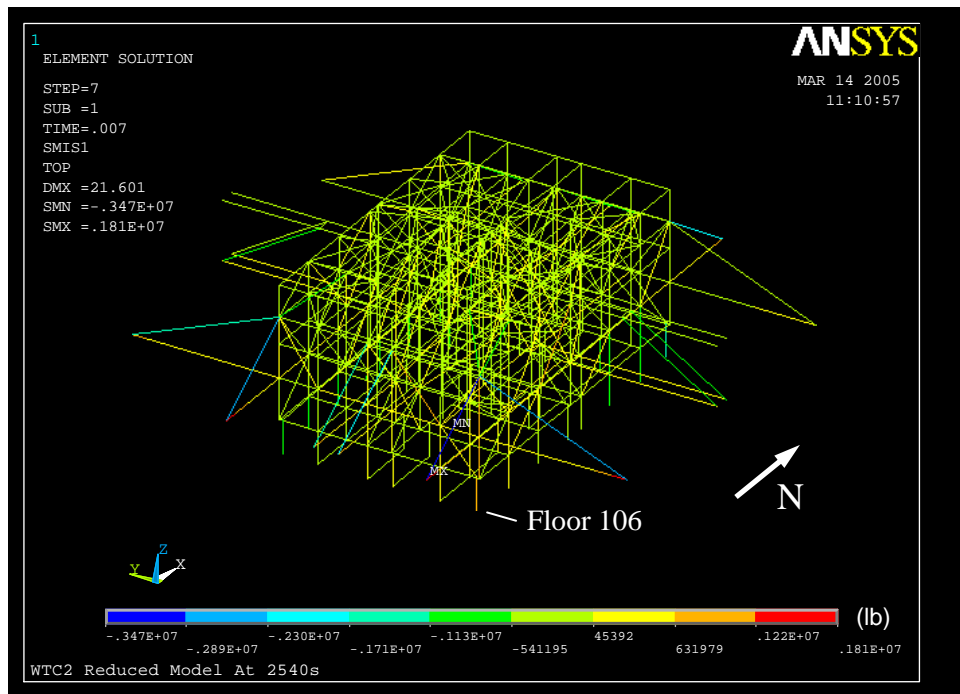


(b) After impact

Figure 4–128. Axial force in hat truss members of WTC 2 for Case D conditions (tension is positive).

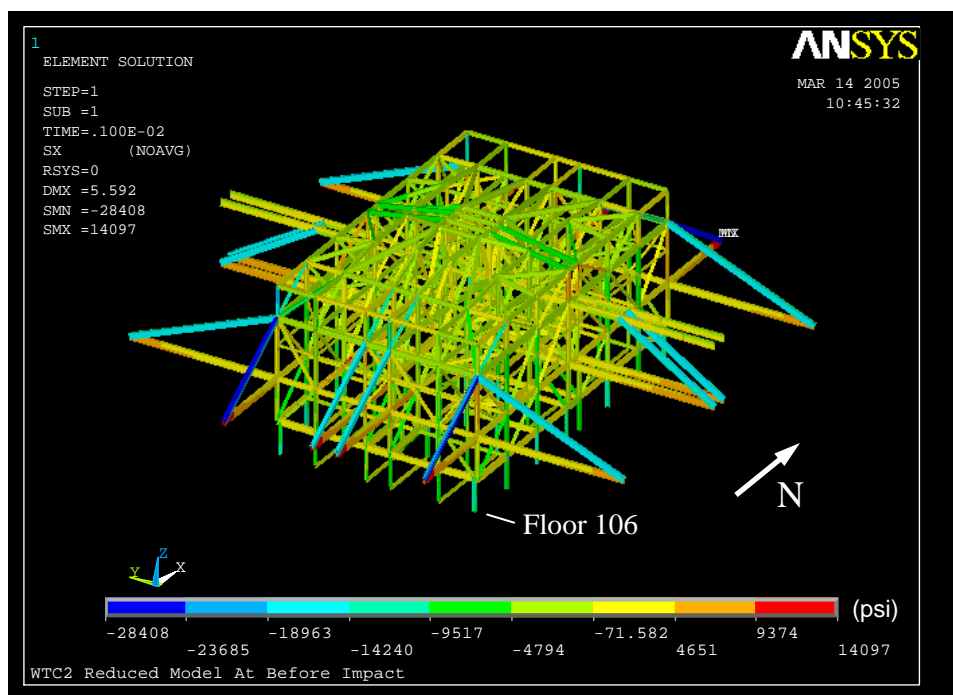


(a) 20 min

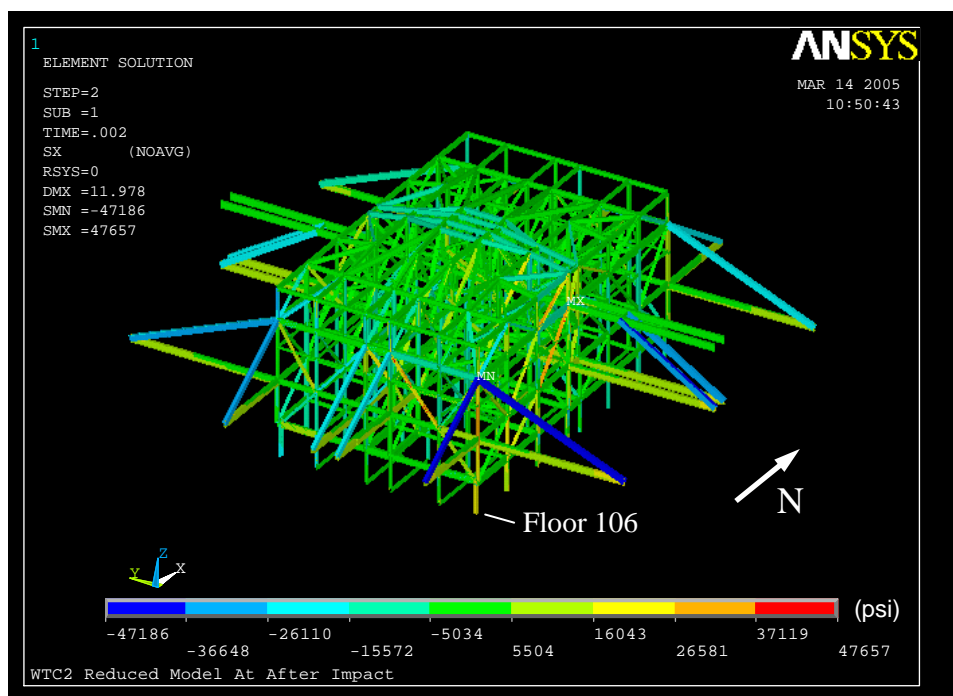


(b) 43 min

Figure 4–129. Axial force in hat truss members of WTC 2 for Case D conditions (tension is positive).

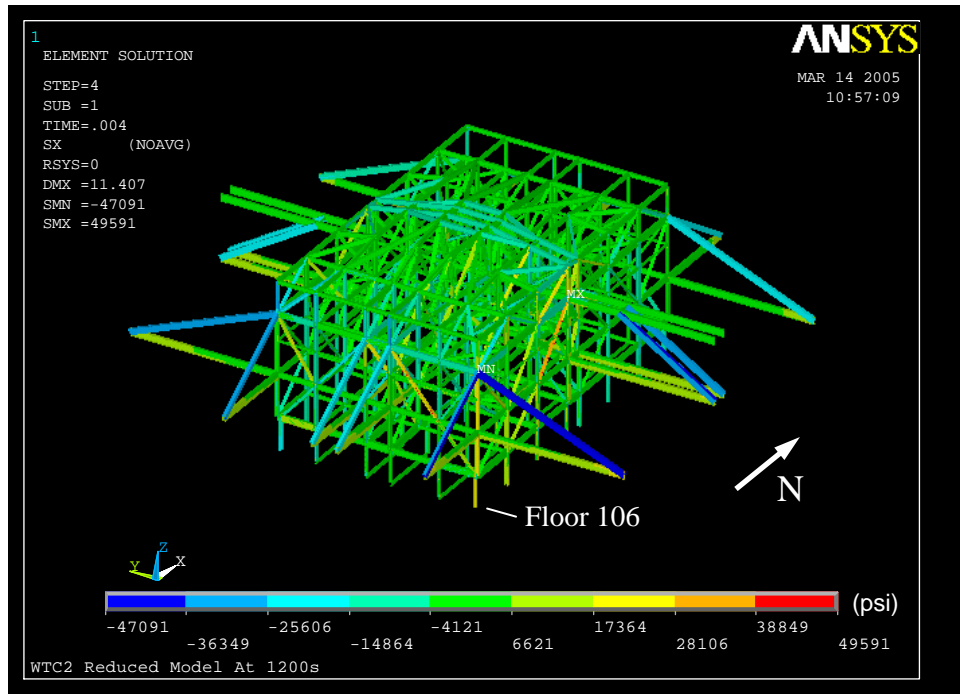


(a) Before impact

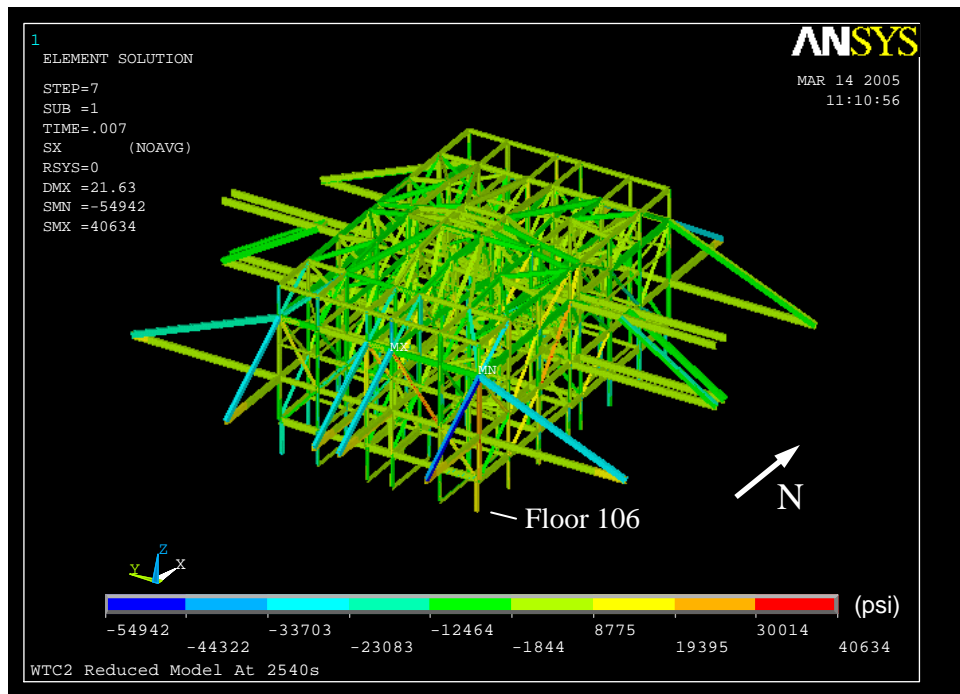


(b) After impact

Figure 4-130. Axial stress in hat truss members of WTC 2 for Case D conditions (tension is positive).



(a) 20 min



(b) 43 min

Figure 4-131. Axial stress in hat truss members of WTC 2 for Case D conditions (tension is positive).

Table 4–32. Demand-to-capacity ratios for outriggers of WTC 2 for Case D conditions (outrigger IDs are shown in Fig. 4–3).

Outrigger ID	Bfr. Imp.	Afr. Imp.	10 min	20 min	30 min	40 min	40* min	40** min	43 min
West									
A	0.23	0.61	0.61	0.64	0.66	0.63	0.63	0.38	0.25
B	0.19	0.30	0.30	0.32	0.33	0.31	0.31	0.25	-0.03***
C	0.19	0.27	0.27	0.28	0.30	0.27	0.28	0.22	-0.07
D	0.21	0.18	0.18	0.19	0.21	0.18	0.20	0.19	-0.29
North									
E	0.29	0.11	0.10	0.10	0.13	0.14	0.17	0.09	-0.01
F	0.21	0.10	0.08	0.08	0.10	0.12	0.13	0.11	0.08
G	0.20	0.11	0.08	0.08	0.11	0.13	0.14	0.13	0.10
H	0.30	0.21	0.16	0.18	0.19	0.18	0.19	0.24	0.24
East									
I	0.22	0.39	0.35	0.34	0.45	0.43	0.42	0.41	-0.18
J	0.18	0.56	0.52	0.53	0.66	0.65	0.61	0.71	0.02
K	0.18	0.62	0.58	0.59	0.72	0.72	0.66	0.79	0.09
L	0.22	1.12	1.09	1.12	1.24	1.30	1.11	0.00	0.72
South									
M	0.30	0.68	0.64	0.64	0.70	0.75	0.52	0.72	0.87
N	0.22	0.34	0.32	0.33	0.36	0.38	0.28	0.34	0.40
O	0.22	0.30	0.28	0.30	0.32	0.33	0.27	0.31	0.33
P	0.31	0.51	0.50	0.52	0.53	0.53	0.50	0.57	0.49

* After load redistribution due to core column splice failures.

** After Outrigger L was removed.

*** Negative value indicates tension

Table 4–33. Demand to capacity ratios for columns supporting outriggers at Floor 107 of WTC 2 for Case D conditions.

Column ID	Bfr. Imp.	Afr. Imp.	10 min	20 min	30 min	40 min	43 min
West							
110	0.26	0.46	0.46	0.47	0.48	0.47	0.28
111	0.26	0.39	0.39	0.40	0.41	0.40	0.26
129	0.27	0.37	0.37	0.38	0.40	0.37	0.06
130	0.31	0.39	0.39	0.40	0.41	0.39	0.09
131	0.27	0.35	0.34	0.36	0.37	0.35	0.05
149	0.25	0.24	0.24	0.25	0.25	0.24	0.08
150	0.25	0.23	0.23	0.23	0.24	0.23	0.00
North							
217	0.17	0.11	0.11	0.11	0.12	0.12	0.07
218	0.23	0.12	0.11	0.11	0.13	0.14	0.05
228	0.27	0.17	0.15	0.15	0.17	0.19	0.15
229	0.22	0.14	0.12	0.12	0.14	0.16	0.13
231	0.26	0.18	0.15	0.15	0.18	0.19	0.17
232	0.26	0.18	0.15	0.15	0.18	0.20	0.18
242	0.20	0.15	0.12	0.13	0.14	0.14	0.17
243	0.19	0.16	0.14	0.14	0.15	0.14	0.17
East							
310	0.25	0.34	0.32	0.31	0.36	0.36	0.05
311	0.27	0.33	0.32	0.31	0.35	0.35	0.13
329	0.26	0.61	0.57	0.58	0.69	0.69	0.12
330	0.31	0.68	0.65	0.66	0.77	0.77	0.19
331	0.27	0.63	0.60	0.61	0.72	0.72	0.16
349	0.26	0.56	0.55	0.56	0.60	0.62	0.42
350	0.26	0.71	0.69	0.71	0.77	0.81	0.51
South							
417	0.18	0.30	0.29	0.29	0.31	0.33	0.37
418	0.24	0.46	0.43	0.44	0.47	0.50	0.57
428	0.28	0.38	0.36	0.37	0.39	0.41	0.43
429	0.23	0.30	0.29	0.30	0.32	0.33	0.34
431	0.26	0.33	0.31	0.32	0.34	0.36	0.36
432	0.27	0.35	0.34	0.35	0.37	0.38	0.38
442	0.21	0.32	0.31	0.32	0.33	0.33	0.31
443	0.20	0.28	0.28	0.28	0.29	0.29	0.27

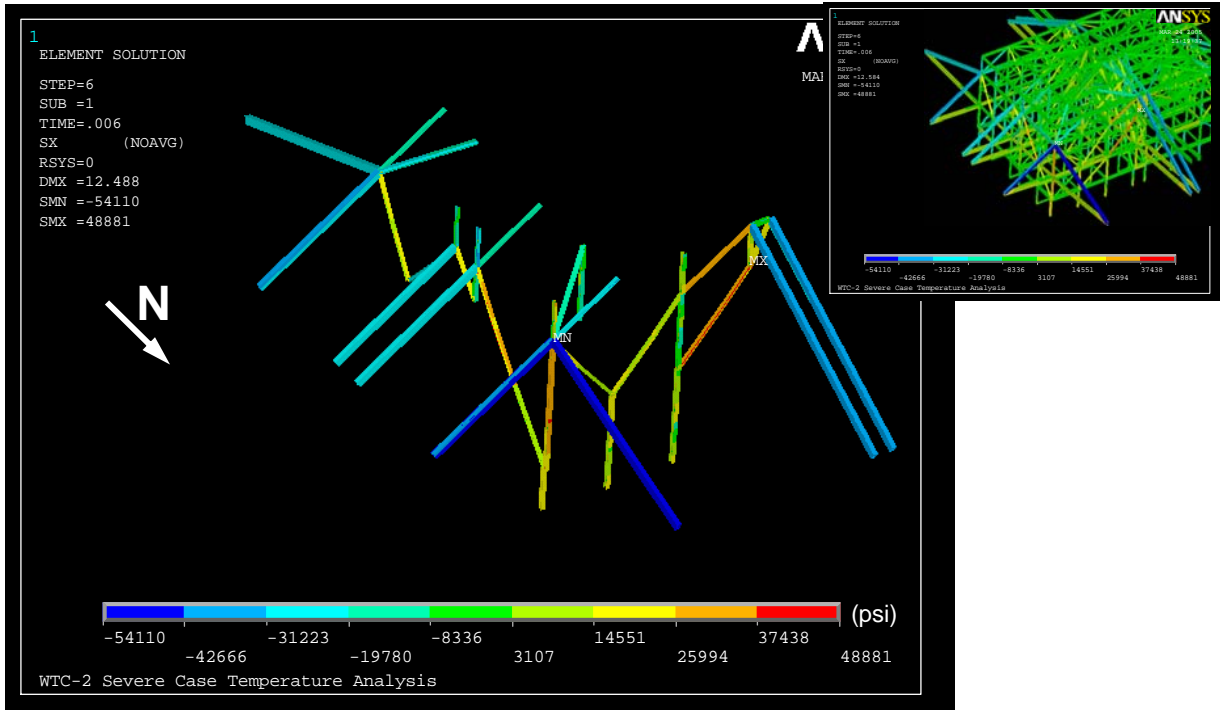


Figure 4–132. Primary load path within the hat truss of WTC 2.

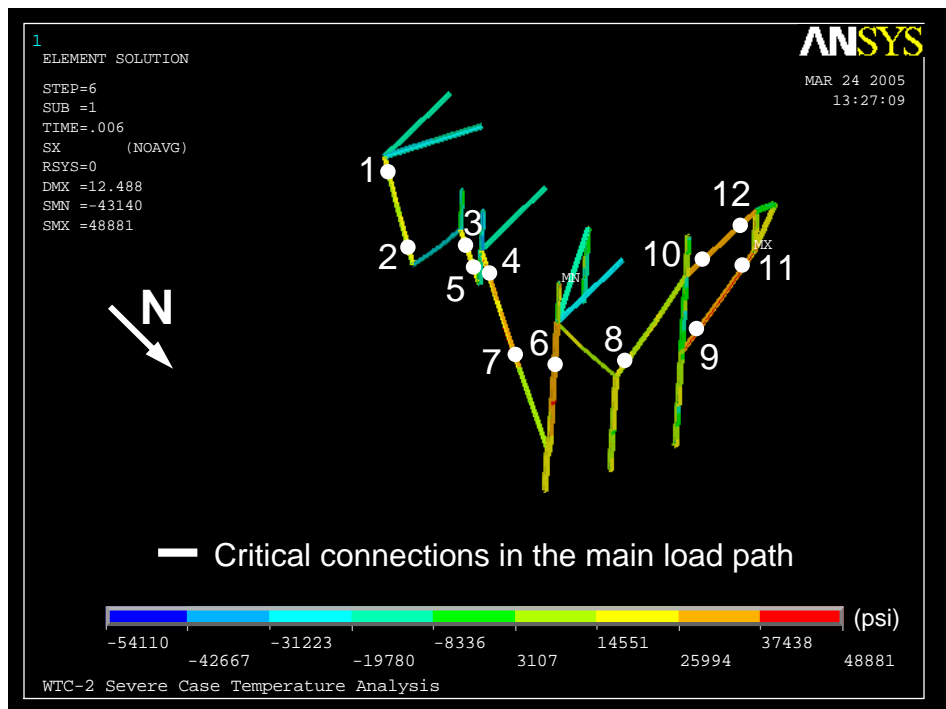


Figure 4–133. Location of hat truss connections that were in the primary load path.

Table 4–34. Demand and capacity of the hat truss connections (kip) in the primary load path at 40 min (connection IDs are shown in Fig. 4–133).

Con. ID	Location		Tension Capacity		Demand Force (tension)		Status	
	Floor	Column	Yield	Ultimate	Before Redist.	After Redist.	Before Redist.	After Redist.
1	110	501	840	1,100	567	512	Safe	Safe
2	108	601	840	1,100	567	512	Safe	Safe
3	110	701	630	870	575	370	Safe	Safe
4	110	801	840	1,100	950	510	Yielded	Safe
5	109	801	630	870	575	370	Safe	Safe
6	110	1001	760	870	1,370	760	Failed	Safe
7	108	901	840	1,100	950	510	Yielded	Safe
8	108	1002	1,250	1,250	440	110	Safe	Safe
9	108	1003	1,470	1,470	1,000	700	Safe	Safe
10	110	1003	1,250	1,250	750	550	Safe	Safe
11	110	1004	1,470	1,470	1,000	700	Safe	Safe
12	111	1004	1,250	1,250	750	550	Safe	Safe

Table 4–35. Total column loads at Floor 83 of WTC 2 for Case D conditions.

Row	Analysis Step	West	East	North	South	Core	Sum
(1)	Before Impact	18,065	18,114	13,567	13,284	61,828	124,857
(2)	After Impact	18,670	22,481	12,193	13,511	57,821	124,676
(3)	10 min	18,728	22,226	11,896	13,358	58,413	124,621
(4)	20 min	18,914	22,208	12,052	13,318	58,124	124,616
(5)	30 min	18,876	23,681	11,770	13,365	56,967	124,659
(6)	40 min	18,531	23,682	11,906	13,473	56,825	124,418
(7)	43 min	15,667	15,143	14,215	16,292	62,422	123,738
(8)	(2)-(1)	604	4,368	-1,374	227	-4,007	-181
(9)	(3)-(1)	662	4,112	-1,670	74	-3,415	-236
(10)	(4)-(1)	849	4,094	-1,515	35	-3,704	-241
(11)	(5)-(1)	811	5,567	-1,797	81	-4,861	-199
(12)	(6)-(1)	466	5,568	-1,661	190	-5,003	-439
(13)	(7)-(1)	-2,398	-2,971	648	3,009	594	-1,119

Note: Compression is positive. Units are in kip.

Table 4–36. Total column loads at Floor 105 of WTC 2 for Case D conditions.

Row	Analysis Step	West	East	North	South	Core	Sum
(1)	Before Impact	8,497	8,572	7,382	7,169	17,123	48,742
(2)	After Impact	9,170	11,272	6,487	8,432	13,382	48,742
(3)	10 min	9,182	11,061	6,250	8,275	13,975	48,742
(4)	20 min	9,279	11,120	6,311	8,351	13,682	48,742
(5)	30 min	9,370	11,859	6,416	8,553	12,544	48,742
(6)	40 min	9,198	11,927	6,524	8,691	12,402	48,742
(7)	43 min	7,086	8,026	6,546	9,169	17,915	48,742
(8)	(2)-(1)	674	2,699	-895	1,263	-3,741	0
(9)	(3)-(1)	685	2,489	-1,132	1,106	-3,148	0
(10)	(4)-(1)	783	2,547	-1,071	1,182	-3,441	0
(11)	(5)-(1)	873	3,287	-965	1,384	-4,579	0
(12)	(6)-(1)	702	3,355	-858	1,522	-4,721	0
(13)	(7)-(1)	-1,411	-547	-835	2,000	792	0

Note: Compression is positive. Units are in kip.

**Table 4–37. Change in total column loads before and after aircraft impact.
(Loads After Impact) – (Loads Before Impact)**

Row	Floor	West	East	North	South	Core
(1)	83	604	4,368	-1,374	227	-4,007
(2)	105	674	2,699	-895	1,263	-3,741
(3)	(2) - (1)	69	-1,668	479	1,035	266

Note: Increase in compression is shown as positive. Units are in kip.

**Table 4–38. Change in total column loads between 40 min and 43 min.
(Loads at 43 min) – (Loads at 40 min)**

Row	Floor	West	East	North	South	Core
(1)	83	-2,864	-8,539	2,309	2,819	5,596
(2)	105	-2,112	-3,901	23	479	5,513
(3)	(2) - (1)	752	4,637	-2,286	-2,340	-84

Note: Increase in compression is shown as positive. Units are in kip.

Table 4–39. Total column loads over the height for the east wall of WTC 2 for Case D conditions.

Step	Before Impact	After Impact	10 min	20 min	30 min	40 min	43 min	(2)-(1)	(3)-(1)	(4)-(1)	(5)-(1)	(6)-(1)	(7)-(1)
Floor/Col	(1)	(2)	(3)	(4)	(5)	(6)	(7)	(8)	(9)	(10)	(11)	(12)	(13)
105	8,572	11,272	11,061	11,120	11,859	11,927	8,026	2,699	2,489	2,547	3,287	3,355	-547
104	8,939	11,668	11,457	11,514	12,273	12,342	8,291	2,729	2,519	2,575	3,335	3,403	-648
103	9,419	12,256	12,048	12,102	12,890	12,968	8,735	2,837	2,628	2,683	3,470	3,549	-684
102	9,752	12,609	12,400	12,454	13,262	13,338	8,927	2,857	2,648	2,702	3,510	3,586	-825
101	10,254	13,235	13,029	13,079	13,917	14,007	9,427	2,981	2,774	2,824	3,663	3,752	-827
100	10,570	13,556	13,349	13,399	14,259	14,342	9,562	2,987	2,780	2,829	3,689	3,773	-1,008
99	11,089	14,217	14,013	14,058	14,950	15,051	10,114	3,128	2,924	2,969	3,861	3,962	-974
98	11,399	14,517	14,312	14,358	15,271	15,363	10,201	3,119	2,913	2,959	3,872	3,965	-1,198
97	11,944	15,223	15,021	15,060	16,009	16,123	10,819	3,279	3,077	3,116	4,065	4,179	-1,125
96	12,240	15,494	15,290	15,332	16,301	16,403	10,844	3,253	3,050	3,092	4,061	4,163	-1,396
95	12,804	16,234	16,035	16,069	17,076	17,204	11,524	3,430	3,232	3,265	4,272	4,400	-1,280
94	13,094	16,484	16,282	16,321	17,348	17,461	11,487	3,390	3,188	3,227	4,255	4,368	-1,607
93	13,673	17,256	17,061	17,088	18,156	18,300	12,235	3,583	3,388	3,415	4,483	4,626	-1,439
92	13,958	17,483	17,284	17,319	18,408	18,533	12,118	3,525	3,326	3,361	4,450	4,575	-1,840
91	14,553	18,287	18,098	18,117	19,250	19,410	12,953	3,734	3,544	3,564	4,697	4,857	-1,600
90	14,830	18,487	18,291	18,323	19,475	19,613	12,724	3,657	3,461	3,494	4,646	4,783	-2,105
89	15,443	19,328	19,147	19,158	20,359	20,538	13,677	3,886	3,704	3,715	4,916	5,095	-1,766
88	15,710	19,500	19,308	19,340	20,559	20,709	13,283	3,790	3,598	3,630	4,849	5,000	-2,426
87	16,341	20,381	20,213	20,211	21,489	21,690	14,400	4,039	3,872	3,870	5,147	5,348	-1,941
86	16,599	20,533	20,347	20,375	21,658	21,819	13,781	3,935	3,749	3,776	5,059	5,220	-2,818
85	17,220	21,438	21,292	21,270	22,636	22,867	15,117	4,218	4,072	4,050	5,416	5,647	-2,103
84	17,466	21,524	21,331	21,379	22,745	22,936	14,151	4,058	3,864	3,913	5,279	5,469	-3,316
83	18,114	22,481	22,226	22,208	23,681	23,682	15,143	4,368	4,112	4,094	5,567	5,568	-2,971
82	18,353	22,540	22,373	22,279	23,713	23,826	14,310	4,187	4,021	3,926	5,360	5,473	-4,043
81	19,036	23,540	23,007	23,275	24,784	24,942	16,763	4,504	3,970	4,239	5,747	5,906	-2,274
80	19,257	23,569	23,570	23,325	24,755	24,924	15,643	4,311	4,313	4,067	5,498	5,667	-3,615
79	19,970	24,634	24,431	24,381	25,821	26,023	17,571	4,665	4,461	4,411	5,851	6,053	-2,398
78	20,169	24,581	24,362	24,299	25,666	25,778	16,729	4,412	4,193	4,130	5,497	5,609	-3,440

Note: Compression is positive. Units are in kip.

Table 4-40. Total column loads over the height for the south wall of WTC 2 for Case D conditions.

Step	Before Impact	After Impact	10 min	20 min	30 min	40 min	43 min	(2)-(1)	(3)-(1)	(4)-(1)	(5)-(1)	(6)-(1)	(7)-(1)
Floor/Col	(1)	(2)	(3)	(4)	(5)	(6)	(7)	(8)	(9)	(10)	(11)	(12)	(13)
105	7,169	8,432	8,275	8,351	8,553	8,691	9,169	1,263	1,106	1,182	1,384	1,522	2,000
104	7,517	8,765	8,606	8,679	8,878	9,019	9,587	1,248	1,089	1,162	1,362	1,502	2,070
103	7,744	8,904	8,743	8,811	9,001	9,136	9,819	1,160	999	1,067	1,257	1,391	2,075
102	8,110	9,266	9,104	9,167	9,354	9,495	10,294	1,156	993	1,057	1,243	1,385	2,183
101	8,308	9,364	9,197	9,258	9,433	9,566	10,462	1,056	889	950	1,125	1,258	2,154
100	8,692	9,758	9,591	9,646	9,819	9,961	10,995	1,067	900	954	1,127	1,270	2,304
99	8,863	9,816	9,644	9,697	9,858	9,988	11,103	953	781	834	995	1,125	2,240
98	9,267	10,247	10,075	10,120	10,280	10,423	11,701	980	808	853	1,013	1,156	2,434
97	9,426	10,277	10,099	10,144	10,291	10,418	11,758	850	673	718	865	992	2,332
96	9,836	10,731	10,554	10,589	10,736	10,879	12,412	895	718	753	900	1,043	2,577
95	9,981	10,732	10,548	10,585	10,718	10,842	12,412	752	568	604	737	861	2,432
94	10,400	11,212	11,030	11,054	11,188	11,332	13,136	812	630	654	789	932	2,737
93	10,532	11,189	10,998	11,026	11,144	11,265	13,072	658	466	495	613	734	2,540
92	10,960	11,697	11,509	11,522	11,643	11,787	13,885	737	549	562	683	827	2,925
91	11,080	11,648	11,449	11,469	11,572	11,689	13,736	569	369	390	493	610	2,657
90	11,521	12,189	11,997	11,996	12,104	12,250	14,673	668	476	476	584	729	3,152
89	11,627	12,110	11,900	11,914	12,001	12,113	14,411	483	273	287	373	486	2,784
88	12,083	12,685	12,490	12,473	12,569	12,717	15,525	603	407	390	486	634	3,442
87	12,176	12,578	12,355	12,362	12,431	12,538	15,099	402	179	187	256	363	2,924
86	12,641	13,182	12,987	12,954	13,043	13,196	16,464	541	346	313	403	555	3,823
85	12,738	13,035	12,795	12,801	12,848	12,948	15,743	297	58	63	111	210	3,005
84	13,224	13,705	13,540	13,459	13,545	13,703	17,525	481	317	236	321	479	4,302
83	13,284	13,511	13,358	13,318	13,365	13,473	16,292	227	74	35	81	190	3,009
82	13,789	14,201	13,851	14,027	14,114	14,280	18,208	413	62	238	325	492	4,419
81	13,851	13,949	13,700	13,722	13,745	13,862	17,024	98	-151	-129	-105	12	3,173
80	14,379	14,645	14,257	14,447	14,522	14,695	18,830	266	-122	68	143	316	4,452
79	14,424	14,325	14,095	14,115	14,143	14,265	17,516	-99	-330	-309	-281	-159	3,092
78	15,000	15,110	14,866	14,916	14,982	15,178	19,109	110	-134	-84	-18	178	4,108

Note: Compression is positive. Units are in kip.

Table 4-41. Total column loads over the height for the north wall of WTC 2 for Case D conditions.

Step	Before Impact	After Impact	10 min	20 min	30 min	40 min	43 min	(2)-(1)	(3)-(1)	(4)-(1)	(5)-(1)	(6)-(1)	(7)-(1)
Floor/Col	(1)	(2)	(3)	(4)	(5)	(6)	(7)	(8)	(9)	(10)	(11)	(12)	(13)
105	7,382	6,487	6,250	6,311	6,416	6,524	6,546	-895	-1,132	-1,071	-965	-858	-835
104	7,738	6,822	6,583	6,648	6,742	6,850	6,946	-916	-1,155	-1,090	-997	-888	-793
103	7,963	7,030	6,790	6,859	6,939	7,052	7,257	-933	-1,173	-1,104	-1,024	-911	-706
102	8,337	7,381	7,139	7,211	7,280	7,395	7,669	-956	-1,198	-1,125	-1,057	-942	-667
101	8,533	7,560	7,316	7,393	7,447	7,565	7,960	-973	-1,217	-1,140	-1,086	-968	-573
100	8,924	7,925	7,680	7,760	7,802	7,923	8,382	-999	-1,245	-1,164	-1,123	-1,002	-542
99	9,096	8,081	7,833	7,919	7,944	8,068	8,659	-1,015	-1,263	-1,176	-1,152	-1,028	-437
98	9,506	8,461	8,212	8,302	8,314	8,440	9,089	-1,044	-1,294	-1,204	-1,192	-1,065	-416
97	9,665	8,608	8,356	8,452	8,446	8,575	9,366	-1,058	-1,309	-1,214	-1,219	-1,090	-299
96	10,081	8,991	8,738	8,837	8,818	8,949	9,793	-1,090	-1,344	-1,245	-1,263	-1,132	-289
95	10,227	9,125	8,869	8,975	8,938	9,071	10,066	-1,101	-1,357	-1,252	-1,289	-1,156	-161
94	10,652	9,514	9,257	9,366	9,315	9,450	10,491	-1,138	-1,395	-1,287	-1,338	-1,202	-161
93	10,785	9,638	9,378	9,494	9,424	9,561	10,763	-1,146	-1,407	-1,291	-1,361	-1,224	-22
92	11,220	10,031	9,769	9,887	9,802	9,941	11,182	-1,189	-1,451	-1,333	-1,418	-1,278	-37
91	11,340	10,148	9,882	10,009	9,904	10,044	11,457	-1,192	-1,458	-1,331	-1,436	-1,296	117
90	11,788	10,546	10,279	10,407	10,286	10,428	11,869	-1,241	-1,509	-1,381	-1,502	-1,359	82
89	11,895	10,658	10,385	10,523	10,381	10,524	12,149	-1,237	-1,510	-1,372	-1,514	-1,371	254
88	12,357	11,061	10,786	10,925	10,764	10,910	12,556	-1,296	-1,571	-1,433	-1,593	-1,448	199
87	12,451	11,166	10,884	11,035	10,851	10,996	12,847	-1,286	-1,568	-1,416	-1,600	-1,455	396
86	12,923	11,571	11,287	11,435	11,232	11,380	13,228	-1,352	-1,637	-1,489	-1,691	-1,543	304
85	13,014	11,686	11,393	11,559	11,327	11,470	13,573	-1,328	-1,620	-1,455	-1,687	-1,544	560
84	13,506	12,101	11,818	11,960	11,693	11,830	13,899	-1,406	-1,688	-1,547	-1,813	-1,676	393
83	13,567	12,193	11,896	12,052	11,770	11,906	14,215	-1,374	-1,670	-1,515	-1,797	-1,661	648
82	14,078	12,616	12,140	12,428	12,134	12,310	14,546	-1,462	-1,937	-1,650	-1,944	-1,768	468
81	14,141	12,725	12,380	12,512	12,121	12,367	14,824	-1,416	-1,761	-1,629	-2,020	-1,774	683
80	14,675	13,157	12,838	13,052	12,756	12,915	15,221	-1,518	-1,837	-1,624	-1,919	-1,761	546
79	14,723	13,259	12,998	13,137	12,873	13,044	15,519	-1,464	-1,724	-1,585	-1,849	-1,679	797
78	15,304	13,767	13,495	13,671	13,441	13,625	15,921	-1,537	-1,809	-1,633	-1,863	-1,679	617

Note: Compression is positive. Units are in kip.

Table 4-42. Total column loads over the height for the west wall of WTC 2 for Case D conditions.

Step	Before Impact	After Impact	10 min	20 min	30 min	40 min	43 min	(2)-(1)	(3)-(1)	(4)-(1)	(5)-(1)	(6)-(1)	(7)-(1)
Floor/Col	(1)	(2)	(3)	(4)	(5)	(6)	(7)	(8)	(9)	(10)	(11)	(12)	(13)
105	8,497	9,170	9,182	9,279	9,370	9,198	7,086	674	685	783	873	702	-1,411
104	8,861	9,544	9,557	9,657	9,743	9,567	7,439	683	696	796	882	706	-1,422
103	9,347	10,028	10,045	10,147	10,229	10,045	7,871	681	698	799	882	697	-1,476
102	9,678	10,370	10,388	10,493	10,570	10,380	8,195	691	710	814	892	701	-1,484
101	10,185	10,873	10,895	11,001	11,075	10,877	8,638	688	710	816	889	691	-1,547
100	10,500	11,199	11,224	11,333	11,401	11,196	8,952	700	724	833	901	696	-1,547
99	11,023	11,714	11,742	11,853	11,917	11,704	9,401	691	719	830	894	681	-1,622
98	11,331	12,038	12,068	12,182	12,240	12,020	9,717	707	737	851	908	689	-1,614
97	11,881	12,573	12,607	12,723	12,776	12,549	10,179	693	727	842	896	668	-1,701
96	12,176	12,886	12,922	13,041	13,088	12,853	10,490	710	746	865	912	678	-1,686
95	12,743	13,433	13,474	13,594	13,636	13,394	10,958	691	731	851	894	651	-1,785
94	13,032	13,742	13,784	13,909	13,944	13,694	11,269	710	753	877	913	662	-1,763
93	13,615	14,299	14,347	14,471	14,502	14,243	11,740	684	732	857	887	628	-1,875
92	13,897	14,606	14,655	14,785	14,808	14,542	12,055	709	758	888	911	644	-1,842
91	14,497	15,171	15,226	15,356	15,373	15,098	12,528	675	729	859	877	601	-1,969
90	14,771	15,476	15,531	15,668	15,678	15,394	12,847	705	760	896	907	623	-1,924
89	15,388	16,050	16,112	16,247	16,251	15,958	13,320	662	724	859	862	570	-2,068
88	15,653	16,352	16,412	16,557	16,553	16,251	13,641	699	760	904	900	598	-2,012
87	16,289	16,933	17,003	17,143	17,132	16,821	14,113	644	714	855	843	533	-2,176
86	16,554	17,233	17,297	17,451	17,433	17,115	14,446	679	743	897	880	561	-2,108
85	17,171	17,801	17,877	18,025	17,996	17,665	14,877	630	706	854	825	494	-2,294
84	17,414	18,100	18,153	18,336	18,300	17,958	15,214	686	739	922	886	544	-2,200
83	18,065	18,670	18,728	18,914	18,876	18,531	15,667	604	662	849	811	466	-2,398
82	18,301	18,970	19,060	19,204	19,155	18,795	15,989	668	758	903	854	494	-2,312
81	18,989	19,559	19,615	19,813	19,764	19,407	16,473	570	626	824	775	418	-2,516
80	19,207	19,846	19,939	20,076	20,019	19,650	16,788	639	733	870	812	443	-2,418
79	19,923	20,461	20,542	20,723	20,672	20,304	17,309	538	619	800	749	381	-2,614
78	20,119	20,723	20,828	20,968	20,912	20,542	17,637	605	710	850	793	423	-2,482

Note: Compression is positive. Units are in kip.

Table 4-43. Total column loads over the height for the core of WTC 2 for Case D conditions.

Step	Before Impact	After Impact	10 min	20 min	30 min	40 min	43 min	(2)-(1)	(3)-(1)	(4)-(1)	(5)-(1)	(6)-(1)	(7)-(1)
Floor/Col	(1)	(2)	(3)	(4)	(5)	(6)	(7)	(8)	(9)	(10)	(11)	(12)	(13)
105	17,123	13,382	13,975	13,682	12,544	12,402	17,915	-3,741	-3,148	-3,441	-4,579	-4,721	792
104	19,100	15,357	15,950	15,657	14,518	14,376	19,892	-3,743	-3,149	-3,443	-4,582	-4,724	792
103	21,069	17,323	17,917	17,624	16,484	16,342	21,862	-3,746	-3,152	-3,445	-4,585	-4,727	793
102	23,022	19,274	19,869	19,575	18,434	18,293	23,815	-3,748	-3,154	-3,448	-4,588	-4,730	793
101	24,980	21,228	21,824	21,529	20,388	20,247	25,773	-3,751	-3,156	-3,450	-4,591	-4,733	793
100	26,927	23,172	23,768	23,473	22,332	22,190	27,720	-3,754	-3,159	-3,453	-4,595	-4,737	793
99	28,873	25,116	25,712	25,417	24,275	24,133	29,667	-3,758	-3,161	-3,456	-4,599	-4,740	794
98	30,816	27,055	27,652	27,357	26,214	26,072	31,610	-3,761	-3,164	-3,459	-4,602	-4,744	794
97	33,524	29,760	30,357	30,062	28,918	28,776	34,318	-3,764	-3,167	-3,462	-4,606	-4,748	794
96	36,232	32,465	33,062	32,767	31,622	31,480	37,026	-3,768	-3,170	-3,465	-4,610	-4,752	794
95	38,203	34,432	35,030	34,734	33,589	33,447	38,997	-3,771	-3,173	-3,469	-4,614	-4,756	794
94	40,190	36,415	37,014	36,718	35,572	35,430	40,985	-3,775	-3,176	-3,472	-4,618	-4,760	794
93	42,144	38,365	38,965	38,668	37,522	37,379	42,938	-3,778	-3,179	-3,475	-4,622	-4,764	795
92	44,098	40,317	40,916	40,620	39,472	39,330	44,894	-3,782	-3,182	-3,479	-4,626	-4,768	795
91	46,071	42,286	42,886	42,589	41,441	41,299	46,867	-3,785	-3,185	-3,482	-4,630	-4,772	796
90	48,045	44,256	44,857	44,560	43,411	43,269	48,841	-3,789	-3,188	-3,485	-4,634	-4,776	796
89	50,020	46,227	46,829	46,531	45,382	45,239	50,816	-3,792	-3,191	-3,488	-4,638	-4,780	797
88	52,014	48,218	48,820	48,522	47,372	47,229	52,811	-3,796	-3,194	-3,492	-4,642	-4,785	797
87	54,008	50,209	50,811	50,513	49,362	49,220	54,806	-3,800	-3,197	-3,495	-4,646	-4,789	798
86	55,974	52,171	52,774	52,475	51,323	51,181	56,772	-3,803	-3,200	-3,499	-4,650	-4,793	798
85	57,967	54,106	54,742	54,460	53,308	53,165	58,648	-3,861	-3,225	-3,507	-4,659	-4,802	681
84	59,946	56,081	56,706	56,425	55,281	55,139	60,637	-3,865	-3,240	-3,521	-4,664	-4,807	691
83	61,828	57,821	58,413	58,124	56,967	56,825	62,422	-4,007	-3,415	-3,704	-4,861	-5,003	594
82	63,815	59,504	60,109	59,798	58,610	58,503	64,091	-4,311	-3,706	-4,017	-5,205	-5,312	276
81	65,866	61,218	61,823	61,382	59,979	60,205	65,813	-4,648	-4,043	-4,484	-5,886	-5,661	-53
80	68,206	63,079	63,687	63,387	62,203	62,100	67,662	-5,127	-4,519	-4,818	-6,003	-6,106	-544
79	70,246	64,597	65,201	64,907	63,760	63,626	69,179	-5,648	-5,045	-5,339	-6,485	-6,620	-1,067
78	72,156	66,093	66,719	66,432	65,277	65,141	70,691	-6,063	-5,437	-5,724	-6,879	-7,015	-1,465

Note: Compression is positive. Units are in kip.

Chapter 5

COLLAPSE SEQUENCE

5.1 INTRODUCTION

This chapter summarizes the sequences of collapse of WTC 1 and WTC 2 from the analyses of global models with creep. The basis of the conclusions derived here are as follows:

- Analyses of subcomponents, such as connections (truss seats and knuckles), components (trusses and columns), subsystems (full floors and exterior walls), preliminary global models, and isolated parts of the final global models (core and exterior wall) subjected to temperature loads from fire, were performed to identify failure modes and failure loads. These models included large deflection effects and temperature-dependent material nonlinearities due to plasticity and creep. *Break elements* were developed to capture various failure modes such as truss seat failure and web diagonal buckling (NIST NCSTAR 1-6C). As they became larger, the models were gradually reduced in complexity to enhance computational efficiency, while ensuring that key failure modes and failure sequences were captured.
- The final global models included large deflection, and temperature-dependent plasticity and creep.
- The final global models were developed based on the following assumptions:
 - Floors were modeled by plate elements with elastic properties without the ability to simulate sagging and its effect on the development of pull-in forces at floor/wall disconnections. Full floor analyses found that floors initially expanded outward but then pulled inward as the floor sag increased. Pull-in forces resulting from floor sagging and floor/wall disconnections were determined based on the results of full floor models and isolated wall models and were modified by visual observations. They were input in the global model analyses at different times as fire-induced damage.
 - Spandrels were modeled by beam elements. The axial degree of freedom of the beam elements was released to enhance numerical efficiency and avoid thermally-induced buckling; spandrel elements continued to transfer shear and bending moments. The exterior wall subsystem analysis showed that large deformations and buckling of spandrels would not affect the stability of exterior columns significantly.
 - Columns were modeled to capture inelastic buckling, but not the kink-type buckling that is initiated by the local buckling of plates and results in significant distortion of the cross section. The analysis of columns showed that when buckling occurred in a column that spanned several floors and was at high temperatures, inelastic buckling, rather than kink-type buckling, governed its load deformation characteristic.

- The building sections below the impact zones were removed, and the vertical stiffness of the removed sections was replaced with equivalent vertical springs. Preliminary analyses of the global models showed that building sections below the impact zone did not contribute much to the overall behavior of the towers.
- Construction sequence was not considered to enhance computational efficiency. A comparative study showed that the total column load on each face of the exterior wall increased by 7 percent to 15 percent and the total column load on the core decreased by about 10 percent when the construction sequence was not included.
- Structural members that were severed or heavily damaged by aircraft impact were removed from the final global models before gravity loads were applied.
- Break elements were not used in the final global models to represent component failures such as failure of column splices. However, the results of the global model analyses were examined to determine whether any component failure occurred and to what extent its failure impacted the collapse sequence.

The key structural events common to both towers are discussed below.

- Floor sagging sufficient to cause the observed inward bowing of the exterior wall was caused by the elevated steel temperatures resulting from loss of thermal insulation. The elevated temperature caused buckling of the truss web diagonals, as shown in Fig. 5–1 (NIST NCSTAR 1-6C), which caused the floor sag to increase significantly and to approach a catenary shape. The catenary action in this study refers to the combined action that results when the bending capacity of the truss is exceeded and additional load is carried by the floor system acting as a tensile structure (Fig. 5–2). Note that in Fig. 5–2, M refers to the residual moment capacity in the floor with highly deformed truss. Sagging of the floor resulted in pull-in forces at floor/exterior wall connections, and led to inward bowing of the exterior wall
- Bowing and buckling of the entire exterior wall of a tower occurred under the combined effects of temperature, redistributed gravity load, pull-in force from sagging floors, and loss of lateral support due to sagging or floor/wall disconnections. Floors with large sag did not restrain the exterior wall columns from buckling.
- Downward displacement of the core was due to severed core columns from the aircraft impact and redistributing column loads to non-severed core columns and due to shortening of the core columns caused by buckling, plasticity, and creep of core columns at elevated temperatures.
- Redistribution of gravity loads among exterior and interior columns resulted from aircraft impact damage, restrained thermal expansion, shortening of core columns, tilting of the tower above the impact area, and bowing and buckling of exterior walls. Gravity loads were redistributed from columns with aircraft impact or fire-induced damage, both in the core and exterior walls, primarily to neighboring columns. Loads were redistributed from the core to the exterior walls and from the exterior walls to the core primarily through the hat truss. Loads were redistributed between adjacent exterior walls primarily through the spandrels, and to a lesser extent through the hat truss. Major load redistribution mechanisms were as follows:

- Aircraft impact reduced the load on the impacted wall and on the opposite wall through the hat truss and redistributed the load to the side walls.
- Restrained thermal expansion caused increased loads in the heated elements.
- Shortening of the core columns caused a redistribution of the load from the core to the exterior walls.
- Tilting of the tower redistributed the load among the exterior walls, resulting in increased load on the compressed part of the exterior walls.

The collapse sequence of each tower is presented in detail below.

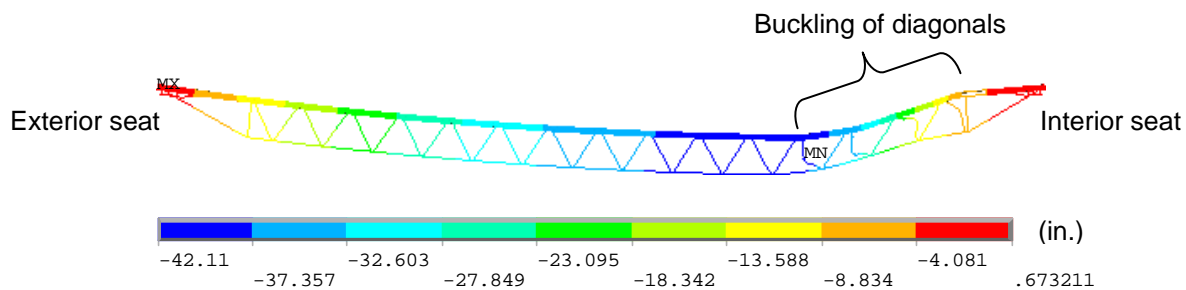


Figure 5–1. Vertical displacement of the truss model under thermal loading.

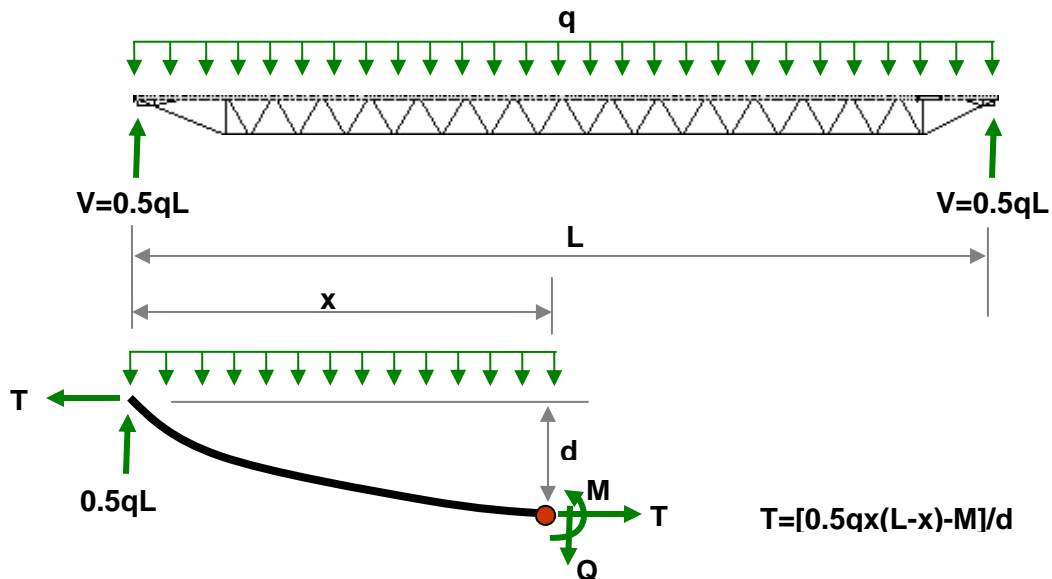


Figure 5–2. Catenary action in the floor system.

5.2 WTC 1 COLLAPSE SEQUENCE

The aircraft impacted the north wall of WTC 1 at 8:46 a.m. The aircraft severed exterior columns and floors on the north side of the tower and core columns and floor members between Floor 93 and Floor 98. The subsequent fires weakened structural subsystems, including the core columns, floors, and exterior walls. The core displaced downward, the floors sagged, and the south exterior wall bowed inward. At 10:28 a.m., about 102 min after the aircraft impact, WTC 1 began to collapse.

The sequence of main structural events that led to the collapse of WTC 1, starting from aircraft impact, and the causes and effects of these structural events along with key observations, are discussed below.

The WTC 1 collapse sequence consists of five main events, listed in Table 5–1, which are discussed below. Actual observations are summarized in Table 5–2, which are based on NIST’s examination of photos and videos (NIST NCSTAR 1-6).

Table 5–1. Summary of main events that led to the collapse of WTC 1.

Event Number	Event
1	Aircraft impact
2	Unloading of core
3	Sagging of floors and floor/wall disconnections
4	Bowing of south wall
5	Buckling of south wall and collapse initiation

Table 5–2. Observations on WTC 1 provided by NIST.

Time	Time from Impact (min)	Observation
8:46:26	0	Aircraft impact on the north wall of WTC 1 between Floor 93 and Floor 99 and Columns 112 and 151.
9:25:28	39	Fire on west side of south wall.
9:40	54	No bowing of columns was observed between Columns 301 and 323 on the east side of south wall.
10:18:43	92	Smoke suddenly expelled on Floor 92 north wall, Floor 94 east side of north wall, Floor 95 to Floor 98 on west side of north wall, Floor 95 and Floor 98 on north side of west wall, lower floor on south side.
10:22:59	97	Inward bowing from Floor 95 to about Floor 99 between Columns 308 and 326 (maybe to 340) on the south wall, maximum amplitude approximately 55 in. at Floor 97.
10:28:18	102	Smoke puff out of north edge and center of west wall; smoke and debris clouds out of the north, east, and west walls on Floor 98. Fire out of windows on the north, east, west, and south walls between Floor 92 and Floor 98, and on Floor 104.
10:28:20	102	WTC 1 began to collapse. First exterior sign of collapse was at Floor 98. Rotation of at least 8 degrees to the south occurred before the building section began to fall vertically under gravity.

Aircraft Impact

The aircraft impacted WTC 1 at the north wall. The aircraft severed or heavily damaged Columns 112 to 151 between Floors 94 and 98 on the north wall. After breaching the building's perimeter, the aircraft continued to penetrate into the building. The north office area floor system sustained severe structural damage between Columns 112 and 145 at Floors 94 to 98. Core Columns 503, 504, 505, 506, 604, 704, 706, 805, and 904 were severed or heavily damaged between Floor 92 and Floor 97. The aircraft also severed a single exterior panel at the center of the south wall from Columns 329 to 331 between Floor 93 and Floor 96. In summary, 38 of 59 columns of the north wall, three of 59 columns of the south wall, and nine of 47 core columns were severed or heavily damaged. In addition, thermal insulation on floor framing and columns was also damaged from the impact area to the south perimeter wall, primarily through the center of WTC 1 and over one-third to one-half of the core width. Figures 2-2, 2-14, and 2-18 summarize aircraft impact damage to exterior and core columns and floors of WTC 1.

Gravity loads in the columns that were severed were redistributed, mostly to the neighboring columns. Due to the severe impact damage to the north wall, the wall section above the impact zone moved downward as shown in Figs. 4-9 and 4-13. The hat truss resisted the downward movement of the north wall and rotated about its east-west axis, which reduced the load on the south wall. As a result, the north and south walls each carried about 7 percent less gravity loads at Floor 98 after impact, the east and west walls each carried about 7 percent more loads, and the core carried about 1 percent more gravity loads at Floor 98 after impact (Table 5-3). Column 705 buckled, and Columns 605 and 804 showed minor buckling.

Unloading of Core

Temperatures in the core area rose quickly, and thermal expansion of the core was greater than the thermal expansion of the exterior walls in early stages of the fire. This increased the gravity loads in the core columns until 10 min after impact (Table 5-3). The additional gravity loads from adjacent severed columns and high temperatures caused high plastic and creep strains to develop in the core columns in early stages of the fire. More columns buckled inelastically due to high temperatures. Creep strain continued to increase to the point of collapse (see Fig. 4-81). By 30 min, the plastic-plus-creep strains exceeded thermal expansion strains. Due to high plastic and creep strains and inelastic buckling of core columns, the core columns shortened, and the core displaced downward. At 100 min, the downward displacement of the core at Floor 99 became 2.0 in. on the average, as shown in Fig. 4-37.

The shortening of core columns was resisted by the hat truss, which unloaded the core over time and redistributed the gravity loads from the core to the exterior walls, as can be seen in Table 5-3. As a result, the north, east, south, and west walls at Floor 98 carried about 12 percent, 27 percent, 10 percent, and 22 percent more gravity loads, respectively, at 80 min than the state after the impact, and the core carried about 20 percent less loads as shown in Table 5-3. The net increase in the total column load on the south wall, where exterior wall failure initiated, was only about 10 percent due to the downward displacement of the core (see Fig. 5-3). At 80 min, the total core column loads reached their maximum. As the floor pulled in starting at 80 min on in the south side, the south exterior wall began to shed load to adjacent walls and the core.

Sagging of Floors and Floor/Wall Disconnections

The long-span trusses of Floor 95 through Floor 99 sagged due to high temperatures. While the fires were on the north side and the floors on the north side sagged first, the fires later reached the south side, and the floors on the south side sagged. Figure 5–4 shows vertical displacements of Floors 95 through 98 determined by the full floor models at 100 min. Full floor models underestimated the extent of sagging because cracking and spalling of concrete and creep in steel under high temperatures were not included in the floor models, and because the extent of insulation damage was conservatively estimated. The sagging floors pulled in the south wall columns over Floors 95 to 99. In addition, the exterior seats on the south wall in the hot zone of Floors 97 and 98 began to fail due to their reduced vertical shear capacity at around 80 min, and by 100 min about 20 percent of the exterior seats on the south wall of Floors 97 and 98 failed, as shown in Figs. 5–4 and 5–5. Partial collapse of the floor may have occurred at Floors 97 and 98, resulting from the exterior seat failures, as indicated by the observed smoke puff at 92 min (10:19 a.m.) in Table 5–2, but this phenomenon was not modeled.

Bowing of South Wall

The exterior columns on the south wall bowed inward as they were subjected to high temperatures, pull-in forces from the floors beginning at 80 min, and additional gravity loads redistributed from the core. Figure 5–6 shows the observed and the estimated inward bowing of the south wall at 97 min after impact (10:23 a.m.). Since no bowing was observed on the south wall at 69 min (9:55 a.m.), as shown in Table 5–2, it is estimated that the south wall began to bow inward at around 80 min when the floors on the south side began to substantially sag. The inward bowing of the south wall increased with time due to continuing floor sagging and increased temperatures on the south wall as shown in Figs. 4–42 and 5–7. At 97 min (10:23 a.m.), the maximum bowing observed was about 55 in. (see Fig. 5–6).

Buckling of South Wall and Collapse Initiation

With continuously increased bowing, as more columns buckled, the entire width of the south wall buckled inward. Instability started at the center of the south wall and rapidly progressed horizontally toward the sides. As a result of the buckling of the south wall, the south wall significantly unloaded (Fig. 5–3), redistributing its load to the softened core through the hat truss and to the south side of the east and west walls through the spandrels. The onset of this load redistribution can be found in the total column loads in the WTC 1 global model at 100 min in the bottom line of Table 5–3. At 100 min, the north, east, and west walls at Floor 98 carried about 7 percent, 35 percent, and 30 percent more gravity loads than the state after impact, and the south wall and the core carried about 7 percent and 20 percent less loads, respectively. The section of the building above the impact zone tilted to the south (observed at about 8°, Table 5–2) as column instability progressed rapidly from the south wall to the adjacent east and west walls (see Fig. 5–8), resulting in increased gravity load on the core columns. The release of potential energy due to downward movement of building mass above the buckled columns exceeded the strain energy that could be absorbed by the structure. Global collapse ensued.

Table 5–3. Total column loads at Floor 98 and Floor 105 of WTC 1 global model for Case B conditions.

Row	Analysis Step	North Wall		East Wall		South Wall		West Wall		Core	
		Floor 98	Floor 105	Floor 98	Floor 105	Floor 98	Floor 105	Floor 98	Floor 105	Floor 98	Floor 105
(1)	Before Impact	10,974	8,026	8,545	6,562	11,025	8,092	8,572	6,604	34,029	20,361
(2)	After Impact	10,137	7,294	9,071	7,028	10,356	7,488	9,146	7,076	34,429	20,761
(3)	10 min	9,796	6,944	8,490	6,461	9,848	6,981	8,536	6,469	36,473	22,790
(4)	20 min	10,437	7,551	9,108	7,075	9,900	7,057	9,202	7,158	34,495	20,806
(5)	30 min	10,913	8,020	10,034	7,998	10,420	7,569	9,715	7,685	32,060	18,377
(6)	40 min	11,068	8,193	10,599	8,571	11,004	8,129	10,178	8,147	30,294	16,608
(7)	50 min	11,149	8,285	10,908	8,878	11,192	8,315	10,458	8,428	29,435	15,743
(8)	60 min	11,205	8,351	11,168	9,130	11,285	8,414	10,716	8,687	28,766	15,069
(9)	70 min	11,286	8,435	11,366	9,319	11,343	8,481	10,939	8,914	28,205	14,502
(10)	80 min	11,376	8,528	11,555	9,497	11,409	8,551	11,119	9,097	27,681	13,978
(11)	90 min	10,916	8,096	11,991	9,847	9,949	7,327	11,657	9,506	28,587	14,876
(12)	100 min	10,828	8,023	12,249	10,076	9,638	7,066	11,905	9,720	28,478	14,767
(13)	(2) - (1)	-837	-732	526	466	-668	-604	574	472	400	400
(14)	(10) - (2)	1,239	1,234	2,484	2,470	1,052	1,063	1,973	2,021	-6,748	-6,783
(15)	(12) - (2)	692	730	3,178	3,048	-719	-422	2,759	2,644	-5,951	-5,993
(16)	(12) - (10)	-548	-504	694	579	-1,771	-1,485	786	623	797	790

Note : Compression is positive. Units are in kip.

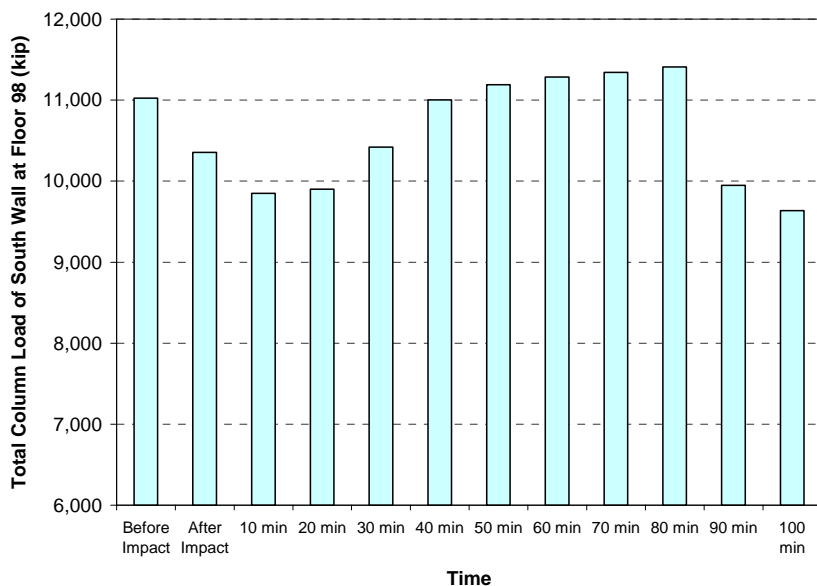
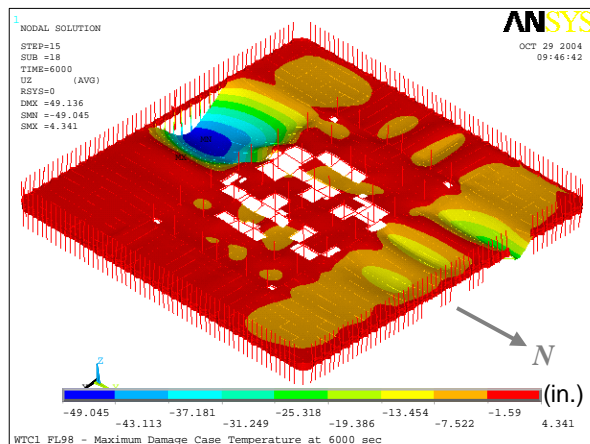
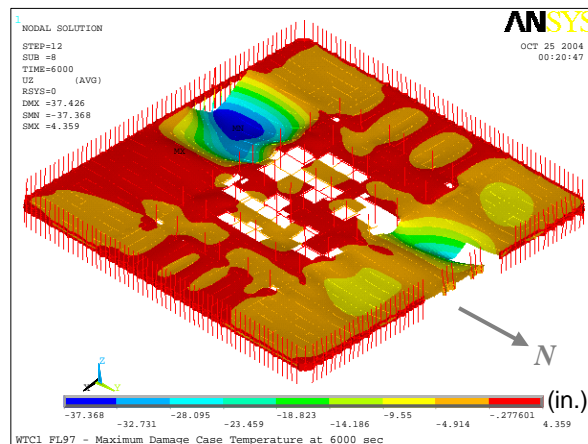


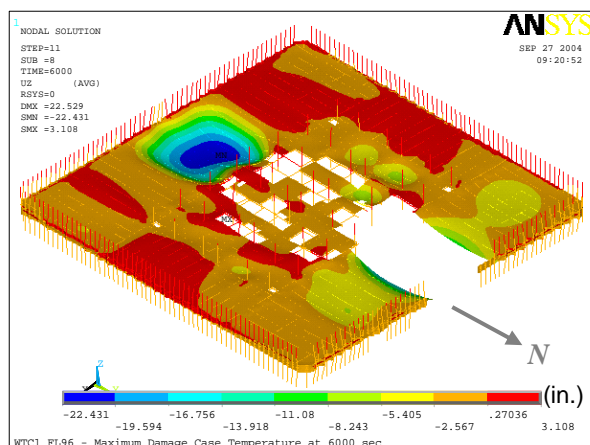
Figure 5–3. Total column loads at Floor 98 of the south wall of WTC 2 global model for Case B conditions (compression is positive).



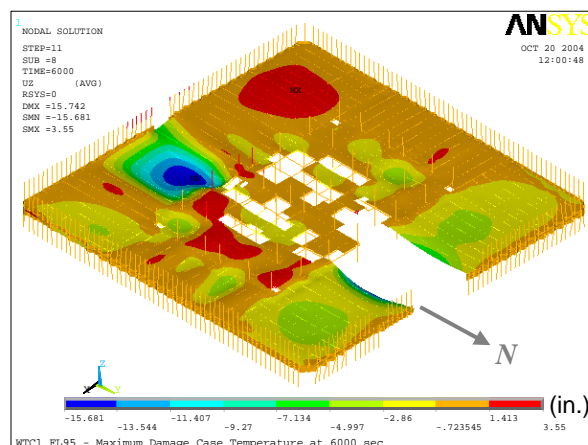
(a) Floor 98



(b) Floor 97

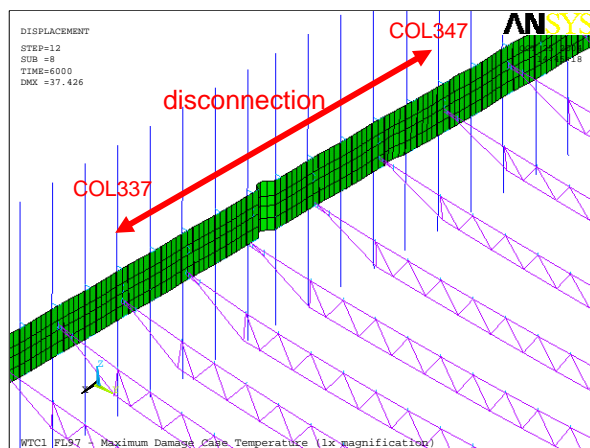


(c) Floor 96

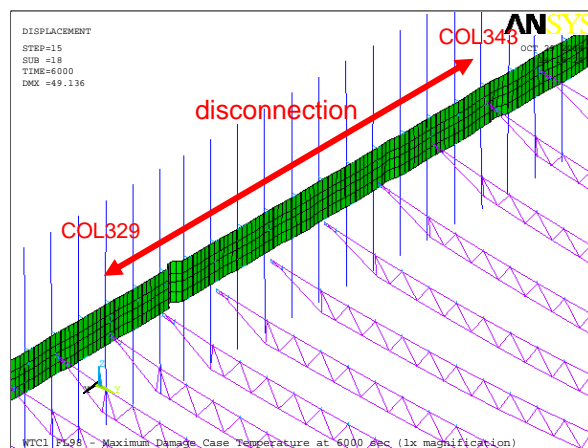


(d) Floor 95

Figure 5–4. Vertical displacements of full floor models of WTC 1 for Case B_i temperature condition at 100 min (downward displacement is negative).



(a) Floor 97



(b) Floor 98

Figure 5–5. Loss of vertical supports obtained in Floor 97 and Floor 98 full floor models of WTC 1 for Case B_i temperature condition at 100 min (1x displacement magnification).

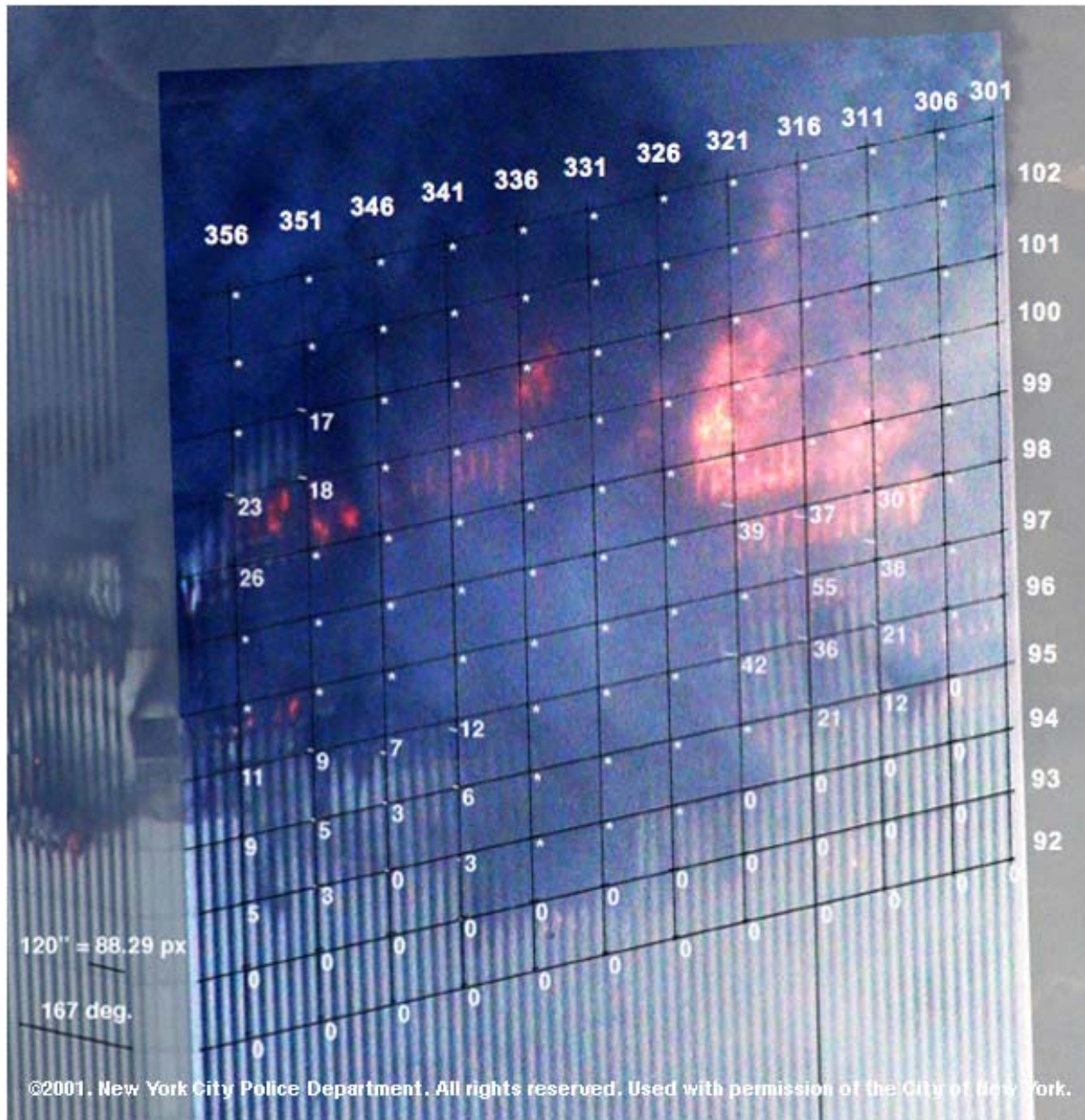


Figure 5–6. Inward bowing of exterior columns of the South wall of WTC 1 at 10:23 a.m. (97 min after impact). Displacements were estimated by NIST from the analysis of this photograph.

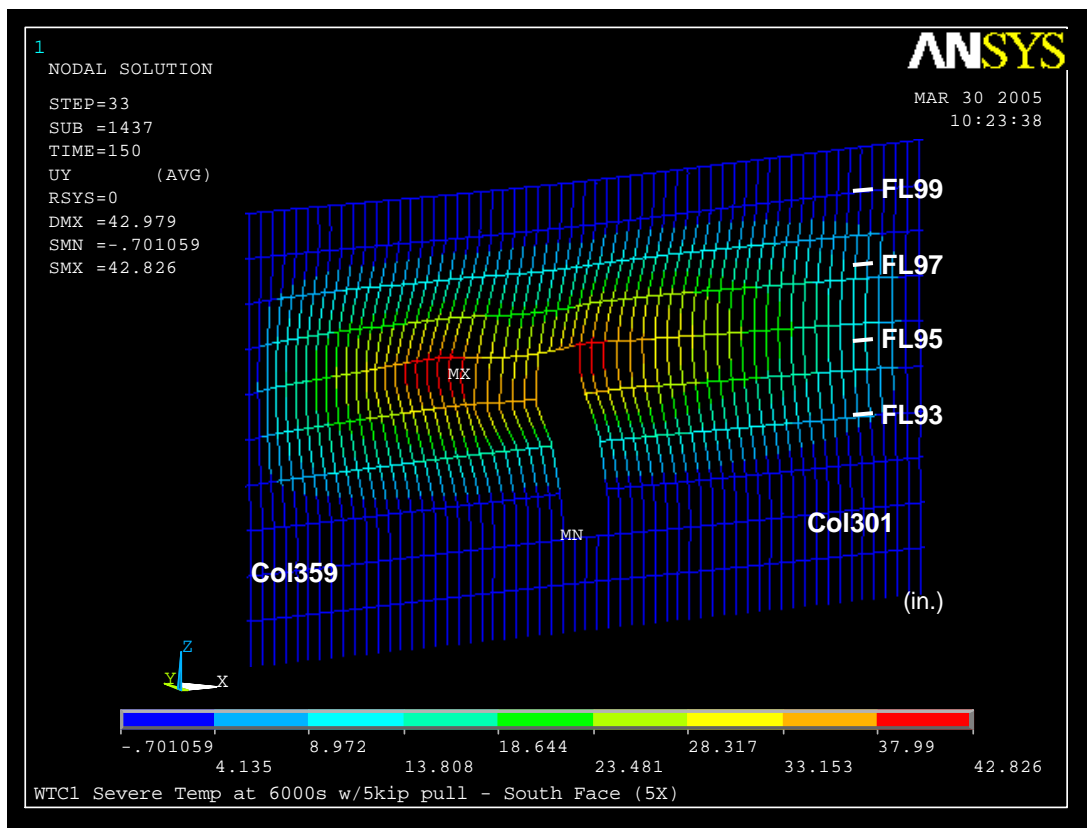


Figure 5–7. Inward bowing of south wall of WTC 1 global model with creep at 100 min for Case B conditions with 5 kip pull-in forces (5x displacement magnification).



Figure 5–8. Collapse initiation and tilting of WTC 1 (view from the northeast).

5.3 WTC 2 COLLAPSE SEQUENCE

The aircraft traveling in a north-northeast direction impacted the south wall of WTC 2 at 9:03 a.m. The aircraft mostly severed columns and floors that were on the east side of the building between Floor 78 and Floor 84. The subsequent fires were also on the east side of the building. At 9:59 a.m., about 56 min after the aircraft impact, the building started to collapse with the east wall buckling inward, followed by tilting of the building above Floor 82 to the east and south.

The section below discusses the sequence of main structural events that led to the collapse of WTC 2, and the causes and effects of these structural events along with key observations, starting from aircraft impact.

The WTC 2 collapse sequence consisted of five main structural events. These events are chronologically listed in Table 5–4 and discussed below. Actual observations for WTC 2 are summarized in Table 5–5, which are based on NIST’s examination of photos and videos (NIST NCSTAR 1-6).

Table 5–4. Summary of main events that led to the collapse of WTC 2

Event number	Event
1	Aircraft impact
2	Sagging of floors and floor/wall disconnections
3	Bowing of east wall
4	Unloading and leaning of core
5	Buckling of east wall and collapse initiation

Table 5–5. Observations on WTC 2 provided by NIST.

Time	Time from Impact (min)	Observation
9:03	0	Aircraft impact on the south wall of WTC 2 between Floors 77 and 85, Columns 404 to 443.
9:21	18	Columns of the east wall bowed inward over the entire width of Floors 78 to 83; maximum of 7–9 in. at Floor 80.
9:38	35	Floor 83 disconnections on the east wall appeared to extend.
9:54	51	Columns of the east wall bowed inward between Floor 78 and Floor 84, 12 – 20 in. at Floor 80. East side of Floor 83 draped between Columns 310 to 342.
9:59	56	WTC 2 began to collapse. Column splices failed at every third panel and columns sprung back from inward bowing as collapse initiated on the east wall near the northeast corner Smoke and debris clouds were expelled from Floor 81 on the east, north, and west walls of the building. WTC 2 appeared to tilt around the base of Floor 82 and initial downward motion was visible at the same location. Tilt of approximately 3 to 4 degrees to the south and 7 to 8 degrees to the east occurred before building section fell. Kink (change in slope) on the southeast corner near Floor 94 (halfway along building section above failure). Kink (change in slope) and offset about at the Floor 106.

Aircraft Impact

The aircraft impacted the south wall of WTC 2, severing a number of exterior columns on the south wall from Floor 78 to Floor 84. The south office area floor system sustained severe structural damage between Columns 410 and 436 from Floor 79 to Floor 83. Core columns 701, 702, 801, 802, 803, 901, 903, 1001, 1002, 1003, and 1004 were severed or heavily damaged between Floor 77 and Floor 84. The aircraft also severed Column 253 of the north wall. The aircraft damaged the floor framing and core columns at the southeast corner of the core. In summary, 32 of 59 columns of the south wall, two of 59 columns of the north wall, and 11 of 47 core columns were severed or heavily damaged. Thermal insulation was damaged from the impact area through the east half of the core to the north and east exterior walls. The floor truss seat connections over about one-quarter to one-half of the east side of the core were severed on Floor 80 and Floor 81 and over about one-third of the east wall on Floor 83. Figures 2–3, 2–15, and 2–19 summarize aircraft impact damage to the exterior wall and core columns and floors of WTC 2.

Gravity loads in the columns that were severed on the south wall and in the southeast corner of the core were redistributed to adjacent intact columns and also to the columns on the east wall (see Table 5–6). In this redistribution, the total axial load on the core columns reduced by 6 percent, and the total axial load on the north wall columns reduced by 10 percent. The total axial load on the east wall columns increased by 24 percent, and the total axial load on the west and south wall columns increased by 2 percent to 3 percent. The large increases in loads on the east wall resulted from their proximity to the severed core columns at the southeast corner of the core. The total load on the south wall at Floor 83 did not change, as some of the loads from the core area were redistributed to that wall through the hat truss.

At Floor 105, splices in the columns at the southeast corner of the core failed (Columns 1001 and 1002 and most likely Columns 701, 801, 901, 902, and 1003). This increased the core tendency to lean toward southeast and also increased the vertical downward displacement of the core at the impact zone. After the core column splices failed, 73 percent of the loads released from the failing core columns were redistributed through the hat truss to the exterior walls.

As can be seen in Table 5–6 for Floor 83, about 20 percent ($= 227 \text{ kip} / 1,263 \text{ kip}$) of the redistributed load at the hat truss level of the south wall was transferred through columns, and the rest of the load (about 1,000 kip) was transferred to the columns of the east and west walls through the spandrels.

After load redistribution following impact, the core was prevented from tilting excessively toward the east by the north and south exterior walls through the action of the floors and the hat truss.

Sagging of Floors and Floor/Wall Disconnections

Aircraft impact and high temperatures due to subsequent fires caused Floor 79 through Floor 83 to sag. The sag was greater at Floor 80 and Floor 81 where the truss seats on the east side of the core failed at aircraft impact (see Fig. 5–9). High temperatures weakened the truss seats on the east exterior wall and caused truss seats to fail at Floor 83 and Floor 82 (see Fig. 5–10) which in turn increased the sag in those floors. Floor sagging induced pull-in forces on the east wall columns, beginning approximately 10 min after impact and increasing with time.

Bowing of East Wall

The east wall columns bowed inward as a result of increasing temperatures (reduced strength and stiffness) and pull-in forces induced by sagging floors (see Fig. 3–98). The inward bowing in the east wall increased with time due to the combined effects of pull-in from sagging floors (see Fig. 4–101), increased axial loads, and a continuous increase in plastic and creep strains. As columns bowed, they shed load to adjacent unbowed columns, but the total column load on the east wall did not change significantly after impact until buckling of the east wall started near the collapse time (see Fig. 5–11).

Unloading and Leaning of Core

With increasing time and temperatures, the core columns developed high plastic and creep strains, especially on the east side of the core. Plastic and creep strains exceeded the thermal expansion strains beginning about 30 min after the aircraft impact (see Fig. 5–12). High plastic and creep strains caused unloading on the east side core columns. This increased leaning of the core toward the east and transferred more loads to the east wall (Table 5–6). Calculations showed that resistance to core leaning was provided by the north and south exterior walls, partly through the floors and partly through the hat truss. Leaning of the core resulted in tilting of the upper part of the tower as the east wall buckled.

Buckling of East Wall and Collapse Initiation

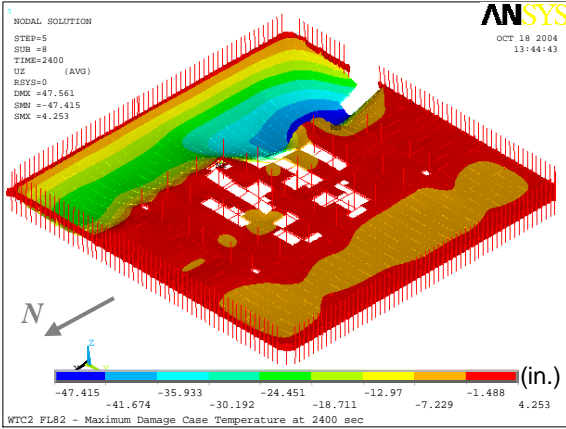
With continuously increased bowing and axial loads, the entire width of the east wall buckled inward. The instability started at the center of the wall and rapidly progressed horizontally toward the sides. As a result of the buckling of the east wall, the east wall significantly unloaded, redistributing its load to the softened core through the hat truss and to the east side of the south and north walls through the spandrels (see Figs. 5–13 and 5–14 and Table 4–38). The section of tower above the buckled wall suddenly moved downward, and the building tilted toward the east (see Fig. 5–15).

The section of the building above the impact zone tilted to the east and south (observed at about 7° to 8° to east and about 3° to 4° to south, Fig. 5–16) as column instability progressed from the east wall to the adjacent south and north walls. The release of potential energy due to downward movement of the building mass above the buckled columns exceeded the strain energy that could be absorbed by the structure. Global collapse ensued.

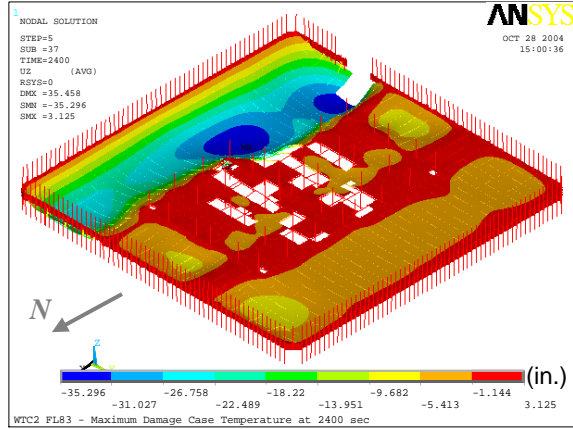
Table 5–6. Total column loads at Floor 83 and Floor 105 of WTC 2 for Case D conditions.

Row	Analysis Step	West Wall		East Wall		North Wall		South Wall		Core	
		Floor 83	Floor 105	Floor 83	Floor 105	Floor 83	Floor 105	Floor 83	Floor 105	Floor 83	Floor 105
(1)	Before Impact	18,065	8,497	18,114	8,572	13,567	7,382	13,284	7,169	61,828	17,123
(2)	After Impact	18,670	9,170	22,481	11,272	12,193	6,487	13,511	8,432	57,821	13,382
(3)	10 min	18,728	9,182	22,226	11,061	11,896	6,250	13,358	8,275	58,413	13,975
(4)	20 min	18,914	9,279	22,208	11,120	12,052	6,311	13,318	8,351	58,124	13,682
(5)	30 min	18,876	9,370	23,681	11,859	11,770	6,416	13,365	8,553	56,967	12,544
(6)	40 min	18,531	9,198	23,682	11,927	11,906	6,524	13,473	8,691	56,825	12,402
(7)	43 min	15,667	7,086	15,143	8,026	14,215	6,546	16,292	9,169	62,422	17,915
(8)	(2)-(1)	604	674	4,368	2,699	-1,374	-895	227	1,263	-4,007	-3,741
(9)	(6)-(2)	-138	28	1,201	656	-287	37	-38	259	-996	-980
(10)	(7)-(6)	-2,864	-2,112	-8,539	-3,901	2,309	23	2,819	479	5,596	5,513

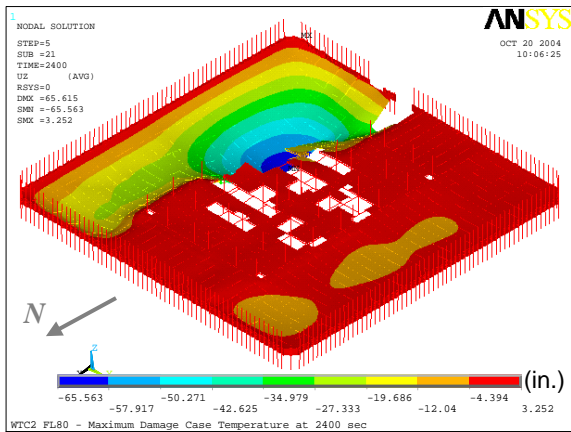
Note: Compression is positive. Units are in kip.



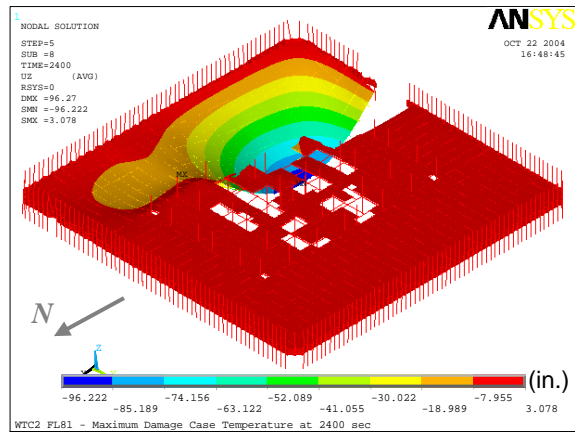
(a) Floor 82



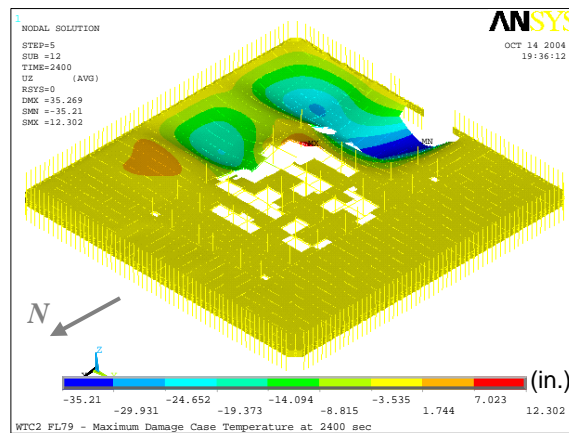
(b) Floor 83



(c) Floor 80

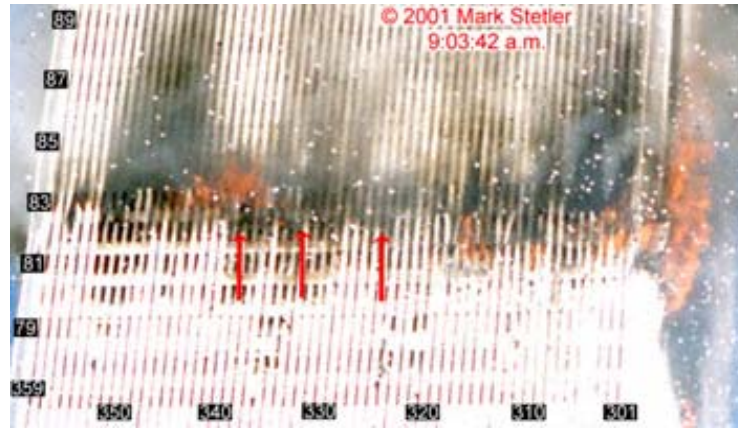


(d) Floor 81

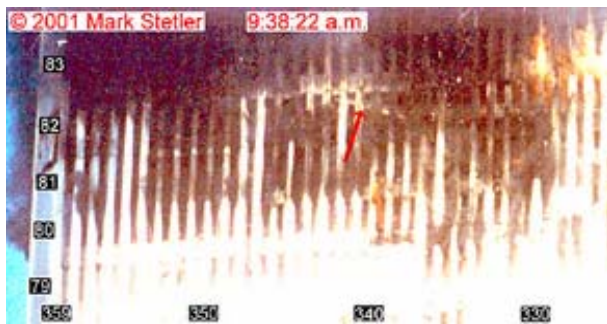


(e) Floor 79

Figure 5–9. Vertical displacements of full floor models of WTC 2 for Case D_i temperature condition at 40 min (downward displacement is negative).



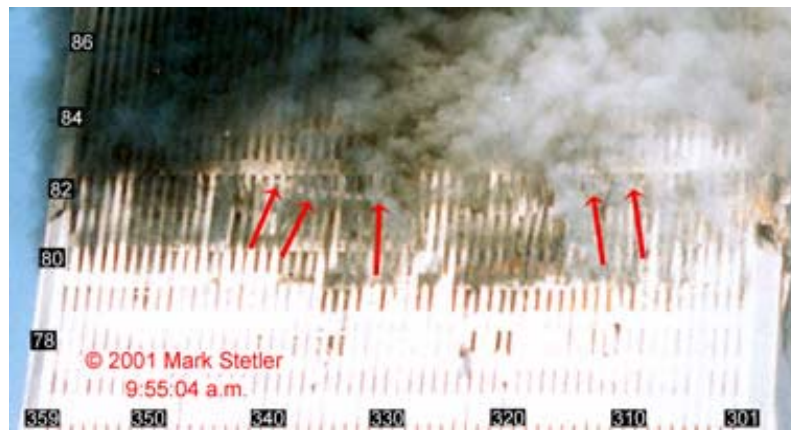
(a) After impact damage



(b) South side at 9:38 a.m.
(35 min after impact)



(c) North side at 9:38 a.m.
(35 min after impact)



(d) At 9:54 a.m.
(51 min after impact)

Figure 5–10. Floor sagging observed on the east wall of WTC 2 at different times.

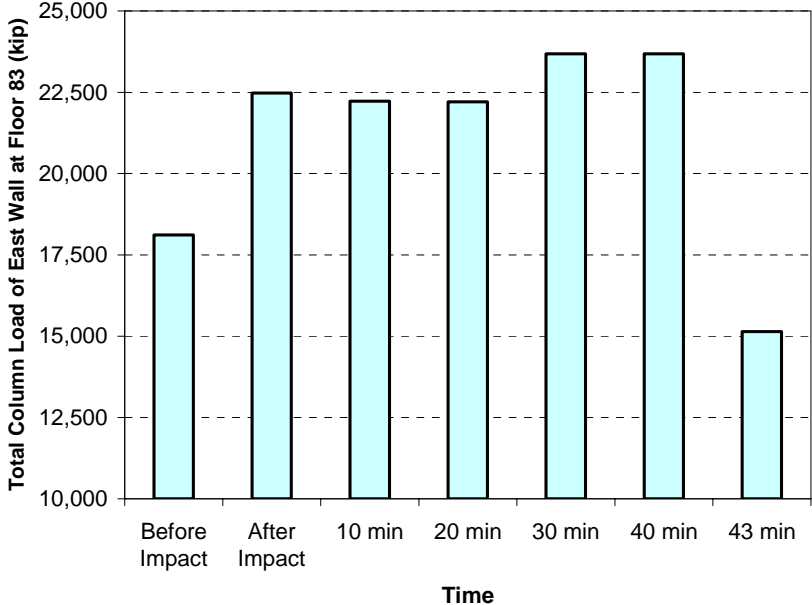


Figure 5–11. Total column loads at Floor 83 of the east wall of WTC 2 global model for Case D conditions (compression is positive).

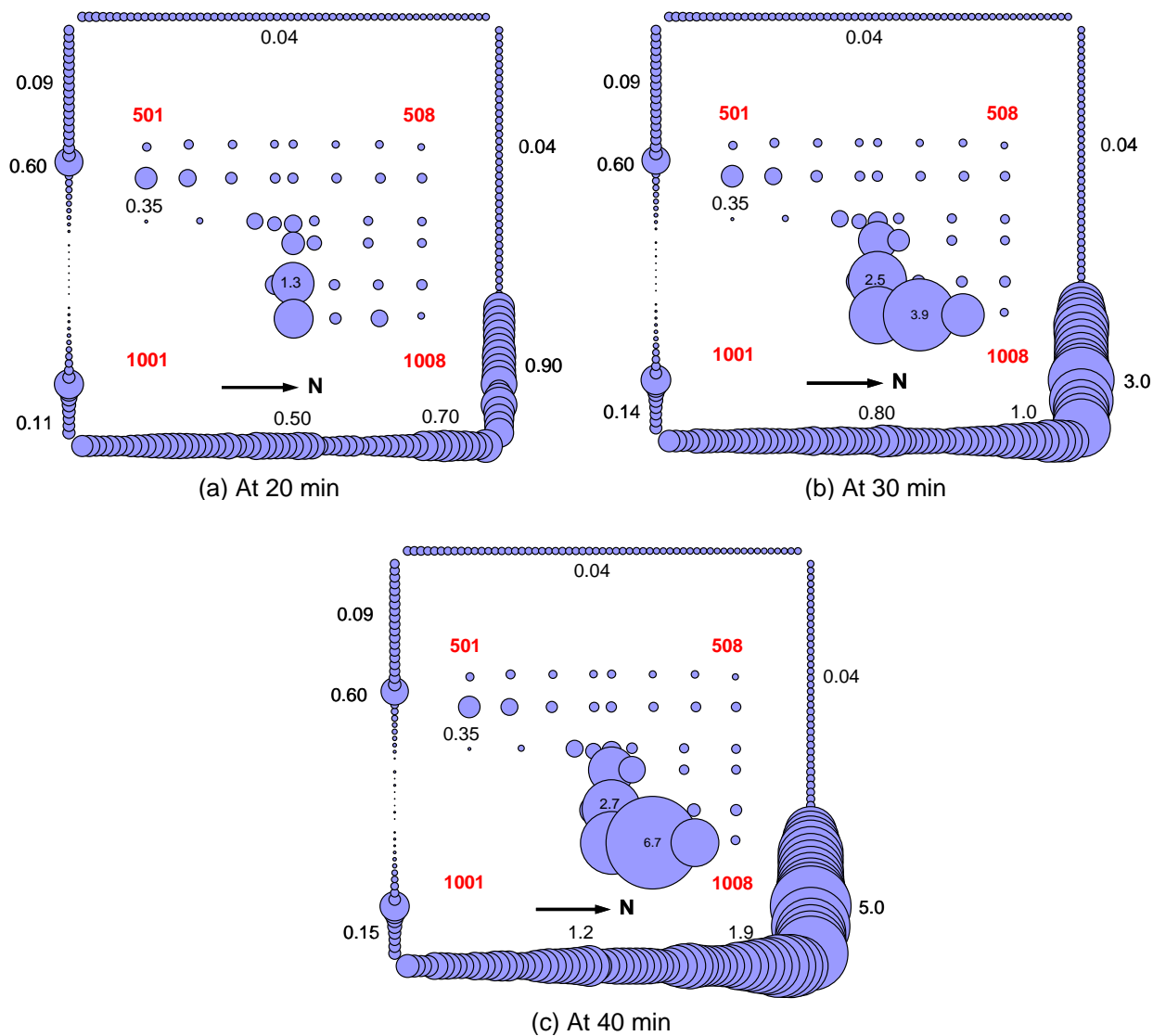
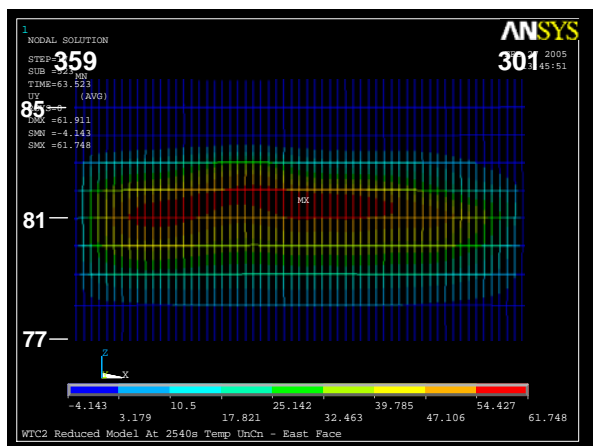
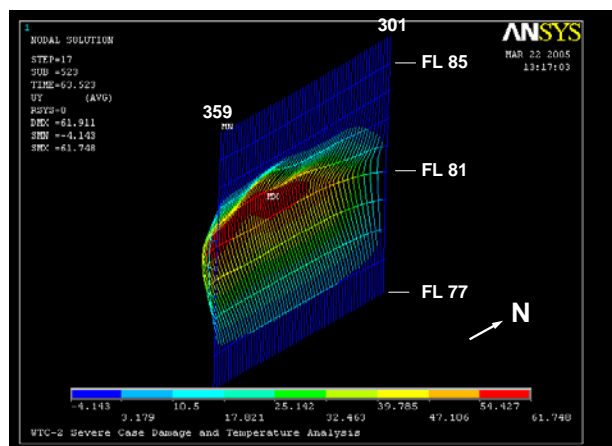


Figure 5-12. Maximum elastic + plastic + creep strain magnitudes for columns between Floor 78 and Floor 83 of WTC 2 global model for Case D conditions at 20 min, 30 min, and 40 min (compressive strain is positive; strain values are in percent).



(a) View from east



(b) View from southeast

Figure 5–13. Inward bowing of the east wall of WTC 2 global model for Case D conditions at 43 min at the instant of collapse initiation (deformed shape scaled four times).

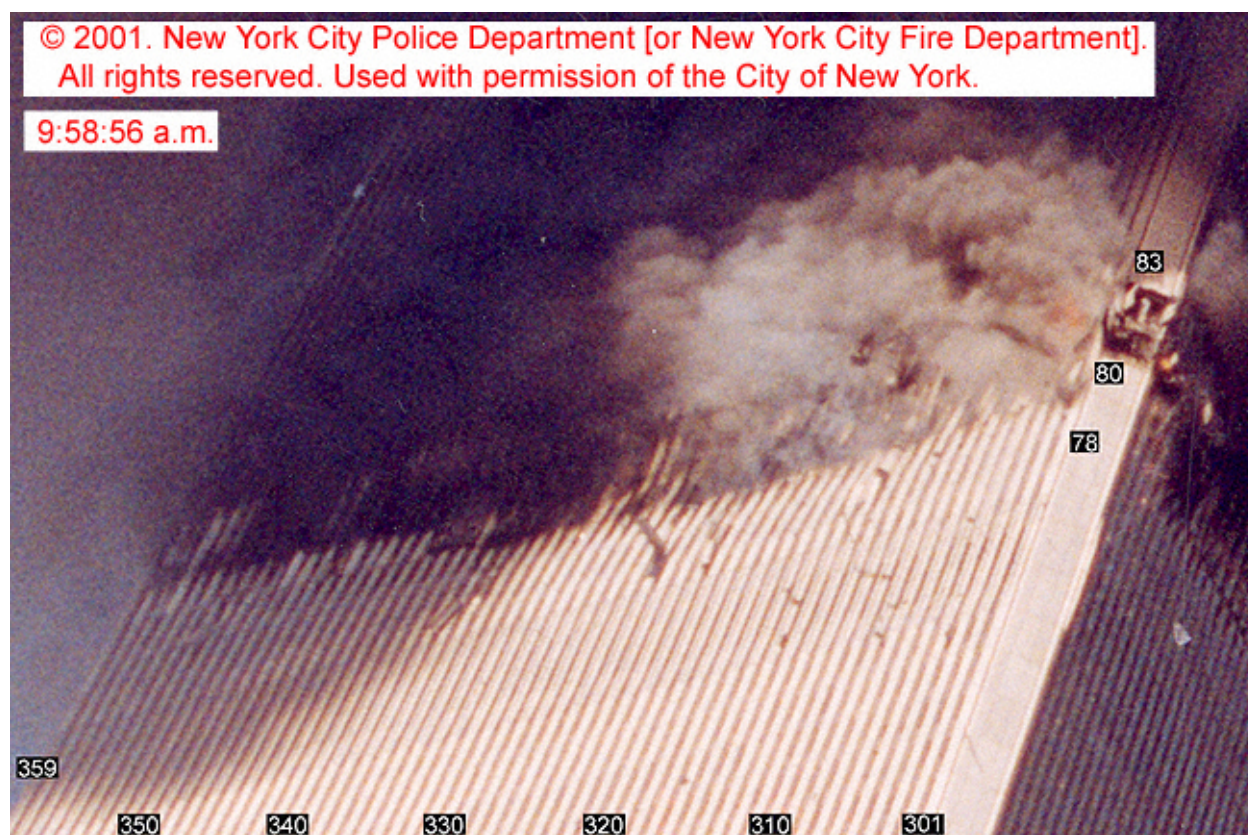


Figure 5–14. Inward bowing of exterior columns of the west wall of WTC 2 just before collapse.

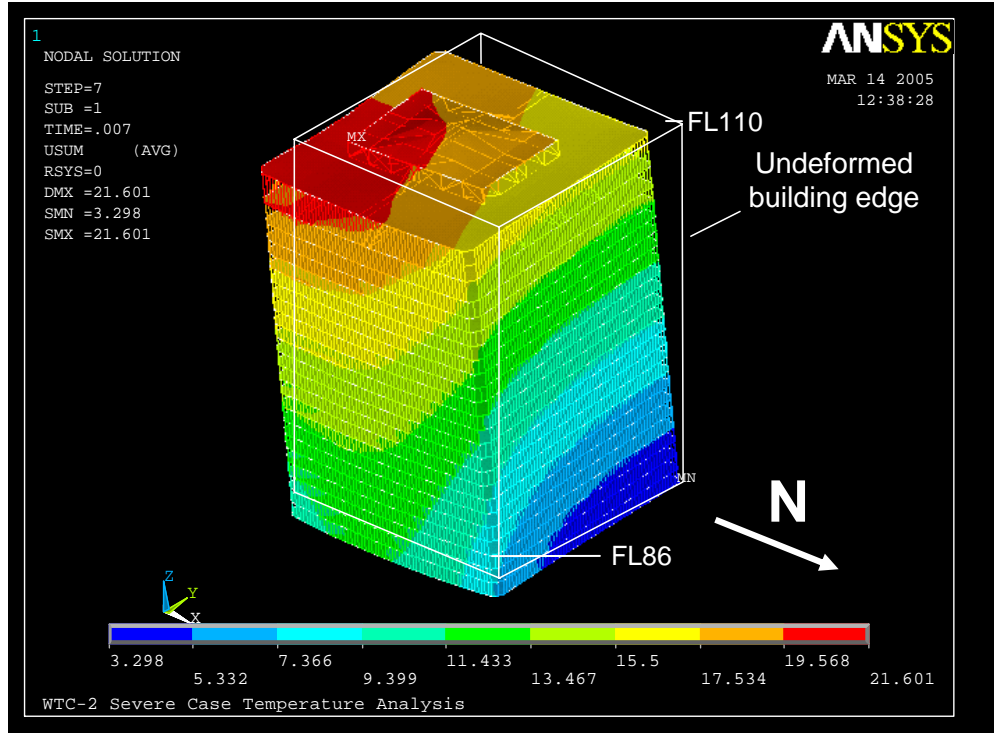


Figure 5–15. Total displacements of WTC 2 global model above Floor 86 for Case D conditions at 43 min at collapse initiation (note the tilt toward east and south; deformed shape magnified 20 times).



Figure 5–16. Initiation of Collapse of WTC 2. Note the tilt toward east and south.

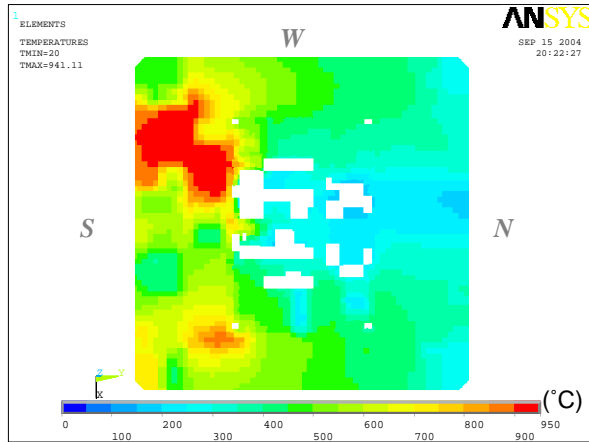
5.4 DISCUSSION

The structural analyses of this study on components, subsystems, isolated exterior walls and cores, and global models of WTC 1 and WTC 2, as well as observations from photos and videos taken during the event, showed that the tower collapses were caused by the combined effects of the structural and thermal insulation damage from aircraft impact and the subsequent intense fires.

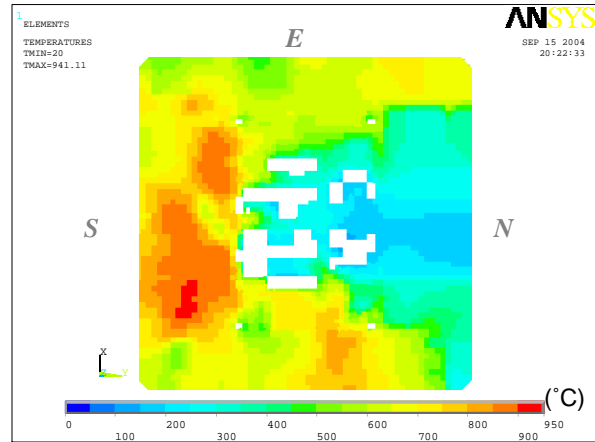
The structural impact damage alone did not cause the collapse of the towers, as they stood for periods of time, and collapsed after fire-induced weakening of the cores, floor systems and exterior walls. In the absence of impact damage, there would have been no insulation damage, and the likelihood of collapse of towers under the intense fires would have been very small.

The damage to insulation was a result of direct impact by debris from the aircraft impact, which knocked down walls and partitions and removed the insulation (NIST NCSTAR 1-6). Insulation is a key fire protection system for steel structural members. Without insulation, steel members may be heated during the “effective duration” of the fires to an extent that causes significant stiffness and strength reduction. According to the results of fire dynamics simulations by NIST (NIST NCSTAR 1-5), fire moved from location to location, and the “effective duration” of the fire at any one location was roughly about 20 minutes, which was much shorter than the time to collapse. It was found in the results of the thermal analysis conducted by NIST that temperatures of floor trusses and columns with insulation were lower than 400 °C during the Case B fire (100 min long) for WTC 1. On the other hand, temperatures of steel members that lost insulation were found to be higher than 600 °C and even higher than 800 °C. Reductions in modulus of elasticity, yield strength, and ultimate tensile strength of steel in the WTC towers were found to be 13 percent, 20 percent, and 10 percent at 400 °C, and 35 percent, 92 percent, and 80 percent at 700 °C. In addition, creep in steel may become more significant than plastic strain when the steel is exposed to temperatures higher than 500 °C under high stress.

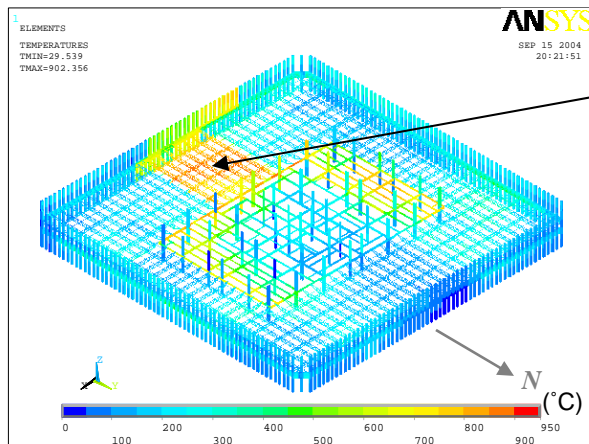
The temperatures in the steel members without insulation damage were lower than those with insulation damage for the same fire (see Fig. 5–17 (c)), and the lower temperatures resulted in much reduced creep, plasticity, and buckling. Without insulation damage, floor sag would have been significantly reduced (see Figs. 5–17 (d) and (e)), and consequently the floors could not and would not have pulled inward on the exterior wall. Without insulation damage, the core columns and the exterior wall would not be significantly weakened, and the likelihood of the exterior wall buckling would be negligibly small. Without insulation damage, the likelihood of collapse of the towers would have been very small.



(a) Temperatures on the top surface of the slab



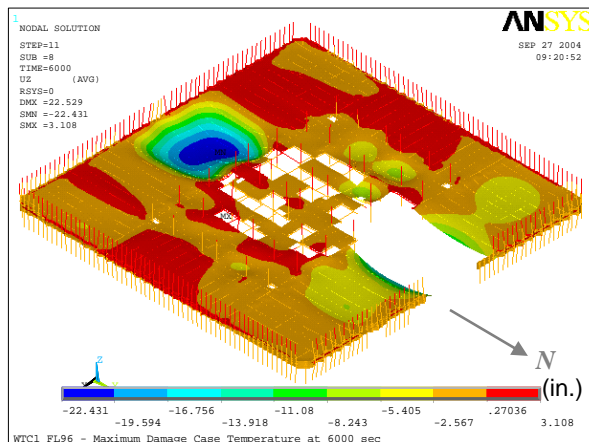
(b) Temperatures on the bottom surface of the slab



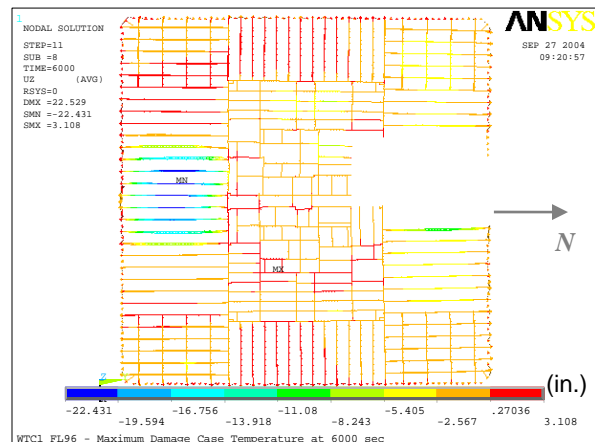
(c) Temperatures of steel members

Area of insulation damage

Note: Structural members that were severed by aircraft impact are also shown in temperature plots (a), (b), and (c)



(d) Vertical displacement (entire model)



(e) Vertical displacement (top view without slab)

Figure 5–17. Full floor model of Floor 96 of WTC 1 for Case B_i temperature condition at 100 min.

Appendix A

FEA OF FLOORS

A.1 MODEL DESCRIPTION

A full floor model includes 1) both exterior and core columns extending from one floor below to one floor above, 2) spandrels of the floor of interest, 3) floor slab, 4) floor trusses including primary and bridging trusses, 5) strap anchors, 6) core beams, 7) deck support angles, and 8) break elements to capture failure modes including truss web diagonal buckling and weld failure, exterior and interior seat failure, stud failure, strap anchor weld failure, connection failure between primary and bridging trusses, and connection failure between long-span and transfer trusses. A full floor model without impact damage is shown in Fig. A-1.

The members listed below were found to fail in the early stage of thermal loading and cause large nonlinearities in the subsequent stages; therefore, they were removed from the model to enhance computational efficiency. Figure A-2 shows the full floor model with these members removed. Deck support angles and bridging trusses buckled due to their thermal expansion in the one-way area. Shear studs and welds between strap anchors and truss top chords failed due to shear force caused by the difference in thermal expansion between the floor and the exterior wall in the direction transverse to the primary trusses. Although these members did not exist in the floor model, they were not expected to control the stability and ultimate failure mode of the full floor system under fire. Analyses performed after removal of the following members showed no premature failure mode such as torsional buckling of primary trusses:

- Deck support angles
- Bridging trusses except in the two-way zone
- Shear studs connecting the slab and the spandrel
- Strap anchors

The visco-elastic dampers that connected the truss bottom chords to the spandrels were not included in the full floor model because dampers were expected to be soft when subjected to slow loading rates.

Truss members (top and bottom chords and web diagonals) were modeled by BEAM188 elements. Columns were modeled by BEAM189 elements. Spandrels were modeled by SHELL181 elements. The concrete slab was modeled by SHELL181 elements with four layers through the thickness. Each layer of the shell element for the slab had one integration point.

Nonlinear steel material properties were assigned to each structural member according to the drawings. A bilinear model with a yield point at its compressive strength was used for the concrete slab, where the yield strength was the same in both tension and compression. Creep in the steel was not included in any of the full floor analyses. It was found that creep in BEAM188/189 elements would cause severe convergence problems when those elements experience thermally-induced buckling.

Both core and exterior columns were fixed in the vertical direction at the bottom. Core columns were free in horizontal directions and fixed in all rotations at the top and bottom. Exterior columns were fixed in translation perpendicular to the face of building and in rotation about the axis parallel to the face of the building at the top and bottom. They were also fixed in torsion at the top and bottom.

Elements corresponding to severed members due to impact were removed from the model in the beginning of the analysis based on the results of the aircraft impact analysis (NIST NCSTAR 1-2 and Chapter 5 of NCSTAR 1-6).

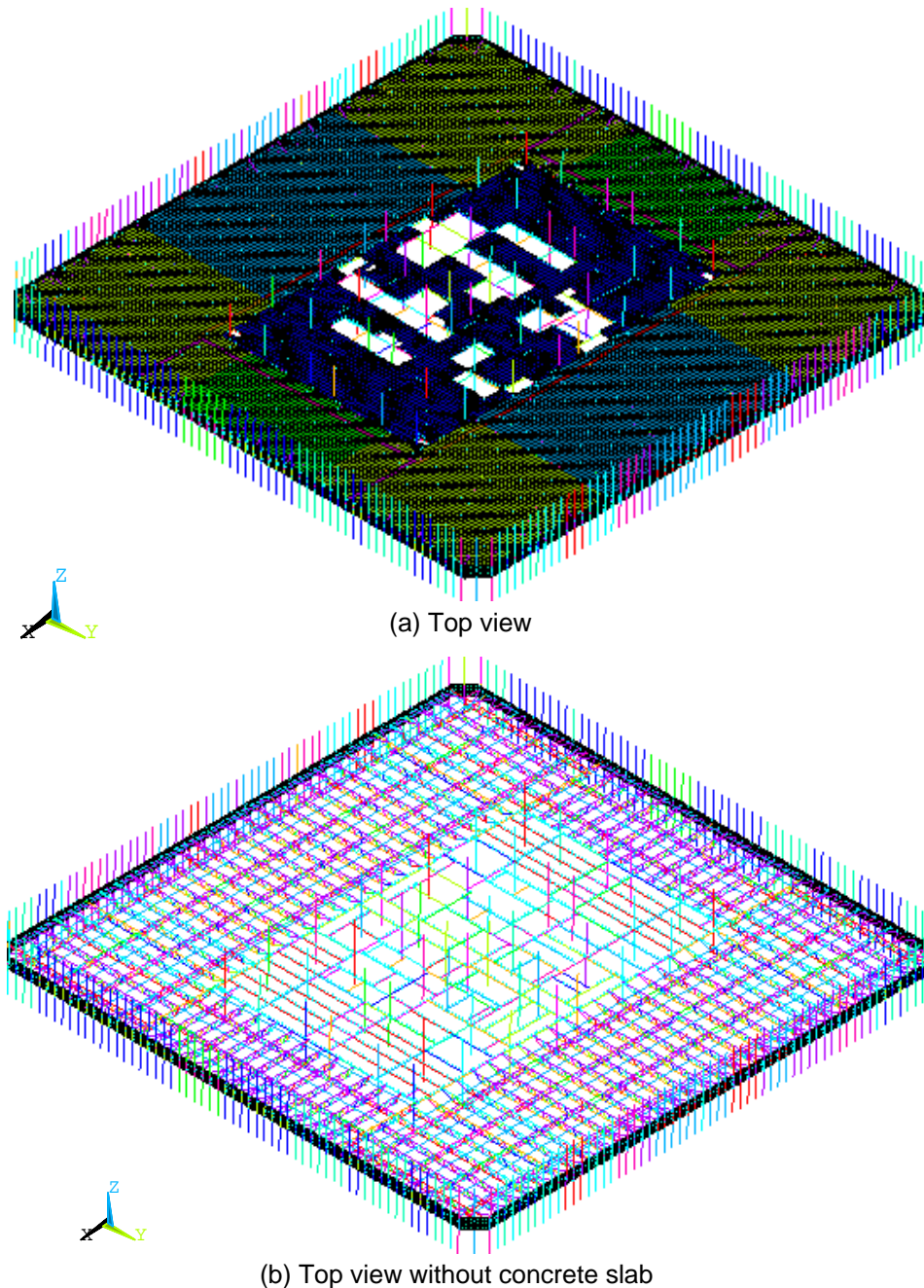


Figure A-1. Full floor model without impact damage.

The full floor model was first analyzed for dead and live loads, and then thermal loads were applied to simulate the path-dependent nonlinear response. Dead and live loads consisted of self-weight, 8 psf superimposed dead load, and 25 percent of design live loads. Design live loads varied from 55 psf to 85 psf in the model. Vertical loads were not applied to columns. For thermal loads, NIST provided two sets of temperature time histories for each building. These temperature cases were designated as “Case A_i temperature condition” and “Case B_i temperature condition” for WTC 1, and “Case C_i temperature condition” and “Case D_i temperature condition” for WTC 2. NIST later refined these temperatures, and refined cases were referred to as “Case A temperature condition” and “Case B temperature condition” for WTC 1, and “Case C temperature condition” and “Case D temperature condition” for WTC 2. Since the largest change in thermal insulation damage and temperatures occurred for WTC 1 Floor 97, Case A_i and Case A temperature conditions were used to analyze the difference in the floor behavior for the two cases. Since results from the WTC 1 Floor 97 analysis under Case A temperature condition was very similar to those from the analysis with Case A_i condition, it was concluded that the refined temperature cases would not change the floor behavior significantly. Therefore, analysis of other floors were not conducted with the refined temperature conditions.

Temperature data sets were provided for every structural node at 10 min intervals up to 100 min for WTC 1 and up to 60 min for WTC 2 for each temperature case. In the first step of the thermal loading, temperature was linearly ramped up from room temperature to the temperature specified at 10 min. After the first step, the temperature was linearly interpolated between two data sets. Figures A–3 to A–8 show NIST temperature distributions for WTC 1 Floor 97 for Case A_i temperature condition, Case A temperature condition, and Case B_i temperature condition. For each case, temperatures were plotted at only 10 min, 50 min, and 100 min. Figures A–9 to A–12 show NIST temperature distributions for WTC 2 Floor 82 for Case C_i and Case D_i temperature conditions. In the figures, severed members were also shown; however, the severed members were removed from the floor models and did not exist in the analysis.

Temperatures for truss members and spandrels were assigned at node locations and did not change within the cross section. Temperatures for columns were assigned at node locations and had a gradient within the cross section. Temperatures for the slab were assigned at node locations, and there were five points to define the temperature distribution through the thickness at each node location.

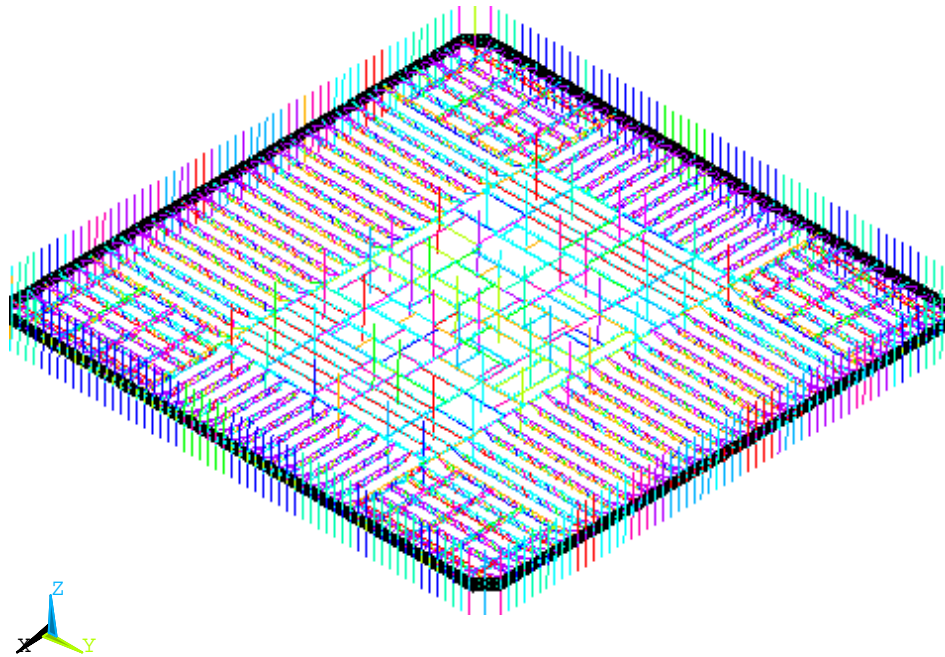
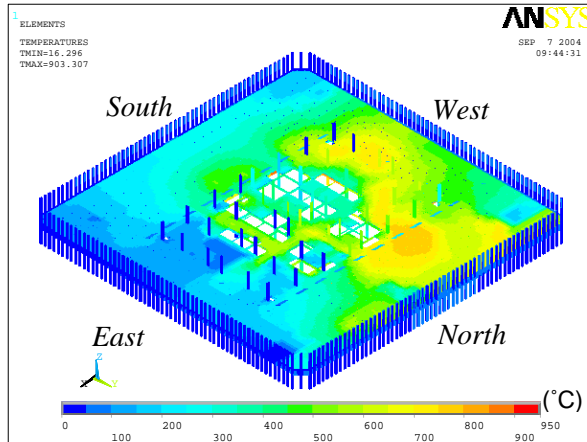
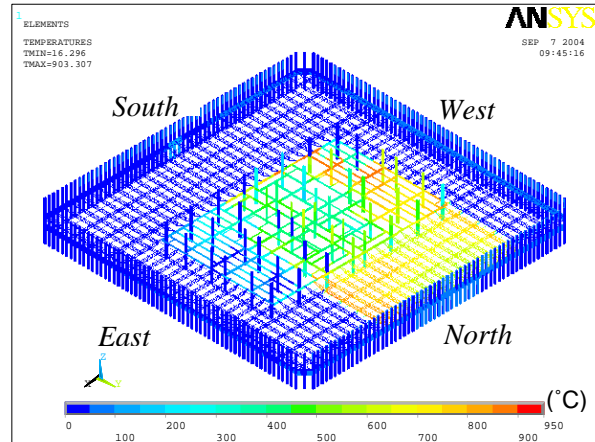


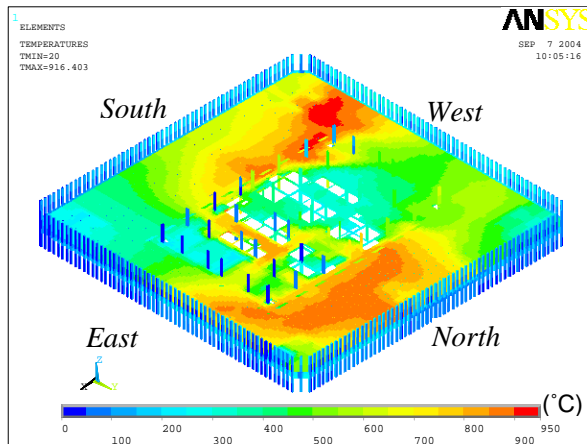
Figure A-2. Full floor model after removal of deck support angles, spandrel studs, bridging trusses outside of two-way zones, and strap anchors.



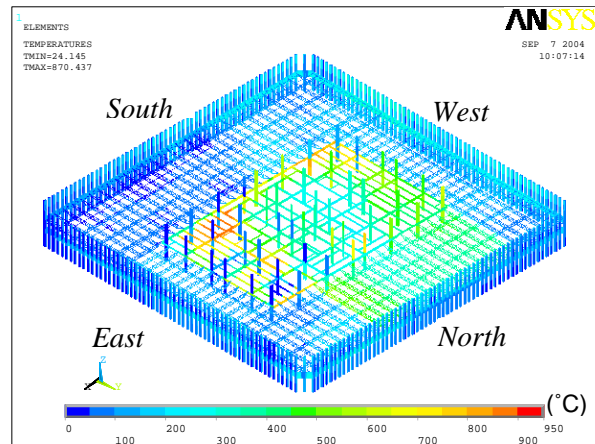
(a) Top view at 10 min



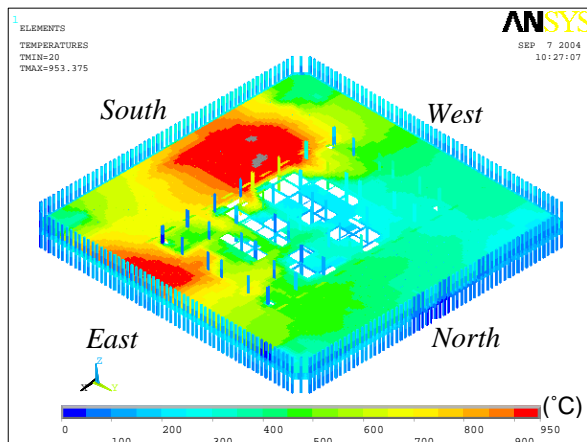
(b) Top view without concrete slab at 10 min



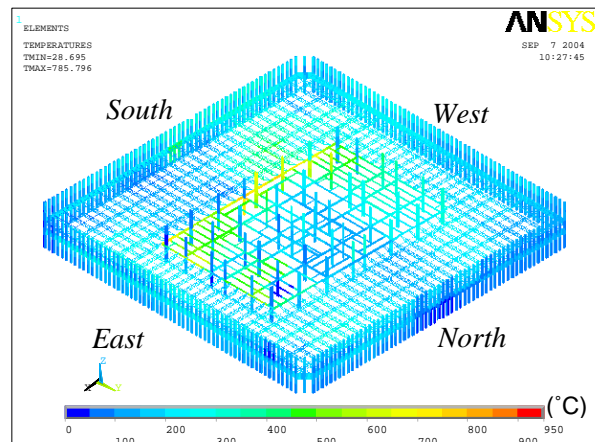
(c) Top view at 50 min



(d) Top view without concrete slab at 50 min

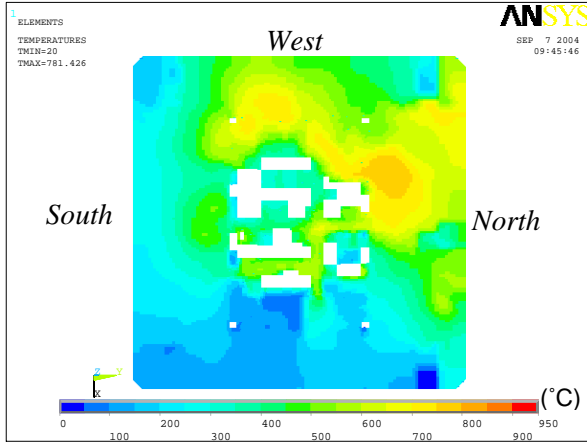


(e) Top view at 100 min

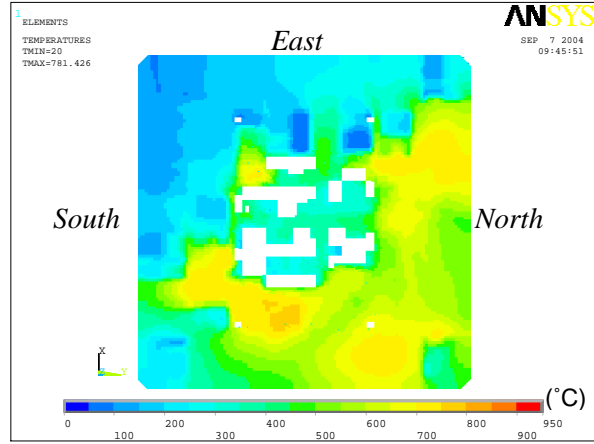


(f) Top view without concrete slab at 100 min

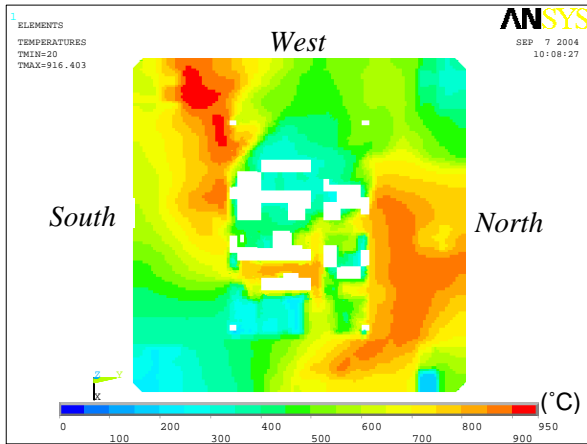
Figure A-3. Case A₁ temperature distribution for Floor 97 of WTC 1.



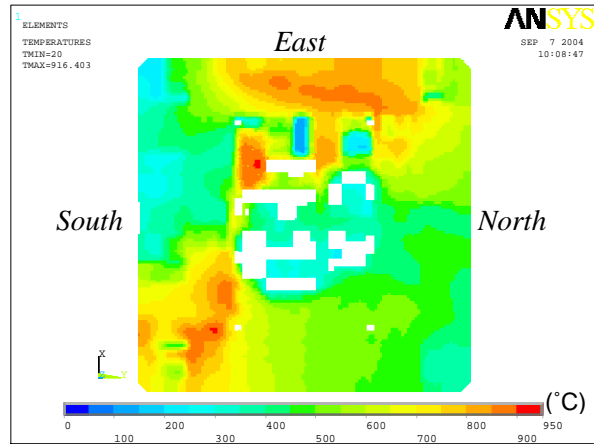
(a) Top surface at 10 min



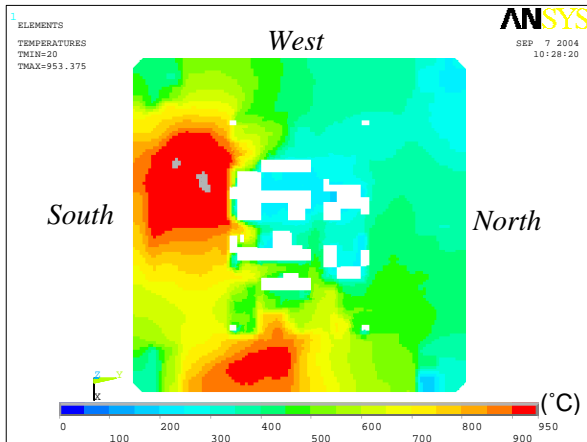
(b) Bottom surface at 10 min



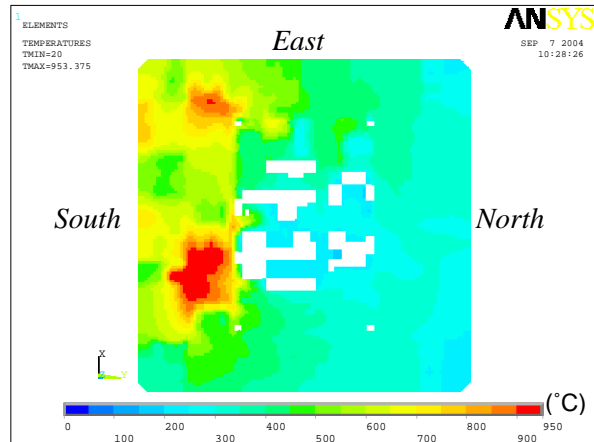
(c) Top surface at 50 min



(d) Bottom surface at 50 min

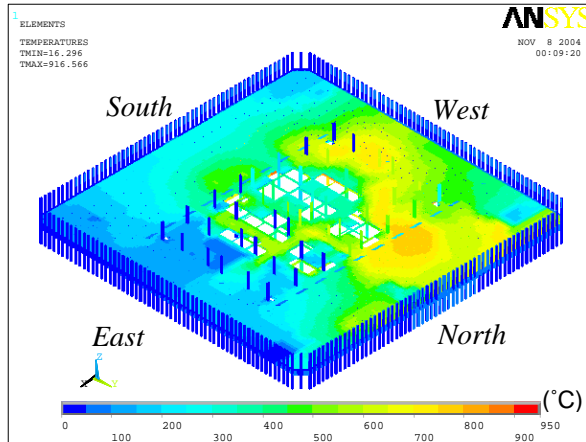


(e) Top surface at 100 min

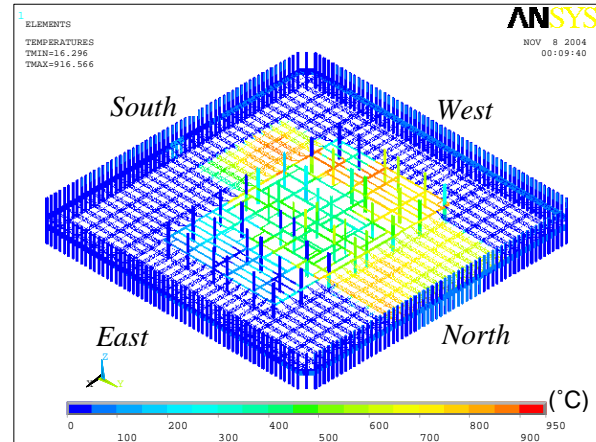


(f) Bottom surface at 100 min

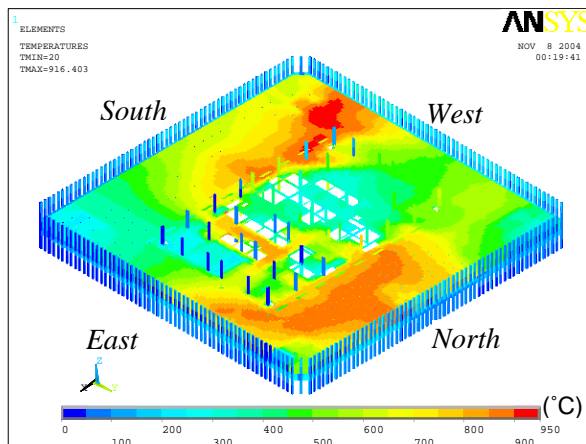
Figure A-4. Case A_i temperature distribution in the slab for Floor 97 of WTC 1.



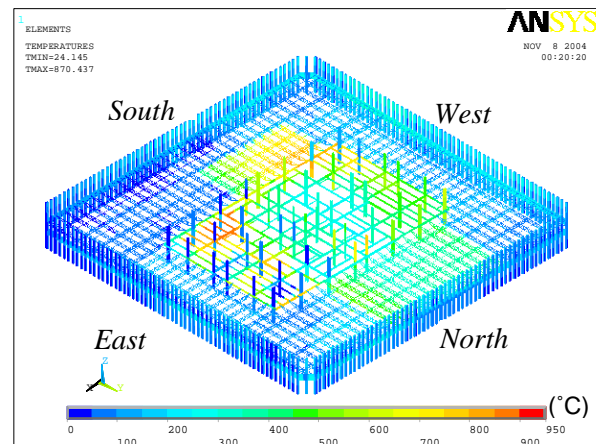
(a) Top view at 10 min



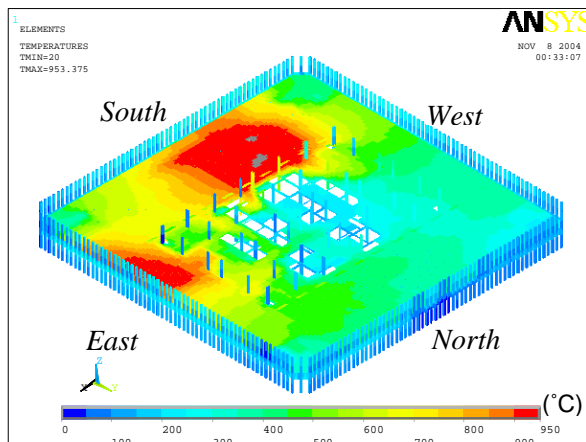
(b) Top view without concrete slab at 10 min



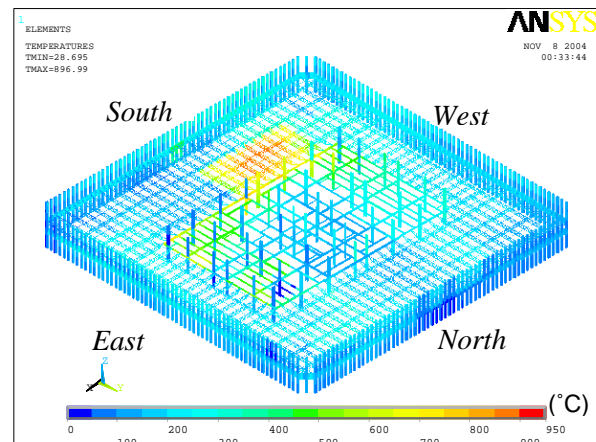
(c) Top view at 50 min



(d) Top view without concrete slab at 50 min

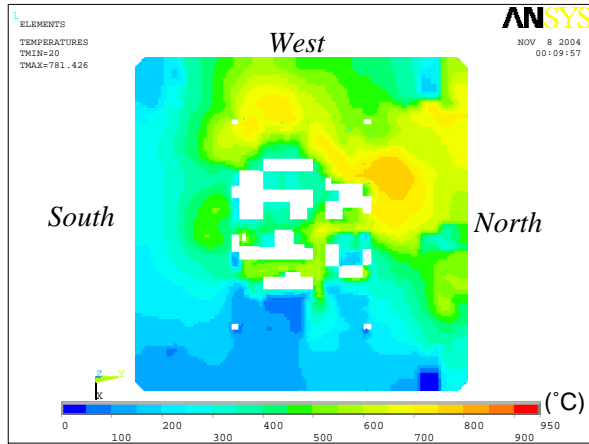


(e) Top view at 100 min

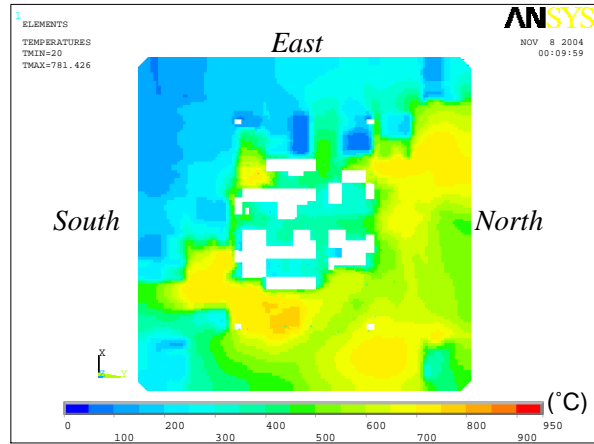


(f) Top view without concrete slab at 100 min

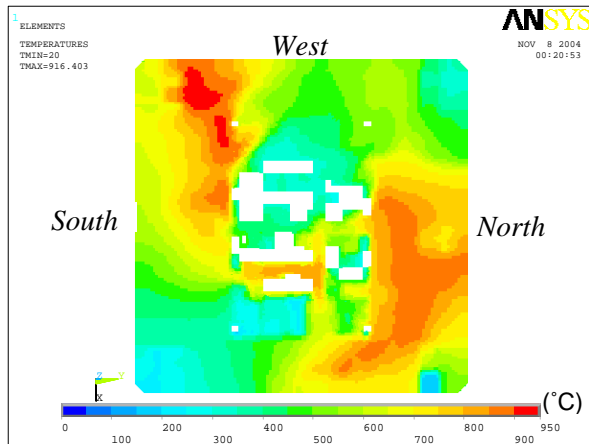
Figure A-5. Case A temperature distribution for Floor 97 of WTC 1.



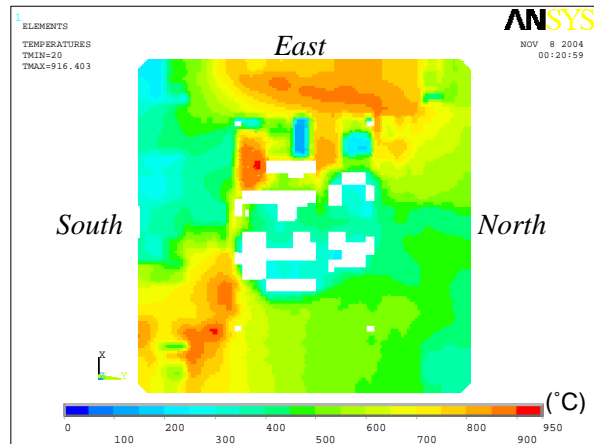
(a) Top surface at 10 min



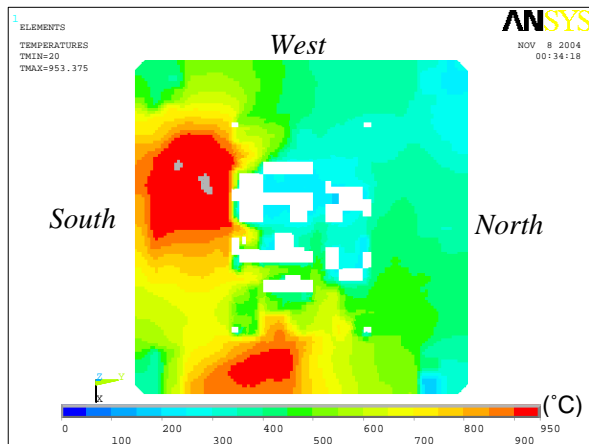
(b) Bottom surface at 10 min



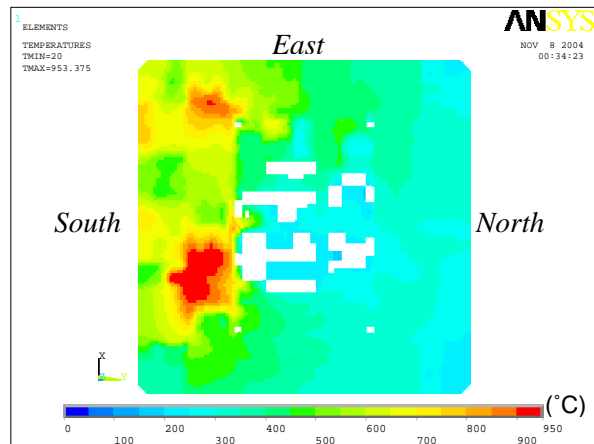
(c) Top surface at 50 min



(d) Bottom surface at 50 min

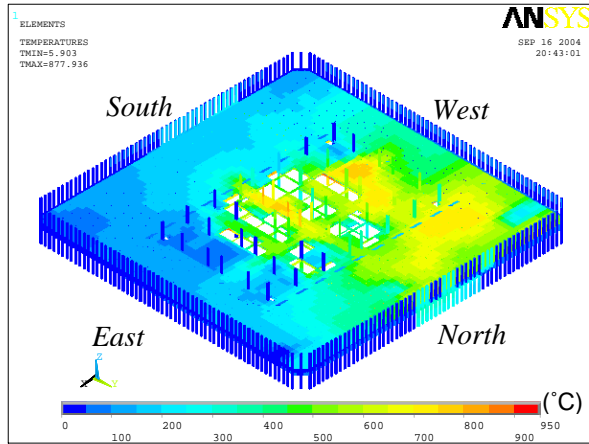


(e) Top surface at 100 min

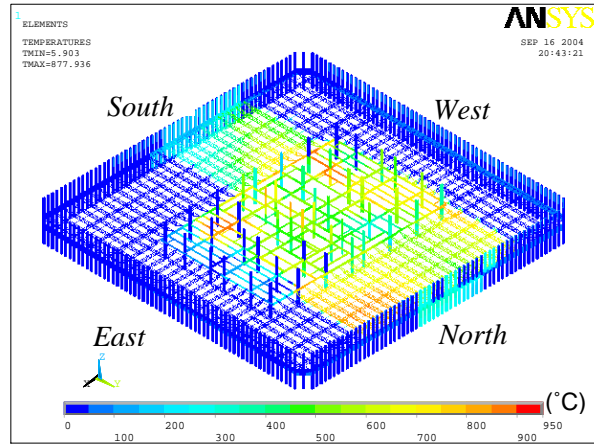


(f) Bottom surface at 100 min

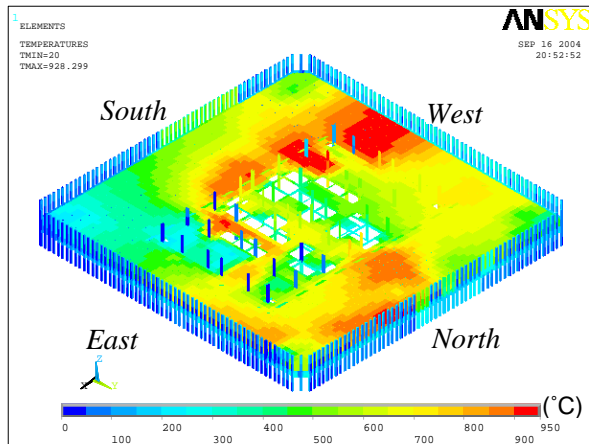
Figure A-6. Case A temperature distribution in the slab for Floor 97 of WTC 1.



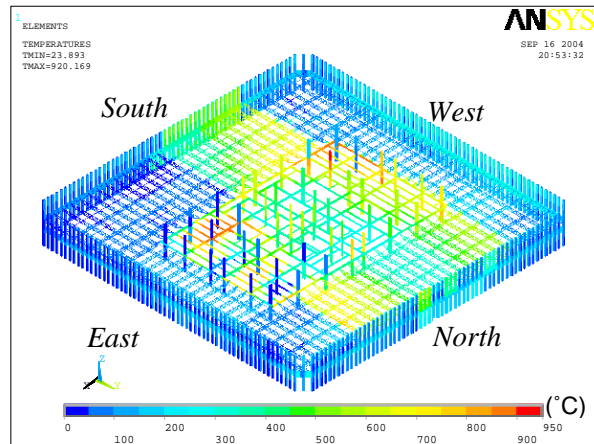
(a) Top view at 10 min



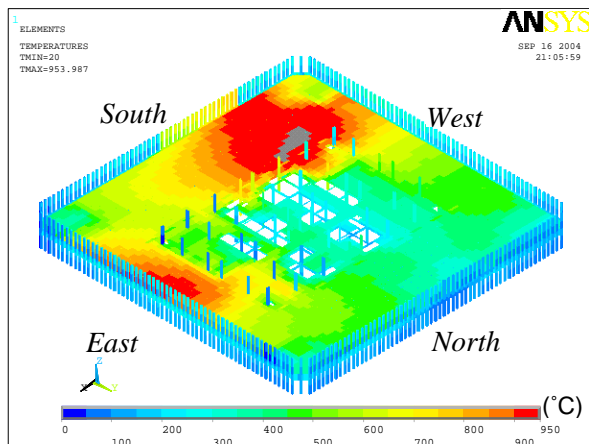
(b) Top view without concrete slab at 10 min



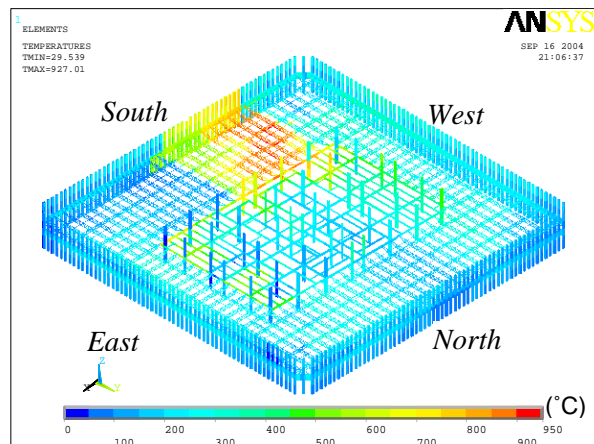
(c) Top view at 50 min



(d) Top view without concrete slab at 50 min

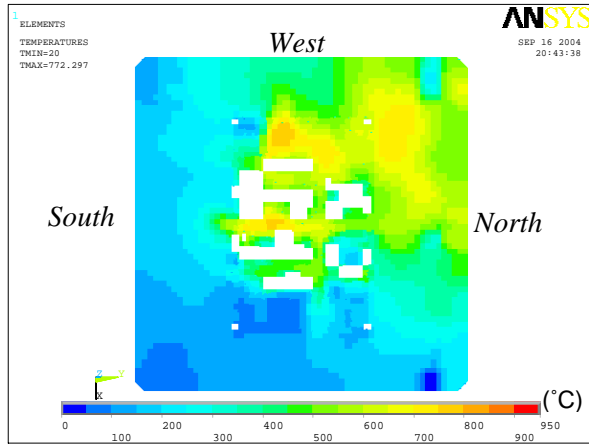


(e) Top view at 100 min

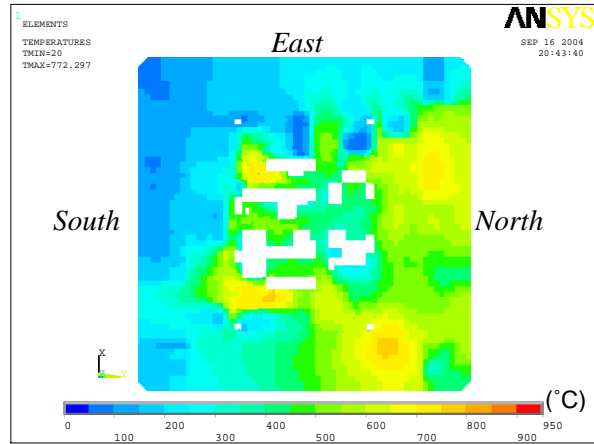


(f) Top view without concrete slab at 100 min

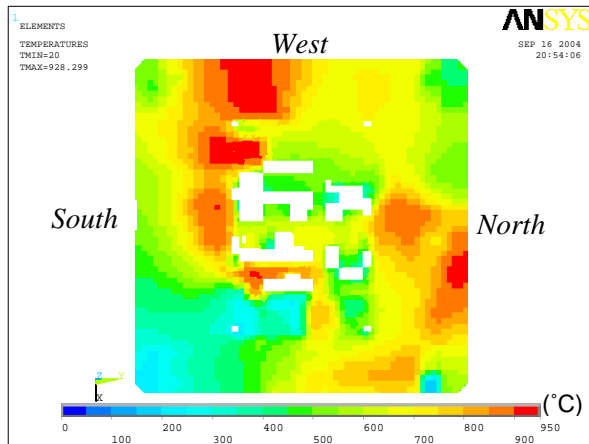
Figure A-7. Case B, temperature distribution for Floor 97 of WTC 1.



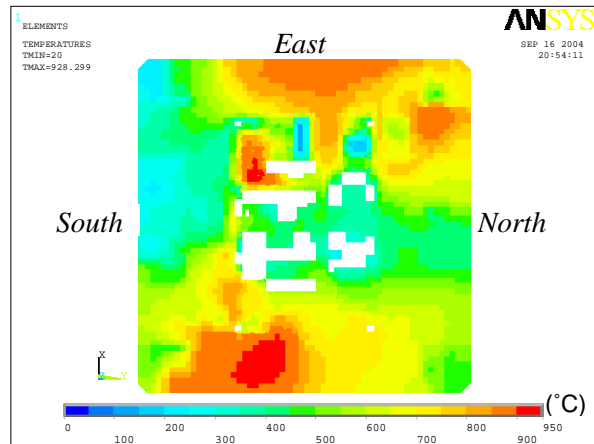
(a) Top surface at 10 min



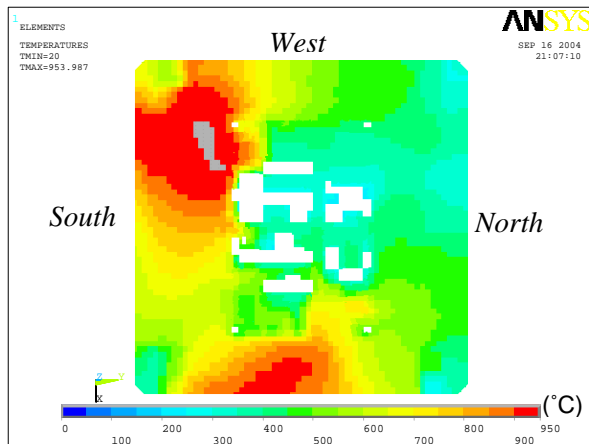
(b) Bottom surface at 10 min



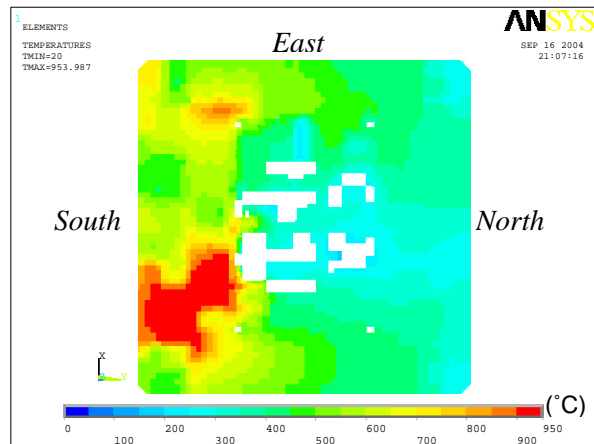
(c) Top surface at 50 min



(d) Bottom surface at 50 min

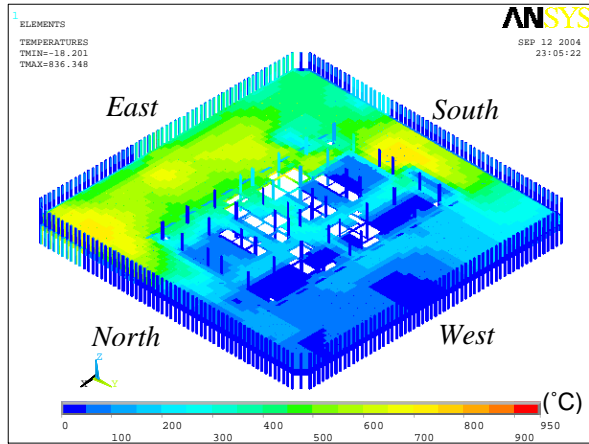


(e) Top surface at 100 min

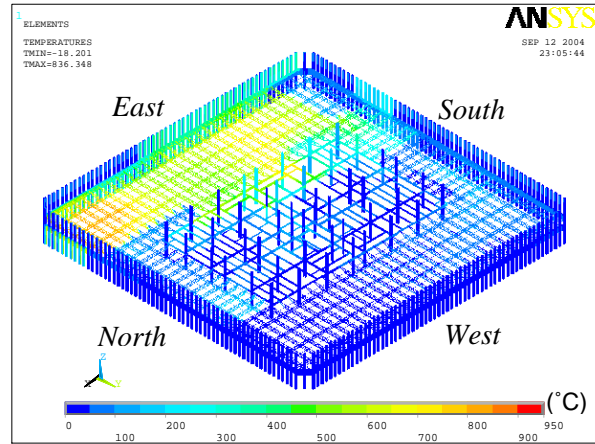


(f) Bottom surface at 100 min

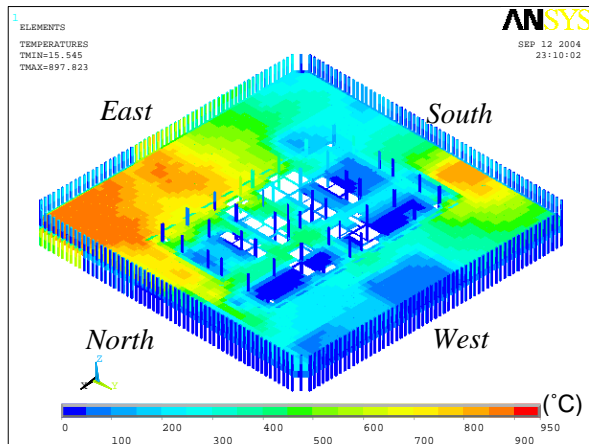
Figure A-8. Case B_i temperature distribution in the slab for Floor 97 of WTC 1.



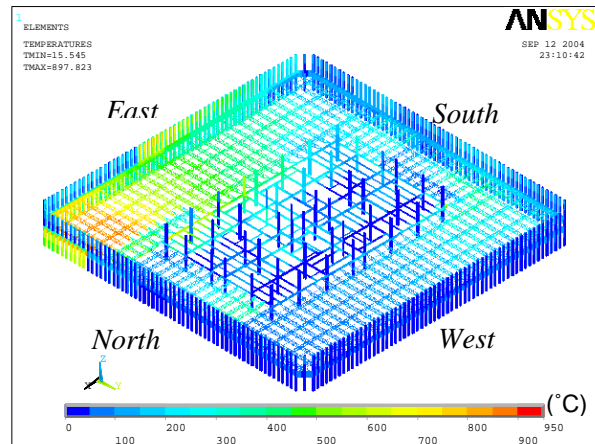
(a) Top view at 10 min



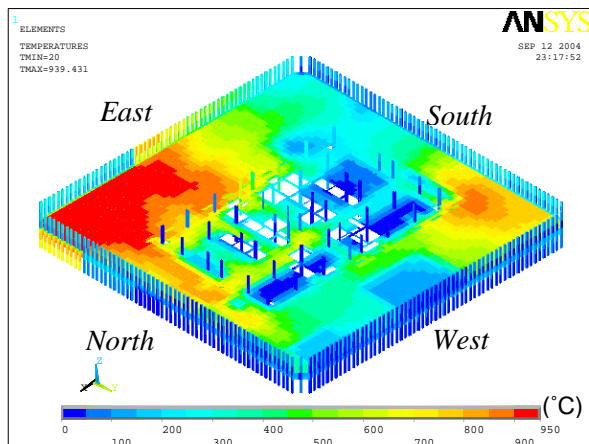
(b) Top view without concrete slab at 10 min



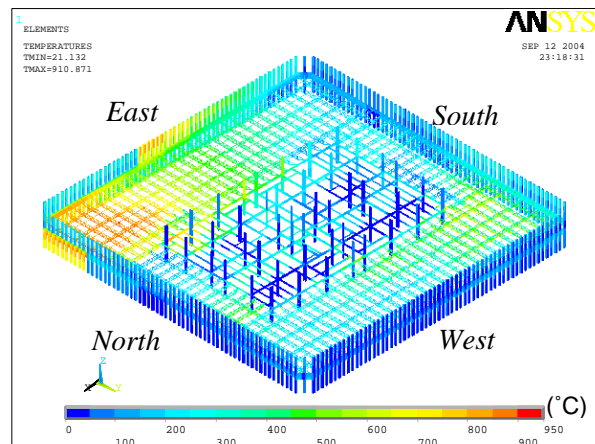
(c) Top view at 30 min



(d) Top view without concrete slab at 30 min

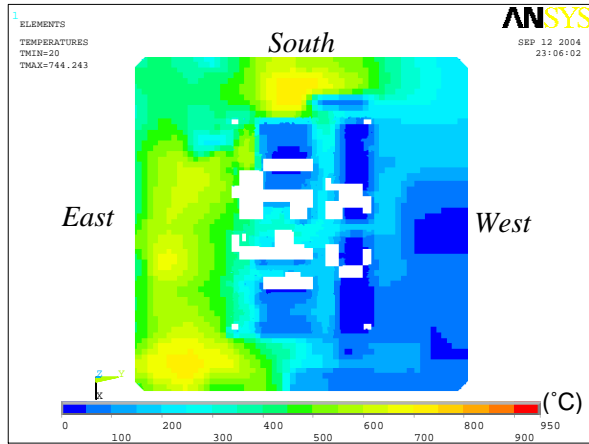


(e) Top view at 60 min

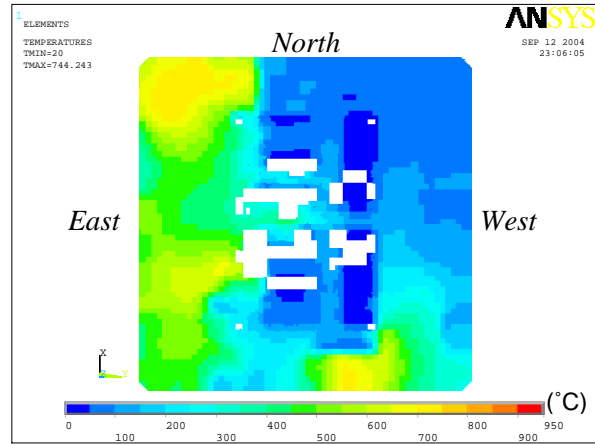


(f) Top view without concrete slab at 60 min

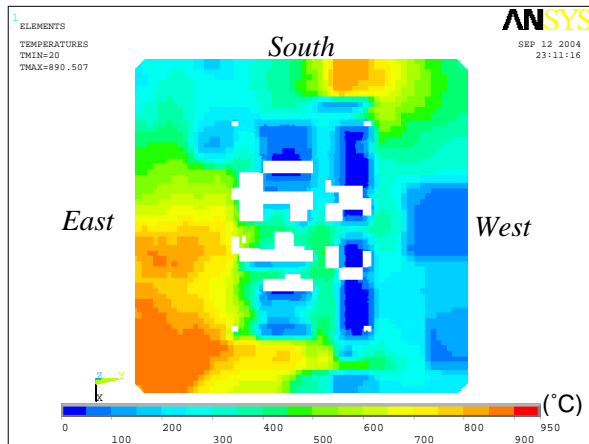
Figure A-9. Case C; temperature distribution for Floor 82 of WTC 2.



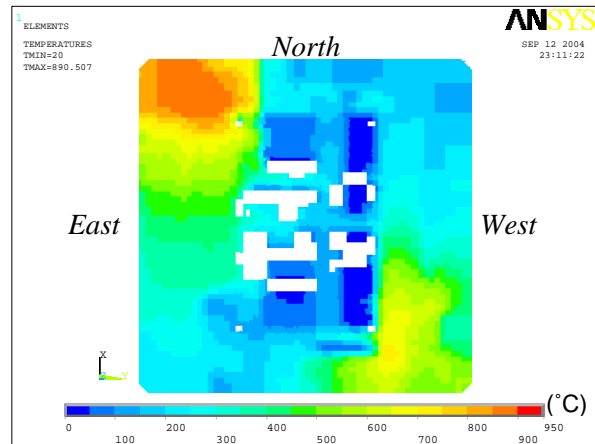
(a) Top surface at 10 min



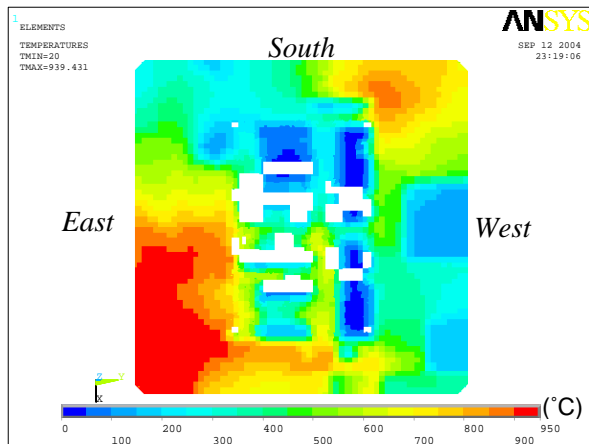
(b) Bottom surface at 10 min



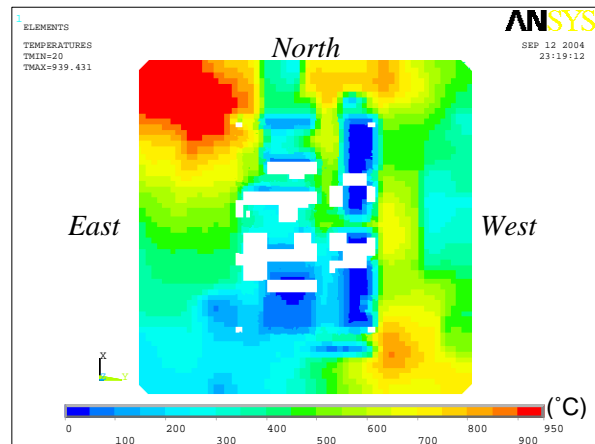
(c) Top surface at 30 min



(d) Bottom surface at 30 min

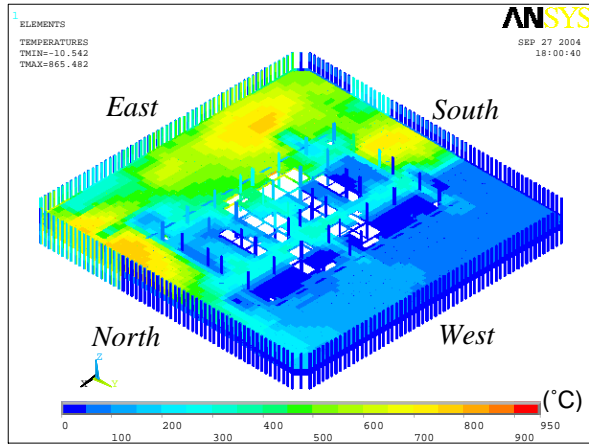


(e) Top surface at 60 min

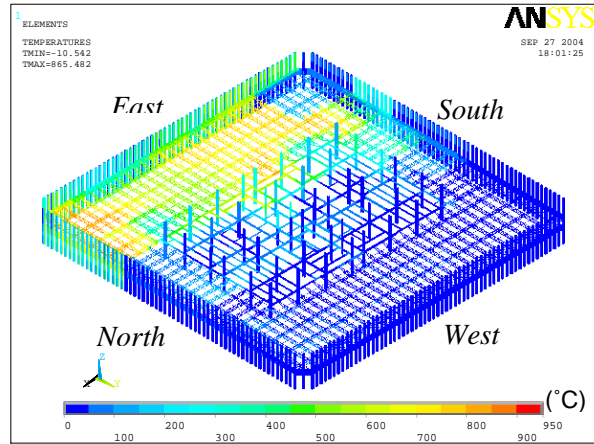


(f) Bottom surface at 60 min

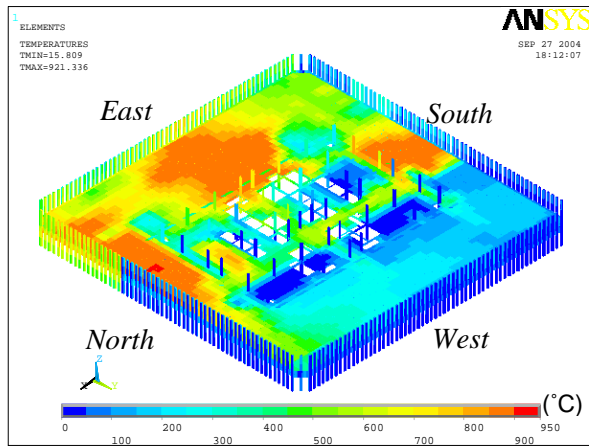
Figure A-10. Case C_i temperature distribution in the slab for Floor 82 of WTC 2.



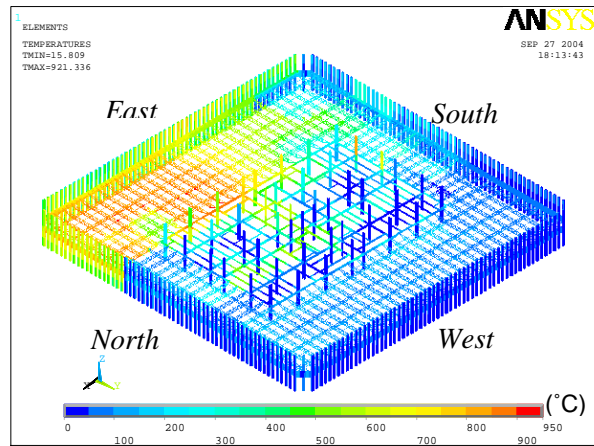
(a) Top view at 10 min



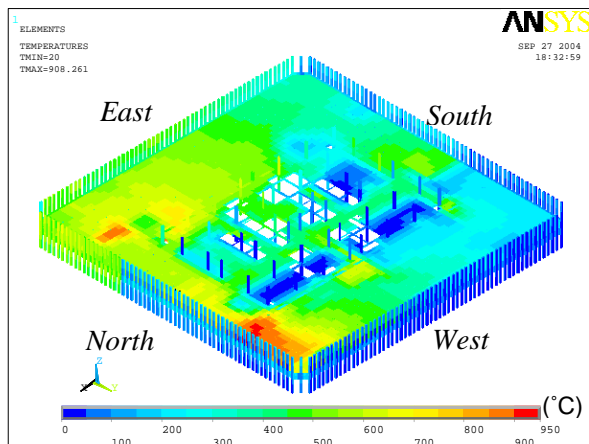
(b) Top view without concrete slab at 10 min



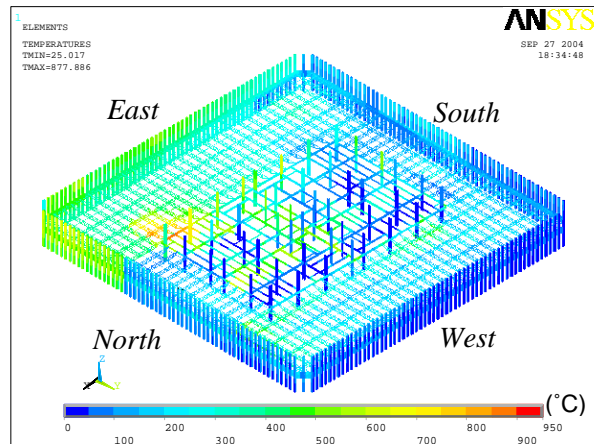
(c) Top view at 30 min



(d) Top view without concrete slab at 30 min

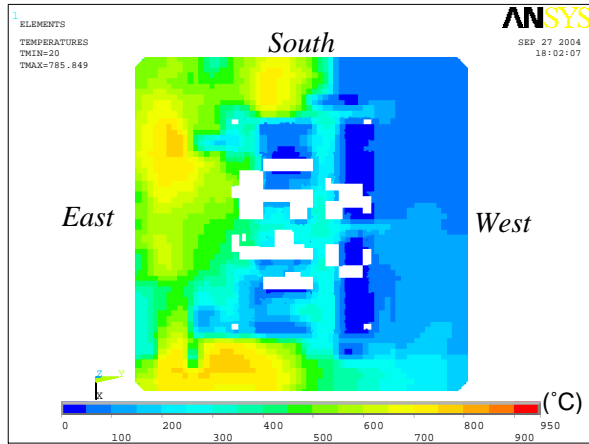


(e) Top view at 60 min

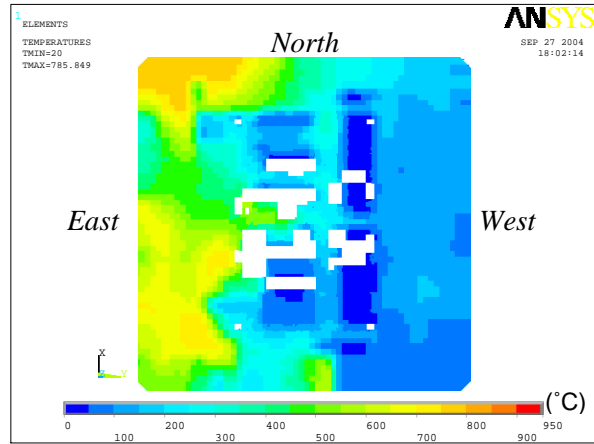


(f) Top view without concrete slab at 60 min

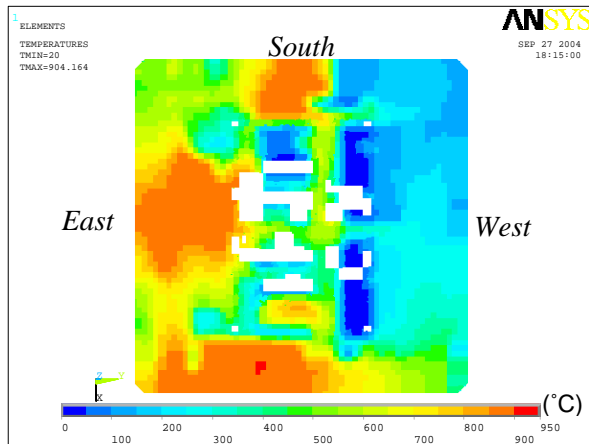
Figure A-11. Case D_i temperature distribution for Floor 82 of WTC 2.



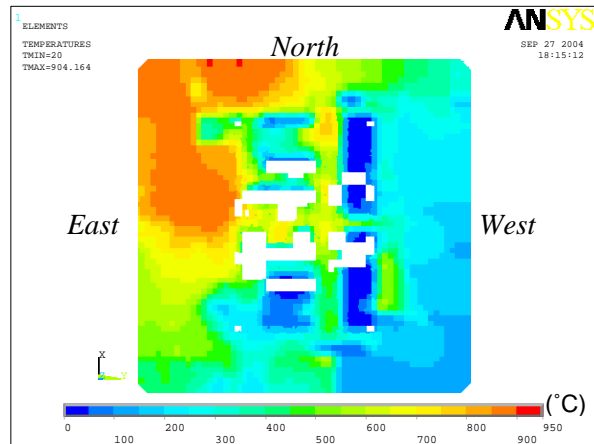
(a) Top surface at 10 min



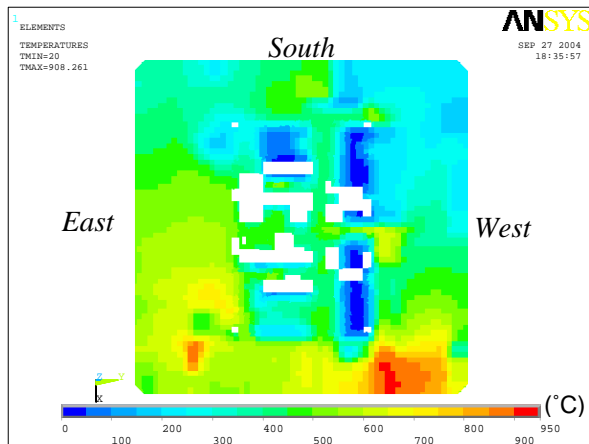
(b) Bottom surface at 10 min



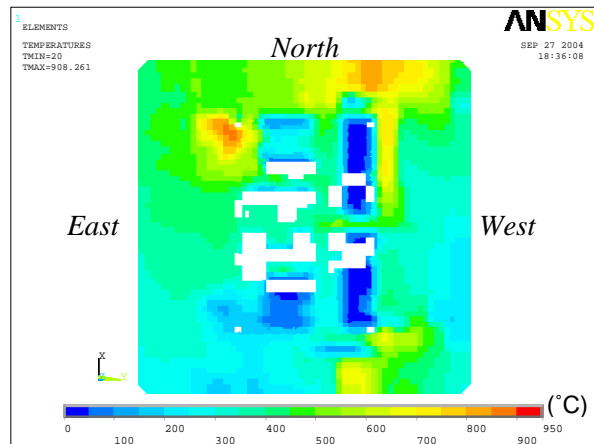
(c) Top surface at 30 min



(d) Bottom surface at 30 min



(e) Top surface at 60 min



(f) Bottom surface at 60 min

Figure A-12. Case D_i temperature distribution in the slab for Floor 82 of WTC 2.

A.2 WTC 1 FLOORS

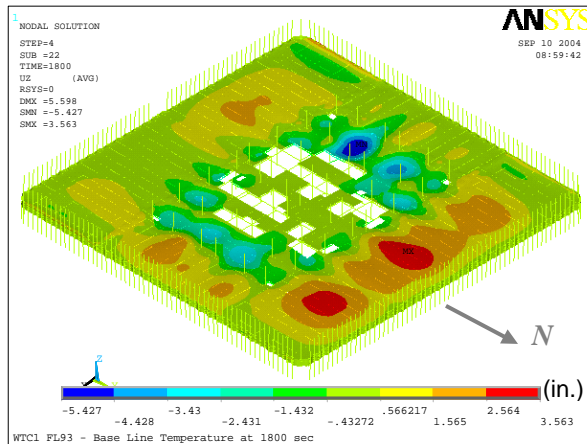
A.2.1 Case A_i Temperature Condition

Table A–1 gives the maximum vertical displacement of WTC 1 floors, and Figs. A–13 to A–19 show the vertical displacements of the floors when the maximum displacement was obtained. Floor 95 to Floor 98 showed a significant vertical displacement in the north office area near the impact damage. The maximum vertical displacement of all floors was 32 in. for Floor 97 at 60 min. The vertical displacement in the south office area was found to be insignificant on all the floors throughout the thermal loading. Figure A–20 shows the average total thermal expansion of floors over the entire width of the building at 100 min in two orthogonal directions. The total floor expansion ranged from 4 in. to 8 in. Many web diagonals of Floor 95 to Floor 98 buckled in the hot zones of the north office area. Although gusset plates fractured at several locations, a complete disconnection of the floor from the exterior wall was not observed. Figure A–21 shows horizontal reaction force at individual columns of the north and south faces of Floor 97. A positive reaction force in the figure means that the column is pulled inward by the floor, and a negative reactions force means that the column is pushed out by the floor. Since columns that were not at floor trusses were not connected to the floor in the model because of the removal of strap anchors and studs, reaction forces at those columns were small, and the plots became jagged. As can be seen in the figure, almost all the columns were pushed out by the floor. This was also the case for other floors.

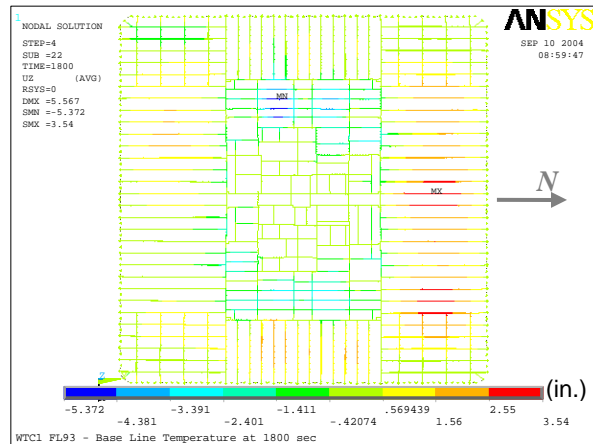
Table A–1. Maximum vertical displacement of WTC 1 floors for Case A_i temperature condition.

Floor	Max. Displacement (in.)	Time at the Maximum (min)
93	5.4	30
94	13.5	100
95	30.9	10
96	23.3	10
97	31.5	60
98	26.4	30
99	7.0	50

Note: Downward displacement is positive.

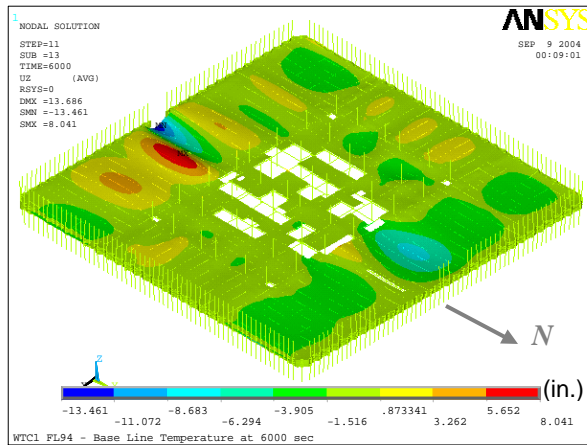


(a) Entire model

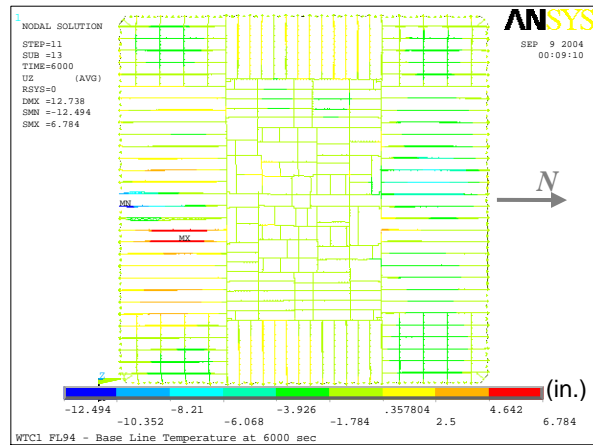


(b) Top view without slab

Figure A–13. Vertical displacement of WTC 1 Floor 93 for Case A_i temperature condition at 30 min (downward displacement is negative; 5x displacement magnification).

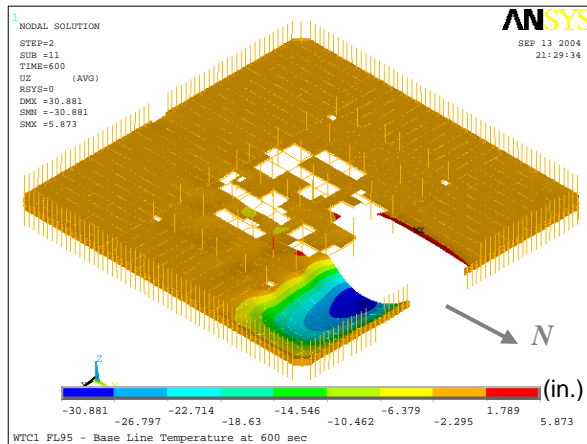


(a) Entire model

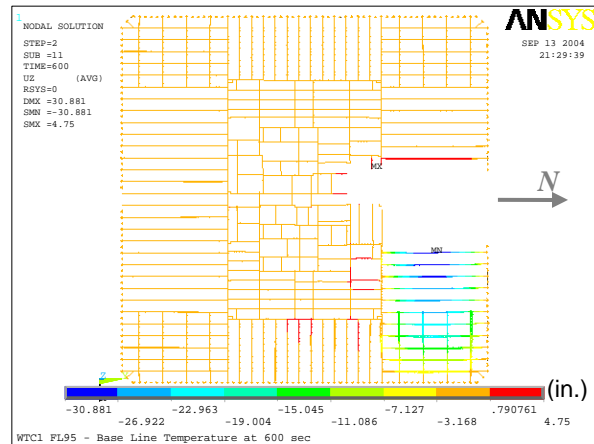


(b) Top view without slab

Figure A–14. Vertical displacement of WTC 1 Floor 94 for Case A_i temperature condition at 100 min (downward displacement is negative; 5x displacement magnification).

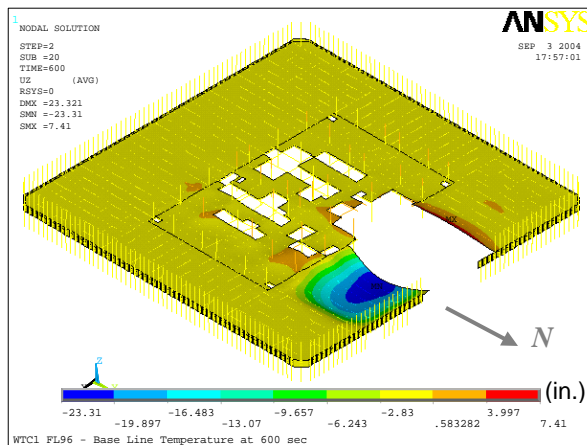


(a) Entire model

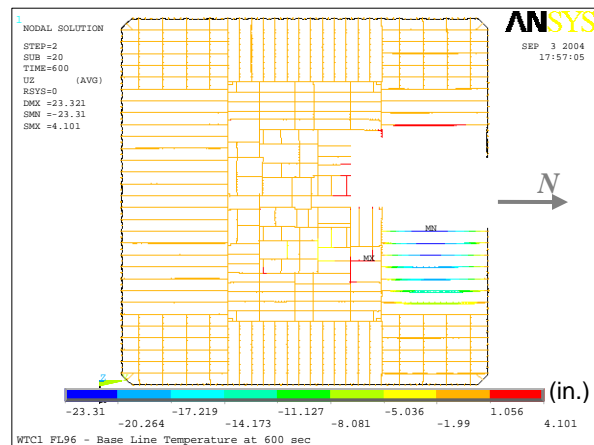


(b) Top view without slab

Figure A–15. Vertical displacement of WTC 1 Floor 95 for Case A_i temperature condition at 10 min (downward displacement is negative; 5x displacement magnification).

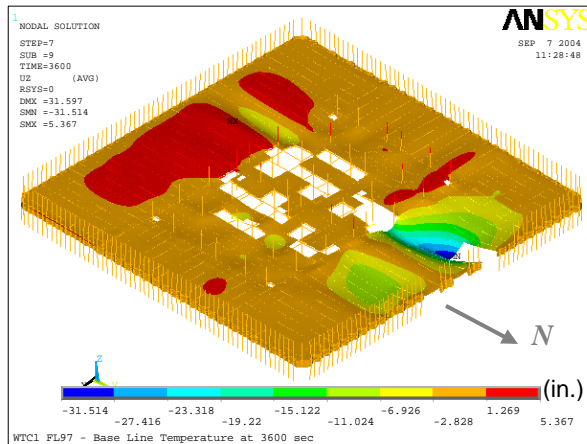


(a) Entire model

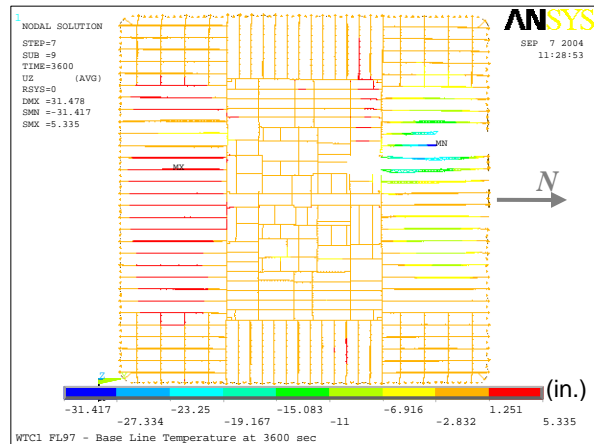


(b) Top view without slab

Figure A–16. Vertical displacement of WTC 1 Floor 96 for Case A_i temperature condition at 10 min (downward displacement is negative; 5x displacement magnification).

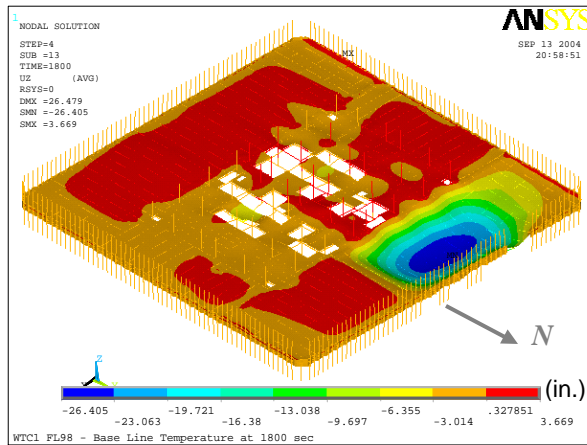


(a) Entire model

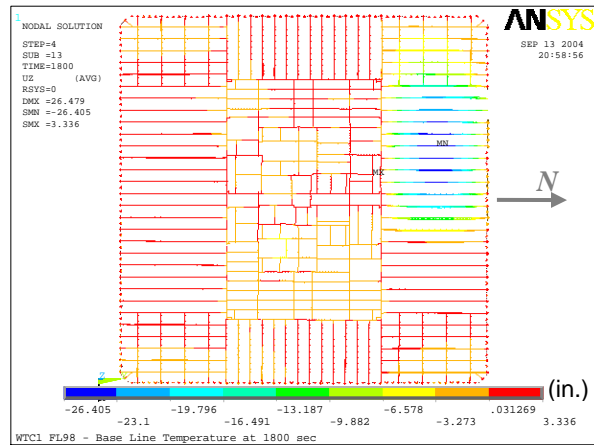


(b) Top view without slab

Figure A-17. Vertical displacement of WTC 1 Floor 97 for Case A_i temperature condition at 60 min (downward displacement is negative; 5x displacement magnification).

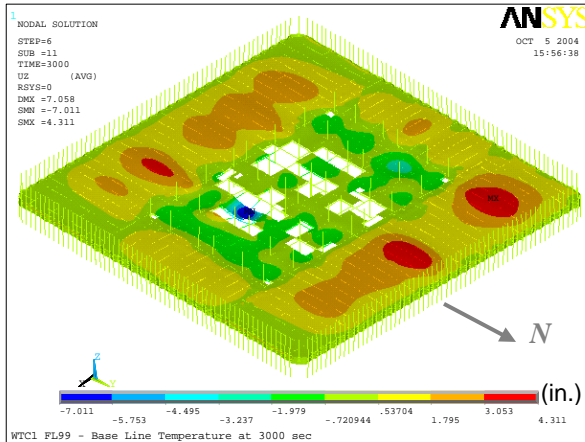


(a) Entire model

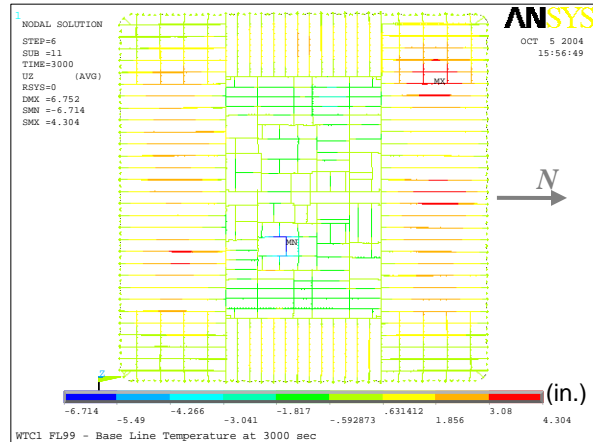


(b) Top view without slab

Figure A-18. Vertical displacement of WTC 1 Floor 98 for Case A_i temperature condition at 30 min (downward displacement is negative; 5x displacement magnification).



(a) Entire model



(b) Top view without slab

Figure A–19. Vertical displacement of WTC 1 Floor 99 for Case A_i temperature condition at 50 min (downward displacement is negative; 5x displacement magnification).

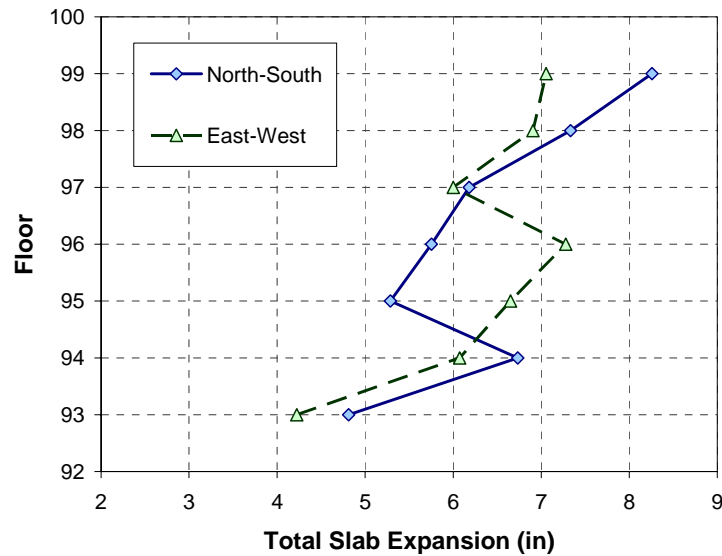


Figure A–20. Thermal expansion of floors of WTC 1 for Case A_i temperature condition at 100 min.

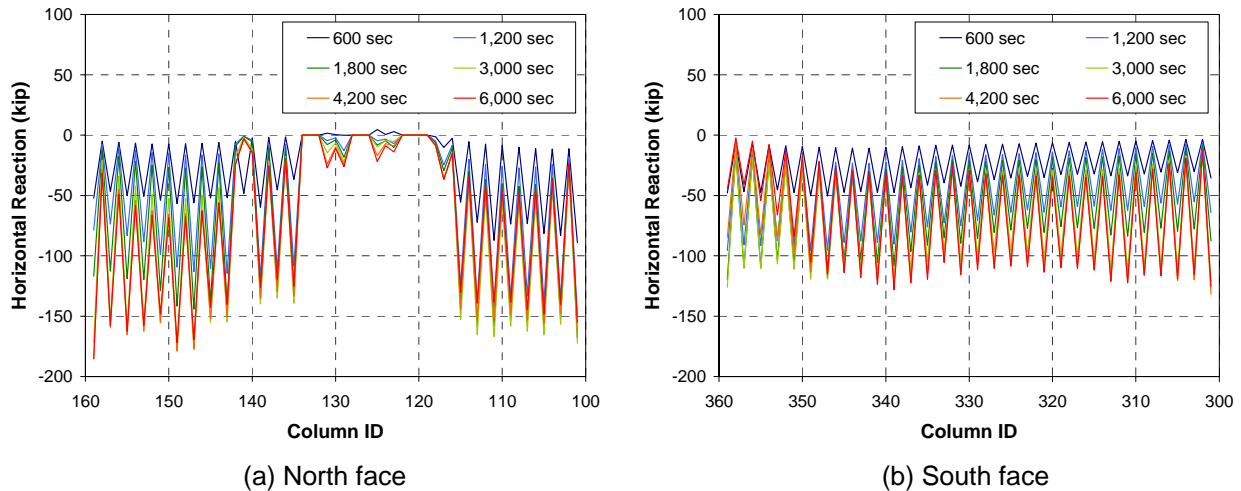


Figure A–21. Horizontal reaction force per column of WTC 1 Floor 97 for Case A_i temperature condition.

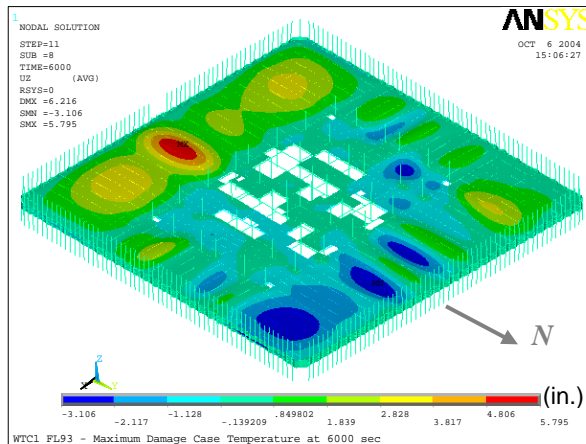
A.2.2 Case B_i Temperature Condition

Table A–2 gives the maximum vertical displacement of WTC 1 floors for Case B_i temperature condition, and Figs. A–22 to A–28 show the vertical displacements when the maximum displacement was obtained. The maximum vertical displacement of Floor 95 to Floor 98 increased due to higher temperature when compared to Case A_i temperature condition. Especially, the vertical displacement in the south office area of those floors became significant. The maximum among the floors was 49 in. in the south office area of Floor 98 as shown in Fig. A–27. The large displacement on the south side of Floor 98 was caused by the exterior seat failure between Column 329 and Column 343 that started at 90 min (see Fig. A–29). Exterior seats between Column 337 and Column 347 of Floor 97 also failed, which caused a vertical displacement of 37 in. in the south office area (see Fig. A–29). These exterior seats failed due to loss of vertical shear strength under the extreme temperatures encountered. Figure A–30 shows the average total thermal expansion of floors over the entire width of the building at 100 min of Case B_i temperature condition. The total floor expansion ranged from 5 in. to 8.5 in. Figure A–31 shows horizontal reaction force at individual columns of the north and south faces of Floor 98. It can be seen in the figure that reaction forces of columns between Column 329 and Column 343 became close to zero after the trusses attached to these column lost their vertical support at the exterior seats. Almost all the columns were found to be pushed out by the floor. This was also the case for other floors.

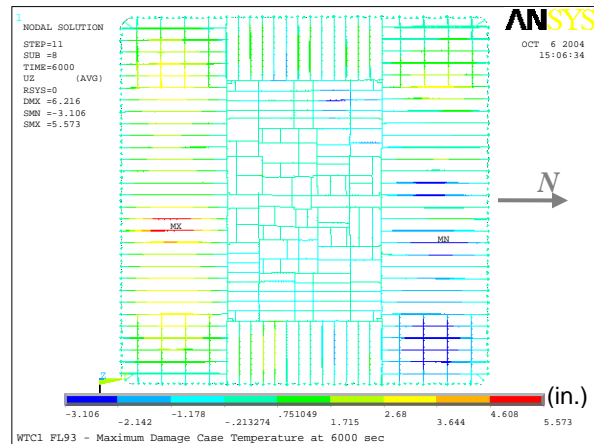
Table A–2. Maximum vertical displacement of WTC 1 floors for Case B_i temperature condition.

Floor	Max. Displacement (in.)	Time at the Maximum (min)
93	-5.8	100
94	12.7	100
95	29.2	10
96	28.6	10
97	37.4	100
98	49.0	100
99	6.8	100

Note: Downward displacement is positive.

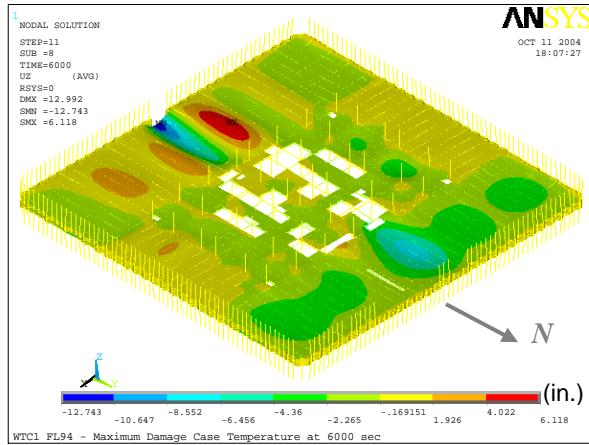


(a) Entire model

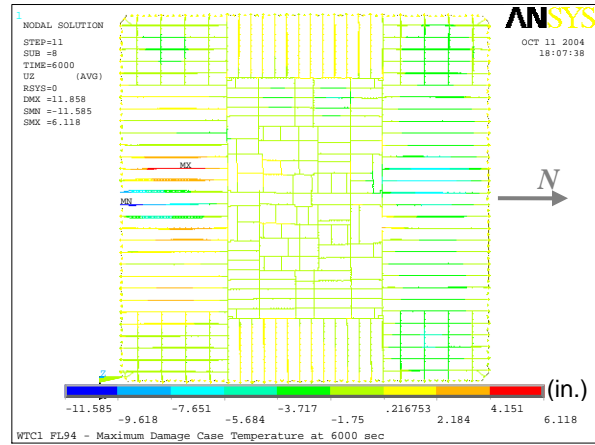


(b) Top view without slab

Figure A–22. Vertical displacement of WTC 1 Floor 93 for Case B_i temperature condition at 100 min (downward displacement is negative; 5x displacement magnification).

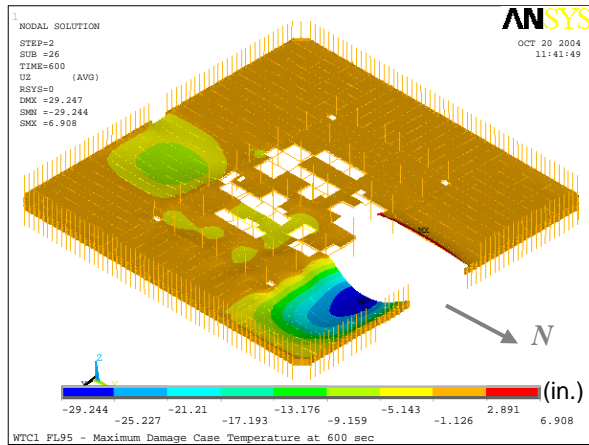


(a) Entire model

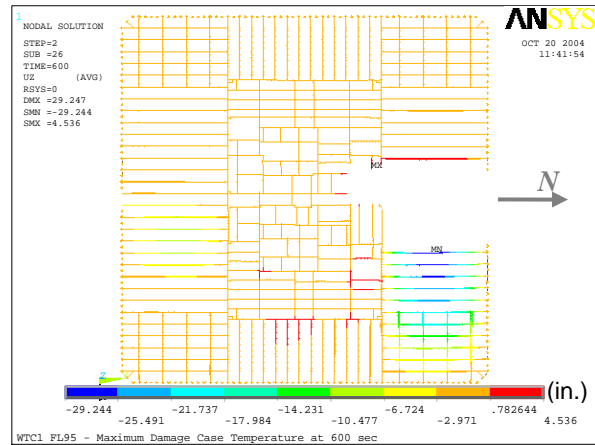


(b) Top view without slab

Figure A–23. Vertical displacement of WTC 1 Floor 94 for Case B_i temperature condition at 100 min (downward displacement is negative; 5x displacement magnification).

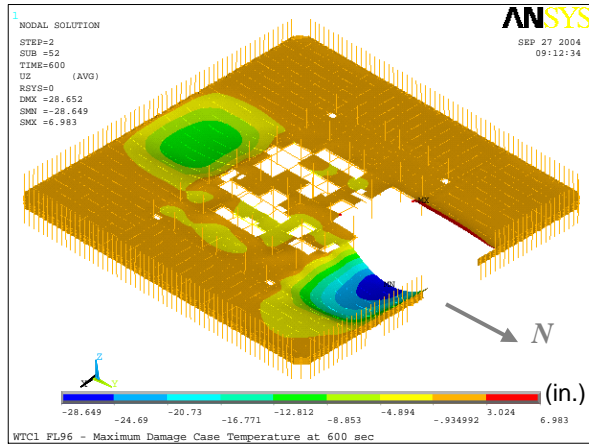


(a) Entire model

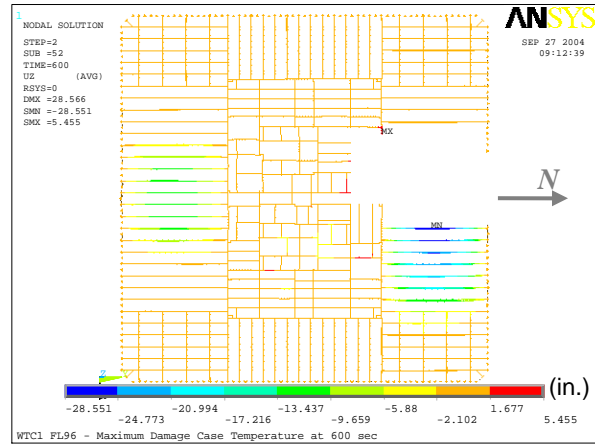


(b) Top view without slab

Figure A–24. Vertical displacement of WTC 1 Floor 95 for Case B_i temperature condition at 10 min (downward displacement is negative; 5x displacement magnification).

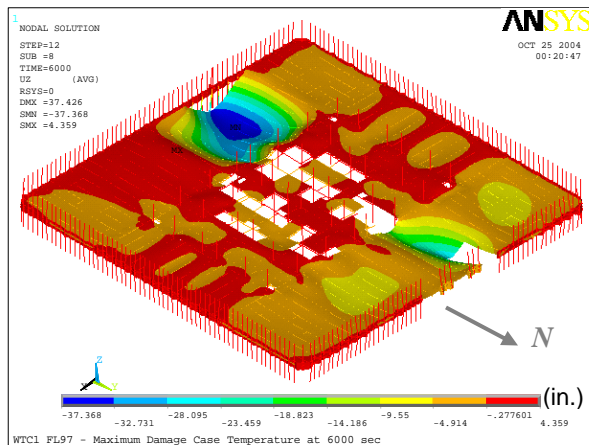


(a) Entire model

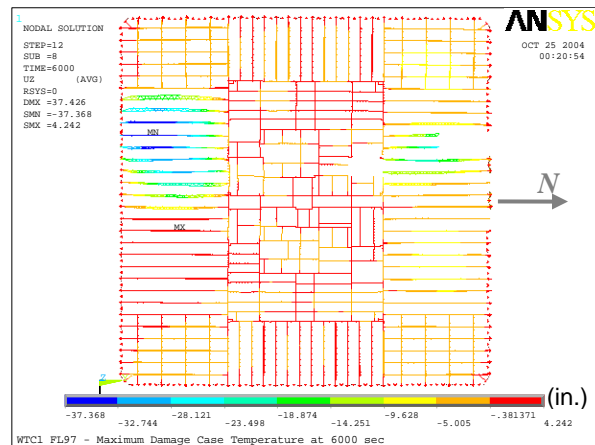


(b) Top view without slab

Figure A–25. Vertical displacement of WTC 1 Floor 96 for Case B_i temperature condition at 10 min (downward displacement is negative; 5x displacement magnification).

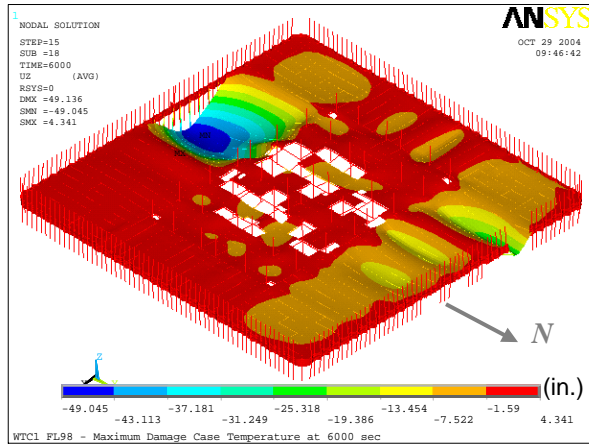


(a) Entire model

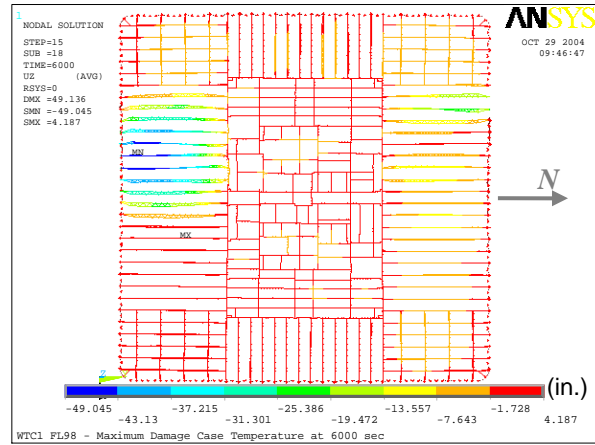


(b) Top view without slab

Figure A–26. Vertical displacement of WTC 1 Floor 97 for Case B_i temperature condition at 100 min (downward displacement is negative; 5x displacement magnification).

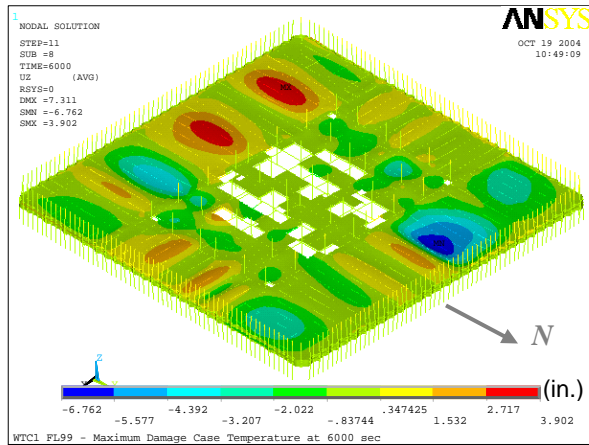


(a) Entire model

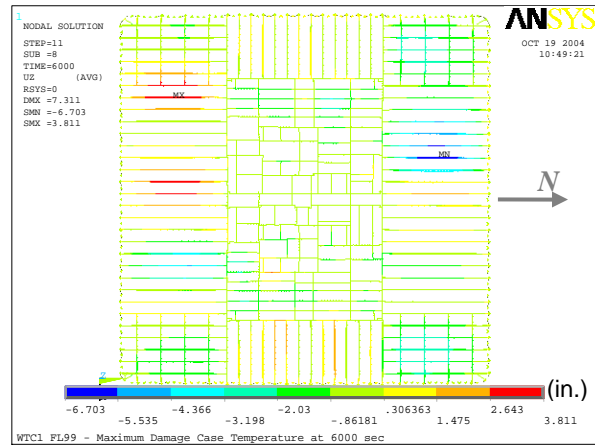


(b) Top view without slab

Figure A–27. Vertical displacement of WTC 1 Floor 98 for Case B_i temperature condition at 100 min (downward displacement is negative; 5x displacement magnification).



(a) Entire model



(b) Top view without slab

Figure A–28. Vertical displacement of WTC 1 Floor 99 for Case B_i temperature condition at 100 min (downward displacement is negative; 5x displacement magnification).

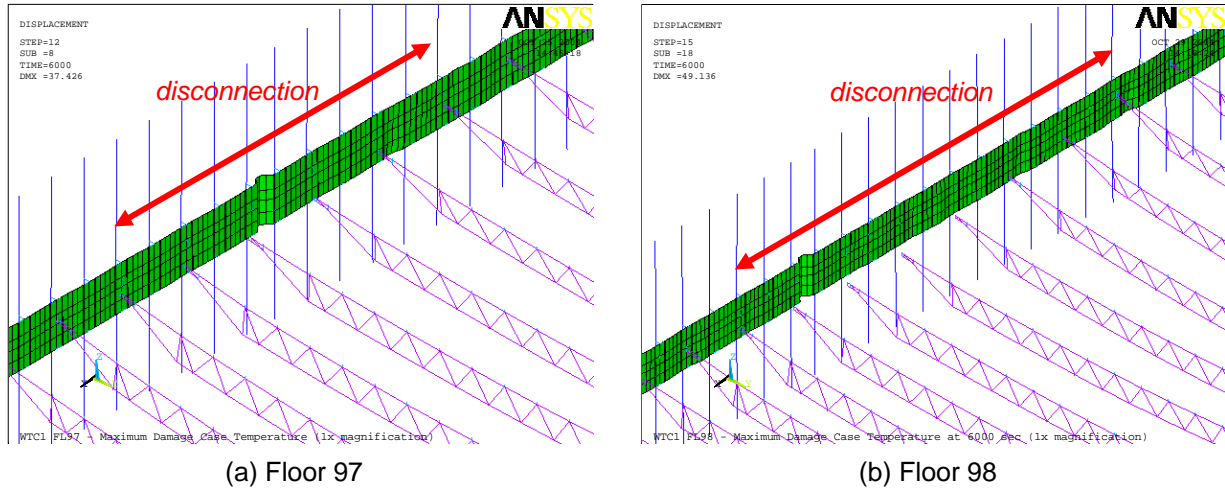


Figure A-29. Loss of vertical supports in WTC 1 Floor 97 and Floor 98 for Case B_i temperature condition at 100 min (1x displacement magnification).

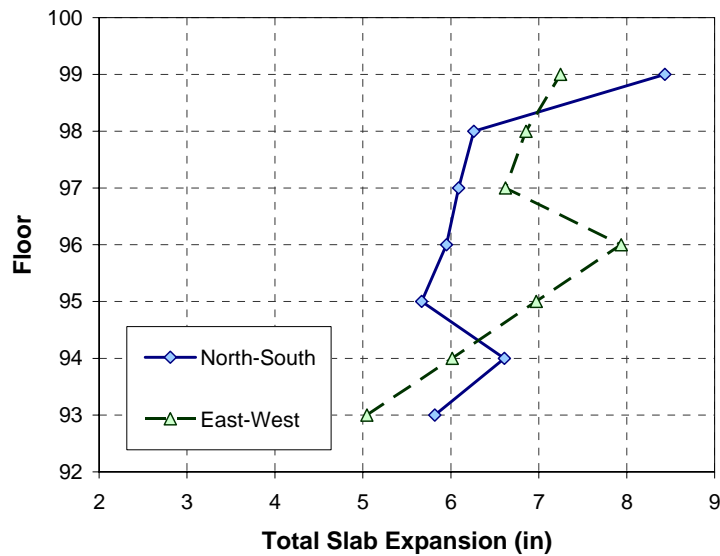


Figure A-30. Thermal expansion of floors of WTC 1 for Case B_i temperature condition at 100 min.

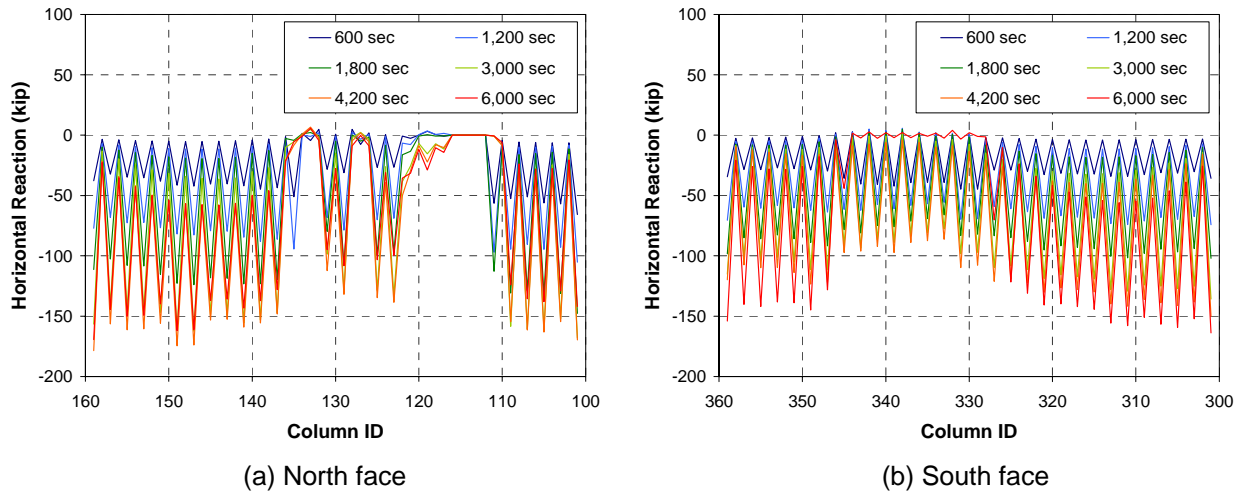


Figure A–31. Horizontal reaction force per column of WTC 1 Floor 98 for Case B_i temperature condition.

A.3 WTC 2 FLOORS

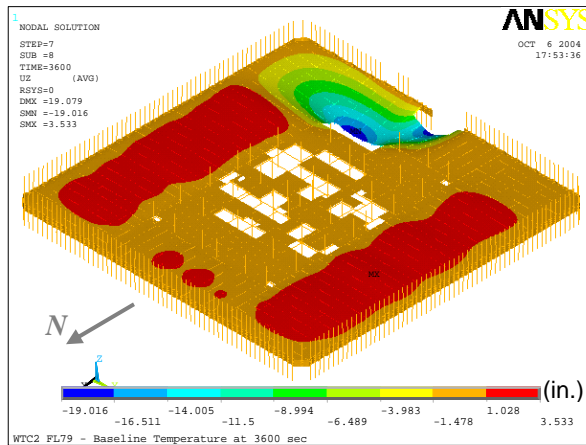
A.3.1 Case C_i Temperature Condition

Table A–3 gives the maximum vertical displacement of WTC 2 floors for Case C_i temperature condition, and Figs. A–32 to A–36 show the vertical displacements when the maximum displacement was obtained. Floor 79 to Floor 83, except Floor 82, had the maximum vertical displacement in the southeast area near the impact damage. Floor 82 had the maximum vertical displacement in the northeast area. The maximum displacement was projected to occur at 60 min on all floors. The vertical displacement in the west office area was found to be insignificant on all the floors throughout the thermal loading. Floor 80 had a fair amount of vertical displacement in the north half of the west office area although the maximum displacement was 15 in. A significant amount of web diagonals of Floor 82 to Floor 83 buckled in the hot zones of the east office area. Seat failures were not observed on Floor 79 to Floor 81. Trusses at Column 301 to Column 317 on the east face of Floor 82 and at Column 325 to Column 333 on the east face of Floor 83 lost their vertical support at the exterior seats at 50 min as shown in Fig. A–37. Figure A–38 shows the average total thermal expansion of floors over the entire width of the building at 60 min in two orthogonal directions. The total floor expansion ranged from 2.5 in. to 5.5 in. Figure A–39 shows horizontal reaction force at individual columns of the north and south faces of Floor 81. When the reaction force is positive, the column is pulled inward by the floor. Columns between Column 353 and Column 359 were pulled in by the floor. This was caused by the floor sagging in the southeast area that was primarily due to the impact damage to the interior truss seats. A few columns at the southeast corner of Floor 80 and Floor 83 were also pulled in by the floor.

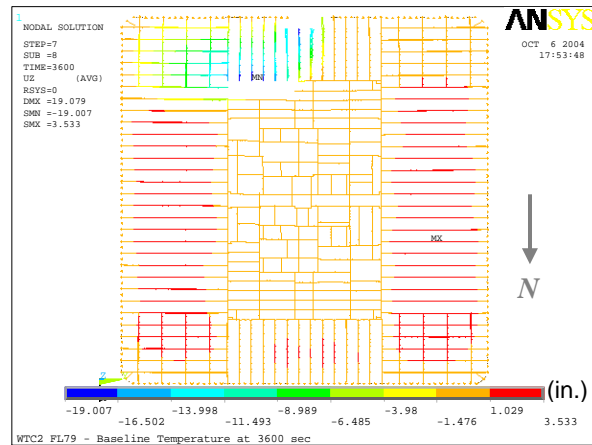
Table A–3. Maximum vertical displacement of WTC 2 floors for Case C_i temperature condition.

Floor	Max. Displacement (in.)	Time at the Maximum (min)
79	19.0	60
80	30.1	60
81	31.0	60
82	45.2	60
83	38.9	60

Note: Downward displacement is positive.

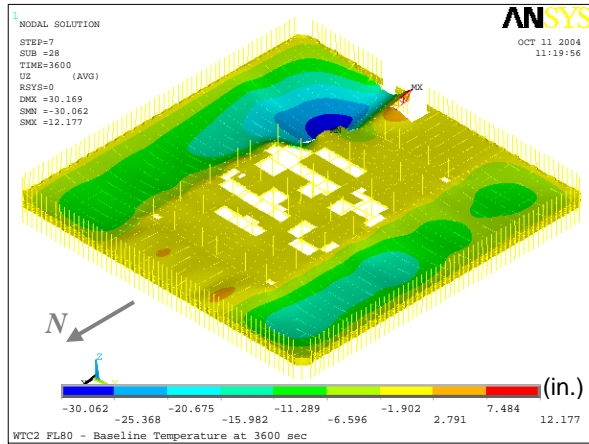


(a) Entire model

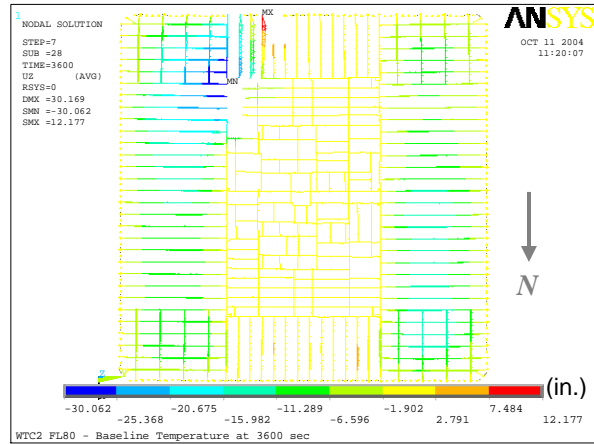


(b) Top view without slab

Figure A–32. Vertical displacement of WTC 2 Floor 79 for Case C_i temperature condition at 60 min (downward displacement is negative; 5x displacement magnification).

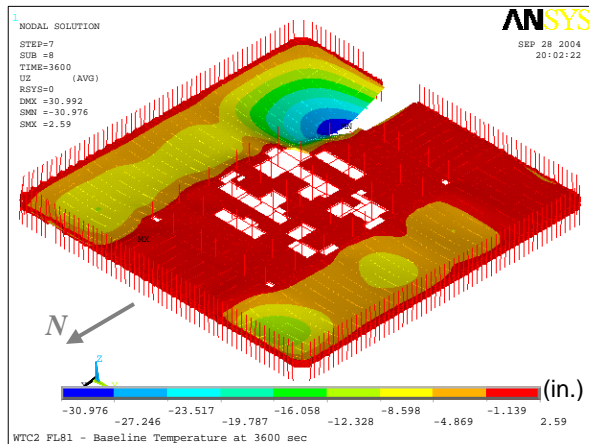


(a) Entire model

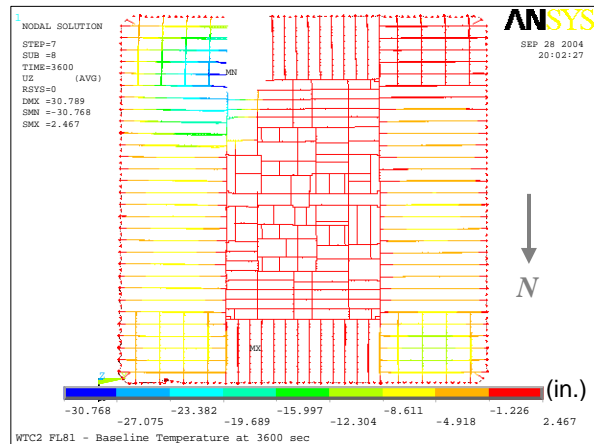


(b) Top view without slab

Figure A–33. Vertical displacement of WTC 2 Floor 80 for Case C_i temperature condition at 60 min (downward displacement is negative; 5x displacement magnification).

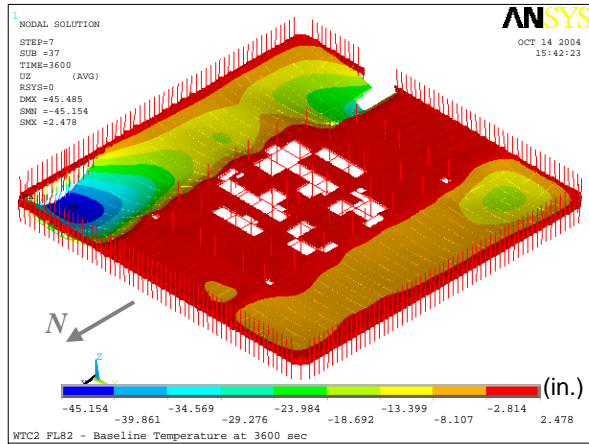


(a) Entire model

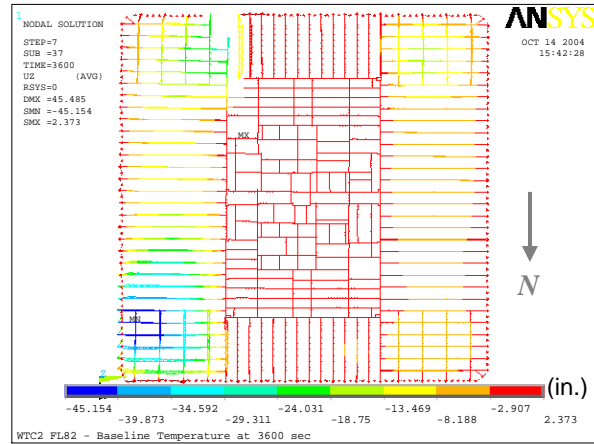


(b) Top view without slab

Figure A–34. Vertical displacement of WTC 2 Floor 81 for Case C_i temperature condition at 60 min (downward displacement is negative; 5x displacement magnification).

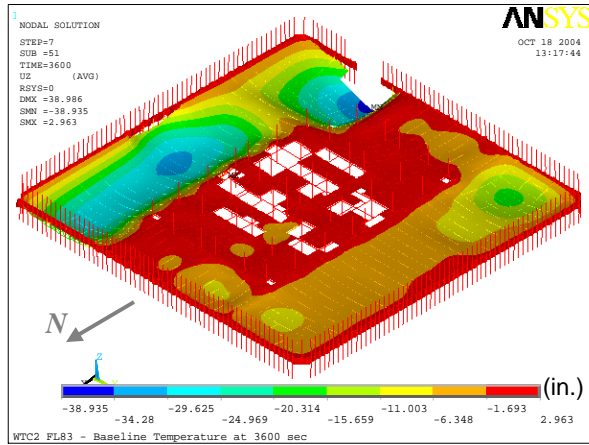


(a) Entire model

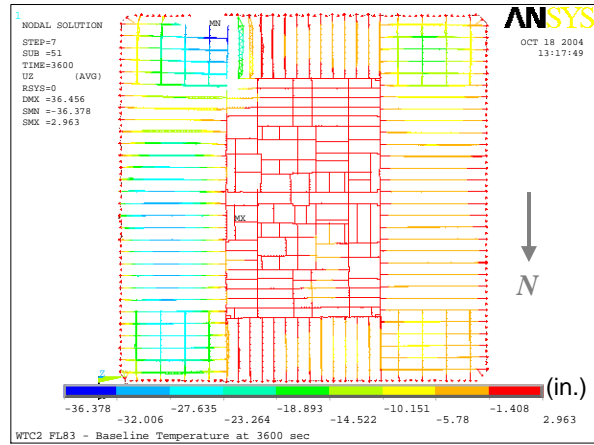


(b) Top view without slab

Figure A–35. Vertical displacement of WTC 2 Floor 82 for Case C_i temperature condition at 60 min (downward displacement is negative; 5x displacement magnification).

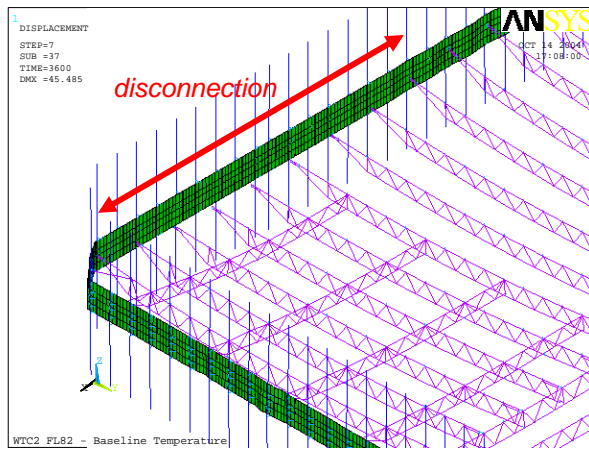


(a) Entire model

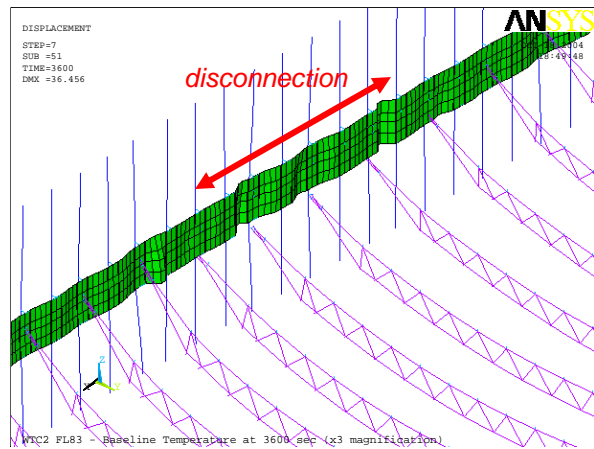


(b) Top view without slab

Figure A–36. Vertical displacement of WTC 2 Floor 83 for Case C_i temperature condition at 60 min (downward displacement is negative; 5x displacement magnification).



(a) Floor 82
(1X displacement magnification)



(b) Floor 83
(3X displacement magnification)

Figure A–37. Loss of vertical supports in WTC 2 Floor 82 and Floor 83 for Case C_i temperature condition at 60 min.

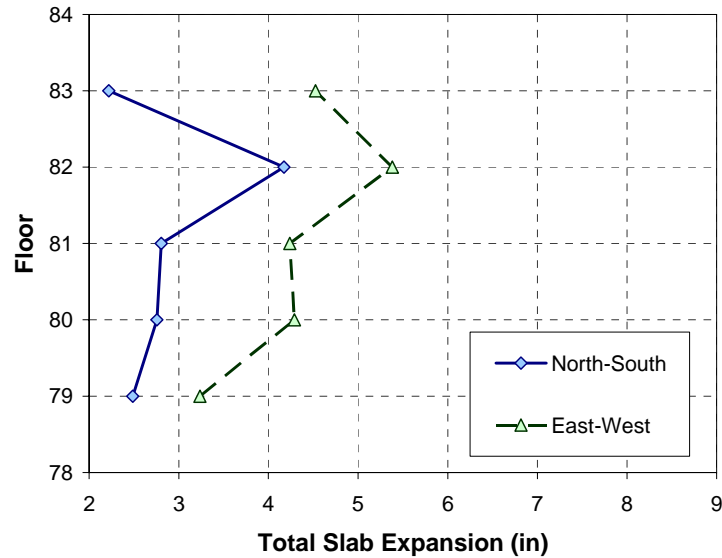


Figure A-38. Thermal expansion of floors of WTC 2 for Case C_i temperature condition at 60 min.

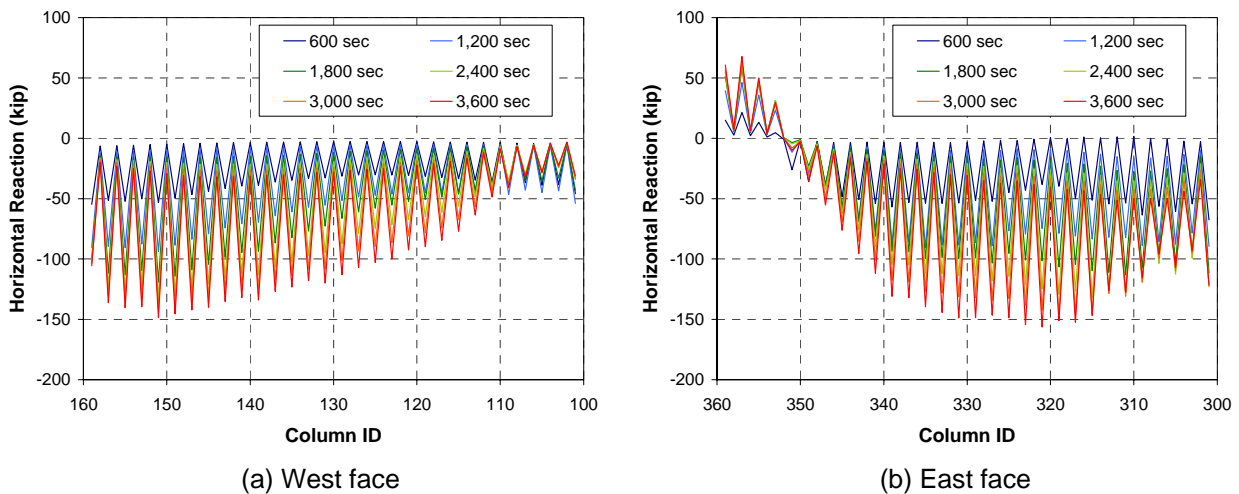


Figure A-39. Horizontal reaction force per column of WTC 2 Floor 81 for Case C_i temperature condition.

A.3.2 Case D_i Temperature Condition

Table A-4 gives the maximum vertical displacement of WTC 2 floors for Case D_i temperature condition, and Figs. A-40 to A-44 show the vertical displacements when the maximum displacement was obtained. Due to more impact damage and different temperature histories than Case C_i temperature condition, all floors had larger vertical displacement. Floor 80 and Floor 81 suffered damage to many interior seats in the east office area due to the aircraft impact. Bridging trusses that had been removed in Case C_i temperature condition were replaced in these two floors in order to support primary trusses of the east

office area after the impact. The maximum vertical displacement of 97 in. was calculated at Floor 81 near the impact damage at 50 min as shown in Fig. A–42. Significant sagging of the floor was observed at Floor 79 to Floor 83. Gusset plates and bolts at more than 75 percent of all the exterior seats of the east face of Floor 82 and Floor 83 failed due to horizontal shear force that was caused by the difference in the thermal expansion between the floor and the exterior wall in the direction transverse to the primary trusses. The truss at Column 357 of Floor 81 was the only truss that lost its vertical support at the exterior seat among all the floors. This truss walked off the truss seat. Figure A–45 shows the average total thermal expansion of floors over the entire width of the building at 60 min of Case D_i temperature condition. The total floor expansion ranged from 1 in. to 5 in. Figures A–46 and A–47 show horizontal reaction force at individual columns of the north and south faces of Floor 80 and Floor 82, respectively. Column 101 to Column 111 on the west face and Column 347 to Column 359 on the east face were pulled in by the floor at 60 min on Floor 80 because of the floor sagging occurring in the southeast area. Since core columns were not restrained in the horizontal directions, when the floor pulled in one face of exterior wall, the opposite face of the exterior wall would also be pulled in. Columns at the southeast corner were pulled in by the floor at Floor 79 and Floor 81. Many columns of the west face of Floor 82 were pulled inward, while reaction forces at many columns of the east face were close to zero. As described above, gusset plates and seat bolts failed at a number trusses on the east face of Floor 82. Because columns at these locations were not supported in the horizontal direction by the floor, the reaction force became close to zero at these columns.

Table A–4. Maximum vertical displacement of WTC 2 floors for Case D_i temperature condition.

Floor	Max. Displacement (in.)	Time at the Maximum (min)
79	35.8	60
80	65.6	40
81	96.7	50
82	49.4	60
83	44.6	60

Note: Downward displacement is positive.

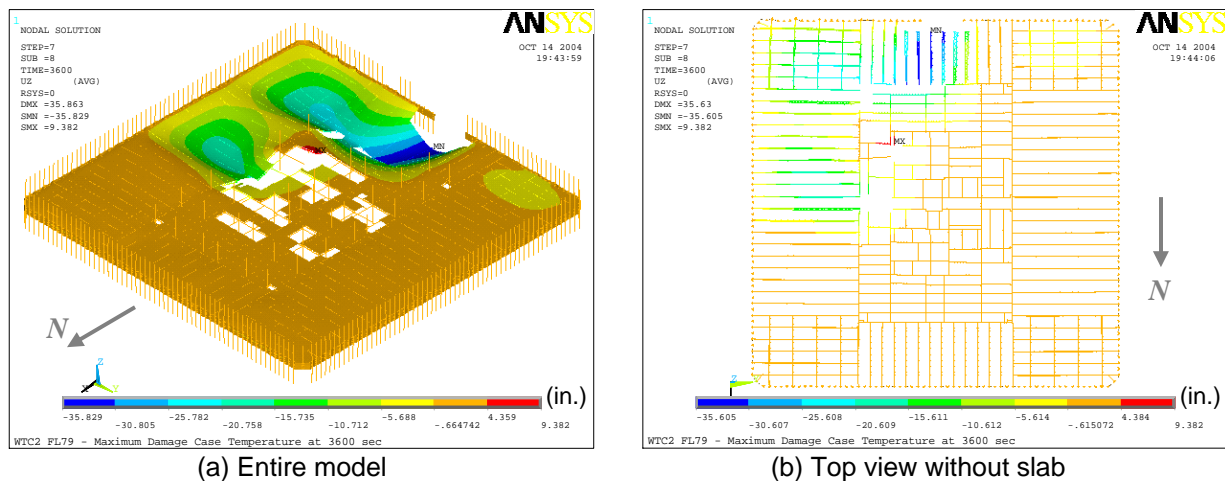
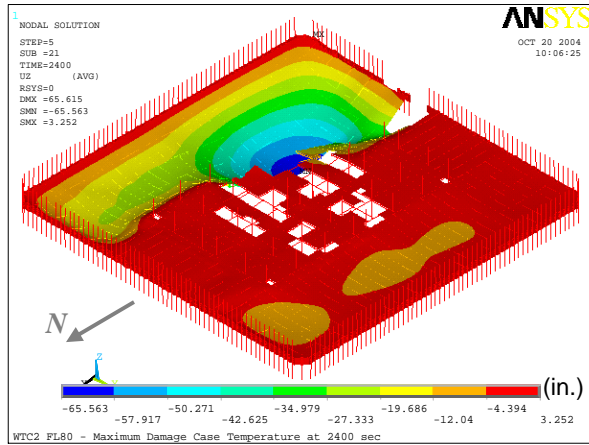
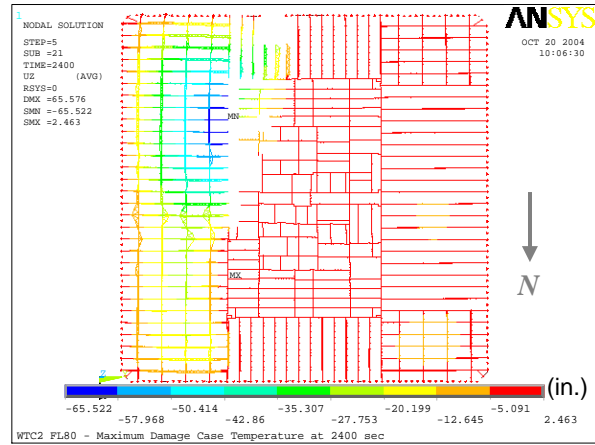


Figure A–40. Vertical displacement of WTC 2 Floor 79 for Case D_i temperature condition at 60 min (downward displacement is negative; 5x displacement magnification).

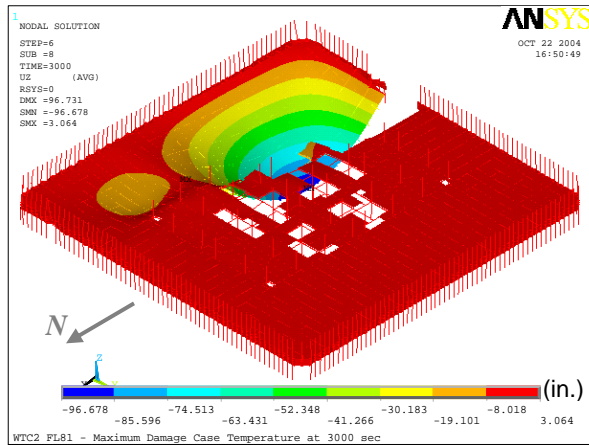


(a) Entire model

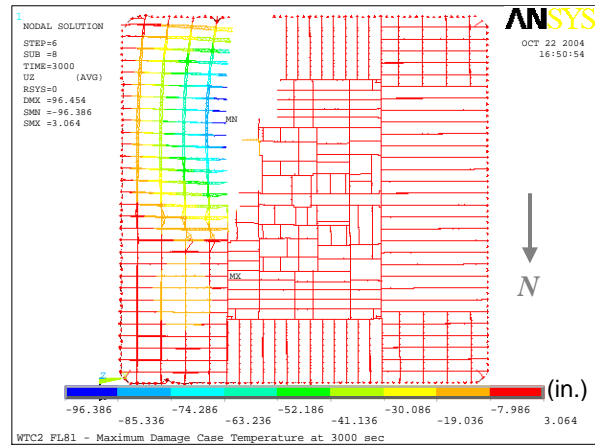


(b) Top view without slab

Figure A–41. Vertical displacement of WTC 2 Floor 80 for Case D_i temperature condition at 40 min (downward displacement is negative; 5x displacement magnification).

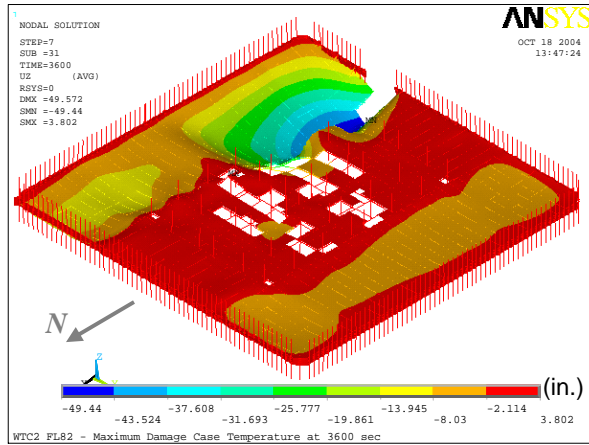


(a) Entire model

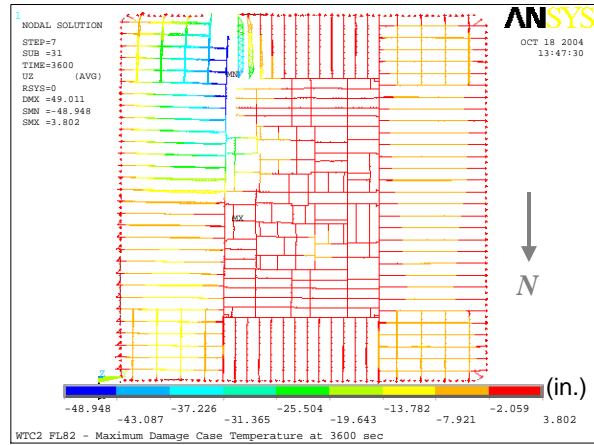


(b) Top view without slab

Figure A–42. Vertical displacement of WTC 2 Floor 81 for Case D_i temperature condition at 50 min (downward displacement is negative; 5x displacement magnification).

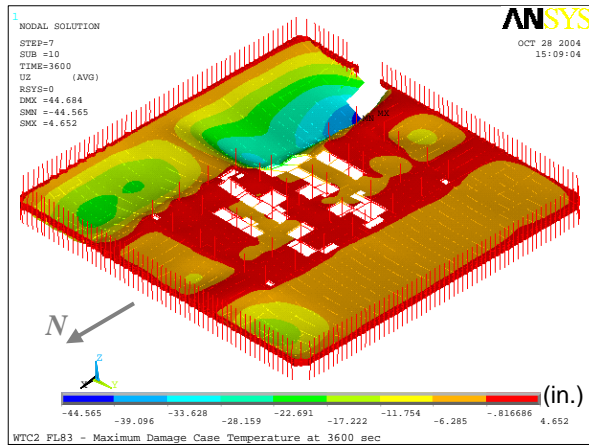


(a) Entire model

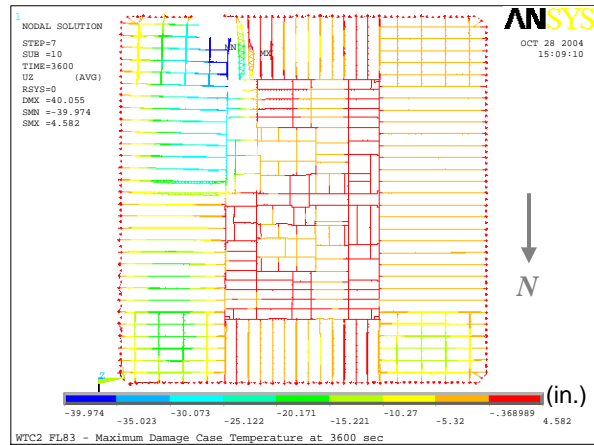


(b) Top view without slab

Figure A–43. Vertical displacement of WTC 2 Floor 82 for Case D_i temperature condition at 60 min (downward displacement is negative; 5x displacement magnification).



(a) Entire model



(b) Top view without slab

Figure A–44. Vertical displacement of WTC 2 Floor 83 for Case D_i temperature condition at 60 min (downward displacement is negative; 5x displacement magnification).

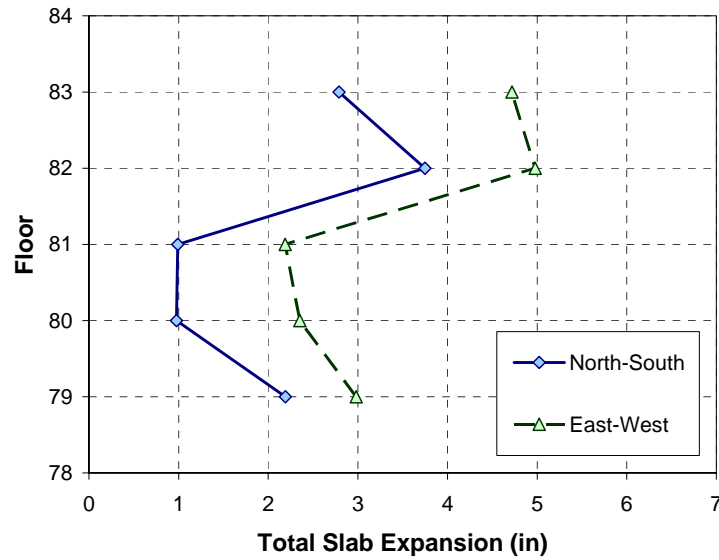


Figure A-45. Thermal expansion of floors of WTC 2 for Case D_i temperature condition at 60 min.

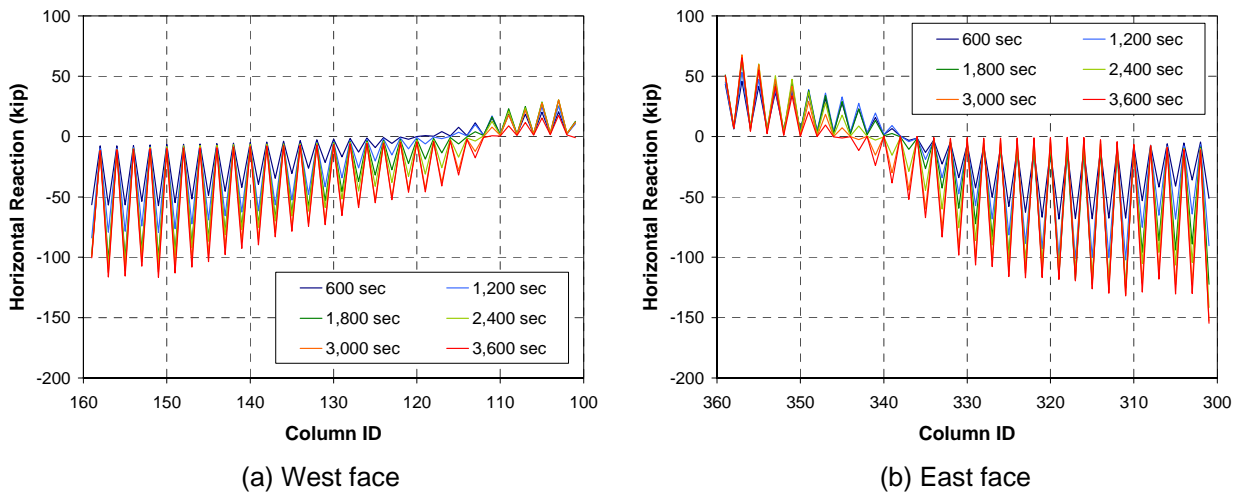


Figure A-46. Horizontal reaction force per column of WTC 2 Floor 80 for Case D_i temperature condition.

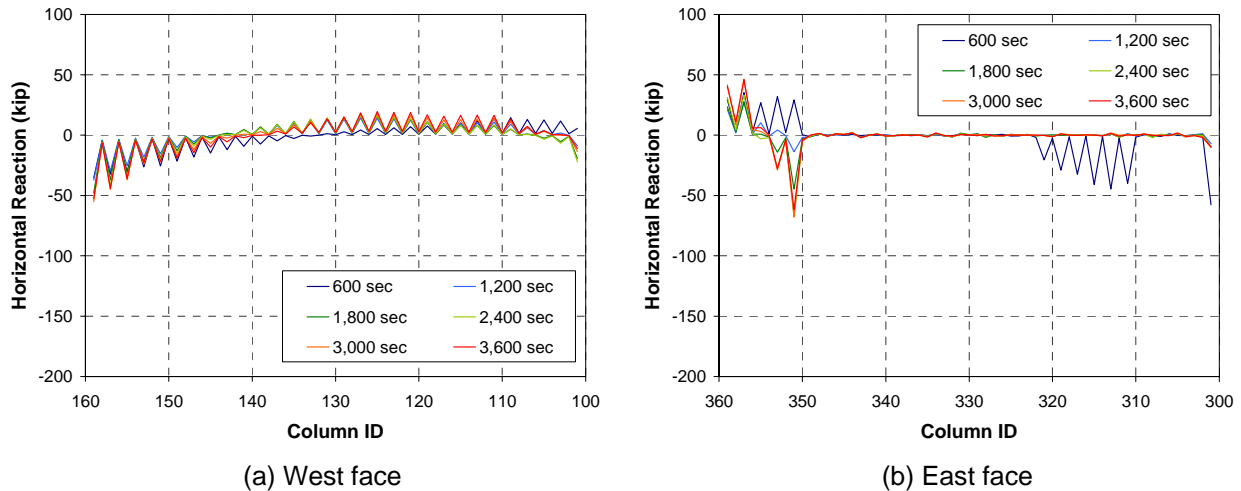


Figure A-47. Horizontal reaction force per column of WTC 2 Floor 82 for Case D_i temperature condition.

A.4 SUMMARY OF RESULTS

Figures A-48 and A-49 show conditions of the connections between the exterior wall and the floors predicted by the WTC 1 floor models at 100 min for Case A_i and Case B_i temperature conditions, and Figs. A-50 and A-51 show conditions of the connections between the exterior wall and the floors predicted by the WTC 2 floor models at 60 min for Case C_i and Case D_i temperature conditions. The figures show the following conditions:

- Condition 1: gusset plate failure + seat failure due to vertical shear (loss of vertical support)
- Condition 2: gusset plate failure + bolt shear-off + truss walk-off (loss of vertical support)
- Condition 3: gusset plate failure + bolt shear-off + significant displacement (>25 in.) of the floor in that area (floor remains vertically supported)
- Condition 4: tensile force between the exterior wall and the floor system (floor remains vertically connected, but exerts pull-in force on the exterior wall)

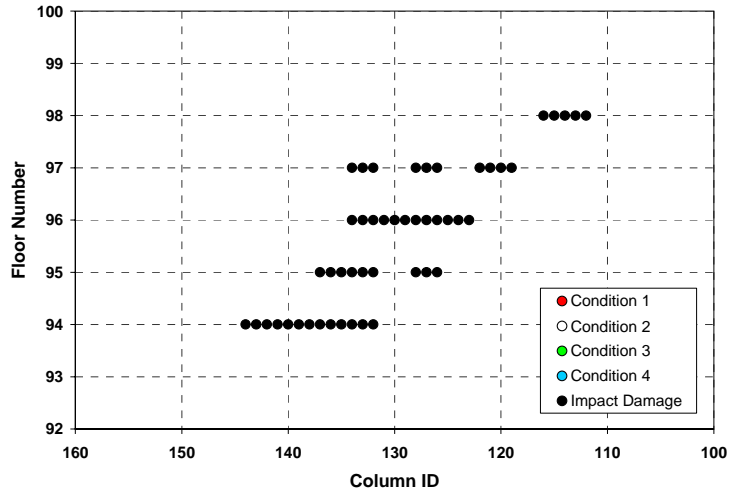
Conditions 1 and 2 were treated as the case of floor/wall disconnections. Conditions 3 and 4 were treated as the case where the floor pulled in the exterior wall.

The behaviors of the floor system found in the full floor models subjected to impact damage and elevated temperatures from the fires can be summarized as follows:

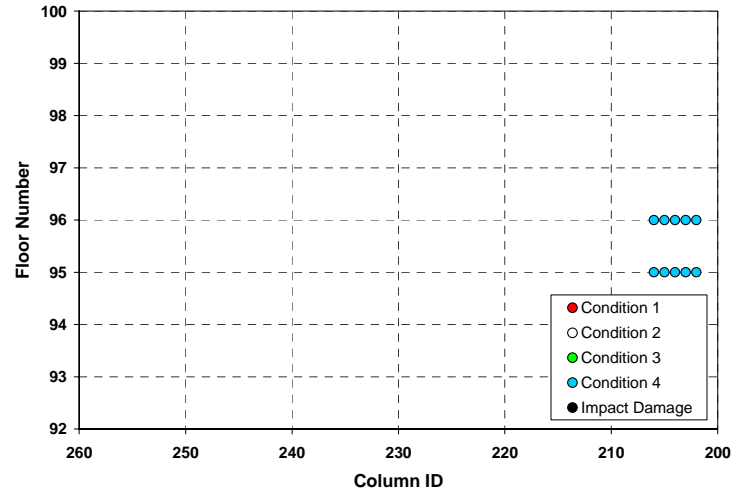
- Bridging trusses subjected to elevated temperatures buckled between primary trusses.
- When significant differences in thermal expansion of floors and exterior walls in the direction transverse to the axes of primary trusses occurred near the corners, studs, diagonal strap anchors, gusset plates, and seat bolts at exterior truss seats failed due to the lateral shear.
- Web diagonals of floor trusses with damaged thermal insulation buckled.

- Floors sagged into catenary forms.
- Truss seats disconnected from the exterior walls.

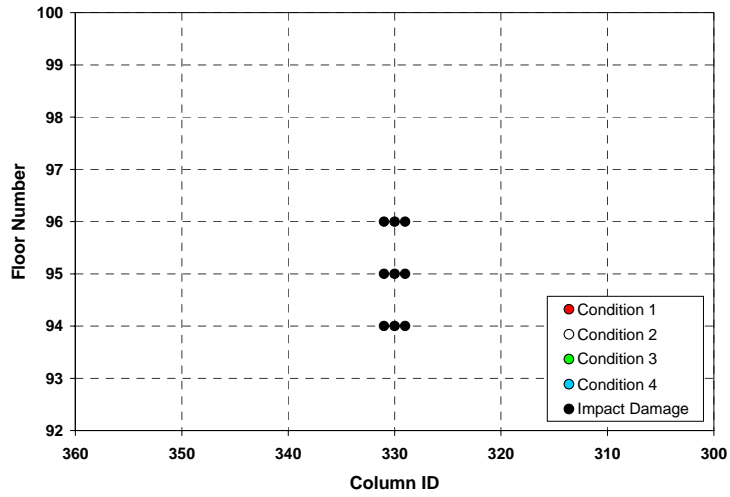
Pull-in forces were expected to develop whenever the floor sagged. Although the floor sagging was captured by the floor models in the heated area, the pull-in force on the exterior columns was not captured in most of the full floor model analyses. To accurately calculate pull-in forces between the floor and the exterior columns in the full floor model, much more detailed modeling would be required. Such modeling includes accurate boundary conditions on columns, creep in steel, friction at the truss seats, accurate evaluation of failure of strap anchors and studs, and concrete cracking and spalling. In addition, temperature time histories that were used in the full floor model analyses may be different if improved estimates of impact damage to insulation were obtained. Further discussion on the pull-in force can be found in Section 2.5.2 of this report.



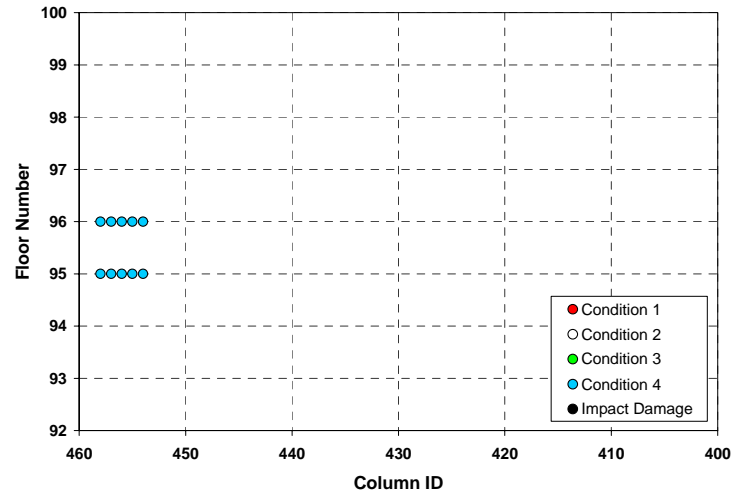
(a) North face



(b) East face

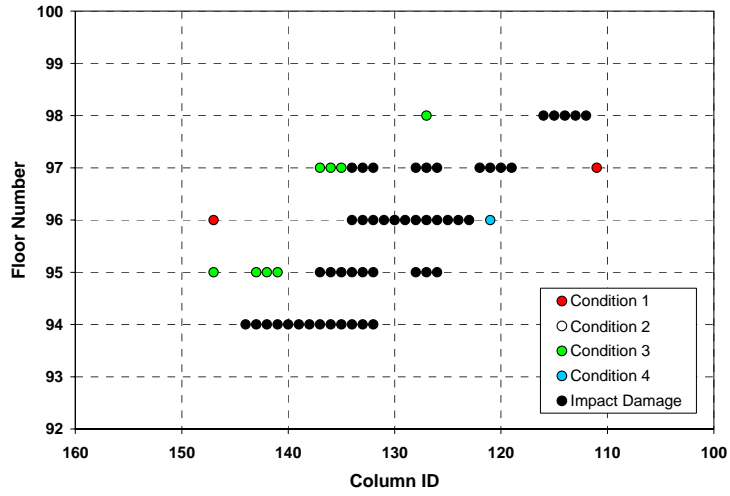


(c) South face

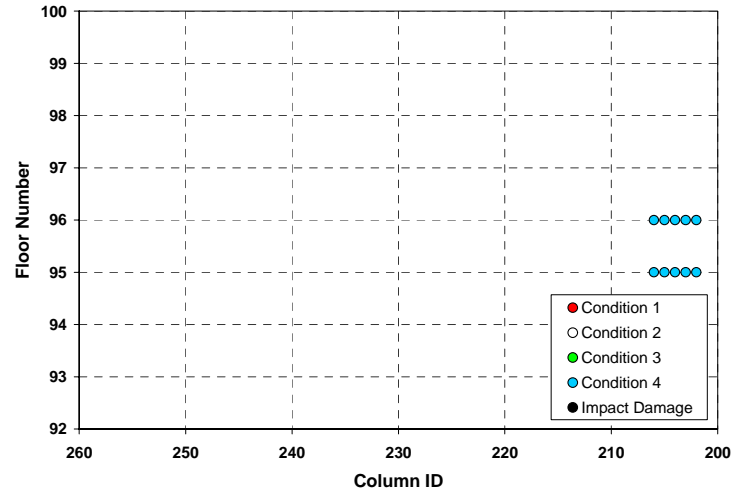


(d) West face

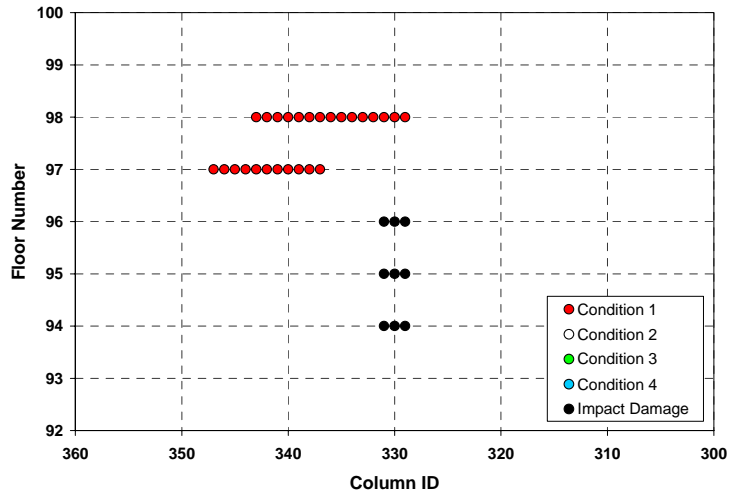
Figure A-48. Conditions of connections between the exterior wall and the floors of WTC 1 predicted for Case A_i temperature condition at 100 min.



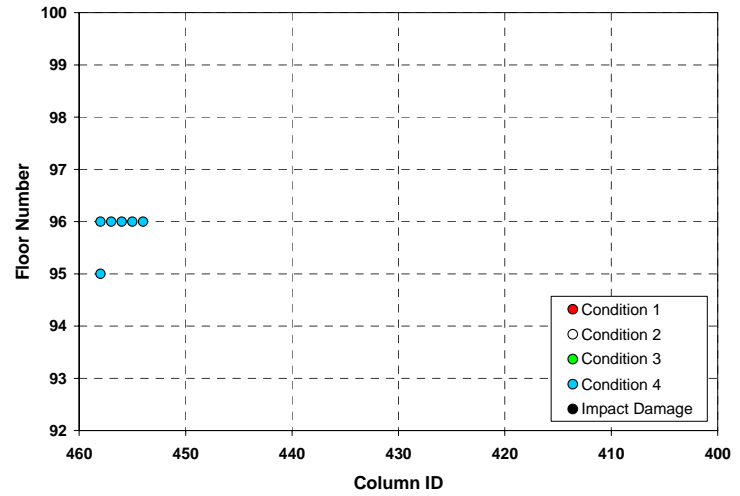
(a) North face



(b) East face

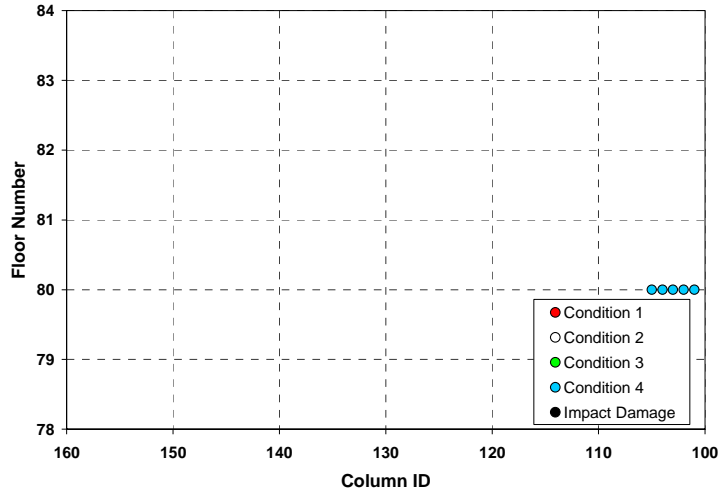


(c) South face

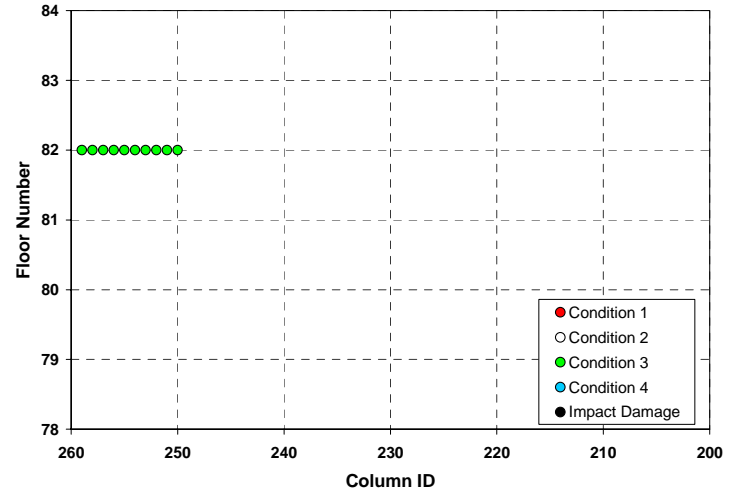


(d) West face

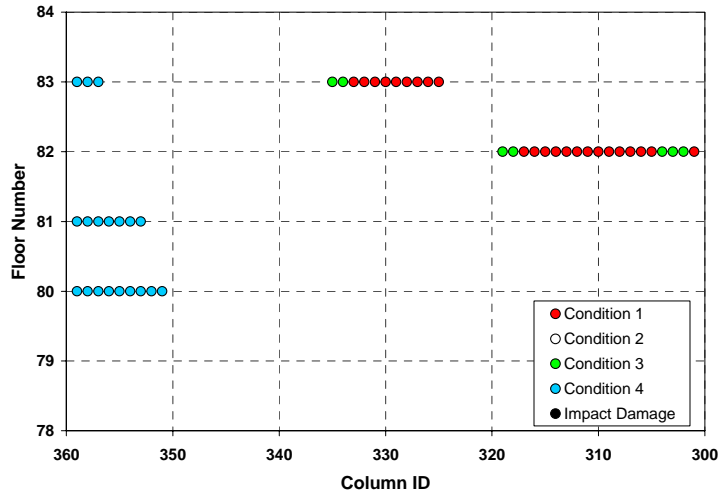
Figure A-49. Conditions of connections between the exterior wall and the floors of WTC 1 predicted for Case B_i temperature condition at 100 min.



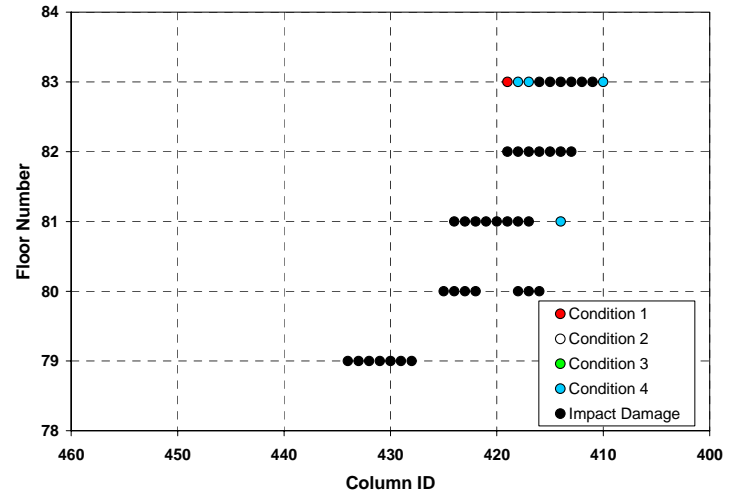
(a) West face



(b) North face

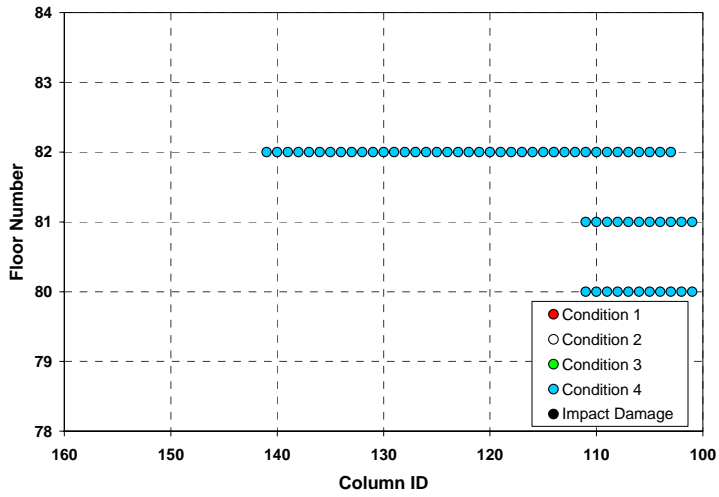


(c) East face

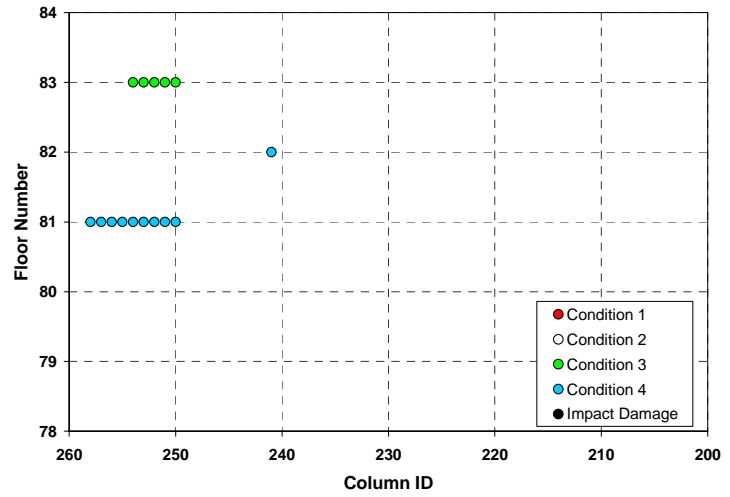


(d) South face

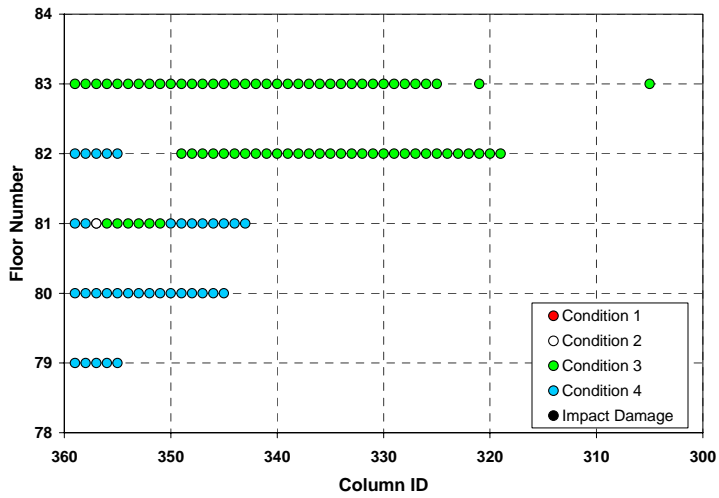
Figure A-50. Conditions of connections between the exterior wall and the floors of WTC 2 predicted for Case C_i temperature condition at 60 min.



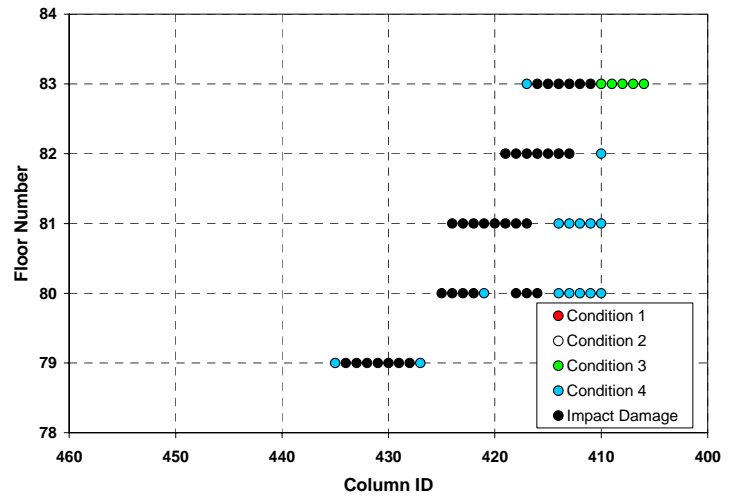
(a) West face



(b) North face



(c) East face



(d) South face

Figure A-51. Conditions of connections between the exterior wall and the floors of WTC 2 predicted for Case D_i temperature condition at 60 min.

This page intentionally left blank.

Appendix B

FLOOR TRUSS DYNAMIC RESPONSE DUE TO IMPACT OF DROPPING FLOOR

B.1 IMPACT OF DROPPING FLOOR

The failure of dropping floor may occur due to thermal and/or additional debris weight on the truss, and/or as a result of the aircraft impact. A floor truss or a group of floor trusses could lose support at both the exterior and interior supporting ends and drop onto the floor below. This failure mode, which is shown in Fig. B-1, will be referred to as *full truss drop*. Alternatively, a floor truss or a group of floor trusses could lose support on one side and drop down to impact the target floor below. This failure mode, which is also shown in Fig. B-1, will be referred to as *partial truss drop*.

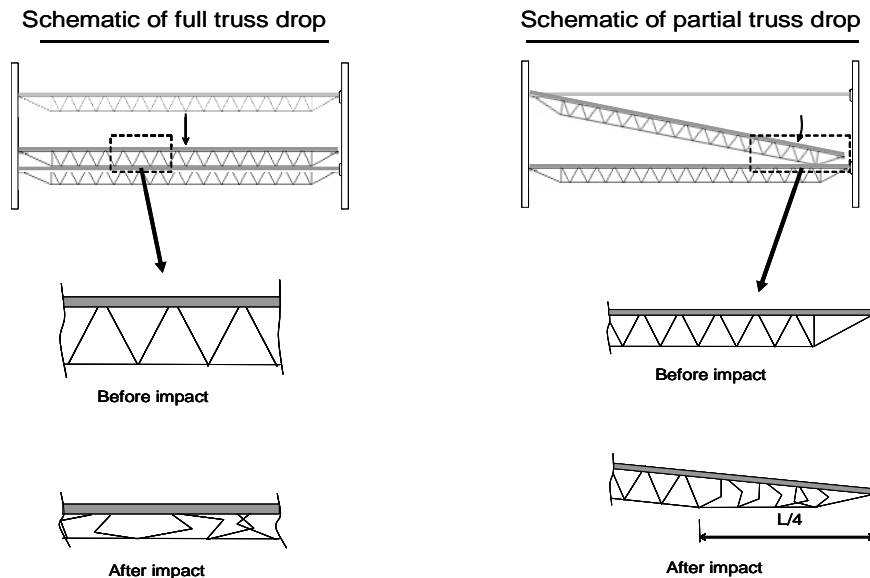


**Figure B-1. Schematic of full truss or partial truss drop
and web diagonal crushing at impact.**

B.2 PURPOSE AND SCOPE

The purpose of this study is to determine the dynamic response of the target truss from the impact of full and partial truss drop, to determine whether the target truss seats can resist such an impact load, and to determine whether the target truss will lose its composite action, sag significantly, and consequently fail to restrain the exterior column to which it is connected against instability.

B.3 METHOD OF ANALYSIS

The simulation of a floor drop is idealized with a truss drop. This has inherent assumptions that all seats for the floor fail simultaneously to cause a full or partial drop. The dynamic response of the target truss from the impact of a dropping truss is calculated using conservation of energy principle. The potential energy of the truss just before drop, which is a function of drop height, converts to the kinetic energy of the truss just before impact. As the dropping truss starts to impact the target truss, the web diagonal members of the dropping truss are assumed to deform plastically to absorb some of the kinetic energy. The energy absorption due to crushing of the furniture and partitions are neglected in this study. The energy absorption due to web diagonal member crushing reduces the kinetic energy available at impact to deform the target truss. All the web diagonal members are assumed to deform plastically for the full truss drop case, while only one quarter of the web diagonal members are assumed to deform plastically for partial truss drop, representing one quarter of the length of the truss that may come in contact at impact with the floor below. The kinetic energy loss at the time of impact of the dropping truss and the target truss is calculated based on conservation of momentum. The two trusses are assumed to travel together after the impact, at one-half of the velocity of the dropping floor before impact.

The dynamic load due to the impact of the dropping truss onto the target truss will cause the target truss to deform plastically beyond the static load due to the weight of the two trusses. The maximum dynamic deformation of the trusses is calculated by conservation of energy principle assuming that the resistance of the truss is a bilinear function of displacement. This assumption is based on fitting the acceleration-deflection relationship of target truss, calculated with finite element analysis, as shown in Fig. B-2.

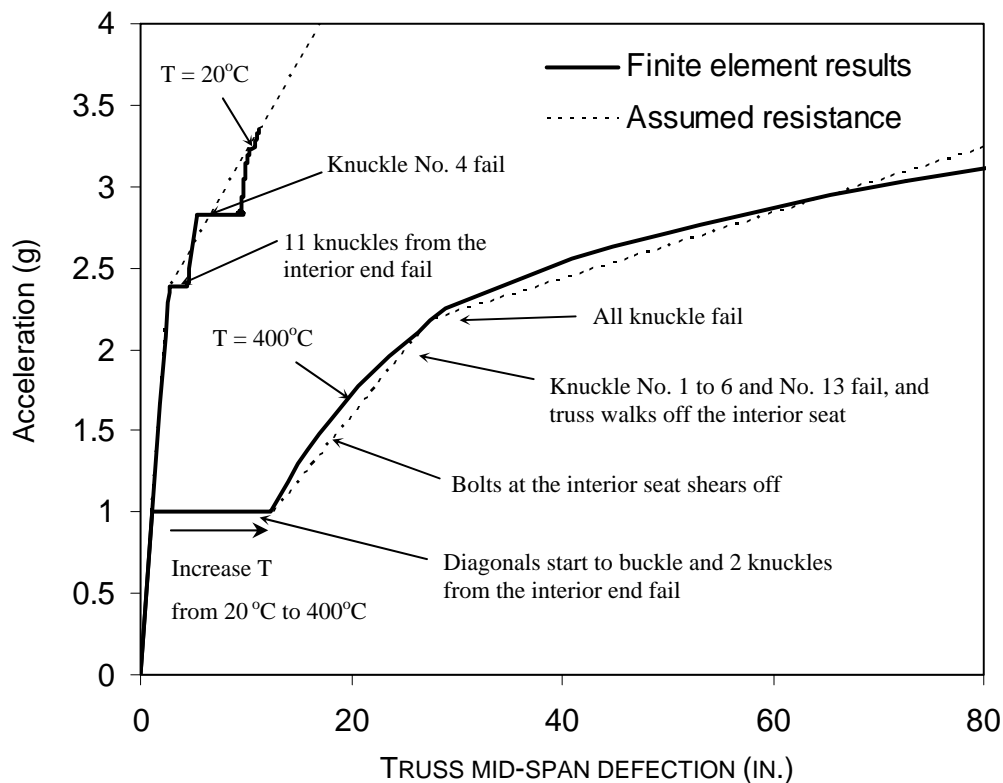


Figure B-2. Target truss resistance against increasing acceleration.

B.4 RESULTS

The ratios of demand-to-seat capacity for the gravity loads of the dropped and impacted trusses moving together for temperatures of 20 °C, 400 °C, 600 °C, and 700 °C, and the gravity plus dynamic impact loads for temperatures of 20 °C and 400 °C, are calculated. A demand-to-capacity ratio of less than one shows that the truss seat has sufficient capacity to resist the load, and a demand-to-capacity ratio of larger than one implies that the seat could fail. The range of the demand-to-capacity ratios is due to the different assumptions for the amount of energy loss due to crushing of the web diagonal members of the dropped truss.

The demand-to-capacity ratio of the long-span truss for gravity loads is shown in Table B–1 and for gravity plus impact loads is shown in Table B–2. The result for gravity loads alone shows the both the exterior and interior truss seats have sufficient capacity to support the weight of two floors for all temperatures considered. The result for gravity plus impact loads shows that at temperatures below 400 °C neither the exterior nor interior truss seats is expected to fail. Peak deflection response due to gravity and the dynamic impact of the dropping truss is given in Table B–3. The results show that at room temperature, and more so at 400 °C, the impacted truss will deflect to an extent that it loses composite action and becomes a catenary. At 400 °C the truss walks off the interior seat. Obviously, a catenary truss is not able to restrain the exterior column against transverse movement and cannot restrain it from instability. Although a truss response to increasing acceleration at 700 °C was not developed, the strength reduction of the truss seats clearly indicates that the failure of truss seats will occur.

Table B–1. Demand-to-capacity ratio of long-span truss for static gravity load.

Temp. (°C)	Demand (kip)	Capacity (kip)		Demand/Capacity	
		Int. Seat	Ext. Seat	Int. Seat	Ext. Seat
20	26.4	187.3	140.0	0.14	0.19
400	26.4	166.9	125.7	0.16	0.21
600	26.4	81.6	77.8	0.32	0.34
700	26.4	37.2	35.5	0.71	0.74

Table B–2. Demand-to-capacity ratio of long-span truss for dynamic impact load from full truss drop.

Temp. (°C)	Demand (kip)			Capacity (kip)		Demand / Capacity					
				Int. Seat	Ext. Seat	Int. Seat			Ext. Seat		
20	38.6	-	65.3	187.3	140.0	0.21	-	0.35	0.28	-	0.47
400	39.1	-	45.2	166.9	125.7	0.23	-	0.27	0.31	-	0.36

Table B–3. Peak deflection response due to static gravity and dynamic impact.

Temp. (°C)	Static Deflection (in.)	Dynamic Deflection (in.)		
20	2.3	7.6	-	25.4
400	24.2	66.4	-	89.6

B.5 CONCLUSIONS

At room temperature, the impact of a dropping truss will not cause failure of truss seats, but will cause the impacted truss to deform into a catenary. At 400 °C, the impacted truss will walk off the interior seat. In either case the impacted floor will not restrain the exterior column against transverse movement and instability. The impact of a dropping truss at 700 °C will cause failure of truss seats.

Appendix C

GLOBAL ANALYSIS WITHOUT CREEP

The analysis results presented in this Appendix were obtained from the preliminary global analyses that were performed neglecting the effects of creep and inelastic buckling of columns. These analyses were primarily used to study the interaction between various structural components in the overall global response of the towers. Because of the significant role that creep played in the collapse process, the results from these analyses are presented without making any conclusive remarks about the collapse sequence of the towers.

C.1 WTC 1 GLOBAL ANALYSIS WITHOUT CREEP

The WTC 1 ANSYS model without creep was analyzed with Case A_i structural damage condition and subjected to Case A_i temperature time histories. Temperature-dependent plasticity and the nonlinear geometry were the major sources of nonlinearity in the model. Table C–1 summarizes the sequence of analyses that were conducted with the WTC 1 ANSYS model with Case A_i conditions (see Section 2.2 for Case A_i structural damage condition). The results of each analysis step were used as the initial conditions for the next. Case B_i was not considered for preliminary global analysis, as the lack of creep and inelastic buckling behaviors limited the usefulness of repeating this analysis.

Table C–1. Analysis Steps of WTC 1 ANSYS global model for Case A_i conditions.

Analysis Step	Description
1	WTC 1 model below Floor 106 was analyzed under its own self-weight.
2	Structures above Floor 106 were added in a stress-free state, and the model was analyzed for dead load including those above Floor 106.
3	Superimposed dead load and 25 percent of the design live loads were superimposed on the model.
4	Columns, spandrels, and floor elements that were severed during aircraft impact were removed, and the model was analyzed.
5	Column and spandrel temperatures were ramped up linearly to temperatures at 10 min.
6	Column and spandrel temperatures were changed linearly from temperatures at 10 min to 20 min.
7	Column and spandrel temperatures were changed linearly from temperatures at 20 min to 30 min.
8	Column and spandrel temperatures were changed linearly from temperatures at 30 min to 50 min.
9	Column and spandrel temperatures were changed linearly from temperatures at 50 min to 100 min.

The model was first analyzed to capture the effects of the construction sequence (analysis steps 1, 2, and 3). The results of analysis for Step 3 represent the state before the aircraft impact. In analysis step 4, the columns, spandrels, and floor elements that were severed during the aircraft impact were removed from the model, and the building was reanalyzed to redistribute the load to the non-severed members. The results of this analysis represent the state of the building after the aircraft impact. After load redistribution, the column and spandrel temperatures provided by NIST at 10 min intervals were applied to the model (analysis steps 5 through 9). Temperatures were calculated by linear interpolation for times in between 10 min intervals. In order to reduce computation time, the temperature data sets for which

temperatures remained approximately linear with time during the interval from the previous and the following temperature data sets were eliminated from the analyses. Based on this elimination, temperature analyses were performed at 10 min, 20 min, 30 min, 50 min, and 100 min. Temperatures were not applied to the floor elements to prevent unrealistic buckling of floors. As discussed earlier, the floors in the global models did not include the floor trusses and were modeled by plate elements to match their membrane stiffness; the bending stiffness of the floors was not modeled accurately.

The results of the WTC 1 global model analyses for Case A_i conditions are summarized in Figs. C-1 through C-9.

Figure C-1 shows the total displacement at different analysis steps. The maximum displacement was obtained right after aircraft impact and was equal to 4.9 in. This displacement was gradually reduced to 4.1 in. at the end of 100 min due to thermal expansion of core and exterior columns between Floor 93 and Floor 98. Figures C-2 and C-3 show the total displacements for north, south, and east exterior walls before and after aircraft impact and at 50 min and 100 min. The total displacements for the west exterior wall are not shown as they were similar to the east exterior wall. The displacements were typically at their maximum right after aircraft impact around the hat truss and gradually decreased with time, reaching their minimum value at 50 min to 100 min in the aircraft damage zone.

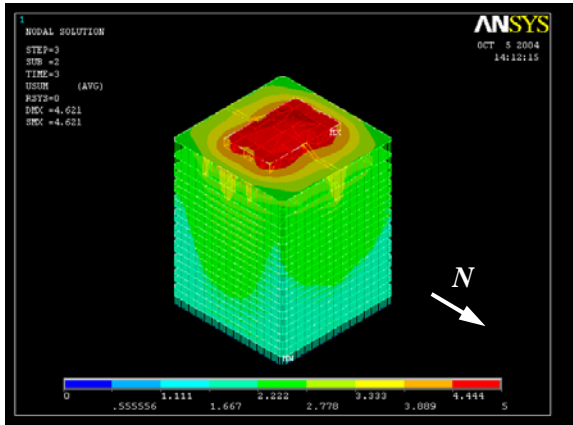
Figures C-4 and C-5 show the axial load variations over north, south, and east exterior wall columns and spandrels before and after aircraft impact and at 50 min and 100 min. After the aircraft impact, the loads carried by the severed columns of the north wall were primarily redistributed to the remaining columns of the north wall and also to the core and other exterior walls. As a result of this redistribution, the maximum column load increased from 265 kip to 1,200 kip on the north exterior wall and from 268 kip to 380 kip on the south exterior wall. The 1,200 kip load occurred in a column adjacent to the impact damage area. The column loads on the east and west walls slightly increased in the south side of the walls. With increasing time, the maximum column load in the south wall increased from 380 kip after aircraft impact to 670 kip at the end of 100 min. This increase was primarily due to the steady increase of column temperatures on the south wall.

Figure C-6 shows the total column loads in the core columns and the north, south, east, and west exterior walls for several floors at the end of each analysis step. Due to the removal of severed columns, spandrels, and floor elements, the total column loads below Floor 98 after aircraft impact did not equal the total column loads before the aircraft impact.

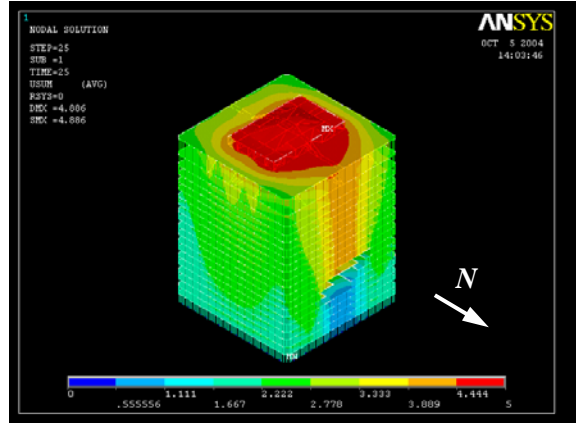
After the aircraft impact, the total load in core columns increased about 1,000 kip, in the east exterior wall columns about 200 kip, and in the west exterior wall columns about 150 kip, whereas the total load decreased in the north wall columns about 1,150 kip and in the south wall columns about 200 kip. With increasing time, the temperatures in the core and the south exterior wall columns increased more than the other exterior wall columns, causing relative thermal expansion. Relative thermal expansion caused the core and the south exterior wall columns to attract more load, and the exterior walls on the north, east, and west sides to unload. The increase in loads due to thermal expansion of the core columns increased the plastic strains with time and the resulting shortening caused the unloading of the core columns at 30 min. As time approaches 100 min, the temperatures of all columns dropped down, and the effects of thermal expansion decreased. This can be seen in the loads at 100 min, where core columns unloaded and redistributed load to each exterior wall (about 3,500 kip). About 32 percent of the redistributed load was

transferred to each of the east and west exterior wall columns, and 18 percent to each of the north and south exterior wall columns.

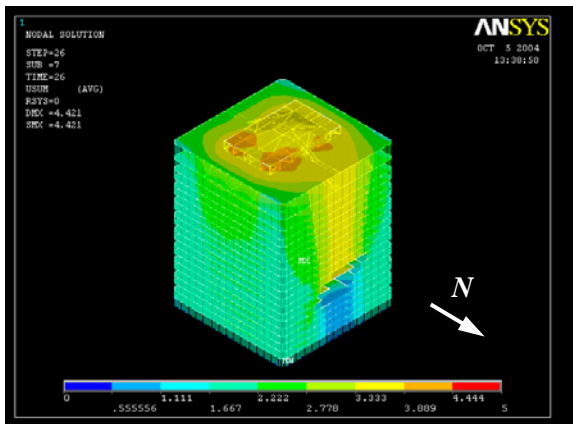
Figures C-7, C-8, and C-9 show the ratio of elastic-plus-plastic strain to the temperature-dependent yield strain of the core columns between Floor 96 and Floor 97 before and after aircraft impact and at 10 min, 20 min, 50 min, and 100 min. As can be noticed, the elastic-plus-plastic strain in the core columns before aircraft impact was typically 50 percent to 60 percent less than the yield strains at room temperature. After the aircraft impact, except for Column 504, the maximum strain ratio did not get beyond 1.0, indicating that almost all core columns remained in the elastic range. With increasing time and temperatures, the strain ratios started to increase, especially in the west and the south sides of the core. Strain ratios reached their maximum at the end of 50 min and remained almost constant till the end at about 100 min. Higher strain ratios were clustered around west and south side core columns, indicating a tendency to tilt toward the south and west.



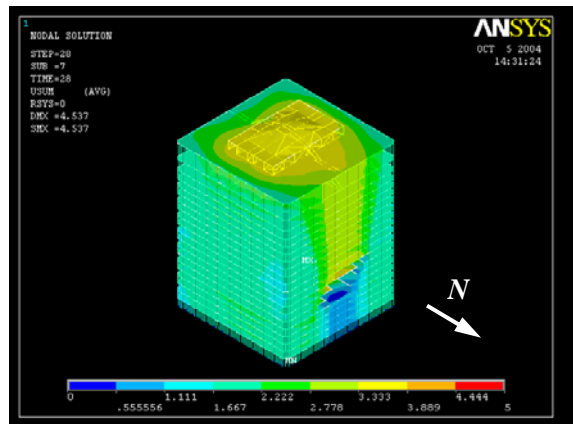
(a) Before impact



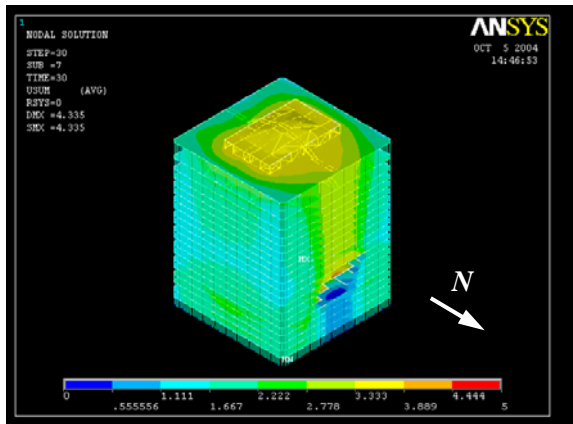
(b) After impact



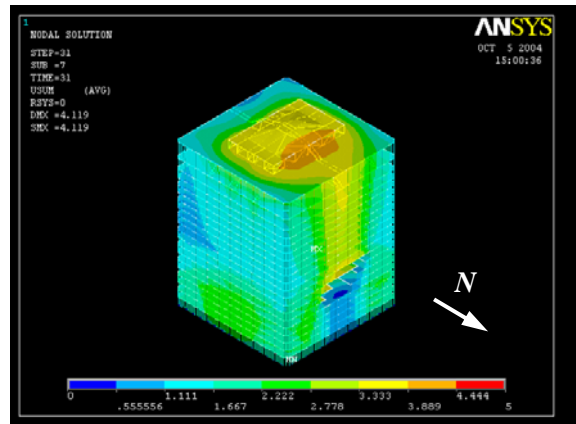
(c) At 10 min



(d) At 30 min

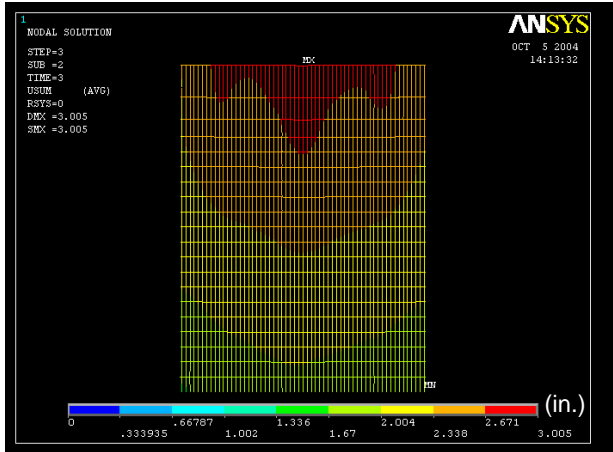


(e) At 50 min

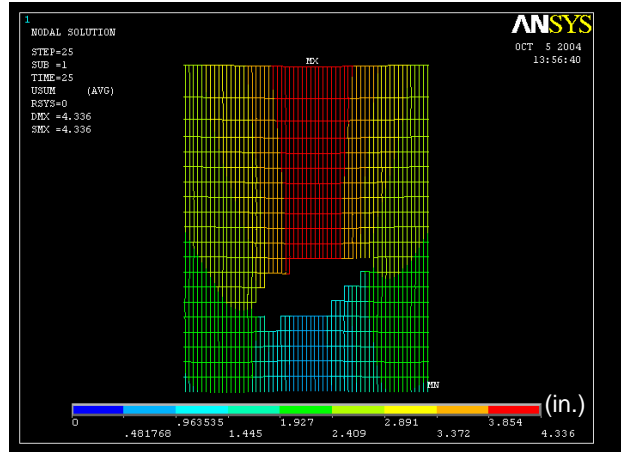


(f) At 100 min

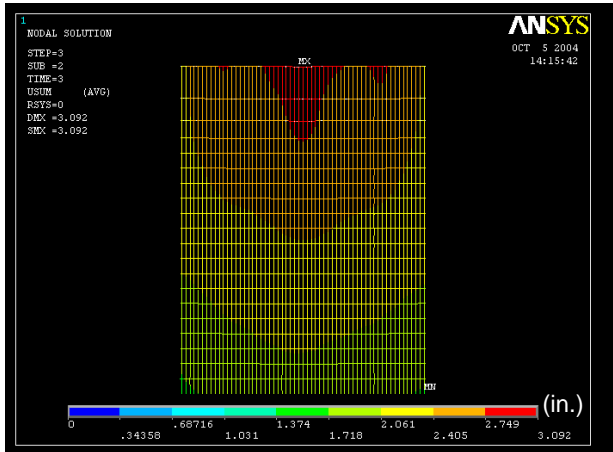
Figure C-1. Total displacement at different stages of WTC 1 for Case A_i conditions.



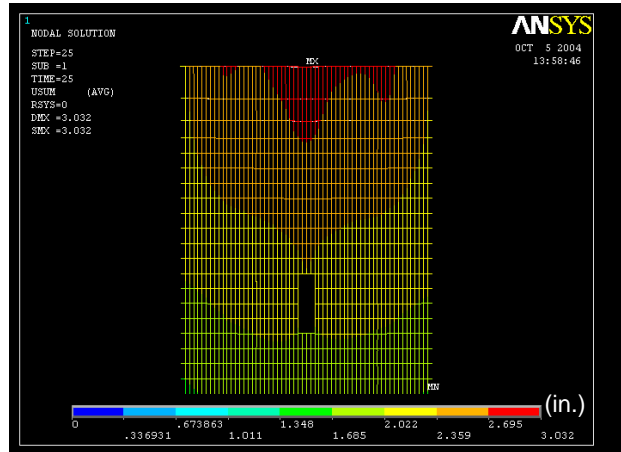
(a) North wall before impact



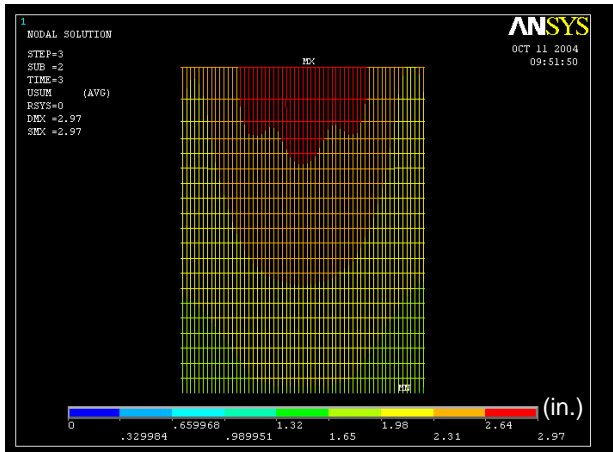
(b) North wall after impact



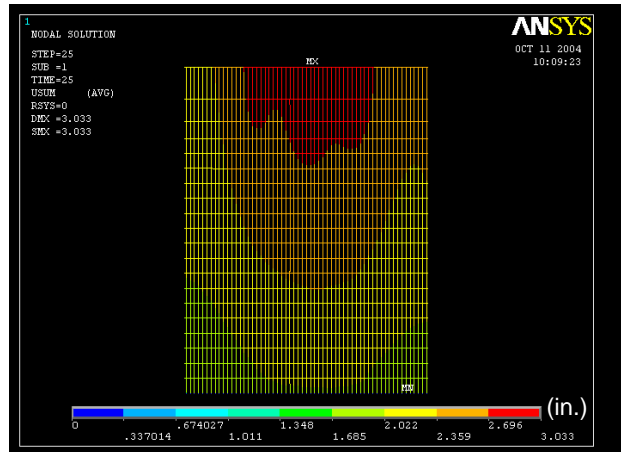
(c) South wall before impact



(d) South wall after impact

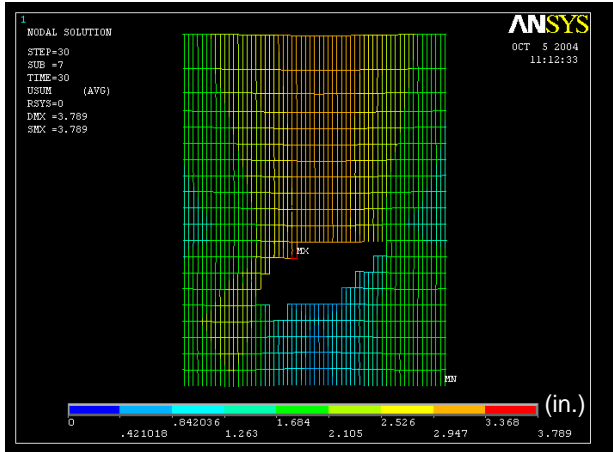


(e) East wall before impact

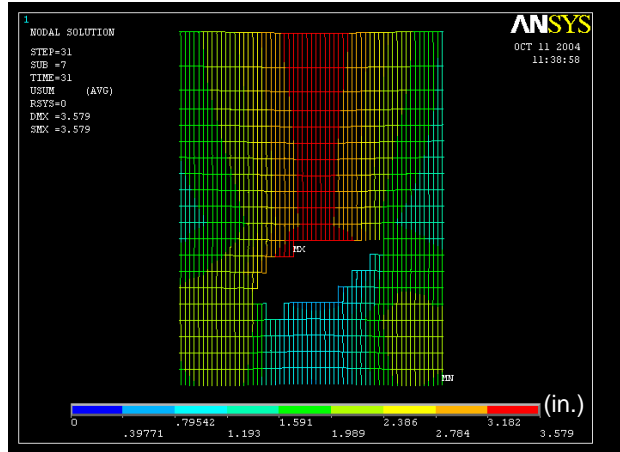


(f) East wall after impact

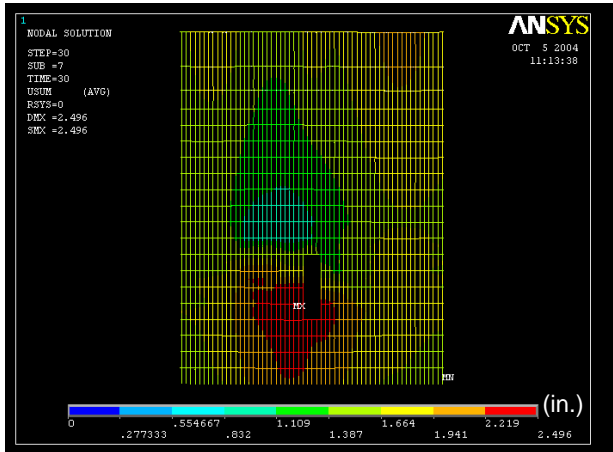
Figure C-2. Total displacement on the north, south, and east faces of the WTC 1 before and after aircraft impact (looking from outside).



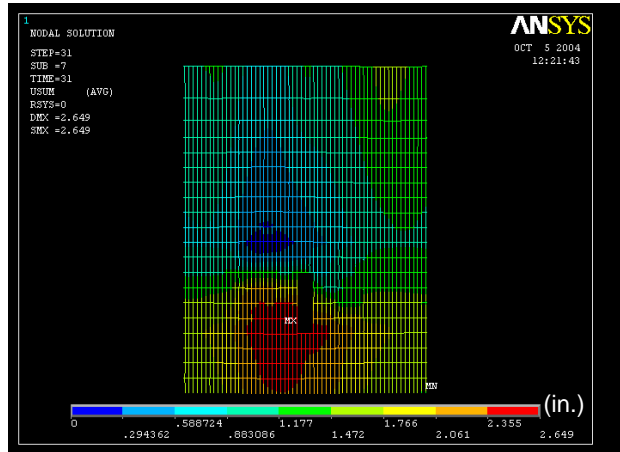
(a) North wall at 50 min



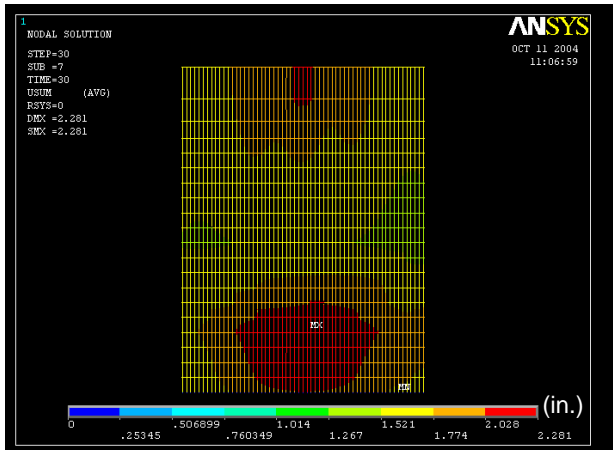
(b) North wall at 100 min



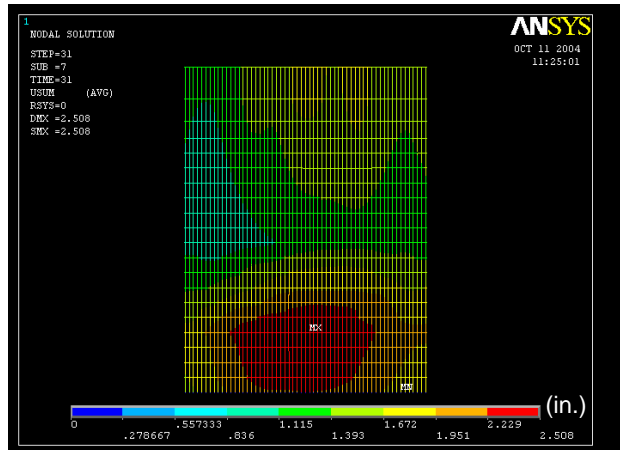
(c) South wall at 50 min



(d) South wall at 100 min

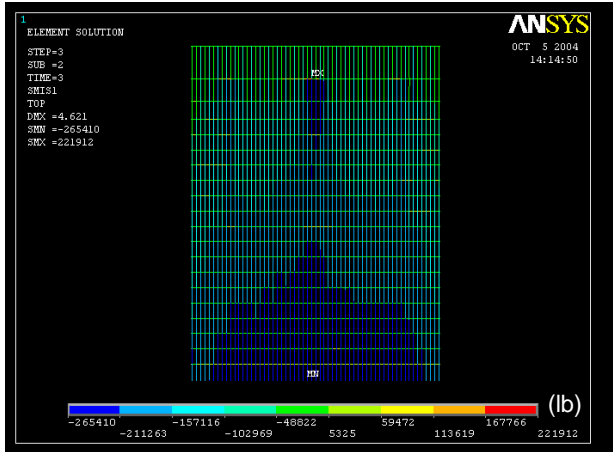


(e) East wall at 50 min

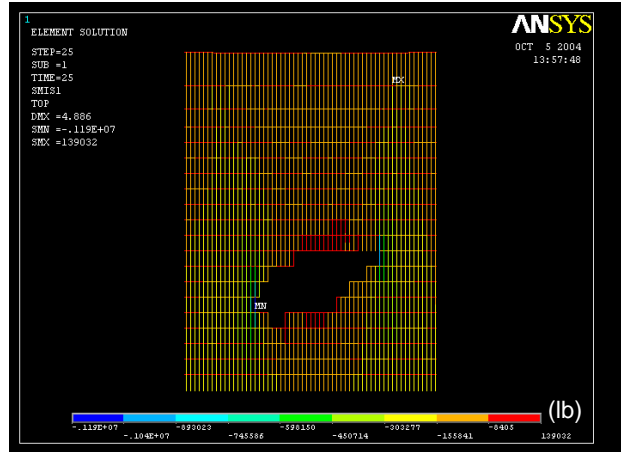


(f) East wall at 100 min

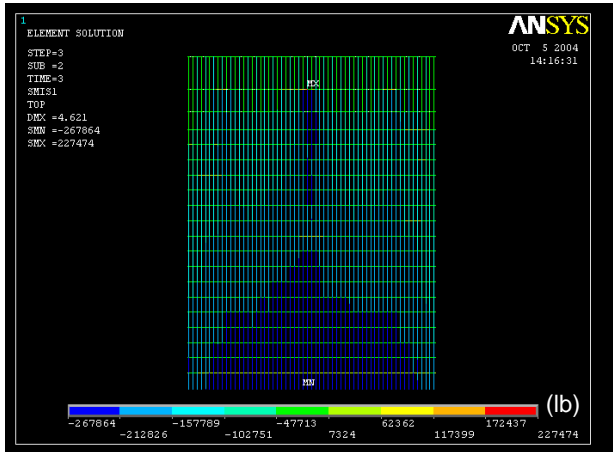
Figure C-3. Total displacement on the north, south, and east faces of the WTC 1 at 50 min and 100 min of Case A_i conditions (looking from outside).



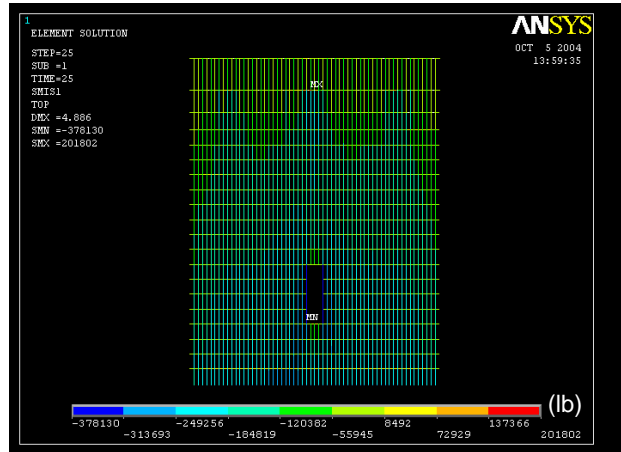
(a) North wall before impact



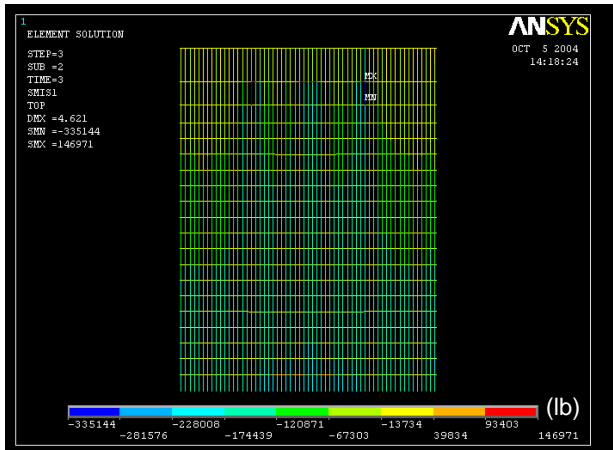
(b) North wall after impact



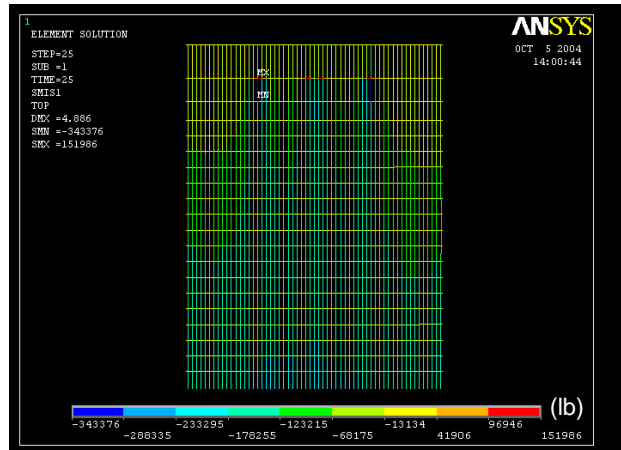
(c) South wall before impact



(d) South wall after impact

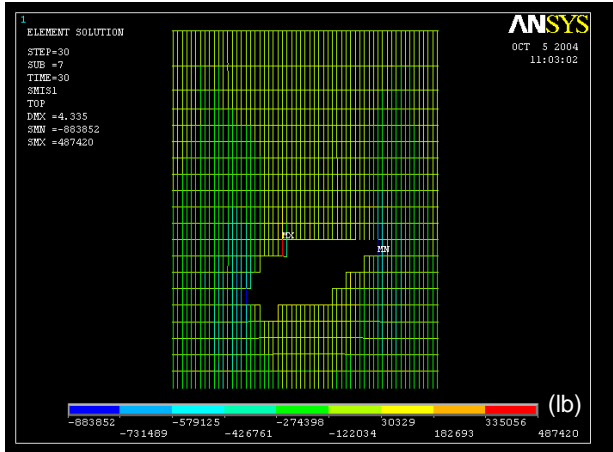


(e) East wall before impact

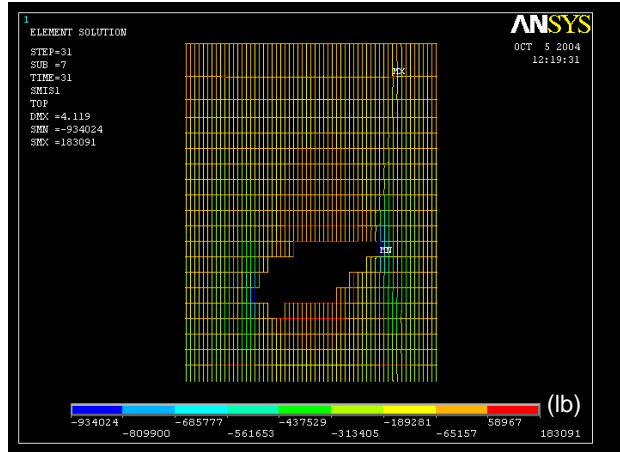


(f) East wall after impact

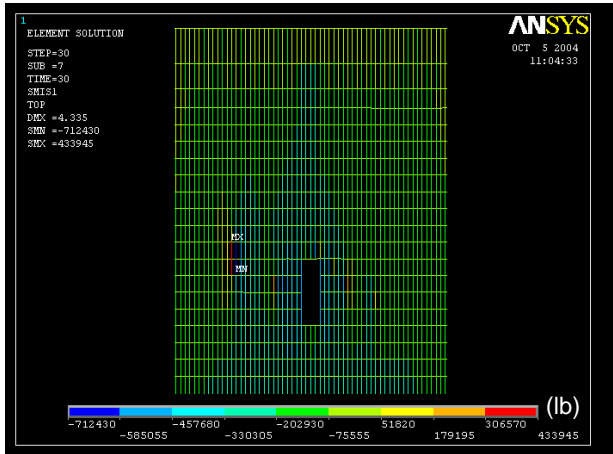
Figure C-4. Axial load variation on the north, south, and east faces of the WTC 1 before and after aircraft impact (looking from outside; compression is negative).



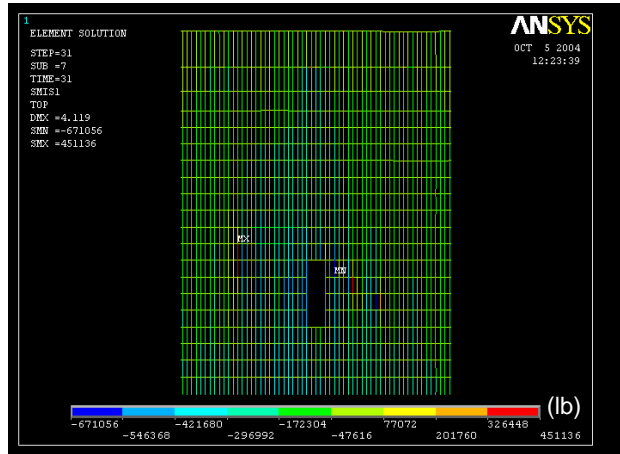
(a) North wall at 50 min



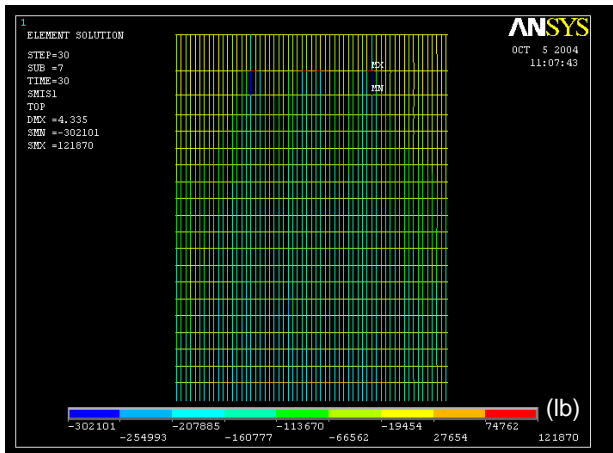
(b) North wall at 100 min



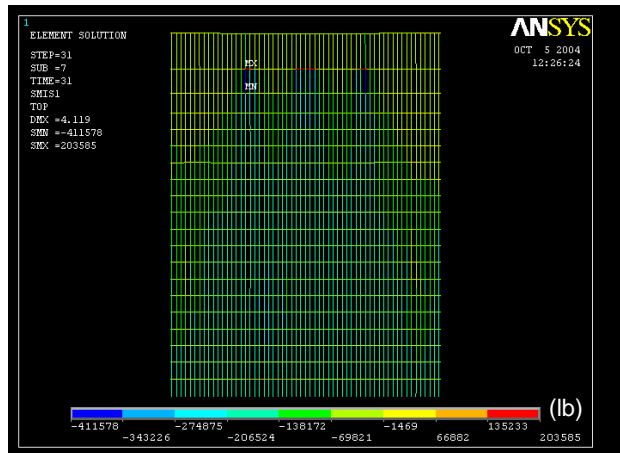
(c) South wall at 50 min



(d) South wall at 100 min



(e) East wall at 50 min



(f) East wall at 100 min

Figure C-5. Axial load variation on the north, south, and east faces of the WTC 1 at 50 min and 100 min of Case A_i conditions (looking from outside; compression is negative).

Row	Analysis Stage	North	South	East	West	Core	Sum
(1)	Before Impact	12375	12459	9006	9045	47101	89986
(2)	After Impact	10330	12151	9222	9242	47812	88757
(3)	10 min	9649	11714	8429	8142	50762	88696
(4)	20 min	9528	11761	8260	8023	51185	88757
(5)	30 min	9564	11931	8421	8060	50781	88757
(6)	50 min	9852	12228	9065	8714	48898	88757
(7)	100 min	10492	12880	10067	9880	45438	88757

(a) Above Floor 93

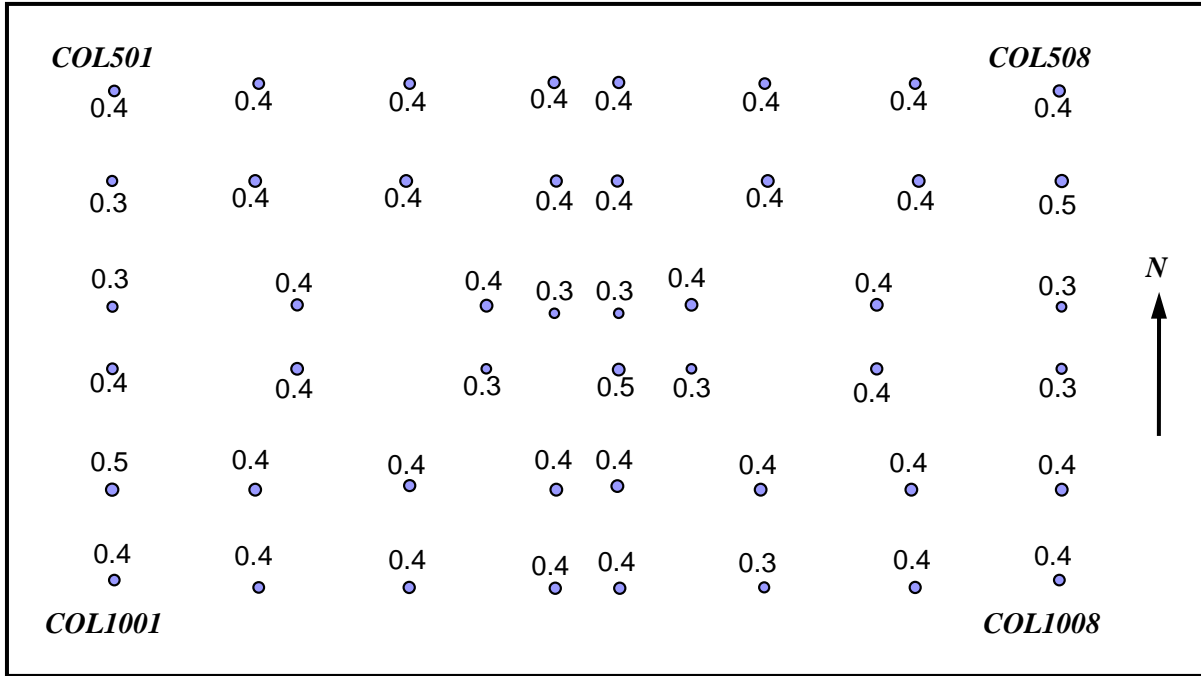
Row	Analysis Stage	North	South	East	West	Core	Sum
(1)	Before Impact	11119	11204	8126	8170	41216	79835
(2)	After Impact	9598	11004	8328	8339	42174	79443
(3)	10 min	8898	10573	7546	7237	45137	79391
(4)	20 min	8757	10620	7387	7128	45552	79444
(5)	30 min	8795	10780	7545	7176	45148	79444
(6)	50 min	9094	11068	8179	7840	43263	79444
(7)	100 min	9771	11668	9192	9014	39799	79444

(b) Above Floor 96

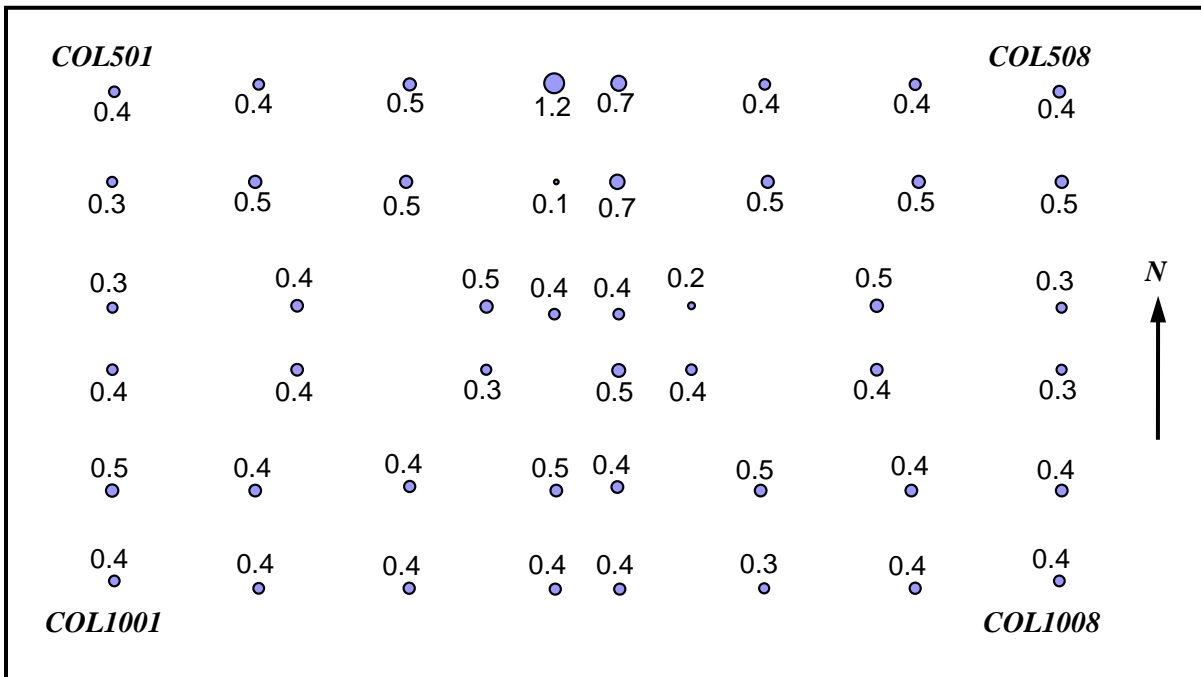
Row	Analysis Stage	North	South	East	West	Core	Sum
(1)	Before Impact	10264	10352	7564	7611	37299	73090
(2)	After Impact	9090	10171	7761	7770	38295	73087
(3)	10 min	8397	9739	6983	6661	41262	73042
(4)	20 min	8261	9783	6828	6546	41669	73087
(5)	30 min	8299	9938	6990	6594	41266	73087
(6)	50 min	8588	10223	7625	7270	39381	73087
(7)	100 min	9250	10824	8628	8466	35919	73087

(c) Above Floor 98

Figure C–6. Total column loads in the core and exterior walls of WTC 1 at different floors and at different times (compression is positive).

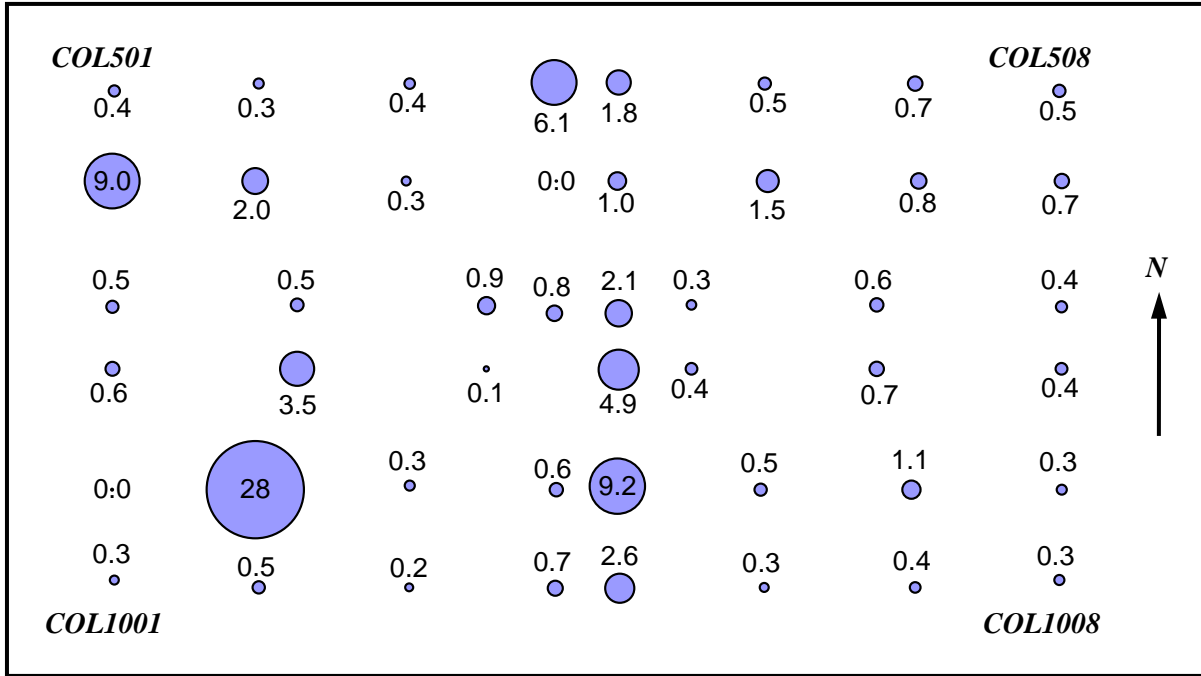


(a) Before impact

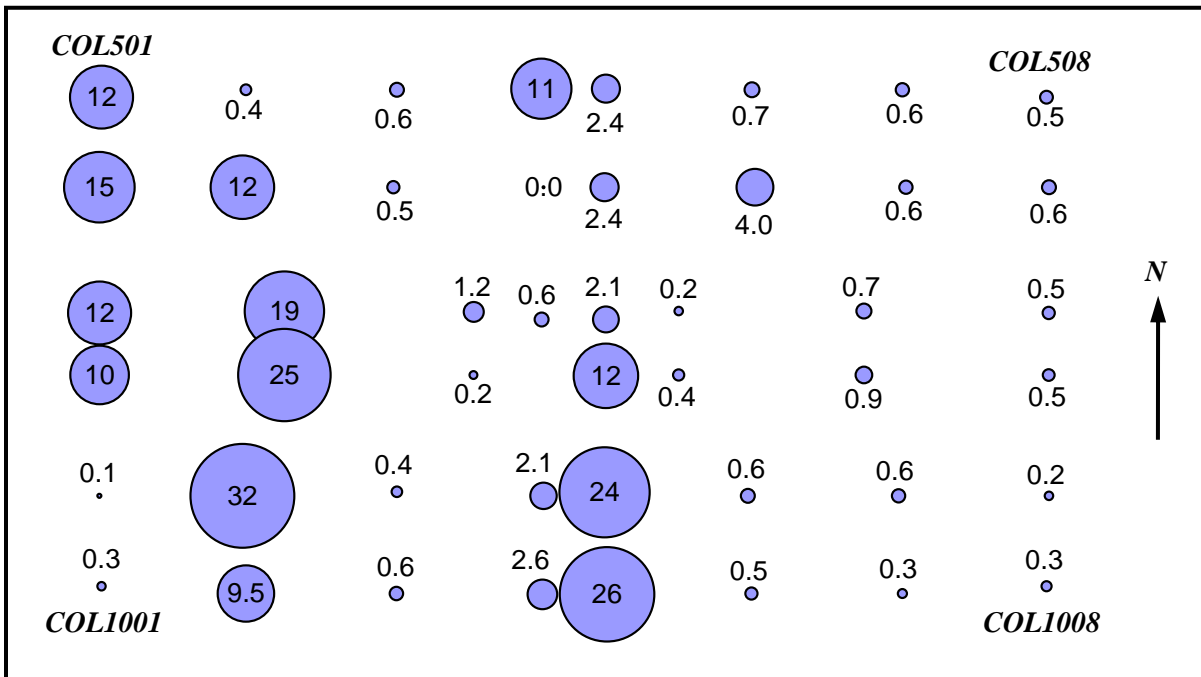


(b) After impact

Figure C-7. Ratios of axial elastic-plus-plastic strain to temperature-dependent yield strain for the core columns at Floor 96 of WTC 1 before and after aircraft impact.

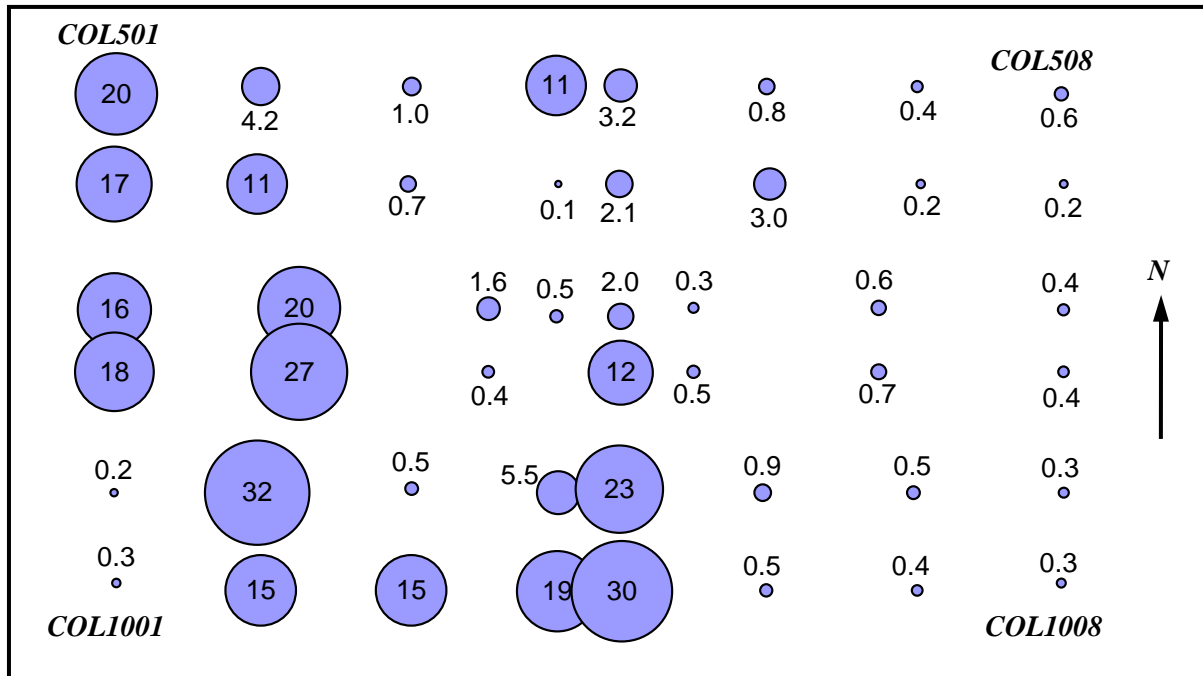


(a) At 10 min

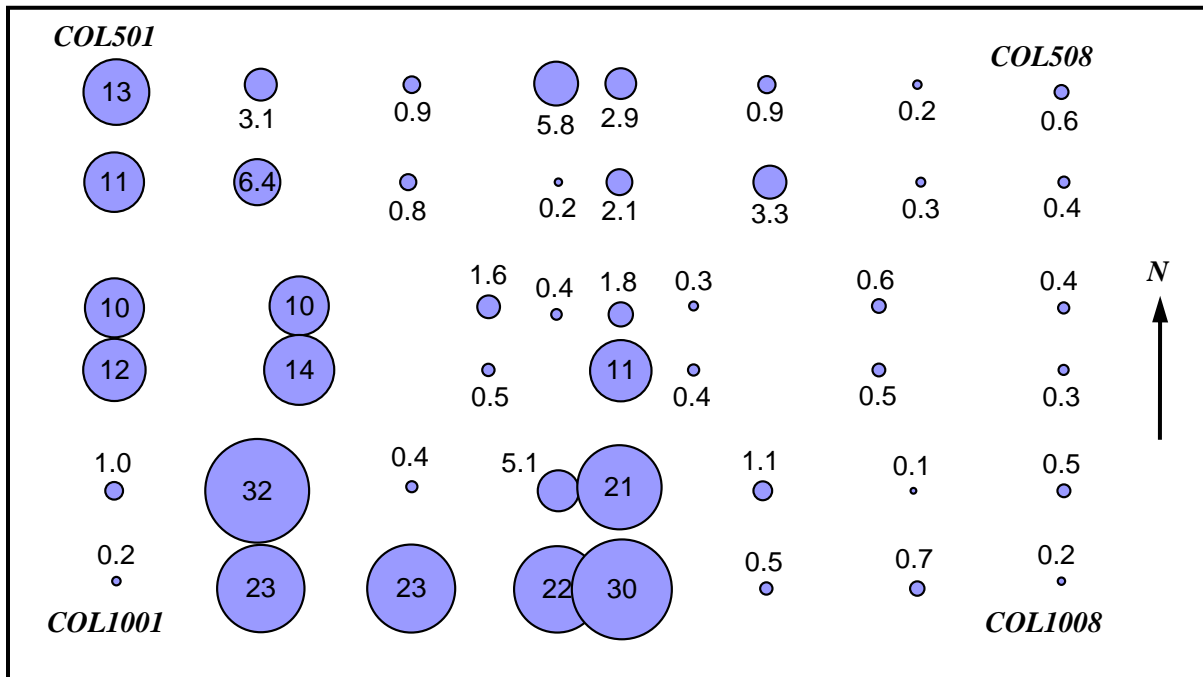


(b) At 20 min

Figure C-8. Ratios of axial elastic-plus-plastic strain to temperature-dependent yield strain for the core columns at Floor 96 of WTC 1 at 10 min and 20 min for Case A_i conditions.



(a) At 50 min



(b) At 100 min

Figure C-9. Ratios of axial elastic-plus-plastic strain to temperature-dependent yield strain for the core columns at Floor 96 of WTC 1 at 50 min and 100 min for Case A_i conditions.

C.2 WTC 2 GLOBAL ANALYSIS WITHOUT CREEP

The WTC 2 ANSYS model with no creep and no inelastic buckling of columns was analyzed with Case C_i and revised Case C_i structural damage condition and subjected to Case C_i and Case D_i temperature conditions. Temperature-dependent plasticity and the nonlinear geometry were the sources of nonlinearity in the model.

Case D_i temperature histories were analyzed with revised Case C_i structural damage as there was little structural response to Case C_i temperature histories, particularly in the core. The application of structural damage to the global model was a lengthy process, hence, only a different temperature history was considered for preliminary analysis purposes.

C.2.1 Case C_i Structural Damage and Temperature Conditions

Table C–2 summarizes the sequence of analyses that were performed with the WTC 2 ANSYS global model with Case C_i conditions (see Section 2.2 for Case C_i structural damage condition). The revised Case C_i structural damage condition was provided by NIST in the middle of the analysis for the thermal loading. Additional core columns were removed in analysis step 6 as shown in Table C–2. The results of each analysis step were used as initial conditions for the next analysis step.

Table C–2. Analysis Steps of WTC 2 ANSYS global model with Case C_i conditions.

Analysis Step	Description
1	WTC 2 model below Floor 106 was analyzed under its own self-weight.
2	Structures above Floor 106 were added in a stress-free state, and the model was analyzed for dead load including those above Floor 106.
3	Superimposed dead load and 25 percent of the design live loads were superimposed on the model.
4	Columns, spandrels, and floor elements severed during aircraft impact were removed, and the model was analyzed.
5	Column and spandrel temperatures were linearly ramped up to temperatures at 10 min.
6	Core Columns 1003 at Floor 80 and 903 between Floors 77 and 84 were removed from the model to represent the additional severed columns that were identified by NIST at later stages of the investigation (see Section 2.2 for the revised Case C _i structural damage condition).
7	Column and spandrel temperatures were changed linearly from temperatures at 10 min to 20 min.
8	Column and spandrel temperatures were changed linearly from temperatures at 20 min to 30 min.
9	Column and spandrel temperatures were changed linearly from temperatures at 30 min to 40 min.
10	Column and spandrel temperatures were changed linearly from temperatures at 40 min to 50 min.
11	Column and spandrel temperatures were changed linearly from temperatures at 50 min to 60 min.

The model was first analyzed to capture the effects of the construction sequence (analysis steps 1, 2, and 3). The results of analysis step 3 represented the structure state before the aircraft impact. In analysis step 4, the columns, spandrels, and floor elements that were severed during the aircraft impact were removed from the model, and the building was reanalyzed to redistribute the load to the non-severed members. This analysis represents the state of the building after the aircraft impact. After load redistribution, the column and spandrel temperatures were applied to the model (analysis steps 5, 7, 8, 9, 10, and 11). The column and spandrel temperatures were provided by NIST at 10 min intervals. For times between these time intervals, temperatures were calculated by linear interpolation. Analyses were

conducted at every 10 min up to 60 min. In Analysis Step 6, after the analysis of 10 min temperatures, two more core columns that were identified as severed during the aircraft impact were removed from the model. Temperatures were not applied to the floors in the global model to prevent floor buckling, as discussed for the WTC 1 global model without creep.

The results of the WTC 2 global model analyses with Case C_i structural damage and temperature conditions are summarized in Figs. C–10 through C–20.

Figure C–10 shows the vertical displacement at different analysis stages. The maximum displacement after the removal of additional severed core columns at analysis step 6 was equal to 7.2 in. This displacement gradually decreased to 7.0 in. at the end of 50 min. This reduction was due to thermal expansion of the core and the exterior wall columns between Floor 79 and Floor 83. Figures C–11 and C–12 show the vertical displacements for south and east exterior walls before and after aircraft impact and at 30 min and 60 min. The displacements were typically at their maximum near the hat truss at analysis step 6, after all severed members were removed, and gradually decreased to their minimum near Floor 77 through Floor 81 at 60 min. Figure C–11 shows that the displacement on the east wall, which was symmetric before the aircraft impact, became greater on the south side of this wall after the aircraft impact. This was due to the load redistribution to the south side of the east wall as a result of the removal of the severed columns on the south wall and in the southeast corner of the core. This was the first sign of tilting of WTC 2 toward the southeast.

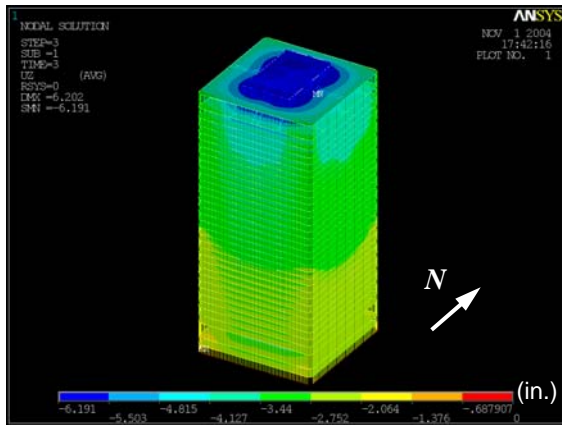
Figures C–13, C–14, C–15, and C–16 show the axial loads before and after aircraft impact and at 30 min and 60 min over the south, east, and north exterior wall columns and spandrels and in the 800, 900, and 1000 core column series. After the aircraft impact, the load carried by the severed columns of the south exterior wall was primarily redistributed to the remaining columns on the same face and also to the core and other exterior wall columns. As a result of this redistribution, the maximum column load increased from 334 kip to 1,410 kip on the south exterior wall and from 451 kip to 485 kip on the east exterior wall. Similar to displacement, the axial load on the east wall, which was symmetric before the aircraft impact, became greater on the south side of this wall after the aircraft impact. This was due to the load redistribution to the south side of the east wall as a result of the removal of the severed columns on the south wall and in the southeast corner of the core. The axial load in core columns also was significantly affected by the aircraft impact and fire-induced temperatures. The maximum column load increased from 4,930 kip to 5,120 kip in the 1000 core-column series, from 1,600 kip to 2,250 kip in the 900 core column series, and from 1,740 kip to 2,630 kip in the 800 core-column series. After the removal of 1003 and 903 core columns, the column loads increased on the east and south side core columns.

With increasing time, the maximum column load on the east exterior wall columns increased from 485 kip after aircraft impact to 630 kip at the end of 60 min. This increase was primarily due to the steady increase of column temperatures on the east wall as a result of the continuous fires. Similarly, the axial loads in the 1000 core column series steadily increased due to continuous fires on the east side of the core.

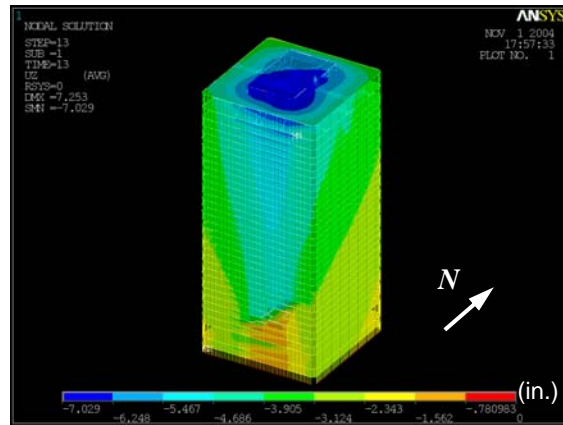
Figure C–17 shows the total column loads over the entire core and north, south, east, and west exterior walls for different floors. Due to the removal of severed columns, spandrels, and floor elements, the total column loads below Floor 83 after aircraft impact are not equal to those before the aircraft impact. Referring to the total column loads above Floor 83 in Fig. C–17, after the aircraft impact (including the effects of additionally removed Column 903 and Column 1003 in the core), the total column load in the

east exterior wall columns increased about 2,600 kip, whereas the total column load decreased in the core by about 1,200 kip, in the north exterior wall by about 750 kip, in the west exterior wall by about 50 kip, and in the south exterior wall by about 600 kip. With increasing time, the temperatures in the east, the north, and the south exterior wall columns increased more than those in the west exterior wall and core columns. The higher temperatures resulted in higher thermal expansions and greater axial loads in the exterior wall columns. In Floor 83, the temperature effect alone resulted in unloading of the core by 1,820 kip and increased the total column loads by 140 kip on the south exterior wall, by 700 kip on the west exterior wall, by 600 kip on the north exterior wall, and by 380 kip on the east exterior wall.

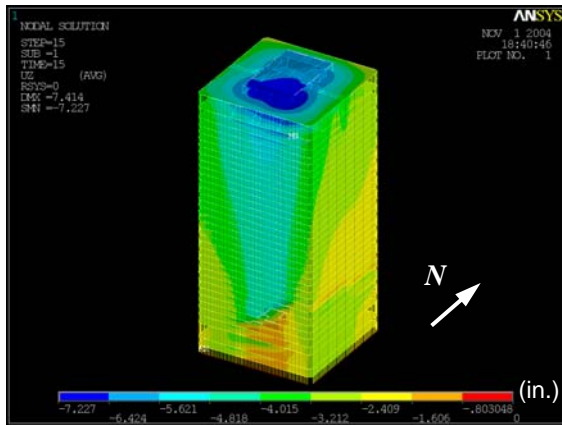
Figures C-18, C-19, and C-20 show the ratio of elastic-plus-plastic strain to the temperature-dependent yield strain of the core columns between Floor 82 and Floor 83 before and after aircraft impact and at 10 min (analysis step 6), 30 min, 40 min, and 60 min. As can be noticed, the elastic-plus-plastic strain in the core columns before aircraft impact was typically 60 to 70 percent less than the yield strains at room temperature. After the aircraft impact, the maximum strain ratio reached 0.6, indicating that all remaining core columns were in their elastic range. After the removal of Core Columns 1003 and 903, Core Columns 1004 and 1005 started to show strain ratios greater than 1.0 (indicating plasticity) with 10 min temperatures. Strain ratios in Core Columns 1004 and 1005 continued to increase with increasing time and temperatures, reaching their maximum at the end of 60 min. High strains were clustered around the east side core columns, demonstrating possible tilting of the core.



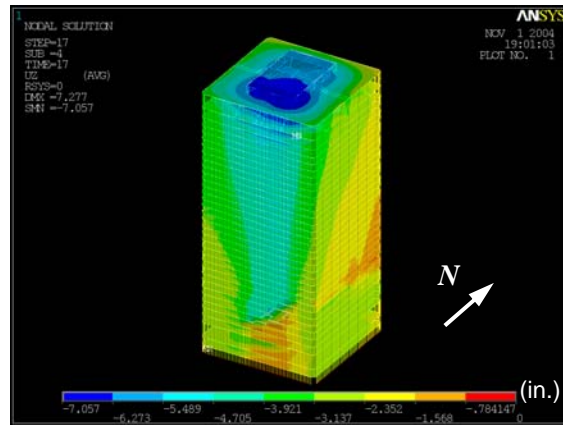
(a) Before impact



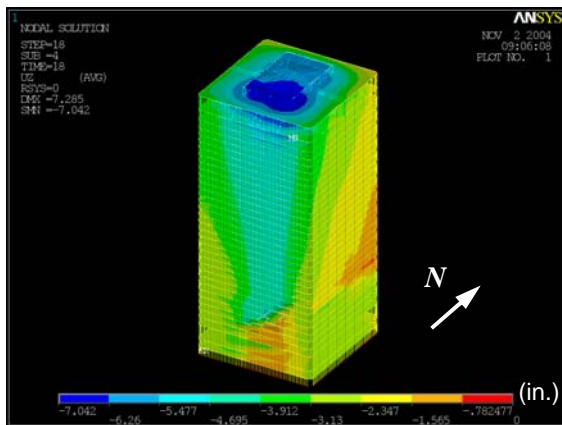
(b) After impact



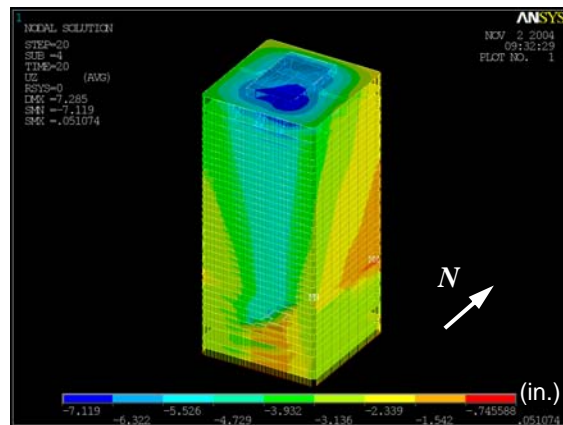
(c) At 10 min (Analysis step 6)



(d) At 30 min

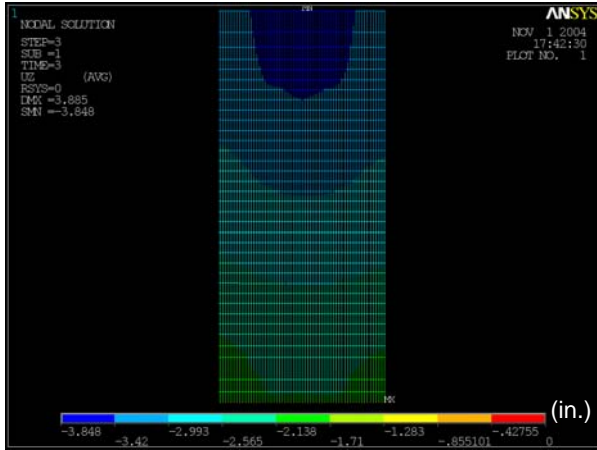


(e) At 40 min

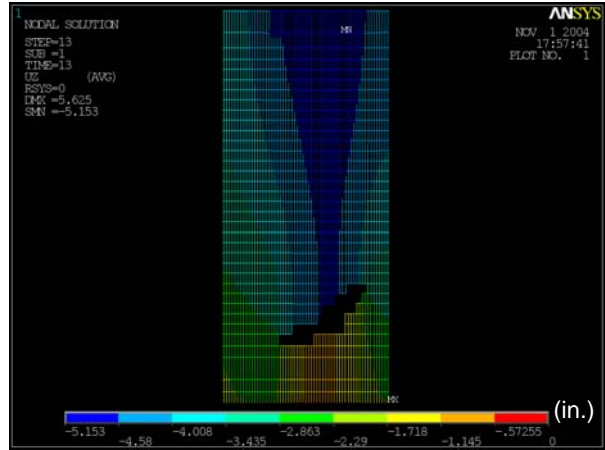


(f) At 60 min

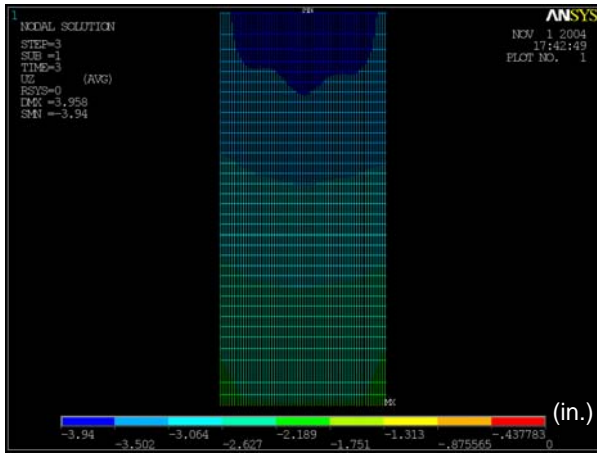
Figure C-10. Vertical displacement at different stages of WTC 2 for Case C₁ conditions.



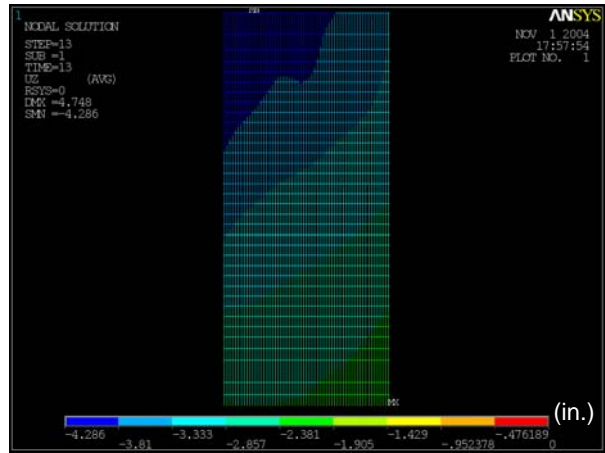
(a) South wall before impact



(b) South wall after impact

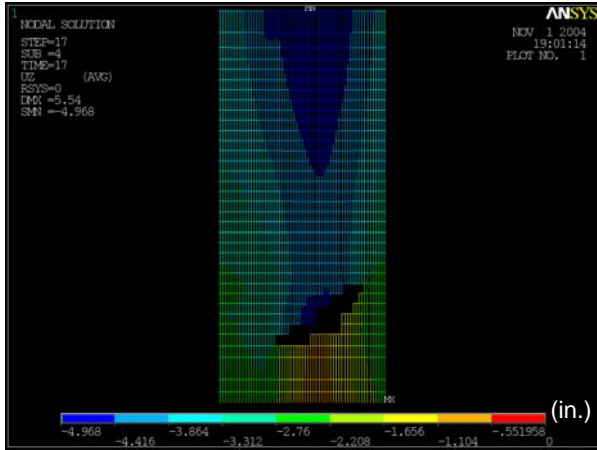


(c) East wall before impact

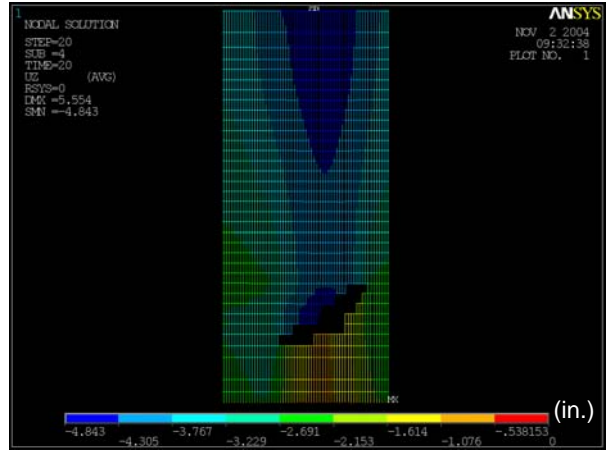


(d) East wall after impact

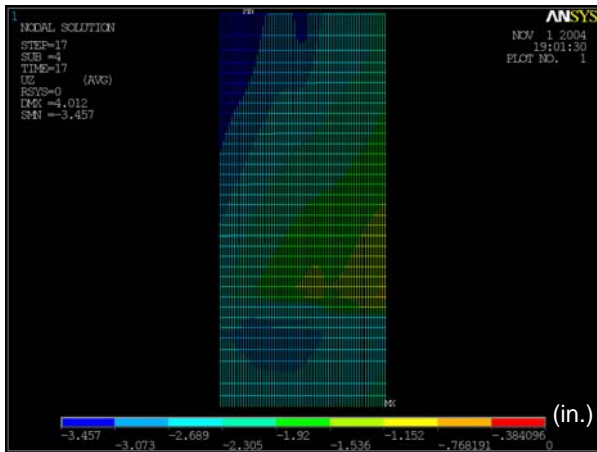
Figure C-11. Vertical displacement on the south and east faces of WTC 2 before and after aircraft impact (looking from outside; downward displacement is negative).



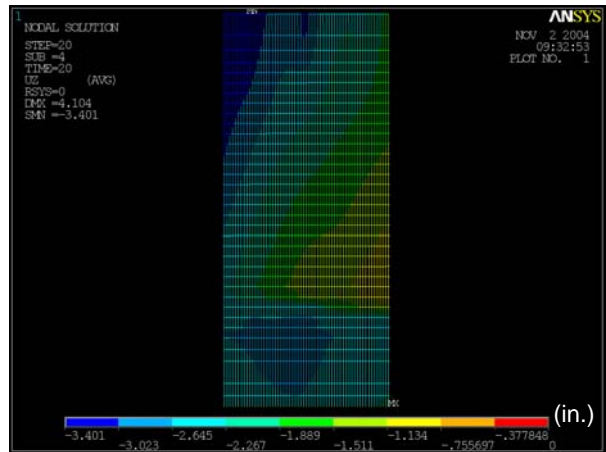
(a) South wall at 30 min



(b) South wall at 60 min

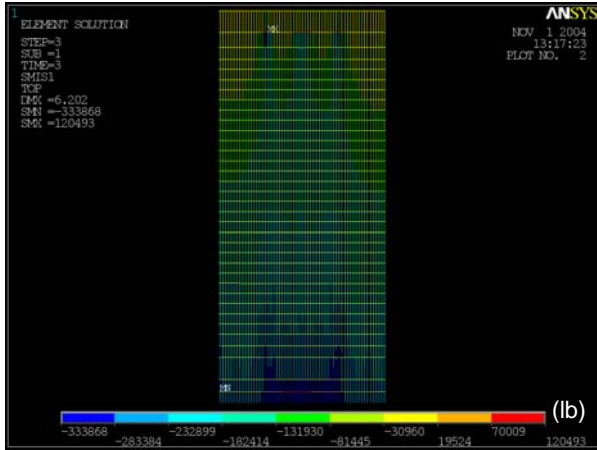


(c) East wall at 30 min

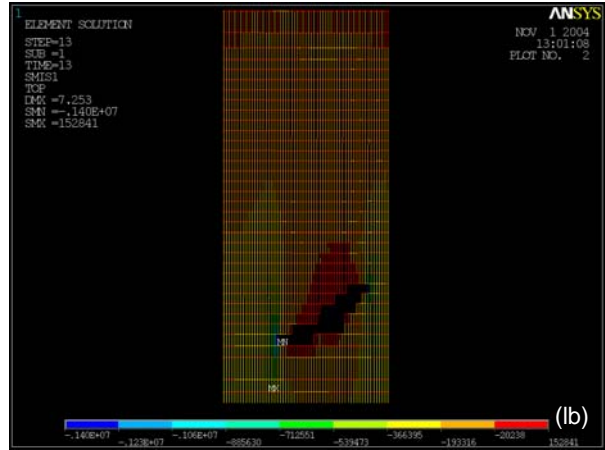


(d) East wall at 60 min

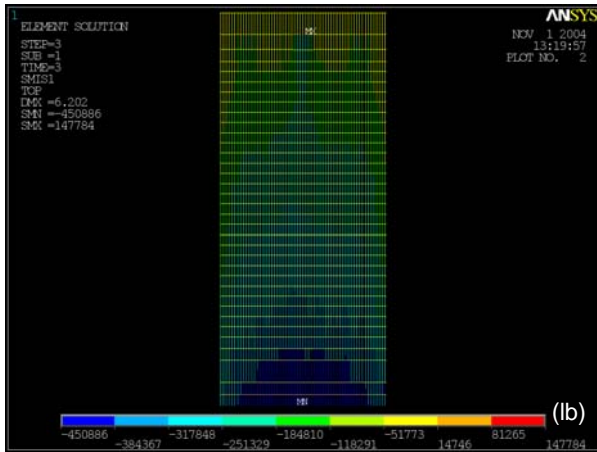
Figure C-12. Vertical displacement on the south and east faces of WTC 2 at 30 min and at 60 min of Case C_i conditions (looking from outside; downward displacement is negative).



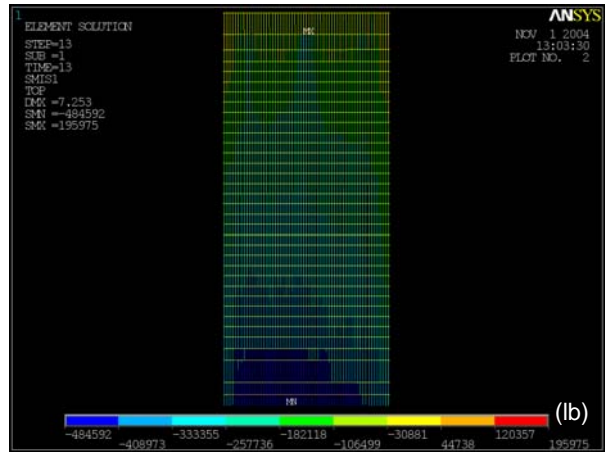
(a) South wall before impact



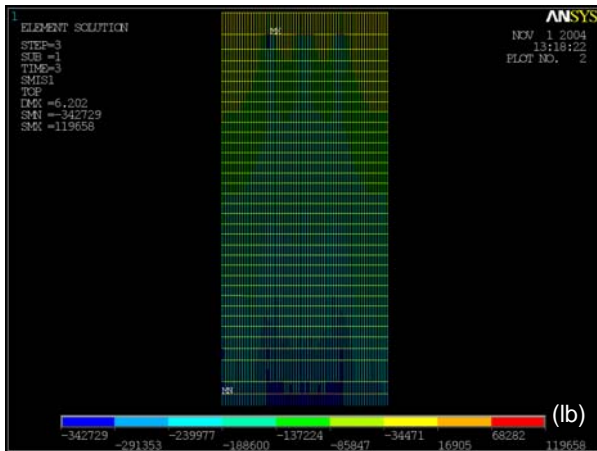
(b) South wall after impact



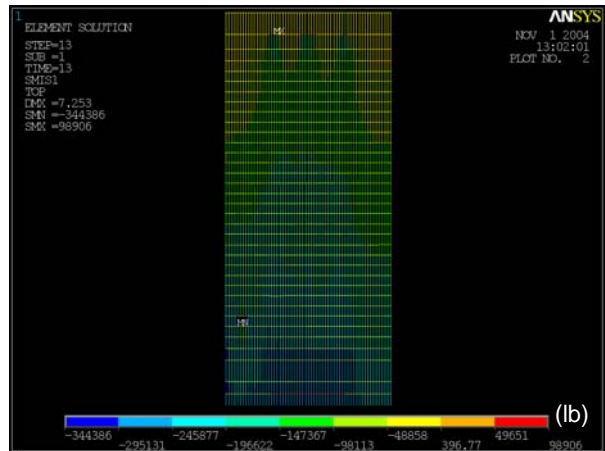
(c) East wall before impact



(d) East wall after impact

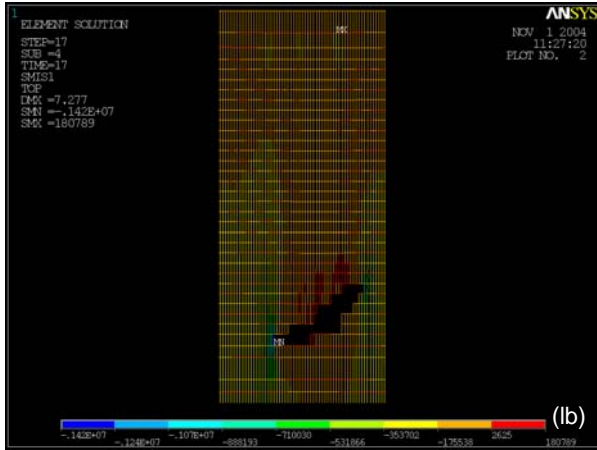


(e) North wall before impact

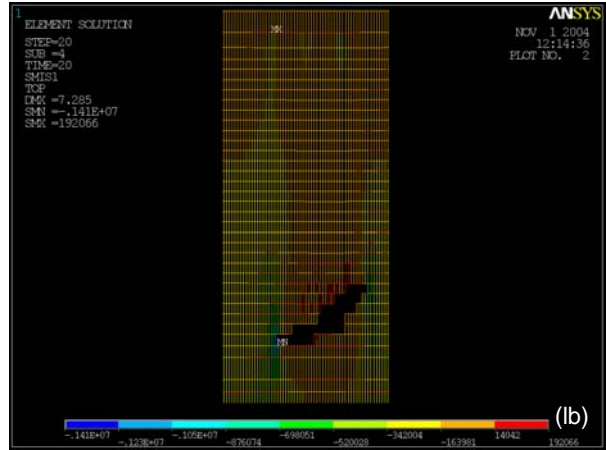


(f) North wall after impact

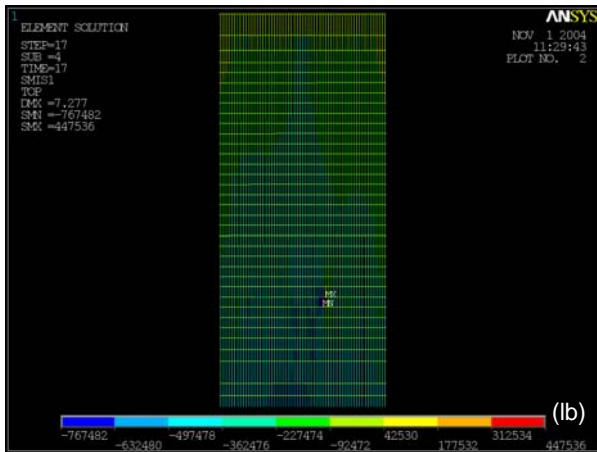
Figure C-13. Axial force variation on the south, east, and north faces of WTC 2 before and after aircraft impact (looking from outside; compression is negative).



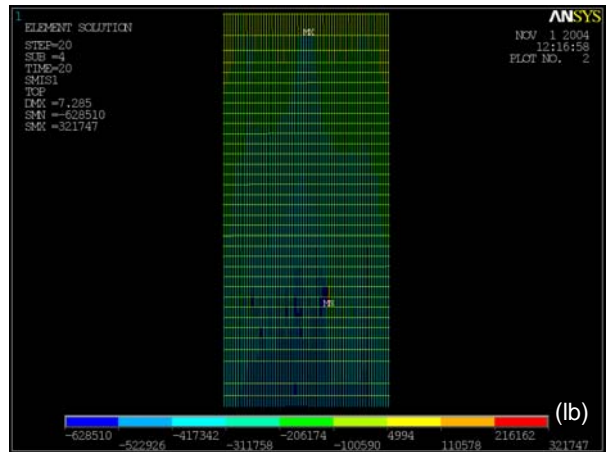
(a) South wall at 30 min



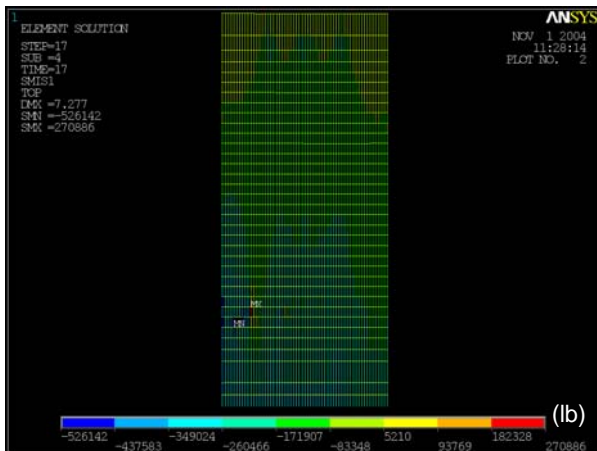
(b) South wall at 60 min



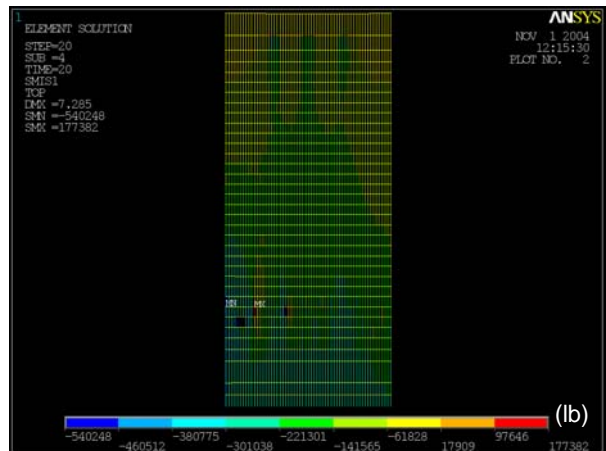
(c) East wall at 30 min



(d) East wall at 60 min

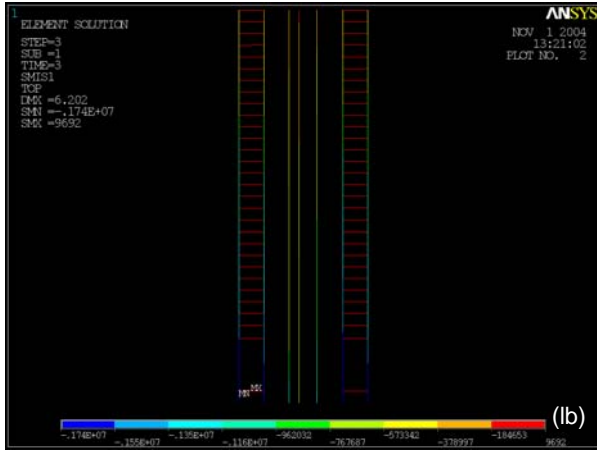


(e) North wall at 30 min

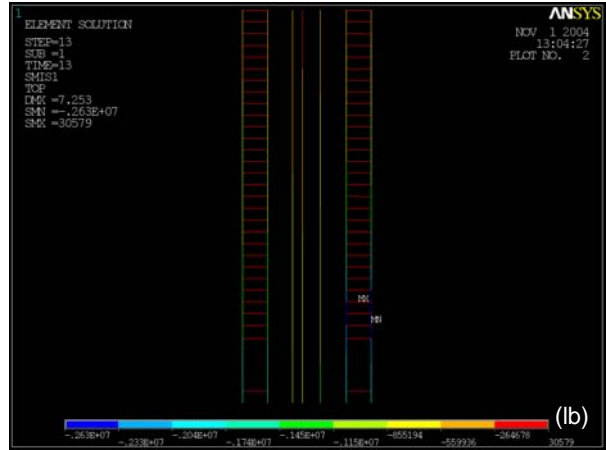


(f) North wall at 60 min

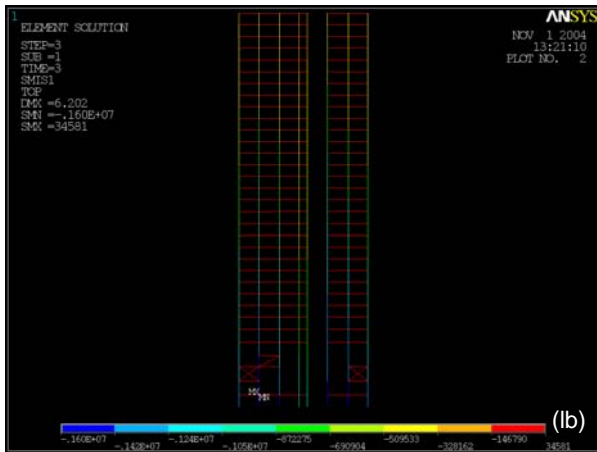
Figure C-14. Axial force variation on the south, east, and north faces of WTC 2 at 30 min and 60 min of Case C_i conditions (looking from outside; compression is negative).



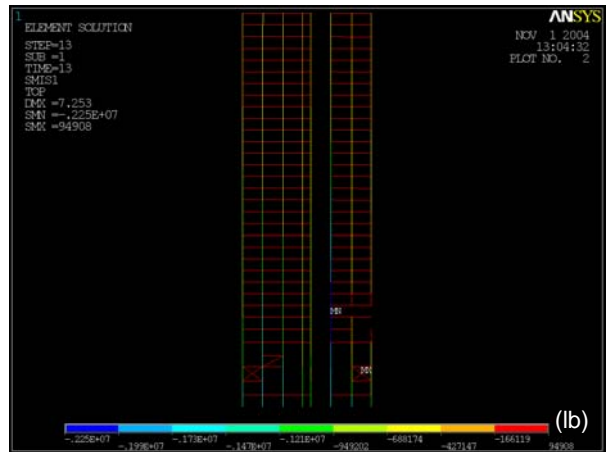
(a) 800 series columns before impact



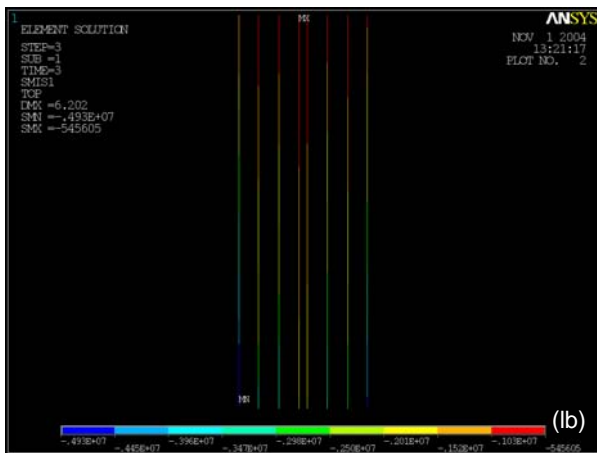
(b) 800 series columns after impact



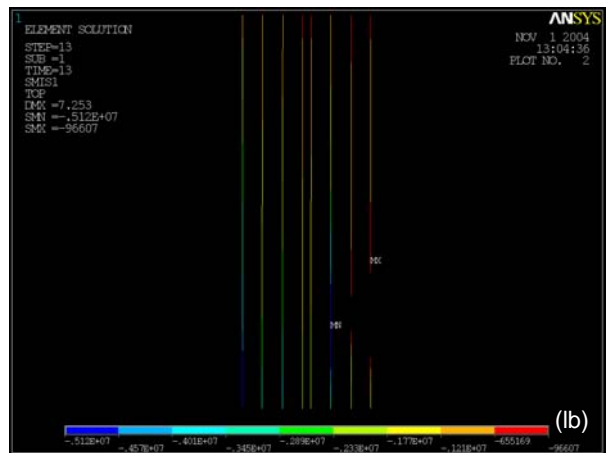
(c) 900 series columns before impact



(d) 900 series columns after impact

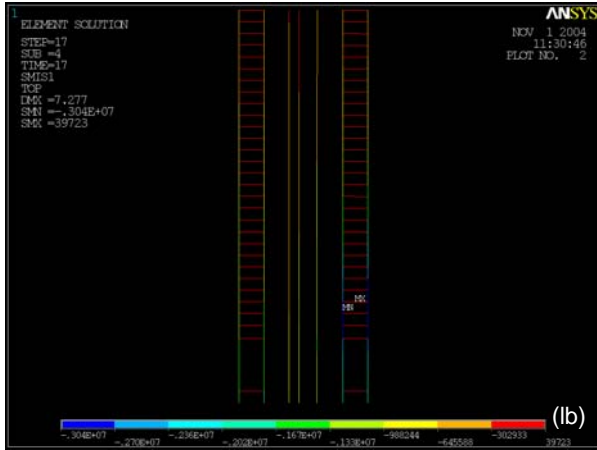


(e) 1000 series columns before impact

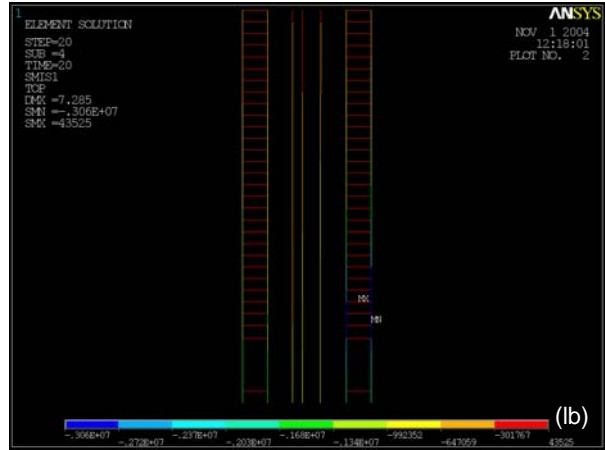


(f) 1000 series columns after impact

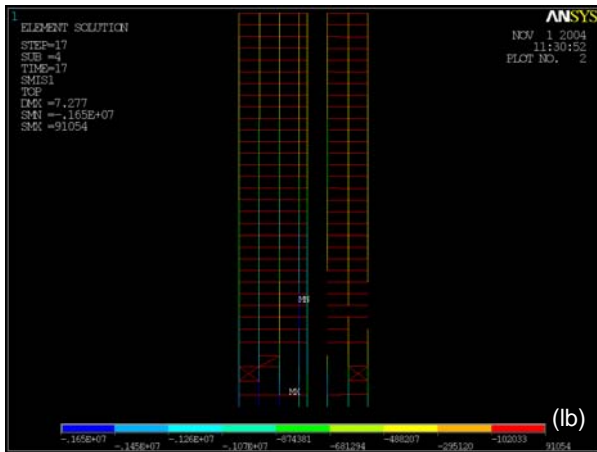
Figure C–15. Axial force variation on the 800, 900, and 1000 series core columns of WTC 2 before and after aircraft impact (looking from west; compression is negative).



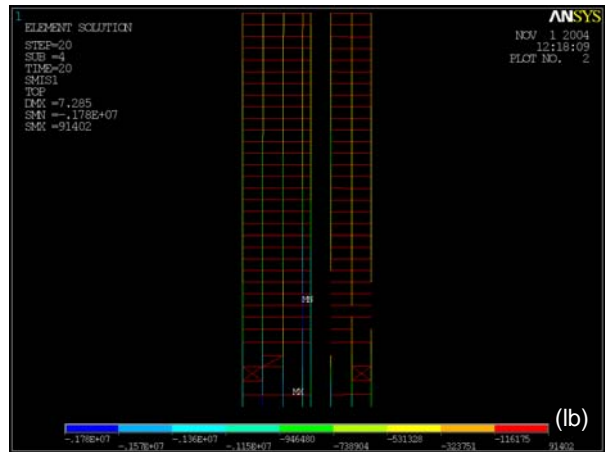
(a) 800 series columns at 30 min



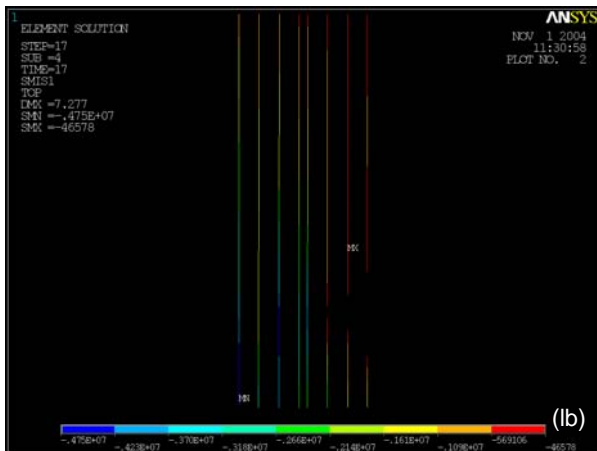
(b) 800 series columns at 60 min



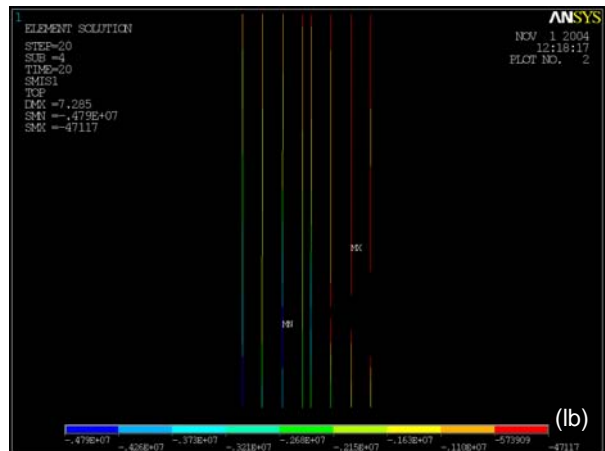
(c) 900 series columns at 30 min



(d) 900 series columns at 60 min



(e) 1000 series columns at 30 min



(f) 1000 series columns at 60 min

Figure C–16. Axial force variation on the 800, 900, and 1000 series core columns of WTC 2 at 30 min and 60 min of Case C_i conditions (looking from west; compression is negative).

Row	Analysis Stage	West	East	North	South	Core	Sum
(1)	Before Impact	18779	18837	13714	13529	77563	142423
(2)	After Impact	18951	20394	12892	11880	76831	140949
(3)	After Impact*	18774	21384	12800	12528	75166	140652
(4)	10 min	19499	20616	12997	11333	76504	140949
(5)	10 min (b)	19322	21606	12905	11981	74839	140652
(6)	20 min	19471	21616	12978	12130	74458	140652
(7)	30 min	19469	21637	13138	12309	74099	140653
(8)	40 min	19462	21692	13246	12427	73826	140653
(9)	50 min	19472	21795	13305	12506	73574	140653
(10)	60 min	19500	21887	13388	12538	73341	140653

* Including the effects of additionally removed Columns 903 and 1003 in the core (= (2) - (4) + (5)).

(a) Above Floor 78

Row	Analysis Stage	West	East	North	South	Core	Sum
(1)	Before Impact	17642	17697	12558	12393	71319	131609
(2)	After Impact	17755	19295	11818	10982	71249	131099
(3)	After Impact*	17557	20305	11756	11599	69754	130972
(4)	10 min	18310	19529	11942	10396	70924	131101
(5)	10 min (b)	18111	20539	11881	11014	69429	130974
(6)	20 min	18258	20479	11960	11230	69048	130974
(7)	30 min	18251	20462	12137	11435	68688	130973
(8)	40 min	18241	20502	12245	11570	68414	130972
(9)	50 min	18238	20603	12309	11660	68162	130972
(10)	60 min	18239	20690	12414	11700	67928	130972

* Including the effects of additionally removed Columns 903 and 1003 in the core (= (2) - (4) + (5)).

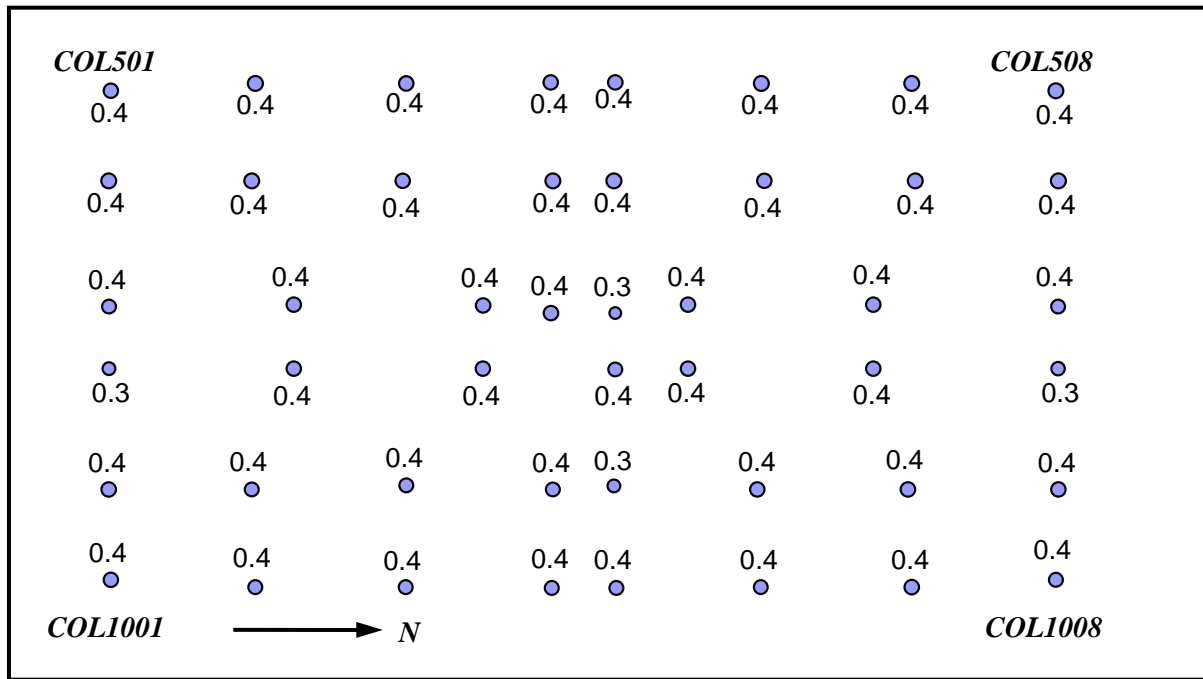
(b) Above Floor 81

Row	Analysis Stage	West	East	North	South	Core	Sum
(1)	Before Impact	16728	16782	11972	11820	67309	124611
(2)	After Impact	16853	18337	11241	10561	67499	124490
(3)	After Impact*	16664	19328	11184	11183	66115	124474
(4)	10 min	17398	18604	11346	9970	67172	124489
(5)	10 min (b)	17209	19595	11288	10592	65788	124473
(6)	20 min	17356	19511	11365	10833	65409	124473
(7)	30 min	17351	19482	11537	11054	65048	124473
(8)	40 min	17344	19521	11644	11191	64773	124473
(9)	50 min	17350	19619	11702	11280	64521	124473
(10)	60 min	17370	19709	11787	11320	64287	124473

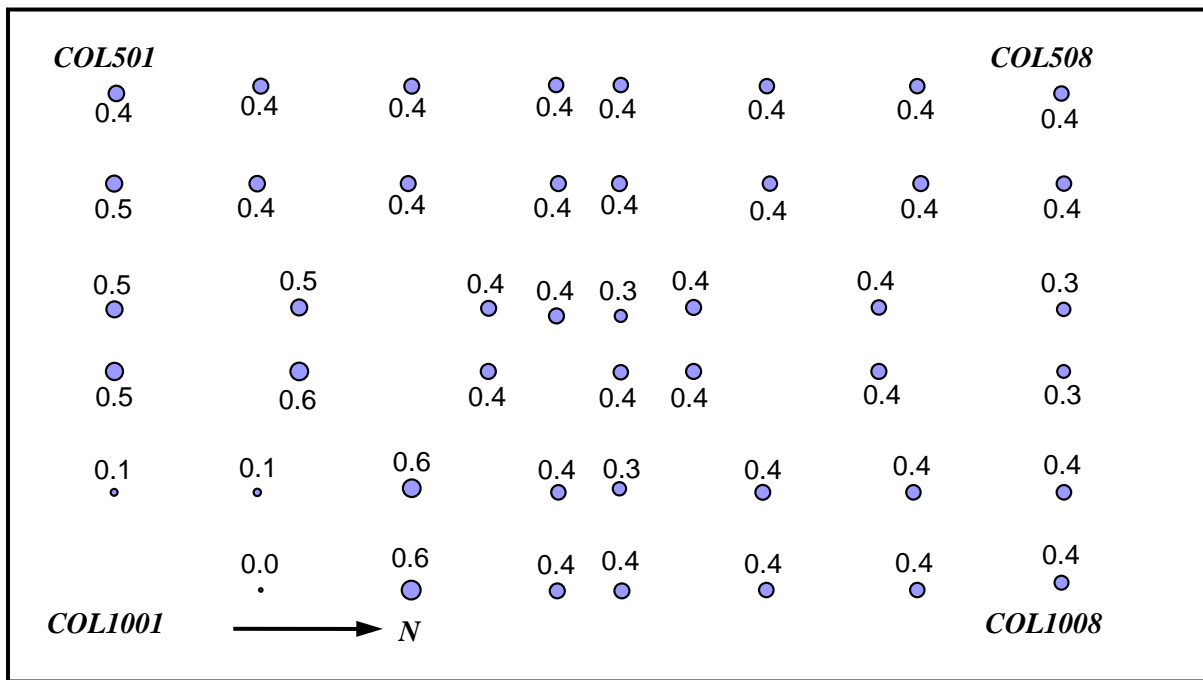
* Including the effects of additionally removed Columns 903 and 1003 in the core (= (2) - (4) + (5)).

(c) Above Floor 83

Figure C–17. Total column loads in the core and exterior walls of WTC 2 at different floors and at different times for Case C_i conditions (compression is positive).

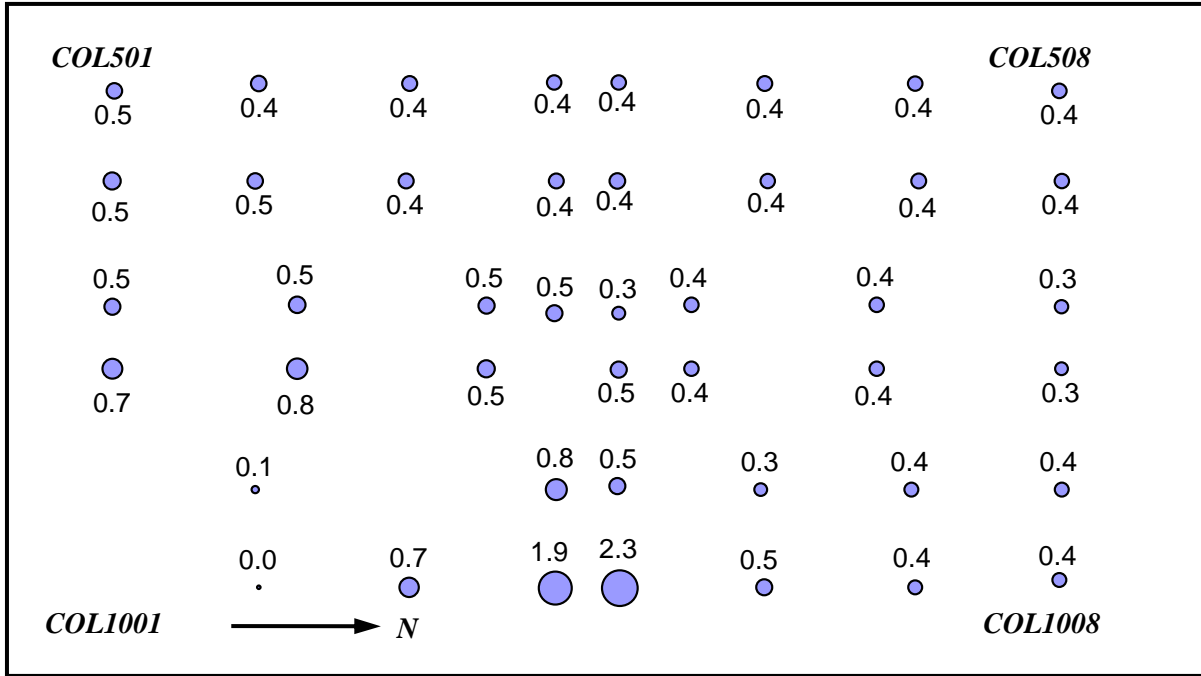


(a) Before impact

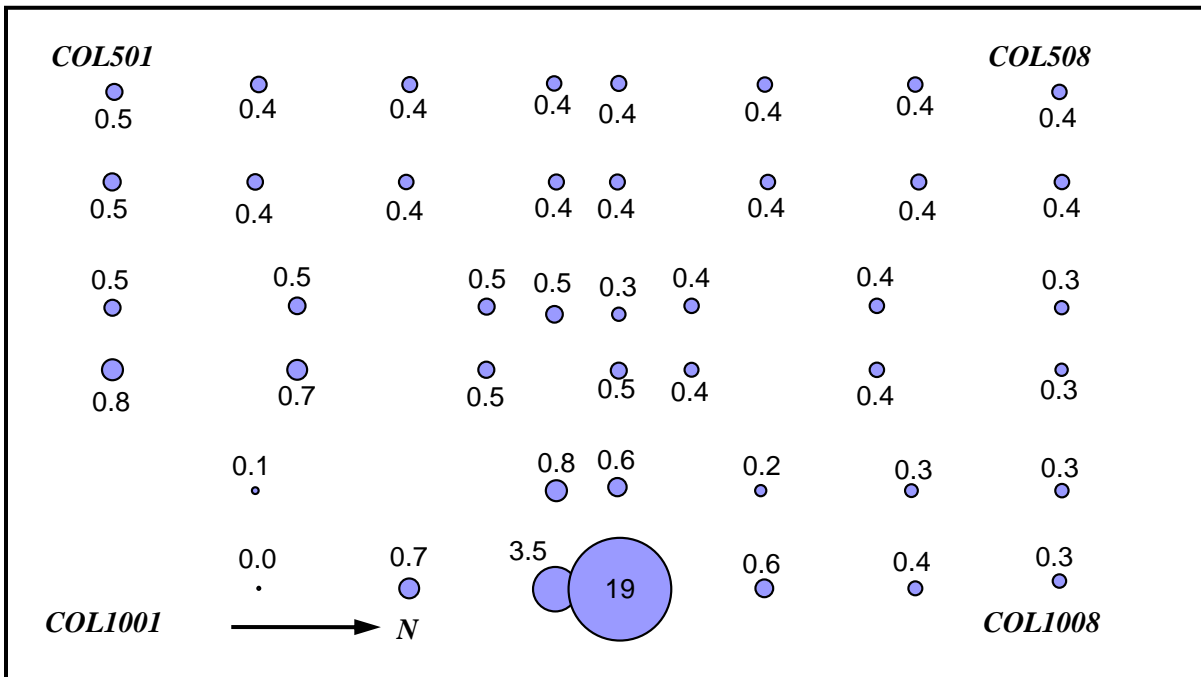


(b) After impact

Figure C-18. Ratios of axial elastic-plus-plastic strain to temperature-dependent yield strain for the core columns at Floor 82 of WTC 2 before and after aircraft impact.

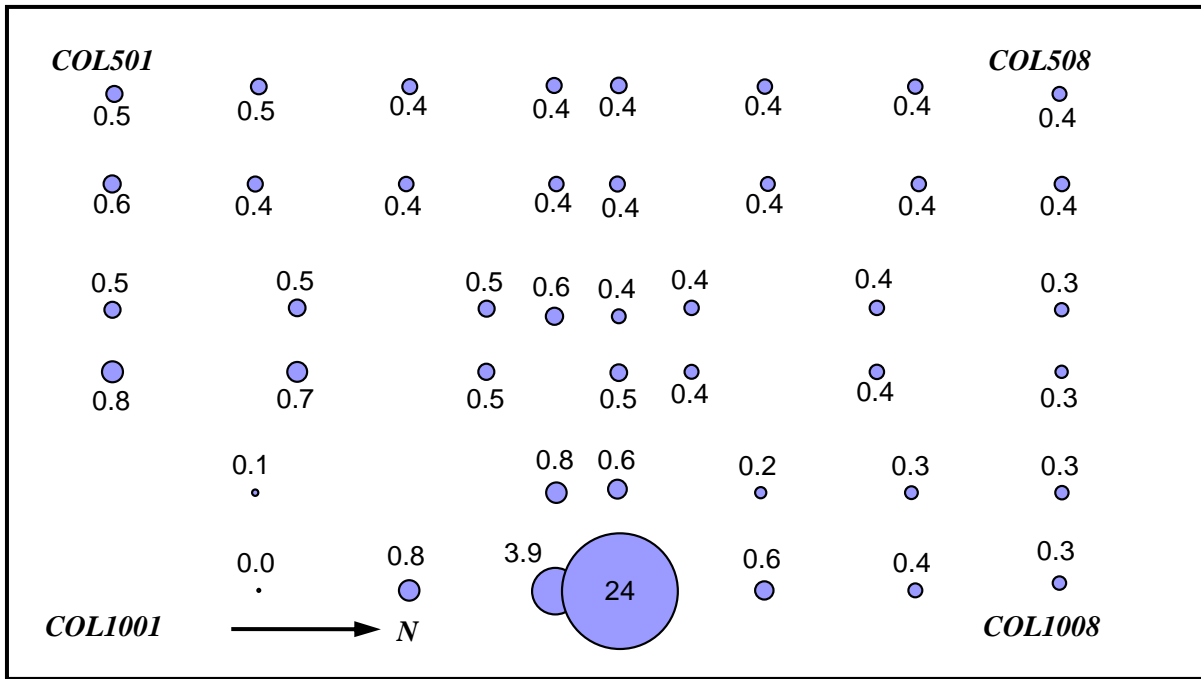


(a) At 10 min (b)

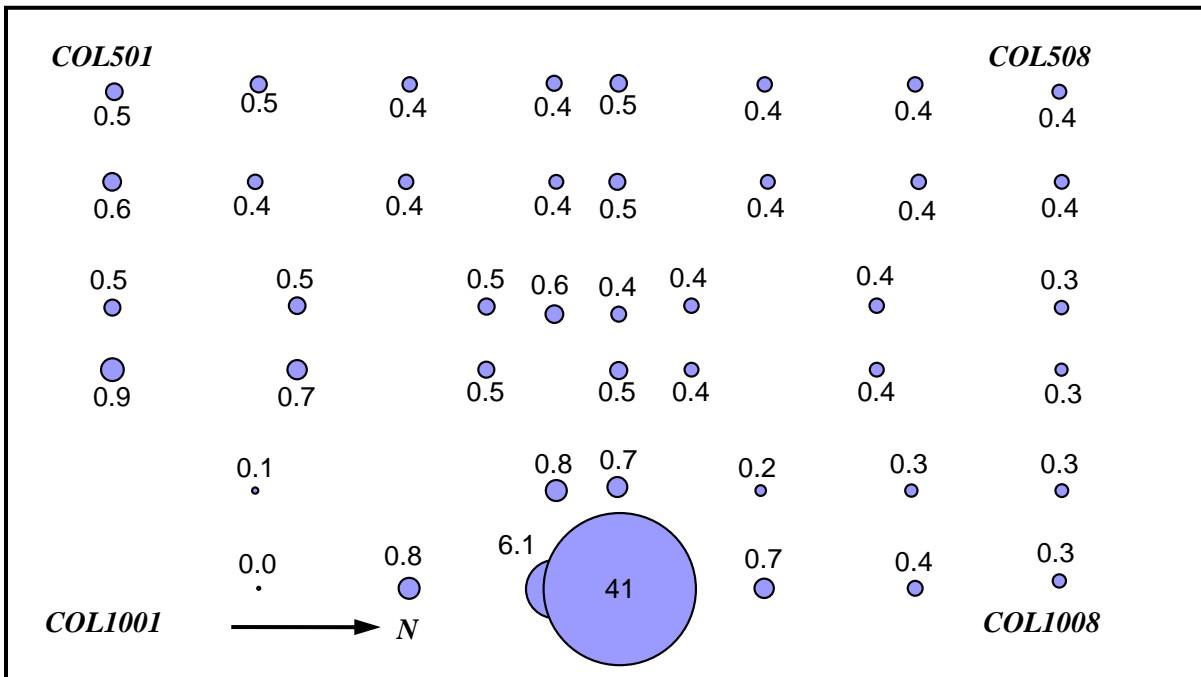


(b) At 30 min

Figure C-19. Ratios of axial elastic-plus-plastic strain to temperature-dependent yield strain for the core columns at Floor 82 of WTC 2 at 10 min and 30 min of Case C_i conditions.



(a) At 40 min



(b) At 60 min

Figure C-20. Ratios of axial elastic-plus-plastic strain to temperature-dependent yield strain for the core columns at Floor 82 of WTC 2 at 40 min and 60 min of Case C_i conditions.

C.2.2 Case D_i Temperature Condition and Case C_i Structural Damage Condition

Table C–3 summarizes the sequence of analyses that were performed with the WTC 2 ANSYS global model with the revised Case C_i structural damage condition from Step 4, and Case D_i temperature condition. Revised Case C_i structural damage refers to the removal of core columns 903 and 1003 in addition to the other core columns that were severed after the aircraft impact as shown in Section 2.2. Case D_i structural damage condition was not used as this structural damage condition was not available at the time of analyses.

Table C–3. Analysis Steps of WTC 2 ANSYS global model with Case D_i temperature condition and Case C_i structural damage condition.

Analysis Step	Description
1	WTC 2 model below Floor 106 was analyzed under its own self-weight.
2	Structures above Floor 106 were added in a stress-free state, and the model was analyzed for dead load including those above Floor 106.
3	Superimposed dead load plus 25 percent of the design live loads were superimposed on the model.
4	Columns (including the 1003 and 903 core columns), spandrels, and floor elements that were severed during aircraft impact were removed, and the model was analyzed (see Section 2.2 for the revised Case C _i structural damage condition).
5	Column and spandrel temperatures were ramped linearly up to temperatures at 10 min.
6	Column and spandrel temperatures were changed linearly from temperatures at 10 min to 20 min.
7	Column and spandrel temperatures were changed linearly from temperatures at 20 min to 30 min.
8	Column and spandrel temperatures were changed linearly from temperatures at 30 min to 40 min.
9	Column and spandrel temperatures were changed linearly from temperatures at 40 min to 50 min.
10	Column and spandrel temperatures were changed linearly from temperatures at 50 min to 60 min.

The model was first analyzed for the effects of the construction sequence (analysis steps 1, 2, and 3). The results of analysis step 3 represent the state of the structure before the aircraft impact. In analysis step 4, the columns, spandrels, and floor elements that were severed during the aircraft impact were removed, and the structure was reanalyzed to redistribute the loads to other members. This analysis represented the structure state after the aircraft impact. The column and spandrel temperatures were applied to the model (analysis steps 5 through 10). The column and spandrel temperatures were provided by NIST at 10 min intervals. Temperatures were calculated by linear interpolation for times in between 10 min intervals. Temperature analyses were performed at every 10 min up to 60 min. Temperatures were not applied to the floor elements, as discussed earlier.

The results of the WTC 2 global model analyses with Case D_i temperature condition and the revised Case C_i structural damage condition are summarized in Figs. C–21 through C–32.

Figure C–21 shows the vertical displacement at different analysis steps. The maximum vertical displacement after the aircraft impact increased from 7.0 in. to 7.7 in. with the inclusion of the additional severed core columns (1003 and 903). The 7.7 in. maximum vertical displacement after aircraft impact gradually increased to 9.2 in. at the end of the 60 min temperature analysis. The exterior columns between Floor 79 and Floor 83 thermally expanded with temperature; however, the core columns shortened due to plastic deformation, and the plastic strains in 1000 series core columns were greater than the thermal expansion strains. Figures C–22 and C–23 show the vertical displacements for the south and east exterior walls after aircraft impact, and at 30 min, 50 min, and 60 min. The displacements of these

exterior walls were typically at their maximum after aircraft impact and gradually decreased to their minimum value with time up to 50 min and then increased slightly beyond 50 min up to 60 min, as temperatures reduced.

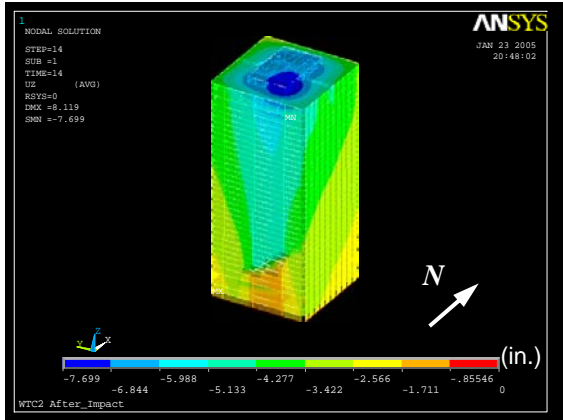
Figures C–24, C–25, and C–26 show the axial load variation over the south, east, and north exterior wall columns and spandrels after impact and at 10 min, 20 min, 30 min, 50 min, and 60 min. The maximum column load on the east exterior wall columns increased from 485 kip after aircraft impact to about 880 kip at the end of 30 min and then dropped down to 800 kip at the end of 60 min. The increase in column forces was mostly concentrated at the center portion of the east wall. The maximum column load on the north exterior wall columns increased from 355 kip after aircraft impact to about 550 kip at the end of 30 min and then dropped down to 440 kip at 50 min; it then increased again to 700 kip at the end of 60 min.

Figures C–27, C–28 and C–29 show the axial load variations over the 800, 900, and 1000 core column series after aircraft impact and at 10 min, 20 min, 30 min, 50 min, and 60 min. Over the duration of the fires, the maximum column load after impact increased from 5,200 kip to 6,250 kip in the 1000 core column series and from 1,700 kip to 2,500 kip in the 900 core column series, and decreased slightly from 3,400 kip to 3,200 kip in the 800 core column series.

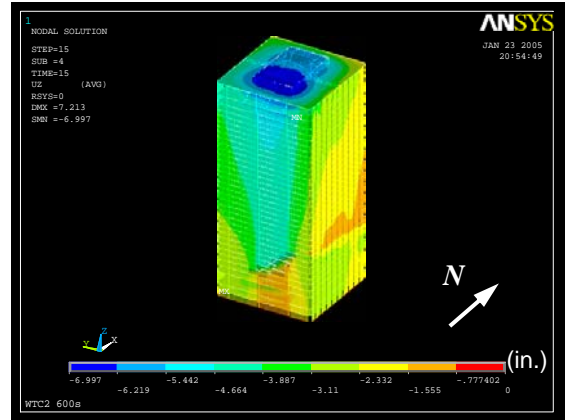
Figure C–30 shows the total column loads in the core and the north, south, east, and west exterior walls for different floors. Total column loads below Floor 83 after aircraft impact did not add up to the total column loads before the aircraft impact. This difference is equal to the self-weight of severed members and floor loads applied to severed columns.

In Floor 83, the temperature effect alone resulted in an unloading of the core columns by 2,000 kip and increased the total load by 630 kip on the south exterior wall, by 300 kip on the west exterior wall, by 540 kip on the north exterior wall, and by 530 kip on the east exterior wall.

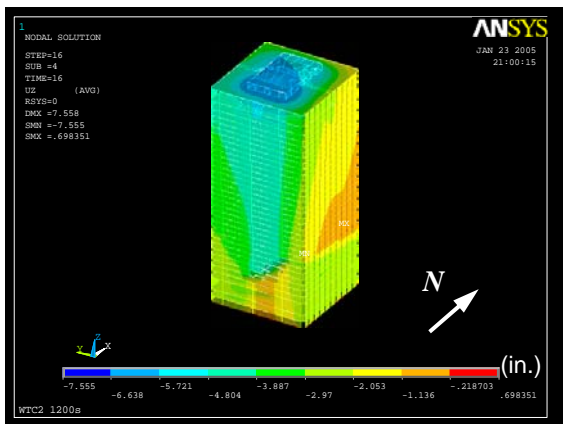
Figures C–31 and C–32 show the ratio of elastic-plus-plastic strain to the temperature-dependent yield strain of the core columns between Floor 82 and Floor 83 at 10 min, 20 min, 50 min, and 60 min. After 10 min, except for Core Columns 801, 1004, and 1005, the strain ratios in the core columns were all less than 1.0. With increasing time, more columns from east side and center region of the core area started to show strain ratios greater than 1.0, indicating the onset of plasticity. A maximum strain ratio of 41 was reached between 40 min and 60 min at Column 1005. Higher strain ratios were clustered around the east side of the core, indicating a tendency of the core to tilt toward east.



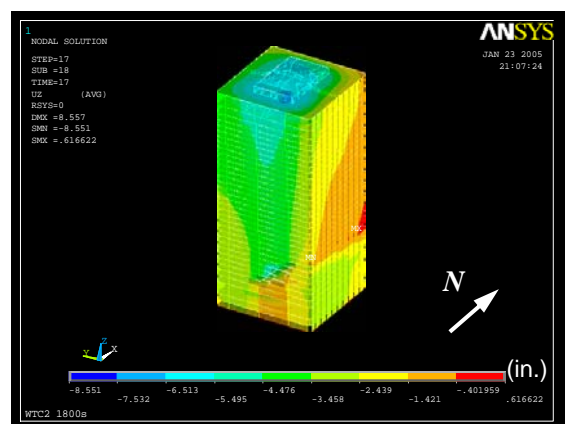
(a) After impact



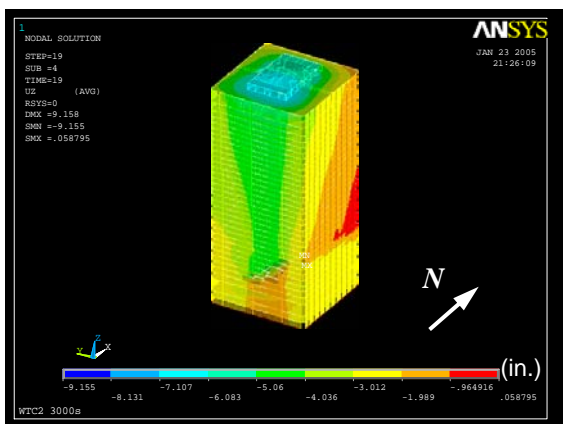
(b) At 10 min



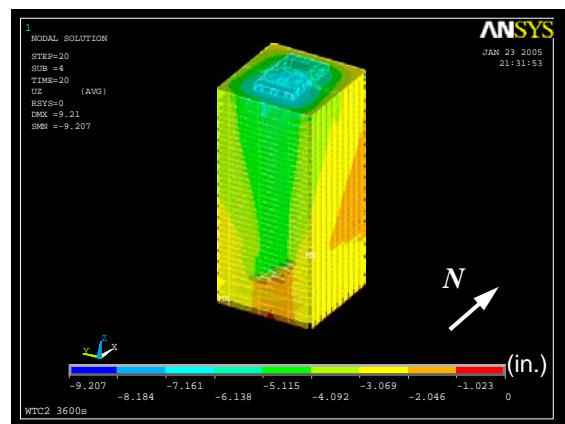
(c) At 20 min



(d) At 30 min

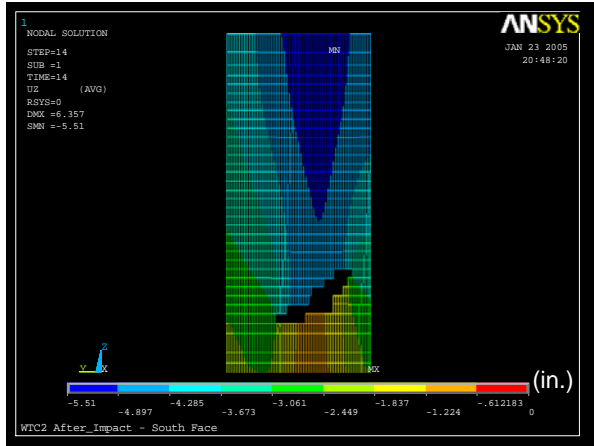


(e) At 50 min

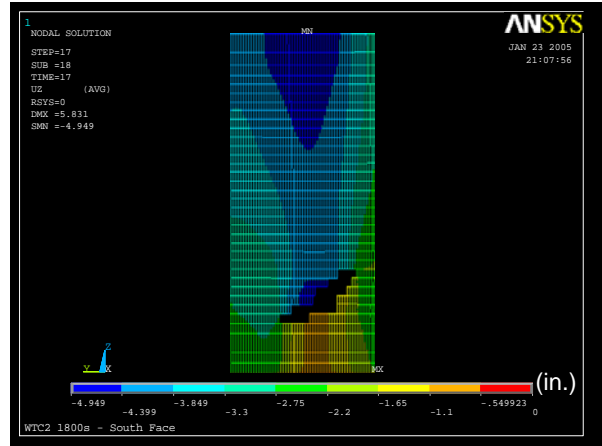


(f) At 60 min

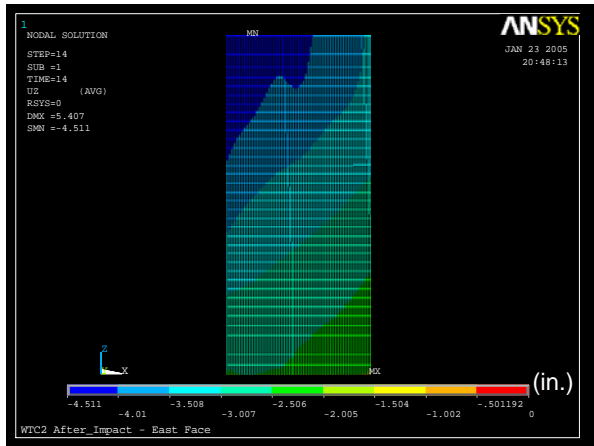
Figure C-21. Vertical displacement at different stages of WTC 2 for Case D_i temperature condition and the revised Case C_i structural damage condition (downward displacement is negative).



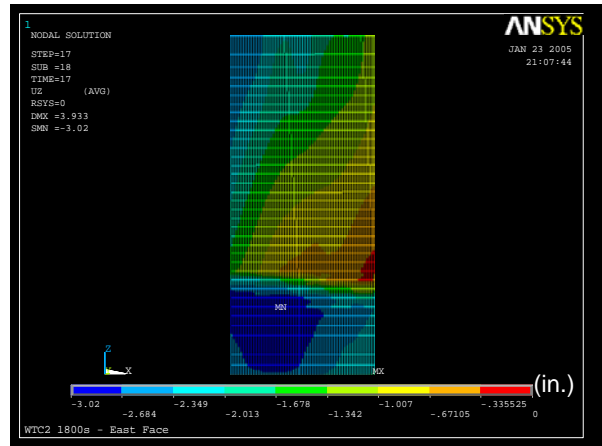
(a) South wall after impact



(b) South wall at 30 min

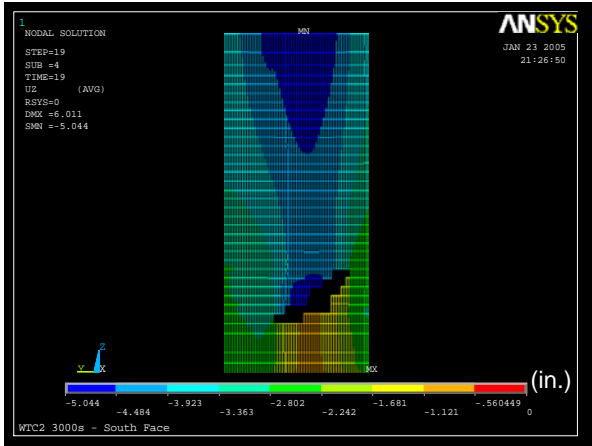


(c) East wall after impact

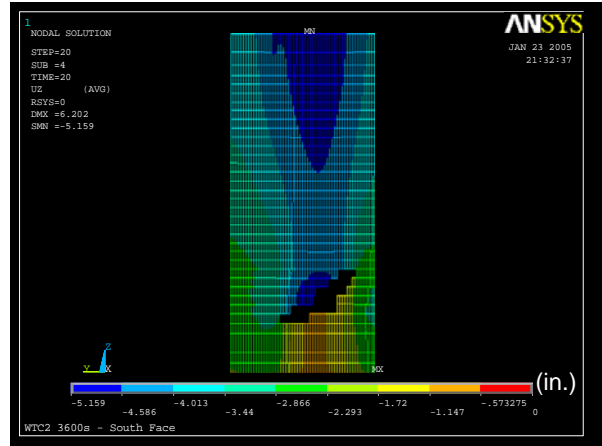


(d) East wall at 30 min

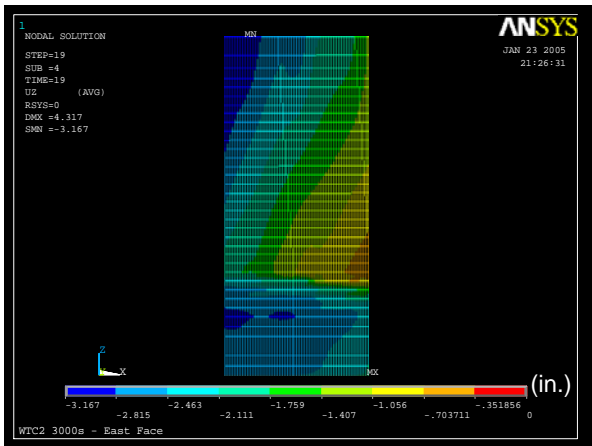
Figure C–22. Vertical displacement on the south and east faces of WTC 2 after aircraft impact and at 30 min of Case D_i temperature condition and the revised Case C_i structural damage condition (looking from outside; downward displacement is negative).



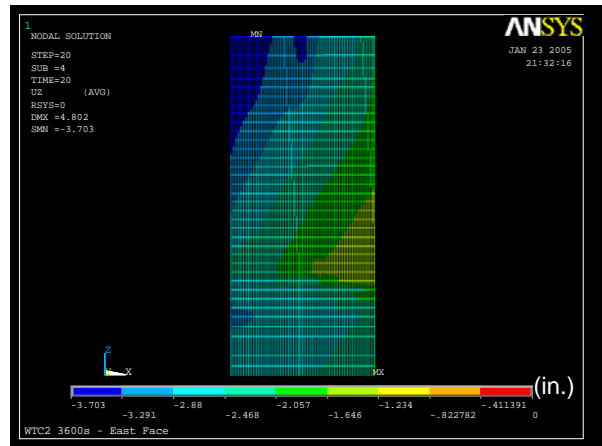
(a) South wall at 50 min



(b) South wall at 60 min

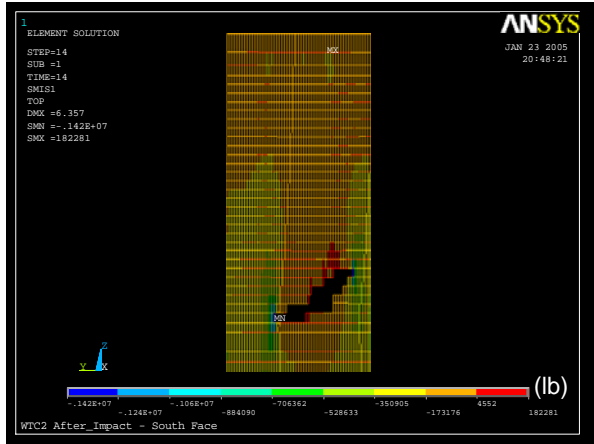


(c) East wall at 50 min

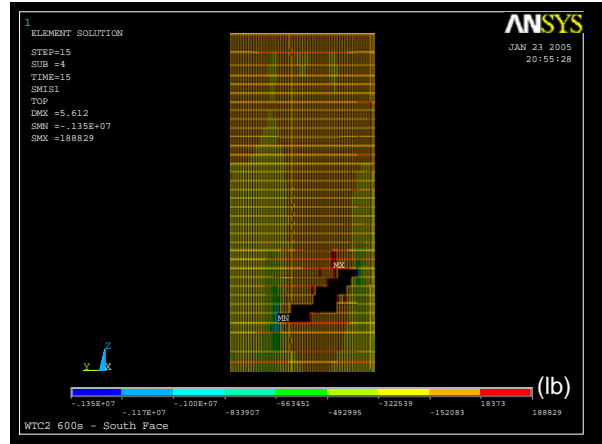


(d) East wall at 60 min

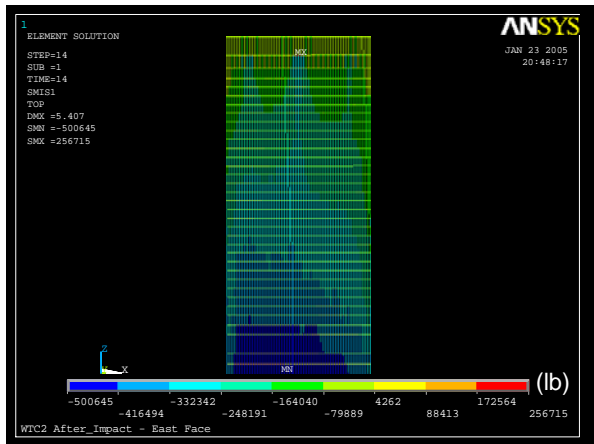
Figure C-23. Vertical displacement on the south and east faces of WTC 2 at 50 min and at 60 min of Case D_i temperature condition and the revised Case C_i structural damage condition (looking from outside; downward displacement is negative).



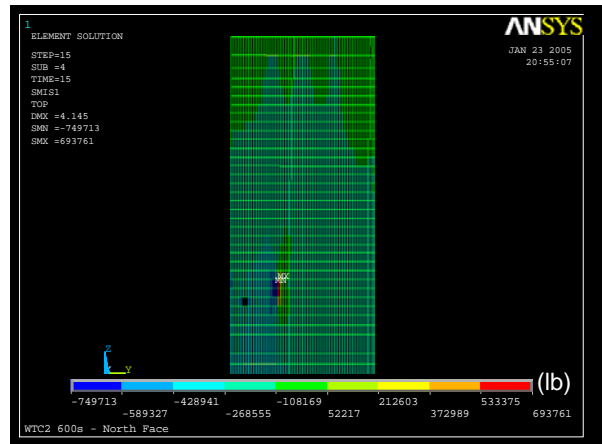
(a) South wall after impact



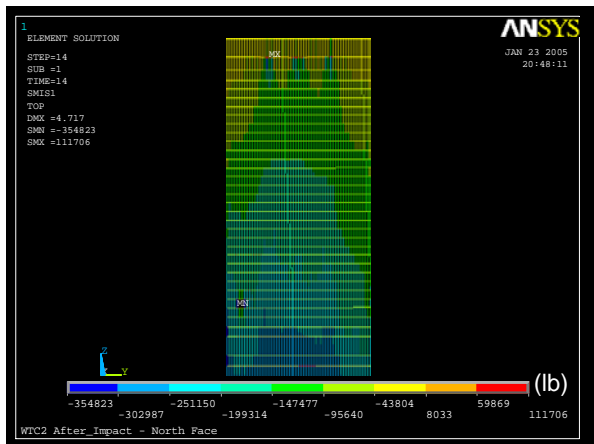
(b) South wall at 10 min



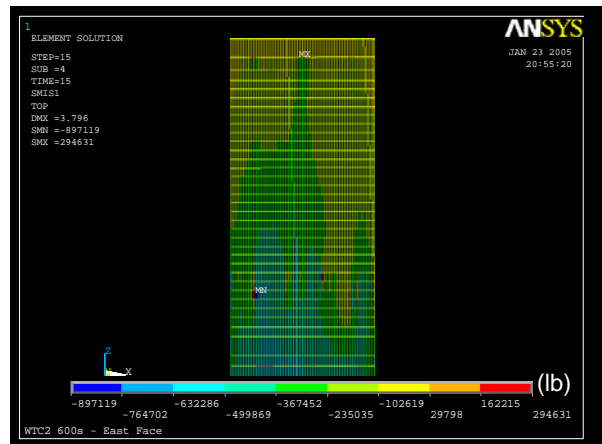
(c) East wall after impact



(d) East wall at 10 min

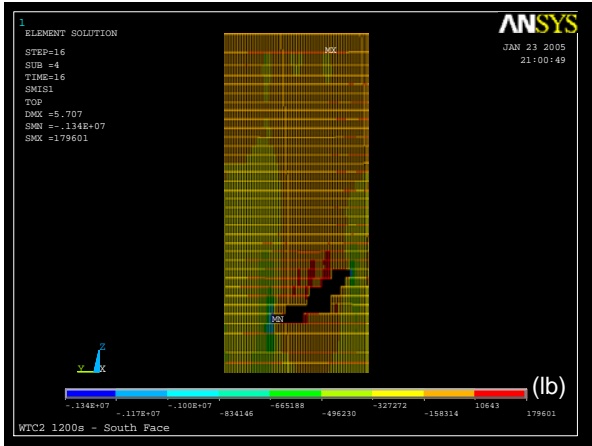


(e) North wall after impact

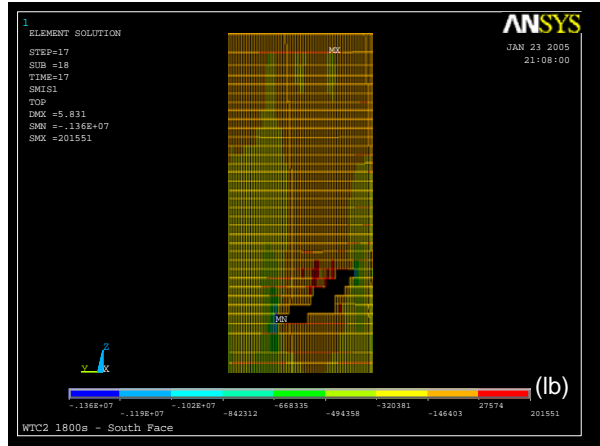


(f) North wall at 10 min

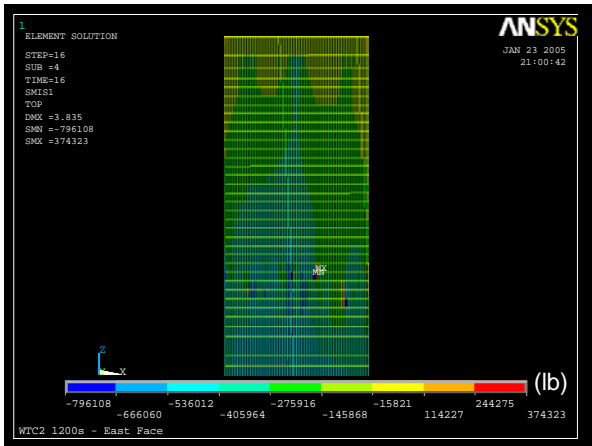
Figure C-24. Axial force variation on the south, east, and north faces of WTC 2 after impact and at 10 min of Case D_i temperature condition and the revised Case C_i structural damage condition (looking from outside; compression is negative).



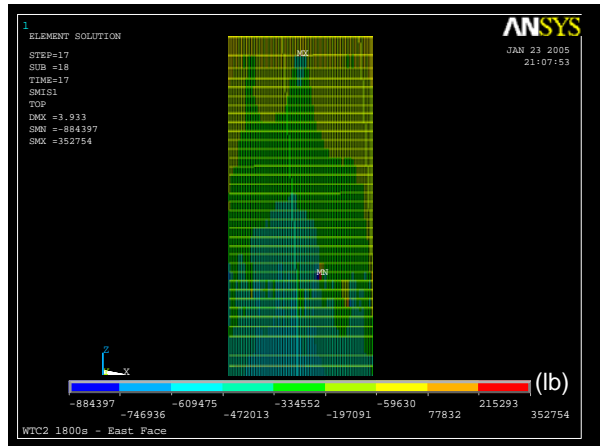
(a) South wall at 20 min



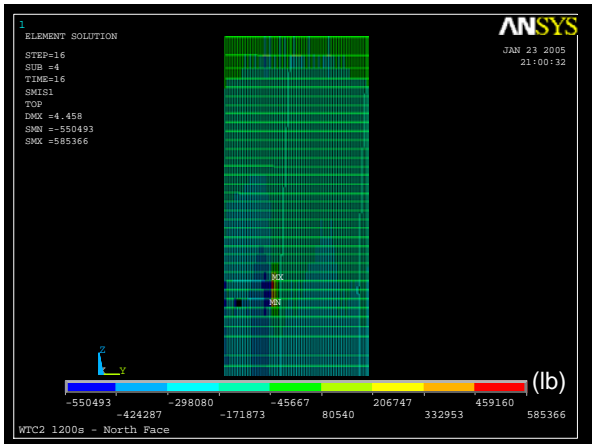
(b) South wall at 30 min



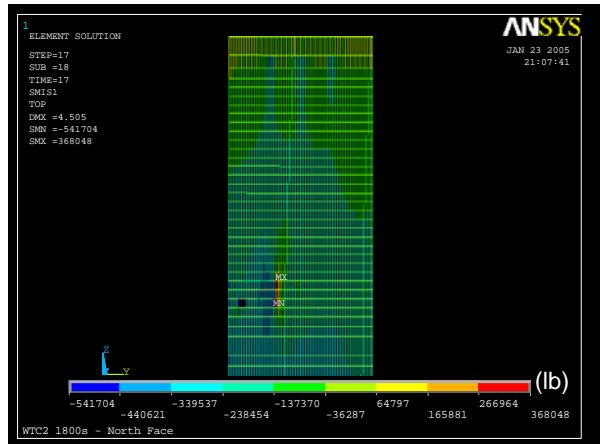
(c) East wall at 20 min



(d) East wall at 30 min

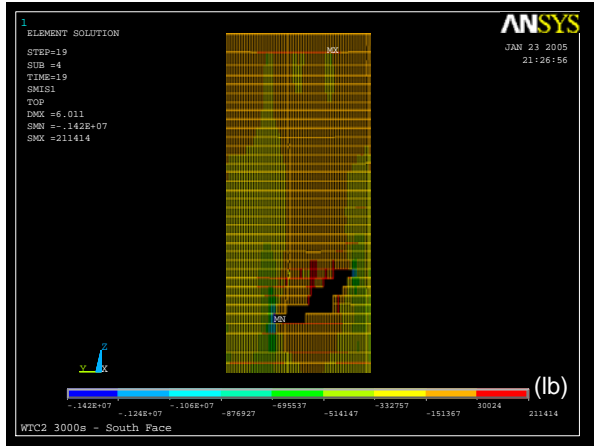


(e) North wall at 20 min

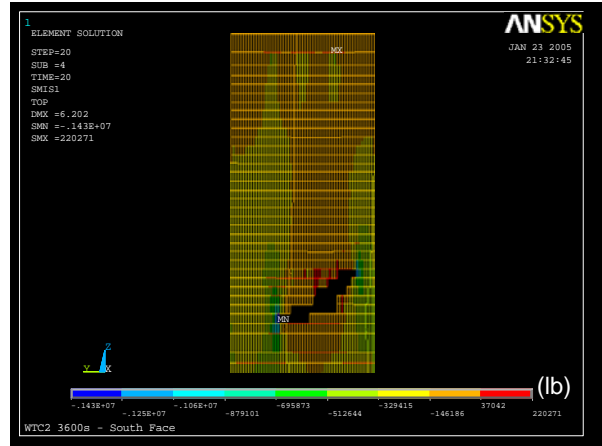


(f) North wall at 30 min

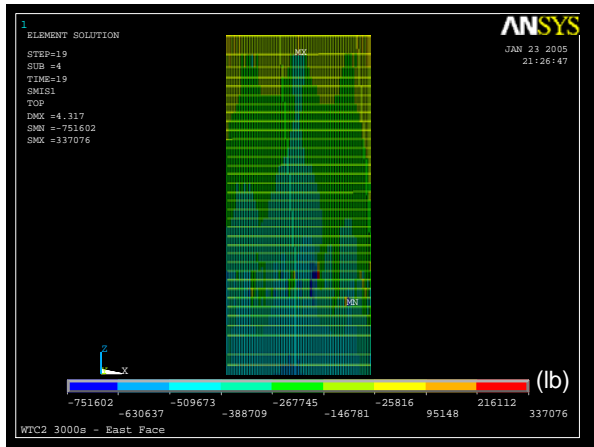
Figure C-25. Axial force variation on the south, east, and north faces of WTC 2 at 20 min and at 30 min of Case D_i temperature condition and the revised Case C_i structural damage condition (looking from outside; compression is negative).



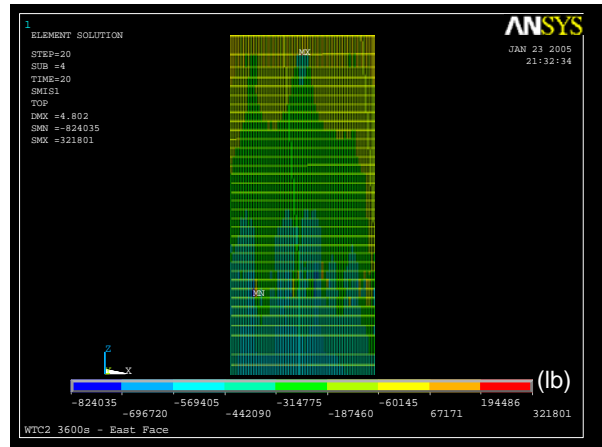
(a) South wall at 50 min



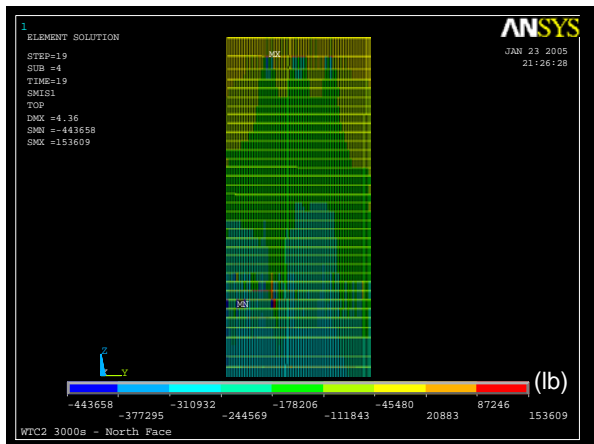
(b) South wall at 60 min



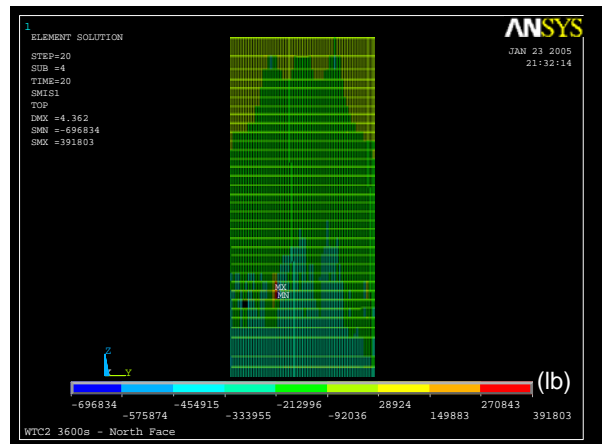
(c) East wall at 50 min



(d) East wall at 60 min

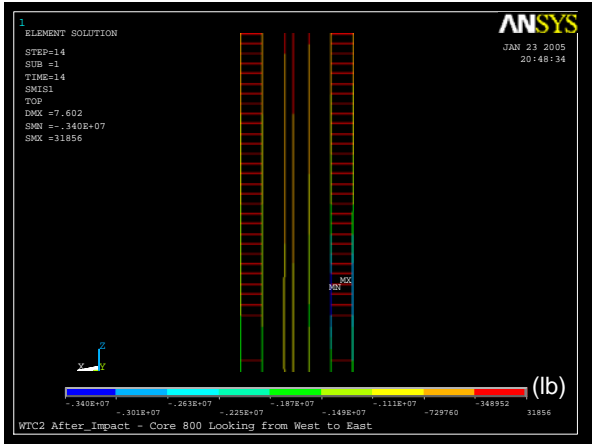


(e) North wall at 50 min

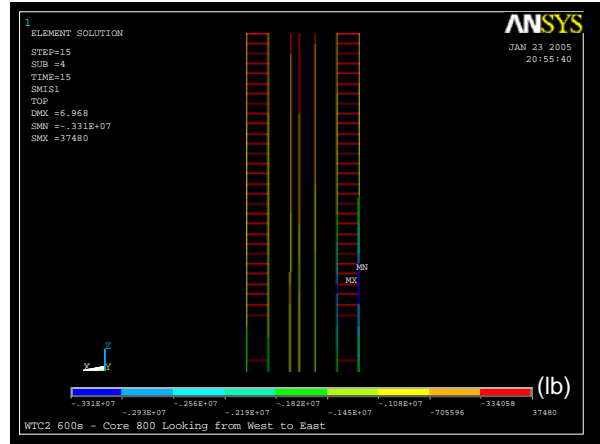


(f) North wall at 60 min

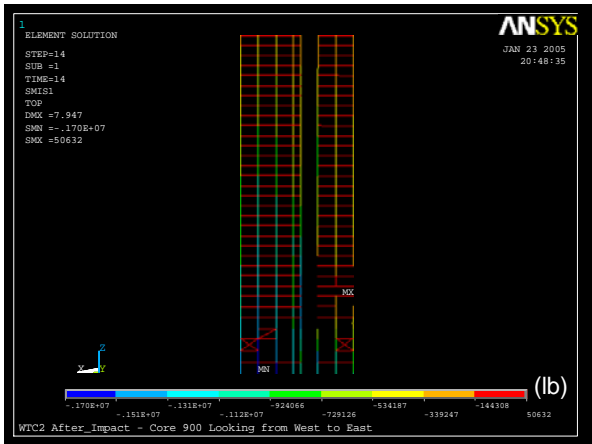
Figure C-26. Axial force variation on the south, east, and north faces of WTC 2 at 50 min and at 60 min of Case D_i temperature condition and the revised Case C_i structural damage condition (looking from outside; compression is negative).



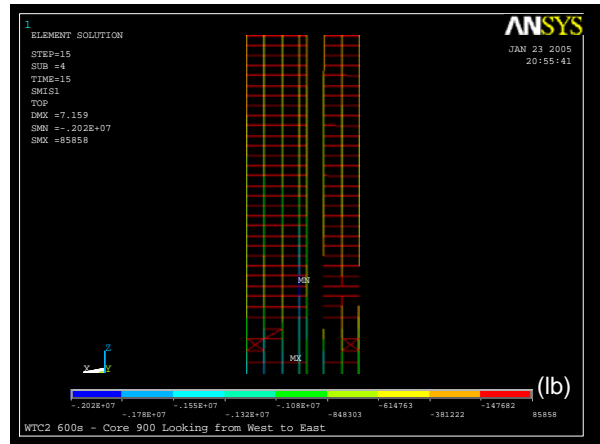
(a) 800 series columns after impact



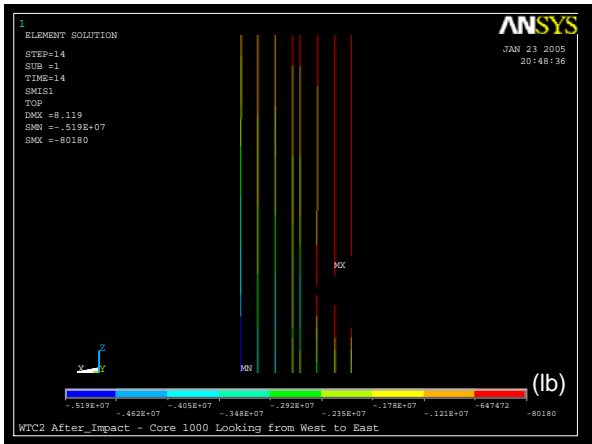
(b) 800 series columns at 10 min



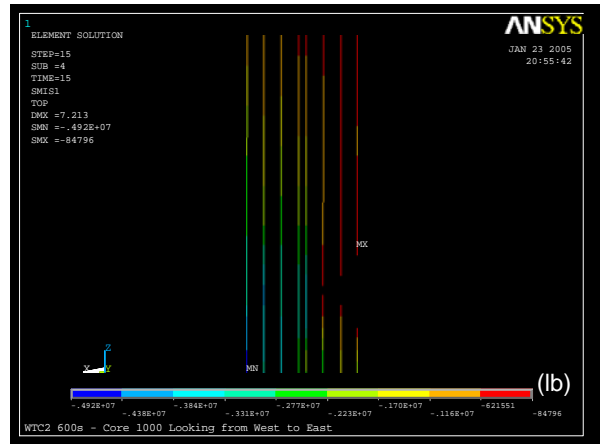
(c) 900 series columns after impact



(d) 900 series columns at 10 min

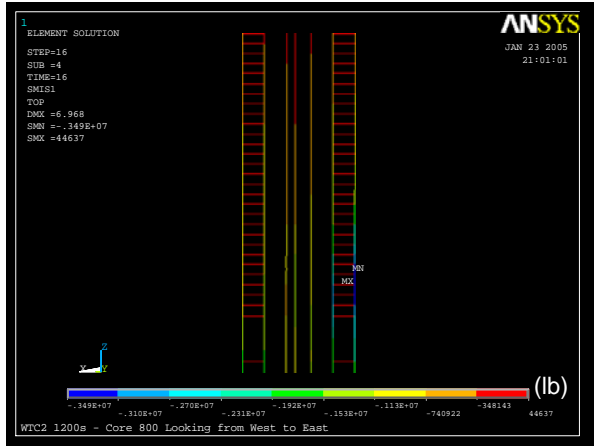


(e) 1000 series columns after impact

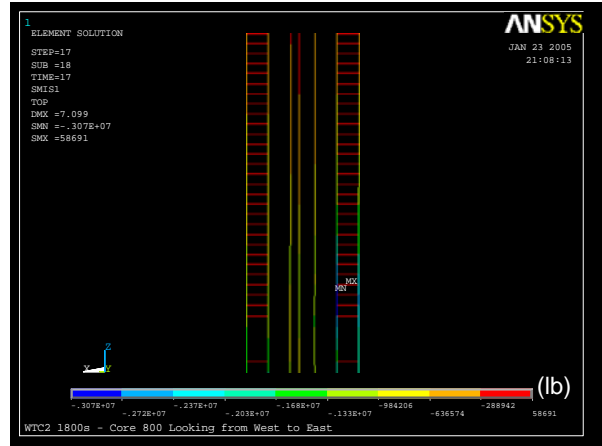


(f) 1000 series columns at 10 min

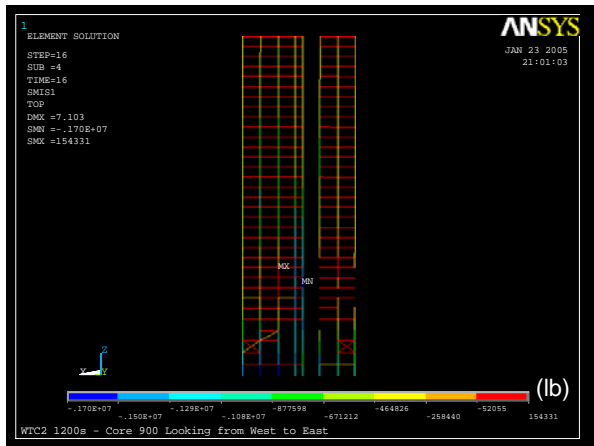
Figure C–27. Axial force variation on the 800, 900, and 1000 series core columns of WTC 2 after impact and at 10 min of Case D_i temperature condition and the revised Case C_i structural damage condition (looking from west; compression is negative).



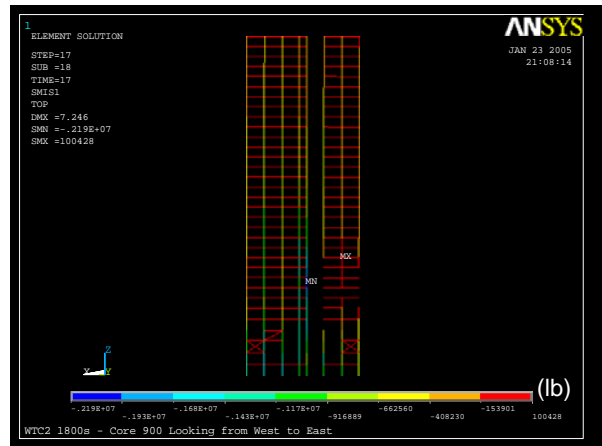
(a) 800 series columns at 20 min



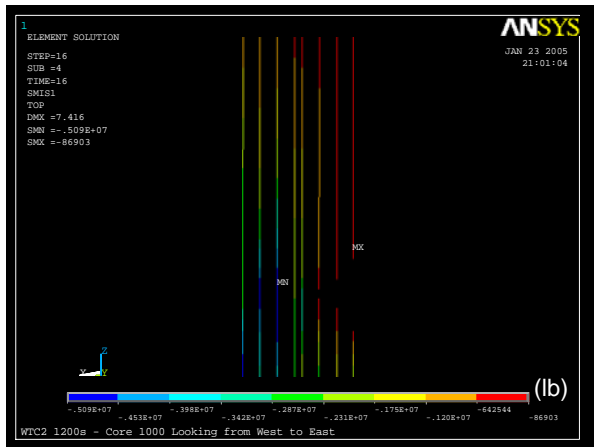
(b) 800 series columns at 30 min



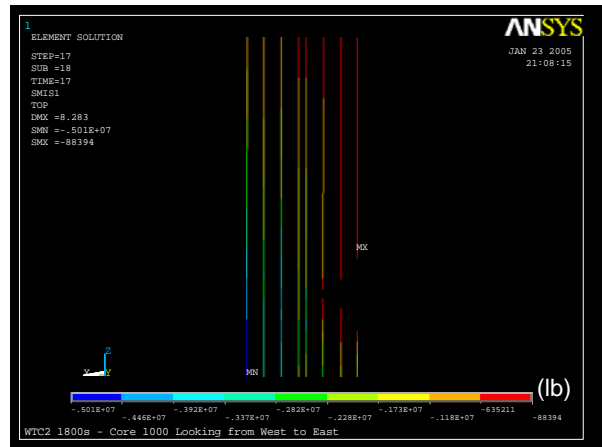
(c) 900 series columns at 20 min



(d) 900 series columns at 30 min

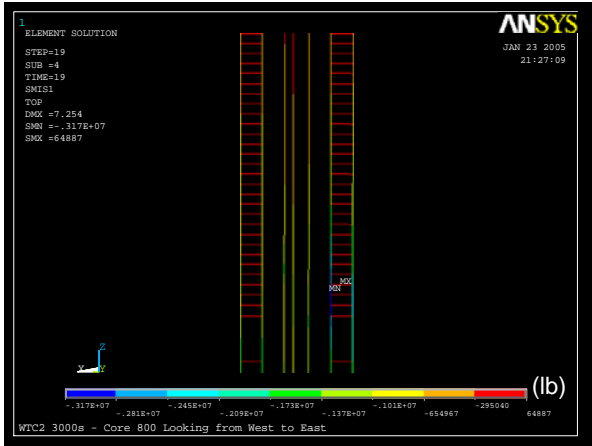


(e) 1000 series columns at 20 min

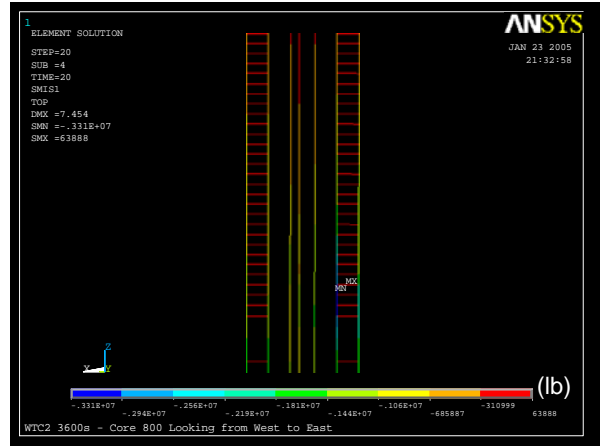


(f) 1000 series columns at 30 min

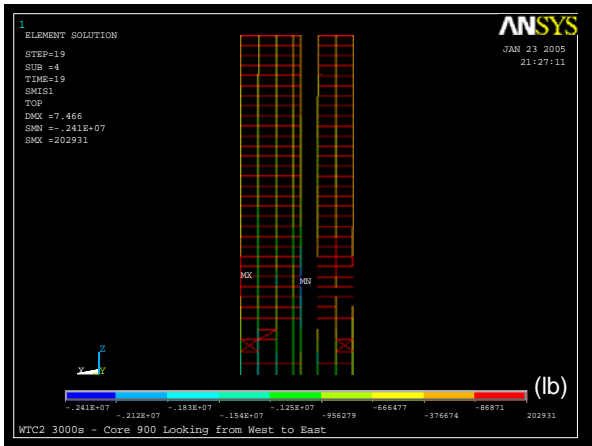
Figure C–28. Axial force variation on the 800, 900, and 1000 series core columns of WTC 2 at 20 min and at 30 min of Case D_i temperature condition and the revised Case C_i structural damage condition (looking from west; compression is negative).



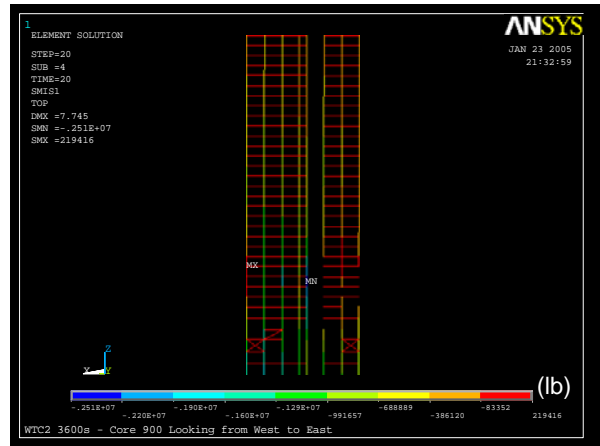
(a) 800 series columns at 50 min



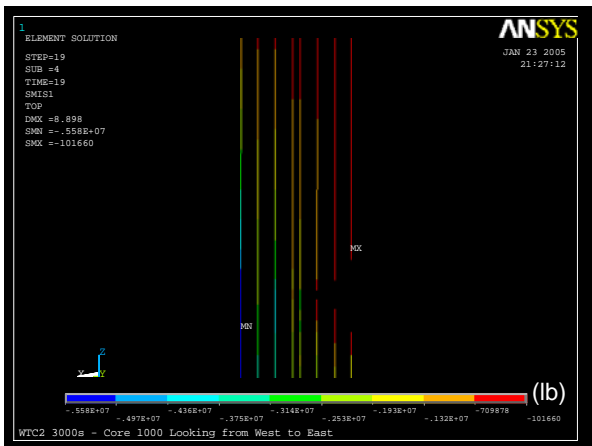
(b) 800 series columns at 60 min



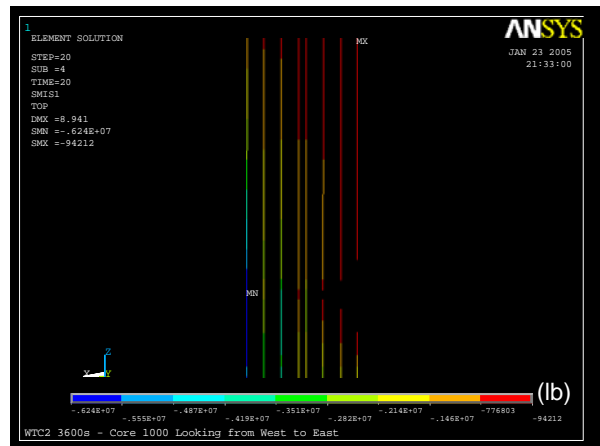
(c) 900 series columns at 50 min



(d) 900 series columns at 60 min



(e) 1000 series columns at 50 min



(f) 1000 series columns at 60 min

Figure C–29. Axial force variation on the 800, 900, and 1000 series core columns of WTC 2 at 50 min and at 60 min of Case D_i temperature condition and the revised Case C_i structural damage condition (looking from west; compression is negative).

Row	Analysis Stage	West	East	North	South	Core	Sum
(1)	Before Impact	18779	18837	13714	13529	77563	142423
(2)	After Impact	18824	21170	12812	12396	75450	140652
(3)	10 min	19668	21636	13148	11694	74506	140652
(4)	20 min	19984	21951	13004	11661	74053	140653
(5)	30 min	20005	22426	13129	11899	73195	140653
(6)	40 min	19980	22260	13252	12156	73005	140653
(7)	50 min	19617	22048	13211	12609	73168	140653
(8)	60 min	19161	21803	13294	12959	73436	140653

(a) Above Floor 78

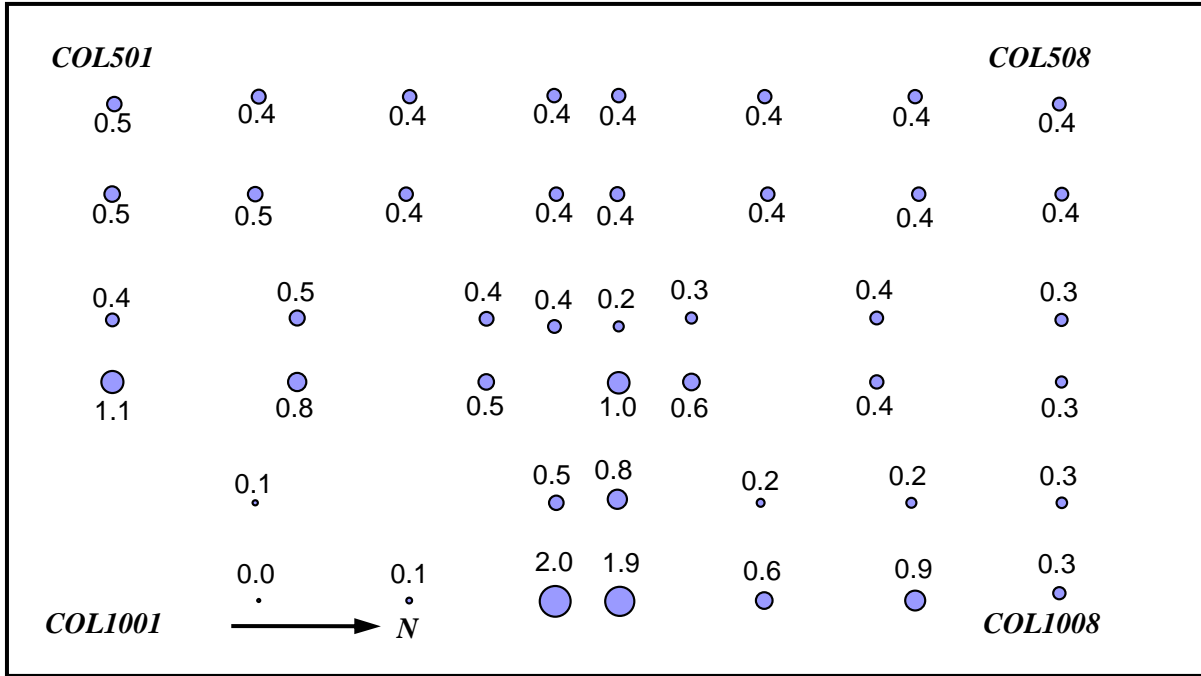
Row	Analysis Stage	West	East	North	South	Core	Sum
(1)	Before Impact	17642	17697	12558	12393	71319	131609
(2)	After Impact	17613	20084	11761	11475	70039	130972
(3)	10 min	18453	20602	12152	10672	69094	130973
(4)	20 min	18759	20889	12005	10680	68640	130973
(5)	30 min	18755	21379	12146	10910	67782	130972
(6)	40 min	18718	21202	12290	11170	67593	130972
(7)	50 min	18340	20983	12237	11655	67756	130971
(8)	60 min	17876	20724	12316	12034	68022	130972

(b) Above Floor 81

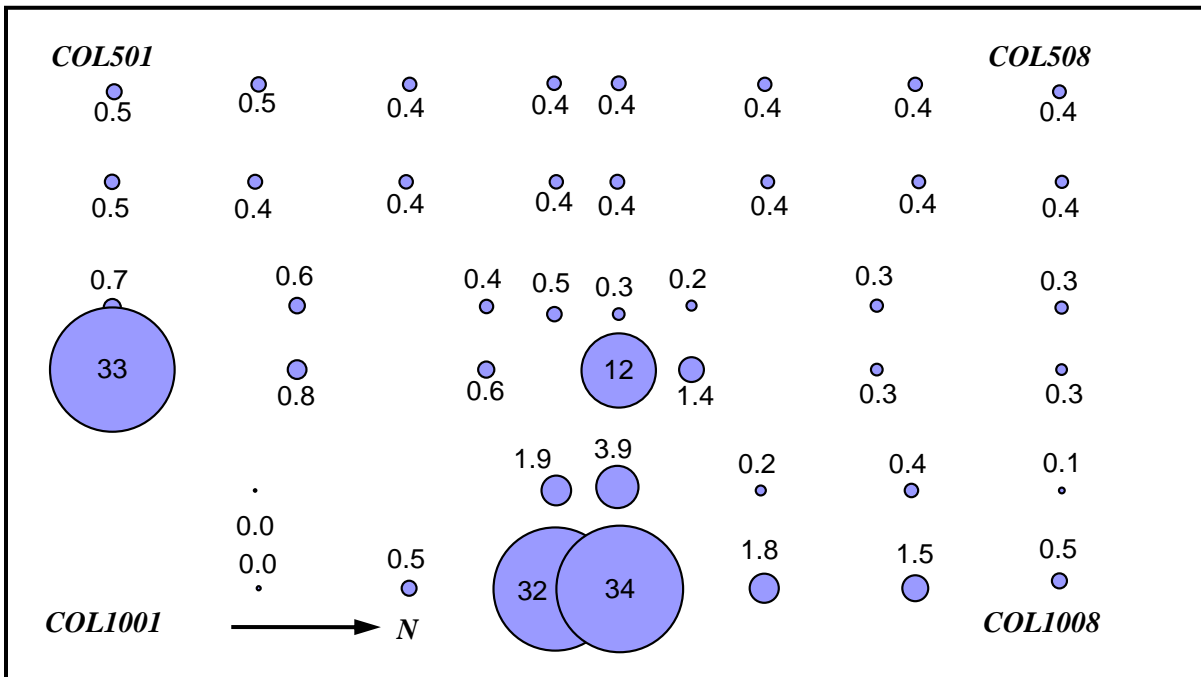
Row	Analysis Stage	West	East	North	South	Core	Sum
(1)	Before Impact	16728	16782	11972	11820	67309	124611
(2)	After Impact	16717	19111	11188	11058	66400	124474
(3)	10 min	17551	19473	11596	10404	65449	124473
(4)	20 min	17864	19739	11443	10431	64996	124472
(5)	30 min	17875	20198	11573	10687	64138	124471
(6)	40 min	17847	20006	11709	10960	63950	124471
(7)	50 min	17482	19841	11651	11384	64113	124472
(8)	60 min	17025	19637	11734	11691	64384	124471

(c) Above Floor 83

Figure C–30. Total column loads in the core and exterior walls of WTC 2 at different floors and at different times for Case D_i temperature condition and the revised Case C_i structural damage condition (compression is positive).

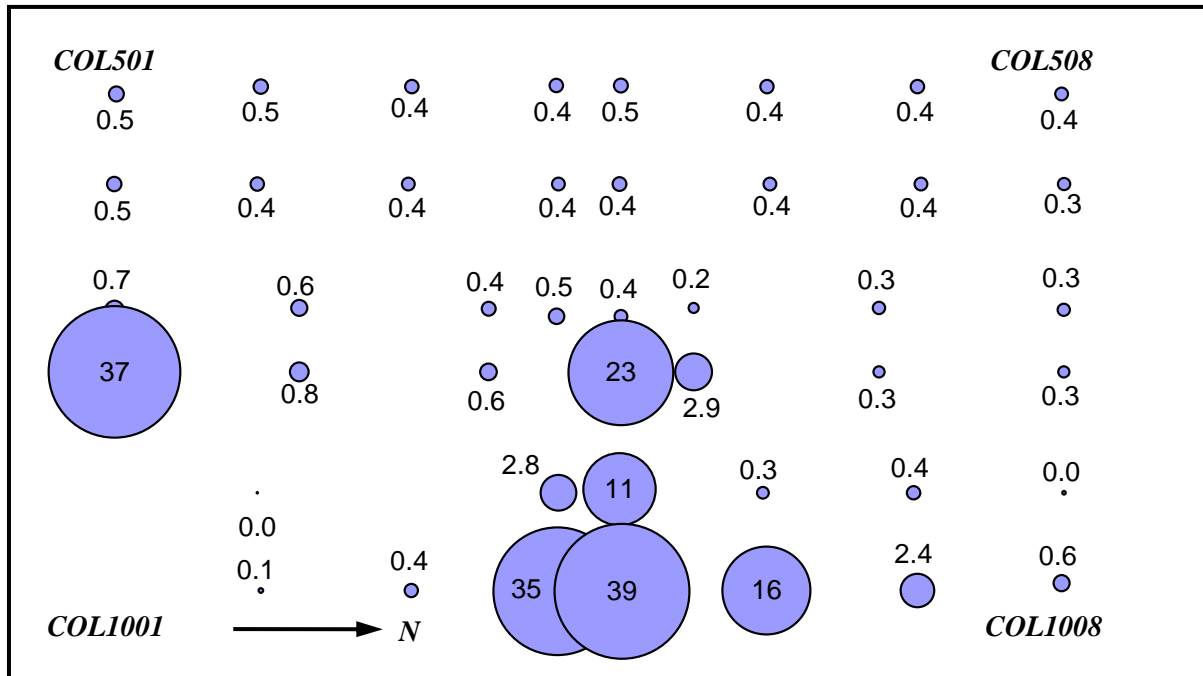


(a) At 10 min

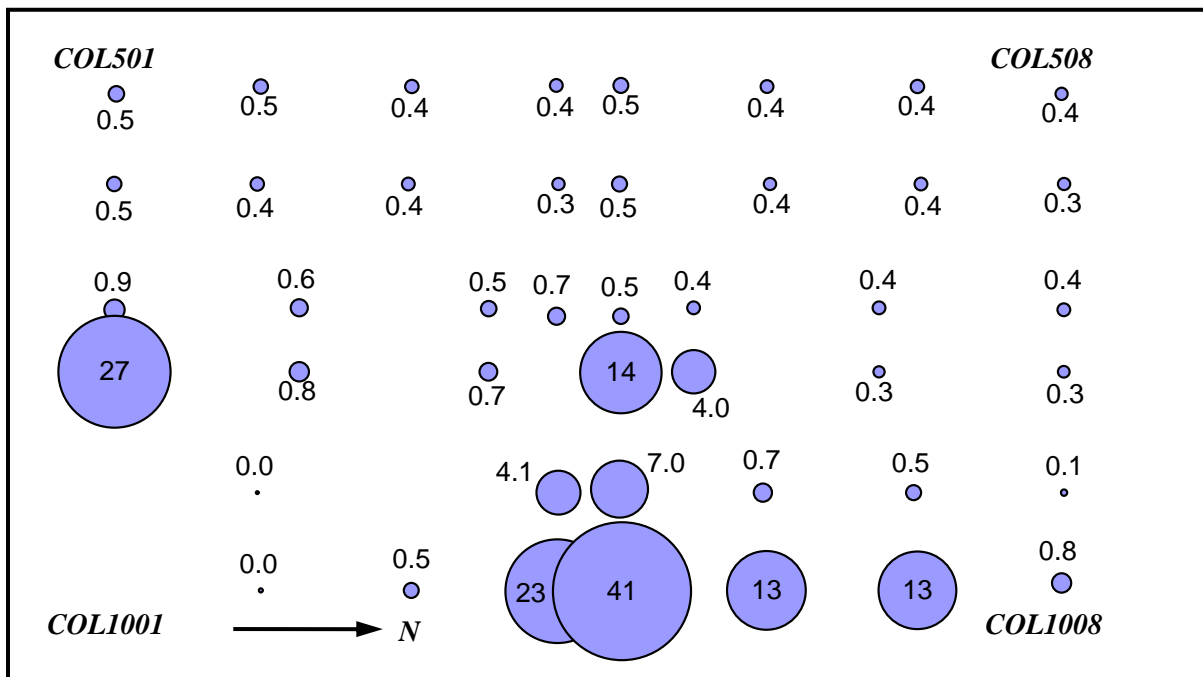


(b) At 30 min

Figure C-31. Ratios of axial elastic-plus-plastic strain to temperature-dependent yield strain for the core columns at Floor 82 of WTC 2 at 10 min and at 30 min of Case D_i temperature condition and the revised Case C_i structural damage condition.



(a) At 40 min



(b) At 60 min

Figure C-32. Ratios of axial elastic-plus-plastic strain to temperature-dependent yield strain for the core columns at Floor 82 of WTC 2 at 40 min and at 60 min of Case D_i temperature condition and the revised Case C_i structural damage condition.